



INŻYNIERIA MINERALNA

CZASOPISMO POLSKIEGO TOWARZYSTWA
PRZERÓBKI KOPALIN

2(48)
2021

NR 2(48) 2021, LIPIEC – GRUDZIEŃ

PL ISSN 1640 - 4920



JOURNAL OF THE POLISH
MINERAL ENGINEERING SOCIETY

NO. 2(48) 2021, JULY – DECEMBER

INŻYNIERIA MINERALNA

Czasopismo Polskiego Towarzystwa Przeróbki Kopalin

JOURNAL OF THE POLISH MINERAL ENGINEERING SOCIETY

REDAKCJA – EDITORIAL BOARD

Redaktor Naczelny – Zastępca Redaktora Naczelnego, Redaktor Techniczny –	Barbara TORA	– Editor in Chief
	Julia OKREGLICKA	– Vice Editor, Technical Editor
Sekretarz Redakcji – Redaktor Statystyczny –	Agnieszka SUROWIAK Tomasz NIEDOBA	– Editorial Secretary – Statistical Editor

REDAKTORZY DZIAŁOWI BRANCH EDITORS

Stanisław CIERPISZ
Andrzej ŁUSZCZKIEWICZ
Stanisława SANAK-RYDLEWSKA
Tomasz SUPONIK
Dariusz PROSTAŃSKI
Alicja BAKALARZ
Jadwiga JARZYNA
Marek BOROWSKI
Tomasz LIPECKI

REDAKTORZY HONOROWI HONOUR ISSUE EDITORS

Prof. Bui Xuan Nam
Assoc.Prof. Nguyen Thi Hoai Nga
Dr. Nguyen Quoc Long
Dr. Nguyen Viet Nghia
Dr. Khuong The Hung

MIEDZYNARODOWA RADA REDAKCYJNA INTERNATIONAL ADVISORY EDITORIAL BOARD

Rosja –	Tatyana ALEXANDROVA	– Russia
Grecja –	Georgios ANASTASSAKIS	– Greece
Polska –	Wiesław BLASCHKE	– Poland
Słowacja –	Peter BLISTAN	– Slovakia
Węgry –	Ljudmilla BOKÁNYI	– Hungary
Czechy –	Vladimir ČABLÍK	– Czech Republic
Czechy –	Pavel ČERNOTA	– Czech Republic
Rosja –	Valentin A. CHANTURIYA	– Russia
RPA –	Johan DE KORTE	– South Africa
Polska –	Jan DRZYMAŁA	– Poland
Słowacja –	Juraj GAŠINEC	– Slovakia
Węgry –	Imre GOMBKÖTŐ	– Hungary
Słowacja –	Gabriel WEISS	– Slovakia
Kanada –	M.E. HOLUSZKO	– Canada
Słowacja –	Slawomir HREDZAK	– Slovakia
W. Brytania –	Douglas E. JENKINSON	– United Kingdom
Polska –	Przemysław KOWALCZUK	– Poland
Rumunia –	Sanda KRAUSZ	– Romania
Polska –	Janusz LASKOWSKI	– Poland
Polska –	Marcin LUTYŃSKI	– Poland
Turcja –	Gülhan ÖZBAYOĞLU	– Turkey
USA –	B. K. PAREKH	– USA
RPA –	David PEATFIELD	– South Africa
Rosja –	Yuliy B. RUBINSHTEIN	– Russia
Polska –	Jerzy SABLİK	– Poland
Indie –	Rai K. SACHDEV	– India
Indie –	Kalyan SEN	– India
Chiny –	Zhongjian SHAN	– China
Słowacja –	Jirí ŠKVARLA	– Slovakia
Czechy –	Hana STANKOVA	– Czech Republic
Australia –	Andrew SWANSON	– Australia
Serbia –	Rudolf A. TOMANEC	– Serbia
Japonia –	Masami TSUNEKAWA	– Japan
Chiny –	Xie WENBO	– China
Ukraina –	Olexandr YEGURNOV	– Ukraine
Niemcy –	Dieter ZIAJA	– Germany

INŻYNIERIA MINERALNA JEST DOSTĘPNA (OPEN ACCESS) NA STRONIE WYDAWCY | WHOLE ISSUES OF INŻYNIERIA MINERALNA ARE AVAILABLE (OPEN ACCESS) ON PUBLISHER
WEBSITE: POLSKA WWW.POTOPK.COM.PL/ARCHIWUM
ENGLISH WWW.POTOPK.COM.PL/AN_ARCHIWUM

INŻYNIERIA MINERALNA JEST INDEKSOWANA I ABSTRAKTOWANA | INŻYNIERIA MINERALNA IS INDEXED AND ABSTRACTED:
SCOPUS (ELSEVIER), WEB OF SCIENCE, MASTER JOURNAL LIST – EMERGING SOURCES CITATION INDEX (CLARIVATE ANALITICS), POL-index, EBESCO, BAZTECH, Chemical Abstracts,
Реферативный Журнал.
Inżynieria Mineralna is a member of CROSSREF.

ADRES REDAKCJI | CORRESPONDANCE ADDRESS:
POLSKIE TOWARZYSTWO PRZERÓBKI KOPALIN | POLISH MINERAL ENGINEERING SOCIETY
MICKIEWICZA 30, 30-059 KRAKÓW
MAIL: TORA@AGH.EDU.PL, C@NWH.PL

SKŁAD/ŁAMANIE/UKŁAD TYPOGRAFICZNY/OBSŁUGA: NOWY WSPANIAŁY HOLDING (NWH)
KONTAKT: C@NWH.PL
DRUK: DRUKARNIA TYPOGRAFIA – WWW.TYPOGRAFIA.COM.PL
KONTAKT: TYPOGRAFIA@TYPOGRAFIA.COM.PL
NAKŁAD: 200 egz.

© Inżynieria Mineralna, ISSN 1640-4920, Kraków 2020 by POLSKIE TOWARZYSTWO PRZERÓBKI KOPALIN
Inżynieria Mineralna is licensed under CC-BY-SA 3.0 Creative Commons.
© Articles by authors

Wydanie Inżynierii Mineralnej jest dofinansowane przez diekana Wydziału Górnictwa i Geoinżynierii Akademii Górniczo-Hutniczej.

Cretaceous Granitic Magmatism in South-Central Vietnam: Constraints from Zircon U–Pb Geochronology

NGUYEN Huu Hiep^{1,*}, PHAM Nhu Sang¹, HOANG Van Long², ANDREW Carter³, BUI Vinh Hau¹, BUI Hoang Bac¹, TRINH Thanh Trung⁴, NGUYEN Lam Anh⁵

¹ Hanoi University of Mining and Geology, 18 Vien street, Hanoi, Vietnam

² Vietnam Petroleum Institute, Hanoi, Vietnam

³ University of London, Malet street, London WC1E 7HX, United Kingdom

⁴ Vietnam Administration of Seas and Islands, 83 Nguyen Chi Thanh, Hanoi, Vietnam

⁵ Vietsovpetro, 105 Le Loi street, Vung Tau, Vietnam

Corresponding author: nguyenuhuuhiep@hmg.edu.vn

Abstract. South-central Vietnam abundantly presents magmatic rocks with larger volumes of Cretaceous granitic rocks. In this study, zircon U–Pb geochronology of granite samples from the Deoca, Ankroet, and Dinhquan complexes in south-central Vietnam are utilized to investigate Cretaceous granitic magmatism. According to U–Pb analysis results, zircon ages of granitic rocks display the Deoca at ~113–92 Ma, the Ankroet at ~103–98 Ma, and the Dinhquan at ~97–113 Ma. The range of ages is narrow from 113 to 92 Ma, with most common ages date at ~100 Ma. Published data and our results display that Cretaceous granitic magmatism was active between ~87–118 Ma and most active at ~100 Ma in south-central Vietnam. Additionally, the Deoca and Dinhquan complexes show inherited ages in Triassic followed by Proterozoic and Carboniferous to Ordovician. The obtained ages indicate that I-type granitic rocks could be derived from melting of basement rocks. Our study suggests that I-type granitic rocks in south-central Vietnam were significantly intruded around 100 Ma.

Keywords: Cretaceous granitic magmatism, Zircon U–Pb, Granitic rock, South-central Vietnam

1. Introduction

South-central Vietnam is situated in the Indochina block of Southeast Asia and abundantly occurs Cretaceous granitic batholiths [1–3]. The formation of Cordilleran-type granitic batholiths mainly shows a close correlation with the subduction of oceanic crust beneath the continental crust, and they can be products of crustal recycling and the presence of liquid water [4–11]. Generally, cordilleran granitic batholiths consist of different chemical characterizations due to they are formed by melting of sedimentary rocks (i.e., S-type granites), differentiation of mafic parental magmas (i.e., A-type granites), and partial melting of dehydrated middle/lower crust (i.e., I-type granites) [11–13]. In south-central Vietnam, granitic batholiths have been considered to be contemporaneous with the granitoid of the South China block. However, only a few studies were carried out on granitic batholiths in this area for investigating Cretaceous magmatism and granite composition [2, 14, 16, 17, 18]. Therefore, Cretaceous magmatism and the formation of granitic batholiths (subducted material (basalt + sediment) or melted basement rock) is still unclear. In this study, granitic rocks of the Deoca, Ankroet, and Dinhquan complexes are collected for zircon U–Pb analysis to investigate Cretaceous magmatism and granite composition in south-central Vietnam.

2. Geological setting

The continental margin of south-central Vietnam belongs to the Indochina Terrane, and it is surrounded by the Kontum Massif to the north, Central Highlands to the west, and the East Sea to the southeast (Fig. 1). The region is dominated by Mesozoic sedimentary rocks and igneous and basaltic rocks (Fig. 2). Precambrian basement is not exposed, although seismic data Khoan et al. [19] suggests that it is composed of granulites and gneisses. Paleozoic rocks are mostly absent in the area due to the region being an emerged continent at that time [20]. The few outcrops are found in the north to northwest in the Dak-Lin area where Upper Paleozoic sedimentary rocks (Carboniferous to Permian) are exposed including intermediate calc-alkaline volcanoes and carbonate rocks [22]. Hence it is considered to have had a similar geological evolution to the Kontum Massif [15, 23, 30].

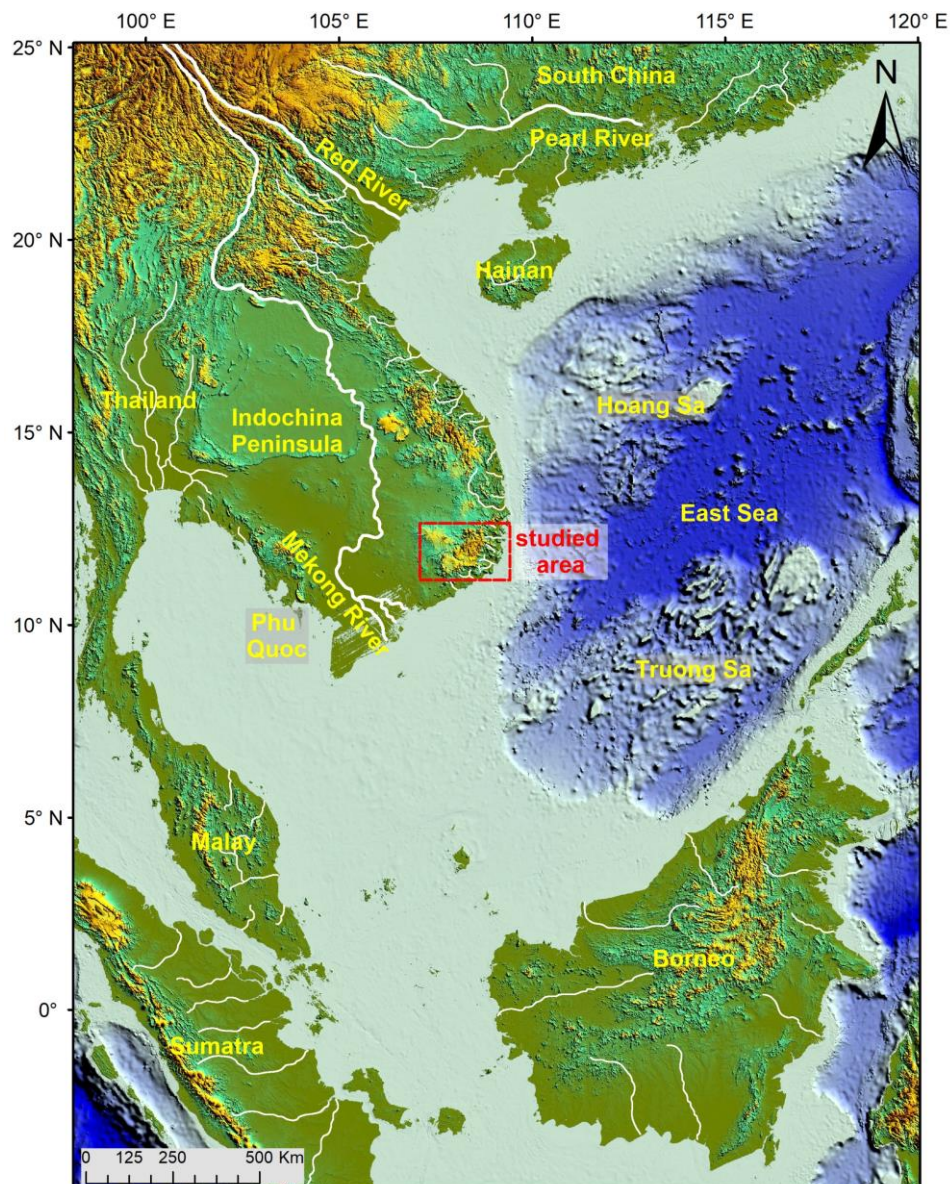


Fig. 1. Topography of the studied area in south-central Vietnam.

Most of the study area is covered by Mesozoic to Cenozoic sedimentary rocks. The Mesozoic formations include widespread Lower to Middle Jurassic shallow marine sedimentary rocks. The Upper Jurassic-Cretaceous sequence consists of the Deo Bao Loc, Nha Trang, and Don Duong formations that formed in a continental environment. These are composed of volcano-sedimentary beds of mainly intermediate, felsic, and alkaline composition [24]. They are slightly folded and display weak contact metamorphism in the aureoles of late Mesozoic plutons. Contemporaneous and widespread volcanic rocks are interpreted as subduction-related products linked to widespread granite plutons [2, 3]. Mesozoic granitoid bodies in the study area are mainly located along the coastline to the south of the Kontum Massif. Early petrological, mineralogical, and structural studies by Vietnamese geologists subdivided these granitoid into three plutonic complexes, called Deoca, Dinhquan, and Ankröet [1], and this scheme was used on the geological map of Vietnam at 1:500.000 scale.

The Dinhquan and Deoca complexes are located northeast-southwest of Kontum and found along the South Vietnamese coast. Petrological characteristics of the Dinhquan Complex comprises hornblende-biotite diorites, granodiorites, and minor granites [23]. The Deoca Complex consists of granodiorite, hornblende-biotite granite (phase I), biotite-hornblende granite, granosyenite, and biotite syenite (phase II), granite porphyry, granular aplite, and pegmatite (dike phase). Sedimentary rocks of the La Nga Formation form smear-slate and were crosscut by granitoid of the Ankröet Complex, and these were overlain by young volcanic rocks of the Don Duong Formation (K₂). K–Ar and Ar–Ar ages of granitic

rock from the Dinhquan and Deoca complexes range from 80 to 118 Ma [22], U–Pb zircon ages range from 88 ± 1.5 to 109 ± 7.0 Ma [2], 115.4 ± 1.2 – 118.2 ± 1.4 Ma [14], 87–104 Ma [17], and 90 ± 0.5 – 135 ± 2 Ma [18].

The Ankroet Complex is less widespread than the Dinhquan and Deoca complexes and is located further inland, at higher elevations. Its characteristics include medium to coarse-grained porphyroid biotite granite, light-grey in color, with low hornblende content. K–Ar isotopic age ranges of granitic rock from 81.0 ± 1.0 to 99.0 ± 1.0 Ma and Rb–Sr are of 94.0– 97.0 ± 1.0 Ma [25] and zircon U–Pb ages of 93.4 ± 2.0 to 96.1 ± 1.1 Ma [2] and 86.8 ± 1.6 Ma [14]. Published granite ages from Nguyen et al. [2] and Shellnutt et al. [14] in this studied area are summarized in Fig. 2.

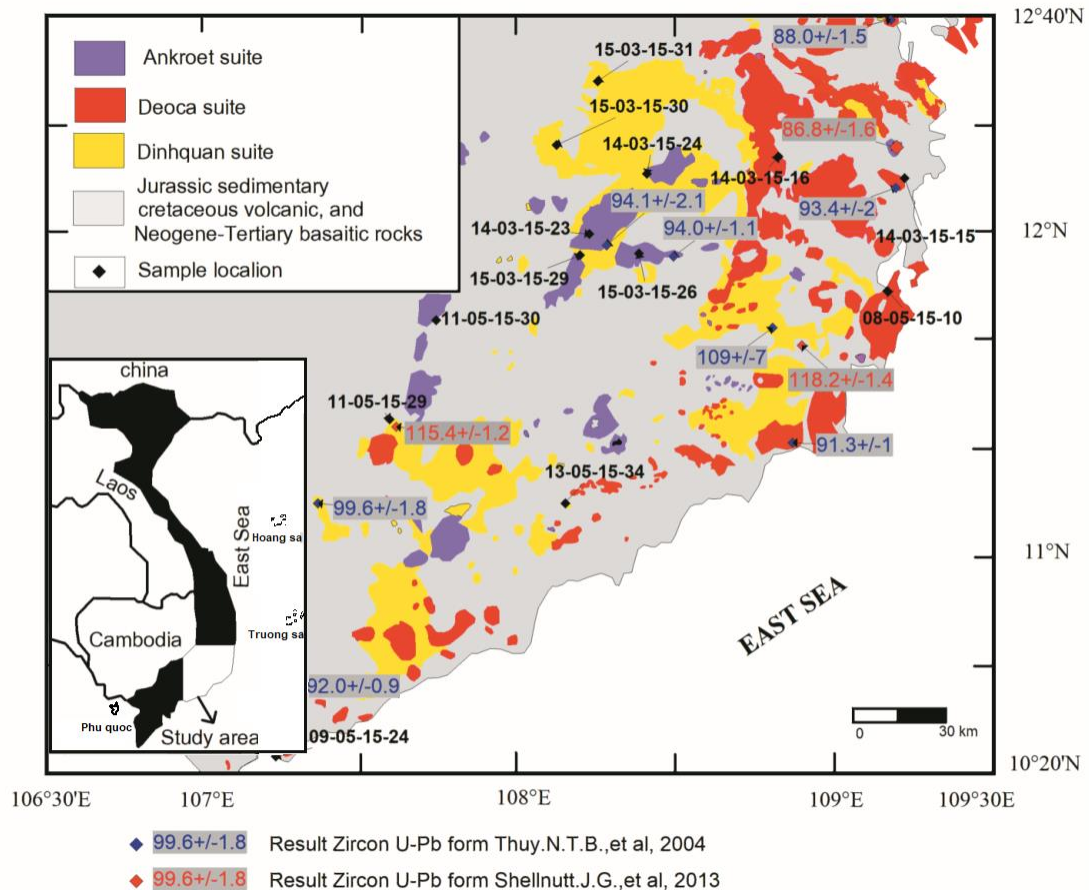


Fig. 2. Simplified geological map of south-central Vietnam, modified from the 1:500,000 Geological Map of Vietnam [20], showing the distribution of sample location and main published zircon U–Pb ages.

The Cretaceous magmatism is associated with an Andean type margin with Meso-Tethyan lithosphere being subduction beneath the margins of South China and Indochina [26]. Geochemical study from Shellnutt et al. [14] shows the Middle Cretaceous granitic batholiths are I-type (partial melting of dehydrated middle/lower crust), whereas the Upper Cretaceous (i.e., ~90 Ma) granitic rocks have compositions similar to A-type (differentiated mafic parental magmas) associated with an extensional tectonic regime, most probably trench retreat caused by slab rollback. The Ankroet rocks are associated with this extensional setting. The cartoon in Fig. 2 shows the plate setting at this time.

During the late Cenozoic widespread volcanism both on the Vietnamese mainland and coastal islands produced extensive basaltic lava flows of variable thickness and composition. Basaltic activity in South Vietnam began in the Middle Miocene and is closely related to the East Sea opening and tectonic reactivation of the continental margin. Local fault zones were re-activated, and this facilitated eruption of lavas [27].

3. Materials and Methods

Fifteen representative granite rock samples of the Deoca, Dinhquan and Ankroet complexes from south-central Vietnam were selected for zircon U–Pb geochronological analyses in this study (Fig. 2).

Each 3–5 kg sample was crushed to a medium sand grain size and then rinsed in water to remove the fine dust. The remaining grains were then placed in an oven at 50–70°C for drying. Grains were then sieved to remove the coarser fraction > 500 µm. After that, detrital zircon grains were separated by standard heavy liquid techniques and mounted on glass slides in epoxy resin. The slides were then polished to expose internal surfaces to enable Cathodoluminescence (CL) imaging and analysis by laser ablation inductively coupled plasma mass spectrometry (LA-ICPMS). Grains for dating were selected randomly from polished grain mounts and analyzed by laser ablation inductively coupled plasma mass spectrometry at the London Geochronology Centre based in University College London using a New Wave 193 nm laser ablation system coupled to an Agilent 7700 quadrupole-based ICP-MS. Typical ablation parameters used 25 µm spots with a 10 Hz repetition rate and an energy fluence of ca. 2.5 J/cm². Instrumental mass bias and depth-dependent inter-element fractionation of Pb, Th, and U were corrected for using Plesovice as an external zircon standard [27]. Time-resolved signals that record evolving isotopic ratios with depth in each crystal were processed using Glitter 4.4 data reduction software. This removed spurious signals caused by inclusions, mixing of growth zones, or fractures. Calculated ²⁰⁶Pb/²³⁸U ages were used for grains younger than 1000 Ma, and the ²⁰⁷Pb/²⁰⁶Pb age for older grains. Grains with a complex growth history or disturbed isotopic ratios, with > +5/–15% discordance, were rejected.

4. Results and discussions

Details of zircon results for granite samples are presented in Tab. 1, without any inherited ages. The range of ages is narrow (from 92 up to 113 Ma), and most of the ages are around ~100 Ma. These ages compare well with the main age range found in river sands and granitic rocks from previous data [2, 14, 29]. Fig. 3 shows the locations of these ages on the geological map. No trends are seen, although older ages tend to be located inland, away from the coast.

Tab. 1. Summary of representative granite zircon U–Pb ages measured in this study.

No	Sample	Unit	U-Pb Age	MSWD	Latitude	Longitude
1	14-03-15-15	Deoca	95.97±0.52	1.9	N12°10'05.1''	E109°11'30.9''
2	14-03-15-16	Deoca	92.01±0.25	4.7	N12°13'52.1''	E108°47'33.3''
3	07-05-15-06a	Deoca	107.5±0.42	2	N13°03'37.0''	E109°17'23.1''
4	07-05-15-06b	Deoca	113.4±0.42	10	N13°03'37.0''	E109°17'23.1''
5	08-05-15-10	Deoca	92.88±0.66	0.68	N11°49'14.8''	E109°08'43.0''
6	09-05-15-24	Deoca	104.3±0.56	4	N10°22'51.6''	E107°15'09.8''
7	13-05-15-34	Deoca	106.9±0.44	11	N11°09'46.2''	E108°08'50.2''
8	14-03-15-23	Ankroet	98.3±0.26	0.84	N11°59'21.0''	E108°12'06.0''
9	14-03-15-24	Ankroet	101.8±0.39	3.9	N12°10'34.2''	E108°22'44.3''
10	15-03-15-26	Ankroet	102.6±0.51	1.9	N11°55'53.5''	E108°21'33.9''
11	11-05-15-30	Ankroet	101.8±0.39	3.9	N11°43'19.5''	E107°43'32.3''
12	15-03-15-29	Ankroet	98.89±0.47	10	N11°55'29.8''	E108°10'24.4''
13	15-03-15-30	Dinhquan	96.85±0.43	1.1	N12°15'44.7''	E108°05'30.0''
14	15-03-15-31	Dinhquan	105.3±0.35	0.67	N12°27'27.6''	E108°12'59.2''
15	11-05-15-29	Dinhquan	113.2±0.37	0.29	N11°24'59.7''	E107°35'08.7''

There are two main published studies on granitic rocks in south-central Vietnam [2, 14]. Both suggest Cretaceous magmatism across the study region was active between 87–118 Ma (by U–Pb method). These studies are well compatible with our research, which also shows bedrock granite ages from 92 to 113 Ma, with most ages falling around 100 Ma. Furthermore, the river sands in south-central Vietnam record magmatic ages between 75–120 Ma, although most ages fall between 85–105 Ma with the greatest abundance around 100 Ma [29]. To get an idea of the timing of Cretaceous magmatism across south-central Vietnam and when magmatism was most active, it is useful to examine the distribution of Cretaceous zircons present in the river sands from Nguyen et al. [29]. This study on river sands showed that zircon grains are widely distributed throughout the Cretaceous period from 85–120 Ma, but the most

common ages, and presumably the main period of magmatism date to 100 ± 10 Ma. Comparing the age range of these zircons to U–Pb age results of granite from previous work by Nguyen et al. [2] and Shellnutt et al. [14] and this study suggests that most zircons in sands from river mouths from Nguyen et al. [29] come from local granites, and therefore the ages reflect the local geology. Therefore, magmatism in the region was most active around 100 Ma and had ended by 85 Ma.

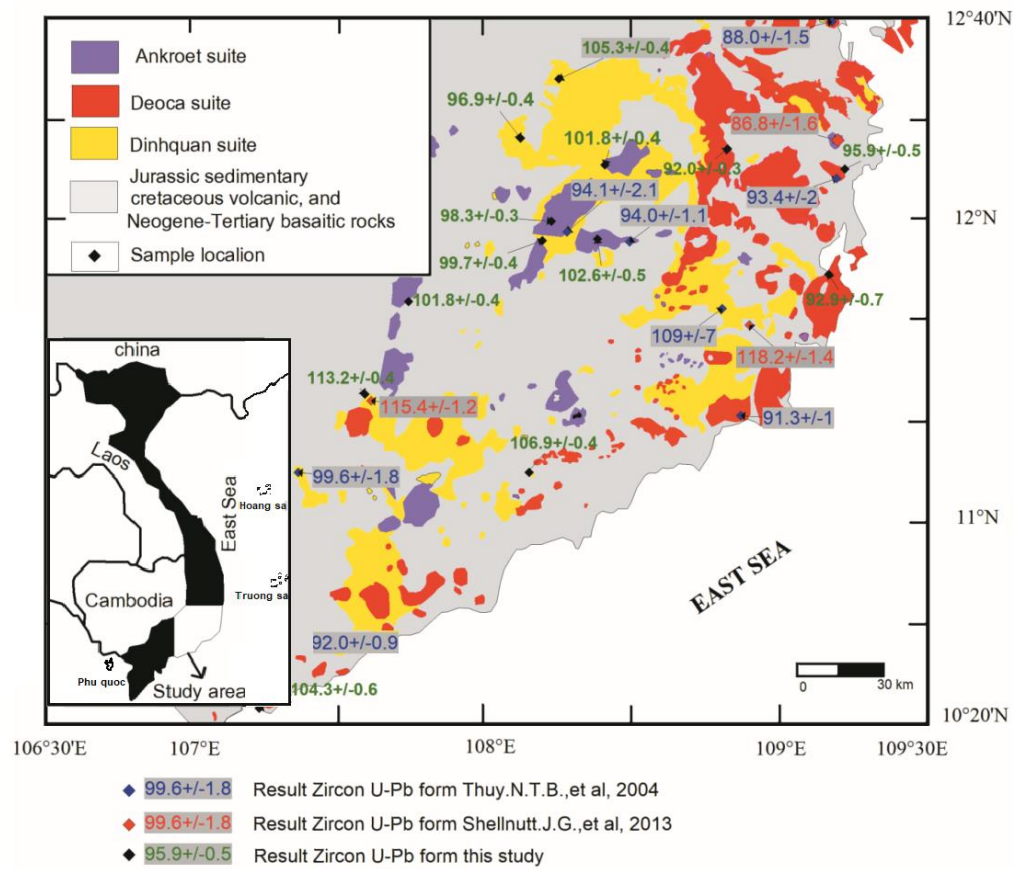


Fig. 3. Geological map to show the location of samples dated for this study as well as main data.

Tab. 2. Summary of zircon inherited ages found in samples from the Deoca and Dinhquan plutons.

Sample	Pluton/Suite	U-Pb Age (Ma)	
07-05-15-06A	Deoca	255±7	961±22
07-05-15-06B	Deoca	253±7	2335±54
		252±6	489±11
		248±6	335±8
		235±6	823±20
		240±7	
		239±7	
		263±7	
		252±7	
08-05-15-10	Deoca	249±3	
13-05-15-34	Deoca	254±7	
11-05-15-30	Ankroet		391±9
			383±10
15-03-15-29	Dinhquan	228±6	1841±70
15-03-15-30	Dinhquan	234±6	1868±49
		211±6	
11-05-15-29	Dinhquan		1872±57

Shellnutt et al. [14] noted that Sr–Nd isotope trends required a portion of the parental magma for the Deoca and Dinhquan granite plutons to have been come from melted basement rocks of the Indochina Block. However, as no inherited grains were found during CL imaging and in situ analysis, Shellnutt et al. [14] could not confirm that mixing between mafic melts and partial melts derived from crustal rocks had taken place. This led authors to propose that the mixing required by their Sr–Nd data was associated with subducted material (basalt + sediment) instead of mixing with assimilated basement. Analyses of granite samples for this study found some inherited grains in granites of the Deoca and Dinhquan complexes, and therefore these relict zircons may help to answer the question about the source of mixing. Tab. 2 summarizes the ages found in this study.

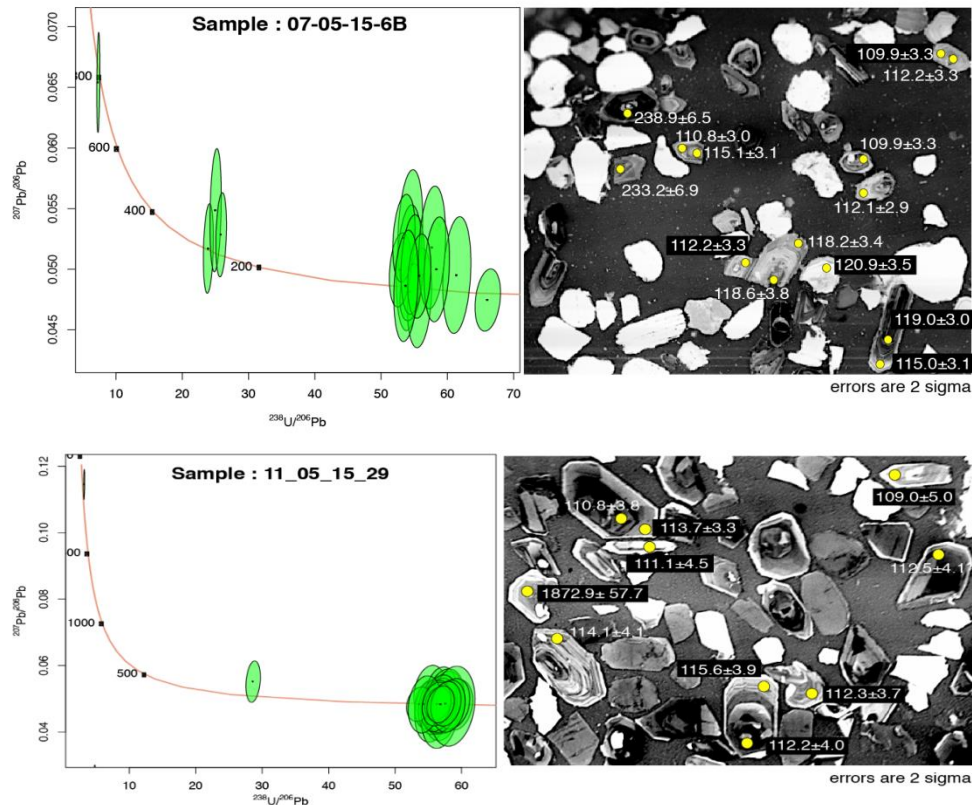


Fig. 3. CL images of zircons from samples 07-05-15-6B and 11-05-15-29 that include grains with inherited cores.

Fig. 3 shows examples of zircon CL images and the location of laser spots and ages. Zircons show oscillatory zoning patterns typical of magmatic grains. Core regions tend to be dark, whilst the analytical strategy was to target grain rims to obtain the youngest ages some grains containing relict zircons and showing both zoned and unzoned cores. The most common inherited ages are Triassic followed by Proterozoic and Carboniferous to Ordovician ages (Tab. 2). These ages match basement rocks in the Kontum region to the north of the study area [21, 23, 29]. Similar basement rocks would be expected to be overlain the sedimentary formations. Shellnut et al. [14] proposed that granite compositions of South Vietnam were the product of either mixing with subducted material (basalt + sediment) or melted basement rock. The inherited core ages found in this study are temporally consistent with basement melting. Based on the inherited core ages in this study and previous publications [2, 14, 18], our study believes that the Ankroet, Deoca, and Dinhquan complexes are primarily I-type granitic rock, which could originate from melting of basement rocks.

5. Conclusions

Granite samples of the Deoca, Dinhquan and Ankroet complexes in south-central Vietnam are analyzed zircon U–Pb to investigate Cretaceous granitic magmatism. This study concludes that:

Bedrock granite ages display the Deoca at ~113–92 Ma, the Ankroet at ~103–98 Ma, and the Dinhquan at ~97–113 Ma. The research confirms that there are much different age values ranging in a wide range between 92 and 113 Ma, with most widespread ages falling around 100 Ma. Comparing with

previous studies, this finding indicates that Cretaceous magmatism was active between 87–118 Ma and most active around 100 Ma in south-central Vietnam.

Inherited ages of the Daoca and Dinhquan complexes are Triassic, followed by Proterozoic and Carboniferous to Ordovician ages. This indicates that I-type granitic rocks in south-central Vietnam could be formed by melted basement rocks.

6. Acknowledgements

The authors acknowledge that this work is a part of our research project, which has been financially sponsored by the National Foundation for Science and Technology Development of Vietnam - NAFOSTED (Grant No.: 105.99-2019.302). We also thank the Birkbeck College, University of London & London Geochronology Centre, Center for excellence in analysis and experiment - Hanoi University of Mining and Geology for providing us excellent experimental facilities to complete our work.

The paper was presented during the 6th VIET - POL International Conference on Scientific-Research Cooperation between Vietnam and Poland, 10-14.11.2021, HUMG, Hanoi, Vietnam.

7. References

1. Bao, N.X., Trung, H., 1980. The distribution of intrusive magma formations, southern Vietnam (in Vietnamese). *Journal of Geology, Hanoi* 41, 35–59.
2. Nguyen, T.B.T., Satir, M., Siebel, W., Chen, F., 2004. Granitoids in the Dalat zone, southern Vietnam: age constraints on magmatism and regional geological implications. *International Journal of Earth Sciences*, 93, 329–340.
3. Nguyen, T.B.T., Satir, M., Siebel, W., Vennemann, T., Long, T.V., 2004. Geochemical and isotopic constraints on the petrogenesis of granitoids from the Dalat zone, southern Vietnam. *Journal of Asian Earth Sciences* 23, 467–482.
4. Campbell, I.H., Taylor, S.R., 1983. No water, no granites-no oceans, no continents. *Geophysical Research Letters* 10, 1061–1064.
5. Wyllie, P.J., Huang, W.L., Stern, C.R., Maaloe, S., 1976. Granitic magmas: possible and impossible sources, water contents, and crystallization sequences. *Canadian Journal of Earth Sciences* 13, 1007–1019.
6. Wyllie, P.J., Carroll, M.R., Johnston, A.D., Rutter, M.J., Sekine, T., Van der Laan, S.R., 1989. Interactions among magmas and rocks in subduction zones regions experimental studies from slab to mantle to crust. *European Journal of Mineralogy* 1, 175–179.
7. Taylor, R.S., McLennan, S.M., 1981. The composition and evolution of the continental crust: rare earth element evidence from sedimentary rocks. *Philosophical Transactions of the Royal Society of London* 301, 381–399.
8. Taylor, R.S., McLennan, S.M., *The Continental Crust: Its Composition and Evolution*: Oxford. England, Blackwell, 312 pp, 1985.
9. Patino Douce, A.E., 1996. Effects of pressure and H₂O content on the compositions of primary crustal melts. *Transactions of the Royal Society of Edinburgh, Earth Science* 87, 11–21.
10. Castro, A., 2013. Tonalite-granodiorite suites as cotectic systems: a review of experimental studies with applications to granitoid petrogenesis. *Earth-Science Reviews* 124, 68–95.
11. Castro, A., Gerya, T., Garcia-Casco, A., Fernandez, C., Diaz-Alvarado, J., Moreno-Ventas, I., Low, I., 2010. Melting relations of MORB-sediment mélanges in underplated mantle wedge plumes; implications for the origin of Cordilleran-type batholiths. *Journal of Petrology* 51, 1267–1295.
12. Chappell, B.W., White, A.J.R., Wyborn, D., 1987. The importance of residual source material (restite) in granite petrogenesis. *Journal of Petrology* 28, 1111–1138.
13. Frost, B.R., Barnes, C.G., Collins, W.J., Arculus, R.J., Ellis, D.J., Frost, C.D., 2001. A geochemical classification for granitic rocks. *Journal of Petrology* 42, 2033–2048.
14. Shellnutt, J.G., Lan, C-Y., Long, T. V., Usuki, T., Yang, H-J., Mertzman, S.A., Lizuka, Y.,

- Chung, S-L., Wang, K-L., Huse, W-Y., 2013. Formation of Cretaceous Cordilleran and post-orogenic granites and their microgranular enclaves from the Dalat zone, southern Vietnam: Tectonic implications for the evolution of Southeast Asia. *Lithos*, 182–183, 229–241.
15. Ngo, T.Xuan, Bui, H.Vinh, Tran, H.Thanh, Phan, B.Van, Dang, B.Van and ., D.Anh Vu 2021. U - Pb geochronology and composition of zircon mineral from granodiorite in the G18 Gold mine, Quang Nam and its significance in regional tectonics (in Vietnamese). *Journal of Mining and Earth Sciences*. 62, 2 (Apr, 2021), 1-11.
 16. Nguyen, T.T.B., 2003. Geochemistry and geochronology of granitoids in the dalat zone, South Vietnam: implications for the mesozoic circum-pacific magmatism and conclusions on the genesis of tin deposits (Doctoral dissertation, Universität Tübingen).
 17. Pham, H.T., 2015. The U-Pb zircon age of granodiorite from Dinh Quan Deo Ca complex of Truong Xuan Khanh Hoa area and its geological significance. *Science and Technology Development Journal*, 18, 5–11.
 18. Hennig-Breitfeld, J., Breitfeld, H.T., Quang, S.D., Kim, V.M., Van Long, T., Thirlwall, M., & Cuong, T. X., 2021. Ages and character of igneous rocks of the Da Lat Zone in SE Vietnam and adjacent offshore regions (Cuu Long and Nam Con Son basins). *Journal of Asian Earth Sciences*, 104878.
 19. Khoan, P., Que, B.C., 1984. Research on the deep geological structures of Kontum area. *Journal of Geology and Minerals* 2, Hanoi, 174–187.
 20. Hutchison, C.S., 1989. The Palaeo-Tethyan realm and Indosinian orogenic system of Southeast Asia. In Sengor AM.C. (Editor), *Tectonic Evolution of the Tethyan region*. Kluwer Academic Publishers, 585–643.
 21. Luc The Trinh, Hai Thanh Tran, Hiep Huu Nguyen, Bac Hoang Bui, Andrew Carter., 2019. New results of the study on isotopic age of the Granodiorite of Chu Lai Complex in North Eastern Quang Ngai by U - Pb zircon isotope dating method. *Journal of Mining and Earth Sciences* 60(1).
 22. Nguyen, X.B., 2001. Tectonics and Metallogeny of South Vietnam, Geological Expedition No. 6. Department of Geology & Mineral of Vietnam (in Vietnamese).
 23. Nam, T.N., Sano, Y., Terada, K., Toriumi, M., Quynh, P.V. and Dung, L.T. (2001). First Shrimp U–Pb zircon dating of granulites from the Kontum massif (Vietnam) and tetonothermal implications. *Journal of Asian Earth Sciences*, 19, 77–84.
 24. Luong, T.D., Bao, N.X., 1988. Geological Map of Vietnam, 1:500,000 Scale. General department of geology and minerals of Vietnam, Hanoi (in Vietnamese).
 25. Phan, L.A., 2001. Petrogenesis of Ca Na peraluminous granite. *Journal of Earth Sciences*, 25, 134–141 (in Vietnamese).
 26. Charvet, J., Lapierre, H., Yu, Y., 1994. Geodynamic significance of the Mesozoic volcanism of southeastern China. *Journal of Southeast Asian Earth Sciences* 9, 387–396.
 27. Bui, M.T., Magma activity in Vietnam. Institute of Geosciences and Minerals, Hanoi, 368 pp, 2010.
 28. Sláma, J., Košler, J., Condon, D.J., Crowley, J.L., Gerdes, A., Hanchar, J.M., Horstwood, M.S., Morris, G.A., Nasdala, L., Norberg, N., 2008. Plešovice zircon—a new natural reference material for U–Pb and Hf isotopic microanalysis. *Chemical Geology*, 249, 1–35.
 29. Nguyen, H.H., Carter, A., Hoang, L.V., Vu, S.Tr., 2018. Provenance, routing and weathering history of heavy minerals from coastal placer deposits of southern Vietnam. *Sedimentary Geology*, 373, 228–238.
 30. Carter, A., Roques, D., Bristow, C., Kinny, P., 2001. Understanding Mesozoic accretion in Southeast Asia: significance of Triassic thermotectonism (Indosinian orogeny) in Vietnam. *Geology*, 29, 211–214.

Automatic Monitoring System Designed for Controlling the Stability of Underground Excavation

MAŁKOWSKI Piotr^{1,*}, NIEDBALSKI Zbigniew¹, BEDNAREK Łukasz¹

¹ AGH University of Science and Technology, Kraków, Poland

Corresponding author: malkgeom@agh.edu.pl

Abstract. Ensuring the stability of mining excavations is a crucial aspect of underground mining. For this purpose, appropriate shapes, dimensions, and support of workings are designed for the given mining and geological conditions. However, for the proper assessment of the adequacy of the used technical solutions, and the calibration of the models used in the support design, it is necessary to monitor the behavior of the excavation. It should apply to the rock mass and the support. The paper presents the automatic system designed for underground workings monitoring, and the example of its use in the heading. Electronic devices that measure the rock mass movements in the roof, the load on the standing support, and on bolts, the stress in the rock mass, are connected to the datalogger and can collect data for a long of time without any maintenance, also in hard-to-reach places. This feature enables the system to be widely used, in particular, in excavations in the vicinity of exploitation, goafs, or in the area of a liquidated exploitation field.

Keywords: Stability of mining excavation, Rock mass monitoring system, Automatic integrated monitoring system, Support control, Rock bolt monitoring

1. Monitoring of underground excavations

Monitoring of the underground excavations is necessary for maintaining their stability. Monitoring not only provides information on the excavation actual condition; it also generates data for verification of the design assumptions and the final design of the working [1-3]. In numerous cases it was a basis for changes or optimization of the assumed support system [4-6]. Proper monitoring of the stability of underground excavation requires concurrent monitoring of the rock mass, and of the support.

Limiting monitoring to the rock mass only causes a lack of data of the load on the support, hence to what degree the support load capacity is engaged. On the other hand, monitoring of the support only precludes identification of the causes of load concentrations i.e., the magnitude of deformation and the intensity of fracturing of the rock mass around the excavation. Monitoring of the excavation may consist of the following measurements:

- convergence of the excavation (linear, peripheral),
- floor heave,
- 3D scanning,
- drillholes inspection by camera,
- stress changes in the rock mass,
- fracturing in the roof rock,
- load on the support (standing support, dowels and bolts, lining),
- deformation of elements of the support,
- stress in the support elements.

Carrying out monitoring of an excavation over a long time allows for determination of trends of rock mass deformation and loads on the support, which can be used for prediction of the behavior of other excavations in similar or specific (e.g. waterlogged rock mass, presence of fault) geological and mining conditions [7, 8]. Shen [9] stresses that the scope and other aspects of monitoring should be adjusted to the possible type of stability loss of the excavation e.g., beam failure, joint-controlled rock falls, roof sag, guttering and shear failure, skin failure, and rib spalling/failure. Skipochka et al. [10] and Mataev et al [11] indicates that it is possible to reduce production costs volume and increase production safety by optimizing the technology of the underground workings support system when simultaneously introducing rock mass monitoring.

Monitoring of roof fracturing and load on the support is particularly important for the design of rockbolt-type support [6, 9, 12, 13], in which case the hazard of sudden failure is much higher than in case of standing

support. Majcherczyk and other authors [3, 4, 7, 8, 14, 15] recommend for the second case measurements of convergence or 3D scanning [16, 17]. Walentek [15] demonstrates in his paper that the support of excavation can be modified together with the advancement of the excavation based on convergence data received progressively, and then used to determine Ground Reaction Curve (GRC), Longitudinal Displacement Profile (LDP), and Support Characteristic Curve (SCC).

An additional parameter that can be monitored and may be used for the stability assessment of the excavation is the stress and its changes within the rock mass [1, 2, 9, 18, 19]. It refers particularly to the situation of the mining front getting closer to the excavation which induces additional stresses [1, 19]. In such cases, useful information may be also obtained from convergence monitoring [14, 20, 21], as well as from endoscopic inspection of boreholes [7, 20, 22, 23]. Endoscopic inspections and measurements show well the development of discontinuities in the rock mass caused by the increasing stress from the approaching exploitation front [5, 6, 14, 15, 20].

Convergence data may also be used for back analysis of the rock mass parameters that were affected by the advancing exploitation [21, 24].

Equally significant are measurements of load on the support as they show how the support load capacity is engaged by the rock mass in terms of magnitude, direction, and distribution. The tensional force measured in the rock bolts should not exceed the nominal rock bolt capacity specified by its manufacturer [2, 4, 5, 6, 7, 13, 14, 19, 15]. Standing support monitoring shows maximum or yielding load [4, 5, 14]. It should be noted that the direction of the load can be inferred from load sensors properly positioned on the perimeter of the support frame, or under the wall arches. Asymmetric load detected on the support signals improper work of the support i.e., no yield on joints, and plastic deformation of the frame [7, 19, 25].

All monitoring data are useful for preparation of the numerical model, and for the calibration of the initially assumed rock mass parameters and stress criterion [7, 9].

Certainly, monitoring of the excavation stability requires proper management. The management covers selection of the parameters to be measured, selection the suitable instrument for each parameter (in terms of accuracy, working range, dimensions, working conditions), number and positioning of the instruments, delegating responsibility of the instruments, measurements, and data processing to the qualified staff [26]. Lack of professional management may cause incompleteness or inaccuracy of data obtained at a high cost, as well as deficient interpretation.

A comprehensive interpretation requires data from a complex monitoring system that covers rock mass and support. Still, the data acquisition and interpretation can be arranged simply and expediently. To achieve that the instrumentation needs to be designed to fully depict the effect of changes of geomechanical situation of the excavation, and the data acquisition possible by just one readout unit. There are known similar monitoring projects in the mines [14, 19], yet most often comprising only single instrument; not an array of instruments combined with automated dataloggers [1, 2, 3, 4, 5, 7].

2. Monitoring of gate roadways

In the case of gate roadways, next to the exploitation panel, the monitoring of the excavation may serve several purposes:

- evaluation of sufficiency of the selected support type,
- observation of working of individual part of the support,
- evaluation of the effect on the rock mass and the support from the approaching longwall face,
- evaluation of the inter-reaction between rock mass and support at changing geological and mining conditions,
- testing of new technological solutions.

Access to the roadway and monitoring devices is safe and unrestricted in a situation where the roadway is still ahead of the exploitation front. Hence, the measurement can be carried out manually, and the devices can be serviced if needed. The situation becomes difficult once the excavation is behind the exploitation front. Often, they are fenced off due to safety reasons e.g., lack of ventilation. However, the monitoring data that can be obtained from them is particularly valuable for correcting further roadway designs. In such cases, automated monitoring is the solution.

Automated dataloggers read the instruments and store the results over a long time depending on memory size e.g., several weeks. Then the results can be downloaded to a portable computer in situ or remotely via telecommunication cable. Moreover, dataloggers can read the instruments at a preset frequency, usually from 1 to 12 hours, which allows for detection of minute changes in the rock mass and the support. Therefore, the example correctly designed monitoring station (Fig. 1) for stand-and-roofbolting support should comprise: multipoint extensometer (minimum 4-point) installed in the roof (marked in orange), load cell installed on the roof-beam of the standing support (marked in yellow), instrumented rock bolt with minimum 4 sensors (marked in red).

In addition, it is recommended to include in the station a biaxial stressmeter for monitoring of stress in the rock mass (marked in purple), and in case of gate roadways advised are load cells on wood cribs, concrete props, and other elements supporting the subsiding roof (marked in blue).

Of course, the station may be equipped with many other sensors e.g., load cells under the side arches, or convergence meters. However, the design of the station is limited by the number of transmission channels of the datalogger (marked in grey on the diagram). If necessary, two or three datalogger may be needed.

As an addition to the station, it is suggested to drill an investigation hole for endoscopic inspections and measurements of apertures of fractures during formation and maintenance of the excavation. Mechanical parameters of the rock types surrounding the excavation can be also obtained from the drillhole core.

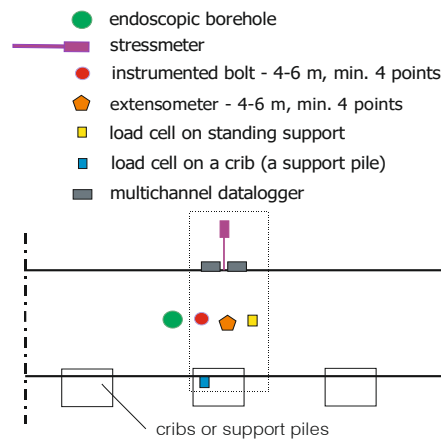


Fig. 1. Diagram of typical automated monitoring station in an excavation with stand-and-roofbolting support.

In this paper the authors present the monitoring system developed for detecting and recording rock mass movements, loads on the support, and loads on additional supports at the near-goaf zone. The system was installed and successfully used in a maingate PW-1 in “Pniówek” coal mine belonging to JSW (Jastrzębska Spółka Węglowa, free transl.: Jastrzębie Coal Company) in Poland.

3. Example of the monitoring system for gate roadway

3.1. Description of monitoring station

In the presented case the monitoring system has been developed for longwall roadway in a coal mine, where the roadway was maintained beyond the exploitation front for ventilation. Therefore, the assumption was that the system had to comprehensively monitor the stability of the excavation, and the readings could be regularly carried out in situ. For this purpose, the instruments for measuring movements in the rock mass and loads on the support were selected and configured that way that they could be read, and the reading stored, by one datalogger or readout unit.

Therefore, when designing the monitoring station, the following aspect had to be considered:

- selection of instruments that suitable for working in mining conditions,
- selection of instruments with measuring range suitable for the expected values,
- selection of instruments powered by the same voltage,

- selection of instruments ready to work as integrated system,
- ensuring the instruments received permit to work in compliance Polish mining regulations,
- ensuring the instruments received ATEX certificate for safe use in explosion hazard zone,
- design the number of instruments and transmission channels matching the capacity of the datalogger.

It appeared that the certificates from other countries issued for the instruments (e.g., by the US or Korea), stating their suitability for working in the mines, do not qualify them for use in Polish mining. Also, some of them did not comply with explosion protection requirements. Since the intended monitoring station was within a methane hazard zone, it was decided that the dataloggers would be protected in legally approved, spark-safe casings.

The objective of monitoring of the maingate PW-1 in coal mine Pniówek was a verification of two novel support systems for longwall roadway maintained behind the longwall front. The two new supports were installed along 200 meters sections each, and their behavior was later compared with the typical support used in the mine. Hence three sections of different support scheme were instrumented and monitored. In each tested section of the maingate PW-1 there were two stations installed comprising (Fig. 2):

- load cell installed on roof arch of the standing support,
- rod extensometer, 6 meter long and with 4 measurement levels,
- rock bolt stressmeter, 6 meter long and with 6 measurement points,
- load cell installed on wooden crib support,
- two biaxial stressmeters.

The stressmeters were installed in the walls at 90° to each other, in the boreholes inclined to the roadway axis, to enable the determination of changes of vertical and horizontal stress, hence the triaxial stress state.

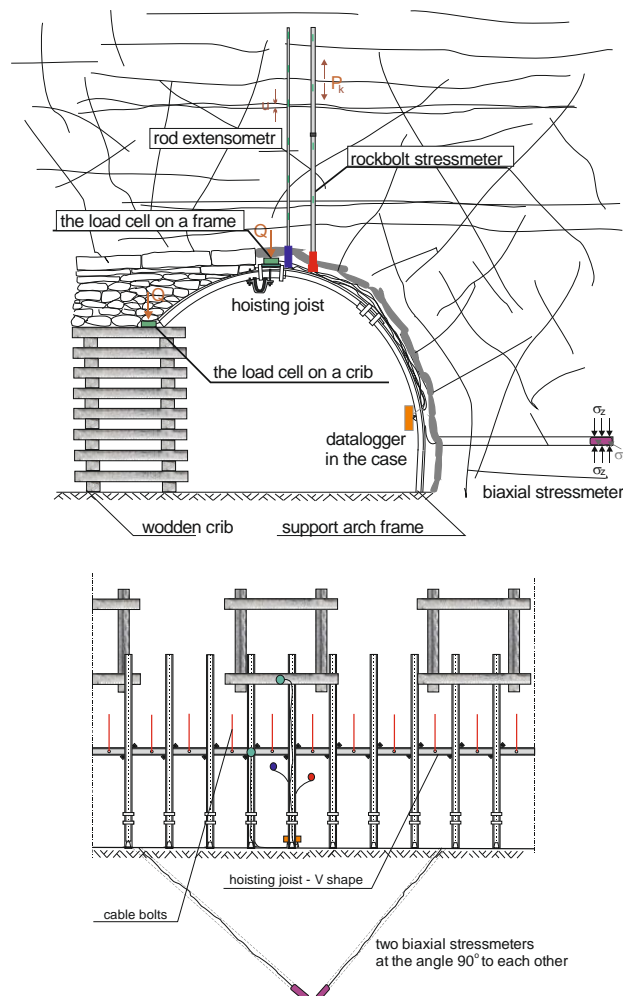


Fig. 2. Diagram of monitoring station in PW-1 maingate.

Moreover, in five of the six stations installed there were investigation holes drilled for endoscopic inspection of development of fracturing since completion of the excavation.

Fig. 2 shows one of the two new support systems tested – with V-profile joist, fixed in the roof along the axis of the gallery with strand bolts, where the excavation borders with goafs supported with wood cribs.

3.2. Monitoring of rock mass

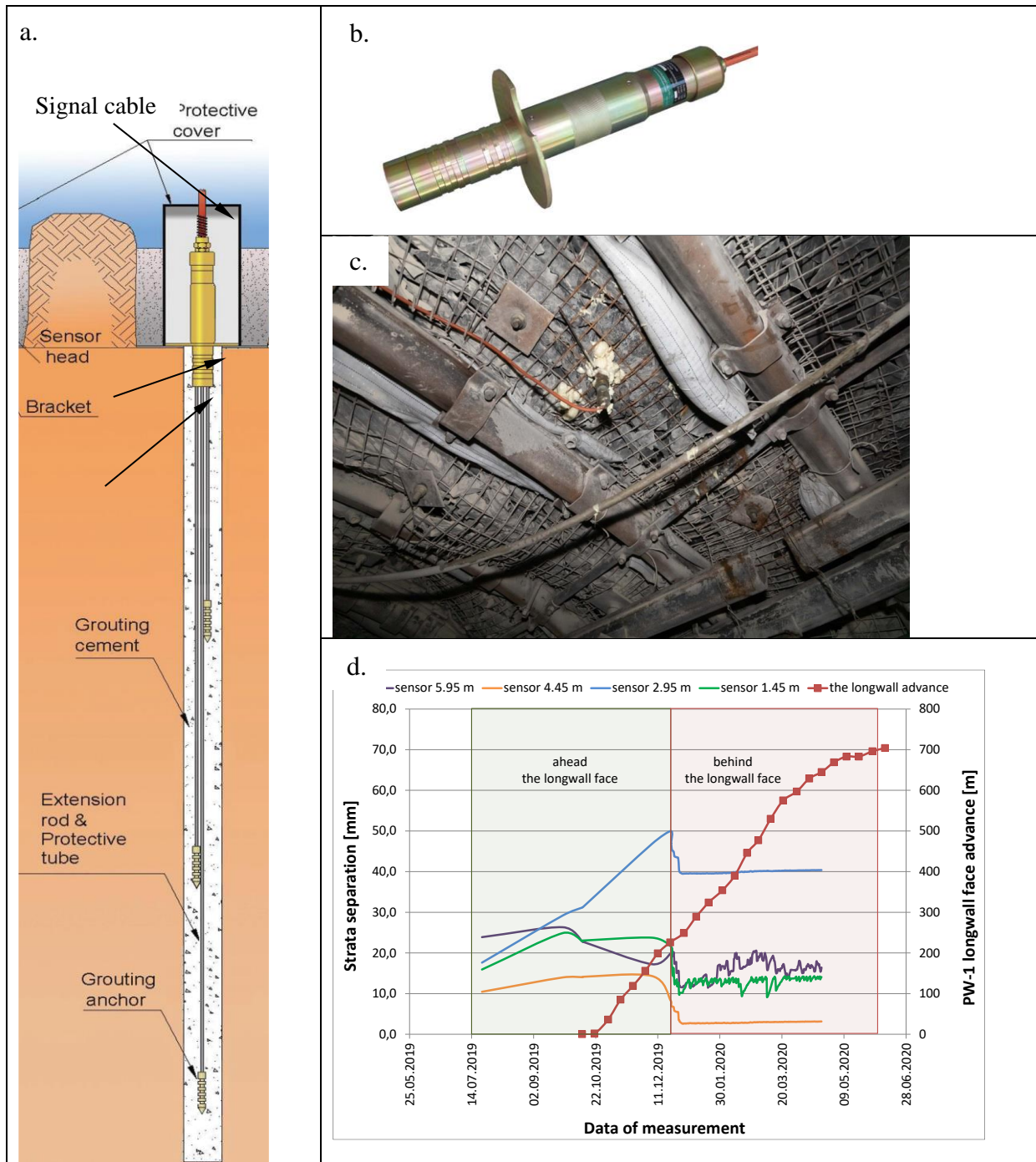


Fig. 3. Rod extensometer MPBX model 1390, a. general view and installation diagram [27], b. extensometer head, c. extensometer grouted into the roof of the gallery, d. readings compiled as graphs.

Rod extensometers with vibrating wire sensors model 1391 by ACE Instruments Co. Ltd were selected for the presented research case for monitoring the development of fracturing within the roof rocks. Extensometers consist of 6 mm diameter polyethylene pipes connected to the reference head equipped with

6 vibrating wire transducers. Fiber glass rods ended with grouting anchor are inserted into the pipes. Once the anchors are grouted at designed levels the rods transmit the anchor movements to VW transducer (Fig. 3a). The distance of the anchors to the reference head can be decided to suit the purpose and the conditions. In this case the anchors were positioned and grouted at 5,95 m, 4,45 m, 2,95 m, and 1,45 m distance from the reference head.

Reference head is made of stainless steel and alloys (Fig. 3b). It is used to set the initial tension on the VW transducers (i.e. zero reading). It also contains a temperature sensor that allows for temperature correction of VW transducer readings. The extensometer was grouted in full length using resin-type glue Verpensin (Fig. 3c).

Figure 3d shows results of readings of one of the sensors that were carried out both before and behind the front of the longwall panel. Visible on the graph is a drop of aperture values which is linked to the passing by longwall and developing collapse of roof, hence subsiding of the roof rocks onto the standing support of the roadway.

Biaxial stressmeters – model 1375 made by ACE Instrument Co. Ltd. were applied for monitoring of changes of stress around the excavation (Fig. 4a). The probe contains an array of three VW sensors directed along a plane perpendicular to the probe axis, and at 120° to each other, hence measuring stress perpendicular to the probe axis and in three directions. The probe, as it is in the extensometer, has an in-built temperature sensor. The probe is made with stainless steel and watertight. The probes were inserted into the holes to around 10 m depth and grouted with cement (Fig. 4b).

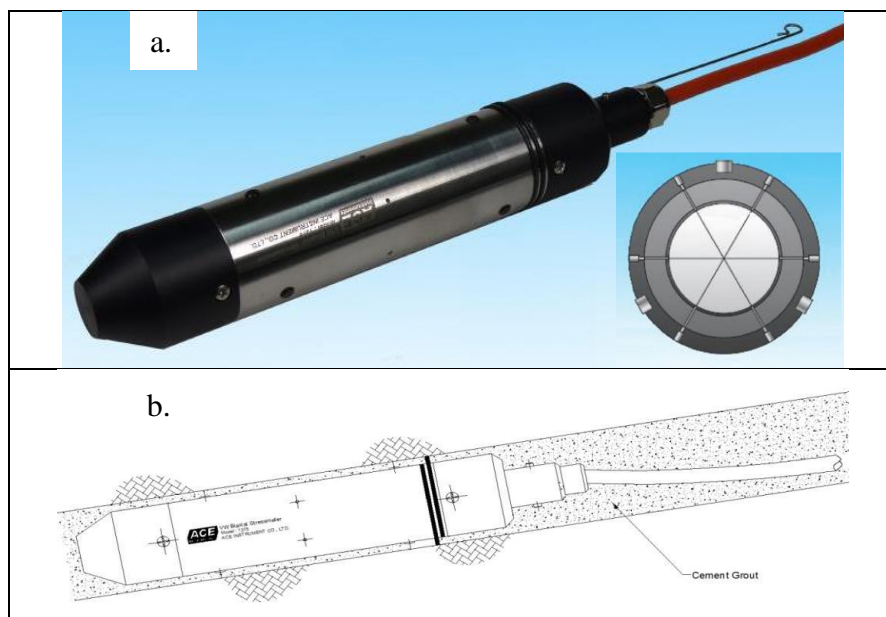


Fig. 4. Biaxial stressmeter, a. general view, b. way of application of the probe [27].

Figure 5 shows stressmeter installed in the wall of the excavation. Visible is the vent tube used for grouting the sensor in the rock.

Biaxial stressmeter allows for determination, not only the stresses in directions perpendicular to the meter axis, but also the tilt angle of the resultant vector of principal stresses. Figure 6a shows the chart of changes of vertical and horizontal stress versus position of the longwall front. The stresses increase together with the approaching exploitation front, and, in case of vertical stress, reach around 1.6 MPa when the longwall is at 100 m distance. Figure 6b demonstrates the method of determination of the resultant of principal stresses, while Figure 6c shows the tilt of the resultant vector. The graph confirms the observations in the excavation that the principal stresses resultant vector is tilted from vertical, in this case of about $60\text{--}75^{\circ}$, and the tilt value is not invariable.

Despite the stressmeter position was around 0.9 m above the floor of the excavation it was damaged by the heaving floor when the longwall was at approx. 110 m distant from the monitoring station.



Fig. 5. Biaxial stressmeter installed in the wall of the excavation. Visible is the vent tube used for grouting the sensor in the rock.

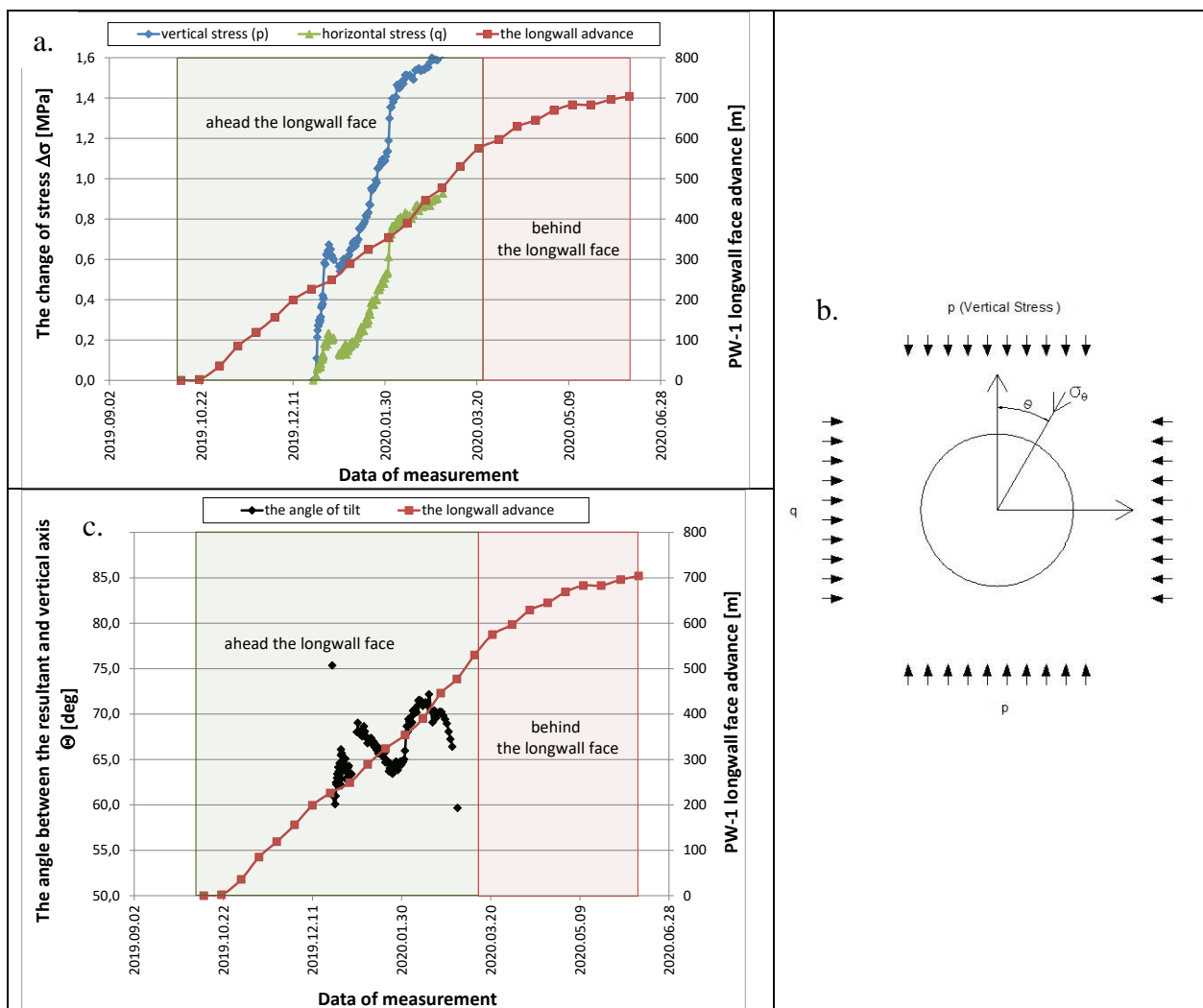


Fig. 6. Evaluation of stress in the rock mass at station no 6 during PW-1 longwall advance, a. chart of changes of stress, b. diagram for determination of the change of the resultant vector of principal stresses, c. change of tilt angle of principal stresses vs. advancement of the longwall.

3.3. Monitoring of support

For monitoring of load on the frame of the standing support the sensors had to be compatible with the datalogger. Therefore, the selected devices were vibrating wire type load cells, model 1102 made by ACE

Instrument Co. Ltd.; 3-wire, specified for load up to 40 T. By the manufacture’s specification the load cells of 1100 series are designed for measurement of load on concrete or steel structures (Fig. 7). It was also assumed that having all the measuring devices from one manufacturer, and built on the same principle, would be advantageous for assembling them into the system. Due to a broad range of load capacity, it was possible to use load cells 1100 series for monitoring both the load on support frames and wooden cribs.

To achieve a good contact between the frame of the support and the rock, the load cell was placed on the roof arch of standing support (Fig. 8) on a purpose-made pad that allowed for wedging it into the V-profile and preventing slipping of the load cell from it.

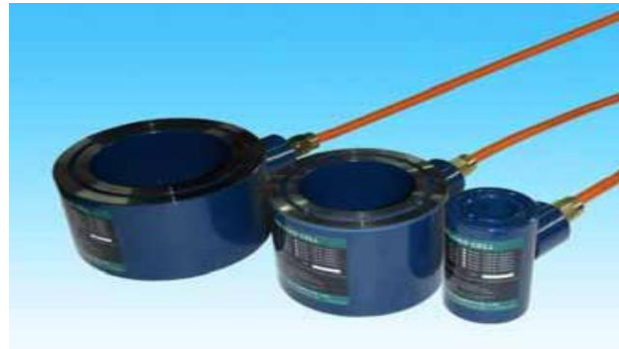


Fig. 7. Dynamometers (load cells) of 1100 series from ACE Co Ltd. [27].

Tab. 1. Parameters of load cells of 1100 series by Ace Co Ltd.

Load cell model	1102	1103	1105	1110	1115	1120
Max. Load [T]	40	80	140	140	140	200
Dimension A [mm]	38.5	50	100	125	75	100
Dimension B [mm]	72	88	138	158	122	150
Dimension C [mm]	80	80	80	80	80	80
Cross-sectional area [cm ²]	29.07	41.18	71.03	73.34	72.72	98.17

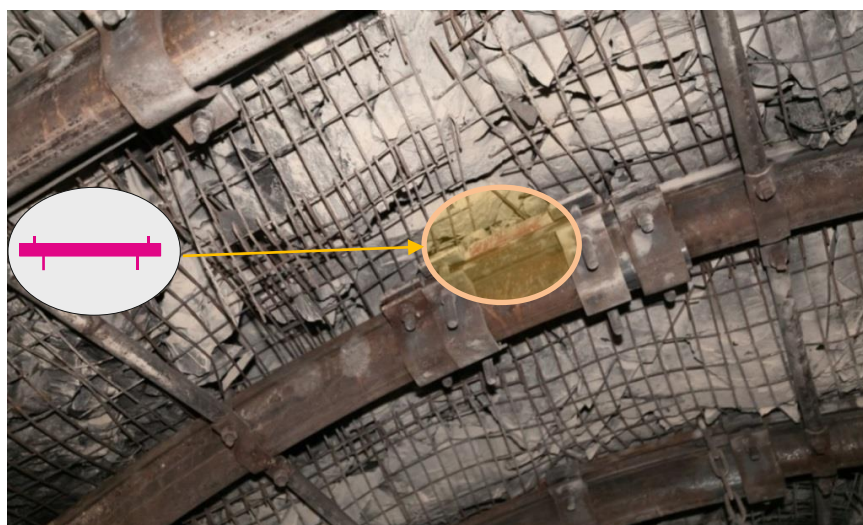


Fig. 8. Load cell type Vibrating Wire installed on a steel plate on top of roof arch in maingate PW-1.

An example of load recorded on the load cell installed between the rock and the roof arch of yielding support in roadway PW-1 versus longwall advancement is shown in Fig. 9. Despite combined standing and rock bolt support installed, visible is an explicit drop of load on the roof arch coinciding with the relaxation of the roof rocks exactly along the longwall face.

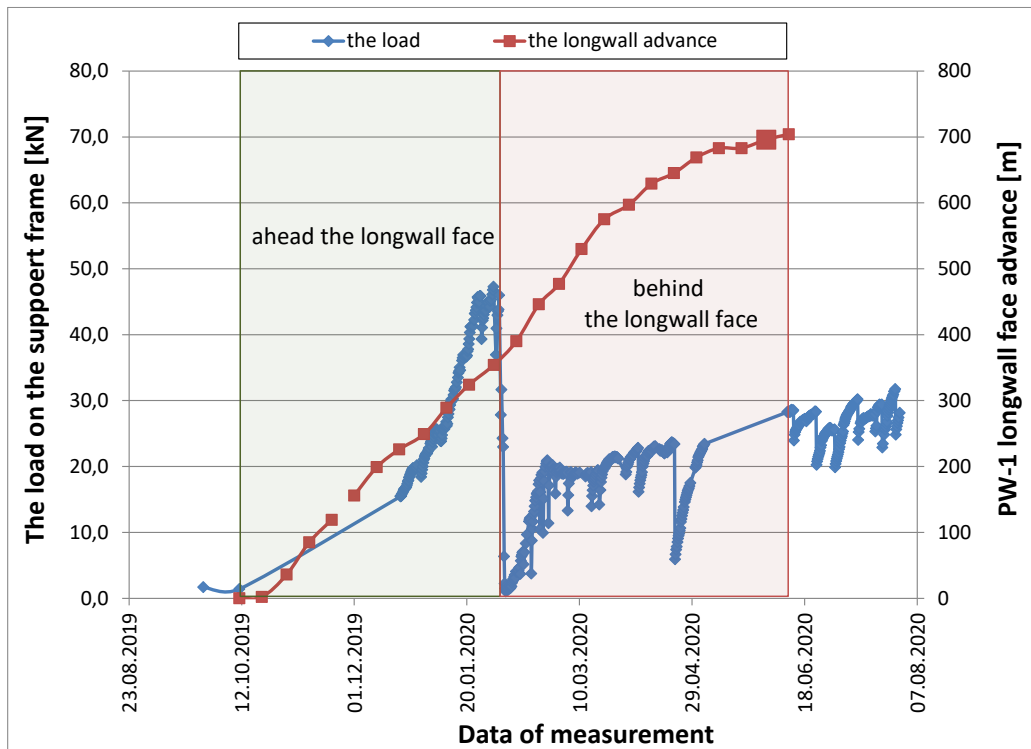


Fig. 9. Readings of load cell installed between rock and roof arch of yielding arch support in maingate PW-1 versus longwall advancement.

Monitoring of load on the rock bolt support was accomplished by introducing 6-levels, instrumented rock bolt stressmeter – model 1350 made by ACE Instrument Co. Ltd. The instrumented rock bolt comprises sections with vibrating wire sensors. These sections, maximum 8, can be distributed along the steel rod which is compressed or tensioned together with rock mass.

There is temperature sensor in the rock bolt head. For the purpose of measuring load on the installed rock bolt support the 6 meters long instrumented rock bolts were selected (Fig. 10a). This length allows for 6 measuring points at around 0.75 m intervals. For this project, the measuring points were fixed into the rock bolts at 0.75 m, 1.50 m, 2.25 m, 3.78 m, 4.25 m, and 5.78 m (Fig. 10b).

Such a long rock bolts, longer than the height of the excavation, require the final assembling of two pre-assembled sections during the installation. These two sections must be connected mechanically with a threaded coupler when inserting to the drill hole (Fig. 10c).

Before the coupler is used, the rock bolt sections have to be joined properly with male and female electrical sockets ensuring connectivity with vibrating wire sensors (Fig. 10d). The instrumented rock bolt grouted with cement into the roof of the excavation is shown in Fig. 11.

Fig. 12 shows an example record of load on the instrumented rock bolt. It appears on the graph, that the loads increase before the approaching longwall face, up to 215 kN on the level 3.75 m. The distribution of the load on the measuring points varies because it depends on what level the rock mass starts discontinuing. After the longwall face passes by the load on the rock bolt still increases.

In the case presented on Fig. 12 the coupler between upper and lower sections snapped due to bending and excessive rock movement still when being ahead of the approaching longwall face. As a result, the three upper sensors were disconnected, and the record is incomplete since the longwall position 15 meters to the station.

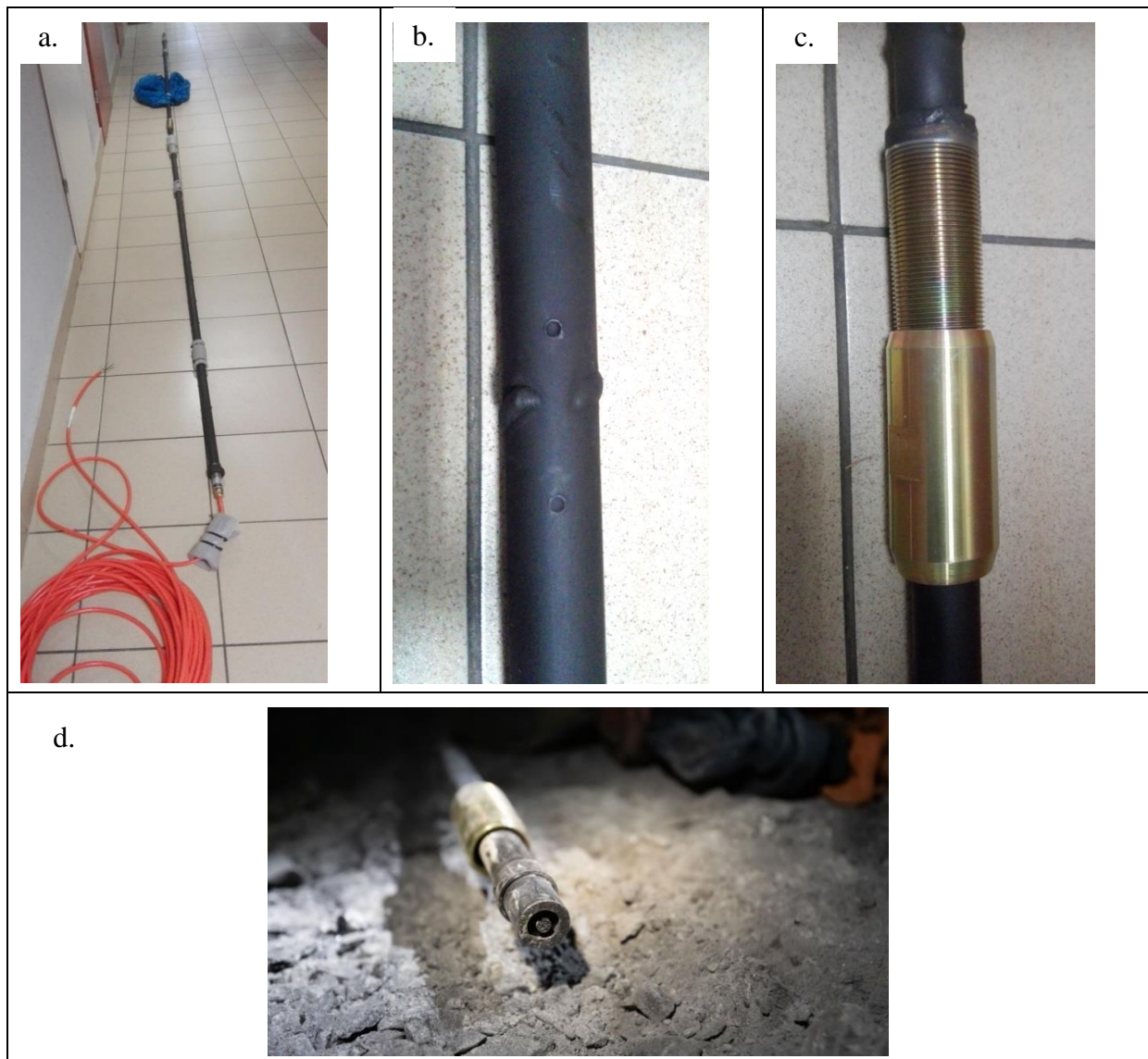


Fig. 10. Rock bolt instrumented with Vibrating Wire sensor, a. general view, b. section of the rock bolt with the Vibrating Wire sensor, c. coupler for rock bolt sections, d. socket for connecting rock bolt sections.



Fig. 11. Instrumented rock bolt installed in the roof of maingate PW-1. Visible is the end of the packer used for grouting.

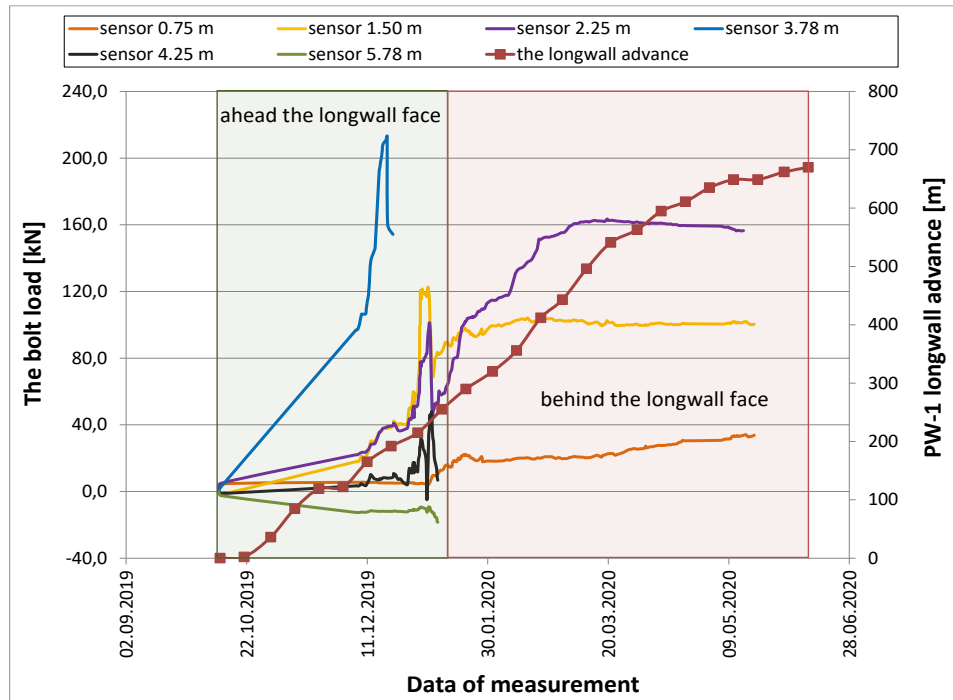


Fig. 12. Distribution of load along instrumented rock bolt in roadway PW-1 (station no 2) versus longwall face advance.

Because the roadway PW-1 was maintained behind the longwall face, the monitoring continued, and additionally included load on wood cribs. For this purpose, the vibrating wire load cell of 200 T capacity, model 1120 made by ACE Instrument Co. Ltd. was applied. The specified parameters of this device are given in Tab. 1. Even though there were no values of load on the wood cribs available from previous experience, yet assuming theoretical capacity of the wood cribs 160 T, the range of the selected load cell 200 T seemed sufficient and with good margin. Fig. 13 shows the monitored wood crib structure.

In practice, it appeared difficult to position the load cell under the rock rubble that way to correctly measure the load on the whole area of the wood crib. The load cell was placed on the roadway side of the crib, where the load was not representing the overall load on the crib.



Fig. 13. View on the monitor wood crib behind the longwall face PW-1.

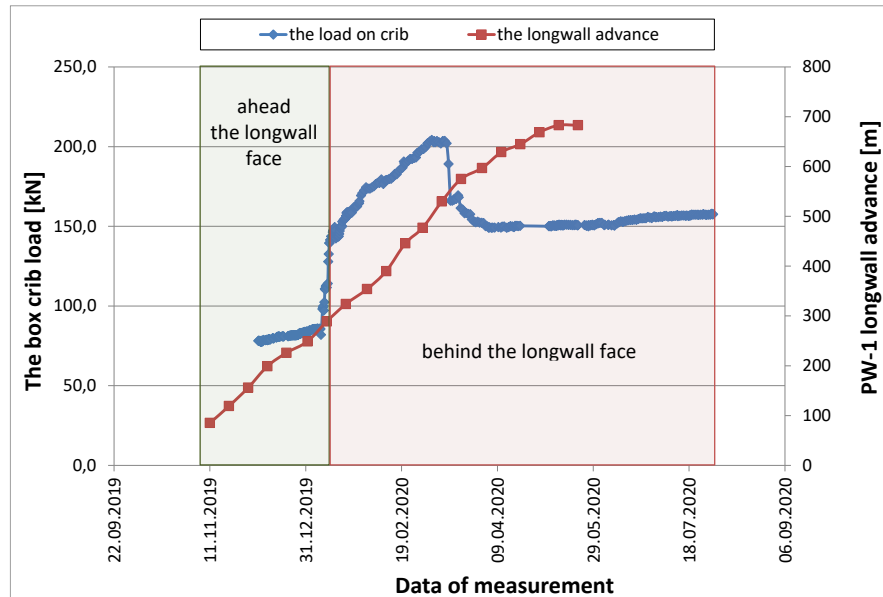


Fig. 14. Load on wood crib built in roadway PW-1 vs. longwall face advance – monitoring station no 2.

The readings show that the load on the wood cribs was not remarkably high (Fig. 14). It did not exceed 210 kN (21 T). In this case, the short, cantilevered section of the subsiding roof did not exert high load on the installed wood cribs. However, it needs to be pointed out that the load cells were installed on the roadway side of the crib where the load was lower and not indicative to the whole load from subsiding roof on the wood crib.

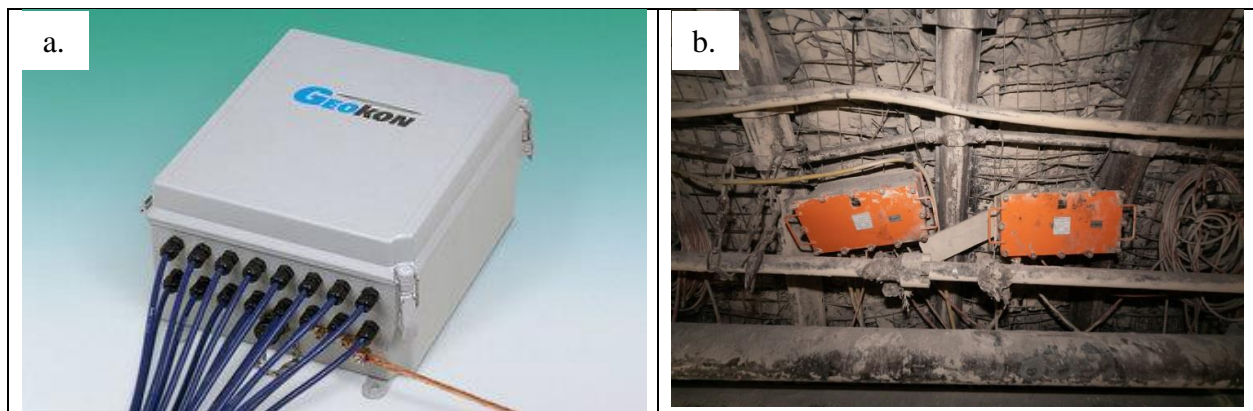


Fig. 15. 16-channel datalogger from Geokon, a. general view [28], b. two dataloggers in casings installed in monitoring station in roadway PW-1.

All readings were taken automatically by 16-channel datalogger from Geokon (Fig. 15a). Because of a large number of needed transmission channels, in each station there were two dataloggers installed, therefore, there were 12 such devices in total in the excavation. Due to the present hazard of methane explosion, as a safety measure, each datalogger was housed in intrinsically safe casing OS253/15/0/B which complies with ATEX requirements (Fig. 15b).

In addition, the dataloggers were not powered from their own batteries. Instead, they were connected to the mine’s power grid which would allow for automatic power cut off in case of detected increase of methane content, fire, or other hazardous situation.

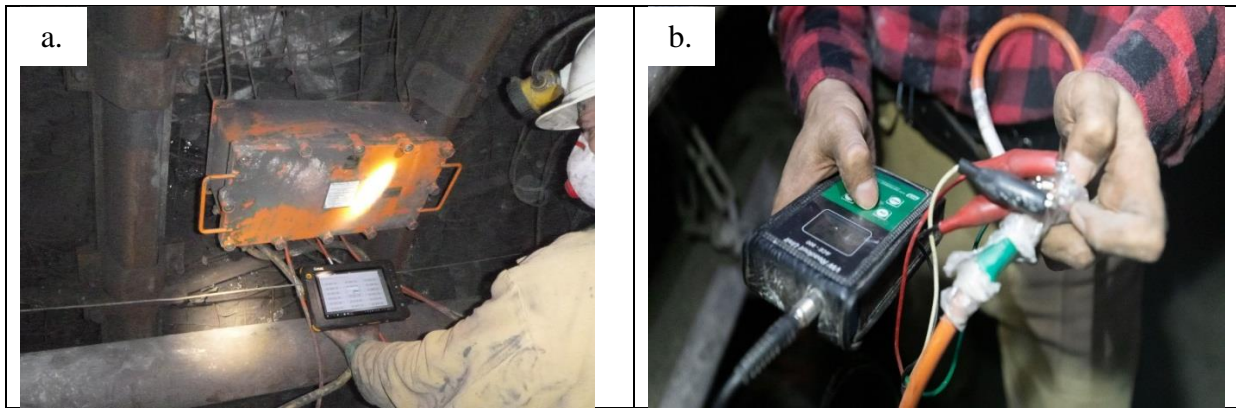


Fig. 16. Acquisition of data from sensors installed in maingate PW-1, a. downloading data from datalogger to tablet computer, b. reading the instrument with the use of portable readout unit.

Measurements were carried out at 6 hours intervals set on the automatic datalogger and then downloaded to the tablet computer (Fig. 16a). Until the automatic data logging system was in place the instruments were read by portable readout unit (Fig. 16b) and providing that way the initial set of reference readings.

It needs to be highlighted that the developed system has the capacity to transmit the data to the mine supervisor control room, either on the given exploitation level or on the surface, via the existing telecommunication network.

4. Summary

Efficient control of stability of the underground excavation requires simultaneous geotechnical monitoring of the rock mass and the support. Monitoring of rock mass should be carried out by extensometers or convergence meters. Whereas behavior of the support should be monitored by load cells placed on support frames, in concrete lining, or by tensometers or vibrating wires built-in rock bolts. It is recommended that the extensometer and instrumented rock bolt readings are spread over several levels. Comparison of that way obtained data with geological and mining charts is a basis for reliable evaluation of the efficiency of the support selected for the given geological and mining conditions.

In case of excavations close to exploitation fronts, or maintained close to the goafs e.g., for ventilation, the most suitable is automated monitoring system. It allows for instruments readings at discretionary set intervals. In such conditions, it is advised carrying out monitoring of load on the additional support like wood cribs, concrete props, etc. In the case of excavations affected by the exploitation, valuable information is provided from monitoring of stress changes within the rock mass which reflect the abutment pressure. Most often these changes are estimated only, while the design of reinforcement of the existing support depends on these values.

In this paper, the authors presented the first case of maingate in coal mines in Poland in which a fully integrated and automated system of rock mass and support monitoring was installed and functioned both ahead and behind the longwall front. The recorded readings explicitly show an increase of stresses before the exploitation front and a decrease behind it. Of course, this effect is well known in general, yet it is rarely quantified by direct measurements for given geological and mining conditions.

The experience gained from maingate PW-1 can be used in further monitoring projects, primarily to eliminate technical and organizational mistakes. The developed system can be advantageous for research projects e.g., on the stability of roadways with rock bolts, innovative support types, or other new technological solutions for mining.

5. Acknowledgements

The paper was presented during the 6th VIET - POL International Conference on Scientific-Research Cooperation between Vietnam and Poland, 10-14.11.2021, HUMG, Hanoi, Vietnam.

6. References

1. Shen, B., Poulsen, B., Kelly, M., Nemcik, J., Hanson, C., 2003. Roadway span stability in thick seam mining – field monitoring and numerical investigation at Moranbah North mine. In: Materials of the 2003 Coal Operators' Conference, Carlton, Victoria, Australia: University of Wollongong, The AusIMM Illawarra Branch, 173-184.
2. Singh, R., Singh, A.K., Mandal, P.K., Singh, M.K., Sinha, A., 2004. Instrumentation and monitoring of strata movement during underground mining of coal. *Minetech*, 25(5), pp. 12-26.
3. Majcherczyk, T., Niedbalski, Z., Małkowski, P., Bednarek, Ł., 2014. Analysis of yielding steel arch support with rock bolts in mine roadways stability aspect. *Archives of Mining Sciences*, 59(3), 641–654, DOI: 10.2478/amsc-2014-0045.
4. Majcherczyk, T., Małkowski, P., Niedbalski, Z., 2008. Rock mass movements around development workings in various density of standing-and-roof-bolting support. *Journal of Coal Science and Engineering*, 14(3), 356–360, DOI: 10.1007/s12404-008-0078-1.
5. Niedbalski, Z., Małkowski, P., Majcherczyk, T., 2013. Monitoring of stand-and-roof-bolting support: Design optimization. *Acta Geodynamica et Geomaterialia*, 10(2), 215–226, DOI: 10.13168/AGG.2013.0022.
6. Xie, Z., Zhang, N., Qian, D., Han, C., An, Y., Wang, Y., 2018. Rapid excavation and stability control of deep roadways for an underground coal mine with high production in Inner Mongolia. *Sustainability*, 10(4), no 1160, DOI: 10.3390/su10041160.
7. Małkowski, P., Niedbalski, Z., Majcherczyk, T., Bednarek, Ł., 2020. Underground monitoring as the best way of roadways support design validation in a long time period. *Mining of Mineral Deposits*, 14(3), 1–14, DOI: 10.33271/mining14.03.001.
8. Małkowski, P., Ostrowski, Ł., Bednarek, Ł., 2020. The Effect of Selected Factors on Floor Upheaval in Roadways - In Situ Testing. *Energies*, 13, 5686; DOI: 10.3390/en13215686.
9. Shen, B., 2014. Coal mine roadway stability in soft rock: A case study. *Rock Mechanics and Rock Engineering*, 47(6), 2225-2238, DOI: 10.1007/s00603-013-0528-y.
10. Skopochka, S., Krukovskiy, O., Serhiienko, S., & Krasovskiy, I., 2019. Non-destructive testing of rock bolt fastening as an element of monitoring the state of mine workings. *Mining of Mineral Deposits*, 13(1), 16-23, DOI: 10.33271/mining13.01.016.
11. Matayev, A.K., Lozynskiy, V.H., Musin, A., Abdrashev, R.M., Kuantay, A.S., & Kuandykova, A.N., 2021. Substantiating the optimal type of mine working fastening based on mathematical modeling of the stress condition of underground structures. *Naukovyi Visnyk Natsionalnoho Hirnychoho Universytetu*, 3, 57-63, DOI: 10.33271/nvngu/2021-3/057.
12. Bigby, D., Mac, A.K., Hurt, K., 2010. Innovations in mine roadway stability monitoring using dual height and remote reading electronic telltales. In: Materials of the 10th Underground Coal Operators' Conference, Carlton, Victoria 2010, Australia: University of Wollongong & the Australasian Institute of Mining and Metallurgy, 145-160.
13. Jena, S.K., Ritesh, D.L., Manoj, P., Kuldip, P., 2016. Analysis of strata control monitoring in underground coal mine for apprehension of strata movement. *Proceedings of the Conference on Recent Advances in Rock Engineering (RARE 2016)*, 505-511, DOI: 10.2991/rare-16.2016.81.
14. Lubosik, Z., Prusek, S., Wrana, A., Walentek, A., 2015. Underground measurement of gateroad stability at the depth around 1000 m. In: *Proceedings of 34th International Conference on Ground Control in Mining, Morgantown*, 1-9.
15. Walentek, A., 2019. Analysis of the applicability of the convergence control method for gateroad design based on conducted underground investigations. *Archives of Mining Sciences*, 64 (4), 765-783, DOI: 10.24425/ams.2019.131065.

16. Kukutsch, R., Kajzar, V., Konicek, P., Waclawik, P., Ptacek, J., 2015. Possibility of convergence measurement of gates in coal mining using terrestrial 3D laser scanner. *Journal of Sustainable Mining*, 4(1), 30–37, DOI: 10.1016/j.jsm.2015.08.005.
17. Majcherczyk, T., Niedbalski, Z., Ulaszek, A., 2015. Roadway stability evaluation on the basis of modern monitoring of displacement. *Studia Geotechnica et Mechanica*, 37(1), DOI: 10.1515/sgem-2015-0006.
18. Waclawik, P., Kukutsch, R., Konicek, P., Ptacek, J., Kajzar, V., Nemcik, J., Stas, L., Soucek, K., Vavro, M., 2017. Stress State Monitoring in the Surroundings of the Roadway Ahead of Longwall Mining. *Procedia Engineering*, 191, 560-567, DOI: 10.1016/j.proeng.2017.05.218.
19. Lubosik, Z., Waclawik, P., Horak, P., Wrana, A., 2017. The Influence of In-Situ Rock Mass Stress Conditions on Deformation and Load of Gateroad Supports in Hard Coal Mine. *Procedia Engineering*, 191, 975-983, DOI: 10.1016/j.proeng.2017.05.269.
20. Majcherczyk, T., Gaiko, G., Małkowski, P., 2002. Deformation process around a heading investigation when front of longwall face advancing. *Ugol*, 11, 27–29.
21. Prusek, S., 2015. Changes in cross-sectional area of gateroads in longwalls with roof caving, ventilated with “U” and “Y” systems. *Archives Of Mining Sciences*, 60(2), 549-564, DOI: 10.1515/amsc-2015-0036.
22. Majcherczyk, T., Małkowski, P., Niedbalski, Z., 2005. Describing quality of rocks around underground headings: Endoscopic observations of fractures. *Eurock 2005 – Impact of Human Activity on the Geological Environment*, 355-360.
23. Małkowski, P., Niedbalski, Z., Majcherczyk, T., 2008. Endoscopic method of rock mass quality evaluation – new experiences. *42nd U.S. Rock Mechanics - 2nd U.S.-Canada Rock Mechanics Symposium, San Francisco 2008, American Rock Mechanics Association, ARMA 08-237*.
24. Małkowski, P., Ostrowski, Ł., 2019. Convergence monitoring as a basis for numerical analysis of changes of rock-mass quality and Hoek-Brown failure criterion parameters due to longwall excavation. *Archives of Mining Sciences*, 64(1), 93–118, DOI: 10.24425/ams.2019.126274.
25. Majcherczyk, T., Niedbalski, Z., Małkowski, P., 2007. Measurements of roof support load in headings: In: *Technical, technological and Economic Aspects of Thin-Seams Coal Mining* (E.J. Sobczyk, J. Kicki eds.), *International Mining Forum 2007*, 37-46.
26. Małkowski, P., 2017. Zarządzanie monitoringiem zagrożeń w górnictwie (Management of mining hazard monitoring). *Journal of the Polish Mineral Engineering Society*, 215-223, DOI: 10.29227/IM-2017-02-24 (in Polish).
27. www.aceco.kr (access: 2021-05-17)
28. www.geokon.com (access: 2021-04-26)

Applying Electrical Impedance Tomography Techniques for Detection of Decay Inside Trees

KIEU Duy Thong^{1,*}, VU Hong Duong¹, NGUYEN Thi Thu Hang¹, NGUYEN Thu Thuy¹

¹ Hanoi University of Mining and Geology, 18 Vien street, Hanoi, Vietnam

Corresponding author: kieuduythong@hmg.edu.vn

Abstract. Trees play a critical role in creating green spaces in public areas such as streets, parks, schools, offices. Over time, the trees often get pests and diseases, and then rotten trees can break. To care for and conserve the trees, it is necessary to determine the condition inside the trunk, especially the possibility of having a hollow or not. Wood decay, modifications of moisture and ion content, density due to biotic and abiotic stress agents of water extremity, salinity, and infection strongly change (di-) electrical properties of wood. Hence, we propose to use electrical impedance tomography to detect the change in electrical properties inside the trees that can link to wood decay. In electrical impedance tomography, an array of electrodes is attached around the tree trunk, and small alternating currents are injected via these electrodes, so the resulting voltages are measured. Processing the data, we can construct the spatial distribution of impedance (or resistivity) of the object. In this work, we will present the preliminary results of our group research. We will show theoretical forward modeling results, followed by laboratory experiments and real data application. The results illustrate that electrical impedance tomography can be useful to define several decay scenarios inside the trees.

Keywords: Electrical impedance tomography, Tree investigation, Resistivity, Conductivity

1. Introduction

Trees play a very important role in creating green space in public areas such as streets, parks, schools, and offices. Over time, trees often suffer from pests and diseases, becoming fragile and susceptible to falling and causing accidents, especially in the rainy season. Thus, determine the tree trunks inside the condition to suggest a suitable treatment plan and minimize damage while keeping the tree intact. In addition, trees are also an important part of historical, cultural, and spiritual works. From 2010 to now, the Vietnam Association for Conservation of Environment and Nature has recognized over 4,000 heritage trees across the country [1]. Since these are perennial plants, a high possibility of having rotten cores inside hollow can occur. A follow-up process is therefore required to care for and preserve these trees. Like people, doctors need X-ray, CT, or nuclear magnetic resonance images to make decisions before treating or operating on patients. Accordingly, we need to have the information of their trunk inside to evaluate the possibility of the trunk being rotten or not. Therefore, it is necessary to apply geophysical techniques to research the tree trunks. The geophysical methods based on electrical properties of the medium such as geoelectrical, electrical resistivity tomography, and electrical impedance tomography are the most used.

The geoelectrical method has been intensively researched and developed both in instruments and data processing [2-4]. This method is very effectively applied in geology, hydrogeology, and engineering [5-7], the study of natural disasters such as landslides [8], research serving agriculture, research branches related to soil [9]. Similarly, electrical tomography has been researched, developed, and applied in many different fields, such as medicine [10, 11] or plant research [12-16].

Techniques similar to impedance tomography have been widely studied and applied in medical imaging [10, 11, 17] and tree investigation [12, 13, 16, 18, 19]. Currently, in Vietnam, according to our research, there is still no research on the application of tomography to determine the hollow capacity inside the trunk. Therefore, our work is the first time in Vietnam focusing on applying geophysical methods to tree investigation.

In the application of geoelectrical methods to image subsurface, the electrodes are usually located above the ground (Fig. 1a). This is related to the boundary conditions between the ground and the air. For the survey to investigate inside the trunk, the electrodes are arranged around the tree trunk (Fig. 1b). In this case, the solution approach of the problem is different from the case of probing underground objects. Therefore, it is necessary to have studies to change the transformation processes of measurement and data

processing to suit the task of tree investigation.

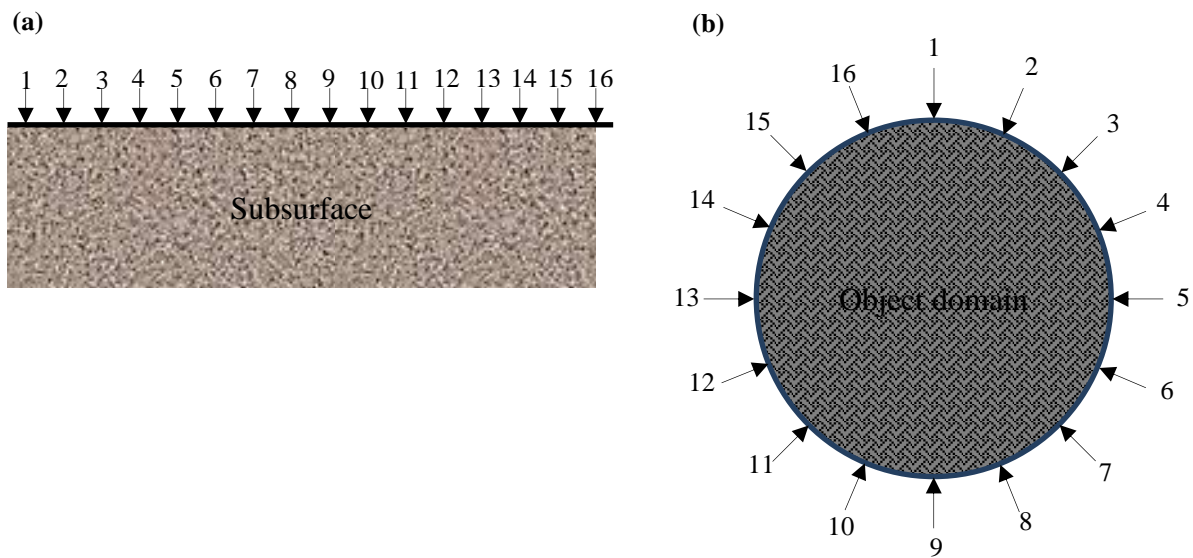


Fig. 1. Electrode’s configuration. Conventional configuration of array in geophysical survey on the surface (a), the configuration around boundaries (b).

2. Theory background

In the Electrical impedance tomography (EIT) method, we inject known amounts of current into a medium that produces current fluxes and induce potentials. We measure the potential electrical field at points on the boundary of the medium (Fig. 1). The current fluxes and potential at the object boundary are influenced by the object impedance. For example, the current conduction within a homogeneous domain (Fig. 2a) differs from that in an inhomogeneous domain (Fig. 2b). As a result, the voltage profile of the homogenous object will be different from the domain with inhomogeneity. It is similar at the boundary; potential profiles will depend on the domain impedance distribution. In other words, we can obtain the information of the impedance distribution of the object domain from the potential boundary data. Also, it is possible to construct a map of the conductivity or resistivity of the region of the object domain.

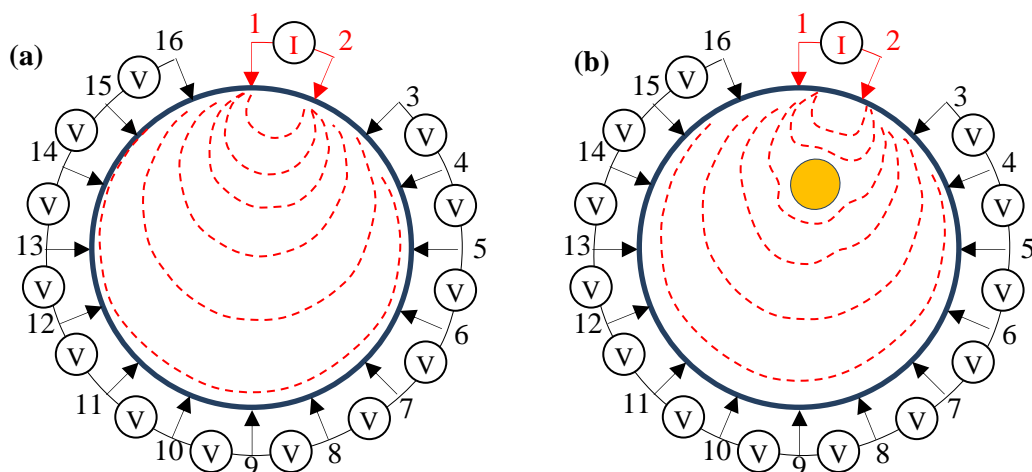


Fig. 2. Variation in boundary data profiles for a homogeneous domain (a) and an inhomogeneous domain (b). The red dash lines show electric current.

a. The governing equations inside the object domain

In an inhomogeneous medium, Maxwell's equations are following:

$$\nabla \times E = -\frac{\partial B}{\partial t}, \tag{1a}$$

$$\nabla \times H = J + \frac{\partial D}{\partial t}, \tag{1b}$$

where E and H is electric and magnetic fields, respectively, B is magnetic induction, D is electric displacement and J electric current density. Moreover, in linear isotropic medium the following relations are valid:

$$D = \varepsilon E, \tag{2a}$$

$$B = \mu H, \tag{2b}$$

$$J = \sigma E, \tag{2c}$$

where ε and μ are electrical and magnetic permittivity, respectively, and σ is the conductivity of the medium. Assuming that the injected currents are time-harmonic with frequency ω , the electric and magnetic fields are of the form (Eqs. 3a and 3b).

$$E = E_0 e^{i\omega t}, \tag{3a}$$

$$B = B_0 e^{i\omega t}. \tag{3b}$$

Using the relations (Eqs. 2a, 2b and 2c), we can rewrite electric and magnetic fields (eqs. 1a and 1b) as follow:

$$\nabla \times E = -i\omega\mu H, \tag{4a}$$

$$\nabla \times H = J + i\omega\varepsilon E. \tag{4b}$$

The quasi-static approximation usually employed in EIT is to assume $\omega\mu H$ is negligible, thus from equation (4a) we have $\nabla \times E = 0$ and hence

$$E = -\nabla\phi, \tag{5}$$

where ϕ is scalar potential.

In EIT, the total current is $J = J_0 + J_s$ where J_s is source current, it is typically zero at frequency ω , and ohmic current $J_0 = \sigma E$. We assume that $\sigma \gg i\omega\varepsilon$, the equation (4b) can be rewritten:

$$\nabla \times H = \sigma E. \tag{6}$$

Substituting E in equation 5 in equation 6 and taking the divergence on both sides, we achieve Laplace's equation (6).

$$\nabla \cdot (\sigma \nabla \phi) = 0. \tag{7}$$

The current density on the boundary is

$$j = -J_s \cdot \mathbf{n} = \sigma \nabla \phi \cdot \mathbf{n}, \tag{8}$$

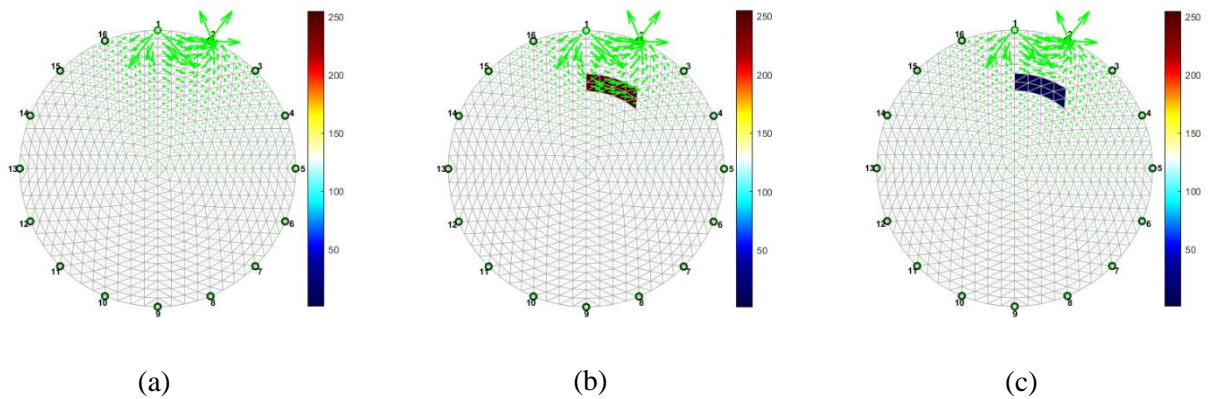
where \mathbf{n} is the outward unit normal to boundary $\partial\Omega$, where j is the negative normal component of the injected current density J_s . Laplace's equation (7) and the boundary conditions (8) is used to build a mathematical model of the EIT method [20].

b. Modeling and inversion

In this work, we use a model of 16 electrodes (Fig. 3). This is the best number to reconstruct the lungs image [21]. The electric resistivity of the wood varies with tree species (Tab. 1), and it is mostly influenced by the water content, chemical elements, which change according to the status of wood and cell structure. Reaction wood does have different resistivity compared to “normal wood”. The models (Fig. 3) represent three scenarios of the trunk: (1) normal status the trunk is homogeneous (Fig. 3a); there is an area inside the trunk, the wood is decayed and contains saline water causing high conductive abnormal (Fig. 3b); and there is an area inside the trunk, the wood is decayed and contains air causing low conductive anomaly (Fig.

3c). In this work, we use an open-source software suite for image reconstruction in electrical impedance tomography and diffuse optical tomography EIDORS [18] for forward and inversion of the data.

Fig. 3. Model of the tree trunk with homogeneous impedance distribution (a), there is a conductive



abnormal area (b), and there is a resistive abnormal area (c). Color bars show relative conductivity of the domain, and dark blue represents more conductive, dark red illustrates more conductive domain. The green arrows show electric current flow; longer arrows represent larger currents.

Tab. 1. Electrical resistivity (ER) parameters (mean \pm SE, minimum and maximum) for tomograms performed at different temperatures (Temp.). For each tree, the stem diameter (Diam.) at measurement height is given [16].

Tree species	ERmean (Ωm)	ERmax (Ωm)	ERmin (Ωm)
<i>B. pendula</i>	136.34 \pm 1.36	755.33	8.66
<i>F. sylvatica</i>	265.08 \pm 4.60	1007.48	8.07
<i>P. nigra</i>	80.22 \pm 0.94	177.82	8.97
<i>L. decidua</i>	276.53 \pm 5.18	1279.42	22.04
<i>P. abies</i>	314.89 \pm 5.19	975.58	25.65

The synthetic data generated from the models in Fig. 3b and c are added 5% Gaussian noise and running inversion process using an approach of Adler and Guardo [22]. The results are shown in Fig. 4. The constructed images show that we can well define the location of decay areas for both models; however, the images of the inverted model are larger than the true areas of the models. Further works of the inversion process are needed to improve the reconstructed images in the future.

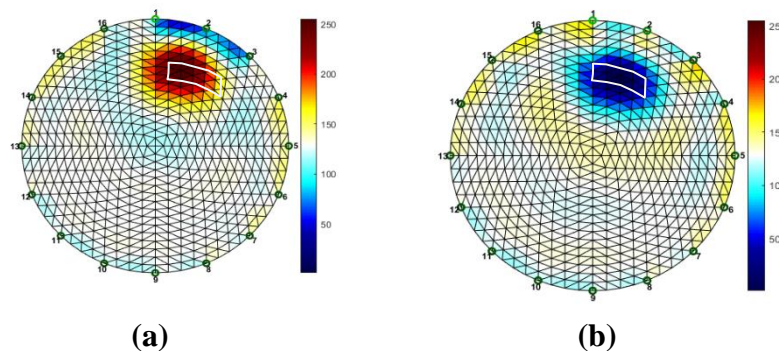


Fig. 4. Inversion results of synthetic data generated by using the conductive model (Fig. 3a) (a) and the resistive model (Fig. 3b) (b). The white polygons mark the true models.

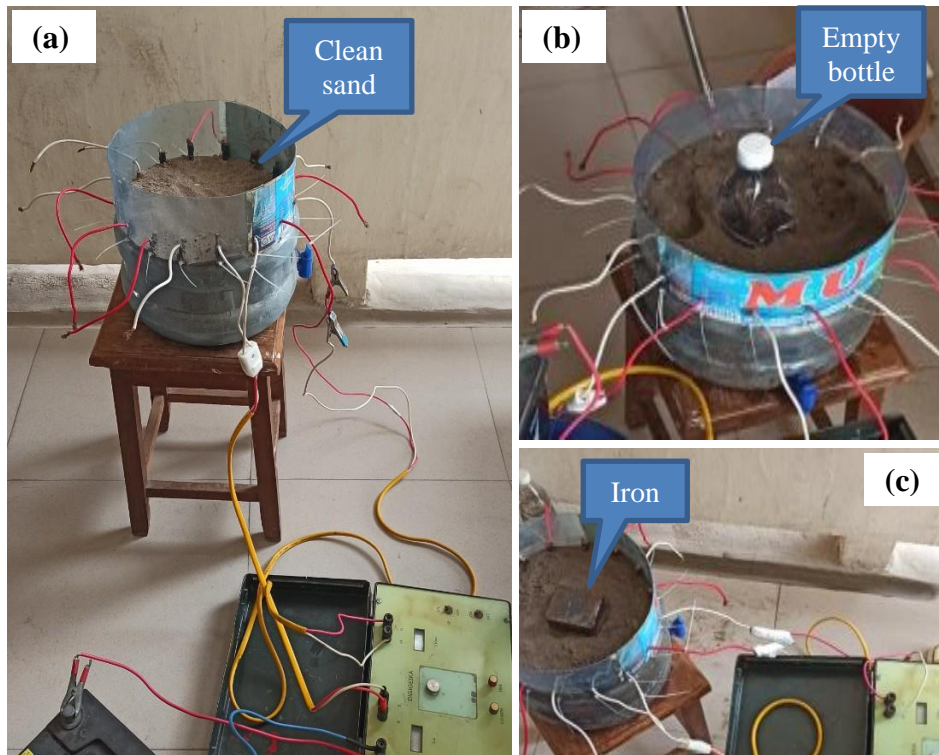


Fig. 5. Experiment models. We use a cylindrical plastic container of sand as the homogeneous model (a), an empty bottle is buried in the center of the cylindrical plastic container represent resistive model (b), and a cubic iron is a conductive model (c).

3. Laboratory experiment

a. Designing experiment models

We use a cylindrical plastic container bottle to make an experiment model (Fig. 5). Copper electrodes are fixed around this cylindrical plastic container. Inside the container, we fill it with moist clean sand to build the homogenous model (Fig. 5a). In one case, we want to build a model with a high resistivity anomaly region, and we use an empty plastic bottle placed in the center of the model (Fig. 5b). In the opposite case, if we want to have a model with a good conductive region, we use iron in the middle of the model (Fig. 5c).

We use a Digigeska electrical instrument made by Geophysical Division, Vietnam, to measure. This is a conventional electrical instrument for four electrodes measurement, a pair of current electrodes, and a pair of potential electrodes. We have a total of 16 electrodes. We have to manually change electrodes at each measurement. First, the current is applied through electrodes 1 and 2 (Fig. 2). The voltage is measured successively with potential electrode pairs 3-4, 4-5, . . . 15-16. Thus, we get 13 voltage measurements. And then, we change the pair of current electrodes to 2 and 3 and measure the voltage of the remaining 13 pairs of electrodes. We continue to change the current electrodes to 16. In total, we obtained 208 measurements.

The data is put in the inversion process, and the results are shown in Fig. 6. We can see that reconstructed images illustrate the models. In the case of the homogeneous model, the container is filled with moist clean sand only. The relative conductivity of the model (Fig. 6b) varies around zero. In the case of the resistive model (Fig. 6a) and conductive model (Fig. 6c), the negative and positive abnormal show the location of the empty bottle and cubic iron, respectively. However, the constructed images do not show the locations and areas of the two objects perfectly, and we can see some artifacts. These may be caused by the highly noisy measured data and the inversion with smooth constraints.

b. Testing on the real wood in the laboratory

We found a solid trunk, which can be seen as a healthy trunk, free from pests and diseases (Fig. 7a). First, we carried out the measurement as described in the experimental model section. We then used a

hollow chisel in the middle to make a model of the hollow trunk (Fig. 7b). Finally, we filled the hollow with hydrated sand to simulate a hollow tree trunk containing water (Fig. 7c). The measurement process is similar to the first case.

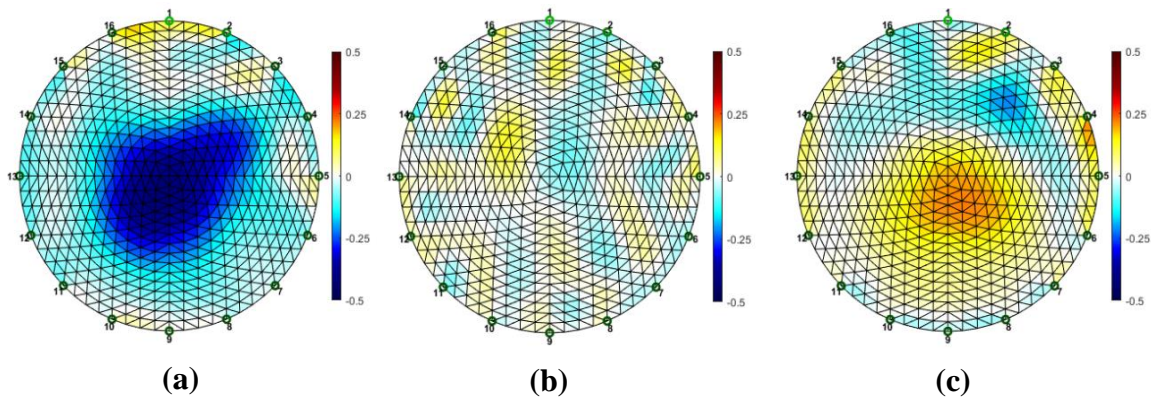


Fig. 6. The inversion results of the experiment data. The constructed image of the resistive model (a), homogeneous model (b), and conductive model (c). The color bars show the relative conductivity of the models; blue and red represent resistive and conductive mediums, respectively.

The inversion process is also applied as similar to the experiment models. The results are shown in Fig. 8. We can see that reconstructed images illustrate the wood models. In the case of the homogeneous model (healthy trunk), the relative conductivity of the model (Fig. 8b) varies around zero. In the case of the resistive model (Fig. 8a) and conductive model (Fig. 8c), the negative and positive anomalies show the locations of the empty hollow and hydrated sand, respectively. The issue is like the container models above; the constructed images do not show areas of the two abnormal areas perfectly. These may be caused by the highly noisy measured data and the inversion with smooth constraints.

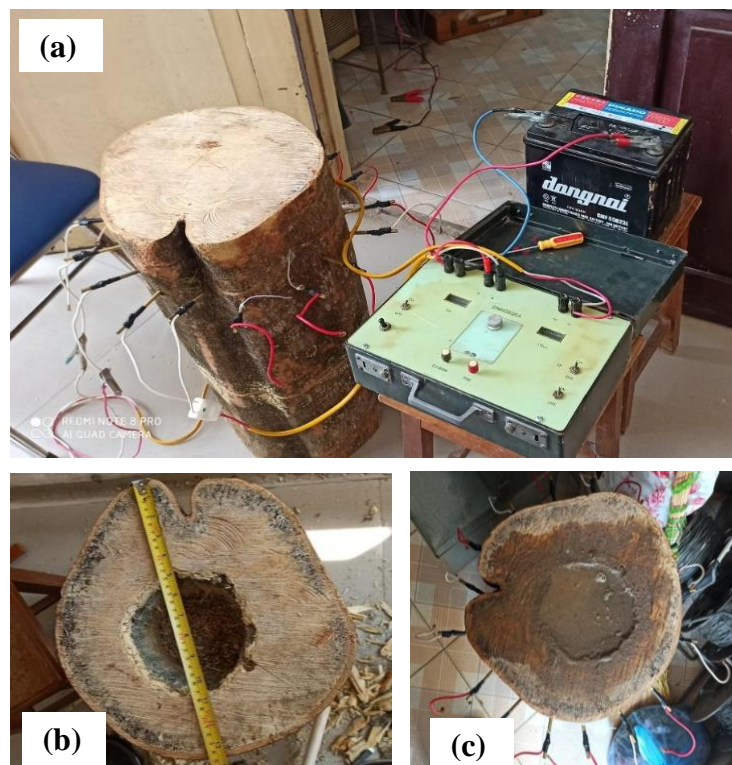


Fig. 7. The wooden models. We have a homogeneous trunk (a), we hollowed out the trunk of the tree to make the model of a hollow trunk containing air (b) and finally we put sand and water inside the hole to make the conductive model of the trunk.

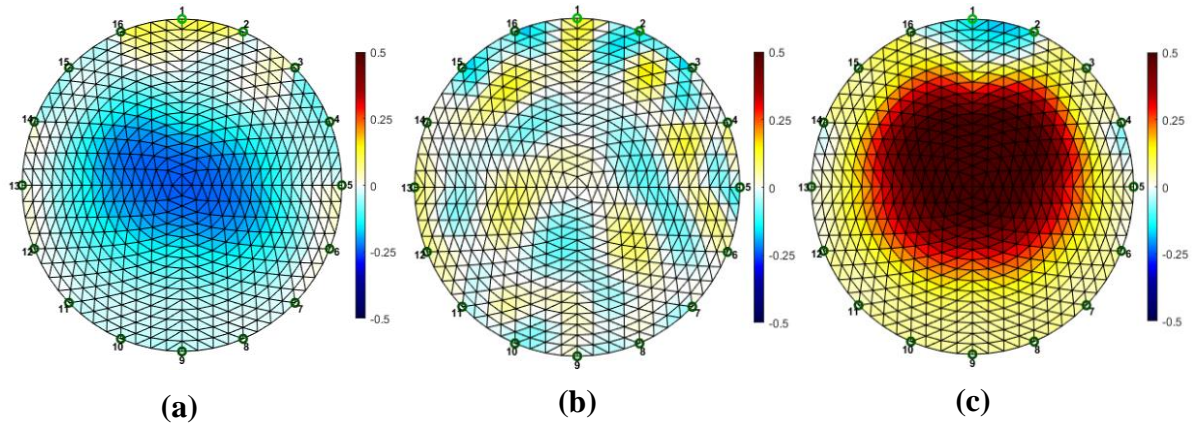


Fig. 8. The inversion results of the experiment data. The constructed image of the resistive model (a), homogeneous model (b) and conductive model (c). The color bars show relative conductivity of the models, blue and red represent resistive and conductive medium, respectively.

4. Real data

The data were measured on two perennial mango trees, planted next to each other and about the same age, about 350 years old. One tree has broken branches due to hollow trunks (Fig. 9). The question is when the remaining tree will break in the future.

The measurement and inversion approaches are similar in the laboratory. We use 16 electrodes and measure the pattern in succession between two electrodes next to each other (Fig. 10a). The constructed image (Fig. 10b) clearly shows the low conductivity part related to the hollow part of the trunk. We made similar measurements on the remainder tree (Fig. 11a) and the results also indicated that there is a hollow in the middle part of the trunk (Fig. 11b).

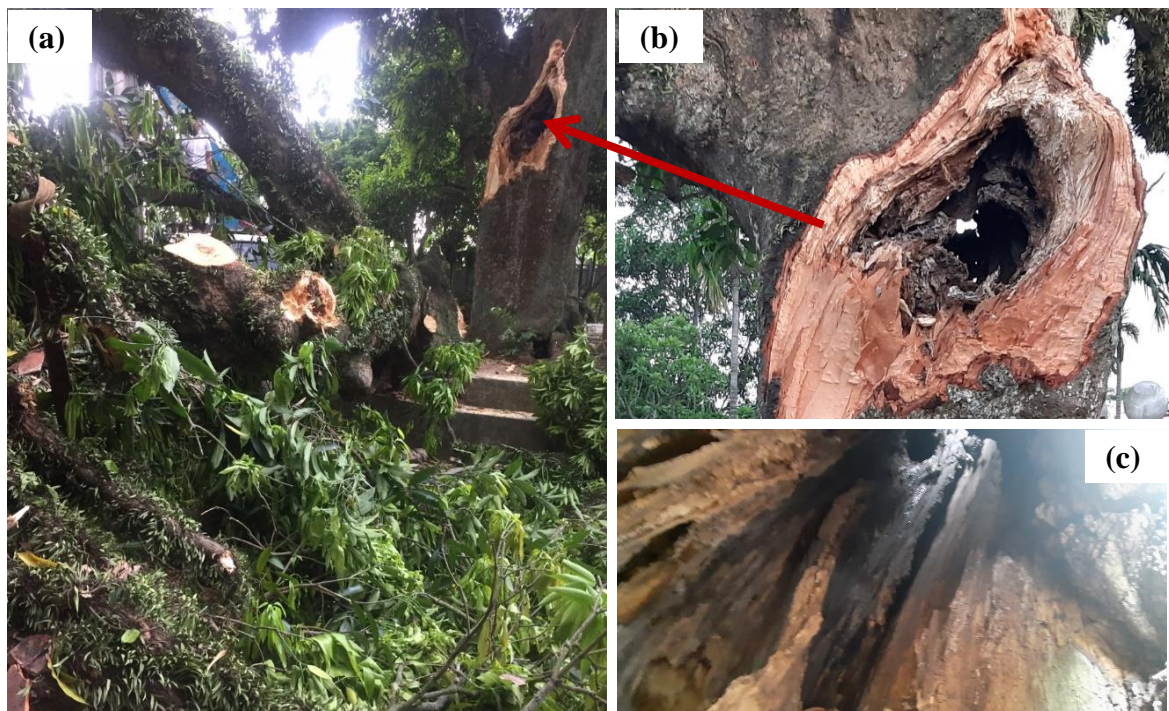


Fig. 9. The hollow tree is the cause of the broken branches (a). Zoom in on the broken branch due to the hollow inside (b). Image of the hollow inside the tree (c).

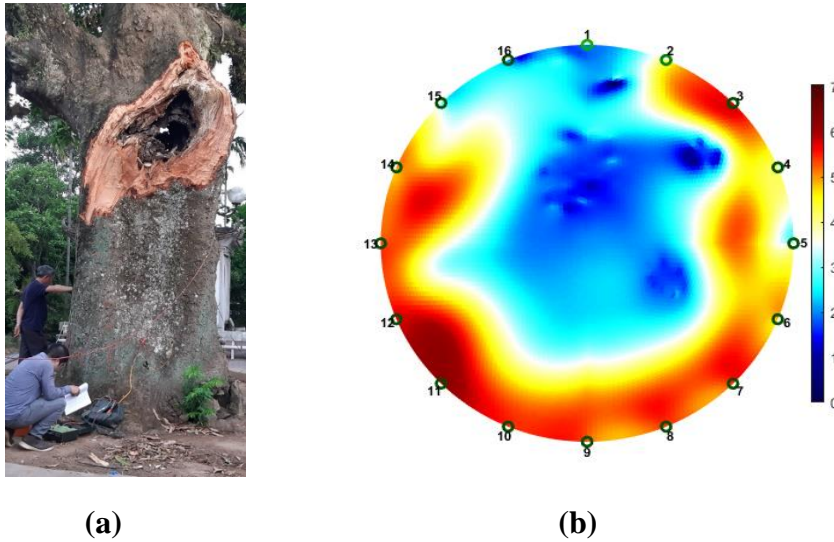


Fig. 10. Measurement of the broken tree (a). The inversion image shows clearly resistive area (blue color) that illustrates the hollow inside the tree (b). The color bar shows relative conductivity of the models. Blue and red represent resistive and conductive media, respectively.

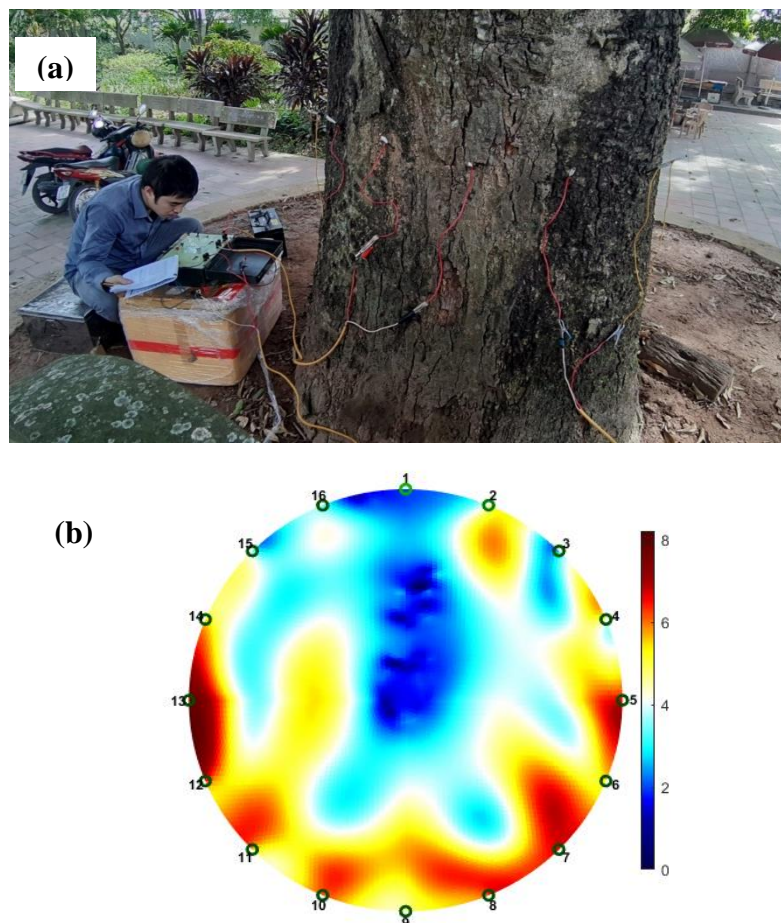


Fig. 11. Measurement of the tree is located near the broken tree (a). The inversion image clearly shows the resistive area (blue color) that may illustrate the hollow inside the tree (b). The color bar shows the relative conductivity of the models; blue and red represent resistive and conductive mediums, respectively.

5. Conclusion

We present the application of the electrical impedance tomography (EIT) method to investigate the inside of trees in Vietnam. The biggest advantage of this method is the non-destructive sample, i.e., the method can be applied to investigate the trees with no damage to them. We have built theoretical models and laboratory experiments and then test in real cases. Our preliminary results demonstrate that the EIT method is robust to investigate the trees. However, the results are not yet perfect, and we believe that further research can improve the results. In the future, a better instrument to acquire data and an improved inversion process to construct the tree image can enhance the robustness of the EIT method.

6. Acknowledgments

This paper is completed as a result of the project funded by the Hanoi University of Mining and Geology, code T21-22. We would like to thank the geophysics students, Pham Van Kien, Nguyen Huu Thang, Tran Phung Trung Hien, Tran Dang Tuan, and Nguyen Tuan Thanh, who assisted us in building experimental models and conducting measurements. We sincerely thank Mr. Nguyen Van Loi, Institute of Ecology and Works Protection, for supporting us in collecting the real data. We would like to thank all the authors of the EIDORS Source code that is used in this work <http://www.sce.carleton.ca/faculty/adler/eidors/programming/programming.shtml>.

The paper was presented during the 6th VIET - POL International Conference on Scientific-Research Cooperation between Vietnam and Poland, 10-14.11.2021, HUMG, Hanoi, Vietnam.

7. References

1. <http://www.vacne.org.vn/4-018-old-trees-across-the-country-have-been-recognized-as-vietnamese-heritage-trees/e3699.html>, 08/07/2021.
2. Loke, M.H., J.E. Chambers, D.F. Rucker, O. Kuras, and P.B. Wilkinson, 2013. Recent developments in the direct-current geoelectrical imaging method. *Journal of Applied Geophysics*, 95: 135-156.
3. Pidlisecky, A., E. Haber, and R. Knight, 2007. RESINVM3D: A 3D resistivity inversion package. *Geophysics*, 72(2): H1-H10.
4. Kieu, T.D., 2020. Inversion of multiple data sets acquired by different array configuration of geoelectrical resistivity method (in Vietnamese) *Journal of Mining and Earth Sciences*, 61(1): 52-60.
5. Kemna, A., J. Vanderborght, B. Kulesa, and H. Vereecken, 2002. Imaging and characterisation of subsurface solute transport using electrical resistivity tomography (ERT) and equivalent transport models. *Journal of Hydrology*, 267(3): 125-146.
6. Chambers, J.E., O. Kuras, P.I. Meldrum, R.D. Ogilvy, and J. Hollands, 2006. Electrical resistivity tomography applied to geologic, hydrogeologic, and engineering investigations at a former waste-disposal site. *Geophysics*, 71(6): B231-B239.
7. Dat, P.N., P.N. Kien, B.V. Thom, L.H. Phong, and D.T. Ninh, 2018. Determining the thickness of the weathering layer overlying the basalt in Cu Mga - Dak Lak area by 2D resistivity imaging, *Journal of Mining and Earth Sciences*, 59(6): 1-10.
8. Perrone, A., V. Lapenna, and S. Piscitelli, 2014. Electrical resistivity tomography technique for landslide investigation: A review. *Earth-Science Reviews*, 135: 65-82.
9. Samouëlian, A., I. Cousin, A. Tabbagh, A. Bruand, and G. Richard, 2005. Electrical resistivity survey in soil science: a review. *Soil and Tillage Research*, 83(2): 173-193.
10. Bera, T.K., 2014. Bioelectrical Impedance Methods for Noninvasive Health Monitoring: A Review. *Journal of medical engineering*, 381251.
11. Luo, Y., P. Abiri, S. Zhang, C.-C. Chang, A.H. Kaboodrangi, R. Li, A.K. Sahib, A. Bui, R. Kumar, M. Woo, Z. Li, R.R.S. Packard, Y.-C. Tai, and T.K. Hsiai, 2018. Non-Invasive Electrical Impedance Tomography for Multi-Scale Detection of Liver Fat Content. *Theranostics*, 8(6): 1636-1647.
12. Sambuelli, L., L.V. Socco, and A. Godio, 2003. Ultrasonic, electric and radar measurements for living trees assessment. *Bollettino di Geofisica Teorica ed Applicata*, 44: 253-279.

13. Attia al Hagrey, S., 2007. Geophysical imaging of root-zone, trunk, and moisture heterogeneity. *Journal of Experimental Botany*, 58(4): 839-854.
14. Jayawickreme, D.H., E.G. Jobbágy, and R.B. Jackson, 2014. Geophysical subsurface imaging for ecological applications, 201(4): 1170-1175.
15. Corona-Lopez, D.D.J., S. Sommer, S.A. Rolfe, F. Podd, and B.D. Grieve, 2019. Electrical impedance tomography as a tool for phenotyping plant roots. *Plant Methods*, 15(1): p. 49.
16. Cimpoişu, M.O., O. Kuras, T. Pridmore, and S.J. Mooney, 2020. Potential of geoelectrical methods to monitor root zone processes and structure: A review. *Geoderma*, 365: 114-232.
17. Malmivuo, J. and R. Plonsey, 1995. Bioelectromagnetism. 26. Impedance Tomography, 420-427.
18. Ehosioke, S., F. Nguyen, S. Rao, T. Kremer, E. Placencia-Gomez, J.A. Huisman, A. Kemna, M. Javaux, and S. Garré, 2020. Sensing the electrical properties of roots: A review, 19(1): e20082.
19. Ganthaler, A., J. Sailer, A. Bär, A. Losso, and S. Mayr, 2019. Noninvasive Analysis of Tree Stems by Electrical Resistivity Tomography: Unraveling the Effects of Temperature, Water Status, and Electrode Installation. *Frontiers in plant science*, 10: 1455-1455.
20. Polydorides, N., 2002. Image reconstruction algorithms for soft-field tomography, in *Electrical Engineering and Electronics*. University of Manchester : UMIST: University of Manchester : UMIST. p. 262.
21. Schullcke, B., S. Krueger-Ziolek, B. Gong, and K. Moeller, 2016. Effect of the number of electrodes on the reconstructed lung shape in electrical impedance tomography. *Current Directions in Biomedical Engineering*, 2.
22. Adler, A. and R. Guardo, 1996. Electrical impedance tomography: regularized imaging and contrast detection. *IEEE Transactions on Medical Imaging*, 15(2): 170-179.

Mining-induced Land Subsidence Detected by Sentinel-1 SAR Images: An Example from the Historical Tadeusz Kościuszko Salt Mine at Wapno, Greater Poland Voivodeship, Poland

KIM Thi Thu Huong^{1,2,*}, TRAN Hong Ha^{2,3}, BUI Khac Luyen², LIPECKI Tomasz¹

¹ AGH University of Science and Technology, Kraków, Poland

² Hanoi University of Mining and Geology, 18 Vien street, Hanoi, Vietnam

³ Institute of Geo-Engineering, Clausthal University of Technology, Clausthal, Germany

Corresponding author: huongktt87@gmail.com

Abstract. There are many mines in Poland that have been in operation for over 100 years, with the Tadeusz Kościuszko mine being a large salt mine in Wapno, northern Poland. The mine was closed in 1977 due to the greatest catastrophe in the history of Polish mining, but in the first days of 2021, a very large hole has been created in this area due to land subsidence. This article uses InSAR technology with Sentinel-1 images to determine settlement and ongoing deformation in this mine. The study results are useful for policymakers, managers, and authorities because land subsidence has caused serious and dangerous effects on people living in the area. The results processed by the Persistent Scatterer InSAR (PSInSAR) method with the Sentinel Application Platform and the Stanford Method for Persistent Scatterers software packages show that deformation in the Wapno village area has been detected in both residential and non-residential areas, with maximum subsidence of up to -19 mm/yr. The subsidence in the mine reaches -12 mm/yr, and that at surrounding area range from 0 to -18.8 mm/yr.

Keywords: PSInSAR, Land subsidence, Mining, Wapno, Poland

1. Introduction

Poland is the biggest mining country in Europe, of which mineral mines concentrate in half of the country, stretching from North-West to South-East (see Fig. 1). Many of them are over 100-year-old excavation mines. As a result, mining-induced land surface deformation is happening, attracting much scientific research in the country.

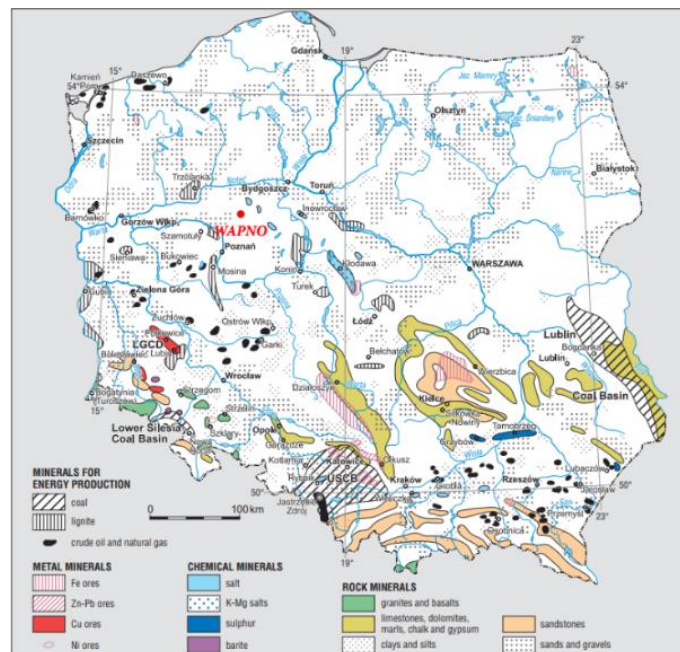


Fig. 1. Distribution of mineral mines in Poland adapted from Kowalczyk Andrzej, Witkowski Andrzej [1]. The red dot is the study area of Wapno, Wielkopolskie, Poland.

Tadeusz Kościuszko is a well-known rock salt mine in Poland, which is located in Wapno, northern Poland. In 1977, the most terrible disaster in the mining history of Poland had happened in this mine, that

a sudden increase of groundwater flooded a level of the mine and broke the insulation layer. A huge sinkhole with a depth of several meters has been created in the village on 28th October 1977. Consequently, 40 buildings were destroyed, and trees, roads, and railway tracks disappeared into the abyss. About 1400 residents had to evacuate, among which some of them have left the village forever. Many years later, the subsidence and appearance of the sinkholes still happened. Other smaller sinkholes also happened in 2007 and 2017. On 26th February 2021, a big sinkhole appeared in the area of the old mine. The risk of ground subsidence is subject to happen at any time [2]. It was shown that from October 2014 to June 2020, the subsiding rate increased from 3 millimeters per year (mm/yr) to 8 mm/yr [3]. Ground deformation in and around an underground mining area frequently occurs. It is a major component of the displacement vector, triggered by underground mining [4]. In Poland, mining-induced land subsidence has been measured by conventional methods, such as geodetic leveling, total stations, or the Global Navigation Satellite System (GNSS). In recent years, it has also been measured by other methods, including Interferometric Synthetic Aperture Radar (InSAR), Unmanned aerial vehicle (UAV), or laser scanning. Conventional methods are labor-intensive and time-consuming [5]. Additionally, these techniques gather data on a point-by-point basis with limited spatial coverage, which does not provide enough information about the whole surface subsidence. Therefore, the monitoring is usually limited to small areas. InSAR, UAV, and laser scanning, in contrast, allow monitoring land surfaces in very large areas with a very high number of measured points. Hence, these technologies are applied more and more in both the science and industry sectors.

Differential InSAR (DInSAR) is a technique in which two SAR scenes acquired over the same area on the Earth, but at different acquired times, are used to derive the Earth's surface deformation [4]. In DInSAR, the contribution of topography is removed from the phase change between the two SAR scenes. It can be used to quantify a small displacement of the land surface [6]. However, the results of DInSAR are affected by the various error and noise sources, e.g., atmospheric artifact, topographical and orbital errors. Therefore, different multi-temporal InSAR (MTInSAR) methods have been proposed, which exploit a big SAR dataset. Small baseline subset (SBAS) [7] and Persistent Scatterer InSAR (PSInSAR) [8] are among the most commonly used MT-InSAR methods [9]. While PSInSAR optimizes pixels with single scatterers, SBAS optimizes those with distributed scatterers [10]. Additionally, SBAS is advantageous in that redundant interferograms can be adopted to reduce noise, particularly in areas of low deformation magnitude affected by high noise [11]. In contrast, in PSInSAR, all interferograms are generated to a single primary, which allows for noise reduction of the primary image as it exists in all interferograms [12].

The PSInSAR method has been employed in the literature worldwide in monitoring Earth's surface deformation, which is associated with groundwater extraction and urbanization [12], mine exploitation [13], [14] among others. In Poland, the first application of PSInSAR for displacement monitoring was published in 1998 by Perski [15] in The Silesian coal mine region. Since then, Zbigniew Perski and his partners started publishing their studies on using InSAR for many areas in Poland: application of satellite radar interferometry in the areas of copper ore mining in LGOM [16], for surface deformation monitoring in the urbanized area of Malbork, northern Poland [17]; analysis of terrain deformation near the Wieliczka salt mine [18] and Nowy Sącz [19]. In 2006, Marek Graniczny and his partners published their article using PSInSAR in observing displacement in the Mining of Silesia Region, Poland [20].

Mapping ground vertical movement caused by salt mining activities with the Sentinel-1 Terrain Observation with Progressive Scanning (TOPS) data was performed by Malinowska, Hejmanowski [21], which was applied to the Wieliczka salt mine in the years 2015-2016. The results have shown the subsidence dynamics in the western part of the Wieliczka town of up to 20 mm/year. Smaller subsidence was observed in the eastern part of the town, not exceed 10 mm/year [21]. Deformation around the Wieliczka salt mine was also studied by [18] and Mirek [22].

However, InSAR has not been employed in the Tadeusz Kościuszko salt mine to date. This study shows the application of InSAR in monitoring the land deformation in the Tadeusz Kościuszko salt mine over the one-year period, between March 2020 and March 2021. The objective of the study is to demonstrate the possibility of the application of the PSInSAR method with Sentinel-1 SAR data to quantify surface deformation around this ancient salt mine and in the Wapno village.

The remainder of the paper is structured as follows: Section 2 introduces the history of the Tadeusz Kościuszko salt mine in Wapno, Grater Poland Region, Poland. In Section 3, the study area, materials, and method are provided. Section 4 provides experimental results, and Section 5 concludes the study.

2. History of the Tadeusz Kościuszko salt mine Wapno, Greater Poland Voivodeship, Poland

Wapno is a large village in west-northern Poland. In 1828, the header of the Wapno village began exploiting the gypsum open-pit mine, which laid shallow under the ground. Then, they realized that there was a big salt layer covered with a gypsum – clay cap with a thickness of 20–160 m. In 1898, the permit for the operation was bought by the German Company Solwerke. In 1910, the drilling of the Wapno I—a mining shaft, was started at 101.5 m depth – due to the enormous inflow of water – this work was stopped. Therefore, during 1912–1917, the Wapno II shaft was exploited. It was reached 420 m underground in 1916. From May 1917 to June 1918, at a depth of 406 m – the first level of mine (later, it is level IV), 450 m main working in the mine was drilled. Then, more four parallel exploded ways in the mine were also drilled. The next levels were created over time according to the depth: 345 m (level I), 365 m (level II), 385 m (level III), 430 m (level V), and 455.5 m (level VI). The salt mine was exploited to level XII at a depth of 648 m and, in the middle of 1960-years, even prepared for the construction of levels VIII and IX [23]. The Wapno salt mine is in the area of 1000×350 m. The salt-mining exploitation was started at level IV. The excavated material was transported to the ground by a steam hoisting machine and a wooden pane tower. Both were replaced in 1930 – 1931 by a modern type of steam hoisting and a steal double-shot over shaft tower. All factory was already electrified at that time, achieved in the 1920s more and more output products - growing from 17234 tons in 1920 to 86422 tons in 1925 (42,1 % of all salt excavation in Poland at that time), and the company’s best result in the entire war period – 100 896 tons salt in 1930 [23].

In 1956, the name of the company was established as the Tadeusz Kościuszko salt mine. From 1950 to 1965, the production of the mine accounted for more than half of the rock salt extracted in Poland during this time. During 1967–1975, the annual production of salt exceeded 400 thousand tons. It was exported to Czechoslovakia, Hungary, Sweden, Finland, Norway, Guinea, Great Britain, Denmark, Nigeria. In the 1970s, the mine’s water hazard increased due to the existence of a very thin layer, which separated the deposit from the water in the overburden formation. In 1976, water leakage into the working place was detected. On 5th August 1977, one of the greatest catastrophes in the history of Polish mining occurred in the mine, that a sudden increase of groundwater flooded the third level. The main causes were the creation of hydraulic connections between the excavation [23–24].

On 28th October 1977, a huge sinkhole appeared in the village, by which over 40 buildings were destroyed while trees, roads, and railway tracks disappeared into the abyss [2]. The Wapno village was inaccessible for about two years between 1978 and 1979. Around 1400 residents were evacuated from the village, many of them left their place forever. As a result of the mining catastrophe, Wapno has lost about half of its inhabitants. According to the data published in December 2018, there were 1650 people living in the village [25]. The financial losses caused by this catastrophe have not been counted. Wapno has never regained its prosperity in the 44 years from 1977 to 2021 that have passed since the disaster. Today, in the mining disaster areas, Obrońcy Stalingradu Ogrodowa, Staszic, and Świerczewski streets do not exist anymore, and the forest has grown instead [25]. Fig. 2 shows examples of typical land subsidence-induced damages in the Wapno village.



Fig. 2. (left) Garages in Karol Swierczewski Street were completely collapsed by a huge sinkhole on 5th August 1977, (middle) railway tracks were broken in the Wapno village [25], (right) A huge hole in the Wapno village, which was allegedly caused by land subsidence triggered by mining exploration in the Tadeusz Kościuszko salt mine [26].

3. Study area, dataset, and method

3.1. Study area and dataset

The study area is located in the northern part of Poland, over the area of the ancient Tadeusz Kościuszko salt mine in the Wapno village, which is located in Gmina Wapno (see Fig. 3, left). Wapno means lime in the Polish language, in which there are large gypsum and lime deposits. There are also large deposits of rock salt, which were started to be excavated from the beginning of the nineteenth century. In addition, Wapno is close to several lakes and thus is called Gniezno Lake District. The study area is limited from 52°52' N to 52°58' N and 17°21' 2.52" E to 17°35' 54.96" E (see Fig. 3, right). It covers all the Wapno village. The Tadeusz Kościuszko salt mine was closed, but people are still living around with kindergarten, primary school, church, post office, grocery store, buildings, and houses.

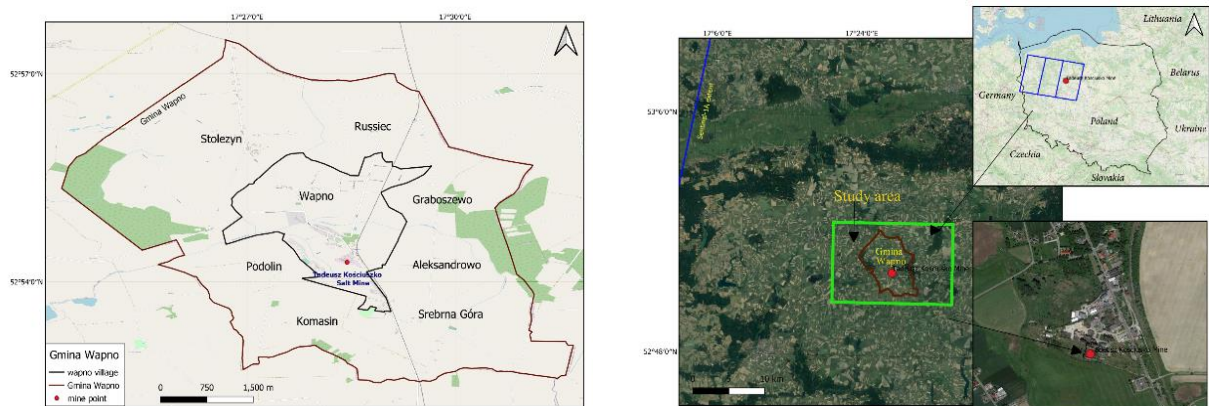


Fig. 3. (left) Location of the Wapno village with the red dot indicating the Tadeusz Kościuszko Salt Mine, (right) The study area (green box). The extent of the Sentinel-1A data sub-swaths is indicated by blue boxes in the right panel. Red dots are the Tadeusz Kościuszko Salt Mine.

In this study, the Sentinel-1A data in the Single Look Complex (SLC) format are utilized. These data can be freely obtained from <http://www.scihub.copernicus.eu>. The dataset is acquired in the descending orbit number 22 and is processed in the Interferometric Wide-swath (IW) mode. We use a total of 32 images covering the 1-year time period, between March 9, 2020, and March 16, 2021, with a 12-day temporal interval. The radar wavelength of Sentinel-1 is ~5.55 cm, which corresponds to the C-band in the microwave spectrum. Tab. 1 shows the information of 32 images with the date of acquisition, perpendicular baseline, and temporal baseline. The image captured on September 29, 2020, was chosen as the primary image. Perpendicular baseline is the spatial distance between the first and secondary observations measured perpendicular to the look direction (means data from the primary and secondary images). It provides an indication of the sensitivity to terrain height, the degree of correlation due to phase gradients, and the effectiveness of the phase unwrapping. Temporal baseline is the time period between two dates of primary and secondary images acquisition.

3.2. Method

The Sentinel-1A data is processed with the PSInSAR method. The interferograms are formed with the image acquired on September 29, 2020, chosen as the primary image (see Tab. 1). The interferogram network is shown in Fig. 4, in which image acquisition times are described along the X-axis, and perpendicular baseline lengths are indicated along the Y-axis. The number shown in the figure for each image indicates the perpendicular baseline w.r.t the primary image. The steps of data processing utilized in this study are shown in Fig. 5. The interferograms are first processed by the Sentinel Application Platform (SNAP) software package by European Space Agency (ESA), then the InSAR time series are analyzed by the Stanford Method for Persistent Scatterers (StaMPS) software package [27]. These steps are described in Tab. 2.

Tab. 1. List of Sentinel-1 SAR scenes used in this study. The image captured on September 29, 2020, is chosen as the primary image.

No	Date of acquisition	Perpendicular baseline (m)	Temporal baseline (days)
1	09 March 2020	100.85	204
2	21 March 2020	40.90	192
3	02 April 2020	-72.80	180
4	14 April 2020	-96.73	168
5	26 April 2020	-23.34	156
6	8 May 2020	-35.85	144
7	20 May 2020	23.31	132
8	1 June 2020	-75.18	120
9	13 June 2020	-41.17	108
10	25 June 2020	-34.47	96
11	07 July 2020	-19.42	84
12	19 July 2020	21.38	72
13	31 July 2020	43.82	60
14	12 August 2020	-73.89	48
15	24 August 2020	-51.59	36
16	05 September 2020	17.96	24
17	17 September 2020	47.80	12
18	29 September 2020	0	0
19	11 October 2020	-24.23	-12
20	23 October 2020	-61.16	-24
21	04 November 2020	43.39	-36
22	16 November 2020	60.71	-48
23	28 November 2020	2.31	-60
24	10 December 2020	-33.10	-72
25	22 December 2020	-31.88	-84
26	3 January 2021	34.62	-96
27	15 January 2021	72.77	-108
28	27 January 2021	97.71	-120
29	08 February 2021	49.32	-132
30	20 February 2021	-87.29	-144
31	04 March 2021	-98.05	-156
32	16 March 2021	-32.23	-168

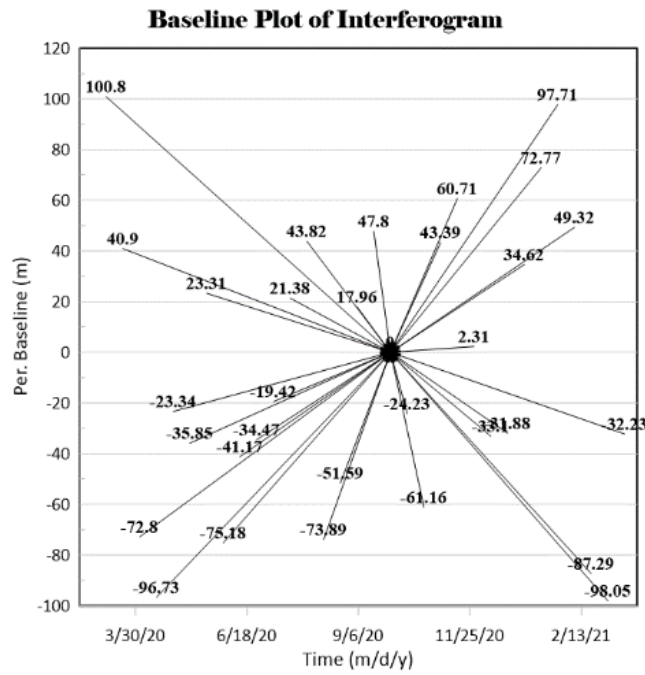


Fig. 4. The interferogram network with the primary image was acquired on September 29, 2020 (black dot).

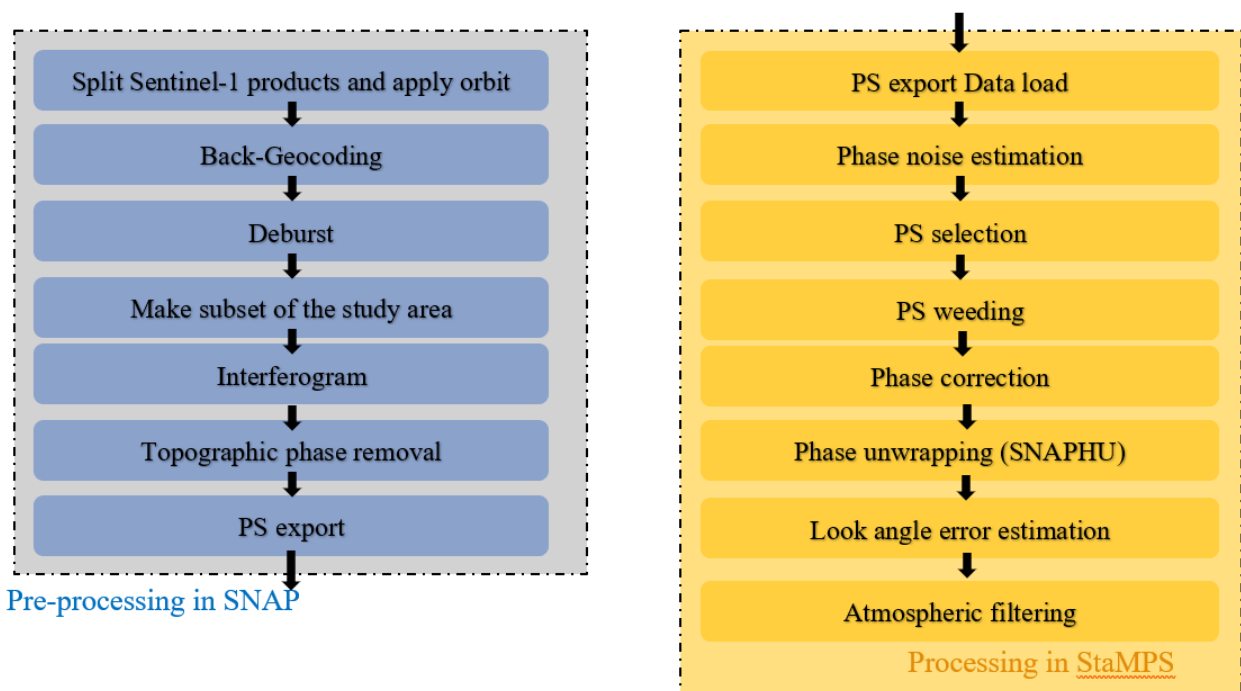


Fig. 5. Workflow of the PSInSAR data processing applied in this study: (left) Steps of interferogram formation by the SNAP software package and (right) PSInSAR time series analysis by the StaMPS software package.

Tab. 2. Description of the main processing steps by the PSInSAR method with the SNAP and StaMPS software packages.

No	Step	Description
1	Split Sentinel-1 products and apply orbit	Split Sentinel-1A images with the selected sub-swath, bursts, and polarization. Based on the accurate information of satellite position and velocity, the orbit state vectors in the metadata of the products are updated.
2	Co-registration	Co-registration of one or more slave images with a master on the same sub-swath using the orbit of the products and the digital elevation model.
3	Deburst	Merging of adjacent bursts in the azimuth direction according to their zero. Remove black path between bursts.
4	Subset	Make a subset to focus on the study area.
5	Interferogram	Form the interferograms.
6	Topographic phase removal	Remove phase due to topography.
7	StaMPS export	Export products to be subsequently processed in StaMPS.
8	Data load	Import the data from SNAP to StaMPS. Save the data in the MATLAB workspaces.
9	Phase noise estimation	Estimation of the phase noise value for each pixel in the interferograms.
10	PS selection	Selection of eligible PS pixel on a noise characteristics basis.
11	PS weeding	Remove PS noise or PS affected by signal contribution from neighboring elements.
12	Phase correction	Correction of the wrapped phase.
13	Phase unwrapping	Phase unwrapping by the SNAPHU method [28].
13	Look angle error estimation	Computation of spatially correlated look angle error
14	Atmospheric filtering	Exploiting triangle mesh generator and Delaunay triangulator.

4. Results

A total of 74 446 points have been generated from the data processing. These points are received from the backscatter of the satellite signal. There are low coherence points located in rural areas but high coherence points in constructions and buildings. Therefore, a coherence threshold of 0.4 is used to filter these low coherence points, by which 9 349 PS points are retained. The deformation rates for the entire study area are shown in Fig. 6b. In this study, positive deformation reveals the movement of the Earth's surface toward the satellite (i.e., uplift), while negative deformation represents the movement away from the satellite (i.e., subsidence). Both indicate the movement along the vertical direction, which is converted from the line of sight (LOS) direction with an assumption that the horizontal component is insignificant by [12]:

$$d_U = \frac{d_{LOS}}{\cos\theta_{inc}}$$

where d_U and d_{LOS} are the deformation in the vertical and LOS directions, θ_{inc} is the radar incidence angle.

No reference area is applied due to no evidence of a stable area (i.e., an area with a low deformation rate); thus, the deformation at detected points have been identified relative to the average deformation of the entire study area. As a result, both subsidence and uplift of the same maximum magnitude (i.e., ± 30 mm/yr) are found in the study area. In the Wapno village, uplift and subsidence spread evenly over the area, as shown in Fig. 6b. In the Wapno village, points of high subsidence (up to -19 mm/yr) are marked by red

dots in Fig. 6b, which are located in non-residential areas (see Fig. 6a). They are distributed in the northern, central, and southern parts of the village marked by blue borders. In residential areas shown by the red borders, the subsidence between 0 and -8.6 mm/yr is found. In the salt mine area, most of the subsidence rates range from 0 to -9 mm/yr, with some points reaching -12 mm/yr.

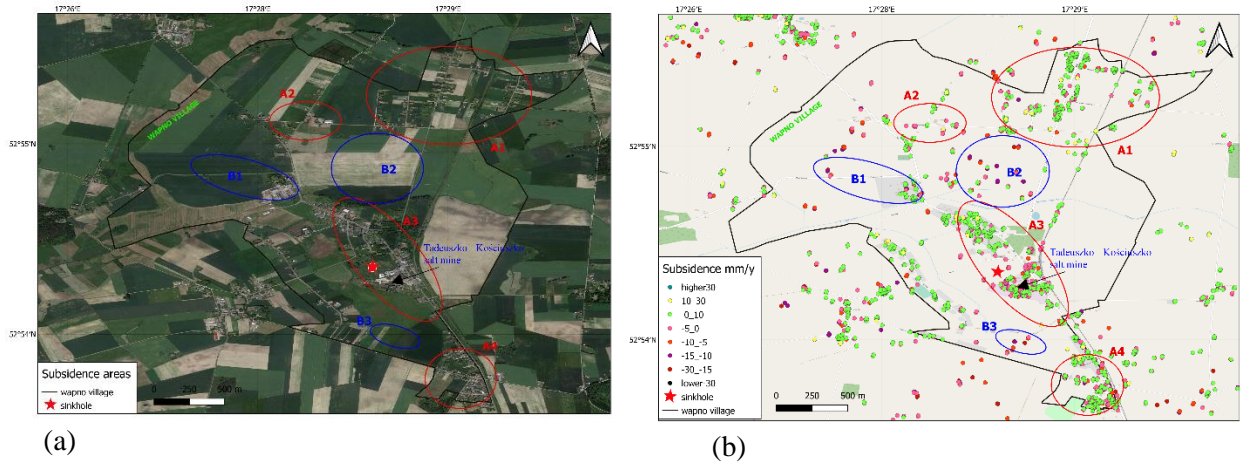


Fig. 6. The deformation rates for the study area between March 9th 2020 and March 16th 2021. The big red star is the sinkhole, which appeared on February 26th 2021.

In each residential or non-residential area with the border shown in Fig. 6, we extract points with the highest subsidence, which are shown in Fig. 7 and

Tab. 3. It is shown that subsidence rates range between ~ -15 mm/yr and ~ -19 mm/yr in non-residential areas (P1 to P9), and ~ -5.5 mm/yr and ~ -14.5 mm/yr in residential areas (P10 to P16).

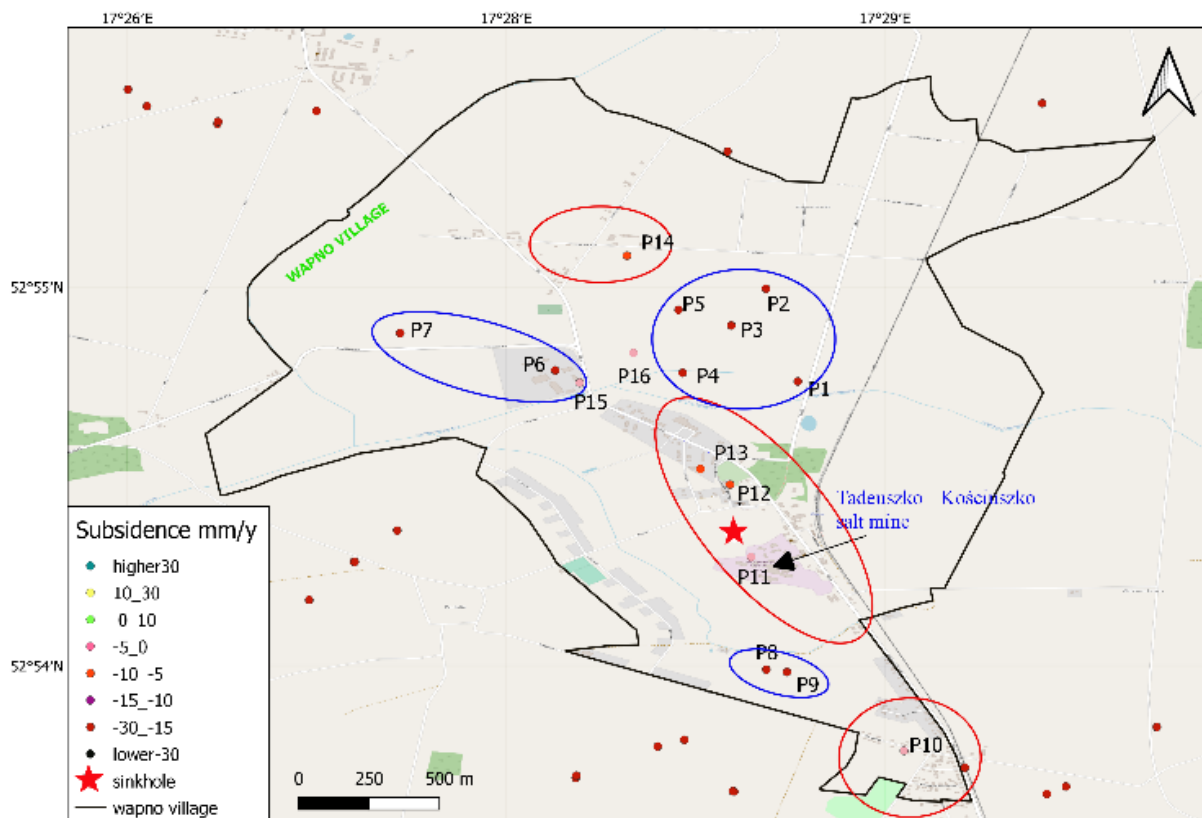


Fig. 7. Points of high subsidence rates were extracted for residential and non-residential areas.

Tab. 3. Coordinates and subsidence rates of high-subsiding points.

No	Points	Latitude (rad)	Longitude (rad)	Subsidence (mm/y)
1	P1	52.91501	17.47541	-19
2	P2	52.91991	17.47373	-17.5
3	P3	52.91796	17.4719	-17.3
4	P4	52.91546	17.46933	-17.9
5	P5	52.91879	17.46911	-15.9
6	P6	52.9156	17.4626	-16.7
7	P7	52.91756	17.45442	-15.3
8	P8	52.8998	17.47375	-18.8
9	P9	52.89967	17.47484	-16.6
10	P10	52.89552	17.48102	-12.1
11	P11	52.90575	17.47295	-12.1
12	P12	52.90957	17.47183	-7
13	P13	52.91039	17.47027	-5.5
14	P14	52.92165	17.46639	-5.6
15	P15	52.91494	17.46389	-13.7
16	P16	52.91652	17.46673	-14.5

Ground deformation around the Tadeusz Kościuszko salt mine is shown in Fig. 8. The maximum subsidence has occurred not only within the mine but also in surrounding areas (A, B, C in Fig. 8). There is a subsidence point with the rate of up to -18 mm/yr on the vacant lot (the southwest of the mine) (area C). As shown in Fig. 8, there is not a special region with high deformation. The subsidence has happened in the entire Wapno village, including the Tadeuszko Kościuszko mine area. We see that the whole region of the Wapno village is under the same risk of land subsidence.

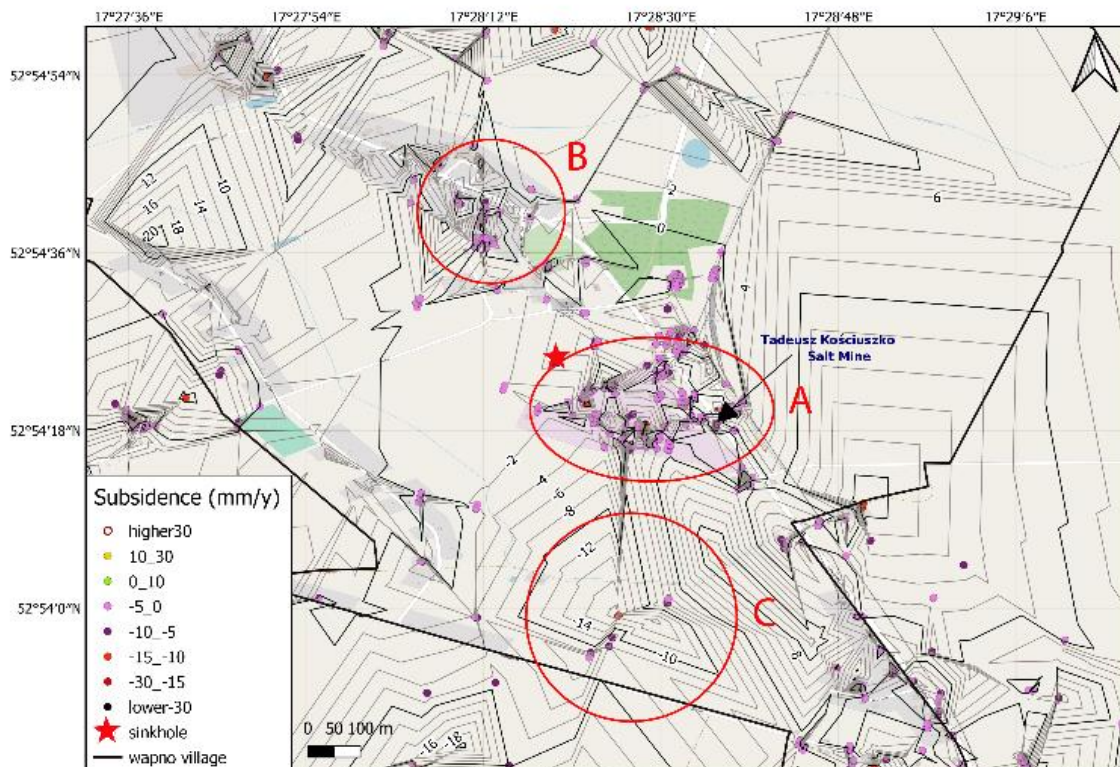


Fig. 8. Contour map of land subsidence in the Wapno village. The red star is the sinkhole, which happened on February 26th 2021.

5. Conclusions

With 32 Sentinel-1B SAR images collected between 9th March 2020 and 16th March 2021, the PSInSAR method was processed by the SNAP and StaMPS software packages to detect surface deformation in the historical Tadeusz Kościuszko salt mine and the surrounding area of Wapno, Poland. The results have shown that:

Sentinel-1 SAR data can be utilized with the PSInSAR method to detect deformation triggered by mining activities in the historical Tadeusz Kościuszko salt mine. Sentinel-1 SAR images, which are free with a regular acquisition interval of 12 days and a large spatial coverage compared to other SAR data, are advantageous.

In this study, deformation in the Wapno village area has been detected with maximum subsidence of up to -19 mm/yr, and the inactive Tadeusz Kościuszko experienced subsidence in most of its area. Subsidence in this mine reach -12 mm/yr and that at surrounding area ranged from 0 to -18.8 mm/yr.

Land deformation has been reported in this study from Sentinel-1 SAR application, but no validation relying on individual measurements, e.g., GNSS or total station data, was conducted. Though the application of PSInSAR and the Sentinel-1 SAR data has been proved to have accurate results of deformation, InSAR measurements are affected by different noise sources, which vary between study areas. Therefore, the confidence of the accuracy of InSAR-derived deformation in the study area should further be validated.

6. Acknowledgments

The paper was presented during the 6th VIET - POL International Conference on Scientific-Research Cooperation between Vietnam and Poland, 10-14.11.2021, HUMG, Hanoi, Vietnam.

7. References

1. Kowalczyk Andrzej, Witkowski Andrzej, Rózkowski Andrzej, Szczepański Andrzej, Rogoż Marek, Przybyłek Jan, and S. Stanisław., 2010; What Polish mining owes to Polish hydrogeology, 58; 9/1; 774-786.
2. <https://www.abandonedspaces.com/uncategorized/salt.html>; 2020 Makeenko, V.; The Salt Mine, Which destroyed a Village in 1977.
3. <https://www.pgi.gov.pl/osuwiska/sopo-aktualnosci/szczegoly/12833-sol-niszczy-wapno-zapadlisko-nad-stara-kopalnia.html>; 2/3/2021 Geozagrożeń, z.C.; Sól niszczy Wapno – zapadlisko nad starą kopalnią.
4. Pawluszek-Filipiak, K. and A.J.E.J.o.R.S. Borkowski, 2021; Monitoring mining-induced subsidence by integrating differential radar interferometry and persistent scatterer techniques, 54; sup1; 18-30.
5. Jung Hahn Chul, Kim Sang-Wan, Jung Hyung-Sup, M.K. Duck, and W. Joong-Sun, 2007; Satellite observation of coal mining subsidence by persistent scatterer analysis, Engineering Geology; 92; 1-2; 1-13.
6. Wempen, J.M.J.I.J.o.M.S. and Technology, 2020; Application of DInSAR for short period monitoring of initial subsidence due to longwall mining in the mountain west United States, 30; 1; 33-37.
7. Berardino Paolo, Fornaro Gianfranco, Lanari Riccardo, and S. Eugenio., 2002; A new algorithm for surface deformation monitoring based on small baseline differential SAR interferograms, IEEE Transactions on geoscience remote sensing; 40; 11; 2375-2383; 10.1109/TGRS.2002.803792.

8. Hooper Andrew, Segall P, and Zebker Howard, 2007; Persistent scatterer interferometric synthetic aperture radar for crustal deformation analysis, with application to Volcán Alcedo, Galápagos, *Journal of Geophysical Research: Solid Earth*; 112; B7; <https://doi.org/10.1029/2006JB004763>.
9. Hooper Andrew, Zebker Howard, Segall Paul, and K. Bert., 2004; A new method for measuring deformation on volcanoes and other natural terrains using InSAR persistent scatterers, *Geophysical research letters* 31; 23; <https://doi.org/10.1029/2004GL021737>.
10. Hooper, A., D.P.S. Bekaert, K. Spaans, and M. Arkan, 2012; Recent advances in SAR interferometry time series analysis for measuring crustal deformation, *Tectonophysics*; 514-517; 1-13; 10.1016/j.tecto.2011.10.013.
11. Bui Luyen Khac, Featherstone WE, and F. MS, 2020; Disruptive influences of residual noise, network configuration and data gaps on InSAR-derived land motion rates using the SBAS technique, *Remote Sensing of Environment*; 247; 111941; <https://doi.org/10.1016/j.rse.2020.111941>.
12. Bui Khac Luyen, Le V.V. Phong, Dao Phuong Duc, Long Nguyen Quoc, Pham Hai Van, Tran Hong Ha, and X. Lei., 2021; Recent land deformation detected by Sentinel-1A InSAR data (2016–2020) over Hanoi, Vietnam, and the relationship with groundwater level change, *GIScience Remote Sensing*; 58; 2; 161-179; <https://doi.org/10.1080/15481603.2020.1868198>.
13. Long Nguyen Quoc, Van Anh Tran, Luyen Bui Khac, 2021; Determination of Ground Subsidence by Sentinel-1 SAR Data (2018-2020) over Binh Duong Quarries, Vietnam, *VNU Journal of Science: Earth Environmental Sciences* 37; 2; <https://doi.org/10.25073/2588-1094/vnuees.4605>.
14. Nam Bui Xuan, Van Anh Tran, Bui Luyen Khac, Long Nguyen Quoc, Ha Thi Le Thu, and G. Ropesh.; 2021; Mining-Induced Land Subsidence Detection by Persistent Scatterer InSAR and Sentinel-1: Application to Phugiao Quarries, Vietnam. in *Proceedings of the International Conference on Innovations for Sustainable and Responsible Mining*. Springer, 108; 18-38; http://doi.org/10.1007/978-3-030-60269-7_2.
15. Perski, Z., 1998; Applicability of ERS-1 and ERS-2 InSAR for land subsidence monitoring in the Silesian coal mining region, Poland, *International Archives of Photogrammetry and Remote Sensing*; 32; 555-558.
16. Krawczyk, A. and Z. Perski, 2000; Zastosowanie satelitarnej interferometrii radarowej na terenach eksploatacji rud miedzi w LGOM, XI Kongres ISM, Kraków.
17. Perski, Z., G. Ketelaar, and M.J.A.F. Mróz, *Kartografii i Teledetekcji*, 2006; Interpretacja danych Envisat/ASAR o przemiennej polaryzacji na obszarach zurbanizowanych w kontekście charakterystyki stabilnych rozpraszaczy (persistent scatterers), 16.
18. Perski Zbigniew, Hanssen Ramon, Wojcik Antoni, and W. Tomasz., 2009; InSAR analyses of terrain deformation near the Wieliczka Salt Mine, Poland, *Engineering Geology*; 106; 1-2; 58-67.
19. Wojciechowski, T., Z. Perski, and A.J.P.G. Wójcik, 2008; Wykorzystanie satelitarnej interferometrii radarowej do badań osuwisk w polskiej części Karpat, 56; 12; 1088-1091;
20. Graniczny Marek, Kowalski Zbigniew, Jureczka Janusz, and C. Magdalena.; 2006; Wykorzystanie technologii PSInSAR dla obserwacji przemieszczeń powierzchni terenu na przykładzie Górnego Śląska. in *Mat. Symp.* 127-129.

21. Malinowska, A., R. Hejmanowski, W.T. Witkowski, and A. Guzy, 2018; Mapping of slow vertical ground movement caused by salt cavern convergence with sentinel-1 tops data, *Archives of Mining Sciences*; 63; 2; 383-396; 10.24425/122453.
22. Mirek, K., 2009; Interferometric Synthetic Aperture Radar InSAR–method for study and monitoring subsidence over mining areas, *Polish Journal of Environmental Studies*; 18; 3A; 270.
23. Urbaniak, M.J.O.D.K., 2018; Kompleks młyna solnego i magazynów byłej kopalni soli w Wapnie. Uwarunkowania i przesłanki do ochrony XX-wiecznych budowli przemysłowych jako trwałej ruiny.
24. https://pl.wikipedia.org/wiki/Kopalnia_Soli_im._Tadeusza_Ko%C5%9Bciuszki_w_Wapnie; 28-07-2019 22:08 Wikipedia; Kopalnia Soli im. Tadeusza Kościuszki w Wapnie
25. Małachowski, K., 2018; The biggest surface mining disaster in Poland and its economic results, *European Journal of Service Management*; 28; 247-255; <https://doi.org/10.18276%2Fejsm.2018.28%2F2-31>.
26. <https://plus.gloswielkopolski.pl/o-katastrofie-w-kopalni-soli-w-wapnie-nie-wolno-bylo-mowic-ani-pisac/ar/12399754>; 19/8/2017 Dziuma, M.; O katastrofie w kopalni soli w Wapnie nie wolno było mówić ani pisać.
27. Tran, V. A., Bui, X. N., Nguyen, Q. L., & Tran, T. A. (2020). Land Subsidence Detection in Tan My-Thuong Tan Open Pit Mine and Surrounding Areas by Time Series of Sentinel-1 Images. *Inżynieria Mineralna*. DOI 10.29227/IM-2020-02-22
28. Chen, C.W. and H.A. Zebker, 2000; Network approaches to two-dimensional phase unwrapping: intractability and two new algorithms, *Journal of the Optical Society of America A*; 17; 3; 401-414; <http://doi.org/10.1364/JOSAA.17.000401>.

Riverbank Filtration – A Potential Water Source Exploitation for the Red River Delta Region

NGUYEN Trung Hieu¹, DOAN Thu Ha^{1,*}, HOANG Van Duy², TONG Thanh Tung³

¹ Thuyloi University, 175 Tay Son, Dong Da, Hanoi, Vietnam

² Institute of Water Resources Science, 8 Phao Dai Lang, Dong Da, Hanoi, Vietnam

³ Division of Northern Water Resources Planning and Investigation, Hanoi, Vietnam

Corresponding author: thuha_ctn@tlu.edu.vn

Abstract. Riverbank filtration technology has been widely applied worldwide because of its high-capacity collection and good water quality throughout natural purification processes. Infiltration water can be extracted from Holocene (qh) layer or the Pleistocene deep layer (qp), replenished with water from the river through hydrogeological windows. Hydrodynamic and isotopic signatures were employed to determine water seepage capacity. The results show that infiltrated water is found in the sand layers along the rivers. However, the seepage rate shows a heterogeneously spatial variation ranging from 30 m³/d in the Dinh Dao river to 33,600 m³/d. Km along the shoreline in the Red River (RRD). Also, the exploitation capacity of seepage water differs widely in order of large (> 3,000 m³/d), medium (1,000-3,000 m³/d), small (500-1,000 m³/d), and very small capacity (200-500 m³/d). This study indicated that RRD could apply riverbank filtration techniques to overcome freshwater scarcity in the delta due to increasing surface pollution and discharge reduction.

Keywords: Seepage water, Hydraulic connection, Hydrogeological window, Red River Delta

1. Introduction

Groundwater in alluvial aquifers is widely used as one of the primary drinking water sources in many countries worldwide because of its high yield and good quality [1]. By pumping wells in an alluvial plain hydraulically connected to a river, it is possible to generate a hydraulic gradient that surface water is forced to flow through the bed and the river banks. During riverbank filtration (RBF) processes, a reduction in the concentration of pollutants is achieved by physical, chemical, and biological processes between the surface water and groundwater and with the substrate [2-5].

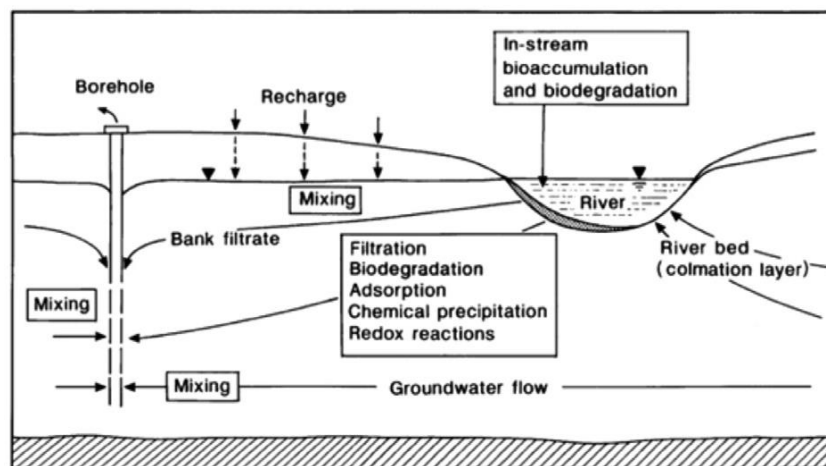


Fig. 1. The basic scheme of riverbank filtration and mail attenuation processes.

The reduction of pollution levels is accomplished by various processes, including physical filtration, microbial degradation, ion exchange, precipitation, sorption, and dilution [6-8]. Other factors that also contribute to the treatment are the river water and the groundwater quality, the porosity of the medium, the water residence time in the aquifer, temperature and pH conditions of water, and oxygen concentrations [9].

In addition to removing pollutants (particles, microorganisms, organic, and inorganic compounds, etc.), there are two additional advantages of RBF. The first is relative to the fact that the flow through the aquifer acts as a barrier against concentration peaks that may result from accidental spills of pollutants. The second

is regulating the temperature variations in the river water: during winter, when air temperatures are low, the filtered water is usually warmer than surface water, and in summer, it is more relaxed. The lowest variation in temperature improves the quality and further processing of the bank filtrate [3].

Riverbank filtration technology has been a common practice in Europe for over 100 years, particularly in countries such as Switzerland, where 80% of drinking water comes from RBF wells, 50% in France, 48% in Finland, 40% in Hungary, 16% in Germany, and 7% in the Netherlands [2]. In Germany, for example, 75% of the city of Berlin depends on RBF, whereas in Düsseldorf, RBF has been used since 1870 as the primary drinking water supply [9-10]. On the other hand, in the United States, this technique has been used for nearly half a century, especially in Ohio, Kentucky, Indiana, Illinois, among others [3]. Other countries that have recently started implementing RBF for drinking water supply are India [11], China, and South Korea [12].

Previous studies show a high possibility of a connection between surface and groundwater, especially in the coastal zones of the Red River [13-14]. In addition, some studies have found that surface water is the primary recharge source for the qp aquifer [15-16]. Also, previous studies illustrated that [13-14] showed hydrogeological windows play an essential role in the hydraulic connection between surface water and shallow groundwater in the RRD. Thus, the research on assessing the potential of river infiltration processes for water supply in the Red River Delta region is essential. Some studies used hydrodynamic and isotope methods to evaluate the potential of infiltration water and determine groundwater extraction reserves via RBF processes [17-22]. The RBF can provide an additional water source for domestic and production activities besides the region's surface and groundwater sources.

2. Study area

The RRD is the flat, low-lying plain formed by the Red River and its distributaries merging with the Thai Binh River in northern Vietnam. The region, measuring some 15,000 square kilometers, is well protected by a network of dikes. It is an agriculturally rich and densely populated area. Most of the land is devoted to rice cultivation. Eight provinces together with two municipalities, the capital Hanoi and the port Hai Phong form the delta. It has a population of almost 23 million in 2019. Spanning some 150 km in width, the Red River Delta is located in the western coastal zone of the Gulf of Tonkin. The Red River is the second largest river in Vietnam and one of the five largest rivers on the East Asia coast. Its catchment covers parts of China and Vietnam, and its water and sediment discharge greatly influence the hydrology in the Gulf of Tonkin (Fig. 2).

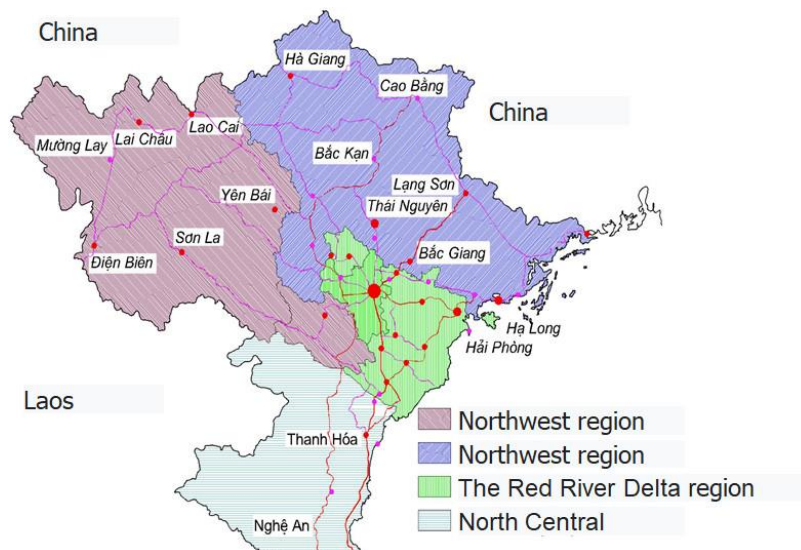


Fig. 2. Position of the Red River Delta region.

The RRD has a flat terrain, slightly declines toward the sea, with dense rivers under the Red -Thai Binh river system. Loose sediments mainly form the delta with a thickness of Quaternary deposit ranging from tens meter in the top and up to 100 m on the sides in the coastal zone. This study considers two aquifers for RBF, including Holocene (q_h) above and Pleistocene (q_p), as shown in Figure 3 below.

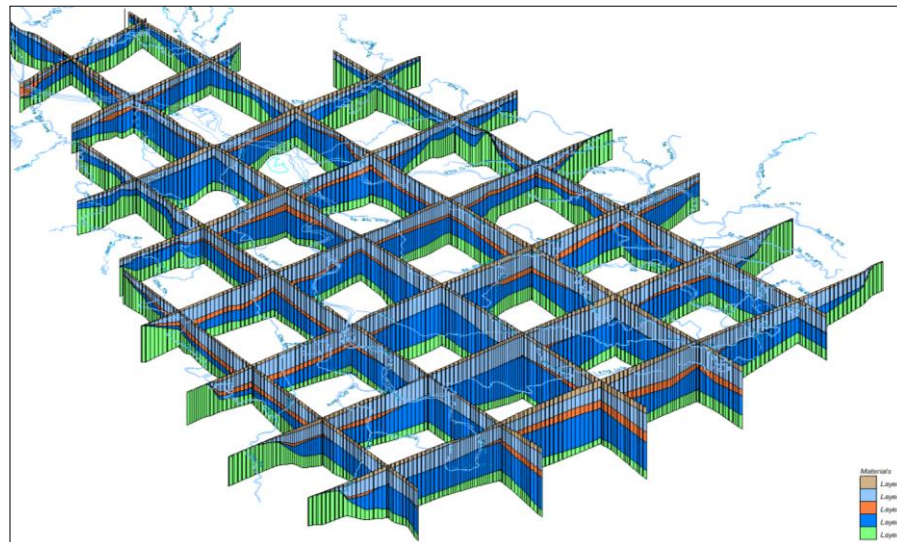


Fig. 3. Hydrogeological structure of the Red River Delta region.

3. Methods

3.1. Estimation of groundwater exploitation

Riverbank infiltration is a complex process; therefore, several issues should be considered, including hydrogeological structure and windows, the hydraulic connection between river surface and groundwater, river replenishment, and groundwater exploitation capacity. Groundwater reserve of a specific region comprises of some components identified according to the following formula:

$$Q_{kt} = Q_{kt} + \frac{V_{dh}}{t} + \frac{\alpha V_{tl}}{t} + Q_{ct} \quad (1)$$

where, Q_{kt} is the exploitation reserve of groundwater (m^3/d); Q_{tn} is the natural dynamic reserve (m^3/d); V_{dh} is elastic static water volume (m^3); V_{tl} is gravity static water volume (m^3); Q_{ct} is entrainment reserve (m^3/d); α is a coefficient infiltrating into gravity static reserve (take like 30% for non-pressure aquifer); t is the calculated exploitation period, typically 104 days.

Among the above-stated components, entrainment reserve (Q_{ct}) happens in the condition of exploitation, including entrainment due to the permeability from the top or from the bottom to the top, entrainment due to the flow from sides, infiltration from surface water sources as rivers, lakes. In favorable conditions, the most considerable entrainment reserve is infiltration from the river.

3.2. Determination of hydraulic connection

In the Red River Delta Region, loose Quaternary sediments are characterized by rhythm distribution; fine-grained formations alternate and interlace coarse-grained ones. The hydrogeological window is a type of hydrogeological structure in which water can penetrate rapidly from the near-surface into deeper aquifers in areas where the continuity of separating low-permeability deposits is disturbed, and their permeability is relatively high. Different aquifers are distinguished in the cross-section, separated by weak water-permeable layers that play a role as water separating layers. The layer separates upper and lowers adjacent layers, creating special hydrogeological features, especially various dynamic hydrogeology. Once the hydrogeological window exists, two aquifers directly overlap, water in the aquifers will interconnect and share the same water level. The hydraulic relationship is the reciprocal interaction between groundwater and river water, either under natural conditions or under human beings intervenes. The study, identification of hydraulic connection is significant to both scientific aspects and problem solutions. The clarification of the hydraulic relationship will contribute to identifying the conditions of dynamic groundwater formation that help assess the groundwater exploitation reserve. Also, it conveys crucial meaning in selecting methods for the construction of coastal infiltration water exploitation works. The hydraulic relationship is studied and identified by: hydrogeological testing, hydrological measurement, monitoring, isotope techniques, hydrogeochemical method, etc.

3.3. Determination of river infiltration water

a) Hydrodynamic Estimation

The method identifying the amount of recharge from the river is based on the permeability resistance in the riverbed and coastal zones, due to deposit of alluvial, bottom sludge which creates a hydraulic resistance and is characterized by the resistance coefficient of sludge layer (A_0), and is identified by the following formula:

$$A_0 = \frac{m_0}{K_0} \tag{2}$$

where K_0 and m_0 is permeability coefficient in vertical direction and thickness of sludge layer on the riverbed.

The volume of infiltration from the river bed is simulated in Figure 4 and identified by the following formula:

$$Q_{cc}^0 = \frac{H_0 - H_1}{A_0} \times 2b \tag{3}$$

where q is the infiltration flow rate from the river (l/s/km); H_0 is the height of river water level (m); H_1 is the height of water level in an aquifer (m); $2b$ is the river stream's width (m).

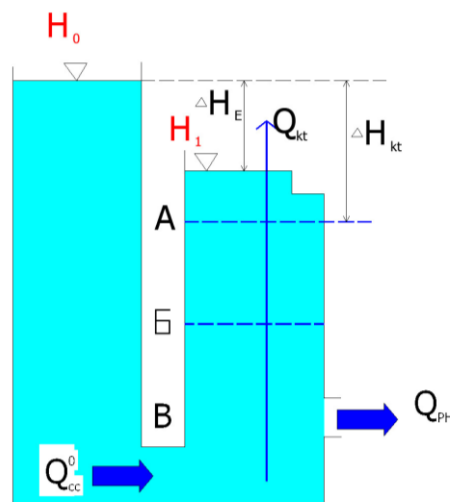


Fig. 4. The diagram on calculating the amount of riverbank infiltration water.

b) Stable isotopes

Based on stable isotope ($\delta^{18}O$) and deuterium (δ^2H) analyzed data, the infiltration value, and relationships among aquifers are identified in the studied area. The amount of infiltration supply and connection among aquifers are determined based on the following equations:

In the rainy season:

$$\delta^{18}O_{nn} = X_1 \times \delta^{18}O_s + (1 - X_1) \times \delta^{18}O_m \tag{4}$$

$$\delta^2H_{nn} = Y_1 \times \delta^2H_s + (1 - Y_1) \times \delta^2H_m \tag{5}$$

In the dry season:

$$\delta^{18}O_s = X_2 \times \delta^{18}O_{nn} + (1 - X_2) \times \delta^{18}O_m \tag{6}$$

$$\delta^2H_s = Y_2 \times \delta^2H_{nn} + (1 - Y_2) \times \delta^2H_m \tag{7}$$

From the above equations, X_1 , Y_1 , and X_2 , Y_2 are defined as follows:

$$X_1 = \frac{\delta^{18} O_{nn} - \delta^{18} O_m}{\delta^{18} O_s - \delta^{18} O_m} \tag{8}$$

$$Y_1 = \frac{\delta^2 H_{nn} - \delta^2 H_m}{\delta^2 H_s - \delta^2 H_m} \tag{9}$$

$$X_2 = \frac{\delta^{18} O_s - \delta^{18} O_m}{\delta^{18} O_{nn} - \delta^{18} O_m} \tag{10}$$

$$Y_2 = \frac{\delta^2 H_s - \delta^2 H_m}{\delta^2 H_{nn} - \delta^2 H_m} \tag{11}$$

where $\delta^{18}O_s$, δ^2H_s are values of isotope oxygen-18 and deuterium in river water (‰) respectively; $\delta^{18}O_m$, δ^2H_s are values of isotope O18 and deuterium in rainwater (‰) respectively; $\delta^{18}O_m$, δ^2H_{nn} are values of isotope oxygen-18 and deuterium in groundwater of Holocene aquifer (‰) respectively; X_1 , Y_1 are respective ratios (%) of river water replenished for Holocene aquifer in rainy season calculated according to isotope ($\delta^{18} O$) and deuterium ($\delta^2 H$); X_2 , Y_2 are respective ratios (%) of groundwater recharged for river water in dry season calculated according to isotope ($\delta^{18} O$) and deuterium ($\delta^2 H$).

4. Results and discussion

4.1. Hydrogeological windows

Identifying a hydrogeological window is essential to apply riverbank filtration techniques successfully in the Red River Delta region. In this study area, three types of hydrogeological windows, including river cuts qh aquifer; river cuts qp aquifer; river cuts both qh and qp aquifers.

Hydrogeological window type 1: The river cuts qh aquifer

This hydrogeological window is prevalent in all rivers within the studied area. For 2 regions on the edge of the delta and the Red River from Viet Tri to Hanoi, the river only cuts the upper layer of qh aquifer, the remaining cuts both layers. A typical cross-section of this type is presented in Figure 5.

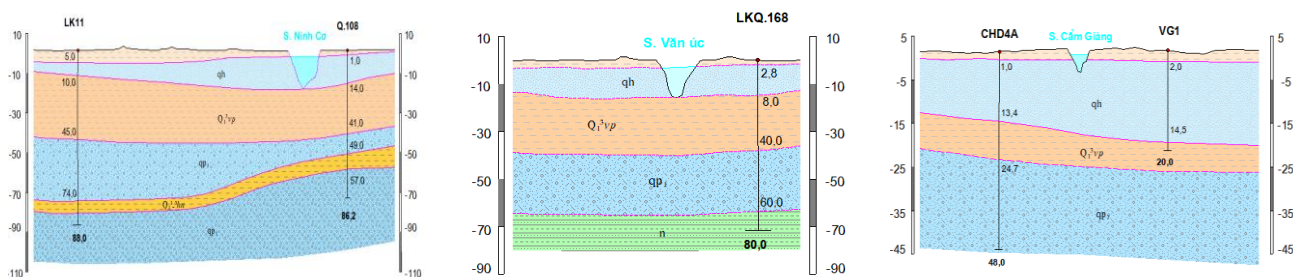


Fig. 5. Hydrogeological section across Ninh Co, Van Uc, and Cam Giang rivers.

Hydrogeological window type 2: The river cuts qp aquifer

This hydrogeological window is typical in the Ca Lo River, Cau river, and rivers on the delta edge. The specific section for this type is displayed in Figure 6.

Hydrogeological window type 3: The river cuts both qh and qp aquifers

This hydrogeological window is popular in Red river, the section from Viet Tri to Nam Du in Vinh Phuc province and Hanoi city, part of Duong river in Dong Anh and Long Bien, Hanoi. The typical section of this type is shown in Figure 7.

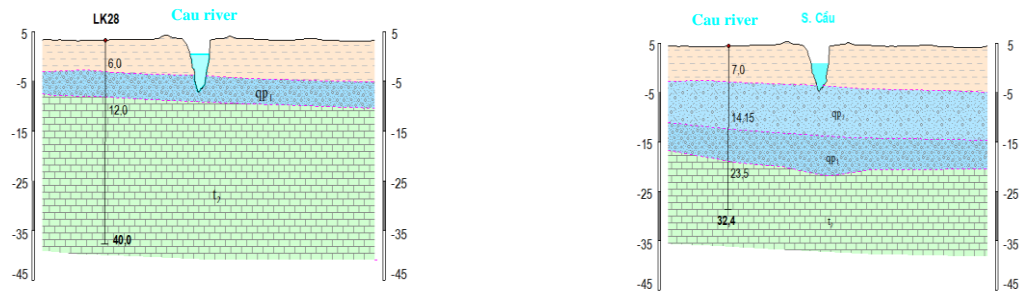


Fig. 6. Hydrogeological section across Ca Lo and Cau rivers.

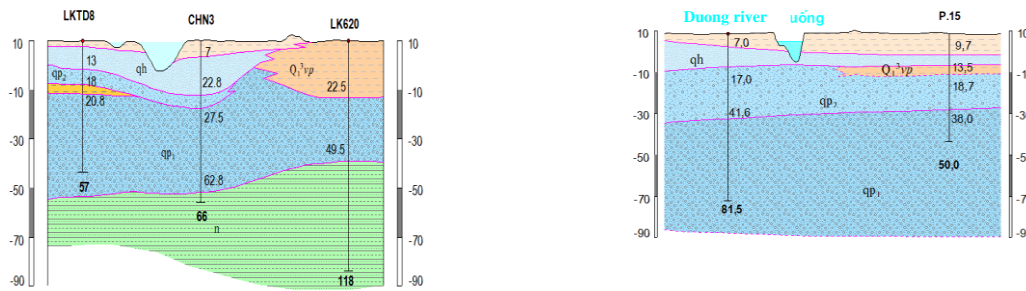


Fig. 7. Hydrogeological section across Red and Duong rivers.

The hydrogeological window described in this type covers the entire Red river bed and extends toward the accretion side at winding sections. The weak infiltration water formations in the upper Vinh Phuc formation are eroded. The river bed directly sits on the qh aquifer, then interconnects to below qp aquifer. This boundary is most clearly identified in Nam Du well field. Of these, 15 drilling wells in the North are located in the winding segments of Red river toward the accretion side in the hydrogeological window where the clay layer separating the qh qp aquifers is absent. Only three wells (H16, H17, H18) in the South have the clay layer separating the qh and qp aquifers.

4.2. Hydraulic relationship between river water and groundwater

The Red River Delta Region covers all four types of hydraulic relationships (Fig. 8) [23-26] with a distribution as follows:

Type 1: Mainly along Red River, the section from Viet Tri to Hanoi, including the beginning section of Duong River. In natural conditions, groundwater plays a vital role in sustaining river flow within the year. However, nearby groundwater river shows a temporal variation, and groundwater is temporarily replenished by river water. Such provision only takes place in the coastal zone where the groundwater flow is directed from the river. The zone's width is from 2 km to 4 km from the edge of river water. If there are any coastal exploitation works, the river water will be provided for those works throughout the year.

Type 2: Mainly in rivers in the center of the delta, typically the South of Cau River, Duong River, where the groundwater is recharged by surface water all around the year. In the flooding period, the replenishment increases and even higher when there are any coastal exploitation works.

Type 3: Popularly in rivers on the delta's edge, typically the North of Cau, Duong, Day, Kinh Thay, and Ca Lo rivers. In these places, groundwater is recharged by river water through the year; however, as the hydraulic decline is not much, the water is still capable of providing for such works when there are exploitation works.

Type 4: Popularly in rivers located in the center of the delta toward the sea. The qp aquifer is deeply situated, and the river does not directly cut the aquifer. The hydraulic relationship still takes place but through separating layers (Fig. 9).

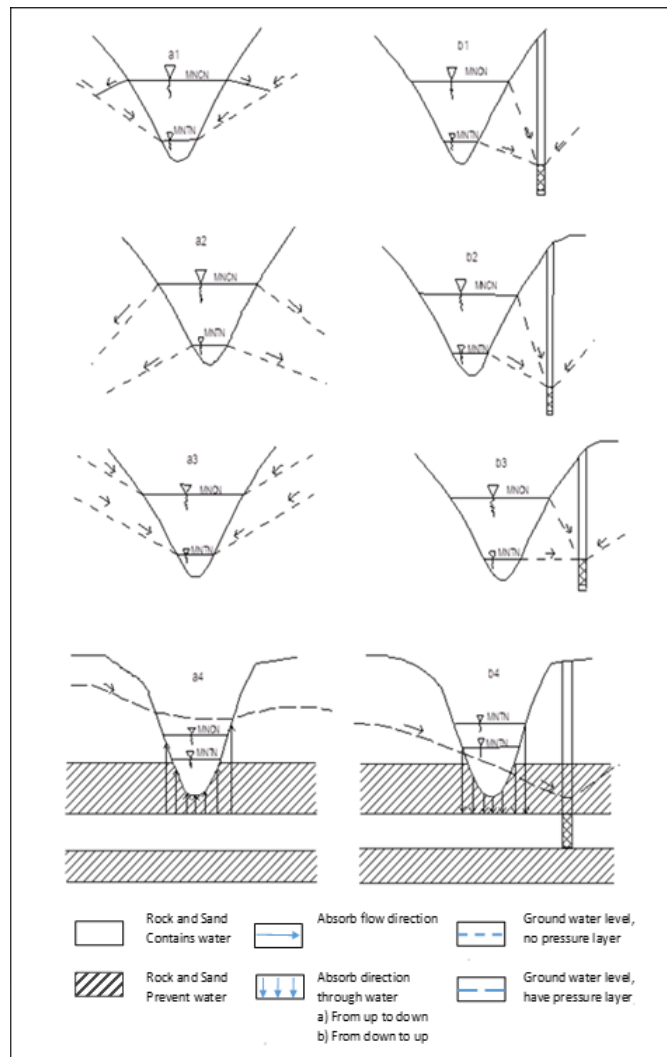


Fig. 8. Types of Surface-groundwater interactions.

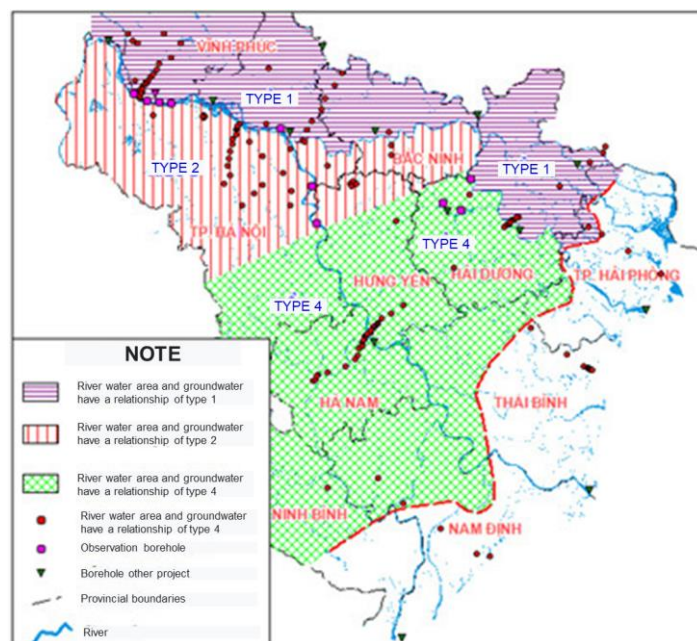


Fig. 9. Zoning Surface-groundwater interactions.

4.3. Amount of permeable water from the river

a) Hydrogeological characteristics

Based on the research results, assessment of water resources implemented [13], the amount of permeable water of studied rivers is calculated, identified, and presented in Table 1.

Tab. 1. Amount of infiltration water of rivers in the Red River Delta Region.

No.	Rivers	Length of river segment (km)	M0 (m)	K0 (m/d)	H0-H1 (m)	2b (m)	Infiltration flow rate (q) (m ³ /d/km)
1	Red	183	0.25	0.1	1.8	540	33,600
2	Cau	69	0.15	0.55	0.51	80	12,925
3	Duong	62	0.35	0.25	0.25	180	2,777
4	Rang	25.5	0.55	0.15	0.1	120	282
5	Kinh Mon	0.505	0.25	0.25	0.1	100	864
6	Lach Tray	19	0.25	0.25	0.1	50	432
7	Luoc	70	0.25	0.025	0.1	120	103
8	Ninh Co	33	0.25	0.25	0.1	100	864
9	Thai Binh	74	0.25	0.015	0.1	250	129
10	Cam Giang	3.5	0.25	0.015	0.1	100	52
11	Ke Sat	14.5	0.15	0.015	0.1	180	156
12	Dinh Dao	16	0.15	0.015	0.1	35	30

b) Isotopic Signatures

The study of infiltration water exploitation results within the scientific research project “Research on application and development of riverbank infiltration exploitation technology in Vietnam for living and production activities” [18] define the ratio of river water replenished to groundwater shown in Table 2 and Table 3 below. The statistical results prove that large rivers have a close relationship with groundwater.

Tab. 2. Calculation of recharge amount between river water and groundwater in dry and rainy seasons through stable isotope (¹⁸O).

Rivers	Rainy season				Dry season				Notes
	$\delta^{18}O_s$	$\delta^{18}O_{nn}$	$\delta^{18}O_m$	X1	$\delta^{18}O_{nn}$	$\delta^{18}O_s$	$\delta^{18}O_m$	X2	
Red Segment 1	-6.85	-7.09	-8.48	85%	-6.48	-5.51	-2.9	73%	Ba Vi – Hung Yen
Red Segment 2	-9.86	-8.89	-8.48	30%	-5.95	-5.04	-2.9	70%	Hung Yen – Thai Binh
Cau	-6.99	-7.53	-8.48	63%	-6.78	-4.72	-2.9	46%	
Thai Binh	-10.27	-6.57	-5.15	28%	-7.48	-4.86	-2.9	42%	
Cam Giang	-10.79	-5.96	-5.15	27%	-8	-4.25	-2.9	26%	

Tab. 3. The amount of recharge between the river and groundwater in dry and rainy seasons by stable deuterium isotope (^2H).

Rivers	Rainy season				Dry season				Notes
	$\delta^{18}\text{O}_s$	$\delta^{18}\text{O}_{nn}$	$\delta^{18}\text{O}_m$	X1	$\delta^{18}\text{O}_{nn}$	$\delta^{18}\text{O}_s$	$\delta^{18}\text{O}_m$	X2	
Red Segment 1	-46.11	-47.73	-55.39	83%	-47.11	-36.12	-9.53	70%	Ba Vi – Hung Yen
Red Segment 2	-63.71	-59.79	-55.39	52%	-34.90	-32.28	-9.53	89%	Hung Yen – Thai Binh
Cau	-42.29	-43.19	-55.39	93%	-43.6	-22.83	-9.53	39%	
Thai Binh	-58.76	-41.98	-35.39	28%	-41.6	-26.56	-9.53	53%	
Cam Giang	-58.39	-40.05	-35.39	20%	-59.24	-24.64	-9.53	30%	

4.3. Determination potential infiltration areas

The potential of water seepage exploitation is determined based on the potential capacity of each infiltration exploitation work. In the RRD, most groundwater extraction works in general and infiltration exploitation, particularly, are drilling wells vertically. According to the actual exploitation results of existing works and results calculating the exploited flow rate of drilling wells in the coastal zone, the areas with potential infiltration exploitation could be divided (Fig. 10).

The area with considerable potential for infiltration exploitation is distributed in the Red River's coastal zone from Viet Tri to Nam Du water treatment plant in Hanoi. The site covers hydrogeological window type 3: Red River cuts both qh and qp aquifers. The hydraulic relationship between surface water and groundwater is of type 1. The Red River's recharge amount is large, the largest among rivers in the Red River Delta Region. The capacity of each well reaches 3,000 m³/d. In places where there is no bottom sludge, the flow rate could increase sharply. In contrast, the flow rate could decrease enormously in areas where the qp aquifer is thin.

The area with the medium potential of filtration exploitation is distributed in the coastal zone of Ca Lo and Cau rivers, one section at the beginning of Duong and Red rivers from Nam Du well field to Hung Yen. The hydrogeological window in this area is as follows: Cau and Ca Lo rivers cut the qp aquifer, Duong River cuts both qh and qp aquifers, Red River cuts qh aquifer and has a weak hydraulic relationship with qp aquifer. The hydraulic relationship between surface water and groundwater is of type 3 for Cau and Ca Lo rivers, types 2 and 4 for Duong and Red rivers. The recharge amount from these rivers is medium. The capacity of each drilling well reaches from 1,000 m³/d to 3,000 m³/d.

The area with a small potential of filtration exploitation is distributed in the coastal Duong River, upper stream of Thai Binh river, and one segment of the Red River from Hung Yen to Nam Dinh. This place exists a hydrogeological window of type 1 that means the river only cuts qh aquifer. The hydraulic relationship between surface water and groundwater is of type 4 with a small recharge from rivers, and the capacity of each drilling well ranges from 500 m³/d to 1,000 m³/d.

The area with the minimal potential of filtration exploitation is distributed in the coastal zone of the remaining rivers. This place has hydrogeological window type 1 that means the river only cuts the qh aquifer. The hydraulic relationship between surface water and groundwater is of type 4 with a small recharge, and the capacity of each drilling well fluctuates from 200 m³/d to 500 m³/d.

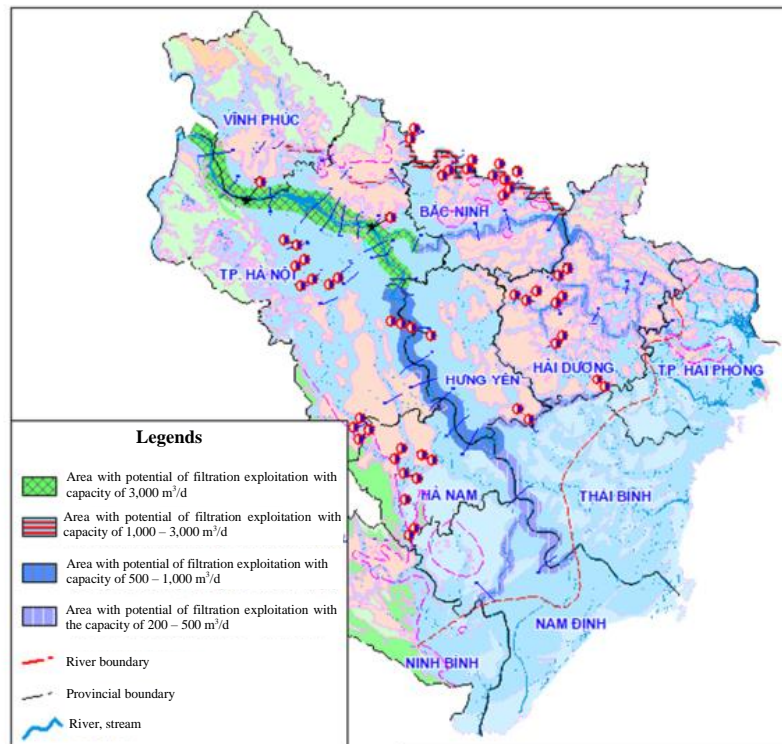


Fig. 10. Zones with potential infiltration water in Red River Delta Region.

5. Conclusion

The study results show that: In the Red River Delta Region, the coastal zone of rivers, there are three types of hydrogeological window: river cuts qh aquifer, qp aquifer, and both qh and qp aquifers. The Red River Delta Region includes four types of hydraulic relationships between groundwater and river water. The river water recharging for groundwater ranges widely from 30 in Dinh Dao river to 33,600 m³/d.km of the Red River shoreline. The Coastal zone of rivers is divided into 04 areas with various potential of infiltration exploitation: large, medium, small, and very small, equivalent to exploitation capacity of each drilling well: > 3,000 m³/d, 1,000-3,000 m³/d, 500-1,000 m³/d, and 200-500 m³/d. The studied results present the potential of infiltration water exploitation in the Red River Delta Region and demonstrate a new water source as potential riverbank filtration, or in other words, permeable water, supplying for living activities and rural areas. It plays a vital role, especially under the existing circumstance of exhausted and polluted water sources.

6. Acknowledgments

It was completed within the frame of Research Project under the protocol between the Ministry of Science and Technology Vietnam and The German Federal Ministry of Education and Research, No. 60.GER-19: “Research on application and development of riverbank infiltration exploitation technology in Vietnam for living and production activities”.

The paper was presented during the 6th VIET - POL International Conference on Scientific-Research Cooperation between Vietnam and Poland, 10-14.11.2021, HUMG, Hanoi, Vietnam.

7. References

1. Doussan, C., Ledoux, E. and Detay, M., 1998. River- groundwater exchanges, bank filtration, and groundwater quality: Ammonium Behavior, *Journal of Environmental Quality*, 27(6), 1418-1427, <https://doi.org/10.2134/jeq1998.00472425002700060019x>.
2. Tufenkji, N., Ryan, J. N. and Elimelech, M., 2002. The promise of bank filtration, *Environmental Science and Technology*, 36(21): 422A-428A, <https://doi.org/10.1021/es022441j>.
3. Hiscock, K.M. and Grischek, T., 2002. Attenuation of groundwater pollution by bank filtration, *Journal of Hydrology*, 266(3-4): 139–144, [https://doi.org/10.1016/S0022-1694\(02\)00158-0](https://doi.org/10.1016/S0022-1694(02)00158-0).
4. Matusiak, M., et al., 2021. Surface water and groundwater interaction at long-term exploited riverbank filtration site based on groundwater flow modelling (Mosina-Krajkowo, Poland), *Journal of Hydrology: Regional Studies*. 37: 100882, <https://doi.org/10.1016/j.ejrh.2021.100882>.
5. Covatti, G. and T. Grischek, 2021. Sources and behavior of ammonium during riverbank filtration, *Water Research*, 191: 116788, <https://doi.org/10.1016/j.watres.2020.116788>.
6. Lee, W., et al., 2020. Spatiotemporal evolution of iron and sulfate concentrations during riverbank filtration: Field observations and reactive transport modeling, *Journal of Contaminant Hydrology*, 234: 103697, <https://doi.org/10.1016/j.jconhyd.2020.103697>.
7. Kondor, A.C., et al., 2020. Occurrence of pharmaceuticals in the Danube and drinking water wells: Efficiency of river bank filtration, *Environmental Pollution*, 265: 114893, <https://doi.org/10.1016/j.envpol.2020.114893>.
8. Ray, C., Grischek, T., Schubert, J., Wang, J.Z. and Speth, T.F., 2002. A perspective of riverbank filtration, *Journal of American Water Works Association (AWWA)*, 94(4): 149-160, <https://doi.org/10.1002/j.1551-8833.2002.tb09459.x>.
9. Kuehn, W. and Mueller, U., 2000. Riverbank filtration: an overview, *Journal of American Water Works Association (AWWA)*, 92(12): 60-69.
10. <https://doi.org/10.1002/j.1551-8833.2000.tb09071.x>.
11. Schubert, J., 2002. Hydraulic aspects of river bank filtration - field studies. *Journal of Hydrology*, 266: 145 - 161, [https://doi.org/10.1016/S0022-1694\(02\)00159-2](https://doi.org/10.1016/S0022-1694(02)00159-2).
12. Sandhu, C., Grischek, T., Kumar, P. and Ray, C., 2010. Potential for riverbank filtration in India, *Clean Techn Environ Policy*, pp. 1-22 (DOI 10.1007/s10098-010-0298-0).
13. Ray, C., 2008. Worldwide potential of riverbank filtration, *Clean Technologies and Environmental Policy*, 10: 223-225, DOI: 10.1007/s10098-008-0164-5.
14. Lan, N.M., 2014. Research on the relationship between river water and ground water, proposal of method system for determining exploitation reserve of groundwater in coastal Red River from Son Tay commune to Hung Yen, Archives of Department of Water Resources Management, Hanoi.
15. Dan, N.V., 2010 Ground water resource in Hanoi city region and orientation for research, investigation, exploitation for use, Proceedings of International Science Conference on 1,000th Anniversary of Thang Long, 1007–1016.
16. Quyen, P.B., 2015. Report on investigation and assessment of water resources in the Hanoi Capital region, Archives of Department of Water Resources Management, Hanoi.
17. Minh, T., 1993. Report on ground water exploration in the Greater Hanoi. Archives of Geology, Hanoi.
18. General Department of Geology and Minerals of Vietnam., 1979. Report on groundwater exploitation in Bai Bang area, Lam Thao, Phu Tho province. Archives of Geology, Hanoi.
19. Dan, N.V., 2012. Possibility of construction of groundwater exploitation well fields with large capacity provided to Hanoi Capital, *Meteorology and Hydrology Journal*, 620: 1–5.

20. Ha, D.T., 2020. Report on research result of the project “Research on application and development of riverbank infiltration exploitation technology in Vietnam for living and production activities”. Scientific research project No. 60.GER–19, Ministry of Science and Technology).
21. Pholkern, K., Srisuk, K., Grischek, T., Soares, M., Schäfer, S., Archwichai, L., Saraphirom, P., Pavelic, P., Wirojanagud, W., 2015. Riverbed clogging experiments at potential river bank filtration sites along the Ping River, Chiang Mai, Thailand. *Environ. Earth Sci.* 73: 7699–7709.
22. Wang, Y., Zheng, C., Ma, R., 2018. Review: Safe and sustainable groundwater supply in China, *Hydrogeol. J.*, 26: 1301–1324, <https://doi.org/10.1007/s10040-018-1795-1>.
23. Wassenaar, L.I., Ahmad, M., Aggarwal, P., Van Duren, M., Pöntenstein, L., Araguas, L., & Kurttas, T., 2012. Worldwide proficiency test for routine analysis of $\delta^2\text{H}$ and $\delta^{18}\text{O}$ in water by isotope-ratio mass spectrometry and laser absorption spectroscopy, *Rapid Commun Mass Spectrom*, 26(15):1641-1648. <https://doi.org/10.1002/rcm.6270>.
24. Dan, N.V., Thanh, T.N., 2000. The characteristics of the formation of groundwater dynamics in the QII-III aquifer of the Northern Delta region and the significance of water supply, *Geology Journal*, Hanoi.
25. Dan, N.V, Thanh, T.N. and Huy. T.D, 2002. On the possibility of building absorbent works along the Red River, *Geological Journal* No. 44 Series A.
26. Dan, N.V., Thanh, T.N, 2000. The characteristics of the formation of groundwater dynamics in the QII-III aquifer of the Northern Delta region and the significance of water supply, *Geology Journal*, Hanoi.

The Influence of the Sample Preparation on the Result of Coal Propensity to Spontaneous Combustion in the High-temperature Adiabatic Method

OBRACAJ Dariusz^{1,*}, KORZEC Marek¹, VU Tien Tung¹

¹ AGH University of Science and Technology, Kraków, Poland

Corresponding author: obracaj@agh.edu.pl

Abstract. The liability of coal to spontaneous combustion is the principal cause of mine fires. Spontaneous combustion is one of the main threats in Polish and Vietnamese coal mines. The article presents an analysis of the spontaneous combustion of coal in mines of both countries. It is related to the natural prone of coal to spontaneous heating and consequently to its self-ignition. Despite the relevant recognition of the methods of preventing this threat, in mines, spontaneous combustion occurs during the exploitation of coal seams with low and very high self-ignition tendency. Apart from the technical factors related to the design of coal seam mining, the properties of coal have a significant impact on the occurrence of spontaneous combustion. Their correct recognition is essential to the precautions against spontaneous combustion for minimalizing the risk of a mine fire. Therefore, it is necessary to study the factors influencing the propensity of coal to spontaneous heating. A review of the methods used to determine the propensity of coal to spontaneous combustion is presented in the article. Based on the high-temperature method of determining the propensity of coals to spontaneous combustion, the influence of selected factors related to samples' preparation for testing on the determination result was investigated. The influence of the fractional decomposition and the moisture content in the prepared samples on the determination result was demonstrated. The presented research results may improve research procedures for determining the propensity of coal to spontaneous combustion.

Keywords: Spontaneous combustion of coal, Propensity to spontaneous combustion, High-temperature method

1. Introduction

Coal is still an essential source of energy for human life. However, people are exposed to many dangerous threats during the coal mining process. One of such threats is the spontaneous combustion of coal. The occurring spontaneous fires cause damage to the health and life of people working in mines and mainly cause significant economic losses. However, spontaneous fire prevention is a complex problem even in countries with world-leading modern mining industries due to coal's natural tendency to self-heating and self-ignition. Generally, there is a view that spontaneous combustion propensity is related to the rank of coal, i.e., the lower the coal rank, the more liability to spontaneous combustion. However, many factors make this propensity ambiguous. Apart from geological and mining factors, other factors affect the spontaneous combustion process related to coal properties. These include, for example, the heat of wetting, the temperature of the coal particles, the oxygen content of coal and coal particles. These factors are investigated while measuring the coal seam's liability to spontaneous combustion in a laboratory. Knowledge of the influence of these factors on the phenomenon's course can improve laboratory tests methods.

One such factor is the size of the coal particles, which is essential in many measurement techniques. There are known studies that use thermal analysis techniques to investigate the relationship between the thermal and fire properties of coal and particle size. On the base of coal samples with grain sizes < 20 µm, 50 µm, 100 µm, and 125 µm Morgan has indicated that the particle size decreases when the coal combustion reaction increases [1].

Yu et al. [2] showed, on samples of Chinese bituminous coal with particle sizes < 63 µm, 63-100 µm, 100-200 µm, and 200-400 µm, that when the particle size decreases, the petrographic composition of the coal sample changes, i.e. primarily vitrinite, the amount of volatile substances, the content of carbon and inert gas is reduced. Samples with smaller particle sizes have better oxygen absorption due to the increase in the sample particles' surface area. The combustion rate of samples is faster for a small particle size than that of samples with a larger particle size [2].

Prepared for laboratory testing samples with pulverised coal have different water absorption capacities.

If pellets (tablets) are prepared from dust samples, a fixed water content, called process water, is used. The samples might have higher external moisture content than raw coal. The influence of coal moisture on the heating and combustion of coal was demonstrated in Beamish's research using the Australian method [3, 4]. It is also an adiabatic method that determines the degree of coal self-ignition on the basis of the heating rate R70. The test results showed that coal samples with lower moisture content had a shorter temperature increase than coal samples with higher moisture content [4]. Coal samples from the same coal seam with different moisture content give different R70 results. It also means that the humidity changes the test results [4, 5].

Therefore, when preparing coal samples using the Olpiński method, in addition to ensuring the correct mixing ratio of water and coal in the amount of 0.4 ml per 2 g of coal, coal samples should be stored in a desiccator during the test to prevent the effect of water evaporation from the sample.

Zhai et al. [6] indicated the susceptibility of water soaked-dried coal samples on spontaneous heating and self-combustion process based on the difference in samples' thermal properties before and after the soaking process. Authors proved that water soaked-dried bituminous coal is more prone to self-heating, resulting in an increase in the rate of coal-oxygen compound reactions and a significantly increased risk of spontaneous combustion. In fact, this thesis is the implication for further research in self-heating of water soaked-dried coal samples [6].

The size of coal particles is a crucial factor that affects real spontaneous combustion behaviour and thus is a primary factor in the assessment of mine fire.

Even though particle size's influence on the course of the coal spontaneous combustion process has been proven, there is little data on the justification of selecting the fractional range of particles in the research procedures. The following part of the article discusses various methods to measure the coal seam's liability to spontaneous combustion against the background of spontaneous fires in Polish and Vietnamese coal mines. For the method used in Polish and Vietnamese coal mining, the influence of particle size on the course of spontaneous combustion was presented using the results of coal tests from three different coking coal seams.

2. Spontaneous fires in Polish and Vietnamese Mines

Poland is one of the countries with a long mining history, especially with the leading technology of mining sciences globally. Polish hard coal deposits belong to the Carboniferous EuroAmerican coal province. They occur in three basins, but coal exploitation continues in the Upper Silesian Coal Basin (USCB) and the Lublin Coal Basin (LCB). Based on the International Classification of Coal, the type of coal in Polish coal basins is bituminous coal. According to International Energy Agency (IEA), there are types of coal in the USCB, steam coal, coking coal and sometimes anthracite. In the LCB, mainly steam coal and coking coal occur.

In Vietnam, coal comes in many types, such as Lignite, Subbituminous, Bituminous, and Anthracite, found in 2 major coal basins, namely Quang Ninh and Song Hong. Anthracite is close to the surface in Vietnam, and Lignite, Subbituminous, and Bituminous are less than 2.5 km from the surface, so now anthracite is mined, mainly in mountainous and hilly areas in the Quang Ninh region. This coal's ash content is 9.73-23.64%, and sulfur 0.29-0.36% [7]. Coal is under extraction using opencast and underground methods. Before 2010, opencast coal mining accounted for 60-80% of Vietnam's total coal production. However, over time, coal mining began to be carried out from greater depths, and the opencast method ceased to be effective. Opencast mines gradually cease to operate and switch to underground mining. Since then, more attention has been paid to underground coal mining. For this reason, spontaneous combustion of coal is increasingly occurring in Vietnam's underground coal mines.

The fire index (W), representing the number of fires per 1 million tons of coal extracted annually, will be provided to illustrate the impact of the intensity of mining activities on mine fire frequency. In the 1950s, in the Polish mining industry, it was within the range of $W=3.74-5.72$ [8]. More and more research projects, new or improving detection methods of spontaneous combustion of coal and fire prevention, were conducted and tested in connection with science and technology development. As a result, the number of coal fires was significantly reduced, and from the second half of the 1990s, the number of coal fires did not exceed 10 per year, and the index W did not exceed the value of 0.07. In the last decade, however, there

was an increase in coal fires (see Tab. 1). However, the fire index reached the value of 0.013 in the years 2018-2019, which indicates an increase in the risk in Polish coal mines. The improvement in fire safety should be noted in 2020 as the fire index fell to 0.04.

Tab. 1. Number of coal fires and fire index in Polish and Vietnamese underground coal mines in the years 2004-2020, according to [7, 9, 10].

State of fires	Year																
	2004	2005	2006	2007	2008	2009	2010	2011	2012	2013	2014	2015	2016	2017	2018	2019	2020
Poland																	
Number of coal fire due to spontaneous combustion	5	8	2	4	5	10	9	6	3	5	1	5	7	9	8	11	2
Fire Index W, 1/mln tones	0.05	0.087	0.02	0.05	0.06	0.13	0.12	0.08	0.04	0.07	0.01	0.07	0.1	0.14	0.13	0.13	0.04
Vietnam																	
Number of coal fire due to spontaneous combustion	1	2	0	2	2	1	0	2	2	1	0	0	0	6	0	3	-
Fire Index W, 1/mln tones	0.11	0.09	0	0.09	0.09	0.014	0	0.09	0.1	0.05	0	0	0	0.27	0	0.13	-

Recording fires in Vietnam did not start until 2004, as there had been a few fires before, but they were considered open fires in mine excavations as it was believed that anthracite was a hard or incapable coal to ignite. From 2004 to date, the total number of fires due to coal's spontaneous combustion is 21 occurred in 7 of 14th underground mines; of which: "Hong Thai" coal mine: 5 cases, "Coal Enterprise 91": 4 cases; "Khanh Hoa Mine": 6 cases, "Mao Khe Mine" 1 fire, "Ha Lam Mine" 2 cases, "Uong Bi": 2 cases; "Thong Nhat": 1 case. The number of fires per year, and the fire index are presented in Table 1.

It is necessary to know the propensity of various types of coal to spontaneous combustion to improve safety and develop the most effective prevention of coal fires. In the following part, the methods of testing the propensity of coals to spontaneous combustion and the conditions of factors influencing the results of one of the methods will be presented.

3. Materials and Methods

Many factors influence the process of coal self-ignition. These are mainly mining and geological factors related to the method of selecting the deposit. Above all, however, the propensity of coal to self-ignition should be emphasized. This tendency depends on the properties of coal, such as the coal metamorphism, the petrographic composition of the coal, moisture and gas content adsorbed on the carbon surface, and the particle size of the coal.

The classic division of the spontaneous combustion process is related to the three stages: the incubation stage, the self-heating stage, and the combustion stage. However, many authors of the investigation on spontaneous combustion suggest that this process should be divided into more stages [11, 12, 13]. Regardless of that, each stage is characterized, among other things, by variations in temperature and exhaust gas concentrations.

In the first stage of spontaneous coal combustion, the physical absorption between oxygen and coal takes place, releasing a small amount of heat and unstable oxides or oxygen-containing free radicals. Reactive sites, which adsorb oxygen, are responsible for this behavior. Subsequent chemical adsorption increases and heat release is higher than heat dissipation. There is an accumulation of heat and a slow increase in the coal temperature to the moment of rapid water evaporation. The external water of coal evaporates faster as the temperature rises, while the internal water does not evaporate yet. The water vapor can be carried away

with the heat, but it can be partially absorbed by the coal pores, which trap heat, as shown by Beamish and Hamilton [4]. However, heat is still removed by the evaporation of moisture, and the self-heating of the coal is significantly delayed. However, more pore channels or fissures are created, thereby increasing the inner surface area for contact with oxygen.

As the coal's outer water is evaporated, the oxidation activation medium on the coal surface increases and the reaction becomes more intense. The internal water starts to evaporate, and the coal temperature stagnates to some extent due to trapping some of the heat for water evaporation. The heat demand associated with the evaporation of internal moisture is much greater than that of external moisture. This state depends on the moisture of the coal. Yoruk and Arisoy [14] developed and validated the new mathematical model based on data from incubation testing of raw coal and moisture removal rate data.

Water evaporation completion is determined by the minimum self-heating start temperature and is called the critical temperature or minimum self-heating or SHT temperature. Depending on the type and grade of coal, SHT ranges from 40°C to 140°C, as reported by Smith and Lazzara [15]. For Polish coals, it ranges from 70°C to 90°C.

Due to the complete evaporation of both the internal and external moisture, the further reaction between the carbon and the oxygen begins actively because the heat generated in this reaction is no longer used for evaporation moisture. Dried coal is more reactive than the original moist coal due to increasing the coal's pore area. During oxygen consumption, heat is released, and qualitative and quantitative changes in discharged gases are visible.

The temperature of the coal rises rapidly up to the critical temperature of coal ignition. If the oxygen supply is sufficient, flame combustion and smoke production occur. However, if the supply of oxygen is insufficient, smoldering will be formed in the coal sample. Generally, as the temperature increases, the coal's activated molecules will appear in higher numbers, and more oxygen will be needed. If the oxygen supply is insufficient, the coal sample will develop smoldering smoke without a flame. In general, when the activated molecules in the coal seam increase with increasing temperature, more oxygen will be required [11]. This process step is highly dependent on the quality of the coal.

When the coal temperature does not reach the critical temperature or after it is reached, changes in external conditions favoring heat dissipation occur, then the self-heating slowly turns into a cooling period, and further air supply to the heated coal causes it to smoldering. A similar phenomenon is observed in the case of oxidation of coals, which are not prone to spontaneous combustion, which quickly turns into a state of weathering. Weathered coal does not ignite spontaneously [16, 17, 18].

4. Methods for determining the liability of spontaneous coal combustion

Many techniques for predicting the spontaneous combustion of coal have been developed all over the world. In methods that have been developed to predict spontaneous combustion, different experimental procedures, both laboratory and field, are used.

In the Russian mining industry U index has been using. In this method, the amount of oxygen absorbed by individual coal samples over 24 hours is measured. The gases obtained in experimental conditions are quantified by evaluating the gas composition. Onifade and Genc [19] reported that the oxygen absorbed during testing is directly proportional to coal's spontaneous combustion liability.

The crossing point temperature methods (CPT) are used to categorize the spontaneous combustion liability of coal in Indian, Polish, Vietnamese, Turkish, and South African mines. These methods are often referred to as the ignobility method [3]. The propensity of coal towards spontaneous combustion is determined with respect to their ignition temperature. The temperature at which the increasing coal temperature is equal to the increasing to steady ambient temperature in the oven or chamber is called the crossing point temperature [3, 20, 21]. An example of one of the CPT-based methods is the method known as XPT [19].

In differential scanning calorimetry (DSC) the changes in energy inputs provided to a sample and a reference material with respect to temperature when these materials are kept at a constant temperature are determined [19]. In thermogravimetric analysis (TGA) the loss in weight of coal samples at variable temperatures due to self-heating is estimated. In this method, the mass of a sample is measured over time

as the temperature changes. The TG curve is referred to as the differential thermogravimetric (DTG) curve and is the difference between the coal curve and the inert material curve.

In Australia, New Zealand, South Africa, UK and USA adiabatic calorimetric method are usually used. In this method, the rate of temperature increase, ignition temperature and the kinetic constant of coal are used to determine the liability of coal for spontaneous combustion [22].

In China, coal's propensity to spontaneous combustion is determined based on measurements of the amount of oxygen absorbed per unit mass of the coal sample, including the type of coal and sulphur content [23]. Coal propensity tests are also performed using the crossing point temperature method using the Temperature-Programmed System (TPS) [24]. The method is often referred to as the ignobility method [3]. The coal's propensity to spontaneous combustion (ISCP) was classified based on the R70 index, calculated based on the temperature rise time from 40 to 70°C in the Australian mining industry. The R70 index is proportional to the coal's spontaneous combustion capacity, which means that the higher the R70, the higher the coal's propensity to self-ignition. The R70 procedure involves drying a 150 g sample of crushed coal at 110°C under nitrogen for approximately 16 hours and served below 212 µm [25].

There are other methods for predicting the spontaneous combustion liability of coal, mentioned by Onifade and Genc [19, 26], such as average heating rate (AHR), Feng, Chakravorty and Cochrane (FCC) liability index, differential scanning calorimetry (DSC), differential thermal analysis (DTA), flammability temperature (FT), wet oxidation potential (WOP), X-ray diffractometer (XRD) used by [27], Wits-Ehac tests used to forecast the propensity of coal and coal-shale by [26, 28, 29, 30, 31, 32] and Wits-CT tests developed by Onifade et al. [26].

Both in Poland and Vietnam, the method known as the Olpiński index is widely used. The Science and Technology Institute in Vietnam launched on October 28, 2016 a laboratory for testing the propensity of spontaneous coal combustion. This method is known as the high-temperature method and is a variation of CPT methods. The propensity of coal to ignite is determined from the self-ignition index Sz^a and activation energy A . For this purpose, coal samples in the furnace are performed for two air temperatures maintained by non-linear heating by fixing the thermostat at a particular point near the coal sample.

The sample is mounted on a thermocouple recording the coal temperature changes over time with an interval of 1 s. Temperature changes are measured for two cycles of air temperatures, 190°C and 237°C, respectively. The sample temperature and air temperature changes with an accuracy of 0.1°C around the sample are recorded by thermocouples connected to a computer.

Two time-temperature curves for samples of the same coal are recorded to determine coal's spontaneous combustion liability. The curves are recorded in two ranges (Zhang, 2002):

1) for CPT of 190°C, the temperature of the coal sample is recorded in the temperature range of 200÷260°C;

2) for CPT of 237°C, the coal sample's temperature is recorded in the temperature range of 165-215°C.

The tangents to curves at the point of 237°C for the temperature range of 200-260°C and at the point of 190°C for the temperature range of 165-215°C are plotted, respectively.

Based on the tangent to the time-temperature curve at a point of 237°C, coal self-igniting index Sz^a (°C/min) is calculated according to the formula:

$$Sz^a = \frac{t_2 - t_1}{\tau_2 - \tau_1} \quad (1)$$

For the tangent to the time-temperature curve in ranges 165-215°C, the self-igniting index of coal $Sz^{a'}$ (°C/min) is calculated according to formula:

$$Sz^{a'} = \frac{t'_2 - t'_1}{\tau'_2 - \tau'_1} \quad (2)$$

where (τ_1, t_1) , (τ_2, t_2) are the coordinates of any two sufficiently distant points lying on the tangent line

to time-temperature curve in the range 200-260°C and $(\tau'_1, t'_1), (\tau'_2, t'_2)$ are the coordinates of any two sufficiently distant points lying on the tangent line to time-temperature curve in the range 165-215°C.

The activation energy A , J/mol is determined from the dependence:

$$A = \frac{R \cdot (\ln Sz^a - \ln Sz^{a'})}{\frac{1}{T'} - \frac{1}{T}} \quad (3)$$

where R is universal gas constant, T', T are absolute temperatures, 463.15 K and 510.15 K, respectively.

Depending on the Sz^a index's value and the activation energy A , the coal seam's liability to spontaneous combustion is divided into five groups, and, in principle, the higher the Sz^a index, the higher the liability is. Table 2 presents the criteria for the division into spontaneous combustion groups.

Tab. 2. Liability of seam coal's spontaneous combustion in EPolish mines [33].

Sz^a index, °C/min	Activation Energy A , kJ/mol	Group of liability	Rank of liability to Spontaneous Combustion
Up to 80	Below 67	I	Very low liability to spontaneous combustion
	From 46 to 67	II	Low liability to spontaneous combustion
	Below 46	III	Medium liability to spontaneous combustion
Above 80 to 100	Above 42		
Above 100 to 120	Below or equal to 42	IV	High liability to spontaneous combustion
	Above 34		
Above 120	Below or equal to 34	V	Very high liability to spontaneous combustion
Above 120	Beyond the standardization		

According to this method, the sample is made of coal particles with a size in the range of 0.063-0.075 mm. However, very often, the results obtained from samples of the same coal are inconsistent. Therefore, it was decided to check how the spontaneous combustion process looks for other ranges of size particle fractions.

5. Experimental investigation

5.1 Coal samples preparation

Coal samples were collected from three different coal seams in Mine B, Uppers Silesian Coal Basin, Poland. After core samples being sealed and stored on-site, they were transported to the laboratory. After peeling off the surface oxide layer, the raw coal samples were crushed and ground to screen out coal powders. Part of the sample masses was transferred to proximate analysis in air-dry condition. Outcomes proximate analyses are presented in Table 3.

Tab. 3. Proximate analysis of tested coal samples.

Coal Seam No.	Symbol of samples	Proximate analysis, mass %				Density, kg/m ³	Gross calorific value, Q_{daf} , kJ/kg
		W_{ad}	V_{daf}	A_{ad}	S_{ad}		
401	P2	0.58	29.2	11.6	0.65	1.37	29856
364/2	P5	0.71	32.4	11.8	0.78	1.33	29494
405/1	P7	0.61	28.6	5.6	0.90	1.16	18450

The remaining sample weight was sieved into five particle size fractions, 0.075-0.125 mm, 0.063-

0.075 mm, and below 0.063 mm, respectively. Then, each of the samples is separately mixed with demineralised water in the proportion of 0.4 ml of water per 2 g of coal. The sample is made at an ambient temperature of 20°C and relative humidity of 50%. The sample mixed in this way is formed in a cylinder-shaped die. The sample in the matrix is compacted with a press with a force of 2.28 kN. Finally, a compacted sample of cylinder shape with a diameter of 7.5 µm, a height of 9 µm, and a centre hole is obtained. Sample and furnace views are shown in Figures 1-2. For each particle size range, three samples were made and placed immediately in the desiccator. Then all samples were weighed on an analytical balance with an accuracy of 10⁻³ g. The results of the sample mass measurements are presented in Table 4.



Fig. 1. View of prepared coal sample mounted on a thermocouple prior to insertion into the furnace.



Fig. 2. View of furnace for Olpiński method.

Tab. 4. Results of the sample mass measurements.

Symbol of coal	Coal particle size ranges					
	< 0.063 mm		0.063-0.075 mm		0.075-0.125 mm	
	Symbol of particle fraction	Mass of coal sample, g	Symbol of particle fraction	Mass of coal sample, g	Symbol of particle fraction	Mass of coal sample, g
P3	A1	0.3085	B1	0.2630	C1	0.2622
	A2	0.2905	B2	0.3572	C2	0.2430
	A3	0.2659	B3	0.3538	C3	0.2366
	A4	0.3228	B4	0.3485	C4	0.2397
P5	A1	0.2583	B1	0.2856	C1	0.2718
	A2	0.2599	B2	0.3324	C2	0.2835
	A3	0.2571	B3	0.3110	C3	0.2878
	A4	0.2784	B4	0.3243	C4	0.2504
P7	A1	0.3217	B1	0.3554	C1	0.3062
	A2	0.2784	B2	0.3296	C2	0.3424
	A3	0.3202	B3	0.3834	C3	0.3410
	A4	0.3941	B4	0.3695	C4	0.3318

5.2 Methodology

To determine the effect of particle size distribution on the change of the sample temperature increase rate, the Olpiński method, which is used in Poland and Vietnam, was used. The two weighed samples were sequentially inserted into continuous mass airflow furnaces, matching the first crossing point temperatures 190°C and 237°C. For each sample, the course of the time-temperature curve was recorded. Next, both indices Sz^a and $Sz^{a'}$, as well as activation energy, were determined. In small surveying projects, rotary-wing UAVs such as DJI Phantom 3, or 4 professional are often utilized widely. In this work, the study sites are small so we use a phantom 4 professional to capture images. The Phantom 4 professional is a quadcopter drone with four powerful rotors (Fig. 2). Its airframe carries the GPS/IMU that enables it to have posture control, stop flight, and automatically take off and land with high stability [6]. The drone is capable of both manual flight mode using the controller and automatic flight mode using the Android or IOS smartphone applications. If you use the automatic mode, you can set the flight path, flight speed, flight altitude, shooting range and overlapping of the photographs, so you can take more aerial photographs. The drone is equipped with a 20 megapixel RGB camera with a focal length of 8.8 mm and sensor a size of 13.2 x 8.8 mm that allows high-resolution aerial photography [7].

6. Results and discussion

Figures 3-5 show the time-temperature curves of the investigated coals. The recording of the coal samples' temperature ended when the critical temperature of ignition of the sample was reached above each set crossing point temperature.

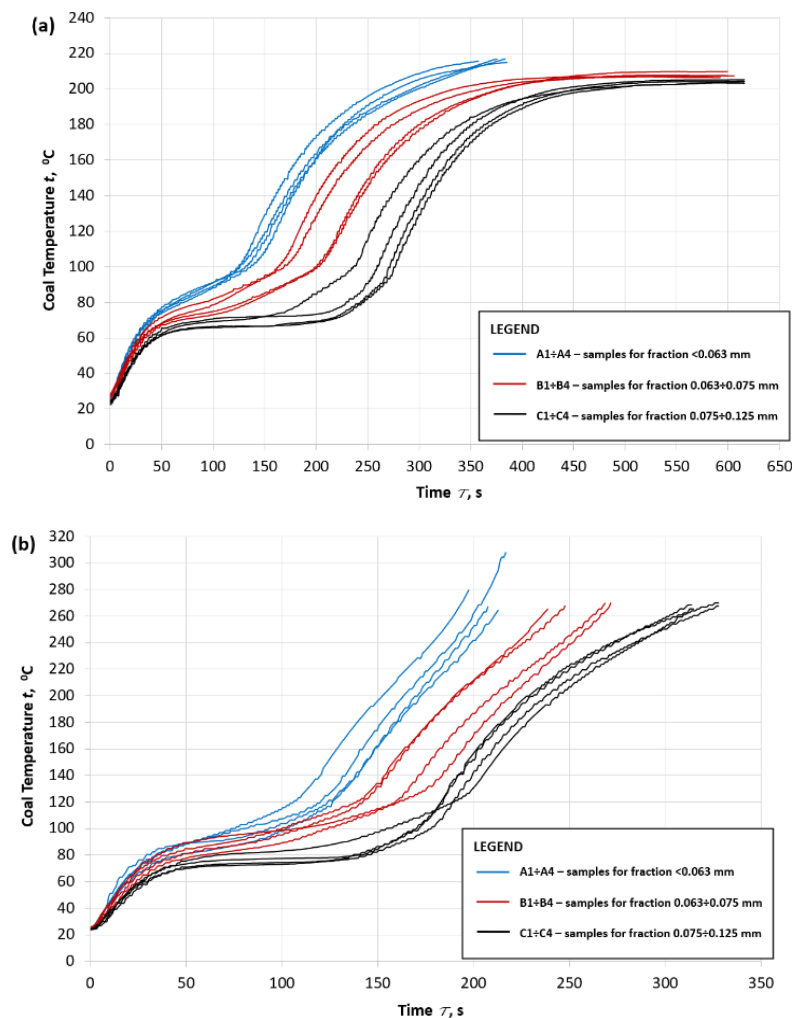


Fig. 3. Thermal curves of temperatures of coal samples P3 for different coal particle fractions, (a) for $t_{CPT} = 190^\circ\text{C}$, (b) for $t_{CPT} = 237^\circ\text{C}$.

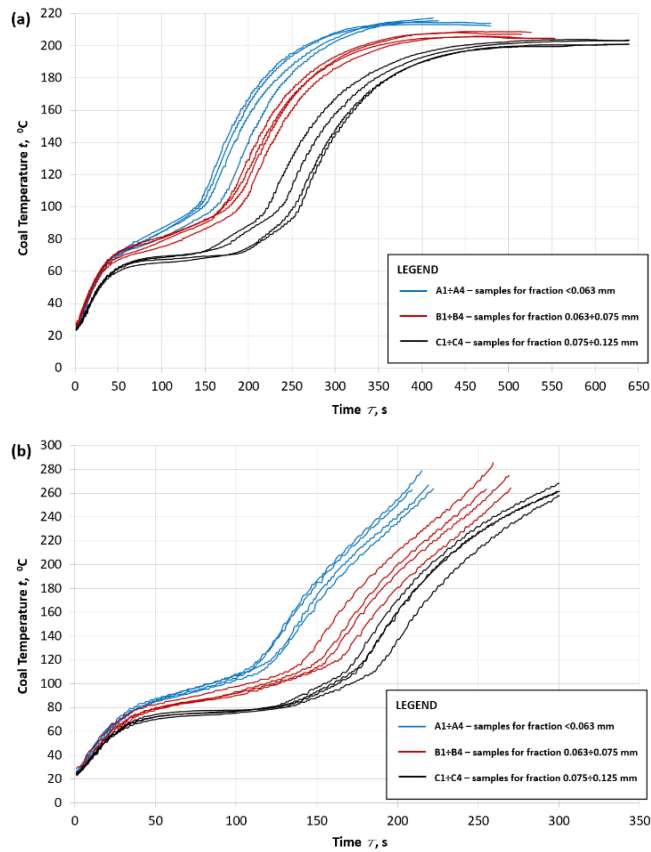


Fig. 4. Thermal curves of temperatures of coal samples P5 for different coal particle fractions, (a) for $t_{CPT} = 190^{\circ}\text{C}$, (b) for $t_{CPT} = 237^{\circ}\text{C}$.

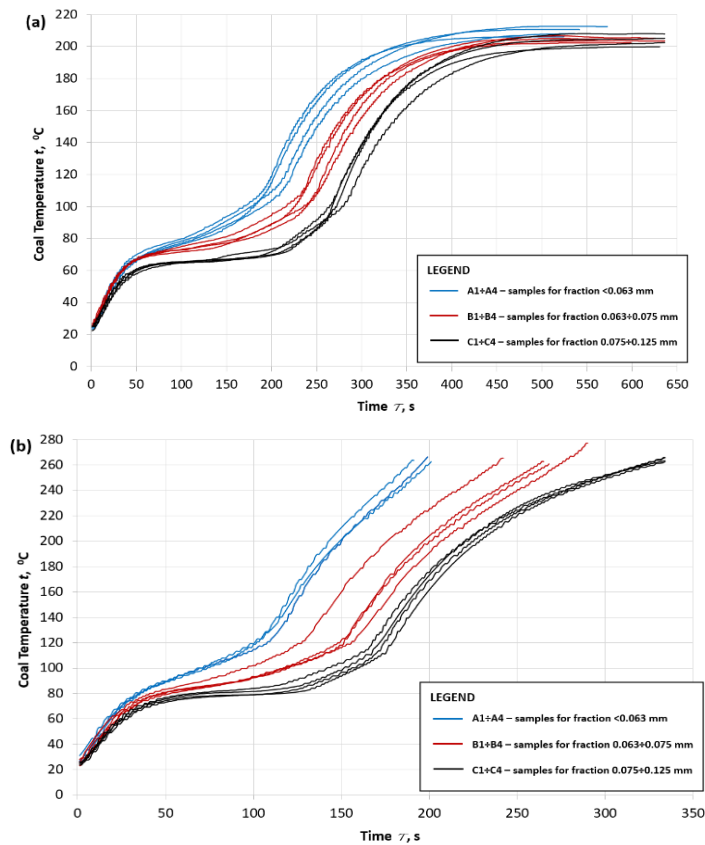


Fig. 5. Thermal curves of temperatures of coal samples P7 for different coal particle fractions, (a) for $t_{CPT} = 190^{\circ}\text{C}$, (b) for $t_{CPT} = 237^{\circ}\text{C}$.

The figures show that the minimum self-heating temperature (SHT) of the starting process for all tested samples is 90°C at a crossing point temperature (t_{CPT}) of 190°C. All samples reached SHT at the same time. The incubation period is strictly dependent on the type of coal and particle size in the sample agglomerate.

Under isothermal conditions of 237°C, the SHT value is no longer as unambiguous as in the case of $t_{CPT} = 190^\circ\text{C}$. For samples with particle size 0.075-0.125 mm, it is clearly visible that SHT is 90°C, but with smaller particle sizes, the temperature increase is higher. The SHT ranges from 90°C to 120°C.

Table 5 shows the incubation period's average times to illustrate the effect of particle size distribution on water evaporation.

Tab. 5. Incubation period of tested coal samples.

Coal No.	Particle size range	Time of incubation period, s	
		For $t_{CPT} = 190^\circ\text{C}$	For $t_{CPT} = 237^\circ\text{C}$
P3	<0.063 mm	80	80
	0.063-0.075 mm	140	105
	0.075-0.125 mm	230	150
P5	<0.063 mm	100	80
	0.063-0.075 mm	140	105
	0.075-0.125 mm	260	150
P7	<0.063 mm	170	80
	0.063-0.075 mm	220	105
	0.075-0.125 mm	270	135

The evaporation period is much more visible at the crossing point temperature of 190°C than at 237°C. Figures 3a-5a show a more extended period of temperature stabilization for coal samples with larger particles (0.075-0.125 mm) than for samples with particles below 0.063 mm. For particles smaller than 0.063 mm, the incubation period is the shortest, and for particle size range 0.075-0.125 mm, the longest. It is natural that at 237°C, this time is shorter than at 190°C. It is the period of evaporation of moisture and steady temperature, which is visible at the temperature of 190°C. At 237°C, the temperature rise rate is already faster, but the rise is also linear (Figs. 3b-3c).

The changes in the temperature curve are due to the moisture removal rate. It may be due to the agglomeration of the dust particles in the cylindrical shape of the sample. The shape of the particle is a rational component of particle agglomeration. The tendency of coal dust to agglomerate increases with decreasing particle size.

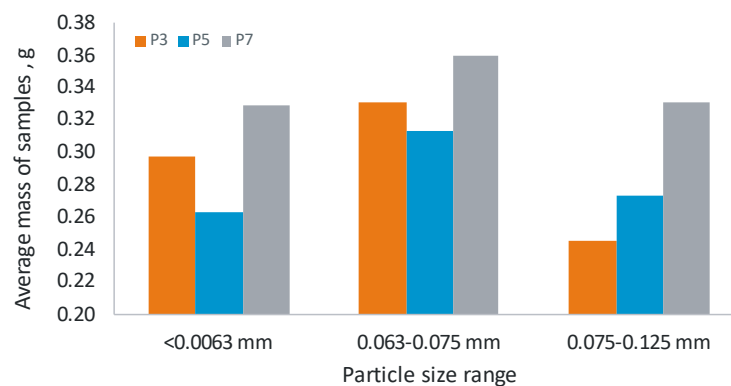


Fig. 6. Average mass of samples of coals P3, P5, P7 for the analysed particle size range.

It should be noted, however, that the samples were prepared with the same proportion of water. Also, the natural moisture content in all three coals was similar (Tab. 3). From Figure 6, it can be seen that the mass of the samples was variable. The highest mass could be expected with the largest particles, probably

resulting from regularly shaped particles on the agglomeration, and yet the samples ranging from 0.063-0.075 mm had the highest mass. On the other hand, samples with sizes 0.075-0.125 mm had the lowest weight. Thus, it is not synonymous with increasing the regular particle size's size - the agglomeration causes more water absorption. Such studies should be repeated using other research methods.

The effect of the particle size distribution on the temperature increase rate Sz^a and the calculated activation temperature A was also checked, and the results are presented in Table 6.

Tab. 6. Incubation period of tested coal samples.

Coal Particles range	No.	τ_1 , s	$t_{1,}$, °C	τ_2 , s	$t_{2,}$, °C	Δt , °C	$\Delta \tau$, s	Sz^a , °C/min	τ'_1 , s	$t'_{1,}$, °C	τ'_2 , s	$t'_{2,}$, °C	$\Delta t'$, °C	$\Delta \tau'$, s	$Sz^{a'}$, °C/min	A, kJ/mol
P2 < 0,063 mm	1	164	200.3	199	257.2	56.9	35	98	190	166.6	349	215.0	48.4	159	18	70.4
	2	173	200.4	211	260.3	59.8	38	94	207	165.1	374	215.0	49.9	167	18	69.8
	3	170	200.0	204	259.4	59.2	34	105	203	165.9	364	214.7	48.8	161	18	73.5
	4	152	200.1	188	258.0	58.2	36	97	194	156.4	384	215.0	58.6	190	19	69.6
P2 0,063÷ 0,075 mm	1	221	201.5	266	259.3	57.3	45	76	261	157.4	479	207.0	49.6	219	14	72.6
	2	211	201.0	261	259.1	57.9	50	69	268	159.2	495	209.0	49.8	227	13	69.9
	3	193	200.9	242	259.7	58.5	49	72	230	155.6	431	205.1	49.4	201	15	66.4
	4	191	200.8	236	260.8	59.5	45	79	220	157.0	418	206.0	49.0	198	15	70.4
P2 0,075÷ 0,125 mm	1	230	201.2	306	260.1	58.4	76	46	310	155.3	557	205.0	49.7	247	12	56.3
	2	232	200.8	302	260.4	59.1	70	51	320	154.2	554	204.2	50.0	234	13	57.8
	3	239	201.0	314	259.1	58.1	75	46	327	154.7	562	203.0	48.3	235	12	55.8
	4	245	202.3	311	261.5	59.2	66	54	290	153.7	528	202.2	48.5	238	12	62.3
P5 < 0,063 mm	1	171	200.4	218	259.3	58.9	47	75	197	165.9	363	214.0	48.1	166	17	61.6
	2	161	200.8	205	257.3	56.5	44	77	199	163.2	380	213.0	49.8	181	16	64.8
	3	160	200.8	204	259.8	59.0	44	80	210	165.3	372	215.0	49.7	162	18	62.0
	4	166	200.1	214	259.6	59.5	48	74	225	166.6	398	215.0	48.4	173	17	62.6
P5 0,063÷ 0,075 mm	1	200	200.1	251	259.5	59.4	51	70	232	155.6	424	205.1	49.5	192	15	63.4
	2	206	201.1	258	259.7	58.6	52	68	245	156.6	455	205.8	49.2	210	14	66.0
	3	191	200.9	241	257.8	56.9	50	68	240	160.3	448	208.9	48.6	208	14	66.5
	4	215	200.3	266	258.7	58.4	51	69	228	158.9	419	208.1	49.2	191	15	62.7
P5 0,075÷ 0,125 mm	1	227	201.0	297	260.0	59.0	70	51	292	152.6	521	202.0	49.4	229	13	57.3
	2	221	201.6	288	259.6	58.0	67	52	277	153.2	513	203.0	49.8	236	13	59.3
	3	226	201.3	298	259.8	58.5	72	49	308	150.8	550	200.4	49.6	242	12	57.9
	4	239	200.8	302	259.2	58.4	63	56	302	149.9	537	199.4	49.5	235	13	62.3
P7 < 0,063 mm	1	150	200.1	194	258.8	58.7	44	80	243	161.4	415	209.0	47.6	172	17	66.2
	2	149	200.2	199	259.8	59.6	50	71	254	159.8	427	209.7	49.9	173	17	59.6
	3	143	200.4	187	257.9	57.5	44	78	231	155.4	409	205.1	49.7	178	17	64.9
	4	163	201.8	204	259.1	57.3	41	84	321	156.8	486	206.0	49.2	165	18	64.9
P7 0,063÷ 0,075 mm	1	197	200.5	261	259.0	58.5	64	55	286	151.7	494	201.6	49.9	208	14	56.2
	2	207	200.7	273	259.2	58.5	66	53	277	154.1	485	203.0	48.9	208	14	55.8
	3	200	200.1	267	259.4	59.3	67	53	281	155.5	498	205.0	49.5	217	14	57.0
	4	176	200.2	238	259.9	59.7	62	58	301	156.8	502	206.4	49.6	201	15	57.2
P7 0,075÷ 0,125 mm	1	220	200.0	323	259.8	59.8	103	35	333	152.4	599	202.0	49.6	266	11	47.8
	2	230	201.2	327	259.8	58.6	98	36	320	155.2	590	204.5	49.3	270	11	49.9
	3	226	201.9	320	259.2	57.3	94	37	312	150.1	576	199.8	49.7	263	11	49.2
	4	221	201.6	320	259.8	58.2	99	35	323	158.3	554	208.0	49.7	231	13	42.3

The results show that as the particle size decreases, the self-ignition index Sz^a and $Sz^{a'}$ increases. The combustion time $\Delta\tau$ and $\Delta\tau'$ is shortened, which means that coal samples with a smaller particle size are more flammable than coal samples with a larger particle size range. The average values of the temperature increase rate and activation energy are presented in Figure 7.

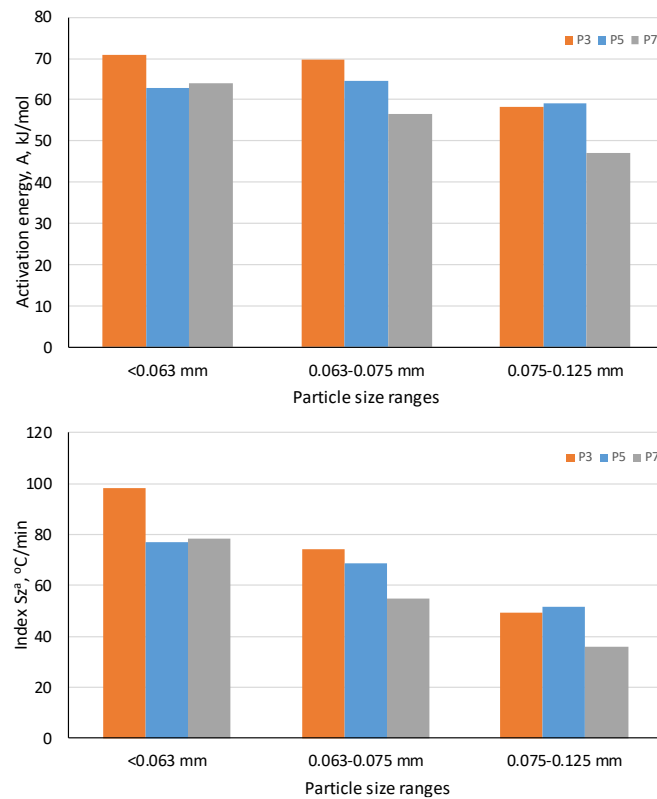


Fig. 7. Average values of index Sz^a and activation energy A for the analysed particle size range of coals P3, P5, P7.

The results show that the P2 coal can be included in the 3rd group of propensity to spontaneous combustion for the sample fraction <0.063 mm, the 1st group for the 0.063-0.075 mm fraction, and the 2nd group for the 0.063-0.075 mm fraction. For all fractions, the P5 and P7 carbons are included in group 2nd. Even though for the coals P5 and P7, the tendency to spontaneous combustion does not depend on the analyzed fractions of coal particles, the differences in the Sz^a index and activation energy A are visible. Further research should be undertaken to determine if the 0.063-0.075 mm fraction is appropriate for this test procedure. The particle size range 0.075-0.125 mm gives as good a course of the process rate curves as the fraction 0.063-0.075 mm. Indeed, too extensive a particle size range should not be used in research methods with prepared samples. The authors are aware of the small research scope in terms of the type and types of coal and the number of research trials. The obtained results may constitute the basis for further research on the improvement of the research method to contribute to the prevention of spontaneous combustion in coal mines.

7. Conclusions

Despite the scientific developments in the spontaneous combustion process, fires still occur during underground coal mining in various countries. The process of spontaneous coal combustion is complex, and its course is influenced by many factors, among which there are particle sizes and the moisture content of coal. There are various methods of testing the propensity of coal to ignite. In order to determine the effect of particle size distribution during the measurements of adiabatic oxidation, the high-temperature Olpiński method, which is used in Poland and Vietnam, was used. The tests performed for the three particle sizes will show differences in the temperature changes of the coal samples. The differences result from the different identification of the moisture evaporation and removal from agglomerated particles in the sample.

For the model course of the phenomenon, samples should be prepared with the smallest possible particle size range. Both the range of 0.063-0.075 mm and the range of 0.075-0.125 mm in the tested shape of the coal sample show the proper character in the course of temperature changes.

8. Acknowledgments

The paper was presented during the 6th VIET - POL International Conference on Scientific-Research Cooperation between Vietnam and Poland, 10-14.11.2021, HUMG, Hanoi, Vietnam.

9. References

1. Morgan, P.A., Robertson, S.D., Unsworth, J.F., 1986. Combustion studies by thermogravimetric analysis: 1. Coal oxidation. *Fuel*, 65(11), 1546-1551, [https://doi.org/10.1016/0016-2361\(86\)90331-5](https://doi.org/10.1016/0016-2361(86)90331-5).
2. Yu, D., Xu, M., Sui, J., Liu, X., Yu, Y., Cao, Q., 2005. Effect of coal particle size on the proximate composition and combustion properties. *Thermochimica Acta*, 439(1–2), 103–109, <https://doi.org/10.1016/j.tca.2005.09.005>.
3. Beamish, B.B., Barakat, M.A., St George, J.D., 2000. Adiabatic testing procedures for determining the self-heating propensity of coal and sample ageing effects. *Thermochimica Acta*, 362(1–2), 79–87, [https://doi.org/10.1016/S0040-6031\(00\)00588-8](https://doi.org/10.1016/S0040-6031(00)00588-8).
4. Beamish, B.B., Hamilton, G.R., 2005. Effect of moisture content on the R70 self-heating rate of Callide coal. *International Journal of Coal Geology*, 64(1–2), 133-138, <https://doi.org/10.1016/j.coal.2005.03.011>.
5. Beamish, B.B., Theiler, J., 2015. Contrast in Self-Heating Rate Behaviour for Coals of Similar Rank. 15th Coal Operators' Conference, University of Wollongong, The Australasian Institute of Mining and Metallurgy and Mine Managers Association of Australia, 11 – 13 February 2015, 300–304.
6. Zhai, X.W., Pan, W.J., Wu, S.B., Ge, H., 2020. Laboratory experimental study on water-soaked-dried bituminous coal's thermal properties. *Journal of Thermal Analysis and Calorimetry*, 139, 3691–3700, <https://doi.org/10.1007/s10973-019-08769-6>.
7. Tuyen, L.T. Study on Susceptibility to Spontaneous Combustion of Anthracite in Vietnamese Coal Mines. Ph.D thesis, 2020, <https://doi.org/10.14943/doctoral.r7062>.
8. Trenczek, S., 2006. Rys historyczny pożarów podziemnych w ostatnim 60-leciu polskiego górnictwa. *Prace Naukowe Instytutu Górnictwa Politechniki Wrocławskiej*, 117, 315-325 (in Polish).
9. Kabiesz, J., 2019. Raport roczny o stanie podstawowych zagrożeń naturalnych i technicznych w górnictwie węgla kamiennego. Główny Instytut Górnictwa, Katowice, 2018 (in Polish).
10. State Mining Authority. Stan bezpieczeństwa w polskim górnictwie, statystyki. Katowice, 2020 (in Polish). https://wug.intracom.com.pl/bhp/stan_bhp_w_gornictwie, 18/03/2021.
11. Zhu, H., Sheng, K., Zhang, Y., Fang, S., Wu, Y., 2018. The stage analysis and counter measures of coal spontaneous combustion based on “five stages” division. *PLOS ONE*, <https://doi.org/10.1371/journal.pone.0202724>.
12. Onifade, M., Genc, B., 2020. A review of research on spontaneous combustion of coal. *International Journal of Coal Science & Technology*, 30(3), 303–311, <https://doi.org/10.1016/j.ijmst.2020.03.001>.
13. Li, B., Li, M., Gao, W., Bi, M., Ma, L., Qin, Q., Shu, C., 2020. Effects of particle size on the self-ignition behaviour of a coal dust layer on a hot plate. *Fuel*, 260, 116269, <https://doi.org/10.1016/j.fuel.2019.116269>.
14. Yoruk, B., Arisoy, A., 2021. Development of a Mathematical Model for Simulating the Self-Heating Behavior of Moist Coal. *Combustion Science and Technology*, <https://doi.org/10.1080/00102202.2021.1885388>.
15. Smith, A., Lazzara, C.P., 1987. Spontaneous combustion studies of US coal. United States Bureau of Mines, Raport of Investigation no. 9079.

16. Maciejasz, Z. Pożary podziemne w kopalniach, część 1. Wydawnictwo „Śląsk”, Katowice, 1977 (in Polish).
17. Strumiński, A. Zwalczanie pożarów w kopalniach głębinowych. Wydawnictwo „Śląsk”, Katowice, 1996 (in Polish).
18. Szlązak, N., Obracaj, D., Swolkień, J., Korzec, M., Piergies, K., 2019. Wybrane problemy zwalczania zagrożenia pożarowego w kopalniach węgla kamiennego (Selected aspects of fighting fire hazard in hard coal mines). AGH University of Science and Technology Press, Kraków (in Polish).
19. Onifade, M., Genc, B., 2019. Spontaneous combustion liability of coal and coal-shale: a review of prediction methods. *International Journal of Coal Science & Technology*, 6(2), 151–168, <https://doi.org/10.1007/s40789-019-0242-9>.
20. Gouws, M.J., 1987. Crossing point characteristics and thermal analysis of South African coals. M.Sc. dissertation, University of Witwatersrand, South Africa, 160–165.
21. Humphreys, D.R., 1979. A study of the propensity of Queensland coals to spontaneous combustion. MSc. Thesis (unpublished), University of Queensland, Brisbane, Australia.
22. Ren, T.X., Edwards, J.S., Clarke, D. 1999. Adiabatic oxidation study on the propensity of pulverized coal to spontaneous combustion. *Fuel*, 78(14), 1611–1620, [https://doi.org/10.1016/S0016-2361\(99\)00107-6](https://doi.org/10.1016/S0016-2361(99)00107-6).
23. Zhang, D.G., 2002. Teoria samozapalenia węgla i praktyka jego zwalczania. Wydawnictwo Przemysłu Węglowego, Pekin, China (in Polish).
24. Xu, Y.-l., Wang, L.-y., Tian, T., Ahang, J., Yu, M., Delichatsios, M.A., 2017. Spontaneous combustion coal parameters for the Crossing-Point Temperature (CPT) method in a Temperature–Programmed System (TPS). *Fire Safety Journal*, 91, 147–154, <https://doi.org/10.1016/j.firesaf.2017.03.084>.
25. Beamish, B.B., Arisoy, A., 2008. Effect of intrinsic coal properties on self-heating rates. 12th U.S./North American Mine Ventilation Symposium, Wallace (ed), ISBN 978-0-615-20009-5, 149–153.
26. Onifade, M., Genc, B., 2018. Establishing relationship between spontaneous combustion liability indices. Proceedings of the 21st International Coal Congress of Turkey ‘ICCET’, 11–13 April 2018, Zonguldak, Turkey, 1–11.
27. Gong, B., Pigram, P.J., Lamb, R.N., 1998. Surface studies of lowtemperature oxidation of bituminous vitrain bands using XPS and SIMS. *Fuel*, 77(9–10), 1081–1087, [https://doi.org/10.1016/S0016-2361\(98\)00002-7](https://doi.org/10.1016/S0016-2361(98)00002-7).
28. Eroglu, H.N., 1992. Factors affecting spontaneous combustion liability index. Ph.D thesis, University of the Witswatersrand, Johannesburg, South Africa.
29. Genc, B., Cook, A., 2015. Spontaneous combustion risk in South African coalfields. *Journal of the Southern African Institute of Mining and Metallurgy*, 115, 563–568, <https://doi.org/10.17159/2411-9717/2015/V115N7A1>.
30. Genc, B., Onifade, M., Cook, A., 2018. Spontaneous combustion risk on South African coalfields: Part 2. Proceedings of the 21st international coal congress of Turkey ‘ICCET’, April 2018, Zonguldak, Turkey, 13–25.
31. Gouws, M.J., Wade, L., 1989. The self-heating liability of coal: predictions based on simple indices. *Mining Science and Technology*, 9(1), 81–85, [https://doi.org/10.1016/S0167-9031\(89\)90797-4](https://doi.org/10.1016/S0167-9031(89)90797-4).
32. Wade, L., 1989. The propensity of South African coals to spontaneously combust. Ph.D Thesis, Department of Mining Engineering, University of the Witwatersrand, Johannesburg.
33. Polish Committee for Standardization PN-93 G-04558. Hard Coal – Determination of autoinflammability index. The Polish Committee for Standardization: Warszawa, Poland, 1993 (in Polish).

Artificial Neural Network Optimized by Modified Particle Swarm Optimization for Predicting Peak Particle Velocity Induced by Blasting Operations in Open Pit Mines

BUI Xuan-Nam^{1,2,*}, NGUYEN Hoang^{1,2}, NGUYEN Truc Anh³

¹ Hanoi University of Mining and Geology (HUMG), 18 Vien street, Hanoi, Vietnam

² Innovations for Sustainable and Responsible Mining Group, HUMG, Hanoi, Vietnam

³ Vinacomin - Mining Chemical Industrial Corporation Limited, Hanoi, Vietnam

Corresponding author: buixuannam@humg.edu.vn

Abstract. Blasting is an indispensable part of the open pit mining operations. It plays a vital role in preparing the rock mass for subsequent operations, such as loading/unloading, transporting, crushing, and dumping. However, adverse effects, especially blast-induced ground vibrations, are considered one of the most dangerous problems. In this study, artificial intelligence was supposed to predict the intensity of blast-induced ground vibration, which is represented by the peak particle velocity (PPV). Accordingly, an artificial neural network was designed to predict PPV at the Coc Sau open pit coal mine with 137 blasting events were collected. Aiming to optimize the ANN model, the modified version of the particle swarm optimization (MPSO) algorithm was applied to optimize the ANN model for predicting PPV, called the MPSO-ANN model. For the comparison purposes, two forms of empirical equations, namely United States Bureau of Mining (USBM) and U Långefors - Kihlström, were also developed to predict PPV and compared with the proposed MPSO-ANN model. The results showed that the proposed MPSO-ANN model provided a better performance with a mean absolute error (MAE) of 1.217, root-mean-squared error (RMSE) of 1.456, and coefficient of determination (R²) of 0.956. Meanwhile, the empirical models only provided poorer performances with an MAE of 1.830 and 2.012, RMSE of 2.268 and 2.464, and R² of 0.874 and 0.852 for the USBM and U Långefors – Kihlström empirical models, respectively.

Keywords: Blast-induced ground vibration, Peak particle velocity, Open pit mine, Artificial neural network, Modified particle swarm optimization, Metaheuristic algorithms

1. Introduction

In open pit mines, the drilling-blasting method has been widely used for rock/ore fragments due to explosive energy's technical and economic advantages. Nevertheless, particularly environmental concerns are significant, and they may arise, such as blast-induced ground vibration, air over-pressure, flyrock, dust, and toxics [1-3]. As a matter of fact, about 20-30% of the generated energy from charged explosives is transmitted to the rock mass and producing fragmentations. The remaining energy is wasted and causes the above environmental effects [4-6]. Of those, blast-induced ground vibration is the most dangerous environmental impact of blasting. Beyond the fragmentation zone, the energy will be transferred to the seismic waves and propagate through the medium as elastic waves. It is also known as ground vibrations with the oscillating particles in the rocky environment in which they travel. Therefore, the intensity of ground vibration induced by blasting can be measured and evaluated by the peak particle velocity (PPV).

For measuring PPV, the aid seismographs were applied, and they provide the most accurate. Nevertheless, the field measurement method is costly, time-consuming, and requires the calibration of the seismographs correctly [7]. Hence, several scholars proposed empirical equations to estimate PPV [8-10]. However, these empirical methods have been recommended as low accuracy and neglect the influence of other parameters [11].

In recent years, artificial intelligence (AI) and soft computing have been widely introduced and applied for predicting PPV, especially in the theme of the Fourth Industrial Revolution [12, 13]. Many AI models were introduced and proposed to predict PPV with promising results. For example, Khandelwal and Singh [14] and Monjezi, Ghafurikalajahi and Bahrami [15] applied an artificial neural network (ANN) model for predicting PPV with the accuracies are pretty high. Khandelwal, Kankar and Harsha [16] also applied the support vector machine (SVM) model for the same purpose with a mean absolute error (MAE) of 0.257 and determination coefficient (R²) of 0.960. Hasanipanah, Faradonbeh, Amnieh, Armaghani and Monjezi [17] applied the classification and regression trees (CART) model for predicting PPV at a cooper mine in

Iran. They found that the CART model can predict PPV with a root-mean-squared error (RMSE) of 0.17 and R2 of 0.950. A new design of the SVM model optimized by a modified firefly algorithm (MFA) was also proposed by Chen, Hasanipanah, Rad, Armaghani and Tahir [18] for predicting PPV with an RMSE of 0.614 and R2 of 0.984. In another study, Nguyen, Drebenstedt, Bui and Bui [19] developed an AI model based on the hierarchical k-means clustering algorithm (HKM) and ANN models for predicting PPV with accuracy is approximately 97%. More recently, Qiu, Zhou, Khandelwal, Yang, Yang and Li [20] applied various metaheuristic algorithms, such as gray wolf optimization (GWO), whale optimization algorithm (WOA), and Bayesian optimization algorithm (BO), for optimizing the extreme gradient boosting (XGBoost) model in predicting PPV. Finally, they found that the WOA-XGBoost became the most reliable model with accuracy was approximately by 97%.

In this study, a modified version of the particle swarm optimization algorithm (MPSO) was considered to optimize the ANN model for predicting PPV in open pit mine, namely the MPSO-ANN model. For comparison purposes, two forms of empirical equations, namely United States Bureau of Mining (USBM) and U Langefors – Kihlstrom [21], were also developed to predict PPV and compared with the proposed MPSO-ANN model.

2. Study areas

Artificial neural network (ANN) is a soft computational system inspired by the human brain and its mechanisms [22]. It is a fact that there are many types of ANN in the AI environment; however, they often have a general structure with one input layer, hidden layer(s), and one output layer (Fig. 1).

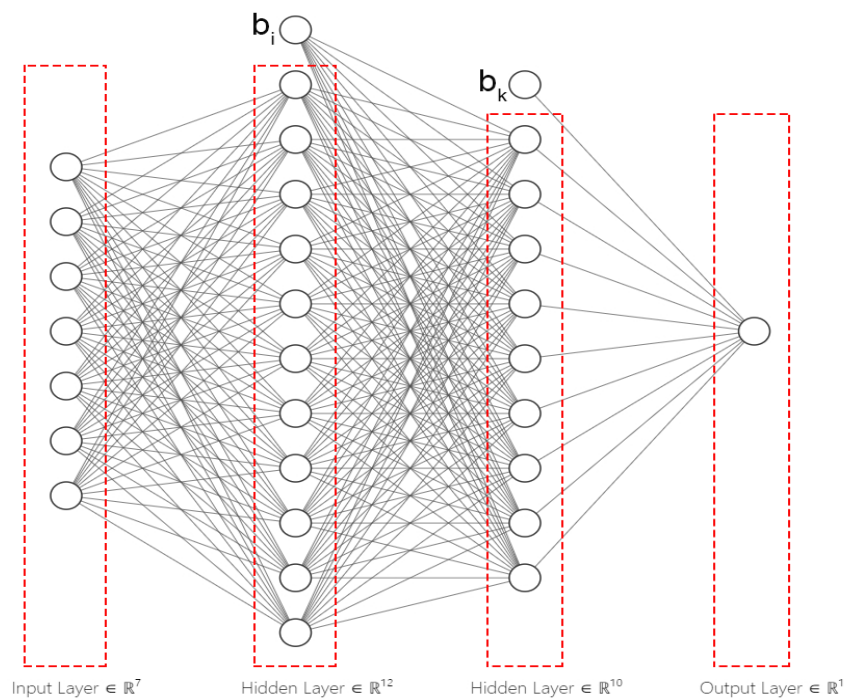


Fig. 1. General architecture of ANN model with one output variable.

The input layer contains input vectors that are gathered by the input neurons, and they are described as in Eq. (1). And then, they are transferred to the hidden layer based on the propagation law in Eq. (2).

$$X^p = (X_1^p, X_2^p, \dots, X_N^p)^T \tag{1}$$

$$S_i^p = \sum_{j=1}^N w_{ji} X_j^p + b_i \tag{2}$$

where N is the number of input variables (input neurons); w_{ji} denotes the weight between the j^{th} neuron in the input layer and the i^{th} neuron in the hidden layer; b_i stands for the bias related to the i^{th} neuron in the hidden layer.

Supposing the activation state of the i^{th} neuron in the hidden layer as the input vector function, then the output can be calculated as follows:

$$y_i^p = f(S_i^p) \tag{3}$$

To calculate the activation state of a neuron from the output layer, the following equation is applied:

$$S_k^p = \sum_{j=1}^L w_{ik} y_j^p + b_k \tag{4}$$

where L is the number of neurons in the hidden layer(s); w_{ik} denotes the weight between the i^{th} neuron in the hidden layer and the k^{th} neuron in the output layer; b_k stands for the bias related to the k^{th} neuron in the output layer.

The error of the network can be computed using the following equation:

$$E^p = \frac{1}{2} \sum_{k=1}^M (d_k^p - y_k^p)^2 \tag{5}$$

As mentioned above, there are many types of ANN, such as MLP neural net, GR neural net, RBF neural net, to name a few. They are often trained by gradient descent-based algorithms. In addition, activation functions, such as elu, relu, sigmoid, tanh, etc., are used to transfer data between layers of the network. In this study, the MLP neural net will be used to predict PPV at the Coc Sau open pit coal mine, Quang Ninh province, Vietnam.

3. Modified particle swarm optimization

PSO was firstly proposed by Kennedy and Eberhart [23] in 1995 based on the behaviors of swarms, such as birds flock, ant, fish, etc. The initial individuals (populations) are generated for each swarm, and each particle in a swarm acts as a searcher in a search space. For each position that is searched by a particle, a solution is defined for a given optimization problem.

Suppose that search space is generated with a D -dimensional space, the particle will fly around the search space with the position is presented by $X_i^d = [x_i^1, x_i^2, \dots, x_i^D]$, and the velocity is presented by $V_i^d = [v_i^1, v_i^2, \dots, v_i^D]$. During searching the optimal position, the particles always exchange their experiences and update their positions and velocities through the Eqs. (6, 7).

$$X_i^d(t + 1) = X_i^d(t) + V_i^d(t + 1) \tag{6}$$

$$V_i^d(t + 1) = V_i^d(t) + c_1 \times r_1 \times (P_{best_i}^d(t) - X_i^d(t)) + c_2 \times r_2 \times (G_{best}^d(t) - X_i^d(t)) \tag{7}$$

where t and $t + 1$ denote the current and the next iteration of the optimization process; P_{best} and G_{best} stand for the local best and global best of the particles; c_1 and c_2 are the positive acceleration coefficients; r_1 and r_2 are random values interval $[0, 1]$.

Although the original version of the PSO algorithm was recommended as a potential solution for optimization problems in engineering; however, it is easy to fall into local optimum in high-dimensional space and has a low convergence rate in the iterative process [24]. Thus, a modified version of the PSO algorithm (i.e., MPSO) has been proposed by adding the bird's weights during updating the particle's velocity [25]. Eq. (7) now can be modified as follows:

$$V_i^d(t + 1) = w(t)V_i^d(t) + c_1 \times r_1 \times (P_{best_i}^d(t) - X_i^d(t)) + c_2 \times r_2 \times (G_{best}^d(t) - X_i^d(t)) \tag{8}$$

With $w(t)$ is the weight of the bird at the current iteration, and it can be calculated using the following formula:

$$w(t) = w_{\max} - \frac{(w_{\max} - w_{\min})}{T_{\max}} \cdot t \tag{9}$$

where w_{\min} and w_{\max} are the minimum and maximum weights of the bird; T_{\max} is the maximum number of iterations.

The pseudo-code of the MPSO algorithm is presented in Fig. 2.

Algorithm: MPSO pseudo-code for the optimization process

```

1  for each particle i
2      for each dimension d
3          Initialize position  $x_{id}$  randomly within permissible range
4          Initialize velocity  $v_{id}$  randomly within permissible range
5      end for
6  end for
7  Iteration  $t = 1$ 
8  do
9      for each particle i
10         Calculate fitness value
11         if the fitness value is better than  $p\_best_{id}$  in history
12             Set current fitness value as the  $p\_best_{id}$ 
13         end if
14     end for
15     Choose the particle having the best fitness value as the  $g\_best_{id}$ 
16     for each particle i
17         for each dimension d
18             Calculate velocity according to the equation
19              $v_j^{i+1} = wv_j^{(i)} + (c_1 \times r_1 \times (local\ best_j - x_j^{(i)})) + (c_2 \times r_2 \times (global\ best_j - x_j^{(i)}))$ ,  $v_{\min} \leq v_j^{(i)} \leq v_{\max}$ 
20             Update particle position according to the equation
21              $x_j^{i+1} = x_j^{(i)} + v_j^{(i+1)}$ ;  $j = 1, 2, \dots, n$ 
22         end for
23     end for
24      $t = t + 1$ 
25 while maximum iterations or minimum error criteria are not attained

```

Fig. 2. The pseudo-code of the MPSO algorithm.

4. MPSO-ANN model

In this study, the MPSO algorithm will be applied to optimize the ANN model for predicting PPV. As introduced in section 2, the main unit of the ANN model is the weights between the neurons. Weights are often calculated and updated by the gradient descent-based algorithm (e.g., backpropagation algorithm), and it will decide the accuracy of the ANN model. However, the main disadvantages of the backpropagation algorithm are premature convergence and trapped to local optimum, and cannot escape [26, 27]. Therefore, the MPSO algorithm was applied to overcome these disadvantages of the backpropagation algorithm to train the ANN model.

For this aim, a number of populations (particles) will be generated first. Subsequently, their fitness was calculated and evaluated. Their fitness will be calculated and updated for each iteration to determine the best position (corresponding to the best solution). For each solution, a set of weights were generated and then imported to the ANN model. Finally, the error of the ANN model was calculated and evaluated through the objective function. During optimization of the ANN model by the MPSO algorithm, the maximum number of iterations is necessary to ensure the algorithm's convergence. To this end, the optimal MPSO-ANN model will be defined based on the lowest value of the objective function with the maximum iterations. The framework of the MPSO-ANN model for predicting PPV is proposed in Figure 3.

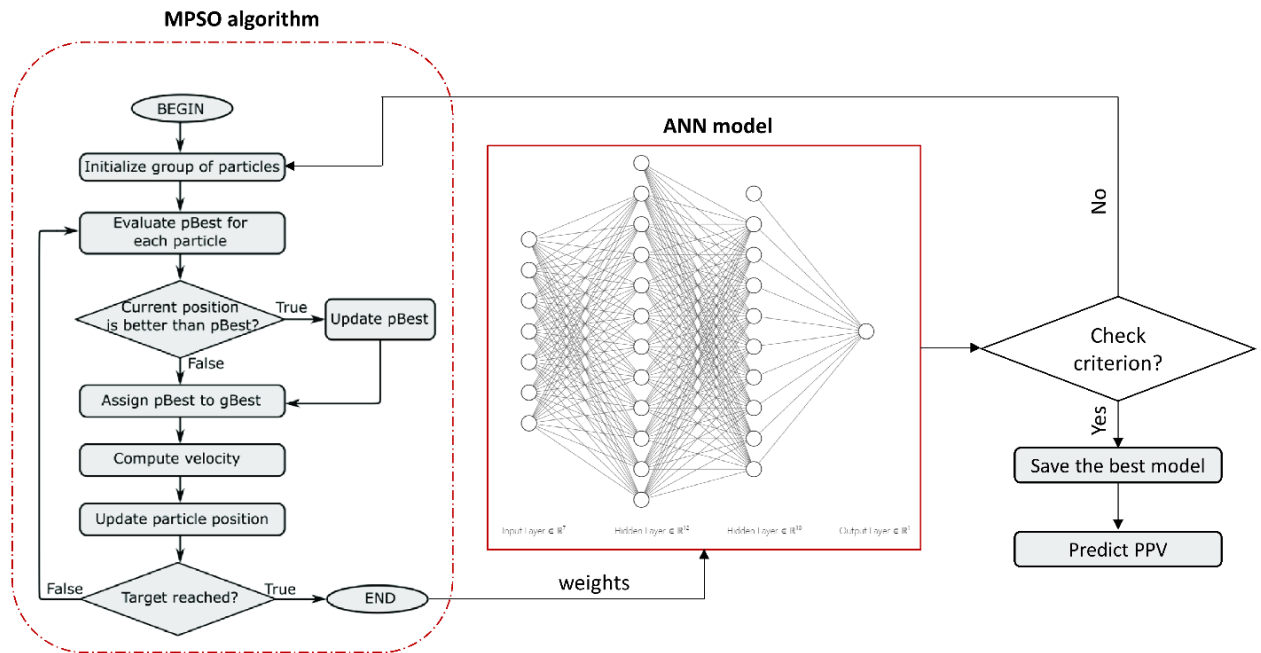


Fig. 3. The framework of the MPSO-ANN model for predicting PPV.

5. Case study

In this study, the Coc Sau open pit coal mine (Quang Ninh – Vietnam) was selected as a case study to investigate the feasibility of the HR model for predicting PPV. The location of the study site is shown in Fig. 4. The Coc Sau open-pit coal mine was covered entirely by sedimentary rocks of Late Triassic Hon Gai Formation (T_3n-rhg). The formation was composed of conglomerate, gritstone, sandstone, siltstone, claystone, shale, and coal seams [28]. In general, these sedimentary rocks are quite hard with the rock strength (f) of 8 to 10 [29]. Therefore, drilling-blasting is taken into consideration as an excellent method for the fragmentation of rock during exploiting coal of the mine. The boreholes diameter of 105 mm was applied for blasting herein with the ANFO explosive was used. Non-electric millisecond detonators were applied to fragment rocks herein. It is considered as an effectiveness blasting method and safety for the human, as well as the surrounding environment [30].

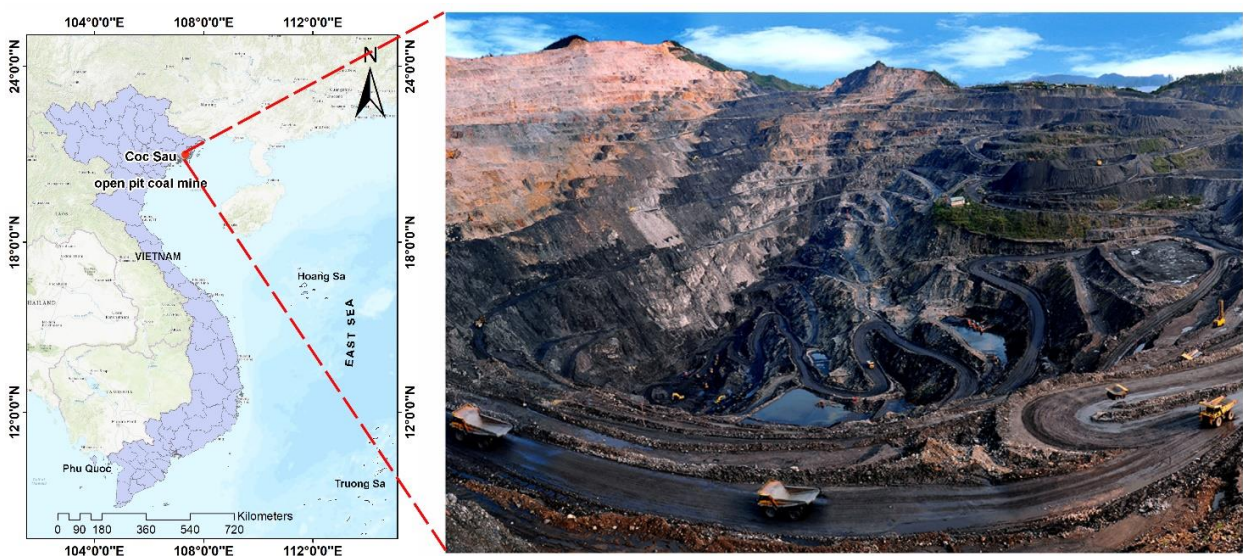


Fig. 4. Location of the Coc Sau open pit coal mine (Vietnam).

In this mine, the millisecond blasting method was applied to fragment rocks, with the ANFO was used

as the main explosive to charge into boreholes. In some boreholes which contain water, emulsion explosives were charged to prevent the pervasion of water to the explosive. To realize this study, 137 blasting events were gathered with three parameters were collected, including explosive charged per delay (Q), monitoring distance (D), and PPV. Of those, Q and D were used as the input variables, and PPV was considered as the output variable.

For the data collection, Q values were extracted from 137 blasting patterns, and D values were determined through the GPS devices that were used at the blast faces and seismograph points. The Micromate device (Instantel - Canada) was used for measuring PPV, and it was calibrated before measuring. The dataset used in this study is summarized in Table 1, and its characteristics are shown in Figure 5.

Tab. 1. Summary of the dataset used.

Q (Kg)	D (m)	PPV (mm/s)
Min. : 320	Min. : 182.0	Min. : 2.25
1st Qu.: 2517	1st Qu.: 326.2	1st Qu.: 8.14
Median : 3276	Median : 408.8	Median : 12.25
Mean : 3184	Mean : 436.4	Mean : 12.57
3rd Qu.: 3845	3rd Qu.: 523.0	3rd Qu.: 16.01
Max. : 6043	Max. : 715.0	Max. : 28.63

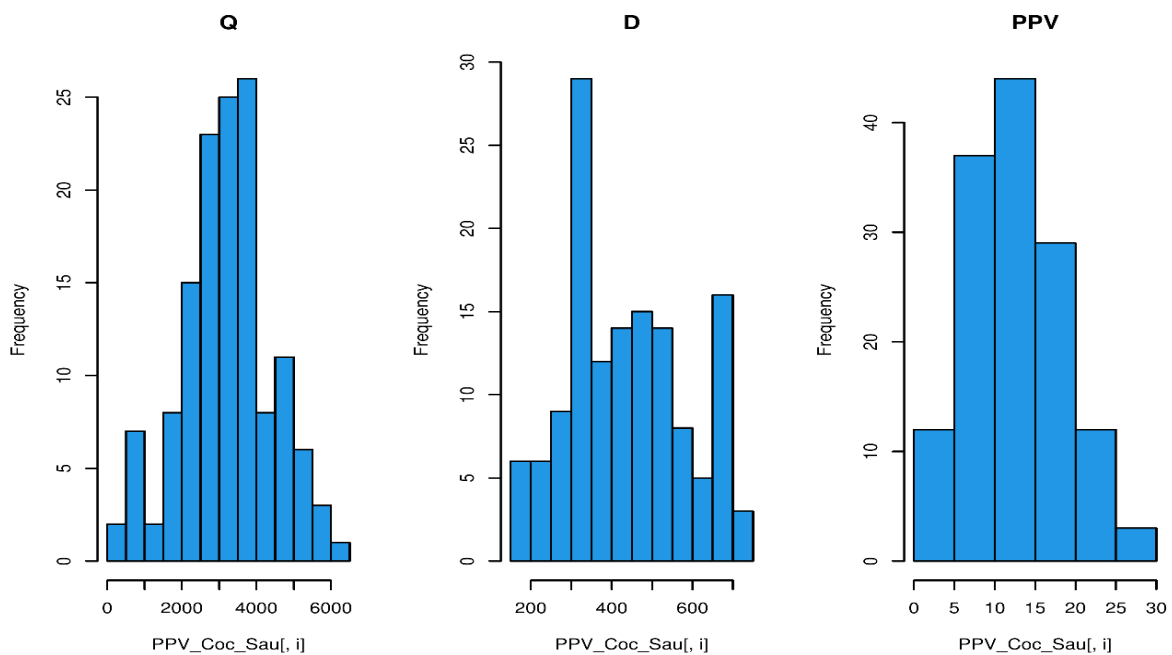


Fig. 5. Histogram of the dataset used.

6. Results and discussion

Before developing the MPSO-ANN model, the dataset was pre-processed aiming to normalize the dataset and improve the performance of the learning of the model. Accordingly, the dataset was divided into two sections: one section contains 70% of the whole dataset for training the MPSO-ANN model, the remaining section contains 30% of the datasets for testing the accuracy of the developed MPSO-ANN model. In order to improve the accuracy of the model, the dataset was normalized interval [0,1]. Subsequently, the proposed framework in Figure 3 was applied to develop the MPSO-ANN model.

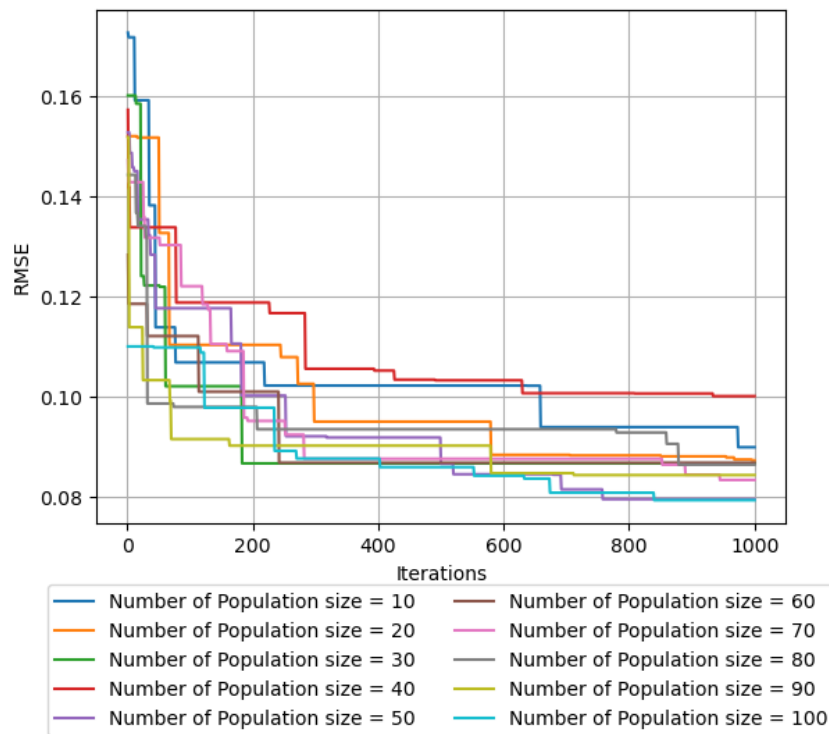


Fig. 6. Training performance of the MPSO-ANN model.

As an optimizer during training the ANN model, the MPSO algorithm was set up first with the following parameters: $c_1 = c_2 = 1.2$; w_{min} ; w_{max} . A different number of populations in the range of 10 to 100 were considered while searching the optimal weights of the ANN model. The searching process was implemented within 1000 iterations. For each MPSO-ANN model developed based on a set of parameters, the performance metrics, such as MAE, RMSE, and R^2 , were computed on both training and testing datasets. Finally, the best MPSO-ANN model was defined based on the performances on both training and testing datasets.

For comparison purposes, empirical equations were considered and developed to predict PPV based on the same datasets. Empirical equations are considered the most straightforward method for predicting PPV in open pit mines. They are often used to express the relationship between the explosive charged and monitoring distance. The first empirical equation was proposed by Duvall and Petkof [8] and used by the United States Bureau of Mining (USBM), as follows:

$$PPV = k \left(\frac{D}{Q^{1/2}} \right)^b \tag{10}$$

where D is the monitoring distance from the blast faces to the seismograph, m; Q is the explosive charged per delay (or per blast), Kg; k and b denote the site coefficients, and they are different in various areas.

Based on the USBM empirical equation, U Langefors and Kihlstrom (1963) proposed an alternative empirical equation, as described in Eq. (11).

$$PPV = k \left(\frac{D}{Q^{1/3}} \right)^b \tag{11}$$

In addition, there are several empirical equations have been proposed based on the relation between blasting parameters and geological conditions and rock properties [31-34]. Nevertheless, due to the lack of geological and geotechnical information, these empirical equations cannot be applied in many cases. In this study, we used Eqs. (10-11) to estimate PPV due to the lack of geological conditions and rock properties, as mentioned above. Based on the original training and testing datasets, the empirical equations for estimating PPV at the Coc Sau open pit coal mine were defined as described in Eqs. (12-13).

- According to the USBM equation form:

$$PPV = 61.756 \left(\frac{D}{Q^{1/2}} \right)^{-0.837} \tag{12}$$

- According to the U Langefors and Kihlstrom (1963) equation form:

$$PPV = 267.752 \left(\frac{D}{Q^{1/3}} \right)^{-0.943} \tag{13}$$

Once the MPSO-ANN and empirical models were well-trained and defined, the training and testing datasets were applied to predict PPV, and their performances were evaluated through three performance metrics MAE, RMSE, and R², which are calculated according to the following equations:

$$MAE = \frac{1}{n} \sum_{i=1}^n |y_i - \hat{y}_i| \tag{14}$$

$$RMSE = \sqrt{\frac{1}{n} \sum_{i=1}^n (y_i - \hat{y}_i)^2} \tag{15}$$

$$R^2 = 1 - \frac{\sum_{i=1}^n (y_i - \hat{y}_i)^2}{\sum_{i=1}^n (y_i - \bar{y})^2} \tag{16}$$

where *n* is the number of blasting events used to calculate the performance; *y_i*, *ŷ_i* stand for the measured and predicted PPVs, *ȳ* denotes the mean of the measured PPVs. The performances of the models are computed in Table 2.

Tab. 2. Performance metrics of the MPSO-ANN and empirical models.

Model	Training dataset			Testing dataset		
	MAE	RMSE	R ²	MAE	RMSE	R ²
MPSO-ANN	1.577	1.968	0.880	1.217	1.456	0.956
USBM	1.870	2.241	0.830	1.830	2.268	0.874
U Langefors and Kihlstrom	2.047	2.443	0.804	2.012	2.464	0.852

As listed in Table 2, it is conspicuous that the proposed MPSO-ANN model yielded superior performance to the empirical models. Whereas the MAE of the MPSO-ANN model is only 1.577 and 1.217 on the training and testing datasets, it is 1.870 and 1.830 on the training and testing datasets for the USBM model, and 2.047 and 2.012 on the training and testing datasets for the U Langefors and Kihlstrom model. The RMSE of the MPSO-ANN model is also better than those of the empirical models, specifically, RMSE = 1.968 and 1.456 on the training and testing datasets. Meanwhile, these values are higher for the USBM and U Langefors and Kihlstrom models, i.e., RMSE = 2.241 and 2.268 for the USBM model; RMSE = 2.443 and 2.464 for the U Langefors and Kihlstrom model on the training and testing datasets, respectively. Remarkably, R² values in Tab. 2 indicated that the dataset was more fit to the proposed MPSO-ANN model with R² = 0.880 on the training dataset and R² = 0.956 on the testing dataset. In contrast, it is in the range of 0.804 to 0.830 on the training dataset, 0.852 to 0.874 on the testing datasets for the empirical models. Fig. 7 interprets the correlation between the measured and predicted PPVs by the MPSO-ANN and empirical models for further discussion.

As depicted in Figure 7, it can be seen that the proposed MPSO-ANN model provided a better correlation between the measured and predicted PPVs. In other words, the predicted PPVs are closer to the actual PPVs than those of the predicted PPVs by the empirical models

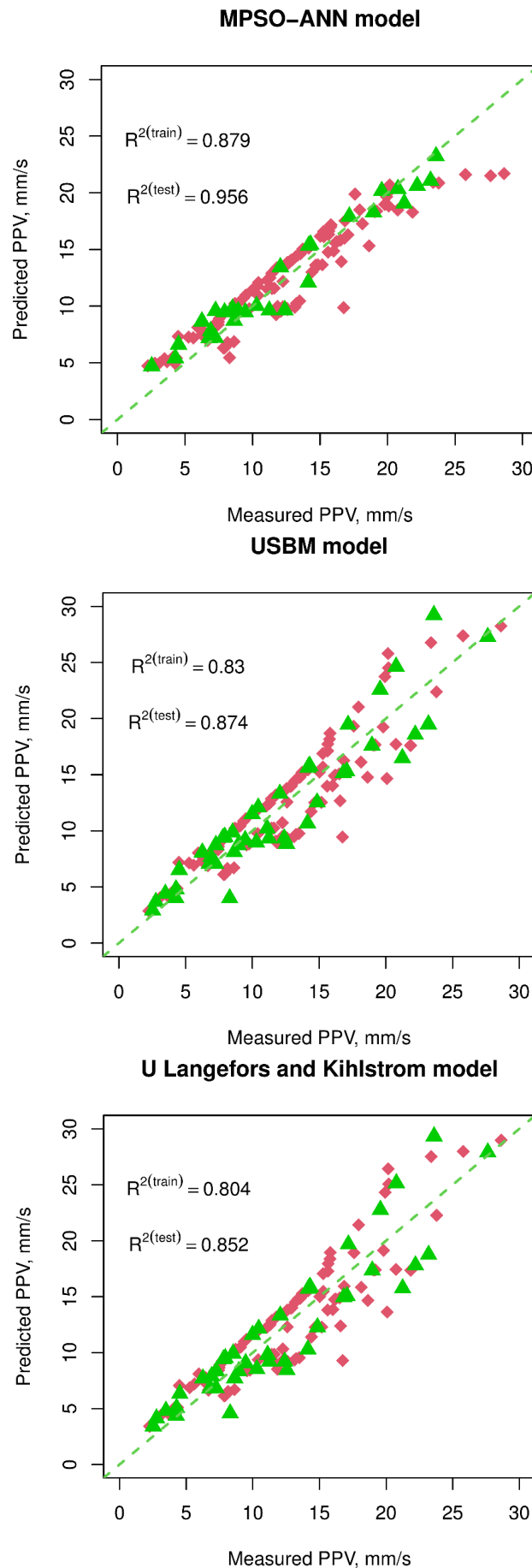


Fig. 7. Correlation between measured and predicted PPVs by the MPSO-ANN and empirical models.

7. Conclusion

Blasting is a crucial stage in open-pit mines even though its adverse effects are significant, especially is the blast-induced ground vibration. The problem now is how to predict, control, and mitigate the intensity of blast-induced ground vibration (i.e., PPV), as well as its side effects on the surrounding environment. This study developed a hybrid AI model, namely MPSO-ANN, for predicting PPV, and it was tested at the Coc Sau open-pit coal mine as a case study. The results showed that the developed MPSO-ANN model could predict PPV with high accuracy than the traditional empirical equations. Based on the developed MPSO-ANN model, the explosive charged per delay can be adjusted to control the PPV induced. This can contribute to reducing the undesirable effects on the surrounding environment in open pit mines.

8. Acknowledgments

This research is funded by Vietnam National Foundation for Science and Technology Development (NAFOSTED) under grant number 105.99-2019.309.

The paper was presented during the 6th VIET - POL International Conference on Scientific-Research Cooperation between Vietnam and Poland, 10-14.11.2021, HUMG, Hanoi, Vietnam.

9. References

1. X.-N. Bui, Y. Choi, V. Atrushkevich, H. Nguyen, Q.-H. Tran, N.Q. Long, H.-T. Hoang, Prediction of Blast-Induced Ground Vibration Intensity in Open-Pit Mines Using Unmanned Aerial Vehicle and a Novel Intelligence System, *Natural Resources Research*, 29 (2020) 771-790.
2. X.-N. Bui, P. Jaronpattanapong, H. Nguyen, Q.-H. Tran, N.Q. Long, A novel Hybrid Model for predicting Blast-induced Ground Vibration Based on k-nearest neighbors and particle Swarm optimization, *Scientific reports*, 9 (2019) 1-14.
3. H. Nguyen, Support vector regression approach with different kernel functions for predicting blast-induced ground vibration: a case study in an open-pit coal mine of Vietnam, *SN Applied Sciences*, 1 (2019) 1-10.
4. H. Nguyen, N.X. Bui, H.Q. Tran, G.H.T. Le, A novel soft computing model for predicting blast - induced ground vibration in open - pit mines using gene expression programming, *Journal of Mining and Earth Sciences*, 61 (2020) 107-116.
5. A.D. Nguyen, B.V. Nhu, B.D. Tran, H.V. Pham, T.A. Nguyen, Definition of amount explosive per blast for spillway at the Nui Mot lake - Binh Dinh province, *Journal of Mining and Earth Sciences*, 61 (2020) 117-124.
6. H.Q. Tran, N.X. Bui, H. Nguyen, T.A. Nguyen, L.Q. Nguyen, Applicable possibility of advanced technologies and equipment in surface mines of Vietnam (in Vietnamese), *Journal of Mining and Earth Sciences*, 61 (2020) 16-32.
7. A.I. Lawal, S. Kwon, O.S. Hammed, M.A. Idris, Blast-induced ground vibration prediction in granite quarries: an application of gene expression programming, ANFIS, and sine cosine algorithm optimized ANN, *International Journal of Mining Science and Technology*, 31 (2021) 265-277.
8. W.I. Duvall, B. Petkof, Spherical propagation of explosion-generated strain pulses in rock, US Department of the Interior, Bureau of Mines 1958.
9. N. Ambraseys, *Rock Mechanics in Engineering Practice*, 1968.
10. U. Langefors, B. Kihlström, *The modern technique of rock blasting*, Wiley New York 1963.
11. H. Nguyen, X.-N. Bui, A Novel Hunger Games Search Optimization-Based Artificial Neural Network for Predicting Ground Vibration Intensity Induced by Mine Blasting, *Natural Resources Research*, (2021).
12. N.X. Bui, G.S. Ho, Vietnamese Surface Mining - Training and scientific research for integrating the Fourth Industrial Revolution, *Journal of Mining and Earth Sciences*, 61 (2020) 1-15.

13. B.D. Tran, T.D. Vu, V.V. Pham, T.A. Nguyen, A.D. Nguyen, G.H.T. Le, Developing a mathematical model to optimize long - term quarrying planing for limestone quarries producing cement in Vietnam, *Journal of Mining and Earth Sciences*, 61 (2020) 58-70.
14. M. Khandelwal, T. Singh, Prediction of blast-induced ground vibration using artificial neural network, *International Journal of Rock Mechanics and Mining Sciences*, 46 (2009) 1214-1222.
15. M. Monjezi, M. Ghafurikalajahi, A. Bahrami, Prediction of blast-induced ground vibration using artificial neural networks, *Tunnelling and Underground Space Technology*, 26 (2011) 46-50.
16. M. Khandelwal, P.K. Kankar, S.P. Harsha, Evaluation and prediction of blast induced ground vibration using support vector machine, *Mining Science and Technology (China)*, 20 (2010) 64-70.
17. M. Hasanipanah, R.S. Faradonbeh, H.B. Amnieh, D.J. Armaghani, M. Monjezi, Forecasting blast-induced ground vibration developing a CART model, *Engineering with Computers*, 33 (2017) 307-316.
18. W. Chen, M. Hasanipanah, H.N. Rad, D.J. Armaghani, M. Tahir, A new design of evolutionary hybrid optimization of SVR model in predicting the blast-induced ground vibration, *Engineering with Computers*, (2019) 1-17.
19. H. Nguyen, C. Drebenstedt, X.-N. Bui, D.T. Bui, Prediction of Blast-Induced Ground Vibration in an Open-Pit Mine by a Novel Hybrid Model Based on Clustering and Artificial Neural Network, *Natural Resources Research*, 29 (2020) 691-709.
20. Y. Qiu, J. Zhou, M. Khandelwal, H. Yang, P. Yang, C. Li, Performance evaluation of hybrid WOA-XGBoost, GWO-XGBoost and BO-XGBoost models to predict blast-induced ground vibration, *Engineering with Computers*, (2021) 1-18.
21. U. Langefors, B. Kihlstrom, *The Modern Techniques of Rock Blasting*, JohnWiley and Sons Inc., New York, 1963.
22. A. Krogh, What are artificial neural networks?, *Nature biotechnology*, 26 (2008) 195-197.
23. J. Kennedy, R. Eberhart, Particle swarm optimization, *Proceedings of ICNN'95-international conference on neural networks*, IEEE, 1995, pp. 1942-1948.
24. M. Li, W. Du, F. Nian, An adaptive particle swarm optimization algorithm based on directed weighted complex network, *Mathematical problems in engineering*, 2014 (2014).
25. M. Dorigo, M.A.M. de Oca, A. Engelbrecht, Particle swarm optimization, *Scholarpedia*, 3 (2008) 1486.
26. S. Yu, K. Zhu, F. Diao, A dynamic all parameters adaptive BP neural networks model and its application on oil reservoir prediction, *Applied mathematics and computation*, 195 (2008) 66-75.
27. M. Li, X. Huang, H. Liu, B. Liu, Y. Wu, A. Xiong, T. Dong, Prediction of gas solubility in polymers by back propagation artificial neural network based on self-adaptive particle swarm optimization algorithm and chaos theory, *Fluid Phase Equilibria*, 356 (2013) 11-17.
28. X.-N. Bui, C.W. Lee, H. Nguyen, H.-B. Bui, N.Q. Long, Q.-T. Le, V.-D. Nguyen, N.-B. Nguyen, H. Moayedi, Estimating PM10 Concentration from Drilling Operations in Open-Pit Mines Using an Assembly of SVR and PSO, *Applied Sciences*, 9 (2019) 2806.
29. M. Protodiakonov, M. Koifman, S. Chirkov, M. Kuntish, R. Tedder, *Rock strength passports and methods for their determination*, Nauka, Moscow, 1964.
30. Q. Gao, W. Lu, P. Yan, H. Hu, Z. Yang, M. Chen, Effect of initiation location on distribution and utilization of explosion energy during rock blasting, *Bulletin of Engineering Geology and the Environment*, 78 (2019) 3433-3447.
31. C. Kuzu, The mitigation of the vibration effects caused by tunnel blasts in urban areas: a case study in Istanbul, *Environmental geology*, 54 (2008) 1075-1080.
32. R. Nateghi, Prediction of ground vibration level induced by blasting at different rock units, *International Journal of Rock Mechanics and Mining Sciences*, 48 (2011) 899-908.

33. R. Kumar, D. Choudhury, K. Bhargava, Determination of blast-induced ground vibration equations for rocks using mechanical and geological properties, *Journal of Rock Mechanics and Geotechnical Engineering*, 8 (2016) 341-349.
34. G. Paneiro, F. Durão, M.C. e Silva, P.F. Neves, Prediction of ground vibration amplitudes due to urban railway traffic using quantitative and qualitative field data, *Transportation Research Part D: Transport and Environment*, 40 (2015) 1-13.

Integration of Delphi Technique and Analytical Hierarchy Process Method in Assessment the Groundwater Potential Influence Criteria: A Case Study of the Ba River Basin

DANG Tuyet Minh^{1,*}, NGUYEN Le Tung Duong²

¹ Thuyloi University, Department of Surveying, Hanoi, Vietnam

²Vietnam National University, Hanoi, Vietnam

Corresponding author: dtminh@tlu.edu.vn

Abstract. Water is a boon for all living beings over the world and groundwater is considered one of the indispensable natural sources of potable water. It is necessary to assess and predict the groundwater potential to provide insights for decision-makers for proper planning and management of groundwater. The occurrence of groundwater depends on hydrological, ecological, climate, geological, and physiographical criteria. The purpose of the present study is to choose and attribute scores to all various factors that affected groundwater prospects in the Ba river basin. Firstly, the Delphi method was applied in the expert-based survey to choose six parameters that are considered as influencing factors, namely, lineament density, rainfall, slope, land cover, drainage density, and geology. Then, the weights for the various factors were generated using the Analytic Hierarchy Process (AHP) approach which allows the pairwise comparison of criteria influencing the potential areas. The consistency analyses show that the findings were consistent with a previous study. The consistency and sensitivity analyses showed that the obtained results were coherent, providing the weight vector of the achievable criteria that affect the groundwater prospect in the study area. The study reveals that lineament density and slope are criteria affecting the most prominent groundwater occurrence with 35.1% and 20.1%, respectively. However, the influence of other factors (rainfall, land cover, drainage density, and geology) is not visible. These criteria are assigned to the small weights and do not have a significant influence on the groundwater potential. The study results provide baseline information, which needs to be taken into account to control and manage groundwater potentiality.

Keywords: Ba river basin, AHP method, Delphi technology, Groundwater, Groundwater potential

1. Introduction

Water covers approximately 71% of the Earth's surface. However, there is a serious shortage of freshwater for drinking, agriculture, industries, and other purposes because 97% of the water on the earth is found in the oceans and seas, about 2% of water is in glaciers in the polar region, and remaining 1% is found in some forms of stream channels and groundwater [1]. The main sources of freshwater are only stream channels and groundwater. According to Ahmadi et al. (2021), groundwater potential supplies almost 30% of freshwater globally, and in general, 65% of groundwater is used for agricultural irrigation, 25% as drinking water, and the remaining 10% is utilized as industrial water [2]. Therefore, groundwater, which is stored in the subsurface geological formations, is one of the Nations' most important natural resources. In Vietnam, groundwater provides the water supply for more than half of Viet Nam's population. More than one-third of the urban population is dependent on groundwater, and almost two-thirds of the rural population [3]. It serves as a natural source for domestic, industrial, and agricultural uses and other developmental initiatives. With exponential growth in population and industrialization, overexploitation of groundwater has been made in many regions, which has contributed to subsequent declination in the groundwater level. Today, many areas around the world are facing a possibility of water scarcity, and shortly, the freshwater sources will depend more on available groundwater resources. The ever-increasing requirement of freshwater for meeting human demands and developments has imposed immense pressure on this limited freshwater resource. Hence, the management of freshwater is very significant to prevent severe water scarcity in arid and semi-arid regions [4] because groundwater remains the ultimate freshwater resource while sources of surface water have been depleted.

The occurrence, distribution, and availability of groundwater are dependent on the various natural and anthropogenic factors. Climate change severely affects the parameters influencing groundwater recharge. Hence, it is necessary to identify and understand which criteria cause groundwater level degradation and what the consequences can be. Different scientists have utilized various parameters for studying groundwater prospects such as Geomorphology, Lineament, Geology, Groundwater Depth, Drainage

Density, Soil, Land use/ Landover, Rainfall, slope, Distance from River, Fault Density, Lithology, Stream Frequency, Relief Ratio, Soil Depth, etc. [5-10]. However, it is rare to combine all criteria because of the non-availability of data. Hence, a sincere evaluation of these factors can give a clear understanding of the groundwater prospect of an area. In addition, assessment of these elements develops a general knowledge concerning the importance of every criterion for groundwater potential in different regions around the world [8]. This proves that determining the dominant influencing factors of groundwater recharge potential and assessing their important information of this rare natural source is indispensability. In other words, it is necessary to identify the major factors affecting groundwater recharge and how to quantify these factors. Using the Delphi-AHP method to survey critical parameters affecting groundwater occurrence and assess their importance in declining groundwater levels has been extensively utilized in groundwater potentiality relevant research.

According to Keeney et al. (2001), although sometimes the reliability of the results obtained from a Delphi method may increase some controversy because of the inappropriate design and study execution, such as shortcomings of the survey instrument, poor choice of experts, weak bias control, unreliable analyses, and limited feedback during the research [11], this approach remains a particularly useful option for the situation when objective data are unapproachable, there is a lack of empirical evidence, or experimental study is not realistic or dishonest [12]. The present study intends to detect prominent factors resulting in the degradation of groundwater level using a Delphi method. It also employs the AHP technique to determine the significance of the criteria in comparison with each other. The combined Delphi-AHP approach is also used in the detection of flood influence criteria in an ungauged basin in Brazil [13], in the identification of factors affecting flood hazard in Lam river basin [14] or in determining the weight of each index used to identify the flood-prone areas of Angkor, Cambodia [15] and the flood hazard potential zone of Nghe An and Ha Tinh province, Vietnam [16]. It is worth saying that the AHP approach is successfully used for solving various problems in groundwater management worldwide [5-10]. This technique is assessed as an effective tool in the determination of the relative importance weight for each hierarchy element [5-10, 13, 15]. With the ability to handle both qualitative and quantitative data as well as the flexibility of the model, the AHP is considered as a powerful tool in calculating the weights of each factor using pairwise comparison matrix basis of judgment formation to support in generating groundwater potentiality maps with a good degree of accuracy. This study has two research objectives: (1) identify the essential factors affecting groundwater occurrence; (2) determine the perceived relative importance of these criteria. To achieve the objectives, this study employed both Delphi and analytic hierarchy process techniques. Delphi can generate new, valuable and reasonable ideas from the respondents, free from group intervention, and strengthening the research validity by enabling a heterogeneity of panelists to contribute without the restriction of geographical distance. AHP is a mathematical technique for pairwise comparisons of multi-criteria, providing relative weights based on the importance of each parameter. It is believed that the results of this study may be considered as a great database for planning and management for groundwater in the study area.

2. Research area

The Ba river basin is the largest river in central Vietnam with a 14×10^3 km² drainage area, 390 km length and the river density is about 0.22 km/km² [17]. The Ba river basin is located in the central region of Vietnam and has an L-shaped shape. The study area lies approximately between 12°35'N to 14°38' N latitude and 108°00'E to 109°55' E longitude. The study area belongs to the administrative boundaries of 20 districts and one city of the three provinces in Central Highlands including Kon Tum, Gia Lai, Daklak, and the Southern Central coastal province of Phu Yen. The highland part of the Ba River drainage basin lies mainly on the central highlands of Vietnam, which includes series of contiguous plateaus with an average elevation of about 800m [18].

The rainfall increases from low to high regions and distributes unevenly in parts of the basin. Annually, the area receives a mean rainfall of 1740 mm. Along the river valley, there is a quite small rainfall, especially in Cheo Reo and Phu Tuc areas where the average annual rainfall does not exceed 1300 mm, meanwhile, the average annual rainfall can reach around 3000 mm upstream of Ba river and Hinh river. The air temperature increases gradually from north to south, from west to east, and from high to low region. The average annual temperature in the uplands is 21.5 – 23.5°C, in the midland region is 25 - 26°C, and in the downstream area is 21 – 26°C. In the Ba river basin, air humidity is closely related to air temperature

and precipitation. In the rainy season, the humidity can reach 80 - 90% but this value is only from 70 - 80% in the dry season months. The lowest air humidity can even be as low as 15-20% [18].

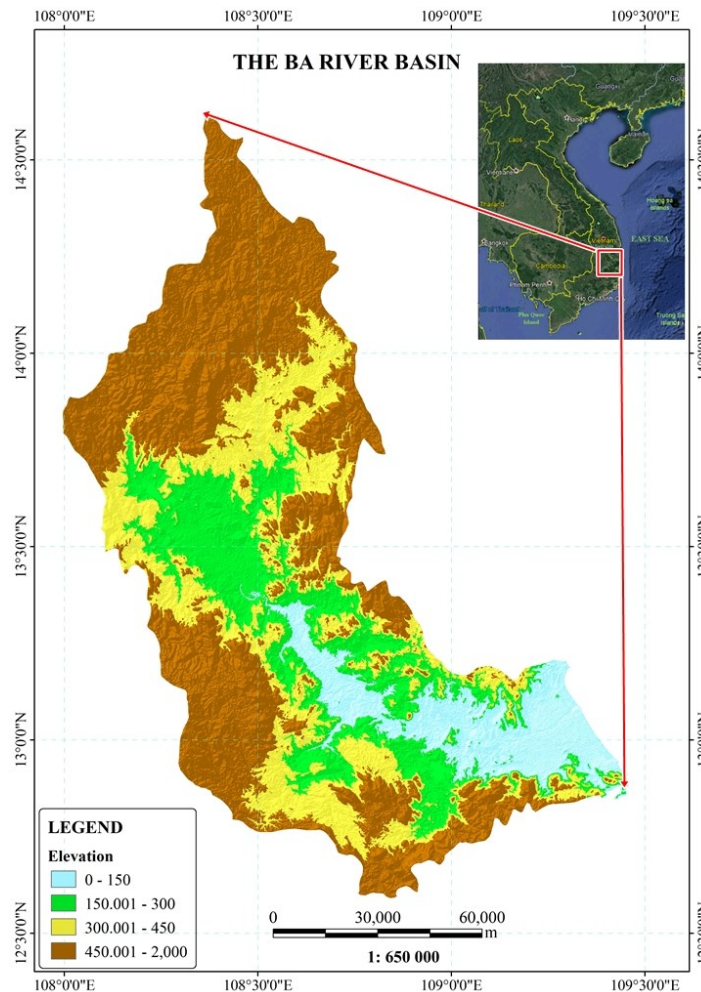


Fig. 1. Ba river basin

3. Methodology and Data

3.1 Methodology

The occurrence and movement of groundwater in an area are governed by several factors such as lithology, geological structures, soil, lineament features, slope, drainage pattern, geomorphology, land use/land cover, etc., and the interrelationship between these factors [19]. These can be divided into three following groups:

Group 1: physical geography factors, for example, lineament features, geological structures rainfall, slope, elevation, drainage density, geomorphology, etc.

Group 2: socio-economy factors, for example, land use, land cover, population density, etc.

Group 3: infrastructure factors, for example, irrigation facilities, reservoirs, etc.

In the groundwater potential zone determination studies, many factors related to groundwater storage based on geologic, hydrologic, hydrogeological, meteorological, and terrain features were used as decision criteria for analyzing groundwater potentiality. According to Yıldırım (2021), selecting the criteria influencing groundwater storage potential depends on the conditions of the region and available data [20]. This paper applies the Delphi method to determine the main factors affecting groundwater occurrence and uses the AHP approach to determine the weights of these main criteria. The combination of Delphi and AHP can determine weight values and increase the objectivity and accuracy of indicators and their relevant variables [21]. The model for the selection of parameters influencing the groundwater potential and

assessment of their importance consisted of three stages: (1) identification of the criteria to be used in the model for evaluating the level of influence using the Delphi technique, b) AHP computation, and c) evaluation of alternatives to determine the final ranking. AHP was applied to give weights and to find the importance degree of each criterion. In the third stage, a ranking of alternatives was done. Fig. 2 shows a flow chart of the study

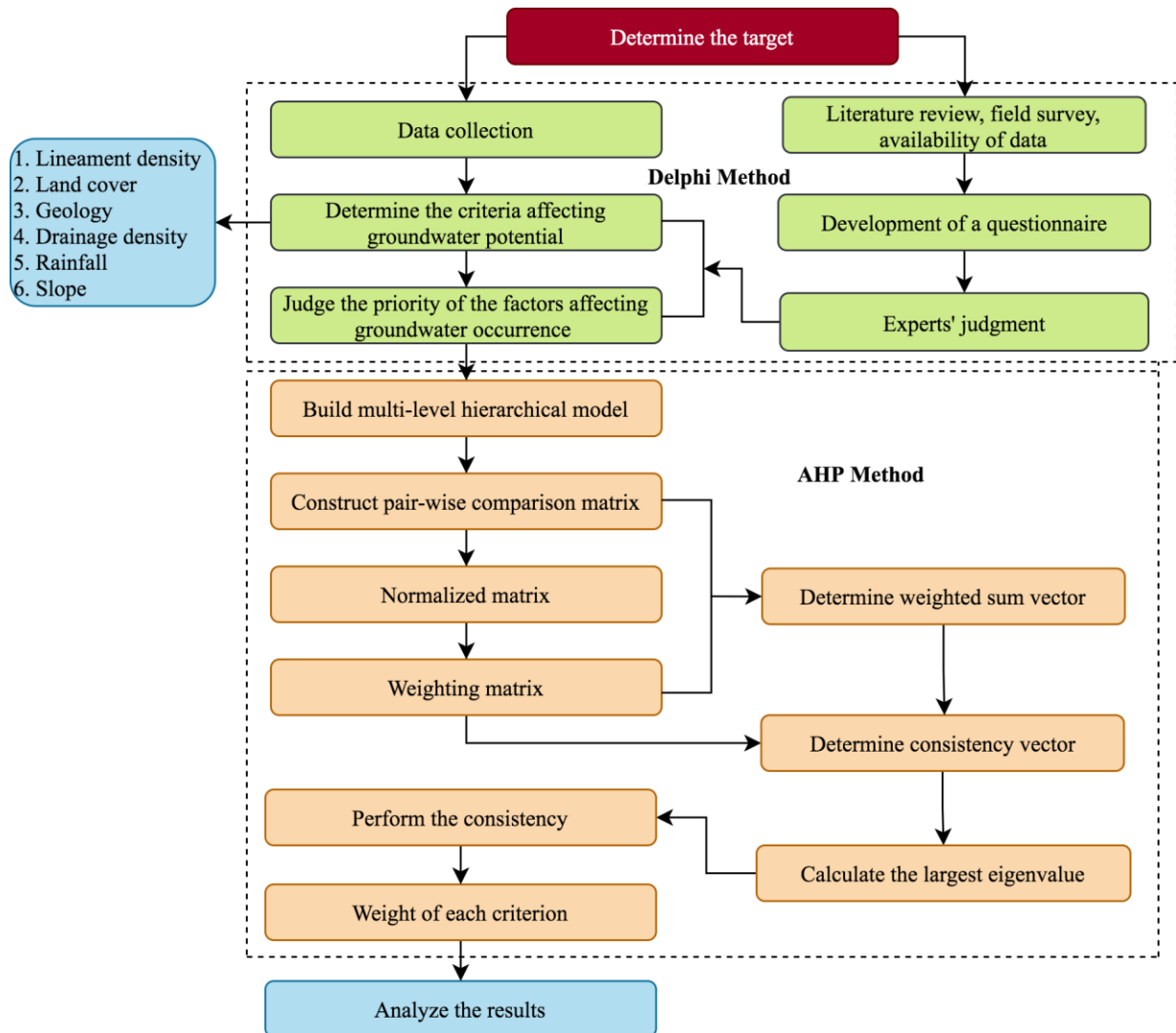


Fig. 2. Flow chart of the study

3.1.1 Delphi method

The Delphi technique was first developed by RAND Corporation in the United States in the 1950s. This technique has been depicted as a method well-suited for consensus-building through the utilization of a series of questionnaires distributed using multiple iteration processes to collect data from a panel of selected experts [22]. It is considered as a qualitative, long-range forecasting approach by some or a mixture of both qualitative and quantitative techniques by some others [23]. This method has been used in a variety of applications, such as planning, environmental impact assessment, social policy, flood hazard, and public health. The wide use of this technique has led to significant deviations from the original technique and the creation of a family of Delphi-related processes [24]. However, the Delphi technique has not yet been widely used in the determination of groundwater potentiality. Since this method is an iterative process designed to achieve consensus among a group of experts on a particular topic, the Delphi approach is the most effective means of querying experts to identify factors causing groundwater decline and depletion. The Delphi method comprises the following steps [25]:

- (1) Design the questionnaire and select the experts

- (2) Perform the first-round survey of anonymous experts
- (3) During the first round survey, provide the experts with the opinion of the others
- (4) According to the survey of the first round, request that each expert answer again the first round problem while observing whether new solutions are proposed or different perspectives are set forth.
- (5) Synthesize expert opinion and reach a consensus
- (6) Repeat steps (3) and (4) until a uniform result is achieved for a particular topic [25].

According to Song et al., the principle of selecting the questionnaire respondents is that they are expected to be professionals with the following qualifications: (1) Relevant education background; [26] (2) Practical experience and abundant expertise in geomorphology, geology, geography, hydrology, water resources, geomatics, soil, environment, metrological; Having been in the relevant fields for a long time and relevant qualification.

3.1.2 AHP method

AHP approach, developed by Saaty (1980), has been studied extensively and used in several applications for many years [27]. The wide AHP applicability is because of its simplicity, ease of use, and great flexibility. The AHP methodology primarily consists of (1) structure the decision into objectives and alternatives; (2) measure objectives and alternatives using pairwise comparison; (3) synthesize objectives; and (4) exploit subjective inputs to reach a prioritized list of alternatives [28].

In the first stage, the assessment criteria were identified and finalized by the Delphi method. Next, the decision hierarchy was created with the main criteria and alternatives. In this stage, the objective was at the first level, criteria at the second, and then ranking of alternatives at the third level of the hierarchy. In the generation of hierarchical structures, it should be noted that human perception is limited. According to George Miller, people can generally deal with seven facts at once, plus or minus two [29]. Therefore, in the AHP approach, several criteria at a given hierarchical level as well as the number of hierarchical levels themselves, for a given study issue should range from 5 to 9 criteria. The number of factors outside that range will lead to an unreliable evaluation. This study mentioned six factors as the main causative parameters for the groundwater decline which are related to the first group, physical geography.

Tab. 1. Fundamental scale of Saaty

Importance	Definition	Explanation
1	Equal importance	Two activities contribute equally to the objective
3	Moderate importance	Experience and judgment slightly favor one over another
5	Strong importance	Experience and judgment strongly favor one over another
7	Very strong importance	Activities are strongly favored and their dominance is demonstrated in practice
9	Extreme importance	Importance of one over another affirmed on the highest possible order
2, 4, 6, 8	Intermediate values	Used to represent a compromise between the priorities listed above

The elements used in groundwater potential assessment would be weighted using AHP in the next step. For this, a pairwise comparison matrix was created to calculate the factors' weights and determine their rankings. To determine the values of the parameters of pairwise comparison matrices A, let C_1, C_2, \dots, C_n denote the set of elements, while a_{ij} represents a quantified judgment on a pair of elements C_i and C_j . The relative importance of the two elements is rated using a Saaty's scale with the values are presented in Table 1 [27]. This yields an $n \times n$ matrix A as follows:

$$A = [a_{ij}] = \begin{matrix} C_1 & \begin{bmatrix} 1 & a_{12} & \dots & a_{1n} \\ 1/a_{12} & 1 & \dots & a_{2n} \\ \dots & \dots & \dots & \dots \\ C_n & 1/a_{1n} & 1/a_{2n} & \dots & 1 \end{bmatrix} \end{matrix} \tag{1}$$

where, $a_{ii} = 1$; $a_{ji} = \frac{1}{a_{ij}}$; $a_{ij} \neq 0$; $i, j = 1, 2, 3, \dots, n$. In matrix A, the problem becomes assigning to the n elements C_1, C_2, \dots, C_n a set of numerical weights W_1, W_2, \dots, W_n that reflect the recorded judgments.

The relative weights are given by the right eigenvector w corresponding to the largest eigenvalue λ_{max} as in Equation (2).

$$A_w = \lambda_{max} * w \tag{2}$$

The consistency measures used for the eigenvector method in the AHP is the consistent index (CI) proposed by Saaty (1980). The expressions for this measure are:

$$CI = (\lambda_{max} - n) / (n - 1) \tag{3}$$

where λ_{max} is the largest eigenvalue derived from the paired comparison matrix, n is the number of criteria or sub-criteria.

For calculating the consistency ratio (CR), the following equation was applied:

$$CR = CI / RI \tag{4}$$

RI is the random consistency index that is shown in Table 2.

If the value of consistency ratio is equal to 10% or smaller ($CR \leq 0.1$), the inconsistency is acceptable. If the consistency ratio exceeds 10% ($CR > 0.1$), it is necessary to revise the subjective judgment to locate the cause of the inconsistency and correct it [30].

Tab. 2. Random Index (RI) used to compute consistency ratios (CR)

n	1	2	3	4	5	6	7	8	9	10
RI	0	0	0.58	0.90	1.12	1.24	1.32	1.41	1.45	1.49

3.2 Data

A judgment from an experienced individual and his/her thorough understanding can be a reliable information source to provide opinions. Furthermore, to avoid bias, it is necessary to utilize more than one expert [31]. The Delphi-AHP model’s primary data were obtained via expert Choice Matrix and were given to 50 specialists with experience in groundwater management from various agencies or departments in Vietnam and other countries. The study conducts two rounds and the second one is four months away from the first round. The main purpose of the survey was to determine the opinion of scholars for their priorities on likely affect groundwater potential, which occurs in the Ba river basin. Table 3 shows the survey respondents by expertise in eight fields.

Tab. 3. The survey respondents by expertise.

No.	Expertise	Number	Percentage
1	Hydrology	6	12%
2	Water resources	8	16%
3	Geology	7	14%
4	Soil	6	12%
5	Environment	5	10%
6	Geography	8	16%
7	Metrological	5	10%
8	Geodesy	5	10%
Total		50	100%

4. Results and discussion

4.1 Questionnaire survey

The questionnaire survey was established in Vietnamese and English language with clear and easy to understand questions. The questionnaire elicits the respondents' viewpoint about the criteria affecting groundwater occurrence in the Ba river basin, their influence degree as well importance. The main content of these questionnaires focuses on 2 following key objectives: First, based on the profound knowledge and experience, the experts selected groundwater potentiality impacts parameters in the Ba river basin. The answer for each question was divided into main five degrees: (1) Very Little Probability; (2) Little Probability; (3) Average Probability; (4) High Probability; (5) Very High Probability. Second, the experts were expected to rank the factors chose from the first question by comparing two elements at a time using a pair-wise comparison matrix based on Saaty's fundamental scale of judgment.

The validity of the questionnaire related to the groundwater potential was then confirmed by returned results from 10 experts in water resources, hydrology, and soil. The review of the questionnaire helped us to correct unclear questions to ensure that respondents understood the questions and give consensus opinions on the groundwater impacts criteria. In this research, experts are selected following the principle: (1) have more than five years of experience in the field related to groundwater; (2) were interested and willing to participate in our study; and (3) have no direct conflict of interest with this study. Through a literature review of scientist publications, we chose some experts who are appropriate to contribute their judgment to this study. As a result, 50 academics with research interests match the objectives of the current study who were invited to take part in the study. We sent an email, had a face-to-face, and made a phone call to introduce the study area, the criteria as well as the implications of each criterion affecting groundwater occurrence and distribution to the contributors.

Tab. 4. Evaluation of the criteria discussed in the last round

No.	Criteria	Concepts raised in the survey	Evaluation
1	Rainfall	The rainfall controls the groundwater recharge of a region	This factor is appropriate to be used in the study. Data is available from rain gauge stations distributed around the Ba river basin.
2	Slope	This parameter affects the speed and flow of water	This parameter is considered suitable for the study. It might be acquired through a Digital Elevation Model (DEM), which is available for the research region.
3	Drainage density	Drainage density is an inverse function of permeability and it indicates the runoff and infiltration of the specific region.	This alternative was judged meet to be applied in the study. It might be accomplished through the river network, a DEM, or topographic map in the Ba river basin
4	Lineament Density	This criterion shows rainfall penetration into the ground as well as controls the movement and storage of the groundwater	This criterion was appropriated essential for this study. It might be resolved using a DEM or topographic map which is gettable in the study area.
5	Land use	This factor impacts runoff, evapotranspiration, and soil infiltration rate, water retention, soil protection capacity, the interrelationship between surface runoff, and groundwater.	This is a necessary criterion and it should be used in the study. It may be achieved by using a current land use map or satellite image.
6	Geology	This element influences the nature of flow, erosion, and sediment transportation	This is a necessary criterion and it should be used in the study. It may be achieved by using a geological map

50 questionnaires were then sent to experts on hydrology, geology, meteorology, water resources, environment, geodesy, soil, and geography from the government offices, academia, university in Vietnam, and foreign. The distribution of the questionnaire to experts who are located in different regions and various

fields leads to reduce the bias in assessing the alternative groundwater potential criteria [32]. In this study, we sent multiple questionnaires in many different rounds to the experts with a request to appreciate and choose factors that can contribute to forming groundwater. The experts and scholars were required to rate the importance of the proposed factors, and the numbers 1–9 were employed to illustrate the importance of the indexes. The larger the number is, the more important it is. For example, the number 9 means that it is very important while number 1 reveals that it is very not important).

In the first Delphi survey, there were 45 returned questionnaires (meet 90% responses). From the results of the first survey, 5 out of the 25 indicators were excluded from the scale for the following reasons. First, some factors were not entirely related to the groundwater potential. Second, some criteria overlapped or have similar properties. In addition, the panelists’ comments suggested that some attributes were not understood or explicitly presented. Consequently, 20 criteria were measured in the second survey. To ensure the validity of the Delphi method, only respondents who participated in the first survey were invited to join the remaining survey rounds. After multiple rounds of information feedback, almost all experts think that many important parameters influence groundwater generation, but six of them are the most preferred alternatives in creating these resources including rainfall, slope, drainage density, lineament density, land cover, and geology. Table 4 shown experts’ opinions in the evaluation of the selected criteria affecting groundwater potential in the final round to give final decisions.

Tab. 5. The summarized results the priority of the factors affecting groundwater potential.

No.	Pairwise Comparison Factors	Average Mark	No.	Pairwise Comparison Factors	Average Mark
1	Lineament Density and slope	2	19	Geology and Lineament Density	-3
2	Lineament Density and rainfall	2	20	Geology and Slope	-2
3	Lineament Density and Geology	3	21	Geology and Rainfall	-2
4	Lineament Density and Drainage Density	5	22	Geology and Drainage Density	2
5	Lineament Density and Land use	7	23	Geology and Land use	7
6	Lineament Density and Lineament Density	1	24	Geology and Geology	1
7	Slope and Lineament Density	-2	25	Drainage Density and Lineament Density	-5
8	Slope and Rainfall	1	26	Drainage Density and Slope	-3
9	Slope and Geology	2	27	Drainage Density and Rainfall	-2
10	Slope and Drainage Density	3	28	Drainage Density and Geology	-2
11	Slope and Land use	5	29	Drainage Density and Land use	7
12	Slope and Slope	1	30	Drainage Density and Drainage Density	1
13	Rainfall and Lineament Density	-2	31	Land use and Lineament Density	-7
14	Rainfall and Slope	1	32	Land use and Slope	-5
15	Rainfall and Geology	2	33	Land use and Rainfall	-5
16	Rainfall and Drainage Density	2	34	Land use and Geology	-7
17	Rainfall and Land use	5	35	Land use and Drainage Density	-7
18	Rainfall and Rainfall	1	36	Land use and Land use	1

4.2 Determination of the weights of criteria affecting groundwater potential

The AHP aimed to weight each indicator in this study after determining six factors influencing groundwater potential by the Delphi method. The decision-makers show preferences or priority for each element in comparison to other factors. The study used six main factors in relation to creating groundwater, thus decision-makers prepare to get relative importance in each level of hierarchy through 6*(6-1)

comparisons. The results of the average evaluation of the priority of the criteria influencing groundwater occurrence are listed in Tab. 5.

The final pairwise comparison matrix is presented in Tab. 6 by the 6 x 6 matrix, where diagonal factors are equal to 1. The values of each row are compared with each column to show the relative importance to achieve a rating score. For example, lineament density is significantly more important from land use and thus assigned the value 7. The row describes the importance of the land use, hence the row has the inverse value of the pairwise comparison (e.g. 1/7 for lineament density). The score matrix was then normalized to obtain the corresponding weight of each criterion. The weight of each factor was calculated by taking the average value of the corresponding row in the normalized matrix.

Tab. 6. Pairwise comparison matrix for six factors influencing Groundwater potential

Factors	Lineament Density	Slope	Rainfall	Geology	Drainage Density	Land use
Lineament Density	1	2	2	3	5	7
Slope	1/2	1	1	2	3	5
Rainfall	1/2	1	1	2	2	5
Geology	1/3	1/2	1/2	1	2	7
Drainage Density	1/5	1/3	1/2	1/2	1	7
Land use	1/7	1/5	1/5	1/7	1/7	1

Each factor was weighted by the AHP method. The higher the weight was, the more important the indicator was [33]. In the first-rank indicators, the weight of the “lineament density” was 35.1%, followed by a “slope” of 20.1%. More details were shown in Table 7. This revealed that the experts regarded the lineament density and slope as the most frequent impact of groundwater occurrence compared with the other factors. The overall result of AHP analysis (Tab. 8) shows that the consistency ratio (CR) is 0.05, which is much lower than the threshold value of 0.1 and this also indicates a high level of consistency in the pair-wise judgments. Hence, the weights (Tab. 7) are acceptable.

Tab. 7. The weight of influential criteria.

Parameters	Weight
Lineament density	0.351
Slope	0.201
Rainfall	0.186
Geology	0.134
Drainage density	0.096
Land use	0.030

Tab. 8. Parameters of AHP.

Parameters	Value
Eigenvalue of a matrix (λ_{max})	6.31
The number of criterion (n)	6
Consistency index (CI)	0.062
Random index (RI)	1.24
Consistency ratio (CR)	0.05

However, our obtained results have some limitations. First, it was challenging to develop a set of criteria affecting groundwater potential that apply to all various areas in the world. Most experts came from Vietnam, and the included literature was only in Vietnamese and English. Second, AHP scores were calculated subjectively by experts, and the weights were mainly based on the judgment of the experts’ experience [34], without objective data to prove. Next, experts’ opinions might not have been adequately included. These factors set mainly considered literature and expert’s experience, without consultation of residents living in areas of shortage and depletion of groundwater. Finally, although details of the survey were described fully in the questionnaire, experts might vary in their understanding of the questionnaire because the survey was mainly conducted by mail instead of face-to-face. To reduce the limitation of identifying criteria affecting groundwater potential and assessing their influence level, face-to-face meetings with experts should be increased. In particular, it is necessary to collect opinions from people living in the study area. These ideas will be a useful information channel to contribute to better results.

5. Conclusion

The current study developed the set of criteria affecting groundwater occurrence in the Ba river basin.

This study was conducted in three rounds. There are 50 experts of eight relevant fields with different ages and years of experience in groundwater management to participate in the Delphi study. Six factors including lineament density, rainfall, slope, land cover, drainage density, and geology were selected as indicators for the groundwater potentiality assessment. Furthermore, each indicator was weighted and ranked and had an acceptable consistency ratio based on the AHP approach. The obtained results revealed that the lineament density is the main criterion of creating groundwater with the highest weight of 0.351 was assigned while the lowest weight of 0.03 to the land use.

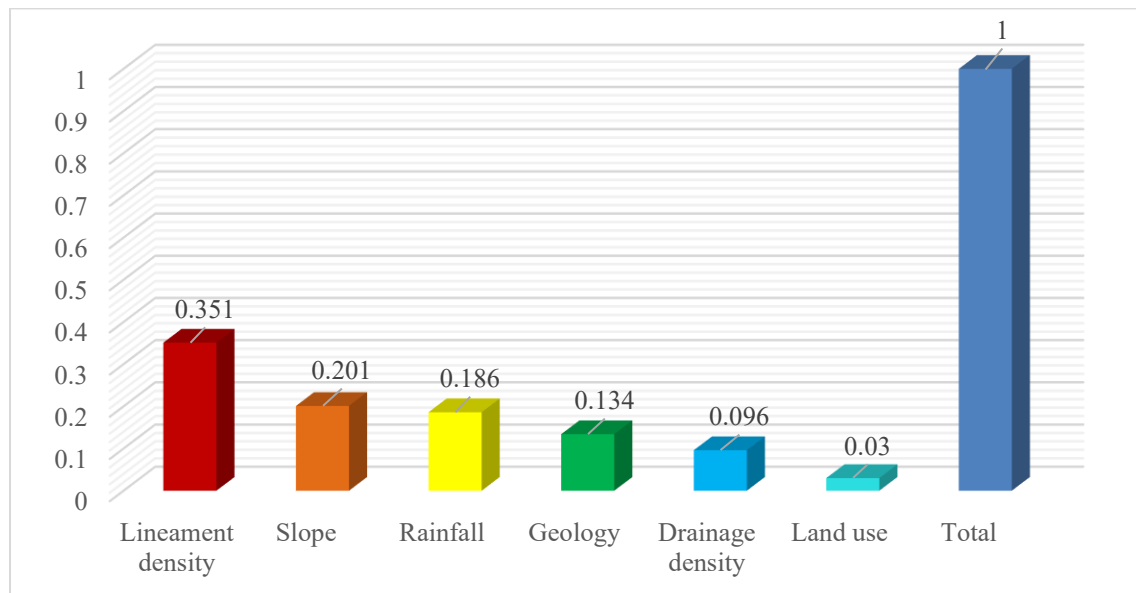


Fig. 3. The weight of criteria affecting groundwater potential in Ba river basin

Although there are some limitations, it can be confirmed that a combined AHP-Delphi method provides a powerful tool for decision-making procedures in groundwater potential analysis. This study describes that the Delphi method is a useful tool for querying and achieving consensus among a group of experts on the major factors affecting groundwater formation. The AHP method was found useful in transforming the preference of all participants regarding each determining factor into a numerical scale. Such scale was then aggregated to produce a numeric indicator that can use to prioritize factors causing groundwater shortage and depletion of groundwater in the study area. Finally, we conclude that the Delphi-AHP method is beneficial to define significant criteria that can impact groundwater generation. In the future, further research is necessary to investigate the applicability of established criteria and the generalizability of these results to other studies.

6. Acknowledgements

The author would like to acknowledge and appreciate the opinions and judgments of researchers, scientists, and professors who came from Thuyloi university, Hanoi University Natural Resources and Environment, Hanoi University of Mining and Geology, Institute of Military Technology, Vietnam, Delft University of Technology, Netherlands, Vietnam Academy of Science and Technology. Also, the author is grateful to engineers with expertise in Vietnam Institute of Geodesy and Cartography, Ministry of Natural Resources and Environment, General Department of Geology, and Minerals of Vietnam for participating in responding to the questionnaire surveys.

7. References

1. World Water Assessment Programme (WWAP), 2009. Water in a changing world. World Water Development Report 3. UNESCO, Paris.
2. Ahmadi, H., Kaya, O.A., Babadagi, E., Savas T., Pekkan, E., 2021. GIS-Based Groundwater Potentiality Mapping Using AHP and FR Models in Central Antalya, Turkey, Environmental Sciences Proceedings, 5(11), <https://doi.org/10.3390>.
3. Asian Development Bank., 2009. Water Vital for Vietnam's Future.

4. Das, S., Pardeshi, S.D., 2018. Morphometric analysis of Vaitarna and Ulhas river basins, Maharashtra, India: using geospatial techniques, *Appl Water Sci*, 8(6):158.
5. Doke, A.B., Zolekar, R.B., Patel, H., Das, S., 2021. Geospatial mapping of groundwater potential zones using multi-criteria decision-making AHP approach in a hard rock basaltic terrain in India, *Ecological Indicators*, 127, <https://doi.org/10.1016/j.ecolind.2021.107685>.
6. Aykut, T., 2021. Determination of groundwater potential zones using Geographical Information Systems (GIS) and Analytic Hierarchy Process (AHP) between Edirne-Kalkansogut (Northwestern Turkey), *Groundwater for Sustainable Development*, 12, <https://doi.org/10.1016/j.gsd.2021.100545>.
7. Hamza, A., Abiyot, L.K., Engida, E.D., & Dereje, L.B., 2021. AHP based analysis of groundwater potential in the western escarpment of the Ethiopian rift valley, *Geology, Ecology, and Landscapes*, DOI: 10.1080/24749508.2021.1952761.
8. Saranya, T., and Saravanan S., 2020. Groundwater potential zone mapping using analytical hierarchy process (AHP) and GIS for Kancheepuram District, Tamilnadu, India, *Modeling Earth Systems and Environment*, 6: 1105-1122.
9. Ahmed, T.H., Al-Manmi, D.A.M., 2019. Delineation of Groundwater productivity Zones with the integration of GIS and Remote Sensing methods, Bazian Basin, Sulaymaniyah, Kurdistan Region, Iraq, *Journal of Basrah Researches (Sciences)*, 45(2): 289-309.
10. Das, S., Pardeshi, S.D., 2018. Integration of different influencing factors in GIS to delineate groundwater potential areas using IF and FR techniques: a study of Pravara basin, Maharashtra, India. *Applied Water Science*, 8(197), <https://doi.org/10.1007/s13201-018-0848-x>.
11. Keeney, S., Hasson, F., McKenna, H. P., 2001. A critical review of the Delphi technique as a research methodology for nursing, *International Journal of Nursing Studies* 38(2): 195–200. [http://dx.doi.org/10.1016/S0020-7489\(00\)00044-4](http://dx.doi.org/10.1016/S0020-7489(00)00044-4).
12. Ameyaw, E.E., Hu, Y., Shan, M., Chan, A.P.C., Le, Y., 2014. Application Delphi method in construction engineering And management research: a quantitative perspective, *Journal of Civil Engineering and Management*, 22(8). <http://dx.doi.org/10.3846/13923730.2014.945953>.
13. Boulomytis, V.T.G, Zuffo, A.C., and Imteaz, M.A., 2019. Detection of flood influence criteria in ungauged basins on a combined Delphi-AHP approach, *Operations Research Perspectives*, 6.
14. Dung, N.B., Long, N.Q., An, D.T., Minh, D.T. 2021a. Multi-geospatial flood hazard modelling for a large and complex river basin with data sparsity: a case study of the Lam River Basin, Vietnam, *Earth Syst Environ*. <https://doi.org/10.1007/s41748-021-00215-8>.
15. Liu, J., Xu, Z., Chen, F., Chen, F., and Zhang, L., 2019. Flood hazard mapping and assessment on the Angkor world heritage site, Cambodia, *Remote Sensing*, 11: 98.
16. Dung, N.B., Minh, D.T., An, B.N., Nga, N.Q. 2021b. Assessment of vulnerability In agricultural land in flood prone Areas and application of mobile smart Phone in providing flood hazard Information in lam river Basin (Vietnam), *Sustainable development of mountain territories*, 2(48): 254-265, DOI: 10.21177/1998-4502-2021-13-2-254-264.
17. Sang, N.P., Dung, T.N., Hung, T.K., Hien, T.T.P., Toan, T.T., Chinh, C.T.V., 2019. The degree of chemical weathering in the Ba River basin, South Central Vietnam: Major-element geochemistry investigations of morden river sediments and sedimentary rocks. *Journal of Mining and Earth Sciences*, 61(1): 82-91.
18. Dung, N.B. 2017. Research on application of geomatics technology to improve the quality of space data for the investigation and planning of water resources. *Ministry-level scientific research project*.
19. Jha, M.K., Chowdary, V.M., Chowdhury, A., 2010. Groundwater assessment in Salboni Block, West Bengal (India) using remote sensing, geographical information system, and multi-criteria decision analysis techniques. *Hydrogeol. J.*, 18 (7):1713-1728.
20. Yıldırım, Ü., 2021. Identification of Groundwater Potential Zones Using GIS and Multi-Criteria Decision-Making Techniques: A Case Study Upper Coruh River Basin (NE Turkey). *ISPRS Int. J. Geo-Inf*, 10(396). <https://doi.org/10.3390/ijgi10060396>.
21. Jabar, A., Wallis, L.A., Ruter, A., and Smith, W.P., 2012. Modified Delphi study to determine optimal data elements for inclusion in an emergency management database system, *African Journal of Emergency Medicine*, 2: 13-19.
22. Grisham, T., 2009. The Delphi technique: A method for testing complex and multifaceted topics. *International Journal of Managing Projects in Business*, 2(1): 112-130. <http://dx.doi.org/10.1108/17538370910930545>.
23. Steward, J., 2001. Is the Delphi technique a qualitative method? *Medical Education*, 35: 922-923. <http://dx.doi.org/10.1111/j.1365-2923.2001.01045.x>.

24. Lee, G., Jun, K.S., Chung, E.S., 2013. Integrated multi-criteria flood vulnerability approach using fuzzy TOPSIS and Delphi technique. *Natural Hazards and Earth System Sciences*, 13: 1293-1312.
25. Arof, A.M., 2015. The application of a combined Delphi-AHP method in maritime transport research – a review, *Asian Social Science*, 11(23): 73-82.
26. Song, G., Yang, C.M., Hao, C., and Ran, Y.P., 2014. Weights of the value assessment indicators in integrated conservation of modern architectural heritage, *Journal of Applied Sciences*, 14: 580-85.
27. Saaty, 1980. *“The Analytic Hierarchy Process”*, McGrawHill, New York.
28. Bertolini, M., Braglia, M. and Carmignani, G., 2006. Application of the AHP methodology in making a proposal for a public work contract, *International Journal of Project Management*, 24(5): 422-430.
29. Miller, G.A., 1967. The magical number seven, plus-or-minus two, some limits to our capacity for processing information, *Brain Physiology and Psychology*. Butterworths: London: 175-200.
30. Saaty, T.L., 2008. Decision making with the analytic hierarchy process, *International journal of services sciences*, 1: 83-98.
31. Ishizaka, A., and Labib, A., 2011. Review of the main developments in the analytic hierarchy process, *Expert systems with applications*, 38.
32. Chen, Y.R., Yeh, C.H., and Yu, B., 2011. Integrated application of the analytic hierarchy process and the geographic information system for flood risk assessment and flood plain management in Taiwan, *Natural Hazards*, 59: 1261-76.
33. Dung, N.B., Long, N.Q., Ropesh, G., An, D.T., Minh, D.T., 2021. The Role of Factors Affecting Flood Hazard Zoning Using Analytical Hierarchy Process: A Review. *Earth Systems and Environment*. <https://doi.org/10.1007/s41748-021-00235-4>.
34. Minh D.T. 2017. ‘Modeling methods and applications in generating flood risk zoning models’. *Journal of Mining and Earth Sciences*, 58(4): 128-136. (In Vietnamese).

Rule-based Classification of Airborne Laser Scanner Data for Automatic Extraction of 3D Objects in the Urban Area

BUI Ngoc Quy^{1,*}, LE Dinh Hien^{1,2}, DUONG Anh Quan¹, NGUYEN Quoc Long¹

¹ Hanoi University of Mining and Geology, 18 Vien street, Hanoi, Vietnam

² Natural resources and Environment one member co., ltd, Hanoi, Vietnam

Corresponding author: buingocquy@humg.edu.vn

Abstract. LiDAR technology has been widely adopted as a proper method for land cover classification. Recently with the development of technology, LiDAR systems can now capture high-resolution multispectral bands images with high-density LiDAR point cloud simultaneously. Therefore, it opens new opportunities for more precise automatic land-use classification methods by utilizing LiDAR data. This article introduces a combining technique of point cloud classification algorithms. The algorithms include ground detection, building detection, and close point classification - the classification is based on point clouds' attributes. The main attributes are height, intensity, and NDVI index calculated from 4 bands of colors extracted from multispectral images for each point. Data of the Leica City Mapper LiDAR system in an area of 80 ha in Quang Xuong town, Thanh Hoa province, Vietnam was used to deploy the classification. The data is classified into eight different types of land use consist of asphalt road, other ground, low vegetation, medium vegetation, high vegetation, building, water, and other objects. The classification workflow was implemented in the TerraSolid suite, with the result of the automation process came out with 97% overall accuracy of classification points. The classified point cloud is used in a workflow to create a 3D city model LoD2 (Level of Detail) afterward.

Keywords: Point cloud, Lidar data, NDVI index, Classification algorithms, 3D city

1. Introduction

Delivering precise and timely data is always an indispensable factor for the management, planning, and landscape pattern analysis of urban land. Recently, alongside satellite images and UAV (Unmanned Aerial Vehicle) data, airborne LiDAR (Light Detection and Ranging) has been widely used as an effective data collection method that helps to produce fast, large scale and accurate geospatial data., it shows the flexibility in flying shooting and data acquisition for small and medium-sized areas. The UAV With UAV technology image data can be used to create digital elevation models (DEM) [1], create 3D map models [2, 3], etc. In addition, point cloud data is processed from UAV images are also classified to create 3D models for terrain objects, especially for open-pit mines [4]. Meanwhile, aviation LiDAR technology shows the ability to fly and capture data in a wide range and is widely used in studies of the earth's surface. In the earliest period, nDSM (normalized Digital Surface Model) extracted from LiDAR data has been used as a criterion for urban land classification [8]. Besides, there were several studies about LiDAR intensity not only for depicting the natural surface condition such as surface moisture [9], flow recognition and aging of lava [10], wetland hydrology [11], and rock properties [12] but also supporting in municipal area cover classification. LiDAR intensity was first utilized by Song, J.H and et al in 2002 [13]; the intensity value of asphalt road, grass, house roof, and the tree was inspected to have an adequate difference for land cover classification. However, using intensity data as a standalone factor was asserted about its limitation in various research [13-18]. Thus, there was plenty of research that integrates LiDAR intensity with height value to eliminate that limitation such as Charaniya, A. et al, 2004 [8] use intensity to separate road from low vegetation, Brennan in 2006 [15] sort out structures with the same height by the intensity and many others [19-22]. Alongside intensity, RGB (Red Green Blue) satellite images and onboard aerial images with direct geo-referencing have also been combined with LiDAR height data for land cover classification [8, 14, 22-28]. Normalized difference vegetation index (NDVI) is another essential factor for land use classification; the adoption of NDVI with LiDAR data has been implemented in various studies [21, 22, 27, 29, 30] that help to raise the efficiency of the classification enormously. Thus, it can be seen that NDVI value from images and the Intensity value of LiDAR data are both good elements to be used in classification. Currently, the use of NDVI and Intensity combination is utilized in land cover classification [31], therefore, if the combination can be used to classify point cloud, it can facilitate the further use of point cloud such as for making 3D city model purpose. This study introduces a method of combining both intensity value of LiDAR data and NDVI, which extracted from onboard high-resolution images with

different LiDAR point cloud classification algorithms in consist of ground detection routine, classification by height compared to ground, building detection routine, and classification by close point and afterward, the classified point cloud is used as material to build a LoD2 city model. The method will help build an automatic classification workflow for LiDAR point cloud into eight different land-use types, including asphalt road, other ground, low vegetation, medium vegetation, high vegetation, building, water, and other objects. TerraSolid suite was used to perform the automation process. The result came out with 97% overall of points were correctly classified. Besides, another workflow to automatically create a 3D city model is also introduced in this study to provide a LoD2 city model which can be used for various applications.

2. Data acquisition and study area

2.1. Lidar system: City Mapper

The LiDAR system used is CityMapper of Leica Geosystem (Fig. 1). It consists of a 0.9 nm wavelength LiDAR scanner, an 80 mm focal length multispectral camera, and integrated with GNSS and IMU system, which provide high accuracy of 5 cm horizontal and 10 cm vertical. The data was captured at 1200 m height with an average point density of 5 pts/m² and 7 cm GSD images. It took 3 flight trips (2 North-South lines and 1 crossed line) to cover the study area in sunny weather. The trajectory was processed in Inertial Explorer, images, and point clouds were processed in HxMap.



Fig. 1. Leica City Mapper system.

2.2. Study area

The chosen study zone is 80 hectares in Quang Xuong town, Thanh Hoa province, Vietnam. It is a plain area located in 19°44'04'' N, 105°46'53'' E with around 5 meters above sea level height (Fig. 2). We select this area because it has enough of 8 land use objects, including asphalt road, other ground, low vegetation, medium vegetation, high vegetation, building, water, and other objects (traffic signs, traffic lights, trash cans, cars, etc.).



Fig. 2. Area of study.

3. Methodology

3.1. Workflow and classification threshold

Workflow: The point clouds of the study area were taken by using the Airborne Lidar system. The lidar signals and images go through the pre-processing with rectification and GCPs adjustment. We used HxMap which is a Leica software to process Leica City Mapper’s data to export the LiDAR point clouds with four bands of color, including Red - Green - Blue - Near Infrared. Based on the point cloud characteristics, we apply the automatic classification process to have point clouds in different classes. The classified point cloud is used in a City 3D modeling workflow to build a LoD2 City Model. The detailed workflow is described in the following Figure 3.

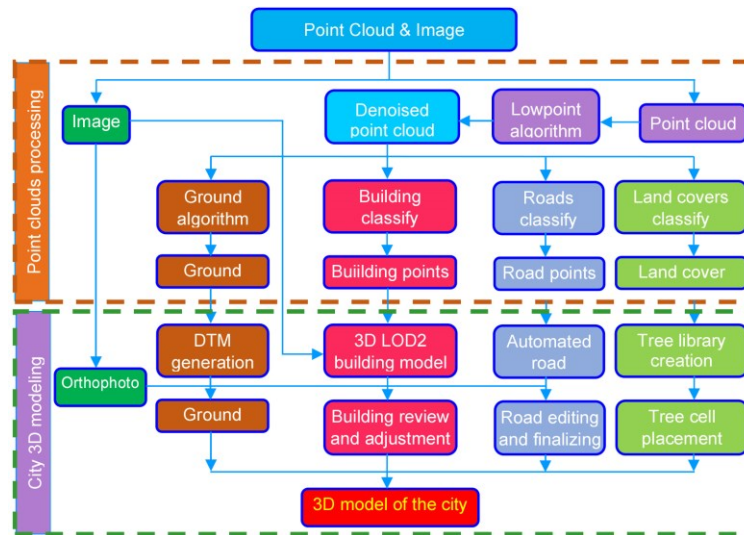


Fig. 3. Point clouds classification & City 3D modeling workflow.

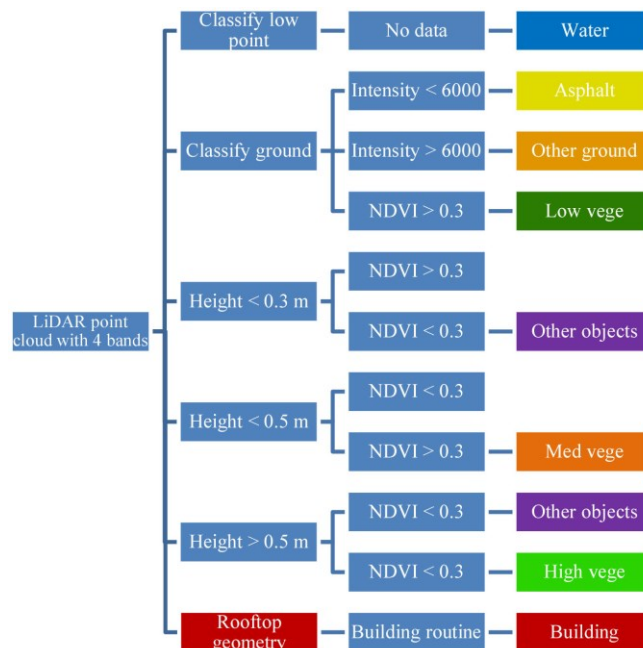


Fig. 4. Classification threshold.

Classification threshold for point clouds: Figure 3 described the overview of the 3D model building workflow. Inside this workflow, the first step is the classification of points in the point clouds to 8 classes. The classification is based on the thresholding levels described in Figure 4.

The threshold level developed base on natural characteristics of object classes in point clouds. There are four characteristics used to develop the threshold level: Intensity, NDVI, Height, and Geometry.

3.1.1. Intensity

Intensity is the ratio of the strength of reflected light to that of emitted light, and the reflectance of the reflecting object has the most impact on its value. Reflectance is different between different material attributes as well as the light used. Therefore, intensity can be used to differentiate point clouds (Fig. 5). We proceeded to manually collect sample intensity values for Asphalt, Concrete, Tile, Soil Lane, and soil to have a table for intensity range below (Tab. 1):

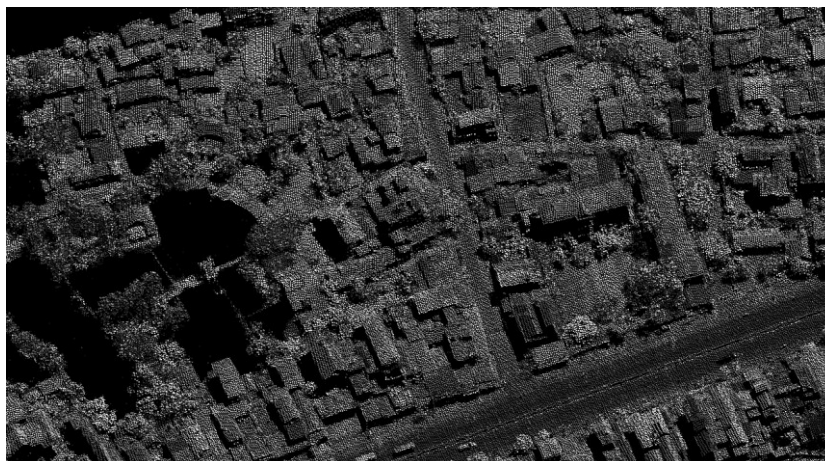


Fig. 5. Point cloud in the display of intensity.

Tab. 1. Intensity range of CityMapper point clouds for different objects.

Order	Objects	Intensity range	Order	Objects	Intensity range
1	Asphalt	2100-5400	3	Tile	7300-9700
2	Concrete	9000-12500	4	Soil lane, soil	7500-13600

From this table, it can be seen that Asphalt can be filtered out from other ground objects by intensity value. Because the flat ground in the area consists of Asphalt, concrete, tile, soil lane, soil.

3.1.2. NDVI

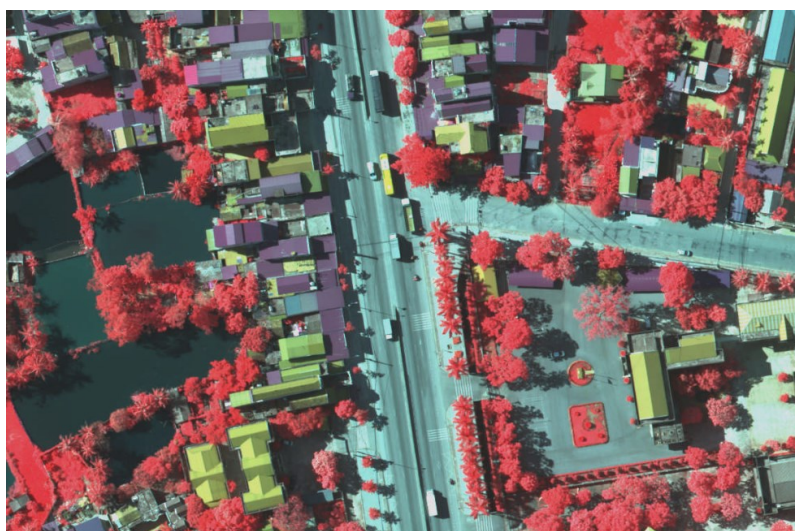


Fig. 6. The area display in the color infrared image.

The NDVI of the CityMapper is calculated by the following formula:

$$NDVI = \frac{(NIR - Red)}{(NIR + RED)}$$

By design, the NDVI itself thus varies between -1.0 and +1.0. Most of the collected vegetation points

samples have the value of intensity above 0.3 since the capture data date is in summer and all kinds of plants here have green leaves. Figure 6 described the point cloud of the study area display in the color infrared image.

3.1.3. The height of points

The height of points is the different elevation of points compared to the ground surface. It is an essential factor to separate different types of objects. For instance, the grass is below 0.3 m in height, while plant pots & bushes range from 0.3 m to 0.5 m and trees are above 0.5 m.

3.1.4. Geometry of points group

A group of points has its geometry; it may present a planar, a curve, or irregular shapes. Based on the shapes, the object can be detected automatically. For example, the rooftop may have planar shapes, and the tree may have irregular shapes (Fig .7).

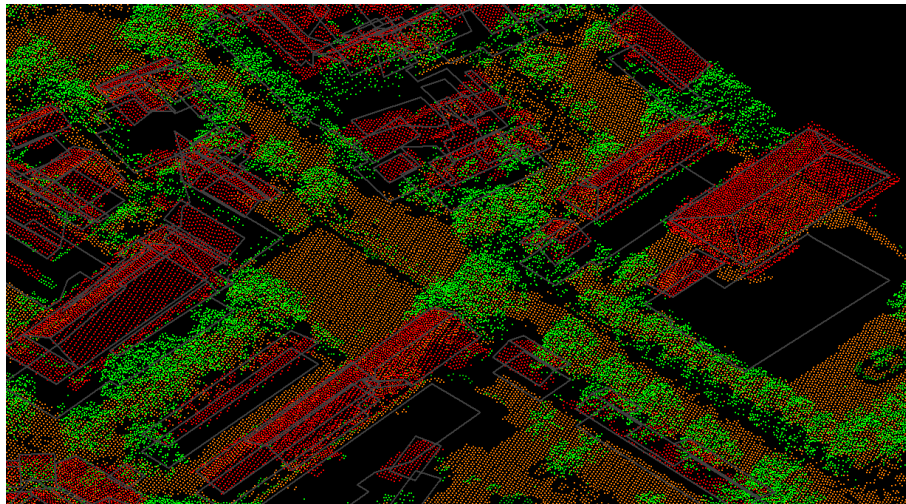


Fig. 7. Rooftop geometry.

3.2. Classification processing

3.2.1 Classify low, isolated point/water

The low-point routine which is used to denoise the point cloud classifies single points or groups of lower points than other points in the surrounding. There might be possible error points that are clearly below the ground. The elevation value of each point or point group with any other point within a given 2D radius will be collated. The routine will classify the point or point group to a low point group if it is lower than any other point.

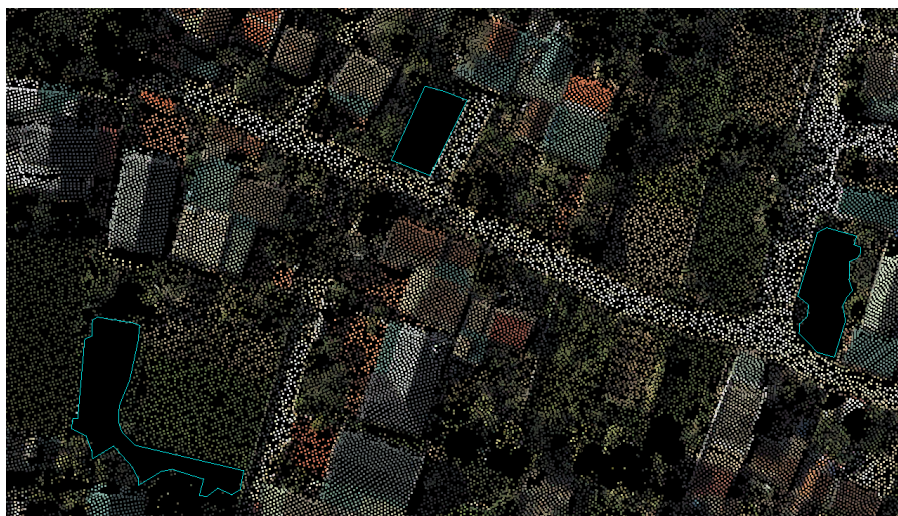


Fig. 8. Water area.

Next, isolated noise points in the air or on the ground will be filtered out by an isolated routine. The loop detects points with fewer neighbor points within a 3D search radius than defined in the routine's settings.

After the low point and isolate routine, an automatic drawing polygon routine will be used to draw boundaries for no data areas for marking as water land use (Fig. 8). The remaining points are ready for the following ground routine.

3.2.2. Classify ground

The classify ground routine automatically searches ground LiDAR points by making a triangulated surface model iteratively. The loop begins by selecting the lowest point with a potential ground surface nearby. Afterward, it makes a surface model (TIN) from the starting point. The model becomes more closely to the proper ground surface by each added point.

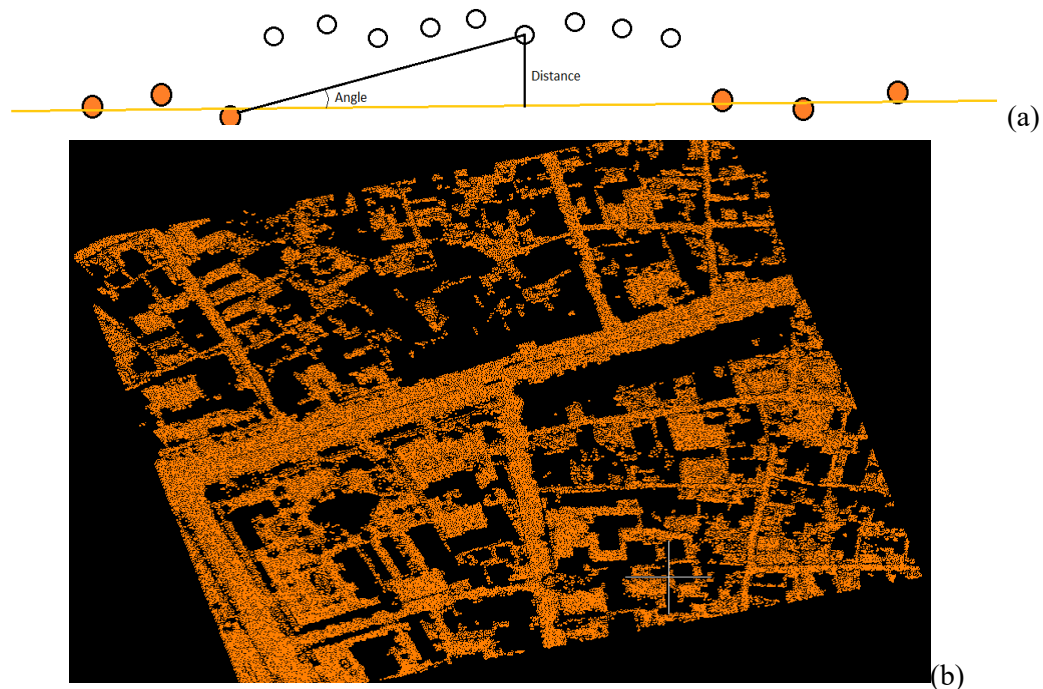


Fig. 9. The ground routine and Ground point.

The chosen algorithm uses parameters of iteration angle and iteration distance (Fig. 9a). Iteration angle is the maximum angle between the line of the ground surface made by two ground points at a far distance and the line which connects the ground point to the search point. Iteration distance ranges from the search point projected in the nadir direction to the ground surface. It helps to prevent detecting points that are too high from the ground.

After this ground routine, a group of ground points was detected (Fig. 9b), then, with the NDVI routine for each point NDVI value >0.3 , mixed in vegetation points will be filtered out. Finally, with the intensity routine, asphalt road points will be classified with an intensity value lower than 6000, and the rest will go to other ground points.

3.2.3. Classify vegetation

Before the vegetation routine, we use a macro to calculate the distance of all remaining points to the ground class. Then, a height algorithm is utilized to classify three types of vegetation.

All points with a height value below 0.3 m go to low vegetation.

Points with a height value below 0.5 m go to medium vegetation.

Points with a height value above 0.5 m go to high vegetation.

Finally, an NDVI routine will be used to filter out other objects from vegetation that have an NDVI value < 0.3

3.2.4. Building routine

The building routine detects points on houses' roofs with a flat distribution from other objects' classes. Holes above the ground class will begin to search for points on planar surfaces first. Minimum acreage and roof thickness of houses need to be set as parameters used for the routine.

Afterward, a close point routine will be applied to bring roof structure from other objects class to building class. The loop looks for nearby points with a set 3D distance compared to the current building class.

3.3. 3D city model

3.3.1. True Orthophoto generation.

The True Orthophoto is created from the Aerial Images (Fig. 10). After a triangulation process, the external orientation of each image is refined to have better accuracy. The Lidar point cloud is used to generate the DSM of the study area. All of the images will be projected to the DSM to form a True Orthophoto of the area.



Fig. 10. Orthophoto of the study area.

3.3.2. DTM generation & textured ground model

DTM is generated as a TIN (Triangulated Irregular Network) model with the input from the ground point layer (Fig. 11). After that, the TIN model will be texturized using the True Orthophoto from the base ground model for the 3D city model.

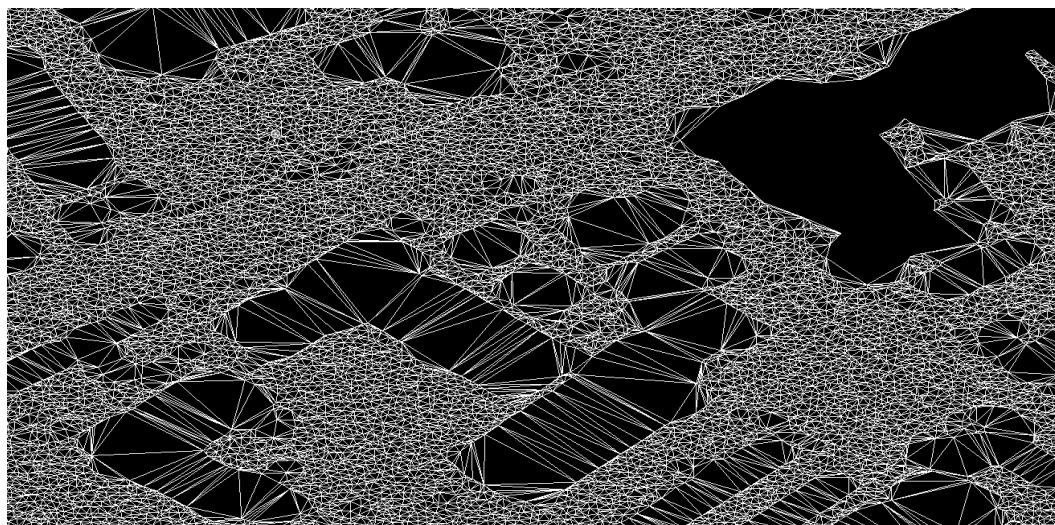


Fig. 11. TIN model.

3.3.3. Building model

The building point cloud layer is the input for this process. An algorithm is used to vectorize buildings automatically. After the automation, every shape of the buildings is checked with manual work. The building models are in the form of LoD2 (Fig. 12) and are texturized by cutting images from the True Orthophoto.

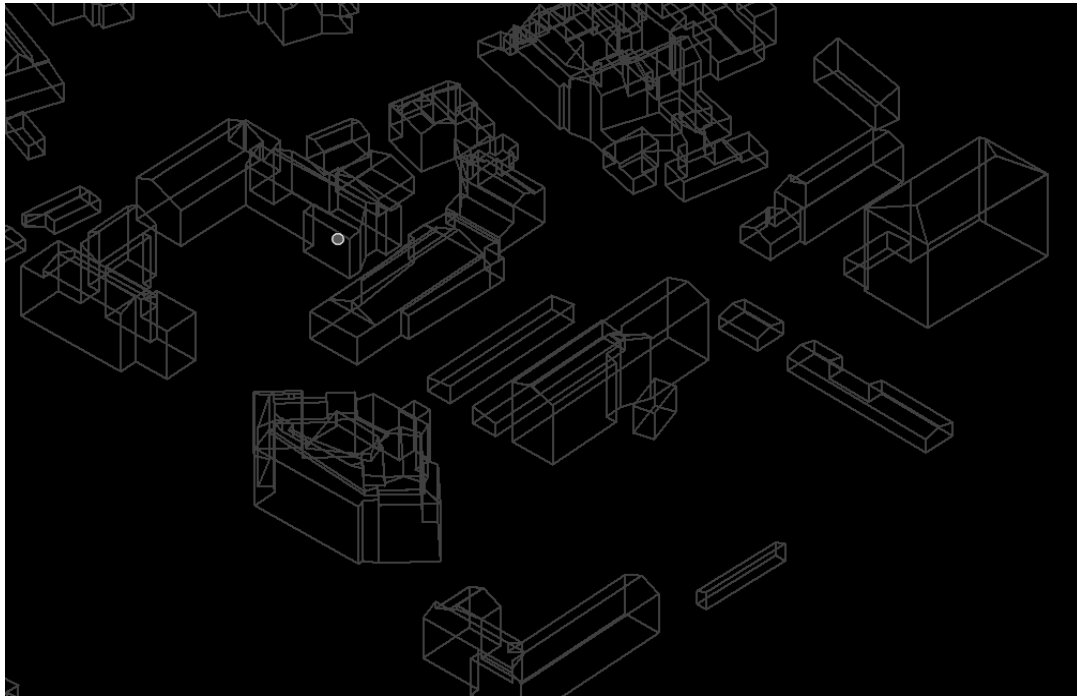


Fig. 12. Buildings models.

3.3.4. The road network

The road network is automatically vectorized by an algorithm with the input of the point cloud from the asphalt class. The road digitation is also checked with a manual process until acceptance.

3.3.5. The tree models

This process requires making a library of trees based on the shape and size of each type of tree (Fig. 13). Three vegetation layers are used as the input, each type of tree is viewed in a vertical section to draw the standard shape and define the parameters of size. A tree model is used correspondingly to each kind.

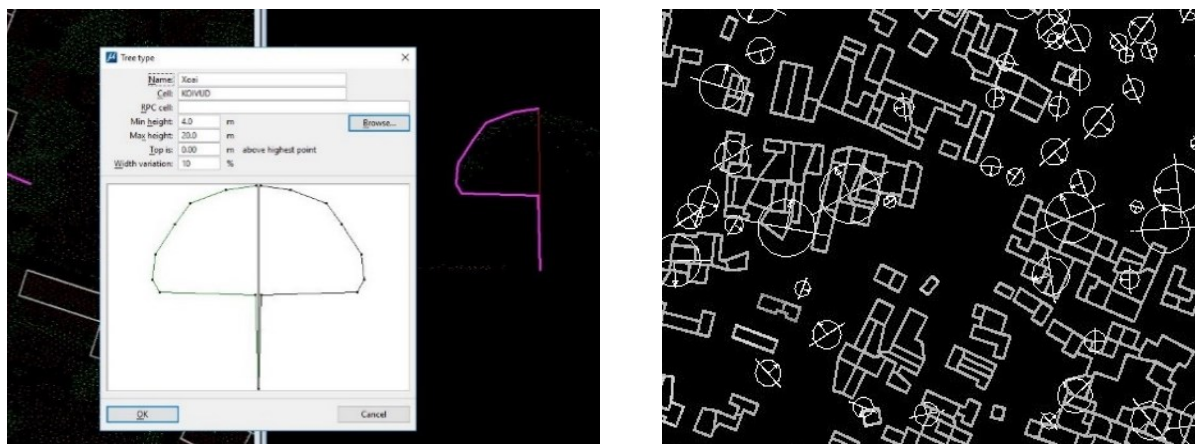


Fig. 13. Trees model.

Afterward, an automatic process is run to sift through the vegetation layer to detect trees. Correspond to each tree, a 3D tree cell from the library is placed on the model. Each tree cell will be present with a tree model from the library, respectively.

4. Result and discussion

4.1. Result

4.1.1. Point cloud classification

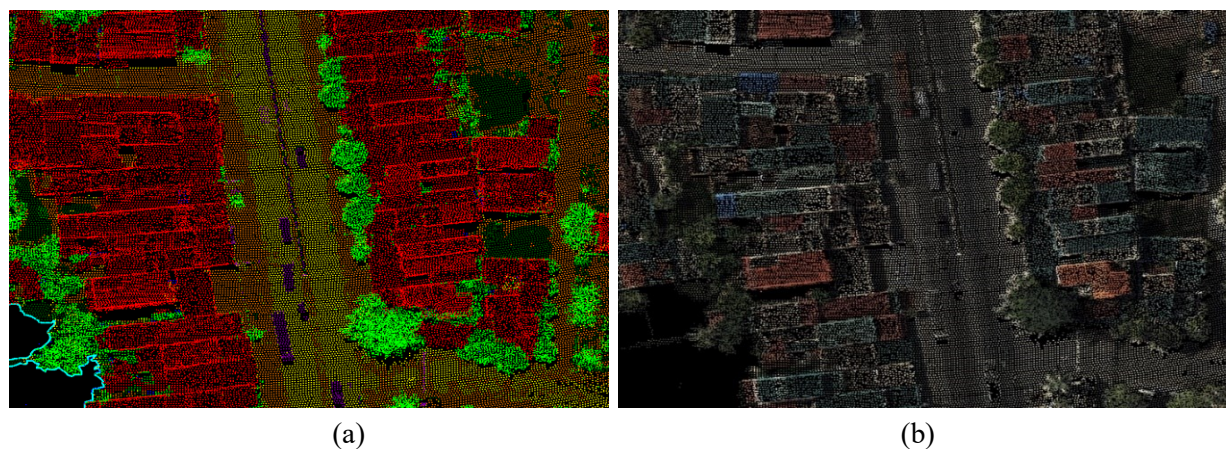


Fig. 14. LiDAR point clouds of Quang Xuong town after the automatic classification process. (a) Point clouds view by class; (b) Point clouds view by color.

After processing through the workflow, the LiDAR point clouds of the study area were automatically classified into seven different classes (Fig. 14): asphalt road, other ground, low vegetation, medium vegetation, high vegetation, building, and other objects (water areas were vectorized as polygons). A manual checking process was performed afterward with the help of referenced orthophoto to collect incorrect classified points.

The result came out with a very promising overall accuracy of 97.18 % as an average value of classification precision of 7 classes totaled up in Table 2.

Tab. 2. Classification accuracy of 7 classes.

	Asphalt	Other ground	Low vegetation	Medium vegetation	High vegetation	Building	Other Objects
Incorrect classified points	s	9637	12519	7398	42361	26521	19841
Total points	169647	745522	600895	234237	1091304	1048832	400823
Accuracy (%)	98.18	98.71	97.92	96.84	96.11	97.47	95.05

The highest accuracy belongs to other ground and asphalt classes (98.71% and 98.18%). It shows that the ground routine worked practically effectively. The intensity value helped filter out asphalt quite thoroughly, thanks to the assistant of NDVI, because most of the low vegetation points were classified as ground points after the ground routine. It has an intensity range quite similar to asphalt. Other objects class has the lowest accuracy due to the complexity of the roof structure of houses in town. NDVI value helps filter vegetation, but the accuracy peaked at 97.92% for low vegetation.

4.1.2. 3D city model

The 3D city model of the study area (Fig. 15) is the combination of 4 layers:

- The 3D textured ground model as the base ground layer
- The road networks drawing layer
- The tree models
- 3D LoD 2 building model

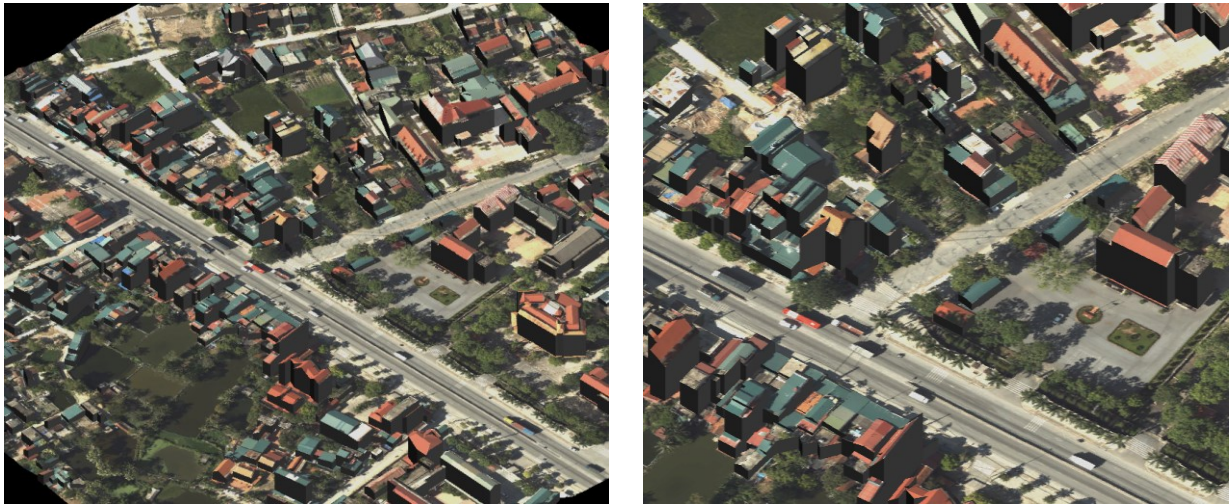


Fig. 15. 3D City model.

4.2. Discussion

The data is captured with the CityMapper with only one nadir camera (the full CityMapper has 4 more oblique cameras), thus, we do not have the oblique images to texture the facades. Therefore the building wall is not used in this research. It is classified into the point class of other objects.

The best setup for a city 3D model is capturing data at around 700-800 m AGL (above ground level) to have the best surface point cloud of the roof building. However, it is very difficult to ask for permission to fly below 1000 m above ground level in Vietnam, yet, the classification still can archive a high accuracy result and be able to create a LoD2 city model.

The outstanding feature of this method is the ability to classify high-density 3D point clouds with many points of different objects in a vertical direction, unlike other [14] that are required to convert LiDAR point clouds to a DTM or DSM surface. The automation process used in the study provides a high accuracy result (above 95% for all classes). With intensity and NDVI value, this method can filter out asphalt and vegetation together to classify up to 8 different classes. However, the data used in this study comes from the Airborne LiDAR system with an average point density of 5 pts/m² and unideal height condition, thus the detail of the point cloud for other objects is not enough to have further classification. Many different objects have to stay in one class - other objects. One suggestion could be the use of the combination data of airborne LiDAR with Mobile Mapping or other ground LiDAR stations to have a more detailed dataset to be able to develop a further classification for other objects. The asphalt and NDVI threshold in this project is localized, other researchers need to choose different values for different areas depending on the type of LiDAR sensors, materials, and trees.

5. Conclusion

This study introduces a method for automatic land use classification by combining many different point cloud routines with their innate value of intensity and NDVI from the onboard multispectral images. The conclusions are as follows.

First, it can be seen that the new airborne LiDAR system is capable of not only collecting data at high speed but also providing abundant and precise data for land use classification.

Second, the method helps eliminate the need for labor-intensive by building an automatic process that can exploit various characteristics of the point cloud to classify it with high accuracy (above 95% for all classes). With the help of onboard high-resolution multispectral images, we can wrap up the workflow by doing correctness by manually classifying the rest of the point cloud to deliver a complete classification.

Last but not least, the point cloud of the area after the classification process can be used to generate a 3D city model. The 3D model introduced in the study is the LoD2 model, which can be used for various purposes like city inventory for buildings, trees, etc.; city management and planning; handling emergencies; tourism, etc.

6. Acknowledgements

This study was supported by the Ministry of Education and Training Science project (N0. B2021-MDA-01), Vietnam.

7. References

1. Nguyen Quoc Long, Ropesh Goyal, Bui Khac Luyen, Le Van Canh, Cao Xuan Cuong, Pham Van Chung, Bui Ngoc Quy, Bui Xuan Nam, Influence of Flight Height on The Accuracy of UAV Derived Digital Elevation Model at Complex Terrain, *Journal of the Polish Mineral Engineering Society*, 1(45): 179 - 186, 2020. DOI: <https://doi.org/10.29227/IM-2020-01-27>.
2. Le Van Canh, Cao Xuan Cuong, Nguyen Quoc Long, Le Thi Thu Ha, Tran Trung Anh, Xuan-Nam Bui, 2020 – Experimental Investigation on the performance of RTK drones on 3D mapping Open-pit coal mines, *Journal of the Polish Mineral Engineering Society*, 2(46): 65–74. DOI: <http://doi.org/10.29227/IM-2020-02-10>.
3. Quy Ngoc Bui, Hiep Van Pham, Research on 3D model from unmanned aerial vehicle (UAV) images, *Journal of Mining and Geology*, 4(58): 1-11, 2017. <http://tapchi.humg.edu.vn/vi/archives?article=873>
4. Bui Ngoc Quy, Le Dinh Hien, Nguyen Quoc Long, Tong Si Son, Duong Anh Quan, Pham Van Hiep, Phan Thanh Hai, Pham Thi Lan, Method of defining the parameters for UAV point cloud classification algorithm, *Journal of the Polish Mineral Engineering Society*, 1(46): 49-56, 2020. DOI: <https://doi.org/10.29227/IM-2020-02-08>.
5. L. Q. Nguyen, 2021. Accuracy assessment of open-pit mine’s digital surface models generated using photos captured by Unmanned Aerial Vehicles in the post-processing kinematic mode (in Vietnamese). *Journal of Mining and Earth Sciences*, Vol. 62, no. 4, Aug. 2021, p 38-47, doi:10.46326/JMES.2021.62(4).05.
6. Nguyen, Q. L., Le, T. T. H., Tong, S. S., Kim, T. T. H., (2020). UAV Photogrammetry-Based For Open Pit Coal Mine Large Scale Mapping, *Case Studies In Cam Pha City, Vietnam. Sustainable Development of Mountain Territories*, 12(4), 501-509. DOI: 10.21177/1998-4502-2020-12-4-501-509.
7. Nguyen Q. L., Ropesh G., Bui, K. L, Cao X. C., Le V. C., Nguyen Q. M., Xuan-Nam B., (2021). Optimal Choice of the Number of Ground Control Points for Developing Precise DSM using Light-Weight UAV in Small and Medium-Sized Open-Pit Mine. *Archives of Mining Sciences*, 66 (3), p 369-384, doi: 10.24425/ams.2021.138594.
8. Charaniya, A., Manduchi, R., Lodha, S., 2004. Supervised parametric classification of aerial LiDAR data. In: *Proceedings of the IEEE 2004 Conference on Computer Vision and Pattern Recognition Workshop*. Vol. 3. Baltimore, pp. 1–8.
9. Garroway, K., Hopkinson, C., Jamieson, R., 2011. Surface moisture and vegetation influences on LiDAR intensity data in an agricultural watershed. *Canadian Journal of Remote Sensing* 37(3): 275–284.
10. Mazzarini, F., Pareschi, M.T., Favalli, M., Isola, I., Tarquini, S., Boschi, E., 2007. Lava flow identification and aging by means of LiDAR intensity: Mount Etna case. *Journal of Geophysical Research: Solid Earth* 112 (B2)
11. Lang, M.W., McCarty, G.W., 2009. LiDAR intensity for improved detection of inundation below the forest canopy. *Wetlands* 29(4): 1166–1178.
12. Burton, D., Dunlap, D.B., Wood, L.J., Flaig, P.P., 2011. LiDAR intensity as a remote sensor of rock properties. *Journal of Sedimentary Research* 81(5): 339–347.
13. Song, J.H., Han, S.H., Yu, K.Y., Kim, Y.I., 2002. Assessing the possibility of land-cover classification using LiDAR intensity data. *International Archives of the Photogrammetry, Remote Sensing and Spatial Information Sciences* 34(Part 3/B): 259–262.

14. Minh, N.Q., Hien, L.P., 2011. Land cover classification using LiDAR intensity data and neural network. *Journal of the Korean Society of Surveying, Geodesy, Photogrammetry and Cartography* 29(4): 429–438.
15. Brennan, R., Webster, T., 2006. Object-oriented land cover classification of LiDAR-derived surfaces. *Canadian Journal of Remote Sensing* 32(2): 162–172.
16. Yoon, J.-S., Shin, J.-I., Lee, K.-S., 2008. Land cover characteristics of airborne LiDAR intensity data: a case study. *IEEE Geoscience and Remote Sensing Letters* 5(4): 801–805.
17. Yan, W.Y., Shaker, A., Habib, A., Kersting, A.P., 2012. Improving classification accuracy of airborne LiDAR intensity data by geometric calibration and radiometric correction. *ISPRS Journal of Photogrammetry and Remote Sensing* 67, 35–44.
18. Yan, W.Y., Shaker, A., 2014. Radiometric correction and normalization of airborne LiDAR intensity data for improving land cover classification. *IEEE Transactions on Geoscience and Remote Sensing* 52(10): 7658–7673.
19. Im, J., Jensen, J.R., Hodgson, M.E., 2008. Object-based land cover classification using high-posting-density LiDAR data. *GIScience & Remote Sensing* 45(2): 209–228.
20. Zhou, W., Huang, G., Troy, A., Cadenasso, M., 2009. Object-based land cover classification of shaded areas in high spatial resolution imagery of urban areas: a comparison study. *Remote Sensing of Environment* 113(8): 1769–1777.
21. MacFaden, S.W., O'Neil-Dunne, J.P., Royar, A.R., Lu, J.W., Rundle, A.G., 2012. High-resolution tree canopy mapping for New York City using LiDAR and object-based image analysis. *Journal of Applied Remote Sensing* 6(1): 063567–1–063567–23.
22. Zhou, W., July 2013. An object-based approach for urban land cover classification: integrating LiDAR height and intensity data. *IEEE Geoscience and Remote Sensing Letters* 10(4): 928–931.
23. Hecht, R., Meinel, G., Buchroithner, M.F., 2008. Estimation of urban green volume based on single-pulse LiDAR data. *IEEE Transactions on Geoscience and Remote Sensing* 46(11): 3832–3840.
24. Huang, M., Shyue, S., Lee, L., Kao, C., 2008. A knowledge-based approach to urban feature classification using aerial imagery with LiDAR data. *Photogrammetric Engineering & Remote Sensing* 74(12): 1473–1485.
25. Guan, H., Ji, Z., Zhong, L., Li, J., Ren, Q., 2013. Partially supervised hierarchical classification for urban features from LiDAR data with aerial imagery. *International Journal of Remote Sensing* 34(1): 190–210.
26. Chen, Y., Su, W., Li, J., Sun, Z., 2009. Hierarchical object-oriented classification using very high-resolution imagery and LiDAR data over urban areas. *Advances in Space Research* 43(7): 1101–1110.
27. Antonarakis, A., Richards, K., Brasington, J., 2008. Object-based land cover classification using airborne LiDAR. *Remote Sensing of Environment* 112(6): 2988–2998.
28. Singh, K.K., Vogler, J.B., Shoemaker, D.A., Meentemeyer, R.K., 2012. Lidar-Landsat data fusion for large-area assessment of urban land cover: balancing spatial resolution, data volume, and mapping accuracy. *ISPRS Journal of Photogrammetry and Remote Sensing* 74, 110–121.
29. Sasaki, T., Imanishi, J., Ioki, K., Morimoto, Y., Kitada, K., 2012. Object-based classification of land cover and tree species by integrating airborne LiDAR and high spatial resolution imagery data. *Landscape and Ecological Engineering* 8(2): 157–171.
30. Hartfield, K.A., Landau, K.I., Van Leeuwen, W.J., 2011. Fusion of high resolution aerial multispectral and LiDAR data: land cover in the context of urban mosquito habitat. *Remote Sensing* 3(11): 2364–2383.
31. Yanjing, J., 2015. Object-based Land Cover Classification with Orthophoto and LIDAR Data. Master of Science Thesis in Geoinformatics TRITA-GIT EX 15-001.

Development of Integrated Reporting in Poland

BARTOSZ Rymkiewicz^{1,*}

¹ AGH University of Science and Technology, Kraków, Poland

Corresponding author: bartosz.rymkiewicz@zarz.agh.edu.pl

Abstract. Organizational reporting is the most important tool of communication between an enterprise and its stakeholders. However, it is not a static tool but continues to develop and adapt to ongoing economic and social changes. Formerly covering only financial information; currently, it is supplemented by a wide range of non-financial information relating to all aspects of the business. The evolution of reporting is particularly fostered by the rapid development of the concepts of corporate social responsibility and sustainable development, as well as the progressing changes in the information needs of stakeholders. Enterprises are increasingly publishing voluntary reports concerning the social, environmental, and employment aspects of their business in addition to reports required by law. This results in the multiplication of reports and duplication of content, which has a negative impact on the reports' usefulness. The solution to this problem may be integrated reporting, which integrates and interconnects financial and non-financial disclosures. A milestone for the development of integrated reporting was the elaboration of integrated reporting guidelines by the International Integrated Reporting Council (IIRC) in December 2013. The aim of the paper is to present the development of integrated reporting in Poland in 2014-2020 on the example of public companies listed on the Warsaw Stock Exchange. The quality of reports was assessed from the point of view of compliance with IIRC guidelines, as well as their usefulness for stakeholders. Content analysis of corporate publications and comparative analysis was used for this purpose.

Keywords: Integrated reporting, Organization reporting, Non-financial disclosures, Reporting evolution, Reporting development

1. Introduction

Organizational reporting is an essential tool for communicating with stakeholders. However, it is not a static tool, but is constantly evolving to adapt to the dynamically changing social and economic environment. The constantly increasing informational expectations of a wide range of stakeholders lead to the emergence of new reporting concepts. In recent decades, reporting has evolved from simple financial statements containing only financial disclosures to complex conglomerates of various types of reports covering financial and non-financial information [1, 2]. However, both traditional financial reporting and the multiplication of reports repeatedly repeating the same content lead to disturbances in communication between the company and its stakeholders [3, 4, 5, 6]. The remedy for these problems is the modern concept of integrated reporting, which integrates and interconnects financial and non-financial disclosures, enabling a better overview of the business. This concept, which focuses on the organization's ability to create value in the short, medium and long term, is key to providing a reliable picture of the company. Integrated reporting differs significantly from traditional reporting. It is manifested in particular through conciseness, strategic focus and future orientation, the connectivity of information and the capitals and their interdependencies [7]. Moreover, it is a two-way communication tool with stakeholders, as it should involve key stakeholders in the content definition process. "An integrated report should provide insight into the nature and quality of the organization's relationships with its key stakeholders, including how and to what extent the organization understands, takes into account and responds to their legitimate needs and interests" [7].

Clearly defining the beginning of integrated reporting is not straightforward. A milestone was the development by the International Integrated Reporting Council (IIRC) of the International <IR> Framework [8] guidelines in December 2013, which included a structural framework for integrated reporting. This date can be described as the beginning of the development of integrated reporting in Poland. More than seven years have passed since then; therefore, it is worth reviewing how the practice of integrated reporting in Poland has changed. In particular, the following questions are worth answering: Has integrated reporting been adopted in Poland? How has the form of reports changed? How has the informational content of reports changed? To achieve this, a research study was conducted on a sample of 95 integrated reports published by companies in Poland between 2014 and 2020. Two main research methods were used - content analysis of corporate publications and comparative analysis.

2. Organizational reporting in Poland

Companies in Poland conduct extensive reporting, often including many diverse financial and non-financial reports. The most frequently used include: financial report, activity report of the entity (Management Commentary), report on payments to the public administration, annual report of marketing and business character, social report (corporate social responsibility report), sustainability report, environmental report, integrated report and others. Companies use a lot of often very extensive reports, repeating specific content many times, which has a negative impact on their reception by users. Generally, organizational reporting in Poland can be divided into obligatory (mandatory) and optional (voluntary). Mandatory reporting is regulated by the Accountancy Act and the International Accounting and Financial Reporting Standards [9a, b]. For all entities obliged to keep accounting books in accordance with the Accounting Act, the obligatory reports include financial statements containing mainly financial disclosures. Certain types of entities indicated in Art. 49.1 of the Accounting Act [9c] are additionally obliged to prepare a activity report (management commentary), which is a report of a non-financial nature. The activity report of the entity should include significant information on the property and financial situation, assessment of the gained results and identification of risk factors and description of threats. In particular, it should include information about events significantly affecting the entity's operations, the expected development of the entity, major achievements in the field of research and development, the current and expected financial situation, treasury shares, branches held by the entity, financial instruments, as well as, if it is important for the assessment of the development, results and situation of the entity - key financial performance indicators related to the entity's operations and key non-financial performance indicators related to the entity's operations, as well as information on employee issues and the environment (Article 49, paragraphs 2 and 3 of the Accounting Act). Moreover, securities issuers are obliged to make a separate statement on corporate governance in their activity report. The transposition of Directive 2014/95/EU into the Polish legal system in 2017 additionally introduced an obligation for the largest entities in Poland [9d] to include a separate statement on non-financial information in their activity report covering: a concise description of the entity's business model, key non-financial performance indicators related to the entity's operations, a description of the policies applied by the entity with respect to social, labour, environmental, human rights and anti-corruption issues, as well as a description of the results of applying these policies, a description of due diligence procedures with respect to the policies indicated, and a description of significant risks related to the entity's operations that may have an adverse impact on social, labour, environmental, human rights and anti-corruption issues (art. 49b of the Accounting Act). Companies operating in the mining industry and in the logging of primary forests that meet certain criteria [9e] are also required to prepare a report on payments to the public administration, including information on the total amount of payments made to the public administration of a given country, divided into payments to the relevant levels of public administration (Art. 63f of the Accounting Act).

In practice, companies in Poland very often go beyond the obligatory reporting by preparing various types of reports referring to specific areas of their activity. This is particularly related to the involvement of entities in modern management concepts, such as corporate social responsibility or sustainable development. The most frequently used reports include, among others, annual report of marketing and business character, social report (corporate social responsibility report), sustainable development report, environmental report, integrated report and other thematic reports. Individual reports are discussed in the Table 1.

Presented types of reports have voluntary character and their structure is not standardized by any regulations. It should be noted, however, that companies in Poland use a variety of standards and guidelines in the report development process. The most popular guidelines include: Global Reporting Initiatives (GRI) [10], IIRC, ISO26000 [11] and AccountAbility1000 [12].

A fundamental problem that has a significant impact on a company's communication with stakeholders is that companies create many very large reports that duplicate specific content. This significantly complicates the process of searching for specific content by the user. As a solution to this problem the modern concept of integrated reporting may be applied, which aims to reduce the number of reports to one containing both financial and non-financial information.

Tab. 1. Voluntary report types prepared by companies in Poland.

TT	Report type	Description
1	Annual report of marketing and business character	<ul style="list-style-type: none"> - a report that is not a simple combination of the financial statements and the activity report of the entity (management commentary); - includes both financial and non-financial disclosures; - prepared in a visually rich form, enriched with photographs and diagrams.
2	Social report (corporate social responsibility report)	<ul style="list-style-type: none"> - a report covering mainly non-financial disclosures; - closely linked to the corporate social responsibility concept which assumes transparency of conducted operations and informing about the impact on society and environment; - discusses the social and environmental impact of the business.
3	Sustainable development report	<ul style="list-style-type: none"> - a report covering mainly non-financial disclosures; - closely linked to the sustainable development concept; - includes disclosures from three primary areas that should balance each other, i.e., social, environmental, and economic areas.
4	Environmental report	<ul style="list-style-type: none"> - a report covering mainly non-financial disclosures; - focuses mainly on the environmental aspects of the business, in particular the company's impact on the environment and activities preventing the negative effects of its operations on this area.
5	Integrated report	<ul style="list-style-type: none"> - a report that integrates and interrelates financial and non-financial disclosures; - the central element of the report is the business model; - future-oriented; - uses a strategic approach.

3. The concept of integrated reporting

The integrated reporting concept is a modern solution to integrate and interrelate financial and non-financial disclosures in one comprehensive report. It is an answer to the most frequently presented problems of traditional reporting, i.e. misalignment with stakeholders' needs or focusing only on the past [3, 4, 5]. The concept currently enjoys great interest among practitioners and theorists of accounting as evidenced by numerous publications [2, 3, 13-19]. The most important objectives of integrated reporting presented in the literature include: full integration of financial and non-financial disclosures (in particular related to the concept of sustainable development and social responsibility) [14], improving the quality of information presented to increase the efficiency of capital allocation, increasing the consistency and efficiency of disclosures, communicating the holistic factors affecting the organization's ability to create value, better understanding of the relationships between individual capitals, supporting integrated thinking, making decisions directed at value creation [7], improving communication with stakeholders [2]. Integrated reporting, unlike traditional reporting, takes as its core point the company's value creation process in the short, medium and long term. As a result, integrated reporting is sometimes referred to as value statement [1]. The value creation process in an enterprise is highlighted by the business model, which is defined as "the chosen system of inputs, business activities, outputs and outcomes that aims to create value over the short, medium and long term" [20]. Accordingly, "the primary objective of business model representation is to provide visibility to the unique way in which the business coordinates resources in order to achieve corporate objectives" [21]. An integrated report should illustrate the way an organization transforms capital (financial, manufactured, intellectual, human, social and relationship, and natural) using business activities into outputs and outcomes that aims to fulfil the organization's strategic purposes and create value over the

short, medium and long term [7]. Equally important in integrated reporting is the different approach to presenting data. Traditional reporting presents mainly historical data about the operational sphere of the business. This approach makes it significantly more difficult for investors and other stakeholders to assess the company's intentions. Integrated reporting changes this approach as the future and strategic orientation becomes crucial [7]. The important thing is not how the company created value, but how it intends to create value in the short, medium and long term.

The structural framework for integrated reporting was developed by IIRC in December 2013 and received its first update in January 2021. The Guiding Principles of the International <IR> Framework [7, 8] set out the principles that should guide a company in preparing an integrated report and the model structure of the report. A total of seven Guiding Principles were identified: strategic focus and future orientation, connectivity of information, stakeholder relationships, materiality, conciseness, reliability and completeness, consistency and comparability. The individual principles are discussed in the Table 2.

Tab. 2. Guiding Principles of International <IR> Framework.

TT	Guiding Principles	Description
1	Strategic focus and future orientation	The integrated report should focus on the organization's strategy and its relationship to the organization's ability to create value over time and to use its capitals.
2	Connectivity of information	The integrated report should provide a holistic view of the relationships between the various factors that affect the organization's ability to create value over time. Information flow within the organization should be integrated with management reporting, analysis, decision making, and ultimately, integrated reporting.
3	Stakeholder relationships	The integrated report should illustrate how the organization relates to its key stakeholders. In particular, it should show how the organization responds to their legitimate needs and interests.
4	Materiality	The integrated report should include material disclosures that have a significant impact on the organization's ability to create value.
5	Conciseness	The integrated report should be concise. It should contain only material information necessary for an understanding of strategy, governance, performance and prospects.
6	Reliability and completeness	The integrated report should include all material information whether positive or negative. It should also be balanced and without material errors.
7	Consistency and comparability	The Integrated Report should present information in a manner that is consistent over time and that ensures comparability.

The model structure of an integrated report compliant with the International <IR> Framework includes eight elements: organization overview and external environment, governance, business model, risks and opportunities, strategy and resource allocation, performance, outlook, basis of preparation and presentation. The individual elements were discussed in the Table 3.

Tab. 3. Content Elements of International <IR> Framework.

TT	Content Elements	Description
1	Organization overview and external environment	Includes a presentation of the organization's activities and the environment in which it operates.
2	Governance	Includes a presentation of the governance structure and its impact on the ability to create value.
3	Business model	Includes a presentation of the organization's business model.
4	Risk and opportunities	Includes a presentation of the risks and opportunities that affect the organization's ability to create value.

5	Strategy and resource allocation	Includes a presentation of the organization's goals and direction.
6	Performance	Includes a presentation of the extent to which the organization has achieved its strategic objectives over the period and what the impact on capital is.
7	Outlook	Includes a presentation of the challenges and uncertainties associated with strategy execution and its impact on the business model and future performance.
8	Basis of preparation and presentation	Includes a presentation of the report content definition process.

4. The evolution of integrated reporting in Poland over the period 2014-2020

4.1. Research purpose

Organizational reporting in Poland is constantly changing, adapting to the rapidly changing social and economic environment. A particularly important factor in the evolution of reporting are legislative changes, especially resulting from European Union directives aimed at increasing the transparency of companies in the value creation process, as well as employee, social and environmental policies. A milestone in the reporting development in Poland was the integrated reporting guidelines - International <IR> Framework developed by IIRC in December 2013. This resulted in the development of a modern form of reporting in Poland, such as integrated reporting. The second milestone was the introduction of Directive 2014/95/EU, which was subsequently transposed into Polish legislation in 2017. It imposed on the largest companies the obligation to disclose non-financial information concerning, for instance, the business model and the policies applied with regard to social, labour, environmental, human rights and anti-corruption issues. However, more than seven years have passed since the end of 2014, therefore it is worth considering how the integrated reporting practice has changed in Poland. Accordingly, a research study was conducted to present the development of integrated reporting in Poland. In particular, focusing on the interest of companies in integrated reporting, the form of reports prepared and the process of defining their content.

4.2. Research sample and research period

The reporting practice of Polish companies is very extensive, many companies publish several different forms of reports, i.e. annual report including financial statements and activity report, report on non-financial information, social report, environmental report, sustainability report, annual report of business-marketing character or integrated report. A number of annual reports of a business and marketing character and social or sustainability reports include both financial and non-financial disclosures. As a result, strictly distinguishing which reports are integrated reports and which are not is extremely difficult. In the study conducted, the assumption was that it is the organization that decides whether to prepare an integrated report. Therefore, the research sample included reports described by companies as "integrated report" or "integrated annual report", as well as reports admittedly called „annual report”, but defined in the description as "integrated report". The research analyzed 95 company reports published between 2014 and 2020. These reports covered 7 reporting periods (reports for 2013-2019). 94 reports were prepared for a single year, while one report covered two years (report prepared by Azoty company for 2016-2017). The study included reports made public by 25 entities, of which 22 are public companies listed on the Warsaw Stock Exchange (WSE) and 3 non-public companies. To determine the beginning of the research period, the development of IIRC guidelines in December 2013 was crucial, providing an impetus for changes in the organizational reporting. The first reports based on the indicated guidelines started to be developed in 2014 (integrated reports for 2013).

4.3. Research methodology

Two research methods were used for the study - content analysis of corporate publications and comparative analysis.

The study focused on two main areas - form and scope of reporting. Under the form, the focus was on answering the question - how does the company present disclosures about its activities? The answer to this

question is extremely important in terms of proper communication with stakeholders. Reporting is one of the most extensive tools for communicating with stakeholders, and therefore should be prepared and published in a user-friendly form. In particular, it should ensure accessibility, ease of use, comparability, reliability and credibility. To this end, five categories have been identified: the type (form) of report produced, the size of the report, the standards used in the report preparation process, the report language, and the report verification.

The form of the integrated report is important in the process of communication with stakeholders. Reports can be produced in two forms: traditional and interactive. The traditional form involves publishing the report as a document, usually in PDF format. All information in this type of report is static. On the other hand, the interactive form involves the development of reports in the form of expanded portals (websites) that allow searching, comparing and preliminary analysis of the content. Interactive reports are in many cases enhanced with video and advanced searching capabilities.

A common criticism of reporting is that it is significantly oversized. Companies publish very extensive reports revealing a lot of information irrelevant from the point of view of stakeholders. Extensive descriptions and frequent repetition of some content significantly reduce the usefulness of reports. Therefore, the study analyzed the size of reports by determining their number of pages. Due to the importance and problem of comparability, this concerned only reports prepared in traditional form.

Standardization is essential to ensure comparability and reliability of reports. Currently, there are many standards and guidelines concerning reporting on non-financial issues. The most widespread worldwide are the guidelines for integrated reporting developed by the IIRC and the guidelines for reporting on sustainable development established by GRI. It should also be noted that these are voluntary guidelines and standards, which include principles and procedures useful in the report preparation process and defining its content. The study analyzes which standards and guidelines are used by companies in Poland in the integrated report preparation process.

In the age of globalization and companies opening up to foreign markets, the number of stakeholders is significantly increasing. This process significantly complicates the communication between companies and their stakeholders. Language is the most significant barrier. In particular, it concerns companies using languages that are not widely used around the world, such as Polish. The study analyzed the language versions of integrated reports used by companies in Poland.

Nowadays, in the age of ubiquitous information, the key issue is its credibility. Organizational reporting provides a huge amount of information about the business activity. However, numerous scandals in recent decades, such as Enron, WorldCom or Amber Gold, have significantly shaken the confidence of stakeholders in the information disclosed in reports. Therefore, verification of the reports by an independent auditor is extremely important. In Poland, financial disclosures included in financial statements are obligatorily audited. Equally important are non-financial disclosures allowing for a more precise view of the company's situation. The audit of non-financial information is not obligatory, but some entities voluntarily submit their reports. The study analyzed whether the report was audited by an independent external auditor for non-financial disclosures.

The second area analyzed in the study, i.e., the scope of the report, attempts to answer the questions - how was the content of the integrated report defined? and what content does the integrated report cover? For this purpose, four elements were focused on: the stakeholder identification process, the stakeholder engagement process, the use of materiality matrix and the business model disclosure.

The integrated report is a tool for communicating with stakeholders, therefore, the first step should be to identify stakeholders. This allows to better customize the content of the report to the users' needs and information expectations. It should be noted, however, that the identification of stakeholders alone is not enough, it is also necessary to involve them in the report content definition process. This process can take different forms, such as conducting interviews, workshops with stakeholders' representatives, surveys, etc. The stakeholder engagement process should lead to the development a catalog of topics that are important from the stakeholders' point of view. However, it should be remembered that not all information can be shared, some of it constitutes company secrets, and its disclosure could result in criminal liability and, in addition, loss of competitive advantage. Therefore, it is necessary to compare issues that are important from the point of view of the stakeholders and the company's capabilities. Stakeholders' expectations and

information needs are extensive, and the integrated report should focus on the most important issues. Therefore, it is necessary to develop a materiality matrix that identifies the most important issues. The study examines the report content definition process from the perspective of stakeholder identification, stakeholder engagement, and the use of materiality matrix.

An integrated report is sometimes referred to as a value creation report. Therefore, the business model (value creation model) should be the central element of any integrated report. The study analyzed the integrated reports content from the perspective of business model disclosures.

4.4. Research findings

In the period 2014-2020, 95 integrated reports were identified. However, it should be noted that there is a wide variation in nomenclature. The most commonly used term is "integrated report" (e.g. "Integrated Report PGNiG 2018"), however, some companies use the term "integrated annual report" (e.g. "ING Bank Śląski 2019 Integrated Annual Report"). In a few cases, companies used the name "annual report", however, in the report content it clearly indicated that it is an integrated report (e.g. "PZU Annual Report 2019"). The number of integrated reports has steadily increased since 2014, from only 5 reports in 2014 to 22 in 2019 and 2020, an increase of 340 percent (see Tab. 4 for details on the number of integrated reports by year). It should be noted that integrated reporting is used mainly by the largest public companies in Poland included in the WIG30 (13 companies in 2020), mWIG40 (3 companies in 2020) and sWIG80 (4 companies in 2020) indices. The reasons for this phenomenon can be sought in particular in greater financial capabilities, greater involvement in modern management concepts, competition with foreign entities and the introduction of Directive 2014/95/EU imposing on the largest entities in the European Union the obligation to publish non-financial information, among others, on the business model.

Tab. 4. Content Elements of International <IR> Framework.

TT	Publication year	2014	2015	2016	2017	2018	2019	2020
1	Reporting period	2013	2014	2015	2016	2017	2018	2019
2	Number of reports	5	8	10	11	17	22	22
3	Year-on-year change	-	60.0%	25.0%	10.0%	54.5%	29.4%	0.0%
4	Public companies	4	6	9	9	15	20	20
5	Change year to year	-	50.0%	50.0%	0.0%	66.7%	33.3%	0.0%
6	Non-public companies	1	2	1	2	2	2	2
7	Year-on-year change	-	100.0%	-50.0%	100.0%	0.0%	0.0%	0.0%

Companies most often prepare integrated reports in two forms simultaneously - traditional and interactive (42 reports). Two approaches of the companies can be observed in this matter. The first one consists in preparing a separate report in the traditional form and in the interactive form. In this case, the report in the traditional form is structured, prepared in an elegant form resembling a folder or a book. Budimex's 2019 report is such an example. The second approach is to be able to create a PDF file that includes all the content of the interactive report. In this variant, the report in the traditional form is characterized by a less structured form, often without a table of contents, including only the content contained in individual pages of the interactive report. Lotos' 2014 report is an example of this approach. More and more companies are choosing only one version of the integrated report - traditional (25 reports in total) or interactive (28 reports in total). This is a much more convenient, less time-consuming and less costly solution for companies. It should also be noted that in the age of progressive computerization it is much easier to reach stakeholders through customized portals. Interactive versions of reports also allow for easier editing in case of identified errors. The main problem with interactive reports is the difficulty of in-depth analysis. It is necessary to repeatedly go through the various sub-pages, open interactive windows, watch videos and animations. This is time-consuming and significantly complicates qualitative analysis. For this type of analysis, it is much more convenient to use traditional reports. Analyzing interactive reports, two forms can be identified. The first is interactive reports which are a kind of visual superstructure over other reports produced in traditional form. They cover some general summary issues, while the details are linked to the traditional report, e.g., financial statements, social report, or report on non-financial

information. The second option is extended interactive reports that include all content in the form of subpages. Orlen's 2018 report is an example of this approach. Analyzing the period of integrated reporting development in Poland, it can be seen that there is a growing interest in the interactive form of integrated reports, and many companies are abandoning traditional form of reporting. In 2020, as many as 9 companies prepared the report exclusively in interactive form (year-on-year increase of 50%), while only 5 companies prepared the report exclusively in traditional form (year-on-year decrease of 28.6%). In addition, companies are abandoning the possibility of obtaining the traditional form of interactive reports (a decrease of 11.1% was recorded in 2020 compared to 2019). It seems that in the future, the interactive form will become the only form of report preparation. Detailed quantitative data on the integrated report forms by year are provided in the Table 5.

Tab. 5. Forms of integrated reports prepared by companies in Poland between 2014 and 2020.

No.	Publication year	2014	2015	2016	2017	2018	2019	2020	Total
	Reporting period	2013	2014	2015	2016	2017	2018	2019	
1	Interactive and traditional form	3	5	4	4	9	9	8	42
2	Year-to-year change	-	66.7%	-20.0%	0.0%	125.0%	0.0%	-11.1%	
3	Traditional only form	2	2	2	3	4	7	5	25
4	Year-on-year change	-	0.0%	0.0%	50.0%	33.3%	75.0%	-28.6%	
5	Interactive-only form	0	1	4	4	4	6	9	28
6	Change year to year	-	-	300.0%	0.0%	0.0%	50.0%	50.0%	

Report size is very important from the point of view of the report users. It is often claimed that reports covering non-financial issues are very voluminous. Analyzing average number of pages of integrated reports prepared by companies in Poland it can be noticed that they are not too extensive. The average is about 200 pages in all years, which seems high, but not very high. It should be remembered, however, that integrated reports are prepared mainly by the largest companies in Poland, which often conduct diverse activities in many countries. It should be noted, however, that the average does not fully show the volume of integrated reports, which range in size from as little as 48 pages to as many as 521. In many cases, the large volume of integrated reports is due to the inclusion of full financial statements that are often 100-150 pages each (e.g. in Lotos' 2014 integrated report), as well as the use of a visually varied form full of photographs and diagrams (e.g. LPP's 2017 report). Detailed quantitative data on the average size of integrated reports prepared in traditional form are presented in the Table 6.

Tab. 6. Content Elements of International <IR> Framework.

Publication year	2014	2015	2016	2017	2018	2019	2020	Total
Reporting period	2013	2014	2015	2016	2017	2018	2019	
Average number of pages	222	169	189	217	180	185	210	194
Year-on-year change	-	-23.74%	11.93%	14.49%	-16.67%	2.77%	13.07%	-
Minimum number of pages	48	60	56	70	73	68	89	48
Maximum number of pages	469	468	351	521	320	442	519	521

Standardisation is extremely important to ensure data comparability published in the integrated reports. Companies in Poland use many standards and guidelines in the integrated reporting preparation process. The most important from the point of view of integrated reporting are guidelines developed by IIRC. It is interesting that only 65 integrated reports were prepared according to these guidelines (68.42% of all integrated reports). It seems that IIRC guidelines should be the core of every integrated report, however some companies ignore them. It should be noted that there are large fluctuations from year to year in the number of companies using the IIRC guidelines - first an upward trend from 60% in 2014 to 80% in 2016, then a decrease to about 64% in 2017, then an increase again to nearly 73% in 2019 and again a decrease in 2020 to about 64%. The sustainability reporting guidelines proposed by GRI are much more popular. As many as 92 of the analyzed integrated reports were prepared according to the indicated guidelines (96.84

percent of all reports). This is related to the greater popularity of GRI standards, which have been developed since 2000. Many companies in Poland had already used these guidelines when preparing their social, environmental, or sustainable development reports. Therefore, it is obvious that effectively implemented and verified reporting procedures are maintained by the companies. Additionally, it should be noted that GRI standards are characterized by voluntariness, a high level of universality, and are constantly developed in order to adapt them to the needs of modern business life. In the period 2014-2020, there were several changes to the applicable GRI standards, therefore GRI G3 (1 report), GRI G3.1 (3 reports), GRI G4 (40 reports) and GRI STANDARDS (48 reports) were used by the companies. The AA1000 standard on building stakeholder relations is also frequently used - 28 integrated reports. This standard is particularly important due to the role of the integrated report as a tool for communication with stakeholders. Identifying and engaging stakeholders in the reporting process is part of building healthy relationships and using integrated reporting as a two-way tool to respond to stakeholders' legitimate information needs. As of 2017, the Sustainable Development Goals (SDGs) [22], which are a United Nations (UN) initiative for the advancement of sustainable development, are also very popular - 29 integrated reports. Less popular guidelines and standards used in the process of preparing integrated reports in Poland include: ISO26000 (17 reports), TCFD (5 reports) [23], CSI (4 reports) [24] and SIN (2 reports) [25-27]. Detailed quantitative data on the standards and guidelines used in the integrated reporting preparation process are presented in the Table 7.

Tab. 7. Content Elements of International <IR> Framework.

Publication year	2014	2015	2016	2017	2018	2019	2020	Total	Share
Reporting period	2013	2014	2015	2016	2017	2018	2019		
IIRC	3	5	8	7	12	16	14	65	68.42%
GRI total, including:	5	7	10	11	17	21	21	92	96.84%
- G3	0	1	0	0	0	0	0	1	1.05%
- G3.1	2	1	0	0	0	0	0	3	3.16%
- G4	3	5	10	11	10	1	0	40	42.11%
- GRI STANDARDS	0	0	0	0	7	20	21	48	50.53%
AA1000	0	1	2	4	6	7	8	28	29.47%
ISO26000	0	1	1	2	4	4	5	17	17.89%
SDGs	0	0	0	3	8	9	9	29	30.53%
TCFD	0	0	0	0	0	0	5	5	5.26%
SIN	0	0	0	0	0	1	1	2	2.11%
CSI	0	0	0	1	1	1	1	4	4.21%

Due to the often worldwide character of the business activity, and therefore having stakeholders from various regions of the world, it is necessary to prepare the report in a language variant enabling proper communication with a wide group of them. Polish is not the leading language in the world, used rather exclusively in Poland, therefore companies preparing integrated reports are often forced to publish them also in other languages. The reporting practice in Poland shows that companies most often choose the global language of business, i.e. English. In the examined sample 74 reports were prepared in two versions, i.e. Polish and English (77.89%). Additionally, four reports by CEMEX were prepared exclusively in English, which is due to the fact that it is a subsidiary of a leading global cement company. Only 17 reports were prepared solely in Polish (17.89%). The reports prepared only in Polish mainly concern companies that choose the traditional form of reporting (e.g. Pekabex). Analyzing integrated reports in Poland one can notice two approaches to preparing traditional reports in two languages. The first variant consists in preparing one report that includes both Polish and English versions, e.g. by dividing the page into two parts, as e.g. LW Bogdanka in the 2016 report. The second practice consists in preparing completely separate integrated reports in Polish and English versions, as e.g. KGHM in the 2019 report. Detailed figures on the language versions used by companies in Poland in integrated reporting are presented in the Table 8.

Tab. 8. Content Elements of International <IR> Framework.

Publication year	2014	2015	2016	2017	2018	2019	2020	Total	Share
Reporting period	2013	2014	2015	2016	2017	2018	2019		
Polish language version only	3	2	1	2	2	3	4	17	17.89%
English language version only	0	0	0	1	1	1	1	4	4.21%
Polish and English language version	2	6	9	8	14	18	17	74	77.89%

Trust is extremely important in the communication process. In the case of reporting this trust is extremely easy to lose as shown by numerous scandals in recent years. Reliability and credibility of the data presented is a key factor in building strong and lasting relations between the company and its stakeholders. Ensuring the credibility and reliability of the presented disclosures may enable the report to be audited by an independent external auditor. In Poland, it is obligatory for public companies to have their financial statements audited by a certified auditor, but there is no obligation to audit non-financial disclosures included in integrated reporting. Nevertheless, some companies have their reports audited by independent auditors - 35 reports representing 36.84% of the total. It should be noted, however, that the percentage of companies auditing non-financial disclosures is decreasing year by year - from 60% in 2014 to only 22.73% in 2020. There are many reasons for this phenomenon. The most important is the difficulty of verifying the truthfulness of disclosures, which in many cases relate to targets or forecasts. It should also be noted that the verification to which the company reports are subjected does not concern the truthfulness of the disclosed information, but only confirms information from a given area being disclosed. Most often, it consists in confirming the fulfillment of the declared GRI indicators. Therefore, this type of verification does not fulfill its basic role, which is to ensure the reliability of the presented data. In addition, one company indicated that it performed an internal verification of the report content (INTERCARS company in the report for 2018). Detailed quantitative data on verification of integrated reports by companies in Poland are presented in the Table 9.

Tab. 9. Content Elements of International <IR> Framework.

Publication year	2014	2015	2016	2017	2018	2019	2020	Total
Reporting period	2013	2014	2015	2016	2017	2018	2019	
Total Report Verification	3	5	5	4	7	7	5	36
Percentage share	60.00%	62.50%	50.00%	36.36%	41.18%	31.82%	22.73%	37.89%
External verification	3	5	5	4	7	6	5	35
Percentage share	60.00%	62.50%	50.00%	36.36%	41.18%	27.27%	22.73%	36.84%
Internal verification	0	0	0	0	0	1	0	1
Percentage share	0.00%	0.00%	0.00%	0.00%	0.00%	4.55%	0.00%	1.05%

Integrated reporting is a tool for communication with stakeholders, therefore it is extremely important to properly identify stakeholders and then engage them in the report content definition process. As the study showed, almost all companies identify their stakeholders by drawing up a stakeholder map and specify which stakeholders are key (92 reports representing 96.84% of the total). Stakeholders are included in the process of defining the content of integrated reports by the vast majority of companies (93 reports representing 97.89% of the total). Stakeholders engagement is most often carried out through workshops, surveys or interviews. The high level of consideration of these elements in the integrated reporting preparation process in Poland results to a large extent from the application of GRI guidelines. One of the GRI principles of defining report content is the stakeholder engagement.

GRI and IIRC guidelines indicate that the report should focus on relevant issues. Stakeholders have different information needs, but not all issues are equally important. Therefore, in addition to identifying

issues, it is crucial to assess their relevance from a stakeholder and corporate perspective. A useful tool for identifying material issues is the materiality matrix. As shown in the research, as many as 87 integrated reports contained a materiality matrix, which is 91.58% of the total reports.

Detailed quantitative data on the identification of stakeholders, their involvement in the report content definition process, and the use of materiality matrixes in integrated reports in Poland are presented in the Table 10.

Tab. 10. Content Elements of International <IR> Framework.

Publication year	2014	2015	2016	2017	2018	2019	2020	Total
Reporting period	2013	2014	2015	2016	2017	2018	2019	
Stakeholder identification	5	7	8	11	17	22	22	92
Percentage share	100.00%	87.50%	80.00%	100.00%	100.00%	100.00%	100.00%	96.84%
Stakeholder Engagement	5	8	8	11	17	22	22	93
Percentage share	100.00%	100.00%	80.00%	100.00%	100.00%	100.00%	100.00%	97.89%
Materiality Matrix	5	7	8	10	16	21	20	87
Percentage Share	100.00%	87.50%	80.00%	90.91%	94.12%	95.45%	90.91%	91.58%

An integrated report is sometimes called a value report. As the IIRC guidelines indicate one of the primary objectives of integrated reporting is to “support integrated thinking, decision-making and actions that focus on the creation of value over the short, medium and long term” [7]. Therefore, one of the most important elements, and even the central element, should be the business model. The analysis showed that 82 integrated reports included the business model.

There was also a big change in the nomenclature used. Initially, there was a great diversity in naming the business model, the terms "business model", "value building model" or "value creation model" were used (this issue was discussed by Bek-Gaik & Rymkiewicz 2016) [26]. Currently, after the introduction of the business model concept in the Accounting Act resulting from Directive 2014/95/EU, most entities already use the term "business model". Another issue related to the business model in integrated reporting is the form of its presentation. In the early years, the business model was usually presented in a schematic form depicting specific segments of the business, often devoid of any description. Currently, the form of presentation of the business model is being systematized by using the capital approach proposed by the IIRC [20, 27].

Detailed quantitative data on business model presentation in integrated reports in Poland are showed in the Table 11.

Tab. 11. Content Elements of International <IR> Framework.

Publication year	2014	2015	2016	2017	2018	2019	2020	Total
Reporting period	2013	2014	2015	2016	2017	2018	2019	
Business model	3	5	7	10	15	21	21	82
Percentage share	60.00%	62.50%	70.00%	90.91%	88.24%	95.45%	95.45%	86.32%

4.5. Research conclusions

The study allowed to draw the following conclusions:

1. Companies should standardize the nomenclature of integrated reports, as currently there is a great variation in their naming.
2. Integrated reporting is used mainly by the largest public companies.
3. Companies are increasingly using the interactive form. It seems that in the future it will become a dominant form.

4. Integrated reports prepared by companies in Poland are voluminous, with the average number of pages oscillating around 200.

5. Companies in many cases do not use IIRC guidelines concerning integrated reporting. Still most popular are guidelines concerning sustainable development issues (GRI). This may indicate that companies do not change their reporting practices, but only rename them, e.g. from sustainability report to integrated report.

6. The majority of companies prepare integrated reports in two versions: Polish and English. Such an action results from the international character of their operations and the desire to reach a wider group of stakeholders who do not speak Polish. The choice of English as the international language of business seems appropriate.

7. About one third of the integrated reports are verified externally. It should be noted, however, that the effectiveness of this type of verification is low and does not ensure the reliability of the presented content. It concerns only the confirmation of information disclosure from a given area and does not confirm the correctness and reliability of non-financial disclosures. It should be noted that verification of non-financial disclosures seems to be impossible, as much information is related to plans and forecasts, which are unverifiable. In addition, a full verification of the truth and accuracy of the published content would entail an enormous time and cost burden, which could further negatively impact the development of integrated reporting.

8. Companies in Poland use integrated reports as a tool for communication with stakeholders, which is confirmed by identifying and engaging stakeholders in the process of defining their content.

9. Business model is presented in most integrated reports. The disclosure of the business model has developed significantly in the period 2014-2020. Initially, there was a large variation in nomenclature, however, after the introduction of the term "business model" in the Accounting Act, it became standardized. There has also been an evolution in the approach to its presentation - from a simple chart showing only business segments to a capital approach in line with IIRC guidelines.

5. Summary

Integrated reporting is a modern approach to reporting that integrates and interconnects financial and non-financial disclosures. Simultaneously, it is one of the most important tools for communicating with stakeholders. Unlike traditional reporting, it is a two-way communication, as it takes into account the needs and expectations of stakeholders. The beginnings of integrated reporting in Poland can be traced back to 2014, when the first reports based on IIRC guidelines began to appear. Since then, integrated reporting in Poland has developed significantly. The number of companies publishing integrated reports is increasing year by year. Nevertheless, such reports are prepared mainly by the largest companies, which are leaders in their industry. In the period 2014-2020 there has been a significant change in the form of integrated reports. Initial integrated reports were not significantly different from social reports or sustainability reports. The structure of the reports was significantly different from the structure proposed by the IIRC. Currently, a major change can be observed in this area. Integrated reports are in most cases constructed according to the structure proposed by IIRC and include organizational overview and external environment, governance, business model, risk and opportunities, strategy and resource allocation, performance, outlook and basis of preparation and presentation. An increasingly popular form of reporting is interactive, which allows for additional content and increased interaction with stakeholders, but complicates deeper analysis. Due to the desire to reach a wider range of stakeholders, a significant number of companies publish reports in two language versions - Polish and English. The volume of reports remains at a constant, relatively high level. A significant part of the reports was audited by an independent external auditor, however, this type of verification does not ensure the reliability of the published disclosures, but only whether the declared contents have been disclosed. The analysis of integrated reports showed that companies in Poland identify and involve stakeholders in the process of defining report contents. This demonstrates that integrated reporting is perceived as a two-way communication tool between the company and stakeholders. The 2014-2020 period has also seen a significant transformation in the presentation of the business model from a simple scheme to a more structured capital approach in line with IIRC guidelines.

Integrated reporting has evolved and standardized significantly over the last seven years. Despite the number of integrated reports published increasing year on year, their popularity is relatively low. They are prepared mainly by large, internationally operating entities with significant capital capabilities. It seems that this situation will not change in the coming years. The prerequisite for greater interest in the concept of integrated reporting is the demonstration of measurable benefits from its use, which would exceed the costs of its application. Costs could be reduced and the reporting process could be accelerated by using XBRL language to automatize it.

6. Acknowledgements

The paper was presented during the 6th VIET - POL International Conference on Scientific-Research Cooperation between Vietnam and Poland, 10-14.11.2021, HUMG, Hanoi, Vietnam.

7. References

1. Walińska, E., 2015. Zintegrowany raport – początek końca sprawozdania finansowego? [Integrated Report – Beginning of the End of Financial Statements?]. *Zeszyty Teoretyczne Rachunkowości* 82 (138), 151-165. <https://ztr.skwp.pl/api/files/view/189204.pdf>.
2. Matuszyk, I., Rymkiewicz, B., 2018a. Integrated reporting and sustainable development reporting – comparison of guidelines IIRC and GRI G4. *Central and Eastern European Journal of Management and Economics* Vol. 6, No.1, 31-43. http://ceejme.eu/wp-content/uploads/2018/09/ceejme_1_8_art_03.pdf.
3. Walińska, E., Bek-Gaik, B., Gad, J., Rymkiewicz, B., 2015. Sprawozdawczość przedsiębiorstwa jako narzędzie komunikacji z otoczenie. Wymiar finansowy i niefinansowy. Wydawnictwo Uniwersytetu Łódzkiego. Łódź, 220 pages.
4. Pounder, B., 2012. Full Disclosure vs. Effective Disclosure. *Strategic Finance*, vol. 94, issue 2 (August), 17-18. <https://cupdf.com/document/full-disclosure-vs-effective-disclosure-strategic-pounder-cma-cfm-editor-financial.html>
5. ICAEW., 2010. New Reporting Models For Business. Information for Better Markets initiative. ICAEW Financial Reporting Faculty, <https://www.icaew.com/-/media/corporate/files/technical/financial-reporting/information-for-better-markets/ifbm-reports/new-reporting-models-for-business-2010-version.ashx>.
6. Matuszyk, I., Rymkiewicz, B., 2018b. Integrated Reporting as a Tool for Communicating with Stakeholders – Advantages and Disadvantages. *E3S Web of Conferences* 35, 06004, 1-7. <https://doi.org/10.1051/e3sconf/20183506004>.
7. IIRC., 2021. International <IR> Framework, <https://integratedreporting.org/wp-content/uploads/2021/01/InternationalIntegratedReportingFramework.pdf> (13.06.2021)
8. IIRC., 2013a. International <IR> Framework, <https://integratedreporting.org/wp-content/uploads/2015/03/13-12-08-THE-INTERNATIONAL-IR-FRAMEWORK-2-1.pdf> (13.06.2021).
9. Accounting Act of 29 September 1994, *Journal od Laws* 2021 item 217.
10. <https://www.globalreporting.org> (13.06.2021)
11. <https://www.iso.org/iso-26000-social-responsibility.html> (13.06.2021).
12. <https://www.accountability.org/standards/> (13.06.2021).
13. Abeysinghe, C., 2020. Integrated Reporting and Integrated Thinking: A Commentary on the Integrated Reporting Framework (2013). *Colombo Business Journal, International Journal of Theory & Practice*, 11(2), December, 142-170. DOI:10.4038/cbj.v11i2.68.
14. Krzus, M., 2011. Integrated reporting: if not now, when? *Journal for International Accounting* 6, 271-276. <https://www.mikekrzus.com/downloads/files/IRZ-Integrated-reporting.pdf>.
15. Eccles, R., Krzus, M., Ribot, S., 2015. Meaning and momentum in the integrated reporting movement. *Journal of Applied Corporate Finance* 27(2), 8–18. [<https://doi.org/10.1111/jacf.12113>]
16. Eccles, R., Krzus, M., 2010. One report: Integrated reporting for a sustainable strategy. John Wiley & Sons. 256 pages.

17. Dragu, I., Tiron-Tudor, A., 2014. Research agenda on integrated reporting: new emergent theory and practice, *Procedia Economics and Finance* 15, 221-227. <https://core.ac.uk/download/pdf/81196232.pdf>.
18. Bek-Gaik, B., Rymkiwicz, B., 2020. Business model disclosure in the integrated reports of Polish companies [in:] Krasodomska J., Chłapek K., Krajewska S. (ed.), *Accounting Reporting and Auditing. Meeting the needs of the information preparers and users*, Difin, Warsaw, 93-111.
19. Fijałkowska, J., Sobczyk-Paterek, M., 2020. Strategy disclosure in the integrated report. *Scientific Papers of Silesian University of Technology, Organization and Management Series* 149, 143-153. DOI:10.29119/1641-3466.2020.149.14.
20. IIRC., 2013b. Business model. Background paper for <IR>, <https://www.ifac.org/system/files/publications/files/Business-Model-IIRC.pdf> (13.06.2021)
21. NIBR., 2018. Business Model in Integrated Reporting: Best Practices and Guidelines. https://integratedreporting.org/wp-content/uploads/2018/03/NIBR_GUIDA-BM_16feb2018_ENG.pdf.
22. <https://sdgs.un.org/goals> (13.06.2021).
23. <https://www.fsb-tcfid.org/> (13.06.2021).
24. <https://www.wbcds.org/Sector-Projects/Cement-Sustainability-Initiative> (12.06.2021).
25. <https://standardy.org.pl/sin/#pobierzsin> (12.06.2021).
26. Bek-Gaik, B., Rymkiwicz, R., 2016. Model biznesu w raportowaniu zintegrowanym [Business model in integrated reporting], *Prace Naukowe Uniwersytetu Ekonomicznego we Wrocławiu* 442, 32-51. DOI:10.15611/pn.2016.442.03.
27. Directive 2014/95/EU of the European Parliament and of the Council of 22 October 2014 amending Directive 2013/34/EU as regards disclosure of non-financial and diversity information by certain large undertakings and groups.

Identifying Correlation of Coal Seams in the Tien Hai Area, Northern Vietnam by Using Multivariate Statistic Methods

KHUONG The Hung^{1,*}, NGUYEN Phuong¹, NGUYEN Thi Cuc¹, PHAM Nhu Sang¹, NGUYEN Danh Tuyen²

¹ Hanoi University of Mining and Geology, 18 Vien street, Hanoi, Vietnam

² Vinacomin - Vietbac Geology Joint Stock Company, 30B Doan Thi Diem, Hanoi, Vietnam

Corresponding author: khuongthehung@humg.edu.vn

Abstract. In northern Vietnam, the Tien Hai area is considered a high potential area of coal deposits. Two hundred fifty-six geochemical coal samples of 13 cores in the Tien Hai area investigate coal seams and coal deposits to identify the correlation of coal seams. According to the statistical method and cluster analysis of geochemical samples, the results indicate that the Mg, V, As, Ca, Zn, Cr, Co, K, Na, Sr, Fe, Ge, Re, U, Mo, Th, and Ga elements are good indicator elements of the major and trace elements in coal. Most of them comply with the normal or lognormal distribution rules. Besides, the Yb, Sc, Ho, Er, Tm, Lu, Y, Tb, Pr, Dy, and Sm elements are also good indicator elements for rare earth elements in the region. Therefore, the selected elements are used to identify the correlation of the coal seams in the Tien Hai area. Based on the similarity degree between studied objects, the results of grouping boreholes in coal seams show that the correlation of coal seam TV2-11 is suitable and acceptable, the coal seams TV3-6a, TV3-6b, and TV3-6c can be grouped into the coal seam TV3-6. These results present that the models can help study geochemical coal samples and identify the correlation of the coal seams in the Tien Hai area. Additionally, the statistical analysis shows a remarkable degree to determine the correlation of the coal seams. Geochemical coal data can help to evaluate the indicator elements of the major, trace elements, and rare earth elements in coal seams and coal rashing of adjoining and pillar rocks in the Tien Hai area, northern Vietnam.

Keywords: Identifying correlation of coal seams, Multivariate statistic methods, Tien Hai area, Northern Vietnam

1. Introduction

Generally, the correlation of coal seams has been one of the most complicated issues that need further research to clarify. Up to the present, investigations on coal seam correlations have mainly focused on stratigraphic correlation and coal seam division, in which properties and composition of major, rare earth, and trace elements play a vital role. These important findings were obtained by geochemical data processing methods based on Dickinson & Suczek (1979) [1], which mainly rely on the mineral composition of sandstones to determine the provenance of sedimentary materials tectonic setting of the basin. Studies on sedimentary basins have proved that the mineral composition of modern sandstones of different tectonic settings exhibits systematic variations in functional correlation with the origin type and tectonic setting [2, 3, 4, 5]. Many similar studies on ancient sedimentary basins have confirmed the relationship between the mineral composition of sandstones, provenance, and the tectonic setting of sedimentary basins [1, 6, 7, 8]. As a result, the information about the chemical composition of major oxides, mainly rare earth and trace elements obtained by qualitative and quantitative data analysis methods, can identify the correlation of the coal seams.

In Vietnam, the Red River basin (RRB) has been recorded as a region with great potential for coal deposits [9, 10]. In the 2000s, the oil and gas prospecting in this area has gained many positive results about the coal resource potential in the Neogene sediments [11, 12]. However, the geological structure conditions are complicated, and coal seams are distributed deep underground, and most geological works through abundant only focus on oil and gas assessment, prospecting, and exploration. These facts have led to limited research on coals and associated minerals. Therefore, it is very difficult and, in some cases, impossible to identify the correlation of coal seams in the Tien Hai area by applying traditional methods. Accordingly, it is necessary to select appropriate methods and processes to identify the correlation of coal seams in the Red River coal basin in general and the Tien Hai area in particular by using geological and geophysical parameters based on multivariate statistic methods and specialized software on computers to contribute to solving actual requirements. This study aims to make a clear context for identifying the correlation of the coal seams in the Tien Hai area, northern Vietnam. This study will help us better understand the contribution of the major and trace elements and rare earth elements in this area and provide valuable tools for correlating

the coal seams in the Red River coal basin.

2. Geological framework

2.1 Structural and tectonic setting of the study area

The Red River coal basin is one part of the RRB in the Vietnam mainland (Fig. 1A). The RRB is about 650 km long, 150 km wide, and has a sediment thickness of more than 10 km at its depocenter. The Tien Hai area is located in the Red River coal basin (Fig. 1B).

The Red River fault zone, which runs northwest to southeast, is bounded by two major northwest to southeast trending faults that form a valley shape in the RRB. Chay River and Lo River faults are the two major faults that dominated the Tertiary sedimentation and deformation of the RRB (Fig. 1A).

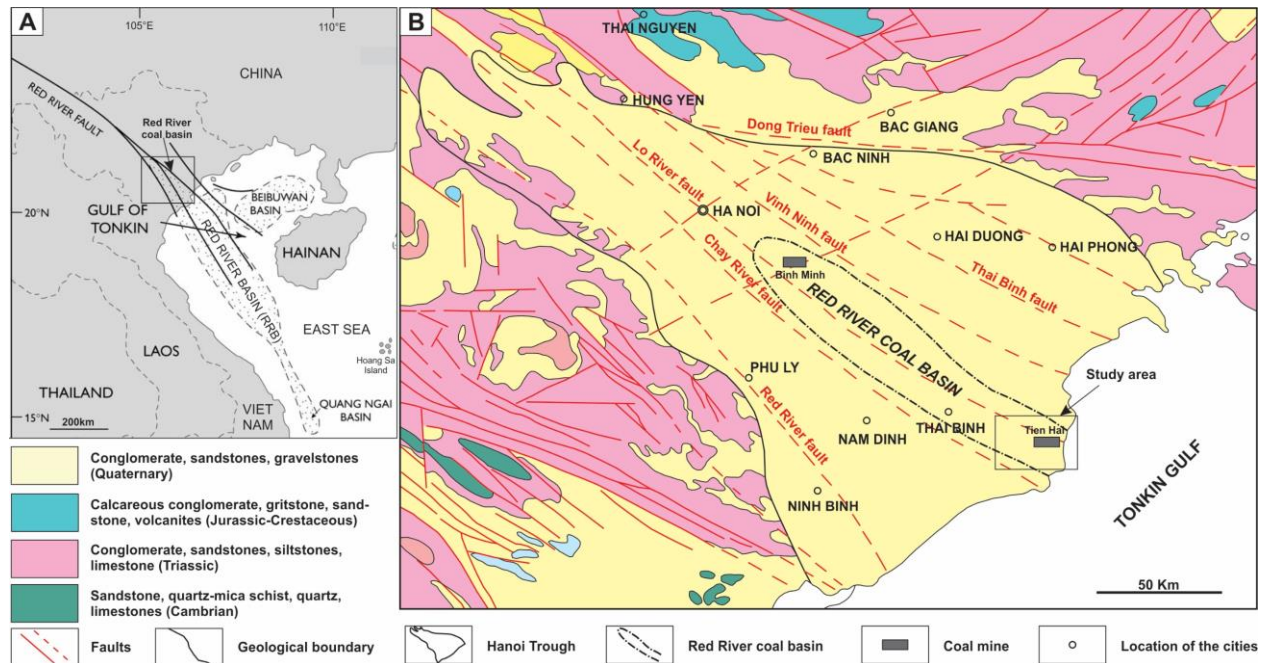


Fig. 1. A-Tectonic sketch map of the Red River basin, showing the location of the Red River coal basin [13], B-Geological map of the Red River coal basin, and location of the Tien Hai area [9, 14].

The RRB was formed and developed as a result of the Indochina block's large-scale extrusion and clockwise rotation induced by the collision of Indian and Eurasian plates. During the early Eocene, the plate began to rift slowly, resulting in forming the NE–SW trending proto-East Sea of Vietnam [11, 13]. Tectonic escape of the Indochina block to the southeast has been exacerbated by the continued collision of the Indian plate with the Eurasian plate during the late Eocene to early Oligocene (40 Ma). The Indochina block's sinistral-slip created a left lateral shear-rifting point followed by rapid clockwise rotation (15–20°). As a result, the forming of the RRB can be attributed to left-lateral displacement of around 200 to 800 km along with the Red River fault system. Strike-slip motions were mostly observed along the Lo River and Chay River faults. Grabens and half-grabens formed during the rifting process in the RRB, which was later filled in by fluvial and lacustrine deposits. When subsidence had to be maintained, the amount of water rose, and the lacustrine setting opened up into a marginal marine or shallow marine ecosystem to create more sedimentation space. The expansion out of the East Sea to the southeast in the late Oligocene, however, induced compression, resulting in the inversion and uplifting of hosts and grabens in the RRB. During the late-early Oligocene, active erosions cut large amounts of earlier deposited Oligocene sections, causing in a pop-up formation on overlying younger sediments. The late Oligocene angular unconformity that divided the syn-rift and post-rift portions were thought to be a significant breakup unconformity caused by erosion.

This basin was further depressed by continuous left-lateral transtension along with the Red River fault systems and thermal cooling after the rifting period. During the early Miocene, widespread subsidence resulted in transgression and back-stepping sedimentation. In the middle Miocene, though, the Sundaland

plate stopped the Indochina from drifting southeast [16, 17]. As a result, relative motions around Red River faults have shifted from left to right lateral. The strike-slip activity, which resulted in fault reversal and the forming of major inversion structures, led to the petroleum system's trapping mechanism in the RRB.

2.2 Stratigraphy

Four major Cenozoic formations have been found and divided in the Tien Hai area [18]. Accordingly, Cenozoic sediments originated from Paleogene with the Eocene-Oligocene Dinh Cao formation, covered by the Miocene formations including the Phong Chau, Phu Cu, and Tien Hung formations, and Pliocene Vinh Bao, Hoa My formations. Overlapping them are Pleistocene sediments of the Hai Duong formation and Holocene sediments of the Kien Xuong formation (Fig. 2). The survey results of the drilling core sample in the Tien Hai area presented sediments of 4 stratigraphic units as follows.

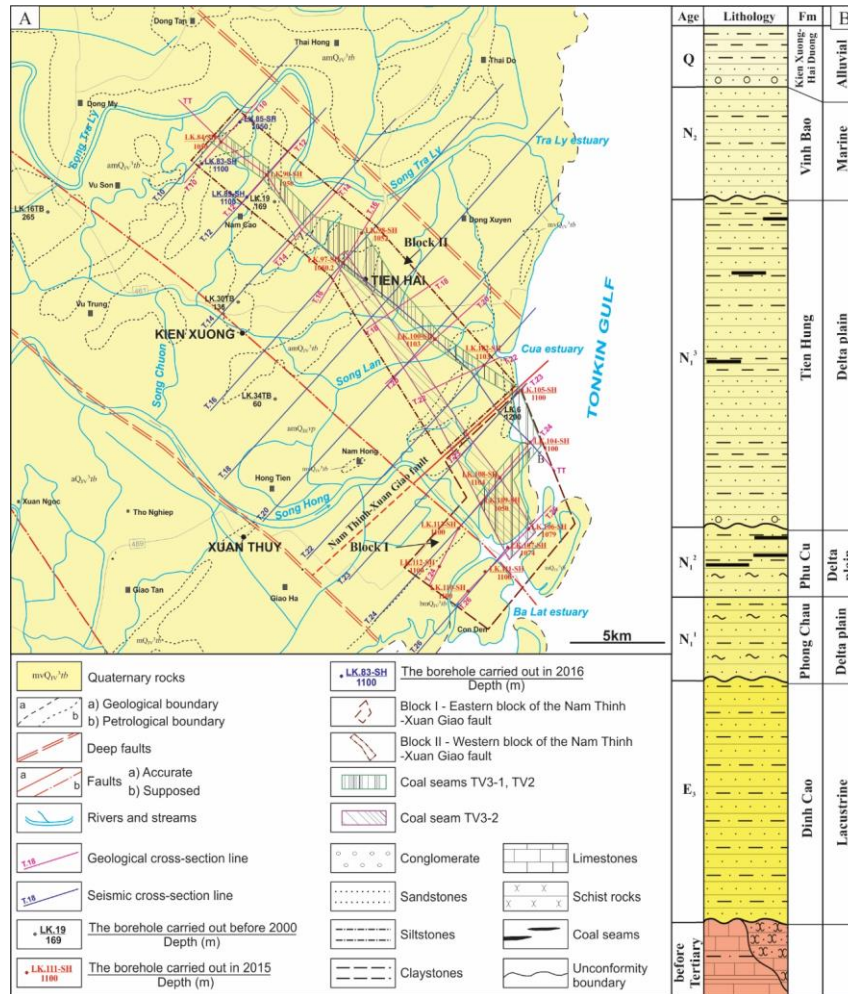


Fig. 2. A - Simplified geological map of the Tien Hai area [9]; B - Generalized stratigraphic column for the northeastern Red River coal basin [14].

The Tien Hung formation was found in all drilled holes that have been under construction in the Tien Hai area; however, only layer 3 of the Tien Hung formation was recorded from a depth of -319 m (LK.98-SH) to -443.3 m (LK.106-SH), at the average depth of -372 m. According to the borehole logs, the lithological composition of the third layer belongs to a coal-forming marsh, composed of large to fine-grained sandstone, siltstone, claystone, and coal. This layer contains 8-15 coal seams with thickness ranging from 0.8 m to 5.1 m, mainly from 2 m to 3m.

The Vinh Bao formation was first described and established in the borehole LK.3-SH [19]. This formation was recorded at the depth from -240 m to -510 m in the Vinh Bao district. The formation was found in all five boreholes in the Tien Hai area [14]. The core samples showed that the sediments of the Vinh Bao formation are characteristic of the lagoon facies, but in very few locations, there can be sand and

gravel in the alluvial-fluvial facies like in the borehole LK.105-SH. The composition of the sediments consists of siltstone interleaved with fine-grained sandstone or a few thin layers of light gray, ash-gray, green-felt claystone. The Vinh Bao formation covers unconformity on the sediments of the Tien Hung formation, and it is also covered unconformity by Quaternary sediments.

The Hai Duong formation was found in all five boreholes, at the depth from -78.4 m to -189.6 m (LK.102-SH), from -79.2 m to -238.6 m (LK.104-SH), from -137.2 m to -195.5 m (LK.106-SH). Its lithological composition includes pebbles, gravel, grit, sand, and a little sandy clay; however, the large-grained rock layer accounts for a higher proportion in the middle part of the formation. The sedimentary composition of the Hai Duong formation is characteristic of the continental alluvial facies. The average thickness of the Hai Duong formation is about 90 m, ranging from 58.3 m (LK.106-SH) to 159.4 m (LK.104-SH). Hai Duong formation covers unconformity on the sediments of the Vinh Bao formation.

The Kien Xuong formation consists mainly of clay sand, sandy clay, clay, powder, and large grain size. Clay sand has dirty gray, ash gray, reddish-brown gray colors, with many plant ruins. The mineral sand is composed of quartz, feldspar, and muscovite. Clay usually has light coffee and a relatively fine pink-brown color, sometimes containing small scales of muscovite. The average thickness of the formation is from -78.4 m (LK.102-SH) to -137.2 m (LK.106-SH). The formation covers conformity on the Hai Duong formation.

Structurally, the Tien Hai area belongs to a small part of the Khoai Chau-Tien Hai zone, limited by two main faults, namely the Vinh Ninh fault in the northeast and the Thai Binh fault in the southwest. The thickness of Cenozoic sediments in this zone is very large, and it can reach over 7,000 m, including Eocene to Quaternary formations (Figs. 2-3).

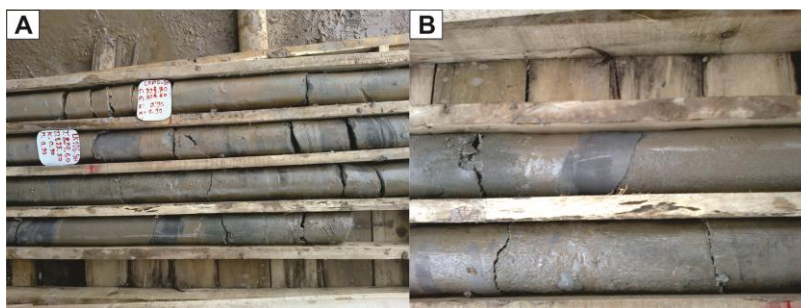


Fig. 3. The core samples of the borehole LK.106-SH in the Con Vanh, Tien Hai area, showing sandstone, siltstone, and gravel in the alluvial-fluvial facies at the depth from -823 m to -827 m [20].

2.3 Properties of coal in the Tien Hai area

The Tien Hai area mainly has brown coal, located in the general structure of the Khoai Chau-Kien Xuong-Tien Hai coal strip [18, 21]. According to the deep borehole and geophysical data, the brown coal distribution in the area is 60-100 km long, with an average length of 70 km, and 7-10 km wide with an average width of 8 km [14].

The borehole drilling successfully identified from 1 to 45 coal seams and coal lenses whose thickness ranges from 0.2 m to 5.0 m, with an average of 1.0 m. Coal seams exist in a large area where the distance between the coal seams in the cross-section is from 30 m to 50 m, even from 10 m to 100 m in some places. Coal seams widen gradually to the southeast, with the dip angle ranging from 8° to 15° and 10° on average. The dip angle of seams can increase from 25° to 40° when it closes to the fault plane. By the end of 2015, 5 coal seams which were concentrated mainly in the Tien Hung formation, were identified. In order from bottom to top of the stratigraphy are coal seam 1 (TV1), coal seam 2 (TV2), coal seam 3 (TV3), coal seam 4 (TV4), and coal seam 5 (TV5) that are distributed at the depth from -120 m to $-1,750$ m. The properties of coal seams are presented in Table 1.

Tab. 1. The properties of coal seams (from TV2 to TV5) [14].

No.	Borehole name	Coal seam name (amount)	Thickness (m)			Sounding rocks of coal seams	
			From	To	Average	Adjoining rocks	Pillar rocks
1	LK.84-SH	TV3 (7)	0.9	3.3	2.1	large grained sandstone	claystone
		TV2 (10)	0.6	10.0	5.3	coal clay	claystone
2	LK.90-SH	TV3 (8)	0.65	3.1	1.875	medium-grained sandstone	claystone
		TV2 (13)	0.65	9.9	5.275	medium-grained sandstone	claystone
3	LK.97-SH	TV4 (1)			0.9	claystone	claystone
		TV3 (12)	0.65	6.4	3.525	claystone	claystone
		TV2 (2)	0.6	8.6	4.6	gritstone	claystone
4	LK.98-SH	TV3 (7)	2.0	6.8	4.4	claystone	siltstone
		TV2 (3)	0.6	8.7	4.65	claystone	claystone
5	LK.100-SH	TV3 (6)	1.6	7.25	4.425	fine-grained sandstone	claystone
		TV2 (2)	3.8	5.8	4.8	claystone	claystone
6	LK.108-SH	TV5 (3)	0.45	4.6	2.525	medium-grained sandstone	siltstone
		TV4 (10)	1.0	7.7	4.35	medium-grained sandstone	claystone
		TV3 (1)			2.9	medium-grained sandstone	claystone
7	LK.109-SH	TV5 (2)	0.9	6.0	3.45	medium grained sandstone	claystone
		TV4 (9)	0.4	7.6	4.0	gritstone	claystone
		TV3 (4)	0.4	4.0	2.2	medium-grained sand	siltstone
8	LK.106-SH	TV5 (2)	0.75	6.5	3.625	medium-grained sandstone	claystone
		TV4 (10)	0.7	6.4	3.55	large grained sandstone	claystone
		TV3 (3)	0.75	8.7	4.725	claystone	claystone
9	LK.107-SH	TV5 (2)	0.5	7.5	4.0	medium grained sandstone	siltstone
		TV4 (5)	0.9	5.6	3.25	fine-grained sand-stone	siltstone
		TV3 (3)	0.4	4.6	2.5	medium grained	siltstone

No.	Borehole name	Coal seam name (amount)	Thickness (m)			Sounding rocks of coal seams	
			From	To	Average	Adjoining rocks	Pillar rocks
						sandstone	
10	LK.110-SH	TV5 (2)	1.1	4.1	2.6	claystone	siltstone
		TV4 (3)	1.2	4.1	2.65	fine-grained sandstone	siltstone
		TV3 (5)	0.85	2.3	1.575	siltstone	siltstone
11	LK.102-SH	TV3 (8)	1.45	5.8	3.625	claystone	claystone
		TV2 (6)	1.3	5.1	3.2	claystone	claystone
12	LK.104-SH	TV4 (6)	2.6	5.05	3.825	large grained sandstone	claystone
		TV3 (3)	1.9	3.9	2.9	large grained sandstone	claystone
13	LK.105-SH	TV4 (6)	0.9	6.0	3.45	gritstone	claystone
		TV3 (2)	2.3	2.6	2.45	fine-grained sandstone	claystone

The coal seam 1 (TV1) was identified in 4 boreholes which are distributed at the depth from –1,200 m to –1,900 m. The seam TV1 is maintained according to the strike direction, the dip format is from relatively stable to unstable, the average thickness of the TV1 is from 1.90 m to 3.27 m, and the average dip angle is 10°. The adjoining rocks of the coal seam are mainly composed of claystone, siltstone, and sometimes sandstone, while its pillar rocks consist mainly of claystone.

The coal seam 2 (TV2) was recorded in 11 boreholes and included 15 coal lenses distributed at the depth from –500 m to –1,400 m. According to the strike direction, the coal seam is maintained, and the dip format is from relatively stable to unstable. The average thickness of the seam TV2 is from 1.28 m to 6.46 m, and the average dip angle is 12°. The adjoining and pillar rocks of the coal seams are mainly composed of claystone, siltstone, sometimes sandstone, and gritstone.

The coal seam 3 (TV3) was found in 19 boreholes. The seam TV3 includes 22 coal lenses distributed at the depth from –295 m to –1,090 m. The coal seam is maintained in the strike direction, the dip format is relatively stable to unstable, the average thickness is from 0.39 m to 4.32 m, and the average dip angle is 13.22°. The coal seam's adjoining and pillar rocks consist mainly of claystone, siltstone, and sometimes sandstone.

The coal seam 4 (TV4) was found in 10 boreholes and consists of 10 coal lenses distributed at a depth of –376m to –1,015m. The seam is maintained in the strike direction, the dip format is relatively stable, the average thickness is from 1.34m to 5.27m, and the average dip angle is from 16° to 17°. The adjoining and pillar rocks of the coal seam are mainly composed of claystone, siltstone, sometimes sandstone, and gritstone.

The coal seam 5 (TV5) was determined in 5 boreholes constructed by the Intergeo Division [12]. The seam TV5 includes 3 coal lenses, distributed at the depth from –432 m to –701 m. The coal seam is maintained in the strike direction, the dip direction is not stable, the average thickness is from 0.39 m to 5.60 m, and the average dip angle is 12.73°. The adjoining and pillar rocks of the coal seam are mainly composed of siltstone and claystone.

The synthesis results of documents in the Tien Hai area show that the drilling works may only be limited at the upper coal beds of the third layer, belonging to the Tien Hung formation, which should be further clarified through research on geological cross-sections according to drilling and geophysical data, especially 2D reflective seismic measurements.

3. Materials and Methods

The geochemical properties of the ancient and modern sandstone formations will clarify the identification marks of the bedrock and the tectonic setting in their composition, helping to speculate the redistribution of chemical elements during and after the sediment deposition process. In the scope of this study, the combination of correlation analysis and geological-geophysical multidimensional statistical methods is applied to identify the correlation of the coal seams in the Tien Hai area.

Based on the results of identifying correlation of coal seams in the Quang Ninh and Thai Nguyen-An Chau coal basins [22, 23] together with analysis results of characteristics of the geological structure, coal seams, core data, and actual geophysical measurements, the correlation models of coal seams in the study area were established in order of its geological and geophysical parameters. The proposed process is shown in Figure 4.

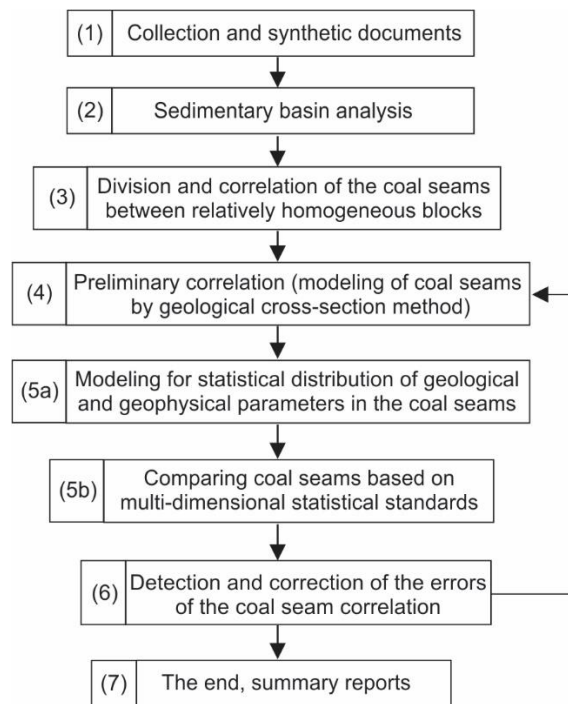


Fig. 4. Seven steps for correlation of coal seams at the Tien Hai area by using geological and geophysical parameters.

3.1 Multivariate statistics

One of the most commonly used algorithms to solve the coal seam correlation problem is the cluster analysis method, also known as dendrogram analysis, which includes the following steps.

Step 1: Determine the similarity $E(x_i, x_j)$ between each pair of objects (coal seams) according to the formula.

$$E(x_i, x_j) = \text{Cov}(x_i, x_j) = \frac{\sum_{p=1}^k a_{ip} \cdot a_{jp}}{\sqrt{\sum_{p=1}^k a_{ip}^2 \sum_{p=1}^n a_{jp}^2}} \quad (1)$$

in which $i, j = 1, 2, \dots, n$; k is the number of study properties, n is the number of study objects, and a_{ip}, a_{jp} are coordinates of the vectors x_i, x_j . The result will create a $Q_{m \times m}$ matrix with terms $\{E_{ij}\}, i, j = 1, \dots, n$.

Step 2: Find the arithmetic mean H from values reflecting the similarity E_{ij} according to the formula.

$$H = \frac{\sum_{i,j=1}^m E_{ij}}{n^2} \quad (2)$$

Step 3: Select $E_t^* = \frac{\max}{t} E_{it}$; $t=1,2,\dots,n$; t^*_i ; where i is the number of rows, t is the number of columns of the matrix $Q_{m,m}$.

Step 4: After selecting E_i^* values, compare E_i^* values with H . When $E_i^* > H$, the study subjects are classified into the same group. When $E_i^* < H$, the study subjects cannot be classified in the same group.

Step 5: Select $t = t^*$, in which $E_{it} = E_i^*$ (the name of column with value E_i^*).

Step 6: Formulate r sets with the following forms.

$$B_s = (t_s^*, i_1^s, \dots, i_\mu^s, \dots, i_{cs}^s; s = 1, \dots, r) \tag{3}$$

where r is the number of different values of t_i^* ; i_1^s, \dots, i_{cs}^s is the symbol of row with the maximum value.

Step 7: Start to synthesize B_1 from the second term i_1^1 compared to the first term of $t_2^* \dots, t_r^*$ of combinations $B_2 \dots, B_r$. Concerning B_v , when $2 \leq v \leq r$, $i_1^1 = t_v$, $B_1^1 = B_i$, t_v^* has such a formula as.

$$B_1' = (t_1^*, i_1^1, \dots, i_{11}^1, i_1^v, \dots, i_{1v}^v) \tag{4}$$

That is, delete the combination B_v and change to the term i_1^2 . If the first term of the combinations $B_2 \dots B_r$ has no terms like i_1^1 continue to compare with the term i_1^2 . Continue like this until all the terms i_1^1 of combination B_1 are considered.

Step 8: The number r' , the number of remaining combinations after step 7 is performed, is reserved for the combination B_1' (If new terms are not included in step 7).

Numbers from 1 to $r'-1$ are reserved for the remaining combinations and combinations with a new number $s=1$ after step 7. Steps 7 and 8 have been repeated until the combinatorial r^* of combination B_s^* with $t_s^* \neq i_{\mu,s}^k$, $k=1,\dots,n$; $\mu=1,\dots,k$.

Step 9: Compare pairs of combinations B_u^*, B_v^* ; $u, v = 1 \dots, r^*$, starting from the second term, $i^u_1 (i^v_1)$. Combine all combinations of the same terms.

Step 10: Calculate the properties of subsets $A_s, s=1,\dots,r^*$; $\hat{X}_s = (\hat{\alpha}_{s_1}, \hat{\alpha}_{s_2}, \dots, \hat{\alpha}_{s_n})$.

$$\hat{\alpha}_{sp} = \frac{\sum_{j,s=1}^{m_s} \alpha_{jsp}}{m_s} \tag{5}$$

with α_{jsp} is the P^{th} coordinate of the X_{js} vector corresponding to the a_{js} condition of the subset A_s ; m_s is the number of objects in a subset.

Step 11: Calculate the similarity values between the subset pairs A_s, A_v , and $s, v = 1 \div r^*$. Then, establish the matrix C with the terms D_{sv} by the formula.

$$D_{sv} = \frac{1}{m_s m_v} \sum_{i_s=1}^{m_s} \sum_{j_v=1}^{m_v} E_{i_s j_v} \tag{6}$$

in which, i_s and j_v are the number of the sum of subsets A_s, A_v ; $E_{i_s j_v}$ is the similarity value between points a_i and a_j calculated in step 1; m_s and m_v are the number of objects in the combinations A_s and A_v , respectively.

3.2 Using multivariate statistics for mapping and comparison of coal seams

Assuming that 2 coal seam beds are belonging to 2 relatively homogeneous blocks (or 2 geological cross-sections according to the exploration route whose properties need to be compared by 2 document term matrices (original data table):

$$T_1 = \{\xi'_1, \xi'_2, \dots, \xi'_1, \dots, \xi'_m\} \text{ and } T_1 = \{\xi''_1, \xi''_2, \dots, \xi''_1, \dots, \xi''_m\}$$

Each seam bed was controlled by the boreholes (corresponding points of view) X_1, X_2, \dots, X_{n1} (belonging block I) and $Y_1, Y_2, \dots, Y_t, \dots, Y_{n2}$ (belonging to block II). In which:

$$X_t = \{X_{t_1}, X_{t_2}, \dots, X_{t_j}, \dots, X_{t_m}\}$$

$$Y_t = \{Y_{t_1}, Y_{t_2}, \dots, Y_{t_j}, \dots, Y_{t_m}\}$$

In order to compare T_1 and T_2 , it is necessary to test the hypothesis $H_0: \mu_1 = \mu_0$ or $H_1: \mu_1 \neq \mu_2$. The hypothesis H_0 can be tested according to multidimensional statistical standard (V), determined by the formula.

$$V = -(n_1 + n_2 - 2) \ln \frac{|S_1|}{|S_0|} \tag{7}$$

where $|S_1|, |S_0|$ are determinants of the matrices S_1 and S_0 determined by the formula (1) and (2).

The hypothesis H_0 is accepted (that is, assuming that the coal seams in two blocks that need to be compared are similar, in other words, they are correlated) when: $V = \chi^2_{q,m}$ (in which $\chi^2_{q,m}$ is the Chi-square standard, q is significance level and m is the number of study properties or parameters).

Accordingly, the terms of the matrices S^0_{ij} and S^1_{ij} are calculated by the following formula.

$$S^0_{ij} = \frac{1}{n_1 + n_2 - 2} \left[\sum_{t=1}^{n_1} X_{t_i} X_{t_j} + \sum_{t=1}^{n_2} Y_{t_i} Y_{t_j} - \frac{1}{n_1 + n_2} \left(\sum_{t=1}^{n_1} X_{t_i} + \sum_{t=1}^{n_2} Y_{t_i} \right) \left(\sum_{t=1}^{n_1} X_{t_j} + \sum_{t=1}^{n_2} Y_{t_j} \right) \right] \tag{8}$$

$$S^1_{ij} = \frac{1}{n_1 + n_2 - 2} \left[\sum_{t=1}^{n_1} X_{t_i} X_{t_j} + \sum_{t=1}^{n_2} Y_{t_i} Y_{t_j} - \frac{1}{n_1} \sum_{t=1}^{n_1} X_{t_i} \cdot \sum_{t=1}^{n_1} X_{t_j} - \frac{1}{n_2} \sum_{t=1}^{n_2} Y_{t_i} \cdot \sum_{t=1}^{n_2} Y_{t_j} \right] \tag{9}$$

After determination of the multidimensional statistical standard (V), compare the V standard with the Chi-square standard ($\chi^2_{q,m}$).

3.3 Testing results of the coal seam correlation

The techniques described above use a mixture of geological and geophysical criteria to compare coal seams in two areas (or cross-sections); however, geologists often have to correlate several areas (cross-sections). They often use the multidimensional statistical standard proposed by Rao (1967) [24] to solve this task.

In order to correlate k geological forms (coal seams or coal seam beds); in which each coal seam or coal seam bed is characterized by a combination of geological and geophysical parameters and presented in the document term matrix in the form of $T_C = T_1, \dots, T_L, \dots, T_K$, with corresponding mathematical expectations $\mu_1, \mu_2, \dots, \mu_k$ and corresponding covariance matrices satisfying the condition: $\sum_1 = \sum_2 = \dots = \sum_k = \sum_0$. Then, the results collected from the boreholes can be expressed as $X_u = \{X_{ct1}, X_{ct2}, \dots, X_{ctj}\}$.

To confirm that the coal seams correlated on the cross-sections and correlation between blocks are suitable (or similar), it is often checked under the assumption: $H_0 = \mu_1 = \mu_2 = \dots = \mu_k = \mu_0$. To test hypothesis H_0 , the multidimensional statistical standard (V) is usually used and determined by the formula.

$$V = - \left(\sum_{i=1}^k n_i - 1 \frac{m+k}{2} \right) \ln \frac{|S_1|}{|S_0|} \tag{10}$$

The formula calculates the terms of the covariance matrices S_1 and S_0 .

$$S^0_{ij} = \frac{1}{n-1} \left[\sum_{L=1}^k \sum_{t=1}^{n_t} X_{L_{t_i}} X_{L_{t_j}} - \frac{1}{n} \sum_{L=1}^k \sum_{t=1}^{n_t} X_{L_{t_i}} \cdot \sum_{L=1}^k \sum_{t=1}^{n_t} X_{L_{t_j}} \right] \tag{11}$$

$$S^1_{ij} = \frac{1}{n-1} \left[\sum_{L=1}^k \sum_{t=1}^{n_t} X_{L_{t_i}} X_{L_{t_j}} - \sum_{L=1}^k \frac{1}{n} \left(\sum_{t=1}^{n_L} X_{L_{t_i}} \cdot \sum_{t=1}^{n_L} X_{L_{t_j}} \right) \right]; N = \sum_{L=1}^k n_i \tag{12}$$

If $V \leq \chi^2_{q,m}$, the assumption is accepted.

4. Results and discussions

Identifying the correlation of coal seams with a combination of geological and geophysical parameters is carried out following 7 steps (Fig. 4). The first step is to set up a database for each selected section, including the number of reflections on stratigraphic, morphological, and structural characteristics of coal seams, their material composition, etc. The second step carries out sedimentary basin analysis. The third step divides and correlates the coal seams between relatively homogeneous blocks. The fourth step models

the coal seams by using geological cross-sections. The fifth step estimates the statistical distribution of the coal seams' geological and geophysical parameters and then compares coal seams based on the multidimensional statistical standards. The sixth step includes detecting and correcting the errors of the coal seams correlation, and the last one summarizes results and reports.

4.1 The characteristics of statistical distribution elements

The rules of the statistical distribution of coal samples and related elements can be recognized by determining their statistical distribution models. Technical features and the element contents of coal in the Tien Hai area expressed through statistical characteristics reflecting coal quality are summarized in Table 2.

The analysis results showed the technical features of W^{pt} (moisture), A^d (ash), V^{ch} (volatile), Q^{ch} (quantity of heat), C^d (carbon), H^d (hydro), O^d (oxy), N^d (nitro), S^d (sulfur), and P (phosphor) in the coal seams with the average values of 16.72, 5.54, 46.70, 7125.61, 69.15, 4.29, 19.34, 0.89, 0.79, and 0.010, respectively (Tab. 2). They also present the coal seams belonging to the low sulfur coal group that is difficult to ignite. Based on the C^d , N^d , and O^d contents, the coal seams are arranged in the low-grade metamorphic ones. Most of the technical parameters of coal seams comply with the normal standard distribution rules; only the ash (A^d) and sulfur (S^d) contents comply with the standard lognormal distribution. The variation of the technical parameters ranges from very even to even, which indicates that coal quality is relatively homogeneous. Remarkably, the ash (A^d) and sulfur (S^d) contents are distributed fairly unevenly.

Similarly, the statistical characteristics of major and trace elements in coal show a clear change among element groups. Accordingly, the group of such elements as Na, V, Ge, As, and Ba has little change in content and complies with the normal standard distribution. On the contrary, the group of elements including Al, Ti, Ni, Zn, Mo, and Th has very strong variations on their contents. It complies with lognormal or gamma standard distribution rules. Moreover, the remaining groups of elements vary from quite even to uneven (Tab. 2).

Otherwise, the contents of the major and trace elements in coal rashing have a very clear change among element groups (Tab. 3). Accordingly, the group of elements including B, Ti, V, Cr, Ni, Zn, Ge, Sr, Tl, Th, and TR_2O_3 has displayed little change in their contents and complies with normal standard distribution models. The group of such elements as Ga, Ba, and Pb has extreme variations and complies with gamma distribution rules. The remaining groups of elements range from quite even to uneven. With this, the statistical characteristics of the contents of the rare earth elements do not affect human health in the coal mining process.

Moreover, most of the contents of the rare earth elements comply with the gamma distribution function, except for Sm, Eu, and Gd elements which comply with normal standard distribution rules. Therein, the contents of rare earth elements vary from uneven to very uneven (Tab. 3). These results indicate that the distribution of the contents of rare earth elements in coal rashing is not high. However, it can still create concentrated accumulations, which should be considered in the future coal mining process.

Tab. 2. Statistical characteristics and distribution models of the technical features and elements in coal seams.

Analyzed samples	Element	Mean (%)	Variance	Coefficient of variation (%)	Skewness	Kurtosis	Distribution model
Technical features	W^{pt}	16.72	3.51	21.01	0.19	-0.84	Normal standard
	A^d	5.54	3.14	56.70	0.94	0.87	Lognormal standard
	V^{ch}	46.70	2.06	4.42	0.35	-0.83	Normal standard
	Q^{ch}	7125.61	273.01	3.83	-0.54	-0.79	Normal standard
	C^d	69.15	3.60	5.20	0.05	-0.84	Normal standard
	H^d	4.29	0.27	6.27	0.23	-0.49	Normal standard
	O^d	19.34	2.26	11.67	-0.10	-0.58	Normal standard
	N^d	0.89	0.14	16.17	-0.58	0.40	Normal standard
	S^d	0.79	0.49	62.20	0.80	-0.19	Lognormal standard

Analyzed samples	Element	Mean (%)	Variance	Coefficient of variation (%)	Skewness	Kurtosis	Distribution model
	P	0.010	0.002	22.22	-0.199	-1.017	Normal standard
Major and trace elements	B	1.00	-	-	-	-	-
	Na	4090.42	1105.38	27.02	0.49	-0.97	Normal standard
	Mg	2007.30	1005.12	50.07	0.07	-0.43	Lognormal standard
	Al	2147.99	2674.92	124.53	2.55	6.78	Gamma
	K	1226.71	1043.03	85.03	1.58	2.23	Lognormal standard
	Ca	5370.13	2978.84	55.47	0.80	-0.04	Lognormal standard
	Ti	227.53	242.92	106.77	1.28	0.20	Gamma
	V	128.38	37.89	29.51	0.04	0.12	Normal standard
	Cr	16.69	9.44	56.60	1.76	3.17	Lognormal standard
	Mn	43.37	37.28	85.95	1.64	1.80	Lognormal standard
	Fe	3610.42	2769.99	2796.99	1.88	3.48	Lognormal standard
	Co	8.45	7.84	7.84	2.01	5.54	Lognormal standard
	Ni	52.75	71.90	71.90	3.73	15.70	Gamma
	Zn	171.55	213.64	213.64	3.65	13.70	Gamma
	Ga	12.96	9.45	9.45	1.85	3.32	Lognormal standard
	Ge	11.15	2.37	2.37	-3.14	12.92	Normal standard
	As	147.27	16.27	16.27	-0.94	1.22	Normal standard
	Sr	135.35	76.31	76.31	0.75	-0.09	Lognormal standard
	Mo	1.32	3.46	3.46	4.39	20.24	Gamma
	Pd	-	-	-	-	-	Normal standard
	Ba	130.99	64.12	64.12	1.14	1.03	Normal standard
	Re	161.64	129.70	129.70	0.53	-1.01	Lognormal standard
	Pt	2.84	2.52	2.52	2.23	5.81	Lognormal standard
Hg	-	-	-	-	-	-	
Tl	-	-	-	-	-	-	
Pb	15.01	10.73	10.73	1.96	2.69	Lognormal standard	
Th	2.15	5.25	5.25	4.37	20.05	Gamma	
U	2.14	1.15	1.15	0.77	-0.69	Lognormal standard	
REE	0.40	0.34	0.34	1.85	2.56	Lognormal standard	
Rare earth elements	La	397.99	517.08	129.92	1.90	2.59	Gamma
	Ce	813.08	1037.97	127.66	1.84	2.29	Gamma
	Pr	93.31	123.08	131.90	1.85	2.30	Gamma
	Nd	342.85	451.89	131.80	1.84	2.26	Gamma

Analyzed samples	Element	Mean (%)	Variance	Coefficient of variation (%)	Skewness	Kurtosis	Distribution model
	Sm	926.16	317.28	34.26	0.73	0.99	Normal standard
	Eu	149.27	50.29	33.69	0.14	-1.14	Normal standard
	Gd	281.72	115.17	40.88	0.96	0.81	Normal standard
	Tb	11.31	13.75	121.49	2.53	6.99	Gamma
	Dy	50.19	80.29	159.99	2.81	8.77	Gamma
	Ho	10.10	17.38	172.10	2.99	9.89	Gamma
	Er	26.30	47.88	182.06	3.04	10.15	Gamma
	Tm	3.57	6.42	179.83	3.21	11.46	Gamma
	Sc	13.71	31.96	233.11	4.09	18.09	Gamma
	Yb	8.96	25.70	286.72	4.19	18.61	Gamma
	Y	253.36	453.68	179.07	2.91	9.17	Gamma
	Lu	3.49	6.40	183.10	3.25	11.77	Gamma

Tab. 3. Statistical characteristics and distribution models of the elements in coal rashing.

Analyzed samples	Element	Mean (%)	Variance	Coefficient of variation (%)	Skewness	Kurtosis	Distribution model
Major and trace elements	B	4.27	0.59	13.80	-0.08	-1.06	Normal standard
	Ti	3900.42	1343.94	34.46	-0.64	-0.63	Normal standard
	V	116.85	47.07	40.28	-0.74	-0.30	Normal standard
	Cr	109.68	32.45	29.58	-0.57	0.00	Normal standard
	Co	22.09	11.19	50.64	2.12	6.63	Lognormal standard
	Ni	68.75	23.68	34.44	1.12	3.59	Normal standard
	Zn	148.60	54.70	36.81	0.03	-0.53	Normal standard
	Ga	13.85	15.48	111.74	2.18	6.16	Gamma
	Ge	3.62	1.33	36.66	-0.34	-1.19	Normal standard
	Sr	135.60	56.13	41.39	3.01	12.04	Normal standard
	Pd	-	-	-	-	-	-
	Ba	807.30	1063.86	131.78	3.14	11.49	Gamma
	Re	92.01	89.50	97.27	0.86	-0.76	Lognormal standard
	Os	-	-	-	-	-	-
	Ir	-	-	-	-	-	-
	Pt	-	-	-	-	-	-
	Pb	14.34	16.80	117.17	0.75	-0.81	Gamma
	Tl	0.78	0.36	46.06	0.78	0.75	Normal standard
	Th	17.88	5.38	30.12	-0.90	0.31	Normal standard
	U	5.57	4.09	73.42	3.21	14.68	Lognormal standard
TR ₂ O ₃	0.51	0.13	26.09	-0.93	0.39	Normal standard	
Rare earth elements	La	495.02	257.10	51.94	0.02	-0.83	Lognormal standard
	Ce	493.35	285.36	57.84	0.15	-1.32	Lognormal standard
	Pr	493.38	331.77	67.24	0.26	-1.54	Lognormal standard

Analyzed samples	Element	Mean (%)	Variance	Coefficient of variation (%)	Skewness	Kurtosis	Distribution model
	Nd	379.53	225.42	59.39	0.54	-0.37	Lognormal standard
	Sm	427.92	269.01	62.87	0.56	-0.45	Lognormal standard
	Eu	259.23	129.59	49.99	1.62	2.06	Normal standard
	Gd	492.44	282.30	57.33	0.08	-1.29	Lognormal standard
	Tb	76.01	25.87	34.04	0.42	1.12	Normal standard
	Dy	382.49	132.23	34.57	0.49	0.92	Normal standard
	Ho	67.69	22.13	32.69	0.35	0.86	Normal standard
	Er	174.46	56.74	32.53	0.34	0.88	Normal standard
	Yb	0.00	-	-	-	-	-
	Tm	24.53	8.02	32.71	0.42	1.13	Normal standard
	Lu	9.41	11.15	118.51	0.71	-1.17	Gamma
	Sc	395.63	156.40	39.53	0.13	-0.38	Normal standard
	Y	355.97	239.60	67.31	0.67	-0.27	Lognormal standard

4.2 Logic models for selecting good indicator elements

Associations of elements as the best indicator elements were selected to eliminate unnecessary elements, reduce computational mass, remove fake anomalous contents of elements, and improve efficiency for the correlation of coal seams. As a result, 256 coal samples (including 25 major and trace elements and 16 rare earth elements) were analyzed and processed.

As a result, the major and trace element concentrations are Mg > V > As > Ca > Zn > Cr > Co > K > Na > Sr > Fe > Ge > Re > U > Mo > Th > Ga > Al > Ti > Ba > Ni > Pt > Mn > REE > Pb for coal seams in the study area (Tab. 4). In particular, 17 elements including Mg, V, As, Ca, Zn, Cr, Co, K, Na, Sr, Fe, Ge, Re, U, Mo, Th, and Ga elements account for more than 90%, representing a clear association for coal seams. Therefore, these elements can be selected as the good indicator ones for coal seams, whereas the remaining elements only account for less than 10%. As the whole, rare-earth elements in coal include 11 elements that also account for more than 90%, namely, Yb, Sc, Ho, Er, Tm, Lu, Y, Tb, Pr, Dy, and Sm, while the remaining elements make up less than 10%. These rare earth elements can also be selected as good indicator elements.

Tab. 4. Frequency analysis of the content of the elements for the coal samples in the study area.

Major and trace elements				Rare earth elements			
Element	Amount of information (AI)	Information combination (IC)	Probability [%]	Element	Amount of information (AI)	Information combination (IC)	Probability [%]
Mg	0.307	0.307	27.6	Yb	0.325	0.325	31.49
V	0.283	0.418	37.5	Sc	0.313	0.451	43.70
As	0.277	0.501	45.0	Ho	0.309	0.547	53.00
Ca	0.276	0.572	51.4	Er	0.309	0.628	60.85
Zn	0.259	0.628	56.4	Tm	0.308	0.700	67.83
Cr	0.256	0.678	60.9	Lu	0.308	0.764	74.03
Co	0.249	0.722	64.9	Y	0.245	0.803	77.81
K	0.237	0.760	68.3	Tb	0.238	0.837	81.11
Na	0.234	0.795	71.4	Pr	0.238	0.870	84.30

Major and trace elements				Rare earth elements			
Element	Amount of information (AI)	Information combination (IC)	Probability [%]	Element	Amount of information (AI)	Information combination (IC)	Probability [%]
Sr	0.230	0.828	74.4	Dy	0.232	0.901	87.31
Fe	0.229	0.859	77.2	Sm	0.227	0.929	90.02
Ge	0.221	0.887	79.7	Gd	0.225	0.956	92.64
Re	0.220	0.914	82.1	Eu	0.204	0.977	94.67
U	0.216	0.939	84.4	Ce	0.197	0.997	96.61
Mo	0.215	0.963	86.5	La	0.195	1.016	98.45
Th	0.213	0.987	88.7	Nd	0.183	1.032	100
Ga	0.201	1.007	90.5				
Al	0.194	1.026	92.2				
Ti	0.191	1.043	93.7				
Ni	0.187	1.060	95.2				
Ba	0.187	1.076	96.7				
Pt	0.155	1.087	97.7				
Mn	0.152	1.098	98.7				
REE	0.138	1.106	99.4				
Pb	0.122	1.113	100				

Note: Amount of information (AI) and Information combination (IC) are mentioned in Hung (et al., 2020) [25].

4.3 Established correlation coefficients between the good indicator elements

The results of correlation analysis can be used to form the pair correlation matrix of the best indicator elements in the coal samples of the study area and each coal seam. The elements of the pair correlation matrix among the good indicator elements are presented in Tables 5, 6, 7, 8, 9, 10, and 11. Among the indicator element associations of the coal seams, the Ca-Mg-Sr, Cr-V-Ga-K-As, and Th-Mo elements display close associations (Tab. 5). The calculated results of each coal seam's associations are also similar to those in the coal deposit. Still, their relation levels vary, particularly in the coal seam TV3-2. Two associations of major and trace elements (including Mg-Ca-Sr, and K-V-Cr-Zn-Mo-Th associations) are established. However, these associations have a closely inverse relationship with each other (Tab. 6). For major and trace elements of the coal seam TV3-1, the Mg-Ca-Cr-K and V-Sr-Mo-Th associations are established. Still, their elements are inversely related; Zn content is inversely related to all other elements (Tab. 7). The contents of the major and trace elements in coal seam TV2 showed two associations as good indicator elements: Ca-Mg-Sr-Mo and V-Zn-K-Th associations. Especially, Cr has a loosely inverse relationship with all elements, except Mo, which has a relatively close inverse relationship with all other elements (Tab. 8). Besides, rare earth elements in coal like the Ho-Er-Tm-Lu-Dy-Sc-Yb-Y association have a very close relationship that is significant in the correlation of coal seams in the study area (Tab. 9).

Herein, correlation coefficient analysis for elements as good indicators in the coal rashing is presented in Tables 10 and 11. Three associations (including V-Zn-Cr, Co-Zn-Ge, and Ge-Co) have a relatively close direct relationship between major and trace elements. The Ge-Co association has an inverse relationship with the Ge element (Tab. 10). Concerning rare earth elements, the results of correlation analysis proved that the group of elements, including Ho-Er-Tm-Dy-Tb, has a very close correlation and is considered an association of elements that go together (Tab. 11).

Generally, the correlation results clearly show that associations of major and trace elements as good indicator elements in the coal deposit and coal seams have relatively clear differences. These associations are often inversely related. Thus, the associations mentioned above of major and trace elements and rare earth elements are important groups that correlate coal seams in the study area.

Tab. 5. The correlation coefficient for major and trace elements as indicator elements in the coal seams.

	Na	Mg	K	Ca	V	Cr	Fe	Co	Zn	Ga	Ge	As	Sr	Mo	Re	Th	U
Na	1																
Mg	0.475	1															
K	0.061	0.035	1														
Ca	0.432	0.867	-0.101	1													
V	-0.075	0.036	0.244	-0.007	1												
Cr	0.058	-0.034	0.766	-0.048	0.571	1											
Fe	0.066	0.15	0.179	-0.139	0.266	0.147	1										
Co	0.199	0.187	0.251	0.206	0.037	0.389	0.246	1									
Zn	0.16	0.402	0.333	0.433	0.236	0.437	-0.041	0.27	1								
Ga	0.196	-0.055	0.687	-0.244	0.533	0.769	0.394	0.255	0.055	1							
Ge	0.051	- 0.369	0.036	- 0.415	0.227	0.086	0.051	-0.176	-0.065	0.283	1						
As	-0.07	-0.057	- 0.367	-0.038	0.645	-0.025	0.027	-0.311	0.062	0.004	0.503	1					
Sr	0.394	0.726	0.029	0.875	0.138	0.115	-0.162	0.281	0.362	-0.021	- 0.393	-0.054	1				
Mo	0.136	-0.002	0.263	0.017	- 0.492	-0.049	-0.033	0.184	-0.114	0.04	-0.075	- 0.66	0.039	1			
Re	0.22	0.353	0.293	0.199	0.313	0.389	0.135	-0.03	0.144	0.449	-0.332	-0.015	0.33	-0.184	1		
Th	-0.003	-0.007	0.284	0.001	-0.334	0.011	0.041	0.212	-0.099	0.082	-0.256	- 0.645	0.08	0.941	-0.047	1	
U	0.275	0.171	-0.011	0.106	-0.115	-0.032	-0.167	-0.006	-0.152	0.158	- 0.443	-0.313	0.127	0.235	0.431	0.338	1

Note: Significant values of correlation coefficients are highlighted in bold-typed.

Tab. 6. The correlation coefficient for major and trace elements as indicator elements in the coal seam TV3-2.

	*Mg	*K	Ca	*V	*Cr	*Zn	*Sr	*Mo	Th
*Mg	1.00								
*K	-0.33	1.00							
Ca	0.69	-0.89	1.00						
*V	-0.36	0.99	-0.91	1.00					
*Cr	-0.70	0.70	-0.92	0.73	1.00				
*Zn	-0.51	0.78	-0.70	0.76	0.39	1.00			
*Sr	0.86	-0.72	0.89	-0.73	-0.78	-0.82	1.00		
*Mo	-0.01	0.87	-0.72	0.88	0.67	0.38	-0.38	1.00	
Th	-0.35	0.99	-0.91	0.99	0.74	0.74	-0.72	0.89	1.00

Tab. 7. The correlation coefficient for major and trace elements as indicator elements in the coal seam TV3-1.

	*Mg	*K	Ca	*V	*Cr	*Zn	*Sr	*Mo	Th
*Mg	1.00								
*K	0.26	1.00							
Ca	0.99	0.26	1.00						
*V	-0.65	-0.72	-0.69	1.00					
*Cr	0.67	0.52	0.67	-0.59	1.00				
*Zn	-0.11	0.32	-0.07	-0.16	0.32	1.00			
*Sr	-0.64	-0.71	-0.67	0.98	-0.52	-0.13	1.00		
*Mo	-0.64	-0.67	-0.68	0.96	-0.70	-0.30	0.92	1.00	
Th	-0.53	-0.58	-0.56	0.81	-0.26	-0.01	0.83	0.69	1.00

Tab. 8. The correlation coefficient for major and trace elements as indicator elements in the coal seam TV2.

	*Mg	*K	Ca	*V	*Cr	*Zn	*Sr	*Mo	Th
*Mg	1.00								
*K	0.40	1.00							
Ca	0.82	-0.14	1.00						
*V	0.11	0.75	-0.33	1.00					
*Cr	-0.41	-0.02	-0.38	0.07	1.00				
*Zn	-0.16	0.57	-0.48	0.78	-0.02	1.00			
*Sr	0.85	0.03	0.91	-0.17	-0.39	-0.50	1.00		
*Mo	0.29	-0.19	0.53	-0.26	-0.51	-0.20	0.46	1.00	
Th	0.26	0.88	-0.19	0.83	0.13	0.80	-0.17	-0.22	1.00

Tab. 9. The correlation coefficients for the rare earth elements as indicators in coal seams.

	Pr	Sm	Tb	Dy	Ho	Er	Tm	Sc	Yb	Y	Lu
Pr	1										
Sm	0.31	1									
Tb	0.884	0.313	1								
Dy	0.813	0.232	0.987	1							
Ho	0.763	0.199	0.971	0.996	1						

	Pr	Sm	Tb	Dy	Ho	Er	Tm	Sc	Yb	Y	Lu
Er	0.737	0.190	0.960	0.992	0.999	1					
Tm	0.711	0.186	0.951	0.986	0.995	0.998	1				
Sc	0.692	0.179	0.927	0.947	0.953	0.951	0.958	1			
Yb	0.464	0.112	0.755	0.793	0.813	0.815	0.844	0.904	1		
Y	0.738	0.179	0.958	0.990	0.998	0.999	0.995	0.940	0.801	1	
Lu	0.704	0.183	0.947	0.983	0.994	0.996	0.999	0.959	0.849	0.993	1

Tab. 10. The correlation coefficient for trace elements as good indicators in the coal rashing.

	V	Cr	Co	Zn	Ge	Re	Th
V	1						
Cr	0.509	1					
Co	0.093	0.022	1				
Zn	0.323	0.404	0.365	1			
Ge	0.077	0.059	0.651	-0.094	1		
Re	-0.101	0.282	-0.229	0.440	-0.534	1	
Th	-0.044	0.103	-0.184	0.096	-0.344	0.327	1

Tab. 11. The correlation coefficient for rare earth elements as good indicator elements in the coal rashing.

	La	Ce	Nd	Gd	Tb	Dy	Ho	Er	Tm	Sc
La	1									
Ce	-0.068	1								
Nd	-0.363	0.057	1							
Gd	-0.005	0.136	0.25	1						
Tb	0.306	0.167	0.239	0.281	1					
Dy	0.319	0.248	0.205	0.299	0.8	1				
Ho	0.344	0.196	0.186	0.257	0.812	0.936	1			
Er	0.327	0.198	0.194	0.256	0.793	0.914	0.993	1		
Tm	0.322	0.2	0.184	0.26	0.781	0.892	0.98	0.993	1	
Sc	0.043	0.198	0.163	0.412	0.12	0.118	0.178	0.225	0.265	1

4.4 Division and correlation of coal seams between relatively homogeneous blocks

The results of calculating the similarity $E(x_i, x_j)$ between each pair of coal seams and grouping the coal seams between relatively homogeneous blocks (blocks I and II) are summarized in Tables 12 and 13.

Comparing similarity coefficient H with similarity coefficient E (Tabs. 12 and 13) shows that the coal seam TV3-6 is unsuitable. Thus, it is necessary to repeat from step 1 to step 10 of the multivariate statistic methods. The comparison results are presented in Table 14, which shows that the coal seam TV3-6 is unreasonable; hence it should be considered and adjusted.

Tab. 12. Similarity coefficients (E) between coal seams.

Coal seam	Similarity coefficient E	Similarity coefficient H			
		Group I	Group II	Group III	Group IV
TV3-6	66	Group I	100	63	65
		Group II	63	100	84
		Group III	65	84	100
TV2-11	79	Group I	100	85	76
		Group II	85	100	82

		Group III	76	82	100	80
		Group IV	89	90	80	100

Tab. 13. The grouping results of boreholes in coal seams.

Coal seam	Borehole groups	
TV3-6	Group I	LK.84-SH, LK.100-SH, LK.104-SH, LK.107-SH, LK.108-SH, LK.109-SH
	Group II	LK.97-SH (SH97/14, SH97/15), LK.106-SH
	Group III	LK.97-SH (SH97/16), LK.102-SH
TV2-11	Group I	LK.84-SH, LK.102-SH, LK.108-SH
	Group II	LK.97-SH (SH90/27), LK.97-SH, LK.98-SH, LK.100-SH
	Group III	LK.90-SH (SH90/29, SH90/30), LK.107-SH
	Group IV	LK.104-SH, LK.106-SH, LK.109-SH

Tab. 14. Similarity coefficient of the coal seam TV3-6.

	Group 1	Group 2
Group 1 (I)	100	66
Group 2 (II)+III)	66	100

The coal seam TV2-11 is as acceptable as the preliminary correlation step; in other words, the correlation of coal seams conducted in step 4 is reasonable. Moreover, the calculation results show that the coal seams TV3-6a, TV3-6b, and TV3-6c (LK.97-SH) can be grouped into the seam TV3-6, which has a relatively complex structure containing many intercalated layered materials. Besides, the coal seams TV2-11a, TV2-11b, and TV2-11c can be grouped into the coal seam TV2-11 (LK.90-SH and LK.100-SH).

From Tables 11, 12, and 13, it can be seen that the preliminary correlation of main coal seams and coal lenses on 02 relatively homogeneous blocks (block I and block II) of the Nam Thinh-Giao Xuan fault zone is suitable and acceptable. However, the preliminary correlation in step 4 between the 02 blocks in the western and eastern blocks of the Nam Thinh-Giao Xuan fault is not appropriate and needs further consideration.

To detect and correct the errors of the coal seam correlation, many quantitative problems can be used; among them is the multidimensional statistical method proposed by Rodinov (1968) [26]. This suggests that the multidimensional statistical standard (V) of the coal seams can follow the equations mentioned above (10), (11), and (12).

Tab. 15. Comparison of coal seams between the eastern block (block I) and western block (block II) of the Nam Thinh - Giao Xuan fault.

Coal seam comparison		Block II		
		TV3-2	TV3-1	TV2
Block I	TV3-1	13.8	229.4	276.8
	TV2	17.6	29.2	22.1

Comparison results showed the Chi-square standard ($\chi^2_{0.5,28}$) of 15.6, which is greater than the multidimensional statistical standard (V) of 13.8 (Tab. 15). This indicates that the seam TV3-1 in the western block (block I) corresponds to the seam TV3-2 in the eastern block (block II) of the Nam Thinh - Giao Xuan fault zone. These results are also completely different from the seam TV3-1 in the eastern block of Nam Thinh-Giao Xuan fault as the results of preliminary correlation in step 4.

Based on the results of step 5 and geological and geophysical data, the unreasonable correlation of coal seams on the geological cross-sections is adjusted. Then step 5a and step 5b are repeated many times until the multidimensional statistical comparison problem (step 5) satisfy comparable standards.

5. Conclusions

Based on 256 geochemical coal and rashing samples of 13 boreholes, several statistical, multivariate, and correlation analysis methods were used to identify the correlation of the coal seams from the Tien Hai area in Northern Vietnam. Throughout this study, the conclusions can be drawn as follows.

The Mg, V, As, Ca, Zn, Cr, Co, K, Na, Sr, Fe, Ge, Re, U, Mo, Th, and Ga elements are strong indicator elements of the major and trace elements in coals and most of them comply with the normal or lognormal distribution, according to the frequency analysis results. Besides, for rare earth elements in coal samples, the Yb, Sc, Ho, Er, Tm, Lu, Y, Tb, Pr, Dy, and Sm elements are also good indicator elements, suggesting that these elements can be selected as the indicator ones for identifying correlation of the coal seams. Additionally, the correlation matrix and cluster analyses can divide the element associations into coal seams (i.e., the Mg-Ca-Sr, and K-V-Cr-Zn-Mo-Th associations of the major and trace elements) V-Zn-Cr, Co-Zn-Ge, and Ge-Co associations in rare earth elements) in the Tien Hai area.

Next, the similarity degree between studied objects is used to group boreholes in coal seams. Generally, the results of identifying the correlation of coal seam TV2-11 are suitable and acceptable; the coal seams TV3-6a, TV3-6b, and TV3-6c can be grouped into the coal seam TV3-6.

Finally, the statistical analysis of the geological and geophysical data from core samples shows a remarkable degree of correlation of the coal seams in the region due to the association with the good indicator elements that are established during the statistical process. Furthermore, geochemical coal data can help to evaluate the indicator elements of the major and trace elements, and rare earth elements in coal seams, and coal rashing of adjoining and pillar rocks in the Tien Hai area, northern Vietnam.

6. Acknowledgments

The paper was presented during the 6th VIET - POL International Conference on Scientific-Research Cooperation between Vietnam and Poland, 10-14.11.2021, HUMG, Hanoi, Vietnam.

7. References

1. Dickinson, W.R., and Suczek, C.A., 1979. Plate tectonics and sandstone compositions, American Association of Petroleum Geologists Bulletin, 110, 1268-1280.
2. Dickinson, W.R., and Valloni, R., 1980. Plate settings and provenance of sands in modern ocean basins, *Geology*, 8, 82-86.
3. Potter, E., 1978. Petrology and chemistry of modern big river sands, *Journal of Geology*, 86, 423-449.
4. Valloni, R. and Maynard, J.B., 1981. Detrital model of Recent deep-sea sands and their relation to tectonic setting: a first approximation, *Sedimentology*, 28: 75-83.
5. Zhifei, L., Yingchun, W., Shuzheng, N., Xu, J., Rongfang, Q., Daiyong, C., 2019. The differences of element geochemical characteristics of the main coal seams in the Ningdong coalfield, Ordos Basin, *Journal of Geochemical Exploration*, 202, 77-91.
6. Crook, A.W., 1974. Lithogenesis and geo-tectonics: the significance of compositional variations in flysch arenites (graywackes), in Dott, R.H., and Shaver, R.H., eds., *Modern and ancient geosynclinal sedimentation*, SEPM Special Publication 19, 304-310.
7. Dyke, M.V., Klemetti, T., Wickline, J., 2020. Geologic data collection and assessment techniques in coal mining for ground control, *International Journal of Mining Science and Technology*, 30(1), 131-139.
8. Schwab, L., 1975. Framework mineralogy and chemical composition of continental margin-type sandstone: *Geology*, 3, 487-490.
9. Hoang Ngoc Ky (ed.). Report on the geological mapping and mineral resources in the Hai Phong-Nam Dinh area at a scale of 1:200.000, Department of Geology and Mineral Resources of Vietnam (in Vietnamese), 1999.
10. Tran Van Tri & Vu Khuc (ed.). *Geology and Earth Resources of Vietnam*. General Department of Geology and Minerals of Vietnam, Publishing House for Science and Technology, Hanoi, 2011.

11. Huyen, T.N., Cuong, D.T., Hieu, T.N., 2019. Non-structural traps in the post-rift succession of Phu Khanh Basin: Classification and Depositional History, *Journal of Mining and Earth Sciences* 60 (3): 1-9.
12. Nga, H.L., Dong, N.P., Huy, Q.B., 2019. Organic petrology and Rock-Eval characteristics in selected coal samples of the Cau Formation, block 07 Nam Con Son Basin, *Journal of Mining and Earth Sciences* 60(3): 10-17.
13. Nielsen, L.H., Mathiesen, A., Bidstrup, T., Vejbnk, O.V., Dien, P.T., Tiem, P.V., 1998. Modeling of hydrocarbon generation in the Cenozoic Red River basin, Vietnam: a highly prospective basin, *Journal of Asian Earth Science* 17(1): 269-294.
14. Dong Van Giap (ed.). Report on the results of Investigation and Assessment of coal resources in the mainland of Red River coal basin and adjacent area, Department of Geology and Mineral Resources of Vietnam (in Vietnamese), 2005.
15. Golonka, J., Krobicki, M., Pajak, J., Giang, N.V., and Zuchiewicz, W. *Global Plate Tectonics and Paleogeography of Southeast Asia*, Faculty of Geology, Geophysics and Environmental Protection, AGH University of Science and Technology, Arkadia, Krakow, Poland, 2006.
16. Hall, R., 1996. Reconstructing Cenozoic SE Asia. In: Hall, R., Blundell, D. J. (eds). *Tectonic evolution of Southeast Asia*, vol 106, Geological Society of London Special Publication, London, 203-224.
17. Lee, T.Y., Lawver, L.A., 1995. Cenozoic plate reconstruction of Southeast Asia, *Tectonophysics* 251:85-138.
18. Vu Xuan Doanh. Report on the degree of coal-bearing in the Hanoi trough (Hung Yen - Thai Binh area), Vietnam Institute of Geosciences and Mineral Resources (in Vietnamese), 1982.
19. Golovenok, V.K., Le Van Chan, 1966. Sediments and formation conditions of Neogene-Quaternary sediments in the Hanoi trough, Vietnam Petroleum Institute, Hanoi (in Vietnamese).
20. Nguyen Van Tinh, Nguyen Phuong, Do Van Nhuan, Nguyen Quoc Phi, Tang Dinh Nam, Dong Van Giap, Dang My Cung, Dang Tran Nhu Thuy. Research on establishing the geological and geophysical parameters as the basis for connection and correlation of the coal seams in the Red River coal basin, a case study of the Tien Hai area, northern Vietnam, Vietnam Institute of Geosciences and Mineral Resources, Vietnam Ministry of Natural Resources and Environment (in Vietnamese), 2015.
21. Ngo Tat Chinh. Report on the results of prospecting mineral deposits in the Khoai Chau-Chau Giang-Hung Yen area, Department of Geology and Mineral Resources of Vietnam (in Vietnamese), 1987.
22. Dong Van Nhi, Nguyen Phuong, 1988. Using geological and geophysical dimensional statistics for identifying correlation of the coal seams in the Quang Ninh area, northeastern Vietnam, *Journal of Mineral Economics and Raw Materials* (in Vietnamese).
23. Tran Manh Quang. Selecting a reasonable combination of borehole geophysical methods for studying and applying the correlation of the coal seams based on the multivariate statistical models of geology and geophysics (an example from the Nga Hai coal mine). PhD thesis, Hanoi University of Mining and Geology (in Vietnamese), 1988.
24. Rao, C.R., 1967. Linear statistical inference and its applications, *Annals of Mathematical Statistics*, 38(1), 281-284.
25. Hung, K.T., Sang, P.N., Phuong, N., Linh, V.T., & Sang, B.V., 2020. Statistical evaluation of the geochemical data for prospecting polymetallic mineralization in the Suoi Thau-Sang Than region, Northeast Vietnam, *Geology, Geophysics and Environment*, 46(4), 285-299.
26. Rodionov, D.A. *Statisticeskie resenija v geologii.*: Izd. "Nedra", Moskva, 231 pp (in Russian), 1968.

Influence of Harmonics on the Working Efficiency of a 6/1.2 kV Transformer in a Pit Mine

NGO Xuan Cuong¹, DO Nhu Y^{2,*}

¹ Hue University, School of Engineering and Technology, Hue, Vietnam

² Hanoi University of Mining and Geology, 18 Vien street, Hanoi, Vietnam

Corresponding author: donhuy@hung.edu.vn

Abstract. Explosion-proof transformers 6/1.2 kV is important electrical equipment responsible for supplying electricity in underground mine electrical networks. A failure of this transformer will cause an interruption in the power supply and loss of safety in underground mining. Usually, explosion-proof transformers in underground mine electrical networks are designed and manufactured to work with ideal parameters such as sinusoidal currents, and the network structure is symmetrical. However, today in underground mine electric networks, many power electronics are connected to the network, such as inverters and soft starters. As a result, a current flowing through the transformer is non-sinusoidal, overloading the transformer even by working with the design specifications. This paper studies the influence of harmonics on the working efficiency of a 6/1.2 kV transformer in a pit mine. Research results suggest reasonable solutions for transformer operation to ensure longevity and not cause damage to the transformer.

Keywords: Harmonics, Working efficiency, Transformer, Pit mine

1. Introduction

The explosion-proof transformer is one of the most important electrical components in an underground power distribution network. The operation and proper preventive maintenance of transformers will ensure a continuous and reliable electrical power supply to end-user customers without power outages or interruptions. Furthermore, the increasing cost of electricity generation has reinforced the importance of using low-loss transformers. Therefore, reducing transformer losses is of interest in today's competitive environment [1].

Traditionally, explosion-proof transformers are designed to operate at a sinusoidal power frequency to provide a linear load. However, the 6kV power network in open-pit mining has characteristics such as long feeder lines, large-capacity equipment, various branches, overuse of power electronics on the grid, which degrades the power quality, leading to increased power loss [2, 3]. Consequently, the performance of the transformer will be impacted. Non-linear loads generate non-sinusoidal currents from electrical networks, and therefore they are considered sources of harmonic currents that produce reverse currents into electrical networks. Such harmonic currents passing through the distribution lines then cause harmonic voltages [4].

Harmonic voltage creates unwanted additional losses, leading to excessive heat generation in the transformer. Excessive temperature rise due to harmonic pollution accelerates the aging of transformer insulation, thereby reducing their service life. As a result, harmonic pollution is becoming an increasingly important concern for power companies. To counter the adverse effects of harmonic pollution, power reduction of transformers is one of the approaches to maintain their expected design life [5].

Transformer losses can be classified into two main groups of no-load and loaded losses. The no-load loss represents the energy required to retain the continuously variable flux in the core and is independent of the transformer load. The load loss arises from the resistance loss of the windings, and it depends on the square of the load current [6]. Continuous no-load losses lead to power loss in network-connected transformers for all 24 h.

The study of core loss of a three-phase transformer with a capacity of 300 VA with different harmonic conditions has been investigated using the three-dimensional finite element method [7]. The results showed that the voltage harmonics contribute to the increase in core losses in the transformer, with a value of up to 67.3% when the input voltage is formed based on the highest harmonic order stated in IEC 61000-3-6 international standards about harmonic emission limits.

Arslan et al. (2014) studied 12.5 MVA, 11 kV/31.5 kV transformer no-load loss on the 2D FEM model under excitation voltage with some content on sub-harmonics [8]. The obtained simulation results have shown that the effect of sub-harmonic voltage on transformer core loss is negligible. However, it has also been found that a small amount of auxiliary harmonic voltage can significantly contribute to winding losses under no-load conditions, and they need to be handled with care for power transformer attenuation [8].

In [9], Yazdani-Asrami et al. (2013) used the experimentally combined finite element method to test non-sinusoidal voltage effects on no-load transformer losses. No-load loss ratio increases from 14% to 20% for harmonics with total harmonic distortion (THD) from 31.7% to 38.2% compared to the sinusoidal condition of the test transformer.

The results of a no-load experiment in [5] showed that the additional core loss due to non-sinusoidal excitation could be increased up to 20.8%. A short-circuit test was also carried out to determine the increase in transformer loss due to the increase in impedance and reactance in the transformer equivalent circuit under the distinct effect of the harmonic orders at different times. The short circuit test results showed that the total resistance and inductance of the coil increases with the applied frequency, and its linear variation can explain the linear increase in reactance with the applied frequency ($X = \omega L$). In contrast, the increase in the total impedance of the coil is due to the skin effect.

This paper builds a loss calculation model for a three-phase transformer and studies the effect of non-sinusoidal voltage on transformer losses in case of no-load and short-circuit and their performance under load in the underground mine electrical network. Thereby, the authors recommend users to have appropriate operating solutions to improve the service life and not cause damage to the mining transformer.

2. Theoretical basis

2.1. Simulation model for a three-phase transformer

A typical transformer commonly used in mining is the 630 kVA mine explosion-proof three-phase transformer. It is used in the experiment in this study with its initial parameters from manual [10] given in Table 1.

Tab. 1. Parameters of mine explosion-proof three-phase transformer 630/6-1.2 from manual [10].

Rated power P_n , kVA	No-load voltage (V)		Rated current, A		Short circuit voltage, $V_{sc\%}$	No-load current, $I_{NL\%}$	Losses, W	
	HV V_{NL1}	LV V_{NL2}	HV I_{1n}	LV I_{2n}			No-load P_{NL}	Short circuit P_{sc}
630	6000	1200	60.6	304.3	3.5	3	2800	4700

This paper uses the “Three-Phase Transformer (Two Windings)” model on MATLAB/ Simulink software as a basis for studying the proposed effects. The Three-Phase Transformer (Two Windings) model uses three single-phase transformers coupled together. Figure 1 shows the equivalent circuit of the single-phase transformer [11]. From the manufacturer’s parameters, the paper builds simulation parameters for a three-phase transformer based on linear transformer combined with hysteresis characteristics on MATLAB/Simulink software. The simulation parameters of a single-phase transformer are given in Table 2 and use the proposed hysteresis characteristic as shown in Figure 2.

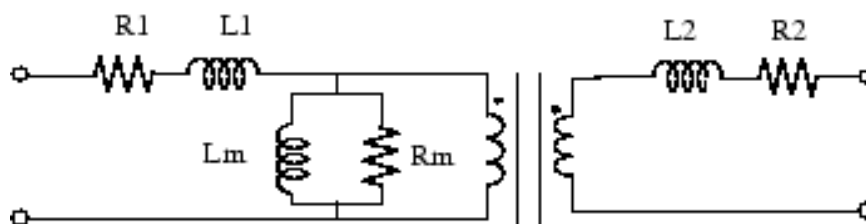


Fig. 1. Equivalent circuit of linear single-phase transformer.

Tab. 2. Simulation parameters of three-phase transformer.

Resistance (ohm)		Inductance (L)		Magnetization resistance, R_m (ohm)
HV, R_1	LV, R_2	HV	LV	
0.2133	0.0085321	0.0031125	0.0001245	13580

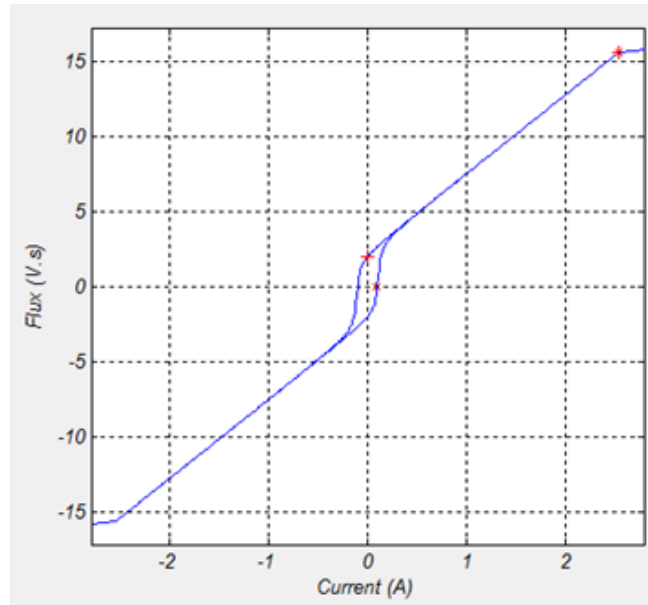


Fig. 2. Hysteresis characteristics.

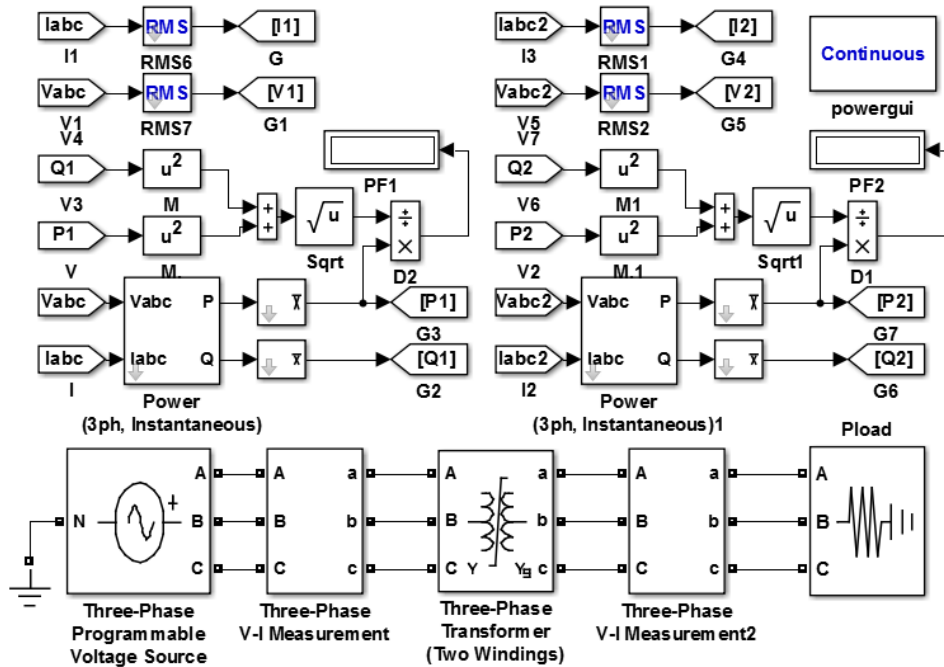


Fig. 3. Simulation model of 3-phase transformer.

The transformer uses a Y/Y connection. In the model, the resistances are constant, which means that the skin effect is ignored. The simulation model of 3-phase transformer on Matlab-Simulink is shown in the figure 3. Where the “Thee Phase Programmable Voltage Source” source block is used, non-sinusoidal modeling is added with a harmonic component to the existing sine source voltage.

2.2. Basis of loss calculation

The losses in the transformer include load and no-load losses, and are calculated by:

$$P_T = P_1 - P_2 = P_L + P_{NL} \quad (1)$$

Where P_1 - 3-phase high-voltage input power, P_2 - low voltage 3 phase power.

The no-load loss is independent of the load and is caused by the induced voltage in the core. It consists of two components: hysteresis loss and eddy current loss [12]. The two-frequency method for transformer [13] to separate the core loss into eddy current loss P_{Fe} and no-load hysteresis loss P_H is expressed by the following formula:

$$P_{NL} = P_{Fe} + P_H \quad (2)$$

Eddy current loss in the proposed model is calculated by:

$$P_{Fe} = 3R_m I_m^2 = 3R_m \sum_{h=1}^{h_{max}} I_{m,h,rms}^2 \quad (3)$$

Where R_m - magnetization resistance, ohm; I_m - true RMS value of magnetizing current, A; $I_{m,h,rms}$ - RMS value of the h harmonic order of the magnetizing current, A.

The load loss in the proposed model is the copper loss, which is proportional to the square of the true root mean square (RMS) value of the load current increased by the current harmonic components.

$$P_L = 3R_1 I_{1,r}^2 + 3R_2 I_{2,h,r}^2 = 3R_1 \sum_{h=1}^{h_{max}} I_{1,h,rms}^2 + 3R_2 \sum_{h=1}^{h_{max}} I_{2,h,rms}^2 \quad (4)$$

Where R_1 - high voltage phase resistor; R_2 - low voltage phase resistance; $I_{1,r}$ - true RMS value of high voltage load current; $I_{2,r}$ - true RMS value of low voltage load current; $I_{1,h,rms}$ - RMS value of the h harmonic order of high voltage load current; $I_{2,h,rms}$ - RMS value of the h harmonic order of low voltage load current.

When the power source has harmonics, PF is calculated according to the following relationship:

$$PF = \frac{P}{\sqrt{P^2 + Q^2}} \quad (5)$$

Where P - the active input power, W; Q - the reactive input power, Var.

The efficiency of a transformer is the ratio of the 3-phase low-voltage output power P_2 to the 3-phase high-voltage input power P_1 :

$$eff = \frac{P_2}{P_1} 100 \quad (6)$$

3. Research results and discussion

3.1 No-load simulation test

The primary purpose of the no-load simulation test is to demonstrate a significant increase in no-load losses when operating at rated voltage and with harmonic distortion. The test transformer is excited on the HV side, and the LV winding is kept open.

In this test, the transformer is operated at different voltages and frequencies, but the V/f ratio is constant. The results are shown in Figure 4. As expected, these losses are proportional to the supply V/f ratio or the frequency ratio applied and the increased voltage level because the flux density is proportional to the excitation. In addition, eddy current losses are the main contributor to core loss. The copper loss component in the no-load test accounts for 0.05-0.1% of the no-load loss.

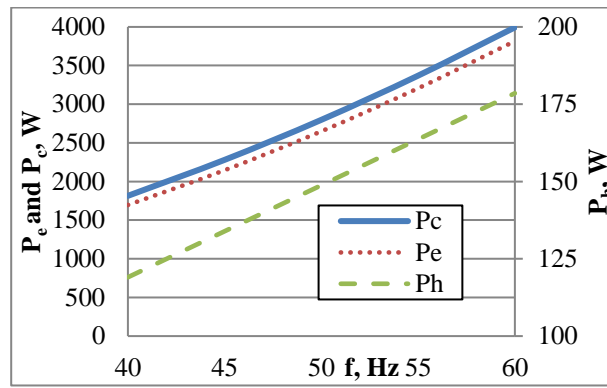


Fig. 4. Core loss in V/f ratio.

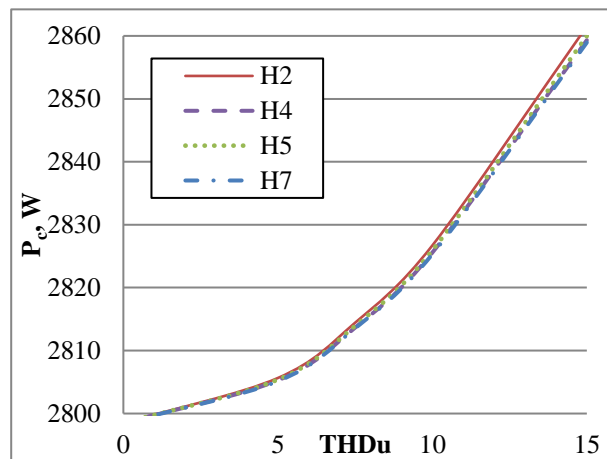


Fig. 5. Core loss under harmonics.

Tests for the effect of harmonics on core losses are carried out by adding high-order harmonic components to the reference voltage with a variable voltage THD, the results of which are shown in Figure 5. It is clear that as the voltage THD increases, so does the core loss proportionally. Tests have also shown that the 3rd and 6th harmonics have no effect and that the 5th harmonic has a significant influence on core losses in the no-load case.

Testing with the effect of input voltage deviation on core losses is also considered. The results in Fig. 6 indicate that when rated voltage increases 8.3%, core loss increases to about 16.6% for the non-harmonic case and 19.4% for the possibility of 5th harmonic sources with a THDu voltage of 15%. These results are significant, considering that the transformer is always on, core losses are always present. Thus, the presence of voltage harmonics will significantly contribute to the total loss in general and the core loss in particular in practice.

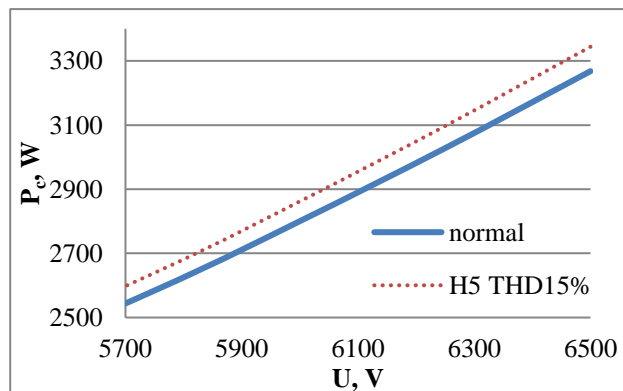


Fig. 6. Core loss under input voltage changer.

3.2 Short circuit simulation test

Here, the short-circuit test transformer is excited on the HV side with the test short-circuit voltage, and the LV winding is kept short-circuited. The results in Table 3 show that the short circuit loss is not affected by the 3rd and 6th harmonics and increases the most when there is the 2nd harmonic. With the increase of voltage THDu, the short-circuit loss also increases correspondingly in Figure 7.

Tab. 3. Short-circuit losses under harmonic with 15% voltage THDu.

Harmonic	H1	H2	H3	H4	H5	H6	H7
P _{sc} , W	4697	4724	4697	4703	4701	4697	4699

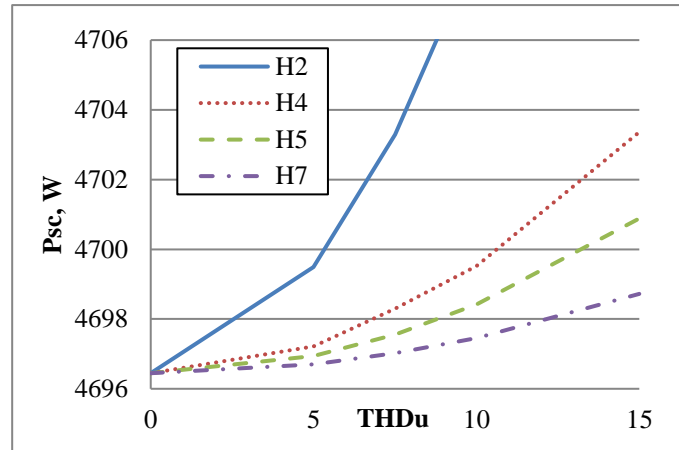


Fig. 7. Short circuit losses with variable THDu.

3.3 Simulation test with load

The simulation test with load gives an overview of the transformer efficiency dependence on voltage harmonics. In Figure 8, the overall efficiency of the transformer depends on the load factor and its power factor PF. Maximum transformer efficiency when unit PF and the efficiency of leading power factor is greater than that of lagging power with the same element. Transformer efficiency with harmonics is lower than the efficiency without harmonics.

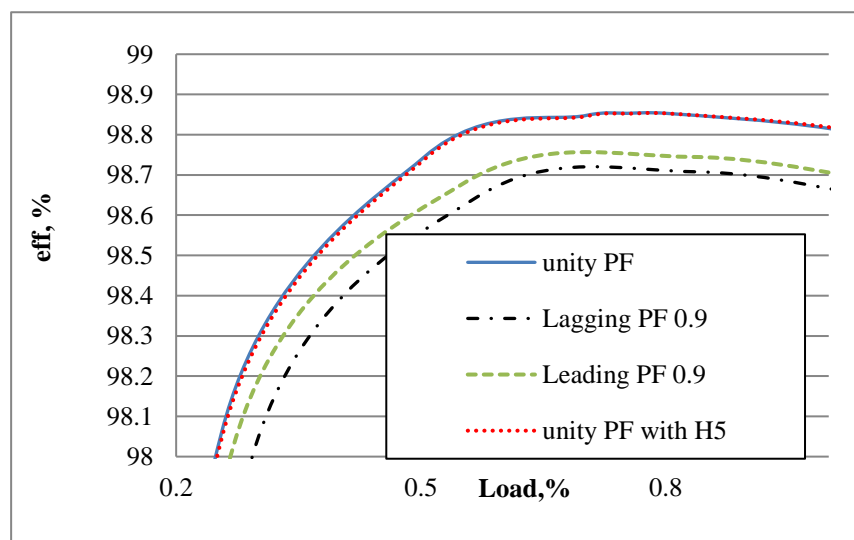


Fig. 8. Transformer efficiency as a percentage of the load.

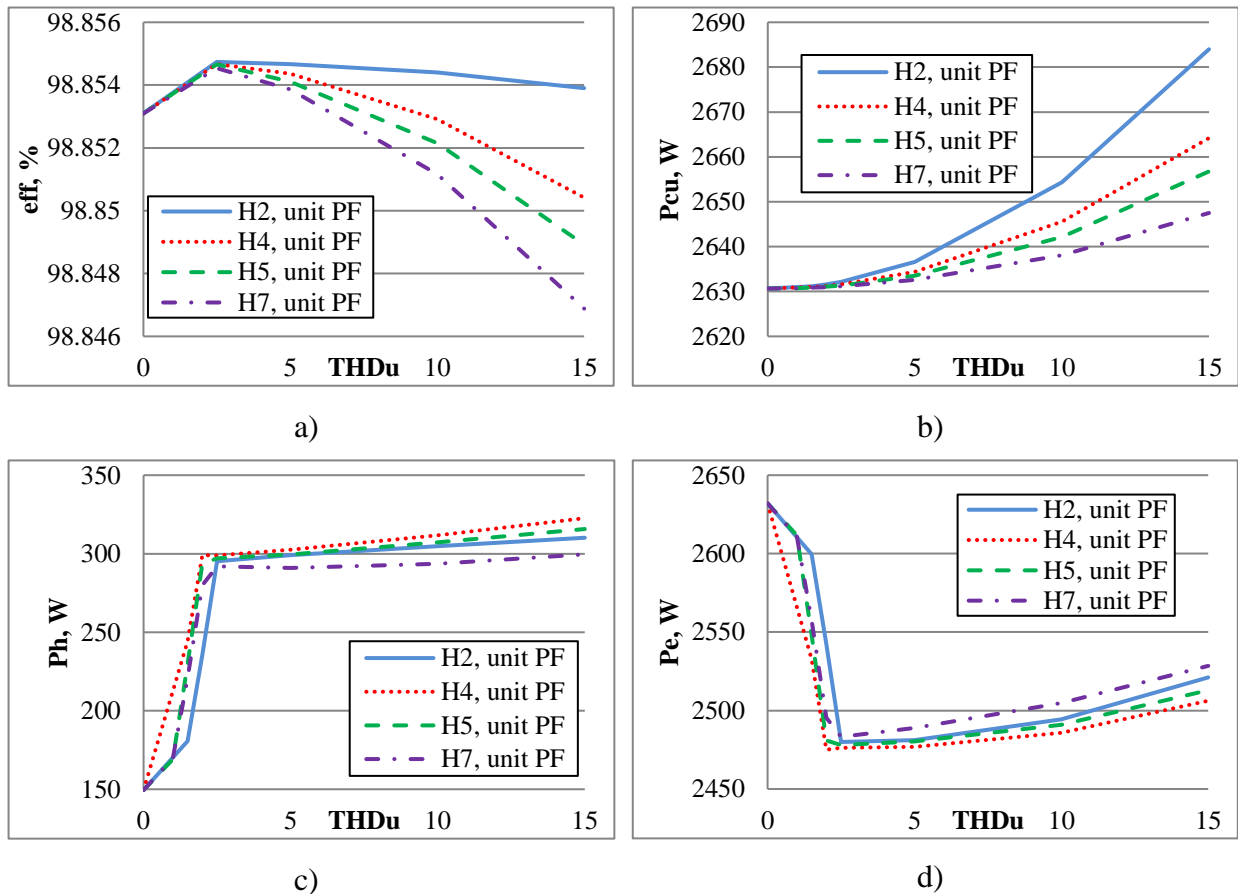


Fig. 9. The efficiency of 3 phase transformer under load with unit PF according to voltage THD.

a) Efficiency; b) Copper loss; c) Hysteresis loss; d) Eddy current loss.

We note that the efficiency peaks at about 2-2.5% voltage THD, plummets as the voltage THD increases, which is explained while increasing THDu from 0-2.5% eddy current loss sharply decreases, hysteresis loss and copper loss increase but not significantly. Hence, the efficiency increases to the maximum point. Then, due to the rise in copper loss and magnetic circuit saturating, the overall efficiency of the transformer gradually decreases with the increase of THD voltage.

The results show that the 5th and 7th harmonics cause the most significant performance degradation, while the 2nd harmonics have a more negligible effect on the overall performance. In addition, increasing voltage THD causes the transformer efficiency to decrease proportionally.

4. Conclusions

This paper has presented a loss calculation model and the influence of non-sinusoidal voltage on 6/1.2 kV transformer loss in underground mines in case of no-load and short-circuit and their performance under load. Simulation tests have shown that the 3rd and 6th harmonics have no influence, and other higher harmonics greatly influence the transformer loss and efficiency. In addition, the increase of THD voltage causes a core loss, and load loss also increases. Testing with the effect of voltage deviation on core losses has also been considered. The results indicated that with an 8.3% increase to rated voltage, core loss increases to about 16.6% for the non-harmonic case and 19.4% for the case of 5th harmonic sources with a THDu voltage of 15%. With the core loss occurring continuously in the transformer, through the influence of harmonics on the core loss, it is possible to determine the total loss in the transformer with a non-sinusoidal operating power supply.

The transformer efficiency is most excellent when the unit power factor and the leading power factor efficiency are more significant than the lagging power with the same factor. Transformer efficiency with harmonics is lower than the efficiency without harmonics. The 5th and 7th harmonics cause the most significant loss of efficiency, while the 2nd harmonics have less impact on overall performance.

From the above analyses, the presence of voltage harmonics in the power supply to the three-phase transformer in underground mines in working modes significantly affects its loss and performance, thereby recommending users to have appropriate operating solutions to improve the service life and not cause damage to the mining transformer.

5. Acknowledgments

The paper was presented during the 6th VIET - POL International Conference on Scientific-Research Cooperation between Vietnam and Poland, 10-14.11.2021, HUMG, Hanoi, Vietnam.

6. References

1. Olivares-Galván, J.C., Georgilakis P.S., and Ocon-Valdez, R., 2009. A review of transformer losses, *J Electric power components systems*, 37(9): 1046-1062.
2. Nguyen, N.X. and Le, T.X., 2017. Evaluating effect of the voltage resonant caused by harmonics of nonlinear loads to capacitor banks located on Nam Mau Coal Company's 6kV electric grid (in Vietnamese), *Journal of Mining and Earth Sciences*, 58(2): 128-136, Available from:<http://jmes.humg.edu.vn/en/archives?article=784>.
3. Ngo, X.C., Do, N.Y., and Tran, Q.H., 2020. The Influence of Voltage Quality on Asynchronous Motor Performance of EKG Excavator in Open Pit Mines–Vinacomin, *Inżynieria Mineralna*, 16(1): 139-145.
4. Do, Y.N., Le, T.X., Nguyen, N.B. and Ngo, T.T., 2020. Impact of asymmetrical phenomena on asynchronous three-phase motors in operation mode, *Journal of Mining and Earth Sciences*, 61(3): 68-74, [https://doi.org/10.46326/JMES.2020.61\(3\).08](https://doi.org/10.46326/JMES.2020.61(3).08).
5. Dao, T., and Phung, B.T., 2018. Effects of voltage harmonic on losses and temperature rise in distribution transformers, *IET Generation, Transmission & Distribution*, 12(2): 347-354.
6. IEEE C57.110-2018 - IEEE Recommended Practice for Establishing Liquid Immersed and Dry-Type Power and Distribution Transformer Capability when Supplying Non-sinusoidal Load Currents.
7. Malekpour, M., Larkin, M., and Phung, T. Core Loss Studies using FEM of a Three phase Isolation Transformer under Harmonic Conditions. in 2019 9th International Conference on Power and Energy Systems (ICPES). 2019. IEEE.
8. Arslan, E., Sakar, S., and Balci, M.E., 2014. On the no-load loss of power transformers under voltages with sub-harmonics. in 2014 IEEE International Energy Conference (ENERGYCON). IEEE.
9. Yazdani-Asrami, M., Mirzaie, M., and Akmal, A.A.S., 2013. No-load loss calculation of distribution transformers supplied by non-sinusoidal voltage using three-dimensional finite element analysis, *J Energy*, 50: 205-219.
10. Dzyuban, V.S., Shirnin, I.G., Vaneev, B.N., Gostishchev, V.M., *Coal Mine Power Engineer Handbook*, Vol. 2., Donetsk: "Yugo-Vostok, Ltd." 447, 2001.
11. Guru, B.S. and Hiziroglu, H.R., 2001. *Electric machinery and transformers*. Vol. 726. Oxford university press New York.
12. Takach, D. and Boggavarapu, R., 1985. Distribution transformer no-load losses, *IEEE transactions on power apparatus and systems*, 1985(1): 181-193.
13. Dao, T., Phung, B., and Blackburn, T., 2015. Effects of voltage harmonics on distribution transformer losses. in 2015 IEEE PES Asia-Pacific Power and Energy Engineering Conference (APPEEC). IEEE.

Stabilization of Deep Roadways in Weak Rocks Using the System of Two-level Rock Bolts

TRAN Tuan Minh^{1,*}, DO Ngoc Thai¹, DANG Trung Thanh¹, NGUYEN Duyen Phong¹, VO Trong Hung¹

¹ Hanoi University of Mining and Geology, 18 Vien street, Hanoi, Vietnam

Corresponding author: tuanminhhung@yahoo.com

Abstract. Large rock mass deformation around deep roadways in the weak rocks was a significant problem in mining activities in Vietnam and other countries. The excavation of roadways leads to high releasing stress, which exceeds the peak strength of spalling surrounding rock and causes it to enter the post-failure stage. Tensile failures then initiate and develop around the roadways, which causes the fragmentation, dilation, and separation of surrounding rock. The capacity of the primary support system is low, which results in a severe contraction in the whole section of roadways, which requires finding solutions to prevent the deformation of rock mass around roadways and technical solutions from stabilizing for deep roadways. To stability analysis of roadways can be applied analytical, experimental, semi-experimental, and numerical methods. This paper introduces the prevention mechanism of large deformation of rock mass around roadways using 2-level rock bolts. The research results show that using the system of two-level rock bolts can reduce the values of tensile stress on the boundary of roadways range from 10 to 15% compared with only one. The importance of the total displacement of rock mass on the boundary of roadways will be reduced from 3.47 to 13.85% using six long cable bolts.

Keywords: Deep roadways, Large deformation mechanism, Control techniques, Numerical simulation, Weak rocks, Rock bolts

1. Introduction

The rapid development of the economy and society in the world and Vietnam requires consuming a significant amount of energy. Therefore, shallow minerals are gradually depleted, and the exploitation requirements of deep mineral resources are imperative. Currently, coal mining countries have carried out the deep mining trend - the depths of exploitation are 1000 m from the surface, which could be seen in the Russian Federation, South Africa, Canada, America, India, Germany, and China [1-12]. The types of rock mass often have variations with the other depths and extreme alterations, so the problem of design and selection of supports is considered different, complicated, and complex. The theories of analysis and calculation of supports for roadways and drifts in case of exploitation at the superficial level are unsuitable for deep roadways and have many inadequacies [13-17]. The deep mining is also accompanied by difficult ventilation conditions in the roadways and drifts; the ventilators also have significant capacity because of fresh air increasing. Drainage has also become complicated and varies complexity, the flow of underground water will be increased.

In Vietnam, the variation of geological conditions has been described in the related geological documents [14-17], especially at underground mines such as Hon Gai, Ha Lam, and Nui Beo coal mines which are located near the sea. Not only is the sea level high, but also many mines are exploited under open pit mining. The drainage and design of supports are specifically complex and dangerous. The excavation of deep roadways could also encounter soft and swelling rock conditions. When underground water appears in the rock mass, the earth pressure will be increased; the rock mass zone consists of tectonic forces that change the initial and the second state of stress around roadways. Because of growing earth pressure, the cross-section of roadways will be reduced during their operation [14-17]. The theoretical analysis application with rock bolts, steel ribs, and rock bolt and shotcrete [14, 16] has become effective in the actual operation of supports.

The trend to design rock supports based on utilizing the bearing capacity of rock mass around roadways and releasing initial stress (Rock mass - supports) [15-17] is more attention to maintaining the stability of roadways and reducing the cost of their excavation. The design ideals utilizing the load-carrying capacity of rock mass around roadways in Vietnam are less focused, requiring further research to ensure sustainable development of national energy security.

With the development of technologies and software, numerical modelings are widely used and brought more efficiency in the design process the stability of roadways [4, 15, 16]. The currently specialized

software can be divided into different groups, such as Discontinuous Deformation Analysis (DDA), Finite Element Method (FEM), Difference Element Method (DEM), Boundary Element Method (BEM), etc [19, 20]. The advantage of these method groups can be simulated problems likely close to the actual conditions, including many influence parameters of geological and hydrogeological conditions of the working areas at the same time. In addition, they can also be simulated for the construction, excavation, and installation of rock supports in the roadways.

2. Background of the theory short rock bolts combination with long rock bolts and other supports in a high-stress rock mass

In a deep coal mine research, the author observed that geological discontinuities in the rock mass become less in density and less opened with an increase in depth. For instance, at a depth of 1000 m, all discontinuities (not many) exposed on excavation faces were closed entirely. Therefore, it can be said that the rock mass quality is improved at great depth due to the reduction of geological discontinuities. However, the in-situ rock stresses increase with depth. At depth, the major instability issue is no longer the falling of loosened rock blocks but rock failure. High pressures could lead to two consequences in underground openings: large deformation in soft and weak rock and rockburst in hard and robust rock (Fig. 1). In some metal mines in Russia, strain burst usually occurs below 600 m and becomes intensive below 1000 m. Rock failure is unavoidable in high-pressure conditions. The task of rock support at depth is not to equilibrate the deadweight of loosened blocks but to prevent the failed rock from disintegration. In high-stress rock masses, the support system must be not only strong but also deformable to deal with either stress-induced rock squeezing in weak rock or rockburst problems.

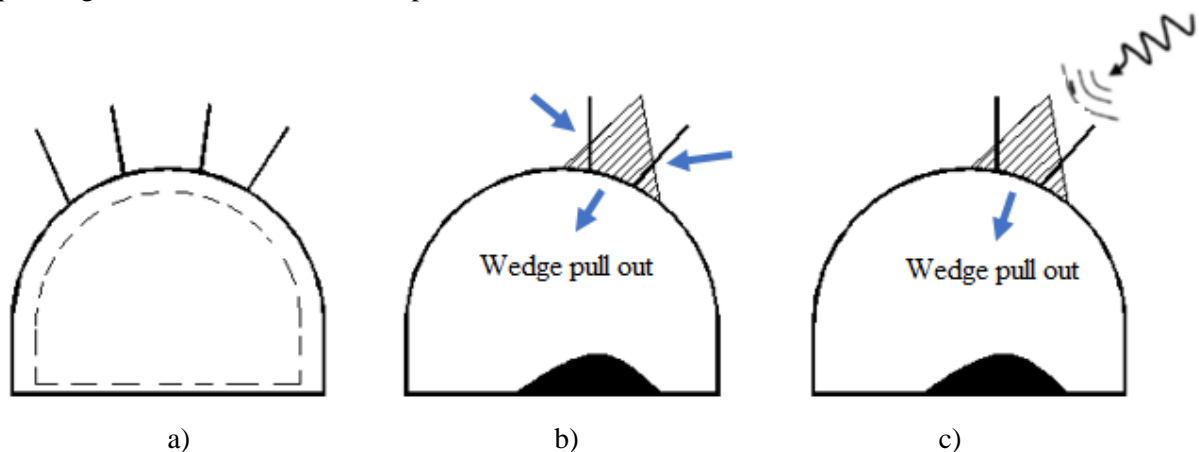


Fig. 1. Loading conditions of rock bolts around roadways: a) squeezing rock; b) strain burst; c) seismic loading or blasting.

A rock supports system may be composed of one or more than one of the following support systems, depending on the loading condition and the expansion of rock failure zone such as (Fig. 2):

Layer 1 - Bolting (short rock bolts): Short rock bolts are installed locally or systematically (Spot bolts or pattern rock bolts on the boundary of roadways).

Layer 2 - Surface retaining: Retaining elements like meshes, straps, lacing, thin liners, shotcrete, and cast concrete lining is installed on the rock surface.

Layer 3 - Cable (length rock bolts): Single - or multi-strand cables are installed into the sharp rock behind the failure zone.

Layer 4 - External support: Structurer elements, including steel ribs, concrete arches, invert, cast concrete lining, and thick shotcrete liners, reinforced concrete lining are set up in tunnels - layer 4A.

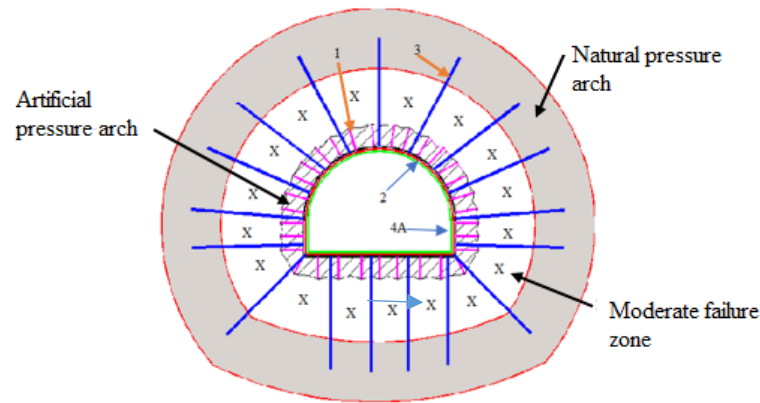


Fig. 2. The characteristic of a reinforced zone by short rock bolts combined with long rock bolts (cable bolts) around roadways: 1 - the short bolts under level; 2 - shotcrete layers; 3 - the long rock bolts; 4A - final (permanent) support layers.

In weak rocks, the failure zone can extend to a depth beyond the length of rock bolts (Fig. 2). In this case, both rock bolts (layer 1) and retaining surface elements (layer 2) are needed. Rock bolts must be tightly installed so that they, together with the surface support elements, help to establish an artificial pressure arch in the failure zone. The artificial pressure arch forms a protective shield over the opening. Either cable bolts (layer 3) or moderately strong external support elements (layer 4A), or both, are added to restrict the movement of the protection shield. The 1-2-3 layer support is often used in deep mines and underground constructions of large span.

Moreover, in the squeezing and swelling rock, the short rock bolts (1) and shotcrete (2) will cause the temporary artificial reinforced arch. This solution leads to reduce the pressure on the permanent supports of roadways (Fig. 2). However, in actual excavation activities, because of the span of roadways, excavated technologies, and geological conditions, the deformation of rock mass around roadways will continuously increase, and the residual deformation will appear. In the points far from the boundary of roadways, the state of stress are initial stress and equal constant. In this case, the conditions are permitted, using the long rock bolts suspended the inner reinforcement layer and external stability and undisturbed rock mass (1+3). Thanks to the advantages of support systems 1 and 3, the pressure impacted on the permanent support system 4A will be declined. Consequently, the thickness of this system will also be reduced, and the cost of roadway excavation will be decreased.

3. The effects of reinforcement in the case of two-level rock bolts

3.1 Support Characteristic Curve for rock bolts

To clearly show the effect of rock bolts combined with other supports, derived from Ground Characteristic Curve (GCC) by Carranza-Torres. Carranza-Torres (2004) proposed the GCC with the sandstone by using the elastoplastic solutions for circular tunnels with extremely initial stress of infinity [1].

It is assuming that the system of short bolts is equally spaced in a circumferential direction, the maximum support pressure (p_{smax}) provided by the support system, and the elastic stiffness (K_s) can be evaluated by using the following equations [1, 5].

$$p_s^{max} = \frac{T_{bf}}{s_c s_1} \tag{1}$$

$$\frac{1}{K_s} = s_c s_1 \left[\frac{4L}{\pi d_b^2 E_s} + Q \right] \tag{2}$$

where:

d_b - diameter of bolt (m);

L - free length of the bolt (m);

T_{bf} - ultimate load obtained from a pull-out test (MN);

Q - deformation load constant for the bolt and the head (m/MN);

E_s - Young's modulus for bolt (MPa);

s_c - circumferential bolt spacing, ($s_c = 2\pi R/n_b$), where n_b is the total number of equally spaced bolts installed in cross-section

s_1 - longitudinal bolt spacing (m).

3.2 Combination effect of support systems

If more than one of the bolt support systems are installed as two-level systems, their combined effect can be calculated by adding the elastic stiffnesses for each of the individual rock bolts, which increases the total elastic stiffness of the whole system. Consider, for example, the case in which two supports characterized by maximum pressure p_{s1max} and p_{s2max} and elastic stiffnesses K_1 and K_2 , respectively, are installed in a section of the tunnel. The stiffnesses K_s for the two systems acting together can be calculated as following [1, 5]:

$$K_s = K_1 + K_2 \quad (3)$$

This value is assumed to remain valid until one of the two supports achieves its maximum possible elastic deformation u_{rmax} calculated by formulas [1, 5]:

$$u_{r1}^{max} = \frac{p_{s1}^{max}}{K_{s1}} \quad (4)$$

$$u_{r2}^{max} = \frac{p_{s2}^{max}}{K_{s2}} \quad (5)$$

$$u_{rmax} = u_{r1max} + u_{r2max} \quad (6)$$

The combined support system is assumed to fail at that point. The support with the lowest value of u_{rmax} determines the maximum support pressure available for the two-level rock bolts acting together because if one assumes that the collapse of the support system, so the maximum support pressure that the system can sustain before destruction is calculated as following [1, 5]:

$$p_s^{max} = u_{rmin}^{max} K_s \quad (7)$$

Safety Factor (SF) will be applied in case of using the method of GCC and Convergence Confinement Method (CCM) to design support in tunnels (Fig. 3) to indicate the role of two-level rock bolt systems in the design process of supports in roadways. The ratio can calculate SF mobilized support pressure P_s and equivalent pressure P_{eq} (the time system of rock mass-support works together - intersection point GCC and SCC). For example, to design rock support by GCC and CCM in Rocsupport 3.0 (Fig. 4).

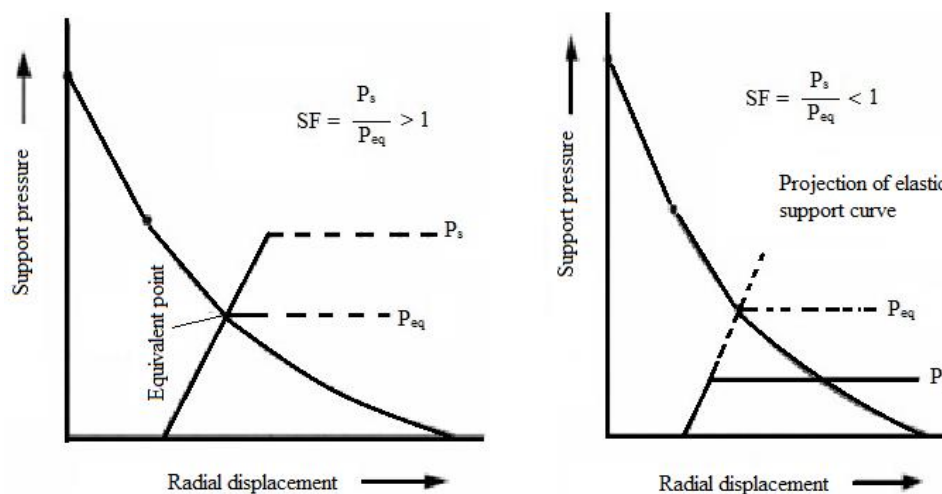


Fig. 3. Defined the design of support according to Safety Factors (SF).

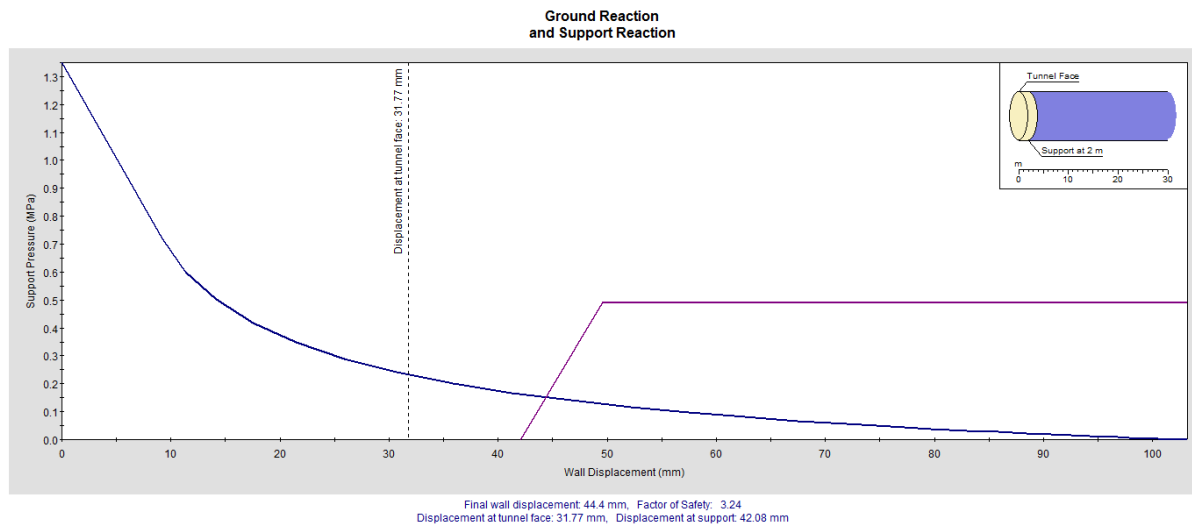


Fig. 4. Example of model analysis by SF coefficient in Rocsupport 3.0.

Currently, a different ideal to design two-level rock bolts in the deep roadways is being used and has become the design standard of the Russian Federation. According to the rules and guidelines of the Russian Federation [13], when the displacement of rock mass on the boundary of roadways exceeds 300 mm, roadways must be applied rock bolts with two levels (shot - long rock bolt system).

The long rock bolts (deeper rock bolts) will be installed near the short rock bolts during excavation roadways and drifts after longwall with the distance 0.1H (H - the depth of roadways or drifts from the surface).

When calculation the parameters of upper-level rock bolts with the theory collapsed arch, the pressure over 1 meter in length P_{cb} , kN/m impact on the rock bolt system can be determined by the following formula [13]:

$$P_{cb} = \frac{2}{3} B_p h_{ph} \gamma \tag{8}$$

where: B_p - width of roadways, h_{ph} - height of collapsed rock mass around roadways can be calculated by formula [13]:

$$h_c = k_{cb} B_p \tag{9}$$

where: k_{cb} - coefficient depending on the properties of type and structures of the rock mass.

The length of rock bolts in upper levels (cable bolts) l_{ka} can be calculated by formula [13]:

$$l_{ka} = h_{cb} + l_z + l_b \tag{10}$$

Where: l_z - length of upper rock bolts located exceeding the boundary of natural arch usually can be chosen $l_z = 0.8 - 1.0$ m or by support passport, l_b selected 0.15-0.20 m. The length of rock bolts is rounded to 0.5 m.

4. Numerical modeling for effects of reinforcement of 2-levels rock bolts in the geological conditions at the deep roadways

In this study, the alteration of stress state around roadways using 2-levels rock bolts will be explained in the geological conditions likely observed and investigation site of roadways in Mong Duong coal company [18]. Roadways were excavated in the geological areas consisting of siltstone and sandstone mixed with thin coal seams. The uniaxial compressive strength $\sigma_{ci} = 20-30$ MPa. The thickness of sandstone ranges 23.0-25.0 m on the roof of roadways, underfloor located siltstone and claystone with $\sigma_{ci} = 40$ MPa, the thickness of layer $m = 5.0$ m, below these layers is sandstone layer with $\sigma_{ci} = 100$ MPa. The service times of roadways are 15 years, the depth of roadways $H = 100$ m from the surface, and roadways are located in the tectonic zone. The underground water exists in the area where roadways, sandstone, and siltstone will be soft and have behaviors of soft and swelling rocks. Tab. 1 describes the properties of rock

mass layers and the surface of stratification layers. The properties of joints and stratification layer can be calculated by criterion Barton and Bandis, 1990 [21].

The numerical modeling was applied to investigate this problem in Phase 2 for two cases: Case 1 - in the homogeneous rock mass, roadways supported by pattern bolts with nine bolts, spacing of bolts 1.5×1.5 m for short level, and three cable bolts for the second level, spacing of cable bolts 1.5×1.5 m. Cable bolts are installed between the short bolts. Case 2 - in the stratification rock mass with an inclined angle of layers - 45° , roadways are applied by nine short and six long cable bolts. The spacing of short bolts and cable bolts are used the same as in case 1. Fig. 5 shows the modeling results, and Figs. 6 - 8 shows the tensile stress distribution and the failure zone around roadways.

Tab. 1. The parameters of sandstone and siltstone.

N0	Parameters	Symbol	Values		Units
			Sandstone	Siltstone	
1	Unit weight of rocks	γ	0.26	0.27	MN/m ³
2	Tensile of rock mass	σ_t	0.5	0.7	MPa
3	Cohesion of rock mass	c	1	2	MPa
4	Friction angle of rock mass	φ	25	35	Degree
5	Elastic modulus of rock	E	1800	2000	MPa
6	Poisson ratio	μ	0.30	0.28	-
7	Residual friction angle	φ_{re}	22	32	Degree
8	Residual cohesion	c_{re}	0.5	1.0	MPa
9	The width of roadways	5	-	-	m
10	Type of material	-	Elasto-Plastic	Elasto-Plastic	-
11	Cohesion on the surface of stratification sandstone/siltstone	c'	0		MPa
12	Friction angle of the surface of stratification sandstone/siltstone	φ'	35		Degree
13	Normal stiffness on the surface of stratification sandstone/siltstone	σ_T	100000		MPa/m
14	Shear stiffness on the surface of stratification sandstone/siltstone	τ	10000		MPa/m

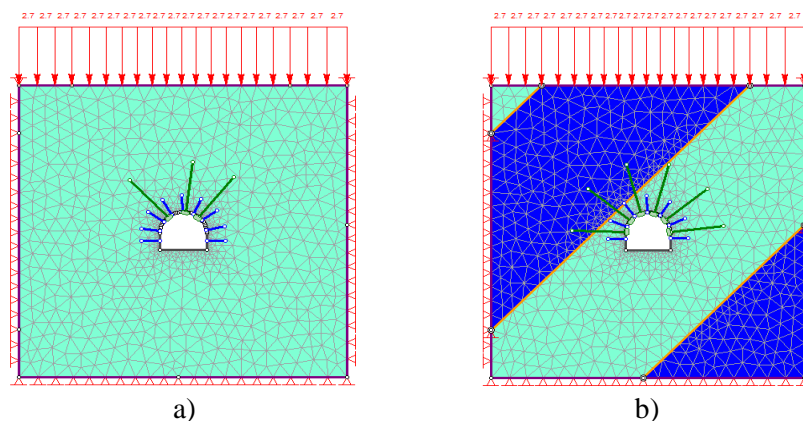


Fig. 5. Using rock bolts with two levels: nine short bolts and three long cable bolts (a), nine short bolts, and six long cable bolts in stratification rock mass (b).

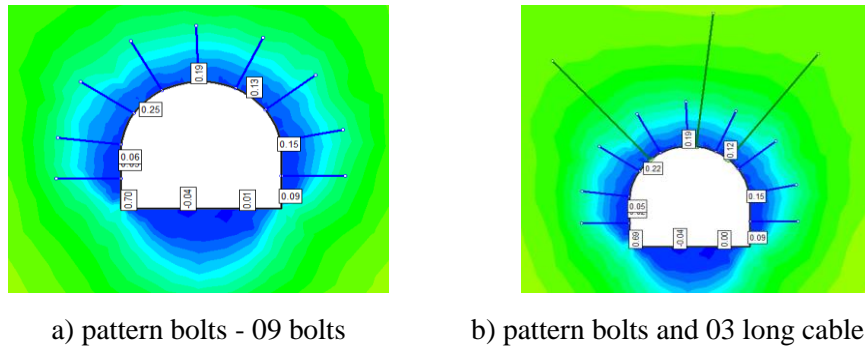


Fig. 6. The tensile stress distribution around roadways in the short rock bolts pattern combination with three long cable bolts.

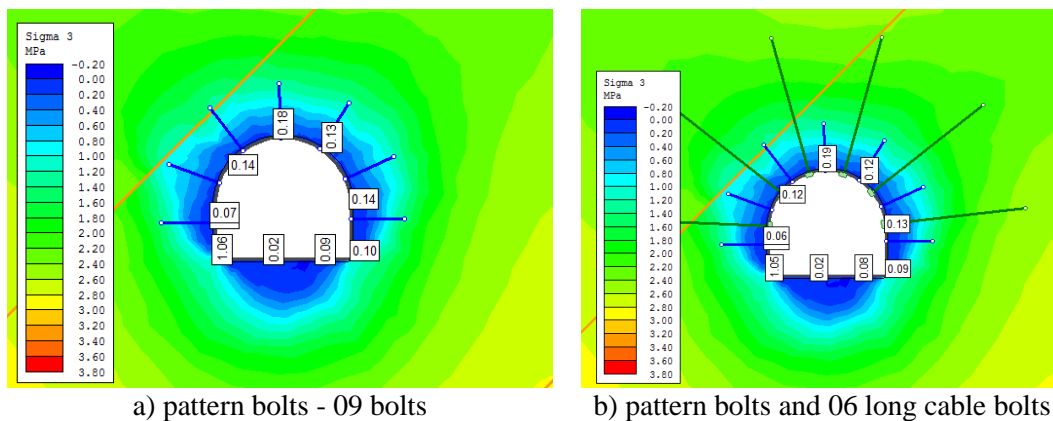


Fig. 7. The tensile stress distribution in case of the short rock bolts pattern combination with six long cable bolts in a stratification rock mass.

The results in Figs. 6-7 show that the tensile stress on the shoulder of roadways is changed using the pattern bolts and long cable bolts. In the detailed conditions applied for three long cable bolts, the tensile stresses are 0.25 MPa; 0.22 MPa; 0.13 MPa; 0.10 MPa, respectively. In long cable bolts in the second level - six bolts are 0.14 MPa; 0.12 MPa; 0.13 MPa; 0.12 MPa. When adding a long cable bolt system, the tensile stresses on the boundary of roadways should be reduced and rock mass around roadways reinforced to become more stable.

Figs. 8-9 describe the failure zone around roadways for two cases in the homogenous and stratification rock mass using rock bolt pattern by nine short bolts, 3 or 6 cable bolts.

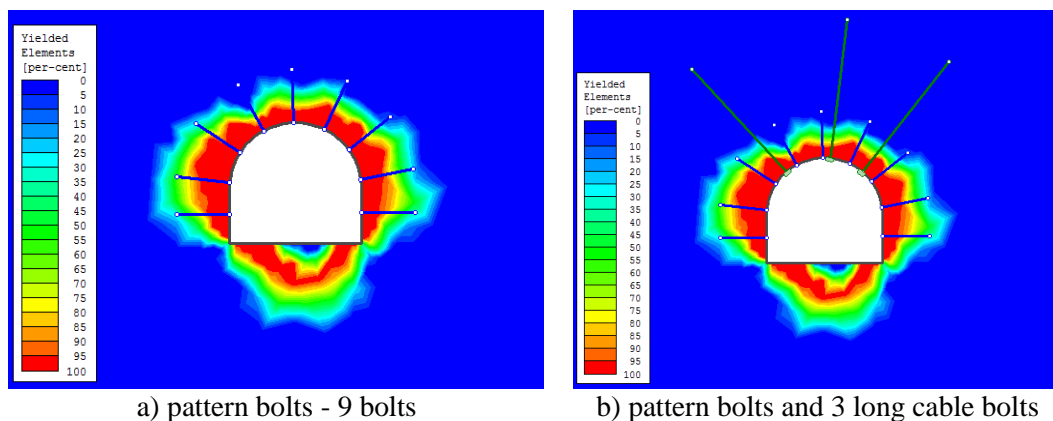
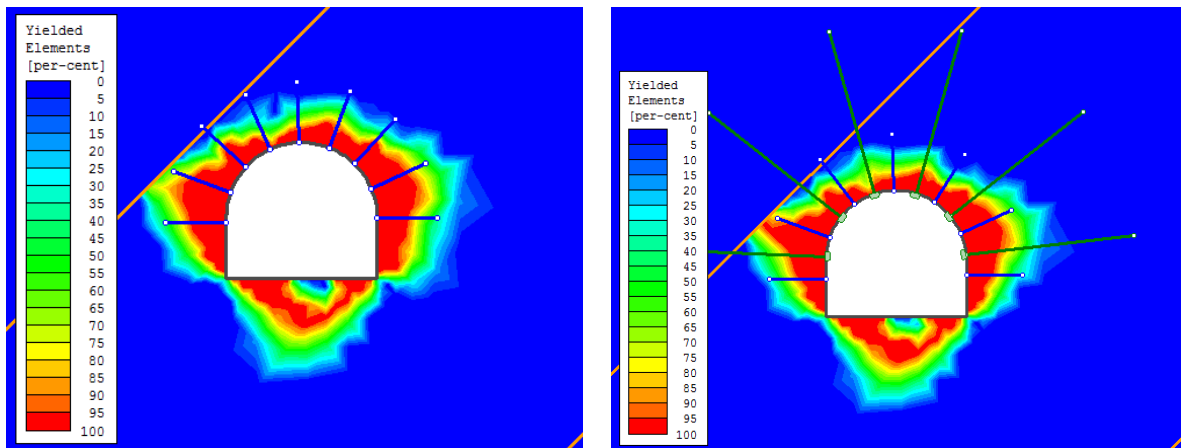


Fig. 8. Failure zone around roadways.



a) pattern bolts - 9 bolts
 b) pattern bolts and 6 long cable bolts
Fig. 9. Failure zone around roadways in the stratification rock mass.

The results indicate that the lengths of the short bolt pattern are small. The efficiency of the bolt system is not inadequate. The long cable bolts prevented the rock mass in the failure arch to the stability rock mass around roadways in the homogenous and stratification rock mass. By statistic can be established the graphics of tensile stress and total displacement on the roadway boundary for two cases in (Figs. 10-11).

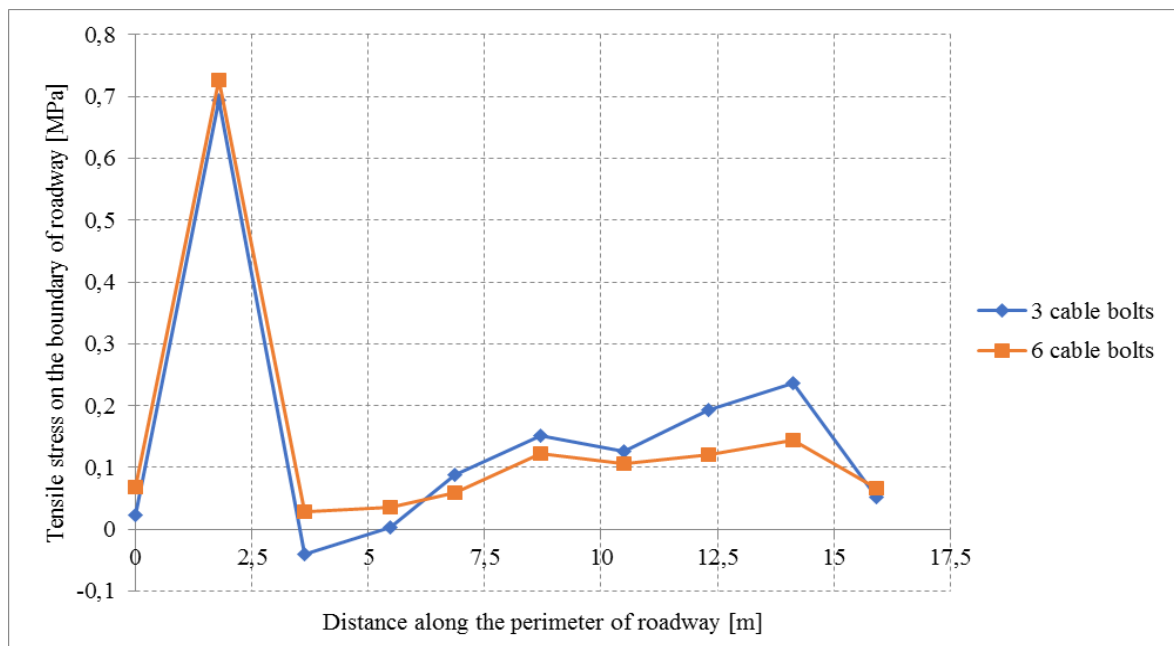


Fig. 10. The tensile stress distribution of rock mass on the boundary of the roadway.

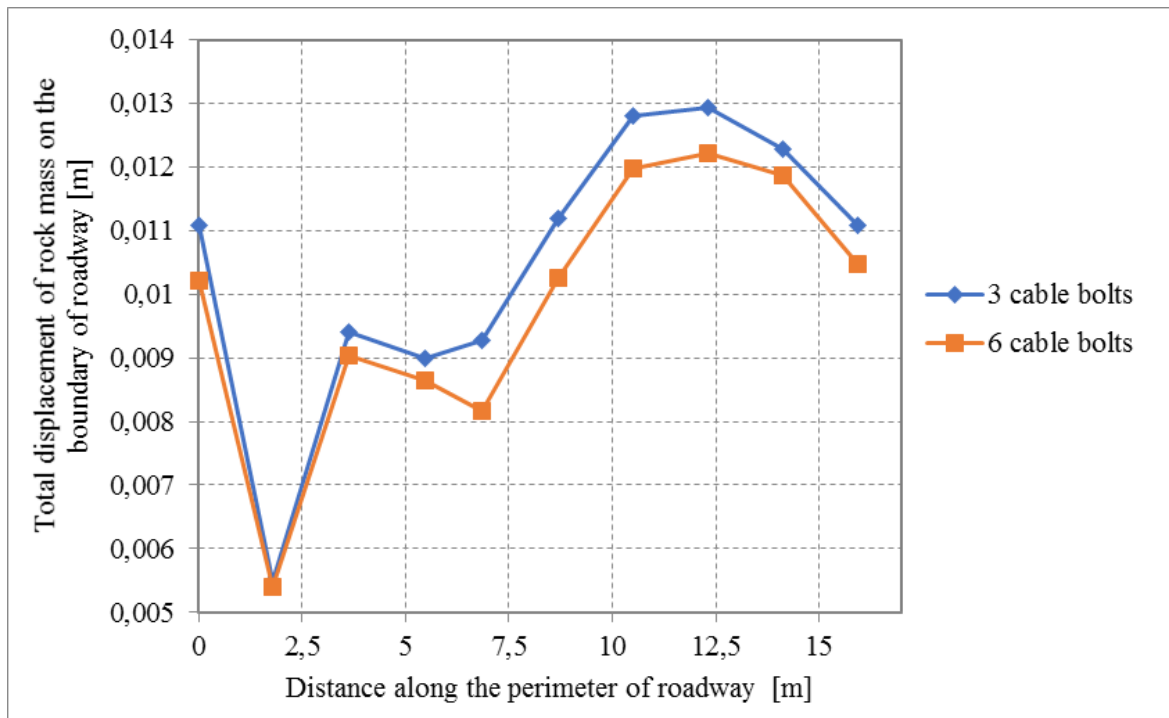


Fig. 11. The total displacement on the boundary of the roadway.

The results on Figs. 10-11 indicate that on the roadway boundary located six cable bolts, the tensile stress and total displacement values are smaller than in the case of three cable bolts. The values of the rock mass displacement on the boundary of roadways will be reduced from 3.47% to 13.85%. This comment explained that the rock mass around the roadway would be more reinforced for similar geological conditions.

5. Conclusions

The above theoretical analysis and the numerical model results show that the rock bolts influence the stability of roadways. Rock bolts can be applied and combined with other supports such as shotcrete, steel ribs, concrete linings, precast concrete, short bolts, and long bolts, as in this research.

The numerical method results also show that in the case of application of short pattern bolts, combined with the long rock bolts, the tensile stress values on the boundary of roadways will be reduced range from 10% to 15%. In the case of applied six long cable bolts, the total rock mass displacement on the boundary of roadways will be reduced from 3.47% to 13.85% compared with three long cable bolts in similar geological conditions, the earth pressure also decreased.

In the stratification rock mass, the distribution of pressure is not symmetrical, and the pattern rock bolts should not be applied because of reinforcement effects. The short rock bolts combination with long rock bolts are not efficient.

Numerical simulation, GCC, and CCM should be applied in the design process to predict the values and distribution of rock pressure early and preliminary selection of temporary supports in analysis. It is necessary to have flexibility, change design ideals of supports, and update each roadway's actual geological conditions.

6. Acknowledgments

The paper was presented during the 6th VIET - POL International Conference on Scientific-Research Cooperation between Vietnam and Poland, 10-14.11.2021, HUMG, Hanoi, Vietnam.

7. References

1. Carranza-Torres, C., 2004. Elasto-plastic solution of tunnel problems using the generalized form of the Hoek-Brown failure criterion, *International Journal of Rock Mechanics and Mining Sciences*, Proceedings of the ISRM SINOROCK 2004 Symposium, edited by J.A. Hudson and Xia-Ting Feng, 41(3).
2. Hoek, E., and Brown, E.T. *Underground Excavations in Rock*. Instn. Min. Metall., London, 1980.
3. Hoek, E., Kaiser, P.K., Bawden, W.F. *Support of underground excavations in hard rock*. Balkema, Rotterdam, 1995.
4. Lee, Y-K., Pietruszczak, S.A., 2014. New numerical procedure for elasto-plastic analysis of a circular opening excavated in a strain-softening rock mass, *Tunnelling and Underground Space Technology*, 23(5), 588-599.
5. Panet, M. *Calculation of tunnels by the Convergence-Confinement Method*. Press of the Ecole nationale des Ponts et Chaussées, Paris, 178p, 1995.
6. Vlachopoulos, N., Diederichs, M.S., 2009. Improved longitudinal displacement profiles for convergence-confinement analysis of deep tunnels, *Rock Mechanics and Rock Engineering* (Accepted - In Press), 16 pgs.
7. Vrakas, A., 2016. A finite strain solution for the elastoplastic ground response curve in tunnelling: rocks with non-linear failure envelopes, *International Journal for Numerical and Analytical Methods in Geomechanics*, 41(7), 1077-1090.
8. Vrakas, A., Anagnostou, G., 2014. A finite strain closed-form solution for the elastoplastic ground response curve in tunnelling, *International Journal for Numerical and Analytical Methods in Geomechanics*, 38(11), 1131-1148.
9. Lei Fan, Weijun Wang, Chao Yuan, Wenqing Peng, 2020. Research on large deformation mechanism of deep roadway with dynamic pressure, *Energy Sci Eng*, 00:1-17. DOI: 10.1002/ese3.672.
10. Guangzhe Xue, Chao Gu, Xinqiu Fang, Tao Wei, 2019. Case Study on Large Deformation Failure Mechanism and Control Techniques for Soft Rock Roadways in Tectonic Stress Areas, *Sustainability*, 11, 3510; doi:10.3390/su11133510.
11. Baklashov, I.V., Kartoziya, B.A., *Mechanics of underground constructions and structures*, Moscow, 543p, 2002.
12. Eremenko, B.A., Razumov, E.A., Zaiatdinov, D.F., 2012., *New technologies of rock bolts*, Mining book, 656p, ISBN 978-5-98672-291-7.
13. Ministry of fuel and energy of the Russian Federation Russian Academy of Sciences. *Instruction for the calculation and application of rock bolts in the coal mines in Russia*. St. Petersburg, 2000.
14. Hung, V.T., Dac, P.M., *Rock mechanics for underground construction and mining*, Scientific and technical publisher, Hanoi, 460p, 2006.
15. Phich N.Q., *Rock mechanics*, Construction publisher, Ha Noi, 356p, 2007.
16. Trang, D.N., 2011. About the determinate support in tunnel by convergence confinement method according to the criterion of Hoek-Brown. *Road and bridge journal*.
17. Minh, T.T., Tuan, D.Q., Huy, N.Q., Dinh, N.V., Nam, P.Q., *The calculation methods for underground structures*, Hanoi polytechnic university publisher, 596p, 2018.
18. *Research on the application tubing precast concrete for roadways in the problematic geological conditions in TKV*, Institute of mining science and technology, code KC.01/16-20, Hanoi 2020.
19. Do, T.Ngoc and Do, T.Duc., 2020. Study of the influence of face pressure on surface settlements by shield tunneling (in Vietnamese). *Journal of Mining and Earth Sciences*. 61, 1 (Feb, 2020), 31-40. DOI:[https://doi.org/10.46326/JMES.2020.61\(1\).04](https://doi.org/10.46326/JMES.2020.61(1).04).
20. Dang, V.Kien, Do, N.Anh, Nguyen, T.Tien, Nguyen, A.Duy Huynh and Pham, V.Vi., 2021. An overview of research on metro tunnel lining in the sub-rectangular shape (in Vietnamese). *Journal of Mining and Earth Sciences*. 62, 4 (Aug, 2021), 68-78. DOI:[https://doi.org/10.46326/JMES.2021.62\(4\).08](https://doi.org/10.46326/JMES.2021.62(4).08).
21. Barton, N.R. and Bandis, S., 1990. Review of predictive capabilities of JRC-JCS model in engineering practice. In *Rock joints, proc. Int. Symp. On rock joints*, Loen, Norway, (eds N. Barton and O. Stephansson), 603-610, Rotterdam.

Stress Distribution Around Mechanized Longwall Face at Deep Mining in Quang Ninh Underground Coal Mine

BUI Manh Tung^{1,*}, LE Tien Dung¹, VO Trong Hung¹

¹ Hanoi University of Mining and Geology, 18 Vien street, Hanoi, Vietnam

Corresponding author: buimanhtung@humg.edu.vn

Abstract. Quang Ninh underground coal mines are currently in the phase of finishing up the mineral reserves located near the surface. Also, in this phase, a number of coal mines have opened and prepared new mine sites for the extraction of the reserves at greater depth. Several mines have mined at -350 m depth and are driving opening excavations at -500 m depth below sea level. The mining at greater depth faces many difficulties, such as a significant increase in support and excavation pressures. The longwall face pressure is mostly manifested in great magnitude that causes support overloaded and jumped and face spall/roof fall. This paper, based on the geological condition of the Seam 11 Ha Lam coal mine, uses the numerical program UDEC for studying the impact of mining depth on stress distribution around the longwall face. The results show that the deeper the mining is, the greater the plastic deformation zone is. The peak front abutment stress moves closer to the coal wall, mainly concentrating on the immediate roof and top coal. The top coal is greatly broken, and its bearing capacity is decreased. Some solutions to the stability of roof strata are proposed, and a proper working resistance of support is determined. Additionally, the paper suggests that the starting depth for deep mining in Quang Ninh underground coal mines should be -350 m below sea level.

Keywords: Stress distribution, Longwall face, Deep mining, Underground coal mine, Quang Ninh

1. Introduction

Deep mining is an inevitable trend for coal mining in the world. According to statistics, there are many countries that perform the coal extraction at -500 m below sea level, such as -514 m in Russia, -928 m in Germany, -610 m in Poland, and -1,024 m in China [1]. These countries have early implemented research on mining at greater depth. Cheng et al [2] used numerical model in combination with theoretical analysis and site observation to interpret the typical stress distribution in roof and floor strata; deformation and failure of coal wall; and typical stress redistribution when mining depth varies. The study found the relationship between face support and roof strata in the condition of competent roof and deep mining. Liu [3] and Bai et al [4], by using the numerical program UDEC 3.0, studied the caving, stress field distribution and roof strata displacement as well as the impact of depth and dip angle on roof rock stability. The results provided scientific evidence and solutions for control of surrounding rock and face support. For studying behaviour of mine pressure and ground control at deep mining, Du [5] and Bai et al [6] used theoretical and practical investigations to predict the mode of failure zone, method for determination of main roof convergence, and relationship between dynamic pressure and mining depth. The results showed that the rock behaviour at deep mining was not clear, the frequency of coal wall spall/roof fall increased as mining depth increased, and the surrounding rock failed significantly. Qi et al [7] analysed ground pressure in deep mining from which fundamental and technical framework for prevention of dynamic impact at different scales in China. At the same time, Li et al [8] found a change in stress distribution at seam floor using numerical model, physical model and site measurement. Recently, Zhang et al [9] studied the stress distribution and failure characteristics of deep inclined seam. They revealed that the vertical taper structure was formed by the roof, interconnection and maingate. Besides, Chen et al [10] investigated deep mining in existence of face fault [10]. Chaoru [11] used regression analysis for studying distribution of in-situ stress in deep underground coal mines. It was found that an increase in mining depth increased the effect of in-situ stress on surrounding rock deformation and failure. However, as the depth increased, the increasing rate of horizontal stress decreases. The ratio of maximum principal horizontal stress to vertical stress was founded in the range of 0.63-2.42. According to Pathegame et al [12], deep mining becomes a common practice in near future, and it is controlled by the understanding of rock mechanics and mining technologies.

It can be seen that in the world, theories and practices for deep mining have been interpreted to some extent through theoretical analysis and site observation. The distribution of stress at great depth, however, is preliminarily studied through mainly numerical modelling. Only several input parameters have been

studied; accordingly, it lacks fundamentals for development of stress distribution around longwall face at great depth. For geological conditions in Vietnam, Le et al [13] used numerical method to study coal mining under competent roof at Quang Hanh coal mine, Quang Ninh coal field. The results showed that the face was affected by overburden pressure more seriously. It caused more face instabilities, especially near two roadways. Nguyen et al [14] developed a numerical model for calculation of failure and subsidence caused by mining for Quang Ninh coal field. An other example can be seen in Le et al in which a safe mining height for extraction of coal under Red River delta was determined and some feasible opening solutions were proposed [1, 15]. In general, the above studies are preliminary and lack detailed investigation for mine design and ground control at great depth.

2. Geological condition of longwall face

The mechanised face belongs to Seam 11 Ha Lam coal mine and in depth from -150 m to -300 m below sea level. The rock units in the mine include conglomerate, sandstone, gritstone, claystone, coal-clay and coal seams. The rock strata alternate each other, resulting in relatively consistent stratigraphic sequence in local scale. The roof and floor rocks are mainly siltstone, claystone and sometime sandstone layers. The rocks are medium strong. Seam 11 is ranks as thick seam but inconsistent in the range of 0.97-29.75 m and an average dip angle of 5 degrees. The longwall dimension in dip and strike directions are 120 m and 430 m, respectively. The rock characteristics are shown in Tab. 1.

Tab. 1. Characteristics of roof and floor rocks.

Surrounding rock	Rock types	Thickness, m	Rock characteristics
Main roof	Conglomerate	16.72	Sandstone-interbedded siltstone, equal distribution, thickness of 16.72 m. Medium to hard roof.
	Siltstone	8.48	
Immediate roof	Sandstone	2.11	Sandstone in thickness of 5-25 m, average of 17 m. Weak to medium stable roof.
Immediate floor	Sandstone, claystone	4.18	Claystone and coal-clay in lens shape of thickness 0.23-1.8 m. Sandstone in equal distribution in thickness of 2-15 m. Floor in stable to medium strong.
Main floor	Conglomerate	5.6	Siltstone-interbedded conglomerate, consistent distribution

3. Stress distribution around longwall top coal caving face in Quang Ninh

3.1 Model development

To study the stress distribution around longwall top coal caving face, this paper uses the numerical program UDEC 3.0 for modelling of longwall face [16]. Based on the geological condition of Seam 11, Ha Lam coal mine, the model has a length of 400 m, height of 126 m, depths of 300 m, 350 m, 400 m and 450 m. The block size is each stratum follows the status in practice.

The top boundary is applied a boundary stress in equal distribution. The bottom boundary is fixed with x- and y-velocity of zero. The side boundaries are fixed in horizontal displacement.

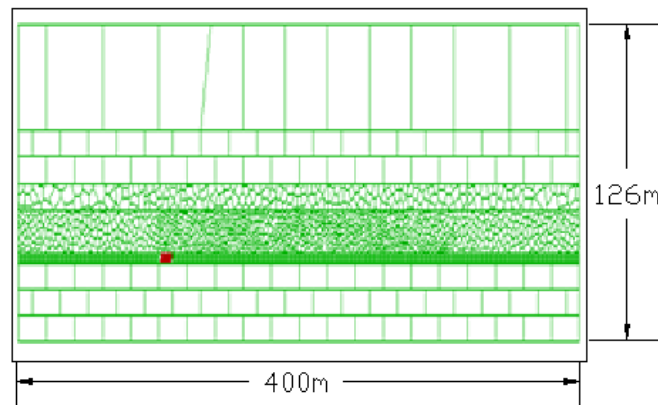


Fig. 1. Initial model.

3.2 Rock strata and coal seam properties

The rock behaviour in model follows Mohr-Coulomb theory. This theory can deal with fundamental rock problems such as slope stability and mining excavation. In coal mining, the theory can capture the failure, rupture and fault, and thus its parameters are of importance for calculation results. From the laboratory test, field observation and modelling experience from past users, the properties are chosen as follows:

Tab. 2. Rock and coal mechanical properties.

Rock strata	Density kg/m ³	Uniaxial compressive Strength, MPa	Young modulus, GPa	Cohesion, Mpa	Internal friction, degree	Tensile strength, MPa
Upper main roof	2500	12	18	4	35	2
Lower main roof	2500	12	10	2	33	1.3
Immediate roof	2200	10	3	1.4	32	0.93
Coal	1400	3.2	1.2	1	33	0.3
Immediate floor	2679	12	3	1.4	35.8	0.93

Tab. 3. Interfaces mechanical properties.

Rock strata	Normal stiffness, GPa/m	Shear stiffness, jGPa/m	Cohesion, MPa	Internal friction angle, degree	Tensile strength, MPa
Upper main roof	10	7	0.08	35	0.05
Lower main roof	9	6	0.06	32	0.04
Immediate roof	7	4.5	0	0	0
Coal	5	3	0.04	15	0.02
Immediate floor	7	4.5	0.04	15	0.04

3.3 Front abutment stress distribution in variation of mining depth

Because the top coal fails under roof pressure, the front abutment stress forms distressed zone, concentrated zone, and pre-mining stress zone. Fig. 2 shows the stress distribution around longwall face when the mining depth is 300 m, 350 m, 400 m and 450 m. When the depth increases, the stress contour of front abutment stress varies. When the depth is 300 m, the concentrated front abutment stress zone locates at immediate roof and about 18 m ahead of coal wall with a peak stress magnitude of 20 MPa. When the depth is 350 m, the concentrated stress zone locates at immediate roof, about 15 m ahead of coal wall with a peak stress value of 27 MPa. When the depth is 400 m, the concentrated stress zone locates below immediate roof. The zone is about 13 m ahead of coal wall with a peak lue of 22 MPa.

When the depth is 450 m, the zone locates at top coal section, about 8 m height compared to face floor and it has a peak stress value of 26 MPa. The numerical results indicate that when the mining depth increases, top coal fails significantly and the bearing capacity of top coal and immediate roof decreases. The concentrated stress zone moves closer to coal wall that in turns facilitates the failure of top coal. This however causes difficulty in face pressure control and support.

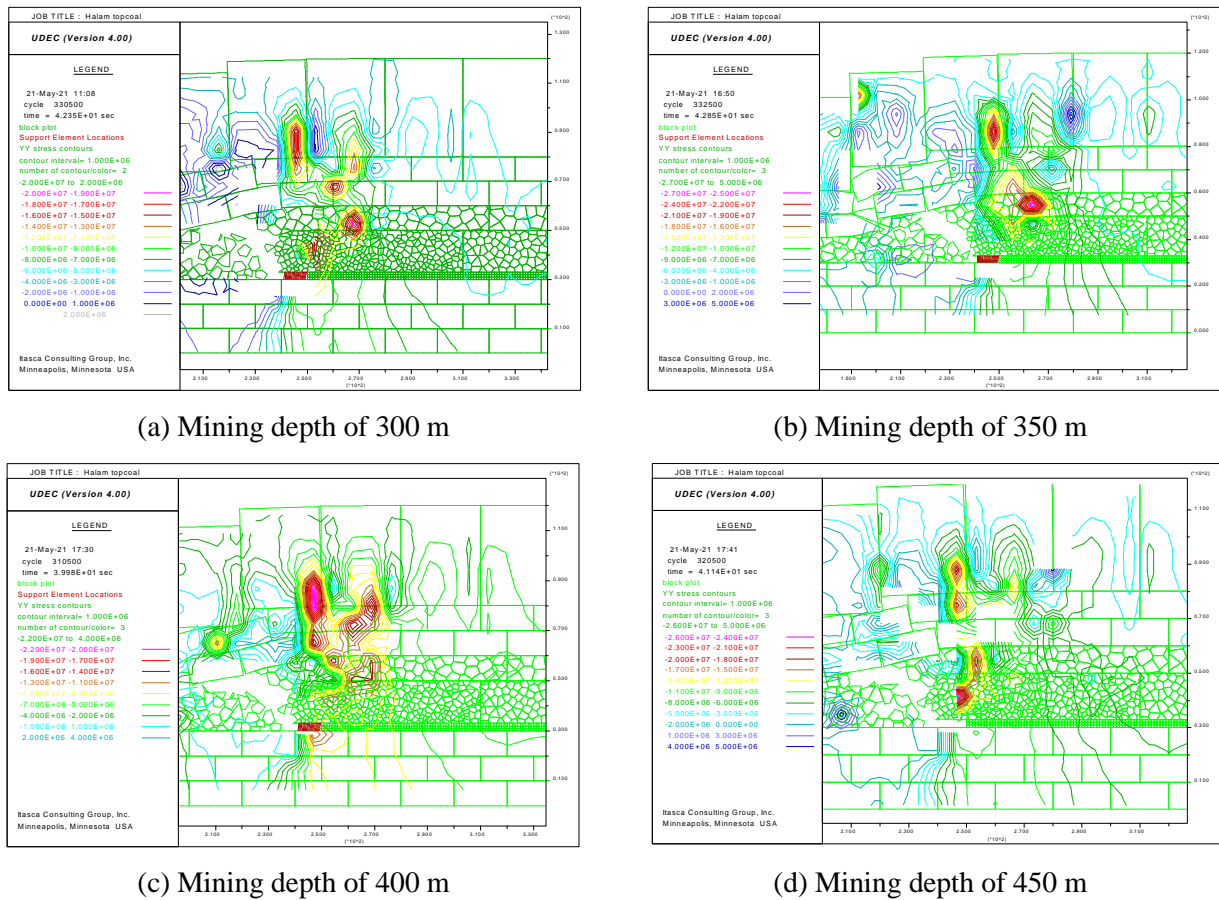
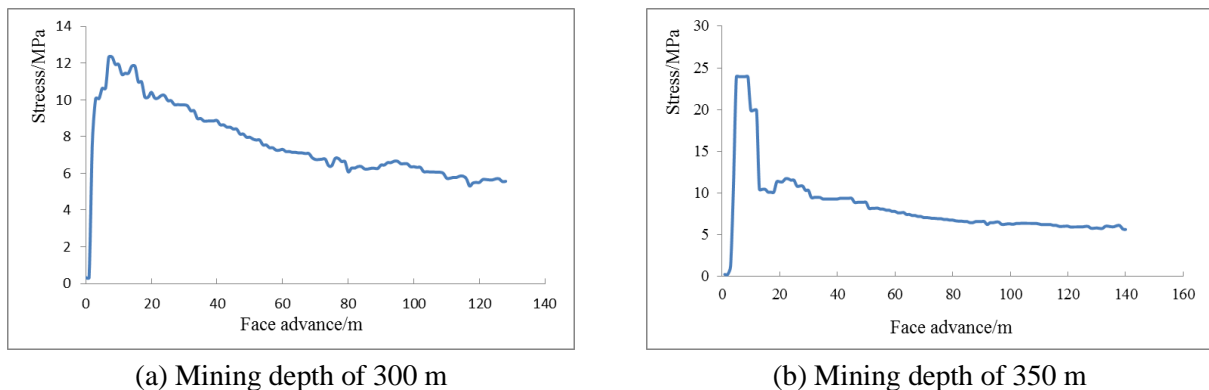
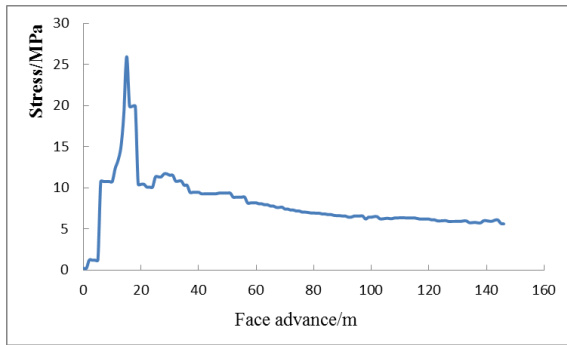


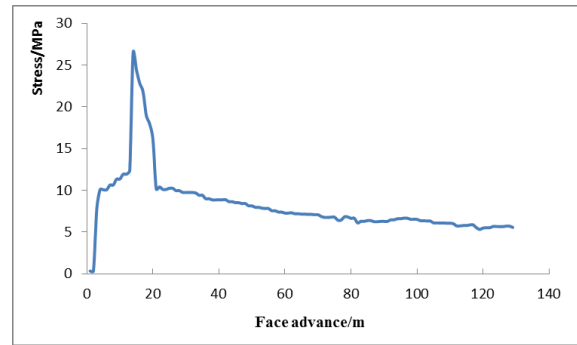
Fig. 2. Stress distribution in vertical direction in variation of mining depth.

To interpret the stress distribution ahead of coal wall, a monitoring line was placed in top coal section and ahead of coal wall. The stress value measured along the monitoring line is shown in Fig. 3:





(c) Mining depth of 400 m



(d) Mining depth of 450 m

Fig. 3. Stress distribution along monitoring line in variation of mining depth.

Following the face movement, as the mining depth increases from 300 m to 350 m, 400 and 450 m, the location and magnitude of peak front abutment stress are 7.2 m, 5.2 m, 11.9 m, 12.1 m and 12.3 MPa, 23.95 MPa, 25.9 MPA, 26.5 MPa, respectively. The location and magnitude of peak front abutment stress are illustrated in Figs. 4-5.

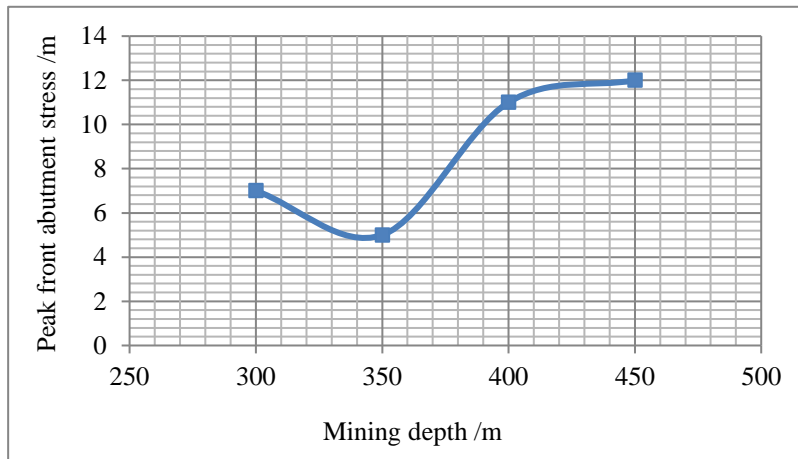


Fig. 4. Location of peak front abutment stress.

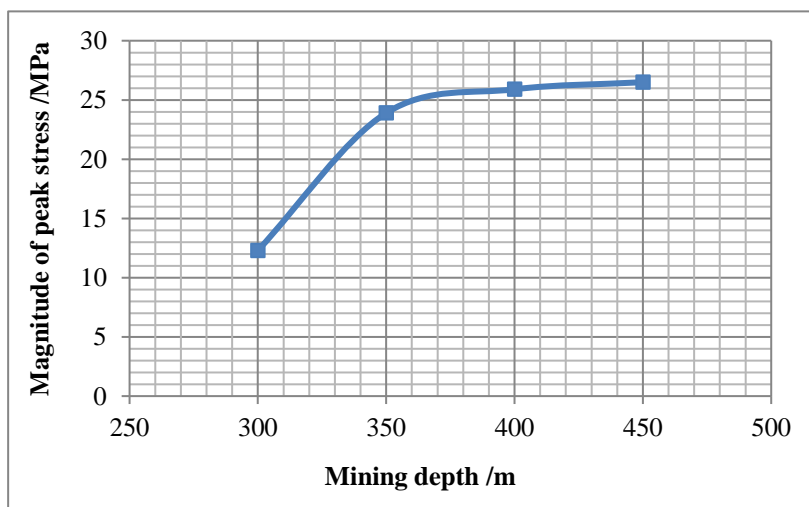


Fig. 5. Magnitude of peak front abutment stress.

Figs. 4 and 5 show that when mining depth increases, the location of peak abutment stress fluctuates. From 300 m to 350 m depth, it decreases from 7.2 m to 5.2 m. However, when the depth increases from

350 m to 450 m, the peak stress' location follows an increasing trend, from 5.2 m to 11.9 m. At the same time, the magnitude of peak front abutment stress follows a clear increasing trend. From the depth of 300 m to 350 m, the stress' magnitude increases significantly, from 12.3 MPa to 23.9 MPa. From 350 m to 450 m, the magnitude increases slightly. The modelling results clear reveal that when the mining depth increases, the peak front abutment stress increases. The decreasing rate of front abutment stress behind the peak point also increases. This study suggests a boundary for separating the shallow and deep mining portion of -350 m for Quang Ninh coal field.

3.4 Distribution of plastic deformation zone around longwall in variation of mining depth

Fig. 6 displays the degree of intact coal failure around longwall face. The top coal and immediate roof fail due to the rotational and shear effect from ruptured main roof and roof pressure from intact main roof. An increase in mining depth affects the stability of coal wall and extent of coal deformation ahead coal wall.

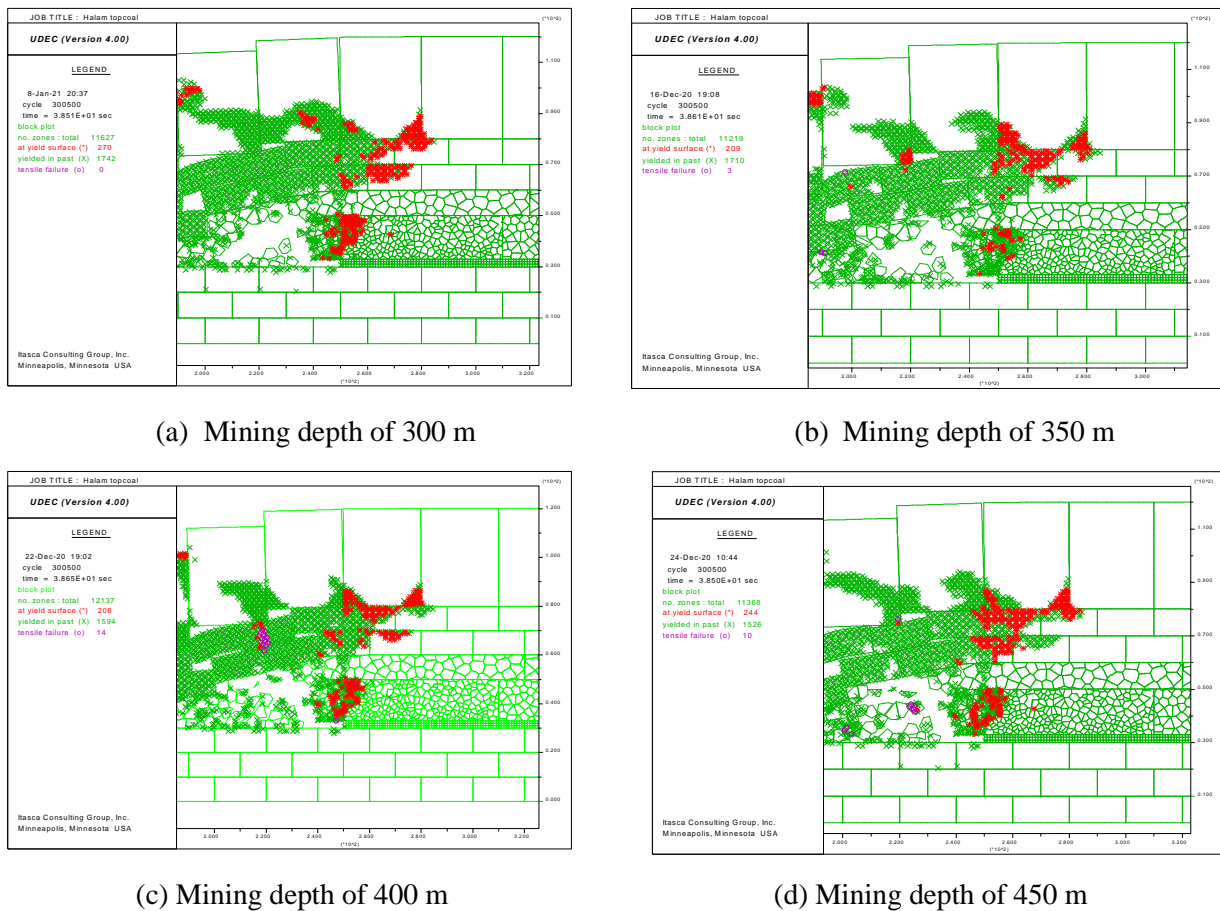


Fig. 6. Distribution law of deformation zone ahead of coal wall.

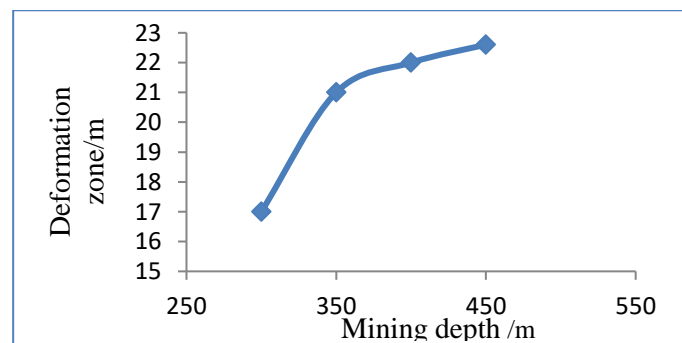


Fig. 7. Distribution of plastic deformation zone ahead of coal wall.

Fig. 7 displays the extent of plastic deformation zone in variation of mining depth. When the depth is 300 m, 350 m, 400 m and 450 m, the extent is 17 m, 21 m, 22 m and 22.6 m, respectively. The figure shows that when the depth ranges within 300-350 m, the deformation zone extent increases significantly by a value of 4.0 m, with an increasing rate of 0.08 m/m. When the depth increases from 350 m to 400 m, the zone extent increases slightly by a value of 0.5 m with a rate of 0.01 m/m. The extent increases greater in the depth range of 400-450 m with a value of 1.6 m and a rate of 0.032 m/m. Therefore, an increase in mining depth increases the extent of deformation zone as well, but with different rate.

4. Distribution of load on face support

Seam 11 Ha Lam coal mine uses support ZF4400/16/28 along panel width and support ZFG4800/18/28 near two roadways. The profiles of immediate support load along panel strike and along panel width in the period of 11/3/2019–28/3/2019 are analysed. The data was collected from the real face.

4.1 Distribution of support load along panel strike

Figs. 8-10 displays the profile of load distribution on support number 85, 15 and 55 along panel strike. The origin (0,0) is 50 m far away from the face entry, meaning that the main roof only collapses due to the mining cycle.

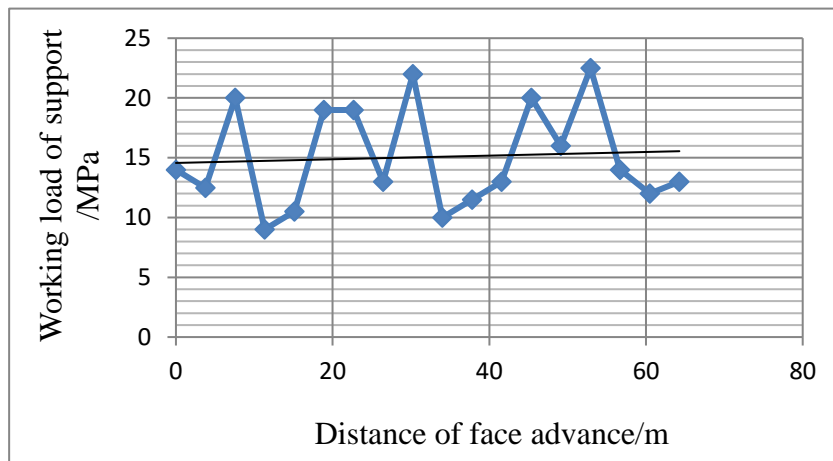


Fig. 8. Load distribution on support No. 85.

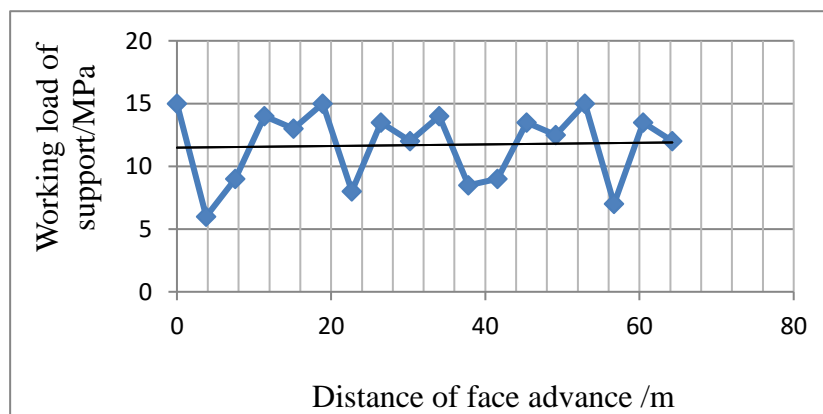


Fig. 9. Load distribution on support No. 15.

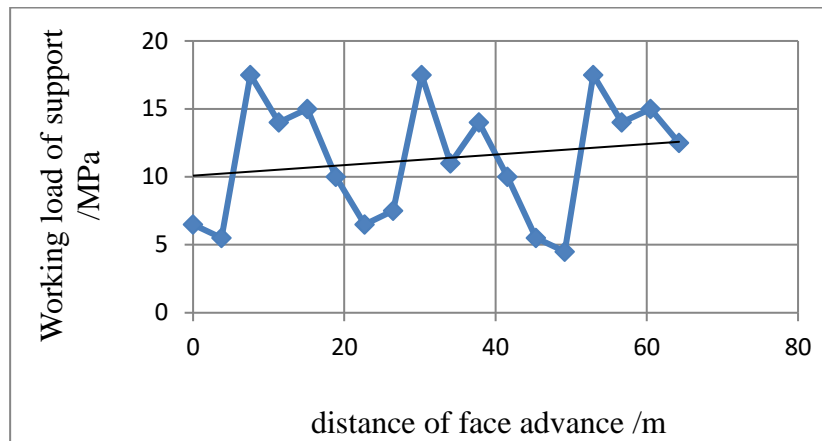


Fig. 10. Load distribution on support No. 55.

The three figures show that for the support No. 85 which is near tailgate, the maximum support load reaches 22.5 MPa with an average of 15.9 MPa. For the support No. 15 near maingate, the maximum support load reaches 15.5 MPa with an average of 12.3 MPa. For the support No. 55 at mid-panel width, the maximum load reaches 17.5 MPa with an average of 12.1 MPa. Therefore, the support load along panel strike follows a cyclically fluctuation. The distance between maximum points also varies in the range of 15-25 m. The result is consistent with the theoretical calculation of main roof fall in the design, which is 20 m [17].

In general, the roof structure in longwall top coal caving face after failure are also in beam form. The load on face support is smaller when the immediate roof ruptures before the rupture of main roof. This load is greater when immediate roof and main roof rupture at the same time. Thus, it is seen that the load support fluctuates cyclically with different values. In comparison with support capacity, the on-site support are totally capable of supporting the roof.

4.2 Distribution of support load along panel width

The distribution of roof load on face support along panel width is shown in Fig. 11. This load distributes unevenly along the dip direction. At about 25 m near maingate and tailgate, the support load is greater than that in the interval between the two locations. Furthermore, the load on front leg pressure is commonly greater than that in rear leg, as shown in Fig. 11.

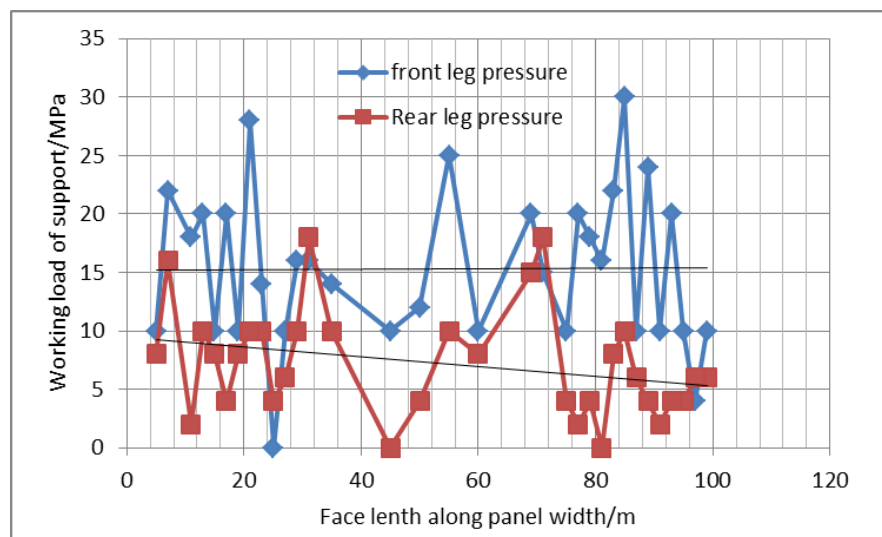


Fig. 11. Distribution of load on support along panel width.

The load distributions of front and rear legs show the difference. The maximum working load of front leg reaches 30 MPa with an average of 16.8 MPa. The maximum working load of rear leg reaches 18 MPa with an average of 8.56 MPa. However, at both face ends, the load is sometimes zero due to the breakage of safety valve as reported by on-site engineers. This also demonstrates the great magnitude of face roof pressure near two roadways.

5. Conclusions

1) When mining depth increases, the location of concentrated stress zone moves closer to coal wall, mainly distributed in immediate roof and top coal. The bearing capacity of top coal and immediate roof significantly decreases. An increase in mining depth therefore facilitates the failure of top coal while it causes difficulty for support and ground control.

2) The magnitude of peak front abutment stress varies clearly in variation of mining depth. When the depth increases from 300 m to 350 m, the stress increases rapidly with high rate, from 12.3 MPa to 23.9 MPa. The stress afterwards increases slightly when the depth increases to -450 m. Accordingly, this study proposes a boundary for separating shallow and deep mining portion of -350 m for Quang Ninh coal field.

3) When mining depth falls in the range of 300-350 m, the plastic deformation zone extends rapidly with a rate of 0.08 m/m. When the depth falls in the range of 350-400 m, the zone extends slightly with a rate of 0.01 m/m. The deformation zone extends greatly again with a rate of 0.032 m/m when the depth increases from 400 m to 450 m. It is concluded that an increase in mining depth causes an increase in extent of deformation zone as well but with different rate.

4) The working load on face support along panel strike changes periodically with an interval of 15-25 m. The load is also not consistent along panel width. It is commonly greater near T-junctions and smaller in the interval between the two junctions. The study confirms that the on-site face support totally meets the requirement of roof control.

6. Acknowledgements

The paper was presented during the 6th VIET - POL International Conference on Scientific-Research Cooperation between Vietnam and Poland, 10-14.11.2021, HUMG, Hanoi, Vietnam.

7. References

1. Le, N.H., Pham, T.H., Nguyen, C.K., Dao, T.C., 2011. Study on the influences during exploring deeper coal mines. 22nd National Conference on Mining Science and Technology. 323-327. (Vietnamese).
2. ChengJia, G., 2004. Characteristics of surrounding rock and support design procedures in working faces of strong roof and high ground pressure in deep mines. Master of philosophy, Shandong University of Science and Technology.
3. Liu, C.Y., Qu, Q.D., Wan, Z., 2002. Numerical simulation on rock stability in fully mechanized coal face under the condition of deep mining and large inclination. Chinese journal of rock mechanics and engineering, June 2002.
4. Bai, Q-S., Tu, S-H., Wang, F-T., Zhang, X-G., Yuan, Y., 2014. Observation and Numerical Analysis of the Scope of Fractured Zones Around Gateroads Under Longwall Influence. Rock Mechanics and Rock Engineering, 47, 1939-1950.
5. Du, J.P., Zhang, X.C., Jia, W., Yong, S., Chun, J., 2016. Characteristics of Strata Behaviors and roof control for longwall faces in deep mining. Journal of China university of mining & technology, 29(1).

6. Bai, Q-S., Tu, S-H., Chen, M., Zhang, C., 2016. Numerical modeling of coal wall spall in a longwall face. *International Journal of Rock Mechanics and Mining Sciences*, 88, 242-253.
7. Qi Q., Pan, Y., Shu, L., Li, H., Jiang, D.Y., Zhao, S., Zou, Y., Pan, J., Wang, K., Li, H., 2018. Theory and technical framework of prevention and control with different sources in multi-scales for coal-rock dynamic disasters in deep mining of coal mines. *Journal of China Coal Society*, 43(07). DOI: 10.13225/j.cnki.jccs.2018.0660-en.
8. Li, J.Z., Xie, Q.X., Wang, L., 2018. Failure Characteristics Induced by Unloading Disturbance and Corresponding Mechanical Mechanism of the Coal Seam Floor in Deep Mining, Preprints, engineering 2018, doi: 10.20944/preprints201804.0207.v1.
9. FengDa, Z., BaoHong, S., WenYan, G., 2020. Stress distribution and failure characteristics of deep inclined seam and overhead mining along strike longwall floor. *International Journal of Mining and Mineral Engineering*, Jan 2020, 11(4):306-322. <https://doi.org/10.1504/IJMME.2020.111933>.
10. Chen, X.H., Li, W.Q., Yan, X., 2011. Analysis on rock burst danger when fully-mechanized caving coal face passed fault with deep mining. *Safety Science*, 50(4): 645-648. <https://doi.org/10.1016/j.ssci.2011.08.063>.
11. Chao ru, L., 2011. Distribution laws of in-situ stress in deep underground coal mines, *Procedia Engineering* 26, 909 - 917, doi:10.1016/j.proeng.2011.11.2255.
12. Pathegama, G.R., Jian, Z., Minghe, J., Radhika, V.S.D., Tharaka, D.R., Adheesha, K.M., Bandara, S., 2017. Opportunities and Challenges in Deep Mining: A Brief Review , *Engineering*, 3, 546–551 , <http://dx.doi.org/10.1016/J.ENG.2017.04.024> .
13. Le, Q.P., Zubov, V.P., Dao, V.C., Vu, T.T.D., 2018. The rules apparition mine pressure and transfigure stone roof in the longwall mechanized furnace TT7.9–area Nga Hai, Quang Hanh coal company, Conference on earth sciences and natural resources for sustainable development (ERSD 2018). 224-229 (in Vietnamese).
14. Nguyen, Q.P., Pham, V.C., 2013. Investigation on development of geomechanical models for collaps and subsidence pridiction in underground coal mining in region Quang Ninh, *Journal of Mining and Earth Sciences*, 43, 64-71 (in Vietnamese).
15. Le, N.H., Nguyen, V.T., Bui, M.T., 2011. Determination of the safe mining depth when exploiting the Red River delta coal basin with underground coal mining and coal gasification methods. 22nd National Conference on Mining Science and Technology. 327-331. (Vietnamese).
16. Itasca Consulting Group, Universal Distinct Element Code (UDEC, FLAC, PFC) Verification Problems and Example Applications, Minneapolis, Minnesota, USA, 2000.
17. Le, T.D., Bui, M.T., Pham, D.H., Vu, T.T. & Dao, V.C., 2018. A modelling technique for top coal fall ahead of face support in mechanised longwall using Discrete Element Method. *Journal of Mining and Earth Sciences*, 59, 56-65.

Geometrical Tests of Powered Roof Support Positioning in a Longwall Complex

SZURGACZ Dawid^{1,*}, ZHIRONKIN Sergey², TRZOP Konrad³,
VÖTH Stefan⁴, SOBIK Leszek⁵, CEHLÁR Michal⁶

¹ Polska Grupa Górnicza S.A., Poland

² T.F. Gorbachev Kuzbass State Technical University, 28 Vesennya street, Kemerovo, Russia

³ 5KWK Ruda Ruch Bielszowice, 160 Halembaska, Ruda Śląska, Poland

⁴ Technische Hochschule Georg Agricola (THGA), 15 Westhoffstraße, Bochum, Germany

⁵ 7KWK ROW Ruch Chwałowice, 4 Przewozowa, Rybnik, Poland

⁶ Technical University of Košice, 9 Letná, Košice, Czechia

Corresponding author: dawidszurgacz@vp.pl

Abstract. A powered roof support protects people and equipment in the longwall from potential danger posed by the surrounding rock mass. The study to determine the position of the powered roof support was conducted in an active longwall. The research team made measurements of the geometric height of the powered roof support structure located in the longwall complex. The main objective of this study was to determine the position of the powered roof support in actual underground conditions. The analysis of the results provided data on whether the assumed height of the longwall was maintained during operation of the complex.

Keywords: Geometrical tests, Powered roof support positioning, Longwall complex

1. Preamble

The longwall systems used in hard coal mining are implemented with the participation of a longwall system which includes three main elements: a mining machine, a longwall conveyor and a powered roof support [1-10]. Powered roof support is an indispensable element of the equipment of the longwall complex. It is used to protect the space between the roof collapse line and the face of the solid coal [11-25].

In this space, there are devices necessary for operation and the movement of employees also takes place there.

The use of powered support is considered individually for a given longwall excavation. Determining the prevailing geological and mining conditions of the exploited deposit is necessary for selecting the support. Additionally, it is necessary to take into account the possibility of cooperation between the powered roof support and the machines and devices included in the elements of the longwall complex. This forces the design of sections with a specific technical configuration and a comprehensive determination of the geometric conditions of powered support operation [7, 9].

The aim of the article is to analyze the geometrical changes occurring in the transverse and longitudinal inclination of the powered roof support operation in underground conditions.

2. Characteristics of the research excavation

The tests were carried out in longwall IV in seam 405 which is located in the PI part of the mine. In relation to the ground surface, the wall begins its course to the west. It is exploited to the north and will end its course to the south-west. The launch of the longwall took place at the beginning of December 2020, while its completion is scheduled for the end of May 2021. The technical parameters of the IV-PI longwall in deck 405 are as follows:

- longwall length ~ 245-250 m,
- wall advance ~ 288-402 m,
- height longwall 3.4-4.4 m,
- exploitation depth 650-710 m.

As a result of the exploitation of longwall IV, the impacts ranging from I to IV mining area categories will appear on the ground surface. The maximum depressions of the area, reaching the value of 2.0 m, will occur in the undeveloped area to the west. There are the following natural hazards in the wall [26-29]:

Tab. 1. Characteristics of natural hazards in the tested longwall excavation.

Longwall	The type of hazards						
	methane [category]	rock bursts [degree]	coal dust explosion [grade]	water [step]	climatic	rock or gas outbursts [category]	fire
IV	I	-	B	I	-	-	IV

3. The sum of the slopes of powered roof support

Measurement tests were carried out in longwall IV to determine the longitudinal and transverse slope of the elements of the powered roof support of the Glinika 22/45 POz type. The measurement of the values made it possible to determine the sum of the longitudinal and transverse slopes of the powered roof support. The sum of the transverse and longitudinal slopes was determined by the formula:

$$\sum \lambda = (Sr\lambda_{\alpha} - St\lambda_{\alpha}) + (Sp\lambda_{\alpha} - O\lambda_{\alpha}) + (L\lambda_{\alpha} - S\lambda_{\alpha}) \cdot \frac{c}{2} \tag{1}$$

where:

$\sum \lambda$ - slope sum, [°]

$Sr\lambda_{\alpha}$ - slope roof timber,

$St\lambda_{\alpha}$ - slope hydraulic prop,

$Sp\lambda_{\alpha}$ - slope hydraulic actuator,

$O\lambda_{\alpha}$ - slope fender,

$L\lambda_{\alpha}$ - slope of the lemniscate,

$S\lambda_{\alpha}$ - slope sill,

c - constant of the calculation factor.

4. Determination of the slopes of the powered roof support in the mining excavation

The slopes were determined using a specially prepared measuring device, the collected measurements made it possible to determine the sum of the transverse and longitudinal slopes, which are illustrated in Figs. 1-2. The next Fig. 3 shows the changes in the value of the slopes in comparison with the height of the span of the support section.

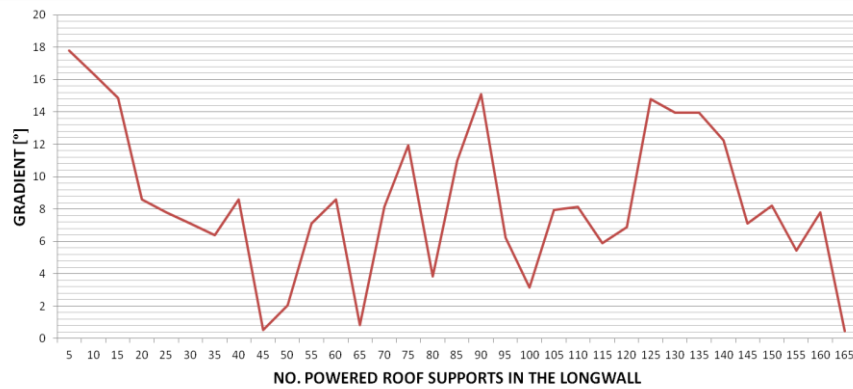


Fig. 1. Longitudinal Slope Graph - Manual Measurement.

The value of the sum of the longitudinal slope is determined by measuring the elements of the powered roof support, i.e. roof timber, hydraulic prop, hydraulic actuator, fender, lemniscate, sill. The measurements of the slopes of these elements are determined perpendicularly to the direction of the face of the longwall excavation, whereas the sum of the transverse slope is determined parallelly to the face of the wall. The method is shown in Figs. 4-5.

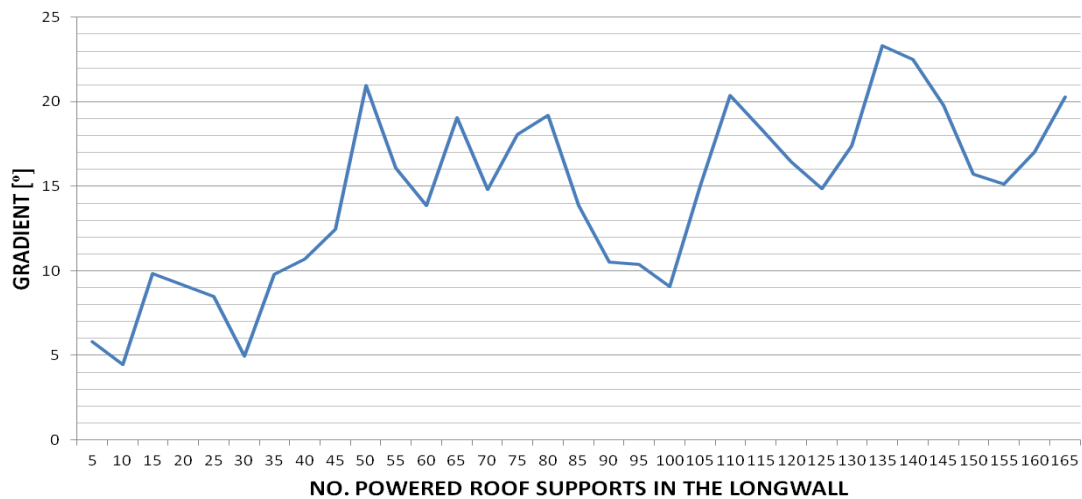


Fig. 2. Cross slope Graph - Manual measurement.

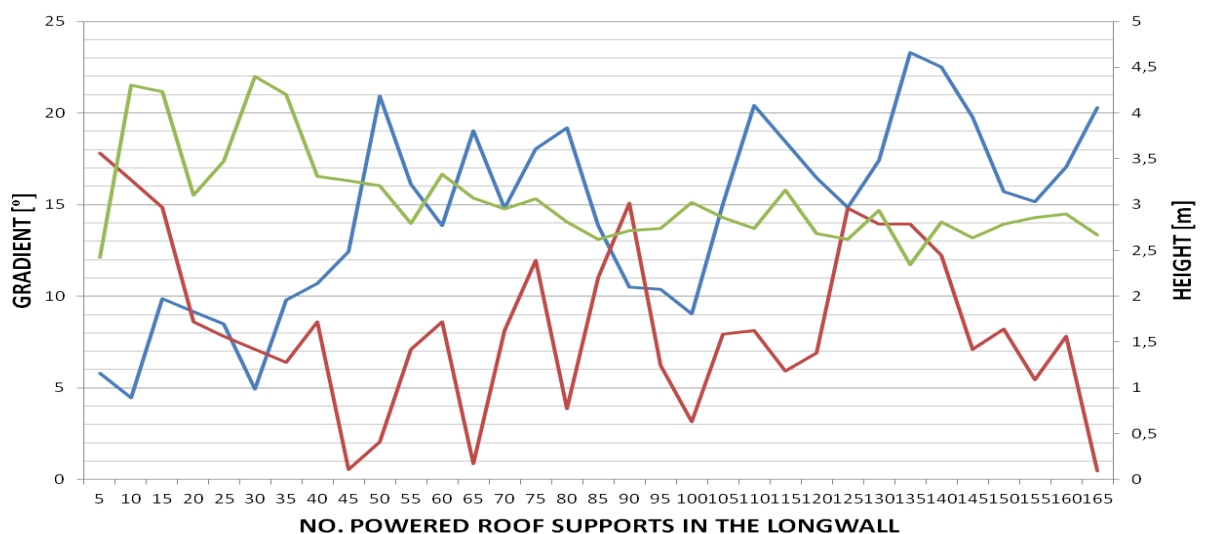


Fig. 3. Graph of the sum of the slopes and the height of the span of the powered roof support - manual measurement.

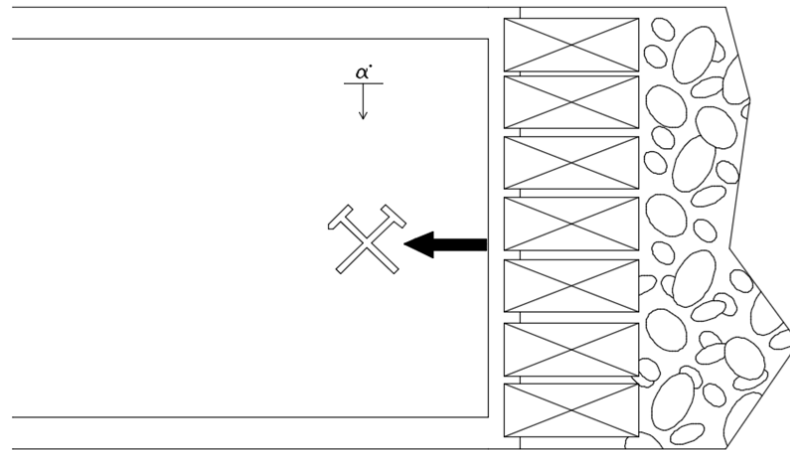


Fig. 4. Longitudinal slope. Own study.

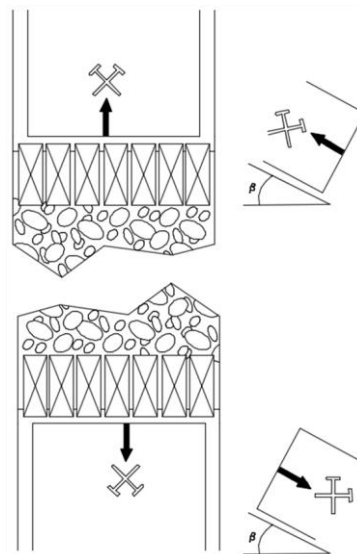


Fig. 5. Transverse slope. Own study.

The sum of the longitudinal slope changes by decreasing its value from 1 to 45 sections, then increases towards section 121. From section 121 to section 165 it decreases assuming a degree of slope close to section 45 of approximately 1° . The cross slope, similar to the longitudinal slope of 1 to 45 sections, changes its value, but in the opposite direction. The transverse slope in this particular working longwall adopts an upward trend. The value of the varying transverse slope has the greatest increase in the area of sections 130-135. The slope at this point is approximately 24° . The longitudinal slope changes its value from 18° to 1° , and the transverse slope increases from about 5° up to 24° . In the vicinity of section 85, the values of the sum of the slopes determine the common point with the superimposed values of the building height of the powered roof support. The slopes shown in the above charts in relation to the designated height of the expansion of the powered roof support in the longwall jointly determine the geometry of the section development in the longwall excavation and the changing topography resulting from from mining and geological conditions.

5. Conclusion

With the help of the measurements of the slope of the mining excavation, we can determine: changes in the height of the wall, the degree of external impacts and the longwall complex development plan. The diagram shows that the wall lowers its height in relation to the longitudinal slope towards the over-panel walkway. The exploitation carried out under the slope conditions, which is illustrated by the graphs of the sum of the transverse and longitudinal slopes in longwall IV, can be classified as difficult or very

difficult. Such conditions force the user to use additional equipment in the powered roof support in order to increase the work safety factor in the longwall excavation. The sections are equipped with, among others a pressure monitoring system and covers protecting against rock fall from the side of the side wall. Carrying out the extraction in a working with a variable slope significantly influences the efficiency of the excavation loading process and increases the power consumption of the drum and feed motor. The increasing slope in the longwall excavation generates changes in the manner of machine operation, operation and crew management. Determining the sum of the slopes of the powered support, which is one of the elements of the longwall complex, will contribute to the improvement of safety and efficiency of exploitation. Obtaining a measurable effect is possible by means of continuous measurement of the changes in the inclination of machines and devices, using systems supporting the monitoring of the slopes of the longwall complex.

6. Acknowledgments

The paper was presented during the 6th VIET - POL International Conference on Scientific-Research Cooperation between Vietnam and Poland, 10-14.11.2021, HUMG, Hanoi, Vietnam.

7. References

1. Biały, W., Czerwińska-Lubszczyk, A., Czerwiński, S., 2019. System monitorowania geometrii sekcji obudowy zmechanizowanej. Systemy wspomaganie w inżynierii produkcji. Górnictwo – perspektywy i zagrożenia.
2. Liu, B., Sang, H., Wang, Z., Kang, Y., 2020. Experimental Study on the Mechanical Properties of Rock Fracture after Grouting Reinforcement. *Energies* 13, 4814.
3. Ziętek, B., Banasiewicz, A., Zimroz, R., Szrek, J., Gola, S., 2020. A Portable Environmental Data-Monitoring System for Air Hazard Evaluation in Deep Underground Mines. *Energies* 13, 6331.
4. Szurgacz, D., S., Zhironkin, M., Cehlár, S., Vöth, S., Spearing, Liqiang, M., 2020. A Step-by-Step Procedure for Tests and Assessment of the Automatic Operation of a Powered Roof Support. *Energies* 14, 697.
5. Szurgacz, D., M., Tutak, J., Brodny, L., Sobik, Zhironkina, O., 2020. The Method of Combating Coal Spontaneous Combustion Hazard in Goafs - A Case Study. *Energies* 13, 17, 4538.
6. Szurgacz, D., Brodny, J., 2020. Adapting the Powered Roof Support to Diverse Mining and Geological Conditions. *Energies* 13, 405.
7. Szurgacz, D., Brodny, J., 2019. Analysis of the Influence of Dynamic Load on the Work Parameters of a Powered Roof Support's Hydraulic Leg. *Sustainability* 11, 2570.
8. Szurgacz, D., Brodny, J., 2019. Tests of Geometry of the Powered Roof Support Section, *Energies* 12, 3945.
9. Szurgacz, D., 2017. Bezpieczeństwo zmechanizowanej obudowy ścianowej w warunkach zagrożenia wstrząsami górotworu. *Wiadomości Górnicze*.
10. Gil, J., Kołodziej, M., Szurgacz, D., Stoiński, K., 2018. Introduction of standardization of powered roof supports to increase production efficiency of Polska Grupa Górnicza S.A. Mining – informatics, automation and electric al engineering.
11. Trzop, K., Szurgacz, D., Zhironkin, S., Kasprusz, A., 2021. Analysis of the impact of mining and geological conditions in longwalls on the introduction of pressure monitoring for powered roof supports. *IOP Conference Series Volume* 1134.
12. Wodecki, J., Góralczyk, M., Krot, P., Ziętek, B., Szrek, J., Worsa-Kozak, M., Zimroz, R., Śliwiński, P., Czajkowski, A., 2020. Process Monitoring in Heavy Duty Drilling Rigs-Data Acquisition System and Cycle Identification Algorithms. *Energies* 13, 6748.

13. Trzop, K., D.Palka, D.Szurgacz, Sobik, L., 2021. Preventive measures to minimize natural hazards in the Polish underground mining industry. IOP Conference Series.
14. Stańczyk, K., 2020. Modelling of Hard Coal Beneficiation Process Utilising Negative Pressure Pneumatic Separato.Energies 13,5174.
15. Bajda, M., Hardygóra, M., 2020. Analysis of Reasons for Reduced Strength of Multiply Conveyor Belt Splices. Energies 14,1512.
16. Beer, M., R.Rybár, M.Cehlár, S.Zhironkin, Sivák, P., 2020. Design and Numerical Study of the Novel Manifold Header for the Evacuated Tube Solar Collector.Energies 13,2450.
17. Beer, M., M.Taušová, R.Rybár, Kaľavský, M., 2020. A Novel Economical Method of Determining the Geometric Characteristic of the Metal Foam Based on Image Analysis.Energies 13, 3378.
18. Mbedzi, M.D., M.van der Poll, J.A.van der Poll, 2020. Enhancing a Decision-Making Framework to Address Environmental Impacts of the South African Coalmining Industry. Energies 13, 4897.
19. Góralczyk, M., P.Krot, R.Zimroz, Ogonowski, S., 2020. Increasing Energy Efficiency and Productivity of the Comminution Process in Tumbling Mills by Indirect Measurements of Internal Dynamics-An Overview. Energies 13, 6735.
20. Sofranko, M., S.Khoury, O.Vegsoova, P.Kacmary, T.Mudarri, M.Koncek, M.Tyulenev, Simkova, Z., 2020. Possibilities of Uranium Deposit Kuriskova Mining and Its Influence on the Energy Potential of Slovakia from Own Resources.Energies 13, 4209.
21. Tutak, M., J.Brodny, D.Szurgacz, L.Sobik, Zhironkin, S., 2020. The Impact of the Ventilation System on the Methane Release Hazard and Spontaneous Combustion of Coal in the Area of Exploitation-A Case Study. Energies 13, 4891.
22. Boroń, P., J.M.Dulińska, Jasińska, D., 2020. Impact of High Energy Mining-Induced Seismic Shocks from Different Mining Activity Regions on a Multiple-Support Road Viaduct.E nergies 13, 4045.
23. Bortnowski, P., L.Gładysiewicz, R.Król, Ozdoba, M., 2020. Energy Efficiency Analysis of Copper Ore Ball Mill Drive Systems. Energies 14, 1786.
24. Borkowski, P.J., 2020. Comminution of Copper Ores with the Use of a High-Pressure Water Jet. Energies 13, 6274.
25. Sivák, P., P.Tauš, R.Rybár, M.Beer, Z.Šimková, F.Baník, S.Zhironkin, Čitbajová, J., 2020. Analysis of the Combined Ice Storage (PCM) Heating System Installation with Special Kind of Solar Absorber in an Older House. Energies 13, 3878.
26. Zhironkin, S., A.Selyukov, Gasanov, M., 2020. Parameters of Transition from Deepening Longitudinal to Continuous Lateral Surface Mining Methods to Decrease Environmental Damage in Coal Clusters Energies 13, 3305.
27. Kawalec, W., N.Suchorab, M.Konieczna-Fuławka, Król, R., 2020. Specific Energy Consumption of a Belt Conveyor System in a Continuous Surface Mine.Energies 13,5214.
28. Chen, Y., H.Wu, H.Pu, K.Zhang, F.Ju, Y.Wu, Liu, J., 2020. Investigations of Damage Characteristics in Rock Material Subjected to the Joint Effect of Cyclic Loading and Impact. Energies 13, 2154.
29. Li, Y., T.Jin, L.Liu, Yuan, K., 2020. Dynamic Performance Simulation and Stable Current Collection Analysis of a Pantograph Catenary System for Trolley Wire Overhead Electrically Actuated LHD. Energies 13, 1015.

General Geometric Model of GNSS Position Time Series for Crustal Deformation Studies – A Case Study of CORS Stations in Vietnam

TRAN Dinh Trong¹, NGUYEN Quoc Long^{2,*}, NGUYEN Dinh Huy¹

¹Hanoi University of Civil Engineering, Hanoi, Vietnam

²Hanoi University of Mining and Geology, 18 Vien street, Hanoi, Vietnam

Corresponding author: nguyenuoclong@hmg.edu.vn

Abstract. In processing of position time series of crustal deformation monitoring stations by continuous GNSS station, it is very important to determine the motion model to accurately determine the displacement velocity and other movements in the time series. This paper proposes (1) the general geometric model for analyzing GNSS position time series, including common phenomena such as linear trend, seasonal term, jumps, and post-seismic deformation; and (2) the approach for directly estimating time decay of postseismic deformations from GNSS position time series, which normally is determined based on seismic models or the physical process seismicity, etc. This model and approach are tested by synthetic position time series, of which the calculation results show that the estimated parameters are equal to the given parameters. In addition they were also used to process the real data which is GNSS position time series of 4 CORS stations in Vietnam, then the estimated velocity of these stations: DANA (n, e, u = -9.5, 31.5, 1.5 mm/year), HCMC (n, e, u = -9.5, 26.2, 1.9 mm/year), NADI (n, e, u = -10.6, 31.5, -13.4 mm/year), and NAVI (n, e, u = -13.9, 32.8, -1.1 mm/year) is similar to previous studies.

Keywords: Geometric model, GNSS position time series, Crustal deformation, CORS stations, Vietnam

1. Introduction

Monitoring the Earth's crust deformation, land deformation using continuous GNSS (Global Navigation Satellite System) stations is now very popular in the world, greatly contribute to the prediction and early warning of seismic activities (e.g., earthquakes, landslides) in the US [1, 2], Japan [3, 4], Taiwan [5], etc.

Continuous GNSS observation allows the calculation of the position time series of GNSS stations. The most basic application of GNSS position time series is in geotectonic studies, such as determining the rates of crustal motion, the seismic displacement, the co-seismic deformation, and the postseismic deformation [6]. Additionally, GNSS position time series are also useful in calculating amplitudes and phases of periodic motions caused by seasonal mass loads; for example, atmospheric, hydrological, or oceanic [7], etc.

Then, the study of GNSS position time series processing in order to determine the most accurate information in the time series such as displacement velocity, seasonal motions, postseismic deformation of the Earth's surface at the continuous GNSS station is very important for the applications mentioned above.

In the processing of the position time series of continuous GNSS station by geodetic approach, the synthetic motion model is often used as a geometric model according to the 3-D coordinate components (XYZ) or (n,e,u) [8]. These geometric models need the parameters describing the basic and the most common motions of the coordinate time series, which are the linear trend, seasonal terms, possibly jumps/offset, and post-seismic deformations. The simpler the model of the position time series, the faster the computation, but the accuracy of the velocity estimated is noticeably reduced, especially with complex position time series.

Using a geometric model with only one linear trend in position time series processing is also common such as [9] in determining the crustal motion in Vietnam and in the surrounding area by continuous GPS, [10] in determining the horizontal displacement of the Earth's crust in the Northwest region of Vietnam by cycle measurement GPS, etc. However, this model does not fully describe the nonlinear motions and discontinuities in the time series used for these studies leading to the estimated velocity field not being accurate.

The geometric model, including linear trend, seasonal motion, and offsets, has been used by [11] to study the effects of the GPS position time series caused by higher-order ionospheric corrections. Similarly,

[12] has also used this model to research the accuracy of the velocity of continuous GPS station, and [13] used it in detecting the jumps automatically in the GPS time series, etc. This model is only suitable for these position time series used in those studies; however, in the case of analyzing complex time series, a synthetic model is needed.

This paper proposes an approach to process GNSS position time series using a synthetic geometric model including linear trend, the seasonal term (annual and semiannual), jumps, and post-seismic deformation, which is suitable for most GNSS position time series cases. This model has also been used in programming the GNSS position time series analyzing software [14, 15], in the study of seismic deformation by GPS [16]. In this way, the time decay of postseismic deformation is estimated directly on the GNSS position time series, from which it is possible to determine the best fit line of time series. It means that the velocity, parameters of seasonal term, the amplitude of jumps, postseismic movements are estimated the most accurately. Moreover, the tool was written by Python 3 to analyze these data and further results. This tool has been tested with the synthetic model position time series and is used to analyze the real position time series of 4 CORS (Continuously Operating Reference Station) stations in Vietnam.

2. Proposed methodology for GNSS time series analyzing

2.1 General geometric model of GNSS time series

GNSS position time series represents the temporal evolution of a point in the 3-D space in the geocentric coordinate system (X, Y, Z) or local geodetic coordinate system (north - n, east - e, up - u). In other words, the GNSS position time series represents the time variation of the coordinates of the GNSS station.

Continuous GNSS stations are built on the land surface, so it is also affected by land surface changes such as displacement, periodic movement due to changes in groundwater levels, geo-tidal, etc., by geotectonic activities such as earthquakes. These influences are evident in the position time series of the GNSS station.

The simplest geometric model for a position time series in terms of coordinate components n, e, u is a linear trend [8]:

$$y(t_i) = a + bt_i + v_i \tag{1}$$

Where t_i is the time of the series positions in a decimal year, a is the initial position at time reference, b is the linear velocity, and v is the measurement errors.

The more common model is a linear trend with the addition of seasonal term (includes annual and semi-annual periodic motion) and jumps in the equation (1) [12, 17, 18], the seasonal term and jumps are described in the square brackets ([]):

$$y(t_i) = [a + bt_i] + [c \sin(2\pi t_i) + d \cos(2\pi t_i) + e \sin(4\pi t_i) + f \cos(4\pi t_i)] + [\sum_{j=1}^{n_g} g_j H(t_i - T_{g_j})] + v_i \tag{2}$$

Where c , d , and e , f are harmonic components of annual motion and semi-annual motion, respectively. g_j is the magnitude of jumps at time T_{g_j} (n_g is the number of jumps). Heaviside function $H(t_i - T_{g_j}) = 0$ if $t_i \leq T_{g_j}$ and $H(t_i - T_{g_j}) = 1$ if $t_i > T_{g_j}$.

A jump (step or offset) in the position time series is a sudden change in the mean coordinates [18], which can occur one or many times in a GNSS position time series at different times with various magnitudes. The cause of the jumps is probably GNSS receiver changes or receiver's firmware update [19], or geophysical phenomena such as land subsidence, earthquakes [17].

The seasonal term is sinusoidal motions with periods of 12 months (annual motion) and six months (semi-annual motion). This is due to cyclical changes over time, such as the effect of the continental water storage loading [20], or the effect of seasonal change of groundwater level [3], etc.

The general geometric model proposed for the GNSS position time series is equation (2) with the addition of the post-seismic motion [8, 14, 15]:

$$y(t_i) = [a + bt_i] + [c \sin(2\pi t_i) + d \cos(2\pi t_i) + e \sin(4\pi t_i) + f \cos(4\pi t_i)] + \left[\sum_{j=1}^{n_g} g_j H(t_i - T_{gj}) \right] + \left[\sum_{j=1}^{n_h} h_j H(t_i - T_{hj}) \right] + \left[\sum_{j=1}^{n_k} k_j e^{-\frac{t_i - T_{kj}}{\tau_j}} H(t_i - T_{kj}) \right] + v_i \tag{3}$$

Where h_j is rate change after an earthquake at the time T_{hj} (n_h is the number of rate changes). k_j is the magnitude of postseismic relaxation at time T_{kj} (n_k is the number of postseismic). τ is decay time (relaxation time) of postseismic deformation in the decimal year.

Thus, the parameters of the general geometric model of GNSS position time series are $a, b, c, d, e, f, g_j (j = 1 \div n_g), h_j (j = 1 \div n_h)$ and $k_j (j = 1 \div n_k)$.

In equation (3), the postseismic deformations that occur after the jumps of earthquakes are described in the square brackets ([]), which includes the rate changes (change in both direction and value) and post-seismic relaxation (described as an exponential decay function with magnitude and decay time).

The GNSS position time series record the seismic, co-seismic, inter-seismic, and postseismic relaxation [21]. Postseismic relaxation can last for years or more. In addition, after an earthquake, the rate of displacement of the GNSS station can change in both direction and value. The earthquake jumps and postseismic relaxations depend on the epicenter, earthquake's magnitude, and the distance between the epicenter to GNSS station [8].

2.2. Determining the parameters of GNSS position time series

Assuming that the times T_{gj} of jumps, T_{hj} of rate changes, and T_{kj} of postseismic relaxation are known. Model (3) is linear with respect to the parameters:

$$x = [a \ b \ c \ d \ e \ f \ g_1 \ \dots \ g_{n_g} \ h_1 \ \dots \ h_{n_h} \ k_1 \ \dots \ k_{n_k}]^T \tag{4}$$

So that

$$y = Ax + v \tag{5}$$

Where A is the design matrix,

$$A = \begin{bmatrix} 1 & \dots & 1 & \dots & 1 & \dots & 1 \\ t_1 & \dots & t_{n_g} & \dots & t_{n_h} & \dots & t_{n_k} \\ \sin(2\pi t_1) & \dots & \sin(2\pi t_{n_g}) & \dots & \sin(2\pi t_{n_h}) & \dots & \sin(2\pi t_{n_k}) \\ \cos(2\pi t_1) & \dots & \cos(2\pi t_{n_g}) & \dots & \cos(2\pi t_{n_h}) & \dots & \cos(2\pi t_{n_k}) \\ \sin(4\pi t_1) & \dots & \sin(4\pi t_{n_g}) & \dots & \sin(4\pi t_{n_h}) & \dots & \sin(4\pi t_{n_k}) \\ \cos(4\pi t_1) & \dots & \cos(4\pi t_{n_g}) & \dots & \cos(4\pi t_{n_h}) & \dots & \cos(4\pi t_{n_k}) \\ 0 & \dots & 1 & \dots & t_{n_h} & \dots & 1 \\ \dots & \dots & \dots & \dots & \dots & \dots & \dots \\ 0 & \dots & 0 & \dots & 1 & \dots & 1 \\ 0 & \dots & t_{n_g} & \dots & t_{n_h} & \dots & t_{n_k} \\ \dots & \dots & \dots & \dots & \dots & \dots & \dots \\ 0 & \dots & 0 & \dots & t_{n_h} & \dots & t_{n_k} \\ 0 & \dots & 1 & \dots & 1 & \dots & 1 \\ \dots & \dots & \dots & \dots & \dots & \dots & \dots \\ 0 & \dots & 0 & \dots & 1 & \dots & 1 \end{bmatrix}^T \tag{6}$$

v is a vector of residual position time series,

$$v = [v_1 \ v_2 \ \dots \ v_n]^T \tag{7}$$

and y is a vector of position time series,

$$y = [y(t_1) \quad y(t_2) \quad \dots \quad y(t_n)]^T \tag{8}$$

The positions in the series are independent observations, then the observation covariance matrix is defined by individual variances σ_i of the position i:

$$C = \text{diag}(\sigma_1^2 \quad \sigma_2^2 \quad \dots \quad \sigma_n^2) \tag{9}$$

The least square for the best linear unbiased estimates of the parameters is:

$$x = (A^T C^{-1} A)^{-1} (A^T C^{-1} y) \tag{10}$$

With parameter covariance:

$$\sigma_{x_i} = \mu \sqrt{\text{diag}(A^T C^{-1} A)} \tag{11}$$

Where μ is weighted root mean square error:

$$\mu = \pm \sqrt{\frac{v^T C^{-1} v}{n - \text{dim}(x)}} \tag{12}$$

From equation (5), the modelled positions (predicted position) are:

$$y = Ax \tag{13}$$

And residual positions are calculated as:

$$v = -Ax + y \tag{14}$$

The amplitude, the phase of the annual and semi-annual motions are calculated from the parameters c, d, e, f [22]:

$$A_{ann} = \sqrt{a^2 + b^2}; \quad \phi_{ann} = \frac{1}{2\pi} \text{atan2}\left(\frac{a}{b}\right) \tag{15}$$

$$A_{semi-ann} = \sqrt{c^2 + d^2}; \quad \phi_{semi-ann} = \frac{1}{4\pi} \text{atan2}\left(\frac{c}{d}\right) \tag{16}$$

The flowchart describes the process of calculating and analyzing the GNSS position time series in Fig. 1.

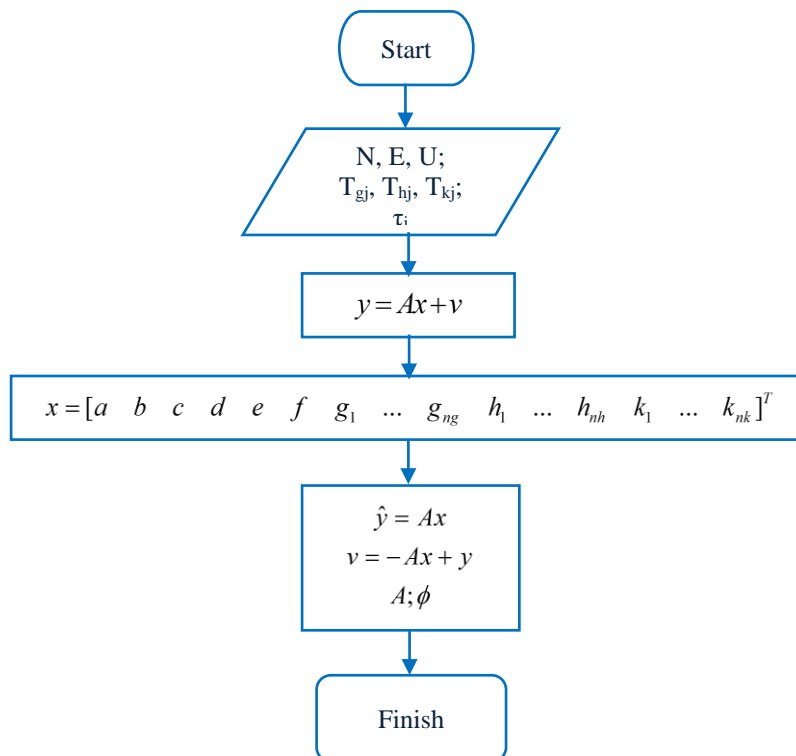


Fig. 1. Flowchart of determining the parameters of GNSS position time series.

In the flowchart (Fig. 1), among the input coefficients for calculation, the decay time (relaxation time) of postseismic deformation τ is known. This coefficient is proposed by estimating directly from the time series and presented in the following section 2.3.

The program has been developed for analyzing GNSS position time series in Python, named **pygps_ts** (GPS time series by Python), which uses the method described above. Pygps_ts helps to solve the most common problems of time series quickly and accurately.

2.3 Determining the time decay of postseismic deformation

The postseismic relaxation time (decay time) is usually determined based on seismic models [23], or the physical process seismicity, or by Omori's law [24, 25]. In this paper, we propose a method to calculate the decay time directly from the position time series based on the equation of the general geometric model (3). τ is iteratively calculated in 2 steps:

First step, choosing the initial value τ^0 (here, we choose $\tau^0 = 0.0027$ yr, equivalent to 01 day [15]). Substituting τ^0 and T_j (time known T_j of seismic jumps) into equation (3) and solving the solution vector:

$$x^0 = [a^0 \ b^0 \ c^0 \ d^0 \ e^0 \ f^0 \ g_1^0 \ \dots \ g_{n_g}^0 \ h_1^0 \ \dots \ h_{n_h}^0 \ k_1^0 \ \dots \ g_{n_k}^0]^T \tag{17}$$

Next in this step, splitting equation (3) into two parts: part one includes the seismic jumps, rate changes, and postseismic displacement; and the other one includes the remaining parameters. These two parts are distinguished in the sign $\{ \}$ in Equation 18.

$$y(t_i) = \{ a + bt_i + c \sin(2\pi t_i) + d \cos(2\pi t_i) + e \sin(4\pi t_i) + f \cos(4\pi t_i) + \sum_{j=1}^{n_g-n_k} g_j H(t_i - T_{gj}) \} + \tag{18}$$

$$+ \{ \sum_{j=1}^{n_k} [g_j H(t_i - T_{kj}) + h_j H(t_i - T_{kj}) t_i + k_j e^{\frac{t_i - T_{kj}}{\tau_j}} H(t_i - T_{kj})] \} + v_i$$

With parameters g_j, h_j, k_j, τ_j ($j = 1 \div n_k$) as unknowns, linearizing equation (18) with partial derivatives with respect to unknowns:

$$y'(t_i) = \sum_{j=1}^{n_k} [g_j^0 H(t_i - T_{kj}) \partial g_j + h_j^0 H(t_i - T_{kj}) t_i \partial h_j + k_j^0 e^{\frac{t_i - T_{kj}}{\tau_j^0}} H(t_i - T_{kj}) \partial k_j + k_j^0 \frac{t_i - T_{kj}}{(\tau_j^0)^2} e^{\frac{t_i - T_{kj}}{\tau_j^0}} H(t_i - T_{kj}) \partial \tau_j^0] \tag{19}$$

Where

$$y'(t_i) = y(t_i) - [a^0 + b^0 t_i + c^0 \sin(2\pi t_i) + d^0 \cos(2\pi t_i) + e^0 \sin(4\pi t_i) + f^0 \cos(4\pi t_i) + \tag{20}$$

$$+ \sum_{j=1}^{n_g} g_j^0 H(t_i - T_{gj}) + \sum_{j=1}^{n_h} h_j^0 H(t_i - T_{hj}) t_i + \sum_{j=1}^{n_k} k_j^0 e^{\frac{t_i - T_{kj}}{\tau_j^0}} H(t_i - T_{kj})]$$

The system of equations (18) in matrix form: $A\partial = y$ (21)

Where,

$$\text{Unknown vector: } \partial = [\partial g_1 \ \dots \ \partial g_{n_k} \ \partial h_1 \ \dots \ \partial h_{n_k} \ \partial k_1 \ \dots \ \partial k_{n_k} \ \partial \tau_1 \ \dots \ \partial \tau_{n_k}]^T \tag{22}$$

$$\text{Vector of free coefficient: } y = [y'(t_1) \ \dots \ y'(t_n)]^T \tag{23}$$

And design matrix A as equation (24).

Then, the unknown vector ∂ is estimated using least squares estimation:

$$\partial = (A^T C^{-1} A)^{-1} (A^T C^{-1} y) \tag{25}$$

Second step, calculating the decay time τ in the next iteration i:

$$\tau_j^i = \tau_j^{i-1} + \partial \tau_j \tag{26}$$

The iterative process stops when the maximum of $\partial \tau_j$ is less than the threshold value, and therefore, convergence is achieved. In practice, we choose the threshold value at 0.003 yr [15].

The process of calculating the decay time of postseismic deformation is summarized in the flowchart Fig. 2.

$$A = \begin{bmatrix} g_1^0 & \dots & g_1^0 & \dots & g_1^0 \\ \dots & \dots & \dots & \dots & \dots \\ 0 & \dots & g_{n_k}^0 & \dots & g_{n_k}^0 \\ h_1^0 t_i & \dots & h_1^0 t_{i+j} & \dots & h_1^0 t_n \\ \dots & \dots & \dots & \dots & \dots \\ 0 & \dots & h_{n_k}^0 t_{i+j} & \dots & h_{n_k}^0 t_n \\ k_1^0 e^{-\frac{t_i - T_{k1}}{\tau_1^0}} & \dots & k_1^0 e^{-\frac{t_{i+j} - T_{k1}}{\tau_1^0}} & \dots & k_1^0 e^{-\frac{t_n - T_{k1}}{\tau_1^0}} \\ \dots & \dots & \dots & \dots & \dots \\ 0 & \dots & k_{n_k}^0 e^{-\frac{t_{i+j} - T_{knk}}{\tau_{n_k}^0}} & \dots & k_{n_k}^0 e^{-\frac{t_n - T_{knk}}{\tau_{n_k}^0}} \\ k_1^0 \frac{t_i - T_{k1}}{(\tau_1^0)^2} e^{-\frac{t_i - T_{k1}}{\tau_1^0}} & \dots & k_1^0 \frac{t_{i+j} - T_{k1}}{(\tau_1^0)^2} e^{-\frac{t_{i+j} - T_{k1}}{\tau_1^0}} & \dots & k_1^0 \frac{t_n - T_{k1}}{(\tau_1^0)^2} e^{-\frac{t_n - T_{k1}}{\tau_1^0}} \\ \dots & \dots & \dots & \dots & \dots \\ 0 & \dots & k_{n_k}^0 \frac{t_{i+j} - T_{knk}}{(\tau_{n_k}^0)^2} e^{-\frac{t_{i+j} - T_{knk}}{\tau_{n_k}^0}} & \dots & k_{n_k}^0 \frac{t_n - T_{knk}}{(\tau_{n_k}^0)^2} e^{-\frac{t_n - T_{knk}}{\tau_{n_k}^0}} \end{bmatrix} \quad (24)$$

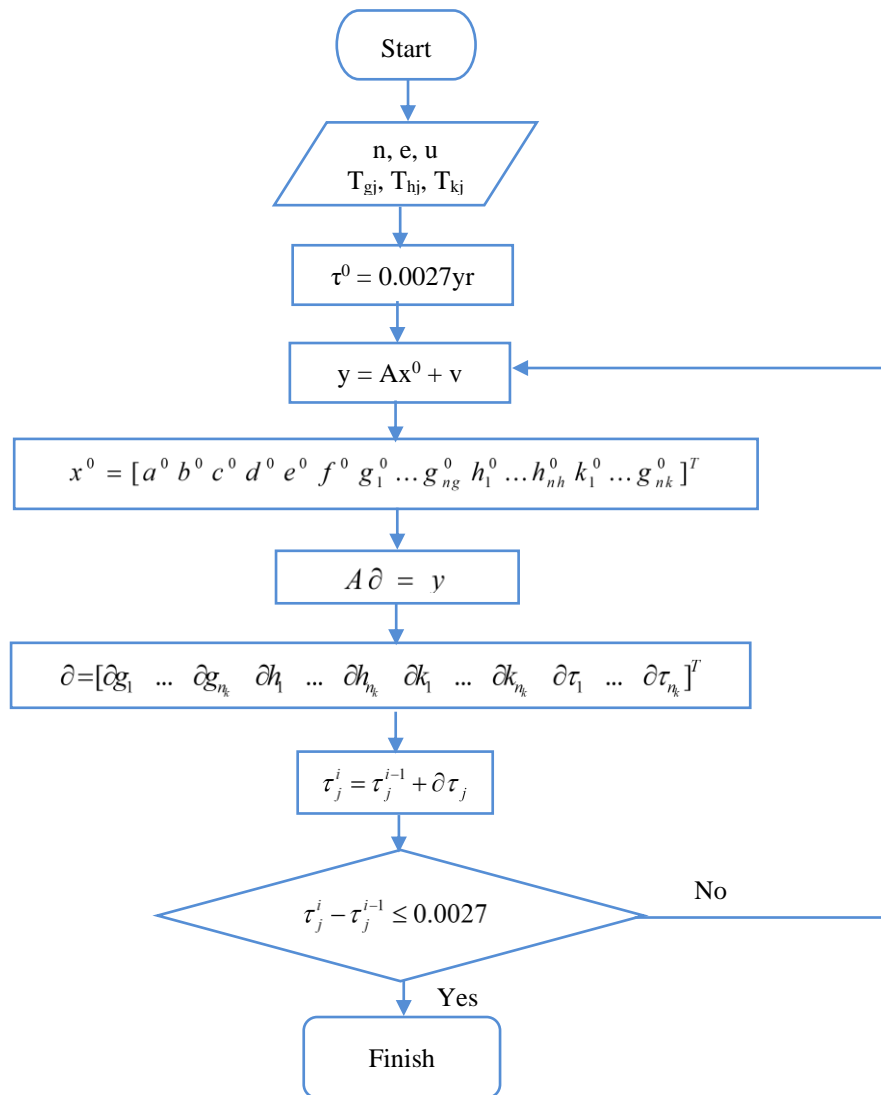


Fig. 3. Flowchart of determining the decay times of postseismic deformation.

In pygps_ts script, we have programmed the τ determination module using this algorithm which will be used if the input data has the times of seismic jumps.

3. Study data and result

3.1 Synthetic data model

It is examined that the performance of this algorithm by a synthetic model produced as a north component of the daily position time series of the GNSS station named SYNT (it mean synthetic) for the period 2015.0-2021.0.

The synthetic model coordinate time series of SYNT is introduced: seasonal motion, coseismic jump at 2018.0, and postseismic relaxation, whose coefficients/parameters are in Tab. 1. Then, this model time series is perturbed by the Normal distribution law $\sigma = 1.0$ mm to create the time series of random coordinates which are illustrated as blue points in Fig. 3 on the left.

Using pygps_ts to process SYNT's coordinate time series, the estimated parameters are obtained and shown in Tab. 1. In addition, the predicted and residual coordinate time series are shown in Fig. 3. Note that the number of iterative estimations of decay time τ is 4, and the processing duration is small, only seconds.

Tab. 1. Comparison of synthetic model and estimated parameters.

Parameters	Linear trend		Seasonal motion				Seismic motion			
	Initial position	Velocity	Annual motion		Semi-annual motion		Jump	Rate change	Amplitude postseismic relaxation	Decay time
	a (m)	b (m/yr)	c (m)	d (m)	e (m)	f (m)	g (m)	h (m/yr)	k (m)	τ (yr)
Model	-0.0050	-0.0010	-0.0002	0.0003	-0.0010	-0.0020	0.0800	0.0100	-0.0500	0.0250
Estimation	-0.0051	-0.0100	-0.0002	0.0003	-0.0010	-0.0020	0.0803	0.0099	-0.0503	0.0249
Difference	0.0001	0.0000	0.0000	0.0000	0.0000	0.0000	-0.0003	0.0001	0.0003	0.0001

Tab. 1 shows that the parameters estimated by using pygps_ts are almost equal to the given parameters of the model time series. The difference between them is mainly in the parameters of seismic motion but is considered insignificant.

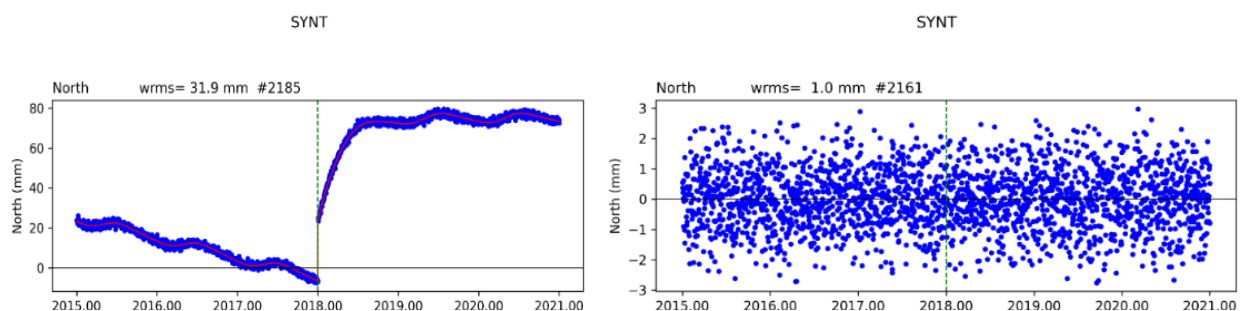


Fig. 3. SYNT's coordinate time series.

In Fig. 3 on the left, the red line (fit line) is the predicted coordinate time series (the correct value of coordinates), while the blue points are the "measurement" coordinate time series. The red line is completely correct with the synthetic model; this line describes the synodal seasonal motion, the seismic jump at 2018.0, and the postseismic relaxation (with decay time $\tau = 0.25$ year and rate change 9.9 mm/year). Fig. 3 on the right is the residual coordinate time series (after the estimated trend, estimated jump, and estimated postseismic relaxation have been removed) with $wrms = 1.0$ mm, exactly equal to the error σ introduced in the data model.

The test result and also our processing results in practice have proved that the proposed geometric model, method, and pygps_ts program for processing GNSS position time series are appropriate and ensure accuracy.

3.2 Some CORS stations in Vietnam

GNSS CORS stations are not only used as a control network for surveying services [26] but also widely used in tectonic plate movement monitoring [27,28], in landslide monitoring [29] (landslide due to mining is regularly monitoring in Quang Ninh [30,31]), etc. This study processes the GNSS position time series of 4 CORS stations in Vietnam: NAVI (Ha Noi), NADI (Nam Dinh), DANA (Da Nang), and HCMC (Ho Chi Minh), which are actual data to verify the algorithm and pygps_ts program.

These CORS stations measure continuously from January 2016 to December 2018, of which 3 stations (DANA, HCMC, and NADI) are designed and operated by Tuong Anh Science and Technology Equipment Joint Stock Company, and one station (NAVI) belongs to The Japan Aerospace Exploration Agency (JAXA). The data of these CORS stations has been [32] processed by the PPP method using PPPC (Precise Point Positioning by using C language software) software to obtain the position time series.

The pygps_ts is used to process the position time series of these 4 CORS stations. The estimated parameters of all these time series only have the linear trend and the seasonal motion according to the 3-D coordinate components n, e, u, but no jumps, no postseismic deformation (illustrated in Fig. 4). The estimated parameters and their accuracy are shown in Tab. 2.

From the estimated parameters describing the seasonal motion, pygps_ts calculates the phase and amplitude of annual and semi-annual motions are shown in Tab. 3.

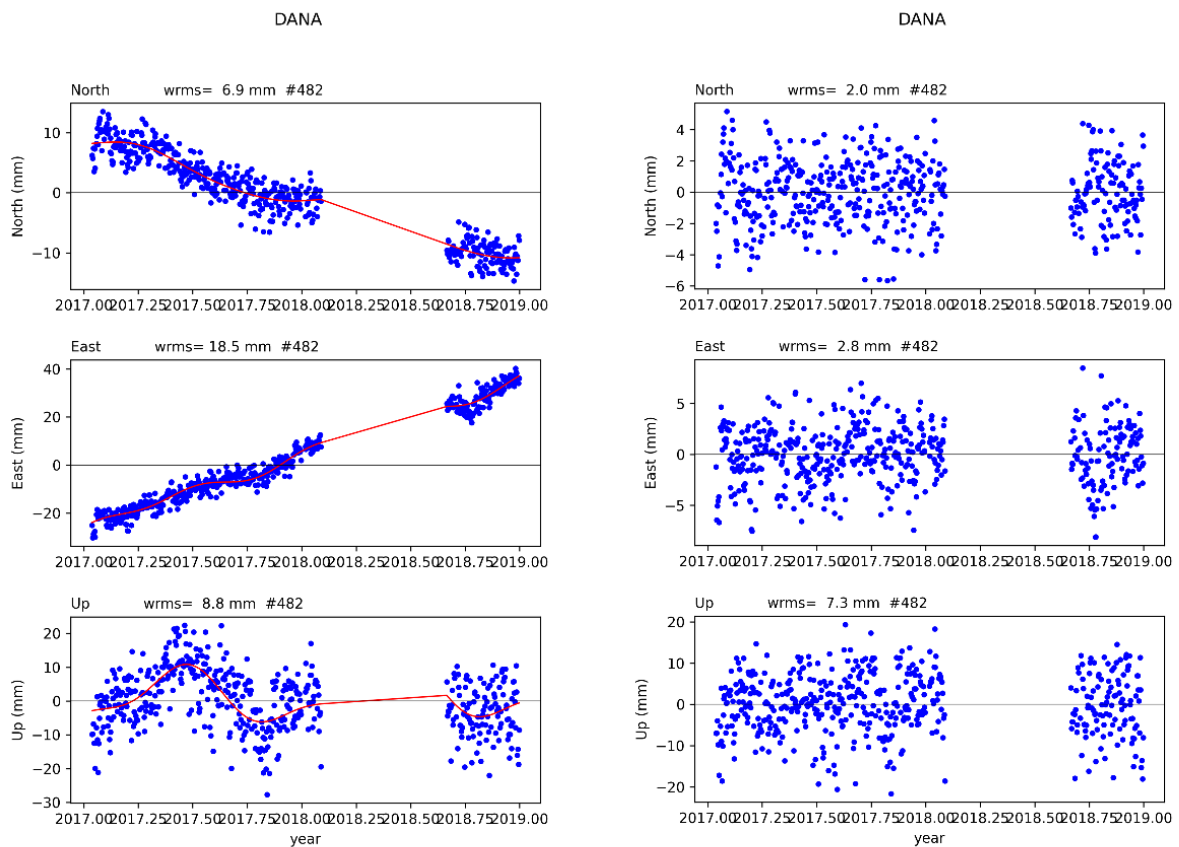
Tab. 2. Estimated parameters and their accuracy.

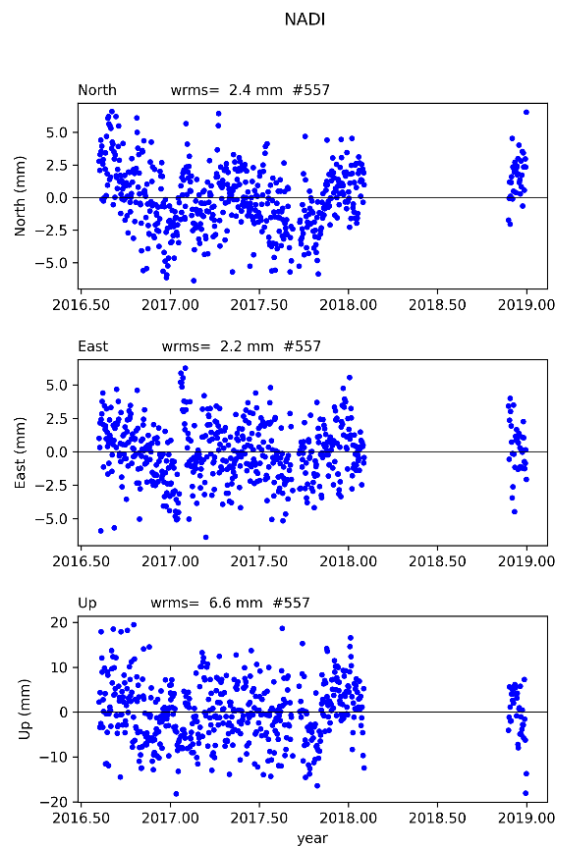
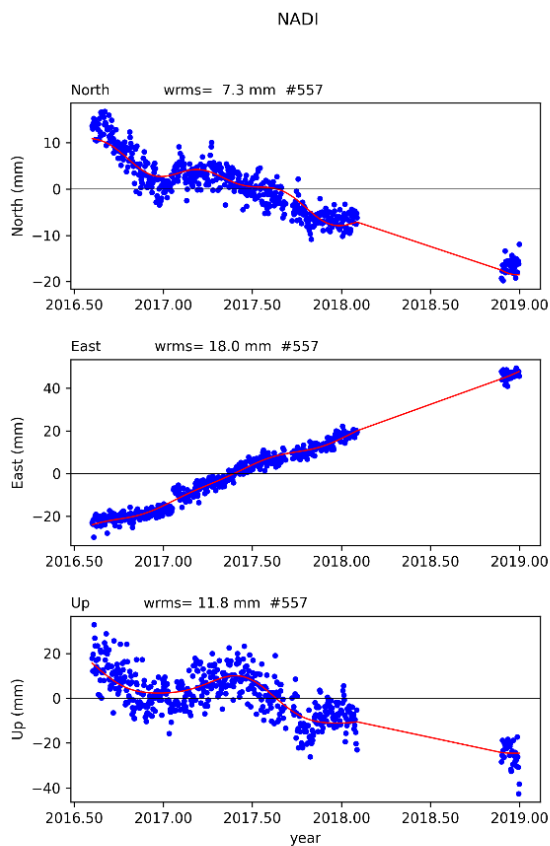
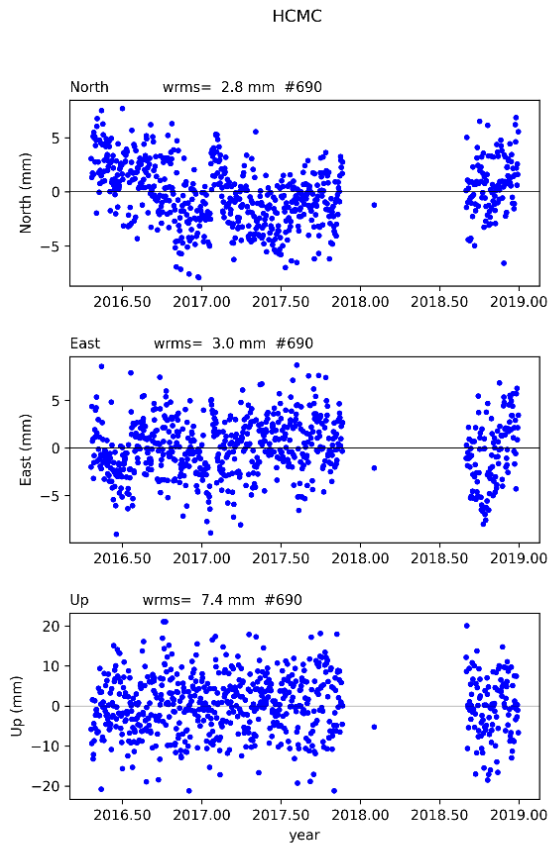
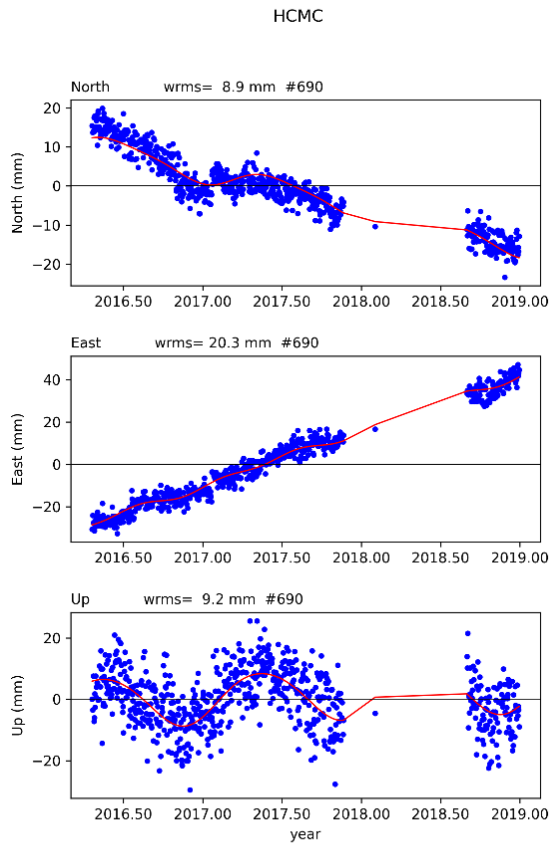
Station	Component	Estimated parameters of a geometric model of position time series					
		a (m)	B (m/yr)	c (m)	d (m)	e (m)	f (m)
DANA	n	-0.0010	-0.0095	0.0017	-0.0002	0.0000	-0.0002
		±0.0001	±0.0002	±0.0002	±0.0001	±0.0001	±0.0001
	e	0.0047	0.0315	0.0016	-0.0005	0.0008	0.0016
		±0.0002	±0.0003	±0.0003	±0.0002	±0.0002	±0.0002
	u	0.0017	0.0015	0.0034	-0.0067	-0.0001	0.0029
		±0.0004	±0.0008	±0.0007	±0.0006	±0.0005	±0.0005
HCMC	n	-0.0058	-0.0095	0.0006	-0.0028	-0.0003	-0.0004
		±0.0002	±0.0002	±0.0002	±0.0002	±0.0002	±0.0002
	e	0.0160	0.0262	0.0003	-0.0010	0.0011	0.0001
		±0.0002	±0.0002	±0.0002	±0.0002	±0.0002	±0.0002
	u	0.0020	0.0019	0.0057	-0.0057	0.0006	-0.0002
		±0.0004	±0.0004	±0.0005	±0.0005	±0.0004	±0.0004
NADI	n	-0.0054	-0.0106	0.0004	-0.0015	0.0008	-0.0009
		±0.0002	±0.0002	±0.0002	±0.0002	±0.0002	±0.0002
	e	0.0181	0.0315	0.0001	-0.0017	0.0006	0.0000
		±0.0001	±0.0002	±0.0001	±0.0001	±0.0001	±0.0001
	u	-0.0059	-0.0134	0.0035	-0.0062	-0.0005	0.0010
		±0.0004	±0.0006	±0.0004	±0.0004	±0.0004	±0.0004
NAVI	n	-0.0143	-0.0139	0.0006	-0.0028	0.0001	-0.0010
		±0.0002	±0.0002	±0.0002	±0.0001	±0.0001	±0.0001
	e	0.0340	0.0328	0.0006	0.0002	0.0009	-0.0002
		±0.0002	±0.0002	±0.0002	±0.0002	±0.0002	±0.0001
	u	-0.0013	-0.0011	0.0038	-0.0086	-0.0008	0.0029
		±0.0006	±0.0005	±0.0004	±0.0004	±0.0004	±0.0004

Tab. 3. Amplitude and phase of seasonal motion.

Station	Component	Annual motion		Semi-annual motion	
		A (mm)	φ (year)	A (mm)	Φ (year)
DANA	n	1.66	0.30	1.77	0.04
	e	1.70	0.26	0.20	0.23
	u	7.46	0.43	2.91	0.00
HCMC	n	1.01	0.45	1.13	0.11
	e	2.81	0.47	0.54	-0.20
	u	8.09	0.38	0.58	0.15
NADI	n	1.72	0.49	0.62	0.13
	e	1.61	0.46	1.22	0.19
	u	7.13	0.42	1.12	-0.04
NAVI	n	0.65	0.21	0.92	0.14
	e	2.89	0.46	0.97	0.25
	u	9.39	0.43	2.96	-0.02

The position time series, the fit line, and the residual position time series of 4 CORS stations are shown in Fig. 4.





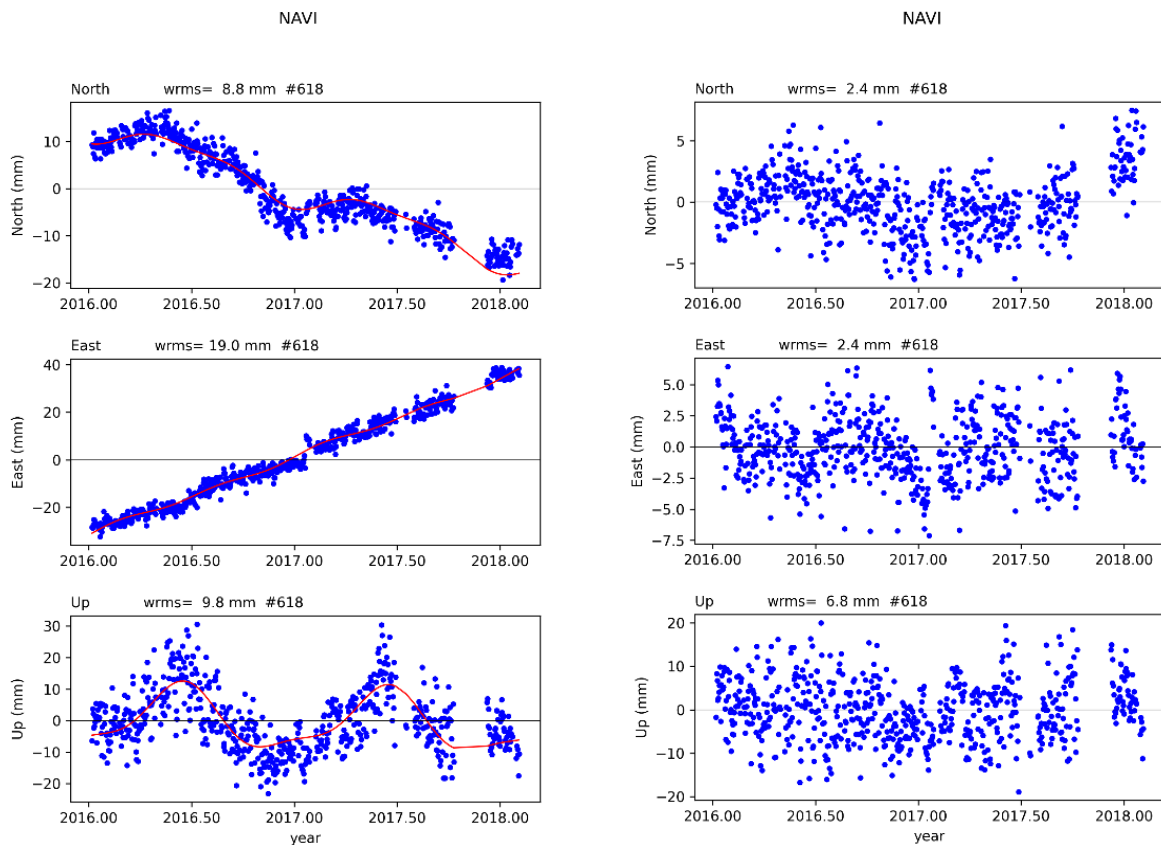


Fig. 4. GNSS position time series of 4 CORS station.

Fig. 4 on the left presents the measurement coordinate time series (blue point) and estimated coordinate time series (red line) according to 3-D coordinate components n, e, u. The estimated coordinate time series are accurate, presented by a fit line with the measured coordinate series, and the wrms is tiny, about 2.0 ~ 3.0 mm for the horizontal components (n, e) and 6.6 ~ 7.4 mm for the vertical components. Fig. 4 presents the residual coordinate time series on the right after calculating and removing the velocity and seasonal motion.

The displacement velocities of the CORS stations are estimated with high accuracy, about tenths of a millimeter, shown in Tab. 3 (column of parameter b). The velocity field of 4 CORS stations is presented in Fig. 5 (also created by pygps_ts).

The displacement velocity and its accuracy according to the coordinate components of the CORS stations DANA is n, e, u = -9.5 ± 0.2 , 31.5 ± 0.3 , 1.5 ± 0.8 mm/year, HCMC is n, e, u = -9.5 ± 0.2 , 26.2 ± 0.2 , 1.9 ± 0.4 mm/year, NADI is n, e, u = -10.6 ± 0.2 , 31.5 ± 0.2 , -13.4 ± 0.6 mm/year and NAVI is n, e, u = -13.9 ± 0.2 , 32.8 ± 0.2 , -1.1 ± 0.5 mm/year. Thus, CORS stations move an average of 3-4cm/year in the East-South direction (e.g. Fig. 5).

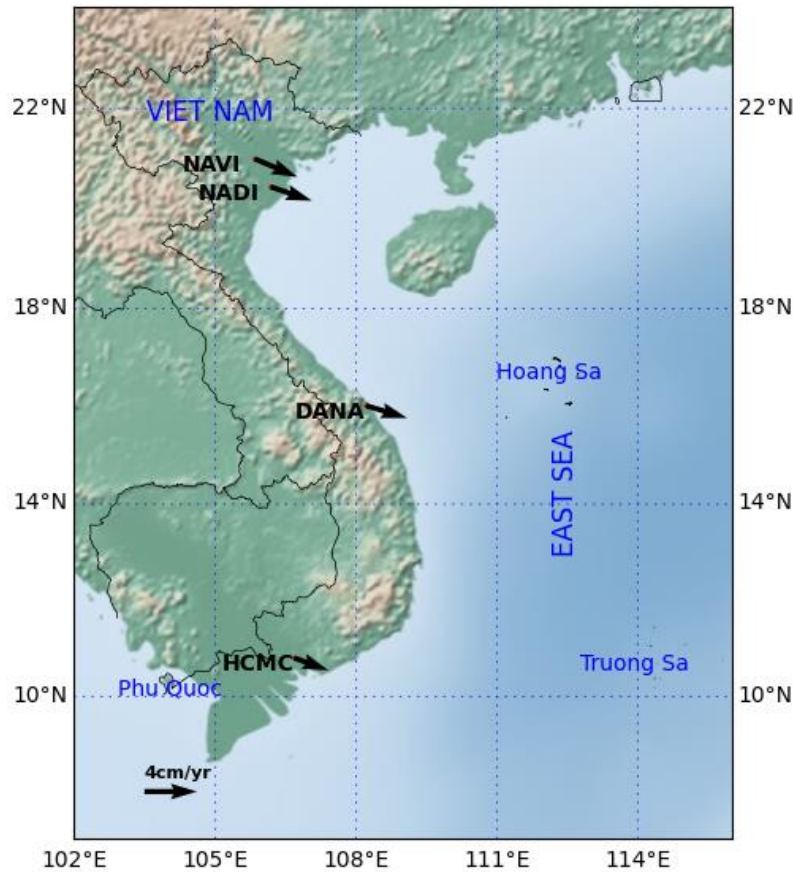


Fig. 5. Velocity field of 4 CORS stations in Vietnam in this study.

4. Discussions and conclusions

The general geometric model mentioned in this study includes common motion phenomena such as linear trend, seasonal motion (including annual and semi-annual displacement), jumps, and postseismic deformations (including rate change and postseismic relaxation) is the complete model for GNSS position time series. However, it is rare that the transient deformation is recorded in the GNSS position time series in areas with complex geotectonic activities such as American Basin and Range [33], Guerrero Mexico [34], etc. Transient deformation is defined as a nonperiodic, nonsecular accumulation of strain in the crust [35], so it is difficult to model geometry like other motions. Note that this phenomenon has not been recorded in GNSS station Vietnam; therefore, it is not mentioned in this paper.

To calculate the magnitude of jumps in the position time series, it is necessary to provide the time of the jumps. The study of automatically determining the jump has also been researched [13, 15] but needs to be improved and examined more closely.

The proposed method of determining the decay time directly from the coordinate time series allows a more accurate description of postseismic deformation. This method's algorithm is programmed in Python, allowing fast and accurate calculations with the data model. However, the GNSS position time series of CORS stations in Vietnam do not record postseismic deformation to verify the method. Therefore, it needs to be tested with real complex data to improve the method-as well as the pygps_ts program.

The general geometric model of the GNSS position time series describes most of the common motions, which is true for most of the position time series in the study of land surface deformation, crustal deformation due to seismic, mining, etc. The calculating results of 4 CORS stations in Vietnam are highly accurate, and the processing time is fast because the data of these CORS stations are quite "beautiful". In the upcoming time, the study will be conducted with more CORS station data in Vietnam.

The estimated velocity field of 4 CORS stations: DANA (n, e, u = -9.5, 31.5, 1.5 mm/year), HCMC (n, e, u = -9.5, 26.2, 1.9 mm/year), NADI (n, e, u = -10.6, 31.5, -13.4 mm/year) and NAVI (n, e, u = -13.9,

32.8, -1.1 mm/year) is similar to the study's results of [32].

Vietnam is in the process of building and developing continuous GNSS networks for geotectonic study, surveying services, etc. the study of methods of processing GNSS position time series is essential to promote the role of GNSS networks in science and practical applications.

5. Acknowledgments

This research has been supported by the Ministry of Education and Training of Vietnam (under grant B2020-XDA-05). The CORS data is provided by Tuong Anh Science and Technology Equipment Joint Stock Company and Japan Aerospace Exploration Agency. We acknowledge Ngoc Lau NGUYEN for providing us the GNSS position time series of 4 CORS stations.

The paper was presented during the 6th VIET - POL International Conference on Scientific-Research Cooperation between Vietnam and Poland, 10-14.11.2021, HUMG, Hanoi, Vietnam.

6. Data Availability Statement

All data, code that support the findings of this study are available from the corresponding author upon reasonable request:

- Code of pygps_ts in Python 3.
- Position time series of SYNT and 4 CORS station.

7. References

1. Hodgkinson, K.M., Mencin, D.J., Feaux, K., Sievers, C., Mattioli, G.S., 2020. Evaluation of earthquake magnitude estimation and event detection thresholds for real-time GNSS networks: Examples from recent events captured by the network of the Americas, *Seismological Research Letters*, 91(3): 1628–1645, <https://doi.org/10.1785/0220190269>.
2. Mattioli, G., Mencin, D., Hodgkinson, K., Meertens, C., Phillips, D., Blume, F., Berglund, H., Fox, O., Feaux, K., 2016. The EarthScope Plate Boundary Observatory and allied networks, the makings of nascent Earthquake and Tsunami Early Warning System in Western North America, *EGU General Assembly Conference Abstracts*, EPSC2016-10953.
3. Sagiya, T., 2004. A decade of GEONET: 1994-2003 - The continuous GPS observation in Japan and its impact on earthquake studies, *Earth, Planets and Space*, 56(8): 1994–2003. <https://doi.org/10.1186/BF03353077>.
4. Hatanaka, Y., Iizuka, T., Sawada, M., Yamagiwa, A., Kikuta, Y., Johnson, J., Rocken, C., 2003. Improvement of the analysis strategy of GEONET, *Bull. Geogr. Surv. Inst*, 49: 11–37.
5. Li, C.K., Ching, K.E., Chen, K.H., 2019. The ongoing modernization of the Taiwan semi-dynamic datum based on the surface horizontal deformation model using GNSS data from 2000 to 2016, *Journal of Geodesy*, 93(9): 1543–1558, <https://doi.org/10.1007/s00190-019-01267-5>.
6. Segall, P., Davis, J.L., 1997. GPS applications for geodynamics and earthquake studies. *Annual Review of Earth and Planetary Sciences*, 25: 301–336, <https://doi.org/10.1146/annurev.earth.25.1.301>.
7. Nicolas, J., Nocquet, J.M., Van Camp, M., van Dam, T., Boy, J.P., Hinderer, J., Gegout, P., Calais, E., Amalvict, M., 2006. Seasonal effect on vertical positioning by Satellite Laser Ranging and Global Positioning System and on absolute gravity at the OCA geodetic station, Grasse, France, *Geophysical Journal International*, 167(3): 1127–1137, <https://doi.org/10.1111/j.1365-246X.2006.03205.x>.
8. Bevis, M., Jonathan, B., Dana J., C.I., The Art and Science of Trajectory Modelling, In J.-P. Montillet M.S. Bos (Eds.), *Geodetic Time Series Analysis in Earth Sciences*, 1st ed., 1–29, Springer International Publishing, 2020.

9. Le, H.M., Masson, F., Bourdillon, A., Fleur, R., Hu, J., Vu, T.H., Le, T.T., Nguyen, C.T., Nguyen, H., 2014. Recent crustal motion in Vietnam and in the Southeast Asia region by continuous GPS data (in Vietnamese), *Vietnam Journal of Earth Sciences*, 36(1): 1–13.
10. Duong, N.A., Sagiya, T., Kimata, F., To, T.D., Hai, V.Q., Cong, D.C., Binh, N.X., Xuyen, N.D., 2013. Contemporary horizontal crustal movement estimation for northwestern Vietnam inferred from repeated GPS measurements, *Earth, Planets and Space*, 65(12): 1399–1410, <https://doi.org/10.5047/eps.2013.09.010>.
11. Deng, L., Jiang, W., Chen, H., Zhu, Z., Zhao, W., 2017. Study of the effects on GPS coordinate time series caused by higher-order ionospheric corrections calculated using the DIPOLE model, *Geodesy and Geodynamics*, 8(2): 111–119, <https://doi.org/10.1016/j.geog.2017.01.004>.
12. Masson, C., Mazzotti, S., Vernant, P., 2019. Precision of continuous GPS velocities from statistical analysis of synthetic time series, *Solid Earth*, 10(1): 329–342, <https://doi.org/10.5194/se-10-329-2019>.
13. Nunnari, G., Cannavo, F., 2019. Automatic offset detection in GPS time series by change point approach, *Proceedings of the 16th International Conference on Informatics in Control ICINCO 2019, Automation and Robotics*, 1(Icinc), 377–383, <https://doi.org/10.5220/0007951503770383>.
14. Wu, D., Yan, H., Shen, Y., 2017. TSAAnalyzer, a GNSS time series analysis software, *GPS Solutions*, 21(3): 1389–1394. <https://doi.org/10.1007/s10291-017-0637-2>.
15. Tran, D.T. Analyse rapide et robuste des solutions GPS pour la tectonique, Thesis, Université de Nice Sophia Antipolis, France, 2013.
16. Nikolaidis, R. Observation of geodetic and seismic deformation with the Global Positioning System, Thesis, University of California, San Diego, USA, 2002.
17. Montillet, J.-P., Williams, S.D.P., Koulali, A., McClusky, S.C., 2015. Estimation of offsets in GPS time-series and application to the detection of earthquake deformation in the far-field, *Geophysical Journal International*, 200(2): 1207–1221, <https://doi.org/10.1093/gji/ggu473>.
18. Gazeaux, J., Williams, S., King, M., Bos, M., Dach, R., Deo, M., Moore, A.W., Ostini, L., Petrie, E., Roggero, M., Teferle, F.N., Olivares, G., Webb, F.H., 2013. Detecting offsets in GPS time series: First results from the detection of offsets in GPS experiment, *Journal of Geophysical Research: Solid Earth*, 118(5): 2397–2407, <https://doi.org/10.1002/jgrb.50152>.
19. Pellegrinelli, A., Perfetti, N., Russo, P., 2005. Time series analysis of daily solutions of IGFN permanent GPS stations, *Bollettino Di Geofisica Teorica Ed Applicata*, 46(2–3): 85–97.
20. Rajner, M., Liwosz, T., 2017. Analysis of seasonal position variation for selected GNSS sites in Poland using loading modelling and GRACE data, *Geodesy and Geodynamics*, 8(4): 253–259, <https://doi.org/10.1016/j.geog.2017.04.001>.
21. Métivier, L., Collilieux, X., Lercier, D., Altamimi, Z., Beauducel, F., 2014. Global coseismic deformations, GNSS time series analysis, and earthquake scaling laws, *Journal of Geophysical Research: Solid Earth*, 119(12): 9095–9109, <https://doi.org/10.1002/2014jb011280>.
22. Klos, A., Bogusz, J.B., Bos, M.S., Gruszczynska, M. Modelling the GNSS Time Series: Different Approaches to Extract Seasonal Signals. In J.-P. Montillet M. S. Bos (Eds.), *Geodetic Time Series Analysis in Earth Sciences*, 1st ed, Springer International Publishing, 2020.
23. Loevenbruck, A., Cattin, R., Le Pichon, X., Dominguez, S., Michel, R., 2004. Coseismic slip resolution and post-seismic relaxation time of the 1999 Chi-Chi, Taiwan, earthquake as constrained by geological observations, geodetic measurements and seismicity, *Geophysical Journal International*, 158(1): 310–326, <https://doi.org/10.1111/j.1365-246X.2004.02285.x>.
24. Vallejos, J.A., McKinnon, S.D., 2011. Correlations between mining and seismicity for re-entry protocol development, *International Journal of Rock Mechanics and Mining Sciences*, 48(4): 616–625, <https://doi.org/10.1016/j.ijrmms.2011.02.014>.
25. Perfettini, H., Avouac, J.P., 2004. Postseismic relaxation driven by brittle creep: A possible

- mechanism to reconcile geodetic measurements and the decay rate of aftershocks, application to the Chi-Chi earthquake, Taiwan, *Journal of Geophysical Research: Solid Earth*, 109(B2): 1–15, <https://doi.org/10.1029/2003jb002488>.
26. Tran, D.T., Nguyen, D.H., Luong, N.D., Dao, D.T., 2020. Impact of the precise ephemeris on accuracy of GNSS baseline in relative positioning technique, *Vietnam journal of earth sciences*, 43(1): 96–110, <https://doi.org/10.15625/0866-7187/15745>.
 27. Uzel, T., Eren, K., Gulal, E., Tiryakioglu, I., Dindar, A.A., Yilmaz, H., 2013. Monitoring the tectonic plate movements in Turkey based on the national continuous GNSS network, *Arabian Journal of Geosciences*, 6(9): 3573–3580, <https://doi.org/10.1007/s12517-012-0631-5>.
 28. El-Mowafy, A., Bilbas, E., 2016. Quality Control in Using GNSS CORS Network for Monitoring Plate Tectonics: A Western Australia Case Study, *Journal of Surveying Engineering*, 142(2), [https://doi.org/10.1061/\(asce\)su.1943-5428.0000157](https://doi.org/10.1061/(asce)su.1943-5428.0000157).
 29. Cong Khai, P., Tran, D.T., Nguyen, V.H., 2020. GNSS/CORS-Based Technology for Real-Time Monitoring of Landslides on Waste Dump – A Case Study at the Deo Nai South Dump, Vietnam, *Inżynieria Mineralna*, 1(2), <https://doi.org/10.29227/IM-2020-02-23>.
 30. Long, N.Q., My, V.C., Luyen, B.K., 2016. Divergency verification of predicted values and monitored deformation indicators in specific condition of Thong Nhat underground coal mine (Vietnam), *Geoinformatica Polonica*, 15, 15–22, <https://doi.org/10.4467/21995923GP.16.002.5479>.
 31. Nguyen, L.Q., Ahmad, A., Cao, C.X., Van Le, C., 2018. Designing observation lines: a case study of the G9 seam in the Mong Duong colliery, *Journal of Mining and Earth Sciences*, 59(6): 28–34.
 32. Nguyen, N.L., Coleman, R., Ha, M.H., 2021. Determination of tectonic velocities of some continuously operating reference stations (CORS) in Vietnam 2016-2018 by using precise point positioning, *Vietnam Journal of Earth Sciences*, 43(1): 1–12, <https://doi.org/10.15625/0866-7187/15571>.
 33. Chamoli, A., Lowry, R.A., Jeppson, T.N., 2013. Implications of transient deformation in the northern Basin and Range, western United States, *Journal of Geophysical Research, Solid Earth*, 119: 4393–4413, <https://doi.org/10.1002/2013JB010605>.
 34. Vergnolle, M., Walpersdorf, A., Kostoglodov, V., Tregoning, P., Santiago, J.A., Cotte, N., Franco, S.I., 2010. Slow slip events in Mexico revised from the processing of 11 year GPS observations, *Journal of Geophysical Research: Solid Earth*, 115(8): 1–18, <https://doi.org/10.1029/2009JB006852>.
 35. Riel, B., Simons, M., Agram, P., Zhan, Z., 2014. Detecting transient signals in geodetic time series using sparse estimation techniques, *Journal of Geophysical Research: Solid Earth*, 119(6): 5140–5160, <https://doi.org/10.1002/2014JB011077>.

Phase Diagrams of the Excitonic Insulator State: Analyzing the Excitonic Susceptibility

DO Thi Hong Hai¹, NGUYEN Thi Hau^{1,*}

¹Hanoi University of Mining and Geology, 18 Vien street, Hanoi, Vietnam

Corresponding author: nguyenthchau@hmg.edu.vn

Abstract. In this paper, the formation of the excitonic insulator state in the rare-earth chalcogenides has been investigated through the extended Falicov-Kimball model. Adapting the unrestricted Hartree-Fock approximation, we have derived a set of explicitly self-consistent equations determining expectation values and the excitonic susceptibility in the system. Analyzing the excitonic susceptibility, we have established phase diagrams of the excitonic insulator state depending on the model parameters. The phase structures confirmed the excitonic insulator state is found at low temperature and between two critical values of the Coulomb interaction. The effect of the external pressure on the formation of the excitonic insulator state is also shown.

Keywords: Unrestricted Hartree-Fock approximation, Falicov-Kimball model, Excitonic insulator, Excitonic susceptibility, Rare-earth chalcogenide

1. Introduction

Excitonic insulator (EI) state has been predicted to occur in semimetal (SM) and semiconductor (SC) materials as the quantum condensation of electron-hole pairs. Although the first theoretical was proposed over a half-century ago [1-3], the nature of this state still has many things yet clarity as well as the ability to observe the experiment remains challenging. Because of the Coulomb attraction between electrons and holes, excitons can be established and if the temperature is low enough with a sufficiently high density, these excitons can condense forming a new spontaneous macroscopic phase-coherent quantum Bose-Einstein condensation (BEC) state [4], the so-called the excitonic insulator state.

In recent years, investigating some mixed-valent rare-earth chalcogenides and transition metal dichalcogenides has strongly supported the theoretical prediction and renewed the interest in the EI state. For instance, electrical and thermal transport properties in the pressure-sensitive mixed-valence rare-earth chalcogenide $\text{TmSe}_{0.45}\text{Te}_{0.55}$ have indicated a stabilized EI state at a temperature below 20 K [5-7]. Most recently, by using the momentum resolved electron energyloss spectroscopy, Kogar and coworkers have shown evidence for the excitonic condensation in the transition metal dichalcogenide semimetal 1T-TiSe₂ [8]. Besides, experimental results of the optical conductivity also have confirmed the existence of the EI state in narrow-gap semiconductor system Ta_2NiSe_5 [9, 10].

As an ordered state, the EI state might be distorted by the thermal fluctuations. Studying the influence of temperature on the EI state, therefore, is helpful. Phase diagrams depending on the temperature of the EI state have been experimentally reported [5, 6]. These phase diagrams show that the EI state occurs at low temperature with intermediate pressure around the semimetal-semiconductor transition. The phase diagrams of the EI state have also been addressed theoretically in a framework of the extended Falicov-Kimball model (EFKM) which covers direct *c*- and *f*-band hopping and admits the pairing of *c*-electrons with *f*-holes via the Coulomb interaction [11, 12]. In the SM regime with small Coulomb interaction, excitons might condense like Cooper pairs in the Bardeen-Cooper-Schrieffer (BCS) theory. On the other hand, in the SC regime, strong Coulomb interaction might formulate tight-binding excitons which then possibly condense like neutral atoms as in the theory of Bose-Einstein. A smooth BCS-BEC crossover of the EI state in the model is then discussed.

However, in the above studies, the description of the EI phase transition is only based on investigating the properties of the condensate order parameter. Moreover, recent studies of optical conductivity give us different views than the initial assumptions about the condensation formation of excitons. For example, in Ta_2NiSe_5 material, the optical conductivity calculated results from the density functional theory based electronic structure calculation and density-matrix renormalization group calculation or electronic states study in real space of low temperature phase release that excitons can be formed before the condensation happens even when the system is in the SM side [13, 14]. This is completely unconventional because one

always believes that this signature happens only in the SC phase, in the SM side the formation of excitons and their condensation state occur simultaneously [15]. Considering the excitonic susceptibility to clearly describe the condensation mechanism of the exciton systems is therefore necessary.

Rare-earth metals and their compounds are mainly used in industry and defense. They are also increasingly used in devices serving modern life such as: computer memory, Digital Video Disc, rechargeable battery, mobile phone, etc. In mixed-valence rare-earth chalcogenides, an exciton binding state of the $4f$ holes with the $5d$ electrons can be formed. At sufficiently low temperature, those excitons condense into the EI state. The effective mass of excitons is so small that they can condense at much higher temperatures than BEC critical temperature of atoms. Therefore, these material systems are being studied extensively in both science and technology [16]. In the present work, the EI state in rare-earth chalcogenides is discussed in the framework of the spinless EFKM, in which the hopping of the f electrons is involved. Using the unrestricted Hartree-Fock approximation, we obtain a set of self-consistent equations which allows us to determine the excitonic susceptibility function. From signatures of the static excitonic susceptibility function, we discuss in detail the phase structures of the EI state due to Coulomb attraction at low temperature.

This paper is organized as follows. In section 2, we introduce the theoretical approach of the present work. Here we present the 2D extended Falicov-Kimball model. and the unrestricted Hartree-Fock approximation developed for this model. In section 3, we outline numerical results where the phase diagrams of the EI state in the system are addressed. The conclusion is given in section 4.

2. Theoretical approach

In order to consider the electron-hole system in rare-earth chalcogenides, we use the EFKM with the Hamiltonian

$$\mathcal{H} = \mathcal{H}_0 + \mathcal{H}_{int} \tag{1}$$

with the non-interacting part of the electron system is given

$$\mathcal{H}_0 = \sum_{\mathbf{k}} \varepsilon_{\mathbf{k}}^c c_{\mathbf{k}}^\dagger c_{\mathbf{k}} + \sum_{\mathbf{k}} \varepsilon_{\mathbf{k}}^f f_{\mathbf{k}}^\dagger f_{\mathbf{k}} \tag{2}$$

where $c_{\mathbf{k}}^\dagger$ ($c_{\mathbf{k}}$) and $f_{\mathbf{k}}^\dagger$ ($f_{\mathbf{k}}$) are the creation (annihilation) operators of c and f electrons carrying momentum \mathbf{k} , respectively. The electronic excitation energies in the tight-binding approximation are given by

$$\varepsilon_{\mathbf{k}}^{c(f)} = \varepsilon^{c(f)} - t^{c(f)} \gamma_{\mathbf{k}} - \mu \tag{3}$$

with $\varepsilon^{c(f)}$ are the on-site energies, $t^{c(f)}$ are the nearest-neighbor particle transfer amplitudes, and μ denotes the chemical potential. In two-dimensional hypercubic lattice, the nearest-neighbor hopping $\gamma_{\mathbf{k}}$ reads $\gamma_{\mathbf{k}} = 2(\cos k_x + \cos k_y)$.

The interacting part of the Hamiltonian \mathcal{H}_{int} reads

$$\mathcal{H}_{int} = \frac{U}{N} \sum_{\mathbf{k}, \mathbf{k}', \mathbf{q}} c_{\mathbf{k}+\mathbf{q}}^\dagger c_{\mathbf{k}'} f_{\mathbf{k}'-\mathbf{q}}^\dagger f_{\mathbf{k}} \tag{4}$$

here U is the Coulomb interaction between conduction c electrons and valence f electrons and N counts the number of lattice sites. In general, $c - c$ and $f - f$ Coulomb interactions might have been taken into account in the interaction part of the Hamiltonian in Eq. (4). However, the additional interactions only lead to mere shifts in the one-particle electronic dispersions and they are neglected from now in our study. Here, we assume that a $c - f$ electron bounding state is equivalent to an exciton state.

Using Hartree-Fock approximation, we introduce the fluctuation operator $\delta A = A - \langle A \rangle$ for an arbitrary operator A , and write the Coulomb interaction operator in Eq. (4) as

$$\begin{aligned} c_{\mathbf{k}+\mathbf{q}}^\dagger c_{\mathbf{k}'} f_{\mathbf{k}'-\mathbf{q}}^\dagger f_{\mathbf{k}} &= [\langle f_{\mathbf{k}}^\dagger f_{\mathbf{k}} \rangle c_{\mathbf{k}'}^\dagger c_{\mathbf{k}'} + \langle c_{\mathbf{k}'}^\dagger c_{\mathbf{k}'} \rangle f_{\mathbf{k}}^\dagger f_{\mathbf{k}}] \\ &+ [\langle c_{\mathbf{k}+\mathbf{q}}^\dagger f_{\mathbf{k}} \rangle f_{\mathbf{k}'-\mathbf{q}}^\dagger c_{\mathbf{k}'} + \langle f_{\mathbf{k}'-\mathbf{q}}^\dagger c_{\mathbf{k}'} \rangle c_{\mathbf{k}+\mathbf{q}}^\dagger f_{\mathbf{k}}] \end{aligned} \tag{5}$$

$$+\left[\langle c_{\mathbf{k}+\mathbf{q}}^\dagger f_{\mathbf{k}} \rangle \langle f_{\mathbf{k}'-\mathbf{q}}^\dagger c_{\mathbf{k}'} \rangle - \langle c_{\mathbf{k}+\mathbf{q}}^\dagger c_{\mathbf{k}'} \rangle \langle f_{\mathbf{k}'-\mathbf{q}}^\dagger f_{\mathbf{k}} \rangle\right]$$

Here, we only focus on the formation and condensation of excitons with momentum \mathbf{q} . Therefore, constants here have been neglected in the approximation. In this case, the Hamiltonian in Eq. (1) reduces to the so-called Hartree-Fock Hamiltonian, which can be read

$$\mathcal{H}_{HF} = \sum_{\mathbf{k}} \bar{\varepsilon}_{\mathbf{k}}^c c_{\mathbf{k}}^\dagger c_{\mathbf{k}} + \sum_{\mathbf{k}} \bar{\varepsilon}_{\mathbf{k}}^f f_{\mathbf{k}}^\dagger f_{\mathbf{k}} + \Lambda \sum_{\mathbf{k}} (c_{\mathbf{k}+\mathbf{q}}^\dagger f_{\mathbf{k}} + f_{\mathbf{k}}^\dagger c_{\mathbf{k}+\mathbf{q}}) \quad (6)$$

here, the electronic excitation energies now have acquired Hartree shifts

$$\bar{\varepsilon}_{\mathbf{k}}^{c(f)} = \varepsilon_{\mathbf{k}}^{c(f)} + U n^{f(c)} \quad (7)$$

with $n^f = \frac{1}{N} \sum_{\mathbf{k}} \langle f_{\mathbf{k}}^\dagger f_{\mathbf{k}} \rangle$; $n^c = \frac{1}{N} \sum_{\mathbf{k}} \langle c_{\mathbf{k}}^\dagger c_{\mathbf{k}} \rangle$ are the densities of f - and c - electrons, respectively, where

$$\begin{aligned} \langle c_{\mathbf{k}}^\dagger c_{\mathbf{k}} \rangle &= \frac{1}{1 + e^{\beta \bar{\varepsilon}_{\mathbf{k}}^c}} = n_F(\bar{\varepsilon}_{\mathbf{k}}^c) \\ \langle f_{\mathbf{k}}^\dagger f_{\mathbf{k}} \rangle &= \frac{1}{1 + e^{\beta \bar{\varepsilon}_{\mathbf{k}}^f}} = n_F(\bar{\varepsilon}_{\mathbf{k}}^f) \end{aligned} \quad (8)$$

Here, $n_F(\varepsilon)$ is the Fermi-Dirac distribution function $n_F(\varepsilon) = \frac{1}{1 + e^{\beta \varepsilon}}$ with $\beta = 1/T$ being the inverse of the temperature.

In effective Hamiltonian (6), Λ is an additional field, reads

$$\Lambda = -\frac{U}{N} \sum_{\mathbf{k}} \langle c_{\mathbf{k}+\mathbf{q}}^\dagger f_{\mathbf{k}} \rangle \quad (9)$$

acts as an order parameter of the EI state. In previous letters, we addressed the EI phase diagrams and also the BCS-BEC crossover in the exciton systems via investigating the properties of the EI order parameter [17-19]. In this paper, we analyze the excitonic susceptibility creating an electron-hole excitation with momentum \mathbf{q} in the system. The excitonic susceptibility function in momentum space is defined

$$\chi(\mathbf{q}, \omega) = -\frac{1}{N} \sum_{\mathbf{k}, \mathbf{k}'} \langle \langle f_{\mathbf{k}}^\dagger c_{\mathbf{k}+\mathbf{q}}; c_{\mathbf{k}'+\mathbf{q}}^\dagger f_{\mathbf{k}'} \rangle \rangle_{(\omega)} \quad (10)$$

Using Hamiltonian (1) and writing the equation of motion for two-particle Green's function, we get

$$\begin{aligned} \omega \langle \langle f_{\mathbf{k}}^\dagger c_{\mathbf{k}+\mathbf{q}}; c_{\mathbf{k}'+\mathbf{q}}^\dagger f_{\mathbf{k}'} \rangle \rangle_{(\omega)} &= \langle n_{\mathbf{k}}^f \rangle - \langle n_{\mathbf{k}+\mathbf{q}}^c \rangle \\ &+ (\varepsilon_{\mathbf{k}+\mathbf{q}}^c - \varepsilon_{\mathbf{k}}^f) \langle \langle f_{\mathbf{k}}^\dagger c_{\mathbf{k}+\mathbf{q}}; c_{\mathbf{k}'+\mathbf{q}}^\dagger f_{\mathbf{k}'} \rangle \rangle_{(\omega)} \\ -\frac{U}{N} \sum_{\mathbf{k}_1, \mathbf{q}_1} \langle \langle (f_{\mathbf{k}}^\dagger c_{\mathbf{k}_1} f_{\mathbf{k}_1-\mathbf{q}_1}^\dagger f_{\mathbf{k}+\mathbf{q}-\mathbf{q}_1} - c_{\mathbf{k}+\mathbf{q}_1}^\dagger c_{\mathbf{k}_1} f_{\mathbf{k}_1-\mathbf{q}_1}^\dagger c_{\mathbf{k}+\mathbf{q}}); c_{\mathbf{k}'+\mathbf{q}}^\dagger f_{\mathbf{k}'} \rangle \rangle_{(\omega)} \end{aligned} \quad (11)$$

According to the principles of Hartree-Fock approximation, the excess operators in the higher order Green's functions are replaced by averages:

$$\begin{aligned} &\sum_{\mathbf{k}_1, \mathbf{q}_1} \langle \langle f_{\mathbf{k}}^\dagger c_{\mathbf{k}_1} f_{\mathbf{k}_1-\mathbf{q}_1}^\dagger f_{\mathbf{k}+\mathbf{q}-\mathbf{q}_1}; c_{\mathbf{k}'+\mathbf{q}}^\dagger f_{\mathbf{k}'} \rangle \rangle_{(\omega)} \\ &= \sum_{\mathbf{q}_1} \langle n_{\mathbf{k}+\mathbf{q}-\mathbf{q}_1}^f \rangle \langle \langle f_{\mathbf{k}}^\dagger c_{\mathbf{k}+\mathbf{q}}; c_{\mathbf{k}'+\mathbf{q}}^\dagger f_{\mathbf{k}'} \rangle \rangle_{(\omega)} \end{aligned} \quad (12)$$

$$\begin{aligned} &-\sum_{\mathbf{k}_2} \langle n_{\mathbf{k}}^f \rangle \langle \langle f_{\mathbf{k}_2}^\dagger c_{\mathbf{k}_2+\mathbf{q}}; c_{\mathbf{k}'+\mathbf{q}}^\dagger f_{\mathbf{k}'} \rangle \rangle_{(\omega)} \\ &\sum_{\mathbf{k}_1, \mathbf{q}_1} \langle \langle c_{\mathbf{k}+\mathbf{q}_1}^\dagger c_{\mathbf{k}_1} f_{\mathbf{k}_1-\mathbf{q}_1}^\dagger c_{\mathbf{k}+\mathbf{q}}; c_{\mathbf{k}'+\mathbf{q}}^\dagger f_{\mathbf{k}'} \rangle \rangle_{(\omega)} \end{aligned} \quad (13)$$

$$= \sum_{\mathbf{q}_1} \langle n_{\mathbf{k}+\mathbf{q}_1}^c \rangle \langle \langle f_{\mathbf{k}}^+ c_{\mathbf{k}+\mathbf{q}}; c_{\mathbf{k}'+\mathbf{q}}^+ f_{\mathbf{k}'} \rangle \rangle_{(\omega)}$$

$$- \sum_{\mathbf{k}_2} \langle n_{\mathbf{k}+\mathbf{q}}^c \rangle \langle \langle f_{\mathbf{k}_2}^+ c_{\mathbf{k}_2+\mathbf{q}}; c_{\mathbf{k}'+\mathbf{q}}^+ f_{\mathbf{k}'} \rangle \rangle_{(\omega)}$$

Replacing Eqs.(12) and (13) into Eq.(11), we obtain

$$(\omega - \omega_{\mathbf{k}}^{cf}(\mathbf{q})) \langle \langle f_{\mathbf{k}}^+ c_{\mathbf{k}+\mathbf{q}}; c_{\mathbf{k}'+\mathbf{q}}^+ f_{\mathbf{k}'} \rangle \rangle_{(\omega)}$$

$$= (\langle n_{\mathbf{k}}^f \rangle - \langle n_{\mathbf{k}+\mathbf{q}}^c \rangle) - \frac{U}{N} (\langle n_{\mathbf{k}}^f \rangle - \langle n_{\mathbf{k}+\mathbf{q}}^c \rangle) \sum_{\mathbf{k}_2} \langle \langle f_{\mathbf{k}_2}^+ c_{\mathbf{k}_2+\mathbf{q}}; c_{\mathbf{k}'+\mathbf{q}}^+ f_{\mathbf{k}'} \rangle \rangle_{(\omega)} \tag{14}$$

with $\omega_{\mathbf{k}}^{cf}(\mathbf{q}) = \bar{\varepsilon}_{\mathbf{k}+\mathbf{q}}^c - \bar{\varepsilon}_{\mathbf{k}}^f$

Finally, we sum over \mathbf{k} Eq. (14) and rename summation indices, the excitonic susceptibility function in Eq. (10) can be written

$$\chi(\mathbf{q}, \omega) = \frac{\chi^0(\mathbf{q}, \omega)}{1 + U\chi^0(\mathbf{q}, \omega)} \tag{15}$$

with

$$\chi^0(\mathbf{q}, \omega) = \frac{1}{N} \sum_{\mathbf{k}} \frac{\langle n_{\mathbf{k}}^f \rangle - \langle n_{\mathbf{k}+\mathbf{q}}^c \rangle}{\omega - \omega_{\mathbf{k}}^{cf}(\mathbf{q})} \tag{16}$$

here $\langle n_{\mathbf{k}}^f \rangle = \langle f_{\mathbf{k}}^\dagger f_{\mathbf{k}} \rangle$ and $\langle n_{\mathbf{k}}^c \rangle = \langle c_{\mathbf{k}}^\dagger c_{\mathbf{k}} \rangle$ have been defined in Eq. (8).

In order to determine the EI phase, we compute the static excitonic susceptibility $\chi(\mathbf{q}, \omega)$ with $\omega = 0$. And in this work, we consider the direct bandgap situation so the order vector of the EI phase as $\mathbf{q} = 0$. Therefore, we focus on the condition for the divergence of the static excitonic susceptibility $\chi_0 = \chi(\mathbf{0}, 0)$ with respect to the temperature and the Coulomb interaction potential.

3. Numerical results and Discussions

To analyze the phase structure of the EI state, in this section, we present numerical results investigating the forming of the EI state in the system caused by the Coulomb interaction and the temperature. The value of excitonic susceptibility represents the exciton fluctuations in the system, in this work, therefore, the formation of the EI phase is indicated by the divergence of the static excitonic susceptibility χ_0 . In doing so, the Eqs. (7), (8), (15) and (16) are solved self-consistently for a system containing $N = 500 \times 500$ lattice sites. The solution of the whole self-consistent calculation is assumed to be achieved if all quantities are determined with a relative error less than 10^{-12} . In our numerical calculation, the results are evaluated in the natural unit system for $\hbar = c = k_B = 1$ and without loss of generality all energies are given in units of the c electron transfer amplitude t^c , i.e., $t^c = 1$. In this work, we choose $\varepsilon^c = 0$ and $t^f = 0.4 < t^c$ to fit the electron system state in rare-earth chalcogenide $\text{TmSe}_{0.45}\text{Te}_{0.55}$.

To discuss the impact of the temperature and the Coulomb interaction on the EI phase structure in the system, firstly, we show in Fig. 1 the dependence of the static excitonic susceptibility χ_0 on the Coulomb interaction U for various values of the temperature T at $\varepsilon^f = -1.5$. We see that the static excitonic susceptibility function only diverges or the EI phase only stabilizes at low temperature. At high temperature such as $T = 0.5$, the bound state of the electron–hole pairs is suppressed by the thermal fluctuations indicated by finite values of the static excitonic susceptibility for all values of U . In other words, at low temperature we always find the divergence of the static excitonic susceptibility at two critical values of the Coulomb interaction U_{c1} and U_{c2} . This means that the EI state only occurs in a confined between two critical values of the Coulomb interaction. Indeed, for $U < U_{c1}$ the weak Coulomb can neither form excitonic bound states nor establish the electron-hole coherence, the system settles in the SM state. Increasing U , the EI phase stabilizes above a critical Coulomb interaction U_{c1} . Similar to some recent studies [18-22], we also yield the upper critical value of the Coulomb interaction U_{c2} , such that the EI phase is confined in between U_{c1} and U_{c2} . As the temperature increases, U_{c1} increases while U_{c2}

decreases, so the window of the EI phase is narrowed. When $U > U_{c2}$, the Hartree shift leads to an electron-hole band splitting, that prevents c - f electron coherence and the system will be stable in the SC state.

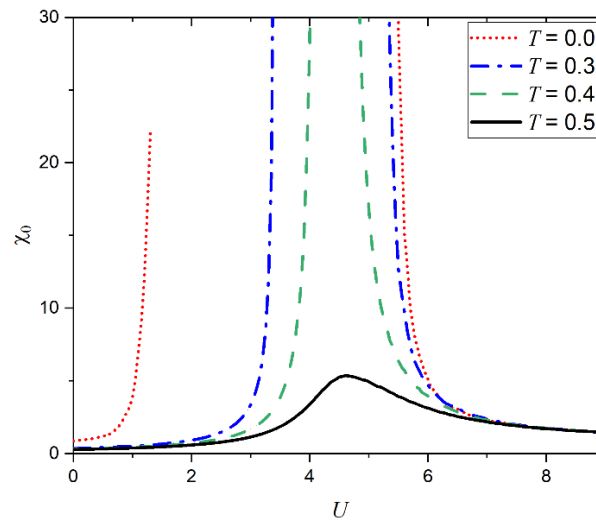


Fig. 1. The static excitonic susceptibility χ_0 as functions of the Coulomb interaction U for several values of temperature T .

Next, we discuss in detail the influence of the temperature on the EI state by investigating the dependence of the static exciton susceptibility function χ_0 on the temperature T for some values of the Coulomb interaction U at $\varepsilon^f = -1.5$ in Fig. 2. In the entire range of Coulomb interactions, we find that at a given Coulomb interaction, the static exciton susceptibility function increases as decreasing temperature. In particular, in low temperature region, the static exciton susceptibility increases strongly and diverges at a critical temperature T_{EI} . This is called the EI phase transition temperature. As $T > T_{EI}$ all excitonic bound states are deformed and the system is in the normal electron–hole liquid state. When $T < T_{EI}$, the system stabilizes in the EI state. Comparing the two panels in Fig. 2 (a and b), we once again affirm that the EI state is only occurred in between two critical values of the Coulomb interaction, a lower critical value U_{c1} and an upper critical value U_{c2} . The diagram also shows that if $U < 3.5$, the EI state exists at low temperature and the critical temperature T_{EI} increases as increasing U (see Fig. 2a), whereas T_{EI} decreases if enlarging from $U = 4.5$ (see Fig. 2b). In particular, if $U < 1.0$ or $U > 5.5$, the value of the static excitonic susceptibility function is so small and remains finite for all T .

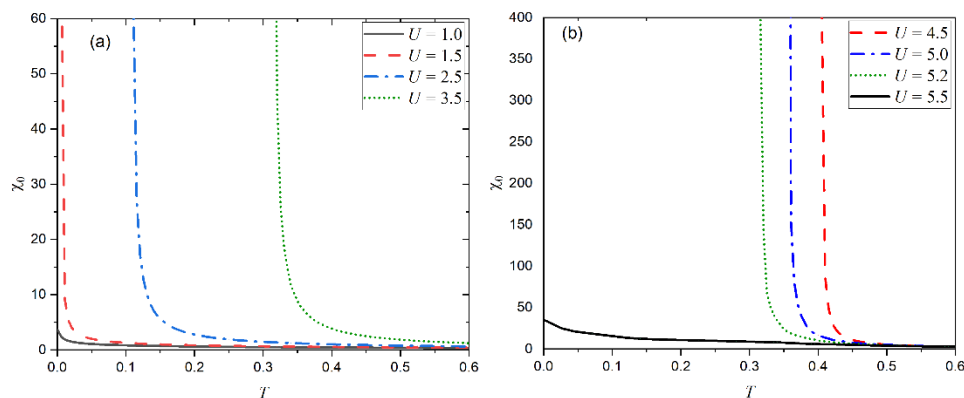


Fig. 2. The static excitonic susceptibility χ_0 as functions of the temperature T for several values of the Coulomb interaction U .

In order to confirm the existence of the EI state depending on the external pressure, we now present in Fig. 3 the static excitonic susceptibility χ_0 as functions of the temperature T for different values of f -electron on-site energy ε^f at the Coulomb interaction $U = 3.5$. Obviously, at a given ε^f , the formation of the EI phase is indicated by the divergence of χ_0 at the critical temperature T_{EI} . The diagram again shows

that the EI phase is only established at sufficiently low temperature. Increasing temperature, the large thermal energy destroys a part of the c - f electron bounding state leading to the EI state is weakened, which is illustrated by a decrease of the χ_0 . As the temperature is larger than the critical temperature T_{EI} , the large thermal fluctuation breaks all the electron–hole couplings and the system settles in the electron–hole plasma liquid, and χ_0 thus becomes insignificant. Fig. 3 also shows that the critical temperature T_{EI} increases when increasing ε^f . Indeed, as ε^f is increased, the overlap between the f -bands and c -bands increases, then some f electrons can be transferred into c -band electrons and exciton bound states may be formed if the Coulomb interaction is sufficiently strong, therefore T_{EI} increases. In fact, the overlap between the energy bands represents the effect of the external pressure on the system. Therefore, increasing ε^f is corresponding to an increase of the external pressure. Our result about the influence of the temperature and the external pressure on the EI state fits quite well with the experimental observation in rare-earth chalcogenide $\text{TmSe}_{0.45}\text{Te}_{0.55}$ of P. Wachter [23]. At sufficiently large pressure, $4f$ - and $5d$ -bands overlap, then electrons from the f -band, which have been thermally excited into the $5d$ conduction band so $4f$ -holes couple to $5d$ -electrons to form excitons and then they can drop into the EI state if the temperature is sufficiently low.

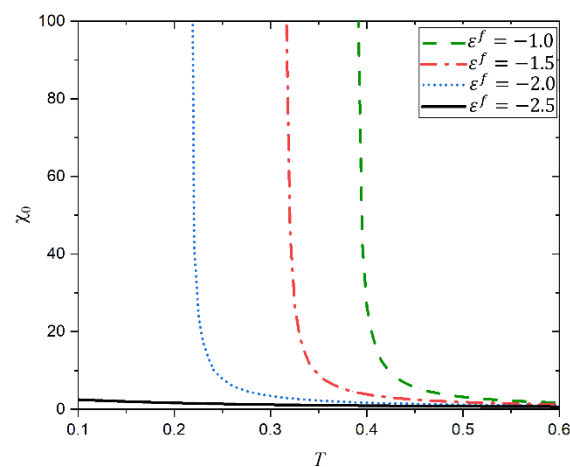


Fig. 3. The static excitonic susceptibility χ_0 as functions of the temperature T for different values of the on-site energy.

4. Conclusions

In this paper, we have adapted the unrestricted Hartree-Fock approximation to the 2D extended Falicov-Kimball model to investigate the EI state in rare-earth chalcogenides via analyzing the static excitonic susceptibility. As functions of model parameters, the phase diagrams of the EI state have been constructed. By analyzing the static excitonic susceptibility, we have found that when decreasing temperature, the exciton fluctuations strongly increase, especially near the temperature of the phase transition. As the temperature is low enough, the static excitonic susceptibility diverges which represents the EI phase transition. The critical temperature of the EI phase transition T_{EI} increases as increasing the Coulomb interaction U in the weak interaction regime. In contrast, T_{EI} decreases as increasing U in the strong Coulomb interaction regime. Our numerical results also have shown that at a given low temperature, the EI phase is found in between two critical values of the Coulomb interaction. When increasing temperature, the EI phase window is narrowed. In particular, the influence of the external pressure on forming of the EI state in the system also has been addressed. The phase diagram indicates that the EI state is formed only if the external pressure is sufficiently large. Considering more meticulously kinetic nature of the EI state in these materials would be a worthwhile goal of our studies in the future.

5. Acknowledgements

This research is funded by the Hanoi University of Mining and Geology, Vietnam, code T21-07.

The paper was presented during the 6th VIET - POL International Conference on Scientific-Research Cooperation between Vietnam and Poland, 10-14.11.2021, HUMG, Hanoi, Vietnam.

6. References

1. Mott, N.F., 1961. The transition to the metallic state. *Philosophical Magazine*, 6(62): 287-309, <https://doi.org/10.1080/14786436108243318>.
2. Knox, R., *Theory of excitons*, in *Solid State Physics*, edited by Seitz F. and Turnbull D., Academic Press, New York, 1963.
3. Kohn, W., *Metals and insulator in Many Body Physics*, edited by DeWitt C. & Balian R., Gordon & Breach, New York, 1968.
4. Moskalenko, S.A., Snoke, D.W., 2000. *Bose-Einstein Condensation of Excitons and Biexcitons*. Cambridge University Press, <https://doi.org/10.1017/CBO9780511721687>.
5. Neuenschwander, J., & Wachter, P., 1990. Pressure-driven semiconductor-metal transition in intermediate-valence $\text{TmSe}_{1-x}\text{Te}_x$ and the concept of an excitonic insulator. *Physical Review B*, 41(18), 12693, <https://doi.org/10.1103/PhysRevB.41.12693>.
6. Wachter, P., Bucher, B., & Malar, J., 2004. Possibility of a superfluid phase in a Bose condensed excitonic state. *Physical Review B*, 69(9): 094502, <https://doi.org/10.1103/PhysRevB.69.094502>.
7. Bucher, B., Park, T., Thompson, J.D., & Wachter, P., 2008. Thermodynamical Signatures of an Excitonic Insulator, Eprint arXiv:0802.3354.
8. Kogar, A., Rak, M.S., Vig, S., Husain, A.A., Flicker, F., Joe, Y.I., Venema, L., MacDougall, G.J., Chiang, T.C., Fradkin, E., et al., 2017. Signatures of exciton condensation in a transition metal dichalcogenide. *Science*, 358(6368): 1314 – 1317, <https://doi.org/10.1126/science.aam6432>.
9. Larkin, T.I., Yaresko, A.N., Pröpper, D., Kikoin, K.A., Lu, Y.F., Takayama, T., Mathis, Y.-L., Rost, A.W., Takagi, H., Keimer, B., & Boris A.V., 2017. Giant exciton Fano resonance in quasi-one-dimensional Ta_2NiSe_5 . *Physical Review B*, 95(19): 195144, <https://doi.org/10.1103/PhysRevB.95.195144>.
10. Lu, Y.F., Kono, H., Larkin, T.I., Rost, A.W., Takayama, T., Boris, A.V., Keimer, B. & Takagi, H., 2017. Zero-gap semiconductor to excitonic insulator transition in Ta_2NiSe_5 . *Nature Communication*, 8, 14408, <https://doi.org/10.1038/ncomms14408>.
11. Ihle, D., Pfafferoth, M., Burovski, E., Bronold, F.X., and Fehske, H., 2008. Bound state formation and the nature of the excitonic insulator phase in the extended Falicov-Kimball model. *Physical Review B*, 78(19): 193103, <https://doi.org/10.1103/PhysRevB.78.193103>.
12. Zenker, B., Fehske, H., & Batista C.D., 2010. Competing chiral and multipolar electric phases in the extended Falicov-Kimball model. *Physical Review B*, 82(16): 165110, <https://doi.org/10.1103/PhysRevB.82.165110>
13. Sugimoto, K., Satoshi, N., Tatsuya, K., & Yukinori, O., 2018. Strong Coupling Nature of the Excitonic Insulator State in Ta_2NiSe_5 . *Physical Review letter*, 120(24): 247602, <https://doi.org/10.1103/PhysRevLett.120.247602>.
14. Lee, J., Kang, C.J., Man, J.E., Jun, S.K., Byung, M., & Han, W.Y., 2019. Strong interband interaction in the excitonic insulator phase of Ta_2NiSe_5 . *Physical Review B*, 99(7): 075408, <https://doi.org/10.1103/PhysRevB.99.075408>.
15. Bronold, F.X., & Fehske, H., 2006. Possibility of an excitonic insulator at the semiconductor-semimetal transition. *Physical Review B*, 74(16): 165107, <https://doi.org/10.1103/PhysRevB.74.165107>.
16. Thang, D.V., Thao, D.T.X., 2012. Study the effect of rare earths Sm over physical $\text{Bi}_{1-x}\text{Sm}_x\text{FeO}_3$ of materials. *Journal of Mining and Earth Science*, 37, 86-91.
17. Hai, D.T.H., Nha, N.H., Giang, N.T., & Nham, P.V., 2016. Temperature effects in excitonic condensation driven by the lattice distortion. *Physica Status Solidi B*, 253(6): 1210-1216, <https://doi.org/10.1002/pssb.201552745>.
18. Hai, D.T.H., Hoi, B.D., & Nham, P.V., 2017. Phonon effects in the excitonic condensation induced in the extended Falicov-Kimball model, *Europhysics Letters*, 119, 47003,

<https://doi.org/10.1209/0295-5075/119/47003>

19. Hai, D.T.H., Nha, N.H., & Nham, P.V., 2019. Thermal Fluctuations in the Phase Structure of the Excitonic Insulator Charge Density Wave State in the Extended Falicov-Kimball Model, *Journal of Electronic Materials*, 48, 2677, <https://doi.org/10.1007/s11664-018-06904-x>.
20. Phan, N.V., Becker, K.W., & Fehske, H., 2010. Spectral signatures of the BCS-BEC crossover in the excitonic insulator phase of the extended Falicov-Kimball model. *Physical Review B*, 81(20), 205117, <https://doi.org/10.1103/PhysRevB.81.205117>.
21. Zenker, B., Ihle, D., Bronold, F.X. & Fehske, H., 2010. Existence of excitonic insulator phase in the extended Falicov-Kimball model: SO(2)-invariant slave-boson approach. *Physical Review B*, 81(11): 115-122, <https://doi.org/10.1103/PhysRevB.81.115122>.
22. Phan, N.V., Fehske, H. & Becker, K.W., 2011. Excitonic resonances in the 2D extended Falicov-Kimball model. *Euro Physics Letter*, 959(1): 17006, <https://doi.org/10.1209/0295-5075/95/17006>.
23. Wachter, P., 2018. Exciton Condensation and Superfluidity in TmSe_{0.45}Te_{0.55}. *Advances in Materials Physics and Chemistry*, 8(3): 120-142, <https://doi.org/10.4236/ampc.2018.83009>.

Geotechnical Properties of Soft Marine Soil at Chan May Port, Vietnam

NGUYEN Thi Nu^{1,*}, NGUYEN Thanh Duong¹, BUI Truong Son¹

¹ Hanoi University of Mining and Geology, 18 Vien street, Hanoi, Vietnam

Corresponding author: nguyenthinu@humg.edu.vn

Abstract. Soft marine soil deposit is distributed under the sea with many special properties. This type of soil is rarely researched in Vietnam because of the difficult geotechnical investigation under the sea level. In this paper, the experimental laboratories were performed to investigate the geotechnical properties of soft marine soil at Chan May port, Vietnam. The field investigation results indicate that the thickness of soft soil varies from a few meters to more than ten meters. Soft soil has a high value of water content, void ratio, and compressibility and a low value of shear strength. The compression index has a good relationship with water content, liquid limit, and dry unit weight. The unit weight, shear strength, and pre-consolidation pressure increase with the increase of depth. These results show that the soil in the study area is unfavorable for construction activities.

Keywords: Geotechnical properties, Soft marine soil, Chan May port

1. Introduction

Chan May Port located in the Chan May embayment, Loc Vinh commune, Phu Loc district, Thua Thien Hue province, Viet Nam (Fig. 1). As reported, Chan May embayment has undergone some progradation stages. Between 6000 and 4000 years ago, the progradation rate is rather fast at around 2.3-2.7 m/year, but it is reduced in the range of 1.3-1.5 m/year from 4000 to 2000 years ago. In the past 2000 years, the rate of coastal progradation is slow at 0.6-0.7 m/year, and it now might be stopped [1]. The Chan May port project includes many items and can be faced with many challenges because the foundation is constructed under sea level [2]. The soft soil distributes at an elevation from -13.0 m, and the thickness of soft soil varies from few meters to more than ten meters. Therefore, it is necessary to research the properties of soft marine soil for construction works at Chan May Port.

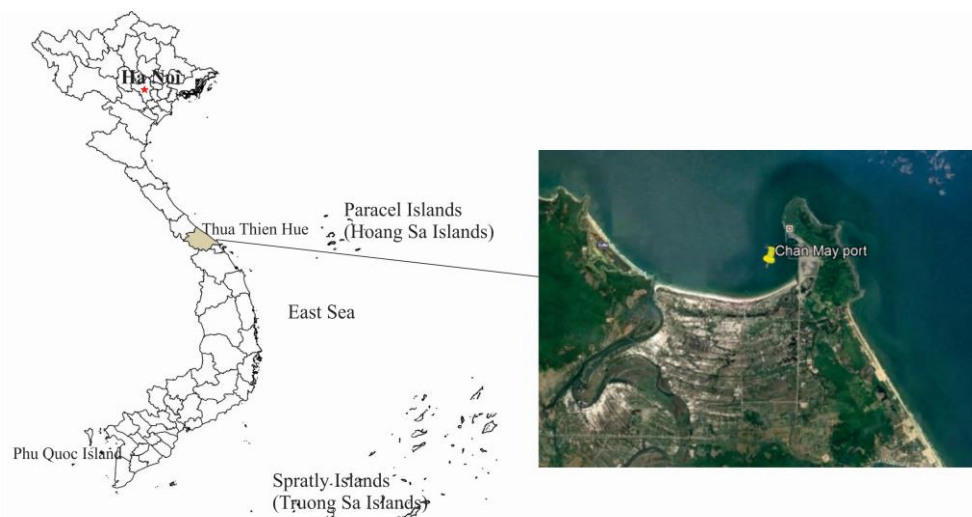


Fig. 1. The study location.

The mineral compositions of marine clays distributed in different areas have been investigated [3, 4, 5, 6, 7, 8, 9,10]. In general, these previous studies showed that the mineral compositions of marine clays depend on the location, the distribution depth, and the age of deposits. Besides mineral compositions, the geotechnical properties of soft marine soil have been studied by some researchers. Chu et al. [11] indicated that the vertical coefficient of consolidation of Singapore marine clay changed from 0.5 m²/year to 2.0 m²/year. The relationship between compression index and water content of marine clay in Northwestern Peninsular Malaysia has been studied by Oh et al. [12]. Miao and Kavazanjian [13] showed that the ratio C_a/C_c of Jiangsu soft marine clay was constant. Ahmad and Harahap [14] investigated some properties of

marine clays in Malaysia and indicated that the compression index varied from 0.177 to 0.797. The undrained shear strengths of marine clay in Singapore and the eastern coast of India were investigated by Arulrajah et al. [15] and Basack and Purkayastha[16], respectively.

From the literature review, the geotechnical properties of some soft marine soil types have been clarified. However, the marine soil distributed under the sea with many special properties needs to be further investigated. In Vietnam, some authors studied the geotechnical properties of soft soil [17-21]. In which, Oanh [21] investigated the undrained shear strength and consolidation yield stress of soft clay distributed in three sites along the coastal area of Vietnam. The research has indicated the suitable methods for the determination of the two parameters for soft soil improvement works. However, the properties of marine soil have not been widely investigated. Thus, this research will focus on soft soil's composition and some physicommechanical properties under the sea at Chan May port. Besides the relationship between physical properties and consolidation parameters, physical properties, and shear strength of soil, the change of soil properties with depth will be discussed.

2. Materials and Methods

In order to investigate the soil profiles, soil samples at different depths were taken from seven boreholes at Chan May port. Based on the soil description, the soft soil at this location is exposed on the seabed, which belongs to the Phu Vang formation. The thickness of the soft layer varies from 4.70 m to 11.6 m. Nineteen soft soil samples were collected from these boreholes to determine the physicommechanical properties. High-quality samples were taken using a thin-walled sampler at different depths (Fig. 2). The SPT values changed from 0 to 2 (blows). Thus, the soil is in a very soft state.

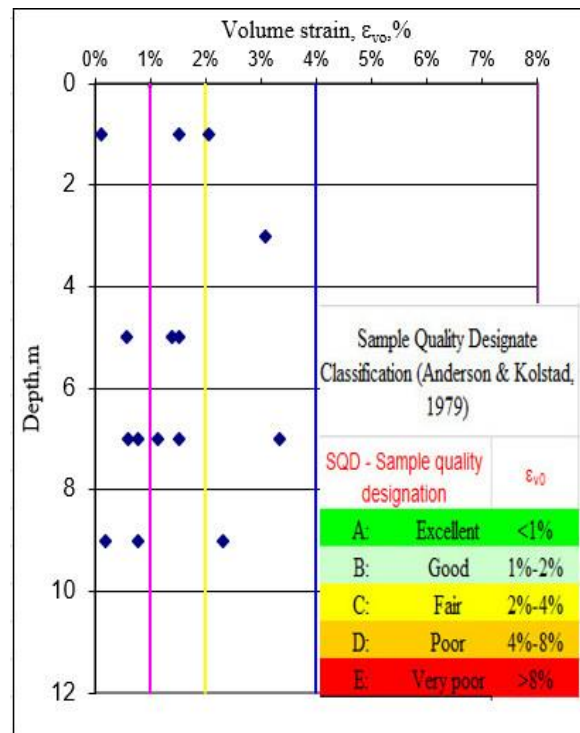


Fig. 2. The quality of the sample in this study.

In this study, particle size analysis and Atterberg limits of soil were determined according to *ASTM D7928 -16e and D6913-17*, *ASTM D4318-17*, respectively. The oedometer tests to determine the consolidation parameters were performed according to the *ASTM D2485-18* standard. The undrained unconsolidated triaxial compression test (*UU*) and unconfined compression test (*Qu* test) were used for determining the undrained cohesion force and undrained friction angle in accordance with *ASTM D2850-15*, *ASTM D 2166 -16* in respective. Finally, the undrained consolidated triaxial compression test (*CU*) was performed in accordance with *ASTM D4767-11* to determine the effective cohesion force and effective friction angle.

3. Results and discussions

3.1 Compositions and physical properties of soft marine soil

Fig. 3 shows the variation of particle size, salt content, organic matter, water content, wet unit weight, and void ratio with increasing depth from 0 to 11m. It can be seen that the salt content varies from 0.2% to 3.1%, with a mean value of 1.1%. The soft soil can be classified as low - saline to high - saline soil [17]. The organic matter content is smaller than 10% and changes from 0.2% to 8.0%, with an average value of 3.5%. As compared with the soft soil distributed in the coastal province of Mekong delta published in Nu et al. [17, 18, 19], the very soft soil in the study area contains a smaller organic matter content and higher salt content. The high salt content in soft soil at Chan May port can be caused by the distribution of soft soil. This very soft soil is distributed under the sea, and it will be affected by seawater.

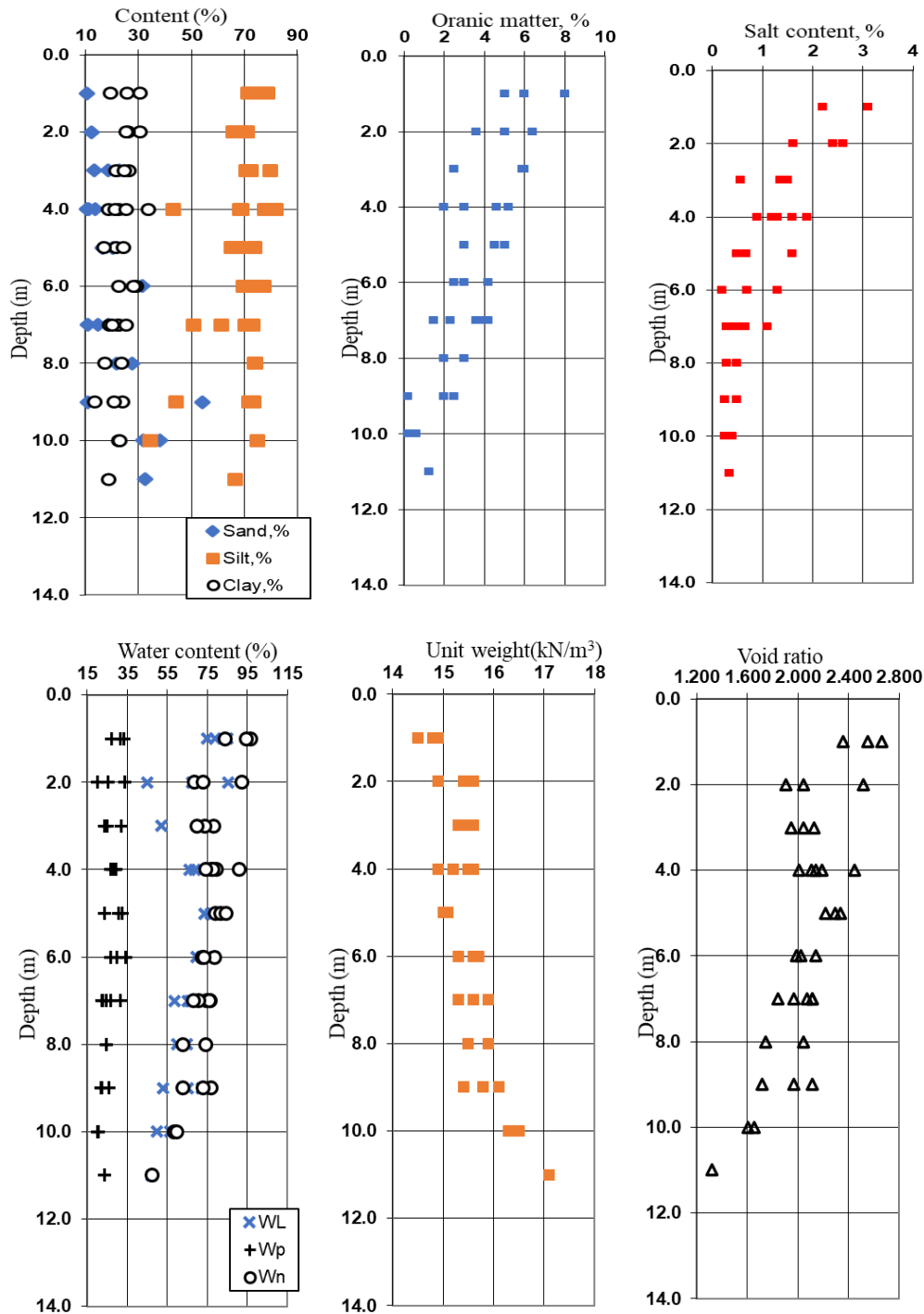


Fig. 3. The variation of soft marine soil properties with depth.

As shown in Fig. 3, the particle size results show that the silt content is highest and varies from 34.3% to 81.7%. The clay content (<0.002 mm) is less than 40% and changes from 13.6% to 33.9%. The sand content significantly varies from 5.3% to 54.2%.

Fig. 3 also shows that the natural water content is higher than the liquid limit, and the soil is very soft. The natural water content varies from 47.2% to 96.4% and tends to decrease with increasing depth. Whereas the unit weight changes from 14.5 kN/m³ to 17.1 kN/m³ and increases with increasing depth. The void ratio is high and changes from 1.319 to 2.662. As compared with [13], the clay and silt contents, the natural water content, the liquid limit of soil in the study area are higher than those of Malaysia marine clays. However, these properties are smaller than those of some other marine clays [3, 22]

3.2 Consolidation properties of soft marine soil

Fifteen oedometer tests were performed to determine the consolidation properties of soft soil and are presented in Figs. 4-6. The soil samples were subjected to pressure levels of 12.5, 25, 50, 100, 200, and 400 kPa. From experimental results, it can be shown that the compression index changes from 0.404 to 0.754, the average value of C_c is 0.671. The swelling index varies from 0.05 to 0.139, with a mean value of 0.112. The compression and swelling indices are higher than those of some other marine clays [14]. The ratios of C_s/C_c range from 0.099 to 0.197. The pre-consolidation pressures (P_c) are determined by the Casagrande method and are plotted in Figure 6, with the values of P_c changing from 10 to 65 kPa. The over consolidation ratio (OCR) equals 1.0, and it can be seen that the soil belongs to normally consolidated soil.

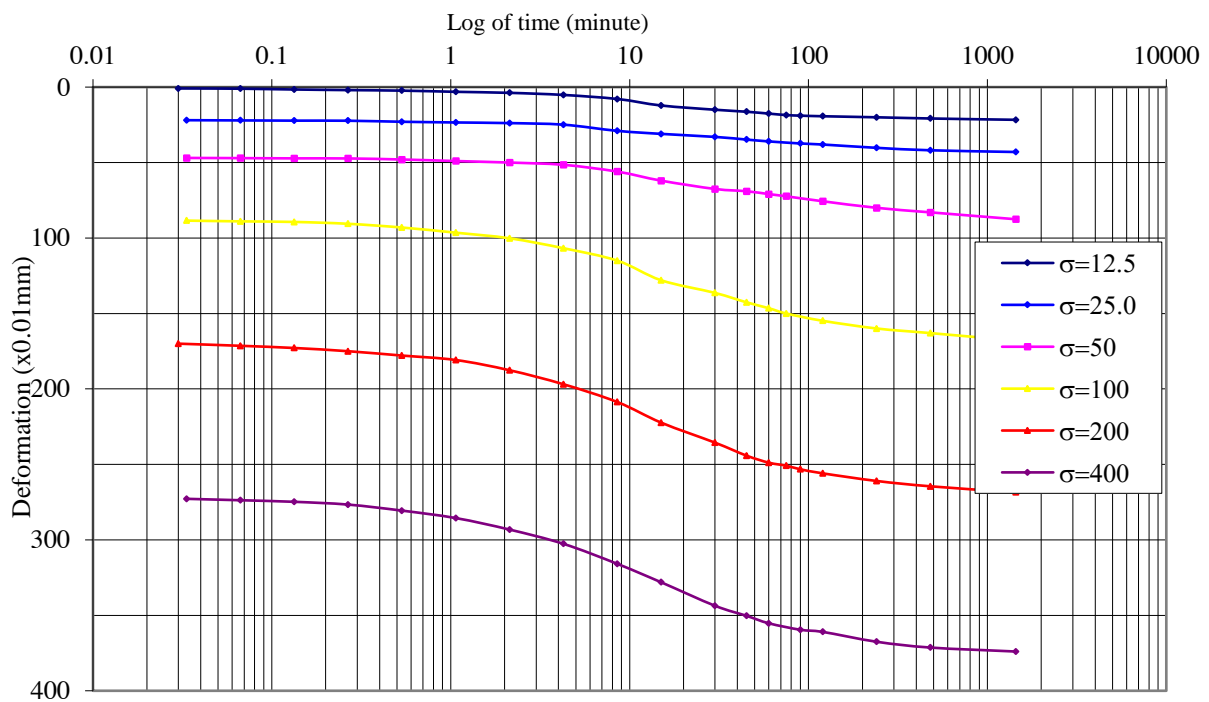


Fig. 4. S-log (t) curve.

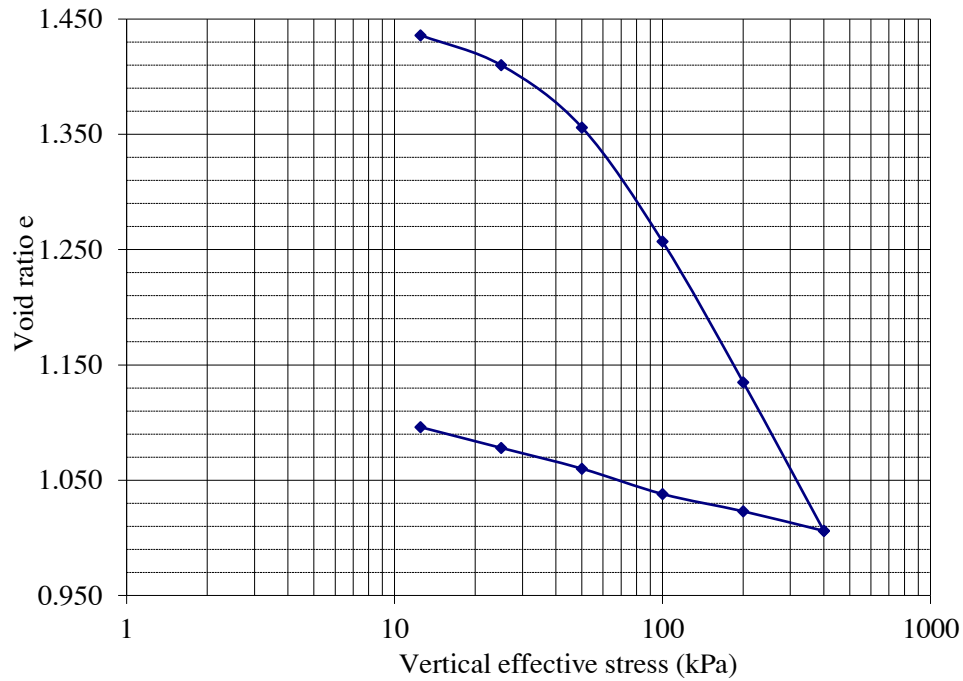


Fig. 5. Effective stress – Void ratio curve.

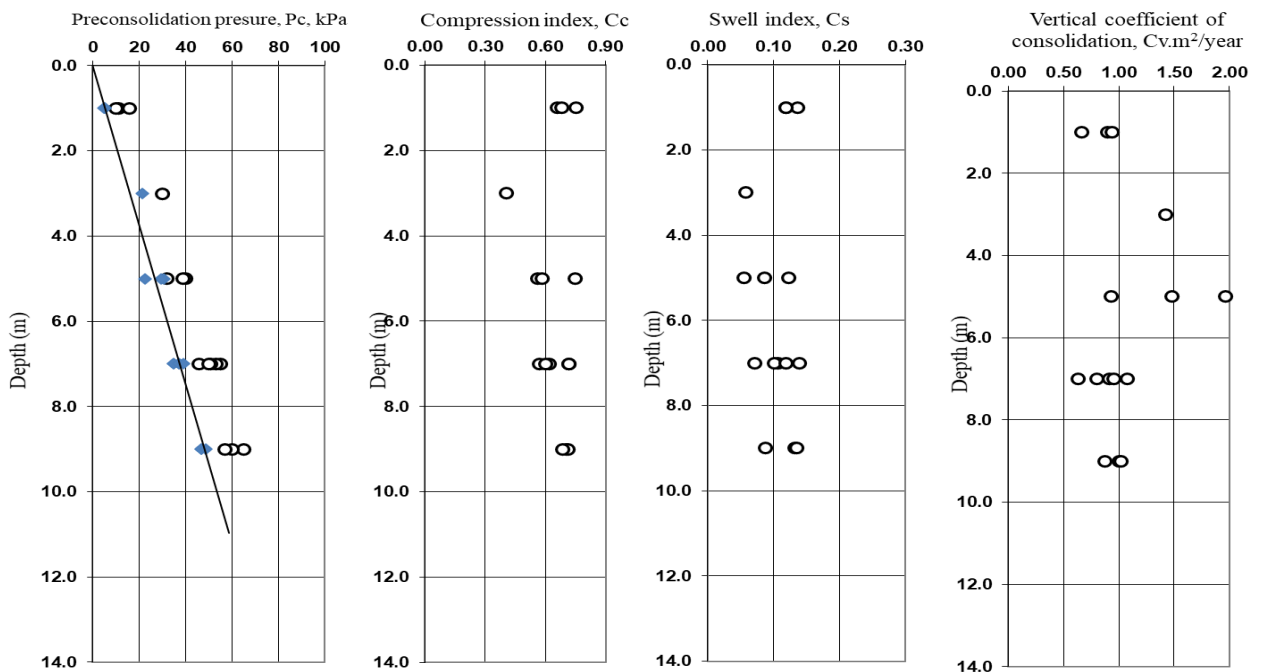


Fig. 6. The variation of consolidation properties of soft soil with depth.

In order to clarify the effect of the physical properties of soft soil on the compression index, the relationship between them was established. These relationships are shown in Fig. 7. As shown, the compression index has a good relationship with water content, void ratio, liquid limit, and dry unit weight with high correlation coefficients (R^2). The increase in water content, void ratio, liquid limit, and decrease in dry unit weight result in an increase in a compression index. Regarding the correlation between C_c and LL of marine clay, Liu et al. [5] established the relationship between compression index and liquid limit of Lianyungang marine clay by equation $C_c = 0.015 (LL - 14)$. For soft clay in Vietnam, Luan et al. (2021) [20] indicated the equation $C_c = 1.6728LL - 0.1888$ for Ho Chi Minh soft clay. This indicated that the correlation between C_c and LL depends on each type of clay, and it cannot be generalized for all types of clay.

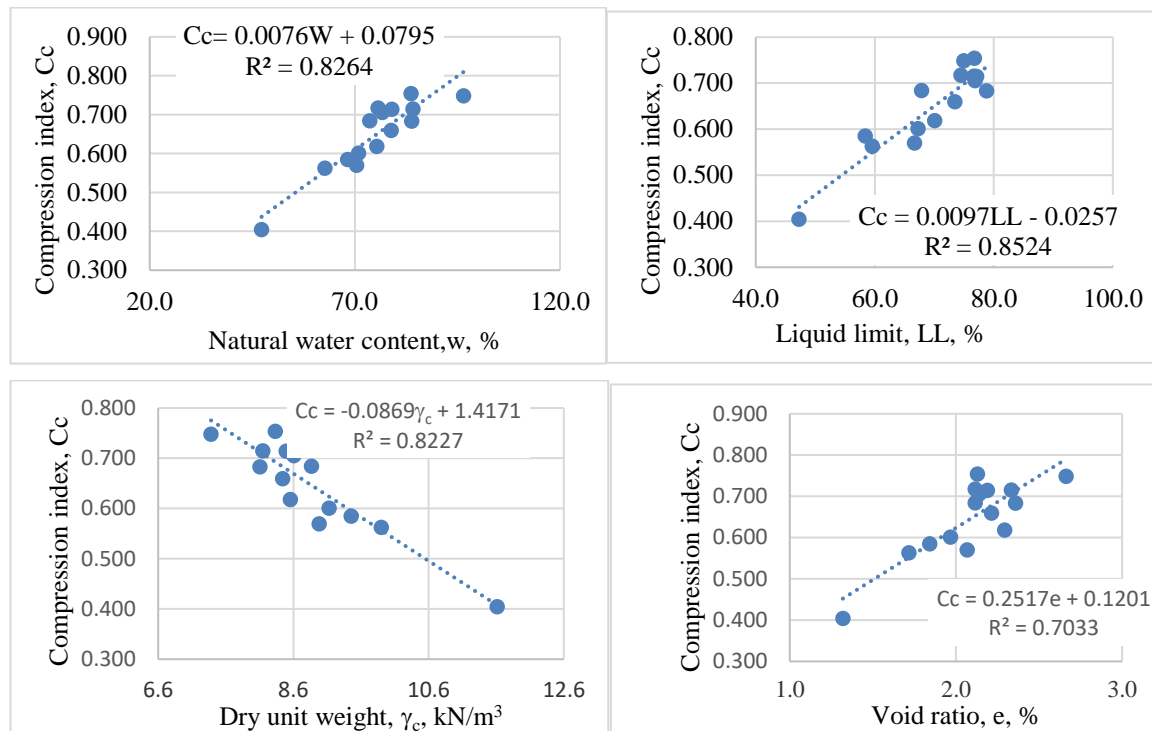


Fig. 7. The relationship between compression index and physical properties of soft marine soil.

3.3 Shear strength of soft marine soil

In this study, the unconfined compression test (Fig. 8a) and UU triaxial test (Fig. 8b) were conducted to determine the undrained shear strength. The test results show that the unconfined compression strength (q_u) is small and varies from 6.06 kPa to 13.76 kPa with the mean value of 8.49 kPa (Fig. 10a). The unconfined compression strength (q_u) increases with increasing depth. It is consistent with the change of physical properties of soil. With increasing depth, the dry unit weight increases, the natural water content decreases, and results in an increase in unconfined shear strength (q_u). Undrained shear strength of soft soil determined from the UU test changes from 3.01 kPa to 11.08 kPa with an average value of 5.16 kPa (Fig. 10b).

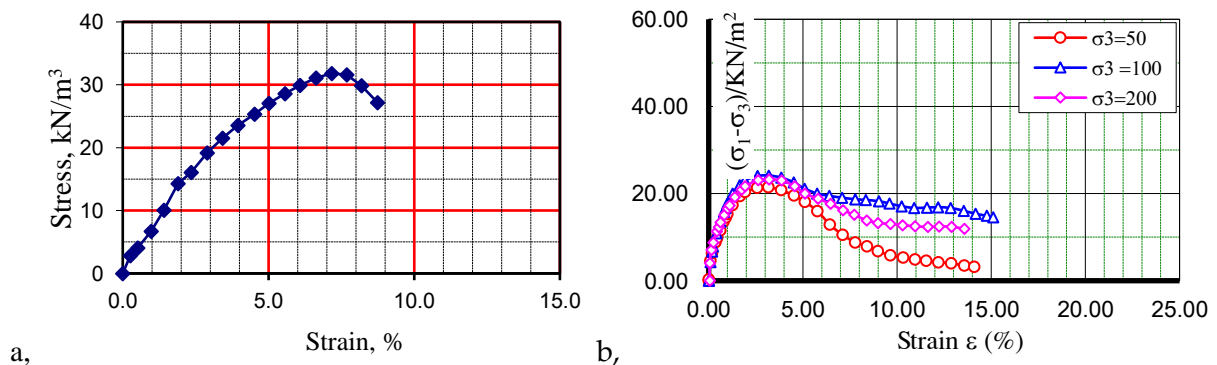


Fig. 8. The stress-strain curves from UCS test (a) and UU test (b).

From CU triaxial compression test (Fig. 9), the effective friction angle of soft marine clay varies from $18^{\circ}50'$ to $24^{\circ}38'$ with the mean value of $22^{\circ}05'$, and effective cohesion changes from 3.44 kPa to 11.0 kPa with an average value of 7.8 kPa. The total cohesion (C_{cu}) and friction angle changes from 5.0 kPa to 15.2 kPa and from $4^{\circ}04'$ to $15^{\circ}08'$ with the average values of 10.30 kPa and $9^{\circ}35'$, respectively. The experimental results indicated that the marine soil belongs to very soft soil and is unfavorable for construction activities such as dredging, excavation. As shown in Fig. 10c, the undrained shear strengths tend to increase with increasing depth. Lumb et al. [23] used vane shear tests, unconfined compression tests, and undrained triaxial tests to determine the undrained shear strength of soft marine clay from Hong Kong and also

indicated that the undisturbed shear strength of the uniform clay increases linearly with depth.

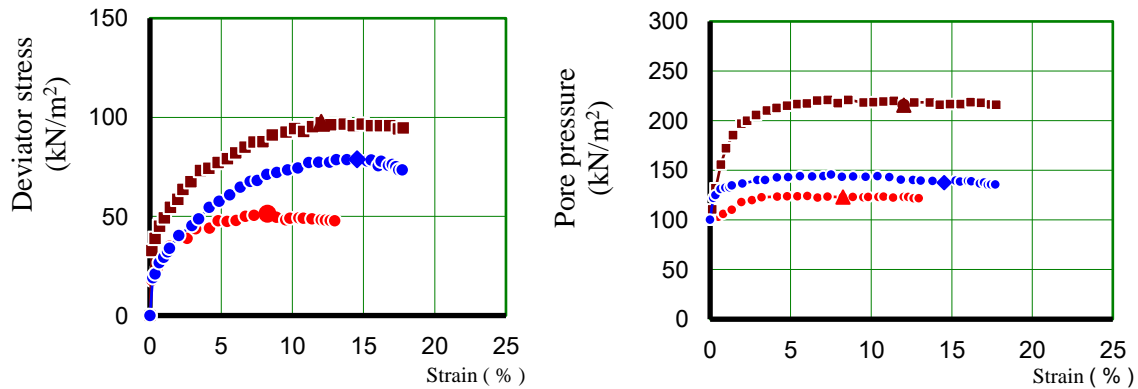


Fig. 9. The stress-strain and pore pressure-strain curves from the CU test.

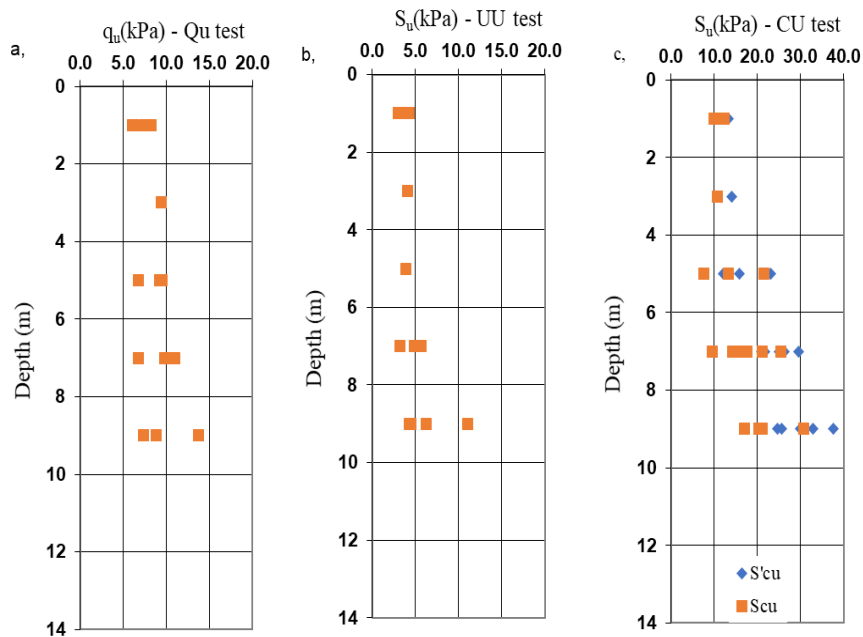


Fig. 10. The variation of unconfined compression strength (a), undrained shear strength – UU test (b), shear strength - CU test (c) of soft marine soil with depth.

Fig. 11 also shows that the relationship between undrained shear strength (S_u) from the UU test and Liquid limit (LL). As shown, this relationship has a high correlation coefficient (R^2). The increase in liquid limit results in an increase in undrained shear strength (S_u).

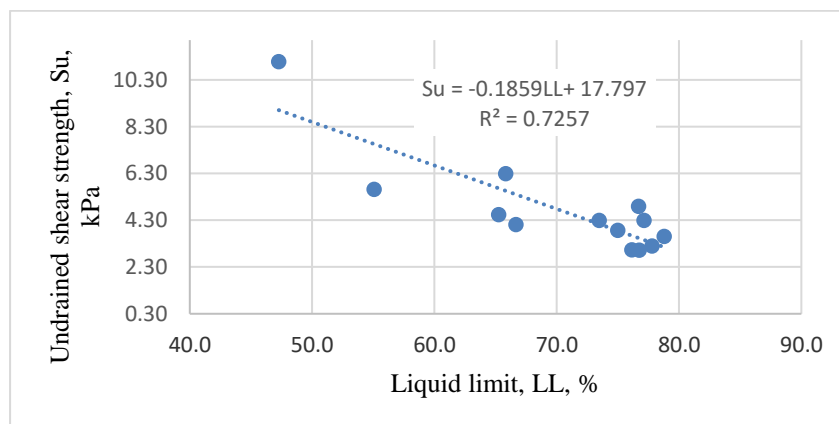


Fig. 11. The relationship between compression index and physical properties of soft marine soil.

4. Conclusions

Based on the experimental results, some conclusions can be made as follows:

- Soft marine soil has high water content, void ratio, and compressibility, and low shear strength.
- The compression index has a good relationship with water content, void ratio, liquid limit, and dry unit weight. The increase in water content, void ratio, liquid limit, and decrease in dry unit weight leads to an increase in a compression index.
- The undrained shear strength is also related to the liquid limit. The decrease in liquid limit results in increasing of undrained shear strength.
- The properties of soft soil change with increasing depth. Accordingly, the water content, void ratio, and liquid limit decrease while the dry unit weight, the undrained shear strength increase with the increasing of depth.

5. Acknowledgments

We would like to thank the Hanoi University of Mining and Geology for the provision of laboratory facilities used in this work.

The paper was presented during the 6th VIET - POL International Conference on Scientific-Research Cooperation between Vietnam and Poland, 10-14.11.2021, HUMG, Hanoi, Vietnam.

6. References

1. Gouramanis, C., Switzer, A.D., Bristow, C.S., Pham, D.T., Mauz, B., Hoang, Q.D., Lam, D.D., Lee, Y.S., Soria, J.L.A., Pile, J., Chi, N.T.K., Nghiem, D., Sloss, C., 2020. Holocene evolution of the Chan May coastal embayment, central Vietnam: Changing coastal dynamics associated with decreasing rates of progradation possibly forced by mid-to late-Holocene sea-level changes. *Geomorphology* 367.
2. Nu, N.T, Son, B.T, Dung, T.L., 2020. The potential of using fine rock for replacing soft soil in construction of abreakwater at Chan May port. *Journal of Mining and Earth Sciences*. 61(4):75-85.
3. Al-Bared, M.A.M, Marto, A., 2017. A review on the geotechnical and engineering characteristics of marine clay and the modern methods of improvements. *Malaysian Journal of Fundamental and Applied Sciences*, 13(4): 825-831.
4. Egashira, K., Ohtsubo, M., 1982. Smectite in marine quick-clays of Japan. *Clays and Clay Miner.* 30(4): 275–280.
5. Liu, S.Y., Shao, G.H., Du, Y.J., Cai, G.J., 2011. Depositional and geotechnical properties of marine clays in Lianyungang, China. *Eng. Geol.* 121, 66–74.
6. Rajasekarana. R, .K, Srinivasaraghavan, R., 1998. Microfabric, chemical and mineralogical study of Indian marine clays. *Ocean Engineering*, 26 (5): 463-483.
7. Rajasekaran, G., Rao, S.N., 2002. Compressibility behaviour of lime-treated marine clay. *Ocean Eng.* 29: 545–559.
8. Yunus, M.N., Marto, A., Pakir, F., Kasran, K., Azri, M. A., Jusoh, S.N., 2015. Performance of lime-treated marine clay on strength and compressibility characteristics. *Inter. J. Geomate*. 8(2): 1232–1238.
9. Bo, M.W., Arulrajah, A., Sukmak, P., Horpibulsuk, S., 2015. Mineralogy and geotechnical properties of Singapore marine clay at Changi. *Soils and Found.* 55(3): 600–613.
10. Nu, N.T., Duong, N.T, Phong, N.V., 2020. The effects of salt contents on the geotechnical properties of some soft soils in the coastal area of Vietnam. *Journal of Mining and Earth Sciences*. 60(6):51-60.

11. Chu, J., Bo, M.W., Chang, M.F., and Choa, V., 2002. Consolidation and permeability properties of Singapore marine clay. *Journal of Geotechnical and Geoenvironmental Engineering*, 128(9): 724 – 732.
12. Oh, E.Y.N., and Chai, G.W.K. Characterization of marine clay for road embankment design in coastal area. *Proceedings of the sixteenth International Offshore and Polar Engineering Conference*. 7–10. 2006.
13. Miao, L., and Kavazanjian, E., 2007. Secondary Compression Features of Jiangsu Soft Marine Clay. *Marine Georesources & Geotechnology* 25 (2): 129–144.
14. Ahmad, N.R., Harahap, I.S.H., 2016. The compression behavior of marine clays in Malaysia. *Proceedings of the 35th International Conference on Ocean, Offshore and Arctic Engineering*. 1–6.
15. Arulrajah, A., Bo, M.W., 2008. Characteristics of Singapore marine clay at Changi. *Geotech. and Geol. Eng.* 26, 431–441.
16. Basack, S., Purkayastha, R.D., 2009. Engineering properties of marine clays from the Eastern coast of India. *J. of Eng. Tech. and Res.* 1(6): 109–114.
17. Nu, N.T., Toan, D.M, Hong, P.T, Son, B.T., 2020. Determination of Particles and Minerals Content in Soft Clay Soil of the Mekong Delta Coastal Provinces, Southern Vietnam for Inorganic Adhesives Stabilization. *Iraqi Journal of Science*, 61(4): 791-804.
18. Nu, N.T, Son, B.T, Ngoc, D.M., 2020. Research on Horizontal Coefficient of Consolidation of Vietnam’s Soft Soil. *Journal of Engineering*, vol. 2020, 13 pages.
19. Ngoc, D.M., Nu, N.T, Toan, D.M, Son, B.T., 2021. Study on Soft Ground Structure in The Mekong Delta Coastal Province, Viet Nam for Embankment Construction. *Journal of Applied Science and Engineering*, 24 (3): 307-314.
20. Luan, V.N, Nu, N.T, Toan, D.M., 2021. Consolidation Properties of Ho Chi Minh City Soil, Vietnam. *Iraqi Geological Journal*, 54 (1A).
21. Oanh, N.C. Undrained shear strength and consolidation yield stress of clay found in three construction sites in Vietnam. *Geotechnics for Sustainable Development - Geotech Hanoi 2013*, 585-591.
22. Zarina Shahri, Chee - Ming Chan. On the Characterization of Dredged Marine Soils from Malaysian Waters: Physical Properties. *Environment and Pollution*; 4(3): 2015.
23. Lumb, P., & Holt, J.K., 1968. The Undrained Shear Strength of a Soft Marine Clay from Hong Kong. *Géotechnique*, 18(1): 25–36. doi:10.1680/geot.1968.18.1.25.

Applying the Lessons Learned from the Economics Nobel Prize 2020 to Land Use Right Auction in Vietnam

PHAM Ngoc Huong Quynh^{1,*}, NGUYEN Thi Ngoc Mai²

¹ VNU University of Economics and Business, Vietnam National University, Hanoi, Vietnam

² National Academy of Public Administration, Hanoi, Vietnam

Corresponding author: quynhpnh@gmail.com

Abstract. This paper mainly relies on qualitative research methodology and secondary data. The paper examines the existing legal framework for land use right auction in Vietnam and its practical implementation, focusing on acquiring agricultural land for non-agricultural purposes. It shows the limitations of sharing information and the disadvantages in distributing and balancing the benefits among different stakeholders who participated in the land use right auction. Also, this paper analyses and propounds the key lessons learned from the 2020 Economics Nobel Prize in creating the information sharing and benefit-sharing mechanism among participants. The paper applies these lessons learned from the 2020 Economics Nobel Prize to create a foundation for policy change the legal regulations of land use right auction in Vietnam in order to bring benefits to households, investors, and the State.

Keywords: Lessons learned, Economics Nobel Prize 2020, Land use right auction, Vietnam

1. Introduction

The 2020 Nobel Prize in Economics acknowledges and honors two economists - Paul Milgrom and Robert Wilson - for their improvements to auction theory and the invention of new auction formats. It advances theory in matching theory, game theory, information in securities markets, and utility pricing. It also has great practical implications for worldwide sellers, buyers, and taxpayers [1].

In Vietnam, private ownership of land is not permitted, the people hold all ownership rights with the State as the administrator, and the laws allow ownership of a right to use land. Consequently, almost all public property auctions in Vietnam are land use right auctions. Land use right auctions are considered one of the basic tools used by the State of Vietnam to allocate and use land more efficiently. Since the economic reform (Doi moi) policy, land use has been affected strongly by industrialization, modernization, and urbanization [2]. The State has implemented the land acquisition and land use right auction policy with the aim to convert a part of agricultural land into the construction of infrastructure, transportation, office buildings, or industrial development, trade and services, and urban and rural residential development [3]. Accordingly, the State acquires land from farming households and then allocates it to different owners through land use right auctions. However, the land use right auction policy has many shortcomings in both policy planning and enforcement [4]. For example, the regulation that the land auction is organized after land acquisition and site clearance is not reasonable; or the starting land price for the auction is usually determined to be lower than the price of the same land sold on the real estate market; or the regulation that farming households whose land is acquired are not involved in land auction is inequity; and the negatives such as “collusion,” “price suppression”, and “price manipulation” appear among auction participants, property owners, and property auction organizations. As a result of the current auction policy and its implementation, the benefit of the farmer whose land is acquired is not possibly ensured, while, except for state budget revenue, most of the profit of land conversion projects belongs to real estate investors [4].

This article examines Vietnam’s land use right auction policy to show the inadequacy in benefit distribution among participating stakeholders, including the State, the farmer households whose land is acquired, and investors whose land is allocated. The scope of this investigation is the project of acquiring agricultural land and converting it to non-agricultural uses. It then proposes applying the main lessons learned from the 2020 Nobel Prize in Economics to revise the legal regulations of land use right auctions in Vietnam to distribute benefits among involved parties better.

2. Materials and Methods

2.1. Literature theories from 2020 Nobel Prize in Economic Sciences

2.1.1. Theory of new format of the auction

Paul Milgrom and Robert Wilson proposed a new form of auction called Simultaneous Multiple Round Auction (SMRA). They have brought theory and practice tightly together. Their invention has established a foundation to train analysts to design new auctions and practitioners to choose wisely among existing auction formats [5].

Through practical observations of “common value”, “personal value” and the behavior of the parties to the auction, Milgrom and Wilson find that the value of an item at auction depends on the value of the same kind elsewhere or in the future [6]. Therefore, two authors have sought to design a suitable auction: a simultaneous multiple-round auction. This allows auctions in different locations to happen simultaneously with low starting prices while participating parties can observe each other’s behavior, reducing information uncertainty. This type of auction can assist buyers, sellers, and businesses participating in the auction in observing and obtaining the best price [7].

In this new auction method, the winning bid is not necessarily the highest selling price nor the lowest buying price. Milgrom and Wilson have incorporated theory and practice closely to answer two of the most fundamental questions in economics: who deserves the goods, and at what affordable price? [8]. Therefore, a good auction must create an information sharing and benefit-sharing mechanism among the participants so that the outcome of auctions can bring benefits to the seller, buyers, taxpayers, and the government.

Thus, the advantage of a multi-session auction form is a mechanism for benefit and information sharing among the auction participants, leading to all of them reaching maximum benefits. In sum, Milgrom and Wilson’s research on auction theory and auction design is highly practical and beneficial for society as a whole [1].

2.1.2. The mechanism for information sharing among participants

Paul Milgrom and Robert Wilson combined the role of information and incentive systems to perfect different auction mechanisms to address the problem of “asymmetric information” in auctions [9]. According to these authors, auction results can be heavily influenced by information [10]. Clearly, the information about the overall value of an item is often unknown and uncertain. Each participant will have different preferences, information, and estimation. When entering the auction, buyers observe, decode signals from the stated prices of others and decide their bid. Each bidder only knows a little bit of information about the value of the item. In the multi-session auction, they can sometimes share information with each other during the auction, and they can even negotiate behind each auction. Therefore, the new auction format has succeeded in creating an information-sharing mechanism among the participants. It can solve the “curse of the winner” to benefit all auction participants [11].

Besides, Milgrom and Wilson have contributed to the notion of affiliation and related concepts to become general tools for finding equilibrium and for carrying out comparative statics [12]. For instance, the monotone likelihood ratio property and supermodel have become important and popular in general information economics and organizational economics, as well as other fields [12]. Especially in the condition of incomplete information or complementary, these tools play important roles in analyzing situations to establish the mechanism of information sharing in an organization.

2.1.3. The mechanism for benefit sharing among participants

Paul Milgrom and Robert Wilson’s auction format also creates a mechanism for benefit sharing among auction participants. It is the result of combining many auction-related theories, such as bilateral bargaining, utility pricing, match theory, and game theory [13].

For example, the analysis of bidding behavior in specific auction settings can be extended to the analysis of mechanisms for bilateral trade-in negotiations in general. In this way, the insights from auction theory help in analyzing different trading institutions [10]. Another example, the problem of determining an optimal reserve price in a single-object auction, turns out to be analogous to finding a seller-optimal trading mechanism in the case of a single buyer [10].

In addition, the best outcomes that can be attained in bilateral bargaining between privately informed parties are tightly connected to equilibrium outcomes of double auctions, where both the buyer and the seller submit bids. Milgrom and Wilson’s simultaneous multi-round auction makes negotiation more convenient on a mutually beneficial basis for all participating parties [11]. As well, the simultaneous multi-session auction model demonstrates the empirical relevance of game theory in situations where participants, strategy, and outcomes can be easily clearly defined [13]. This is because, through this auction, it is possible to clarify the essential things that influence the participants’ decisions, such as their preferences, information, and knowledge, which in turn leads to action that can be optimized for their benefits.

Thus, the successful application of negotiation theory, valuation, match theory, and game theory has helped create an effective benefit-sharing mechanism among auction participants.

2.1.4. Lessons learned from 2020 Nobel Prize in Economic Sciences

Paul Milgrom and Robert Wilson’s auction theory shows that if designing suitable auctions and choosing wisely among existing auction formats, both buyers and sellers can observe and obtain the most suitable price [12]. Key lessons learned include:

- (i) Sufficient and transparent information plays an important role in an auction;
- (ii) An appropriate auction form, including auction time, method of bidding, and the starting price, is a necessity;
- (iii) A good auction must create optimal welfare for the auction participants.

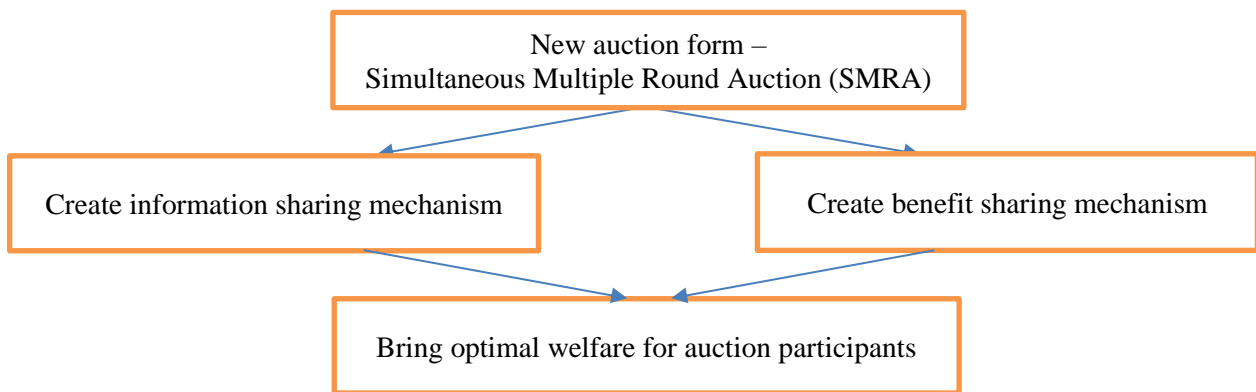


Fig. 1. Suggestions from the 2020 Nobel Prize in Economics for auction in Vietnam.

This is a lesson for changing auction policy in Vietnam in order to create information sharing and benefit-sharing mechanisms in order to achieve optimal welfare for the State and land auction participants.

2.2. Method and analytical framework

This paper employs a qualitative method that is suitable for reviewing, analyzing, evaluating, and synthesizing both theoretical and practical problems. Documents under review were from journals and books to analyze the content of the 2020 Nobel Prize in Economics. Therefore, it helps explore and synthesize main theories and ideas about auction design. Policies, frameworks, directives, and regulations on land use right auction in Vietnam were gathered from the Ministry of Natural Resources and Environment, the Ministry of Finance, the Ministry of Justice, and other State management agencies. Finally, other relevant studies and reports from land-related organizations have been rigorously reviewed and synthesized. This provides a clear insight into the context to understand the characteristics of land use right auctions in Vietnam. Based on the analysis and synthesis of the above documents, the article analyzes and explains how to apply ideas from Paul Milgrom and Robert Wilson’s auction theory to revise the land use right auction framework in Vietnam.

Furthermore, the preliminary findings of the research have been reviewed and consulted by experts, researchers, and other organizations. Conclusion and suggestions of interventions were given by considering and applying ideas from the auction theory of the 2020 Nobel Prize in Economics to change

the regulations of land use right auction to optimize and harmonize benefits for the State and other stakeholders.

The analytical process of this paper is illustrated in several below stages. First, the article analyzes the new contributions of the 2020 Economics Nobel Prize of the new form of the simultaneous multi-session auction to create information sharing and benefit-sharing mechanisms among auction participants. Second, the lessons learned for Vietnam are drawn. Third, the paper examines the legal provisions on an auction of land use rights in Vietnam, focusing particularly on acquiring agricultural land for non-agricultural uses, in order to highlight the inadequacies in information sharing and benefit-sharing among stakeholders. Finally, the article proposes to change a number of legal provisions on land use right auction in Vietnam, with the aim to create a mechanism for information sharing to maximize and balance the interests among the auction participants.

3. The data of land use right auction in Vietnam

Recently, the State has promulgated a number of essential documents to establish the legal foundation for land use right auction - for example, Decision No. 216/2005/QĐ-TTg dated 31/08/2005 about the promulgation of the Regulation on land use right auction to allocate land with collection of land use fees or to lease land; Decree No. 17/2010/NĐ-CP dated 04/03/2010 of the Government on property auction; Decree No. 44/2014/NĐ-CP dated 15/05/2014 of the Government on land prices, 2014; Decree No. 01/2017/NĐ-CP dated 06/01/2017 of Government on Amending and supplementing a number of decrees detailing the implementation of the Land Law; Land Law 2003, Land Law 2013; and Property Auction Law 2017 [14, 15, 16, 17, 18, 19, 20].

In December 2019, there were 1,008 auctioneers, more than 410 property auction businesses, and 63 Property Auction Service Centers nationwide [21].

Tab. 1. Auction data in Vietnam between 2017-2019.

Period	Number of auctions	Total starting price (billions VND)	Total sale value (billions VND)	Profit for property owners and the State budget (billions VND)	Taxes to the State budget (billions VND)
1/2017-12/2019	86.607	194.755	233.053	38.185	100

These statistics show that 86,607 successful auctions were held, with a total starting price of more than 194,755 billion VND. The total value of selling was more than 233,053 billion VND, generating more than 38,185 billion VND profit for property owners and the State. Total tax paid was nearly 100 billion VND from the period of January 2017 to December 2019 [22].

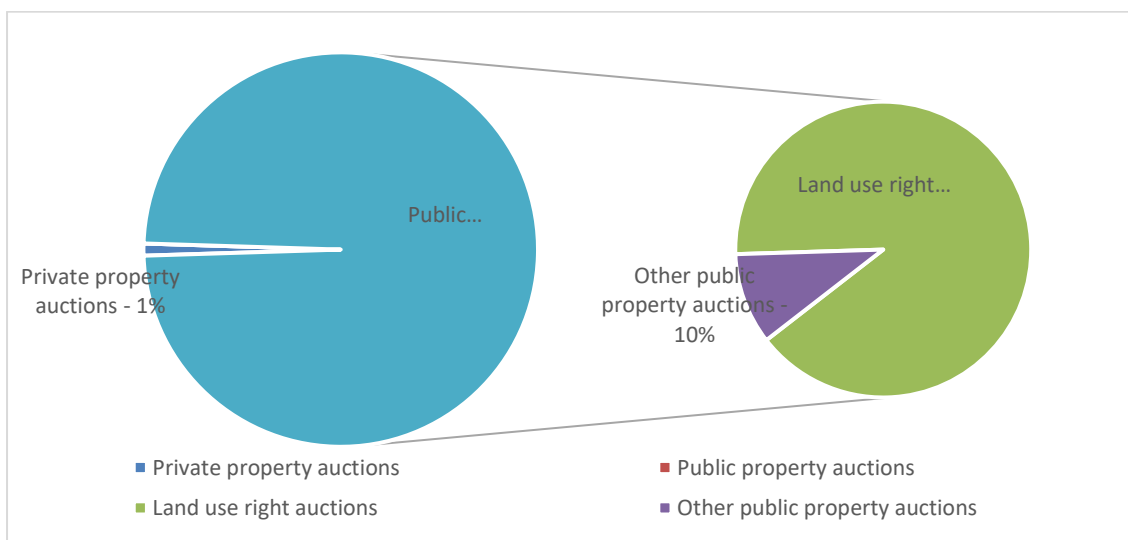


Fig. 2. Vietnam asset auction.

According to the Ministry of Justice, up to 90% of the public assets that are required to be auctioned are auctions of land use rights. Assets owned by individuals and organizations put up for sale through auctions accounted for nearly 1% of the number of compulsory asset auctions [21].

4. Current regulations on an auction of land use rights in Vietnam

Tab. 2 below documents the formal legal provisions and procedures of the land use right auctions. These include auction timing, auction participants, auction form, and State's starting price.

Tab. 2. Current land use right auction regulations in Vietnam.

Content	Current regulations	Legal Document
Time to organize land use right auction	<ul style="list-style-type: none"> - After having the annual district-level land use plan approved by a competent state agency - After having the land use right auction plan approved by a competent state agency - After land acquirement and clearance 	Article 119 Land Law 2013 [18]
Organizations and individuals are allowed to participate in land use right auction	<ul style="list-style-type: none"> - Households and individuals are allowed to participate in land use right auction to allocate residential land; economic organizations are allowed to participate in land use right auction to allocate land to execute investment projects on housing construction for sale or for sale and for lease - Overseas Vietnamese, foreign-invested enterprises are allowed to participate in land use right auction to allocate land to execute investment projects on housing construction for sale or for sale in combination with lease - Economic organizations are allowed to participate in land use right auctions to allocate land to execute investment projects on the infrastructure of cemeteries and graveyards 	<ul style="list-style-type: none"> - Articles 55 and 56 of the 2013 Land Law [18] - Article 58 of the 2013 Land Law [18]
Forms and methods of land use right auction	<ul style="list-style-type: none"> - Forms of auctions: direct verbal auction; direct voting auction; indirect voting auction; online auction. - Methods of the auction: bidding up; bidding down. 	Article 40 of the Law on Property Auction 2016 [19]
Determination of the starting price for land use right auction	<ul style="list-style-type: none"> - The Ministry of Finance is responsible for determining the starting price for land use right auction in coordination with the Ministry of Natural Resources and Environment. - Methods of determining the starting price include the direct comparison method, extraction method, income method, surplus method, and land price adjustment coefficient method. 	<ul style="list-style-type: none"> - Clause 3 Article 3 of Decree 01/2017/ ND-CP [16] - Clause 1, Article 15 of Decree 44/2014/ND-CP [15] - Decree 44/2014/ ND-CP [15]

5. Result and discussion

5.1. Evaluating the current framework of land use right auctions in Vietnam

5.1.1. Regarding information sharing mechanism among stakeholders

The existing framework of land use right auctions in Vietnam does not help to overcome challenges resulting from the emergence of collusion among auction participants, asymmetric information, and uncertainty in value evaluation [3]. This is because, during the auction of land use rights, the participants do not know each other's movements. There is no negotiation or bargaining, and there are no other sources of price reference in the auction.

Currently, there is no mechanism for information sharing through the State's regulations. There is only the requirement that competent authorities announce information about auction organizations and auction land plots through various channels. For instance, it is required to post information about land auctions on specialized websites of the central or local agencies and notify that information at the Commune People's Committee [3].

However, due to the massive press volume, it is not easy for interested parties to access posted information on land auctions in mass media. Besides, advertising that information at the Commune People's Committee where the auctioned land is located is also very difficult for out-of-province people to access. This is because in many localities, the website of the Commune People's Committee has not been completed or licensed by the Ministry of Justice [23]. In addition, searching for specific auction information on a common website can cause difficulty for the majority of people, especially the poor living in rural areas, ethnic minorities living in remote areas, and people with disabilities. Furthermore, there is a lack of reputed and good asset auction organizations in some localities [23]. While the Commune People's Committee does not play a favorable role in supervising and monitoring, the regulations on publicly announcing land auctions have not been implemented well and seriously.

Furthermore, currently, auctioned land prices are totally determined by state authorities. There is no consultation with independent agencies or experts to help to evaluate land prices. The law has prescribed and guided procedures for hiring a consultant to determine specific land prices [3]. However, there is no mandatory regulation requiring to use of this consultancy for the auction. There are a number of private organizations providing consultancy on land prices, but the valuation capacity has not been evaluated. There are no state professional organizations assigned to take responsibility for the appraisal of land valuation results by consultancy organizations, nor is there any legal corridor to unify the management of the private valuation. The Ministry of Natural Resources and Environment, Ministry of Construction and Ministry of Finance are involved in this management [22]. Regulations on technical standards for land pricing services and on the mechanism of delimitation when there are disputes over valuation results are also still lacking.

5.1.2. Regarding benefit-sharing mechanism among stakeholders

Currently, the land use right auctions for allocating land are separated from the agricultural land acquisition process of the State. In this case, the land put up for auction is "clean land" after land clearance, and the auctioned land price is set by the state agency [3]. With the current implementation, there is absolutely no benefit-sharing mechanism among the farmer households whose land is acquired, the investors whose land is allocated and the State. In projects in which agricultural land is acquired and auctioned for non-agricultural purposes or commercial and profitable activities, the benefits and risks of these projects are shared not only by households and the community but also by investors. There is currently no mechanism for benefit and risk-sharing among stakeholders involved in these projects. This problem is analyzed below.

Specifically, in the projects of acquiring agricultural land for the non-agricultural purpose, by the State's decision of land acquisition and land allocation through land use right auctions, the purpose of using agricultural land is converted to non-agricultural land. After that, land prices usually increase sharply because of the fact that the price of residential and service land is much higher than that of agricultural land [24]. The gains from the increase in land prices mainly benefit investors who are usually the winners in the auction and allowed to own the land use rights [25]. Investors, including enterprises, organizations, and individuals after winning in auctions, are allowed to convert land use from agricultural land to non-agricultural purposes, such as investing in business and housing. They can collect a large profit from the change of land price before and after the auction. If investors can buy land at low prices in the auction, their income from the auction increases many times over. Even if investors pay high prices in the auction, they are still able then to sell that land slot at a larger profit in the estate market [25].

On the other hand, the farmers, despite losing land - their main source of income - receive only compensation and support based on the land price bracket set by state agencies. The benefits obtained from auctions are completely denied to the farmers. In many cases, farmers suffer a lot of disadvantages as a result of land acquisition, such as losing income, property, livelihood, resulting in extreme poverty or impoverishment [26]. This is because the land is the primary means of production and the main source of income for farmers. The vast majority of them do not have any job other than farming, although they do some secondary jobs when not actually working on the farm. Moreover, when agricultural land is acquired,

the spiritual and cultural life of the farmer is greatly affected. In the rural context of Vietnam, agricultural land carries the identity of the family, lineage, history, culture, and spirituality, which has been passed down through generations [23]. These cultural and spiritual values cannot easily be erased or replaced. Many farmers cannot accept abandoning their agricultural land, which was left to them by their ancestors and took much effort to develop and persevere. Often, this land is forcibly recovered by the State, then auctioned and transferred to real estate development, and eventually sold at much higher prices than the compensation received by the farmers. Compared to the profit obtained by investors, farmers whose land is acquired gain a lot less [26].

Furthermore, land price determined by state authorities to compensate for forcibly acquired land is not close to the market price if that land were to be freely transferable in the market [23]. This is a limitation of evaluating and determining land prices because of the incapacity to investigate, survey land prices in the market. This also comes from the weaknesses in applying modern methods of determining land prices or collusion and bribery in the implementation auction process. As a result, the auctioned land price is always determined to be lower than the market price of that land, leading to a number of investors who have no real need for land participating in the auction with the aim to speculate on land [2].

Thus, through the land use right auctions after acquiring agricultural land, the State has created great added value by changing the purpose of land use. While investors get the greatest benefit from this added value, the direct benefit of farmers is less. They may even take a disadvantage if the compensation price is too low compared to the increase of land prices in the market after land-use conversion.

5.2. Suggestions for changing regulations of land use right auction in Vietnam

Building a suitable auction form that can create mechanisms for information sharing and benefit sharing in order to achieve optimal welfare for land auction participants in Vietnam is necessary. Some legal provisions of land use right auction should be changed. These include (i) the time to organize the auction, (ii) the organizations and individuals allowed to participate in the auction, (iii) the forms and methods of the auction, and (iv) determining starting price.

Firstly, the auctions of land use rights should be organized before land acquisition and site clearance. Second, it is recommended that organizations, individuals, and households whose land is acquired should be added to the list of compulsory participants. Thirdly, it is recommended that multiple round auctions of land use rights with different land plots in different areas at the same time should be organized. Fourth, in terms of land price valuation, the State should add a provision allowing that the participants whose land is acquired have the right to request the land price determination from authorized agencies, and this price could become the starting price of auctions.

Tab. 3 below compares the benefits and drawbacks of land use right auctions under the existing framework and the new proposal.

Tab. 3. Comparison of Changes in Land Use Right Auction Form and Process.

Content change	Auction format	
	Current regulation	New proposal
Auction time	After land acquisition and site clearance - Advantages: separating the process of land acquisition and land auction, creating a “clean land” fund for auction. - Limitations: benefits are not guaranteed for farmers whose land is acquired	Before land acquisition and site clearance - Advantages: ensuring harmonious benefits for farmers whose land is acquired - Limitations: complexity in formulating, implementing, examining, and monitoring policy implementation
Participants	Farmers whose land is acquired may or may not participate in the auction. - Advantages: flexible - Limitations: benefits are not guaranteed for farmers whose land is acquired	Farmers whose land is acquired are required to participate in the auction. - Advantages: ensuring benefits for farmers whose land is acquired - Limitations: complexity in formulating, implementing, examining, and monitoring policy implementation

Auction method and form	- Direct verbal auction; direct voting auction; indirect voting auction; online auction - Method of the auction includes: bidding up method; bidding down method	- Organize multi-round auctions; multi-session auctions at the same time - Additional regulations on information disclosure - Additional regulations on online auction venues
	- Advantages: easy to implement, fast, low cost - Limitations: asymmetric information arises in price manipulation	- Advantages: creating an information-sharing mechanism - Limitations: complexity in formulating, implementing, examining, and monitoring policy implementation
Determine starting price	Authorized by state management agencies	The participants whose land is acquired have the right to request the land price determination
	- Advantages: easy to implement, fast, low cost - Limitations: land prices are determined not corresponding to market prices, not ensuring harmonious benefits for farmers whose land is acquired.	- Advantages: enhancing stakeholder's participation, ensuring the interests of participants whose land is acquired - Limitations: complexity in formulating, implementing, examining, and monitoring policy implementation

6. Conclusion

The primary goal of this paper is to synthesize existing auction of land use right frameworks in order to apply the lessons learned from the 2020 Nobel Prize in Economics to support designing a new method for land use right auctions in Vietnam. Focusing on auctions of land that was formerly agricultural land, the research shows that the existing land use right auction framework fails to harmonize interests among stakeholders, especially farmer households whose agricultural land is acquired. The paper applies the lessons learned from the Economics 2020 Nobel Prize in creating information sharing and benefit-sharing mechanisms to change current land use right auction regulations. The paper recommends that the State should rethink and adopt the proposed effective provisions of land use right auction, including provisions about the time to organize auctions, the organizations and individuals required to participate in auctions, the forms and methods of auctions, and the determination of the starting price.

7. Acknowledgements

The paper was presented during the 6th VIET - POL International Conference on Scientific-Research Cooperation between Vietnam and Poland, 10-14.11.2021, HUMG, Hanoi, Vietnam.

8. References

1. The Royal Swedish Academy of Sciences, 2020. Improvements to auction theory and inventions of new auction formats, The Committee for the Prize in Economic Sciences in Memory of Alfred Nobel.
2. Nguyen, D.B., Research on renovating land management system to form and develop real estate market in Vietnam, National scientific research project, Hanoi, Vietnam, 2005.
3. Nguyen, N.D., 2013. Land use rights auction and specific recommendations for the draft amendments and supplements to the Land Law, Journal of Legislative Studies, 14(246): 137-146.
4. Ministry of Justice, Implementation of the Law on Property Auction from 2017, 2018, 2019 to 2020.
5. The Royal Swedish Academy of Sciences, 2020. The quest for the perfect auction, The prize in economic sciences.

6. Sonin, K.I., 2021. The principles of auction theory (Nobel Memorial Prize in Economic Sciences 2020), *Voprosy Ekonomiki*, 2021(1): 5-32, <https://doi.org/10.32609/0042-8736-2021-1-5-32>.
7. Hung-po, C., Shmuel, S.Oren, Robert, B.W., 2020. Beyond the 2020 Nobel prize for economic sciences, *Energy Economics*, 95(3): 105-120, <https://doi.org/10.1016/j.eneco.2020.105020>
8. Janssen, M.C.W., 2021. Reflections on the 2020 Nobel Memorial Prize Awarded to Paul Milgrom and Robert Wilson, *Erasmus Journal for Philosophy and Economics*, 13(2): 177–184, <https://doi.org/10.23941/ejpe.v13i2.533>
9. Ausubel, L.M., 2004. An Efficient Ascending-Bid Auction for Multiple Objects, *American Economic Review*, 94(5): 1452-1475, <https://doi.org/10.1257/0002828043052330>.
10. Kasberger, B., 2020. When Can Auctions Maximize Post-Auction Welfare?, SSRN, <http://dx.doi.org/10.2139/ssrn.3519866>.
11. Klemperer, P., 2002. What Really Matters in Auction Design, *Journal of Economic Perspectives*, 16(1): 169-189, <https://doi.org/10.1257/0895330027166>.
12. Milgrom, P., Mollner, J., 2018. Equilibrium selection in auctions and high stakes games. *Econometrica*, 86(1): 219-261, <https://doi.org/10.3982/ECTA12536>.
13. Cao, Z, Qiao, H, Yang, Z., 2020. Auction Theory and Design: A Review of the Contributions of the 2020 Nobel Prize Winners in Economics, *Management Review*, 2020, 32(10): 3-10, http://journal05.magtech.org.cn/jweb_gpl/EN/Y2020/V32/I10/3.
14. Government, Decree No. 17/2010/ND-CP dated 04/3/2010 of the Government on property auction, Hanoi, Vietnam, 2010.
15. Government, Decree 44/2014/ND-CP dated 15/05/2014 of the Government on land prices, Hanoi, Vietnam, 2014.
16. Government, Decree 01/2017/ND-CP dated 06/01/2017 of Government on Amending and supplementing a number of decrees detailing the implementation of the Land Law, Hanoi, Vietnam, 2017.
17. National Assembly, Land Law, Hanoi, Vietnam, 2003.
18. National Assembly, Land Law, Hanoi, Vietnam, 2013.
19. National Assembly, Law on Property Auction, Hanoi, Vietnam, 2017.
20. Prime Minister, Decision No. 216/2005/QD-TTg dated 31/8/2005 promulgating regulations on auction of land use rights.
21. Ministry of Natural Resources and Environment, Implementation of the Land Law 2013 on the period 2015-2020, Hanoi, Vietnam, 2021.
22. Ministry of Finance, Decision No. 22/2003/QD-BTC dated 18/02/2003 On the financial mechanism in the use of land fund to create capital for infrastructure construction, Hanoi, Vietnam, 2003.
23. Hanoi People's Committee, Decisions on promulgating regulations on auction of land use rights to generate capital for infrastructure construction in Hanoi City in 2002, 2003, 2004, 2005, Decisions planning approval for land auction, decisions on land allocation, Hanoi, Vietnam, 2006.
24. Nguyen, T.T., Pham, N.H., Efficiency of land use right auction through some projects in Hanoi, Research project, Hanoi Agricultural University, Hanoi, Vietnam, 2018.
25. Nguyen, T.T., 2012. Auction of land use rights: A tool to deal with pressing land issues, *Financial Magazine*, 10(12): 54-61.
26. Dang, H.V., Dao, T.C., Nguyen, T.T., 2013. Evaluation of practical implementation of land acquisition, compensation, support, and resettlement in accordance with the law, *Journal of Sciences and Development*, 11(3): 328-336.

An Overview of Rare Earth Ores Beneficiation in Vietnam

NHU Thi Kim Dung^{1,*}, PHAM Van Luan¹, VU Thi Chinh¹, TRAN Van Duoc¹

¹ Hanoi University of Mining and Geology, 18 Vien street, Hanoi, Vietnam

Corresponding author: nhuthikimdung@humg.edu.vn

Abstract. Rare earth metals are used in electricity, electronics, nuclear, optics, space, metallurgy, superconducting and super magnetic materials, glass and ceramics, and agriculture. Some rare earth elements are added to fertilizers for crops and some trials for animal feed. Rare earth elements, except for radioactive promethium, are relatively abundant in the earth's crust. Vietnam has a tremendous rare earth potential, distributed mainly in the Northwest, including Nam Xe, Dong Pao, Muong Hum, and Yen Bai. There are many research projects on rare earth ores of different types globally, but the focus is mainly on the essential minerals, including monazite, xenotime, and bastnaesite. This report summarizes research data on rare earth ore intending to produce a general assessment of rare earth ore and its beneficiation technology in Vietnam.

Keywords: Rare earth, Monazite, Xenotime, Bastnaesite

1. Introduction

Rare earth is the common name for a group of rare metallic elements or rare earth metals, including 17 chemical elements of Mendeleev's periodic table such as scandium, yttrium, and 15 elements of the Lanthanide group, which have a relatively large percentage in the earth's crust. Nowadays, about 250 minerals containing rare earth elements have been discovered in the earth's crust. About 1/2 have been identified in mineral lattice structures, and more than 60 minerals contain not less than 5,0 - 8.0% REO. It is noteworthy that there are six different ore minerals processed in the industrial productions, which include bastnaesite [(Ce,La)(CO₃)F], monazite [(Ce,La)PO₄], xenotime (YPO₄), loparite [(Ce,Na,Ca)(Ti,Nb)O₃], apatite [(Ca,REE,Sr,Na,K)₃Ca₂(PO₄)₃(F,OH)], and ion-adsorption clays [1-3]. The first three minerals, known as the commercial rare earth elements (REE) mineral sources, contribute to almost 95% of the world's reserves: bastnaesite (70–75% rare earth oxides REO), monazite (55–60% REO), and xenotime (55-60% REO). The mainly exploited rare earth minerals of industrial values are bastnaesite, monazite, xenotime, and gadolinite, which bastnaesite occupies one-third of the world's rare earth production. Recently, rare earth in clays with ionic adsorption has been found in the weathered laterite crust [4-7].

Rare earth elements (REEs) are classified into two groups, "heavy" and "light", depending on the density of their atom. "Light" REEs include lanthanum (La) (number 57 in the periodic table) to europium (Eu) (number 63 in the periodic table). In contrast, 'heavy' REEs include gadolinium (Gd) (64) to lutecium (Lu) (71), and yttrium.

The common rare earth minerals in nature are shown in Table 1.

Tab. 1. The common rare earth minerals in nature [11-13].

No	Minerals	Chemical formula	Distribution of main rare earths	The grade of REO; %
<i>I - Phosphate group</i>				
1	Monazite	(Ce,La,Th).(PO ₄ ,SiO ₄)	Light group	60.6
2	Apatite	(Ca,Ce) ₅ .(PO ₄) ₃ .(F,Cl)	Light group	0-5
3	Xenotime	YPO ₄	Heavy group	61.4
4	Fluorexite	(Y,Al ₃).(PO ₄) ₂ .(OH) ₆	Heavy group	32
5	Rapdofanite	(Ce,Y).PO ₄ .H ₂ O	Light group	36-65
<i>II - Carbonate and Fluor carbonate group</i>				
6	Bastnaesite	(Ce,La).CO ₃ . F ₂	Light group	74.77

7	Pazisite	$\text{CaCe}_2 \cdot (\text{CO}_3)_3 \cdot \text{F}_2$	Light group	60.89
<i>III – Oxide group</i>				
8	Loparite	$(\text{Ce,Ca, Na}) \cdot (\text{Ti,Nb})\text{O}_3$	Light group	16-19
9	Fecgusonite	$(\text{Y,Er,Ce,U,Th,...}) \cdot (\text{Nb,Ta,Ti}) \cdot \text{O}_4$	Heavy group Light group	54 3
10	Samacskite	$(\text{Y,Er,Ce,U,...})_4 \cdot (\text{Nb,Ta})_6 \cdot \text{O}_{21}$	Heavy group Light group	9.13-27.86 1.36-9.11
11	Euxenite	$(\text{Y,Ce,Ca,U,Th}) \cdot (\text{Nb,Ta,Ti})_2 \text{O}_6$	Heavy group Light group	16-27.8 0.4-3.5
12	Priorite	$(\text{Y,Er,Ca,U,Th}) \cdot (\text{Nb,Ti})_2 \cdot \text{O}_6$	Heavy group Light group	21.1-28.7 3.7-4.3
13	Branerite	$(\text{U,Ca,Y,Fe, Th})_3 \cdot \text{Ti}_2 \text{O}_{16}$	Heavy group	3.9
14	Conopite	$(\text{Ce,Ca}) \cdot (\text{Ti,Fe}) \cdot \text{O}_3$	Light group	7
15	Piroclo	$(\text{Na,Ca,Ce,Y,...})_2 \cdot (\text{Nb,Ti,...})_2 \cdot \text{O}_6 \cdot (\text{F,OH})_7$	Heavy group Light group	5 2 - 13.3
<i>IV – Silicate group</i>				
16	Gadolinite	$(\text{Ca,Y})_2 \cdot \text{Fe} \cdot (\text{Be}_2\text{Si}_2\text{O}_{10})$	Heavy group	55.4
17	Eudialite	$(\text{Ce,Y,Ca})_4 \cdot (\text{Fe,Zr}) \cdot (\text{Si}_8\text{O}_{18}) \cdot (\text{OH,Cl})$	Light group	0.3-2.9
18	Xerite	$(\text{Ce,Ca})_{10} \cdot (\text{SiO}_4)_6 \cdot (\text{OH,F})$	Light group	50
19	Orthite (Allanite)	$(\text{Ca,Ce,Y}) \cdot (\text{Mg,Al})_2 \cdot [(\text{Si}_2\text{O}_7) \cdot (\text{SiO}_4) \cdot (\text{O,OH})]$	Heavy group Light group	18 8
20	Rincolite (Lopchorite)	$(\text{Ca,Na,Ce})_3 \cdot (\text{Ti,Nb}) \cdot (\text{SiO}_4)_2 \cdot (\text{F,OH})_2$	Light group	13-20
<i>V – Fluorine group</i>				
21	Fluxerite	$(\text{Ca,Y}) \cdot \text{F}_3$	Heavy group	70

In recent years, an increase in demand for REEs has been observed because of their unique properties and various applications. By the mid-twentieth century, rare earth materials were only used in the military field. Since 1987, their use has expanded to include glass, ceramics, catalysts in the oil refining and metallurgical industries. Over time, less than 5% of rare earth production was used in the electronics industry to produce high-strength magnets. Nowadays, with the high development of the metallurgical industry, rare earth alloy products are widely used in many sectors, such as the food industry, healthcare, ceramics, computers, color television screens, and environmentally friendly cars, magnets, batteries, petrochemical catalysts, rockets, radar, etc. [8-10].

2. Mining and processing of rare earth in Vietnam

2.1 Rare earth mining

Vietnam is one of the countries possessing rare earth resources. As a result of research and exploration works carried out since 1958, many rare earth deposits have been discovered in Nam Xe North, Nam Xe South, Dong Pao (Lai Chau), Muong Hum (Lao Cai), and Yen Phu (Yen Bai).

Placer REEs are mainly monazite, xenotime, a kind of rare earth phosphates, while silicate REEs (orthites) are less common. In the mainland and coastal areas, REEs are distributed in the river and stream

shelves, such as REEs mines in the Bu Khang North region (Nghe An). In this area, small mines are in Pom Lau - Ban Tam, Chau Binh, and Ban Gio, with the monazite grade accounts for 0.15-4.8 kg/m³, and simple mining and processing conditions are applied. There should be evaluation for further exploration and exploitation when a need appears. In the coastal areas, many active mines and ilmenite placer deposits contain rare earth minerals (monazite, xenotime) with concentrations from 0.45-4.8 kg/m³, such as Ky Ninh, Ky Khang, Cam Hoa, Cam Thuong (Ha Tinh), Ke Sung (Hue), Cat Khanh (Binh Dinh), Ham Tan (Binh Thuan) mines, etc. However, to date, REEs in those mines have not been fully evaluated [13-15].

Despite the tremendous rare earth potential of the country, rare earth mining in Vietnam is almost small-scale, and processing technology is still outdated. The mining method is mainly manual. Consequently, large resource losses (up to 60%) and disadvantages are low capacities and incapability for completely separating REEs. Besides environmental problems, it would be no value added of REEs if Vietnam cannot process raw materials.

Each year, Vietnam only mines a few tens of tons of bastnaesite ores from Dong Pao mine and a few thousand tons of monazite ores with a grade of 35-45% REO from the central coastal placer mines for limited sale by quota. Dong Pao rare earth mine, Tam Duong district (Lai Chau), is the largest rare earth mine in Vietnam at the moment, with a total area of more than 11 km², reserves of over 5 million tons of oxides. The main ore bodies are F3 and F7, which contain REEs suitable for electronic factories. The Dong Pao mine project is an open-pit type of surface mining utilizing a sequence of mining, mineral processing, and hydrometallurgy for treating 1,088,000 tons capacity of the run of mine ores in the future [16,17].

It is necessary to prevent pollution from the first stage of project investment and pollution control from the first step of the project's operation to exploit REEs efficiently, protecting the environment and safety. Along with the excavation of rare earth mines such as Dong Pao, Nam Xe, etc. it is necessary to continue to invest in discovering and fully evaluating this precious mineral in other regions of Vietnam.

2.2 Research on beneficiation of rare earth ores in Vietnam

Until now, all rare earth ore processing technologies in Vietnam have remained mainly laboratory-scale and semi-industrial-scale research projects, with almost no significant applications in industrial production scale. Based on semi-industrial scale tests, several studies on ore processing technology of Nam Xe South, Dong Pao, Yen Phu mines, some marine placer deposits, and several processing flowsheets have been proposed. There is the suggestion that the research results can be applied to production. However, currently, only some research results on monazite recovery from marine placers have been applied. The research in the field of hydrometallurgy and extraction is still limited due to not insufficient data and conditions to evaluate the capability and economic efficiency.

2.2.1 Dong Pao rare earth ores

The Dong Pao rare earth ore is a type of "multi-metallic" complex ore that is very difficult to beneficiate. The total rare earth oxide grade is not high at 5.98% REO. The ore has relatively high barite and fluorite grades which are of 21.58% BaSO₄ and 12.35% CaF₂ respectively. Many other minerals are associated with rare earth, such as Ca, Al, Fe, Si, S, Mn, Pb, Mg, etc. Rare earth minerals exist mainly in the form of bastnaesite. Barite minerals account for the largest percentage in quantity as well as the content. In addition, a few REEs exist in the form (Ca,Y)F₂₋₃ - Yttrifluorite, and fluorite exists in the form CaF₂·[(CaF₂)_{0.75}(YF₃)_{0.25}] [13].

The Dong Pao rare earth ore processing tests were conducted in 1986 to explore and excavate the mining area between Vietnam and Germany. The test flowsheet is shown in Figure 1, and the results are shown in Table 2 [18].

Tab. 2. Results of direct flotation of Dong Pao rare earth ore.

Stage	Product	Yield, %	Grade, %			Recovery, %		
			REO	BaSO ₄	CaF ₂	REO	BaSO ₄	CaF ₂
	Feed	100.00	11.25	49.53	10.44	100.00	100.00	100.00
Grinding, screening	Rare earth concentrate I (1)	13.62	38.09	14.71	4.12	46.37	4.07	5.40
	Particle size +0.03 mm	86.38	6.99	55.05	11.44	53.63	95.93	94.60
Flotation	Concentrate BaSO ₄ (7)	51.79	0.77	86.50	1.65	3.54	90.44	8.19
	Tailings CaF ₂ (8)	7.66	15.60	7.45	5.04	10.53	1.14	3.66
	Concentrate CaF ₂ (9)	15.88	13.58	5.00	39.10	49.18	1.60	59.48
	Rare earth concentrate (10)	11.95	20.74	12.3	21.90	20.38	2.75	23.27
	Rare earth concentrate (1) + (10)	24.47	30.34	13.65	12.10	66.75	6.82	28.67

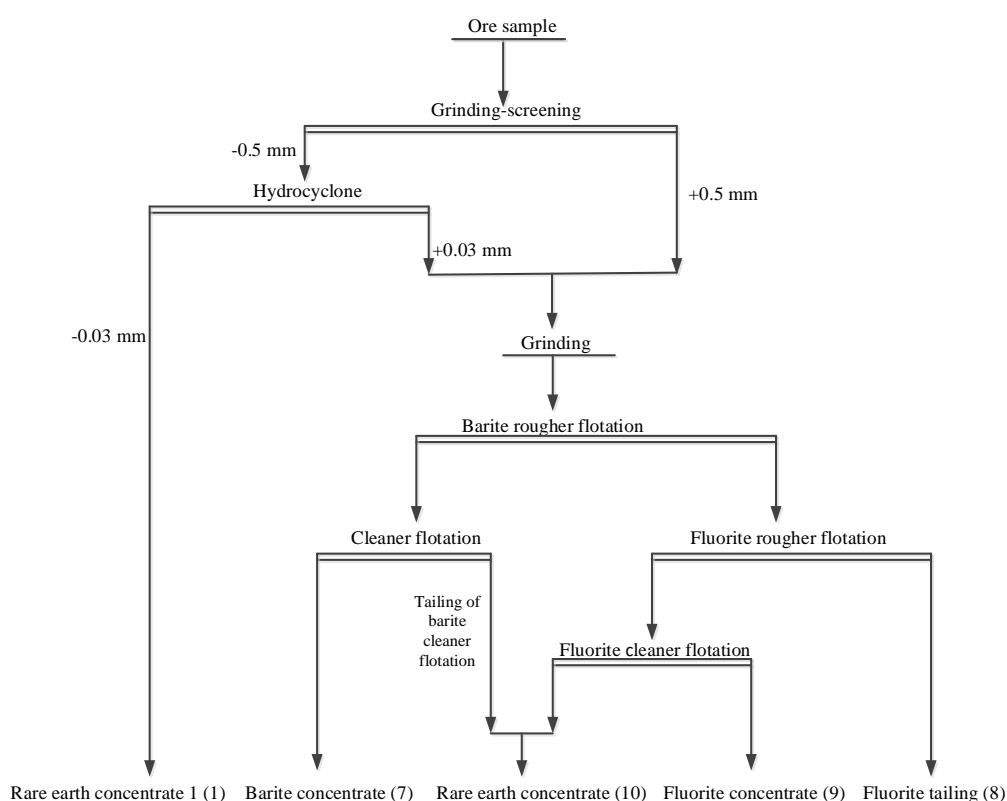


Fig. 1. Flotation flowsheet of the Dong Pao rare earth ore in research cooperation with Germany.

The Dong Pao rare earth ore sample was sent to Lakefield Research Laboratory in Ontario, Canada, for further flotation studying. Preliminary research has been conducted on three different processing flowsheets: Direct flotation REO from the feed ore, CaF₂ - BaSO₄ - REO selective flotation, and BaSO₄ - CaF₂ - REO selective flotation. REO direct flotation flowsheet, similar to bastnaesite treatment flowsheet of Mountain Pass flotation plant. The results of direct flotation REO and selective flotation CaF₂ - BaSO₄ - REO, respectively, are shown in Tables 3-4, indicating that these two flowsheets are not adequate for the concentrates of BaSO₄, CaF₂, REO separately.

The selective flotation flowsheet of BaSO₄ - CaF₂ - REO respectively is much more efficient because barite has a good float ability. The criteria of the separate concentrates are also higher than the other two flowsheets. The processing flowsheet and results are shown in Tables 5-6. However, all the results obtained, the concentrates of REO did not exceed 40%, and the highest recovery obtained less than 70% [18, 19].

Tab. 3. The result of rare earth direct flotation from the feed.

Products	Yield, %	Grade, %			Recovery, %		
		CaF ₂	BaSO ₄	REO	CaF ₂	BaSO ₄	REO
Test 1							
Concentrate REO of the third cleaner flotation	33.63	6.50	38.60	6.76	49.10	21.20	45.40
Concentrate REO of the first cleaner flotation	62.06	5.82	54.20	5.96	81.10	54.90	73.90
Concentrate REO of rougher flotation	87.89	5.03	58.60	5.58	99.40	84.20	98.00
Tailings REO of rougher flotation	12.11	0.21	80.00	0.81	0.60	15.80	2.00
Feed ore (calculated)	100.00	4.45	61.20	5.00	100.00	100.00	100.00

Tab. 4. The result of CaF₂ - BaSO₄ - REO selective flotation.

Products	Yield, %	Grade, %			Recovery, %		
		CaF ₂	BaSO ₄	REO	CaF ₂	BaSO ₄	REO
Test 2							
Concentrate CaF ₂ of the third cleaner flotation	15.33	7.63	79.70	2.39	25.90	18.80	5.70
Concentrate CaF ₂ of the second cleaner flotation	16.94	7.24	79.30	2.61	27.20	2.07	6.90
Concentrate BaSO ₄ of the third cleaner flotation	55.54	3.29	86.20	1.34	40.50	74.00	11.70
Concentrate BaSO ₄ of the second cleaner flotation	58.64	3.61	82.89	2.14	47.00	74.90	19.70
Concentrate REO of the third cleaner flotation	10.73	8.40	23.40	34.30	20.00	3.90	57.60
Concentrate REO of rougher flotation	13.42	8.41	20.00	30.90	25.00	4.10	65.00
Tailings REO of rougher flotation	11.00	0.35	1.40	4.89	0.90	0.20	8.40
Feed ore (calculated)	100.00	4.51	64.90	6.39	100.00	100.00	100.00

Tab. 5. The result of BaSO₄ - CaF₂ - REO selective flotation.

Products	Yield, %	Grade, %			Recovery, %		
		CaF ₂	BaSO ₄	REO	CaF ₂	BaSO ₄	REO
Concentrate BaSO ₄ of the fourth cleaner flotation	58.70	0.06	97.10	0.55	1.60	85.20	5.10
Concentrate BaSO ₄ of the third cleaner flotation	62.88	0.09	96.20	0.82	2.50	90.40	8.20
Concentrate CaF ₂ of the third cleaner flotation	9.47	11.20	42.20	4.48	49.10	6.00	6.70
Concentrate CaF ₂ of the second cleaner flotation	10.96	10.60	41.70	5.57	53.80	6.80	9.60
Concentrate REO of cleaner flotation	13.88	6.26	11.70	30.60	40.20	2.40	67.10
Concentrate REO of rougher flotation	19.50	4.69	9.01	25.00	42.40	2.60	76.90
Tailings REO of rougher flotation	6.66	0.41	1.28	4.97	1.30	0.10	5.20
Feed ore (calculated)	100.00	2.60	66.90	6.33	100.00	100.00	100.00

Dong Pao rare earth ore samples were studied and concentrated by Sumitomo Metal Mining Company (Japan) using a flotation flowsheet to separate barite - fluorite - rare earth; the experimental results are shown in Table 7. The results show that obtained rare earth concentrates reached a grade of 45.9-48.4% REO. The recovery is in the range of 75.6-76.1% [20].

Nguyen Van Hanh (2005) studied the separation of rare earth, fluorite, and barite from weathered ores of Dong Pao mine and concluded that the main mineral of Dong Pao rare earth ores is bastnaesite. From his works, the ore samples, containing an average of 8-10% REO, were selectively ground and then cleaned by hydraulic classification and magnetic separation. A concentrate of 31.77% REO at a recovery of 84.46% on a laboratory and semi-industrial scale can be produced. Besides, the study determined the ability to separate barite and fluorite by flotation with reagents such as fatty acids and alkyl sulfates [15].

Tab. 6. The results of BaSO₄ - CaF₂ - REO selective flotation of the F3 and F4 ore bodies of the Dong Pao rare earth mine.

Samples	Products	Yield, %	Grade, %			Recovery, %		
			BaSO ₄	CaF ₂	REO	BaSO ₄	CaF ₂	REO
F3	Concentrate BaSO ₄ of the third cleaner flotation	27.52	84.20	3.33	2.94	90.80	3.20	4.80
	Concentrate BaSO ₄ of the second cleaner flotation	31.83	73.80	9.95	7.60	92.10	10.90	8.10
	Concentrate CaF ₂ of the third cleaner flotation	17.34	1.23	82.30	10.70	0.80	49.30	11.00
	Concentrate REO of the third cleaner flotation	31.20	3.22	30.10	32.70	3.90	32.40	60.30
	Concentrate REO of the second cleaner flotation	39.56	3.58	27.80	32.20	5.50	38.00	75.20
	Concentrate REO of rougher flotation	45.87	3.63	24.90	29.50	6.50	39.50	79.90
	Tailings REO of rougher flotation	4.95	2.59	1.60	3.35	0.50	0.30	1.00
	Feed ore (calculated)	100.00	25.50	28.90	16.90	100.00	100.00	100.00
F4	Concentrate BaSO ₄ of the third cleaner flotation	27.83	74.40	2.33	2.21	92.00	3.70	4.00
	Concentrate BaSO ₄ of the second cleaner flotation	35.41	59.40	4.80	11.50	93.50	9.70	8.80
	Concentrate CaF ₂ of the third cleaner flotation	15.90	1.33	47.80	21.00	0.90	43.50	21.80
	Concentrate REO of the third cleaner flotation	30.25	1.62	22.40	28.40	2.20	38.80	56.20
	Concentrate REO of the second cleaner flotation	36.65	1.77	20.50	26.90	2.90	42.90	64.40
	Concentrate REO of rougher flotation	37.81	1.82	19.90	26.50	3.10	43.00	65.50
	Tailings REO of rougher flotation	10.88	5.15	6.08	5.43	2.50	3.80	3.90
	Feed ore (calculated)	100.00	22.50	17.50	15.30	100.00	100.00	100.00

Duong Van Su (2010) mentioned a combination of magnetic separation and flotation circuit to separate Dong Pao rare earth ores. The REEs content increased from 8.7% REO up to 31.66% REO at a recovery of 63.52%. However, this research has not recovered barite and fluorite minerals from the F7 orebody of the Dong Pao mine [13].

2.2.2 Nam Xe North rare earth ores

There are two main types of ores at the Nam Xe North mine, the weathered and the lode ores; thus, the technological samples here should be studied accordingly in two directions. The rare earth mineral is bastnaesite, with a relatively small mineral content of 5-7%. Non-ore mineral composition accounts for

the main proportion, including barite, quartz, illite, kaolinite, feldspar, goethite, chlorite...

In 1971, the Institute of the Nonferrous Metallurgy studied the weathered ores from the Nam Xe North mine. An ore sample at 14.8% REO was taken and tested. The sample was tested in two alternative magnetic separation and flotation circuits. The magnetic separation circuit increased the magnetic concentrate by 19.5 % REO. The flotation circuit consisted of a rougher and five cleaners, obtained a concentrate of 18.5% REO [21].

In 2013, the National Institute of Mining - Metallurgy Science and Technology studied the technological experiment of rare earth ore extraction at Nam Xe North rare earth mine. The technological sample has chemical compositions as follows: 4.6% REO, 19.63% BaSO₄, 0.15% CaF₂, 21.8% SiO₂, 15.31% Fe. The research has used the flotation method to recover rare earth concentrate and barite concentrate. The results are as follows: The obtained rare-earth concentrate ore has more than 30% REO content, corresponding to the total recovery of 59.40%. In addition, barite concentrate with BaSO₄ content of more than 95% was also obtained, equivalent to a total recovery of 63.56%. The tailings contain about 2% REO, corresponding to a rare earth recovery of about 35.90% [21].

2.2.3 Nam Xe South rare earth ores

Fong-Sam (2013) reported proven reserves at Nam Xe South to be 199,300 tonnes of REO and probable reserves to be 3.0 Mt of REO [22]. REE concentrations reported for the Nam Xe South carbonatites are as follows: TREE from 3,400 ppm to 6,100 ppm in calciocarbonatites, and from 43,200 ppm to 163,900 ppm in ferrocyanatites, respectively [23, 24]. Detailed mineralogical studies [25] revealed that parisite Ca(REE)₂[CO₃]₃(F,OH)₂ is the main REE-bearing mineral in the ores of Nam Xe South. Other rare earth fluoro-carbonates, such as bastnaesite (REE)[CO₃](F,OH) and synchysite Ca(REE)(CO₃)₂(OH,F) occur only in minor amounts. The ore contains considerable amounts of baryte celestine, i.e., minerals of the baryte-celestine solid solution series [26], calcite, biotite, and magnetite. Especially the barytocelestine is finely intergrown with parisite on a sub-100µm-scale [25].

The results of the beneficiation research on Nam Xe South rare-earth were as follows: The mineral composition of Nam Xe South rare earth ores is complex with fine dissemination and intimately associated barite, calcite, mica, magnetite, quartz. The raw ore of grade 7 - 10% REO was ground and directly floated with sodium, NaF, dextrin, liquid glass according to Mountrin Pass's circuit to produce a rare-earth concentration containing 30 - 35% REO, at a recovery of 80 - 85%. In addition, the study had recovered barite by flotation separation. The barite concentrate grading of 85% BaSO₄ was obtained at a recovery of 54%. However, the content of rare earths in barite concentrate is still quite high, up to about 7% REO. A principal flowsheet is shown in Figure 2 [27, 28].

Robert Möckel et al. (2019) has studied the flotation of Nam Xe South rare earth ore. Flotation tests were redesigned with a two-step rougher flotation and a scavenger where the concentrate is re-feed into the wet milling followed by a wet re-grind of the rougher concentrate to minus 40 µm feeding into a 3 step cleaner flotation with a scavenger of the first cleaner tailing. The more sterile scavenger concentrate is re-feed into the regrinding stage before the cleaners. TREO concentrate grades of more than 40 wt% could be reached in the cleaner stage. The most effective way turned out to be a combination of cold (rougher) flotation on de-slimed ore at a coarser grain size (-100 µm) and a subsequent hot (cleaner) flotation after regrinding down to minus 40 µm. The REE loss of the de-sliming procedures was found to be below 8%. In contrast to the initial liberation evaluation, the regrinding step needed a better grade than 35% REO [29].

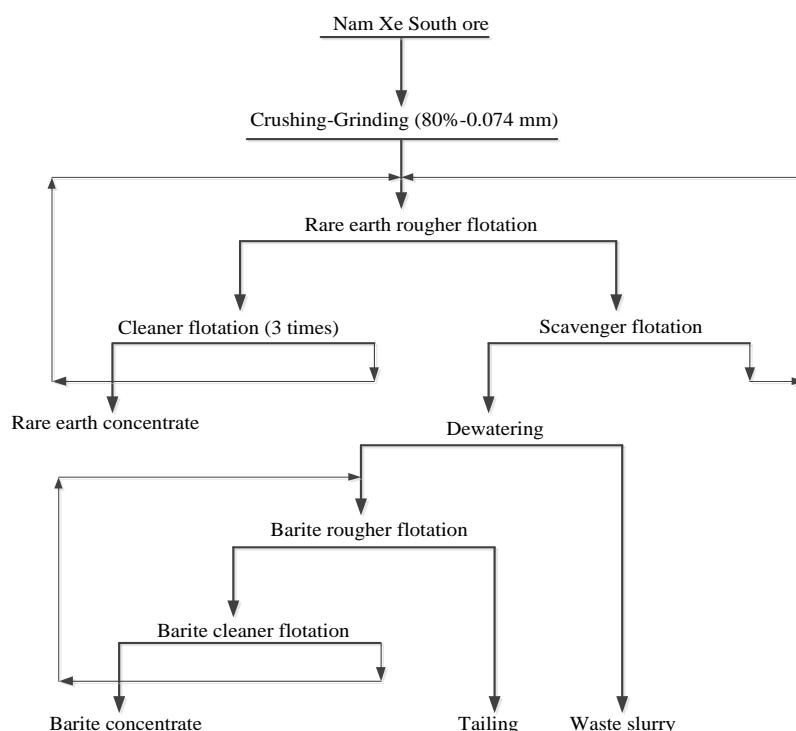


Fig. 2. Experimental flotation flowsheet for Nam Xe South rare earth ores.

2.2.4 Yen Phu rare earth ores

The Yen Phu rare earth mine has a reserve of about 28,000 tons of REO. Rare earth minerals are xenotime in small content. Iron minerals include goethite and magnetite, which account for 18-20% and 24-26%, respectively. Other components include mainly quartz 41-43%, kaolinite + chlorite 3-5%, feldspar 2-4%, talc 1-3%, etc. The ore has an average content of ~ 1.2% REO, ~33% Fe, ~40% SiO₂, etc [30]. Yen Phu rare earth mine is the primary one of Vietnam to implement both mining and processing of rare earth ores. After more than two years of operation (since 2019), the achieved processing performance is low with the rare earth recovery of less than 50% REO, the average tailings are about 0.7% REO. The processing flowsheet of the plant includes a combination of gravity concentration- magnetic separation - flotation. Gravity separation uses the washing–classifying process. There are three stages of magnetic separation to recover iron concentrate of the desired grade. Flotation recovering rare earth minerals includes 01 rougher, 03 cleaner, and three scavenger flotation. Chemicals used include soda ash (pH = 9); water glass, lignin, corn starch as depressants; Berol and diesel oil as a collector. An outline of the flowsheet is shown in Figure 3 [31].

3. Conclusions

Vietnam's rare earth resources are relatively large. However, the application of REEs so far is still minimal and currently mainly stands at laboratory-scale or semi-industrial studies. Rare earth mining and processing in the country is still very modest.

Many research has concentrated on separating rare earth ores with different ore types, focusing mainly on the most critical minerals of bastnaesite, monazite, and xenotime.

The methods for extraction and recovery of minerals in rare earth ores are mainly combinations of gravity concentration, magnetic separation, electrostatic separation, and flotation. Flotation is the only method in the beneficiation flowsheets of Nam Xe North and Nam Xe South ores. For Dong Pao and Yen Phu ores, combinations of gravity-magnetic separation -flotation methods are used.

There should be further studies of technological processes and proper equipment for each rare earth ore type to maximize resource recovery, improve economic efficiency, and protect the environment in Vietnam and worldwide.

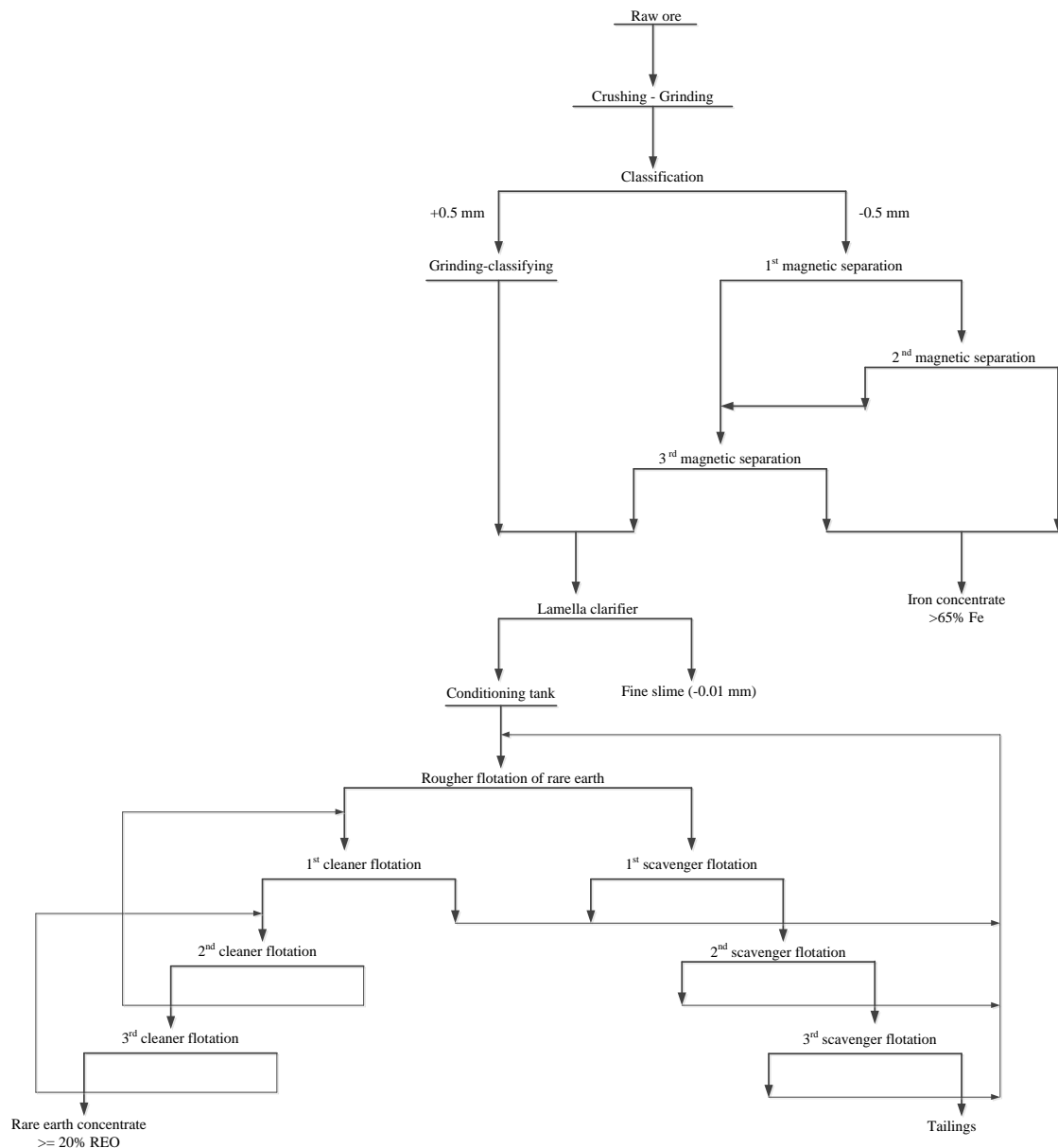


Fig. 3. Outline flowsheet of the Yen Phu rare earth ores in 2020.

4. Acknowledgments

The paper was presented during the 6th VIET - POL International Conference on Scientific-Research Cooperation between Vietnam and Poland, 10-14.11.2021, HUMG, Hanoi, Vietnam.

5. References

1. C.K. Gupta, and N. Krishnamurthy, 1992. Extractive metallurgy of rare earths, *International Materials Reviews*, 37(1): 197-248 .
2. C. Zhou, 1993. Rare earth industry of China, *Journal of Alloy Compd*, 192: 111-3.
3. Massari S, and Ruberti, M. Rare earth elements as critical raw materials: focus on international markets and future strategies. *Resource Policy*; 38(1): 36-43, 2013.
4. A. Jordens, Y.P. Cheng, K.E. Waters, 2013. A review of the beneficiation of rare earth element bearing minerals, *Minerals Engineering*, 41: 97-114.
5. A.V. Naumov, 2008. Review of the world market of rare-earth metals Russian, *Journal of Non Ferr Met*; 49(1):14-22.
6. F. Xie, T.A. Zhang, D. Dreisinger, and F. Doyle, 2014. A critical review on solvent extraction of rare earths from aqueous solutions, *Minerals Engineering*, 56: 10-28.

7. S.C. Chelgani, M. Rudolph, T. Leistner, J. Gutzmer, and U.A. Peuker. A review of rare earth minerals flotation: Monazite and Xenotime, *International Journal of Mining Science and Technology*, 25(6): 877-883, 2015.
8. Liyanadirah Mat Suli, Wan Hanisah Wan Ibrahim, Badhrulhisham Abdul Aziz, Mohd Rizauddin Deraman, Nurul Ain Ismail, A Review of Rare Earth Mineral Processing Technology, 2017.
9. Moustafa, M.I., Abdelfattah, N.A., 2010. Physical and chemical beneficiation of the Egyptian Beach Monazite, *Resource Geology* 60 (3): 288–299.
10. Nagaiyar Krishnamurthy, Chiranjib Kumar Gupta, 2016. *Extractive Metallurgy of Rare Earth*, 2nd Editor, Chapter 3.
11. Cheng Jianzhong, Hou Yunbing and Che Liping, 2007. Flotation Separation on Rare Earth, *Minerals and Ganges*. 25(Spec.Iss.): 62, Dec.2007.
12. Chelgani, S., Chehreh, Rudolph, M., Leistner, T., Gutzmer, J., Peuker Urs A., 2015. A review of rare earth minerals flotation: Monazite and xenotime, *International Journal of Mining Science and Technology*.
13. Duong Van Su, 2014. Study on technology for processing rare earth - barite - fluorite ore from Dong Pao mine (Lai Chau), Ministry of Industry and Trade.
14. Nguyen Ngoc Anh, 1983. Report on search-preliminary exploration of Nam Xe North rare earth mine, Geological Team 151.
15. Nguyen Van Hanh, 2005. Study on separation of rare earth, fluorite, and barite from weathered ores of Dong Pao mine, Technical PhD Thesis.
16. Nguyen Thi Hong Ha, 2010. Study on technology for processing weathered rare earth with F7 ore body, Dong Pao mine, Institute of Mining Science and Technology.
17. <http://vinacom.vn/>, 15/07/2013.
18. Lai Chau Rare Earth Joint Stock Company – VIMICO, 2009. Investment project on mining and processing of rare earth ore with F3 ore body, Dong Pao mine.
19. Nguyen Duy Phap, 2011. Study on Processing technology of rare earth ores Dong Pao, Tam Duong District, Lai Chau Province, Institute of Rare and Radioactive Elements.
20. Naoto Yamagishi, 2010. Feasibility study report of F3 body, Dong Pao, Lai Chau, Toyota Tsusho, Sojit Company.
21. Tran Thi Hien, 2013. Study report on rare earth ore technology samples at Nam Xe North rare earth mine, The National Institute of Mining - Metallurgy Science and Technology.
22. Fong-Sam, Y., 2013. The Mineral Industry of Vietnam, Mineral Yearbook. USGS.
23. Nguyen, T., 2013. Study on geochemistry of the South Nam Xe carbonatites, north-west Vietnam, Shizuoka University.
24. Nguyen, T., Wada, H., Ishikawa, T., Shimano, T., 2014. Geochemistry and petrogenesis of carbonatites from South Nam Xe, Lai Chau area, northwest Vietnam, *Mineralogy and Petrology*, 108(3): 371–390.
25. Heinig, T., Burisch, M., Möckel, R., Phan, Q.V., Ebert, D., Gutzmer (in prep.) Mineralogy, petrography and genesis of REE bearing carbonatite dykes, Nam Xe deposit, Vietnam.
26. Hanor, J.S., 2000. Barite-celestine geochemistry and environments of formation: Sulfate Minerals, *Crystallography, Geochemistry and Environmental Significance*, 40: 193-275.
27. Nguyen Van Hanh, 1988. Experimental research on semi-industrial technology of Nam Xe South rare earth ore processing, Institute of Nonferrous Metallurgy.
28. Tran Van Minh, 1984. Report on research project on Nam Xe South rare earth ore processing technology at laboratory scale, Institute of Nonferrous Metallurgy.
29. Robert Möckel, Thomas Heinig, Alan Fernando Cardenas Vera, Jens Gutzmer, Gerhard Merker, Van Phan Quang, 2019. Beneficiation of parisite-rich rare earth ore from the Nam Xe South deposit, Vietnam, *Life with Ore Deposits on Earth – 15th SGA Biennial Meeting 2019, Volume 4*
30. Luong Quang Khang, 2012. Characteristics of rare earth ore at Yen Phu mine, Yen Bai, *Journal of Mining and Earth Sciences*, 40: 23-29.
31. Pham Duc Phong, 2020. Study on technological equipment solutions and selective chemicals to process fine-grained rare earth ores in Yen Phu rare earth mine, The National Institute of Mining - Metallurgy Science and Technology.

Technological and Economic Analysis of the Application of Surface Miner on the Example of a Limestone Deposit in Poland

ZAJĄCZKOWSKI Maciej^{1,*}

¹ AGH University of Science and Technology, Kraków, Poland

Corresponding author: maciejz@agh.edu.pl

Abstract. Mining a deposit utilizing surface miner is very popular in many countries. Presently, a surface miner has also experimented with extracting different deposits: bauxite, hematite, sandstone, shale etc. Surface miners can completely eliminate drilling and blasting operation and primary crushing unit, thus reducing their associated environmental hazards. Apart from this, the sized excavated material increases transport or conveying efficiency and saves the energy requirement in processing. So far, these machines have not been used in Poland. To evaluate this technology, tests were carried out on one of the limestone deposit in Poland. During these tests, basic parameters of efficiency, output quantity and mining costs were defined. The conducted tests have shown that this technology cannot be used in all geological and mining conditions. Therefore, the article presents the advantages and disadvantages of using surface miner, taking into account the Polish geological and mining conditions.

Keywords: Limestone deposit, Surface miner, Technology of extraction, Non-blasting extraction

1. Introduction

In surface mining, there are increasing restrictions on the use of drilling and blasting operations, which are the primary means of mining rocks with compressive strength exceeding 20 MPa. These limitations are due to the fact that significant impacts from paraseismic vibration, flyrock, and shock waves occurring during these operations negatively affect protected structures or residential clusters in the vicinity of surface mines. In such cases, it is necessary to replace drilling and blasting operations with mechanical mining methods that would allow the extracted mineral to remain economically competitive [1].

Among the many decision-making problems in the process of designing and managing exploitation, and, at the same time, one of the most important ones is the appropriate choice of technical equipment for the implementation of the main technological processes in extraction, which include mining, transport and processing of the mineral. At the same time, it is necessary to ensure appropriate quantitative and technological links between these processes in order to achieve the full efficiency of both the extraction and processing system. It is essential to ensure the quality of the aggregate according to the in-house production control of aggregates [2].

For rocks, with compressive strength of 20 MPa and higher (e.g. limestone, dolomite, sandstone, marl, travertine, etc.) the lowest unit costs (in PLN/Mg of material) are achieved when the blasting technique is applied. Therefore, it is the primary method of mining rock raw materials, but with the existing constraints of paraseismic vibration, airborne shock waves, or rock debris scatter, mines do not have the option of using it close to the mining boundary adjacent to residential areas or protected structures [3]. This restriction may also be established due to the impact of noise from operating machinery [4]. In this situation, despite higher mining costs, other solutions for mining hard rocks are currently being sought.

Market availability of machinery, amount of capital expenditure, operating costs including maintenance etc. are also considered. Each of the factors cited above can be decisive in selecting the method of mechanical rock mining to be implemented.

2. Test site

The first tests of the Wirtgen surface miner for mining rock raw material deposits in Poland were conducted at the "Raciszyn" limestone deposit.

Since it is impossible to use the blasting technology to mine this deposit, it was decided to conduct tests using the Wirtgen 2200 surface miner.

The important fact was that the mine is focused on the production of limestone aggregate with a fraction of 0-31.5 mm. This fraction is widely used in the road construction industry, as a mix for the base road layer, and is the basic raw material for the production of lime powder. In addition, this product is supplied to the conventional power generation sector and, after grinding, is used as a sorbent in flue gas desulfuring

processes. In the case of the analyzed mining company, the 0-31.5 mm fraction accounted for about 70% of the sales volume of all aggregates and is therefore the most representative commercial product for many players in this sector [5].

Table 1 shows the basic physical and mechanical parameters of the "Raciszyn" limestone deposit.

Tab. 1. Physical and mechanical parameters of the "Raciszyn" limestone deposit.

Parameters	Unit	Average values
Bank density	Mg/m ³	2.22
Porosity	%	17.45
Absorbability by weight	%	6.07
Compressive strength	MPa	57
Boehme abrasion test	cm	1.15
Deval abrasion test	%	12.56

The classification of cutability by surface miner includes 5 physical and mechanical parameters of the deposit and divides them into 5 cutability groups [6]. The parameters of the "Raciszyn" limestone deposit, according to the above classification, pointed to the "economic excavation" group.

3. Technical specifications of the Wirtgen 2200 SM surface miner

The tests on the "Raciszyn" limestone deposit were carried out with the use of the only Wirtgen 2200 SM surface miner available on the Polish market. Table 2 shows the exact technical specifications of the Wirtgen 2200 SM surface miner.

Tab. 2. Technical specification of the Wirtgen 2200 SM [7].

Parameter	Unit	Size
Cutting width	[mm]	2 200
Cutting depth with a direct loading/windrowing	[mm]	0÷300/0÷250
Spacing between the cutting cutters on the drum	[mm]	38
Number of cutters	[Pcs.]	76
Diameter of cutting drum with cutters	[mm]	1115
Maximum tilt of the drum	[°]	5
Motor power	[kW/KM]	708/950
Motor speed	[min ⁻¹]	2 100
Driving speed	[km/h]	0÷5
Maximum inclination	[%]	90
Kerb weight	[kg]	44 500
Operating weight	[kg]	50 780

The Wirtgen 2200 SM surface miner made a single course of 150 to 200 m during the test, then returned by reversing to the beginning of the work area. This system of work was dictated by a significant limitation, which is the size of the accessible deposit roof, and thus the limited length of the work area. Bulk measurements were made by accurately weighing the excavated raw material on scales installed on the wheel loader and measurements of fuel consumed.

Figure 1 presents the operation of the Wirtgen 2200 SM surface miner with direct loading onto dump trucks at the "Raciszyn" limestone deposit.



Fig. 1. Operation of the Wirtgen 2200 SM combine with direct loading onto technological trucks on the "Raciszyn" limestone deposit.

4. Production results of tests

The operation of the Wirtgen 2200 SM surface miner at the "Raciszyn" limestone deposit can be divided into two working stages: preparation and production. In the preparatory stage, the surface miner levelled the deposit floor in the area to be tested. This stage, which lasted about a week, was characterized by a higher travel speed of the surface miner and a lower efficiency of the machine. Proper operation at full capacity of the surface miner occurred at the production stage. The output obtained during the test was loaded directly onto technological trucks, or, in the second variant, it was left on the floor of the working level for further loading.

To efficiently operate the Wirtgen surface miner, 3 dump trucks (Volvo A40 articulated dump trucks) were required to directly collect the output. Providing a standby technological truck waiting to be loaded in addition to the one currently being loaded was a necessary element in maintaining the smoothness of the milling process. This system ensured continuous operation of the Wirtgen 2200 SM surface miner without the need to stop the process due to an inability to collect the output.

Operating tests carried out on the "Raciszyn" limestone deposit were used to determine the performance of the Wirtgen 2200 SM surface miner. The test results are presented in Table 3.

Tab. 3. The test extraction results of the Wirtgen SM 2200 on the "Raciszyn" limestone deposit.

Item	Unit	Size
Average cutting speed	[m/min]	7.2
Machine test time	[h]	204
Production volume	[Mg]	39,485
Total fuel consumption	[liters]	17,800
Average hourly capacity	[Mg/h]	194
Average fuel consumption per hour	[liters/h]	87.3
Average fuel consumption per tonne	[liters/Mg]	0.45

During the entire test, the Wirtgen 2200 SM operated for 204 hours (according to the machine's timer) and consumed 17,800 liters of diesel fuel. These figures were then used to determine the actual output of the Wirtgen 2200 surface miner at the "Raciszyn" limestone deposit at 194 Mg/h, and average fuel consumption - at 87.3 liters/h.

With a limestone average compressive strength of 57 MPa, the Wirtgen 2200 SM achieved an average cutting speed of 7.2 m/min.

The output produced by the Wirtgen 2200 SM was highly ground. Figure 2 shows the grain size distribution curve of the output produced by the Wirtgen 2200 surface miner at the "Raciszyn" limestone deposit.

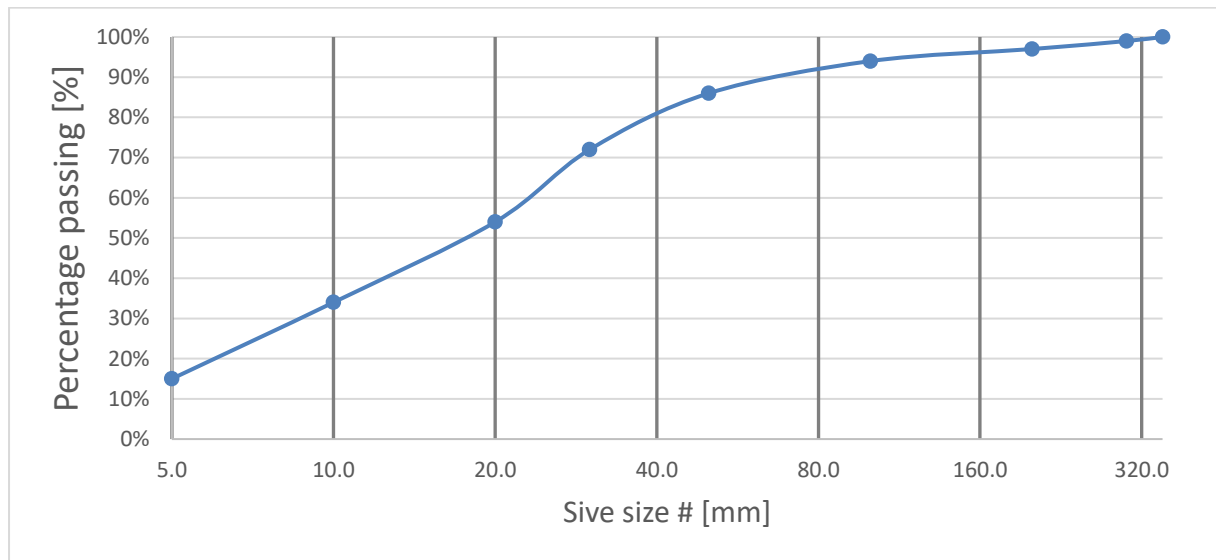


Fig. 2. Grain Size Distribution Curve of the output obtained with the use of the Wirtgen 2200 SM on the "Raciszyn" limestone deposit.

The grain size distribution curve of the excavated material obtained with the Wirtgen 2200 SM confirms the high level of fineness of the raw material. Its size does not exceed the 0-350 mm fraction, and the P80 index for the obtained feed was 38 mm.

The uniformity of the output is also relatively favourable. The degree of uniformity of grain size was determined as:

$$U = \frac{d_{60}}{d_{10}} = \frac{23}{4} = 5,75 \tag{1}$$

where:

U - degree of uniformity of grain size;

d_{60} - diameter of 60% of grains [mm];

d_{10} - diameter of 10% grains [mm].

5. Economic results of the tests

In the economic analysis of the operation of the Wirtgen SM 22200 surface miner on the "Raciszyn" limestone deposit, only the direct costs of the cutting process were considered and related to 1 Mg of the excavated material.

The most significant share in the costs of excavation with the Wirtgen 2200 SM surface miner on the "Raciszyn" limestone deposit was attributed to the cost of renting the machine. If a machine is purchased, a similar level of cost is to be expected due to the depreciation of the machine. Fuel consumption was another important component of the overall costs. Together, these two costs accounted for 71% of total costs.

The cost also included the salaries of 2 operators and the cost of replacing the cutters on the cutting

drum.

The results of the mining test with the Wirtgen SM 2200 surface miner on the "Raciszyn" limestone deposit are presented in Table 4.

Tab. 4. Economic results of the test of extraction of the Wirtgen SM 2200 on the "Raciszyn" limestone deposit.

Types of costs	Unit	Amount	Share
Surface miner rental	[PLN]	90,533	38%
Flat rate for additional mileage	[PLN]	26,306	11%
Service/insurance/transport	[PLN]	8,458	4%
Interchangeable tools (cutters)	[PLN]	3,303	1%
Operator service	[PLN]	31,570	13%
Total fuel cost	[PLN]	78,320	33%
Cost of water and other costs	[PLN]	2,000	1%
Total	[PLN]	240,489	100%

Considering the fact that 39,485 Mg of limestone were excavated during the tests and the costs amounting to PLN 240,489 were incurred, the unit cost of excavation with the Wirtgen 2200 surface miner on the "Raciszyn" limestone deposit was PLN 6.09/Mg.

6. Conclusions

The tests of the surface miner were the first of such tests carried out in Poland. To date, hydraulic hammers, vibration rock breakers or rippers have been used to mechanically mine hard rock materials.

These tests provided an excellent opportunity to conduct empirical measurements of the main parameters of the Wirtgen 2200 surface miner on the "Raciszyn" limestone deposit.

In addition to such parameters as effective capacity, fuel consumption per hour, output grain size, and, finally, the unit cost of mining, other important factors have been indicated that should be taken into account when designing the exploitation of deposits with the use of this mining machine.

An important factor affecting the milling combine's performance is the effectiveness of the workplace length. Having to manoeuvre and change the direction of cutting significantly increases the machine's downtime, limiting its productivity. Therefore, the optimal way to operate the surface miner is in a circular motion to ensure its uninterrupted operation. However, this requires a large surface area of the workplace.

Small caverns and inhomogeneities in the deposit were also significant impediments to the operation of the surface miner. When a cavern was encountered, it was necessary to identify it, open it by hydraulic hammer, and backfill it with additional material so that the surface miner would be able to drive over it.

Two operators were required to operate the machine on the Raciszyn limestone deposit. One of them controlled the machine from the operator's cab, and the other one supervised the machine's progress while standing next to it.

The surface miner creates smooth surfaces, both on the slopes and on the floor of the working level. This results in improved geotechnical safety and fewer transport road maintenance problems.

The disadvantages include a high excavation cost, which amounted to PLN 6.09/Mg on the "Raciszyn" limestone deposit. This result is incomparably higher than for the blasting technique (1.5-2.0 PLN/Mg).

However, it should be noted that the surface miner allows direct loading onto technological trucks, eliminating the need to load the excavated material with an additional machine (hydraulic excavator or wheeled loader). The specified cutting cost, therefore, already includes the cost of loading and the first processing stage, in some cases.

The last of the important issues noticed during the tests was that, in addition to fuel consumption, the surface miner required a large amount of water to cool the cutting drum. This needs to be factored into the logistics of fuel and water deliveries.

7. Acknowledgements

The paper was presented during the 6th VIET - POL International Conference on Scientific-Research Cooperation between Vietnam and Poland, 10-14.11.2021, HUMG, Hanoi, Vietnam.

8. References

1. Kolleth, H., 1990. Overview of open pit mines for mining technologies with high outputs, *Bulk Solid Handling*, 10(1): 29-35.
2. Kubuszewski, T., Góralczyk, S., 2015. Analiza systemu zakładowej kontroli produkcji kruszyw po wejściu w życie rozporządzenia nr 305/2011 (CPR), *Mining Science - Mineral Aggregates*, 22(1): 93-100.
3. Volk, H.J., 2016. Wirtgen drives the development of surface mining, *Procedia Engineering*, 138: 30-39.
4. Dey, K., Bhattacharya, J., 2012. Operation of Surface Miner: Retrospect of a Decade Journey in India, *Procedia Engineering*, 46: 97-104.
5. Będkowski, T., Kasztelewicz, Z., Zajączkowski, M., Sikora, M., 2016. Technical and economic analysis of mechanical rock extraction based on "Raciszyn" deposit, *Inżynieria Mineralna - Journal of the Polish Mineral Engineering Society*, 38(2): 107-112
6. Dey, K., Ghose, A.K., 2008. Predicting "Cuttability" with Surface Miners – A Rockmass Classification Approach, *Journal of Mines, Metals and Fuels*, 56(5-6): 85-91.
7. Schimm, B., Georg, J., 2014. Wirtgen Surface Miner – The First Link of a Simple Extraction and Materials Handling Chain in "Medium Hard"-Rock, *Proc. of the 12th Int. Symp Continuous Surface Mining – Aachen*, 511-521, DOI: 10.1007/978-3-319-12301-1_44.

Determination of Land Fund for the Development of Static Road Traffic Demand in Hanoi (Vietnam)

PHAN Anh^{1,*}, VO Thi Hong Lan², PHAN Huy Duong³

¹ Hanoi Academy of Banking, Hanoi, Vietnam

² Hanoi Department of Finance and Planning, Ministry of Public Security, Hanoi, Vietnam

³ Dai Nam University, Hanoi, Vietnam

Corresponding author: duongph@vnu.edu.vn

Abstract. Determining a reasonable proportion of land fund for urban static traffic will meet the current needs and future development of urban areas, contributing to improving the operational quality of urban transport systems and improve the quality of life of people in urban areas [1]. Hanoi, the capital of Viet Nam, is facing difficulties in meeting the land fund for static traffic development. In 2020, the city's land fund meets only 38.73% of the demand for traffic system development in general, static traffic in particular [2]. By using a regression model on the relationship between GDP per capita and demand for means of transport in Hanoi, the article forecasts the demand for urban static traffic development in Hanoi city, demand for land fund for its static traffic development to 2025 and 2030. From the forecast results, the article proposes some solutions on meeting the land fund demand for static traffic development in order to achieve efficiency of the government's policies on static traffic development in Hanoi.

Keywords: Static traffic, Determination of land fund for static road traffic

1. Introduction

Static traffic means the entire facilities serving passenger and cargo vehicles during the non-moving time of modes of transport. Static traffic related to space is ground, overhead and underground [1]. Components of static traffic: garages, parking lots, terminals serving intercity transport, inner-city transport, transshipment of goods and passengers [3].

Static traffic ensures the systematic, synchronous, and compatible features of the urban transport system. Static traffic is an essential element of the transport system. The transport system can only operate effectively when the details in the synchronous system are compatible, so it is necessary to put static traffic on par with its importance. This should be considered right from the stage of planning, implementation, and operational exploitation. The main criteria considered here are (1) land fund for static traffic compared to the total urban land area (6-8%), (2) the ratio of static traffic land fund compared to land fund or urban traffic (25-30%), and (3) investment capital for static traffic in the structure of investment capital for urban traffic [4]. In the recent years, the Ministry of Transport has accelerated the investment progress of construction of urban transport infrastructure works, wharves, parking lots, inland waterway ports; urban traffic infrastructure works connecting key airports and seaports; strengthen inspection of the maintenance, maintenance and assurance of convenient bridges and roads for smooth and safe traffic. However, because of the rapid population growth in urban areas along with large travel demand, the land area for static traffic does not meet the demand for static traffic development [4] and the lack of parking spots has led to sidewalks, roadways, parks being occupied and parking lots, parking vehicles are rampant in many urban areas [5].

According to calculations by the Institute of Strategy and Transport Development, in 2025 there will be 600 thousand cars and 7.9 million motorbikes; the number will be nearly 1 million cars and 10.5 million motorbikes in 2030, therefore, it is necessary to increase investment in static traffic development of Hanoi [6]. The article forecasts the demand for static traffic development of the city, thereby determining the demand for land fund for its static traffic development. The article also proposes policy recommendations to improve the ability to meet the land fund for static traffic development, contributing to improving the effectiveness of the policy of static traffic development of the city.

2. Modeling and Research Methodology

2.1. Modeling

Urban static traffic is the entire physical and technical infrastructure serving traffic of the city but not directly involved in the traffic process. Large-scale static traffic is bus station, pier, port and the small scale is parking lot, parking place, etc. [7].

Urban static traffic development is the development of systems of wharves, grounds and space areas to serve various types of transport in non-moving time, optimally meeting the demand for static traffic [8]. According to Tran Thi Lan Huong (2011), one of the criteria to evaluate the results of the proposed static traffic development is the target of land fund for static traffic [8], the author also assumes, the demand for static transport system depends on GDP per capita, and it can be determined through GDP per capita. According to Ngoc Hai (2017), in order to develop static traffic in Hanoi in the context of the limited urban land fund, many measures are needed to expand the space for static traffic, in which, emphasizing the importance of exploiting the above and underground space [3]. Tuan Luong (2021) also said that one of the solutions to improve the effectiveness of Hanoi's static traffic development policy in Hanoi city is to determine the land fund for static traffic development and propose solutions to enhance the traffic capacity, meet the land fund for static traffic development [2].

Thus, the relationship between GDP per capita and demand for land fund to develop the urban static traffic is shown in Figure 1.

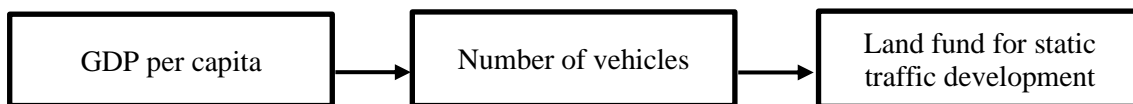


Fig. 1. Model of forecasting demand for land fund to develop the urban static traffic.

With the hypothesis: When GDP per capita increases, the number of vehicles will increase, the relationship between GDP per capita (GDPP) and the number of vehicles (NV) is represented by the model [9] as follows:

$$NV_i = \beta_1 + \beta_2 * Ln(GDPP_i) + U_i \tag{1}$$

Demand for land fund (LD) for static traffic development in year (t) is determined by the formula [1]:

$$LD^t = \sum_{j=1}^m a_j * NV_j^t * S_j \tag{2}$$

In which:

LD^t - Demand for land fund for static traffic development in year t, m^2 ;

NV_j^t - Number of vehicles of type j in year t, unit;

a_j - Percentage of vehicles type j using public parking, %;

S_j - Usable area of vehicles type j at the public parking lot, m^2 .

2.2. Research Methodology

The article uses secondary data on GDP per capita and the number of vehicles in Hanoi to determine the sample regression function between GDP per capita and the number of vehicles according to the model (1). Secondary data are collected in the period 2008-2020, the regression model is estimated by the Ordinary Least Squares method, the fit of the sample regression function is evaluated through the coefficient of determination R^2 ; The level of statistical significance of the regression coefficient is tested through the T-test with Sig. < 0.05, The appropriate of the regression function is tested through Anova analysis. Based on the estimated regression model, the article forecasts the number of vehicles in the year of 2025 and 2030 corresponding to the GDP per capita in those years.

Demand for land fund for static traffic development is calculated according to formula number 2 and the data on the average rate of each type of vehicle using public parking, the forecasted quantity of each type of transport means of public parking, the average square of usable area at the public parking lot of each type of transport.

3. Results

3.1. Descriptive statistics on land fund for static traffic development in Hanoi

Parking lots and parking spots for cars and motorcycles: There are 1,178 authorized parking spots for cars and motorcycles (car parking spot: 553 spots, motorcycle parking spot: 625 spots) land area for parking lots and parking spots is 429,269 m^2 [10].

The bus station system in Hanoi consists of 11 inter-provincial bus stations and 30 intra-provincial bus stations in the districts on a small scale. The main bus stations in Hanoi area are from 10,000 m^2 to more

than 30,000 m². The smaller bus stations vary from 100 m² to over 1,000 m² (mainly of districts and communes).

Besides, there are ten inter-provincial truck stations with a total area of 5.9 ha. Most truck stations are transformed from ancillary works associated with the wholesale market system or spontaneous ones in the areas of non-fixed traffic hubs. The stability of the truck dock system is low.

The land fund reserved for authorized public parking lots and parking spots counted and surveyed currently meets only 8-10% of the demand for parking spots. Other infrastructures can fulfill the shortage of more than 90% of parking spots. Apartment buildings and urban areas (accounting for about 24%, equivalent to 93.4 ha); offices and private houses (accounting for 63.5% or 245.3 ha); roadbed, sidewalks, dead-end lanes, and schoolyards with areas for toll parking name a few. However, parking spots in the yard of toll collection agencies are not declared by organizations and agencies. Therefore, the exact capacity of parking lots and parking spots is not determined (accounting for about 12% or 46.36 ha); parking spots in the vacant areas of projects that have not yet started construction (accounting for about 0.5%, equivalent to 1.9 ha).

Most bicycle and motorcycle parking spots are narrow in size and small in scale. All the parking spots take advantage of sidewalks and are not built specifically for bicycle and motorcycle parking. Car parking lots are mainly small ones and lack facilities to meet the demand. Most of these parking lots take advantage of sidewalks and roadbeds. Eight new spots are planned and built standardly, among which the most extensive area of 16,000 m² with the capacity of 400 cars per day and night is located in the city center. Other parking spots are at the entrance to Hanoi, where incoming and outgoing vehicles are not many. The most significant parking spot is in My Dinh, with two components of 22,000 m² and 72,000 m², primarily for buses or important sports events at My Dinh National Stadium. Eight current parking lots occupy a total area of 185,250 m² with a capacity of 2830 vehicles.

Lack of parking lots is becoming a problem for a long time in Hanoi, particularly after the city expansion of the administrative boundaries. The prominent parking spot is still roadbed with a localized sign without a large-scale parking lot in the main streets. As the minimum standard for a parking spot is 25 m² of land, an area of 429,269 m² for parking lots (including the parking area on the roadbed and sidewalks) meets 30% of the parking demand in Hanoi, accounts for 0.45% of the urban land fund. Meanwhile, according to the standards of a modern city, static traffic requires 4-7% of the land fund.

Although the land area for static traffic in inner-city districts is insufficient, these districts do not have land funds to expand the number and size of parking spots. Newly built offices have basements for parking, but the capacity is negligible. In the newly constructed buildings in the central area, parking aside from the buildings is an alternative for the insufficient parking lots in the basements. The tunneling, raising the floor, or using the automated parking system of Hanoi has not been conducted due to the high construction cost of these projects. Besides, the parking fees at these spots are very high and not appropriate for living standards. The immediate measure is expanding the parking lots around the entrance to the city.

Tab. 1. Parking lots and parking spots in Hanoi.

No.	District	Number of parking stations and spots	Total area (m ²)	Capacity (vehicle)	Parking area on (m ²)		Name of station
					Roadbed, sidewalks	Parking station built according to planning	
1	Hoan Kiem	63	21,190	1,513	21,190		
2	Hai Ba Trung	27	15,038	1,034	15,038	0	
3	Ba Dinh	26	39,848	1,215	23,173	16,657	Ngoc Khanh
4	Dong Da	11	8,416	385	8,416		
5	Tay Ho	2	320	28	320		
6	Hoang Mai	2	26,717	400	4800	21,917	Kim Nguu
7	Cau Giay	11	41,148	1,236	20,248	20,900	Dich Vong
8	Long Bien	1	12,993	180		12,993	Gia Thuy
9	Tu Liem	2	93,000	1530		93,000	My Dinh 1, 2 Nam Thang Long
10	Dong Anh	1	20,000	160		20,000	Hai Boi
Total		146	27,610	7681	93,185	185,425	8

Source: Hanoi City People's Committee 2019

According to the municipal plan, roads must account for 15-20% of urban land, including 5-6% of urban land for static parking lots. In Hanoi, the land fund for transport accounts for a meager ratio, including land for static traffic. In addition, the improper use of the land fund also contributes to traffic congestion, especially in inner-city districts.

Location and arrangement of parking spots in cities

The ratio of parking lot types by scale in each district is presented in Table 2, in which the outdoor and campus parking lots are listed as “other”. The ratio of parking lots on sidewalks and roadbed is 10-15%. The rest of the demand is provided by campus and public outdoor or private parking lots.

Tab. 2. Location of parking lots for vehicles in 2019.

District	Sidewalk	Roadbed	Other	Unidentified
1 Ba Dinh	5%	9%	67%	19%
2 Hoan Kiem	7%	9%	65%	20%
3 Hai Ba Trung	6%	6%	66%	21%
4 Dong Da	6%	9%	64%	21%
5 Tay Ho	5%	8%	70%	18%
6 Thanh Xuan	4%	5%	64%	27%
7 Cau Giay	5%	7%	63%	25%
8 Hoang Mai	4%	6%	66%	24%
9 Long Bien	2%	8%	53%	37%
10 Tu Liem	1%	10%	64%	25%
11 Thanh Tri	2%	11%	65%	23%
12 Soc Son	3%	7%	68%	21%
13 Dong Anh	2%	8%	63%	27%
14 Gia Lam	1%	6%	67%	26%

Source: Hanoi City People's Committee 2019

Current parking lots in Hanoi mainly take advantage of the sidewalks and roadbeds. In some places, parking on the sidewalks is a ban for bicycles and motorcycles. Still, they are kept on the roadbed, such as Hang Bong and Hang Gai Streets, Hoan Kiem District, which makes the roadbed overloaded for vehicles and is now used to keep vehicles, causing the regular occurrence of traffic congestion on the streets.

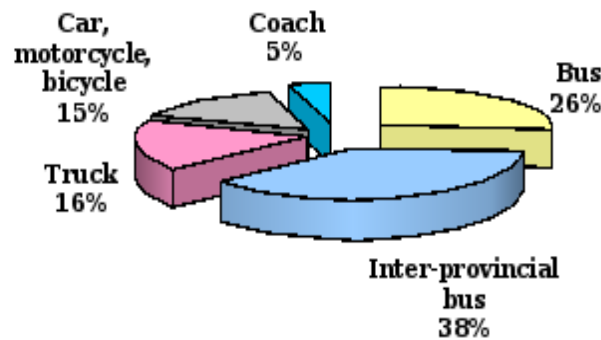


Fig. 2. Parking structure by vehicle type in Hanoi.

Analysis of land funds and parking spots for static road traffic in Hanoi shows that the ratio of land reserved for static traffic is too low. Simultaneously, the means of transport has increased dramatically, significantly personal cars are overgrowing. Lack of parking lots and parking spots for oversized vehicles such as trucks, coaches, and current car parking lots is only suitable for cars and small trucks. The inter-provincial transport stations are usually small in scale, connected to the primary market system, and there has not been a large-scale hub truck station. The gateway areas and traffic hubs lack stops to support the traffic organizations, so the vehicles have to park on the roadbed and sidewalks, causing more congestion. The network of parking spots is not rational in terms of density, location, and distance. Many new cities have not been calculated correctly and sufficiently for parking lots but only arranged separately for high-rise buildings. Many hotels and commercial centers do not have parking space; hence, guests occupy streets

instead of parking. The construction process is always in demand, even in determining the location and size of the land fund. The technical infrastructure of parking spots and parking lots is lacking, the form of parking lots is monotonous, mainly on the ground, equipment and facilities are lacking and inconsistent, etc. Many organizations and individuals involved in the business and operation of the parking spots lead to uncontrolled and cursory management, causing confusion, insecurity, disrupting planning, and losing the city's revenue. Organization and management are still fragmented and limited. Although the City People's Committee has approved the planning for parking lots, the plan implementation is still slow due to insufficient and inconsistent policies, especially the lack of capital.

3.2. Determination of static traffic development demands in Hanoi

Planning a public parking network aims to meet about 66% of Hanoi's total parking demands. The remaining demand for parking is allocated to construction works (offices, training schools, high-rise buildings, etc.) in the direction of an increasing basement and parking area to meet the demands themselves and a part of public demands of the surrounding area.

Hanoi's different transportation types include cargo vehicles, individual cars, coaches, buses, motorcycles, special-purpose vehicles, rudimentary vehicles, and bicycles. The number of bikes has not increased in recent years and remains the same in the future. Special-purpose vehicles are in small quantity and used and preserved separately without affecting public land funds. The rudimentary cars are on a downward trend, so they also do not affect the demand for static traffic in the future. Thus, the construction of vehicle models is as follows: Trucks, coaches, cars, motorcycles, and buses.

Suppose the relationship between the number of vehicles and the GDP per capita correlates through the two-variable function.

Tab. 3. Statistics of GDP and the number of road vehicles in the inner-city areas 2008-2020.

Year	GDP per capita (VND)	Number of motorcycles	Number of cars	Number of coaches	Number of trucks
2008	57862880	785969	96679	5128	6710
2009	62832523	951083	103748	6302	6984
2010	68827318	1112976	112126	7485	8213
2011	72862880	1197166	126478	9050	8571
2012	77432523	1600000	150000	10775	9618
2013	82827318	2154646	177986	13057	10202
2014	85,430,000	2466114	187883	16137	11732
2015	89930000	2850068	209695	19525	11078
2016	93840000	3306079	244295	21380	11300
2017	98375000	3785460	285825	22983	11865
2018	112270000	4277570	332986	25282	12695
2019	120100000	4812266	369614	27304	12885
2020	125700000	5437861	401032	29134	13568

Source: Hanoi City People's Committee 2020

*** The regression results for forecasting the number of motorcycles**

Tab. 4. The results of regression analysis with motorbikes.

	Coefficients				R ²	ANOVA ^a	
	β	Std. Error	t	Sig.		F	Sig.
(Constant)	-112,730352.35	7,089,170.683	-15.902	.000	0.960	265.039	.000 ^b
GDPP	6,316,585.65	387,996.490	16.280	.000			

The sample regression function of GDP per capita and number of motorcycles is described as follows:

$$NV_i = 6,316,585.65 * \ln(GDPP_i) - 112,730352.35$$

With $R^2 = 0.99$ the sample regression function is considered to be relatively concordance.

With T- test, the values of $Sig = 0.000 < 0.05$: regression coefficients are statistically significant.

Anova analysis results: $F = 265.039$, $Sig = 0.000 < 0.05$: the population regression function is considered to be concordance.

*** The regression results for forecasting the number of cars**

Tab. 5. The results of regression analysis with cas.

	Coefficients				R ²	ANOVA ^a	
	β	Std. Error	t	Sig.		F	Sig.
(Constant)	-7,446,466.894	529,075.619	-14.074	.000	0.950	209.743	.000 ^b
GDPP	419,366.647	28,956.770	14.483	.000			

The sample regression function of GDP per capita and number of cars is described as follows:

$$NV_i = 419,366.65 * \ln(GDPP_i) - 7,446,466.89$$

With $R^2 = 0.95$, the sample regression function is considered to be relatively concordance.

With T- test, the values of $Sig = 0.000 < 0.05$: regression coefficients are statistically significant.

Anova analysis results: $F = 209.743$, $Sig = 0.000 < 0.05$ the population regression function is considered to be concordance.

*** The regression results for forecasting the number of coaches**

Tab. 6. The results of regression analysis with coaches.

	Coefficients				R ²	ANOVA ^a	
	β	Std. Error	t	Sig.		F	Sig.
(Constant)	-606,796.760	35,677.169	-17.008	.000	0.965	305.194	.000 ^b
GDPP	34,112.291	1,952.643	17.470	.000			

The sample regression function of GDP per capita and number of coaches is described as follows:

$$NV_i = 34,112.29 * \ln(GDPP_i) - 606,796.76$$

With $R^2 = 0.965$ the sample regression function is considered to be relatively concordance.

With T- test, the values of $Sig = 0.000 < 0.05$: regression coefficients are statistically significant.

Anova Analysis results: $F = 305.194$ the population regression function is considered to be concordance; ensures tightness to make the forecast:

*** The regression results for forecasting the number of trucks**

Tab. 7. The results of regression analysis with trucks.

	Coefficients				R ²	ANOVA ^a	
	β	Std. Error	t	Sig.		F	Sig.
(Constant)	-155,585.346	11,377.457	212.916	.000 ^b	0.951	212.916	.000 ^b
GDPP	9,086.185	622.698	212.916	.000 ^b			

Coaches Analysis and calculation of model for forecasting number of trucks as follows:

$$NV_i = 9,086.185 * \ln(GDPP_i) - 155,585.35$$

With $R^2 = 0.951$ the sample regression function is considered to be relatively concordance.

With T- test, the values of $Sig = 0.000 < 0.05$: regression coefficients are statistically significant.

Anova analysis results: $F = 212.916$, $Sig = .000 < 0.05$ the population regression function is considered to be concordance; ensures tightness to make the forecast

*** Using the model for forecasting the number of vehicles according to GDP per capita in Hanoi.**

Calculation results show that the demand for land fund for static traffic development is 22,780,610.05 m² by 2025 and 28,921,103.73 m² by 2030. The calculation of total parking demand in the table above is based on the area norm for each vehicle type and assumes the total number of vehicles mentioned above but has not considered the static traffic land fund for rail transport, air transport, and waterway transport.

Tab. 8. Forecast results in the inner-city of Hanoi.

Year	Norms	Type of transport			
		Motorcycles	Cars	Coaches	Trucks
2025	GDPP	197,000,000			
	MT	7,908,312	562,896	44,704	17,949
	a	92.67	6.60	0.52	0.21
	S	3	21	52	65
	LD _j	21,985,898.19	780,173.86	12,087.96	2,450.04
	LD	22,780,610.05			
2030	GDPP	276,000,000			
	MT	10,038,246	704,306	56,206	21,012
	a	92.78	6.51	0.52	0.19
	S	3	21	52	65
	LD _j	27,940,453.92	962,856.73	15,198.10	2594.98
	LD	28,921,103.73			

4. Solutions to develop the static traffic system in Hanoi

According to the city's static traffic planning project to 2030, with a vision to 2050, Hanoi will have: 7 inter-provincial bus stations, 8 truck stations; 18,300,000 m² of land for public parking; ensure the ratio of land for static traffic reaches 3-4% of urban construction land [2]. However, this plan only meets 60-70% of the land fund for urban static traffic development, so in the coming time, in order to ensure the land fund for the development of static traffic in Hanoi, some solutions can be suggested, include:

Firstly, the investment for smart parking lots is Increase to take advantage of underground and overhead space for static traffic.

High-rise smart parking lots can meet the demand for land fund 3-4 times higher than the traditional parking lots. However, the amount of investment is very large, so in order to strengthen the construction of smart parking lots, the Government should have policies to socialize investment activities for building smart parking lots.

In addition, investment in the construction of underground parking lots also contributes to a increase in the land fund for static traffic development. Hanoi is planning to invest in parking lots in the underground space at 295 Le Duan, Dong Da district with the scale of 1.03 ha, the total estimated investment of 600 billion VND; parking lot in front of the gate and in Thong Nhat Park, adjacent to Tran Nhan Tong street, Hai Ba Trung district with a scale of 0.3 ha, total estimated investment of 450 billion VND; Youth Park parking lot (Thanh Nhan, Hai Ba Trung district) with a scale of 1.12ha, total estimated investment of 800 billion VND; 19/8 Square car park (including the area under the flower garden) in Hoan Kiem district with a scale of 0.32ha, total estimated investment of 350 billion VND; Underground parking lot at Quan Ngua stadium, Ba Dinh district with a scale of 1.12 ha, total estimated investment of 800 billion VND [2]. For achieving the efficiency of planning, it is necessary to issue specific regulations and standards for point and parking projects for investors to implement. Strengthen the management of investment activities, support administrative procedures, prioritize loans, remove obstacles on price mechanism, site clearance, etc. create the most favorable conditions for investors

Secondly, organizations, businesses, hotels, buildings should be encouraged to invest in building parking lots to meet their parking needs. The investment on building parking lots of that organizations will contribute to increasing the land fund for the city's static traffic development. For newly built areas, it is mandatory to fulfill the parking space requirement for the sites and partly support the surrounding. The arrangement of parking spots needs to consider the function of the city's automotive engineering services in this area. It is also obligatory to have independent parking lots and parking spots with an additional 20% of the land fund for greenery to ensure the critical coverage of parking lots reaches over 60% of the total land area. For high-rise apartment buildings, apartment buildings must have adequate parking spaces. High-rise garages should utilize the land fund, such as apartment buildings of over ten floors must have independent high-rise garages, less than ten floors must have underground garages. It is possible to arrange high-rise garages for some alternative low-rise apartment complexes. For sports and entertainment areas, if possible, parking lots should be arranged right on campus. Taking public transportation as the primary form of transportation to reduce the land fund for parking, put into operation in public parking service for the parking places with low use time and the parking places that are often not fully used up their capacity. It is also essential to tree planting to ensure landscape and thermal stability to protect vehicles.

Thirdly, space along some roads, the space of agencies and schools can be enhancing the use of as night parking places.

Some streets and administrative offices with large campuses in the area can be sites for parking, especially at night. Another proposal is arranging parking spots in the vicinity, especially in new cities, specialized in service of restricted development areas. A convenient parking location, combined with low fares and synchronized vehicle engineering services, can be an appropriate solution. Due to the restrictions of the traffic network, when investing in the construction of new routes, parking spots and parking lot systems must be additionally designed and connected to the road.

Fourthly, public transport with the se bus system should be encouraged to develop

Hanoi is the capital of Vietnam, in which most of the Party and State agencies are located, where important diplomatic activities of the country take place. Therefore, the use of public passenger transport services is an urgent need that cannot be separated from the lives of citizens of the capital, creating an urban landscape. Moreover, the increased provision of bus transportation services will contribute to reducing the demand for private means of transport, thereby enhancing the development of static traffic in Hanoi.

Fifthly, the planning on land fund for static traffic development must be complied

The land fund should not be converted to other functional purposes for sites with limited development and expansion but prioritize parking lots and retain the existing parking lots with good positions. It is possible to build an underground garage under park gardens and even lakes. The land of factories and enterprises in the city that must be relocated to the suburbs can transform into parking lots by building high-rise garages or take underground floors as parking spots, depending on the scale.

5. Conclusion

The development of urban static traffic with the demand for land fund is required indispensably to meet the travel demands of the people and achieve the social - economic growth of Hanoi city. To meet the demand for land fund for static traffic development, Hanoi needs to promote the completion and implementation of the land fund development plan for static traffic, increase investment attraction for smart parking lots, underground parking lots, and make use of the space of agencies and organizations. Organizations, hotels, buildings for parking as well as encouraging people in the city to travel by public transport such as buses... To implement the solutions, it is necessary to mobilize resources to socialize and invest in urban static traffic infrastructure development to build a sustainable urban space, to have the mechanisms and policies to encourage and attract the investors' participation, to issue appropriate regulations and standards for parking lots and parking spots projects to guide the investors to contribute to the future's static traffic development.

6. References

1. Tran Thi Lan Huong., 2008. Method of determining urban static traffic area, Scientific Journal of Transport No 24, 2018.
2. Tuan Luong., 2021. Increasing land fund for traffic in Hanoi: Prioritizing infrastructure development, hanoimoi.com.vn, 1/1/2021.
3. <https://kinhtedothi.vn/phat-trien-giao-thong-tinh-ha-noi>, 20/5/2021.
4. Nguyen Hong Thai., 2012. Public-private cooperation in investment and development of transport infrastructure, Journal of the University of Transport (Vietnamese).
5. <http://www.tapchigiaothong.vn/bai-toan-kho-trong-quan-ly-giao-thong-tinh-tai-ha-noi>, 21/4/2021.
6. <https://phuongnam.reatimes.vn/giai-bai-toan-phat-trien-giao-thong-tinh>, 20/3/2021.
7. <http://ttz.vn/bai-do-xe-thong-minh-tu-dong-la-tuong-lai-cua-giao-thong-tinh-do-thi.htm>, 19/5/2021.
8. Decision No. 1259/QĐ-TTg., 2011. Approving the "General Plan of Construction of Hanoi Capital to 2030, outlook to 2050" by the Prime Minister (Vietnamese).
9. Tran Thi Lan Huong., 2011. Research on methods of determining needs and solutions to develop urban static traffic, PhD thesis on organization and management of transportation, University of Transport and Communications.
10. Ministry of Transport., 2013. Decision No. 4403/QĐ - BGTVT dated December 31st , 2013 on approval of the project to mobilize breakthrough resources to invest in developing transport infrastructure (Vietnamese).

Assessment of Change in Urban Green Spaces Using Sentinel 2 MSI Data and GIS Techniques: A Case Study in Thanh Hoa City, Vietnam

NGUYEN Viet Nghia^{1,*}, TRINH Le Hung², NGUYEN Thi Thu Nga², LE Thi Le³,

¹ Hanoi University of Mining and Geology, 18 Vien street, Hanoi, Vietnam

² Le Quy Don Technical University, 236 Hoang Quoc Viet street, Hanoi, Vietnam

³ Thu Dau Mot University, Binh Duong, Vietnam

Corresponding author: nguyenvietnghia@hung.edu.vn

Abstract. This paper presents the results of an assessment of change in urban green spaces in Thanh Hoa city (Vietnam). Sentinel 2 MSI data in 2015 and 2021 are used to calculate 3 parameters: percentage of green, weight of green types, and weight of proximity to green. These parameters are used to calculate the Weighted Urban Green Space Index (WUGSI). The final result shows the distribution of green space in the study area consisted of very high-quality green, high-quality green, moderate quality green, and low quality green. The obtained results show that the quality of urban green space in Thanh Hoa city has changed significantly in the period 2015-2021, in which the area with category “low quality green space” increased from 7.17% up to 9.48%; areas with category “very high-quality green space” reduced from 65.02% to 47.39%.

Keywords: Urban green space, Weighted Urban Green Space Index, Sentinel 2, Thanh Hoa city

1. Introduction

Urbanization is an inevitable development trend of all countries in the world, especially for developing countries like Vietnam. In general, urbanization contributes to economic growth, changes the economic and labor structure, and to changes the population distribution. However, besides these positives, the urbanization process also creates many challenges for the development of big cities, such as high population density, traffic congestion, and environmental pollution. Urbanization has also led to a drastic change in land cover/land use, with an increase in built-up land and a decrease in vegetative cover.

Urban green spaces are one of the indispensable elements for design and development of cities. UGS are considered as “lung” of cities as well as one of the elements reflecting the quality of life [1]. Therefore, the quantity and quality of UGS are of prime concern for planners and city administrators [2]. Recently, researchers have objectively measured UGS using remote sensing data by estimating the percentage of green and built-up density in many cities of the world. The percentage of green is usually estimated from the Normalized Difference Vegetative Index (NDVI) using multi-spectral remote sensing image [3]. This index has been used in various studies to distinguish between vegetated and non-vegetated areas. Meanwhile, several urban indices have been proposed to classify urban land use/land cover from multispectral satellite imagery, such as UI (Urban index), IBI (Index based built-up index), NDBI (Normalized Difference Built-up Index), NDBaI (Normalized Difference Bareness Index), EBBI (Enhanced Built-up and Bareness Index), etc [4-10].

Gupta et al. (2012) developed the Urban Neighborhood Green Index (UNGI), which considers four parameters: percentage of green, built-up density, proximity to green, and height of structures to assess the quality of UGS [2]. In a study (Gupta et al., 2012), the type of green was used for defining the proximity to green by applying a single buffer of 20 m. Li et al. (2014) estimated the green spaces at the building level using Building Proximity to Green Spaces Index (BPGI) [11]. However, in this study, the authors used only one parameter (proximity to green) to assess the greens without using other parameters.

In this study, we use 03 parameters, including the percentage of green, weight of green types, and weight of proximity to green to assess urban green space. Two Sentinel 2 MSI images taken on December 21, 2015, and January 13, 2021, are used to evaluate the change in green space quality in Thanh Hoa city, Vietnam. The NDVI index is used to calculate the percentage of green based on the green/non-green classification. The weight of green types and weight of proximity to green parameters are determined on the basis of the results of the urban land cover classification. Finally, the Analytic Hierarchy Process method (AHP) of Saaty (1980) has been used for determining the weights of individual parameters and calculating the Weighted Urban Green Space Index (WUGSI) map.

2. Materials and Methodology

2.1 Study areas and Materials

Thanh Hoa city is the administrative, economic, cultural, political, and scientific-technical center of Thanh Hoa province. The city is an urban gateway linking the northern Vietnam key economic region with the North Central region. After nearly 30 years since its establishment, Thanh Hoa city has grown strongly with a high rate of urbanization and became a class I city in 2014. Currently, Thanh Hoa city has a natural area of 146.77 km² with 20 wards and 17 communes, a population of more than 400 thousand people. This is one of the cities with a large population and area in the Northern region of Vietnam. The location map of the study area is presented in Figure 1 [12].

In this study, two multispectral cloud - free Sentinel 2A images acquired from December 21, 2015, and January 13, 2021 (Fig. 2) were used to calculate 3 parameters: the percentage of green, weight of green types, and weight of proximity to green to assess urban green space.

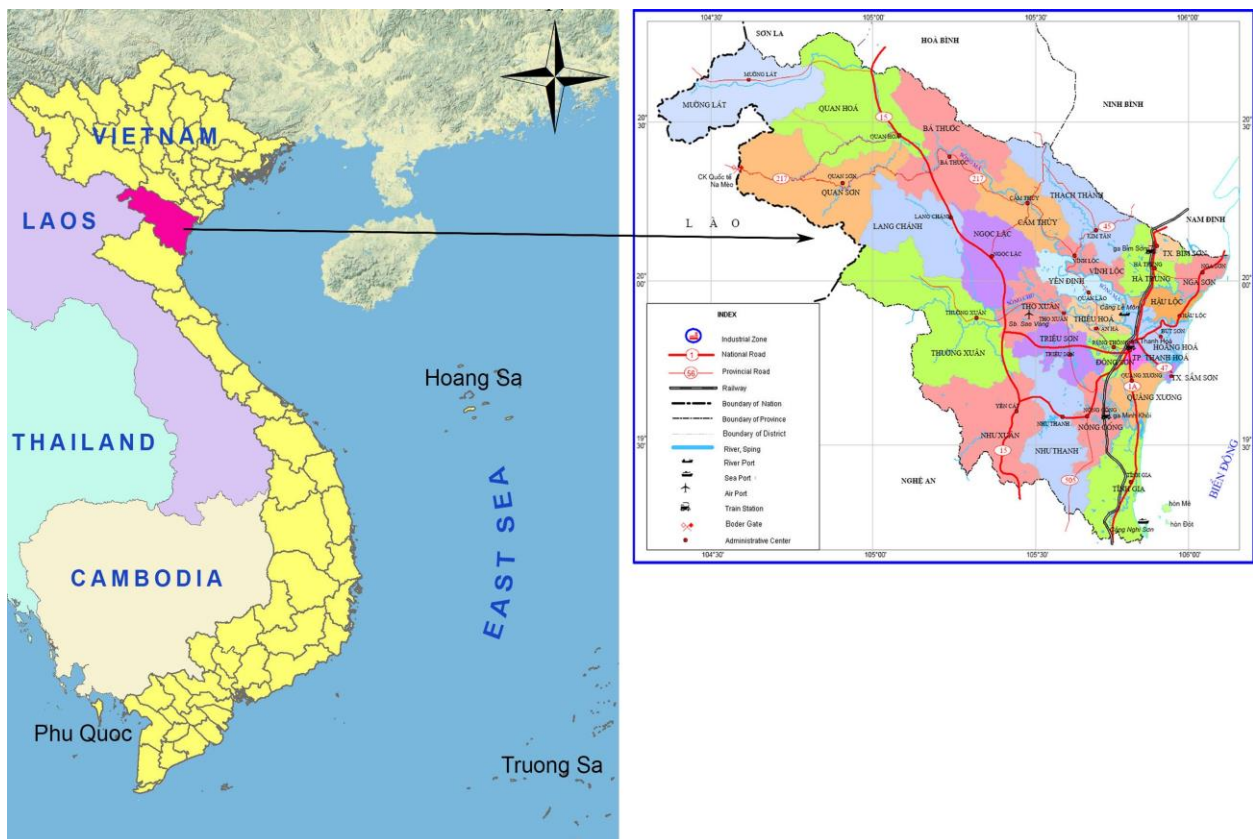


Fig. 1. Study areas in Thanh Hoa city, Vietnam.

The Sentinel-2 mission consists of two satellites developed to support vegetation, land cover, and environmental monitoring. The Sentinel-2A satellite was launched by ESA on June 23, 2015 and operates in a sun-synchronous orbit with a 10-day repeat cycle. A second identical satellite (Sentinel-2B) was launched on March 7, 2017. Together they cover all Earth’s land surfaces, large islands, and inland and coastal waters every five days. The Sentinel-2 Multispectral Instrument (MSI) acquires 13 spectral bands ranging from Visible and Near-Infrared (VNIR) to Shortwave Infrared (SWIR) wavelengths along a 290 km orbital swath [13]. The spectral bands used to calculate the NDVI index have a spatial resolution of 10 m, consistent with studies at a detailed level.

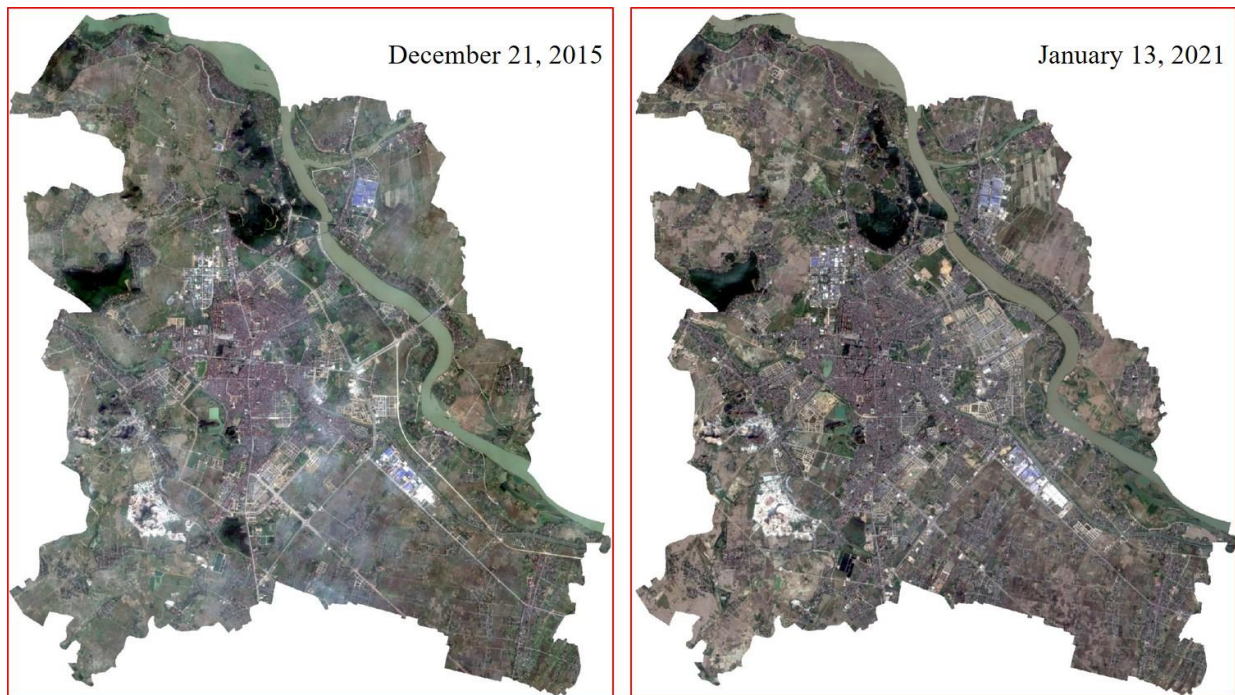


Fig. 2. Sentinel 2 MSI data in Thanh Hoa city, Vietnam, RGB=RED:GREEN:BLUE.

Characteristics of Sentinel 2 satellite bands are showed in Table 1 [14].

Tab. 1. Characteristic of Sentinel 2 satellite imagery.

Sentinel - 2 Bands	Central wavelength (µm)	Resolution (m)
Band 1 - Coastal aerosol	0.443	60
Band 2 - Blue	0.490	10
Band 3 - Green	0.560	10
Band 4 - Red	0.665	10
Band 5 - Vegetation Red Edge	0.705	20
Band 6 - Vegetation Red Edge	0.740	20
Band 7 - Vegetation Red Edge	0.783	20
Band 8 - NIR	0.842	10
Band 8A - Vegetation Red Edge	0.865	20
Band 9 - Water vapour	0.945	60
Band 10 - SWIR-Cirrus	1.375	60
Band 11 - SWIR	1.610	20
Band 12 - SWIR	2.190	20

2.2 Methodology

The Sentinel 2 MSI images after collection and pre-interpreter were cut according to the study area boundary. Spectral reflectance at the red, near-infrared (NIR), and shortwave infrared (SWIR1) bands was used to calculate the NDVI [3] using the following formula:

$$NDVI = \frac{\rho_{NIR} - \rho_{RED}}{\rho_{NIR} + \rho_{RED}} \tag{1}$$

where: ρ_{RED} , ρ_{NIR} - the spectral reflectance values of red (band 4) and near-infrared (band 8) of Sentinel 2 image.

The thresholding method is used to classify green and non-green classes from NDVI. Then, the 100m × 100m grid was overlaid over the binary image, and the percentage of green was calculated as the ratio between the green area in each cell and the area of 1 cell. The buffer zone at a distance of 100 m was chosen because it is consistent with the 10m spatial resolution of the Sentinel 2 MSI data (visible and NIR bands) used in the study. Based on the percentage of green, each cell has been classified into four green quality classes: low (GI value less than 25%), moderate (25-50%), high (50-75%), and very high green quality (>75%). These classes are assigned values of 0.25, 0.50, 0.75 and 1.00, respectively [2].

The object-oriented method was applied for urban land cover classification, then calculate 2 parameters: weight of green types and weight of proximity to green. In this study, 6 basic urban land cover classes were classified: dense vegetation; shrubs, sparse vegetation; agricultural land; vacant; water body, and built-up land, then each class will be weighted according to studies. In addition, the buffer distance 100 m was created based on the land cover map to calculate the weight of proximity to green parameter. A grid of 100m × 100m size was overlaid on buffers for each land cover class and the weight of proximity to green map generated [1, 15].

To assess the change in urban green spaces quality in Thanh Hoa city, the study was used the Weighted Urban Green Space Index (WUGSI), which proposed by Duong et al. (2015) follow the formula:

$$WUGSI_i = \sum_{j=1}^{i=1 \text{ to } n} W_j \times P_{ij} \tag{2}$$

Where: W_j - the relative weight of j^{th} parameter ($j = 1$ to 3); P_{ij} - the value of j^{th} parameter in the i^{th} cell.

Flowchart for the methodology used in this study to assess urban green spaces based on Sentinel 2 MSI data is shown in Figure 3.

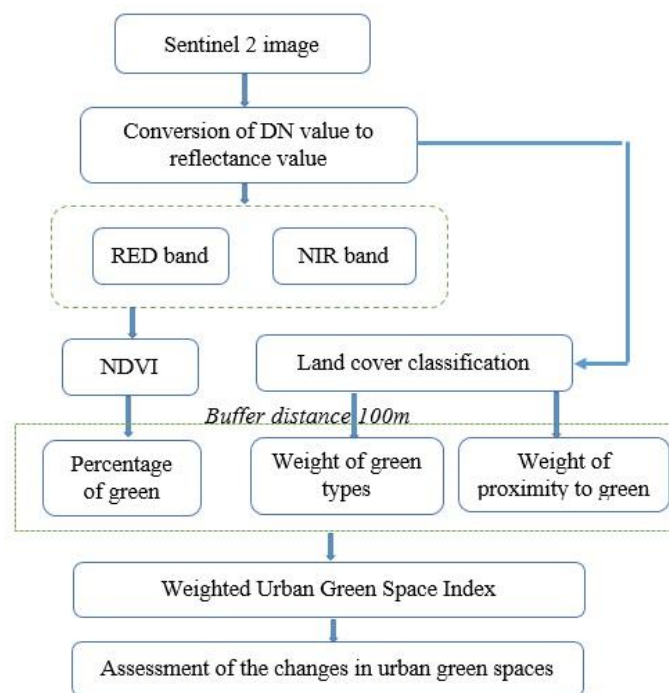


Fig. 3. Flowchart of the methodology for urban green spaces assessment.

3. Result and Discussion

After pre-processing, the reflectance values of red and NIR bands of Sentinel 2 multispectral imagery were used to calculate the NDVI index (Eq. 1). These indices will continue to be used to calculate percentage of the green parameter. The obtained percentage of the green parameter is presented in Figure 4.

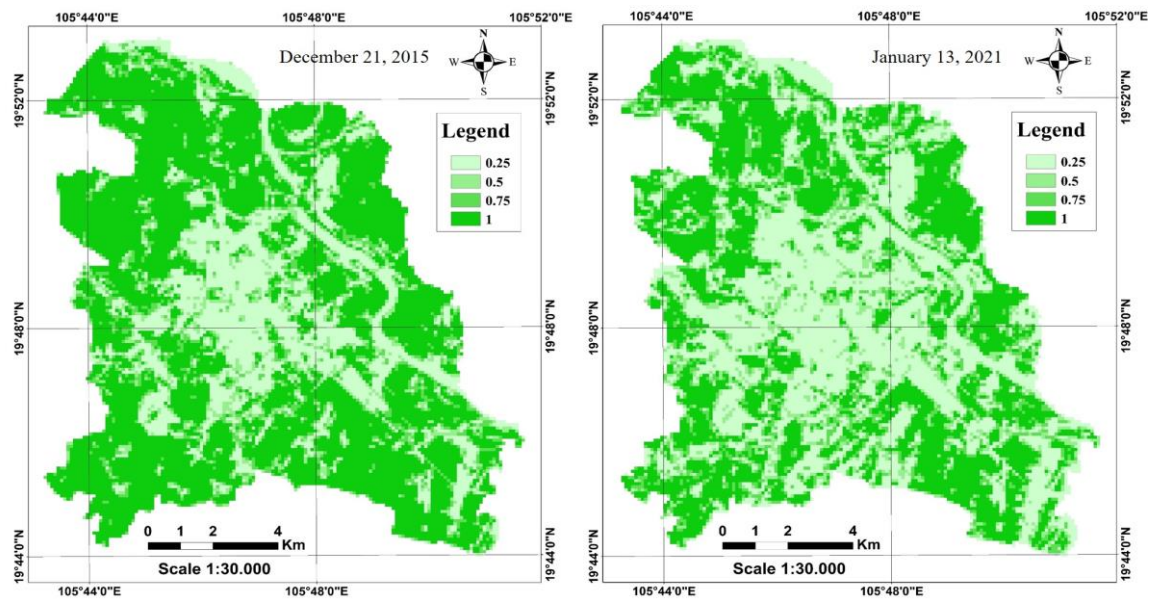


Fig. 4. The percentage of green parameter in Thanh Hoa city, December 21, 2015, and January 13, 2021.

The land cover in Thanh Hoa city is classified into 6 types (dense vegetation; shrubs, sparse vegetation; agricultural land; vacant; water body and built-up land), then create the buffer at a distance of 100 m. In this study, we use the eCognition Developer program to classify the land cover by using an object-oriented method. The land cover maps of Thanh Hoa city established from the Sentinel 2 MSI image on December 21, 2015, and January 13, 2021, are presented in Fig. 6. In this case, the overall accuracy of land cover classification reached 90.8% and 92.0%, the Kappa values were 0.86 and 0.89 respectively for Sentinel 2 images in 2015 and 2021.

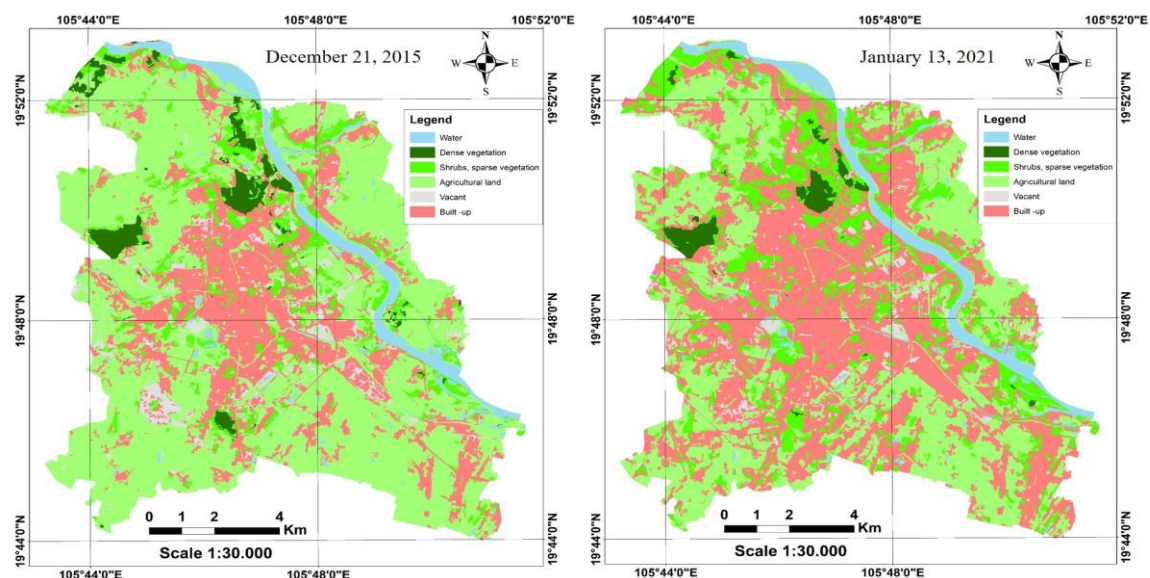


Fig. 5. Land cover maps in Thanh Hoa city, December 21, 2015, and January 13, 2021.

The results of land cover classification in Thanh Hoa city from Sentinel 2 images in 2015 and 2021 are presented in Table 2. It can be seen that the built-up land in Thanh Hoa city has increased significantly in

the period 2015-2021, from 3,554.38 ha in 2015 to 6,433.81 ha in 2021, equivalent to nearly 2 times. The agricultural land has decreased markedly, from 8,741.91 ha in 2015 to 5,151.57 ha in 2021, equivalent to more than 41%. Bare land (vacant) and dense vegetation classes also decreased, while the area of shrubs and sparse vegetation increased about 2 times.

Tab. 2. Land cover classification in Thanh Hoa city from Sentinel 2 MSI images.

No.	Land cover types	Area (ha)	
		December 21, 2015	January 13, 2021
1	Dense vegetation	476.89	293.90
2	Shrubs, sparse vegetation	1,218.13	2,412.60
3	Agricultural land	8,741.91	5,151.57
4	Vacant	583.14	309.96
5	Water body	772.99	745.63
6	Built-up land	3,554.38	6,433.81

These land cover types will be assigned weight values, then define proximity to green parameters according to studies [1, 2]. The weight of green types and weight of proximity to green parameters created from Sentinel 2 MSI image acquired on December 21, 2015, and January 13, 2021, in Thanh Hoa city, are presented in Figures 7 and 8.

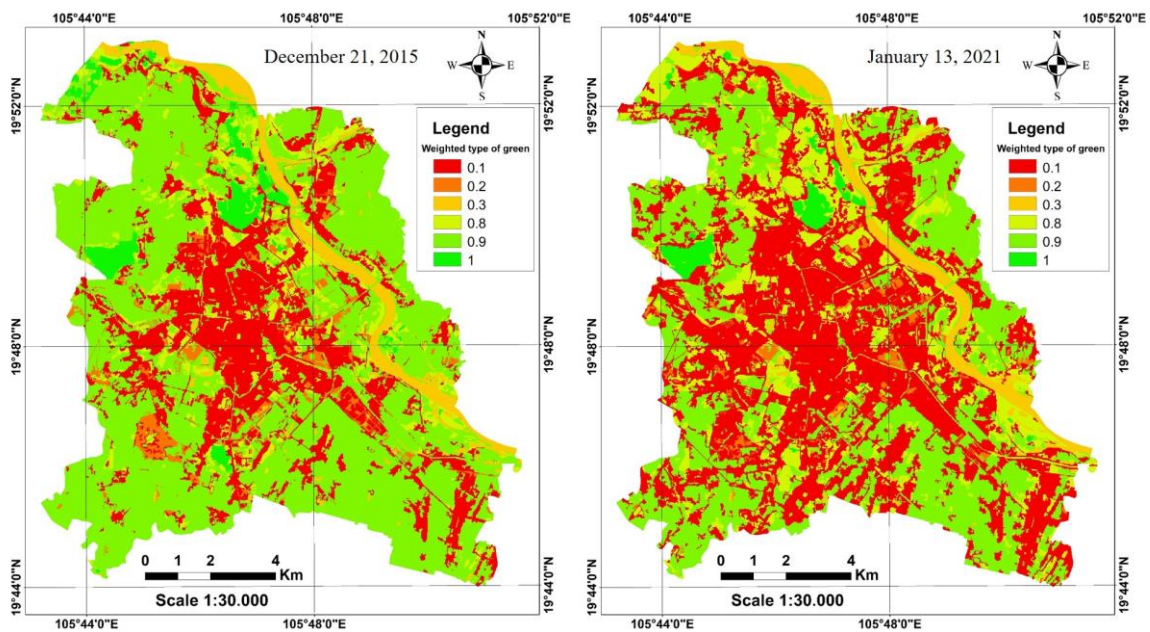


Fig. 6. The weight value of green types calculated from Sentinel 2 MSI data.

To calculate the WUGSI index according to formula 2, it is first necessary to determine the weight value W_j of each parameter: percentage of green, the weight of green types, and weight of proximity to green. The Analytic Hierarchy Process (AHP) method [16] was used to calculate the weights of individual parameters. Saaty’s method describes the level of importance of parameters and their relationship on a scale of 1 to 9. After calculating the weights, the consistency ratio index (CR) was computed to test the consistency of weights. In a study [17], Saaty indicates that the value of CR needs to be less than 0.1. The results of determining the weights of 3 parameters (percentage of green, weigh of green types, the weight of proximity to green) and the CR index values in this study are presented in Table 3. It can be seen that

the green type has the most influence on the quality of green space in urban areas, expressed in the weighted value of 02 parameters: percentage of green (0.590) and weight of green types (0.291). In this case, the CR value reaches 0.042.

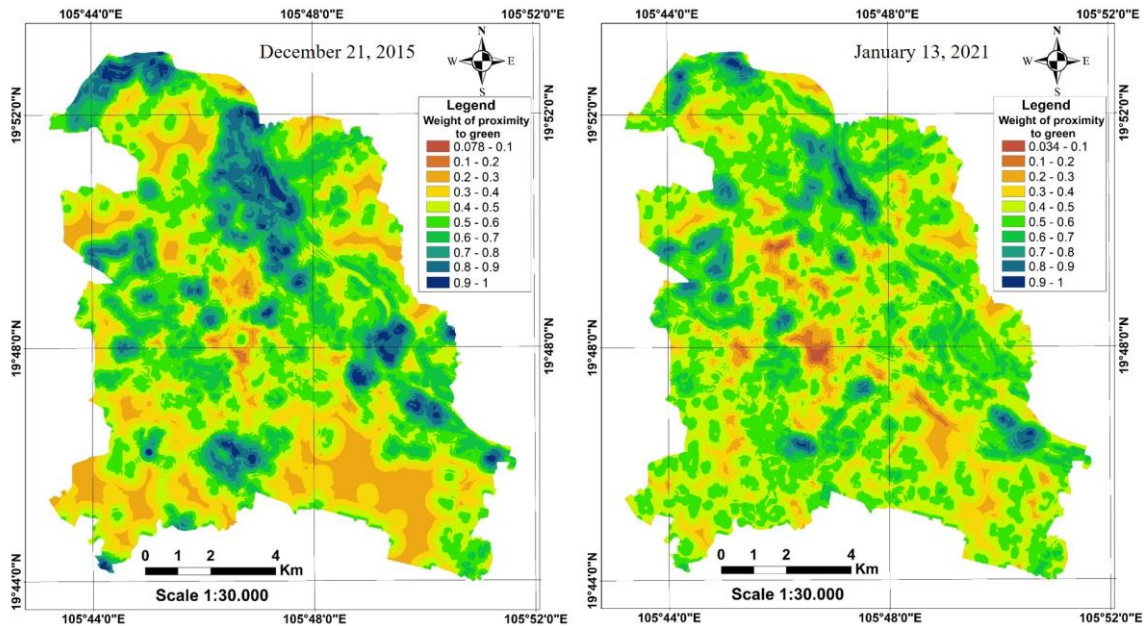


Fig. 7. The weight of proximity to green parameters calculated from Sentinel 2 MSI data.

Tab. 3. The weights of individual parameters and CR index.

No.	Parameter	The weight value	CR index
1	Percentage of green	0.590	0.042
3	Weight of green types	0.291	
4	Weight of proximity to green	0.119	

The result of the WUGSI mapping in Thanh Hoa city from the Sentinel 2 MSI images dated December 21, 2015, and January 13, 2021, are presented in Figure 8. The WUGSI index has a value between 0 and 1, in which the quality of urban green space is divided into 4 categories: low green space quality (< 0.30), moderate green space quality (0.30-0.50), high green space quality (0.50-0.70) and very high green space quality (> 0.70). The results of green space quality zoning in Thanh Hoa city from Sentinel 2 MSI images dated December 21, 2015, and January 13, 2021, are presented in Table 4.

The results obtained show that most of Thanh Hoa city has good green space quality, corresponding to 65.02% and 47.39% of the study area at category “very high green space quality” respectively for 2015 and 2021. The area with the category “high green space quality” also occupies a considerable area, equal to 6.34% and 7.34% of the total study area in 2015 and 2021. This can be explained by the relatively large area of agricultural land and shrubs, sparse vegetation land in Thanh Hoa city, especially after the city was expanded.

In contrast, the areas at categories “low green space quality” and “moderate green space quality” in 2021 both increased compared to 2015. In the 2015-2021 period, the area at category “low quality green space” increased from 7.17% of Thanh Hoa city area to 9.48%; the area at category “moderate level of green space” increased from 21.46% of the total study area to 35.79%. Thus, the area with poor quality of green space (low and moderate quality green space) has increased by more than 1.5 times after more than 5 years, from December 21, 2015 to January 13, 2021. In addition, Figure 7 shows that the area in low green space quality

is mainly concentrated in the central of Thanh Hoa city, mainly in Dong Tho, Dong Huang, Truong Thi, Dong Ve wards. Meanwhile, the wards outside the center city have green space levels ranging from high to very high green space quality. The areas with good green space quality are also similar to areas with a high percentage of green (> 0.5) (Fig. 4).

Tab. 4. The green space quality level in Thanh Hoa city, December 21, 2015, and January 13, 2021.

No.	Green space quality level	Area (%)	
		December 21, 2015	January 13, 2021
1	Low quality green spaces	7.17	9.48
2	Moderate quality green spaces	21.46	35.79
3	High quality green spaces	6.34	7.34
4	Very high quality green spaces	65.02	47.39

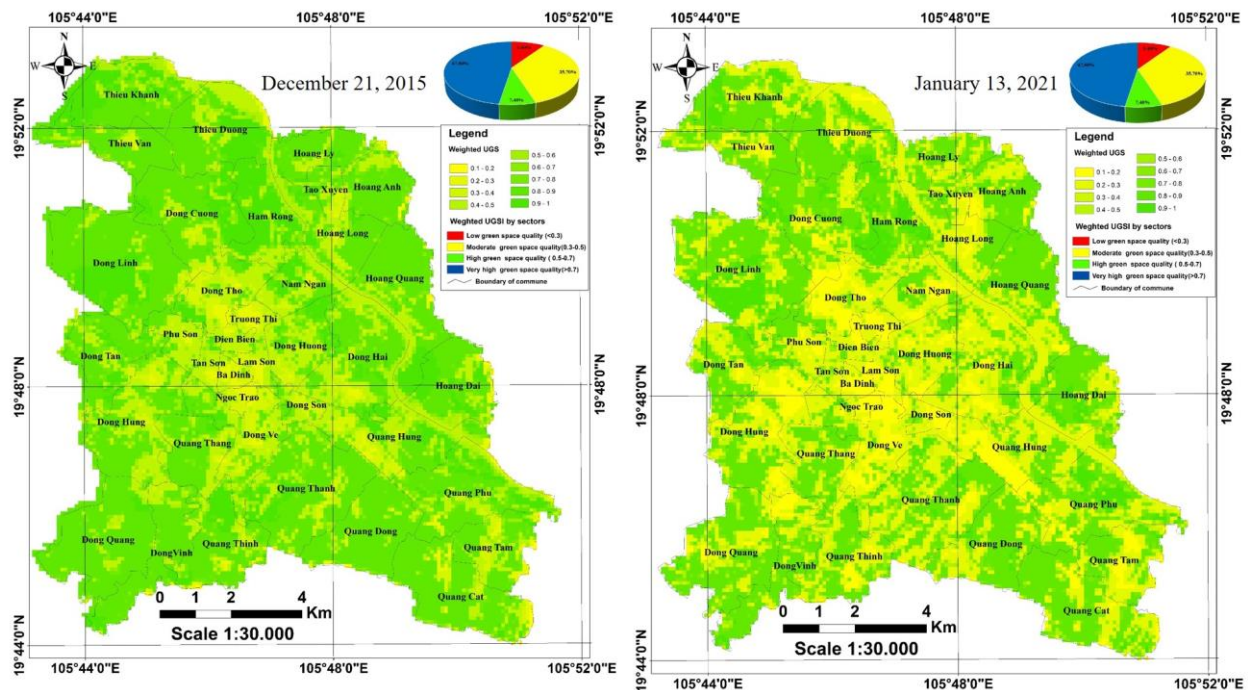


Fig. 8. WUGSI maps in Thanh Hoa city, December 21, 2015, and January 13, 2021.

4. Conclusion

Thanh Hoa is a fast-growing city and has good green space quality due to the relatively large area of agricultural land and shrubs, sparse vegetation land. The results obtained in the study show that most of the city area has very high quality of green space. However, the area with high quality of green space is rapidly decreasing in the period 2015-2021 due to the increase in built-up land. Along with that, the area at category low and moderate green spaces quality have increased significantly.

Remote sensing imagery with high spatial resolution and GIS data can be effectively used in preserving and monitoring green and open spaces in the urban area. Sentinel 2 MSI images with the highest spatial resolution up to 10 m are perfectly suitable for urban cover classification, thereby calculating parameters such as percentage of green, percentage of built-up land, the weight of green types, weight of proximity to green. These are the input parameters to calculate the WUGSI index to classify the quality level of urban green space. The results obtained in the study are objective and timely information, helping managers in

monitoring and planning land use in urban areas.

5. Acknowledgements

We would like to send our deepest thanks to the Mine-Surveying department of HUMG and Le Quy Don Technical University for providing us with good facilities in research and unconditional help to carry out the study.

The paper was presented during the 6th VIET - POL International Conference on Scientific-Research Cooperation between Vietnam and Poland, 10-14.11.2021, HUMG, Hanoi, Vietnam.

6. References

1. Duong Thi Loi, Pham Anh Tuan, Gupta., K., 2015. Development of an index for assessment of urban green spaces at city level, *International Journal of Remote Sensing Applications*, 5: 78-88.
2. Gupta, K., Kumar, P., Pathan, S.K., Sharma, K.P., 2012. Urban neighborhood green index – A measure of green space in urban areas, *Landscape and Urban Planning*, 105(3): 325-335
3. Rouse J.W., Hass R.H., Schell, J.A., Deering, D.W., 1973. Monitoring vegetation systems in the Great Plains with ERTS. In: *Earth Resources Technology Satellite-1 Symposium*, 3, Washington-DC, 309-317.
4. As-syakur Abd. R., Adnyana, I.W., Arthana, I.W., Nuarsa, I.W., 2012. Enhanced built - up and bareness index (EBBI) for mapping built - up and bare land in an urban area, *Remote Sensing*, 4: 2957-2970.
5. Trinh Le Hung, Le Thi Thu Ha, Le Duc Loc, Nguyen Thanh Long, 2021. A development of the Enhanced Built-up and Bareness Index (EBBI) based on combination of multi-resolution Landsat 8 and Sentinel 2 MSI images, *Journal of Mining and Earth Sciences*, 62(1): 1-9.
6. Xu, H., 2008. A new index for delineating built-up land features in satellite imagery, *International Journal of Remote Sensing*, 29: 4269-4276.
7. Zha, Y., Gao, J., Ni, S., 2003. Use of normalized difference built-up index in automatically mapping urban areas from TM imagery, *International Journal of Remote Sensing*, 24(3): 583-594.
8. Zhao, H., Chen, X., 2005. Use of Normalized Difference Bareness Index in quickly mapping bare areas from TM/ETM+, *International Geoscience and Remote Sensing Symposium (IGARSS) 3*, 1666-1668, DOI: 10.1109/IGARSS.2005.1526319.
9. Le, H.Thu Thi, Hoang, L.Van and Nguyen, T.Van 2021. Object-oriented classification for land cover of North Thang Long Industrial area using Worldview-2 data (in Vietnamese). *Journal of Mining and Earth Sciences*. 62, 1 (Feb, 2021), 10-18. DOI:[https://doi.org/10.46326/JMES.2021.62\(1\).02](https://doi.org/10.46326/JMES.2021.62(1).02).
10. Nguyen, N.Viet and Trinh, H.Le 2020. Determination of water quality parameters in the Tan Rai exploiting area (Lam Dong province) using Sentinel-2 MSI and Landsat 8 data (in Vietnamese). *Journal of Mining and Earth Sciences*. 61, 2 (Apr, 2020), 126-134. DOI:[https://doi.org/10.46326/JMES.2020.61\(2\).14](https://doi.org/10.46326/JMES.2020.61(2).14).
11. Li, X., Meng, Q., Li, W., Zhang, C., Jansco, T., Mavromatis S., 2014. An explorative study on the proximity of buildings to green spaces in urban areas using remotely sensed imagery, *Annals of GIS*, 20(3): 193-203.
12. <https://thanhhoa.gov.vn/portal/Pages/default.aspx>

13. <https://scihub.copernicus.eu/dhus/#/home>
14. Pahlevan, N., Sarkar, S., Franz, B., Balasubramanian, S., He, J., 2017. Sentinel-2 MultiSpectral Instrument (MSI) data processing for aquatic science applications: Demonstrations and validations, *Remote Sensing of Environment*, 201: 47-56.
15. Meng, Q., Yu, Q., Li, X., 2014. Urban green space remote sensing retrieval with LIDAR and multispectral satellite data, *Open GIS Conference*, Szekesfehervar, Hungary.
16. Saaty, T.L., 1970. How to make a decision: The Analytic Hierarchy Process, *European Journal of Operational Research*, 48: 9-26.
17. Saaty, T.L., 2008. Decision making with the Analytic Hierarchy Process, *International Journal of Services Sciences*, 1(1): 83-98.

Mineralogical and Geochemical Characteristics of Lead-zinc Ore Deposits, and Potential Accompanying Components in the Cho Don - Cho Dien Area, Bac Kan Province, Vietnam

NGUYEN Tien Dung¹, NGUYEN Khac Du^{1,2,*}, NGUYEN Ngoc Thom²

¹ Hanoi University of Mining and Geology, 18 Vien street, Hanoi, Vietnam

² Center for Excellence in Analysis and Experiment HUMG, Hanoi, Vietnam

Corresponding author: nguyenkhacdu@humg.edu.vn

Abstract. The Pb-Zn mineralization in the Cho Don - Cho Dien ore districts often occurs in 2 types: (1) oxidized ore near to the surface and (2) sulfide ore at deeper section. Based on microscopic observations, sulfide ores can be divided into sphalerite-galena-pyrite and/or galena-sphalerite mineralization types. To examine the geochemical features of the Pb-Zn ores, SEM-EDX and ICP-MS analytical methods were performed in this study. Previous $\delta^{34}\text{S}$ data of Pb-Zn concentrates, and sulfide minerals from various deposits suggest that the Pb-Zn ore-forming fluids might be related to the felsic-granitic magmatic activities rather than a genesis of stratiform type. Geochemical data show that the major, minor, and trace element compositions of lead-zinc ores have wide ranges of variation even in each deposit. The sulfide ores are generally higher in economic components than those in the oxidized ores. The positive correlations between Pb-Ag can be found in the entire dataset, whereas excellent Zn-Cd correlation can only be observed from Cho Don ore samples. Apart from the principal components (Pb and Zn), the ores also contain other accompanying elements that supply high-technological manufacturing industries. Of which As, Cu, Ag, Sb, and Cd could be potential by-products and can be extracted during smelting Pb/Zn concentrate processes, and need more detailed studies for every deposit.

Keywords: Cho Don-Cho Dien Pb-Zn ore deposits, Mineralogy and geochemistry, Accompanying components, By-products

1. Introduction

Bac Kan province, situated at about 200 km from Ha Noi to the north (Fig. 1a), is one of the most abundant lead-zinc ore resource localities in Viet Nam. Most of the ores, high in essential metal concentration, distribute in Cho Don, Cho Dien ore districts and scattered in other places such as Ngan Son, Pac Nam, Bach Thong, and Cho Moi. Many deposits have been exploiting from the 19th Century up to the present, resulting in a few hundred thousand tons of zinc, lead, silver, cadmium, and indium have been extracted.

Based on the occurrences, lead-zinc ores can be divided into two ore types: (1) sulfide and (2) oxidized ores, of which the latter often appear at a depth from a few tens to a few hundred meters below the surface. Both are primarily present in Paleozoic carbonate and/or terrigenous-carbonate formations in northern Vietnam [1-3]. Although the lead-zinc deposits are formed spatially in the carbonatic rocks, the ore-forming fluids could have derived from magmatic and/or metamorphic processes [4, 5]. In those deposits, apart from primary metals lead (Pb) and zinc (Zn), some trace elements could be considered as by-products such as silver (Ag), cadmium (Cd), indium (In) [1, 6-11]. Those components are often formed as accompanying elements and/or inclusions in other sulfide phases [12-18]. However, the relationship between each ore deposit type and its accompanying elements remains controversial.

In the presenting manuscript, on the basis of microscopic observations, geochemical data combined with isotopic data presented in previous studies, we will clarify the mineralogical, genesis, geochemical characteristics of Pb-Zn ores, and potential by-products from the various deposits in the Cho Don-Cho Dien ore district in the north of Viet Nam.

2. Outline of regional geology and analytical methods

2.1 Outline of Cho Don - Cho Dien geology

The Cho Don and Cho Dien ore districts are distributed in the Lo Gam structure, which is the southernmost part of the South China plate (Fig. 1a). The Pb-Zn deposits in Cho Don are located mainly-

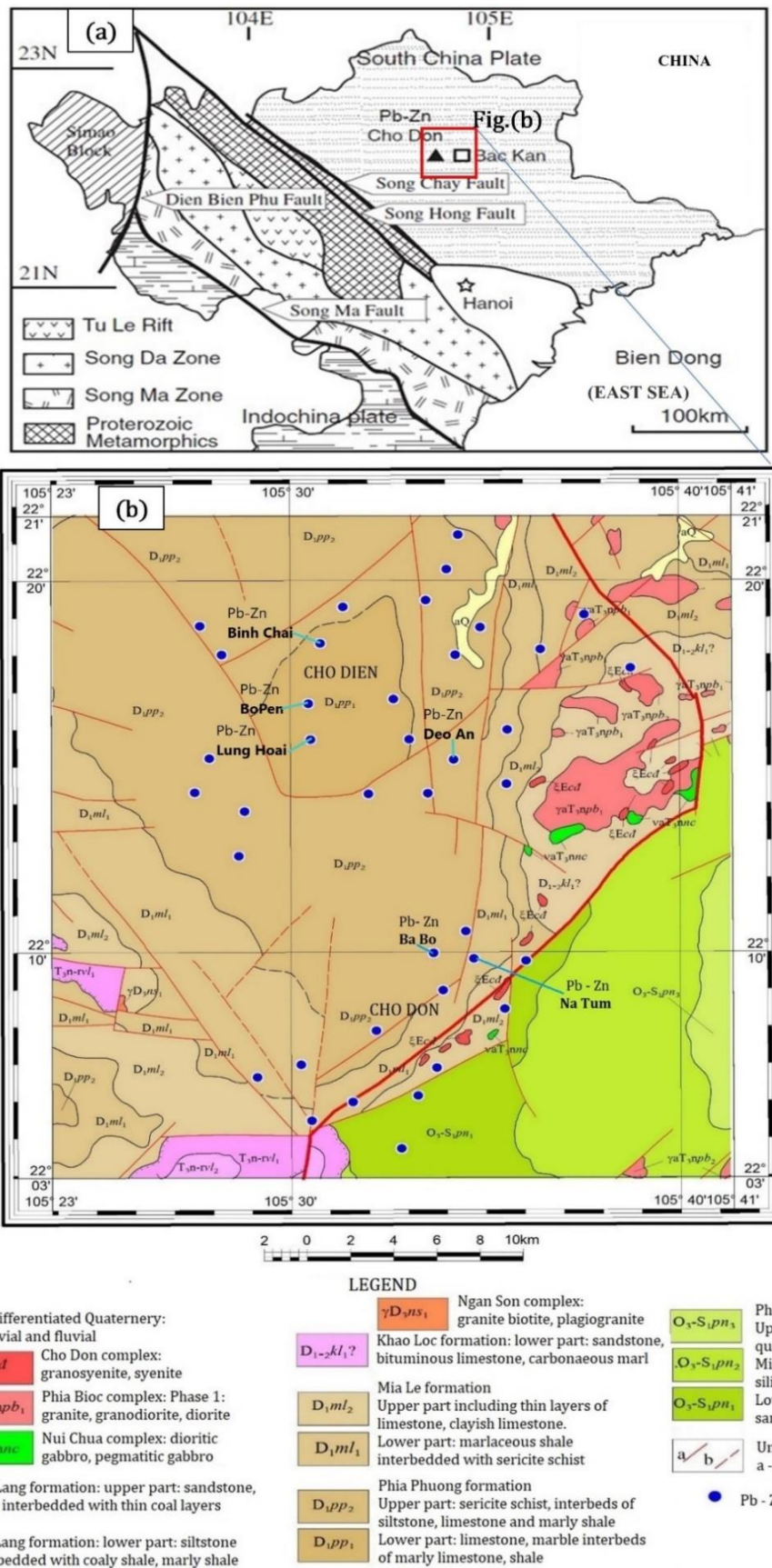


Fig. 1. (a) Tectonic sketch map of northern Vietnam and (b) Simplified geological map of the Cho Don-Cho Dien area, Bac Kan province showing the location of the studied Pb-Zn mines in highlight (modified from [1, 5]).

in Lower Devonian ($D_{1ml} - D_{3pp}$) sedimentary rocks of Mia Le and Phia Phuong formations, and a few

occurrences are recorded in terrigenous sedimentary of Phu Ngu formation ($O_3 - S_{1pn}$) in Upper Ordovician and Lower Silurian. The hosted rocks comprise sericite-quartz schists, shales, interbedded with limestones, cherty limestones, quartzites, tuffs, and tuffaceous sandstones. Grayish limestone, siltstones, shales, and sandstones are commonly observed at the mineralization zones. Lead-zinc deposits in the Cho Don area consist of Ba Bo, Na Tum, Lung Vang, Na Bop - Pu Sap deposits. The main economic minerals are galena and sphalerite; however, the former is predominated. These minerals always associate with pyrrhotite, pyrite, arsenopyrite, and chalcopyrite. Their optical characteristics will be described in detail in a later section.

The Cho Dien ore district is located about 20 km to the north of the Cho Don district (Fig. 1b). The Pb-Zn deposits and occurrences comprise Lung Hoai, Binh Chai, Bo Luong, Dam Van, Deo An, Suoc, and Bo Pen. All of the deposits are distributed in Lower Devonian ($D_{1pp} - D_{1ml}$) sedimentary rocks. The host rocks contain shales, bituminous mudstones, dolomitic limestones, and marbles. Ores from all deposits are similar in primary mineral composition, including sphalerite, pyrite, arsenopyrite, and a lesser amount of galena. Pyrrhotite and chalcopyrite are commonly observed and are reported as secondary minerals. Oxidized ores are composed of smithsonite, cerussite, siderite, rhodochrosite, and iron hydroxides, limonite [3, 5, 19].

The Pb-Zn deposits in the Cho Don-Cho Dien ore districts are generally classified into the stratiform ore deposit type, which appears worldwide (i.e., Russia, Kazakhstan, Bulgaria, Poland, Austria, France, China, and other countries). It is notified recently that stratiform deposits are typified by the intimate association with carbonatic rocks of Paleozoic-Mesozoic is the stratigraphic control of mineralization without the appearance of igneous complexes ([3] and references therein). However, the felsic magmatic rocks appear widely in this area with various compositions, their relationship with ore-forming fluids remains controversial.

2.2 Samples and Analytical methods

We collected twenty-six samples from various deposits, occurrences (i.e., in a tunnel, outcrops, and drill cores) (Fig. 2), and ore types in the Cho Don and Cho Dien ore districts to examine the ore mineralogy and geochemistry (major, minor, traces including rare earth elements). Thin and polished sections were prepared from rock chips at Hanoi University of Mining and Geology. Microscope (Carl Zeiss – Axio Scop. A1) and Scanning electron microscope (SEM) coupled with energy-dispersive X-ray spectroscopy (EDS) (Quanta 450, FEI Company, Hillsboro, OR, USA) were initially applied to determine and estimate mineral modes qualitatively (Fig. 4).

Major, minor, and trace element compositions of twenty-two selected lead-zinc ore samples including fourteen sulfides and two oxidized ores, four Pb/Zn concentrates, and two ore tailing were obtained using Inductively Coupled Plasma Mass Spectrometry (ICP-MS, Agilent 7700x) at Center for Radioactive and Rare Elements Analysis and Experiment, Geological Division for Radioactive and Rare Elements, Viet Nam. Sample preparation processes strictly follow the Standard Basis of Viet Nam (TCCS 01/XH: 2012). The detection limit for most of the elements is ten parts per billion (ppb). Results are presented in Tables 1, 2, and Figure 5.

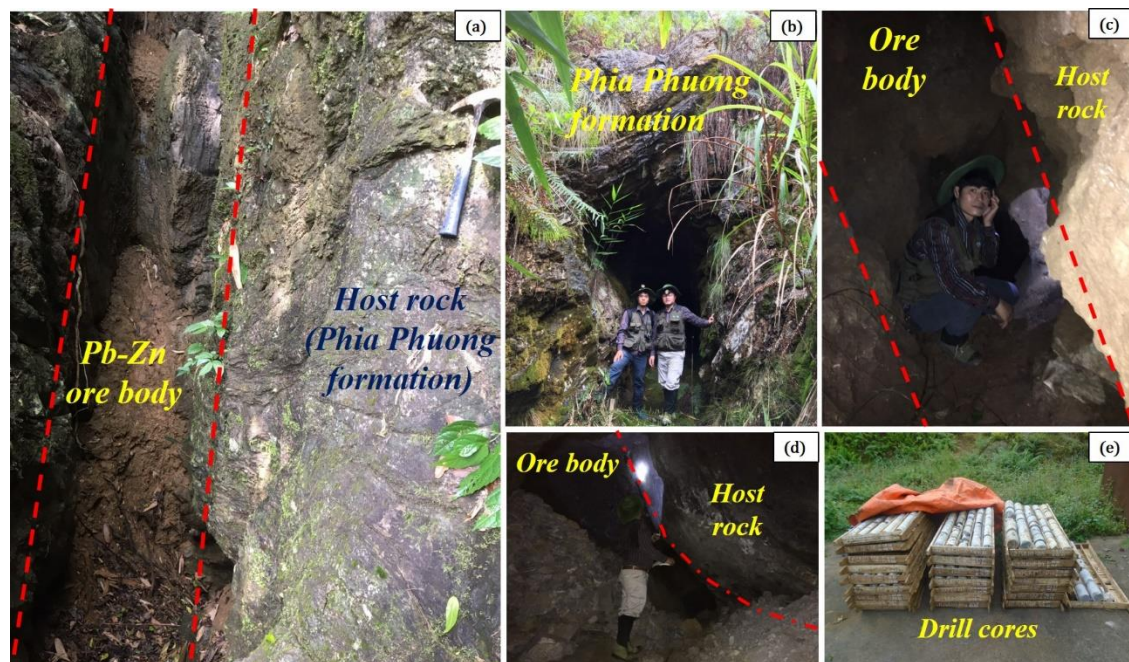


Fig. 2. Field survey and Sampling in Cho Don-Cho Dien ore districts: (a) outcrop showing the distribution of Pb-Zn ore body coincident with a fault plane; (b-d) Pb-Zn ore extraction by tunneling and relationship between ore body and host rock. (e): Drill cores from the Cho Dien mine group.

3. Results

3.1 Ore Mineralogy

As mentioned in the earlier section, the lead-zinc ores are formed spatially related to the carbonatic rocks of lower Devonian (D_{1pp} and D_{1ml}), rock-forming minerals are composed of calcite, dolomite, clay minerals group, quartz, barite, and organic material. Dissolution and embayment textures of rock-forming minerals are commonly observed in contact with opaque minerals (Fig. 3c). The abundances of quartz, barite, hydrothermal calcite, and dolomite in rocks and/or mineralization zone seem to be related to the occurrence of sulfide minerals.

In oxidized ore samples, minerals assemblage mainly comprises smithsonite, hydrozincite, calamine, cerussite, rhodochrosite, bornite, and limonite [5], making the dark brown color of the ores. The lead-zinc sulfide ores could be either massive sulfides or banded, varying in each deposit (Figs. 3a, b). Primary ore minerals are various in size and shape, ranging from coarse- to fine-grained, euhedral to anhedral. Predominant phases comprise galena and sphalerite. The samples recovered from the Cho Don ore districts are generally higher in galena (up to 70 vol %) but much lower in sphalerite compositions than those collected from the Cho Dien ore district (up to 75vol % sphalerite). Pyrite appears with significant amounts in few samples recovered from both Cho Don and Cho Dien ore districts (up to 75 vol %). Small amounts (1-2%) of chalcopyrite, pyrrhotite, marcasite, and arsenopyrite present as accessory phases in some polished sections. Geochemical characteristics of essential ore minerals were semi-quantitatively determined by SEM-EDX and are depicted in Figure 4.

Sphalerite and galena commonly occur in samples as anhedral crystals with grain sizes varying from 0.2-2.6 mm, rarely up to >4 mm. They are closely associated with pyrite (Fig. 3d-i), replacing the earlier rock-forming minerals (Fig. 3c). The texture of sphalerite and galena filling in the microcrack systems, forming veinlets or branches, is commonly recorded.

Pyrite is often euhedral to subhedral in most of the studied samples, with grain size varying from 0.1-2.5 mm. The rim of pyrite is often corroded and replaced partly by sphalerite, suggesting that pyrite is the earliest crystallized phase of the ore. Chalcopyrite is a trace mineral in the studied samples, occurring widely as tiny rounded grains, blebs (10-20 μm) in larger grains of sphalerite, forming typical emulsion texture of the ores (Figs. 3g-i).

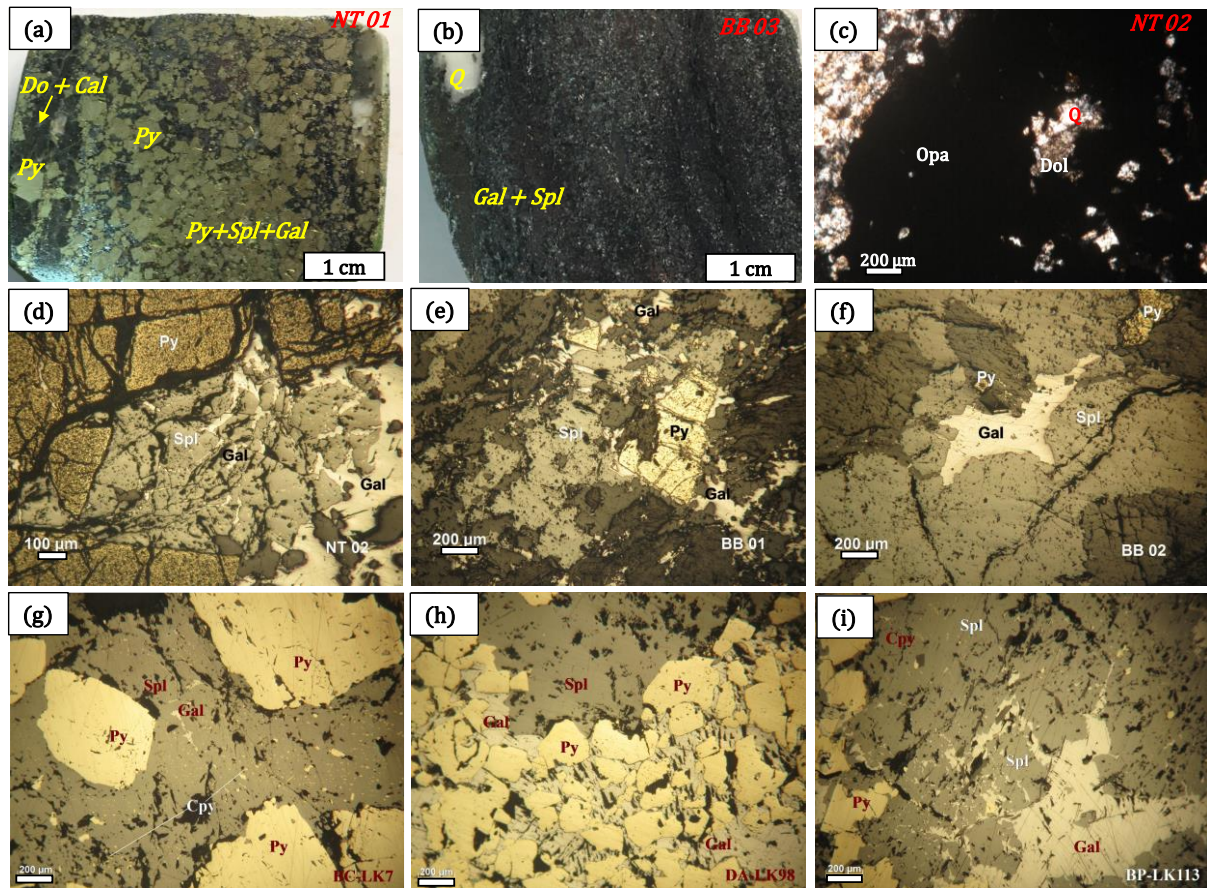


Fig. 3. Representative photos of Pb-Zn ores (a: massive pyrite-sphalerite-galena ore; b: banded galena-sphalerite-pyrite ore) and microphotographs showing (c: embayment and dissolution texture of rock-forming mineral in ore background), (d-i) mineral assemblages of the studied Pb-Zn ores. NT, BB, BC, DA, BP: Na Tum, Ba Bo, Binh Chai, Deo An, Bo Pen deposits, respectively. Py: Pyrite. Spl: Sphalerite. Gal: Galena. Dol: Dolomite. Cal: Calcite. Q: Quartz. Sul: Sulphides.

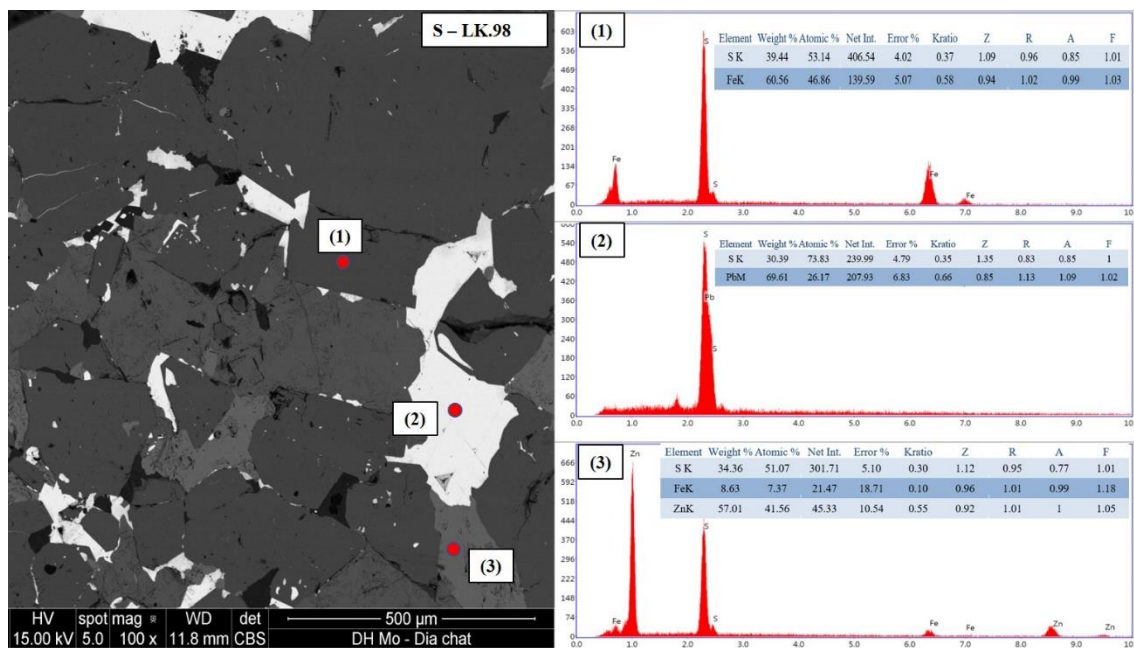


Fig. 4. Representative SEM results for minerals: (1) Pyrite; (2) Galena; (3): Sphalerite (Sample LK.98 in the Suoc deposit).

Tab. 1. Major and trace element compositions of ore samples from the Cho Don ore district.

Deposit	Na Tum				Ba Bo							
Samples	NT.01	NT.02	NT.04	NT.05	BB.01	BB.02	BB.03	BB.04	BB.07	BB.08	BB.09	
Ore Type	Sul.	Sul.	Ox.	Ox.	Sul.	Sul.	Sul.	Sul.	Tail.	Pb-Con.	Zn-Con.	
Na ₂ O	0.61	0.58	0.59	0.51	0.57	0.40	0.49	0.49	0.56	0.51	0.49	
K ₂ O	0.30	0.24	0.43	0.19	2.07	0.45	1.23	1.68	1.94	0.33	0.27	
MgO	1.18	1.07	0.99	1.37	1.38	9.94	1.74	2.40	3.18	1.53	1.26	
Al ₂ O ₃	0.44	0.50	3.38	0.79	6.48	1.34	3.49	4.70	7.41	0.77	0.70	
Fe ₂ O ₃	28.36	19.43	34.82	36.05	1.13	7.87	6.26	22.54	13.78	8.15	8.86	
P ₂ O ₅	0.02	0.02	0.04	0.05	0.02	0.01	0.02	0.03	0.03	0.03	0.03	
MnO	1.37	0.44	15.54	7.83	0.09	2.21	2.38	9.68	2.44	1.08	1.06	
Zn	10.08	5.12	0.56	5.64	20.94	8.62	1.51	0.18	1.89	3.69	44.56	
Pb	14.59	8.74	2.25	4.32	5.49	0.32	41.46	6.11	0.33	55.46	0.54	
As	3.761	0.69	0.03	2.79	0.53	0.01	0.01	0.003	0.85	0.95	0.03	
Ba	642.85	631.51	1,405.98	691.72	521.70	1,430.68	1,042.37	882.87	1,100.73	909.00	1,349.74	
Th	8.20	12.14	8.23	2.84	10.11	3.82	4.49	9.24	15.80	33.66	3.68	
Ti	19.65	23.98	139.52	28.35	291.28	39.44	140.55	161.70	168.77	101.41	45.34	
Ge	2.97	1.84	4.21	3.74	0.27	1.17	0.76	2.85	1.78	0.87	1.07	
Cd	34.70	19.14	2.18	21.19	126.78	66.38	12.79	1.11	11.07	23.52	2,412.36	
In	273.53	7.71	3.45	128.51	0.53	0.25	0.52	0.13	1.32	1.20	1.14	
Y	3.41	8.27	41.73	26.05	1.41	11.95	4.50	11.91	20.86	9.50	4.14	
Cr	7.33	10.12	14.38	12.32	8.26	6.70	9.98	13.80	15.94	11.23	8.30	
Co	12.67	10.55	24.00	14.68	12.33	4.78	13.97	9.26	13.90	11.19	9.29	
Ni	13.50	14.73	27.68	14.74	19.85	13.15	13.76	15.76	26.75	34.17	20.26	
Cu	2,373.57	1,290.90	21.72	1,369.38	33.68	16.47	483.81	15.85	21.50	3,124.05	1,182.53	
Ag	170.65	9.87	2.05	9.83	9.67	2.03	527.10	14.72	2.98	1,089.13	9.30	
Sb	23.14	2.62	2.56	4.84	21.18	4.41	918.01	12.72	6.15	2,144.37	16.06	
Sn	698.71	30.36	7.40	171.57	16.96	4.94	8.30	17.29	16.19	21.47	43.31	
Ga	13.58	12.17	26.23	15.22	8.89	23.29	18.73	16.67	21.33	16.72	24.77	
Mo	6.73	5.13	14.71	7.31	3.62	2.97	3.45	4.55	8.57	17.40	3.96	
La	6.51	3.93	6.25	6.56	4.94	5.39	4.55	4.14	7.88	7.55	4.24	
Ce	10.28	6.20	10.07	9.44	9.51	11.37	6.41	8.47	12.87	10.70	8.43	
Pr	0.81	0.39	0.81	0.95	0.68	0.65	0.57	0.59	1.11	1.00	0.65	
Nd	2.22	0.98	2.42	2.98	2.09	1.75	1.46	1.62	3.07	2.12	1.71	
Sm	2.31	0.94	3.56	4.27	2.54	1.79	2.16	2.33	5.45	4.99	1.50	
Eu	1.78	1.09	4.18	2.36	1.31	2.63	1.87	4.18	5.15	7.39	2.67	
Gd	2.79	2.10	6.00	5.07	2.69	3.55	2.24	3.62	7.65	7.03	2.64	
Tb	0.45	0.19	0.67	0.57	0.17	0.36	0.23	0.42	2.04	4.90	0.15	
Dy	0.73	0.83	3.87	2.64	0.40	2.27	1.13	2.11	5.10	5.38	0.66	
Ho	0.27	0.17	0.88	0.57	0.10	0.40	0.18	0.39	2.01	4.57	0.15	
Er	0.43	0.59	2.59	1.93	0.22	1.01	0.52	1.61	2.75	5.09	0.44	
Tm	0.18	0.10	0.34	0.26	0.02	0.19	0.07	1.61	1.67	4.45	0.02	
Yb	0.28	0.30	2.38	1.35	0.15	1.11	0.37	0.24	2.46	4.16	0.26	
Lu	0.19	0.09	0.29	0.17	0.01	0.18	0.08	0.01	1.61	4.26	0.04	
Σ REE	29.24	17.88	44.31	39.13	24.84	32.65	21.85	31.34	60.81	73.59	23.57	

Note: Na₂O – As in %, Ba – Mo in ppm. Sul. – Sulfide ore, Ox. – Oxidized ore.
 Pb-Con. – Pb Concentrate. Zn-Con. - Zn-Concentrate. Tail.- Tailing.

Tab. 2. Major and trace element compositions of ore samples from the Cho Dien ore district.

Deposit	Lung Hoai		Binh Chai		Bo Pen		Deo An	Suoc	Ore concentrate		Tailing
Samples	LK44/2	LK63A/2	LK7	LK3	LK111	LK113	LK90	LK98	TQ.01	TQ.02	DT
Ore Type	Sul.	Sul.	Sul.	Sul.	Sul.	Sul.	Sul.	Sul.	Pb-Con.	Zn-Con.	Tailing
Na ₂ O	0.28	0.25	0.27	0.27	0.28	0.27	0.28	0.29	0.24	0.28	0.29
K ₂ O	0.09	0.08	0.26	0.17	0.42	0.31	0.66	0.09	0.06	0.08	0.28
CaO	12.47	3.40	1.24	0.47	0.43	0.47	2.13	0.92	0.78	1.17	15.56
MgO	1.97	0.23	0.36	0.24	0.27	0.25	1.13	0.20	0.27	0.38	3.59
Al ₂ O ₃	2.37	0.27	0.73	0.77	1.26	0.87	1.83	0.15	0.11	0.22	0.94
Fe ₂ O ₃	11.29	0.99	29.47	29.06	19.97	11.62	25.39	8.28	7.03	9.02	11.63
P ₂ O ₅	0.05	0.02	0.03	0.03	0.04	0.03	0.05	0.06	0.03	0.03	0.05
MnO	1.41	0.13	0.06	0.04	0.02	0.04	0.25	0.12	0.04	0.14	1.38
Zn	17.85	55.36	6.74	13.78	18.43	38.79	2.28	51.60	7.70	53.89	0.69
Pb	0.42	0.66	0.42	7.02	8.46	13.06	2.78	0.16	54.36	0.95	0.32
Cu	0.08	0.11	0.03	0.03	0.09	0.20	0.03	0.08	0.37	0.27	0.02
As	0.02	0.00	0.39	0.27	0.33	0.09	0.94	0.01	0.34	0.23	1.19
Ba	24.20	14.53	25.97	22.79	32.31	23.13	60.44	19.13	17.89	11.36	32.49
Th	3.60	0.64	1.52	1.31	1.76	1.16	2.40	0.47	0.91	2.22	1.46
Ti	112.55	80.41	73.85	78.72	146.71	82.38	199.36	39.76	40.13	46.18	97.66
Ge	6.26	3.05	16.54	16.40	12.15	5.60	14.72	3.78	3.43	5.11	8.20
W	61.31	36.13	500.38	193.18	207.39	56.88	324.00	51.48	13.04	16.59	89.05
In	4.63	7.53	4.20	0.54	0.44	0.63	0.58	411.41	3.21	64.20	1.45
Y	7.88	0.83	0.30	0.31	0.69	0.30	1.25	0.58	0.29	1.29	3.95
Cr	258.47	88.95	187.58	191.77	225.67	212.80	212.84	135.38	251.64	257.75	159.67
Co	9.89	8.87	45.82	46.20	9.51	5.30	17.12	18.17	4.67	6.39	11.44
Ni	22.35	18.62	14.41	25.01	18.53	12.54	28.92	17.88	15.84	14.30	14.00
Ag	45.72	144.97	36.78	261.17	143.21	246.26	115.66	36.90	1,573.12	287.75	20.95
Sb	2.25	48.52	4.88	30.77	20.01	36.59	15.58	1.22	92.37	4.73	3.64
Sn	52.05	61.44	38.29	53.74	228.78	406.86	133.38	129.16	67.78	131.72	47.34
Ga	5.62	5.64	2.45	2.75	5.06	6.60	4.94	2.90	1.01	4.30	2.56
Mo	6.53	4.73	3.33	3.03	2.70	1.81	1.93	1.60	3.93	2.48	1.75
La	10.20	2.01	0.68	1.16	1.16	0.84	7.18	2.00	1.59	7.26	5.13
Ce	33.01	3.30	1.22	1.83	1.86	1.27	12.95	3.48	2.41	14.37	9.46
Pr	2.29	0.39	0.16	0.23	0.26	0.17	1.41	0.39	0.31	1.51	1.05
Nd	7.87	1.42	0.53	0.71	0.98	0.62	4.67	1.26	0.99	4.16	3.93
Sm	1.45	0.30	0.11	0.15	0.18	0.13	0.63	0.25	0.19	1.21	0.79
Eu	0.48	0.07	0.05	0.04	0.05	0.03	0.11	0.06	0.04	0.64	0.27
Gd	1.52	0.22	0.08	0.12	0.17	0.10	0.51	0.22	0.14	1.03	0.77
Tb	0.29	0.04	0.03	0.02	0.03	0.02	0.06	0.03	0.02	0.59	0.11
Dy	1.37	0.16	0.07	0.06	0.13	0.07	0.24	0.11	0.08	0.77	0.60
Ho	0.37	0.04	0.02	0.02	0.03	0.02	0.05	0.03	0.02	0.62	0.13
Er	0.98	0.08	0.05	0.04	0.08	0.04	0.15	0.06	0.04	0.67	0.38
Tm	0.22	0.03	0.02	0.01	0.02	0.01	0.02	0.01	0.01	0.61	0.05
Yb	0.99	0.08	0.04	0.04	0.06	0.04	0.14	0.05	0.04	0.59	0.33
Lu	0.23	0.02	0.02	0.01	0.02	0.01	0.02	0.01	0.01	0.60	0.04
∑ REE	61.27	8.18	3.07	4.45	5.02	3.39	28.15	7.95	5.88	34.64	23.04

Note: Na₂O–As in %, Ba–Mo in ppm. Sul. –Sulfide ore. Pb-Con. –Pb Concentrate. Zn-Con.- Zn-Concentrate.

3.2 Ore geochemistry

In order to examine the variation in the chemical composition of Pb-Zn ores in the Cho Don - Cho Dien area, 22 samples containing various ore types (rich/poor ores as well as sulfide/oxidized ores, Pb/Zn concentrates, and tailing) have been selected for detailed ICP-MS analyses. Results are presented in Figure 5 and Tables 1, 2.

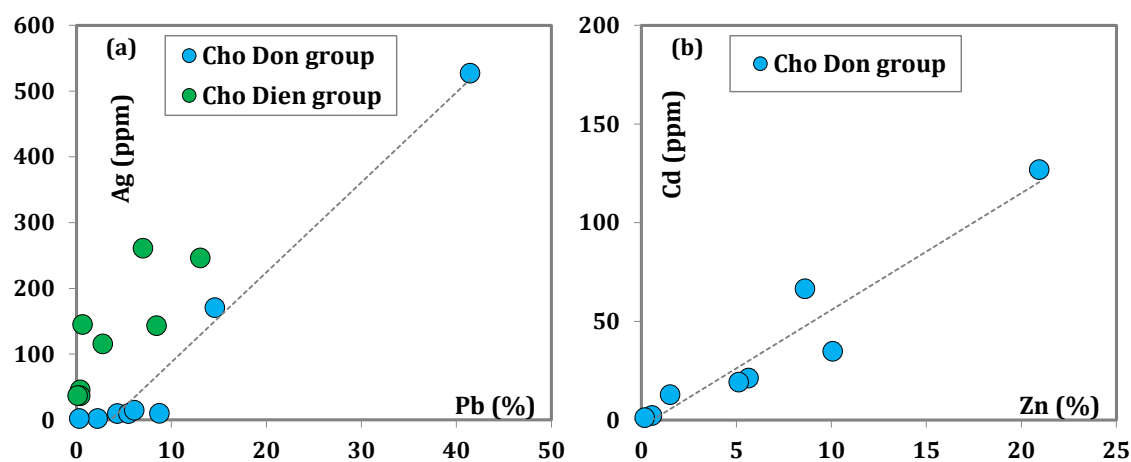


Fig. 5. Binary diagrams for (a) Pb-Ag, and (b) Zn-Cd of the studied Pb-Zn ores.

In general, the chemical compositions of lead-zinc ores have wide ranges of variation. The sulfide ores are commonly higher in Pb, Zn but lower in Fe contents than those in the oxidized samples. The total Pb-Zn content in ores from Cho don and Cho Dien ranges from 2.81-42.97% and 5.07-56.03%, respectively. The values commonly exceed 8% in rich ores, reaching the maximum of 41.46% Pb; 20.94% Zn (Cho Don), and 13.06% Pb; 55.36% Zn (Cho Dien). After flotation, the ore concentrates in the Cho Don area are up to 55.46% and 44.56% of Pb and Zn components. The total Pb and Zn content is 1.01-2.22% in the tailing.

Overall, there are excellent correlations only between Pb-Ag in the entire data and between Zn-Cd in only samples from the Cho Don area (Fig. 5). Most of the trace elements have low concentrations in the studied ore samples. The concentration of many components (i.e., Ge, Cr, Co, Ni, etc.), and the radioactive elements (Th, U), rare earth elements, and yttrium do not exceed the Clarke values. However, several components are enriched during the flotation process. These characteristics will be discussed more in detail in section 4.2.

4. Discussion

4.1 Genetic type of the Cho Don-Cho Dien ore district

Based on microscopic observations and paragenetic relationships of various hydrothermal minerals, the mineralization process in the Cho Don-Cho Dien ore districts can be classified into three stages (Tab. 3): (1) sedimentary diagenesis through (2) hydrothermal mineralization, ending by (3) supergene oxidization.

The hydrothermal process forming Pb-Zn ore in the Cho Don-Cho Dien areas can be divided into early-stage and late-stage based on distinct mineral assemblages. The early stage of mineralization mainly produces massive ores, containing euhedral to subhedral coarse- to medium-grained sulfide minerals (pyrite, sphalerite, and galena). The process continues to form lesser amounts of veins or disseminated ores comprising fine subhedral to anhedral grains (dominated by galena). The late-stage mineralization ends with the formation of hydrothermal dolomite, calcite, and barite. Therefore, the mineralization in the Cho Don-Cho Dien ore districts can be divided into pyrite-sphalerite-galena and/or galena-sphalerite mineralization types in terrigenous carbonate rocks. These observations are well consistent with the descriptions presented in previous studies, such as [1, 5, 7, 8, 19].

Regarding the geneses of sulfide ore deposits, sulfur isotopic ratios ($\delta^{34}\text{S}$) of PbS and/or ZnS are commonly applied. Because most of the Pb-Zn ore deposits in the Cho Don district appear in Paleozoic sedimentary (carbonatic rocks, shale, and sandstone), it is generally believed that the ore geneses are of stratiform (Mississippi Valley-MVT or even SEDEX) type. To conclude the origin of Mississippi Valley-type ores, the sulfur isotopic values should be similar to those of Pb-Zn ores in the Mississippi Valley area,

ranging from +0.5 to +15.3 ‰ with an average of +11.0 ‰. However, such a wide range of variation and high $\delta^{34}\text{S}$ values and low Fe content as those in Pb-Zn ore deposit of the MVT ores are absent from the data of Pb-Zn ores in the Cho Don-Cho Dien areas (Fig. 6).

Tab. 3. Mineral paragenesis in the Cho Don-Cho Dien areas.

Mineral	Sedimentary diagenesis	Hydrothermal		Supergene Oxidation
		Early-ore stage	Late-ore stage	
Calcite	—————			
Dolomite	—————			
Quartz		—————	—————	
Pyrite (marcasite)		—————	-----	
Chalcopyrite		—————		
Sphalerit		-----	—————	
Galena		-----	—————	
Hydrothermal Calcite		-----	—————	
Hydrothermal Dolomite			-----	
Barite			—————	
Limonite				—————
Smithsonite				—————
Calamine				—————
Hydrozincite				—————
Rhodocrosite				—————
Cerussite				—————
Bornite				—————

----- Locally occurring ————— Minor ————— Main

The $\delta^{34}\text{S}$ values of zinc concentrate from the Cho Don district do not vary much, ranging from +6.9 (one sample from Na Bop - Pu Sap deposit) to +7.5 ‰ (both two values from Na Tum mine) [4]. In addition, the $\delta^{34}\text{S}$ values of lead-zinc ore and concentrates from Cho Dien district are even much lower, varying from -3.4‰ to +1.1‰ [4, 5]. These clearly suggest that the ore-forming fluids that formed Pb-Zn deposits in the Cho Don-Cho Dien ore districts are probably related to the felsic-granitic rocks occurring widely in the area rather than the stratiform ore deposit type.

Although the essential ore minerals in the Cho Don area are similar to those in the Cho Dien district, the ores from Cho Don are generally richer in galena but less abundant in sphalerite compositions than those from the Cho Dien district. Based on these observations and the $\delta^{34}\text{S}$ values from various deposits (Fig. 6), we propose that the nature of the Pb-Zn mineralization process in the Cho Don district might differ from that in the Cho Dien ore district, leading to further variation in accompanying economic elements and need more detailed studies in the future.

4.2 Accompanying elements and potential by-products

As presented in the previous section, the crude ores and Pb/Zn concentrates from the Cho Don-Cho Dien ore districts include some minor and trace elements with noticeable concentrations. Of which As, Cu, Ag, Sb, and Cd could be of commercial interest (Tabs. 1, 2). Geochemical characteristics and sources of those elements are as follows:

Arsenic presents mainly as arsenopyrite in sulfide ores; therefore, it also appears in oxidized samples, ranging from 0.003-3.761% in studied samples. In the Pb concentrates, it is 0.95%. Since arsenic is toxic,

it is necessary to recover in flotation and smelting processes. Unfortunately, most of the factories do not pay much attention to this yet.

Copper is often present as chalcopyrite and bornite in sulfide and oxidized ores, respectively. The Cu contents vary widely in the crude ores, generally higher abundances in samples from the Cho Dien than in representatives from the Cho Don ore district. It is enriched up to 0.37% and 0.27% in Pb and Zn concentrates. It could be economically extracted as one of the by-products during smelting processes.

Silver and antimony concentrations also have wide ranges of variation in studied samples, occasionally up to 527.1 (ppm) and 918.01 (ppm) in samples from the Cho Don area. They are enriched in the Pb concentrates, showing a strong positive correlation to the lead content in the bulk ores (Fig. 5, Tab. 4). Although some trace minerals containing high contents of Ag, Sb (i.e., tetrahedrite) were observed in the Cho Don-Cho Dien area and were reported [16, 20], they could not play an essential role as a source for those trace elements in the bulk ore analyses. The Ag, Sb contents increase sharply in the commercial Pb-concentrates (1089.13 and 2,144.37 ppm) in samples from the Cho Don ores, suggesting an intimate relationship between these elements and the galena mineral. A strong positive correlation between Pb-Ag is also observed in ore from the Cho Dien district.

Tab. 4. Correlation coefficients for major and selected trace elements in Pb-Zn ores. Data applied in the calculation are compiled from references [1, 9], and this study.

<i>Element</i>	<i>Zn</i>	<i>Pb</i>	<i>As</i>	<i>Cd</i>	<i>In</i>	<i>Cu</i>	<i>Ag</i>	<i>Sb</i>	<i>Sn</i>	<i>Ga</i>
<i>Cho Don ore district</i>										
Zn	1									
Pb	0	1								
As	0.12	0.13	1							
Cd	0.53	-0.22	-0.11	1						
In	-0.06	-0.07	0.56	-0.06	1					
Cu	0.04	0.41	0.34	0.21	0.51	1				
Ag	-0.13	0.89	0.03	-0.15	-0	0.52	1			
Sb	-0.09	0.9	-0.08	-0.14	-0.14	0.47	0.96	1		
Sn	-0.09	-0.11	0.52	-0.03	0.54	0.43	0.06	-0.02	1	
Ga	-0.3	-0.3	-0.14	0.3	0.38	0.49	-0.05	-0.1	0.38	1
<i>Cho Dien ore district</i>										
<i>Element</i>	<i>Zn</i>	<i>Pb</i>	<i>As</i>	<i>W</i>	<i>In</i>	<i>Cu</i>	<i>Ag</i>	<i>Sb</i>	<i>Sn</i>	<i>Ga</i>
Zn	1									
Pb	-0.26	1								
As	-0.29	-0.11	1							
W	-0.33	-0.06	-0.13	1						
In	0.42	-0.12	-0.14	-0.14	1					
Cu	-0.23	0.30	-0.08	-0.08	0.07	1				
Ag	-0.17	0.97	-0.12	-0.09	-0.11	0.19	1			
Sb	-0.28	0.04	0.97	-0.20	-0.17	-0.04	0.03	1		
Sn	-0.14	0.31	-0.16	0.05	0.06	0.88	0.18	-0.12	1	
Ga	0.01	0.10	-0.20	-0.01	0.04	0.88	-0.01	-0.18	0.90	1

Note: Significant values of correlation coefficients are highlighted in bold-typed.

Geochemical behavior of cadmium shares a lot of similarities to that of Ag and Sb. There is no independent mineral of Cd found and reported in the studied area, and its concentrations strongly correlate to the occurrence of sphalerite. Despite the poor Cd composition in both sulfide and oxidized ores, the Cd content in Zn-concentrate from the Cho Don reaches 2,412.36 ppm. It could be considered as one of the

by-products during the smelting of the Zn concentrates processes. The sphalerite is relatively abundant in samples from the Cho Dien ore district; however, Cd might not be a by-product of ore from the Cho Dien area (Cd contents in the bulk ores do not exceed the Clarke value: data are not presented here).

Last but not least, indium is often paid much attention in the Pb-Zn deposits due to their utilities in high-technological industries. It is also pointed out that the Cho Don - Cho Dien ore districts have a high potential of In and that sphalerite is the host for the element [4]. However, the indium concentrations are often very low not only in the crude ores but also in both the Pb/Zn concentrates and the tailing, suggesting that the sphalerites from different deposits have various amounts of the element. The indium contents are markedly high in 2 samples from the Na Tum (Cho Don) deposit (273ppm and 128 ppm in the samples NT.01 and NT.05, respectively), where are also high in Sn, Cu, As contents (Tabs. 1, 2). These observations, coupled with the strong correlations between In and (Sn, Cu, As) but weak correlation between In and Zn (Tab. 4), suggesting that indium might be presented mostly in (Sn, Cu/As)-rich phases rather than in the sphalerite as recorded earlier in the Cho Don ore district.

5. Conclusion

The main results of this work can be summarized as follows:

- The Pb-Zn mineralization in Paleozoic terrigenous carbonate rocks from the Cho Don-Cho Dien ore districts can be divided into sphalerite-galena-pyrite and/or galena-sphalerite mineralization types. Based on $\delta^{34}\text{S}$ values from previous studies, ore-forming fluids might be driven from the felsic-granitic magmas in the area rather than a genesis of stratiform ore deposits (MVT or SEDEX types).
- The chemical compositions of the ores have wide ranges of variation, even in each deposit from Cho Don-Cho Dien ore districts. Apart from the essential ore components (Pb and Zn), several minor and trace elements concentrate with significant amounts in the ores; some are enriched during flotation. Of which As, Cu, Ag, Sb, and Cd could be potential by-products and can be extracted during smelting Pb/Zn concentrates processes, but this is required more detailed studies in the future.

6. Acknowledgments

We would like to thank Dr. Khuong The Hung from Hanoi University of Mining and Geology for the initial discussion on the genesis of lead-zinc ore deposits. This is really helpful in improving the quality of the presenting manuscript.

The paper was presented during the 6th VIET - POL International Conference on Scientific-Research Cooperation between Vietnam and Poland, 10-14.11.2021, HUMG, Hanoi, Vietnam.

7. References

1. Ishihara, Shunso, Tuan Anh Tran, Yasushi Watanabe, and Trong-Hoa Tran, 2010. Chemical Characteristics of Lead-Zinc Ores from North Vietnam, with a Special Attention to the In Contents. Bulletin of the Geological Survey of Japan, 61(9-10): 307-23, <https://doi.org/10.9795/bullgsj.61.307>.
2. Tran Van Tri and Vu Khuc (Editor), 2011. Geology and Earth Resources of Vietnam. Hanoi: Publishing house for Science and Technology, 2011. ISBN: 9786049130472.
3. Tran Tuan Anh, Gas'kov, I.V., Tran Trong Hoa, Nevol'ko, P.A., Pham Thi Dung, Pham Ngoc Can, 2012. Complex Deposits in the Lo Gam Structure, Northeastern Vietnam: Mineralogy, Geochemistry, and Formation Conditions. Russian Geology and Geophysics, 53(7): 623-35, <https://doi.org/10.1016/j.rgg.2012.05.001>.
4. Ishihara, S., Tuan Anh Tran, Kezhang, Q, 2010. Reconnaissance Study on Sulfur Isotopic Ratios of Lead-Zinc Ores from North Vietnam. Bulletin of the Geological Survey of Japan, 61(11-12): 485-88, <https://doi.org/10.9795/bullgsj.61.485>.
5. Dao Thai Bac. Study on Characteristics and Distribution Rules of Lead - Zinc Mineralisation in Viet Bac Region, Ph.D Thesis, University of Mining and Geology, Ha Noi, 2011 (In Vietnamese with abstract in English).

6. Tran Trong Hoa, 2004. Investigation and Assessment the Prospect of Accompanying Minerals in Some Lead-Zinc and Copper Deposits in the North of Viet Nam. Institute of Geological Sciences, Vietnamese Academy of Science and Technology, Hanoi, Vietnam. (In Vietnamese with abstract in English).
7. Do Quoc Binh. Investigation and Assessment the Prospect of Lead-Zinc, Gold and Accompanying Minerals at Phia Da - Na Cang Area, Cao Bang and Bac Kan Province. General Department of Geology and Minerals of Vietnam, Hanoi, 2005 (In Vietnamese with abstract in English).
8. Do Quoc Binh. Assessment the Prospect of Copper, Lead-Zinc and Accompanying Minerals at Quan Ba - Pac Nam Ore Band in Ha Giang, Cao Bang and Bac Kan Province. General Department of Geology and Minerals of Vietnam, Hanoi, 2009 (In Vietnamese with abstract in English).
9. Tran Tuan Anh. Study on Accompanying Components in Promising Deposits of Basic Metal and Rare Metal in the North of Vietnam to Improve the Efficiency of Mineral Exploitation and Processing, and Environmental Protection. Institute of Geological Sciences, Vietnamese Academy of Science and Technology, Hanoi, Vietnam, 2010, 376 (In Vietnamese with abstract in English).
10. Phuong Nguyen, Hang Thu Thi Nguyen, Nam Dinh Tang, Houmphavanh Phatthana, 2017. Application of some geological properties for surveillance prospects and Pb-Zn prospects forlands capeonly. *Journal of Mining and Earth Sciences*, 58 (5): p. 363-378. (In Vietnamese with abstract in English).
11. Phuong Nguyen, Dong Phuong Nguyen, Huong Thi Nguyen, Huong Thi Le, Dinh Van Do, 2020. Features of lead-zinc mineralization in the Phia Dam -Khuoi Man region. *Journal of Mining and Earth Sciences*, 61 (5): p. 120-134, [http://doi.org/10.46326/JMES.2020.61\(5\).14](http://doi.org/10.46326/JMES.2020.61(5).14). (In Vietnamese with abstract in English).
12. Sangameshwar, S.R., Barnes, H.L., 1983. Supergene Processes in Zinc-Lead-Silver Sulfide Ores in Carbonates. *Economic Geology*, 78(7): 1379-97, <https://doi.org/10.2113/gsecongeo.78.7.1379>.
13. Tran Tuan Anh, Gaskov, I.V., Tran Trong Hoa, Nevolko, P.A., Pham Thi Dung, Bui An Nien, Pham Ngoc Can, 2011. Mineralogical and Geochemical Characteristics and Forming Conditions of Lead-Zinc Deposits in Lo Gam Structure, Northern Vietnam. *Vietnam Journal of Earth Sciences*, 33(3): 393-408, <https://doi.org/10.15625/0866-7187/33/3/348>. (In Vietnamese with abstract in English).
14. Jiayi, ZHOU, HUANG Zhilong, ZHOU Guofu, LI Xiaobiao, DING Wei, and BAO Guangping, 2011. Trace Elements and Rare Earth Elements of Sulfide Minerals in the Tianqiao Pb-Zn Ore Deposit, Guizhou Province, China. *Acta Geologica Sinica - English Edition* 85(1): 189-99, <https://doi.org/10.1111/j.1755-6724.2011.00389.x>.
15. Bui An Nien, Tran Trong Hoa, Tran Tuan Anh, Pham Thi Dung, Pham Ngoc Can, Tran Van Hieu, Tran Quoc Hung, Ngo Thi Phuong, 2011. New Research Results on Distribution and Compositional Characteristics of the Na Son Lead-Zinc Ore. *Vietnam Journal of Earth Sciences*, 33(1): 63-77, <https://doi.org/10.15625/0866-7187/33/1/278>.
16. Pham Thi Dung, Tran Tuan Anh, Tran Trong Hoa, Ngo Thi Phuong, Nguyen Viet Y, Shunsho Ishihara, Pham Ngoc Can, Tran Van Hieu, 2012. Indium-Potential by-Product in Lead-Zinc Ore of the Cho Don Deposits. *Vietnam Journal of Earth Sciences*, 32(4): 9, <https://doi.org/10.15625/0866-7187/32/4/1032>.
17. Frenzel, M., Tamino, H., Jens, G., 2016. Gallium, Germanium, Indium, and Other Trace and Minor Elements in Sphalerite as a Function of Deposit Type - a Meta-Analysis. *Ore Geology Reviews*, 76: 52-78, <https://doi.org/10.1016/j.oregeorev.2015.12.017>.
18. Li, Z., Lin, Y., Yusi, H., Chen, W., Zhilong, H., Yulong, Y., Leonid, D., 2020. Trace Elements in Sulfides from the Maozu Pb-Zn Deposit, Yunnan Province, China: Implications for Trace-Element Incorporation Mechanisms and Ore Genesis. *American Mineralogist*, 105(11): 1734-51, <https://doi.org/10.2138/am-2020-6950>.
19. Nguyen Tuan Anh. Ore Chemical Characteristics and Orientation of Prospecting and Exploration

- of Lead-Zinc Ore in Northeast Vietnam. Ph.D Thesis, Hanoi University of Mining and Geology, Hanoi, 2014. (In Vietnamese with abstract in English).
20. Tran Trong Hoa, Tran Tuan Anh, Pham Thi Dung, Tran Quoc Hung, Bui An Nien, Tran Van Hieu, Pham Ngoc Can, 2012. By-Products in Lead-Zinc and Copper Ores of Northeast Vietnam. Vietnam Journal of Earth Sciences, 32(4): 10, <https://doi.org/10.15625/0866-7187/32/4/1031>.

State Governance of Coal Mining Industry towards Sustainable Development in Vietnam

CHU Thi Khanh Ly¹, PHAM Ngoc Huong Quynh², PHAM Tu Phuong³, NGUYEN Quynh Nga^{1,*}

¹ National Academy of Public Administration, Hanoi, Vietnam

² VNU University of Economics and Business, Vietnam National University, Hanoi, Vietnam

³ Investment Consulting Joint Stock Company, Hanoi, Vietnam

Corresponding author: nganq@napa.vn

Abstract. Coal is one of the most precious mineral resource, mining and mineral processing contributes to the economic development. In Vietnam, coal mining industry is economically profitable. However, this industry shows several disadvantages such as low productivity, wasting resources, negative environmental impact. Therefore, the State of Vietnam need to improve the coal mining governance to raise revenues, avoid wasting resources and meet the requirements of sustainable development. The paper aims to evaluate State governance of coal mining industry in Vietnam, and shows the advantages and disadvantages of this governance. Therefore, this paper proposes the strategies and solutions to improve coal mining governance in Vietnam towards sustainable development. The structure of the paper includes: (i) Literature review of the importance and requirements of state governance of coal mining industry towards sustainable development; (ii) State governance of coal mining industry in Vietnam; (iii) Proposals to improve State governance of coal mining industry towards sustainable development in Vietnam.

Keywords: State governance, Coal mining industry, Sustainable development, Vietnam

1. Introduction

“Sustainable development” was mentioned in the early 80s of the twentieth century in the Strategy of World Conservation proposed by the International Union for Conservation of Nature, the World Wildlife Fund, and the United Nations Environment Program. And then, this concept was officially introduced and worldwide used in 1987 by the World Commission on Environment and Development (WCED) in the Brundtland Report - “Our Common Future”. According to the Brundtland Report, sustainable development is defined as “development that meets the needs of the present without compromising the ability of future generations to meet their own needs” [1]. In other words, the sustainable development must ensure the effectively economic development, social equity, and protected and preserved environment. Therefore, all socio-economic sectors, state authorities, social organizations in the economy together take a responsibility to make and implement development policies to reach socio-economic goals as well as environmental protection.

The WCED’s definition of sustainable development mainly emphasizes the effective using of natural resources and ensuring the work place and living environment in the socio-economic development process. The sustainable development is also the transformational model that optimizes the economic and social benefits in the present while potential benefits in the future could not be damaged (Goodian and Hecdue, 1988, Prof. Grima Lino) [2].

The nature of the sustainable development concept was reaffirmed in the Summit Conference on Environment and Development in Rio de Janeiro (Brazil) in 1992 and was supplemented and completed in the World Summit Conference on Sustainable Development in Johannesburg (Republic of South Africa) in 2002. Accordingly, “sustainable development” is a development process that is a combination of three aspects including: economic development (economic growth), social development (social progress and justice, poverty alleviation and hunger elimination, and job creation), and environmental protection (reducing environmental pollution, restoring and improving environmental quality; preventing wildfires; reducing and preventing deforestation; rationally exploiting and effectively using natural resources) [2].

There are more than seventy different definitions of “sustainable development”. Depending on different approaches, different research purposes and contents, authors can define the concept of “sustainable development”. However, the sustainable development seeks to attain a balance between economic development, environmental protection, community benefits. The sustainable development is the requirement of country’s development that is a combination of economic development, social development, natural resources and environment protection, national defense and social safety [3].

Figure 1 below illustrates the content of sustainable development that balances economic development, social benefits, and environmental protection.

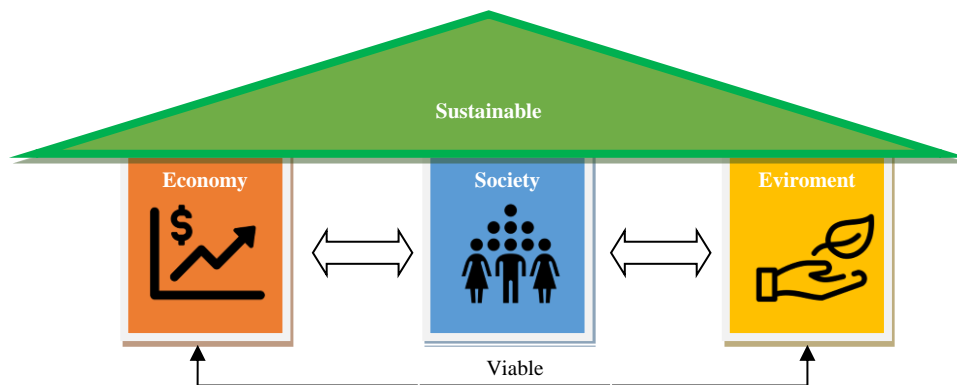


Fig. 1. Sustainable development.

Basing on the sustainable development definition, the paper illustrates the concept “the mineral resources sustainable development”. “Sustainable development of mineral resources is the level of use that does not exceed the capacity to discover new minerals, acceptable alternative materials and the ability to recycle to use wastes. And also, it is always necessary to apply processing technology to prolong the life of the exploited resource to the most extent” [4].

Inevitably, the mineral activities cause significant impacts on the surrounding environment such as destroying natural landscapes, contaminating surface water and groundwater, affecting air quality in the project area and local area. This leads to contaminate and erode arable land, and disturb wildlife, crops and livestock. Therefore, the state should address the ability to prevent environmental impacts in the beginning of project implementation to develop coal mining industry while protecting ecological environment and gaining economically viable.

This paper analyses the state governance of coal mining toward sustainable development in Vietnam. This includes different management functions and solutions that are promulgated and implemented by the State to ensure transparency and fairness in the coal mining industry to exploit economic value while ensuring the sustainable regeneration of coal mineral resources and environmental protection.

2. State governance of coal mining industry in Vietnam

2.1 Policy promulgation

Currently, the competent authorities have issued many legal regulations that is considered as management instrument of the State of Vietnam. Accordingly, the licensing of mineral mining activities has been adjusted more and more closely. Some documents are Directive No. 02/CT-TTg of the Prime Minister dated January 9, 2012 on strengthening the State management of mineral exploration, mining, processing, use and export; Directive No. 02/CT-TTg of the Prime Minister dated September 29, 2020 on strengthening the State management of exploration, mining, processing, use and export of minerals; Decree No. 40/2019/ND-CP dated May 13, 2019 of the Government amending and supplementing the decrees detailing and guiding the implementation of the Environmental Protection Law [5]; Decree No. 91/2019/ND-CP dated November 19, 2019 of the Government on sanction in land; Decree No. 96/2019/ND-CP dated December 19, 2019 of the Government on the Land Price Framework; Decree No. 06/2020/ND-CP dated January 3, 2020 of the Government amending and supplementing Article 17 of Decree No. 47/2014/ND-CP dated May 15, 2014 of the Government on compensation, support and resettlement when the State recovers land; Decree No. 67/2019/ND-CP dated July 31, 2019 of the Government on the method of calculating and collecting fees for granting mineral mining rights; Decree No. 03/2019/ND-CP dated January 4, 2019 of the Government on remote sensing activities; Decree No. 27/2019/ND-CP dated March 13, 2019 of the Government detailing a number of articles of the Surveying and Mapping Law; Decision No. 1746/QĐ-TTg dated December 4, 2019 of the Prime Minister promulgating the national action plan on ocean plastic waste management by 2030; Decision No. 417/QĐ-TTg dated April 13, 2019 of the Prime Minister promulgating the Master Action Program to carry out Resolution No. 120/NQ-CP and Directive No. 23/CT-TTg dated September 5 /2019 of the Prime Minister on accelerating the implementation of Resolution No. 120/NQ-CP, and many relevant documents.

Besides, the State has also issued a lot of regulations that are consulted by different stakeholder before and after promulgating the natural resources and environment policies and laws. Several documents are the draft on Environmental Protection Law; Decree replacing Decree No. 22/2012/ND-CP dated March 26, 2012 of the Government regulating the auction of mining rights; National action plan on ocean plastic waste management by 2030; The Government's master plan, 5-year plan for implementation of Resolution No. 36/NQ-TW dated October 22, 2018 of the Central Committee on sustainable development of Vietnam's marine economy by 2030, towards 2045 [4]; Decision of the Prime Minister promulgating the National Action Plan to respond to climate change from 2021-2030; Strategy for environmental protection from 2021-2030, towards 2040; Strategy for development of three surveying industries in Vietnam and national spatial infrastructure by 2030, toward 2040; Strategy for environmental protection from 2021-2030, toward 2040; National environmental protection planning from 2021-2030 toward 2050; National marine spatial planning from 2021-2030, toward 2050; National master planing on water resources from 2021-2030, toward 2050; National action plan to respond to climate change from 2021-2030, and many relevant documents [6].

Furthermore, while implementing the 2010 Mineral Law, the State of Vietnam issued many relevant legal documents to clarify mineral management institution and improve mineral resource governance, such as, Decree No. 33/2017/ND-CP of the Government on sanctioning of administrative violations in water resources and minerals. This document stipulates different types of fines for negatives in mineral mining. Accordingly, if an individual does not build the mine map during mining, he will be fined 200 million VND. Similarly, this fine for an organization will be 400 million VND [3]. There are many other relevant documents including Decision No. 89/2008/QD-TTg dated July 7, 2008 of the Prime Minister approving the development strategy of Vietnam's coal industry by 2015, toward 2025; The coal mining industry development plan to 2020, toward 2030, approved by the Prime Minister under Decisions No. 60/QD-TTg dated January 9, 2012, Decision No. 403-TTg dated 14/3/2016 and No. 1265/QD-TTg dated 24/8/2017 [5].

In general, the current legal documents can create a foundation to manage and ease the operation of enterprises in coal and mineral mining industry.

2.2 Policy implementation

The Vietnam National Coal and Mineral Industries Holding Corporation Limited - Vinacomin and the Ministry of Natural Resources and Environment (MONRE) take the main responsibility to implement the coal mining industry policy and strategy. Many other ministries and state agencies also contribute to State's coal mining industry policy and strategy implementation.

Coal mining license

The MONRE has granted the permits for coal mining activities in accordance with the Mineral Law. Accordingly, there are 128 licenses issued, including 27 exploration licenses and 101 coal mining licenses until 2020 [7].

From 2014 to June 30, 2019, the MONRE and local governments approved 582 mining auction projects. There were 304 successfully auctioned plans (including 13 types of minerals) accounted 52.23 % of the total projects. The auctions that are completed mineral exploration were 56 (accounting for 18.4 % of the total projects), gaining 272,516 billion VND revenue. While the data of auctions that are uncompleted mineral exploration were 248 (accounting for 81.6 % the total projects), gaining 768,306 billion VND revenue. The total revenue from 304 auction plans was at 1,040,823 billion VND, and more 466.210 billion VND than the total starting price auction (576,504 billion VND). Therefore, state budget revenue increased by 466,210 billion VND through mining auction [8].

Besides, the MONRE approved 94 projects of mineral investigation and exploration, earning 866.6 billion VND, while the local government licensed 152 mineral mining projects (accounting for 50 % of the total projects) and earned 354,358 billion VND to state budget [8].

Coal mining processing

According to the MONRE's reports, there are currently 3,000 organizations and individual be conducting mineral exploration and mining. Until 2020, there are 55 projects of mining investment and expansion, including 38 coal mining projects. Accordingly, there are 46 progressing projects, 35 completed projects, and 9 not started yet projects [7].

Unit: Billion VND

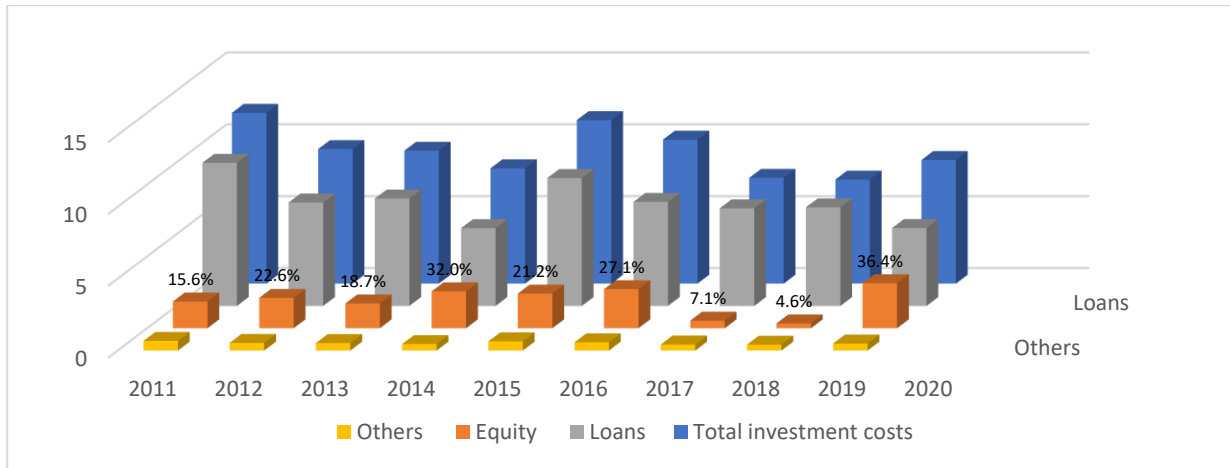


Fig. 2. Coal and mineral industry's investment from 2011-2020.

The coal and mineral mining investment is continuously fluctuated from 2011 to 2020. Figure 2 illustrates that the total investment cost for coal and mineral mining increases from 7.24 billions VND to 11.887 billions VND from 2011 to 2020. The figures in 2011, 2016 and 2020 are highest (11.887 billions VND, 11.381 billions, and 11.23 billions VND, respectively). Besides, majority of coal and mineral mining investment comes from the bank loans. The Chart 2.1 also shows that the capital from private equity is accounted for 4.6 % to 38.5 % of total investment cost [9].

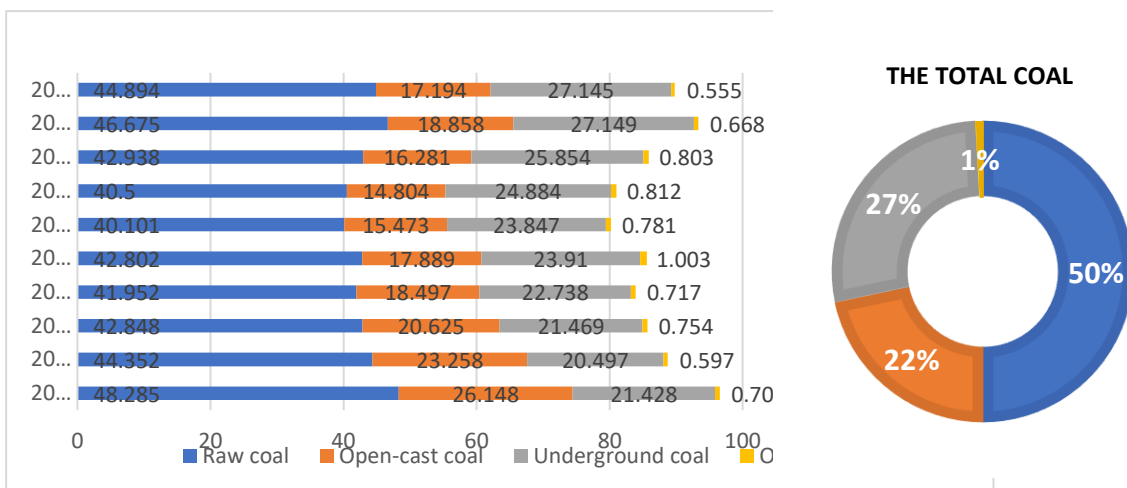


Fig. 3. Coal production from 2011 – 2020 (Unit: Thousand tons).

Figure 3 illustrates the coal production is fluctuated from 2011 to 2020. the data that the coal output is 48.285 tons in 2011, but from 2012 to 2018, this figure decreases from 44.325 tons to 40.5 tons. This is because of the decrease of mining investment; the decrease of households' consumption demand; the tightened State's management on mineral resources protection to protect ecological environment. From 2018 - 2020, the rate of coal mining increases from 42.938 to 26.676 tons [9]. This is due to the increase investment cost and the improvement of electronic government with online services and electronic one-stop model.

Accordingly, raw coal accounts for 50 % of total coal production, while the proportion of open-cast coal and underground coal is 22 % and 27 %, respectively. Because open-cast coal resources have become to be exhausted, many enterprises have switched to underground mining. This shift is inevitable, leading to use resources more effectively and to ensure sustainable ecological environment.

Besides, Vietnam has accelerated the construction of new mines as well as maximized the domestic mining capacity, the Vietnamese coal industry has invested in building several vertical well mines due to domestic units that design, construct and supply equipment themselves, have joint ventures or hire the foreign subcontractors. The Figure 4 compares the different output of raw coal and commercial coal from 2011-2020.

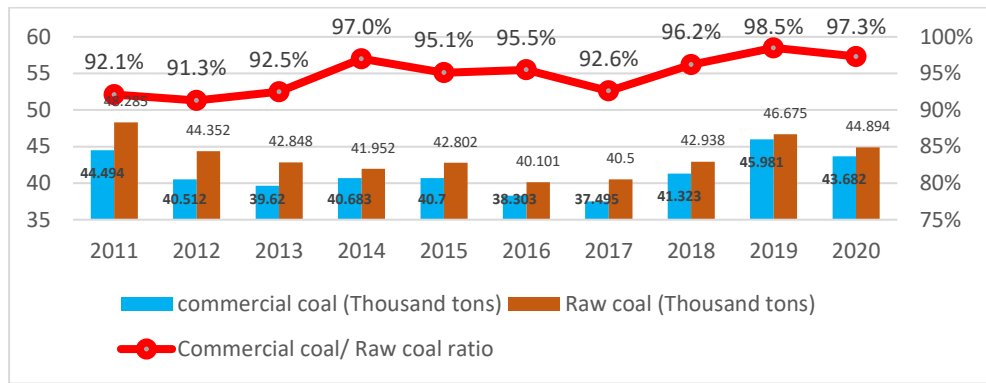


Fig. 4. Mining output of raw coal and commercial coal from 2011-2020.

Furthermore, mining production significantly depends on investment. Figure 5 shows the correlation between investment capital and coal mineral mining products. Accordingly, total investment costs are proportional to mining output from 2011-2020. From 2011 to 2014, the investment costs for production decreased from 11,887 billion VND to 9,251 billion VND, and mining output in this period also tended to decrease accordingly. However, in 2015, the investment costs increased by 11,381 billion VND, but the product did not increase significantly [9]. This is because investment cost has not been used effectively.

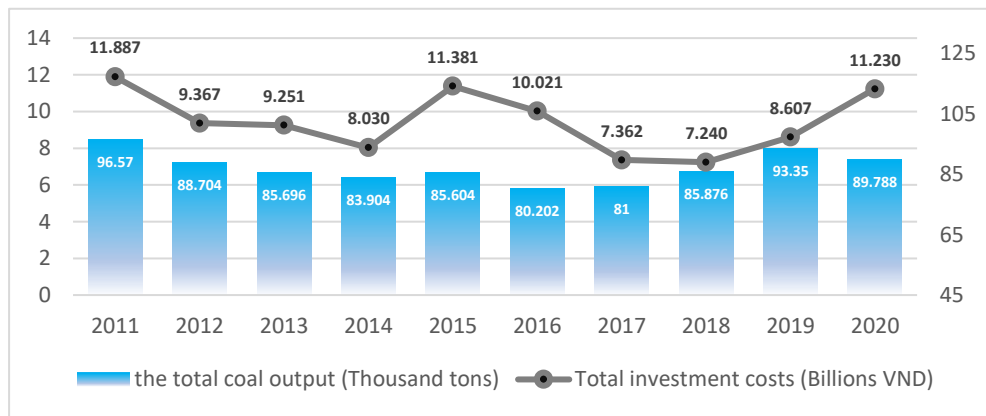


Fig. 5. Mining output of raw coal and commercial coal by 2011-2020.

The mining production also significantly depends on equity investment. The Figure 6 illustrates that from 2011 to 2020, the coal mining efficiency increases from 91.3% to 98.5%. This is because the improvement of equity proportion that grows from 4.6% to 38.6% [9]. Therefore, the exploiting natural resources efficiency strongly depends on the equity. If the equity is low, the mining efficiency decreases and vice versa. This result has shown the limitations in investment policy as well as state management in coal mining.

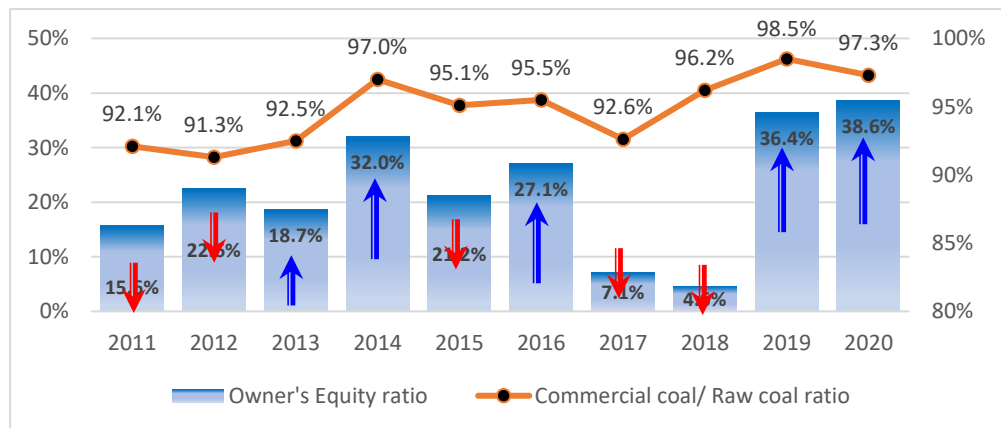


Fig. 6. Correlation between ratio of owner's investment capital and mining output of raw coal and commercial coal by 2011-2020.

2.3 Evaluating State governance of coal mining industry in Vietnam

Advantages

First, mineral exploration and mining are managed and licensed in accordance with the 2010 Mineral Law. The mineral deposit investigation, exploration, and assessment are also seriously managed in accordance with the 2010 Mineral Law. Therefore, mining enterprises can easily invest capital in undertaking, design mining projects, assessing environmental impact, design renovation projects, and deposit the Environmental Restoration Fund to apply for a mining license. Mining enterprises also can promote new mining technology and equipment to increase business efficiency, reduce environmental pollution, and save resources.

Second, due to the inspection of mineral exploration, mining and processing activities have been strengthened. The negatives of coal mining have been handled more effectively than in the earlier period, leading to limit the disadvantages in coal mining and raise the awareness of compliance with the law on minerals of organizations, individuals, people and agencies and organizations. Therefore, illegal coal mining has decreased, the awareness of compliance with the minerals law of organizations and individuals as well as agencies has been enhanced.

Third, due to the proactive implementation of environmental protection solutions according to the approved planning, the impact of coal production on the environment and population has become much minimized, the production environment has strongly changed, the ability to adapt to climate change has been enhanced. This contributes to the improvement of the general landscape and environment and the development of localities.

In general, the mining and mineral resources protection are strictly adhered to the approved planning, achieve positive results, and contribute to socio-economic development, economic structure transformation, and industry proportion.

Disadvantages

There are many challenges posed in coal mining. After the Prime Minister's Directive No. 29/CT-TTg dated December 2, 2019, this is fierce competition between domestically produced coal and imported coal, between coal production and business units in importing coal. While the mines are getting deeper and deeper with increasingly difficult and complex mining conditions (underground mines) and increasing waste supply (open-pit mines). Moreover, many inputs used for production and business activities (most types of machinery and equipment; petrol and oil; raw materials for the production of industrial explosives, etc.) depend on imports. The beneficial effects of weather and climate change will also be challenges for coal enterprises [4].

Accordingly, the coal reserves in favorable mining areas are gradually being exhausted. In the near future, coal mining will be mainly by underground mining method, while the investment rate for underground coal mining is currently very high. The mining area is getting deeper and deeper, the mine pressure is great, the mining conditions are increasingly unfavorable, leading to the increasing costs of exploration, mining, environment, and labor safety. The taxes on natural resources in Vietnam are still high, higher than the common tax rates of other countries in the region, leading to high domestic coal production costs, reduced competitiveness and disadvantages compared to imported coal.

In addition, there is a shortage of high-quality human resources due to the heavy and toxic mining working environment affecting the workers' health, leading to the fact that mining enterprises have to face the labor shortage, especially the direct labor force (underground miners, open-pit mines). Currently, remuneration policies have been improved, but still not satisfactory, even lower than that of some countries in the region, while the developing domestic economy creates conditions for the workers to have many career choices. As a result, labor productivity is low compared to some countries in the region.

Besides, the requirement of environmental protection and sustainable development have been set more rigorously for the mining of mineral resources.

Therefore, improving the state governance in the mining of mineral and coal resources is necessary to ensure the sustainable development of the national mineral resources.

3. The importance of State governance in the coal mining industry towards sustainable development in Vietnam

3.1. Guiding the national coal-mineral resource mining strategy

The coal mining industry is an important sub-sector in the overall energy sector of Vietnam. The development of the coal mining industry is currently being implemented in accordance with the

Development Planning of Vietnam's coal industry by 2020, towards 2030, approved by the Prime Minister in Decision No. 403/QD-TTg dated 14/14/ 3/2016 [4] and adjusted some contents in Decision No. 1265/QD-TTg dated August 24, 2017 [9]. In the past, the planning of sectors was carried out almost independently, but now the energy sectors such as electricity, oil, gas, coal and renewable energies integrated into the “National Energy Master Planning for the period of 2021-2030, toward 2050”.

The strategic orientation of coal mining industry development has been stated in Resolution No. 55-NQ/TW on “*Strategic Orientation for National Energy Development of Vietnam by 2030, toward 2045*” by the Ministry of Political Affairs. The main tasks and solutions are: (i) building a new coal mining industry development strategy associated with the task of effective investment abroad and long-term coal import; (ii) implementing appropriate coal reserves to meet requirements for production activities, especially electricity generation; (iii) expanding search, exploration, improve the quality of assessment of reserves and resources; (iv) stepping up domestic coal mining on the basis of ensuring safety, efficiency and saving resources; urgently research technology to be able to exploit the coal basin of the Red River Delta; improve the clean coal recovery coefficient in underground mining; (v) rapidly deploying the construction of a large-scale coal port, storage and transit system; increasing mechanization and modernization of coal sieving, sorting and mining equipment; (vi) reviewing and assessing the demand, developing plans and optimizing solutions for stable coal supply for power production in line with the market mechanism” [10].

The Master Plan is also a condition for coal mining enterprises to meet the requirements of the 2010 Mineral Law. According to the Article 40 of the 2010 Mineral Law, “organizations and individuals with mineral exploration licenses must have an exploration project in accordance with the planning”. The Article 53 shows that organizations and individuals with mineral mining licenses must have an investment project to exploit the minerals in the area where the reserves have been explored and approved in accordance with the planning” [10].

Currently, the government is restructuring the economy and transforming the growth model, enforcing intellectual property rights, making investment and bidding activities transparent, creating a more open mechanism. This is the driving force for the coal industry to realize strategic goals, improve competitiveness, and improve the quality of goods and services.

3.2. Promoting national socio-economic development strategy

The coal mining industry plays the role of a key economic sector providing operating fuel for most industries, especially electricity, fertilizer, paper, and cement, which use the most coal in production. This shows that the output of the coal industry is very stable. The State pays strongly attention to issue and implement policies and directly invest to coal mining industry, so that the risks of the industry’s operation due to fluctuations in the monetary market are limited. The workers and officers of the coal mining industry is rich in revolutionary tradition, always upholding the spirit of “Discipline and Coordination”, ready to face and overcome all challenges. In addition, Vietnam has changed from an energy exporter to an energy importer, the demand for coal for power generation and other domestic economic sectors has increased, even exceeding the domestic mining capacity, creating great opportunities for the coal industry. While the world coal price is on an upward trend and the domestic coal price in 2021 and the following years is expected increase.

4. Some suggestions

In order to improve the effectiveness of State governance in coal mining industry towards sustainable development in Vietnam, there are some following recommendations.

Firstly, the State should soon complete legal documents on mineral resource mining in general and coal mining in particular. In which, the State should soon issue specific and update regulations to increase the participation of different stakeholders in coal mining investment. Besides, the administrative reform and application of information technology in governance is very important to control and supervise coal mining activities and coal mining capital sources.

Secondly, the State should design and implement specific coal mining policies and measures to ensure the requirements and principles in the exploration and mining of mineral resources to ensure sustainable development. Accordingly, coal and mineral mining activities should comply with the principles of law, the principles of professional expertise leading to gain economic profits, ensure the ecological environment, and respect traditional cultural values.

Thirdly, the State should encourage enterprises to more invest and apply modern science and technology in coal production. This is a sustainable development strategy to increase productivity, mining output and

especially save mineral resources for the country. Particularly, at underground mines, enterprises should apply mechanization and synchronous automation systems in coal mining to improve working conditions for miners and limit the impact on the environment.

Fourthly, the State should delineate and publicize scattered and small coal areas for local management, and effectively calculate fees for granting coal mining rights, fees for using data and information of coal investigation and exploration.

Finally, the inspection and examination of coal exploration and mining activities should be promoted. Accordingly, the State should conduct statistics on actual coal production, inventory of exploited coal reserves and remaining coal reserves nationwide accurately and efficiently.

5. Conclusions

In general, State governance in the mineral resources mining in general and coal mining in particular in recent years has achieved certain results. The details are as follows:

The State has oriented the development strategy of coal mining by formulating and promulgating legal regulations to ensure the legal implementation. Besides, State's investment capital for coal mining from 2010 to 2020 is relatively large, especially in 2012, 2014, 2020. State policies also have been more open in enhancing the participation of different stakeholders in coal mining investment, leading to more attract capital sources of enterprises and business owners, and bringing a lot of coal mining output and economic value for the State's budget.

However, State governance of coal mining still has certain limitations. Specifically, although the current legal regulations on coal mining have been promulgated by the State, the current regulations still show overlapping and lack of regulatory contents. Currently, there is still a lack of regulations on the participation of stakeholders in capital investment in coal mining activities. Regulations on ensuring sustainable coal mining and the environment are also still lacking. The management of the State's investment capital in coal mining is less effective, so that using State's investment capital in coal mining is less effective than that of business owners.

Therefore, State governance has not focused only on the efficient mining of coal production but also on the sustainability of mineral resources upon coal mining and ensuring the ecological environment. Environmental protection and renewable resources in coal mining should be seriously concerned by the State. The State should issue specific legal documents in coal mining to ensure the sustainability of mineral resources and living environment. The State also should improve the inspection, supervision on environmental assurance in coal mining.

6. Acknowledgements

The paper was presented during the 6th VIET - POL International Conference on Scientific-Research Cooperation between Vietnam and Poland, 10-14.11.2021, HUMG, Hanoi, Vietnam.

7. References

1. World Commission on Environment and Development, 1887.
2. Nguyen Duc Quy, Dang Huy Huynh, Nguyen Thuong Hung, Nguyen An Phong, 2011. On the mining and rational use of some natural resources of Vietnam, Anthology "Environmental Resources" Science and Technology Publishing, Hanoi.
3. Strunk, Jr. W., White, E.B., The Elements of Style, fourth ed., Longman, New York, 2000.
4. Vu Van Hien, 2014. Sustainable Development in Vietnam. Communist Review, 1(4): 67-69.
5. <https://thuvienphapluat.vn/van-ban/Tai-nguyen-Moi-truong/Nghi-quyet-55-NQ-TW-2020-dinh-huong-Chien-luoc-phan-tien-nang-luong-quoc-gia-cua-Viet-Nam-435381.aspx> 15/5/20121.
6. <https://tulieuvankien.dangcongsan.vn/he-thong-van-ban/van-ban-cua-dang/nghi-quyet-so-36-nqtw-ngay-22102018-hoi-nghi-lan-thu-tam-ban-chap-hanh-trung-uong-dang-khoa-xii-ve-chien-luoc-phan-tien-ben-4810>, 15/05/2021.
7. Debra Lam, Vietnam's Sustainable Development Policies: Vision VS Implementation, World Science Book, Hanoi, 2014.
8. <http://baochinhphu.vn/Chinh-sach-moi/De-xuat-quy-dinh-ve-dau-gia-quyen-khai-thac-khoang-san/395960.vgp>, 10/05/2021.
9. Vietnam National Coal and Mineral Industries Group - Vinacomin (TKV) and Dong Bac Corporation.
10. <https://nhandan.com.vn/tin-tuc-xa-hoi/minh-bach-trong-quan-ly-khai-thac-khoang-san-330362,10/5/2021>.

Life Cycle Inventory (LCI) Stochastic Approach Used for Rare Earth Elements (REEs), Considering Uncertainty

SALA Dariusz^{1,*}, BIEDA Bogusław¹

¹ AGH University of Science and Technology, Kraków, Poland

Corresponding author: dsala@zarz.agh.edu.pl

Abstract. The purpose of the paper is to present the results of the stochastic modelling with uncertainty performed with the use of Monte Carlo (MC) simulation with 10,000 cycles and a confidence interval of 95 %, as recommended. Analysed REEs were fitted by lognormal distributions by using the Crystal Ball® (CB) spreadsheet-based software after defining the geometric mean value (μ_g) and the standard deviation (σ), automatically calculated (matches) the lower, as well as, upper boundaries of lognormal distribution. The number of replications of a simulation affects the quality of the results. The principal output report provided by CB and presented in this study consists of the graphical representation in the form of the frequency chart, percentiles summary, and statistics summary. Additional CB options provide a sensitivity analysis with tornado diagrams. The data that was used for MC simulation of the LCI model includes available and published data concerning associated with the REEs. This paper discusses the results and show that the adopted approach is applicable for any REEs used in the LCI studies under uncertainty. The results obtained from this study can be used as the first step in performing a full LCA analysis and help practitioners as well as decision-makers in the environmental engineering and management.

Keywords: Life cycle inventory (LCI), Stochastic approach, Rare earth elements (REEs)

1. Introduction

The REEs are grouped into two different categories on the basis of their atomic numbers. REEs with atomic numbers 57-63 are classified as light-rare earths (LREEs), and REEs with atomic numbers 64-71 are classified as heavy-rare earths (HREEs) [1]. According to Xie et al. [2] the term “rare” earth is a misnomer; because they are relatively abundant in the Earth’s crust, as well as they are typically dispersed and only rarely occur in concentrated and economically exploitable mineral deposits [3].

The Socialist Republic of Vietnam has many of mineral resources located in the northern part of the country [4]. The large resource of rare earth metals in Vietnam is located in the Namxe rare earth deposit which belongs to Namxe commune, Phongtho district, Laichau province (Fig. 1) [5]. Based on the previous studies presented in [6], the rare earth deposit contents include about 80 different minerals.



Fig. 1. Location of Namxe rare earth deposit [5, 7, 8].

2. Materials and Methods

2.1 Uncertainty analysis

In this study uncertainty is performed by using the Monte Carlo (MC) simulation. The applicability of the MC approach for assessing parameter uncertainty was presented as follows by Warren-Hicks and Moore [9]:

- 1/ select a distribution to describe possible values of each parameter;
- 2/ specify properties of each parameter;
- 3/ generate data from the distribution;
- 4/ use the generated data as possible values of the parameter in the model to produce output.

Ribal et al. [10] quoted the definition of uncertainty given by Huijbregts [11] which is as follows: “Uncertainty is defined as incomplete or imprecise knowledge, which can arise from uncertainty in the data regarding the system, the choice of models used to calculate emissions and the choice of scenarios with which to define system boundaries, respectively”. Suter [12] proposed uncertainty definition as follows: „imperfect knowledge concerning the present or future state of the system under consideration”. This definition is similar to the definition given in Reinert et al. [13], and is as follows: „process that assesses the imperfect knowledge concerning the present or future state of the system under study; may be qualitative and/or quantitatively addressed.

In our case the REEs were fitted by lognormal distributions with σ equal 1.1 obtained by using the Crystal Ball® (CB) spreadsheet-based software. The graphic illustration of log-normal probability distributions used to assess the La, Ce and Nd, offered in CB software (Lognormal Distribution tab windows), are shown in Figures 2, 6 and 10, respectively. The simulation outputs after 10,000 runs have been given in the form of frequency forecast charts (Figs. 3, 7 and 11), and statistic reports (Figs. 4, 5, 8, 9, 12 and 13, respectively).

In order to obtain an accurate value, the MC method should be based on a large number of simulations [13]. The number will vary from problem to problem at least in hundreds and, even better, in thousands [14], through 5000 runs [21] to up 10,000 runs [10, 15, 16]. Further guidance to MC simulation is provided by the ILCAD handbook - General guide for Life Cycle Assessment - Detailed guidance [17]. Each realization, or trial, involves random selection of a value for each uncertain quantity (according to a probability or frequency distribution).

Probabilistic methods are distinguished from deterministic methods in that exposure is characterized not as a point estimate but as a probability distribution (or frequency distribution) of possible estimates, based on the use of distributions to characterize some or all of the uncertain input quantities [18]. Moreover, probabilistic methods improve accuracy in risk characterization by capturing a more realistic range of possible outcomes than from deterministic methods in that deterministic methods [18].

The data used in the current study is obtained from the Deliverable D1.2 Report and Deliverable D1.3 Report – with both coming from the ENVIREE (ENVIRONMENTALLY friendly and efficient methods for extraction of Rare Earth Elements from secondary sources) - funded grant within the second ERA-NET ERA-MIN Joint Call Sustainable Supply of Raw Materials in Europe 2014 [19]. The each REEs analyzed in this study is independent (uncorrelated) of the others and comes from the same source, in this case from laboratory. A stochastic (probabilistic) analysis considering uncertainty and using MC, has been performed on three selected REEs, namely Lanthanum (La), Cerium (Ce) and Neodymium (Nd).

This project aims to increase the knowledge on the stochastic modelling (used random probability distribution) considering uncertainty and performed by the use of the Monte Carlo (MC) simulation.

The graphic illustration of log-normal probability distributions used to assess of the La, Ce and Nd, adopted in CB software (Lognormal Distribution tab windows), are shown in Figures 2, 6 and 10, respectively.

The simulation outputs after 10,000 runs have been given in the form of frequency forecast charts (Figs. 3, 7 and 11), and statistic reports (Figs. 4, 5, 8, 9, 12 and 13, respectively).

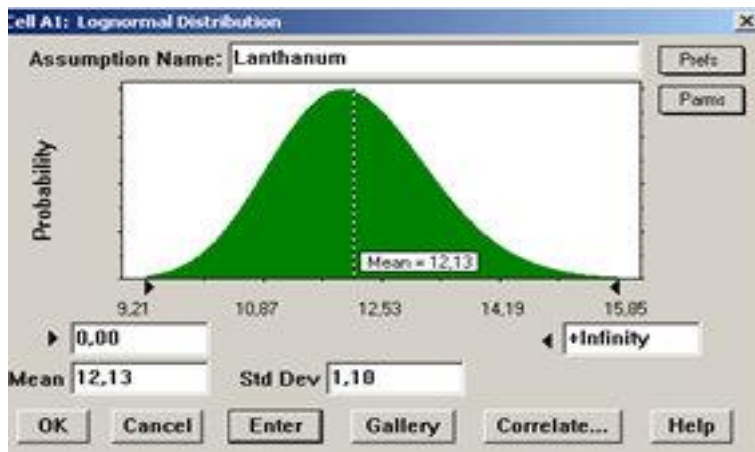


Fig. 2. The dialog windows of log-normal probability distribution of La, as obtained in CB software (source: own work).

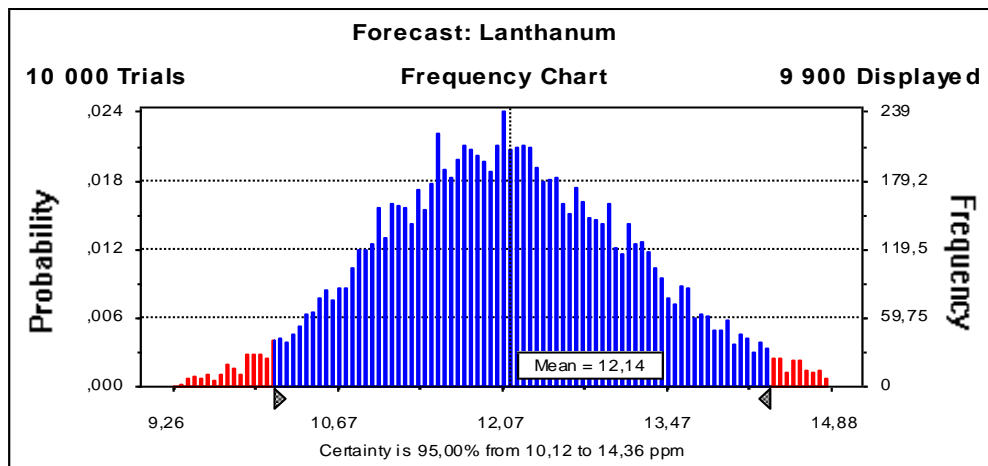


Fig. 3. The Frequency chart of the La forecast with 95% confidence level (source: own work).

Statistic	La (ppm)
Trials	10 000
Mean	12.14
Median	12.10
Mode	---
Standard deviation	1.09
Variance	1.19
Skewness	0.24
Kurtosis	3.14
Coeff. of variability	0.09
Range maximum	8.09
Range minimum	18.46
Range width	10.37
Mean std. error	0.01

Fig. 4. The statistics report of the forecast of the La – Statistics (source: own work).

Percentile	La (ppm)
0%	8.09
10%	10.78
20%	11.21
30%	11.55
40%	11.82
50%	12.10
60%	12.37
70%	12.69
80%	13.06
90%	13.58
100%	18.46

Fig. 5. The statistics report of the forecast of the La – Percentiles (source: own work).

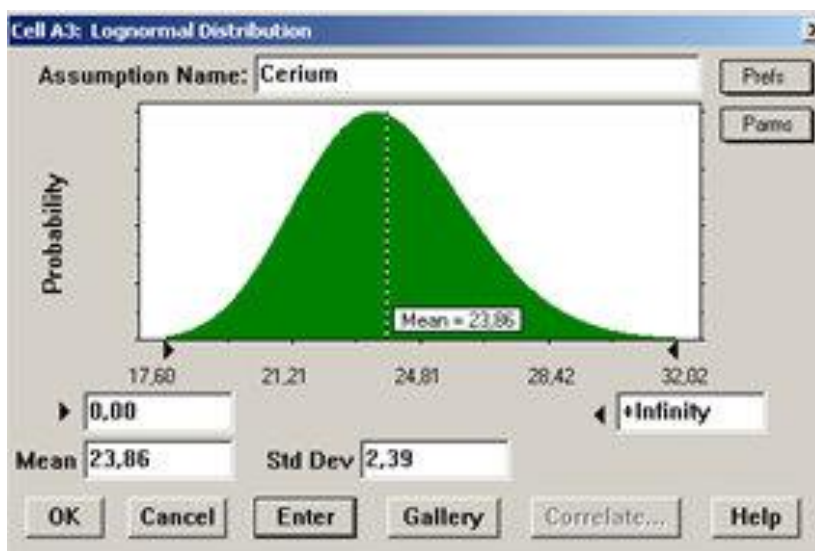


Fig. 6. The dialog windows of log-normal probability distribution of Ce, offered in CB software (source: own work).

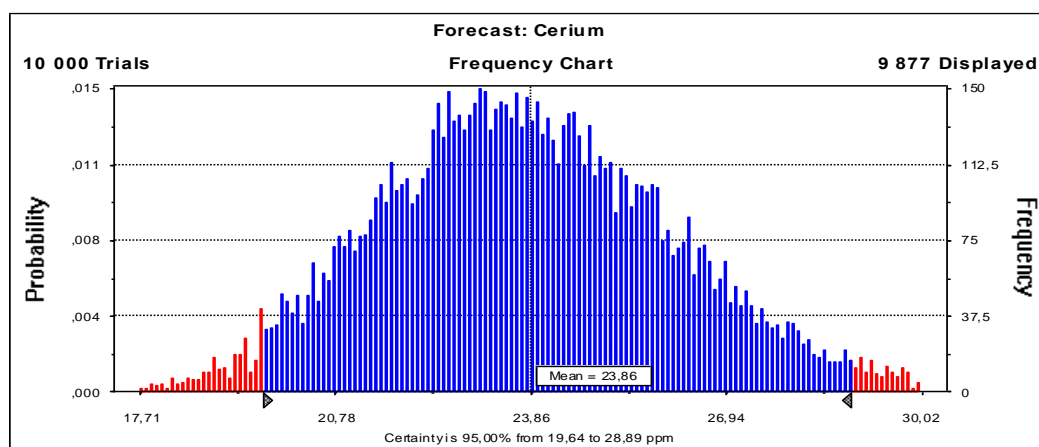


Fig. 7. The Frequency chart of the Ce forecast with 95% confidence level (source: own work).

Statistic	Ce (ppm)
Trials	10,000
Mean	23.86
Median	23.73
Mode	---
Standard deviation	2.37
Variance	5.61
Skewness	0.33
Kurtosis	3.20
Coeff. of variability	0.10
Range maximum	16.03
Range minimum	33.18
Range width	17.15
Mean std. error	0.02

Fig. 8. The statistics report of the forecast of the Ce – Statistics (*source: own work*).

Percentile	Ce (ppm)
0%	16.03
10%	20.91
20%	21.84
30%	22.56
40%	23.14
50%	23.73
60%	24.34
70%	25.00
80%	25.79
90%	26.93
100%	33.18

Fig. 9. The statistics report of the forecast of the Ce – Percentiles (*source: own work*).

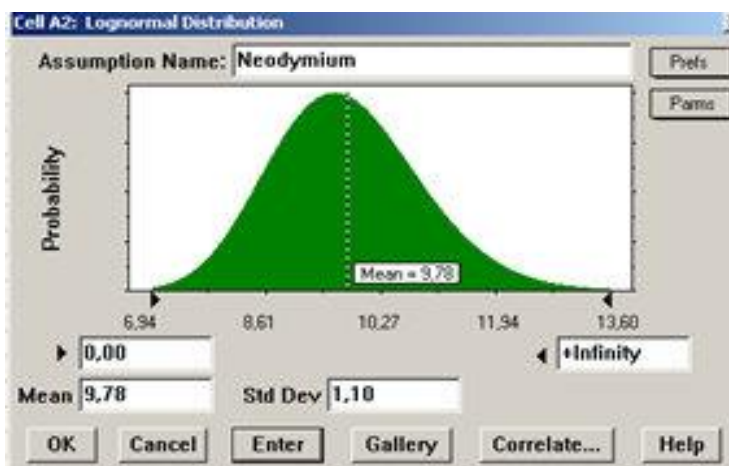


Fig. 10. The dialog windows of log-normal probability distribution of Ne, offered in CB software (*source: own work*).

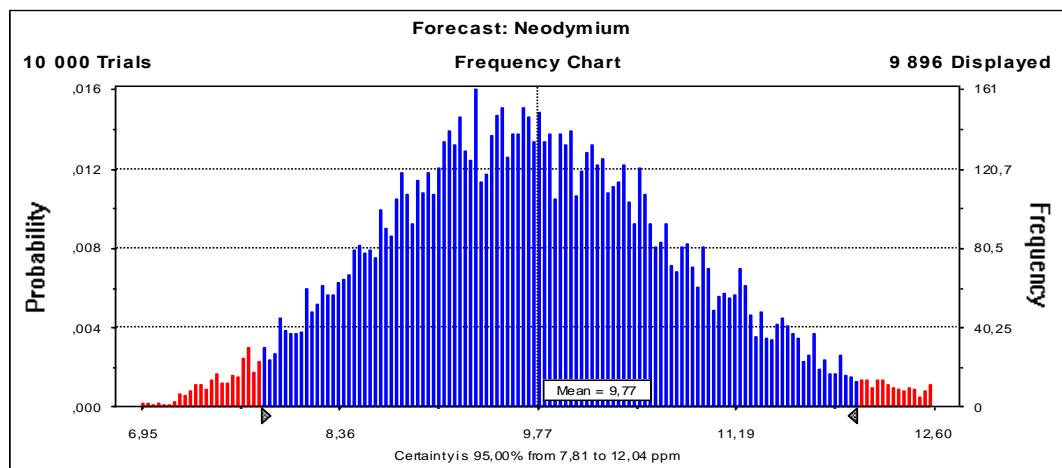


Fig. 11. The Frequency chart of the Nd forecast with 95% confidence level (Source: own work).

Statistic	Ne (ppm)
Trials	10 000
Mean	9.77
Median	9.72
Mode	---
Standard deviation	1.09
Variance	1.18
Skewness	0.34
Kurtosis	3.26
Coeff. of variability	0.11
Range maximum	6.47
Range minimum	16.71
Range width	10.24
Mean std. error	0.01

Fig. 12. The statistics report of the forecast of the Ne – Statistics (source: own work).

Percentile	Ne (ppm)
0%	6.47
10%	8.42
20%	8.85
30%	9.17
40%	9.45
50%	9.72
60%	9.99
70%	10.30
80%	10.66
90%	11.21
100%	16.71

Fig. 13. The statistics report of the forecast of the Ne – Percentiles (source: own work).

Tab. 1. Overview of the REEs taken into account in the study (all values in ppm).

REEs	Distribution type	Atomic number	μ_g	σ_g	Quality	Reference
Lanthanum (La)	Lognormal	57	12.13	1.10	12.19	CB® analysis result
Cerium (Ce)	Lognormal	58	23.86	2.39	23.89	CB® analysis result
Neodymium (Nd)	Lognormal	60	9.78	1.10	9.83	CB® analysis result

3. Results and discussions

MC simulation has received considerable attention in the literature, especially when MC simulation is used for making decisions that will have a large social and economic impact [20]. This is best seen in [21-26]. Di Maria et al. [14] proposed novel approach for quantifying uncertainty propagation in LCA and recommended MC simulation for carrying out an uncertainty analysis in LCA studies.

Bieda and Grzesik [23] provided definition of the uncertainty in the Article 3(6) of the Monitoring and Reporting Regulation - Guidance on Uncertainty Assessment No. 4, Final Version of 5 October 2012, part of a series of documents provided by the Commission services for supporting the implementation of Commission Regulation (EU) No. 601/2012 of 21 June 2012 (on the monitoring and reporting of greenhouse gas emissions pursuant to Directive 2003/87/EC of the European parliament and of the Council).

In the current study uncertainty analysis at the LCI level is conducted using Oracle Crystal Ball® (CB) associated with Excel spreadsheet models for carrying MC simulation. LCI data was defined as probability distributions instead of deterministic values.

The confidence interval is 95%. The total forecast value ranges of Ce, La, and Ne forecast value amounted to the mean values of 23.86 ppm, 12.13 ppm, and 9.78 ppm, respectively. The range centered about the mean from 19.64 ppm to 28.89 ppm for Ce, from 10.12 ppm to 14.36 ppm for La, and from 7.81 ppm to 12.04 ppm for Ne, respectively. Just below the horizontal axis at the extremes of distribution there are two small triangles, called endpoint grabbers. The confidence limits, presented in the frequency charts, are fixed using the above-mentioned grabbers (the area of the frequency charts covered by them is darker) [25].

4. Conclusions

This study aimed to express application of the stochastic approach to the neodymium, cerium and lanthanum, extracted from secondary sources of the REEs, classified as waste, and obtained during gold processing. The study also hope to promote the use of uncertainty analysis in environmental science based on the use of MC simulation. Furthermore, the goal of this study was to provide LCI data which can be further treated and used to the full LCA analysis of REEs recovery processes from secondary sources.

Under real conditions, primary data parameters are usually loaded with uncertainty. The uncertainty analysis for stochastic simulation requires that all parameters are described by probability distributions. In order to assess the credibility of the LCA results, which are burdened with a certain degree of uncertainty, the stochastic analysis, using the MC simulation has been adopted with the aim of evaluating the uncertainty in LCA.

This study combines the knowledge and insights from previous works about modelling of recycling with environmental data for REEs and continue to evaluate and discuss focus on the usefulness of stochastic modelling concerning uncertainty in the environmental engineering. This study also highlights the needs for further studies of REEs recovery. Presented study could be helpful in explaining the problems of stochastic analysis to scientific researchers, and to industry managers.

Acknowledgments

The authors are grateful for the input data provided as part of the environmentally friendly and efficient methods for extraction of rare earth elements from secondary sources (ENVIREE) project funded by NCBR within the second ERA-NET ERA-MIN Joint Call Sustainable Supply of Raw Materials in Europe 2014.

The paper was presented during the 6th VIET - POL International Conference on Scientific-Research Cooperation between Vietnam and Poland, 10-14.11.2021, HUMG, Hanoi, Vietnam.

References

1. Navarro, J., Zhao, F., 2014. Life-cycle assessment of the production of rare-earth elements for energy application: a review. *Frontiers in Energy Research*, <https://doi.org/10.3389/fenrg.2014.00045>.
2. Xie, F., Zhang, T.A., Dreisinger, D., Doyle, F., 2014. A critical review on solvent extraction of rare earths from aqueous solutions. *Minerals Engineering*, 56: 10-28.
3. Sala, D., Bieda, B., 2019. Life Cycle Inventory (LCI) Approach Used for Rare Earth Elements (REEs) from Monazite Material, Considering Uncertainty. Editors. 2019: Nasser S. Awwad and Ahmed T. Mubarak. *LANTHANIDES*, Chapter 3. InTechOpen. London, SE19SG – United Kingdom.
4. Mijał, W., Polek, D., 2019. Phosphate and copper resources in Lao Cai area and their beneficiation (in Polish). *Czasopismo Techniczne*, 180-181: 31-35.
5. Phan, Q.V., Dao, T.T., Nguyen, P., Trinh, D.H., Heinig, T., 2019. An Assessment of Natural Radioactivity in the Namxe Rare Earth Deposit, Laichau Province, Vietnam. *Minerals*, 9(10): 602, doi:10.3390/min9100602.
6. Bui, T.H., Trinh, D.H., Nguyen, P., 2010. Overview of rare earth in Vietnam. *Geological Journal Ser. A.*, 447–456.
7. Lai Chau Map. Available online: <http://vietnamtravels.vn/Vietnam-travel-information/Lai-Chau.htm>.
8. Vietnam Map. Available online: <http://www.vietnamtours.ws/Map.html>.
9. Pellston Workshop on Uncertainty Analysis in Ecological Risk Assessment (23-28 August 1995: University of Michigan Biological Station), Pellston, Michigan, Pensacola, FL, USA. Editors. 1998: Warren-Hicks, W.J. and Moore, D.R.J., Society of Environmental Toxicology and Chemistry (SETAC).
10. Ribal, J., Ramírez-Sanz, C., Estruch, V., Clemente, G., Sanjuán, N., 2017. Organic versus conventional citrus. Impact assessment and variability analysis in the Comunitat Valenciana (Spain). *International Journal of Life Cycle Assessment*, 22(4): 571-586.
11. Huijbregts, M.A.J., 1998. Application of uncertainty and variability in LCA. Part I: A general framework for the analysis of uncertainty and variability in life cycle assessment. *International Journal of Life Cycle Assessment*, 3(5): 273-280.
12. Suter, G.W.II., 1993. *Ecological risk assessment*. Lewis Publishers. CRC Press Boca Raton, FL, USA. 538 pages.
13. Reinert, K.H., Bartell, S.M., Biddinger, G.R., 1998. Ecological risk assessment decision-support system: a conceptual design. Proceedings from SETAC Ecological Risk Assessment Modeling Workshop, 23-28 August 1994, Pellston Michigan Pensacola FL. Society of Environmental Toxicology and Chemistry (SETAC).
14. Di Maria, F., Micale, C., Contini, S., 2016. A novel approach for uncertainty propagation applied to two different bio-waste management options. *International Journal of Life Cycle Assessment*, 21: 1529-1537.
15. Escobar, N., Ribal, J., Clemente, G., Rodrigo, A., Pascual, A., Sanjuán, N., 2015. Uncertainty analysis in the financial assessment of an integrated management system for restaurant and catering

- waste in Spain. *International Journal of Life Cycle Assessment*, 20: 1491-1510.
16. Willers, C.D., Maranduba, H.L., de Almeida Neto, J.A., Rodrigues, L.B., 2017. Environmental Impact assessment of a semi-intensive beef cattle production in Brazil's Northeast. *International Journal of Life Cycle Assessment*, 22: 516-524.
 17. ILCD-Handbook-General-guide-for-LCA-DETAILED-GUIDANCE. <https://eplca.jrc.ec.europa.eu/uploads/ILCD-Handbook-General-guide-for-LCA-DETAILED-GUIDANCE-12March2010-ISBN-fin-v1.0-EN.pdf>. 2010.
 18. Federal Contaminated Sites Action Plan (FCSAP) Ecological Risk Assessment Guidance. https://www.canada.ca/content/dam/eccc/migration/fcs-scf/B15E990A-C0A8-4780-9124-07650F3A68EA/ERA-20Guidance-2030-20March-202012_FINAL_En.pdf. 2012.
 19. Dias, M.I.M., Borcia, C.G., Menard, Y., 2016. Deliverable D1.2 report on the physical-chemical properties of available materials for the recovery of REE and Deliverable D1.3 chemical and mineralogical data of secondary REE sources. http://www.enviree.eu/fileadmin/user_upload/ENVIREE_D1.2_and_D1.3.pdf.
 20. Saltelli, A., Tarantola, S., Campolongo, F., Ratto, M., 2004. *Sensitivity Analysis in Practice. A Guide to Assessing Scientific Models*. 2004: John Wiley & Sons, Ltd, Chichester, West Sussex, England.
 21. Bieda, B., Grzesik, K., 2017. Application of stochastic approach based on Monte Carlo (MC) simulation for life cycle inventory (LCI) of the rare earth elements (REEs) in beneficiation rare earth waste from the gold processing: case study. In *ASEE17 Conferences Wrocław, Poland*, July 2-5, 2017. Wrocław, Poland, DOI: 10.1051/e3sconf/20172200018.
 22. Bieda, B., Grzesik, K., 2017. Uncertainty analysis of the life cycle inventory of rare earth elements from secondary flotation of rare earth elements in beneficiation rare earth waste from the gold processing: case study. In *SGEM Conference 2017, Albena, Bulgaria*.
 23. Bieda, B., Grzesik, K., 2017. Stochastic modelling using the Monte Carlo simulation for life cycle inventory of the rare earth elements (REEs) in beneficiation rare earth waste from Covas mining site, Portugal case study. In *23rd SETAC Europe LCA case study symposium, 27–28 November 2017, Barcelona, Spain*.
 24. Sala, D., Bieda, B., 2019. Life Cycle Inventory (LCI) Approach Used for Rare Earth Elements (REEs) from Monazite Material, Considering Uncertainty. *Lanthanides*, Editors, 2019: IntechOpen, London, United Kingdom. <http://dx.doi.org/10.5772/intechopen.80261>.
 25. Evans, J.R. and Olson, D.L. *Introduction in Simulation and Risk Analysis*, Prentice Hall, Inc. New Jersey 1998. 279 pages.
 26. Bieda, B., *Stochastic analysis in production process and ecology under uncertainty*. Springer Verlag. Berlin 2012, Heidelberg, 168 page

Estimation of Suspended Sediment Concentration in Downstream of the Ba River Basin using Remote Sensing Images

NGUYEN Ba Dung¹, BUI Ngọc An², DANG Tuyet Minh^{2,*}

¹ Hanoi University of Natural Resources and Environment, Hanoi, Vietnam

² Thuyloi University, Department of Surveying, Hanoi, Vietnam

Corresponding author: dtminh@tlu.edu.vn

Abstract. Assessing the tendency of suspended sediment concentration (SSC) in the river watersheds enables a better understanding of the hydromorphological properties of its basins and the associated processes. In addition, analyzing this trend is essential to address several important issues such as erosion, water pollution, human health risks, etc. Therefore, it is critical to determine a proper method to quantify spatio-temporal variability in SSC. In recent years, remote sensing and GIS technologies are being widely applied to support scientists, researchers, and environmental resource investigators to quickly and synchronously capture information on a large scale. The combination of remote sensing and GIS data will become the reliable and timely updated data source for the managers, researchers on many fields. There are several tools, software, algorithms being used in extracting information from satellites and support for the analysis, image interpretation, data collection. The information from satellite images related to water resources includes vegetational cover, flooding events on a large scale, rain forecast, population distribution, forest fire, landslide movements, sedimentation, etc., and especially information on water quality, sediment concentration. This paper presents the initial result from LANDSAT satellite image interpretation to investigate the amount of sediment carried downstream of the Ba river basin.

Keywords: Remote sensing image, Suspended sediment concentration, Downstream of the Ba river basin

1. Introduction

Suspended sediment, representing most of the total amount of sediment transported downstream and being easier to monitor than other components [1], is commonly used to estimate sediment loads within a stream [2]. Suspended sediment is a water quality constituent of particular concern to many rivers, lakes because this parameter increases turbidity and can influence the transport of particle-bound contaminants such as nutrients, organic compounds, pesticides, and trace metals [3]. Timely information on total suspended matter plays an important role in assessing the effects of a wide range of issues caused by poor water quality. In order to study changes in the sediment-related environment, such as alterations of river morphology, degradation of water quality, or negative influences on aquatic ecology, it is indispensable to accurately supervise the transport and discharge of suspended matter in rivers [4, 5, 6]. In fact, many rivers in the world have either not been gauged or their sediment data are not readily available. Therefore, estimating the sediment load in turbid systems is an important aspect at the catchment level [7]. Unfortunately, the acquisition of reliable suspended sediment concentration data at the necessary spatial and temporal resolution can often be prohibitively time-consuming and expensive in large rivers.

Several methods have been mentioned to predict suspended sediment concentration, ranging from field measurement, basic sediment rating curves [4, 7, 8, 9, 10], remote sensing [11, 12, 13, 14] to more complex models such as support vector regressions [15, 16], artificial neural networks, regression trees and model trees [17, 18]. In the field measurement method, observations are typically collected using cumbersome in situ samplers deployed along bridges, boats, or cableways for monitoring SSC and local sediment transport in large fluvial systems [19]. The main advantage of on-site sampling is that it can provide accurate measurements of suspended sediments within a given location at a given time. However, this measurement is constrained by severely limited spatial and temporal samplings of suspended sediment due to the high cost and time-consuming methods currently used for in-situ observation, especially in a large area [13]. Furthermore, employing datasets gathered by in situ monitoring devices or stations for local analysis and large-scale sediment quantification can lead to high uncertainties and potential error [20]. The complex models are suitable to the complexity of the sediment dynamics sometimes requires more sophisticated approaches to explain most of the variability in SSC [21].

Alternatively, a remote sensing approach may provide an appreciated tool for quantifying SSC in river systems. As Marrinez et al. (2015) indicated that, remote sensing is an efficient tool for hydrological monitoring in large rivers, because it allows relate the color of the water to its content using satellite [22].

With its advantages, satellite images are used in many studies on the distribution of factors on the surface. Besides using remote sensing imageries for studying the surface temperature distribution [23], many studies have used this technology to predict the SSC distribution. Remote sensing tools can provide the images with a high spatial and temporal resolution to estimate surface suspended sediment concentration in large rivers that are not available from traditional in situ measurements [24, 25]. Over the last several decades, satellite image has been used to retrieve SSC data because it has wide spatial coverage and high temporal repeatability, and various visible and NIR bands have been proposed as the SSC indicators [13]. The sensors have been used to analyze water quality parameters including suspended sediment. Based on the relationship between SSC and spectral reflectance, prediction SSC has been implemented using a range of statistical modeling techniques and satellite data. Therefore, a remote sensing approach has been used to determine the SSC, through models and algorithms showing potential at regional, multi-temporal and synoptic levels. Costs involved in this procedure are considerably lower than those of in situ samplings and laboratory analysis [26].

Previously, models associating SSC and spectral reflectance using different multispectral satellite sensors have been generated by many scientists. They utilized from coarse spatial resolution such as MODIS and MERIS [27, 28] to relatively finer spatial resolution, for example, the Landsat series [29, 30, 31, 32]. There are few studies mentioned on estimating SSC in rivers utilizing MODIS satellite images because of the coarse spatial resolution of the data comparing to the size of the rivers [33]. With the launch of the Landsat 8 Satellite, in 2013, this sensor has a high potential for monitoring the aquatic environment and so the possibilities of studies in hydrology fields have expanded. The Landsat 8 data are already being used to predict turbidity and sediment concentration [34, 35, 36, 37]. Our literature review has revealed that SSC is highly correlated with the first four bands of the Landsat sensors [38] and the use of an appropriate single band from the sensor series can provide an accurate estimate of SSC [39]. Gholizadeh et al. (2016) indicated that sensors from the Landsat satellite series (TM, ETM+, OLI) are the most regularly used remote sensing platforms to predict SSC [40]. Results from previous studies also have proven Landsat 8 as a proper satellite asset for a robust estimation of SSC.

Besides on the main rivers, suspended sediment formed in the fields and canals is mostly fine-grained. This material is capable of providing a good source of nutrients for the ecosystem. The distribution of alluvial particles fluctuates greatly according to the season and different locations in the basin. Furthermore, the monitoring data in a concentration of suspended sediment is often very little, so it is not enough to assess the evolution and change trend of sediment in the basin. Therefore, the interpretation of remote sensing images to estimate the SSC partly meets the demand for SSC data as well as provide the initial scientific basis for the assessment of the SSC in the river basin for developing agricultural and forestry field.

In order to map the SSC, it is necessary to process, analyze, and interpret the satellite image, especially focus on image editing, image interpretation, publishing documents from images. Up to now, the research on the application of remote sensing in predicting the SSC has continued to develop by analyzing images and the measured spectrum or images and field measurements. This study aimed to estimate SSC in downstream of the Ba river basin from the use of Landsat satellite imagery and the obtained results are validated by field documents at different times and locations.

2. Research area

The Ba River is one of the major river systems in the Central Highlands and Central Coast area with a basin natural area of 1,413,204 ha (including the Ban Thach branch). The geographical position of the basin is about 12°55' to 14°38' north latitude and 108°00' to 109°55' east longitude on the northern borders of the Sesan river basin and the Tra Khuc river, the southern borders of the Cai river basin and the Srepok river, and the eastern borders of the basin of Kon river, the Ky Lo river, and the East sea. Ba river basin is located in the area of both Western Truong Son and Eastern Truong Son, accounting for 4.3% of the country's area, belonging to three provinces of Central Highlands, namely Gia Lai, Dak Lak, Phu Yen, and a very small part of Kon Tum [41]. The Ba River has a drainage area of 14x10³ km², and provides 1x10⁶ tons of suspended sedimentary material annually into the East Sea [42].

The downstream area of the Ba river basin has mountain ranges with an elevation of 200 - 500m, covering all three north, west, and south directions. The estuary and coastal areas have elevations ranging from 0.5 to 2 m, with long stretches of sand dunes along the coast. The average rainfall in the basin is about 1730 mm with a flow modulus of 23.6 l/s/km², annually the Ba River flows into the East Sea with more than 10 billion m³ of water. The sediment in the river is generated by the interaction between the water flow

and the basin surface. There are many factors affecting SSC in the river such as the slope of the basin, runoff, topography, buffer surface, etc. But the flow factor has the greatest influence on the amount of sediment in the river [41].

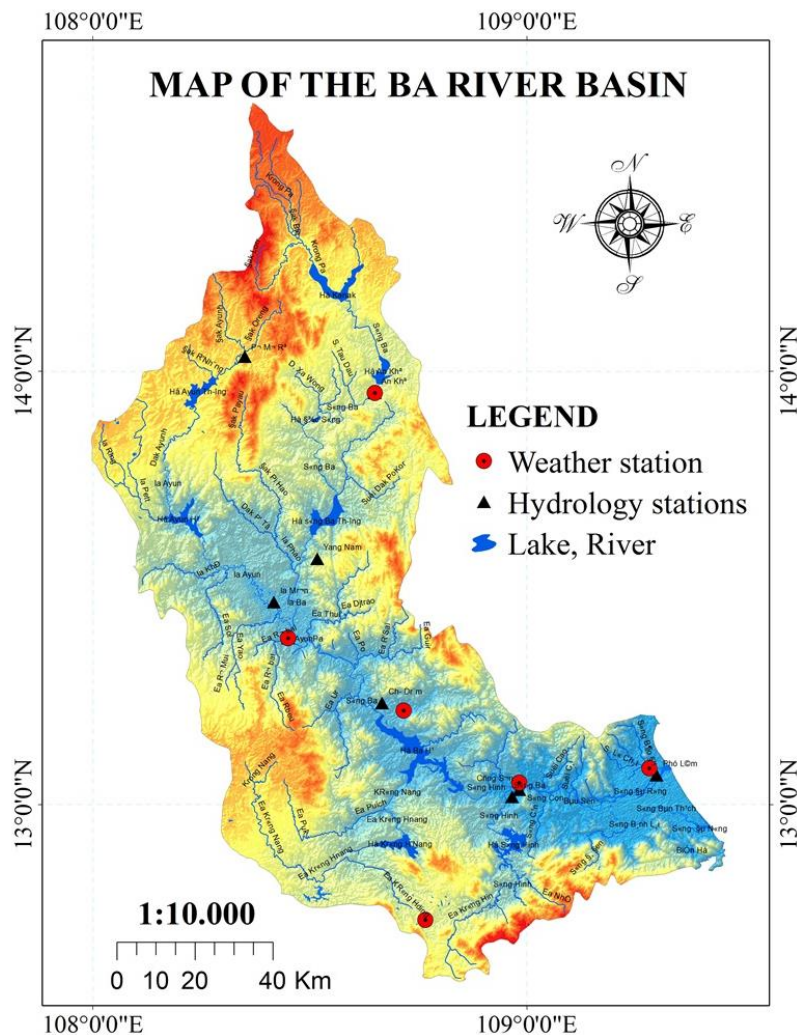


Fig. 1. Ba river basin.

3. Methodology and Data

The Landsat 8 images have been analyzed in the present study due to its wide range of spatial and temporal data available for the Ba river basin, and it has an acceptable spatial resolution of 30 m x 30 m for mapping large rivers. Data obtained from all four Landsat satellites were used to study the Ba river basin including both Landsat 4 and Landsat 5 Thematic Mapper (TM), Landsat 7 Enhanced Mapper Plus (ETM+), and Landsat 8 Operational Land Imager (OLI), for the upstream and midstream area with Path = 123, Row = 50, downstream area with Path = 123, Row = 51. Imagery with adequate meteorological conditions was searched from various dates with no clouds present (0% of clouds). Each satellite crosses every point on Earth once every 16 days with 8 days offset data acquisition, while two Landsat satellites were in operation [43] (Sutari et al., 2020). Landsat Level-1 surface-reflectance data products were downloaded from the <http://glovis.usgs.gov/> website from 1991 to 2016 for the study area to create the Landsat database. All scenes were projected into UTM Zone 49/WGS 84 and radiometrically and geometrically corrected to account for differences in sun and sensor angles as well as atmospheric conditions.

Atmospheric corrections: The purpose of atmospheric correction is to determine true surface reflectance values by removing atmospheric influences from satellite images. The atmospheric conditions influence the radiometric response of the acquired images [44]. These impacts can be eliminated by Radiometric and atmospheric corrections and converted digital levels in physical and biophysical variables. In the present study, photographs were adjusted using physical models of radiative transference, usually based on a series

of standard atmospheres [45]. There are many methods to correct atmospheric effects with Landsat-8 images such as using commercial software such as FLAASH of Envi, ATCOR of ERDAS or ACOR, 6S, etc. In this study, ACOLITE tool was used to adjust atmospheric effects. This tool a very popular applied to the studies of the aquatic environment.

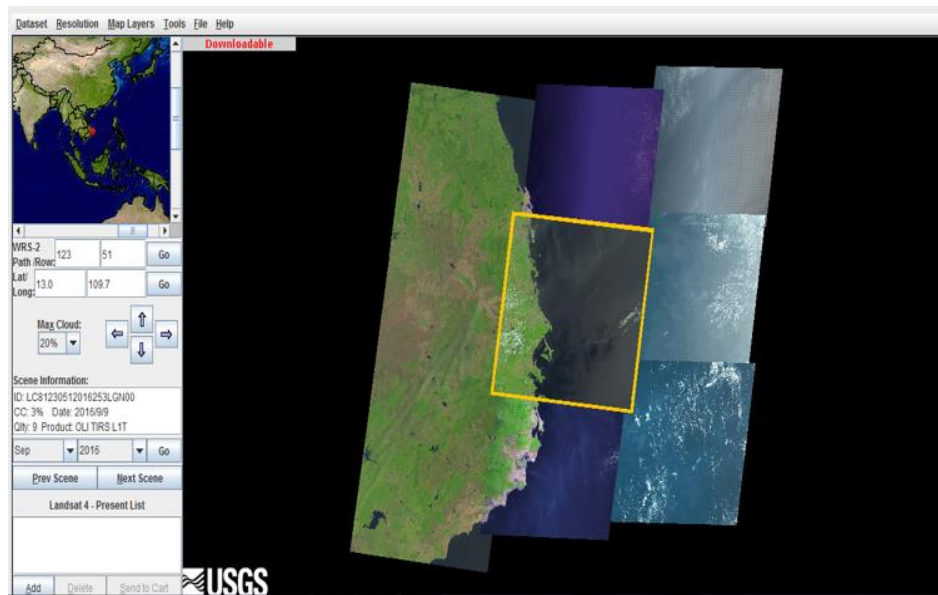


Fig. 2. Landsat satellite data of downstream of the Ba river basin.

Image processing: After the atmospheric and radiometric corrections, the image was cut according to the study area. The salt and pepper error was adjusted by applying a media filter with a 3×3 kernel. The Normalized Difference Vegetation Index (NDVI) is employed to reach the goal of isolating water and non-water features. This index was used to separate the reflectance of the green portion of vegetation from any other surface. However, it was proven useful to detect water surfaces [46]

Features related to water resources that can be collected on remote sensing image data include the length of rivers and streams, the width of riverbeds, catchment slope, branching coefficient, meandering coefficient, the roughness of the buffer surface, the speed of the flow, etc. The relationship between them is expressed by the following equation [47]:

$$V = \frac{R^{2/3} S^{1/2}}{n}; R = \frac{A}{P} \tag{1}$$

where:

A- Cross-sectional area of rivers and streams (m^2); P - Wetted perimeter (m); S – The slope of energy grade line; n – The coefficient of the roughness of the buffer surface. V - Average flow rate (m/s); In the real case, the speed V can be calculated based on the analysis of sample images with moving objects in the image.

In addition, it is necessary to determine the spectral coefficient for the Landsat image with bands 5, 6, 7 to calculate the amount of solid flow for a basin according to the following formula [48,49]:

$$X = \frac{N_4}{\sum_{i=1-4}^6 N_i}; Y = \frac{N_5}{\sum_{i=1-4}^6 N_i} \tag{2}$$

where:

N_i is the radiation coefficient on the i -th band; X and Y are values on the colormap axes, and $X' = X + \Delta X$, $Y' = Y + \Delta Y$; ΔX and ΔY are correction factors due to the atmosphere in each region on the colormap.

The amount of sediment for each basin is determined by the following formula [48,49]:

$$S_{YI} = EA * V * D * 100 / A \tag{3}$$

where

EA: Erosion coefficient of the basin; A: Basin area; V: Flow rate; D: The distribution ratio of the river
The total amount of turbidity can be determined by the following formula [48,49]:

$$T_{ss} = a + b(Z_6)^{1/2} + C(Z_7)^2 + d(Z_5)^{1/3} \tag{4}$$

where:

T_{ss} : Total Turbidity (mg/l)

$Z_5 = X_5 / 2.8132$; $Z_6 = X_6 / 2.7002$; $Z_7 = (X_7 - 0.5524) / 0.4265$

X_5 : Average value on band 5; X_6 : Average over band 6; X_7 : Average over band 7

$a = 399.850$; $b = 135.787$; $c = -0.0115$ and $d = 321.630$ (empirical coefficient)

4. Results and Validation

The study uses Landsat 8 image data to analyze the sediment flow for the Ba River downstream area with the boundary of the downstream area calculated from behind Ba Ha reservoir towards the estuary. Figure 3 shows the study area (downstream of the Ba River) on a DEM map with a resolution of 30x30 m including a river network system and hydro-meteorological stations in the basin. Color composite used in this paper are band 6, band 5, band 2 as red, green, blue from Landsat 8 imagery data. A natural color map is obtained that reflects the current state of the Ba River's buffer surface, in which the green color represents the vegetation cover, the red color represents the soil layer and blue color represents water areas such as rivers, streams, reservoirs, hydroelectric dams, lagoons, etc. (Fig. 4).

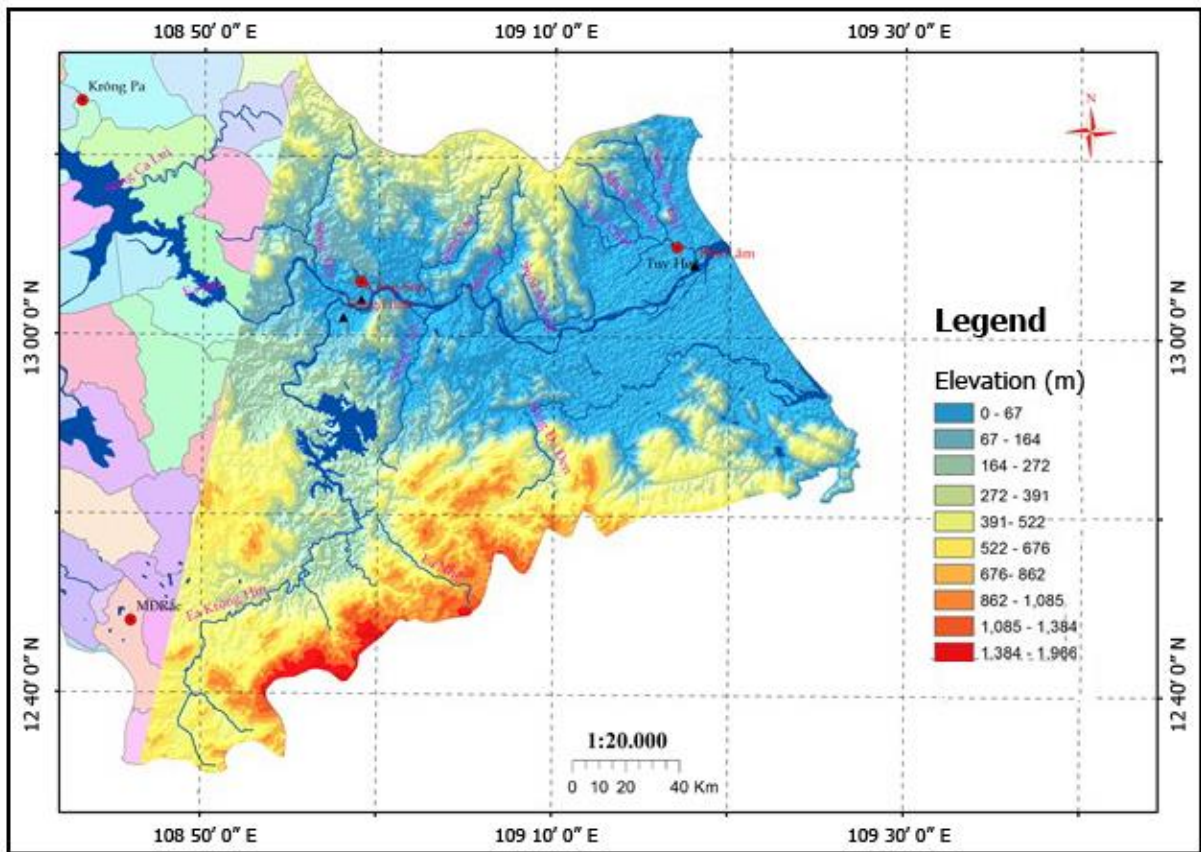


Fig. 3. Downstream of the Ba River basin on a DEM map .

Using Image Analysis, Classification tools, and sediment survey data at some locations in the Ba River downstream, remote sensing image interpretation and obtained results were shown in Figures 5 and 6. From Figure 6, it can be seen that the SSC in downstream of the Ba river is quite evenly distributed, areas with large SSC are mainly concentrated in rivers and lakes and fluctuate in the range of 10 mg/L - 15 mg/L. The area spread throughout the basin has SSC ranging from 2 mg/L to 5 mg/L (76% of the downstream area). Thus, downstream area of the Ba river, the potential for SSC is low compared to other basins in our country.

The study uses data from the Cung Son hydrological station (about 12 km downstream from Ba Ha lake and 45 km from the Da Dien estuary) to verify the estimated results. According to the South Central regional hydrometeorological center, measurement data at Cung Son station on the main Ba river, the average amount of the SSC in many years varies from 70 - 180 g/m³. The maximum amount of sediment can reach 1730 g/m³, while the lowest SSC is in the dry season months and usually below 50g/m³, even some days this

value is only 0 g/m^3 . The obtained results show that the sediment concentration in the area of Cung Son station is estimated in the range of 10-15 mg/L, much smaller than the actual measured average SSC value of many years. The reason is that the data used to estimate the SSC in the study area is collected in the dry season when the flow in the river is small and the amount of sediment transported is also much smaller.

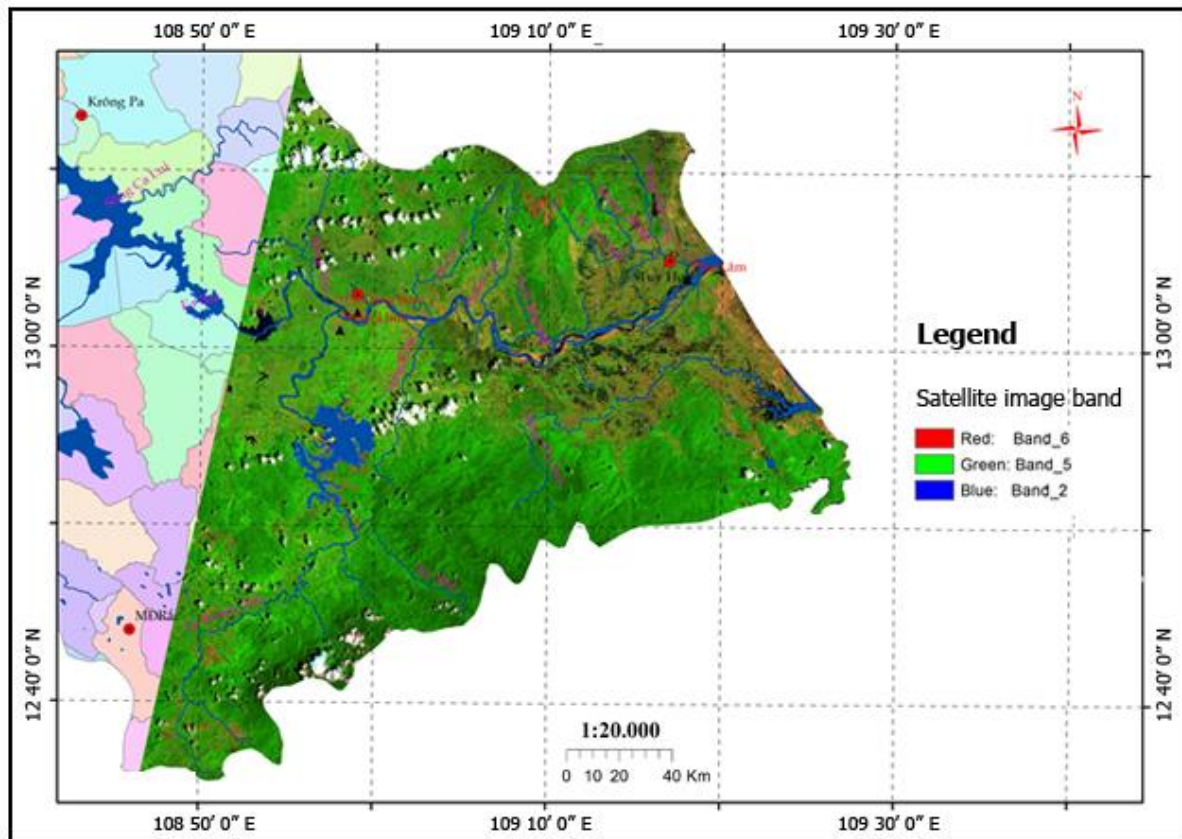


Fig. 4. Current map of buffer surface in the Ba river basin.

In addition, the remote sensing image data for this study were taken at the time after the operation of Ba Ha reservoir. Research results of Giang et al. (2017) shows that the Ba Ha reservoir has a significant impact on the SSC in the Ba river basin [50]. In particular, when considering the total amount of sediment for the whole year at Cung Son hydrological station, we can clearly see the shortage of sediment in the period after Ba Ha reservoir is operational. Therefore, with the SSC in Cung Son station of 10-15 mg/L, it is consistent with the law of sediment change of the downstream under the impact of the reservoir. It is very difficult to determine SSC because the alluvium of the study area has fine particles and precipitates, so this result can be used for calibration service of sediment transport models. Thus, obtained results are objective and can be acceptable. This proves that the method used in the study is reliable and this allows the usage of image analysis to calculate the SSC in the future. This is a useful data source to supplement data for studies and applications in cases where actual measured data are limited.

Besides the obtained results, using satellite images to estimate SSC has some limitations. Because optical satellites are completely dependent on weather conditions, it is difficult to obtain satellite images with optical cloud conditions corresponding to the time of field sampling for verification. The study area is often cloudy, while clouds are one of the factors that greatly hinder the interpretation of satellite images since it will cover observed objects, create shadows on the objects' surface affecting the quality of interpretation causing difficulty in evaluating the spatial distribution of the SSC.

In addition, the field measurement depends on the satellite transit time, so the survey route must be designed so that the sampling time coincides with the time of the Landsat-8 satellite pass (approximately 10h17) [51]. Besides, according to Nguyen Khac Thoi et al. (2011), light intensity will decrease exponentially with increasing depth when entering the water. Light that is weakened to a certain depth will have no reflection and is completely absorbed in the water. The degree of attenuation is different with wavelengths of electromagnetic radiation, especially in the visible spectral bands, the higher depths, the

worse the reflection [52]. Therefore, this is one of the factors affecting the accuracy as well as the difficulty of image interpretation to estimate SSC for the study area.

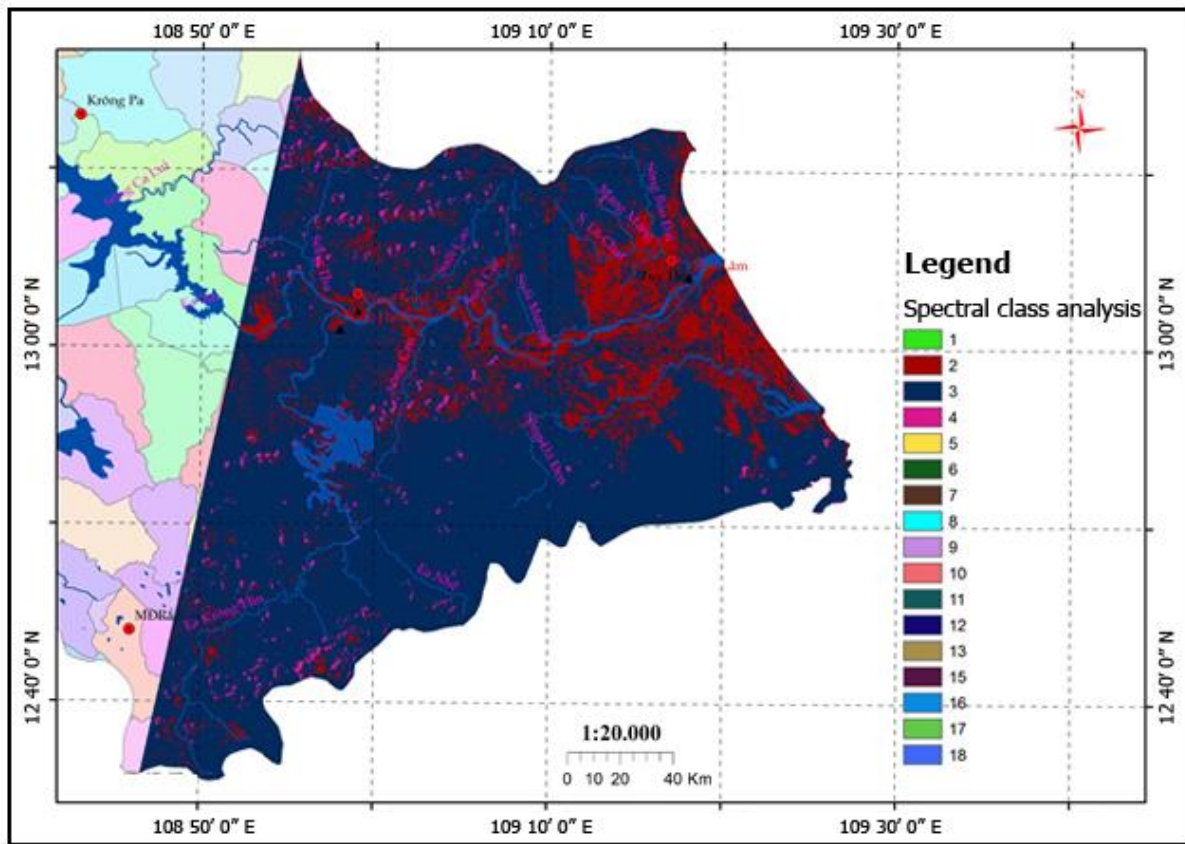


Fig. 5. Spectral analysis from Landsat image of the Ba river basin.

5. Conclusion

The results of this investigation show that it is feasible to use Landsat image data for quantifying, assessing, and mapping suspended sediment concentration of an Ba river basin. Moreover, the researches show that the Landsat 8- derived green-red band ratio is minimally susceptible to uncertainties in the atmospheric correction allowing for its utility for river water management. Map of SSC distribution in the Ba river basin revealed that the SSC is highly related to the seasonal variation and the area with high SSC is mainly concentrated in the lake and river. The results of SSC estimation for the whole study area accurately reflect the trend of SSC fluctuations over time in the year compared to the measured data as well as consistent with the influence of river hydrodynamic factors in the study area.

Through careful analysis and interpretation of satellite images, it is shown that we can study suspended sediment changes by approaches using remote sensing image data. Nowadays there are many websites that provide free quality satellite images with a resolution of about 30 m. Therefore, it is necessary to focus in this research direction to obtain a SSC database in space and time, ensuring a scientific basis for the assessment and analysis of the impact of the upstream dam, the impact of the internal area of the embankment system, etc. on the SSC in the basin. The combination of satellite image interpretation and hydrological measurement data allows us to calculate the amount of the SSC and sediment spilled into the field. The research results can be used to develop a plan for the transmission of sediment to clean the fields and support the development of agriculture more effectively.

Due to the limitation of actual measured data at different locations, it is necessary to collect more measured data at different locations to increase accuracy. In addition, it is necessary to use a combination of satellite images with different spatial and temporal resolution levels to support better assessment of the SSC distribution as well as limit the influence of clouds on the research results

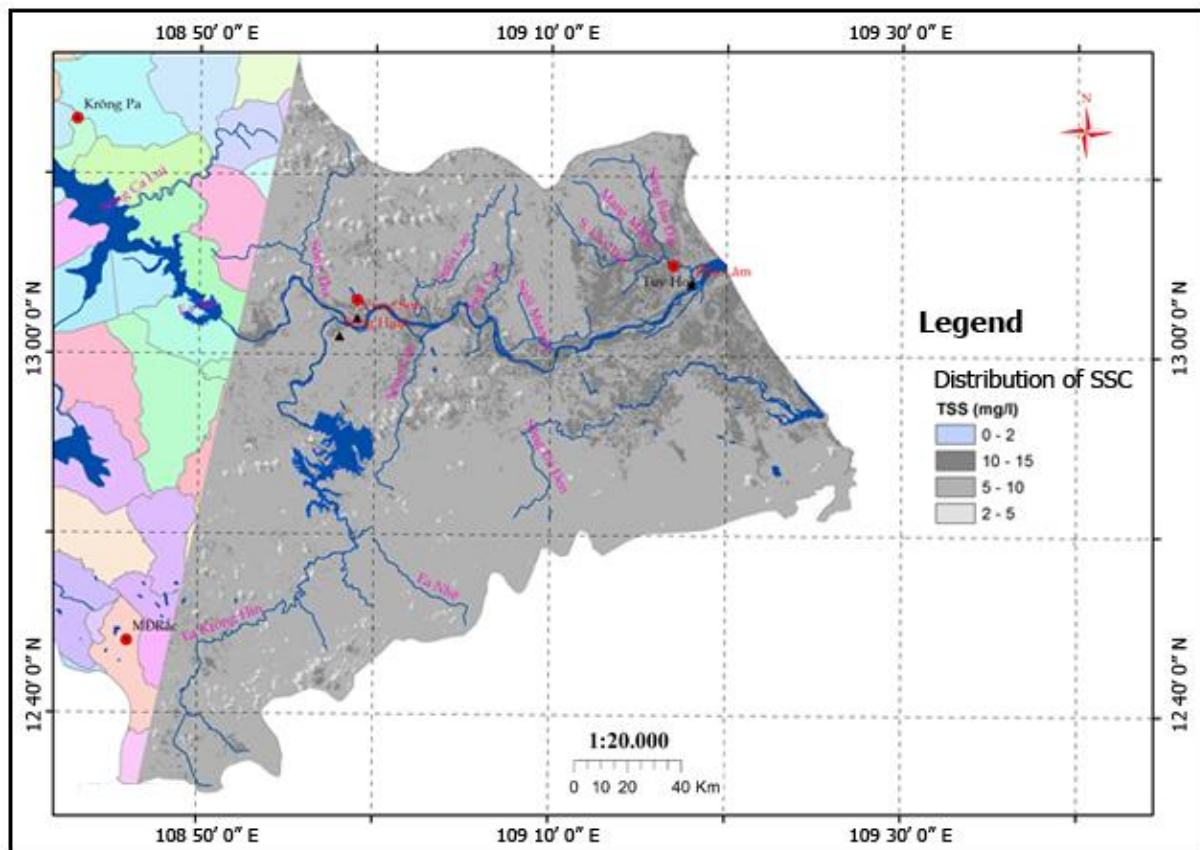


Fig. 6. Distribution of SSC in the Ba river basin from Landsat image.

6. Acknowledgements

The authors are grateful to South Central regional hydrometeorological center, Vietnam for providing data to complete this paper. In addition, the author thanks unnamed reviewers for their valuable comments which helped us to improve the quality of the manuscript.

The paper was presented during the 6th VIET - POL International Conference on Scientific-Research Cooperation between Vietnam and Poland, 10-14.11.2021, HUMG, Hanoi, Vietnam.

7. References

1. Meade, R.H., Yuzyk, T.T., Day, T.J.,1990. Movement and storage of sediment in rivers of the United State and Canada. In: M.G. Wolman and H.C. Riggs, eds. *The geology of North American, surface water hydrology*. Co: Geological Society of American, 1: 255-280.
2. Knighton, A.D., 1998. *Fluvial forms and processes: a new perspective*. London, UK: Arnold, 383p
3. Markert, K.N., Schmidt, A.M., Griffin, R.E., Flores, A.I., Poortinga A.; Saah D.S.; Muench R.E.; Clinton N.E.; Chishtie F.; Kityuttachai K.; Someth P.; Anderson E.R.; Aekakkararungroj A.; Ganz D, 2018. Historical and Operational Monitoring of Surface Sediments in the Lower Mekong Basin Using Landsat and Google Earth Engine Cloud Computing. *Remote sensing*, 10(6).
4. Harrington, S.T., Harrington, J.R., 2013. As assessment of the suspended sediment rating curve approach for load estimation on the Rivers Bandon and Owenabue, Ireland. *Geomorphology* 2013, 185: 27–38.
5. Collins, A.L., Walling, D.E., 2004. Documenting catchment suspended sediment sources: problems, approaches and prospects. *Prog Phys Geogr*, 28: 159–169.
6. Ouillon, S., Douillet, P., Andrefouet, S., 2004. Coupling satellite data with in situ measurements and numerical modeling to study fine suspended-sediment transport: a study for the lagoon of New Caledonia. *Coral Reefs*, 23: 109–122.

7. Zheng, M., 2018. A spatially invariant sediment rating curve and its temporal change following watershed management in the Chinese Loess Plateau. *Sci. Total Environ*, 630: 1453–1463.
8. Asselman, N.E.M., 2000. Fitting and interpretation of sediment rating curves. *Journal of Hydrology*, 234: 228–248, doi:10.1016/S0022-1694(00)00253-5
9. Horowitz, A.J., 2003. An evaluation of sediment rating curves for estimating suspended sediment concentrations for subsequent flux calculations. *Hydrological Processes*, 17: 3387–3409, doi:10.1002/(ISSN)1099-1085
10. Jung, B.M., Femandes, E.H., Mojjer, Jr O.O., Rodrihuez, F.G., 2020. Estimating Suspended Sediment Concentrations from River Discharge Data for Reconstructing Gaps of Information of Long-Term Variability Studies, 12(2382), doi:10.3390/w12092382
11. Hung, N.T., Luan, N.T., Cuong, V.D., Thanh, D.H., Long, V.H., Giang, N.V., 2017. Research and application of remote sensing to determinate the concentration of the suspended sediment in the Hoi estuary, Ma river. *Journal of Water Resources Science and Technology*, 37: 13-25, in Vietnamese
12. Tinh, T.V., Hung, T.D., 2019. Research and application of remote sensing to determinate the concentration of the suspended sediment in the Southern coastal estuary area. *Journal of climatechange science*, 12: 16-23, in Vietnamese.
13. Wang, J.J., Lu, X.X., 2010. Estimation of suspended sediment concentrations using Terra MODIS: An example from the Lower Yangtze River, China. *Science of the Total Environment*, 408: 1131-1138.
14. Peterson, K.T., Sagan, V., Sidike, P., Cox, A.L., Martinez, M., 2018. Suspended Sediment Concentration Estimation from Landsat Imagery along the Lower Missouri and Middle Mississippi Rivers Using an Extreme Learning Machine. *Remote sensing*, 10(10). <https://doi.org/10.3390/rs10101503>
15. Gao, P., 2008. Understanding watershed suspended sediment transport. *Progress in Physical Geography*, 32(3): 243–263. doi:10.1177/0309133308094849
16. Kisi, O., 2012. Modeling discharge-suspended sediment relationship using least square support vector machine. *Journal of Hydrology*, 456-457(110–120), doi:10.1016/j.jhydrol.2012.06.019
17. Bhattacharya, B. and Solomatine, D.P., 2006. Special issue: machine learning in sedimentation modelling. *Neural Networks*, 19: 208–214, doi:10.1016/j.neunet.2006.01.007
18. Shiri, J. and Kişi, Ö., 2012. Estimation of daily suspended sediment load by using wavelet conjunction models. *Journal of Hydrologic Engineering*, 17: 986–1000, doi:10.1061/(ASCE)HE.1943-5584.0000535
19. Edwards, T.K., Glysson, G.D., 2018. Field Methods for Measurement of Fluvial Sediment. Available online: <https://pubs.er.usgs.gov/publication/ofr86531> (accessed on 17 September 2018).
20. Meade, R.H., 2018. Setting: Geology, Hydrology, Sediments, and Engineering of the Mississippi River. Available online: <https://pubs.usgs.gov/circ/circ1133/geosetting.html> (accessed on 17 September 2018).
21. Proulx, S.O., Hilaire, A.S., Courtenay, S.C., Haralampides, K.A., 2016. Estimation of suspended sediment concentration in the Saint John River using rating curves and a machine learning approach. *Hydrological Sciences Journal*, 61(10), <https://doi.org/10.1080/02626667.2015.1051982>
22. Martinez, J.M., Espinoza-Villar, R., Armijos, E., Silva Moreira, 2015. The optical properties of river and floodplain waters in the Amazon River Basin: Implications of satellite-based measurements of suspended particule matter. *Journal of Geophysical Research. Earth Surface*, 120(7): 1274-1287. <http://dx.doi.org/10.1002/2014JF003404>.
23. Ha, T.T.L., Trung, V.N., Lan, T.P., Le, T.L., Huong, T.D., Long, H.N., 2018. Impact of urbanization on land surface temperature using remote sensing and GIS: A case of Tay Ho district, Hanoi city, Vietnam. *Journal of Mining and Earth Sciences*, 59(6): 66-75.
24. Park, E., Latrubesse, E.M., 2014. Modeling suspended sediment distribution patterns of the Amazon River using MODIS data. *Remote Sens. Environ*, 147: 232–242.
25. Umar, M., Rhoads, B.L., Greenberg, J.A., 2018. Use of multispectral satellite remote sensing to assess mixing of suspended sediment downstream of large river confluences. *J. Hydrol*, 556: 325–338.

26. Nooren, K., Hoek, W.Z., Winkels, T.G., Huizinga, A., van der Plicht, J., Van-Dam, R., Van-Heteren, S., Van-Bergen, M., Prins, M.A., Reimann, T., Wallinga, J., Cohen, K., Minderhoud, P., Middelkoop, H., 2017. The Usumacinta-Grijalva beach-ridge plain in southern Mexico: A high-resolution archive of river discharge and precipitation. *Earth Surface Dynamics*, 5(3): 529-556.
27. Son, S., Wang, M., 2012. Water properties in Chesapeake Bay from MODIS-Aqua measurements. *Remote Sens. Environ*, 123: 163-174.
28. Feng, L., Hu, C., Chen, X., Tian, L., Chen, L., 2012. Human induced turbidity changes in Poyang Lake between 2000 and 2010: Observations from MODIS. *J. Geophys. Res*, 117: 1-19.
29. Montanher, O.C., Novo, E.M.L.M., Barbosa, C.C.F., Renno, C.D., Silva, T.S, 2014. Empirical models for estimating the suspended sediment concentration in Amazonian white water rivers using Landsat 5/TM. *Int. J. Appl. Earth Obs. Geoinf*, 29: 66-77.
30. Pereira, L.S.F., Andes, L.C., Cox, A.L., Ghulam, A., 2018. Measuring suspended-sediment concentration and turbidity in the middle Mississippi and lower Missouri Rivers using Landsat data. *J. Am. Water Resour. Assoc*, 54: 440-450
31. Shahzad, M.I., Meraj, M., Nazeer, M., Zia, I., Inam, A., Mehmood, K., Zafar, H., 2018. Empirical estimation of suspended solids concentration in the Indus Delta Region using Landsat-7 ETM+ imagery. *Journal of Environmental Management*, 209: 254-261. <http://dx.doi.org/10.1016/j.jenvman.2017>
32. Duarte, C.R., Cordeiro, E.F., Araujo da costa, J.H.B., Sabadia, J.A.B., Salgueiro, A.R., Souto, M.V.S., Silva Filho, W.F., 2016. Principal component analysis and morphostructural characterization of a portion of the eastern continental shelf of Ceará, Brazil, using Landsat 5-TM images. *Journal of Sedimentary Environments*, 1(3): 324-333. <http://dx.doi.org/10.12957/jse.2016.25905>.
33. Mangiarotti, S., Martinez, J.M., Bonnet, M.P., Buarque, D.C., Filizola, N., Mazzega, P., 2013. Discharge and suspended sediment flux estimated along the mainstream of the Amazon and the Madeira Rivers (from in situ and MODIS Satellite Data). *Int. J. Appl. Earth Obs. Geoinf*, 21: 341-355.
34. Wu, G., Cui, L., Liu, L., Chen, F., Fei, T., Liu, Y., 2015. Statistical model development and estimation of suspended particulate matter concentrations with Landsat 8 OLI images of Dongting Lake, China. *Int. J. Remote Sens*, 36: 343-360.
35. Market, K.N., Schimt, C.M., Griffin, R.E., Flores, A.I., Poortinga, A., Saah, D.S., Muench, R.E., Clinton, N.E., Chishtie, F., Kityuttachai, K., Someth, P., Anderson, E.R., Aekkapol Aekakkararungroj, A., Ganz, D.J., 2018. Historical and operational monitoring of surface sediments in the lower mekong basin using landsat and Google Earth engine cloud computing. *Remote Sensing*, 10(909). <http://dx.doi.org/10.3390/rs10060909>.
36. Manzo, C., Braga, F., Zaggia, L., Brando, V.E., Giardino, C., Bresciani, M., Bassani, C., 2018. Spatio-temporal analysis of prodelta dynamics by means of new satellite generation: the case of Po river by Landsat-8 data. *Int J Appl Earth Obs Geoinformation*, 66: 210-225. <http://dx.doi.org/10.1016/j.jag.2017.11.012>.
37. Ko, N.T., Rutten, M., Conallin, J., 2017. Remote Sensing Analysis of Temperature and Suspended Sediment Concentration in Ayeyarwady River in Myanmar. *Global Journal of Engineering and Technology Review*, 2(3): 30-47.
38. Brezonik, P., Menken, K.D., Bauer, M., 2005. Landsat-based remote sensing of lake water quality characteristics, including chlorophyll and colored dissolved organic matter (CDOM). *Lake Reserv. Manag*, 21: 373-382.
39. Overeem, I., Hudson, B.D., Syvitski, J.P.M., Mikkelsen, A.B., Hasholt, B., van den Broeke, M.R., Noël, B.P.Y., Morlighem, M., 2017. Substantial export of suspended sediment to the global oceans from glacial erosion in Greenland. *Nat. Geosci*, 10(859).

40. Gholizadeh, M.H., Melesse, A.M., Reddi, L.A., 2016. Comprehensive Review on Water Quality Parameters Estimation Using Remote Sensing Techniques. *Sensors*, 16(1298).
41. Dung, N.B., 2017. Research on application of geomatics technology to improve the quality of space data for the investigation and planning of water resources. Ministry-level scientific research project. In Vietnamese.
42. Sang, N.P., Dung, T.N., Hung, T.K., Hien, T.T.P., Toan, T.T., Chinh, C.T.V, 2020. The degree of chemical weathering in the Ba River basin, South Central Vietnam: Major-element geochemistry investigations of modern river sediments and sedimentary rocks, *Journal of Mining and Earth Sciences*, 61(1): 82-91, DOI: 10.46326/JMES.2020.61(1).09
43. Sutari, C.A.T., Van der Perk M., Middelkoop, H., 2020. Estimation of suspended sediment concentrations in the Rhine River using Landsat Satellite Images. *IOP Conf. Series: Earth and Environmental Science*, 451. doi:10.1088/1755-1315/451/1/012079
44. Richards, A.J., 2013. *Remote Sensing Digital Image Analysis (5th Ed.)*. Springer, Berlin.
45. Hhernández-cruz, B., Vásquez-ortiz, M., Canet, C., Prado-molina, J., 2019. Algorithm to calculate suspended sediment concentration using Landsat 8 imagery. *Applied Ecology and Environmental Research*, 17(3): 6549-6562, http://dx.doi.org/10.15666/aeer/1703_65496562
46. Rokni, K., Ahmad, A., Selamat, A., Hazini, S., 2014. Water feature extraction and change detection using multitemporal imagery. – *Remote Sensing*, 6(5): 4173-4189.
47. Cherrymar, R.A., Ricardo, I.R., 2008. Assessment Monitoring of Suspended Sediment of Alpine Glaciers, using Remote Sensing Techniques. Department of Geology, University of Puerto Rico.
48. Shafaie, M., Ghodosi, H., Mostofi, K.H., 2015. River sediment monitoring using remote sensing and GIS. Department of Civil Engineering, Faculty of Engineering, University of Shahid Chamran, The International Archives of the Photogrammetry, Remote Sensing and Spatial Information Sciences, Volume XL-1/W5, 2015, International Conference on Sensors & Models in Remote Sensing & Photogrammetry, Kish Island, Iran, 675-680, DOI: 10.5194/isprsarchives-XL-1-W5-675-2015
49. Minwei Zhang, QingDong, Tingwei Cui, CunjinXue, SongliZhang (2014). Suspended sediment monitoring and assessment for Yellow River estuary from Landsat TM and ETM+ imagery. Institute of Remote Sensing and Digital Earth, Chinese Academy of Sciences, Beijing, China, 146: 136-147, DOI: 10.1016/j.rse.2013.09.033
50. Giang, N.T., Thao, H.T., Vinh, T.N., Binh, P.D.H., Quan, V.D., 2017. Study on Sediment Regime Changes in Downstream of the Ba River, Vietnam under the Impact of Reservoirs System. *VNU Journal of Science: Earth and Environmental Sciences*, 33(4): 127-134.
51. Hung, N.T., Luan, N.T., Cuong, V.D., Thanh, D.H., Long, V.H., Giang, N.V., 2017. Application satellite images to determine the concentration of suspended sediment at Hoi estuary, Ma river. *Journal of Water Resources Science and Technology*, 37: 13-24.
52. Linh, V.T.P., Thanh, V.Q., Hoang, L.V., 2019. Application of Landsat images to estimate suspended sediment concentration in the Hau and Tien rivers. *Can Tho University Journal of Science*, 55: 134-144.

A Numerical Method for the Design of the U-Shaped Segmental Tunnel Lining under the Impact of Earthquakes: A Case Study of a Tunnel in the Hanoi Metro System

NGUYEN Chi Thanh^{1,*}, DO Ngoc Anh¹, PHAM Van Vi¹, GOSPODARIKOV Alexandr²

¹Hanoi University of Mining and Geology, 18 Vien street, Hanoi, Vietnam

²Saint Petersburg Mining University, Saint Petersburg, Russia Federation

Corresponding author: nguyenthanh.xdctn47@gmail.com

Abstract. Circular tunnels are usually encountered when excavation tunnel. However, the U-shaped tunnel lining is used a lot in practice because of its advantages. However, there are not many studies in the world to calculate and design for underground structures with U-shaped tunnel lining, especially in the case of tunnels being affected by earthquakes. This paper proposes a new numerical-HRM method approach for the analysis of U-shaped segmental tunnel lining under the impact of earthquakes. Hanoi is the capital of Vietnam, this is a big city with more than 8 million people. Hanoi is located between two major fault systems, the Red River fault system and the Son La-Dien Bien-Lai Chau fault system. Therefore, the Hanoi area is assessed as likely to be affected by earthquakes of magnitude $M_w = 6.1$ up to 6.5 Richter. The Hanoi metro system is constructed by TBM and the U-shaped segmental tunnel lining is also one of the types of tunnel lining considered for use in the construction of metro tunnels in Hanoi. The improved HRM method has been used to investigate the effect of joints in the tunnel lining from the Hanoi system metro under the impact of earthquakes is conducted considering from the results of the tunnel lining behavior in terms of bending moment (M), normal forces (N) and tunnel lining displacements (δn) in both cases: the U-shaped continuous tunnel lining and the U-shaped segmental tunnel lining.

Keywords: Numerical method, U-Shaped segmental tunnel lining, Impact of earthquakes, Hanoi metro system

1. Introduction

In the construction process and the design for tunnels, the U-shaped tunnel lining is used a lot by its construction ability, usability, and bearing capacity. Some researchers in the world have conducted research and calculations for the U-shaped tunnel lining to serve the needs of using this type of tunnel lining in underground constructions in hydroelectricity, transportation, and infrastructure. Yin and Yang, (2000) together with the topology optimization method [1], Barpi et al., (2011) with a method for the study of the U-shaped tunnel lining based on a fuzzy approach and the bedded-beam-spring model [2], Some other authors with the Hyperstatic Reaction Method (HRM) [3, 4, 5, 6, 7, 8]. In which, the HRM method is a numerical method that is quite focused on developing and used because of its advantages, such as fast calculation results, simple input parameters, ease to use. However, there is still no study using the HRM method to calculate the U-shaped segmental tunnel lining affected by earthquakes.

In fact, could use numerical methods with software such as FLAC^{3D}, Plaxis^{2D}, Abaqus^{2D}, etc. studying and calculating the effect of earthquakes on the U-shaped segmental tunnel lining. However, the use of these software requires a large initial investment, the computer configuration used must be strong enough, the time to build the tunnel model that is affected by the earthquake, and processing research results for quite a long time. The HRM method, one numerical method was developed and used to calculate the U-shaped continuous tunnel lining by Nguyen et al., (2020) [7] which used the following theories: the reaction of soil mass around the tunnel caused by the deformation of the tunnel lining that is a function of the tunnel lining stiffness. This reaction is determined using the geometrical parameters and mechanical characteristics of the tunnel lining. The active loads depend on the displacements in the tunnel lining along with the structure/ground interface.

The ground is linked with the tunnel lining through two types of springs: normal springs and tangent springs. Sections of the segmented lining of the tunnel are linked through joints. These joints work through characteristic stiffnesses, including K_{R0} is rotational stiffnesses, K_A is axial stiffness and radial stiffness K_R .

This paper presents the HRM method and provides some improvements to the methodology so that the method could calculate the U-shape tunnels when the tunnels are affected by earthquakes, in both cases of the U-shaped continuous tunnel lining and the U-shaped segmental tunnel lining.

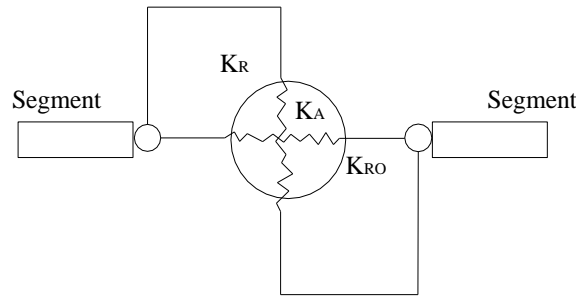


Fig. 1. Joint and properties.

K_{RO} is rotational stiffnesses, K_A is axial stiffness and radial stiffness K_R .

2. Hyperstatic Reaction Method for the U-shaped tunnel lining

The HRM method was proposed and developed by; Oreste, 2007 [3]; Do, 2014 [4, 5, 6]; Du et al., (2020) [9]; Duddeck and Erdmann (1985) [10]; Leca and Clough (1992) [11]. Firstly, the HRM method was used to calculate the circular tunnel. This is a numerical method that is likely to account for the effects of the ground's parameters, these can change under load, and to 2014, Do et al. [4] have used the HRM method in cases of circular tunnels are affected by static load and in case of the circular tunnels are affected to dynamic loads with the tunnel lining is segmental lining.

2.1. The HRM method for the U-shaped continuous tunnel lining

Du et al., (2020) used the HRM method to calculate and design for the U-shaped tunnel lining in case of the continuous tunnel lining and under static load [9]. Nguyen et al., 2020 [7] improved the HRM for use in the design of the U-shaped tunnel lining in the case of that the tunnel is affected by an earthquake and the tunnel lining is continuous.

In the HRM method, the tunnel lining interacts with the ground by springs. There are two types of springs used: tangential springs and normal springs. The tunnel lining in the HRM method is represented by a number of one-dimensional elements. The "i" element in the tunnel has two nodes. The length of each element is the distance between the two bounding nodes of that element, with the parameters of the tunnel element, including the inertia modulus J , area A of the element transversal section, the elastic modulus E , and length are parameters of each element in the tunnel lining [6].

The interaction between ground mass and the tunnel lining could be analysed through springs distributed over the nodes and applied active loads. When the displacement of the nodes in the elements of the tunnel lining under the effect of external load is determined, it is possible to determine the stress occurring inside the elements of the tunnel lining [12]:

$$Z_i * S_i = R_i + G_i \tag{1}$$

where S_i is the vector displacements at node "h" and node "j" of the element "i" (Fig. 5); G_i is the external nodal forces of the element "i"; R_i is the forces at nodal applied by the neighboring elements.

$$\begin{bmatrix} \frac{E.A}{L_i} & 0 & 0 & -\frac{E.A}{L_i} & 0 & 0 \\ \frac{12.E.J}{L_i^3} & \frac{6.E.J}{L_i^2} & 0 & -\frac{12.E.J}{L_i^3} & \frac{6.E.J}{L_i^2} & 0 \\ & \frac{4.E.J}{L_i} & 0 & -\frac{6.E.J}{L_i^2} & \frac{2.E.J}{L_i} & 0 \\ & & \frac{E.A}{L_i} & 0 & 0 & 0 \\ & & & \frac{12.E.J}{L_i^3} & -\frac{6.E.J}{L_i^2} & 0 \\ & & & & \frac{4.E.J}{L_i} & 0 \end{bmatrix} \begin{bmatrix} u_{h,i} \\ v_{h,i} \\ \theta_{h,i} \\ u_{j,i} \\ v_{j,i} \\ \theta_{j,i} \end{bmatrix} = \begin{bmatrix} R_{sh,i} + G_{sh,i} \\ R_{yh,i} + G_{yh,i} \\ R_{\theta h,i} + G_{\theta h,i} \\ R_{sj,i} + G_{sj,i} \\ R_{yj,i} + G_{yj,i} \\ R_{\theta j,i} + G_{\theta j,i} \end{bmatrix} \tag{2}$$

With K is the matrix of the global stiffness, K in the global Cartesian reference system had been setup:

$$Kq=F \tag{3}$$

$$\begin{bmatrix} (k_{n,a}+k_{1,a}) & k_{1,b} & 0 & 0 & 0 & k_{n,c} \\ k_{1,c} & (k_{1,d}+k_{2,a}) & k_{2,b} & 0 & 0 & 0 \\ 0 & k_{2,c} & (k_{2,d}+k_{3,a}) & k_{3,b} & 0 & 0 \\ 0 & 0 & k_{3,c} & (k_{3,d}+k_{4,a}) & \dots & 0 \\ 0 & 0 & 0 & \dots & \dots & k_{n-1,b} \\ k_{n,b} & 0 & 0 & 0 & k_{n-1,c} & (k_{n-1,d}+k_{n,a}) \end{bmatrix} \begin{bmatrix} q_1 \\ q_2 \\ q_3 \\ q_4 \\ \dots \\ q_n \end{bmatrix} = \begin{bmatrix} F_1 \\ F_2 \\ F_3 \\ F_4 \\ \dots \\ F_n \end{bmatrix} \tag{4}$$

The sub-matrices of k_i , each of which has 3×3 dimension with $k_{i,a}$; $k_{i,b}$; $k_{i,c}$, $k_{i,d}$ are the sub-matrices of k_i :

$$k_i = \begin{bmatrix} k_{i,a} & k_{i,b} \\ k_{i,c} & k_{i,d} \end{bmatrix} \tag{5}$$

$q_1, q_2, q_3, \dots, q_n$: the sub-vectors composed of the three displacements of each node in the element of the tunnel lining. $F_1, F_2, F_3, \dots, F_n$: the sub-vectors composed of the three external forces applied to each node of the element.

$$\begin{aligned} K_{3i-2,3i-2}^* &= K_{3i-2,3i-2} + k_{n,i} \cdot \cos^2\left(\frac{\alpha_{i+1}}{2} + \frac{\alpha_i}{2} - \frac{\pi}{2}\right) + k_{s,i} \cdot \sin^2\left(\frac{\alpha_{i+1}}{2} + \frac{\alpha_i}{2} - \frac{\pi}{2}\right) \\ K_{3i-1,3i-1}^* &= K_{3i-1,3i-1} + k_{n,i} \cdot \sin^2\left(\frac{\alpha_{i+1}}{2} + \frac{\alpha_i}{2} - \frac{\pi}{2}\right) + k_{s,i} \cdot \cos^2\left(\frac{\alpha_{i+1}}{2} + \frac{\alpha_i}{2} - \frac{\pi}{2}\right) \\ K_{3i-1,3i-2}^* &= K_{3i-1,3i-2} + (k_{n,i} - k_{s,i}) \cdot \sin\left(\frac{\alpha_{i+1}}{2} + \frac{\alpha_i}{2} - \frac{\pi}{2}\right) \cdot \cos\left(\frac{\alpha_{i+1}}{2} + \frac{\alpha_i}{2} - \frac{\pi}{2}\right) \\ K_{3i-2,3i-1}^* &= K_{3i-2,3i-1} + (k_{n,i} - k_{s,i}) \cdot \sin\left(\frac{\alpha_{i+1}}{2} + \frac{\alpha_i}{2} - \frac{\pi}{2}\right) \cdot \cos\left(\frac{\alpha_{i+1}}{2} + \frac{\alpha_i}{2} - \frac{\pi}{2}\right) \end{aligned} \tag{6}$$

where “ i ” is the number of the generic node; $k_{s,i}$ is the stiffness of the tangential interaction spring connected to node “ i ” of the element; $k_{n,i}$ is the stiffness of the normal interaction spring connected to node “ i ” of the element; α_i and α_{i+1} are the angle between the local systems and global reference systems, for element i and for element $(i + 1)$ in the tunnel lining.

By two ways: through the active loads that have an effect on the tunnel lining and through the normal springs and tangential springs over the nodes of the tunnel lining. The interaction between the tunnel lining with the ground was setup.

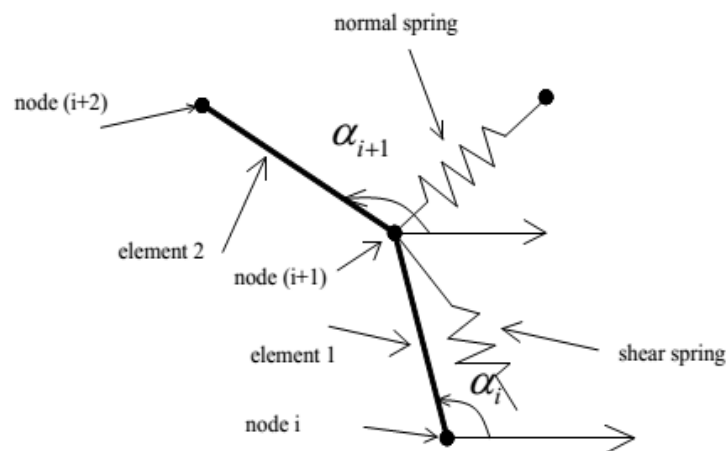


Fig. 2. The tunnel lining-soil surrounding interaction through the Winkler springs linked to support nodes of the tunnel lining.

The equation about the relationship between the deformation of the tunnel lining and the reaction pressure was given [3]:

$$p = p_{lim} * \left(1 - \frac{p_{lim}}{p_{lim} + \eta_0 \delta}\right) \tag{7}$$

where p is reaction pressure (MPa), p_{lim} is the maximum reaction pressure of ground (MPa), η_0 is the initial stiffness of the ground (N/m³), δ is deformation of the tunnel lining (m).

The relationship between the initial normal stiffness ground and tangential stiffness ground had determined by the equation [13, 14]:

$$\eta_{n,0} = \beta \frac{1}{1 + \nu} * \frac{E}{R} \tag{8}$$

$$\eta_s = \frac{1}{3} \eta_n \tag{9}$$

where E is Young’s modulus of the ground (MPa); ν is Poisson’s ratio of the ground; R is the tunnel radius (m); β is the dimensionless factor, β could be known as a function depending on factors such as: the grounds elastic modulus, the elastic modulus of the tunnel lining, the thickness of the tunnel lining. In this study, $\beta=2$; η_s is the tangential stiffness of the ground.

$$p_{n,lim} = \frac{2c * \cos \omega}{1 - \sin \omega} + \frac{1 + \sin \omega}{1 - \sin \omega} * \Delta\sigma_{conf} \tag{10}$$

$$\Delta\sigma_{conf} = \frac{\sigma_h + \sigma_v}{2} * \frac{\nu_s}{1 - \nu_s} \tag{11}$$

The maximum shear reaction pressure was determined:

$$p_{s,lim} = \frac{\sigma_h + \sigma_v}{2} * tg \omega \tag{12}$$

$$\sigma_h = K_o * \sigma_v \tag{13}$$

$$k_{n,i} = \frac{p_{n,lim}}{\delta_{n,i}} * \left(1 - \frac{p_{n,lim}}{p_{n,lim} + \eta_{n,0} * \delta_{n,i}}\right) * \frac{(L_{i-1} + L_i)}{2} \tag{14}$$

$$k_{s,i} = \frac{p_{s,lim}}{\delta_{s,i}} * \left(1 - \frac{p_{s,lim}}{p_{s,lim} + \eta_{s,0} * \delta_{s,i}}\right) * \frac{(L_{i-1} + L_i)}{2} \tag{15}$$

$$\tau = \gamma_c * G \tag{16}$$

where G is the shear modulus of the ground (MPa); τ is shear stress (MPa) and γ_c is shear strain (%); σ_v and σ_h are the respectively vertical and horizontal loads effect to the tunnel lining (MPa); K_o is the lateral earth pressure coefficient; $k_{n,i}$ and $k_{s,i}$ are the stiffnesses of each spring in the ground interaction with the tunnel lining [15-19].

The HRM method has been improved [7] when using the HRM method to calculate and design for the U-tunnel, the continuous tunnel lining and effected by earthquakes. The cross-section of the U-tunnel is now divided into five regions. Each region is determined by the centre corners of the cross-section tunnel as shown in Figure 3, when dividing the tunnel lining into 360 elements, each element that has been determined by a corresponding angle $\phi=1$ degree at the point centre of the cross-section tunnel. According to Nguyen et al., (2020) [7], the length of each element of the tunnel lining will be changed according to the respective angle ϕ , that had been made by the vertical line and the location of the element on the tunnel lining, rotate counter-clockwise.

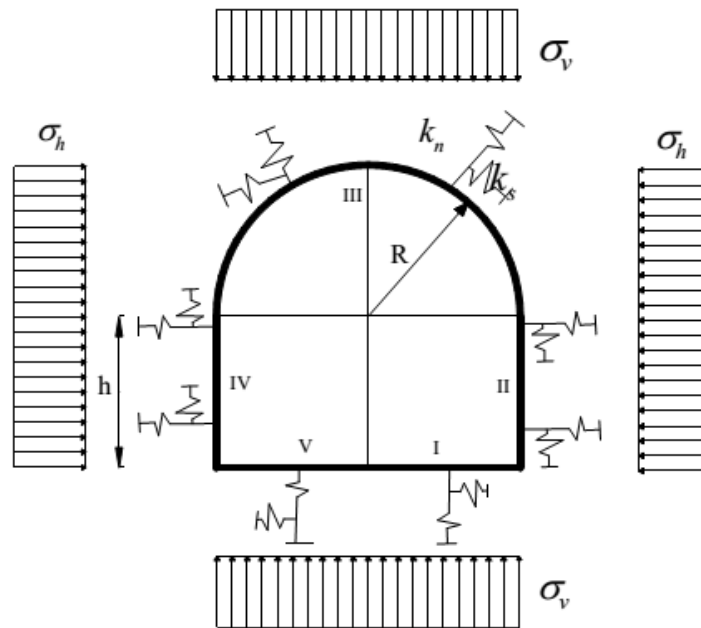


Fig. 3. Calculation diagram of tunnel lining with the HRM method in case the U-shaped tunnel lining σ_v -vertical load in the model tunnel–surrounding soil; σ_h -horizontal load in the model tunnel–surrounding soil; k_n -normal stiffness of the interaction springs; k_s -tangential stiffness of the interaction springs; R -tunnel radius; EJ and EA -bending and normal stiffness of the tunnel lining.

In the region I, the length of elements, when $0^\circ \leq \varphi \leq \arctan\left(\frac{R}{h}\right) - 1$:

$$L_1 = h * \left[\tan\left(\frac{3.1415 * \varphi}{180} + \varphi\right) - \tan\left(\frac{3.1415 * \varphi}{180}\right) \right] \quad (17)$$

In the region II, the length of elements in the region II, $\arctan\left(\frac{R}{h}\right) \leq \varphi \leq 90^\circ$:

$$L_2 = R * \left[\tan\left(\frac{3.1415 * (90 - \varphi)}{180}\right) - \tan\left(\frac{3.1415 * (90 - \varphi)}{180} - \varphi\right) \right] \quad (18)$$

In the region III, the length of elements in the region III, when $90^\circ \leq \varphi \leq 269^\circ$:

$$L_3 = 2 * R * \sin\left(\frac{\varphi}{2}\right) \quad (19)$$

In the region IV, the length of elements in the region IV is determined by the equation, when $270^\circ \leq \varphi \leq 270^\circ + \arctan\left(\frac{h}{R}\right)$:

$$L_4 = R * \left[\tan\left(\frac{3.1415 * (\varphi - 270)}{180} + \varphi\right) - \tan\left(\frac{3.1415 * (\varphi - 270)}{180}\right) \right] \quad (20)$$

In the region V, $270^\circ + \arctan\left(\frac{h}{R}\right) \leq \varphi \leq 359^\circ$, the length of elements:

$$L_5 = h * \left[\tan\left(\frac{3.1415 * (360 - \varphi)}{180}\right) - \tan\left(\frac{3.1415 * (360 - \varphi)}{180} - \varphi\right) \right] \quad (21)$$

where R is the radius of the dome; h is the length of the column of the tunnel.

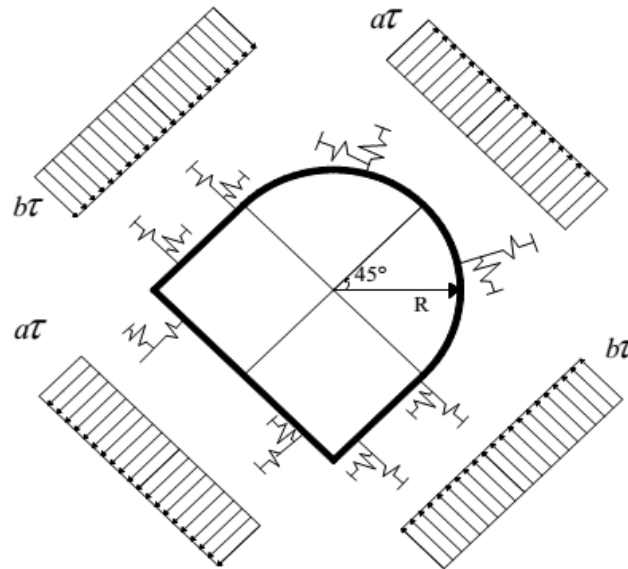


Fig. 4. The external load applied to the tunnel under the effect of earthquakes in the HRM method in case the U-shaped tunnel.

In case the tunnel is affected by an earthquake, as in case the static load diagram on the tunnel lining but the horizontal load components are in opposite direction, the external loads have the impact to tunnel lining are rotated counter-clockwise 45° . Parameters in the equations for determining the diagram of the load acting on the tunnel under the impact of an earthquake are: The parameter “ b ” = 5, the parameter “ a ” depends on the tunnel radius R -the circular tunnel cross-section has the equivalent area than the area of the U-shaped tunnel cross-section and can be defined using the following the equation [7]:

$$a = -0.7\ln(R) + 0.885 \tag{22}$$

2.2 The HRM method for the U-shaped segmental tunnel lining

In this paper, the author used the formulas to calculate the fixity factor of joints in the segmental tunnel lining r_j (which is used extensively in semi-rigid frame analysis and determined at each link node of the tunnel lining element), which could describe the working of the segmental tunnel lining [4] to improve the HRM method in case of the HRM method has been used to calculate the U-shaped segmental tunnel lining under the impact of an earthquake.

$$r_j = \frac{1}{1 + \frac{3E_s J_s}{K_{RO} L_i}} \tag{23}$$

The joints can work between two cases: joints are a pinned link with fixity factor $r_j=0$ and a fully rigid connection is unity with the fixity factor $r_j=1$. The joints are considered semi-rigid links with a fixity factor of between zero and unity ($0 < r_j < 1$).

Working of joints in the segmental tunnel lining is shown in the equation:

$$K_i^{SR} = z_i * C_i \tag{24}$$

$$C_i = \begin{bmatrix} 1 & 0 & 0 & 0 & 0 & 0 \\ 0 & \frac{4r_2 - 2r_1 + r_1r_2}{4 - r_1r_2} & \frac{-2L_i r_1(1 - r_2)}{4 - r_1r_2} & 0 & 0 & 0 \\ 0 & \frac{6(r_1 - r_2)}{L_i(4 - r_1r_2)} & \frac{3r_1(2 - r_2)}{4 - r_1r_2} & 0 & 0 & 0 \\ 0 & 0 & 0 & 1 & 0 & 0 \\ 0 & 0 & 0 & 0 & \frac{4r_1 - 2r_2 + r_1r_2}{4 - r_1r_2} & \frac{2L_i r_2(1 - r_1)}{4 - r_1r_2} \\ 0 & 0 & 0 & 0 & \frac{6(r_1 - r_2)}{L_i(4 - r_1r_2)} & \frac{3r_2(2 - r_1)}{4 - r_1r_2} \end{bmatrix} \quad (25)$$

where K_i^{SR} is the stiffness matrix of member “i”; L_i is the length of the element “i”; C_i is the stiffness matrix of the element “i” was represented by a semi-rigid correction matrix; rotational stiffness modulus at two ends of the element K_{R01} and K_{R02} .

It should be noted that, in the calculation of the U-shaped segmental tunnel lining, due to the change in the length of the elements of the tunnel lining, the fixity factor of joints in the tunnel lining is also changed.

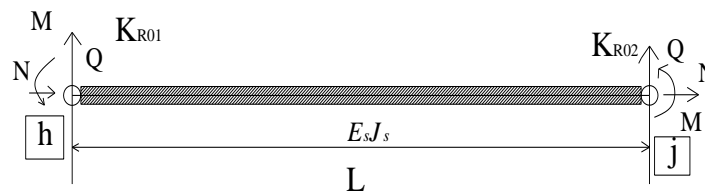


Fig. 5. The beam-type finite element in the tunnel lining with reference to the local Cartesian coordinates.

3. A case study: calculation for the tunnel lining from Hanoi metro system

3.1 Characteristics of earthquakes, soil and tunnel in Hanoi metro system

The hydrogeological and geological conditions of the Hanoi center are as follows in Table 1. In the Hanoi center, the groundwater level is three meters below the surface.

Tab. 1. The properties of the ground in Hanoi center [7, 17].

Number of soil layers	Elastic module of soil, E , MPa	Poisson's ratio of soil, μ	Thickness of soil layer (d), m	Measured SPT blow count, N	Density of the soil, ρ , g/cm ³
1	9.25	0.41	4.6	2	1.75
2	7.68	0.38	1.1	1	1.76
3	15.3	0.35	11.8	3	1.81
4	35.02	0.33	12.5	7	1.78
5	53.9	0.32	11.0	10	1.83
6	65	0.3	7.0	12	1.86

The parameters of the tunnel in the Hanoi metro system are shown in Table 2: the tunnel has a depth of between 15 and 20 m below the ground surface. The U-shaped tunnel with the size is shown in Figure 7, the radius of the dome R with the length of the column-wall h , $R=h=2.95$ m. The tunnel lining is reinforced concrete with properties in Table 2. In the case of the segmental tunnel lining with joints. Arrange 6 joints

at the positions at the reference angle is 0° , 60° , 120° , 180° , 240° , 300° (the reference angle is 0 degrees to the horizontal).

The strongest earthquakes that can occur in the Hanoi center have properties [7, 20]: highest magnitude $M_w=6.5$ Richter; distance from the epicenter of the earthquake to Hanoi is 20 km to 50 km and peak ground acceleration $a_{max} = 0.2g$. In this method, using data of El Centro earthquake (Fig. 7).

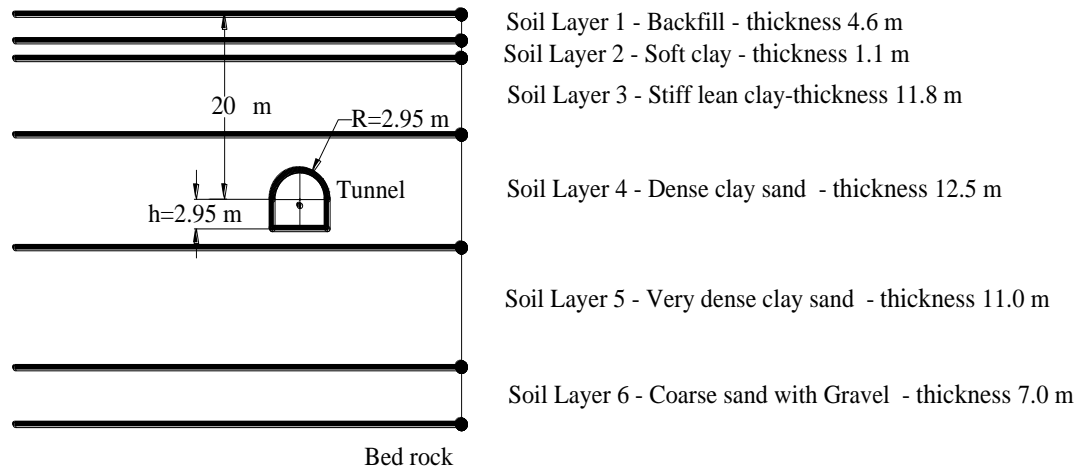


Fig. 6. Parameters of ground and tunnel.

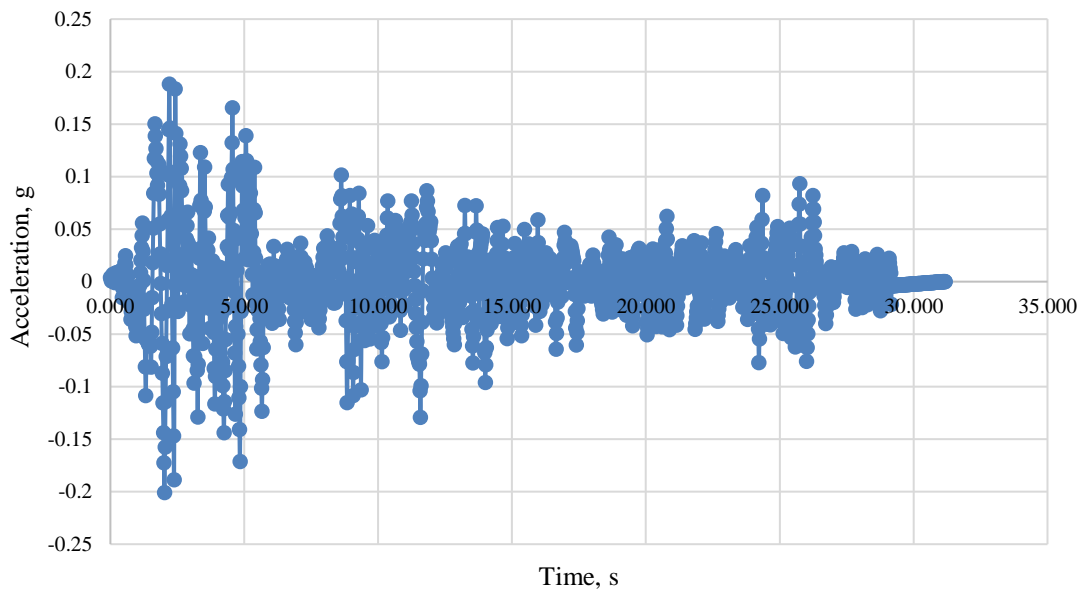


Fig. 7. Data of El Centro earthquake [21, 22, 23, 24, 25].

Tab. 2. The parameters of the tunnel lining [7].

Young's modulus E_l	MPa	35500
Poisson's ratio ν_l	-	0.15
Lining thickness t	m	0.35
Overburden H	m	20
The radius of the dome R	m	2.95
The length of the column-wall h	m	2.95

3.2 Results and Discussions

In the case of the continuous tunnel lining, the finite element method Abaqus^{2D} (FEM) and the HRM method are used to calculate for the tunnel from Hanoi metro system in Hanoi central. In HRM method and FEM, there is no influence of the groundwater on the tunnel model. The tunnel lining and the surrounding ground are considered to be an environment elastic, homogeneous, and isotropic. The characteristics of surrounding ground: $E = 37.75$ MPa, Poisson's ratio $\nu = 0.34$.

Phases of the construction process of the tunnel and soil in the FEM:

Phase 1 - Set up the model: setting up the model and assigning boundary conditions and the initial stress state. There is no reflection wave at the boundary of the model (using the CINPE4 infinite elements);

Phase 2 - Excavation tunnel: The excavated ground inside the tunnel boundary is deactivated. It should be mentioned that there is not influence of the groundwater on the tunnel model and the soil. All the external loads caused by the soil were applied to the tunnel lining in order to consider the worst case of tunnel lining stress.

Phase 3 - Installation of the tunnel lining: the tunnel lining is activated on the tunnel boundary (the continuous tunnel lining). Set up to the peak ground acceleration of the earthquake in the model;

Phase 4 - Run the model with conditions established in the above phases and obtain the results.

Table 3, and Figures 9, 10, 11, 12 indicate small differences for the maximum stress, the maximum bending moment and maximum displacement in the tunnel lining obtained by the HRM method and the FEM (Abaqus^{2D}). The HRM method gives the maximum stress which is 7.415% smaller than those of the FEM (Abaqus^{2D} model). The differences of the maximum bending moment and maximum displacement in HRM method are 5.84% and 2.513%. These differences are not big.

Tab. 3. Analysis results of different methods for the U-shaped continuous tunnel lining.

The internal forces in tunnel lining	HRM	The FEM (reference case)
M_{max} (kN.m/m)	273.60	289.6
σ_{max} (MPa)	14.821	15.92
Maximum displacement of the tunnel lining	5.365	5.39
% difference with the reference case		
ΔM	5.84	-
$\Delta \sigma$	7.415	-
Δd	2.513	-

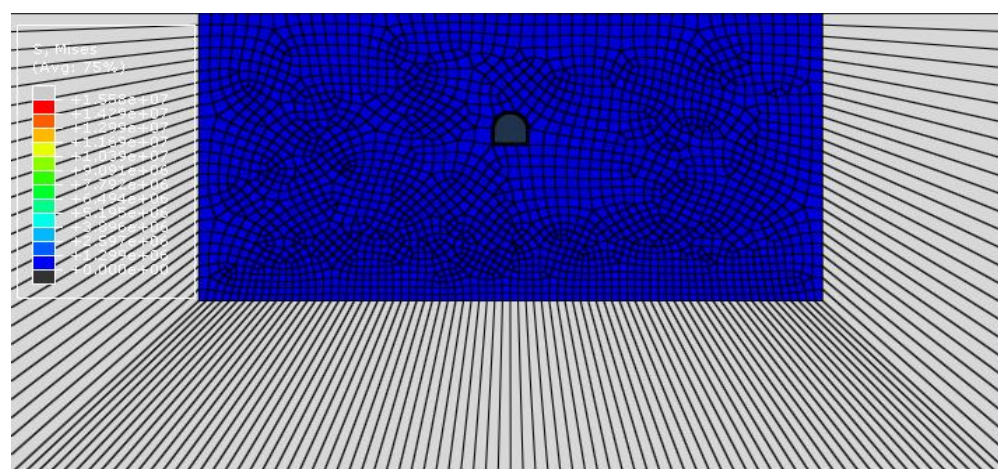


Fig. 8. Model the U-tunnel continuous lining by the FEM.

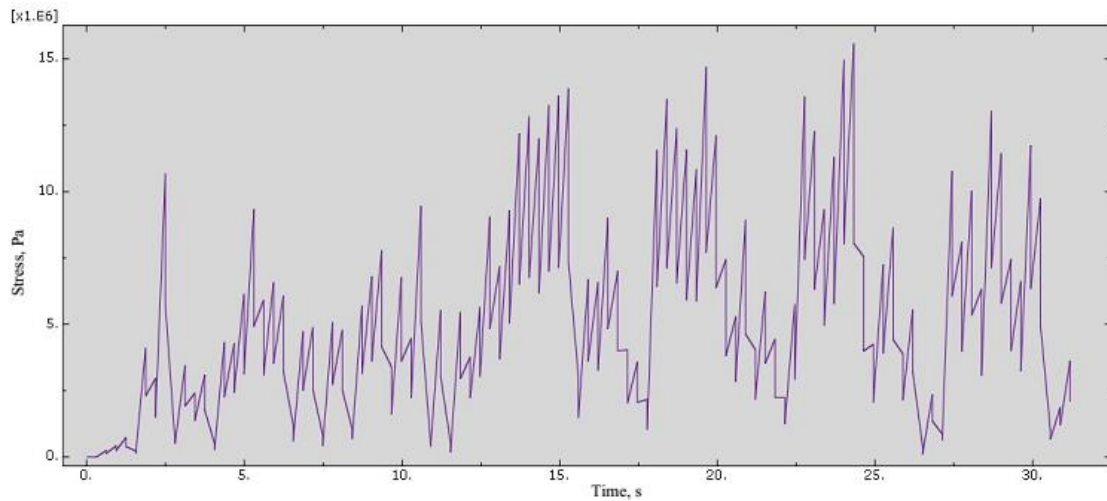


Fig. 9. State stress on the one point in the U-tunnel continuous lining by the FEM.

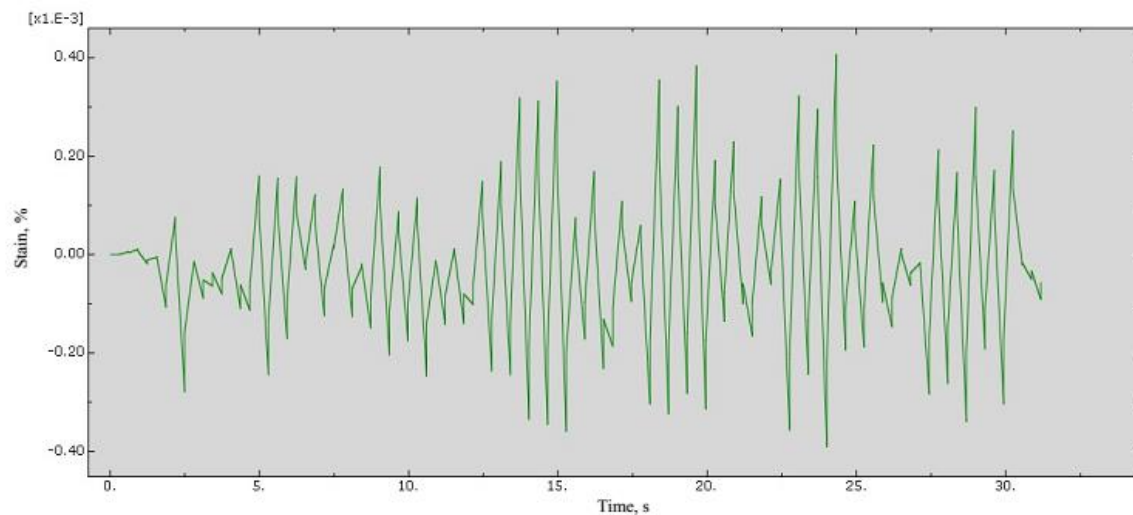


Fig. 10. Strain of the one point in the U-tunnel continuous lining by the FEM.

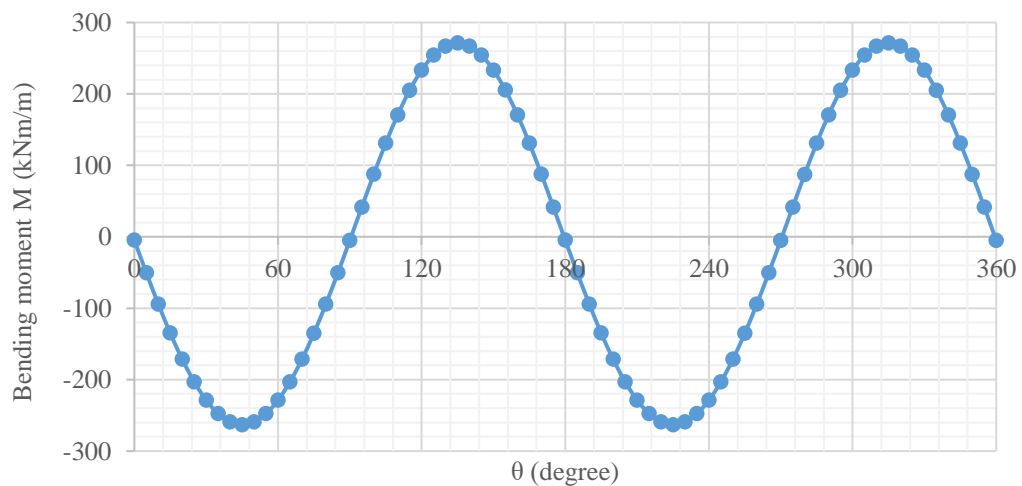


Fig. 11. Bending moment M in the tunnel lining by HRM method in case of the U-tunnel continuous lining.

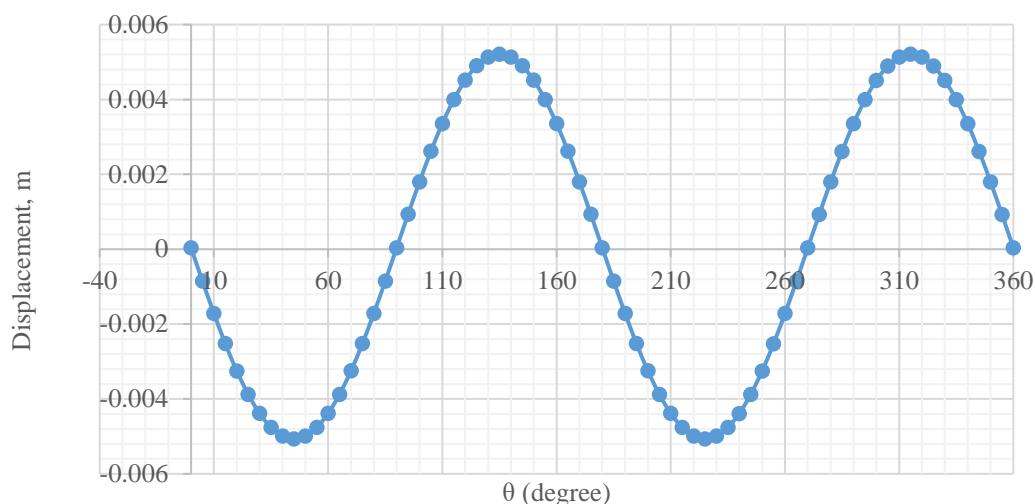


Fig. 12. Displacement of the tunnel lining by HRM method in case of the U-tunnel continuous lining.

In case the segmental tunnel lining with joints, using the HRM method to calculate the tunnel of the Hanoi metro system when the tunnel under the effect of the strongest earthquake that may occur in Hanoi centre. In the tunnel lining cross-section, 6 joints were evenly distributed, and the tunnel lining cross-section is made up of 6 segments that were distributed evenly along the tunnel border. The joints of the tunnel lining these are located at angles of 0°, 60°, 120°, 180°, 240° and 300°, measured counter-clockwise from the spring line on the right. These results are shown in Table 4, and Figures 13, 14, 15, 16.

Tab. 4. Analysis results in case the U-shaped segmental tunnel lining.

The internal forces in the tunnel lining	The continuous lining (reference case)	The segmental tunnel lining			
		$\lambda=1.5$	$\lambda=1$	$\lambda=0.5$	$\lambda=0.25$
M- Maximum bending moment (kN.m/m)	273.60	256.90	251.20	238.0	220.90
% difference with the reference case -M	-	6.104	8.187	13.011	19.261
T-Maximum normal force (kN/m)	465.28	462.40	461.70	460.0	457.60
% difference with the reference case -T	-	0.619	0.769	1.134	1.65
σ -Stress (MPa)	14.821	13.904	13.623	12.971	12.127
% difference with the reference case - σ	-	6.187	8.083	12.482	18.176
d- Maximum displacement, (mm)	5.932	7.699	8.935	12.422	18.765
% difference with the reference case -d	-	29.787	50.623	109.41	216.355

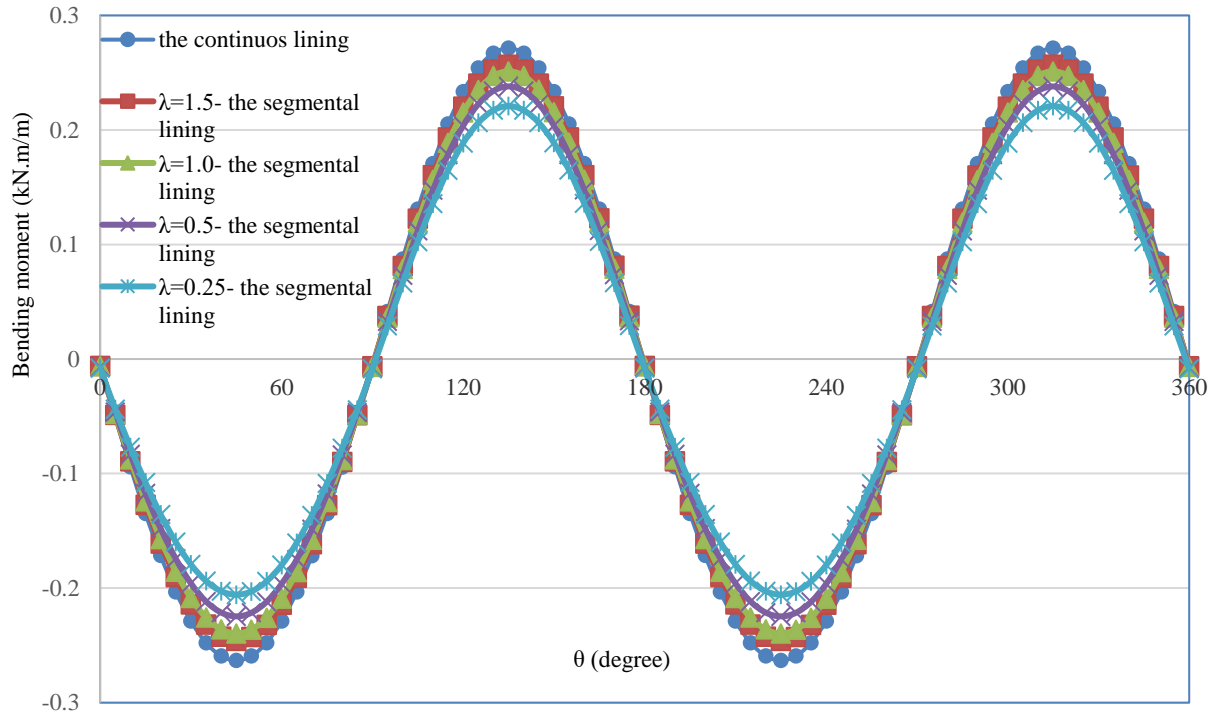


Fig. 13. Bending moment M in the U-shaped segmental tunnel lining by the HRM method.

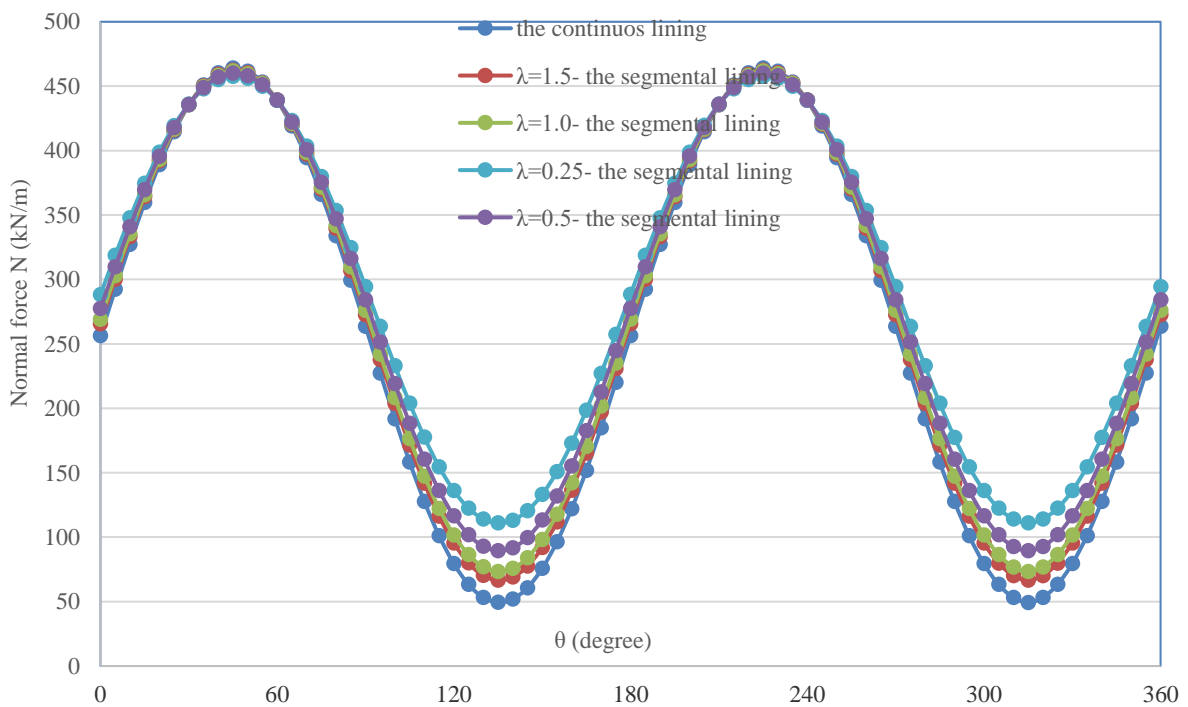


Fig. 14. Normal force in the U-shaped segmental tunnel lining by the HRM method.

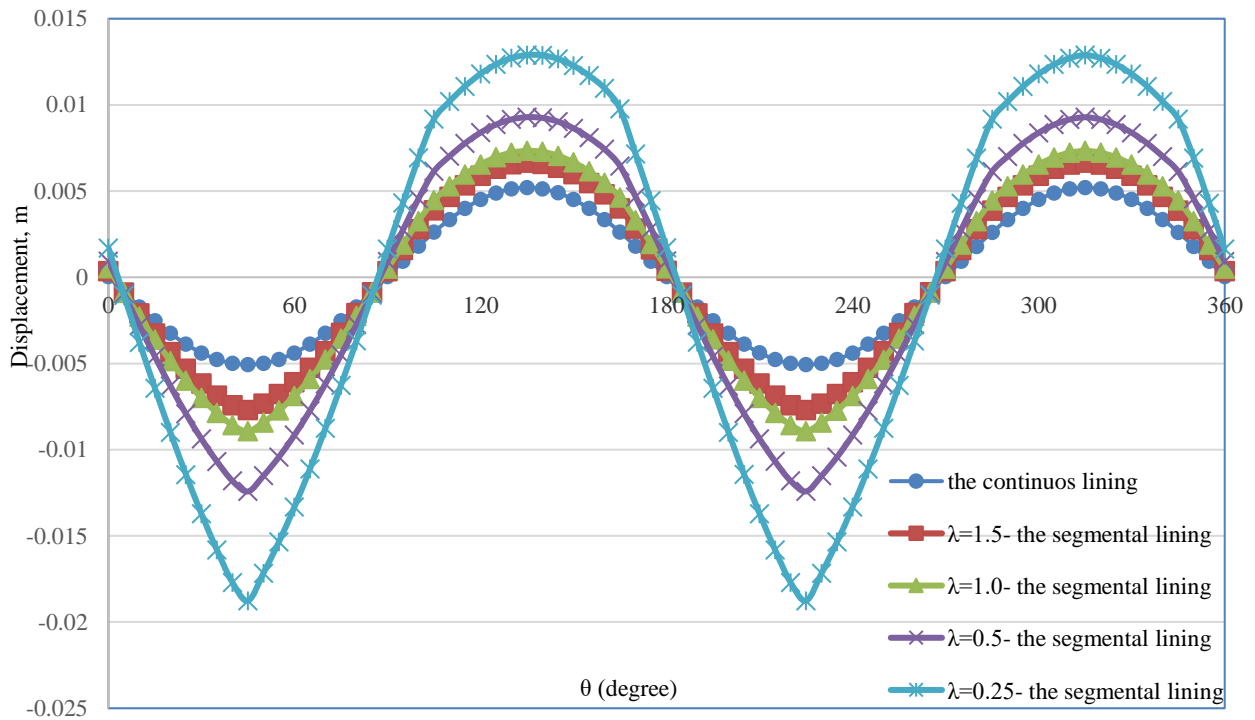


Fig. 15. Displacement of the U-shaped segmental tunnel lining by the HRM method.

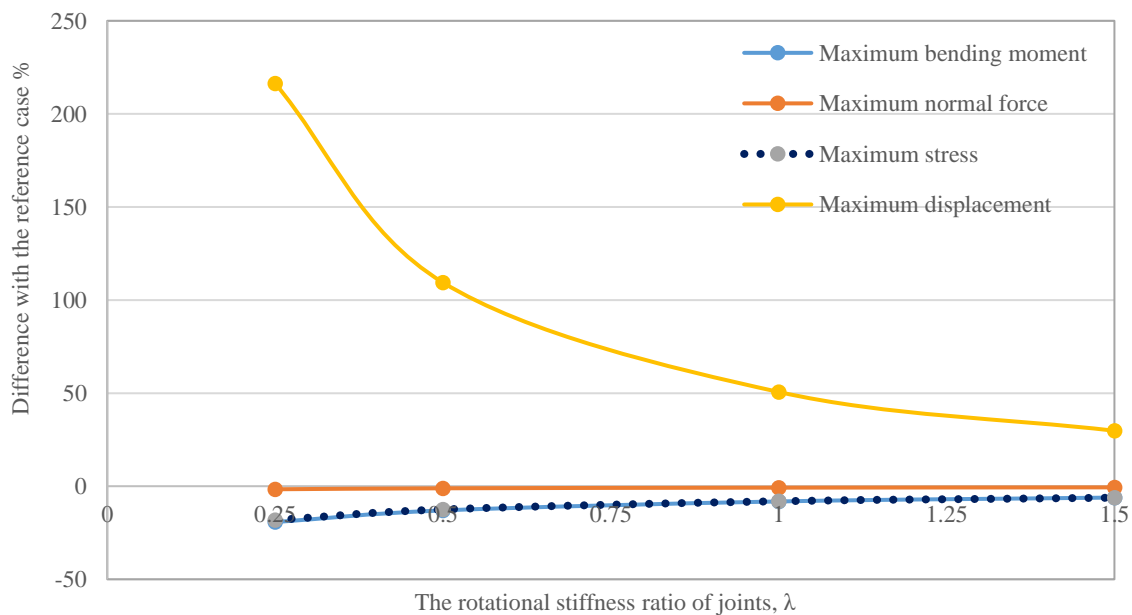


Fig. 16. Effect of the rotational stiffness ratio of joints on the internal forces and displacements on the U-shaped segmental tunnel lining.

The results in the case of the continuous tunnel lining are reference values. When the rotational stiffness ratio of joints has a value $\lambda=1.5$, the maximum bending moment in the tunnel lining with the reference case is 6.104%, smaller, the maximum normal force with the reference case is smaller 0.619% and the absolute maximum displacement with the reference case is 29.787%, bigger.

When the rotational stiffness ratio of the joints has a value $\lambda=1.0$, the maximum bending moment in the tunnel lining with the reference case is 8.187%, smaller, the maximum normal force with the reference case is smaller 0.769% and the absolute maximum displacement with the reference case is bigger 50.623%.

With the rotational stiffness ratio of the joints has a value $\lambda = 0.5$, the maximum bending moment in the tunnel lining with the reference case is 13.011%, smaller, the maximum normal force with the reference case is smaller 1.134% and the absolute maximum displacement with the reference case is bigger 109.41%.

When the rotational stiffness ratio of the joints has a value $\lambda = 0.25$, the maximum bending moment in the tunnel lining with the reference case is 19.261%, smaller, the maximum normal force with the reference case is smaller 1.65% and the absolute maximum displacement with the reference case is 216.355%, bigger.

On the basis of the above analysis, it is reasonable to conclude that:

- The internal force and the displacement of the tunnel lining when the tunnel is effected by the earthquakes depend on the rotational stiffness ratio of the joints in the tunnel lining;

- In both cases, the tunnel lining is continuous and the tunnel lining is segmental, the maximum stresses in the tunnel lining under the effect of the strongest earthquake that can occur in the central of Hanoi is less than the limited stress value of material tunnel's ($\sigma_{\text{limit}}=22$ MPa), so the tunnel could work safely and stable under the influence of the strongest earthquake that can occur in Hanoi center.

4. Conclusions

This study proposed some improvements of the method numerical HRM for designing the U-shaped segmental tunnel lining under the impact of earthquakes. The paper mentioned the influence of the geometrical parameters and mechanical characteristics of the tunnel lining on the content of the HRM method. In the case of the continuous tunnel lining, the internal forces in the tunnel lining under the impact of the strongest earthquake that can occur in the Hanoi center were calculated by using the improved HRM method and the FEM. The difference in results of the two methods is not large and the maximum stress value that occurs in the tunnel lining under the influence of the strongest earthquake is located at the intersection of the column and the dome of the tunnel lining. On the base these results above, it can confirm the accuracy of the HRM method when HRM method was used to design the U-shaped tunnel under the impact of an earthquake with the outstanding advantage of the HRM method: the time calculation is very short (10s to 15s); the input data is simple and easy to access.

In case of the segmental tunnel lining under the effect of the earthquake, the improved HRM method was used to calculate the U-shaped segmental tunnel from the system Hanoi metro. On the basis of the internal forces in the tunnel lining and the displacement of the tunnel lining with the rotational stiffness ratio of joints in the lining respectively, the conclusion that can be drawn is that:

- When joints have a big rotational stiffness ratio, the internal force in the tunnel lining is big and vice versa;

- When joints have a small rotational stiffness ratio, the displacement of the tunnel lining has a value big and vice versa.

This means the rotational stiffness ratio of the joints is directly proportional to the internal force and stress in the lining and inversely proportional to the displacement of the tunnel lining. With the presence of joints, if the tunnel lining has big displacement, the internal forces in the tunnel lining that has value small and vice versa. The presence of joints in the tunnel lining could increase the flexibility of the tunnel lining and could increase the stability of the tunnel under the impact of an earthquake.

5. Acknowledgements

This research is supported by Vietnam National Foundation for Science and Technology Development (NAFOSTED) under grant number 17/2020/STS02, Vietnamese Ministry of Education and Training under grant number B2021-MDA-09, and Hanoi University of Mining and Geology under grant number T21-30. We thank two anonymous reviewers for their comments that were very valuable for revising the manuscript.

The authors would like to thank the Board of Directors of Dong Bac Corporation and the Board of Directors of Nam Khe Tam mine, Company 86, for providing the 10T seam documents. Company 86 is acknowledged for approval of the field visit at the 10-2 face. In particular, Nam Khe Tam mine has used

the research results to produce and bring good results.

6. References

1. Yin, L., Yang, W., 2000. Topology optimization for tunnel support in layered geological structures, *International Journal for Numerical Methods in Engineering*, 47(12): 1983-1996, DOI:10.1002/(SICI)1097-0207(20000430)47:123.3.CO;2-E.
2. Barpi, F., Barbero, M., Peila, D., 2011. Numerical modelling of ground-tunnel support interaction using bedded beam-spring model with fuzzy parameters. *Gospodarka Surowcami Mineralnymi*, 27: 71-87.
3. Oreste, P.P., 2007. A numerical approach to the hyperstatic reaction method for the dimensioning of tunnel supports. *Tunnelling and Underground space technology*, 22: 185-205, DOI: 10.1016/j.tust.2006.05.002.
4. Oreste, P., Spagnoli, G., Ramos, C.A.L., Sebille, L., 2018. The hyperstatic reaction method for the analysis of the sprayed concrete linings behavior in tunneling. *Geotech. Geol. Eng.*, 36: 2143-2169, DOI: 10.1007/s10706-018-0454-6.
5. Do, N.A., Dias, D., Oreste, P.P., Djeran-Maigre, I., 2014. The behaviour of the segmental tunnel lining studied by the Hyperstatic Reaction Method. *European Journal of Environmental and Civil Engineering*, 18(4): 489-510, <https://doi.org/10.1080/19648189.2013.872583>.
6. Do, N.A., Dias, D., Oreste, P.P., Djeran-Maigre, I., 2014. 2D tunnel numerical investigation - the influence of the simplified excavation method on tunnel behaviour. *Geotechnical and Geological Engineering*, 32(1): 43-58, <https://doi.org/10.1007/s10706-013-9690-y>.
7. Do, N.A., Dias, D., Oreste, P.P., Djeran-Maigre, I., 2014. A new numerical approach to the Hyperstatic Reaction Method for segmental tunnel linings. *International Journal for Numerical and Analytical Methods in Geomechanics*, 38(15): 1617-1632, DOI: 10.1002/nag.2277.
8. Nguyen, T.C., Gospodarikov, A.P., 2020. Hyperstatic reaction method for calculations of tunnels with horseshoe shaped cross-section under the impact of earthquakes. *Earthquake Engineering and Engineering Vibration*, 19(1): 179-188, DOI: 10.1007/s11803-020-0555-0.
9. Du, D., Daniel, D., Do, N.A., Vo, T.H., 2020. U-shaped tunnel lining design using the Hyperstatic Reaction Method– Influence of the invert. *Soil and Foundations*, 60(3): 592-607, DOI: 10.1016/j.sandf.2020.02.004.
10. Duddeck, H., Erdmann, J., 1982. Structural design models for tunnels in soft soil. *Underground Space*, 9(5).
11. Leca, E., Clough, G.W.J., 1992. Preliminary design for NATM tunnel support in soil. *International Journal of Rock Mechanics and Mining Sciences & Geomechanics Abstracts*, 29(6): 558-575, DOI: 10.1016/0148-9062(92)92087-s.
12. Huebner, K.H., Dewhirst, D.L., Smith, D.E., Byrom, T.G. *The finite element method for engineers*. John Wiley and Sons, New York, 2001.
13. Möller, S., 2006. Tunnel induced settlements and structural forces in linings. Ph.D Dissertation. Stuttgart University.
14. Moller, S.C., Vermeer, P.A., 2008. On numerical simulation of tunnel installation. *Tunnelling Underground Space Technology*, 23: 461-475, DOI: 10.1016/j.tust.2007.08.004.
15. Penzien, J., Wu, C., 1998. Stresses in linings of bored tunnels. *Journal of Earthquake Eng. Structural Dynamics*, 27: 283–300, DOI: 10.1002/(SICI)1096-9845(199803)27:3<283::AID-EQE732>3.0.CO;2-T.
16. Penzien, Z., 2000. Seismically induced racking of tunnel linings. *Int. J. Earthquake Eng. Struct. Dynamic*, 29: 683–691, DOI: 10.1002/(SICI)1096-9845(200005)29:5<683::AID-EQE932>3.0.CO;2-1.

17. Naggar, H.E., Hinchberger, S.D., 2008. An analytical solution for jointed tunnel linings in elastic soil or rock. *Canadian Geotechnical Journal*, 45: 1572-1593, DOI:10.1139/T08-075.
18. Takano, Y.H. Guidelines for the design of shield tunnel lining. 2000. *Tunneling and Underground Space Technology*, 15(3): 303-331, DOI: 10.1016/S0886-7798(00)00058-4.
19. Zhang, D., Huang, H., Hu, Q., Jiang, F., 2015. Influence of multi-layered soil formation on shield tunnel lining behavior. *Tunnelling Underground Space Technology* 47(3): 123-135, DOI: 10.1016/j.tust.2014.12.011.
20. Systra. Hanoi Pilot Light Metro Line 3, Section Nhon - Hanoi Railway Station, Package number: HPLMLP/CP-03 (Ver. 2), 2011.
21. <http://scedc.caltech.edu/>, 09/2018. The Southern California Earthquake Data Center (SCEDC). Data of El Centro earthquake.
22. Nguyen, TA., Nguyen, DA., Vu, VG., Tran, VQ., 2018. Prediction of ground vibration due to blasting: case study in some quarries in Vietnam. *Journal of Mining and Earth Sciences* 59(3): 1-8.
23. Gospodarikov, AP., Nguyen, TC, 2017. Liquefaction possibility of soil layers during earthquake in Hanoi. *International Journal of GEOMATE*, 13(39): 148-155, DOI: 10.21660/2017.39.50721.
24. Gospodarikov, AP., Nguyen, TC, 2018. The impact of earthquakes of tunnel linings: A case study from the Hanoi metro system. *International Journal of GEOMATE*, 14(41): 151-158, DOI: 10.21660/2018.48.26210.
25. Nguyen, TC., Do, NA., Pham, VV., 2021. Research on calculating the effects of earthquakes on the lining tunnel in Hanoi metro system. *Journal of Mining and Earth Sciences* 62(2): 35 - 46. DOI:10.46326/JMES.2021.62(2).04.

Development of Support Plan and Operation Scheme for Semi-mechanized Longwall Face of Coal Seam 10T, Nam Khe Tam Mine – 86 Company, Dong Bac Corporation

VU Trung Tien^{1,*}, LE Tien Dung¹, VU Thai Tien Dung¹

¹Hanoi University of Mining and Geology, 18 Vien street, Hanoi, Vietnam

Corresponding author: vutrongtien@hmg.edu.vn

Abstract. Support plans and operation schemes of mine faces are critical technical documents in underground coal mining management. The development and selection of a reasonable support plan and operation scheme of the face are complicated because they involve many factors. In specific mining conditions, developing and selecting an appropriate support plan and operation scheme will improve the working efficiency of equipment, increase labor productivity, and ensure workers' safety. This article researched a mining technology for the thin seams, focusing on coal seam 10T in Nam Khe Tam coal mine, 86 Coal Company. From the analysis of geo-mining conditions, the article developed and selected a reasonable support plan and operation scheme for the face in coal seam 10T. After being used in the field, the support plan and operation scheme have brought the face efficiency and safety.

Keywords: Mining technology, Semi-mechanized, Hydraulic prop, Box bar, Operation scheme, Support plan

1. Introduction

Semi-mechanized mining technology is a type of technology that uses shearer or plow with non-mechanized supports to extract raw coal block [1]. This technology has been used in many countries, especially in China [2, 3], where semi-mechanized mining techniques applied to thin coal seams with a gently sloping angle are also relatively effective. However, this technology for thin coal seams is still new for underground mines in Quang Ninh coal basin, Vietnam.

To date, Dong Bac Corporation's coal mines are managed and exploited mainly by the underground method. With a limited mining area, the annual mining output at the mines is not high. The Nam Khe Tam mine of Company 86, Dong Bac Corporation, is an exception. In Dong Bac, underground sites include Bac Quang Loi, Tay Bac Khe Cham (Company 790), Tay Bac Nga Hai, Tay Nam Khe Tam (Company 35), Dong Ri (Company 45), Nam Khe Tam (Company 86), Khe Chuoi (Company 91), Ho Thien (Company 618), Dong Quang La, and Tay Quang La (Thang Long Company) occupy total geological reserves of about 66.9 million tons.

Due to different geological conditions, Dong Bac Corporation has applied a few mining systems and supporting and mining technologies. Nowadays, the Corporation has researched and used different types of supports for each geological condition. Hydraulic props, moveable hydraulic supports, moveable frame supports, support shields “ZRY”, and recently, flexible mechanized support are being deployed at Company 35, Company 618, and Company 790. However, most faces in the Corporation are using mining technology of drilling and blasting method. The advantage of drilling and blasting technology is mobility and flexibility, applied to all geological conditions. However, the disadvantages of this technology are low safety, interruption in the technological chain, releasing harmful gases, and low productivity.

To eliminate the disadvantages of the drilling and blasting mining method, along with the determination to modernize technology in underground mining, Dong Bac Corporation has cooperated with Company 86 to find suitable areas for applying mechanized mining technology. The first problem is choosing the type of mechanization technology (semi-mechanized or fully mechanized). The second is human resources to operate the equipment because the Corporation has no experience applying such technology. Based on research results and consultation and a practical study on the application of semi-mechanized mining technology at some Chinese longwall faces for thin and gently sloping coal seams, the efficiency has been realized. Therefore, the Corporation decided to apply for the same conditions at Nam Khe Tam [3, 4].

From the above practical issues, the article has researched and proposed a design for support plan and operation scheme for longwall face in seam 10T. Nam Khe Tam mine can apply and deploy these proposal designs in actual production to improve synchronous equipment's supporting and working efficiency in the longwall face, thereby increasing mining efficiency and productivity.

2. Geological features and mining technology of Face № 10-2, Nam Khe Tam mine, Company 86

2.1 Geological characteristics of Face № 10-2

Basic geological parameters of the designed area are as follows [5, 6]:

- Name of the face: № 10-2
- Mining levels: +70/+90
- Coal seam: 10T
- Average thickness of coal seam: $m = 1.3$ m;
- Average seam dip angle: $\alpha = 20^\circ$;
- Volumetric weight of coal: $\gamma = 1.58$ T/m³;
- Average length in dip direction: $L_d = 88$ m;
- Length in strike direction: $L_p = 250$ m;
- Immediate roof is siltstone with an average thickness of 3.3 m, hardness f of $4 \div 6$; the main roof is sandstone with an average thickness of 8 m, Protodyakonov scale of hardness f of $6 \div 8$;
- Immediate floor is siltstone with a thickness of 6 m, hardness f of $4 \div 6$; the main floor is sandstone, an average thickness of 5.5 m, Protodyakonov scale of hardness f of $6 \div 8$.

From the results of geological exploration and data collected from the preparatory excavation process, the coal in the designed area is of the semi-anthracite type, without spontaneous combustion. Coal seam has a simple structure. The roof and floor are of medium to stable stability, and the main roof is stable to very stable. With the above geological conditions, applying semi-mechanized mining technology for longwall face № 10-2 is appropriate. Seam 10T is thin and gently sloping, so selecting and applying equipment with small capacity used in the face is entirely feasible.

+ Location of Face № 10-2

For opening the deposit at Seam 10T, Company 86 drove an adit level +45 and drove transport drift level +70 from ventilation raise +45/+70. From collar level +195 drove ventilation raises +100/+195 and +70/+90, therefore drove ventilation drift level +90. On that basis, drove raise +90/+70 to form Face № 10-2 at Seam 10T. Figure 1. show the location of the longwall face № 10-2.

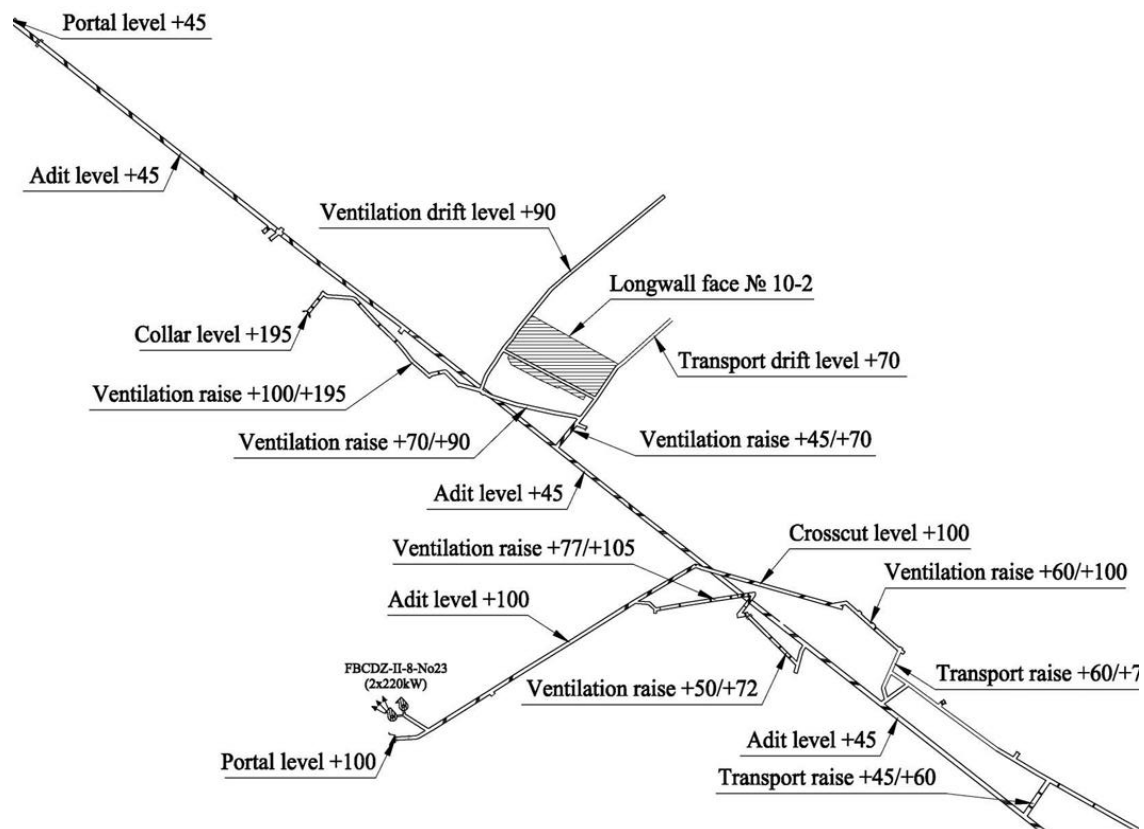


Fig. 1. Location of the longwall face № 10-2 at coal seam 10T, Company 86.

2.2 Mining technology of the longwall face № 10-2

+ Mining technology

The selection of coal mining technology depends on many factors in which the geological conditions of mine are the decisive factors. Coal seam 10T in Nam Khe Tam mine has an average slope angle of 20 degrees, an average thickness of 1.3 m; this is a thin and gently sloping seam. According to a preliminary assessment of geological conditions, the seam is relatively stable, and it is possible to use mechanized technology. Currently, this technology is used in many different underground mines and has shown fairly good results. The application of mechanized technology at underground coal mines of Dong Bac Corporation has been approved based on geological conditions assessment of a few mines having suitable conditions. The application of mechanization technology ensures the requirements of output, productivity, and a high level of safety [4].

+ Main synchronized equipment at the longwall face [7]

Many different factors and regulations influence the selection of synchronous equipment at the longwall face. This selection is a problem of the technological system and a problem of the most optimal combination. The synchronous selection of equipment achieves the most relevant results for overall longwall face design. The equipment synchronization must be consistent with the geological conditions of the designed area and technical and economic factors of Company 86.

- Shearer

To extract coal in the longwall face № 10-2, Company 86 has chosen the China shearer MG125/150-WD (Fig. 2) with specifications shown in Table 1.

Tab. 1. Specifications of shearer MG125/150-WD.

(№)	Parameters	Unit	Value
1	Cutting range	m	0.8 ~ 2.2
2	Cutting drum web	m	1.0
3	Operational Haulage speed	m/min	0 ~ 3.5
4	Maximum Haulage pull	KN	150
5	Number of cutting drum	drum	1
6	Cutting drum diameter	mm	800
7	Cutting drum speed	r/min	82
8	Chain type	mm	Φ18×64
9	Operation angle of ranging arm	degree	+45 ÷ -16
10	Coal hardness		f ≤ 3.5
11	Slope angle	degree	≤ 35
12	Speed adjustment method		inverter
13	Maximum power installed on cutting drums	Kw	125
14	Supply voltage	V	660/380
15	Cooling method		by water
16	Maximum power installed on haulage drive	Kw	22
17	Total weight	Ton	~8
18	Outer Dimensions (Length x Width x Height)	mm	6500 x 1600 x 700

- Roof support

From analysis and comparison of different types of roof supports, the support selected for application at the longwall face № 10-2 is a combination of single hydraulic prop DW22-300/100 and steel box bar DFB 2800/300. Specifications of single hydraulic prop DW22-300/100 and steel bar DFB 2800/300 are shown in Tables 2 and 3.



Fig. 2. Shearer MG125/150-WD.

Tab. 2. Specifications of single hydraulic prop DW22-300/100.

N ^o	Parameters	Unit	Value
1	Rated working resistance	kN	300
2	Rated working pressure	MPa	38.2
3	Setting load	kN	118 - 157
4	Hydraulic pump pressure	MPa	15 - 20
5	Max height	mm	2240
6	Min height	mm	1440
7	Piston range	mm	800
8	Cylinder diameter	mm	110

Tab. 3. Specifications of steel box bar DFB 2800/300.

N ^o	Parameters	Unit	Value
1	Bar length	mm	2800
2	Weight	kg	65
3	Allowable load of bar	kN.m	300

- Transport equipment

The transport equipment used in the longwall face N^o 10-2 is a conveyor coded SGZ 630/2*90, synchronized with the shearer MG125/150-WD (see Fig. 3). Table 4 shows the technical parameters of this conveyor.



Fig. 3. Armored face conveyor SGZ 630/2*90.

Tab. 4. Specifications of conveyor SGZ 630/2*90.

N ^o	Parameters	Unit	Value
1	Transport capacity	Ton/h	250
2	Conveyor length	m	150
3	Moving speed	m/s	0.868
4	Electric motors		DSB-90, 90Kw × 2
	Motor speed	r/min	1480
	Voltage	V	660
5	Hydraulic coupling		D450
	Rated power	Kw	90 × 2
	Cooling method		by water
	Coolant water flow	lit	14
6	Chain type		two middle chains
	Chain specification		φ18×64
7	Dimensions of plate (Length × Width × Height)	mm	1500×630×190

3. Design of support plan and operation scheme for longwall face N^o 10-2

Support plan and operation scheme are two closely related technical documents. They must fit together in both time and space. These documents are prepared by professionals and are used to direct the production and management of the mine [8].

3.1 Design of support plan for the longwall face N^o 10-2

The support plan is a document that shows necessary information for viewers to use to build and install the roof supports, ensuring the safety of workers and equipment. This plan offers the status of longwall face according to each extraction cycle, type of used mining technology, distance between supports, number of supports, movement of shearer and support, and pressure control method in the face. In addition, the support plan also shows the progress of moving face in one day and the procedure for creating a room placing shearer.

+ **Design basis** [6, 9, 10]

- Documents on the mine geology of design area; parameters on properties of the roof and floor rock;
- Mining technology in the longwall face, technical parameters of equipment;
- Hypothesis to determine mine pressure (console beam hypothesis);
- Method of creating a room for placing shearer (head or tail);
- Method of controlling mine pressure in the longwall face;
- Skill level of workers;
- Requirements of actual production;
- Technical, safety, and efficiency requirements.

+ **Support plan for the longwall face N^o 10-2**

According to the calculation, the length of the longwall face is 88 m, the number of single hydraulic props is 1057 pillars, and the number of steel bars is 23 units. In the longwall face, there are three rows of props. The distance between the prop rows is 0.8 m, the distance between the props in each row is 0.5-1 m (Fig. 4).

3.2 Design of operation scheme in the longwall face N^o 10-2

The operation scheme in the longwall face shows how to arrange the work in a specific space and time relationship. It also shows the required labor to complete each assignment, ensuring that the longwall face moves on schedule to reach the designed capacity. It is imperative to establish a suitable operation scheme for each different condition, which is helpful to managers because it determines the working efficiency of the selected synchronous equipment and ensures the safety of workers.

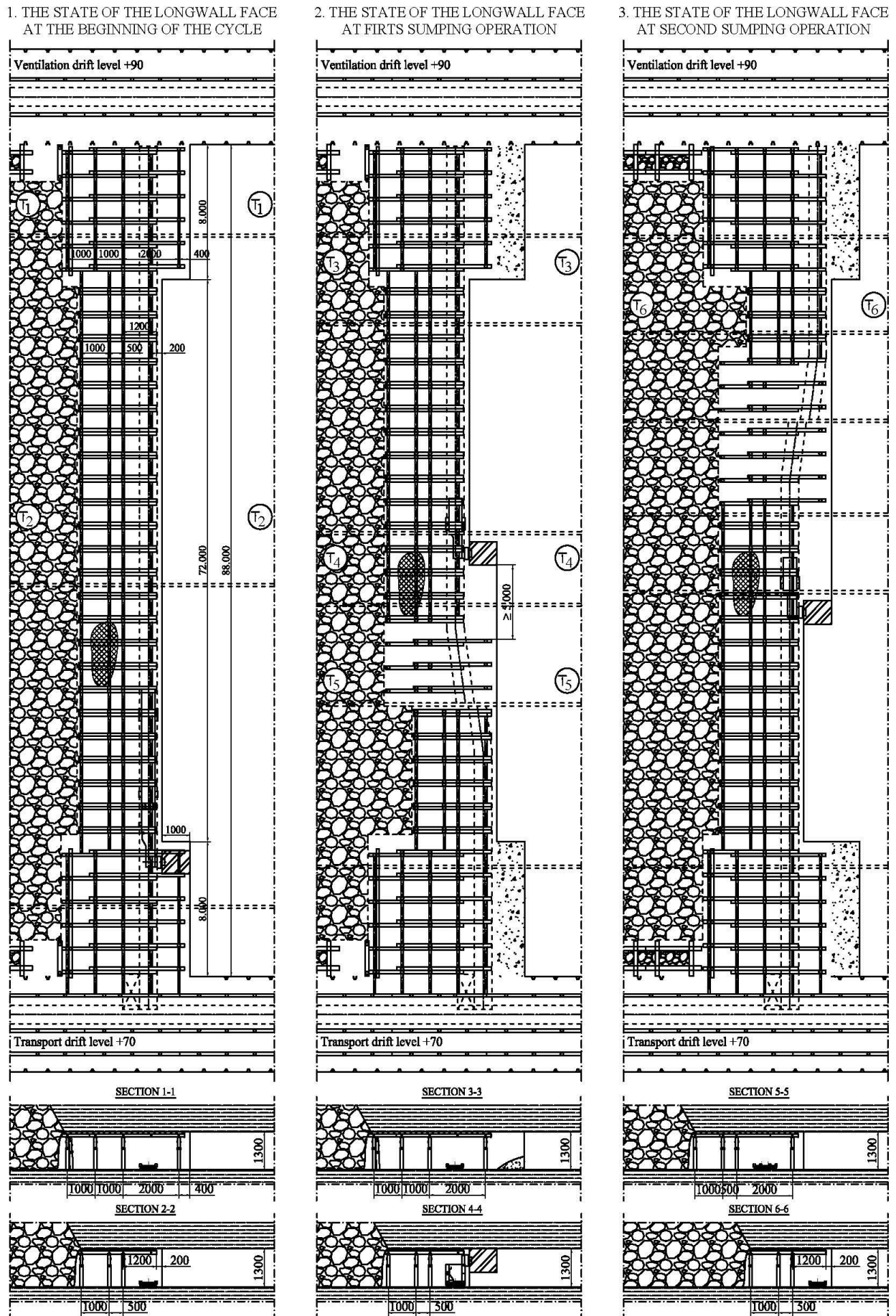


Fig. 4. Support plan for the longwall face № 10-2, Nam Khe Tam mine.

Detailed research and calculation based on initial geological data to establish a close relationship between technological stages are essential, aiming to maximize the working efficiency of the shearer and other equipment at the longwall face. The operating efficiency of shearer is one of the factors affecting the economic efficiency in the mining process. It is necessary to arrange a reasonable operation scheme so that shearer can promote its advantages to achieve high productivity in longwall face.

+ **Design basis** [1, 8, 11, 12]

- Factors regarding characteristics of geological conditions of the design area;
- Technical and technological factors;
- The parameters directly affect the productivity of the shearer;
- Movement speed of shearer;
- Tasks need to be completed in one mining cycle: cutting face, strengthening face, repairing face, operating face supports and conveyors...);
- Norms to complete each task;

+ **Operation scheme for the longwall face № 10-2**

The production tasks in the longwall face № 10-2 are organized and performed in cycles. A cycle of two web cuts is completed within two shifts, equivalent to the face moving progress of three meters per day (Fig. 5). A web cut includes the following stages: cutting face and installing supports with an advance rate of 1.0 m, recovering supports at transport, and ventilation drifts. The inspection and maintenance of equipment are carried out at the end of each shift, including maintenance, repair, and replacement of spare parts if necessary for shearer, roof supports, conveyors, electrical equipment and emulsifier pump systems, dust filter system, power supply system, water supply system, methane warning system, and pressure test of roof supports. The number of workers in the face is arranged depending on the specific work of each shift. According to calculations, the required number of workers is 29 people for the first shift and 27 people for the second shift (Fig. 6).

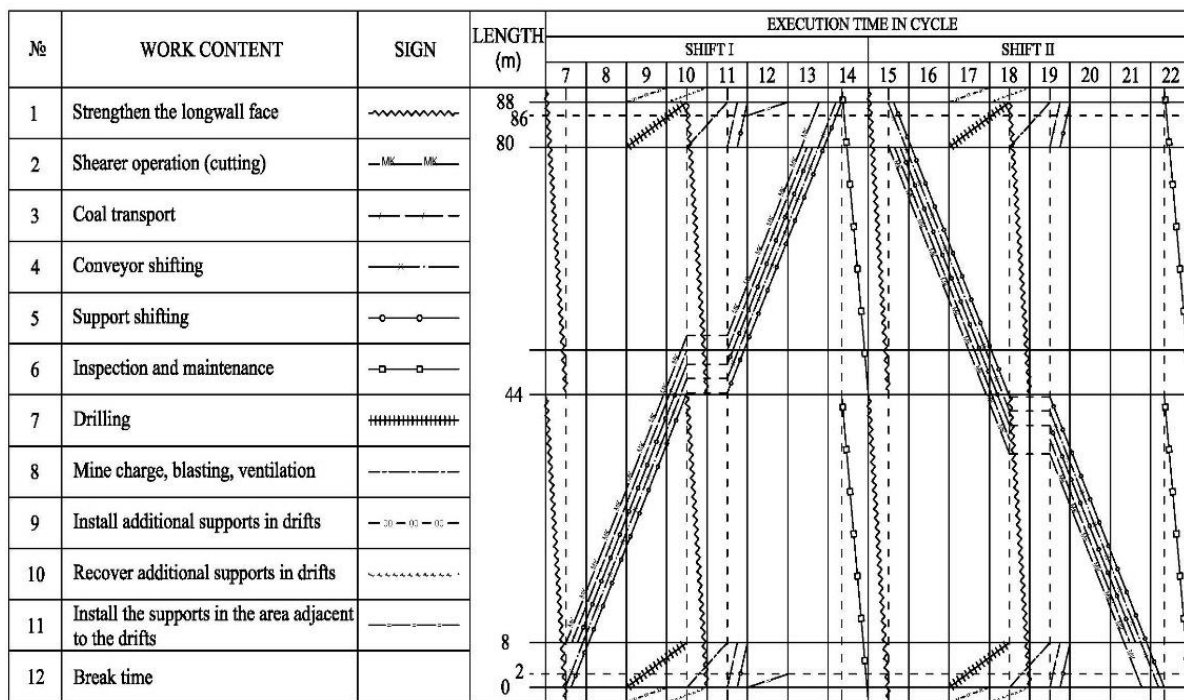


Fig. 5. The operation scheme in the longwall face № 10-2.

№	WORK CONTENT	Number of people			EXECUTION TIME IN CYCLE														
					SHIFT I							SHIFT II							
		SHIFT I	SHIFT II	TOTAL	7	8	9	10	11	12	13	14	15	16	17	18	19	20	21
1	Strengthen the longwall face	(10)	(10)	(10)															
2	Shearer operation (cutting)	2	2	4															
3	Conveyor operation in longwall face	1	1	2															
4	Conveyor operation in transport drift	1	1	2															
5	Loading	4	4	8															
6	Conveyor shifting	4	4	8															
7	Support shifting	8	8	16															
8	Inspection and maintenance	8	8	16															
9	Drilling	4	-	4															
10	Mine charge, blasting, ventilation	4	-	4															
11	Install additional supports in drifts	2	2	4															
12	Recover additional supports in drifts	-	4	4															
13	Install the supports in the area adjacent to the drifts	-	4	4															
14	Transfer materials, food	2	2	4															
15	Control area manager	1	1	2															
16	Electromechanical manager	1	1	2															
17	General production manager	1	1	2															
18	Break time	-	-	-															
TOTAL		29	27	56															

Fig. 6. Chart of human resource arrangement in the longwall face № 10-2.

3.3 Economic and technical indices

After researching and establishing a support plan and operation scheme for Face 10-2 seam 10T Nam Khe Tam mine, which is exploited by semi-mechanized technology, with the above equipment combination, the calculated main economic-technical indices are shown in Table 5.

4. Results and discussions

To bring the best coal cutting efficiency of shearer, we need to arrange it to work correctly. Therefore, the arrangement of shearer to work in the face is also the process of calculating and establishing the support plan and operation scheme in the longwall face. It determines the labor productivity in the longwall face and thus should be arranged to work properly.

The article has built a support plan (Fig. 4) and an operation scheme (Figs. 5, and 6) for Face 10-2 seam 10T Nam Khe Tam mine, Company 86. Based on the established support plan and the operation scheme of Face10-2, 10T seam, Nam Khe Tam mine, the authors calculate the economic-technical indices for the face. The results (Table 5) show that this technology has good efficiency, completely meets technical and economic requirements, and at the same time ensures safe conditions in exploitation.

Compared to other studies, the new point of this study is the development of a support plan and operation scheme for the semi-mechanized face (currently, Quang Ninh coalfield has nine faces, which have been used fully mechanized technology). The type of shearer used is the single-drum shearer. The cutting depth of the shearer is 1 m (the shearers currently used in nine faces in Quang Ninh are double-drums shearer, cutting depth 0.63 m) [13, 14, 15, 16, 17].

Tab. 5. Economic and technical indices of the longwall face № 10-2.

№	Indices	Unit	Amount
1	Average thickness of coal seam	m	1.3
2	Average slope angle of coal seam	degree	20
3	Volumetric weight of coal	Ton/m ³	1.58
5	Strike length	m	250
6	Average length in dip direction	m	88
7	Face advance in one web cut	m	1.0
8	Cycle completion coefficient	-	0.95
9	Number of shifts in a day	shift	3
10	Extraction coefficient	-	0.95
12	Coal output of one face cut (1 shift)	ton	171.7
13	Coal output of a day	ton	489.4
14	Coal output of a month	ton	12.724
15	Coefficient of change in location of longwall face	-	0.8
16	Capacity of longwall face	T/year	122.150
17	Number of workers in a day	worker	84
18	Direct labor productivity	T/ labor	5.8
19	Wood consumption for 1000 tons of coal	m ³	26.5
20	Explosive consumption for 1000 tons of coal	kg	76.87
21	Detonator consumption for 1000 tons of coal	unit	128
22	Consumption of wire mesh for 1000 tons of coal	kg	1506.7
23	Consumption of emulsifying oil for 1000 tons of coal	kg	481.8

5. Conclusions

The proposed mining technology diagram has been applied at Nam Khe Tam mine, and it gradually shows the efficiency in exploiting thin and gently sloping seams. Thereby, it is recommended that Nam Khe Tam mine - Company 86 continue to report and evaluate so that this technology can be applied to other areas with similar geological conditions. At the same time, this is also a premise for Dong Bac Corporation to comprehensively evaluate other mines with thin, gently sloping seams in the Corporation to put this technology into application.

6. Acknowledgements

The authors would like to thank the Board of Directors of Dong Bac Corporation and the Board of Directors of Nam Khe Tam mine, Company 86, for providing the 10T seam documents. Company 86 is acknowledged for approval of the field visit at the 10-2 face. In particular, Nam Khe Tam mine has used the research results to produce and bring good results.

The paper was presented during the 6th VIET - POL International Conference on Scientific-Research Cooperation between Vietnam and Poland, 10-14.11.2021, HUMG, Hanoi, Vietnam.

References

1. Vu Dinh Tien, Tran Van Thanh. Underground coal mining technology. Transport Publishing, Hanoi, 2008
2. Dou, L., Cao, S. Strata control in coal exploitation, China university of mining and technology press, China, 2010.
3. Yuanwei, S., Yu, N., Qingxin, Q. Strata control and technology optimization for fully mechanized coalface using top-coal caving, China university of mining and technology press, China, 2006.
4. Vu Trung Tien, Nguyen Van Ngoc, 2018. Proposing and applying reasonable mining technical solutions for the conditions of some underground mines belonging to Dong Bac Corporation. Journal of Mining Industry, 3: 27-33.
5. 86 Company, Dong Bac Corporation. General report of geological data of Nam Khe Tam mine, 2020.
6. Vu Trung Tien, Do Van Vien, 2019. Research on reasonable initial roof caving control solution for the longwall at Company 86, Dong Bac Corporation. Journal of Mining Industry, 1: 14-20.
7. 86 Company, Dong Bac Corporation. Current status of coal mining technology and support technology of Nam Khe Tam mine, 2020.
8. Tran Van Thanh, Vu Trung Tien, 2008. The arrangement of rationalized production in the longwall coal cutting by narrow-web . Journal of Mining and Earth Sciences, 23(7): 66-70.
9. wenping GUO, jinsheng CHEN. Longwall mining, Beijing science press, China, 2010.
10. Vu Trung Tien, Do Anh Son, 2019. Causes of local roof fall and face spall phenomena in the full mechanized longwall and preventive measures. Journal of Mining Industry, 1: 14-20.
11. Nguyen Van Dung, Vu Thai Tien Dung, Dao Van Chi, Bui Manh Tung, Nguyen Phi Hung, Vu Tien Quang, Dinh Thi Thanh Nhan, 2019. Setup knotting model to determine influencing factors and effective working time in the organizational structure of mechanized longwall production. Journal of Mining and Earth Sciences, 60(5): 60- 66.
12. Tran Van Thanh, 2006. The productivity of the shearer and the organization of continuous production in the longwall. National Mining Science and Technology Conference, Da Nang, 93-99.
13. Le Tien Dung, Bui Manh Tung, Pham Duc Hung, Vu Trung Tien, Dao Van Chi, 2019. A modelling technique for top coal fall ahead of face support in mechanised longwall using Discrete Element Method. Journal of Mining and Earth Sciences, 59(6): 56-65.
14. Vu Trung Tien, Pham Duc Hung, Do Anh Son, 2018. The problems often happening at the fully mechanized longwall in Quang Ninh province and methods of remedy. National conference of earth sciences and natural resources for sustainable development, 163-167.
15. Vu Trung Tien, 2016. Research on selective mining technology by coal cutting machine for thick, gently sloping seams of Vang Danh mine in Quang Ninh province. International conferences on earth sciences and sustainable geo-resources development, 254-260.
16. Vu Trung Tien, Do Anh Son, 2016. Research on the application of the control solutions for the weak and loose roof in the fully machanized longwall. International conferences on earth sciences and sustainable geo-resources development, 92-95.
17. Pham Duc Hung, Le Tien Dung, Nguyen Van Quang, 2020. Safe exploitation solution and reduction of resources loss for the L7 Seam at the West Wing area of the 790 Open Pit site of the Mong Duong Coal Mine. Journal of the Polish Mineral Engineering, 1(2): 231-238.

Research the Integration of Geodetic and Geotechnical Methods in Monitoring the Horizontal Displacement of Diaphragm Walls

PHAM Quoc Khanh^{1,*}, TRAN Ngoc Dong², NGUYEN Thi Kim Thanh¹, PHAM Van Chung¹

¹ Hanoi University of Mining and Geology, 18 Vien street, Hanoi, Vietnam

² Institute for Building Science and Technology (IBST), Hanoi, Vietnam

Corresponding author: phamquockhanh@hung.edu.vn

Abstract. This article investigates the integration of geodetic and geotechnical methods for monitoring the horizontal displacement of diaphragm walls. The results show that when the horizontal displacement is measured by the geotechnical method using an inclinometer sensor, the center point at the bottom of the guide pipe is usually chosen to be the origin to calculate displacements of the upper points. However, it is challenging to survey the bottom point for checking its stability directly. If this bottom point moves, the observation results will be incorrect. Thus, the guide pipe must be installed in the stable rock layer. But in the soft ground, this rock layer locates more deeply than the diaphragm walls, so the guide pipe cannot be laid out at the required location. Geodetic methods can directly observe the displacement of the center point on the top of the guide pipe with absolute displacement values at high accuracy. Because the displacements of observation points are determined at stable benchmarks, these values are considered the pipe's displacement. Thus, an integrated solution allows the center point on the top of the pipe to be the origin to calculate the displacements of different points located inside the diaphragm wall. Then, the calculated values are calibrated back to the inclinometer observed values to achieve highly reliable displacement, which reflects the moving of diaphragm walls. An experiment integrating the geodetic and geotechnical methods is conducted with an observation point at a depth of 20 meters at a construction site in Ho Chi Minh city. The deviations of the top point that are observed by the two methods are -4.37 millimeters and -3.69 millimeters on the X-axis and the Y-axis, respectively. The corrected observed results prove that the integrated solution has a good efficiency in monitoring the horizontal displacement of diaphragm walls. The bottom point observed by an inclinometer is unconfident enough to choose to be a reference point.

Keywords: Deformation monitoring, Diaphragm wall, Engineering surveying, Soft ground

1. Introduction

In Vietnam, big cities are usually located in delta regions with unstable geologic conditions, especially Hanoi and Ho Chi Minh cities. When huge projects such as high-rise buildings, super-high buildings with 4-6 basements, and subway are constructed, foundation pits need to be excavated down from several to tens of meters. The diaphragm walls of foundation pits are usually kinds of temporary ones as Larsen steel plates or types of permanent ones as continuous barrette piles lying underground [1, 2]. The displacements of diaphragm walls have to be monitored while constructing pits to prevent incidents [3]. Nowadays, a popular solution for observation is geodetic methods (i.e., to observe the movement on the top of diaphragm walls) and geotechnical methods using inclinometer sensors (i.e., to monitor the displacement according to the depth direction of the diaphragm walls). The advantage of geodetic methods is that the absolute displacement can be obtained at high accuracy.

In contrast, a disadvantage is that they can only detect the displacement at the top points of the diaphragm wall. The advantage of the inclinometer geotechnical method is monitoring the displacement of diaphragm walls according to the depth for early warning and giving timely handling solutions. However, inclinometer displacement values are relative because the original point chosen for comparison is at the bottom of the guide pipe, which is deeply under the ground and difficult to observe. Additionally, with the weak geological background, the bottom point is unstable, and thus the observed values reflect the displacement of diaphragm walls inaccurately.

There are several studies on this. Some documents mentioned the application of the inclinometer method in monitoring the diaphragm walls' displacement and emphasized the discrepancies between results from geodetic methods and inclinometer sensors [4, 5], or numerical modeling experimental monitoring for a full-scale diaphragm wall [6]. The displacement of diaphragm walls is the construction of the foundation pit in soft ground, which has been shown in [7, 8, 9, 10]. From the advantages and disadvantages of each method, it can be expected that the integrated solution of geodetic and geotechnical methods in deformation

monitoring is a good choice [11].

In Vietnam, no studies have ever mentioned the combination of the inclinometer and geodetic methods. This article shows the research on the integrated solution to improve the reliability of the observation results in the construction of a deep excavation pit on soft ground. The integrated method has a great significance in which the displacement of the top point measured by an inclinometer has a significant deviation in theory. The observation results are used to recommend the construction team choosing a suitable regime of work later. Through an experiment in an actual project, it is concluded that the integrated solution is appropriate to monitor the diaphragm walls of a deep excavation pit when projects are constructed on the soft ground in Vietnam.

2. Monitoring the displacement of diaphragm walls by geodetic methods

Geodetic methods are usually used to monitor the horizontal displacement of points at the top of diaphragm walls. The nature of these methods is to determine the coordinates of observation points to obtain the displacement at different periods. The popular observation instruments are high precision total stations. Common surveying methods include triangulation, polygon, intersection, standard direction, and automatic monitoring using an electronic tacheometer in real-time [12]. The process of monitoring the horizontal displacement by geodetic methods is shown in Figure 1.

Observation results obtained by geodetic methods are absolute and high accuracy displacement values because the displacement of monitoring points is determined at stable benchmarks. However, the most significant disadvantage of this method is that it can only detect the displacement of the top points of diaphragm walls. In constructing a foundation pit, monitoring displacement of diaphragm walls according to the depth is essential because of its effect on the construction of the basement later. At present, the geotechnical method using inclinometer sensors is usually applied to monitor the diaphragm wall's horizontal displacement according to the depth.

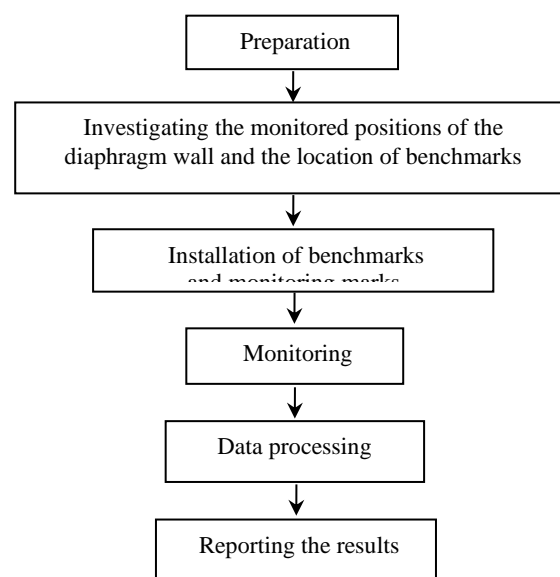


Fig. 1. The process of monitoring the horizontal displacement by geodetic methods.

3. Monitoring the horizontal displacement of diaphragm walls by geotechnical methods

3.1 Components of an inclinometer

The inclinometer device monitors the horizontal displacement of rock layers according to the depth in landslide areas and dykes, dams, transportation roads; to observe the horizontal deformation of the diaphragm walls and piles. The main components of an inclinometer are shown in Figure 2 (left and middle), including guide pipe (1), probe head (2), signal cable (3), and reading device (4). The cross-section of guide pipe is shown in Figure 2 (right).

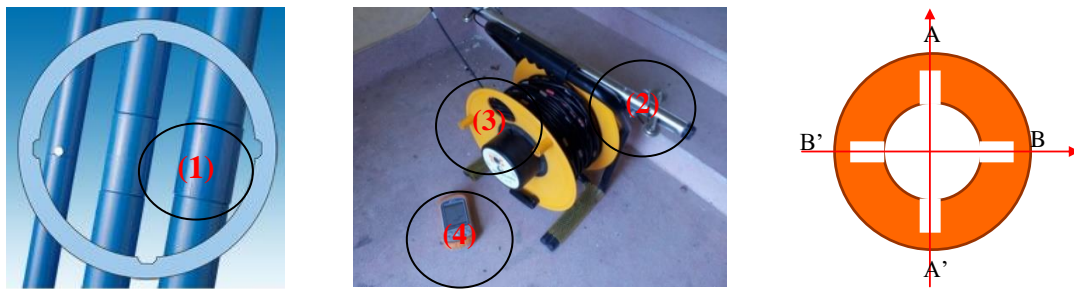


Fig. 2. An inclinometer device and the cross-section of guide pipe.

3.2. Principles of monitoring the horizontal displacement by an inclinometer

Monitoring the horizontal displacement by an inclinometer is a method that observes the displacement of objects indirectly through the movement of the guide pipe. When the diaphragm walls are the type of barrette, the guide pipe is installed inside the wall. If the diaphragm walls are Larsen steel sheet piles, the guide pipes will be installed outside those piles. The basic principle of monitoring the horizontal displacement by an inclinometer is that the point at the bottom of the guide pipe is used as the origin to calculate the displacement of the upper points. The displacement of the pipe is calculated in two perpendicular directions AA' and BB', with formulas shown in Figure 3.

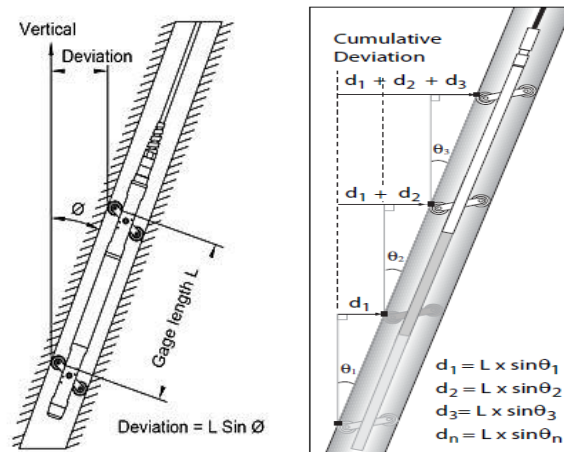


Fig. 3. Diagram of calculation in monitoring the horizontal displacement by an inclinometer.

The way to install the guide pipe and how to monitor by an inclinometer were mentioned in detail in literary studies, e.g., [1, 13, 14]. Monitoring of the horizontal displacement of diaphragm walls by an inclinometer has process shown in Figure 4.

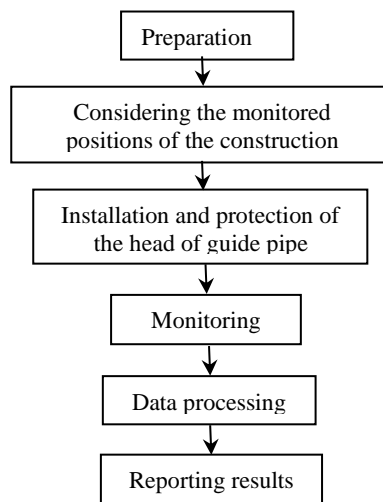


Fig. 4. Process of monitoring the horizontal displacement by an inclinometer.

As mentioned above, the displacement is compared with the reference point at the bottom of the guide pipe. In this case, the guide pipe was anchored to the original rock layer so that it had no movement, thereby without error. The higher the probe head moves, the bigger the observation error is; thus, the top of the guide pipe on the ground has the most significant error. According to device specifications provided by the producer, the reading head of the inclinometer is displayed to 0.01 mm. Each time the probe head moves 0.5 m in the guide pipe, the reading error is 0.25 mm. When the length of the guide pipe is 25 m, the accumulated error in one axis is 6 mm.

The geotechnical method using inclinometer sensors has advantages such as detecting the displacement in-depth and early warning about dangerous deformations of the diaphragm walls. Therefore, safety precautions are proposed as soon as the deformation begins, or there is even no deformation, and they will help solve any situations more simply and less expensively. However, the disadvantage is that it can only determine the relative displacement of the diaphragm wall at different depths compared with the original point at the bottom of the guide pipe. At this point, surveyors cannot observe it.

If the bottom point of the guide pipe is unstable, the observed values reflect the displacement of the diaphragm wall inaccurately. Thus, to accurately monitor the diaphragm wall's horizontal movement, the combination of inclinometer sensors with geodetic methods should be applied.

4. Integration of geodetic and geotechnical methods in monitoring the displacement of diaphragm walls

This article proposed an integrated approach to monitor the horizontal displacement of diaphragm walls in constructing a foundation pit to overcome the disadvantages of the two abovementioned methods. The objectives of the study are:

- If the bottom of the guide pipe (in the inclinometer method) is anchored to a stable rock layer, the integrated method helps to improve the precision of monitoring at the points located deeply inside the diaphragm wall. Because high accurate electronic total stations are used to survey the displacement of the top of the tube, the result is much better than the inclinometer-only measurement.
- If the bottom of the guide pipe is anchored to an unstable rock layer, the purpose of using the integrated method is to determine the movement of that bottom point and the accurate displacement values of points inside the diaphragm wall.

4.1. The bottom of the guide pipe is anchored to a stable rock layer

When the bottom of the guide pipe is attached to a stable rock layer, using the integrated solution helps to increase the accuracy of monitoring the horizontal displacement at points inside the diaphragm walls, and the surveying plan, in this case, is shown as follows:

- Put a cap on the top of the inclinometer tube and draw two rectangular coordinate axes (Fig. 5). The distances from the center point to all points on the axes (A, B, C, D) are measured by a ruler accuracy of ± 0.1 mm. The A-B axis coincides with A0-A180, and the C-D axis is B0-B180 of the guide pipe.

In each period, the horizontal displacement is measured in-depth by an inclinometer and the center point on the guide pipe's top. Thus, this point has two displacement values. Displacements were surveyed in the geodetic coordinate system $q_{x_{tb}}^{(o)}$, $q_{y_{tb}}^{(o)}$ and the values were obtained in the inclinometer coordinate system $q_{x_{icl}}^{(o)}$, $q_{y_{icl}}^{(o)}$ (Fig. 6).

Based on Figure 6, the formula of transformation of coordinates between the two systems (i.e., from the geodetic coordinate system to the inclinometer coordinate system) for the center point on the top of the guide pipe is established as follows:



Fig. 5. Designation of a lid whose center point coincides with the center of the guide pipe.

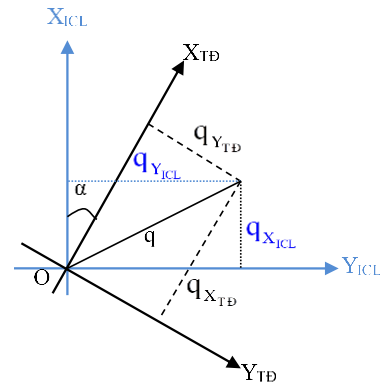


Fig. 6. Coordinate systems in monitoring the displacement by geodetic and inclinometer methods.

$$\left. \begin{aligned} q_{X_{TB-ICL}}^{(o)} &= q_{X_{TB}}^{(o)} \cdot \cos \alpha - q_{Y_{TB}}^{(o)} \cdot \sin \alpha \\ q_{Y_{TB-ICL}}^{(o)} &= q_{X_{TB}}^{(o)} \cdot \sin \alpha + q_{Y_{TB}}^{(o)} \cdot \cos \alpha \end{aligned} \right\} \quad (1)$$

where $q_{X_{TB}}^{(o)}$, $q_{Y_{TB}}^{(o)}$ measured by the geodetic method are the displacement values of the point at the top of the guide pipe (O) in the geodetic coordinate system;

$q_{X_{TB-ICL}}^{(o)}$, $q_{Y_{TB-ICL}}^{(o)}$ measured by the geodetic method are the displacement values of the point on the top of the guide pipe in the inclinometer coordinate system;

α is the rotation angle between the geodetic coordinate system and the inclinometer coordinate system (Fig. 6).

Thus, on the top point of the tube, two displacement values were observed by the two devices with different accuracies. Because of higher accuracy, the values surveyed by the geodetic method are considered the actual displacement. The difference between the two types of observations is called the error of closure of monitoring by the inclinometer. The following equation calculates the errors of closure in coordinate axes:

$$\left. \begin{aligned} \omega_X^{(o)} &= q_{X_{ICL}}^{(o)} - q_{X_{TB-ICL}}^{(o)} \\ \omega_Y^{(o)} &= q_{Y_{ICL}}^{(o)} - q_{Y_{TB-ICL}}^{(o)} \end{aligned} \right\} \quad (2)$$

In Eq. (2), $q_{X_{ICL}}^{(o)}$, $q_{Y_{ICL}}^{(o)}$ were observed by the inclinometer in the corresponding coordinate system and are displacements of the top point of the tube.

According to the principles of monitoring and calculating the horizontal displacement in the inclinometer method, it is easy to realize that the points close to the reference point have higher accuracy than the far ones. It means the accuracy of the upper points is worse than that of the lower ones, and the top point of the tube has the most significant error. The series of observations are adjusted by distributing the error of closure of the center point on the top of the guide pipe to all points. This is conducted relying on the principle of proportion to the height. From that the adjusted data of the displacement values are calculated:

$$\left. \begin{aligned} q_{X_{ICL-TB}}^{(i)} &= q_{X_{ICL}}^{(i)} - \frac{H_i}{H} \omega_X^{(o)} \\ q_{Y_{ICL-TB}}^{(i)} &= q_{Y_{ICL}}^{(i)} - \frac{H_i}{H} \omega_Y^{(o)} \end{aligned} \right\} \quad (3)$$

where $q_{x_{iCL}}^{(i)}$, $q_{y_{iCL}}^{(i)}$ are the displacements of the point i that were monitored by the inclinometer at the height H_i , $q_{x_{iCL-TB}}^{(i)}$, $q_{y_{iCL-TB}}^{(i)}$ are corrected displacements of the point i , H_i , H are the heights of the monitoring point i and the top point of the tube, calculated from the pipe's bottom point.

4.2. The bottom of the guide pipe is anchored to an unstable rock layer

As mentioned above, displacement values are calculated in a coordinate system with the reference point at the guide pipe's bottom. Therefore, when this original point is unstable, the observed values are inaccurate. It is difficult to directly observe the displacement of this bottom point, so it is necessary to choose another reference point that can be located quickly by a geodetic method. The new reference point is the center of the top of the inclinometer guide pipe on the ground. Fortunately, the inclinometer device has the associated software to calculate the displacement of monitoring points in a system, with the reference point at the top of the guide tube. Therefore, the reference point must be chosen again on the guide pipe's top in the calculation procedure. Then, displacement values $q_{x_{iCL}}^{(i)}$ and $q_{y_{iCL}}^{(i)}$ of all points inside the diaphragm wall are calculated. Although all points on the top of the guide pipe are unstable, their displacements can be surveyed using a geodetic method [15,16], e.g., a total electronic station. Thus, in each monitoring period, the center of the top of the guide pipe has to be located precisely in the geodetic coordinate system. The difference of coordinates between the two periods is the displacement values $q_{x_{TB}}^{(o)}$ and $q_{y_{TB}}^{(o)}$ of the center point.

The conversion calculation of the displacement values of the top of the guide pipe from the geodetic coordinate system to the inclinometer coordinate system can be conducted using eq. (1) by which the values $q_{x_{TB-iCL}}^{(o)}$ and $q_{y_{TB-iCL}}^{(o)}$ are determined. The coordinates which were surveyed by geodetic methods have high accuracy, so the displacements of the top of the tube $q_{x_{TB-iCL}}^{(o)}$, $q_{y_{TB-iCL}}^{(o)}$ are considered to be actual values (i.e., without error) and are used to rectify in inclinometer observations $q_{x_{iCL}}^{(i)}$, $q_{y_{iCL}}^{(i)}$ as the following equation:

$$\left. \begin{aligned} q_{x_{iCL-TB}}^{(i)} &= q_{x_{iCL}}^{(i)} + q_{x_{TB-iCL}}^{(o)} \\ q_{y_{iCL-TB}}^{(i)} &= q_{y_{iCL}}^{(i)} + q_{y_{TB-iCL}}^{(o)} \end{aligned} \right\} \quad (4)$$

5. Experiment

To verify the proposed approach, an experiment combining an inclinometer with geodetic methods is established. This is to monitor the displacement of the diaphragm wall of a high building with two basements in Ho Chi Minh city. The experiment is conducted at the time of construction of the underground part (the underground part is constructed by the semi-top down method). The observation points on the diaphragm wall are eight (denoted by P01, P02, P03, P04, P05, P06, P07, P08). The depth of the diaphragm wall is 20 m. The guide pipe for inclinometer monitoring is a specialized plastic tube (D70) of the slope indicator installed inside the steel pipe D114 (the D114 tube was fixed by concrete mortar without shrinking inside the diaphragm wall in the phase of construction). The A axis of the guide pipe is perpendicular to the diaphragm wall, while the B axis is parallel to the diaphragm wall. On the top of the guide pipe, there is a lid (Fig. 5) for monitoring the horizontal displacement of the center point by the geodetic method.

Steps of monitoring in the experiment are:

- Monitoring the displacement of the diaphragm wall in depth by the GK-604D-50m inclinometer device of the American Geokon manufacturer;
- The horizontal displacement of the center point on the top of the tube is surveyed by the geodetic method as follows:
 - + Establishment of the geodetic coordinate system that the X and Y axes are respectively parallel to the A and B axes of the inclinometer;
 - + Three benchmarks were drilled down 40 m in the surrounding area;
 - + The total station TCR1201+ is used that has an accuracy of angular measurement $m_\beta = \pm 1.0''$ and an accuracy of distance measurement $m_s = \pm (1 + 1.5D) \text{ mm}$, D is the length of the edge in kilometer;

+ A network is established between the three benchmarks and the monitoring points. All angles and edges are then measured. The coordinates of the observation points are calculated after the adjustment of the network in two periods. The benchmarks are stable, and the mean square error of position m_P of all observation points is less than 2 mm.

Using the calculation process of the integrated solution in two cases of the bottom point of the guide pipe: stability and instability at P05 in two periods. Results are as follows:

+ The displacement of the center at the top of the pipe is measured by an inclinometer (its bottom point is the reference point): 30.97 mm on axis XICL and 0.27mm on axis YICL.

+ The displacement of the center at the top of the pipe is measured by the geodetic method: -24.30 mm on axis XTD and -1.10 mm on axis YTD.

The first case: Assume that the bottom of the inclinometer guide tube is stable:

When the geodetic method is used to monitor the displacement, the mean square error of the position has very high accuracy ($m_P < 2.0$ mm); it can obtain the absolute displacement values because of the stable benchmarks. Therefore, the displacement of the center point on the top of the tube is the actual value. Based on the displacement results, the error of closure is calculated as Eq. (2) with the obtained results of -6.67 mm and 1.37 mm. The closure errors are distributed to all points inside the guide pipe using Eq. (3), so their displacement values are more accurate. Table 1 shows the inclinometer displacement values after the error of P05 is corrected.

Tab. 1. The inclinometer displacement values after correcting the error (point P05).

The monitoring depth (m)	The inclinometer displacement values (mm)		Correction number according to pipe length ratio (mm)		The integrated displacement values (mm)	
	$q_{XICL}^{(i)}$	$q_{YICL}^{(i)}$	$\frac{H_i}{H} \omega_x^{(o)}$	$\frac{H_i}{H} \omega_y^{(o)}$	$q_{XICL-TD}^{(i)}$	$q_{YICL-TD}^{(i)}$
0.0	-30.97	0.27	-6.67	1.37	-24.30	-1.10
0.5	-30.33	0.44	-6.50	1.34	-23.83	-0.90
1.0	-29.62	0.47	-6.34	1.30	-23.28	-0.83
1.5	-28.97	0.49	-6.17	1.27	-22.80	-0.78
2.0	-28.39	0.50	-6.00	1.23	-22.39	-0.73
...
18.0	-6.02	-0.26	-0.67	0.14	-5.35	-0.40
18.5	-4.45	-0.32	-0.50	0.10	-3.95	-0.42
19.0	-2.89	-0.29	-0.33	0.07	-2.56	-0.36
19.5	-1.51	-0.15	-0.17	0.03	-1.34	-0.18
20.0	0.00	0.00	0.00	0.00	0.00	0.00

After all the observation values were corrected for their errors, we could draw a chart of axial displacement. Figure 7 shows the diagram of the P05 position before and after the error is corrected. It shows the inclinometer displacement values according to the depth of the diaphragm wall (the graph line of measuring by inclinometer) and the values with improved accuracy after the inclinometer sensor is integrated with the geodetic method (the graph line of measuring by integration of the inclinometer and geodetic methods).

The second case: Assume that the bottom of the inclinometer guide tube is unstable:

The point at the bottom of the tube is the source. Thus, the inclinometer displacement values of the point at the top of the pipe must be added with the source's displacement value. As mentioned above, the monitoring results by the geodetic method have high accuracy ($m_P < 2.0$ mm), which are determined from stable benchmarks. Thus, the displacement of the center point at the top of the pipe is considered the actual value. The inclinometer observed values are recalculated when the reference point is at the top of the pipe. The geodetic displacement values that are transformed to the inclinometer coordinate system are corrected in all inclinometer values as Eq. (4). The updated results of P05 are shown in Table 2.

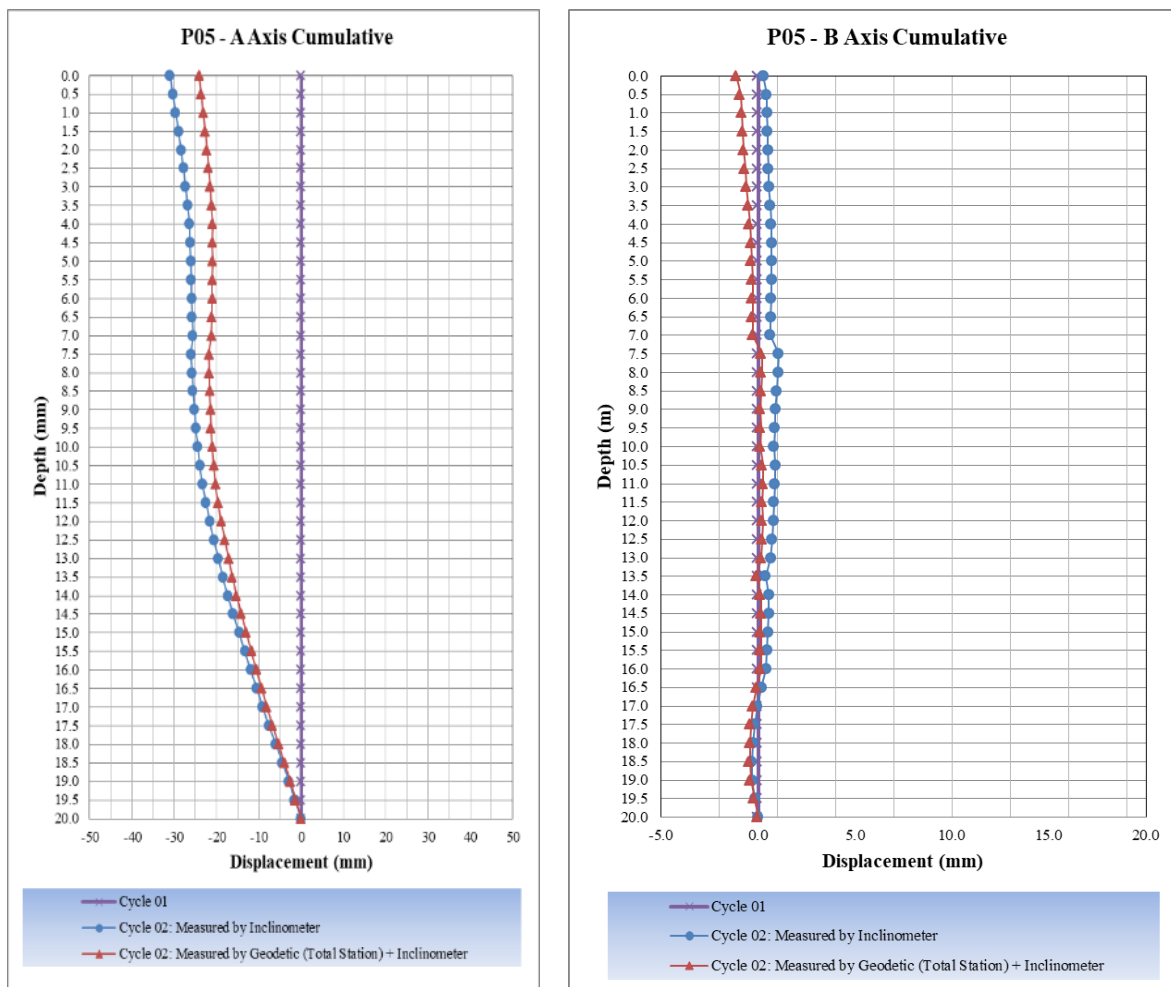


Fig. 7. Charts of P05 observation points before and after correcting the error.

Tab. 2. Displacement values of all observation points measured by the inclinometer after correcting the displacement of the origin.

Monitoring depth (m)	Inclinometer displacement values (mm)		Correction number (mm)		Integrated displacement values (mm)	
	$q_{X_{ICL}}^{(i)}$	$q_{Y_{ICL}}^{(i)}$	$q_{X_{TD-ICL}}^{(o)}$	$q_{Y_{TD-ICL}}^{(o)}$	$q_{X_{ICL-TD}}^{(i)}$	$q_{Y_{ICL-TD}}^{(i)}$
0.0	0.00	0.00	-24.30	-1.10	-24.30	-1.10
0.5	0.64	0.17	-24.30	-1.10	-23.66	-0.93
1.0	1.35	0.20	-24.30	-1.10	-22.95	-0.90
1.5	2.00	0.22	-24.30	-1.10	-22.30	-0.88
2.0	2.58	0.23	-24.30	-1.10	-21.72	-0.87
...
18.0	24.95	-0.53	-24.30	-1.10	0.65	-1.63
18.5	26.52	-0.59	-24.30	-1.10	2.22	-1.69
19.0	28.08	-0.56	-24.30	-1.10	3.78	-1.66
19.5	29.45	-0.42	-24.30	-1.10	5.15	-1.52
20.0	30.97	-0.27	-24.30	-1.10	6.67	-1.37

Table 2 and Figure 8 indicated that the integrated solution can monitor the displacements of all points inside the diaphragm more accurately. In this solution, the origin at the top of the tube is chosen.

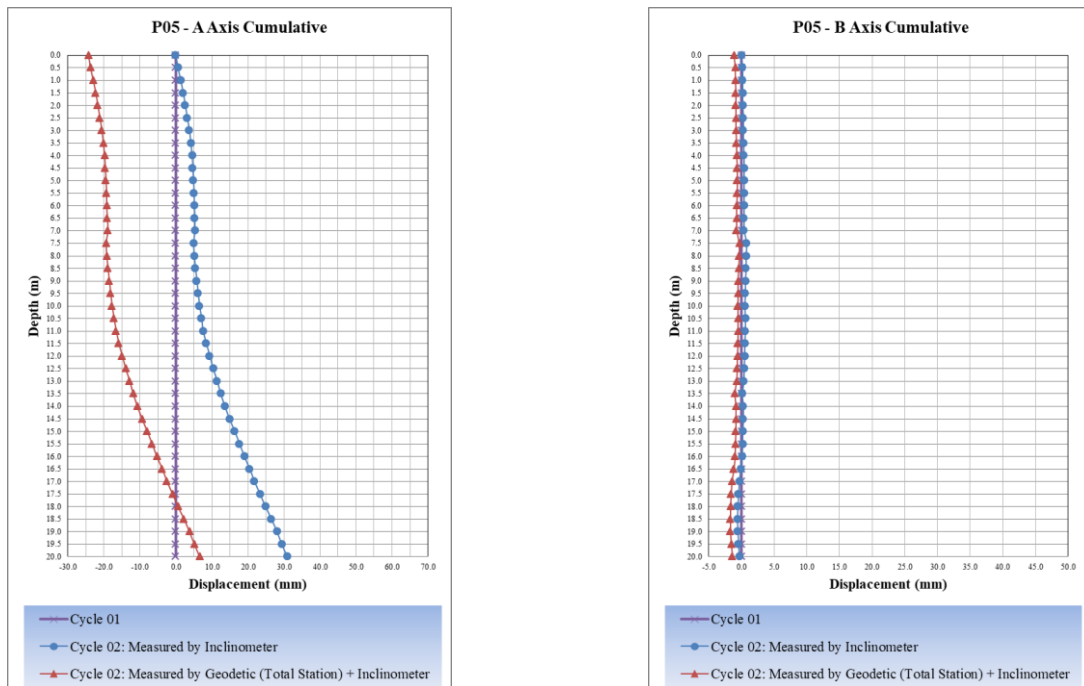


Fig. 8. Charts of P05 point before and after correcting the displacement of the origin.

6. Discussions

In the geotechnical method using inclinometer sensors, the origin is the guide pipe's bottom point, and it is difficult for surveyors to observe. Therefore, this method only determines the relative displacement values of points at different depths inside the diaphragm wall. If the bottom point of the guide pipe is unstable (e.g., because it is installed in the soft ground), the observed values will inaccurately reflect the level of displacement.

The geodetic method can survey the displacement of the center point on the top of the tube with high accuracy, with an error of position less than ± 2.0 mm. Additionally, it can obtain the absolute displacement values.

When an inclinometer is integrated with geodetic methods, the obtained displacements are absolute values. Suppose the guide pipe is not anchored to a stable rock layer. In that case, it is necessary to combine the inclinometer with the geodetic method in monitoring the horizontal displacement of diaphragm walls to achieve more accurate results. In contrast, when the inclinometer guide pipe is attached to a stable rock layer, an inclinometer is used to measure the displacement. Additionally, in some periods, geodetic methods should also be used to check and correct the inclinometer displacement values. This is to improve the reliability of the derived displacement and to avoid costing money.

7. Conclusion

The integration of geodetic methods and inclinometer sensors in monitoring the horizontal displacement of the diaphragm wall of a deep excavation pit on the soft ground helps advance precision of observation (the bottom of the guide pipe is attached to a stable rock layer). In the experiment conducted in this article, the displacement values between the two methods are -6.67 mm on the X-axis and +1.37 mm on the Y-axis.

Choosing the center at the top of the pipe to be the origin for determining precisely displacement of points in the diaphragm wall is allowed. However, if the displacement measured by the inclinometer is smaller than in theory, it is unnecessary to observe geodetic methods.

This integrated method has a good efficiency in monitoring the displacement of diaphragm walls on the soft ground, especially when the center of the bottom of the pipe measured by an inclinometer is unable to affirm the stability to choose as a reference point.

The integrated method can be applied for monitoring different works, such as irrigation-hydroelectric dams, excavation pits, retaining walls, landslides, mining, or in areas with leveled foundations. It is necessary to carefully study the geological engineering documents and the design of the diaphragm wall before deciding to combine geodetic and geotechnical methods to avoid costing money and time.

8. Acknowledgments

The paper was presented during the 6th VIET - POL International Conference on Scientific-Research Cooperation between Vietnam and Poland, 10-14.11.2021, HUMG, Hanoi, Vietnam.

9. References

1. Astm D6230–98. Standard Test Method for Monitoring Ground Movement Using Probe-Type Inclinometers, 2005.
2. Nisha, J.J., Muttharam, M., 2017. Deep excavation supported by diaphragm wall: A case study, *Indian Geotechnical Journal*, 47(3): 373-383.
3. Castelli, F., Lentini, V., 2016. Monitoring of full scale diaphragm wall for a deep excavation. *Proceedings of 1st IMEKO TC-4 international workshop on metrology for geotechnics*. Benevento, Italy, 103-108.
4. Grodecki, M., Toś, C., Pomierny, M., 2018. Excavation supported by diaphragm walls—inclinometric monitoring and numerical simulations. *Czasopismo Techniczne*, 5: 129-140.
5. Chen, S.L., Ho, C.T., Gui, M.W., 2014. Diaphragm wall displacement due to creep of soft clay. *Proceedings of the Institution of Civil Engineers-Geotechnical Engineering*, 167(3): 297-310.
6. Castelli, F., Lentini, V., 2019. Numerical Modelling and Experimental Monitoring of a Full-Scale Diaphragm Wall. *International Journal of Civil Engineering*, 17(6): 659-672.
7. Liu, G.B., Jiang, R.J., Charles, W.N., Hong, Y., 2011. Deformation characteristics of a 38 m deep excavation in soft clay. *Canadian Geotechnical Journal*, 48(12): 1817-1828.
8. Wu, S.H., Ching, J., Ou, C.Y., 2013. Predicting wall displacements for excavations with cross walls in soft clay. *Journal of geotechnical and Geoenvironmental engineering*, 139(6): 914-927.
9. Chen, S.H., Ho, C.T., Gui, M.W., 2014. Diaphragm wall displacement due to creep of soft clay. *Proceedings of the Institution of Civil Engineers-Geotechnical Engineering*, 167(3): 297-310.
10. Teparaksa, W., Teparaksa, J., 2018. Displacement of Diaphragm Wall for Very Deep Basement Excavation in Soft Bangkok Clay. *International Journal*, 14(46): 57-62.
11. Kalkan, Y., Baykal, O., Alkan, R.M., Yanalak, M., Erden, T., 2002. Deformation Monitoring with Geodetic and Geotechnical Methods: A case study in Ambarli Region. *International Symposium on GIS*, 1-12.
12. Tran Khanh, Nguyen Quang Phuc. *Structural deformation and displacement monitoring*. Transportation Publisher, Hanoi, 2010.
13. Diem Cong Huy, Ngo Van Hoi, Tran Ngoc Dong, Nguyen Anh Dung, Dinh Quoc Dan and the other people. *Training curriculum on construction monitoring*. Construction Publisher, Hanoi, 2016.
14. *Guide To Geotechnical Instrumentation*. Durham Geo Slope Indicator, 2004.
15. Pham, K.Quoc and Nguyen, T.Kim Thi 2021. Application of the method of robust estimation by posterior variance in detecting the raw error of geodetic control network (in Vietnamese). *Journal of Mining and Earth Sciences*. 62, 2 (Apr, 2021), 57-64. DOI:https://doi.org/10.46326/JMES.2021.62(2).06.
16. Pham, K.Quoc 2021. Application of statistical test on determining the unstable points in the basic network of horizontal displacement monitoring (in Vietnamese). *Journal of Mining and Earth Sciences*. 62, 1 (Feb, 2021), 35-41. DOI:https://doi.org/10.46326/JMES.2021.62(1).05.

Influence of Single-Phase Voltage Loss and Load Carrying Mode on Mine Drainage Pump Motor in Vietnam

DO Nhu Y¹, NGO Xuan Cuong^{2,*}

¹Hanoi University of Mining and Geology, 18 Vien street, Hanoi, Vietnam

²School of Engineering and Technology, Hue University, Hue, Vietnam

Corresponding author: ngoxuancuong@hueuni.edu.vn

Abstract. Mine drainage pump is the most important load in mining which requires high reliability when operating. Currently, the power supply of a mine drainage pump is connected to the same power line with many nonlinear loads, and is equipped with power electronic converters, which makes the power supply nonsinusoidal. During the working process of a mine drainage pump, the load-carrying factor often changes, and many types of failures occur, among which single-phase voltage loss is the most common problem. In the case of a nonsinusoidal power supply, if a single-phase voltage loss occurs in different load modes, it will greatly affect the working mode of the mine drainage pump leading to influences on the working efficiency, the life of the pump, and sometimes it is necessary to recalculate the protection parameters. This paper studies the influence of single-phase voltage loss and load carrying mode on the working mode of mine drainage pump motor in case the of nonsinusoidal power supply. Research results show that, in the case of nonsinusoidal power supplied with single-phase voltage loss, copper losses in the rotor and stator circuits increase with increases in voltage total harmonic distortion (THD) and load-carrying factor, 5th order reverse harmonic increases copper loss in asynchronous motor the most, and higher harmonic components have less effect on copper loss in the motor. At the same time, the speed ripple decreases with the increase of the motor load factor and decreases in the presence of the 5th order negative sequence harmonic, and increases significantly in the presence of the 7th order positive sequence harmonic. 5th order negative sequence harmonic increases, the torque ripple increases, while the 7th order positive sequence harmonic reduces the torque ripple in the case of single-phase voltage loss. The results of the paper will help improve the operational efficiency of the mine drainage pump in Vietnam's mines.

Keywords: Mine drainage pump, Single-phase voltage loss, Asynchronous motor, Harmonics

1. Introduction

The mine drainage pump is responsible for draining water during the mining process, ensuring timely drainage in mining even in adverse cases such as heavy rain, water breaks. Drainage pump is the most important load with the largest power consumption in mining [1]. Improving the performance of drainage pumps is of interest to many researchers. Drain pump performance needs to be checked periodically and it is always necessary to implement solutions to improve the energy efficiency of the pumping system [2, 3]. The characteristics of mining are wet and harsh environment, strong vibrations on working equipment due to drilling and blasting, transportation and unstable geology. This leads to many problems with the drainage pump motor in the mine, the most common being a single-phase voltage loss. In the case of a single-phase voltage loss, the motor will continue to operate but will also heat up very quickly and it is necessary to have solutions to improve operating efficiency as well as take measures to protect the motor when this operating mode occurs [4, 5, 6].

The progression to a single-phase voltage loss can take a long time from uncertain electrical contacts, loose connections, and gradually progressing to the single-phase voltage loss. The above progression results in an electrical imbalance. Under an unbalanced voltage, the amplitude of the current deviation can be many times larger and generate torque impulse. These problems lead to reduced performance of the motor, overheating, damage [7, 8]. The article [9] studied the impact of unbalanced voltage supply on the performance of a 3-phase induction motor. The results showed that the voltage imbalance leads to reduced motor efficiency and reduces power factor. Unbalanced voltages in a voltage source can lead to problems such as excessive losses, overvoltage, mechanical oscillations, and interference with electrical equipment [10]. Unbalanced voltage has a marked effect on the losses in the induction motor, which greatly affects the winding temperature rise and the slip coefficient. Several literary studies have also shown that the power factor of the asynchronous motor is inversely proportional to the positive sequence, while the efficiency is directly proportional to the positive sequence [11, 12, 13, 14].

The effect of voltage asymmetry on the operation of the asynchronous motor has been analyzed in [15] [16]. Gnacinski et al. [16] revealed that the voltage imbalance causes coil heating much faster than the effects of other power quality standards [17]. The characteristics of the 6kV power network supplying power to mine water pump systems in Vietnam have along outgoing lines, use high-powered equipment, multiple branches, and increasing use of power electronics on the grid, this reduces the quality of the voltage supplied to the drain pump motors and affects the performance characteristics of the motors [18, 19]. The voltage quality of the power supply to a mine water pump motor when connected through the converter is often influenced by harmonic components [20, 21].

In [8], Bhattarai identified power quality problems and their impact on power systems and loads. It was also suggested in that paper that harmonics have a significant influence on the current capacity of various electrical components, such as cables, transformers and power transmission lines and electric motors. The supply of pulse-width modulation inverter causes an additional loss, which is manifested as a temperature rise in the asynchronous motor. The temperature rise due to additional losses is significant compared with machines operated from sinusoidal sources [22]. In [23], the authors have shown the existence of harmonics in power systems generated by non-linear loads, such as power electronic devices, electric arc furnaces, and the presence of this harmonic greatly affects the performance of the asynchronous motor. When powered with a high harmonic voltage, an asynchronous motor will experience increased vibration [24].

The selection of mine drainage pump capacity is based on the rated working capacity of the mine drainage design. However, the drainage pump is operated in different modes depending on the actual requirements of the mine drainage, the quality of mine wastewater changes causing the pump load to change. At the same time, the use of drainage pumps in the whole mining cycle is also the difference in pump capacity compared to the design capacity, which affects the working mode of the mine drainage pump [1]. In [25], the authors have shown the effect of unbalance due to frequency deviation according to the load-carrying factor of the motor on the loss, temperature rise, torque, efficiency of the motor as well as vibration and reliability when the motor is working. Different case studies were presented with different load conditions to study the performance of electromechanical systems widely used in the mining industry [26]. The results indicated that severe torque will be generated on the motor shaft during starting. This severe torque can lead to an effect on the life of the crankshaft if appropriate countermeasures are not taken.

From the above analyses, it is necessary to study the effect of single-phase voltage losses and the load-carrying mode considering the influence of the power supply on the mine drainage pump motor. The research results are important data for users to have suitable operating solutions to improve the operating efficiency and life of the mine drainage pump motor in different operating modes.

2. Materials and Methods

2.1 Model of asynchronous motor

Mine drainage pumps in Vietnam are usually driven by asynchronous motors (AM). The AM electrical part is represented by a quaternary state space model and the mechanical part by a quadratic system [19, 27]. All stator and rotor quantities are in an arbitrary biaxial reference frame (dq frame) in Fig. 1. The physical model is considered to be linear and the inductance is assumed to be constant. Therefore, the saturation of the magnetic circuit is not considered here.

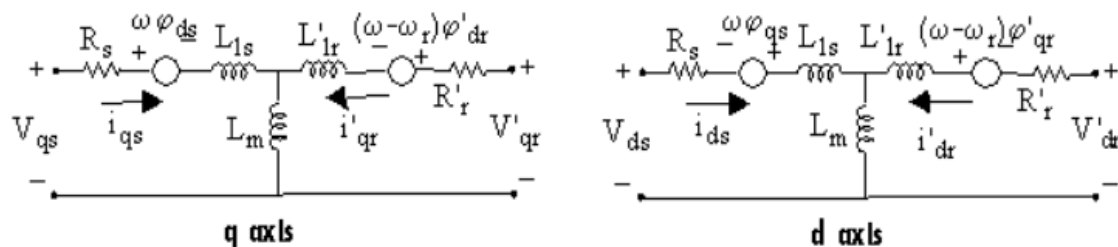


Fig. 1. The AM Model on the qd frame.

Synchronous speed is determined by:

$$N_s = \frac{60 \cdot f}{p} \tag{1}$$

where f - frequency, p - number of double poles. Rated torque is determined by:

$$T_n = \frac{30 \cdot P_n}{\pi \cdot N_n} \tag{2}$$

where P_n - power, N_n – speed.

When the power source has harmonics, power factor (PF) is calculated according to the following relationship:

$$PF = \frac{P_{in}}{\sqrt{P_{in}^2 + Q_{in}^2}} \tag{3}$$

where P_{in} - the active input power in W, Q_{in} – the reactive input power in Var. The mechanical power is calculated according to the following formula:

$$P_{-M} = T_e \cdot \omega_m \tag{4}$$

where T_e - electromagnetic torque in Nm, ω_m - angular velocity of the rotor in rad/s. The mechanical loss is determined according to the following formula

$$P_{loss-m} = F \cdot \omega_m^2 \tag{5}$$

where F represents the friction factor in N.m.s. The losses in the motor mainly occur in the rotor, stator circuit and ferromagnetic losses. In this model of asynchronous motor, ferromagnetic losses are ignored. The copper loss on the rotor is determined by:

$$P_{Cu2} = R'_r (I_{ra}^2 + I_{rb}^2 + I_{rc}^2) \tag{6}$$

where I_{ra} , I_{rb} , I_{rc} - RMS value of rotor current in phase a, b, c, R'_r - rotor resistance. The copper loss on the stator is determined by:

$$P_{Cu1} = R_s (I_{sa}^2 + I_{sb}^2 + I_{sc}^2) \tag{7}$$

where I_{sa} , I_{sb} , I_{sc} - RMS value of stator current in phase a, b, c, R_s - stator resistance.

Finally, we determine the AM efficiency using the direct method as follows:

$$\eta = \frac{P_{-M} - P_{loss-m}}{P_{in}} 100 \tag{8}$$

where P_{in} - the active input power in W, P_{-M} - the total mechanical power of motor in W, P_{loss-m} - the mechanical losses (friction and windage losses), in W.

2.2 Model to evaluate the single-phase voltage loss

Assuming that the asynchronous motor is working, a single-phase voltage loss occurs with a replacement diagram shown in Fig. 2 [4].

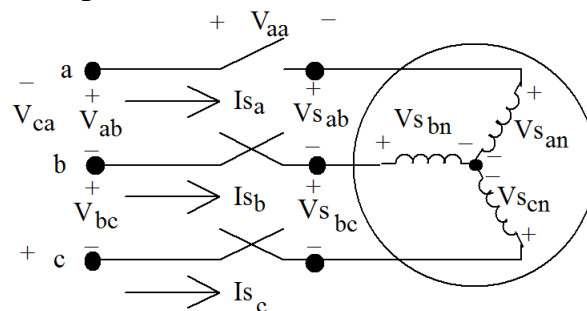


Fig. 2. Loss of phase a of asynchronous motor [4].

where V_{ab}, V_{bc}, V_{ca} - line-to-line voltage of the system, $V_{sab}, V_{sbc}, V_{sca}$ - working line voltage at motor terminal, $V_{s.an}, V_{s.bn}, V_{s.cn}$ - stator line-to-neutral voltage, I_{sa}, I_{sb}, I_{sc} -line current.

When a motor has a single-phase voltage loss, the voltage and current on the motor can be decomposed into the components of positive order (index 1), negative order (index 2) and zero order (index 0). The replacement diagram for single-phase voltage loss is shown in Figure 3.

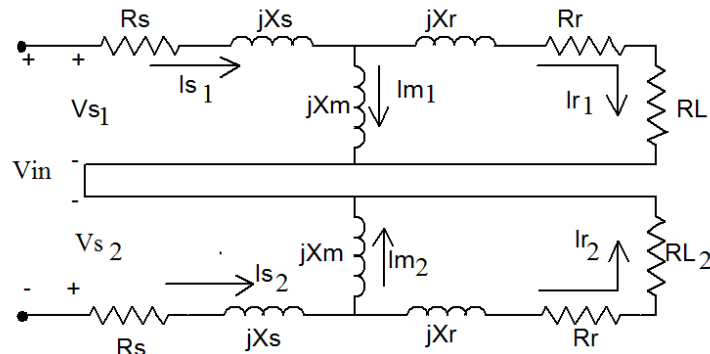


Fig. 3. Sequence Network Connection [4].

where V_{in} - input voltage, R_s, X_s – resistance and reactance of stator circuit, R_r, X_r – resistance and reactance of rotor circuit, X_m - magnetizing reactance, RL – load impedance.

The input voltage is given by:

$$V_{in} = V_{s1} - V_{s2} \tag{9}$$

The input voltage according to the case of phase loss can be calculated as:

$$\begin{aligned} V_{s1} &= \frac{1}{3}(V_{s.an} + aV_{s.bn} + a^2V_{s.cn}); \\ V_{s2} &= \frac{1}{3}(V_{s.an} + a^2V_{s.bn} + aV_{s.cn}) \\ V_{in} = V_{s1} - V_{s2} &= j\frac{\sqrt{3}}{3}(V_{s.bn} - V_{s.cn}) = j\frac{V_{s.bc}}{\sqrt{3}} \end{aligned} \tag{10}$$

Then the negative sequence slip is given by:

$$s_2 = 2 - s_1 \tag{11}$$

The load resistances of the two networks are:

$$\begin{aligned} RL_1 &= \frac{1 - s_1}{s_1} R_r \\ RL_2 &= \frac{1 - s_2}{s_2} R_r = \frac{1 + s_1}{2 - s_1} R_r \end{aligned} \tag{12}$$

The general equation for the input equivalent impedance at the terminals of the networks is given by:

$$Z_{eqi} = Z_{si} + \frac{Z_r - RL_i}{jX_m + Z_r + RL_i} \tag{13}$$

where $i = 1$ for the positive sequence and $i = 2$ for the negative sequence.

The stator sequence currents are:

$$\begin{aligned} I_{s1} &= \frac{V_{in}}{Z_{eq1} + Z_{eq2}} \\ I_{s2} &= -I_{s1} \\ I_{s0} &= 0 \end{aligned} \tag{14}$$

Because the motor is connected to a three-wire delta line, the zero sequence stator current must be zero. The stator input line currents are computed by:

$$\begin{bmatrix} I_{sa} \\ I_{sb} \\ I_{sc} \end{bmatrix} = \begin{bmatrix} 1 & 1 & 1 \\ 1 & a & a^2 \\ 1 & a^2 & a \end{bmatrix} \begin{bmatrix} I_{s0} \\ I_{s1} \\ I_{s2} \end{bmatrix} \quad (15)$$

The sequence rotor currents are determined by:

$$I_{ri} = I_{si} - \frac{jX_m}{jX_m + Z_r + RL_i} \quad (16)$$

- Motor Terminal Voltages:

$$\begin{aligned} V_{s0} &= 0 \\ V_{si} &= Z_{eqi} - I_{si} \end{aligned} \quad (17)$$

The sequence line-to-neutral stator voltages are:

$$\begin{bmatrix} V_{s.an} \\ V_{s.bn} \\ V_{s.cn} \end{bmatrix} = \begin{bmatrix} 1 & 1 & 1 \\ 1 & a & a^2 \\ 1 & a^2 & a \end{bmatrix} \begin{bmatrix} V_{s0} \\ V_{s1} \\ V_{s2} \end{bmatrix} \quad (18)$$

The line-to-line stator voltages are:

$$\begin{bmatrix} V_{s.ab} \\ V_{s.bc} \\ V_{s.ca} \end{bmatrix} = \begin{bmatrix} 1 & -1 & 0 \\ 0 & 1 & -1 \\ -1 & 0 & 1 \end{bmatrix} \begin{bmatrix} V_{s.an} \\ V_{s.bn} \\ V_{s.cn} \end{bmatrix} \quad (19)$$

It needs to be pointed out that the stator line-to-line voltages will not be the same as the secondary line-to-line voltages. Because this voltage will appear across the switch (fuse), it is given by:

$$V_{aa} = V_{ab} - V_{s.ab} \quad (20)$$

- Converted Power

The total converted sequence powers are given by:

$$P_{convi} = 3 \cdot I_{ri}^2 \cdot RL_i \quad (21)$$

We recall that the negative sequence load resistance is a negative number so that the converted negative sequence power will be negative, which adds to the effective rotor power loss. The total converted power is:

$$P_{convi} = P_{conv1} + P_{conv2} \quad (22)$$

- Stator and Rotor Power Losses

The total stator and rotor power losses are:

$$\begin{aligned} P_{loss.rotor} &= 3(I_{r1}^2 + I_{r2}^2)R_r \\ P_{loss.stator} &= 3(I_{s1}^2 + I_{s2}^2)R_s \end{aligned} \quad (23)$$

2.3 Model of harmonics

Drain pump motors in Vietnam's mines are usually powered by power converters (i.e., soft starters or inverters) with the actual form shown in Figure 4. Power converters often cause a large number of harmonics on the grid, so it is necessary to build a harmonic effect on the motor.

The equation for the motor supply voltage can be written as:

$$\begin{aligned} v_a &= V_m \sin \omega t \\ v_b &= V_m \sin \left(\omega t + \frac{2\pi}{3} \right) \\ v_c &= V_m \sin \left(\omega t - \frac{2\pi}{3} \right) \end{aligned} \quad (24)$$

A non-sine waveform can be constructed by adding two or more sine waves. The synthesis of a particular non-sine waveform is a problem of combining signals of appropriate frequency, amplitude, and phase. Using the "Thee Phase Programmable Voltage Source" block in Simulink can generate non-sine waveforms to power an asynchronous motor.



Fig. 4. Power supply of a mine water pump motor in Vietnam: a mine drainage pump (left) and a conversion device (right).

Harmonic is a sinusoidal voltage whose frequency is an integer multiple of the fundamental power system frequency. Harmonics have the positive order ($k_p = 3n + 1$), the negative order ($k_n = 3n + 2$) and the zero order ($k_z = 3n$). In an asynchronous motor, when the motor windings are connected in a three-wire Y configuration with an isolated neutral, zero-sequence current harmonics is null. The total harmonic distortion (THD) in the current can be calculated by:

$$THD = \frac{\sqrt{\sum_{n=2}^{\infty} I_n^2}}{I_1} = \frac{\sqrt{I_1^2 + I_2^2 + I_3^2 + I_4^2 + \dots}}{I_1} \quad (25)$$

Harmonics will affect the motor's losses according to Eq. (6) and Eq. (7), leading to a decrease in motor efficiency.

2.4 Modeling and simulation of research models

The main mine drainage pump motor parameter in this study is the FD450-60x4 motor type, whose nominal data and other characteristic dimensions are indicated in Table 1. This is a 3-phase squirrel cage rotor asynchronous motor, class F insulation, connected in the shape of Y. The model of mine drainage pump is show on Figure 5. We use a 3-phase asynchronous motor model in the Matlab-simulink library, version R2014a. The simulation parameters of the motor are calculated based on the parameters shown in Table 1.

Tab. 1. Main pump specifications FD450-60x4.

Parameter	Value	Parameter	Value
Flow (m ³ /h)	450	Rated power, Pn (kW)	630
Push height (m)	262	Rated voltage, U (kV)	6
Pump efficiency (%)	80	RPM, Nn (rpm)	1493
NPSH (m)	5	Efficiency, η (%)	96.4
Diameter of straws (mm)	450	PF (%)	87
Diameter of push tube (mm)	350	Starting torque multiples	0.8
Total pump weight (kg)	7520	Starting current multiple	6.5

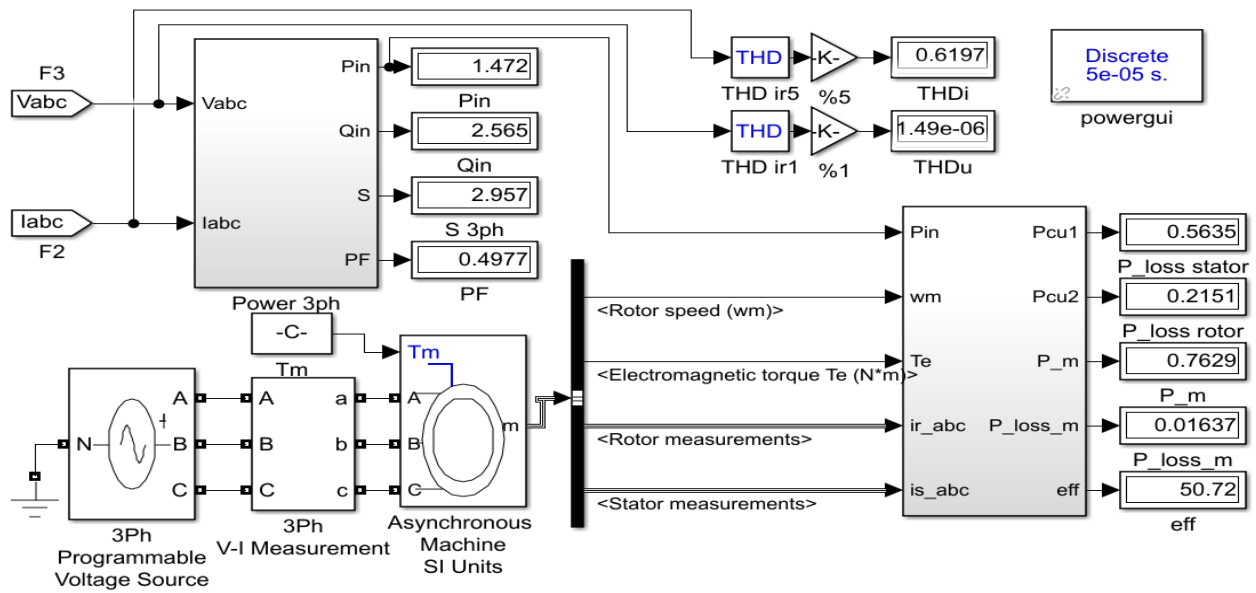


Fig. 5. Simulation model of the mine drainage pump motor.

Investigate motor working in the normal mode with three-phase power supply, we use sinusoidal power supply and motor's load-carrying factor $K=100\%$. The results tested on the model are shown in Table 2 and in Figure 6.

Tab. 2. Parameters of the motor with sinusoidal voltage source.

Motor Load, %	Parameter							
	THD, %	Pcu ₁ , pu	Pcu ₂ , pu	N, rpm	Te, Nm	P_loss_m, pu	PF	η , %
75	0	0.0105	0.0027	1495	3089	0.0166	0.81	96.18
100	0	0.0160	0.0049	1493	4097	0.0165	0.87	96.40
125	0	0.0232	0.0076	1491	5104	0.0165	0.90	96.36

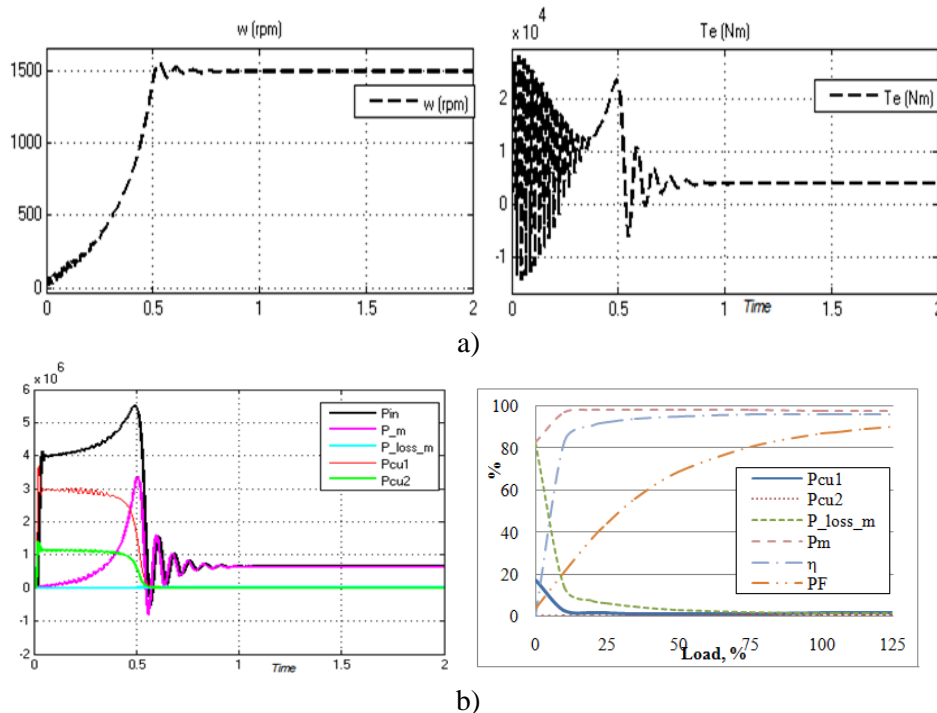


Fig. 6. Characteristics of the drainage pump motor when working in a normal mode with $K=100\%$: a) Motor speed and torque, b) Loss components and motor efficiency.

The results in Tables 2 and Figure 6 are similar to the rated parameters of the motor in Table 1. Thus, the model is built reliably.

3. Results and discussions

Using the simulation model built in Figure 5, the working mode of the mine drainage pump motor in different cases is tested. The proposed case study is a power supply containing harmonic components and single-phase voltage loss at 1.5s, the motor operates with a load factor of 75%, 100%, and 125%, respectively. THD of power supply is considered with values of 5%, 10%, 15%. Copper loss, ripple of torque and speed analyzed in source cases containing 5th, 7th, 11th and 13th harmonic components (corresponding to symbols are H5&LP, H7&LP, H11&LP, H13&LP). The obtained results are presented in Table 3.

Figure 7 shows the transient characteristics of the motor, torque and motor losses in the case of single-phase voltage loss at 1.5s with 100% load and 5th harmonic with THD=5%. From the results shown in Figure 7, when a single-phase voltage loss is accompanied by a harmonized power supply, the speed and torque of the asynchronous motor strongly fluctuate. This causes vibrations when working and an increase in the loss of the motor, leading to a reduction in the efficiency of the motor compared to the normal working mode.

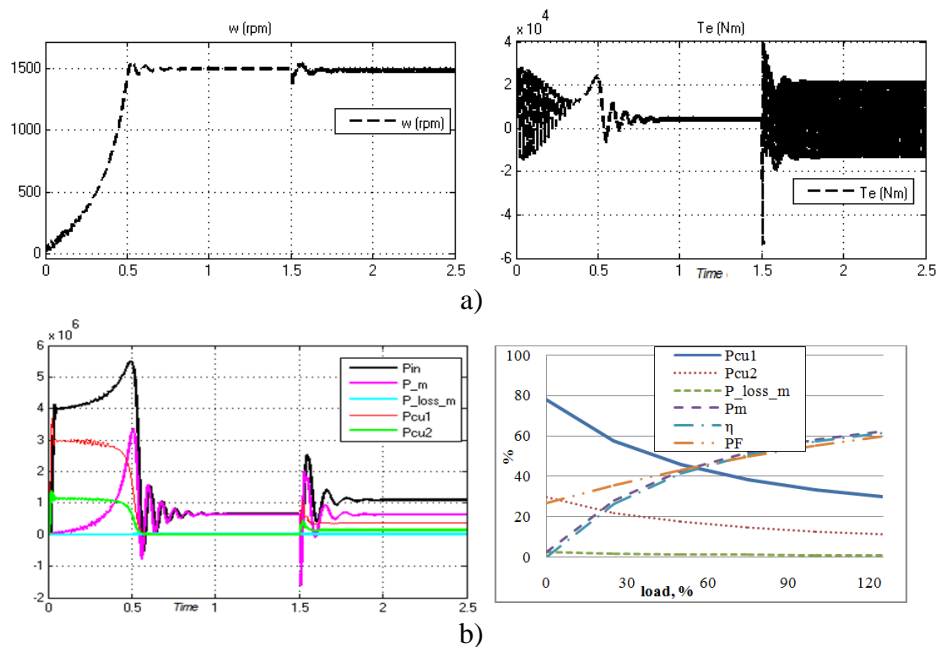


Fig. 7. Characteristics of the drainage pump motor with $K=100\%$ in the case of single-phase voltage loss at 1.5s: a) Motor speed (w) and torque (T_e), b) Loss components and motor efficiency.

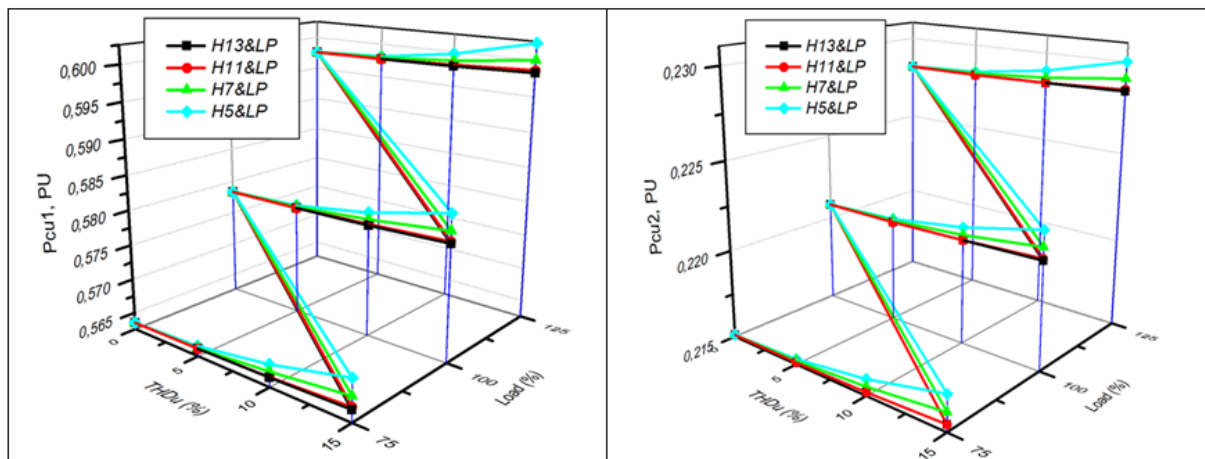


Fig. 8. Copper losses of the motor: Copper loss on stator (P_{Cu1}) and copper loss on rotor (P_{Cu2}).

Tab. 3. Motor performance parameters in the case of a single-phase voltage loss considering the load carrying factor and the effect of harmonics.

Load (%)	Harmonic	THDu, %	P_{cu1} , W pu	P_{cu2} , W pu	Ripple N, %	Torque ripple, %	P_{loss} , W pu	
75	phase loss	0	0.5635	0.2151	1.575	1134	0.7786	
	5 th order harmonic (H5&LP)	5	0.5640	0.2153	1.561	1163	0.7793	
		10	0.5656	0.2159	1.548	1194	0.7815	
		15	0.5682	0.2169	1.536	1226	0.7851	
	7 th order harmonic (H7&LP)	5	0.5637	0.2152	1.586	1112	0.7789	
		10	0.5646	0.2155	1.596	1091	0.7801	
		15	0.5659	0.2160	1.607	1073	0.7819	
	11 th order harmonic (H11&LP)	5	0.5636	0.2151	1.577	1120	0.7787	
		10	0.5639	0.2152	1.578	1112.4	0.7791	
		15	0.5645	0.2154	1.58	1112.8	0.7799	
	13 th order harmonic (H13&LP)	5	0.5636	0.2151	1.573	1146	0.7787	
		10	0.5638	0.2152	1.572	1158	0.779	
		15	0.5642	0.2154	1.571	1171	0.7796	
	100	phase loss	0	0.5783	0.2208	1.561	845	0.7991
		5 th order harmonic (H5&LP)	5	0.5788	0.221	1.547	867.6	0.7998
10			0.5804	0.2216	1.533	891	0.802	
15			0.583	0.2226	1.52	915	0.8056	
7 th order harmonic (H7&LP)		5	0.5786	0.2209	1.572	827.6	0.7995	
		10	0.5794	0.2212	1.583	810	0.8006	
		15	0.5807	0.2217	1.594	795	0.8024	
11 th order harmonic (H11&LP)		5	0.5784	0.2208	1.563	836	0.7992	
		10	0.5788	0.2209	1.565	832	0.7997	
		15	0.5793	0.2211	1.567	833.9	0.8004	
13 th order harmonic (H13&LP)		5	0.5784	0.2208	1.559	853	0.7992	
		10	0.5786	0.2209	1.557	861	0.7995	
		15	0.579	0.221	1.555	871	0.8	
125		phase loss	0	0.5976	0.2282	1.544	669.13	0.8258
		5 th order harmonic (H5&LP)	5	0.5981	0.2284	1.53	687.46	0.8265
	10		0.5997	0.2290	1.516	706.35	0.8287	
	15		0.6023	0.230	1.503	725.73	0.8323	
	7 th order harmonic (H7&LP)	5	0.5979	0.2283	1.556	654.72	0.8262	
		10	0.5987	0.2286	1.567	640.52	0.8273	
		15	0.6	0.2291	1.579	626.83	0.8291	
	11 th order harmonic (H11&LP)	5	0.5977	0.2282	1.547	663.18	0.8259	
		10	0.5981	0.2283	1.549	661.59	0.8264	
		15	0.5986	0.2285	1.552	664.17	0.8271	
	13 th order harmonic (H13&LP)	5	0.5977	0.2282	1.542	674.44	0.8259	
		10	0.5979	0.2283	1.54	680.84	0.8262	
		15	0.5983	0.2284	1.537	687.95	0.8267	

From the results in Table 3, a graph depending on the working parameters of the motor is built. Figure 8 shows that copper losses in the rotor and stator circuits increase as the load-carrying factor and the voltage THD increase. When the motor loses single-phase voltage, the losses in the motor increase, and are highest in the case of a power source containing 5th harmonics. The increase in the THD harmonic index makes the motor loss increase. Therefore, it is necessary to limit the 5th harmonic component and

reduce the harmonic amplitude in the power supply network to reduce the losses in the motor.

When the mine drainage pump motor with 75% load factor is working under a power supply containing 5th harmonics with THD={5%, 10%, 15%}, the stator copper loss increases by {1.05, 1.20, 1.45} times and the rotor copper loss increases by {1.07, 1.29, 1.66} times respectively compared with the symmetric sine power supply case. When the mine drainage pump motor with 100% load factor is working under a power supply containing 5th harmonics with THD={5%, 10%, 15%}, the stator copper loss increases by {1.03, 1.13, 1.29} times and the rotor copper loss increases by {1.04, 1.16, 1.37} times respectively compared with the symmetric sine power supply case.

When the mine drainage pump motor with 125% load factor is working under a power supply containing 5th harmonics with THD={5%, 10%, 15%}, the stator copper loss increases by {1.02, 1.09, 1.20} times and the rotor copper loss increases by {1.03, 1.11, 1.24} times respectively compared with the symmetric sine power supply case. When the mine drainage pump motor is overloaded with a load carrying factor of 125%, if a single-phase voltage loss occurs, the total copper loss in the motor will increase to 3.3% compared to the total copper loss when the single-phase voltage loss occurs at rated load $K=100%$ and increases 39.8 times more than the rated mode without phase loss.

When the motor is under-loaded with a load-carrying factor of 75%, if a single-phase voltage loss occurs, the copper loss in the motor will be reduced by more than 2.7% compared to the total copper loss in phase loss at the rated load $K=100%$ and increases 37.3 times more than that in the rated mode without phase loss. Losses in the motor produce heat that heats the motor, reducing efficiency, lifetime, and causing motor damage. Thus, when a single-phase voltage loss occurs, there must be a suitable motor protection method according to the load mode as well as the quality of the power supply to the motor.

Figure 9 shows speed ripple and torque ripple. Speed ripple is defined as the difference in the percentage between the maximum and minimum speeds relative to the mean speed. Torque ripple is defined as the difference in the percentage between the maximum and the minimum torques compared to the average torque.

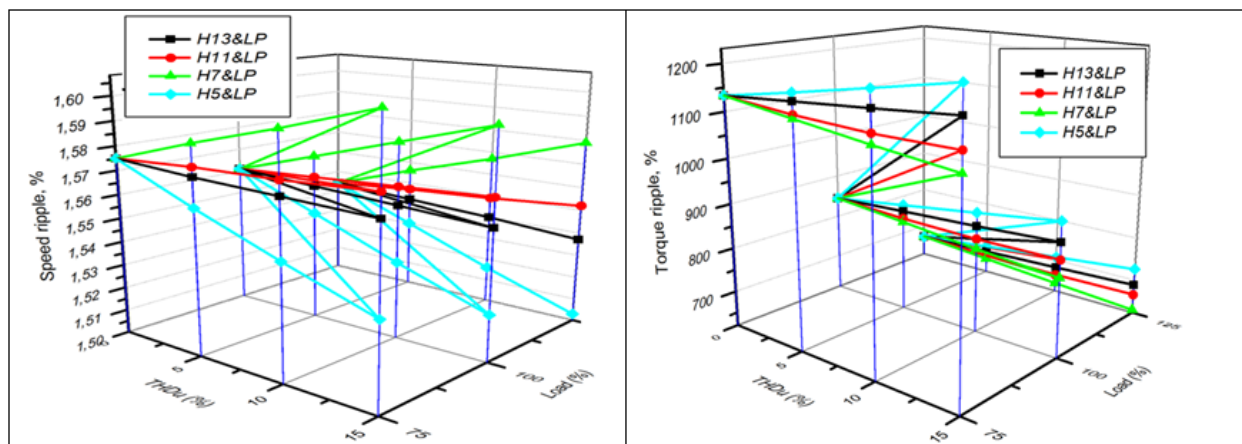


Fig. 9. Mechanical characteristics: Speed ripple and torque ripple.

Speed ripple decreases when a 5th order inverse harmonic is present and increases significantly when there is a 7th order harmonic in the case of a single-phase voltage loss. Speed ripple decreases with the increase of the load-carrying factor of the motor. As the 5th order harmonic increases, while the torque ripple increases leading to an increase in the vibration, the 7th order harmonic reduces the torque ripple in the case of single-phase voltage loss.

In the case when the power supply contains harmonics with the load factor $K=\{75\%, 100\%, 125\% \}$, the speed and torque ripples in the motor reach the highest of 0.0749% and 161.87% respectively. The torque ripple in the case of single-phase voltage loss with rated load ($K=100%$) is 1.26 times higher than the under-load case ($K=75%$) and 0.75 times lower than in the overload case ($K=125%$). In addition, the torque ripple in this case is 23 times higher than in the normal working case

The speed ripple in the case of single-phase voltage loss with rated load ($K=100%$) is 1.01 times higher than in the overload case ($K=125%$) and 0.99 times lower than in the under-load case ($K=75%$). In

addition, the speed ripple in this case is 113 times higher than in the normal working case.

4. Conclusions

The paper has presented the influence of the single-phase voltage loss and the load-carrying mode on the working mode of the mine drainage pump motor in the nonsinusoidal power supply case. The results showed that when the single-phase voltage loss occurs, the speed and torque of the asynchronous motor decrease and fluctuate strongly, the copper losses on the stator and the rotor increase strongly, leading to an increase in the total loss in motor even in the case of underload, full load or overload.

In the case of nonsinusoidal power supply with single-phase voltage loss, copper losses in the rotor and stator circuits increase with increased voltage THD and load-carrying factor. The 5th order reverse harmonic increases copper loss in asynchronous motor the most. Higher harmonic components have less effect on copper loss in the motor.

The speed ripple decreases with the increase of the motor load factor. Additionally, it decreases in the presence of the 5th order negative sequence harmonic but increases significantly in the presence of the 7th order positive sequence harmonic. If the 5th order negative sequence harmonic increases then the torque ripple increases. In contrast, the 7th order positive sequence harmonic reduces the torque ripple in the case of single-phase voltage loss.

From the above analyses, the study of single-phase voltage loss in the case of nonsinusoidal power supply in the mine pump motor with different load-carrying modes is essential to determine the loss, working efficiency, thereby recommending users to have a suitable operating solution to improve the life of the mine drainage pump motor.

5. Acknowledgements

Paper was presented during the 6th VIET-POL International Conference Scientific-Research Cooperation between Vietnam and Poland, 10-14.11.2021, HUMG, Hanoi, Vietnam.

6. References

1. Ovchinnikov, N.P., 2020. Recommendations for improving the operation efficiency of electric pumping units of mine drainage installations. In IOP Conference Series: Earth and Environmental Science. 548(5): 20-48.
2. Shang, D., 2017. Application research on testing efficiency of main drainage pump in coal mine using thermodynamic theories. International Journal of Rotating Machinery.
3. Papa, F., Radulj, D., Karney, B., Robertson, M., 2014. Pump energy efficiency field testing and benchmarking in Canada. Journal of Water Supply: Research and Technology-AQUA, 63(7): 570-577.
4. Kersting, W.H., 2005. Causes and effects of single-phasing induction motors. IEEE Transactions on Industry Applications, 41(6).
5. AQ 1012-2005 The Main Drainage System Safety Testing Inspection Specifications in Coal Mine. 2005. China Standards Press, Beijing, China.
6. Samir, M., Singh, G., Ahmed, N., Ahmed, H., 2013. Dynamic Performance Analysis of Three Phase Induction Motor with Single Phasing. In Proceedings of the Conference on Advances in Communication and Control Systems, Atlantis Press.
7. Donolo, P., Bossio, G., De Angelo, C., Garcia, G., Donolo, M., 2016. Voltage unbalance and harmonic distortion effects on induction motor power, torque and vibrations. Electric power systems research.
8. Bhattarai, P.D., 2013. Study on effects of supply voltage asymmetry and distortion on induction machine. A thesis, the Louisiana state University and Agricultural and Mechanical College. Faculty of the Louisianan State University and Agricultural and Mechanical College.
9. Lee, C.Y., 1999. Effects of unbalanced voltage on the operation performance of a three-phase induction motor. IEEE Transactions on Energy Conversion, 14(2): 202-208.

10. Mirabbasi, D., Seifossadat, G., Heidari, M., 2009. Effect of unbalanced voltage on operation of induction motors and its detection. In 2009 International Conference on Electrical and Electronics Engineering-ELECO. 1-189, IEEE.
11. Kersting, W.H., Phillips, W.H., 1997. Phase frame analysis of the effects of voltage unbalance on induction machines. *IEEE Transactions on Industry Applications*, 33(2): 415-420.
12. Gnacinski, P., 2008. Effect of unbalanced voltage on winding temperature, operational life and load carrying capacity of induction machine. *Energy Conversion and Management*, 49(4): 761-770.
13. Wang, Y.J., 2001. Analysis of effects of three-phase voltage unbalance on induction motors with emphasis on the angle of the complex voltage unbalance factor. *IEEE Transactions on energy conversion*, 16(3): 270-275.
14. Dekhandji, F.Z., Refoufi, L., Bentarzi, H., 2017. Quantitative assessment of three phase supply voltage unbalance effects on induction motors. *International Journal of System Assurance Engineering and Management*, 8(1): 393-406.
15. Quispe, E., Gonzalez, G., Aguado, J., 2004. Influence of unbalanced and waveform voltage on the performance characteristics of three-phase induction motors. In: *Proceedings of international conference on renewable energy and power quality applications*. Barcelona: Espana.
16. Gnaciński, P., Peplinsski, M., Hallmann, D., Jankowski, P., 2019. Induction cage machine thermal transients under lowered voltage quality. *IET Electric Power Applications*, 13(4): 479-486.
17. NEMA. Standard publications No. MG1. Motors and generators. Washington: published by national electrical manufactures association; 1993. Part 21 and part 30, 1-2.
18. Ngo, X.C., Do, N.Y., Tran, Q.H., 2020. The Influence of Voltage Quality on Asynchronous Motor Performance of EKG Excavator in Open Pit Mines–Vinacom. *Inżynieria Mineralna*, 16(1): 139-145.
19. Nguyen, N. X. and Le, T. X., 2017. Evaluating effect of the voltage resonant caused by harmonics of nonlinear loads to capacitor banks located on Nam Mau Coal Company's 6kV electric grid (in Vietnamese), *Journal of Mining and Earth Sciences*, 58(2): 128-136, Available from: <http://jmes.humg.edu.vn/en/archives?article=784>.
20. Do, Y. N., Le, T. X., Nguyen, N. B. and Ngo, T. T., 2020. Impact of asymmetrical phenomena on asynchronous three-phase motors in operation mode, *Journal of Mining and Earth Sciences*, 61(3): 68-74, [https://doi.org/10.46326/JMES.2020.61\(3\).08](https://doi.org/10.46326/JMES.2020.61(3).08).
21. Sousa, S.V., Cabello, E.JJ., Sagastume, G.A., Cabello, U.MJ., 2019. Assessment of the energy efficiency estimation methods on induction motors considering real-time monitoring. *Measurement*, 136, 237-247.
22. Ding, X., Mi, C.C., 2011. Impact of inverter on losses and thermal characteristics of induction motors. *International Journal of Power Electronics*, 3(6), 641-651.
23. Al-Badri, M., Pillay, P., Angers, P., 2017. A novel in situ efficiency estimation algorithm for three-phase induction motors operating with distorted unbalanced voltages. *IEEE Transactions on Industry Applications*, 53(6), 5338-5347.
24. Yacamini, R., Chang, S.C., 1995. Noise and vibration from induction machines fed from harmonic sources. *IEEE Transactions on energy conversion*, 10(2), 286-292.
25. El-Kharashi, E., Massoud, J.G., Al-Ahmar, M.A., 2019. The impact of the unbalance in both the voltage and the frequency on the performance of single and cascaded induction motors. *Energy*, 181: 561-575.
26. Amin, K.E., Hamouda, R.M., Abu-Siada, A., El Dessuki, M.A., 2016. Electromechanical oscillations of common-shaft cascaded induction motors driving a large mechanical load. *Eighteenth International Middle East Power Systems Conference (MEPCON)*, pp. 645-650, IEEE.
27. Beleiu, H.G., Maier, V., Pavel, S.G., Birou, I., Pică, C.S., Dărab, P.C., 2020. Harmonics Consequences on Drive Systems with Induction Motor. *Applied Sciences*, 10(4): 1528.

Method of Air Temperature Forecast in Mechanized Longwall Workings in the Conditions of Vietnamese Mines

TRUONG Tien Quan^{1, 2, *}, Rafał ŁUCZAK¹, Piotr ŻYCZKOWSKI¹, Marek BOROWSKI¹

¹ AGH University of Science and Technology, Kraków, Poland

² Institute of Mining Science and Technology, Hanoi, Vietnam

Corresponding author: truongtienquan@gmail.com

Abstract. In the most recent years, the Vietnam National Coal - Mineral Industries Holding Corporation Limited (VINACOMIN) has been dynamically developing mechanization technologies in underground coal mines. The climatic conditions of Vietnam, as well as increasing the depth of the coal seams and the production capacity, contribute to an air temperature increasing in mining excavations. The article presents statistical equations enabling air temperature forecasting at the outlet of mechanized longwall workings. The results of numerical calculations, obtained from the solutions of the adopted mathematical descriptions, were compared with the measurement results and the statistical significance of the obtained deviations was determined. The performed analysis allowed to assess the practical usefulness of the adopted model for the air temperature forecasting in the workings of mechanized underground mines in Vietnam. The presented method can be used as a tool for mining services in the fight against the climate threat in underground excavations.

Keywords: Climatic conditions, Temperature forecasting, Statistical data analysis

1. Introduction

Air temperature is one of the most important variables for environmental conditions in an underground mine. Environmental conditions in underground mine workings are critical to the health, safety and efficiency of miners, as well as to the operation of machinery and equipment. These factors must be taken into account when planning mining.

According to the regulations in force in Poland, the permissible air temperature in the workplace should not exceed 28°C [1], and in Vietnam - the maximum air temperature is 30°C [2]. In order to achieve the climatic conditions in the mine workings required by the regulations, it is necessary to ensure proper airflow or use cooling devices. However, it is not possible to provide the required and time invariant microclimate conditions in an underground mine. Very often the mine ventilation system is ineffective and insufficient due to limitations related to the maximum air velocity specified by mining regulations and the topology of the ventilation network. In addition, an increase in the power of energomechanical equipment in high performance longwall systems contributes to an increase in temperature and causes changes in the microclimate at workplaces [3, 4, 5, 6]. Underground mines in Vietnam, Poland as well as around the world are exploiting deposits at increasing depths and using more advanced mechanised systems as global demand for minerals continues to drive rising production rates.

Only a deep analysis of air parameters, heat sources, operating conditions and energomechanical equipment used in longwall areas can be used to predict air temperature. Based on the forecast air temperature, technical and organisational measures can be taken to achieve the required air parameters. Besides, the improvement and adjustment of the ventilation system and the use of cooling equipment will contribute to ensuring microclimate parameters at workplaces.

Currently, the prediction of air temperature in underground mine workings is performed using various models, taking into account the characteristic parameters of the workings and the prevailing climatic conditions. Shiyue Wu et al. [4] proposed mathematical models to predict temperatures in groups of workings in an underground mine, such as: vertical workings (e.g. shaft), horizontal and inclined workings (e.g. crosscut, drift, gallery, ramp, slope mine, etc.), corridor faces and longwalls. Air parameters in the corridor workings were also predicted using CLIMSIM software developed at the University of Nottingham [7]. The CLIMSIM model was developed to simulate climate conditions in workings with streamlined air currents. In 2004, the authors modified the mathematical model to predict climatic conditions in blind workings with separate ventilation [8]. A model of environmental and climatic parameters in mine workings was developed and written in C++ [9]. Artificial Neural Network (ANN) based on nonlinear autoregressive

time series algorithm with external input (NARX - Nonlinear Autoregressive Exogenous) was applied as a novel method to predict temperature in mining and ventilation shafts. In [10], an ANN model based on the NARX algorithm is presented for predicting air temperature at the shaft station and for assessing air quality [11]. The models for predicting the temperature in the workings use the principles of energy conservation and it is necessary to consider the heat sources such as autocompression of air, mining machinery and equipment, heat input from the rock mass to the air, etc. The prediction of temperature in the streamlined air current is determined from a linear regression model in which the dependent variable includes inlet temperature, volume air flow rate, and working length [12]. Compared with measured results, these models achieve sufficient accuracy for mining to predict air temperature in pits. However, in order to improve the accuracy of air temperature prediction modeling, more local heat sources in mine workings should be considered.

This paper presents an integrated approach for predicting air temperature at the outlet of mechanised longwalls in Vietnam using statistical models. The main goal is to create accurate linear and nonlinear equations between the dependent variable and the independent variables. In these equations, the dependent (explained) variable is the outlet air temperature (t_p). On the other hand, the independent (explanatory) variables are: air temperature at the longwall inlet (t_o), relative humidity (φ), volume air flow rate (V), heat source power (Q) and working depth (z). The thermodynamic parameters of working air, volume air flow rate, and working depth are mostly well known or easily measured by ventilation and power services at the mine. Therefore, the criteria given in this paper for predicting the air temperature at the outlet of mechanised longwalls can be useful for temperature prediction by ventilation services. The models presented can serve as a tool for mine services to deal with climate hazards in underground workings in Vietnamese underground mines.

2. Research results of selected mechanised longwalls in Vietnam

By the end of 2021, most underground coal mines in Vietnam will use mechanised mining [13]. Mechanised longwalls use machines and equipment that have high electrical power, such as in Ha Lam mine (the total power of the electrical equipment working in the I-11-16 mechanised longwall was 1503 kW) [14], Duong Huy coal company (in the TT-11-6 mechanised longwall, the total power of electrical equipment was 1389.5 kW) [15], the total power of electrical equipment used in the working was 1689 kW in the I-8-3A mechanised longwall in Vang Danh mine [16], etc. Mechanised longwalls were also ventilated with the system at U. The volume air flow rate was high and varied from 1045 to 1609 m³/min. The average working depth of the studied longwalls (calculated from the ground surface) varies from 163.2 to 293.2 m. The primary temperature of the rock mass in the excavated workings ranged from 30.9 to 32.9°C. On the other hand, daily coal extraction from these longwalls averaged approx. 1150 to 1975 Mg. Figure 1 shows the ventilation scheme of the I-8-3A mechanised longwall area in Vang Danh mine. The figure shows the layout of the excavations with the direction of air flow marked on it. Besides, points P1 and P2 mark the places where air parameters are measured.

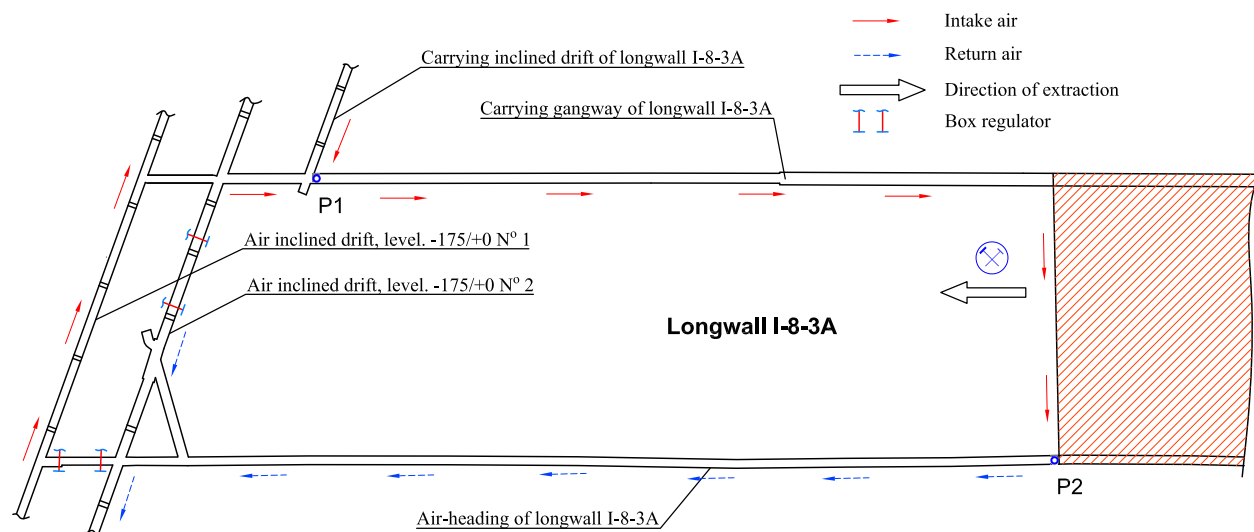


Fig. 1. Diagram of ventilation in the area of the I-8-3A longwall of deposit No. 8 in the Vang Danh mine, P₁ - inlet to the longwall region; P₂ - outlet from the longwall [16].

To create a mathematical model using statistical tools to predict the air temperature at the outlet of longwalls, the data of measurement points P1 and P2 from mining workings in Vang Danh, Ha Lam, Duong Huy mines were used. Ventilation measurements were taken at the designated measuring stands, including measurements of the air velocity and the area of working cross-sections to calculate the volume air flow rate (*V*), measurements of the air temperature (*t_i*) at the inlet (at point P1) and the air temperature (*t_p*) at the outlet (at point P2), measurements of the relative humidity of the air (*φ*). Heat source power (*Q*) was determined based on the calculation of heat from equipment, dredged material transport process and coal oxidation. The depth of the workings was determined by the average depth values of the longwall working sections to the surface. The data used is from May 2018 to September 2020. The results of air temperature measurements at the longwall outlet and air parameters at the inlet, heat source power, and working depth for all 198 alternatives are shown in Figure 2.

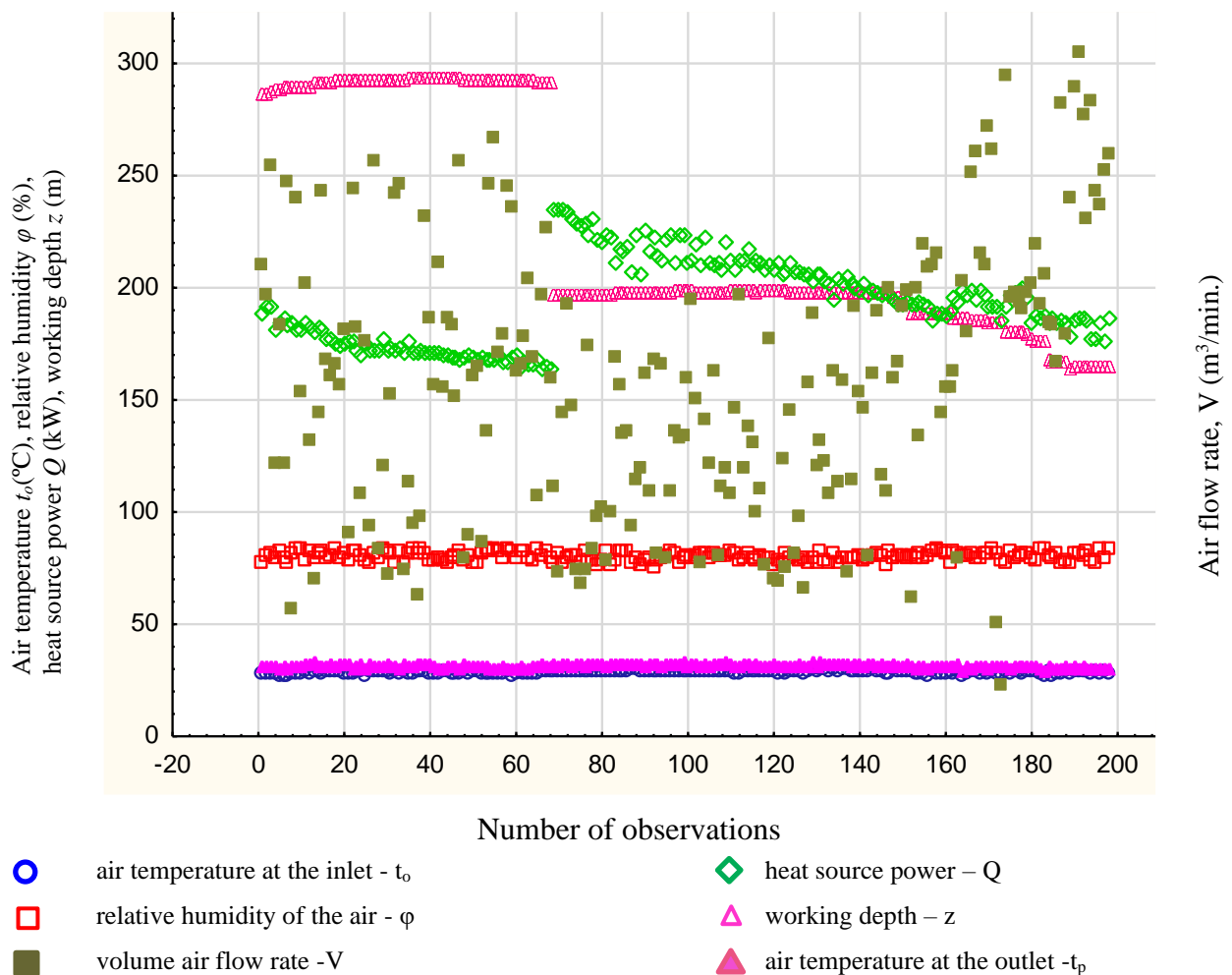


Fig. 2. Results of measurements of air temperature at the longwall outlet and air parameters at the inlet, heat source power and working depth used.

3. Analyses of basic statistical parameters

This paper analyses and evaluates the influence of technical and thermodynamic factors on the variation of air temperature at the outlet of mechanised longwalls. All independent variables and the dependent variable were verified for the type of statistical distribution by comparing them with a standardised normal distribution. Descriptive statistics characterise parameters such as arithmetic mean, geometric mean, median, mode, mode count, minimum, maximum, standard deviation, coefficient of variation, skewness, kurtosis.

When data are not normally distributed and measurements are at best expressed on an ordinal scale, then

the calculation of standard descriptive statistics (e.g. mean, standard deviation) is not the best way to represent data collectively. Nonparametric statistics and distributions allow us to define a number of different measures of position (mean, median, mode, etc.) and dispersion (variance, mean deviation, fractional interval data, etc.), thus providing a complete picture of the variability of the data. Nonparametric statistics and distributions allow the calculation of a wide range of different measures of location, thus giving a complete picture of the data [17, 18]. Table 1 shows the basic descriptive statistics determined for the variables analysed for the mechanised longwalls.

Tab. 1. Descriptive statistics of predictors and dependent variable for mechanised longwalls in a 198 element study sample.

Parameter	Air temperature at the inlet, t_o [°C]	Relative air humidity, φ [%]	Volume air flow rate, V [m ³ /min]	Power heat source, Q [kW]	Working depth, z [m]	Air temperature at the outlet, t_p [°C]
Arithmetic mean	28.552	80.114	1317.343	193.365	225.320	31.141
Geometric mean	28.546	80.090	1311.994	192.456	220.328	31.132
Median	28.7	80.1	1319.0	192.3	198.0	31.2
Mode	29.1	79.4	Multiple	172.2	Multiple	31.2
Mode count	22	8	3	4	10	14
Minimum	26.8	75.5	1045.0	163.6	164.2	28.9
Maximum	29.7	83.9	1609.0	234.7	293.2	33.1
Standard deviation	0.5986	1.9720	119.3295	18.8999	49.0107	0.7796
Coefficient of variation	2.0966	2.4615	9.0583	9.7742	21.7516	2.5033
Skewness	-0.7223	-0.0315	0.2091	0.2845	0.5522	-0.3652
Kurtosis	0.1296	-0.8484	-0.6425	-0.9355	-1.5285	-0.0245

It is clear from this table that there is not much difference between the arithmetic mean and the geometric mean. Except for the z variable, the differences between the arithmetic mean and the median are very small. For the working depth variable (z), this difference is 27.32 m, which is approx. 12%. For the individual variables, the largest difference in standard deviation was determined for the working depth and is approximately 22%. When evaluating measures of clustering and dispersion and inferring the normality of the data distribution, kurtosis and skewness deserve attention. The analysis of skewness (asymmetry of distribution) and kurtosis (flattening of distribution) measures allows us to conclude that in all cases we are dealing with normal distributions or distributions close to normal ($|\text{skewness}| < 1.5$, $|\text{kurtosis}| < 3$) [19]. For all variables, the skewness value ranges from -1.0 to 1.0. Analysis of the flattening measures showed that the distributions of all variables are close to the normal distribution in this respect. The modal value, or dominant, is the value that occurs most often, with the highest probability. For volume air flow rate and working depth, the distribution shows features of multiple mode. Multiple mode is common; in fact, many physical phenomena have multiple mode distributions. This regularity of a characteristic often occurs in situations where the human factor and the repeatability of a phenomenon play a role in the measurement procedure [20, 21].

According to the [22, 23] important element of variable description is the shape of its distribution, which informs about the number of values of this variable in different areas of its variability. The normal distribution (with its characteristic "bell curve" shape, symmetrical with respect to the mean) is a theoretical probability distribution commonly used in statistical inference as an approximation to the sample

distribution. The nature of the distributions of the measurement data was apparently examined on the basis of the prepared histograms and using the statistical Kolmogorov-Smirnov test modified by Lilliefors and the Shapiro-Wilk test at the 0.05 significance level. Figs. 2-7 present graphs in the form of histograms of the variation of the values of all the variables used in the statistical analysis for the mechanised longwalls. The figures also show the results of the performed tests of normality of distributions, the symbols used mean respectively: K-S - Kolmogorov-Smirnov test, d - value of K-S test statistic, S-W - Shapiro-Wilk test, W - value of S-W test statistic, p - significance level.

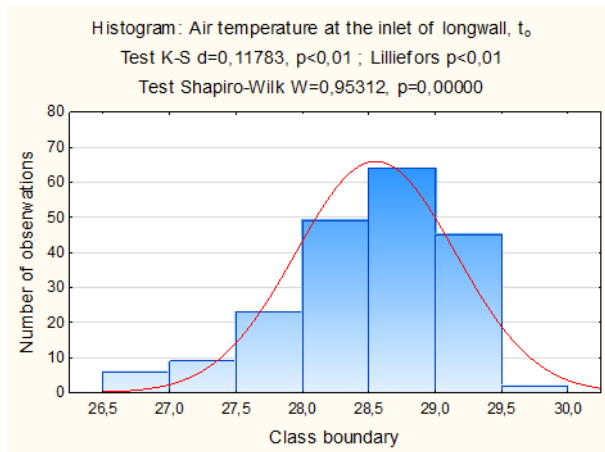


Fig. 3. Air temperature distribution at the outlet for mechanised longwalls.

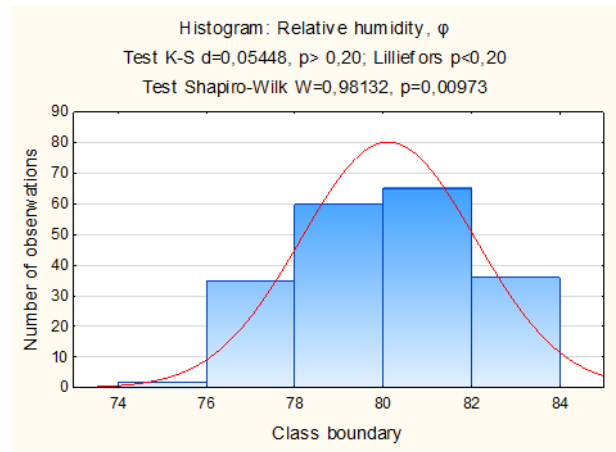


Fig. 4. Air humidity distribution for mechanised longwalls.

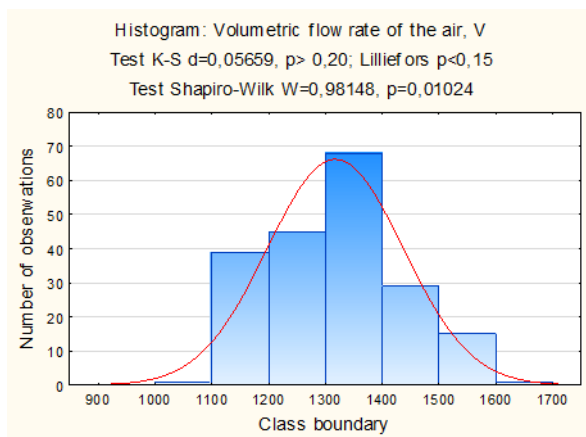


Fig. 5. Volume air flow rate distribution for mechanised longwalls.

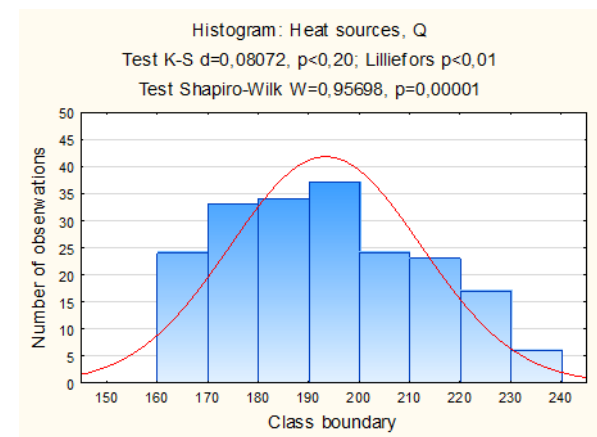


Fig. 6. Power distribution of heat power sources for mechanised longwalls.

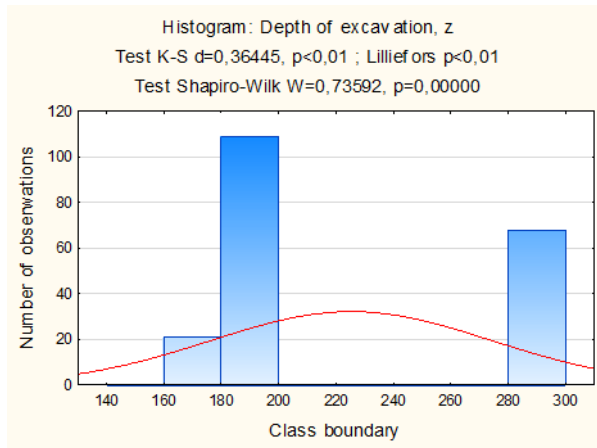


Fig. 7. Working depth distribution of for mechanised longwalls.

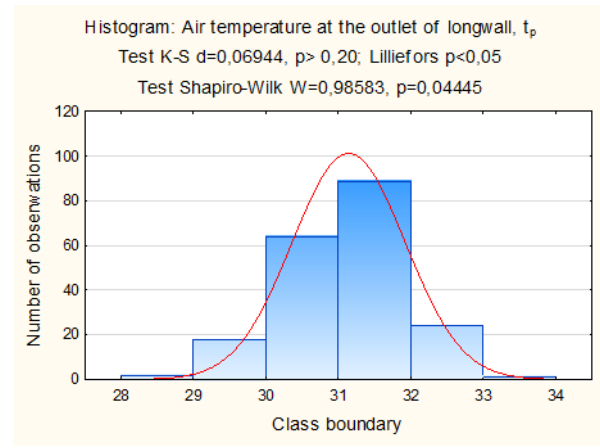


Fig. 8. Air temperature distribution for mechanised longwalls.

Based on the graphs and Shapiro-Wilk test results for all variables, the significance level values were found to be less than 0.05. Therefore, the H_0 hypothesis was rejected in favor of the alternative hypothesis that the variables t_o , φ , V , Q , z , t_p are not normally distributed. For the Kolmogorov-Smirnov test, the value of p-significance is also less than 0.05. Therefore, like the Shapiro -Wilk test, the H_0 hypothesis is rejected and the variables t_o , φ , V , Q , z , t_p do not have a normal distribution. However, by visually evaluating the test values obtained for these variables and the shape of the graph, it can be concluded that the distributions of these variables are close to a normal distribution. For variable (z), it can be observed that values between 180-200 m and 280-300 m are dominant, as there is not much variation in the level of coal seams and their exploitation in the longwall region. The difference in depth is due to the change in depth of the inlet and outlet of the mining longwall.

After an initial multiple regression analysis of the first model, several residuals were found that did not fit the standardised straight line. Which shows that there are outliers in the model. These values reduce the estimation efficiency of the linear regression model. On this basis, 30 variants were eliminated from the model. Table 2 collects the basic descriptive statistics determined for the 168 element sample.

Tab. 2. Descriptive statistics of predictors and dependent variable for mechanised longwalls in a 168 element study sample.

Parameter	Air temperature at the inlet, t_o [°C]	Relative air humidity, φ [%]	Volume air flow rate, V [m ³ /min]	Heat power sources, Q [kW]	Working depth, z [m]	Air temperature at the outlet, t_p [°C]
Arithmetic mean	28.548	79.945	1,320.506	192.982	223.818	31.133
Geometric mean	28.541	79.921	1,315.056	192.105	218.815	31.125
Median	28.700	79.800	1,321.000	192.050	197.900	31.200
Mode	29.1	79.4	1158.0	172.2	197.3	Multiple
Mode count	20	8	3	3	9	12
Minimum	27.0	75.5	1,045.0	163.6	164.2	28.9
Maximum	29.7	83.9	1,609.0	234.6	293.2	32.4
Standard deviation	0.6002	1.9943	120.5605	18.5504	49.0535	0.7060
Coefficient of variation	2.1024	2.4945	9.1299	9.6125	21.9167	2.2676

Parameter	Air temperature at the inlet, t_o [°C]	Relative air humidity, φ [%]	Volume air flow rate, V [m ³ /min]	Heat power sources, Q [kW]	Working depth, z [m]	Air temperature at the outlet, t_p [°C]
Skewness	-0.6905	0.0789	0.1890	0.2786	0.5931	-0.5111
Kurtosis	-0.0146	-0.8121	-0.6192	-0.8937	-1.4726	-0.0544

Table 2 shows that, as in the first model, there is no significant difference between the arithmetic mean and the geometric mean. Except for the z variable, the differences between the arithmetic mean and the median are very small. For the working depth variable, the difference is 25.92 m, which is approx. 12%. For the individual variables, the greatest difference in standard deviation was found for the working depth and this value is approximately 22%. When evaluating measures of clustering and dispersion and inferring the normality of the data distribution, kurtosis and skewness deserve attention. Analysis of skewness and kurtosis indices allows us to conclude that in all cases we are dealing with normal or near-normal distributions ($|\text{skewness}| < 1.5$, $\text{kurtosis} < 3$). For all variables, the skewness values range from -1.0 to 1.0. The kurtosis values of all variables are less than 0. Thus, the variables have a platocurtic (more flattened) distribution. Analysis of the flattening measures showed that the distributions of all variables are close to the normal distribution in this respect. In the case of the air temperature at the outlet, the distribution shows the characteristics of a multiple mode.

In the absence of statistically significant differences in the histograms and their effect on the multiple regression process with reduced sample size, the histograms for the 168 element sample are not presented in this paper.

4. Linear and nonlinear regression analyses

Linear and nonlinear statistical equations were determined for a set of measurements consisting of 168 observations to predict the air temperature at the outlet of the mechanised longwalls. All statistical calculations were performed using Statistica version 13, IBM SPSS Statistics version 25 and EViews version 8.

The general equation of air temperature at the outlet of the longwall t_L for the multiple linear regression model determined by the least squares method presents the relationship (1):

$$t_L = \beta_1 \cdot t_o + \beta_2 \cdot \varphi + \beta_3 \cdot V + \beta_4 \cdot Q + \beta_5 \cdot z + \beta_0 \tag{1}$$

where: $\beta_1 - \beta_5$ – regression coefficients expressing the direct effect of variables t_o , φ , V , Q , z .

β_0 – absolute term, is the coefficient of freedom (coefficient of intersection), which is the starting point of the theoretical regression line, showing the influence of other factors on the value of the explained variable than the independent variables used in the model.

The best fit of the results of a model built using linear regression is obtained when the following assumptions are met: the residuals of the model must have a normal distribution, there are no outliers, the residuals of the model are homoskedastic, there is no collinearity between the independent variables, and there is no autocorrelation of the model residuals [18, 20, 23, 24].

After meeting the above requirements, the dependent variable t_L is described by the independent variables t_o , φ , V , Q , with a linear regression equation in the form (2):

$$t_L = 0,7340 \cdot t_o - 0,0334 \cdot \varphi - 0,0021 \cdot V + 0,0089 \cdot Q + 0,0045 \cdot z + 12,8567 \tag{2}$$

The value of the coefficient of determination $R^2 = 0.793$ of the model indicates a strong correlation relationship of the t_L variable with the independent variables. The results of VIF test (collinearity test), Jarque-Bera test (normal distribution test of residual component), White test and Breusch - Pagan test (heteroskedasticity test of residuals), Durbin-Watson test and Breusch - Godfrey test (autocorrelation test of residuals) meet the criteria of linear regression. The model presented in equation 2 is a good fit to the measured data analysed, explaining the variation in air temperature at the t_L longwall outlet.

In order to simplify the model and obtain a more convenient form of the equation for practical use, a modification was made to the values of the coefficients of function (2). The modification was done to get the best possible functional representation. Thus, equation (2) after modifying the values of the function coefficients has the form (3).

$$t_{L-z} = 0,73 \cdot t_o - 0,03 \cdot \varphi - 0,002 \cdot V + 0,009 \cdot Q + 0,005 \cdot z + 12,5 \tag{3}$$

where by t_{L-z} the air temperature at the outlet of the mechanised longwalls after modifying the function coefficients.

Figure 9 shows the relationship between the measured values of air temperature at the outlet of the mechanised longwalls and the values of this temperature determined from the statistical equations created, before and after modification of the function coefficients (Eqs. 2 and 3).

Analysing the results obtained, it can be observed that the largest deviation for which the difference between the air temperature at the longwall outlet resulting from the measurements and the value obtained from the linear equation is 0.6°C (2%). In contrast, the deviation calculated from the linear equation with corrected function coefficients for this variant is 0.7°C (2.2%). Comparison of t_L and t_{L-z} values from the two models shows that there are not very large differences between the models, the largest being 0.1°C (0.27%).

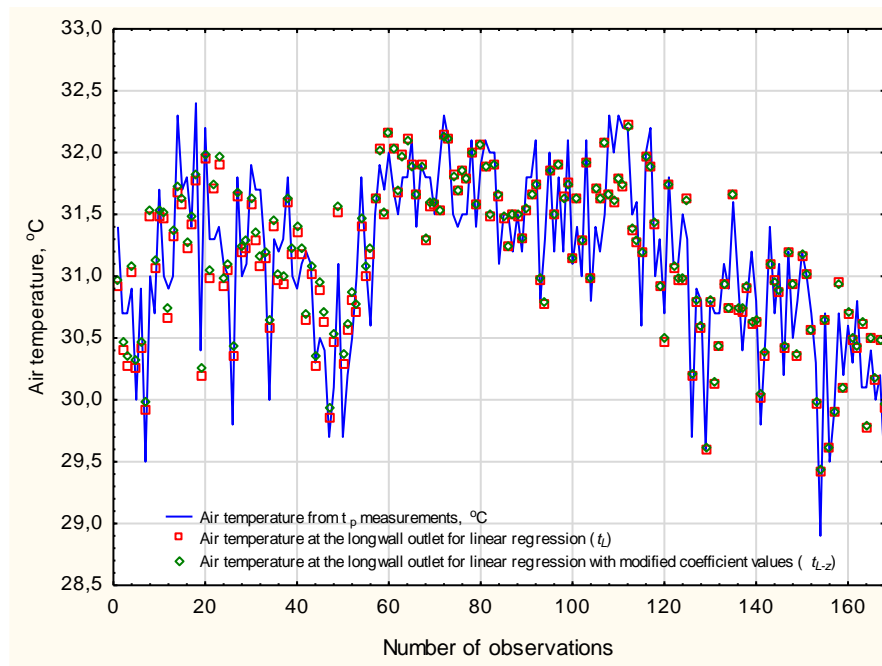


Fig. 9. Correlation of observed and predicted values of air temperature at the longwall outlet for linear regression before and after modification of function coefficients.

To determine better model fit than the linear regression model, correlation analysis between the dependent variable and each independent variable was conducted for the linear, logarithmic, quadratic, power, and exponential models. In most cases, the correlation between the factors analysed and air temperature at the longwall outlet is significant or high. Only the correlation relationship of air humidity (φ) and working depth (z) is small. Except for variable (z), the values of p-significance of tests for the other variables are less than 0.05, which indicates the statistical significance of these variables in the regression model. Considering the results of the partial correlation analysis, the fit of the linear function was found to be as good as that of the power or exponential function, so this paper presents the analysis of the linear function.

Based on the Levenberg-Marquardt nonlinear estimation of the system displacement for the above variables, a nonlinear model of the change in air temperature at the longwall outlet (t_K) was determined in the form (4):

$$t_K = -0,0342 \cdot t_o^2 - 2,21 \cdot 10^{-4} \cdot \varphi^2 + 6,619 \cdot 10^{-7} \cdot V^2 - 9,838 \cdot 10^{-5} \cdot Q^2 - 5,788 \cdot 10^{-5} \cdot z^2 + 8,864 \cdot 10^{-7} \cdot t_o \cdot Q \cdot V + 2,449 \cdot t_o - 84,43 \cdot 10^{-4} \cdot V + 0,0135 \cdot Q + 0,0321 \cdot z - 8,9727 \tag{4}$$

The value of the coefficient of determination is $R^2 = 0.804$ and indicates a very strong correlation relationship between air temperature at the outlet t_K and the independent variables used.

As in the case of linear regression, in equation 4, the values of the coefficients standing by the independent variables were modified, resulting in a new form of the function, equation (5):

$$t_{K-z} = -34,2 \cdot 10^{-3} \cdot t_o^2 - 22,1 \cdot 10^{-5} \cdot \varphi^2 + 66,2 \cdot 10^{-8} \cdot V^2 - 98,4 \cdot 10^{-6} \cdot Q^2 - 57,9 \cdot 10^{-6} \cdot z^2 + 88,6 \cdot 10^{-8} \cdot t_o \cdot Q \cdot V + 2,5 \cdot t_o - 84,4 \cdot 10^{-4} \cdot V + 0,014 \cdot Q + 0,032 \cdot z - 10,5 \tag{5}$$

where by t_{K-z} is the air temperature at the outlet of the mechanised longwalls after modifying the function coefficients.

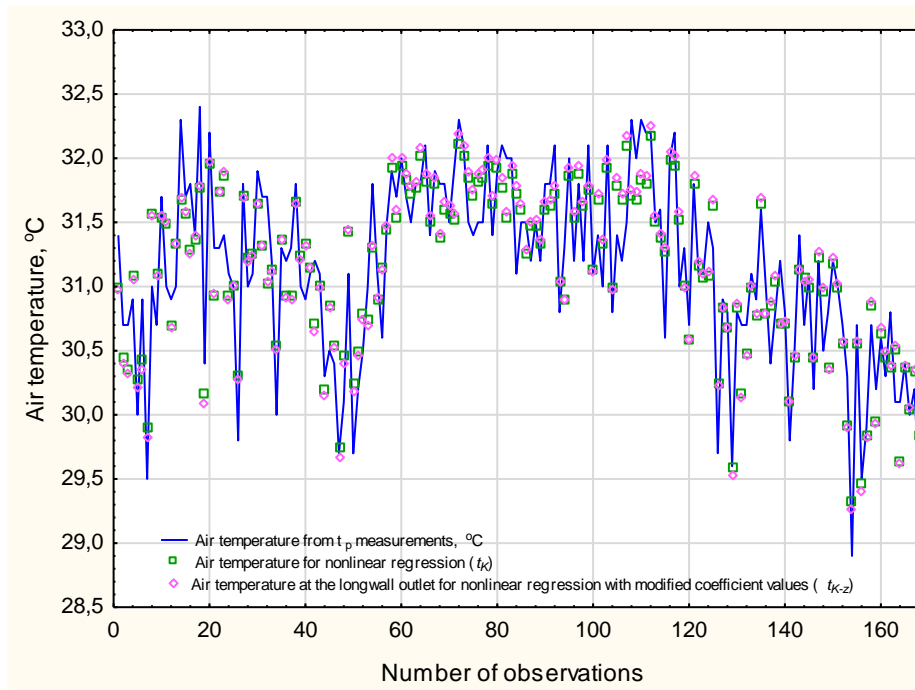


Fig. 10. Correlation of observed and forecasted air temperatures at longwall outlet for nonlinear regression before and after modification of function coefficient.

After analysing the air temperature values at the longwall outlet obtained from the statistical equations created (Eqs. 4 and 5), it can be concluded that the largest deviation of the air temperature value obtained from the measurements and the model value calculated from the nonlinear equation is 0.7°C (2.2%). In contrast, the deviation calculated from the linear equation with corrected function coefficients for this variant is 0.7°C (2.3%). The comparison of the values of t_K and t_{K-z} from the two equations shows that there is no significant difference in value between the two models. The largest difference between t_K and t_{K-z} is 0.1°C (0.25%). The distribution of air temperature values at the outlets of the t_p , t_K , t_{K-z} longwalls is shown in Figure 10.

5. Air temperature prediction under Khe Cham III mine conditions

In the 14-5-5 longwall in Khe Cham III mine, the air flow rate at the inlet of the longwall varied from 1165 to 1475 m³/min. This longwall was ventilated by a U-system, and the primary temperature of the rock mass was 31.1°C. Figure 11 shows the ventilation scheme for the area of the 14-5-5 longwall in Khe Cham III mine. A longwall shearer MG150/375-W of 375kW power and two longwall conveyors SGZ630/264 with drives of total power of 528kW (upstream and downstream of the powered roof support) operated in the longwall. The transport gallery was equipped with a scraper conveyor type SZZ630/110, a belt conveyor type DSJ100/80/110, a crusher type PLM 800 and some other equipment. The total power of the electrical equipment operating in the workings was 1358 kW. The longwall output ranged from 600 to 2610 Mg/day.

In the analysed example of mechanised longwall 14-5-5 in Khe Cham III mine, the determined criterion equations (3) and (5) with modified values of function coefficients were used to predict the temperature at the longwall outlet. Table 3 shows the values of the characteristic parameters-required for air temperature modeling, the measured air temperature values at the outlet of the 14-5-5 longwall (shown in gray), and the predicted air temperature values t_{L-z} and t_{K-z} .

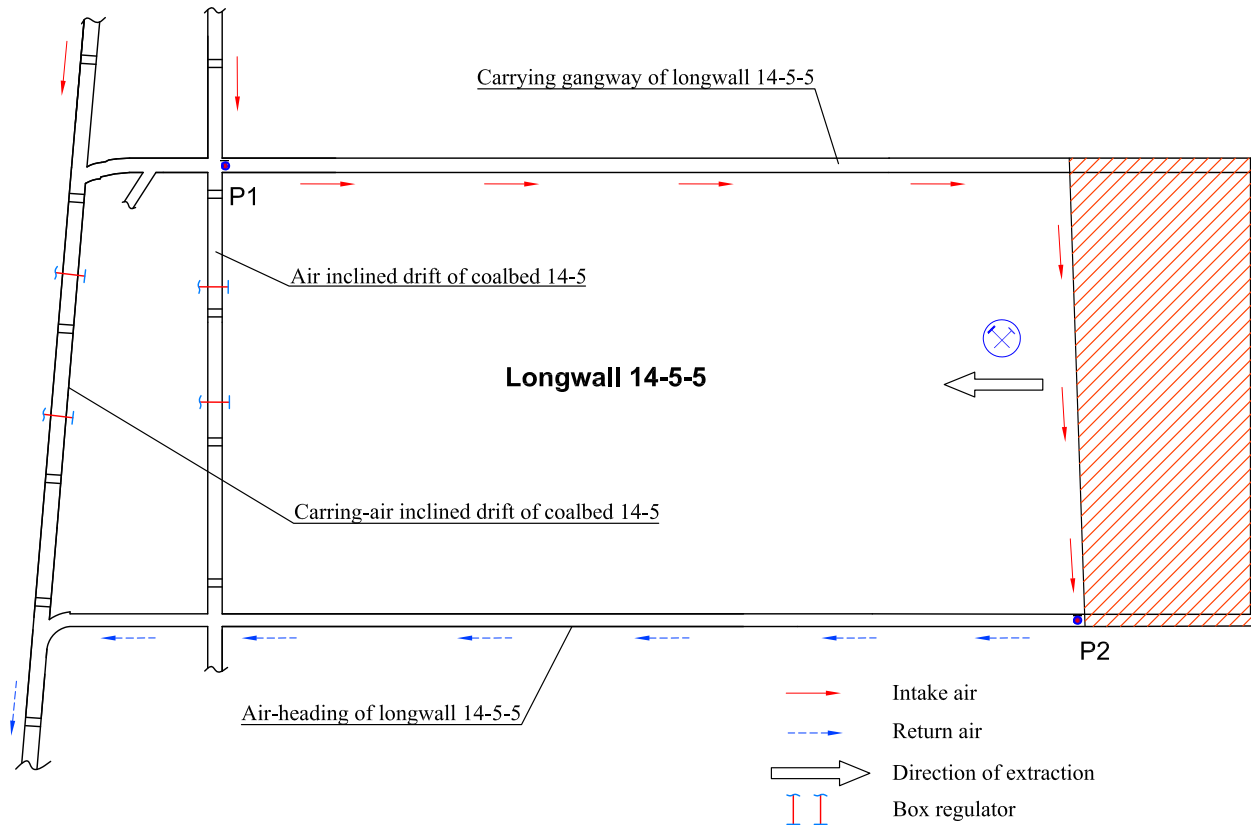


Fig. 11. Ventilation scheme for longwall area 14-5-5 in Khe Cham III mine [25].

Tab. 3. Results of measuring and predicting air temperature at the outlet of the 14-5-5 mechanised longwall in Khe Cham III mine.

Ordinal	Air temperature at the inlet	Relative air humidity	Volume air flow rate	Heat source power	Working depth	Air temperature at the outlet		
	t_o	φ	V	Q	z	t_p	t_{L-z}	t_{K-z}
	°C	%	m ³ /min.	kW	m	°C		
1	27.8	82.0	1165	204.4	277.5	31.8	31.2	31.2
2	28.2	80.3	1206	203.1	276.5	31.5	31.5	31.5
3	28.7	81.1	1327	200.3	276.5	31.7	31.5	31.6
4	28.7	81.8	1416	200.2	276.5	31.2	31.3	31.4
5	28.4	81.5	1261	212.4	276.5	30.9	31.6	31.5
6	28.1	81.2	1370	202.1	276.4	30.7	31.0	31.1
7	27.3	81.3	1347	201.8	275.1	31.3	30.5	30.4
8	27.3	81.5	1463	195.6	275.0	29.9	30.2	30.2
9	26.9	79.3	1254	193.1	275.0	30.7	30.4	30.3
10	27.0	77.5	1475	195.7	274.9	30.1	30.1	30.0

Based on the analysis of the obtained results, it can be concluded that the average error between the measured values and the forecast values is 0.3 °C (1.1%) (linear equation) and 0.4 °C (1.2%) (nonlinear equation). The largest temperature deviation for the linear equation is 0.81°C (2.60%) and for the nonlinear

equation is equal to 0.85°C (2.73%). Such small deviations of the predicted air temperature for the 14-5-5 longwall in Khe Cham III mine, allow to use the created statistical models with modified function coefficients (Eqs. 3 and 5). The models obtained by statistical analysis can be used as a tool for mine services to predict the air temperature at the outlet of the exploited longwall.

6. Summary

This paper discusses methods for predicting air temperature at the outlet of mechanised longwalls in Vietnamese underground mines. The equations obtained by the method of multiple regression and nonlinear estimation determine the dependence of the air temperature at the longwall outlet on the air temperature at the longwall inlet, relative humidity of the air, volume air flow rate, heat source power and working depth. Modifying the values of the function coefficients to a simpler form yielded new equations that are less complex and more convenient for practical use. Using the criterion equations formed by statistical methods, a prediction of the air temperature at the outlet of the 14-5-5 mechanised longwall at the Khe Cham III mine was made. By analysing the obtained results, it can be concluded that there is a high fit between equation (3) and equation (5), and the measured longwall outlet temperature, where the differences of the obtained temperatures do not exceed 1.2%. The criterion equations presented with modified function coefficients allow for simple modeling and prediction of air temperature at the longwall outlet. The function models presented can serve as a tool for mine services to predict the air temperature at the outlet of mechanised longwalls under Vietnamese mine conditions.

Acknowledgements

We are grateful to the Faculty of Civil Engineering and Resource Management, AGH University of Science and Technology for providing essential equipments for this study. Data used for this study were provided from the Mining Safety Center – Institute of Mining Science and Technology (IMSAT), Vinacomin – Khe Cham Coal Company, Vinacomin – Vang Danh Coal Joint Stock Company, Vinacomin – Duong Huy Coal Company and Vinacomin – Ha Lam Coal Joint Stock Company.

References

1. Ministra Środowiska, Rozporządzenie Ministra Środowiska W sprawie Zagrożeń Naturalnych w Zakładach Górniczych (Dz. U. z 2015 r. Poz. 1702 i 2204, z 2016 r. Poz. 949 Oraz z 2017 r. Poz. 1247), Warszawa, 2019.
2. Ministry of Industry and Trade of Vietnam, National technical regulation on safety in underground coal mining QCVN 01: 2011/BCT (Issued together with Circular No. 03/2011/TT-BCT of February 15, 2011) of the Minister of Industry and Trade), Hanoi, 2011.
3. Borowski, M., Truong Tien, Q., Łuczak, R., Życzkowski, P., 2020. Selection and Calculation of Air Cooling Solutions in Underground Coal Mines in Vietnam, *Inżynieria Mineralna*, 2(2): 237-244, <http://doi.org/10.29227/IM-2020-02-68>.
4. Knechtel, J., 2007. Zwalczanie Zagrożenia Klimatycznego w Polskich Kopalniach Węgla Kamiennego w Odniesieniu Do Górnictwa Światowego, *Górnictwo zrównoważonego rozwoju*, Politechnika Śląska, 279: 225–240.
5. Truong Tien, Q., Łuczak, R., Życzkowski, P., 2019. Climatic Hazard Assessment in Selected Underground Hard Coal Mines in Vietnam, *Inżynieria Mineralna*, 2(44); 155-163, <http://doi.org/10.29227/IM-2019-02-67>.
6. Dao, C.Van and Tran, H.Xuan 2020. Study on status and solution to improve the ventilation system of Quang Hanh coal mine (in Vietnamese). *Journal of Mining and Earth Sciences*. 61, 4 (Aug, 2020), 110-117. DOI:[https://doi.org/10.46326/JMES.2020.61\(4\).12](https://doi.org/10.46326/JMES.2020.61(4).12).
7. Gibson, K.L., *The Computer Simulation of Climatic Conditions in Underground Mines*. Ph.D., University of Nottingham, Nottingham, 1976.
8. Lowndes, I.S., Crossley, A.J., Yang, Z.-Y., 2004. The Ventilation and Climate Modelling of Rapid Development Tunnel Drivages, *Tunnelling and Underground Space Technology*, 19(2): 139-150, doi:10.1016/j.tust.2003.09.003.
9. Lyu, W., Cai, S., Yang, P., Zhang, Y., 2017. Underground environment parameter prediction in a deep mine, in J Wesseloo (ed.), *Deep Mining 2017: Proceedings of the Eighth International Conference on Deep and High Stress Mining*, Australian Centre for Geomechanics, Perth,

- p. 949–960, doi:10.36487/ACG_rep/1704_65_Lyu.
10. Roghanchi P. i Kocsis K. C., 2019. Quantifying the thermal damping effect in underground vertical shafts using the nonlinear autoregressive with external input (NARX) algorithm, *Int. J. Min. Sci. Technol.*, Vol. 29, Issue 2, 255–262, doi: 10.1016/j.ijmst.2018.06.002.
 11. Stupnicka, T.Ł., Monika, T., 2005. Zastosowanie Modeli Sieci Neuronowych w Ocenie i Prognozowaniu Jakości Powietrza. *Inżynieria środowiska*, 10(2): 121-134.
 12. Bascompta, M., Rossell, J.M., Sanmiquel, L., Anticoi, H., 2020. Temperature Prediction Model in the Main Ventilation System of an Underground Mine, *Applied Sciences*, 10(7238): 1-11, doi:10.3390/app10207238.
 13. Dao, C.Van, Tran, H.Xuan and Le, D.Tien 2021. Determination of reasonable working mode for main fan stations during pilot operation of fan station VO - 22/14AR in Lo Tri area, Thong Nhat coal mine (in Vietnamese). *Journal of Mining and Earth Sciences*. 62, 4 (Aug, 2021), 15-20. DOI:https://doi.org/10.46326/JMES.2021.62(4).02.
 14. Vinacomin-Ha Lam Joint Stock Company, Explanatory statement about exploiting the longwall of CGH 11-1-16 in the Coal Seam 11 in the Ha Lam Mine (document not public), Quang Ninh, 2018.
 15. Mining Safety Center - Institute of Mining Science and Technology - Vinacomin, Investigation of air composition parameters in the longwall TT-11-6 in the coal Seam 11 in the Central Part of the Duong Huy mine (document not public), Quang Ninh, 2020.
 16. Mining Safety Center - Institute of Mining Science and Technology - Vinacomin, Investigation of air temperature in the longwall I-8-3A in the area Gieng Vang Danh, Vang Danh mine (document not public), QuangNinh, 2019.
 17. Domański, C., Krystyna, P., 2000. Nieklasyczne metody statystyczne, Polskie Wydawnictwo Ekonomiczne, Warszawa.
 18. Hellwig, Z., *Linear Regression and Its Application to Economics*, Oxford, London, 1963.
 19. Sanisz, A., 2006. *Przystępny Kurs Statystyki z Zastosowaniem STATISTICA PL Na Przykładdach z Medycyny*; Statsoft (www.StatSoft.pl), 1: Statysyki podstawowe, 2006.
 20. Hoàng Trọng, Chu Nguyen Mong Ngoc, 2008. *Analyze Research Data with SPSS*, University of Economics Ho Chi Minh City, Ho Chi Minh city.
 21. Krysicki W., Bartos J., Dyczka W., Królikowska K., Wasilewski M., 2004. *Rachunek prawdopodobieństwa i statystyka matematyczna w zadaniach*, Wydawnictwo naukowe PWN, Warszawa, 2.
 22. Vittinghoff, E., Shiboski, S.C., Glidden, D.V., Charles, E.Mc., 2005. *Regression Methods in Biostatistics: Linear, Logistic, Survival, and Repeated Measures Models*; Vittinghoff, E., Ed., *Statistics for biology and health*; Springer, New York, 2005.
 23. Weisberg, S., 2005. *Applied Linear Regression*, Wiley series in probability and statistics; third ed., Wiley-Interscience: Hoboken, New Jersey (Canada).
 24. Bingham, N.H., Fry, J.M., 2010. *Regression*, Springer Undergraduate Mathematics Series; Springer London, London.
 25. Mining Safety Center - Institute of Mining Science and Technology - Vinacomin, Investigation of air composition parameters in the longwall 14-5-5 in the coal seam of the Khe Cham III mine (document not public), Quang Ninh, 2017.

VISION ZERO – Tools for Safety, Health, and Well-being Management and the Application in the Vietnamese Coal Mining Industry

NGUYEN Nga^{1,*}, MEESMANN Ulrich², TRUONG Ngoc-Linh³, TRINH Vu-Hoa⁴

¹ Hanoi University of Mining and Geology, Department of Mining Management, Hanoi, Vietnam, International Social Security Association – Prevention in Mining (ISSA Mining)

² Association for Raw Materials and Chemical Industry (BG RCI), Bochum, Germany, ISSA Mining

³ Ha Lam Coal Joint Stock Company, Halong, Quang Ninh, Vietnam

⁴ Duong Huy Coal Company, Campha, Quang Ninh, Vietnam

Corresponding author: nguyenthihoinga@humg.edu.vn

Abstract. The Vietnamese mining industry is one of the most dangerous industries in the country. Mining companies understand safety and health for sustainable development at the mining sector and the national level. Thus, they have been applying many measures to improve their safety and health management achievements. Besides technology measures, organizational and personal measures are priorities. At the international level, VISION ZERO is a global movement based on the belief that all accidents, diseases, and harm at work are preventable. VISION ZERO develops its Seven Golden Rules to guide leaders, managers, and workers to create a safe and healthy working environment for the well-being of employees. The paper focuses on VISION ZERO, its theoretical aspects, and the application process in the Vietnamese coal mining companies.

Keywords: Vision Zero, Safety and health, Vietnamese coal mining industry

1. Introduction

VISION ZERO (VZ) is a transformational approach to prevention that integrates the three dimensions of safety, health, and well-being at all levels of work [1]. In June 2015, all thirteen prevention sections of the International Social Security Association (ISSA) decided to adapt the VISION ZERO prevention strategy and the Seven Golden Rules as the harmonized tools to reach the aim of zero harm, in all sectors of industry across the globe. Today, many resources have been developing to support the VZ campaign and promote it worldwide. Besides PowerPoints, videos, articles, App, tools like the 7 Golden Rules, and Guides can be widely used for leaders and managers in companies. The mining industry worldwide is benefiting from VZ, and its guiding documents, which mining companies in Chile, Germany, Pakistan, Peru, Thailand, Zambia, etc., are examples. As of 2019, 1100 companies, partners, and trainers are engaging in VZ. In Vietnam, the mining industry is a pillar of the economy regarding its contribution to other manufacturing industries, a significant taxpayer, and a big employer. However, the Vietnamese mining industry is also facing safety and health management problems when the production conditions become complicated, the acceptance of society to an industry with images of danger, negative impacts on the environment, and solutions to protect the climate change, and reduce cultivation areas [2]. Therefore, for the sustainable development of the nation and the mining sector, besides economic benefits, environmental protection, safety, and social acceptance are significant. Fortunately, safety, health, and well-being of labor are now priorities in the general strategic development of Viet Nam to 2045, as stated in the Resolution of the Party Congress in 2021. Thus, a focus on Vision Zero and the application in the Vietnamese mining industry becomes very helpful.

2. Study objectives and areas

Vision Zero and its documents, especially the Seven Golden Rules are objectives in the theoretical part of the paper.

The Seven Golden Rules for Vision Zero are as follows:

1. Take leadership – demonstrate commitment
2. Identify hazards – control risks
3. Define targets – develop programs
4. Ensure a safe and healthy system – be well-organized
5. Ensure safety and health in machines, equipment, and workplaces

6. Improve qualifications – develop competence

7. Invest in people – motivate by participation

These golden rules are developed by various questions with three rates of (1) action required, (2) room for improvement, and (3) fully implemented so that leaders, managers, and other employees can use them as a checklist to see how things look in their companies. The Seven Golden Rules contain 23 statements, under which 110 questions are used for the evaluation [3].

Ha Lam Coal Mining Company is in Halong City, and Duong Huy Coal Mining Company is in Cam Pha City, Quang Ninh. Ha Lam Coal Mining Company (HLC) was founded in 1950, and today it is one of the forerunners in the coal mining industry regarding the innovation of technology to meet the demand of deeper excavation in a vertical shaft, safety, and health culture, and quantity of output and profit from the production. HLC has been employing more than 3,100 people. From 2015 – 2019, there were 132 accidents happened, causing three deaths [4]. The annual production of HLC is approximately 2.5 million tons in the last five years. Duong Huy Coal Mining Company (DHC) was established more than 40 years ago. Recently, the annual output is more than two million tons. DHC is a big employer in the area with over 3,400 employees. Despite many safety management measures, during 2016 – 2020, there were 310 people have been suffering from serious and minor accidents, of which are eight fatalities [5]. The two companies are implementing modern technology in their excavation to improve safety. Consequently, there are also adjustments in the organization and labor force.

In HLC, the Seven Golden Rules were adjusted to evaluate the safety culture of the company in 2020. These rules once again were modified to survey the safety and health management in DHC in 2021.

Besides, a few training activities for staff and middle-level managers of the coal mining companies and mining engineering students about VZ and the Seven Golden Rules from 2017 to 2020 are also research objectives.

3. Materials and Methods

3.1 Documents and guidelines about Vision Zero

Vision Zero has offered resources for people who wants to use VZ as a helpful tool in companies, such as the Seven Golden Rules and guides, Powerpoints, videos, visual identity, articles, proactive leading indicators, app, and resources produced by VZ supporters [6]. There are several guidelines for mining industry, which is developed by the International Social Security Association – Prevention in Mining [3], seeing if in a mining company how the safety, health, and well-being are implemented, or if there is a need for improvement, or whether it needs to take corrective action.

Golden rule 1: Take leadership – demonstrate commitment: Safety and health are not only duties of the executive or a manager, or an employee, but of the whole company's system. However, the safety competence of companies' leaders is significant, so are leader skills regarding communication, management culture and role models. Thus, a good leader with demonstrate commitments about safety is a decisive factor for the success or failure of safety and health in a mining company

Golden rule 2: Identify hazards – control risks: Risks cannot be controlled if they are not fully identified. Once hazards are identified, the assessment of risks' damages and losses, either visible or invisible, or time is more precise. Accidents, injuries and near misses should also be recorded.

Golden rule 3: Define targets – develop programs: Success in occupational safety and health requires clear goals and concrete steps for implementaion, which should be established in a program. In another words, plans for safety management in short-term, midium-term and long-term are important to utilize the companies' resources.

Golden rule 4: Ensure a safe and healthy system – be well-organized: To implement this rule, leaders should understand the advantages of an adequate and a systematic occupational safety and health organization. As disruptions, production downtime and other quality issues can be protected with the system, productivity can be increased and the companies can be more profitable.

Golden rule 5: Ensure safety and health in machines, equipment, and workplaces: Safe production includes all technical, organizational and personal measures, in which technical issues should be first improved. Although companies cannot use the latest technology most of the time, when they can maintain the newest occupational and health standards, the companies' employees, assets, and images can be protected.

Golden rule 6: Improve qualifications – develop competence: This rule requires the understanding of investment in the training and skills of employees is bringing the readiness of knowledge and competence for the workers, managers and leaders of the companies.

Golden rule 7: Invest in people – motivate by participation: This rule relates to the leadership and the role model of the leader to engage their employees talk openly about risks and hazards, and the employees feel that they are part of the safety strategy and safety culture.

Tab. 1. The Seven Golden Rules to implement VISION ZERO.

Rule	Statement (Scale)	Number of breakdown categories
Rule 1: Take leadership – demonstrate commitment	I demonstrate safety and health, set the standards, and serve as a role model for the employees and managers	6
	The importance of safety and health is known to everyone in my enterprise – and we talk about it openly	5
	I act consistently and demonstrate the importance of safety and health at work	4
	I invest in safety and health in the enterprise	4
Rule 2: Identify hazards – control risks	I make sure that a risk assessment is prepared in my enterprise, documented, and updated at regular intervals	6
	Occupational accidents, near misses and critical incidents are reported, recorded statistically, and evaluated to determine the potential for improvements	6
	We use the insights gained from the risk assessment and from accident analysis to make improvements	3
Rule 3: Define targets – develop programs	I have established clear goals for safety and health	4
	I plan concrete activities to reach my goals	4
	I establish performance figures to verify the effectiveness of my measures	5
Rule 4: Ensure a safe and healthy system – be well-organized	Structure, responsibilities, competencies, procedures and processes – my enterprise is well-organized in regard to occupational safety and health	7
	Safety and health in the enterprise is an important factor when filling management positions	5
	The organization of safety and health in my enterprise meets the applicable legal requirements as a minimum	9
Rule 5: Ensure safety and health in machines, equipment, and workplaces	We make sure that the current safety standards are met in the construction and/or procurement of new production facilities, machines, and equipment, and in the design of workplaces	5
	In the daily operation of production facilities, machines, and equipment, I make sure that the safety devices work reliably and are used	6
	We make sure that our production facilities, machines, and equipment do not pose any health hazards, and that these are minimized	3
Rule 6: Improve qualifications – develop competence	We know what qualifications and competencies we need for the safe and healthy operation of our production technology and to avoid disruption	4
	I invest in the systematic training and continuing education of my employees and also support their personal further development	4
	I put the expanded or new competencies of my employees to use and assign them suitable new responsibilities	3

	Knowledge leads to safety – which is why I highly value practical, comprehensible instructions for the employees	3
Rule 7: Invest in people – motivate by participation	I demonstrate my personal appreciation to the employees, I also expect this from all managers and senior staff	3
	I use the topics of safety and health at work for the establishment and further development of a positive company culture	5
	In our enterprise, we have established structures that are helpful for participation and motivation	6

3.2 Data collection from HLC and DHC

Both HLC and DHC comply regulations from the authorities regarding occupational safety and health (OSH) structures, issuing internal OSH regulations and guidelines, collecting and storing statistic data, conducting regular reports, training, practicing etc.

At HLC, safety culture was established throughout the years by many regulations, campaigns and activities. Besides, HLC is also the first coal company of Vietnam that proposed a safety strategy to 2025, concentrating on improving leadership and organization in OSH, assuring the safety management effects by investment in technology innovation, upgrading safety training and creating rewards and sanctions in safety management, reducing numbers of incidents, accidents, and death tolls. At top managers level, HLC ensure the implementation of technology renovation in OSH, with strong commitments about safety. At the middle managers level, statistic data about OSH, including near-missed incidents and accidents are fully recorded, which are much helpful to mitigate risks. In 2020, HLC also assessed its safety culture under the consultation of an ISSA Mining expert to recommend solutions for better safety culture and safety competence for the staff and workers of the company [4]. VZ checklist (Tab. 1.) was modified to a questionnaire with some open-ended questions, getting to know the safety competence of the interviewees, and 7 golden rules with various scales. The following categories are the focus of the survey: Role model, Responsibility, Standards and benchmarks establishment, Monitoring, Motivation, Discussion, Compliance (Rule 1), Forecasting, Recording and Communication, Evaluation and Investigation (Rule 2), Company targets and personal goals, Instruction, (concrete) Plans to achieve targets (Rule 3), Safety organization, Safety procedure, Monitoring and early warning system, Safety legal regulation (Rule 4), Safety machines and equipment, Safety production, Safety workplaces (Rule 5), Design safety programs, Training, Training effects (Rule 6), Payrolls and rewards scheme, Spiritual motivation (Rule 7). The survey was applied to 4 focus groups of leaders and managers (42 scales), officer staff (46 scales), foremen (46 scales), and workers (46 scales). Of the 483 correspondents, 373 handed completed questionnaires. The data collection process was exclusively conducted and administered by the researchers throughout the implementation period of this research study, which took practically 3 months - from beginning of March 2020 to end of May 2020.

All scales were scored on a 3-point Likert-type format from (1) action required – 1 point, (2) room for improvement – 2 points and (3) fully implemented – 3 points. The checklist transferred to participants in Vietnamese. Surveying questionnaires were sent to participants via the hard copy version.

At DHC, the Seven Golden Rules was applied in March and April 2021 to evaluate the current situation of OSH management. The focus groups are safety managers (middle and first-line) and safety staff, and workers. The questionnaire includes also open-ended questions, aiming to understand the current situation OSH, evaluating OSH measures of DHC, identifying risks and hazards, and collecting appropriate safety measures. Of the 500 correspondents, 472 handed completed questionnaires. The scales were scored on a 5-point Likert scale from (1) Strongly disagree to (5) Strongly agree. The scale concentrated on legal – policies, technology, organization, personal and leadership. The checklist also transferred to participants in Vietnamese. Surveying questionnaires were sent to participants via the hard copy version.

Both in HCL and DHC the distribution of interviewees regarding ages and seniorities are of reliable and precise evaluation.

Tables 2 and 3 describes the sample information after collected and processed in HLC and DHC, respectively.

Tab. 2. Distribution of sample by title in HLC, 2020.

		Frequency	Percent	Valid Percent	Cumulative Percent
Valid	Leaders and department managers	26	6.97	6.97	6.97
	Department officers	86	23.06	23.06	30.03
	Foremen	36	9.65	9.65	39.95
	Workers	225	60.32	60.32	100.0
	Total	373	100.0	100.0	

Tab. 3. Distribution of sample by title in DHC, 2021.

		Frequency	Percent	Valid Percent	Cumulative Percent
Valid	Middle and first-line managers	93	24.54	24.54	24.54
	Workers	379	75.46	75.46	100.0
	Total	472	100.0	100.0	

3.3 Methods

Authors organized surveys and group discussions in HLC and DHC. All scales Observation happened in training activities of VZ and the Seven Golden Rules to staff (approximately 100 persons) for coal mining companies in the Vietnam National Coal – Minerals Holding Corporation Limited (Vinacomin), the representative of the Vietnamese mining industry.

From the questionnaire responses, descriptive statistics were used to identify reality of safety culture and management in HLC and DHC.

The collected data was then analyzed using SPSS 20 to obtain Minimum, Maximum, and Mean.

4. Results and discussions

Generally, the foremen of HLC highly evaluated the OSH management with 2.934. The lowest point comes from workers with 2.705. This number shows that the OSH management in HLC still needs improvement. Table 4. Show results of safety culture in HLC following the checklist from VZ golden rules.

Tab. 4. Results of safety culture in HLC.

Rule	Leaders and managers		Department officers		Foremen		Workers	
	Mean	Rank	Mean	Rank	Mean	Rank	Mean	Rank
Total	2.712		2.896		2.934		2.705	
Rule 1: Take leadership – demonstrate commitment	2.669	5	2.903	2	2.938	4	2.743	2
Rule 2: Identify hazards – control risks	2.715	3	2.902	3	2.897	6	2.738	3
Rule 3: Define targets – develop programs	2.746	2	2.899	4	2.901	5	2.712	5
Rule 4: Ensure a safe and healthy system – be well-organized	2.669	5	2.887	6	2.889	7	2.717	4

Rule 5: Ensure safety and health in machines, equipment, and workplaces	2.762	1	2.935	1	2.972	2	2.633	6
Rule 6: Improve qualifications – develop competence	2.646	7	2.853	7	2.978	1	2.774	1
Rule 7: Invest in people – motivate by participation	2.692	4	2.893	5	2.961	3	2.588	7

Although safety culture is an essential aspect of HLC in their safety strategy, the evaluation differs among each focus group. From the point of view of leaders and managers, as well as department officers of HLC, the company have been invested in safety machines and equipment. They also build and maintain a safety and healthy working environment for the employees, especially workers underground (Rule 5). The leaders of the company can have a close look into their leadership and commitment, understanding that they must do more to maintain and increase the leadership effects in OSH at the company (Rule 1). So do the foremen, who are the leaders onsite. From that understanding, following the advice from ISSA Mining experts, top leaders of HLC raise the awareness of leadership and commitment in safety by the slogan: Safety is moral, our employees are the first and foremost. This commitment is nowadays the strongest commitment in the Vietnamese mining industry ever.

The foremen and workers of HLC through the questionnaires think that they are well trained to adapt to the production. However, the leaders and managers, as well as the department officers in HLC recognized that they must improve in the Rule 6 Improve qualifications – develop competence, especially in the training for employees to prepare a skillful labor force with high safety competence to meet the demand of their production in the future. Based on the evaluation from the workers’ views, HLC issued its guidelines to comply Rule 5 Ensure safety and health in machines, equipment, and workplaces for their staff and workers in the beginning of 2021.

Regarding the Rule 7, despite the understanding of the importance of the labor force from the leaders, payrolls and rewards scheme and spiritual motivation for workers at HLC still require better improvement. The evaluation from 205 workers (60.32% of interviewees) is the lowest point in the whole survey at HLC.

In DHC, the Seven Golden Rules was developed to 31 scales for managers and 28 scales for workers. Tables 5 and 6 shows the top 5 and bottom 5 results of OSH management in DHC, evaluated by managers and workers, respectively.

Tab. 5. Results of the OSH management in DHC by managers (top 5 and bottom 5).

Scale	N	Minimum	Maximum	Mean
You always comply with OSH regulations	93	3.0	5.0	4.505
You always promote OSH for other employees	93	1.0	5.0	4.495
Your company regularly updates OSH regulations and policies from the government and authorities, specifying to the internal ones	93	1.0	5.0	4.484
You always remind your colleagues about OSH at short meetings before shifts start	93	1.0	5.0	4.484
You are the role model to other colleagues regarding OSH	93	2.0	5.0	4.452
...		.		
Departments and production units have good connection and communication for OSH	93	2.0	5.0	4.043

You understand well the OSH regulations	93	2.0	5.0	4.032
Employees of DHC always comply OSH regulations	93	1.0	5.0	4.032
Employees of DHC always improve their competence and skills for better OSH	93	1.0	5.0	3.978
Machines and equipment are always maintained and prepared in time to ensure OSH	93	2.0	5.0	3.978

Tab. 6. Results of the OSH management in DHC by workers (top 5 and bottom 5).

Scale	N	Minimum	Maximum	Mean
Talking about OSH is always a topic of short meetings before shift start	379	1.0	5.0	4.492
You are always communicated about OSH	379	2.0	5.0	4.347
You are usually trained and coached about OSH	379	1.0	5.0	4.347
DHC built appropriate sanctions for people who cause unsafety	379	2.0	5.0	4.329
You always want to improve your competence and skills for better OSH at your production units	379	1.0	5.0	4.310
...		.		
PPE is in good conditions and ready to use	379	1.0	5.0	4.077
Equipment to fix incidents always function well	379	1.0	5.0	4.021
You understand well the OSH regulations	379	2.0	5.0	4.016
Machines and equipment are always maintained and prepared in time to ensure OSH	379	1.0	5.0	4.005
Your production unit is always equipped in time to fix incidents	379	1.0	5.0	3.995

The managers of DHC recognized that they must comply with OSH regulations and promote OSH for other employees of the company. However, it seems sometimes they did not understand well the OSH regulations (one of bottom 5) and this situation needs to be improve. To managers, leadership and its role were practiced better at DHC, but it still needs to develop ensure safety and health in machines and equipment and workplaces, as well as improve capacity of workers, regarding the bottom 5 with the lowest points. To workers, leadership, identify hazards to control risks, and improve capacity of employees were implemented well in DHC, meanwhile ensure safety and health in machines and equipment and workplaces still had room to improve. DHC is now conducting its action plans to improve OSH with a strong commitment from the leaders to reduce 20 – 25 % accidents of the company in comparison to previous years. They expect the results of improving productivity and benefits both for DHC and the employees. Their solutions concentrate on technology renovation, organizational reform and personal OSH programs.

Training activities with VZ documents and resources have been applying for reserve directors, middle managers, first-line managers, etc. in mining and auxiliary companies of Vinacomin since 2019. By participatory training methods, such as group discussion, teamwork, etc. learners can easily form knowledge and skills. Using OSH clips as a resource of VZ help learners increase their ability to remember. Observations from Wrap-ups and Feedback sessions of trainings show their evaluation that learners are more motivated, improving their awareness of OSH, respecting skillful workers and their roles in mining coal company, and the precious asset of a company is the labor force.



Fig. 1. Resources of ISSA Mining used in an OSH training to staff of Cua Ong Coal Processing Company in 2019 (Photo/Trainer: NGUYEN, Nga).

5. Conclusions

Generally, VISION ZERO and the Seven Golden Rules is gradually introduced into coal mining companies in Vietnam at different level of training for awareness, implementation the rules and development into various activities such as designing handbooks and guidelines at mines. Pilot programs in Ha Lam Coal Joint Stock Company and Duong Huy Coal Company show the possibility of the Seven Golden Rules' application widely in the Vietnamese coal mining industry, regardless production conditions and cultural aspects. Coal mining companies can also use scales of the Seven Golden Rules and broaden the Linkert scales, besides using statistic numbers, to evaluate in a period for better understanding about the OSH improvement.

6. Acknowledgments

The paper was presented during the 6th VIET - POL International Conference Scientific-Research Cooperation between Vietnam and Poland, 10-14.11.2021, HUMG, Hanoi, Vietnam.

The authors are thankful to colleagues of the International Social Security Association – Prevention in Mining, the Mining Management Department of HUMG and coal mining companies of Vinacomin for their supports and cooperation.

7. References

1. <https://visionzero.global/resources>, 19/05/2021
2. Nguyen, N., 2020. A review of social license to operate in Southeast Asian mining, *The Extractive Industries and Society*, 8(2), <https://doi.org/10.1016/j.exis.2020.11.007>
3. <https://visionzero.global/sites/default/files/2017-12/2-Vision%20Zero%20Guide-Web.pdf>, 19/5/2021
4. <https://halamcoal.com.vn/>, 19/5/2021
5. <http://thanduonghuy.com.vn/>, 19/5/2021
6. <https://visionzero.global/guides>, 19/5/2021

Current Status of Coal Mining and Some Highlights in the 2030 Development Plan of Coal Industry in Vietnam

NGUYEN Quynh Nga¹, NGUYEN Van Hau¹, PHAM Tu Phuong², CHU Thi Khanh Ly^{1,*}

¹ National Academy of Public Administration, Hanoi, Vietnam

² Investment Consulting Joint Stock Company, Hanoi, Vietnam

Corresponding author: khanhly@napa.vn

Abstract. Coal mining is one of the key mining industries in Vietnam. Coal is also an important fuel for many other industries. Currently, coal mining is mainly concentrated in Quang Ninh coal basin, the proportion of open-pit coal mining and underground mining is quite similar. However, according to Decision 403/QĐ-TTg on approving the adjustment of the Vietnam coal industry development plan up to 2020, considering the prospects by 2030, the mining output will be from 51 to 54 million tons by year 2025 and from 55 to 57 million tons by 2030. In which, the proportion of underground coal mining will increase gradually compared with that of open-cast mining, specifically, by 2030, the proportion of the later compared to that of the former will be only 11%. According to this plan, open-pit coal mines have been shifting to underground mining technology, due to the increasingly deep conditions of coal seams. The following article will analyze the current status of coal mining in Vietnam and some highlights of the coal industry development plan to 2030, in order to provide a general picture of Vietnam's coal industry in the future.

Keywords: Coal mining, Development plan, Mining technology, Environmental protection

1. Current status of coal mining in Vietnam

1.1 Distribution of coal resources in Vietnam

Vietnamese coal is distributed in all three regions: the North, the Central and the South. In the mainland, coal is found in some main coal basins: Northeast, An Chau, Lang Son, Red River, Nong Son. There are also several small, scattered coal storage areas such as Song Da (Muom Lum, Suoi Bang, Doi Hoa), Nghe Tinh (Dong Do, Huong Khe), Chay river (Hong Quang), etc., in which coal reserves and resources are concentrated in the Northeast and Song Hong basins. Coal in the continental shelf of Vietnam is distributed in the Red River, Hoang Sa, Truong Sa, Phu Khanh, Cuu Long, Nam Con Son [1, 2].

1.2 Exploration work

Coal exploration in Vietnam has gradually clarified the geological structure, resources, and coal reserves in the coal basins in the mainland. The Northeast, An Chau, Lang Son and Red River basins are identified as essential coal basins.

Coal in the Northeast basin has been searched, explored and exploited since the 19th century. Up to now, the geological structure of the Northeast basin has been thoroughly evaluated. This is Vietnam's leading coal mining area with large reserves such as Mao Khe, Vang Danh, Ha Lam, Khe Cham. Most of the coal mines in the Northeast basin have been assigned by the State to Vietnam National Coal-Minerals Holding Corporation Limited (Vinacomin) and Dong Bac Corporation to manage and exploit. Currently, the exploration work in the Northeast basin has been completed to the level of -300m (except for the new mines: Dong Trieu - Pha Lai, Bao Dai, Cuoc Be). However, exploration work in the Northeast basin continues to be carried out to increase the reliability of the remaining coal reserves [1, 2, 3, 4].

Some mines with large reserves and resources such as Khanh Hoa, Nui Hong, Lang Cam, Phan Me in An Chau coal basin have been invested and explored through many stages. The geological structure has been basically clarified. However, Khanh Hoa mine and Nui Hong mine need to continue exploring correct coal reserves and resources [2].

1.3. Coal mining

Vinacomin and Dong Bac Corporation are two leading coal production and trading units in Vietnam, which supply 95% of domestic coal production.

There are 5 large open-pit mines with over 2.0 million tons/year (Cao Son, Coc Sau, Deo Nai, Ha Tu, Tay

Nam Da Mai), the remaining open-pit mines with a total of 100 to 200 thousand tons/year and some open seam mining points with a capacity of fewer than 100 thousand tons/year. There are about 30 underground mines currently in operation, of which 11 have large deposits, have relatively comprehensive technology and infrastructure, with a capacity of 1.0 million tons/year or more, such as Mao Khe (2.0 million tons), Trang Bach (1.2 million tons), Nam Mau (2.5 million tons), Vang Danh (3.7 million tons), Binh Minh (1 million tons), Ha Lam (2.4 million tons), Nga Hai (1.5 million tons), Khe Cham III (2.5 million tons), Khe Tam (2.5 million tons), Lo Tri (2.0 million tons) and Mong Duong (1.5 million tons) [5]. New mines are under construction, such as Nui Beo (2.0 million tons) and Khe Cham II-IV (3.5 million tons). The remaining mines have a capacity of fewer than 1.0 million tons/year. The mining area is narrow, reserves are small or scattered, and there are no conditions to develop high output and apply synchronously.

1.4. Mining Technology

a. Open-pit mining technology

Implementing the sustainable development policy, the coal industry has promoted technological innovation over the years, invested in modern equipment and large capacity. At present, the technical level of open-pit mines has reached an advanced level.

- Increased application of technology to loosen the soil by mechanical methods, especially in residential areas, works that need to be protected by hydraulic dam heads, and large-capacity plough up to 670 KW (Komatsu D575A); using advanced blasting methods (creating edges, creating breakwaters, differential blasting, etc.) with high-performance, environmentally-friendly explosives, etc.; tested and applied the automatic fuel distribution and monitoring system; are conducting research and applying software to design, manage and operate mines equivalent to countries with developed mining industries [6, 7, 8, 9].

- The plan to connect 3 mines Deo Nai - Coc Sau - Cao Son brings high efficiency, reducing the peeling coefficient, the transport arc. Open-pit coal production units have invested many excavators with bucket capacity from 10-12 m³; cars with a tonnage of 90-100 tons and are testing 04 cars with a load of 130 tons; gradually apply computerization and automation to monitor the operation of equipment, towards the application of centralized monitoring and control [6, 7].



Fig. 1. Synchronization of large-capacity equipment in open-pit coal mining.

Presently, the used equipment fleet is as follow:

- + Drill with diameter $d_k = 200 \div 300$ mm;
- + Hydraulic excavator with bucket capacity $E = 3,5 \div 12$ m³, power shovel with $E = 5 \div 10$ m³;
- + For hauling waste rocks, use of dump trucks with payload of 55÷60 tonnes and 90÷120 tonnes;
- + For hauling coal, use of dump trucks with payload of 30÷40 tonnes;

+ Equipment fleet for mining and hauling comprise hydraulic excavators with $E=3,0\div 6,7$ m³, maximal digging depth $h_s \geq 8\div 9$ m and dump trucks of 25÷58 tonnes to transport coal from the working face to the bunker of crush station.

+ Beside that, at present Vinacomin (Cao Son surface coal mine) has invested the belt conveyor system and crush station with hauling capacity of 20 million m³ of waste rocks to the waste dumps.

+ For hauling coal, use of dump trucks with payload of 30÷40 tonnes.

b. Underground mining technology

Currently, coal industry units have promoted the application of mechanization (CGH) of stages from mining, transportation (people, coal, materials) in underground mining, the application of mining CGH today. It is being replicated in both quantity and variety of technologies. Significantly, the synchronous CGH furnace lines, lowering the ceiling to recover top coal at Ha Lam Coal Company, have a capacity of 1.2 million tons/year, contributing to improving coal production by CGH in the past year. The coal industry is contributing to improving working conditions, improving labour safety for workers in the pits, improving labour productivity and overall production efficiency for the coal industry.

Advanced technologies of countries with developed mining industries (Russia, Japan, Poland, China, etc..) have been gradually put into testing, evaluation and application; Specifically:

- Longwall mining technology, fully mechanised (mining by shearer, supporting by shield support), top coal caving (or single-pass longwall), roof controlled by full caving.

- Longwall mining technology, supported by hydraulic props (self-moving frame, chain-linked frame, light shield support, XDY support, hydraulic prop)

- Mining technology in dip direction, supported by 2ANSH support, mining by plough, roof controlled by full caving

- Mining technology in diagonal direction, supported by soft shield support, mining by drilling-and-blasting, roof controlled by full caving;

- Mining technology in horizontal-inclined slice, supported by hydraulic props (or frame), mining by drilling and blasting, roof controlled by full caving;

- Other technologies: sub-level stoping, room and raise, room and diagonal raised, supported by hydraulic props (or wood), mining by drilling and blasting, roof controlled by full caving to extract medium-thick seam, seam dip angle $>45^\circ$, protective pillars, resources loss and coal loss.

Currently, Vietnam's coal industry is deploying a variety of underground coal mining technologies. However, the application of mining technologies by synchronous mechanization and advanced technologies to increase the kiln's capacity depends significantly on the geological conditions of the area. While countries in the world have a significant advantage, especially reserves of pit coal are concentrated in coal seam thickness, angle slope, length according to the large and stability, in Vietnam, most of the coal mine tunnel furnaces with coal seams with thickness from thin to medium, large slope angle, according to the short length and often divided by milling out the geology.

Therefore, the application of synchronous mechanization technology and advanced technologies to increase the capacity of the market furnace in recent years is still only at the level of selecting several qualified units. Favourable to apply and expected to be replicated in units with similar geological conditions, the rest are mainly traditional mining technologies.

The output of underground coal mining by technology from 2015 to 2020 is as shown in Table 1. The distribution of underground coal mining output by technology in 2020 is as shown in Fig. 2 [8].

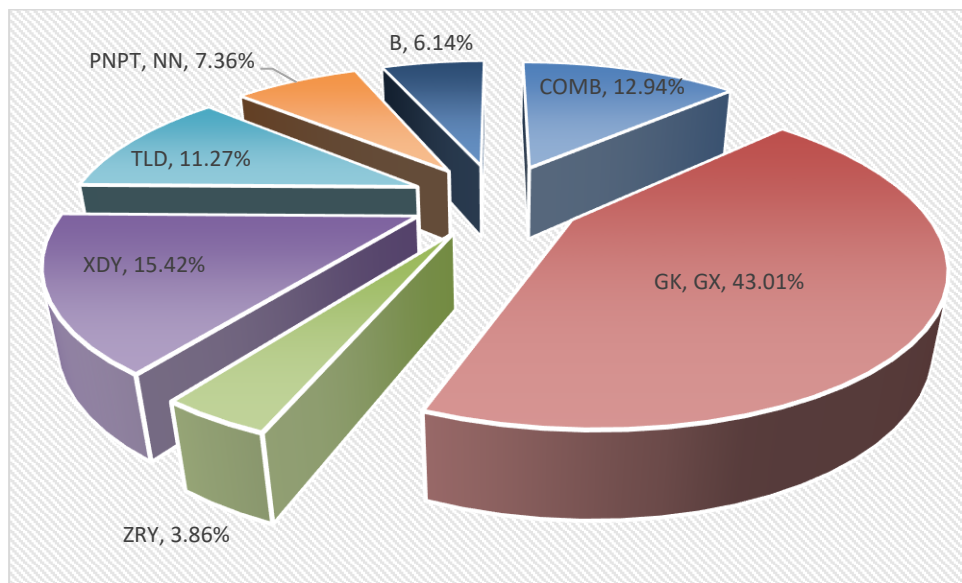


Fig. 2. Distribution chart of underground mining output by technology in 2020.

Tab. 1. The output of underground coal mining by technology from 2015 to 2020.

No.	Technology	Coal production, 10 ³ ton					
		2015	2016	2017	2018	2019	2020
	Coal production by technology	19,820	20,296	21,716	22,420	23,486	23,532
1	COMB	701	1,336	2,537	2,951	2,868	3,045
2	GK.GX	5,409	7,143	8,044	8,862	9,728	10,120
3	ZRY	23	128	265	857	800	909
4	XDY	5,796	5,148	4,468	3,989	4,146	3,629
5	TLD	4,336	3,722	3,135	3,180	2,814	2,652
7	PNPT, NN	2,896	1,994	2,151	1,912	1,732	1,733
8	B	659	825	1,116	669	1,398	1,444



(a)



(b)

Fig. 3. Synchronized mechanized furnace at Ha Lam Coal Company (a) and Mong Duong (b).

1.5. Environmental protection work

Concerning environmental protection, currently, the coal industry has achieved achievements in many areas such as [9]:

- Collection and treatment of all kinds of waste: Invested in building more than one hundred wastewater treatment stations to ensure that mines have wastewater treatment stations that meet environmental standards (Fig. 4a); coal mining plants invest in large-capacity sludge filtration systems, using circulating water that is not discharged into the environment; Built and maintained an industrial hazardous waste treatment plant in Quang Ninh; waste soil and rock generated from coal sifting screens are dumped into planned waste dumps. Ordinary industrial solid waste and daily-life solid waste generated in production shall be collected and treated under regulations.

- Environmental improvement and restoration: Planted trees to improve and restore the environment. Implement the plan of planting trees with high density to green the mine waste dumps, limiting soil quickly and rock washing, reducing dust emissions, quickly improving the general landscape environment, especially in the Ha Long city (Fig. 4b). Carrying out more than projects to build dykes and dams to prevent soil and rock from being swept away, renovate and restore the environment, renovate and dredging drainage systems, and settling lakes.



(a)



(b)

Fig. 4. (a) Wastewater treatment and (b) landfill rehabilitation of Vinacomin.

- Dust prevention: Invested in coal transport conveyor lines. Currently, the transportation of coal to the port and the power plants in Quang Ninh, Thai Nguyen, and Lang Son is carried out by conveyors and railways to overcome the dust situation, contributing to improving the environmental landscape of the cities; Installed nearly one hundred high-pressure misting machines (both mobile and fixed) for coal production units. Invest in specialized mine road irrigation vehicles to improve the capacity and efficiency of dust suppression on mine routes. Other anti-dust solutions in production have been enhanced: making hard dust covers on wagons, building car and wagon washing stations, making dust nets for coal warehouses, covering coal trucks and warehouses with tarpaulins piles, invest in the additional capacity of dust suppression water trucks, anti-dust water supply systems on waste dumps.

- Environmental pollution control: The coal industry cooperates with Quang Ninh province to invest and install automatic environmental monitoring systems for coal mine wastewater and transmit data directly to the Resource base and environment under the provisions of the law on environmental protection. Continue to

conduct concentrated environmental monitoring for residential areas at risk of being affected outside the management boundary to control and detect pollution risks and promptly direct preventive measures. Carry out periodic ecological tracking at the member unit following the approved environmental impact assessment report (congdoantkv.vn).

- Climate change response: Construction of many dams and dykes to prevent soil and rock at the bottom of the landfill, currently, the coal mine waste dumps have enough dykes as planned, preventing soil and rock from flowing, ensuring safety for production and population; Building nearly three dozen reservoirs upstream of streams for drainage, regularly dredging the system of rivers and streams to reduce sedimentation and prevent flooding; Relocating hundreds of households in dozens of areas at risk of dangerous landslides and floods due to the influence of coal mining areas under the overall migration scheme of Quang Ninh province to ensure safety. population during the rainy season.

- Innovating technology to contribute to environmental protection: The investment in coal mining technology towards mechanization and hydraulics in underground mining (hydraulic struts, hydraulic struts, excavators), synchronous investment in large-capacity equipment in open-pit mining has reduced the consumption of wood against furnaces, reduced coal loss, and reduced emissions. The screening plants invest in large capacity sludge filtration equipment to increase the coal recovery rate, use circulating water, and reduce discharge to the environment. Invest in a soft-start system of electrical equipment to save electricity. Take advantage of the lousy quality coal outside the standard, invest in recruiting stations to upgrade the quality to take advantage of resources.

2. Some highlights in the coal industry development plan to 2030

According to the forecast of the Master Plan, Vietnam will have to import a large amount of coal, and domestic exploitation can only meet about 50% of the total coal demand. The orientation of the coal industry is to continue investing in renovating and expanding existing mines and investing in deep and new mines on the principle of maximum exploitation and efficiency of coal resources; ensure the socio-economic efficiency of coal mining; ensure the harmonization of the interests of enterprises, employees, the coal region and the economy in association with national energy security and sustainable development of the coal industry. Specifically, as follows [3, 4]:

- Regarding coal exploration: To step up exploration and improve the reliability of resource and reserve supply to meet the coal mining target according to the master plan and the stable and long-term development of the industry. Expand search and exploration; step up exploration and assessment of reserves to the bottom of the coal bed; improve the quality of assessing reserves and resources.

- Underground coal mining: To focus on developing large-volume underground mines according to the criteria "Green mine, modern mine, high-yield mine"; Connecting underground mines with the same mining conditions into large capacity mines; Continue to invest in coal mines as planned, meeting the highest coal demand for the economy. Units focus on ensuring the progress of coal mine projects; Continue to research and innovate mining technology in the direction of modern advanced associated with mechanization, automation and computerization; synchronously implement solutions to increase labour productivity.

- Open-pit coal mining: To develop and expand existing open-pit mines in the direction of improving the limiting coefficient of peeling, suitable to technical conditions and coal selling price; maximize the exploitation capacity following the planning on dumping, transportation, water drainage and environmental protection; Maximize the exploitation of resources assigned to management, including the resources in the areas protecting the underground works, the remaining resources after the underground mining... Continue to change synchronously and modernized equipment of mining and transportation lines in the direction of putting into use mobile equipment with large capacity, continuous transportation systems suitable to the conditions and scale of each mine. ; Optimize the technical parameters of the applicable mining system; increasing the application of vertical layer mining system, selective mining and thin-seam mining technology; technology for dumping temporary and internal waste dumps.

Any technology must apply the most advanced technology and management solutions to minimize the loss rate and dirty coal in mining and reduce energy consumption.

- Environmental protection: With the goal of green growth, developing in harmony, being environmentally

friendly, the need to develop a circular economy and a substantial transformation under the strategy from brown to green needs to continue implementing a number of contents such as [8]: Implement environmental protection policies for the coal industry in association with the goal of reducing greenhouse gas emissions, promoting circular economy and sustainable development; Strictly control waste sources that pollute the environment, strengthen the prevention of environmental incidents, effectively use all kinds of resources, respond to climate change and epidemics; Invest in a mine wastewater treatment system to ensure environmental standards; complete installation of automatic ecological monitoring system for waste water and exhaust gas; Research to increase recycling and reuse of wastes for production and supply to other businesses; Continue to strengthen industrial hygiene, plant trees to improve the landscape and environment of factory premises and other production areas; Proactively adapting to climate change, ensuring the safety of landfills, minimizing soil and rock backflow, and preventing the risk of flooding; reduce greenhouse gas emissions, enhance resource utilization, and limit climate change impacts; Planning the entire mine space including waste dumps, ground, excavation pits to be renovated into: mine park with regulating lake; Continuing the idea of renovating the landfill into a world-class golf course; Or renovate and build apartment buildings for coal industry officials or apartment buildings for low-income people in the province. Early application of approved scientific topics into practice, such as applying lime nanotechnology in mine wastewater treatment (instead of using conventional lime powder at present, the cost is high, which is not as effective as using nano lime). Using environmentally friendly Neoweb technology to improve the quality of mine roads. Recycling quarry waste stone into standard building materials.

3. Overall rating

In recent years, the coal industry has performed well to ensure sufficient coal for domestic demand, especially coal for electricity production, ensuring national energy security.

Mining engineering is interested and focused by the coal industry, especially in mining, excavation, ventilation - drainage, electromechanical - transportation, mechanics - manufacturing. There are many breakthroughs, bringing excellent efficiency, contributing to the overall achievement of coal production and business, affirming a critical role, throughout which is "technology is the root of all problems" that determines the success of the coal industry, the existence and development of the coal industry.

Currently, the coal industry has been promoting investment to promote growth based on development in both breadth and depth by applying new, advanced and modern technologies to improve labour productivity, quality and efficiency products and business performance; concentrate resources to implement approved coal mine projects; develop coal mines according to the criteria "Clean mine, safe mine, modern mine" [9].

The management of exploitation and protection of mineral resources closely followed the approved planning, achieved positive results, and made significant contributions to the country's socio-economic development, transforming the country's economic structure and increasing the proportion of industry.

To step up research and investment in the application of advanced technologies, increase mechanization, computerization and automation to coal production, processing and trading. At the same time, it is determined that the development of mechanization, computerization, and automation in line with the trend of the fourth industrial revolution must be paid attention to, and is a critical task in the management work to improve labour productivity, safety, reduce costs, improve working conditions for employees, protect the environment, ensure overall business and production efficiency and the sustainable development of the coal industry.

It is necessary to invest heavily in the mechanization of coal mining and quarrying while gradually automating some stages such as transportation, drainage pumping, ventilation control, mine gas, power stations, and production process in coal sieving and sorting plants, etc. towards connecting centralized monitoring and control systems and building advanced, modern coal mines with few people.

4. Conclusions

Vietnam's demand for coal energy balance is enormous but challenging because of its limited potential, technology and management experience.

The coal industry continues to carry out planning, investment, exploration and exploitation of domestic

coal to supply coal to the economy. Currently, there are large mining projects such as anthracite mining in Quang Ninh and the construction of mining infrastructure.

To sustainably develop the coal industry, it is necessary to research and apply advanced and appropriate science and technology in coal mining and processing as well as environmental protection activities...; strengthen cooperation with organizations and businesses from other countries to develop coal mining and use technologies in an environmentally friendly and safe manner, and at the same time research and find foreign coal sources to contribute ensure quality security for Vietnam.

5. Acknowledgements

Paper was presented during the 6th VIET-POL International Conference Scientific-Research Cooperation between Vietnam and Poland, 10-14.11.2021, HUMG, Hanoi, Vietnam. We thank two anonymous reviewers for their comments that were very valuable for revising the manuscript.

6. References

1. Government, 2008. Decision No. 89/2008/QĐ-TTg dated 07/07/2008 by the Prime Minister of Vietnam on: Approving the strategy for the development of Vietnam's coal industry until 2015, with a 2025 orientation (in Vietnamese).
2. Informatics, Technology, and Environment Joint Stock Company – Vinacomin, 2015. Planning of coal exploration up to 2020 and a 2030 orientation (in Vietnamese).
3. Government, 2016. Decision No. 403/QĐ-TTg dated March 14, 2016 by the Prime Minister of Vietnam on: Approving the adjustment of the plan of development of Vietnam's coal industry up to 2020, considering the prospects for the year of 2030 (in Vietnamese).
4. Government, 2017. Decision No. 1265/QĐ-TTg dated August 24, 2017 by the Prime Minister of Vietnam on: Approving the adjustment and supplementation of the master plan on development of Vietnam's coal industry up to 2020, with the consideration of development outlook to 2030 (adjusted), (in Vietnamese).
5. Vietnam Coal-Mineral Industry Group, 2021. Report on evaluating the results of implementation of Joint Resolution No. 33-NQLT/DUTKV-ĐUTQN, dated April 18, 2018 on strengthening leadership at all levels of Communist Party Committees in the implementation of environmental protection in the period of 2018 - 2020 (in Vietnamese).
6. Ministry of Industry and Trade, 2021. Technical report on developing and updating the action plan to respond to climate change in the industry and trade sector in the 2021-2030 period. (in Vietnamese)
7. Mining and Industry Investment Consulting Joint Stock Company – Vinacomin, 2021. the National Energy Plan for the period of 2021-2030, with a vision to 2050 (coal sub-sector) (in Vietnamese).
8. Informatics, Technology and Environment Joint Stock Company – Vinacomin, 2021. Project on environmental protection of Quang Ninh coal region for the period from 2020 to 2025 and a 2030 orientation (in Vietnamese).
9. Vietnam Coal and Mineral Industries Group (2021), Report on summarizing S&T research (in Vietnamese).
10. Report on results of application of annual technologies in the period from 2015 to 2020 By Vietnam National Coal - Mineral Industries Holding Corporation Limited and Dong Bac Corporation (in Vietnamese).

Cause and Solution to Roadway Deformation in Vietnam Underground Coal Mines

LE Quang Phuc^{1,*}

¹ Hanoi University of Mining and Geology, 18 Vien street, Hanoi, Vietnam

Corresponding author: lequangphuc@humg.edu.vn

Abstract. The deformation and support method of roadways have always been important issues in safe mining and production. Vinacomin's statistics show that, by 2021, there will be 64.19 km of roadways that need to be repaired (accounting for 25% of the total new roadways). Thus, the problem of maintaining roadway stability is facing difficulties in underground coal mines in Vietnam. To find out the causes of roadway failures, a case study at roadways of the Khe Cham I and Khe Cham III coal mines, Vietnam, is presented in this paper. Based on the results of a detailed field survey, the deformation characteristics of roadways and the failure mode of support structures were investigated. The results show that the roadway deformation is severe and the main support cannot control surrounding rock mass. Also, the destruction of support structure is frequent on reused roadways, affecting production efficiency and work safety. Therefore, to reduce deformation and increase roadway stability, a new support method called "multi-stage anchor of rock bolt + cable bolt" has been developed and a new longwall mining system with critical coal pillar width has been proposed. The new findings of the research can provide references for scientific studies, and apply them in Vietnam's underground coal mine practices.

Keywords: Roadway deformation, Coal pillar, Longwall mining system, Underground coal mine

1. Introduction

In coal production by underground mining method, controlling and maintaining roadway stability is an important task and has a positive influence on safety and high-efficiency production. Controlling roadway deformation using appropriate support and retention measures has become an extremely important area of focus in the study of rock mechanics and mining [1]. The deformation characteristic of roadways have been one of the hot research topics and have received considerable attention from researchers around the world. Coggan et al. [2] or Huang et al. [3] investigated the effect of an intercalated rock layer in the coal seam on roadway deformation. They found that the weak interstitial rock layer had a significant effect on the degree of roadway failure, causing asymmetric stress around the roadway. Tu et al [4] presented a mechanical model based on theoretical analysis and a prediction of the stress distribution around the roadway. Yan et al. [5] explored the influence of faults on the deformation mechanism of roadways and found that roadway strain increased when they were located near faults. Yu et al. [6] studied the deformation law of the roadway next to gob based on numerical simulation and field survey method. Chang et al. [7] or Gao et al. [8] discussed the characteristics of roadway deformation. They show that the high stress in rock mass, the stress caused by exploitation of adjacent panels, and the low strength of rock mass cause deformation of the roadway. Chen et al. [9], Kang et al. [10] or Yang et al. [11] used numerical simulations such as UDEC and FLAC3D to investigate the damage characteristics due to deformation of deep roadway.

For the conditions of Vietnam's underground coal mines, the deformation and failure mechanism of roadways in the area impacted by longwall faces have not been studied specifically and in detail. The width of protective coal pillar and the roadway support solution are usually taken from the experience of other regions. This implementation causes unsafe and roadway stability problems, which incurs a lot of repair costs. The roadway often suffers large deformations, the supports are destroyed, and the roadway stability cannot be guaranteed. The main remedial solution used was the repair and replace new support. This increases production cost and reduces economic efficiency and labor safety. Vinacomin's statistics show that, by 2021, there will be 64.19 km of roadways that need to be repaired (accounting for 25% of the total new roadways). Thus, the problem of maintaining roadway stability is facing difficulties in underground coal mines in Vietnam.

With these existences, performing field investigations and a detailed assessment of the status of roadways support in Vietnam's underground coal mines in the current period is of high urgency. The research results are practical scientific evidence to develop and apply solutions suitable to specific conditions, ensuring safety and economic efficiency.

2. Study areas and Methods

The study area was carried out at Khe Cham I and Khe Cham III coal mines in the Quang Ninh coal basin. The Field research method was carried out with the help of colleagues and mine engineers. After that, a numerical model is developed for preliminary evaluation of the proposed solution.

3. Results and discussions

3.1 Field research results

Conducting field investigations is a suitable way to understand roadway deformation in detail and visually. In this study, it was carried out on ventilation roadways No. 11.1.3 & No.11.1.4 on coal seam 11 of Khe Cham I coal mine, ventilation roadway No. 14.5.2A on coal seam 14.5 Khe Cham III coal mine. The roadways are located 300 m below the terrain surface. The cross-sectional area of the roadways when designed is about 8.4-9.5 m². The width of the protective coal pillars is 18-20 m. Steel supports "SVP" or anchors are used in the roadways. [12, 13].

Roadways No.11.1.4 & No. 14.5.2A used steel support "SVP". Support structures include two support columns linked to beams by sliding connection. The distance between support is 0.7 m and $\Phi 90$ mm wood is used to make wall and roadway roof inserts.

Roadway No. 11.1.3 using anchor support - rock bolt of type $\Phi 22.0$ mm and length of 2.4 m is used; internal length of rock bolts to roof and roadway wall is 2.3 m, the exposed length is 0.1 m, the tensile strength of rock bolt is 260 KN, the layout space is 900 mm x 900 mm.

To provide visual data for the application of appropriate support measures, the survey includes - a survey of rock mass structure, support structure, roadway deformation, construction method, and other factors that affect roadway stability. The visual research results are shown in Figures 1, 2, and 3.

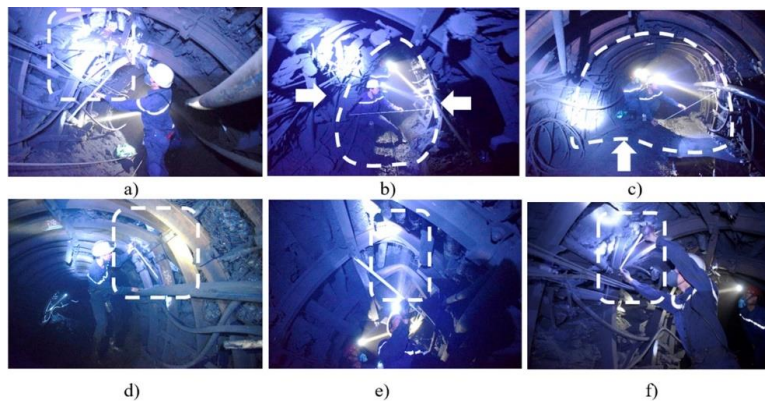


Fig. 1. Visual study results at roadway No.11.1.4, where "SVP" steel support is used.

- a - Break of supports; b - Rib bulge; c – Floor heave; d - Break of sliding connection; e - Break beam;
- f - Steel column tearing.

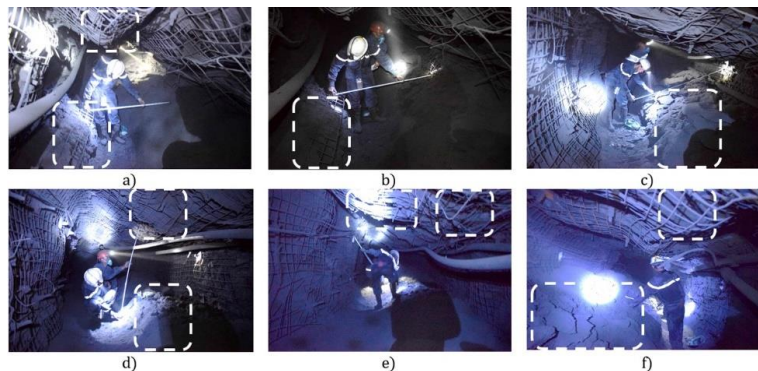


Fig. 2. Visual study results at roadway No.11.1.3, where rock bolt is used.

a - Roof sag and rib bulge; b - Rib bulge; c - Rib bulge and floor heave; d - Roof sag and floor heave; e - Roof sag; f - Floor heave and rib bulge.

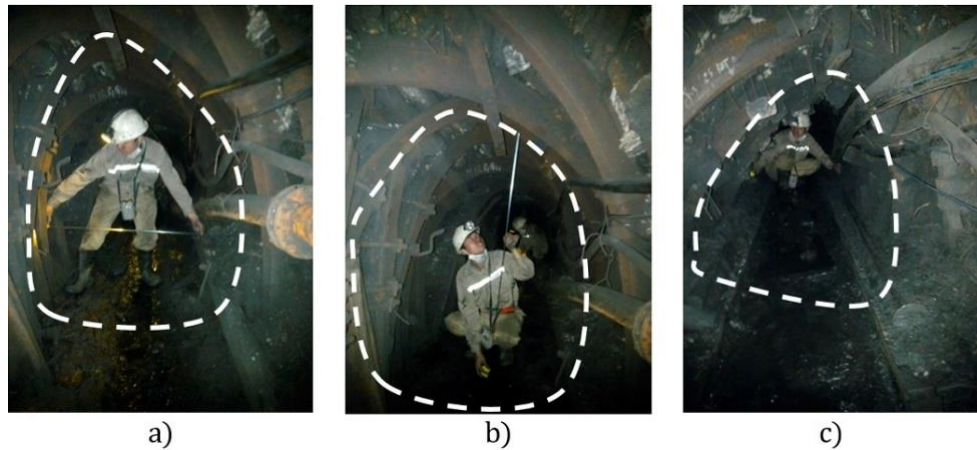


Fig. 3. Visual study results at roadway No.15.5.2A, where "SVP" steel support is used.

Figures 1-3 show the roadway deformation patterns in this area can be arranged as follows: unsymmetrical pressure, rib bulge, floor heaving, broken sliding connection, broken support beam "SVP" or sag roof (rock bolt), the support frame is destroyed.

In addition, monitoring of roadway convergence is carried out with two measuring stations located on the headgates No.11.1.3 and No.11.1.4 (corresponding to two types of supports). At the time of measurement, the upper mining panels have been fully mined. Figure 4a shows the location of this measuring station in the typical area of headgate No.11.1.3. A detailed description of the measurements, including equipment, station installation, and data collection is as follows: For each measuring station, permanent paint marks (solid red circles in Figs. 4c, 4d) are marked respectively on the roof, and the two ribs of the road, and on the floor is fixed with pegs of 50 cm long. The roof and floor are installed in the middle of them, and the ribs are marked on support columns or anchor locks.

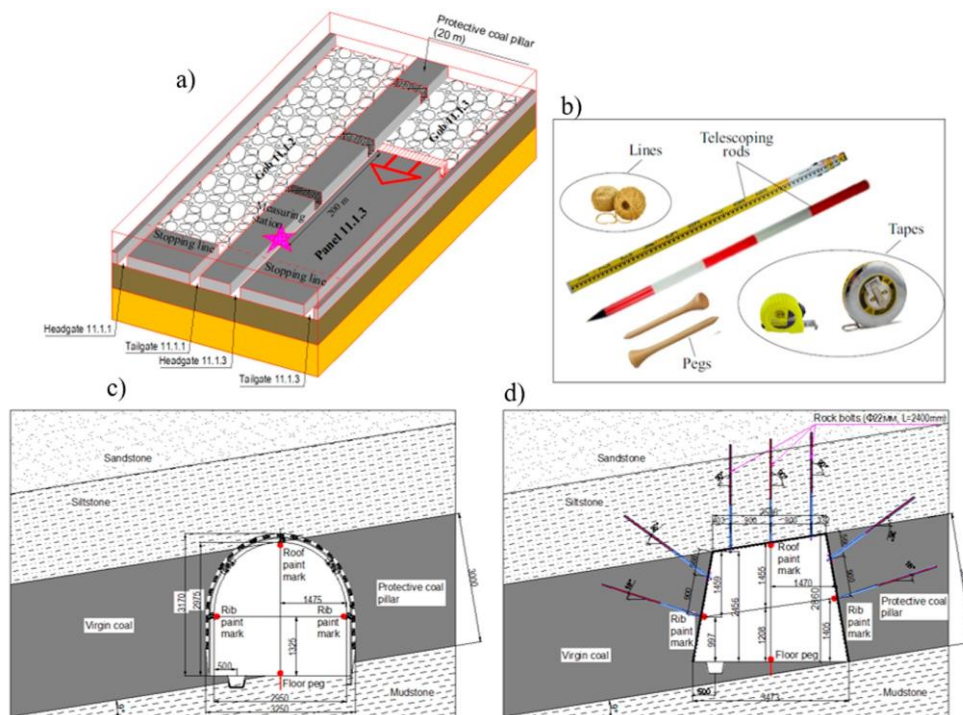


Fig. 4. The layout of roadway and roadway convergence measurement in the field.

a – The layout of roadways, typically at panel 11.1.3; b – Measurement devices; c, d – The layout of the measurement station of roadways No.11.1.4 & No.11.1.3.

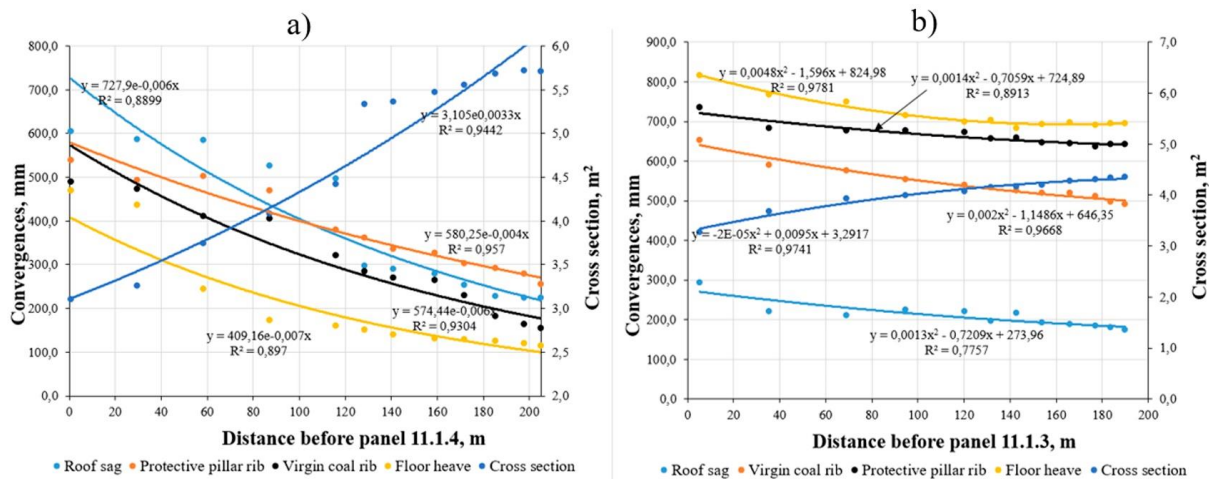


Fig. 5. Measured convergences in headgate during panels retreat.

a - convergences of headgate No.11.1.4; b - convergences of headgate No.11.1.3.

Figure 5 shows the result of the convergence of roadways No.11.1.3 & No.11.1.4 during the reuse period for the lower panel. It should be noted that, at the time of measurement, the roadway had a significant convergence due to the influence of the previous mining panel. The results have shown that about 200 m ahead of the 2nd longwall face, the deformation of the headgate with SVP support is much more intense than that of the headgate with anchor support. For example, at headgate No.11.1.4, the increasing amplitude of roof convergence is from 220 mm to 730 mm, of coal pillar rib is 265-578 mm, of virgin coal rib is 185-575 mm, and of floor heave is 100-405 mm. This shows that the SVP steel support has a good stability during the first panel's exploitation period, but cannot guarantee its integrity when it is in the abutment pressure zone of the second longwall face. A Typical example is the breakdown of the support structure and roadway deformation, as shown in Figs. 1 and 3. Meanwhile, for headgate No.11.1.3, where anchor support is used, the opposite is true. Most of the deformation occurs during the exploitation of the first panel, and when it is in the bearing pressure area of the second working surface, the amplitude of convergence is not large with roof convergence in the range of 190-275 mm, coal pillar rib 650-735 mm, virgin coal rib 500-640 mm and floor heave 700-810 mm. In actual monitoring at the field, the convergence amplitude of headgate No.11.1.3 is not as high as that of headgate No.11.1.4 due to the addition of two rows of reinforced hydraulic columns at a distance of 25 m in front of the second longwall face. However, in general, both types of supporting structures do not meet the technical and safety requirements. The SVP steel support is easily broken, and the 2.4 m rock bolts are too short and not long enough to penetrate the plastic deformation zone of the surrounding rock mass. The final used cross-section of the roadway is only 2-3 m².

3.2 Discussions the results

Based on the above data, we have carried out a comprehensive analysis of the field survey results, and can reveal several causes of roadway deformation with the following characteristics:

3.2.1. Roadway deformation is influenced by the main stress

In the distribution area of the roadways of the longwall mining system, the vertical stress from the main roof is very high, leading to a large horizontal stress growth at the ribs and floor. Fieldwork results have shown that rib bulge, floor heaving, broken sliding connection, broken support beam "SVP", all related to lateral stresses, account for about 70% of the total deformation locations of the roadway. When the roadway is under a lateral force, the weak structural surfaces in the coal pillar and coal massive move towards the free surface, and support structure failures occur if this force exceeds its limiting resistance. In particular, the roadways are within the influence area of the longwall face from the adjacent panel, the deformation of the roadway becomes more severe. Furthermore, we can see from Fig. 1b that the direction of the asymmetric pressure is roughly consistent with the direction of action of the primary stress that thrives from

the (almost horizontal) side of the coal pillar.

3.2.2. *The influence of the time factor*

The effects on the deformation of the roadway from the time factor include two aspects: the deformation rate and the deformation time. In the longwall mining system with the protection of coal pillars, after the first longwall face passes, the unloading and collapse of the surrounding rock mass are very severe because of the stress change in the roof rock layer, which is adjacent to the gob. Depends on the type of support, roadway deformation occurring during this period can account for more than 40% of the total deformation of the surrounding rock (example headgate 11.1.3). After the stress state is redistributed to a new equilibrium, the strain rate slows down and has a linear direction with time until it is in the stress region of the second longwall face. Rock mass deformations accelerate in magnitude under the abutment pressure of the longwall face. Here, the deformation is accelerated strongly with the average speed according to the measurement and statistical results in the study area: the roof convergence is 1.3 mm/day, left rib bulges 4.7 mm/day, right rib bulges 0.6 mm/day and floor heaving 4.1 mm/day. According to the monitoring results, the roadway does not achieve stability when lying in this area, the entire supporting structure is almost destroyed, so it has to be repaired locally to ensure production safety.

3.2.3. *The influence of spatial factors*

Similar to the time factor, the roadway deformation is greatly influenced by their distribution in relation to the surrounding structures. Previous studies have shown that, in the longwall mining system, the deformation process of the reusable roadway takes place in three main stages:

- During the panel preparation stage - the deformation is very small, the roadway is stable;
- In the second stage when the roadway is in the area of influence of the abutment pressure from the first longwall face, and then the pressure disturbance area from the gob next to the coal pillar - the roadway is deformed strongly and quickly;
- In the third stage, the roadway deformation is slow and linear because the rock layers and coal pillar are in a new equilibrium, and until it is in the abutment pressure area of the second longwall face, its deformation is increasing rapidly and strongly.

Thus, roadway deformation mainly occurs at the 2nd stage and at the end of stage 3. If the roadway support structure is not good, it will lead to deformation and collapse. In the results of the field study, at the end of stage 3, the roadways were greatly deformed and had to be repaired locally.

3.2.4. *Influence from the width parameter of the protective coal pillar*

In the longwall mining system, besides the role of the supporting structures, the protective coal pillar is a very important factor for the roadway to be reused next to it. The width of coal pillar and its load capacity have been studied in many workings. Many mechanical models have been proposed to analyze the stability of coal pillars such as the nonlinear rheological model of Wang et al. [14], simulating the simple spring model and the curved roof model of Mroz et al. [15]. In addition to mechanical models, mathematical models have also been introduced, for example, logistic regression and symmetry matrices in the study of Salamon [16] or Wattimena et al. [17]. In addition, the studies of Li et al., Wang et al., Mao et al. and Zubov et al. [18, 19, 20, 21, 22, 23, 24, 25] based on the limit equilibrium rule, numerical simulation and experimental research to evaluate the load capacity of coal pillars and the stability of the roadway. These studies all reveal that the coal pillar is stable only when there is an elastic region in the center of the coal pillar. A simulation of this state is shown in Fig. 6.

Fig. 6a shows that the plastic deformation region running through the coal pillar makes it weak and unstable. The coal pillar pushed into the roadway space by the strong development of cracks across its entire width. This causes the roadway to be strongly compressed and asymmetrical between the two sides, the steel support is easily destroyed.

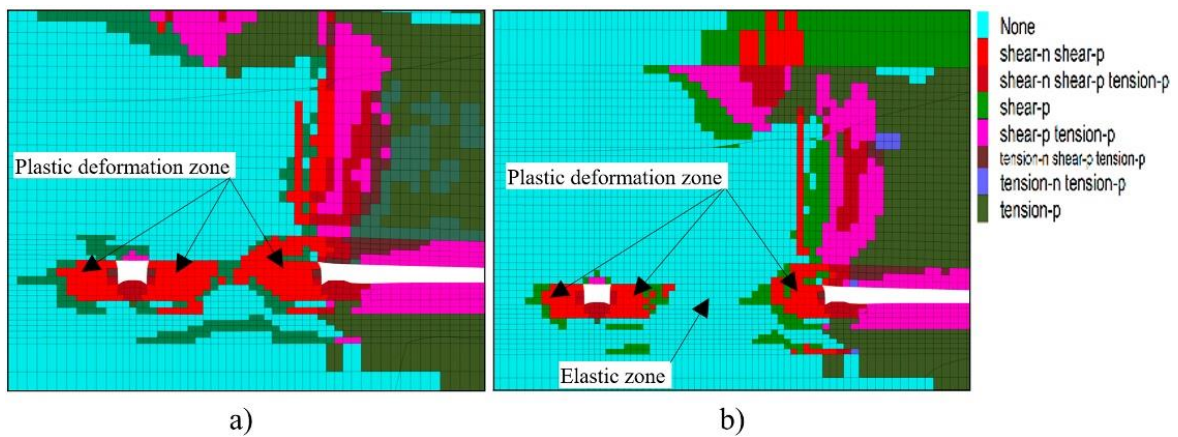


Fig. 6. The distribution of deformation and elastic regions of coal pillars in the longwall mining system, a – Coal pillar 20 m width according to reality; b – 30 m width coal pillar.

Fig. 6b shows that, when the coal pillar width is large enough, an elastic region appears in its center. This is the main bearing area and maintains stability of the coal pillar. The plastic deformation areas only grow to a certain limit. Therefore, if a reasonable supporting structure is used, the roadway will completely ensure the stability and safety of production, reducing the repair costs incurred.

3.1.5. Recommendation of applicable solutions

According to the above analysis, the disadvantages leading to the failure of roadway stability control at underground coal mines in Quang Ninh coal basin of Vietnam are:

(1) Load bearing capacity of the steel support "SVP" according to the current passport is not enough to ensure the stability of the reuse roadway in the area affected by longwall face, the steel support is prone to bending and breaking.

(2) Due to the influence of loads and displacements of the upper rock strata, the coal pillar and surrounding rocks tend to move into the reuse roadway space, and form cracks and plastic deformation in the coal pillar. When the coal pillar is not wide enough, this plastic deformation area will run through and occupy its entire area. The growth of this fissure zone is responsible for the weakening, deformation and even collapse of the coal pillar. This is a dangerous threat to occupational safety and the instability of the reused roadway.

(3) The short rock bolts are not capable of anchoring the rock mass around the roadway with the stable rock deep within. Because their length (2.4 m) is not enough to overcome the plastic deformation area to anchor the surrounding weak rock mass to the more stable rock mass. Therefore, the sole use of these rock bolts in the support structure will not guarantee the effect of roadway stability and safety of production

Thus, from the existing situation of the stability control of the reuse roadway in the longwall mining system, the first problem that needs to be overcome is to determine the critical width of the coal pillar, which capable of guaranteeing its own stability. This means that the coal pillar must be wide enough to ensure its stability, which in turn leads to the stability of the roadway being protected. In addition, the loss of coal in these coal pillars also needs to be studied. Therefore, to compensate for the shortcomings of the current mining system, a scheme is recommended to be applied as shown in Figure 7b [21, 22].

In the recommended diagram, a coal pillar of sufficient width will improve the protection and stability of the reuse roadway. After the function expires, coal pillars will be extracted along with the next longwall face to reduce coal resource loss.

In addition, the support structure of the roadway also needs to change. Steel support with current passport is no longer suitable under high mine pressure conditions. Especially, large rib pressure will easily destroy it. Moreover, the heavy weight of the steel support will be an important drawback when using it for deep roadways [26].

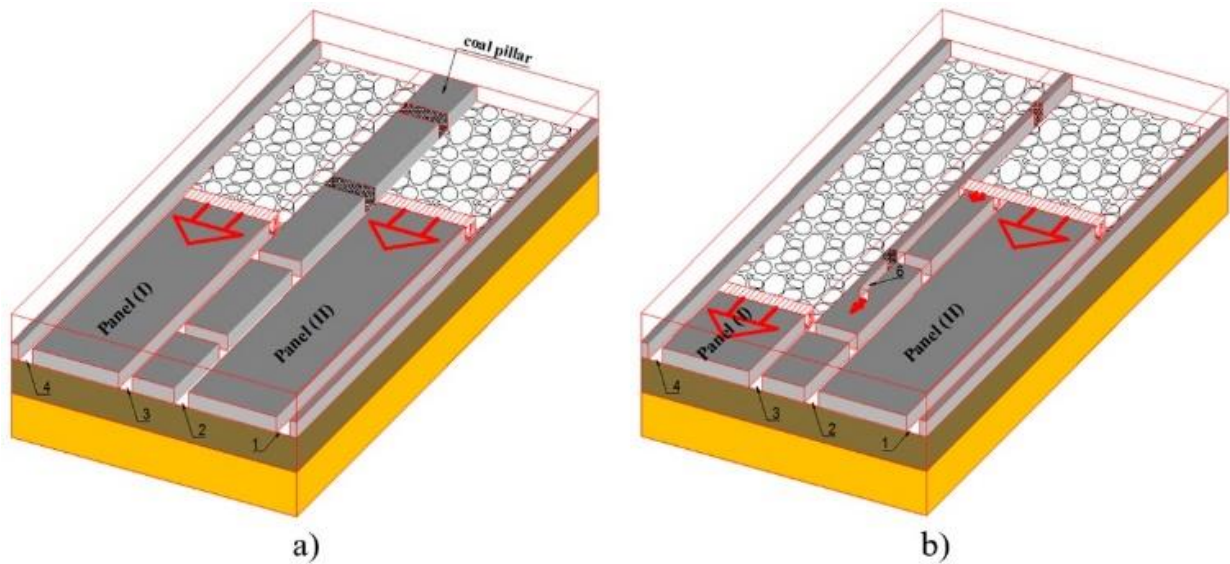


Fig. 7. Diagram of longwall mining system,

a – Current applicable diagram; b – Recommended application diagram.

At present, most of the underground coal mines in the world prefer to use the self-loading support method of the rock mass - the anchor support method. However, in order to improve the efficiency of use, the anchor length must overcome the plastic deformation around the roadway to anchor them to the hard rock mass. On that basis, the article recommends using a multi-stage anchor system combining rock bolts and cable bolts for roadways. The structure of the proposed multi-level anchoring system is as follows:

- Rock bolts: 2.4 m long, with a spacing of $0.9\text{ m} \times 0.9\text{ m}$, applied immediately after roadway excavation. The rock bolts pass through the plastic deformation zone around the roadway, securing them to prevent the falling rock into the roadway and collapsing during construction. This kind of flexible support can also release the initial rock stress to some extent, relieving the stress on the cable bolt.

- Cable bolts: 5 m (or 7 m) long, installed on locations where great convergence and deformation often occur, to fully correct the horizontal deformation of the road. Furthermore, cable bolts combine with rock bolts to connect the surrounding rock mass and to form a support system with strong resistance to deformation. This will greatly improve the stability and integrity of the surrounding rock.

The shallow area of broken rock around the roadway has poor stress transfer capacity. Through the multistage anchoring system, an effective superposition of the surrounding rock stress has been achieved, and its combined effect is capable of maintaining good roadway stability. It also fully mobilizes the capacity of the deep rocks, stabilizing the surrounding and inhibiting the development of deformation.

To evaluate the results of the proposed solution, the numerical modeling method with FLAC3D software was used. The input parameters of the model are made similar to roadway No.11.1.3 (in depth $H = 300\text{ m}$) on the seam 11 of Khe Cham I coal mine. In the proposed solution, the coal pillar is designed with a width of 30 m, the roadway is supported with the system multi-level anchor system (Fig. 8). The parameters of rock bolts and cable bolts are taken according to its manufacturing specifications. The dimensions of the model are $260\text{ m} \times 210\text{ m} \times 150\text{ m}$. Panels 11.1.1 & 11.1.3 and the gate roads system have been included in the model. A vertical stress of 6.5 MPa was applied at the top model boundary to simulate an overburden pressure by assuming the overburden unit weight is 0.025 MN/m^3 , and gravity force was applied. The horizontal displacements of the four vertical planes of the model were restricted in the normal direction, and the vertical displacement at the base of the model was set to zero. Mohr - Coulomb deformation model is used in the research process [27].

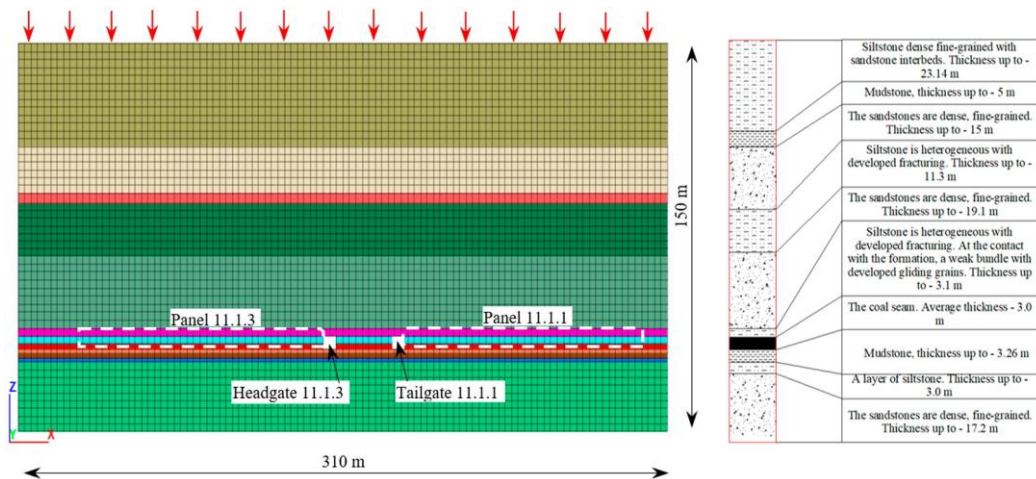


Fig. 8. Configuration of the model performed using FLAC3D and lithological profile.

Tab. 1. Mechanical properties of the rock strata used in numerical modeling.

Strata	Tensile strength (MPa)	Bulk modulus (GPa)	Shear modulus (GPa)	Poisson ratio	Cohesion (MPa)	Friction angle (deg)	Density (kg/m ³)
Sandstone	1.6	7.456	3.244	0.31	3.2	34	2780
Siltstone	0.9	2.333	0.955	0.32	2.1	30	2550
Mudstone	1.2	1.822	0.607	0.35	1.8	26	2250
Coal	0.4	0.748	0.484	0.26	1.5	19	1450

The simulation results of the plastic deformation regions around the roadway and the stress state on the coal pier are presented in Figure 9.

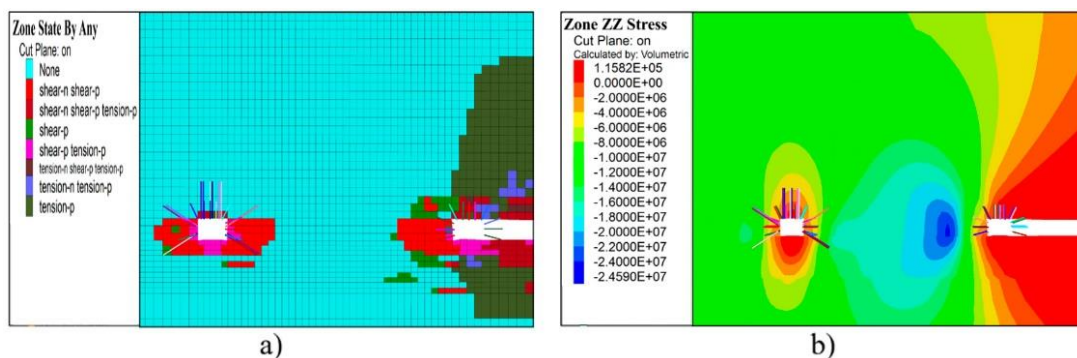


Fig. 9. Numerical simulation with the proposed solution, a – The state where the plastic deformation area appears; b – Vertical stress distribution on the coal pillar and around the roadway.

The simulation results show that the size of the elastic zone in the coal pillar is quite sufficient to ensure the stability of the pillar. With this solution, two vertical stress peaks are formed in the coal pillar, so the roadway is safe from the influence of gobs. The multi-level anchoring system has linked the plastic deformation around the roadway with the hard rock to form a stable and stable block. Therefore, the effect of roadway deformation control effect with the proposed solution is completely feasible.

4. Conclusions

This article has discussed the deformation breakdown and stability control results of reused roadways

in the longwall mining system at underground mines of the Quang Ninh coal basin. Characteristic data are obtained through the results of fieldwork at Khe Cham I and Khe Cham III mines. On the basis of detailed field investigation, the types and deformation characteristics of the roadway have been identified. Some proposed solutions to minimise roadway deformation have also been implemented. The main conclusions of the study are as follows:

(1) The types of roadway deformation failures can be classified into unsymmetrical pressure, rib bulge, floor heaving, broken sliding connection, broken support beam "SVP" or sag roof (rock bolt). Moreover, the main causes affecting the roadway deformation include roadway lifetime effect, spatial effect, effect of main stress and width of the protective coal pillar.

(2) Investigation and measurement results have shown that the roadway deformation occurs very strongly when it is in the abutment pressure area of the longwall faces. Most roadways require local repairs to ensure ventilation and production safety. These roadways have demonstrated that the correlation between the width of the protective coal pillar and the existing roadway support structure does not meet the safety and efficiency requirements.

(3) A new scheme of the proposed longwall mining system and a multi-level anchorage structure has been developed. The elastic zone at the center of the coal pillar completely guarantees the stability of itself and the roadway. In addition, support with multi-tiered anchors and surrounding rock mass forms a hierarchical support system that can cooperate and work together. The evaluation results show that the effectiveness of the proposed solution is completely feasible for the reusable roadway in the longwall mining system.

5. Acknowledgements

Paper was presented during the 6th VIET-POL International Conference Scientific-Research Cooperation between Vietnam and Poland, 10-14.11.2021, HUMG, Hanoi, Vietnam. The author would like to thank the staff of Ha Long Coal Company and Khe Cham Coal Company for their help to complete this research.

6. References

1. Guo, Z., Yang, X., Bai, Y., Zhou, F., Li, E., 2012. A study of support strategies in deep soft rock: The horsehead crossing roadway in Da qiang coal mine. *Int. J. Min. Sci. Technol*, 22: 665-667, <https://doi.org/10.1016/j.ijmst.2012.08.012>
2. Coggan, J., Gao, F., Stead, D., Elmo, D., 2012. Numerical modelling of the effects of weak immediate roof lithology on coal mine roadway stability. *Int. J. Coal Geol*, 90: 100-109, <https://doi.org/10.1016/j.coal.2011.11.003>
3. Huang, F., Zhu, H.H., Zhu, Q.W., Xu, Q.W., 2013. The effect of weak interlayer on the failure pattern of rock mass around tunnel-Scaled model tests and numerical analysis. *J. Tunn. Undergr. Space Technol*, 35: 207-218, <https://doi.org/10.1016/j.tust.2012.06.014>
4. Hong-sheng, T., Shi-hao, T., Chen, W., Ding-yi, H., De-fu, Z., 2018. Mechanical analysis of a vertical-wall, semicircular-arch roadway and a repair technique using double-shell support. *Environ. Earth Sci*, 77: 509, <https://doi.org/10.1007/s12665-018-7680-3>
5. Yan, S., Bai, J.B., Li, W.F., Chen, J.G., Li, L., 2012. Deformation mechanism and stability control of roadway along a fault subjected to mining. *Int. J. Min. Sci. Technol*, 22: 559-565, <https://doi.org/10.1016/j.ijmst.2012.01.020>
6. Yu, Y., Bai, J., Wang, X., Zhang, L., 2020. Control of the Surrounding Rock of a Goaf-Side Entry Driving Heading Mining Face. *Sustainability*, 12, p 2623, <https://doi.org/10.3390/su12072623>
7. Chang, Q.L., Zhou, H.Q., Xie, Z.H., Shen, S.P., 2013. Anchoring mechanism and application of hydraulic expansion bolts used in soft rock roadway floor heave control. *Int. J. Min. Sci. Technol*, 23: 323-328, <https://doi.org/10.1016/j.ijmst.2013.05.017>
8. Gao, F.Q., Stead, D., Kang, H.P., 2015. Numerical simulation of squeezing failure in a coal mine roadway due to mining-induced stresses. *Rock Mech. Rock Eng*, 48: 1635-1645, DOI 10.1007/s00603-014-0653-2
9. Chen, X., Guo, H., Zhao, P., Peng, X., Wang, S., 2011. Numerical modeling of large deformation and nonlinear frictional contact of excavation boundary of deep soft rock tunnel. *J. Rock Mech. Geotech. Eng*, 3: 421- 428, <https://doi.org/10.3724/SP.J.1235.2011.00421>

10. Kang, Y.S., Liu, Q.S., Xi, H.L., 2014. Numerical analysis of THM coupling of a deeply buried roadway passing through composite strata and dense faults in a coal mine. *Bull. Eng.Geol. Environ*, 73: 77-86, DOI 10.1007/s10064-013-0506-3
11. Yang, S.Q., Chen, M., Jing, H.W., Chen, K.F., Meng, B., 2017. A case study on large deformation failure mechanism of deep soft rock roadway in Xin'An coal mine, China. *Eng. Geol*, 217: 89-101, <https://doi.org/10.1016/j.enggeo.2016.12.012>
12. Phuc Le Quang, Vladimir Zubov, Thang Pham Duc, 2020. Design a Reasonable Width of Coal Pillar Using a Numerical Model. A case study of Khe Cham basin, Vietnam. *E3S Web of Conferences*, 2020 174 01043. "Vth International Innovative Mining Symposium". 10p. DOI: 10.1051/e3sconf/202017401043.
13. Le Quang Phuc, V. P. Zubov, Phung Manh Dac, 2020. Improvement of the Loading Capacity of Narrow Coal Pillars and Control Roadway Deformation in the Longwall Mining System. A Case Study at Khe Cham Coal Mine (Vietnam). *Inżynieria Mineralna - Journal of the Polish Mineral Engineering Society*, 2: 115-122. <http://doi.org/10.29227/IM-2020-02-15>
14. Dong Wang, Yujing Jiang, Xiaoming Sun, Hengjie Luan, Hui Zhang, 2019. Nonlinear Large Deformation Mechanism and Stability Control of Deep Soft Rock Roadway: A Case Study in China. *Sustainability*, 11, p 6243, <https://doi.org/10.3390/su11226243>
15. Mroz, Z., Nawrocki, P., 1989. Deformation and stability of an elasto-plastic softening pillar. *Rock Mech Rock Eng*, 22: 69-108.
16. Salamon MDG, 1970. Stability, instability and design of pillar workings. *Int J Rock Mech Min Sci Geomech Abstr*, 7: 613-631, [https://doi.org/10.1016/0148-9062\(70\)90022-7](https://doi.org/10.1016/0148-9062(70)90022-7)
17. Wattimena, R., Kramadibrata, S., Sid,i I., Azizi, M., 2013. Developing coal pillar stability chart using logistic regression. *Int J Rock Mech Min Sci*, 58: 55-60, <https://doi.org/10.1016/j.ijrmms.2012.09.004>
18. Li, C., Xu, Jh., Panm Jz., Ma, C., 2012. Plastic zone distribution laws and its types of surrounding rock in large-span roadway. *Int J Mining Sci Technol*, 22(1): 23-28, <https://doi.org/10.1016/j.ijmst.2011.06.002>
19. Wang, B., Jiang, F., Wang, C., Zhang, B., 2019. Experimental Study on the Width of the Reasonable Segment Pillar of the Extremely Soft Coal Seam in the Deep Mine. *Geotechnical and Geological Engineering*, 37: 4947-4957, <https://doi.org/10.1007/s10706-019-00954-6>.
20. Li, M., Mao, Xb., Yu, Yl., Li, K., Ma, C., Peng, Y., 2012. Stress and deformation analysis on deep surrounding rock at different time stages and its application. *Int J Mining Sci Technol*, 22(3):301-306, <https://doi.org/10.1016/j.ijmst.2012.04.003>
21. Zubov В. П., 1998. Метод оценки параметров областей с повышенной нарушенности пород кровли над краевыми частями угольного массива / В. П. Zubov, Г. И. Козовой, А. Б. Соколов. Доклады III Международной конференции "Горное оборудование, переработка минерального сырья, новые технологии, экология" / Санкт-Петербургский горный институт. СПб, С. 44-50.
22. Zubov, V.P., 2013. Scientific school "Development of solid mineral deposits": stages of formation, main research results, directions of development. *Journal of Mining Institute*. T.205. SPB, p 11-17.
23. Kazanin, O.I., Yaroshenko, V.V., 2020. Decrease in coal losses during mining of contiguous seams in the near-bottom part at Vorkuta deposit. *Journal of Mining Institute*, 244: 395-401. DOI:10.31897/PMI.2020.4.1.
24. Quang Phuc Le, Tien Dung Le, Duc Thang Pham, Anh Tuan Nguyen, 2019. Strata movement when extracting thick and gently inclined coal seam from a physical modelling analysis: a case study of Khe Cham basin, Vietnam. *Scientific journal "Sustainable development of mountain territories"*, 11(42): 561-567, DOI: 10.21177/1998-4502-2019-11-4-560-566.
25. Kazanin, O.I., Sidorenko, A.A., Sirenko, Y.G., 2019. Analysis of the methods of calculating the main roof caving increment in mining shallow coal seams with long breaking faces. *ARNP Journal of Engineering and Applied Sciences*, 14(3): 732-736.
26. Pham, N.Thi and Nguyen, N.Viet 2021. The effects of dynamic pressure on the stability of prepared drifts near the working surface areas (in Vietnamese). *Journal of Mining and Earth Sciences*. 62, 1 (Feb, 2021), 85-92. DOI:[https://doi.org/10.46326/JMES.2021.62\(1\).10](https://doi.org/10.46326/JMES.2021.62(1).10).
27. Le, D.Tien and Bui, T.Manh 2021. Numerical modelling techniques for studying longwall geotechnical problems under realistic geological structures. *Journal of Mining and Earth Sciences*. 62, 3 (Jun, 2021), 87-96. DOI:[https://doi.org/10.46326/JMES.2021.62\(3\).10](https://doi.org/10.46326/JMES.2021.62(3).10).

Research and Development of Real-time High-precision GNSS Receivers: A Feasible Application for Surveying and Mapping in Vietnam

PHAM Cong Khai^{1,*}, NGUYEN Gia Trong¹, NGUYEN Van Hai², TRAN Trong Xuan³

¹Hanoi University of Mining and Geology, 18 Vien street, Hanoi, Vietnam

²Thuyloi University - Second campus, Ho Chi Minh, Vietnam

³North Technical World Joint Stock Company, Hanoi, Vietnam

Corresponding author: phamconghai@hmg.edu.vn

Abstract. In recent years, the Global Navigation Satellite System (GNSS) has been widely applied in surveying and mapping. Currently, in Vietnam, dual-frequency GNSS receivers are quite extensively applied with the real-time kinematic (RTK) measurement technique using a continuously operating reference station network. However, high-accuracy GNSS receivers are often expensive, sometimes not meeting the needs of users for specific applications. This research develops two types of low-cost high-precision GNSS receivers for RTK positioning for different purposes. First, the millimeter precision GNSS receiver used in real-time displacement monitoring is based on Trimble's BD970 mainboard technology and some other modules. These components are interconnected according to a standard design scheme and assembled in an enclosure to form a GNSS receiver. In addition, a GNSS data transmission in the National Marine Electronics Association standard format by Networked Transport of Radio Technical Commission for Maritime Services via Internet Protocol (NTRIP) has been designed and developed. The GNSS receiver after development is loaded with program code written in the C# programming language, using the Arduino programming tool. Second, the GNSS receivers have the centimeter accuracy for RTK positioning used in surveying and mapping based on U-blox's mainboard technology and some other modules. These modules are also connected together according to a standard design scheme and assembled in an enclosure to form a complete GNSS receiver. The evaluation results show that the designed and developed GNSS receivers completely meet the requirements of surveying and mapping in coal mines in Vietnam, such as real-time monitoring of landslides, surveying and topographical mapping and other surveying works to serve the mining process.

Keywords: GNSS/CORS, Low-cost high-precision GNSS receivers, Real-time high-precision GNSS receivers, NTRIP, BD970 Trimble, ZED-F9P

1. Introduction

Nowadays, the Global Navigation Satellite System (GNSS) is widely used in surveying and mapping. With GNSS technology, positioning on the ground is conducted by establishing a continuously operating reference station (CORS) network. Then RTK positioning is widely applied in surveying. The application of the RTK positioning technique using CORSs has brought great efficiency in surveying, reducing time and low cost. The advantage of GNSS technology is providing 3D data in real time, working continuously in all weather conditions, positioning in real time and high accuracy.

Currently, a network of CORSs has been built in Vietnam (VNGEONET), based on which users will be provided with many more applications. The GNSS/CORS/RTK positioning technique is then performed by dual-frequency GNSS receivers to achieve highly accurate and precise results. In recent times, there has been an increasing interest in low-cost high-precision GNSS receivers. For example, in [1], the authors developed a low-cost single-frequency Global Positioning System (GPS) receiver and concluded that this GPS receiver can be used for RTK positioning. The research and development of a high-sensitivity sensor locator in unfavorable measuring conditions has been successfully carried out by Trajkovski et al. (2010) [2]. The integration of GPS positioning with inertial navigation system (INS) sensors has been performed by Lee (2010) [3] to accurate RTK positioning with long baselines. A study by Hwang et al. (2012) [4] has successfully developed GPS-RTK receivers in both hardware and software, which are installed in a smartphone. It provides wireless communication, transmission data over the Networked Transport of RTCM via Internet Protocol (NTRIP). Performance evaluation of the developed GNSS receiver showed that the RTK positioning accuracy is a few centimeters at 20 Hz. The optimal methods integrating GPS-RTK with an accelerometer have been developed by Hwang et al. (2012) [5] to determine the displacement of the structures.

The study by Wisniewski et al. (2013) [6] compared different positioning methods based on the open-source software called RTKLIB with GNSS receivers developed based on the U-blox's GNSS LEA-6T satellite signal receive module. The effect of the Network Real Time Kinematic (NRTK) positioning method with the use of a low-cost RTK navigation board for Arduino environment, an open-source software application that runs in the Android operating system of smartphones and receives correction data from the CORS service was analyzed by Pepe (2018) [7]. A recent study by Manurung et al. (2019) [8] has researched and developed a GNSS receiver with reasonable cost, RTK positioning using CORS stations. The development of a GNSS receiver based on Ublox's satellite receiver board costing just a few hundred dollars that captures the L1 GPS frequency and the B1 Beidou frequency has been carried out by Parluhutan et al. (2019) [9]. A comparison of the results measured with a GPS receiver with the L1+L2 frequency, which costs several thousand dollars, showed that the low-cost GNSS receiver has the same positioning performance as the high-cost GNSS receiver [10, 11].

The tests and evaluations of the developed GNSS receiver based on the U-blox's NEO-P7 module and the low-cost Tallysman TW2410 antenna showed that RTK positioning is of the centimeter accuracy [12]. In [13], the authors have developed two types of low-cost receivers; U-blox's LEA-6T and NEO-7P. The quality assessment of the two types of receivers was carried out within the framework of published standards of the International Organization. The test results showed that the two types of receivers achieve centimeter accuracy. The accuracy of low-cost GNSS receivers is also of concern. A study was performed with two types of GNSS receivers, which are a Leica GS10 GNSS receiver with AS10 antenna and the low-cost receivers based on U-blox's NEO-M8P board [14]. The results of the assessment of the accuracy of the two types of GNSS receivers showed that, for the Leica GS10 GNSS receiver, the horizontal error is ± 2.5 mm and the vertical error is ± 4.5 mm, and the U-blox's NEO-M8P receivers have a horizontal error of ± 5.5 mm and a vertical error of ± 11 mm.

In Vietnam in recent years, there have been a few research and projects working on GNSS receivers used in real-time displacement monitoring deformation [15, 16, 17]. The design and development of GNSS positioning equipment with centimeter-level accuracy were also carried out by the International Collaboration Centre for R&D on Satellite Navigation Technology in South East Asia of Hanoi University of Science and Technology [18]. The Ho Chi Minh City University of Technology in collaboration with Dai Nam Company has researched and developed high-precision dual-frequency P2 Elite GNSS receivers used in surveying for mapping. Vietnam Aitogy Infrastructure Technology Joint Stock Company has developed Ainav-RTK-R receivers used for RTK positioning according to CORS station technology with centimeter-level accuracy. However, the Ainav-RTK-R receivers are still under design and manufacture separately between the antenna and the GNSS receiver.

With the above assessment, it can be seen that GNSS/CORS technology is increasingly widely applied. Currently, in Vietnam's coal mines, CORS/RTK positioning techniques are applied, so the demand for GNSS receivers is increasing. But currently, GNSS receivers on the Vietnamese market are mainly purchased from large global corporations such as Trimble, Leica, Topcon that are of high cost, thereby reducing the applicability of this technology. Therefore, the development of real-time high-precision GNSS receivers and low-cost that meets user requirements is of great economic and technical significance. In this study, two real-time high-precision GNSS receivers were developed; the first receiver for real-time displacement monitoring, the second receiver for surveying and mapping.

2. Development of GNSS receivers for real-time displacement monitoring systems

2.1. Components of a real-time displacement monitoring system

A real-time displacement monitoring system is designed based on GNSS/CORS/RTK technology and consists of two main parts: a) The CORS System and b) Continuously Monitoring Station System (CMSS) [19]. The CORS system includes CORS GNSS antennas (1), data transmission cables (2), CORS GNSS Receivers (3), Wi-Fi modem and internet connection (4), host computers with specialized software (5), and electricity supply (6). The CMSS system includes GNSS antennas (7), GNSS receivers (8), data transmitters (9), Uninterruptible Power Supply (UPS) (10), power converters (11), solar panels (12), warning equipment (13). The components of the real-time displacement monitoring system are shown in Fig. 1.

The operating principle of the real-time displacement monitoring system is built based on the operating principle of the GNSS/CORS system. CORS is responsible for data processing to determine the correction for the monitoring station according to the standard of the Radio Technical Commission for

Maritime Services (RTCM). The monitoring station that receives the correction from the CORS will determine the exact coordinates. The monitoring data is received according to the National Marine Electronics Association-0183 (NMEA-0183) standard. The correction data from the CORS is sent to the monitoring station and the monitoring data sent to the server is performed by the NTRIP.

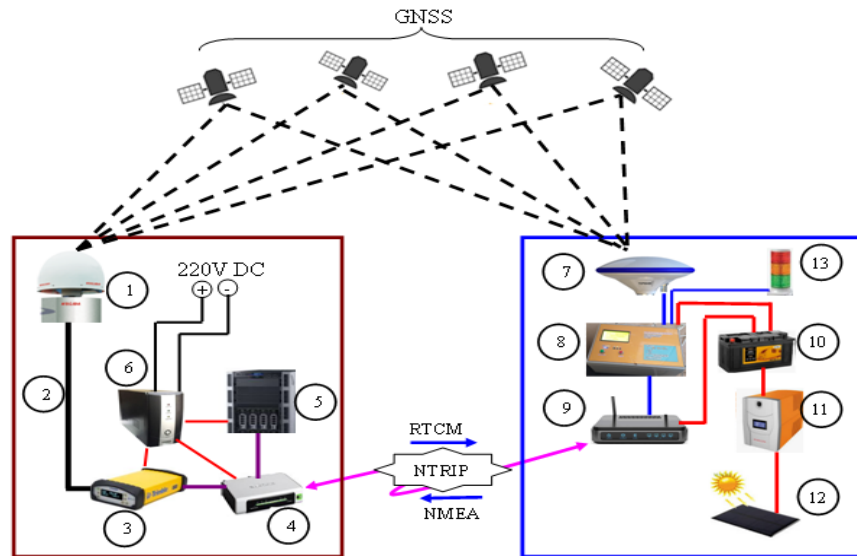




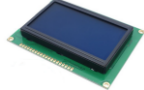



Fig. 1. Components of a real-time displacement monitoring system: CORS (left) and CMSS (right).

2.2. Development of GNSS receivers for monitoring station

Receiving data from the monitoring station and transmitting it to the CORS must ensure continuous operation and provide the 3D position of the monitoring station in real-time. The GNSS receiver and data transmission are designed and developed, including the main modules described shown in Table 1.

Tab. 1. Main modules for developing GNSS receivers for monitoring station.

No	Module name	Description	Module image
1	Trimble BD970	Receive 220 channels of constellation including GPS L2C/ L5, Global Navigation Satellite System, GLONASS L1/L2, BeiDou B1/B2, Galileo L1/E5A/E5B/E5C1	
2	LM2596	This module is used to lower the output voltage from 1.23V to 30V. It is used in voltage converter circuits or circuits that need to reduce voltage.	
3	RS232 to TTL	This module uses Chip MAX232 to transfer data between standard RS232 and transistor-transistor logic (TTL). It helps to communicate with the microcontroller without any additional peripherals.	
4	Atmega328P	This is the central control module. It is responsible for controlling other modules to operate. All codes are loaded directly into the ATmega 328 microprocessor. In the signal transmission protocols, the ATmega328 module is responsible for receiving calculation data and returning it to other modules.	
5	Display screen LCD12864	It is used to display information, message lines about the status of the GNSS receiver	
6	Warning	This module is our self-developed for the monitoring station to warn by sound and light when the displacement occurs beyond the limit.	

The modules of the GNSS receiver for the real-time displacement monitoring station are connected to each other according to the diagram as shown in Figure 2. According to the connection diagram in Figure 2, the assembly process is as follows:

- Module BD970 is assembled with a circuit board connected by male-female pins.
- The input of the LM2596 module is connected to a 12V power supply. The output of the LM2596

module is connected to the input of the connecting board.

- The RS232 to TTL module is connected to the Com1 port of the connecting board.
- The Atmega328P module is connected to the RS232 to TTL module.
- The Atmega328P module is connected to the alarm module.
- The alert module is connected to the display.

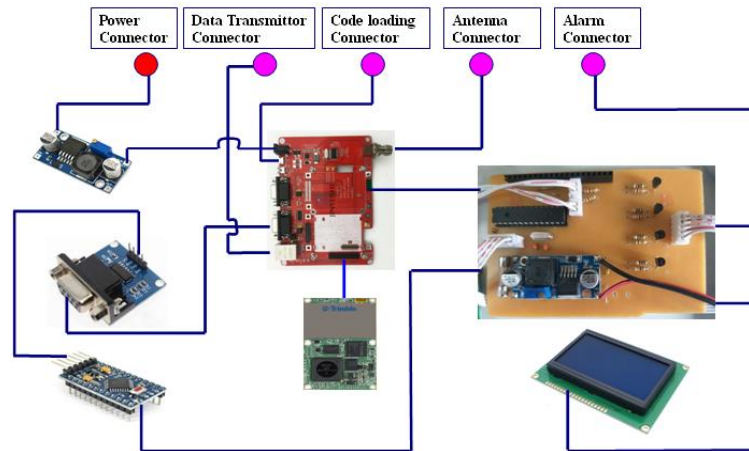


Fig. 2. Connection diagram of GNSS receiver components.

The modules are connected and assembled in a standard design enclosure and form a complete GNSS receiver as shown in Figure 3.

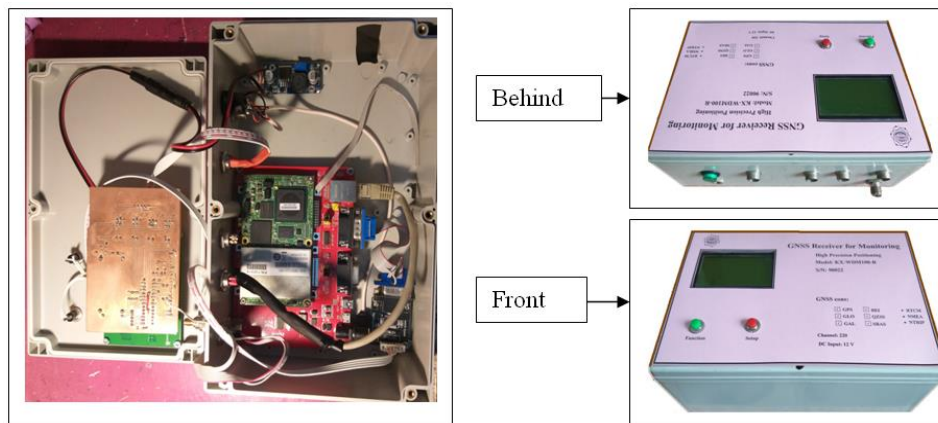


Fig. 3. GNSS receiver: incomplete (left) and complete (right)

After the GNSS receiver is assembled completely, the software controls operation in our self-developed system. The software written in the NMEA's standard data format using the Arduino programming tool and the C# programming language is shown as Figure 4.

```

File Edit Sketch Tools Help
max232
byte rx = 6;
byte SWval;

void setup() {
  pinMode(rx, INPUT);
  delay(2);
  digitalWrite(13, HIGH); //turn on debugging LED
  SWprint('h'); //debugging hello
  SWprint('i');
  SWprint(10); //carriage return
}

int SWread()
{
  byte val = 0;
  while (digitalRead(rx));
  //wait for start bit
  if (digitalRead(rx) == LOW) {
    delayMicroseconds(halfBit9600Delay);
  }
}
Done Saving.
    
```

Fig. 4. Program source code that controls operation of the GNSS receiver.

When software source code has been written and checked for errors, it is loaded into the GNSS receiver via the USB connector to the computer by Arduino's programming tool. Software controls GNSS

data acquisition and transmission functions as follows: The satellite signal collected from receivers in the NMEA standard format is directly transmitted to Arduino via an RS232 port. The received Arduino signals are divided into two types \$GPGGA, \$GNGGA and other NMEA signals. The \$GNGGA signals are transmitted to the server according to the NTRIP server protocol and other NMEA signals are simultaneously transmitted to Ethernet W5100 and stored in an SD memory card, which is integrated into Ethernet W5100 in the text file format. \$GNGGA signals are processed then the results are sent to the software in the server to provide instant location. These data are automatically processed by our self-developed software called GNSS CORS WDM (GNSS CORS Works Deformation Monitoring) and deformation and displacement quantities are determined with high accuracy.

2.3. Development of the GNSS data transmitter for monitoring station

The transmission of RTCM correction data and monitoring data in accordance with the NMEA format is carried out over the internet according to the NTRIP [20] protocol using a developed data transmitter (Fig. 4). The GNSS data transmitter is developed based on TP-Link's mainboard with high power, using Qualcomm's chip to receive, decode and process incoming and outgoing signals, broadcast Wi-Fi, transmit port signals LAN, the antenna receives and transmits the signal. The mainboard is also integrated with USB Dcom 4G to used telecommunications services. The data transmitter uses a 12V electricity supply with the voltage change module LM2596 when the input voltage is greater than 12V.



Fig. 4. GNSS data transmitter by NTRIP.

2.4. GNSS antenna

The antenna used for the monitoring station system with model GN-GGB0710 has a low cost (only a few tens of dollars). It can provide comprehensive GNSS tracking of satellite systems, which are GPS (L1/L2/L5), GLONASS (G1/G2), Beidou (B1/B2/B3), Galileo (L1/L6/E1/E2/E5/E6) and QZSS (L1, L2, and L5). The GNSS antenna is shown in Figure 5.



Fig. 5. GNSS antenna GN-GGB0710.

The GNSS data receiver and transmitter together with the GNSS antenna and other ancillary equipment form a complete monitoring station system. The GNSS receivers have been developed with the product code KX-WDM100-R.

3. Development of RTK GNSS receivers

3.1. Hardware system design

Nowadays, dual-frequency GNSS receivers are widely applied for surveying and mapping because they can fully receive satellite signals at the L1 and L2 frequencies, which gives the dual-frequency receivers a wide operating range and higher accuracy than single-frequency receivers. The components of a dual-frequency GNSS receiver include the main modules shown in Figure 6.

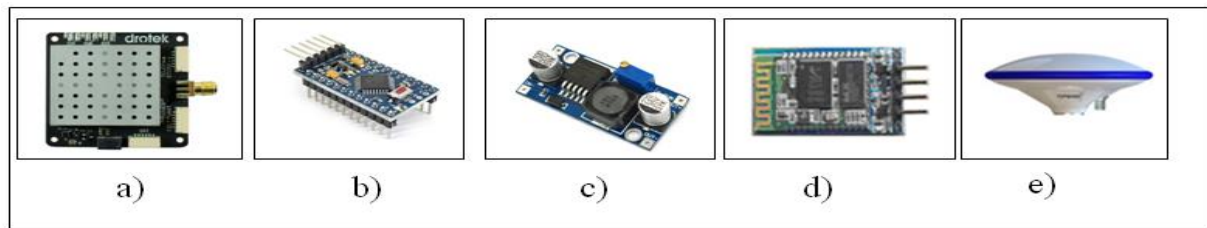


Fig. 6. Modules for developing a GNSS RTK receiver.

3.1.1. GNSS positioning module

The GNSS positioning module used to design the receiver is the U-blox's ZED-F9P (Fig. 6a). This is a module that receives signals of GPS, GLONASS, GALILEO, Beidou satellite systems. The U-blox's ZED-F9P module has a compact size, small power consumption, and supported formats of correction messages are RTCM, so it is suitable for developing GNSS receivers used in RTK positioning. The U-blox's ZED-F9P positioning module has a horizontal error of 10 mm and a vertical error of 15 mm [21].

3.1.2. Atmega328P Module

The Atmega328P module (Fig. 6b) used to design the GNSS RTK receiver is the same type as the module used for the GNSS receiver of the monitoring station as shown in Table 1.

3.1.3. LM2596 Module

The LM2596 module (Fig. 6c) is used to lower the output voltage of the GNSS RTK receiver to 1.23V ÷ 30V. It is the same type as the module used for the GNSS receiver of the monitoring station as shown in Table 1.

3.1.4. Bluetooth Module

Bluetooth is a wireless communication standard for exchanging data over short distances. This communication standard uses radio waves (UHF radio) in the Industrial Scientific Medical (ISM) frequency, ranging from 2.4 to 2.485 GHz. The data transmission distance of the Bluetooth module is about 10 m. The HC-05 Bluetooth module was used to develop the GNSS RTK receiver in this study (Fig. 6d).

3.1.5. GNSS antenna

The antenna used to design the GNSS RTK receivers is of the same type as the antenna used in the monitoring station system as shown in Table 1. The modules are assembled in housing designed using specialized software and printed with a 3D printer. This GNSS receiver has model KX20-R as shown in Figure 7.



Fig. 7. Developed GNSS RTK receivers KX20-R: incomplete (left) and completed (right)

3.2. Design and build software for GNSS RTK receivers

We have developed software called RTK KX Rover (Fig. 8) to control the operation of GNSS receivers. It is written in C# programming language in the Android environment and set up on smartphones. The function of the software is to manage measurement jobs, input coordinates, convert parameters, set up parameters of CORS station, manage measurement data files among other functions.



Fig. 8. Interface of RTK KX Rover software installed in a smartphone.

4. Evaluation of the performance of the two developed GNSS receivers

4.1. Evaluation of the performance of the KX-WDM100-R GNSS receiver for monitoring station

To evaluate the performance of the KX-WDM100-R GNSS receiver, an experiment was performed on 09-06-2021 at 04:37:13.00 (UTC time) i.e., at 11:37:13.00 (Hanoi time). A Leica's single CORS station was established at the main campus of the Hanoi University of Mining and Geology and the KX-WDM100-R GNSS receiver was set up on the roof of the apartment building 184 in Hoang Quoc Viet street. The distance from the CORS station to the KX-WDM100-R GNSS receiver is about 2.836 km (Fig. 9).

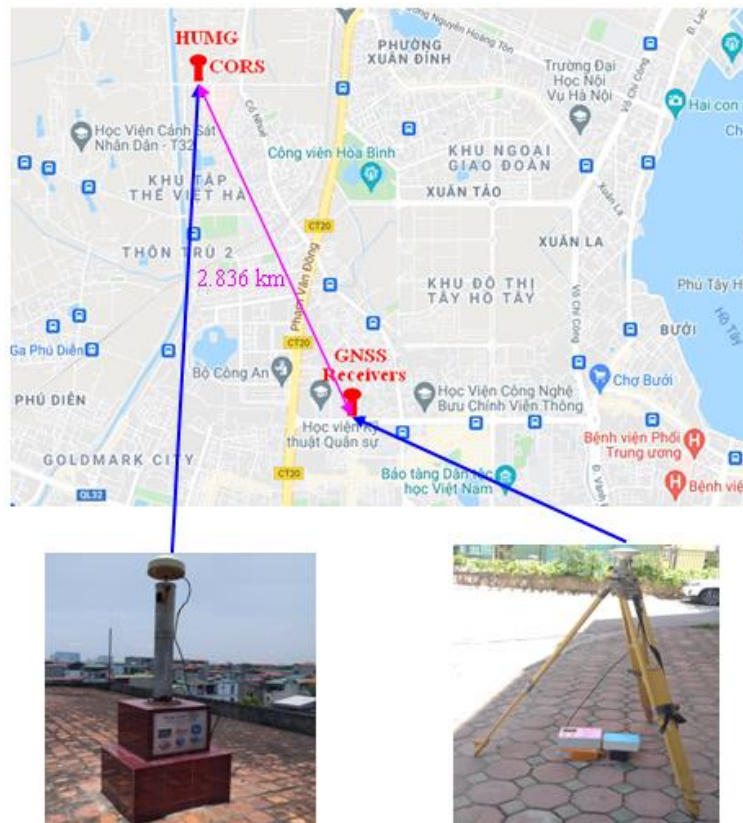


Fig. 9. Locations of the CORS station and the KX-WDM100-R GNSS receiver.

The KX-WDM100-R GNSS receiver is connected to the CORS station through the static IP address: 118.70.171.179 and port 8001 to transmit correction data to the GNSS receiver in the RTCM standard format. The data at the GNSS receiver are corrected in the NMEA standard format. The evaluation of positioning performance shows that the error in the X-axis is 0.004 m, the error in the Y-axis is 0.003 m, and the error in the altitude component is 0.009 m (Fig. 10). With such errors, the KX-WDM100-R GNSS receiver is suitable for real-time displacement monitoring.

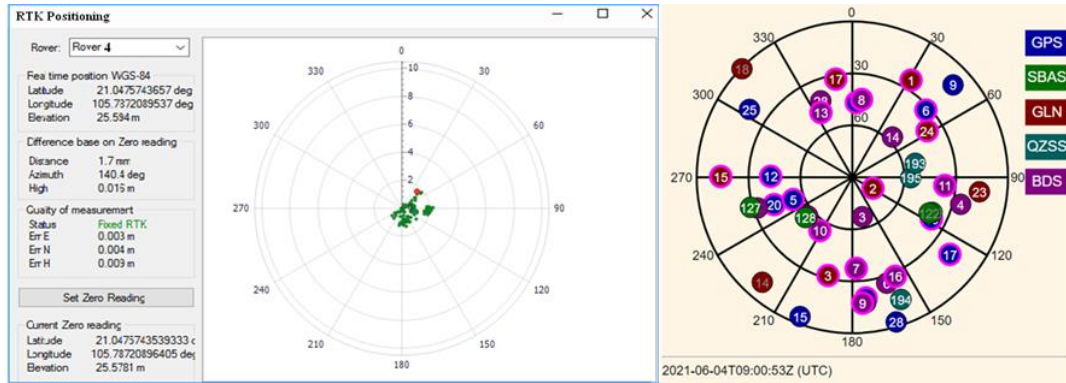


Fig. 10. Positioning performance of GNSS receivers and observable satellite constellation.

Those errors can be obtained by solving the relative position problem in the RTK method as [22] :

$$\mu = \pm \sqrt{\frac{V^T P V}{n - t}} \tag{1}$$

where n is the number of observations, t is the number of unknowns, V is the correction calculated from the system of correction equations in the matrix form using Eq. (2) [23].

$$V = A.X_{XYZ} + B.X_N + L \tag{2}$$

where A is the coefficient matrix of the real unknown of the size $n_i(n_j - 1)$ rows and 3 columns, B is the coefficient matrix of integer unknowns of the size $n_i(n_j - 1)$ rows and $(n_j - 1)$ columns.

$$B = \begin{bmatrix} B_1 \\ B_2 \\ \dots \\ B_{n_i} \end{bmatrix}; \quad X_N = \begin{bmatrix} N_{A,B}^{j,1} \\ N_{A,B}^{j,2} \\ \dots \\ N_{A,B}^{j,(j-1)} \end{bmatrix}_{(n_j-1) \times 1}$$

Then, the error components for each coordinate axis are calculated using Eq. (3) :

$$m_i = \mu r_{ii} \tag{3}$$

with i is the i axis, r_{ii} value determined from relative dilution of precision (RDOP).

Data from the KX-WDM100-R GNSS receivers are transmitted to the CORS central server in the standard format NMEA-0183 with the lowest frequency of 1Hz and the highest of 50Hz, depending on the user's requirements. Table 2 shows a segment of data collected in 1 second using KX-WDM100-R GNSS receivers. In this experiment, only GGA, GST, GSV and GSA messages in the NMEA-0183 standard format are collected.

Tab. 2. A segment of NMEA data collected by KX-WDM100-R GNSS receivers.

\$GNGGA,043714.00,2102.85446475,N,10547.23254501,E,4,21,0.7,25.590,M,-28.232,M,1.0,0000*4B
\$GNGST,043714.00,0.063,0.002,0.001,80.1,0.001,0.002,0.004*74
\$GPGSV,11,1,39,30,37,202,46,1,17,036,21,6,45,239,45,17,45,348,45*41
\$GPGSV,11,2,39,7,11,170,40,28,61,351,46,14,74,032,46,22,16,050,39*71
\$GPGSV,11,3,39,19,36,313,45,3,33,073,42*7C
\$GPGSV,11,4,39,40,29,254,33,42,40,114,,41,54,229,47*73

\$GLGSV,11,5,39,80,20,161,39,68,8,074,38,69,10,121,43,74,52,322,48*62

\$GLGSV,11,6,39,83,13,031,23,85,22,263,46,84,45,332,36,73,70,185,50*5B

\$GBGSV,11,7,39,114,10,065,37,116,6,179,,109,11,198,34,105,32,250,37*62

\$GBGSV,11,8,39,104,26,104,38,108,88,330,46,102,54,227,42,127,43,299,49*52

\$GBGSV,11,9,39,128,43,018,48,103,65,167,44,123,34,167,47,101,40,114,42*52

\$GBGSV,11,10,39,107,67,081,45,110,69,359,46,113,68,220,49*6D

\$QGSV,11,11,39,193,22,123,38,195,51,048,44,194,49,138,45*7D

\$GNRSA,A,3,17,7,22,14,19,3,28,6,30,,,,,1.2,0.7,1.0*19

\$GNRSA,A,3,80,84,85,69,73,,,,,,1.2,0.7,1.0*2B

\$GNRSA,A,3,109,107,110,105,113,101,108,,,,,1.2,0.7,1.0*19

The collected data files are processed by our self-developed software and installed on the central server computer of the CORS station. The data processing is carried out by the following steps:

1. Check the integrity of each message line in the NMEA data file. If these message lines are incomplete, they must be discarded. Inspection of messages is performed by analyzing all characters in the range from \$ to * of the NMEA message.

2. Filter the GGA and GST messages to separate the message lines with the most accurate coordinates (minimum position error).

3. Transform the coordinates from the geodetic coordinate system to the VN2000 coordinate system. The transformation of the coordinates from the geodetic coordinate system to the VN2000 coordinate system is carried out by the following steps:

Firstly, the conversion from geodetic coordinates (B, L, H) to Cartesian coordinates (X, Y, Z) in the World Geodetic System 1984 (WGS84) is conducted using Eq. (4) [23].

$$\left. \begin{aligned} X &= (N+H)\cos B \cdot \cos L \\ Y &= (N+H)\cos B \cdot \sin L \\ Z &= [N(1-e^2)+H] \cdot \sin B \end{aligned} \right\} \quad (4)$$

where B is the geodetic latitude, L is the geodetic longitude, H is the ellipsoidal height, and N is the radius of curvature in the prime vertical at the point of consideration:

$$N = \frac{a}{\sqrt{1-e^2 \sin^2 B}}$$

where e is the first eccentricity of the ellipsoid:

$$e = \frac{\sqrt{a^2 - b^2}}{a}$$

where a is the semi-major axis and b is the semi-minor axis of the ellipsoid.

Then, Cartesian coordinates are transformed from WGS84 to the VN2000 coordinate system (Vietnam's coordinate system) using Eq. (5):

$$\left. \begin{aligned} X_{VN2000} &= \Delta X_o + k(X + \epsilon_o Y - \psi_o Z) \\ Y_{VN2000} &= \Delta Y_o + k(-\epsilon_o X + Y + \omega_o Z) \\ H_{VN2000} &= \Delta Z_o + k(\psi_o X - \omega_o Y + Z) \end{aligned} \right\} \quad (5)$$

where X_{VN2000} , Y_{VN2000} , H_{VN2000} are the coordinates in the VN2000 reference system, X, Y, and Z are the coordinates in the WGS84 system, and 7 parameters of Helmert transformation includes:

- ΔX_o , ΔY_o , ΔZ_o are the translation.

- ω_o , ψ_o , ϵ_o are 3 rotation angles about the X, Y and Z axes.

-k is the scale factor.

The seven parameters of Helmert transformation from WGS84 to the VN2000 coordinate system were published by the Ministry of Natural Resources and Environment, Vietnam as shown in Table 3 [24].

Tab. 3. Seven parameters of Helmert coordinate transformation.

No	Parameters	Values of the parameters	Unit
1	ΔX_o	-191.90441429	meters
2	ΔY_o	-39.30318279	meters
3	ΔZ_o	-111.45032835	meters
4	ω_o	-0.00928836	seconds
5	ψ_o	0.01975479	seconds
6	ϵ_o	-0.00427372	seconds
7	k	1.000000252906278	-

After that, Cartesian coordinates are converted to geodetic coordinates in VN2000.

Secondly, Universal Transverse Mercator (UTM) coordinates (x, y) is computed from geodetic coordinates (B, L) in VN2000 using Eq. (6), [21].

$$\begin{aligned}
 x &= k_0 \left(X + \frac{1}{2\rho^2} N.t \cos^2 B.l^2 + \frac{1}{24\rho^4} N.t(5 - t^5 + 9\eta^2 + 4\eta^4) \cos^4 B.l^4 \right. \\
 &\quad \left. + \frac{1}{720\rho^6} N.t(61 - 58t^2 + t^4 + 270\eta^2 - 330\eta^2 t^2) \cos^6 B.l^6 + \dots \right) \\
 y &= k_0 \left(\frac{N}{\rho} \cos B.l + \frac{1}{6\rho^3} N(1 - t^2 - \eta^2) \cos^3 B.l^3 + \right. \\
 &\quad \left. + \frac{1}{120\rho^5} N(5 - 18t^2 + t^4 + 14\eta^2 - 58\eta^2 t^2) \cos^5 B.l^5 + \dots \right)
 \end{aligned} \tag{6}$$

where $t = \tan B$, $\eta = e' \cdot \cos B$, $1 = \frac{(L - L_o)''}{\rho''}$, $k_0 = 0.9996$ corresponds to a 6° projection zone, $k_0 = 0.9999$ corresponds to a 3° projection zone, L_o is the central meridian. In Hanoi, $L_o = 105^\circ 00'$.

From the data in Table 2, the processing and filtering GGA messages with the most accurate coordinate components are shown in Table 4.

Tab. 4. A segment of GGA data according to the NMEA 0183 standard format.

No	GGA Messages according to the NMEA standard format
1	\$GNGGA,043713.00,2102.85446474,N,10547.23254501,E,4,21,0.7,25.590,M,-28.232,M,1.0,0000*4D
2	\$GNGGA,043714.00,2102.85446475,N,10547.23254501,E,4,21,0.7,25.590,M,-28.232,M,1.0,0000*4B
3	\$GNGGA,043715.00,2102.85446474,N,10547.23254502,E,4,21,0.7,25.590,M,-28.232,M,1.0,0000*48
4	\$GNGGA,043716.00,2102.85446474,N,10547.23254504,E,4,21,0.7,25.589,M,-28.232,M,1.0,0000*45
5	\$GNGGA,043717.00,2102.85446473,N,10547.23254504,E,4,21,0.7,25.589,M,-28.232,M,1.0,0000*43
6	\$GNGGA,043718.00,2102.85446474,N,10547.23254505,E,4,21,0.7,25.590,M,-28.232,M,1.0,0000*42
7	\$GNGGA,043719.00,2102.85446474,N,10547.23254506,E,4,21,0.7,25.590,M,-28.232,M,1.0,0000*40
8	\$GNGGA,043720.00,2102.85446474,N,10547.23254509,E,4,21,0.7,25.589,M,-28.232,M,1.0,0000*4D
9	\$GNGGA,043721.00,2102.85446474,N,10547.23254507,E,4,21,0.7,25.589,M,-28.232,M,1.0,0000*42
10	\$GNGGA,043722.00,2102.85446474,N,10547.23254506,E,4,20,0.7,25.590,M,-28.232,M,1.0,0000*49
11	\$GNGGA,043723.00,2102.85446474,N,10547.23254505,E,4,20,0.7,25.590,M,-28.232,M,1.0,0000*4B
12	\$GNGGA,043724.00,2102.85446474,N,10547.23254505,E,4,20,0.7,25.590,M,-28.232,M,1.0,0000*4C

13	\$GNGGA,043725.00,2102.85446474,N,10547.23254503,E,4,20,0.7,25.590,M,-28.232,M,1.0,0000*4B
14	\$GNGGA,043726.00,2102.85446473,N,10547.23254502,E,4,20,0.7,25.590,M,-28.232,M,1.0,0000*4E
15	\$GNGGA,043727.00,2102.85446474,N,10547.23254502,E,4,20,0.7,25.590,M,-28.232,M,1.0,0000*48
16	\$GNGGA,043728.00,2102.85446474,N,10547.23254502,E,4,20,0.7,25.589,M,-28.232,M,1.0,0000*4F
17	\$GNGGA,043729.00,2102.85446474,N,10547.23254501,E,4,20,0.7,25.589,M,-28.232,M,1.0,0000*4D
18	\$GNGGA,043730.00,2102.85446473,N,10547.23254502,E,4,20,0.7,25.589,M,-28.232,M,1.0,0000*41
19	\$GNGGA,043731.00,2102.85446473,N,10547.23254505,E,4,20,0.7,25.589,M,-28.232,M,1.0,0000*47
20	\$GNGGA,043732.00,2102.85446473,N,10547.23254505,E,4,20,0.7,25.589,M,-28.232,M,1.0,0000*44
...

Geodetic coordinates in the WGS84 coordinate system are transformed to those in the VN2000 coordinate system and shown in Table 5.

Tab. 5. Results of coordinate transformaion from WGS84 to VN2000.

No	Experiment times	Latitude (B)	Longitude (L)	Ellipsoid Altitude (H)	X _{VN2000} (meters)	Y _{VN2000} (meters)	h (meters)
1	04:37:13.00 6/9/2021	21 04 51.267884	105 47 13.952701	0.7219	2331412.081	581575.262	25.773
2	04:37:14.00 6/9/2021	21 02 51.267885	105 47 13.952701	0.7229	2327722.718	581593.483	25.711
3	04:37:15.00 6/9/2021	21 02 51.267884	105 47 13.952701	0.7245	2327722.718	581593.483	25.713
4	04:37:16.00 6/9/2021	21 02 51.267884	105 47 13.952702	0.7233	2327722.718	581593.483	25.711
5	04:37:17.00 6/9/2021	21 02 51.267884	105 47 13.952702	0.7226	2327722.718	581593.483	25.711
6	04:37:18.00 6/9/2021	21 02 51.267884	105 47 13.952703	0.7261	2327722.718	581593.483	25.714
7	04:37:19.00 6/9/2021	21 02 51.267884	105 47 13.952704	0.7209	2327722.718	581593.483	25.709
8	04:37:20.00 6/9/2021	21 02 51.267884	105 47 13.952705	0.7241	2327722.718	581593.483	25.712
9	04:37:21.00 6/9/2021	21 02 51.267884	105 47 13.952704	0.7209	2327722.718	581593.483	25.709
10	04:37:22.00 6/9/2021	21 02 51.267884	105 47 13.952704	0.7225	2327722.718	581593.483	25.711
11	04:37:23.00 6/9/2021	21 02 51.267884	105 47 13.952703	0.7278	2327722.718	581593.483	25.716
12	04:37:24.00 6/9/2021	21 02 51.267884	105 47 13.952703	0.7243	2327722.718	581593.483	25.712
13	04:37:25.00 6/9/2021	21 02 51.267884	105 47 13.952702	0.7271	2327722.718	581593.483	25.715
14	04:37:26.00 6/9/2021	21 02 51.267884	105 47 13.952701	0.7202	2327722.718	581593.483	25.708
...

4.2. Accuracy evaluation of the RTK KX20-R GNSS receiver used for surveying and mapping

A method to evaluate the accuracy of coordinates measured by the RTK KX20-R GNSS receiver is developed by using two GNSS receivers set up at the same point of a control network with exact coordinates. The control network used for accuracy evaluation is established by GPS technology and adjusted by the Trimble Business Control (TBC) 3.5 software. In this work, the KX20-R GNSS receiver, which is developed in this study, and a South's GNSS S82 receiver are used. The S82 receiver is a dual-frequency GNSS receiver that can receive 220 channels of the GPS, GLONASS, Compass systems. The RTK positioning errors are 10 mm ±1 ppm in the horizontal component and 15 mm ±1 ppm in the vertical component. The communication is carried out via USB, Bluetooth, RS-232 serial ports. Thus, the S82 receiver is quite similar to the KX20-R receiver. When conducting the experiment, the two S82 and

KX20-R receivers are used and set up at the points of the control network. A Leica's CORS station (Fig. 10) is used to correct the positions for the receivers. Based on the coordinates determined by the S82 and KX20-R GNSS receivers and their known coordinates, the deviations in horizontal coordinates of the two receivers are calculated and shown in Tables 6 and 7.

Tab. 6. Horizontal coordinate deviations of the KX20-R receiver.

No	Points	Known coordinates (m)		Measured coordinates (m)		Coordinate deviation (m)		Horizontal error (m)
		X _{Kn}	Y _{Kn}	X _{KX20-R}	Y _{KX20-R}	δX	δY	
1	KH-1	2331078.161	580952.520	2331078.153	580952.529	-0.008	0.009	0.012
2	KH-4	2328976.440	580430.385	2328976.428	580430.371	-0.012	-0.014	0.018
3	KH-3	2330112.400	581855.510	2330112.386	581855.494	-0.014	-0.016	0.021
4	KH-6	2326970.116	580887.986	2326970.135	580888.008	0.019	0.022	0.029
5	KH-2	2333147.615	582109.681	2333147.640	582109.708	0.025	0.027	0.037
6	KH-5	2327466.300	582693.099	2327466.273	582693.068	-0.027	-0.031	0.041
7	KH-7	2326251.236	582094.451	2326251.208	582094.486	-0.028	0.035	0.045
8	KH-8	2324291.465	581377.192	2324291.429	581377.231	-0.036	0.039	0.053
9	KH-10	2323870.602	579504.400	2323870.559	579504.354	-0.043	-0.046	0.063
10	KH-9	2323643.828	581962.164	2323643.781	581962.213	-0.047	0.049	0.068

Tab. 7. Horizontal coordinate deviations of the S82 receiver.

No	Points	Known coordinates (m)		Measured coordinates (m)		Coordinate deviation (m)		Horizontal error (m)
		X _{Kn}	Y _{Kn}	X _{S82}	Y _{S82}	δX	δY	
1	KH-1	2331078.161	580952.520	2331078.157	580952.526	-0.004	0.006	0.007
2	KH-4	2328976.440	580430.385	2328976.432	580430.376	-0.008	-0.009	0.012
3	KH-3	2330112.400	581855.510	2330112.410	581855.524	0.010	0.014	0.017
4	KH-6	2326970.116	580887.986	2326970.095	580888.008	-0.021	0.022	0.030
5	KH-2	2333147.615	582109.681	2333147.635	582109.702	0.020	0.021	0.029
6	KH-5	2327466.300	582693.099	2327466.278	582693.076	-0.022	-0.023	0.032
7	KH-7	2326251.236	582094.451	2326251.207	582094.480	-0.029	0.029	0.041
8	KH-8	2324291.465	581377.192	2324291.425	581377.235	-0.040	0.043	0.059
9	KH-10	2323870.602	579504.400	2323870.560	579504.356	-0.042	-0.044	0.061
10	KH-9	2323643.828	581962.164	2323643.786	581962.212	-0.042	0.048	0.064

The horizontal errors of points measured from the two GNSS receivers are calculated and shown in Tables 7 and 8, and Fig. 11.

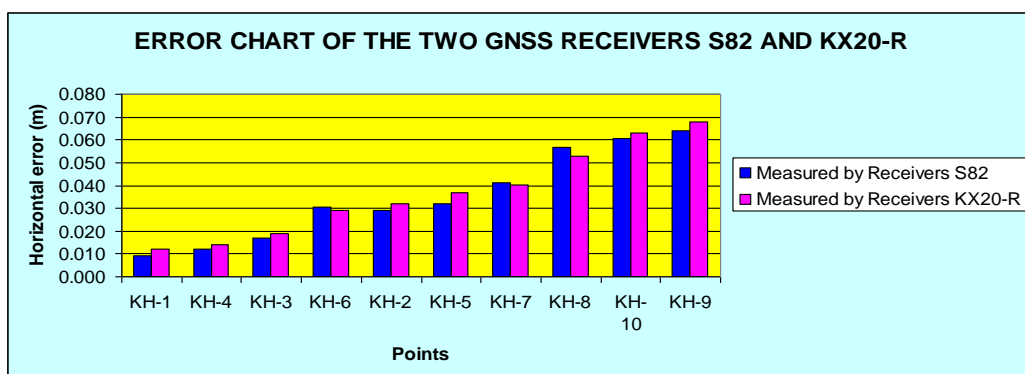


Fig. 11. Comparison of horizontal coordinate accuracy of the S82 and KX20-R receivers.

It can be seen from Fig. 11 that the horizontal errors of points measured by the two receivers KX20-R and S82 are approximately the same and both increase as the distance from the CORS station to the receivers increases. The maximum errors at the KH-9 point measured by the S82 receiver is 0.064 m and by the KX20-R receiver is 0.068 m. Thus, the KX20-R GNSS receiver, which is designed and developed

in this study, meets the needs of surveying and mapping in Vietnam.

5. Conclusions

With GNSS/CORS technology, dual-frequency GNSS receivers are widely used for various purposes, especially for real-time high accuracy requirements. This study has developed two types of real-time high-precision GNSS receivers that can be used for geodetic works in Vietnam. The receiver was developed based on Trimble BD970 motherboard technology and several other modules are connected together according to the synchronous design scheme. These modules are assembled according to the design scheme and form a complete GNSS receiver with model GNSS KX-WDM100-R. This receiver could perform high-precision real-time positioning, with errors in the X-axis being 0.004 m, in the Y-axis being 0.003 m and in the altitude component being 0.009 m.

The method of transmitting rectified data in the RTCM format and monitoring data according to the NMEA standard is carried out over the internet according to NTRIP protocol thanks to the data transmitter developed in this study. The experimental measurement results conducted with the developed KX-WDM100-R GNSS receiver connecting to the Leica CORS station showed that positioning data is instantly transmitted to the server of the CORS station with millimeter-level positioning error. Thus, the KX-WDM100-R GNSS receiver developed in this study can be used to monitor real-time landslides in Vietnam.

In addition, in this study, a low-cost GNSS receiver was also developed based on U-blox's ZED-F9P motherboard technology. This receiver, together with the self-developed RTK KX Rover software installed on a smartphone device, has the functions of measuring job management, setting parameters for calculating coordinates and CORS station parameters, and managing the measurement data file to create a complete GNSS receiver. The test results of the RTK method using the S82 and KX20-R GNSS receivers showed that the KX20-R GNSS receiver centimeter accuracy meets the requirements of surveying and mapping in Vietnam.

6. Acknowledgment

This research was supported financially by Hanoi Department of Science and Technology (Project 01C-01/02-2020-3). We also thank the Hanoi city People's Committee, Hanoi University of Mining and Geology for helping us in experimental measurements.

7. References

1. Takasu, T., Yasuda, A., 2008. Evaluation of RTK-GPS Performance with Low-cost Single-frequency GPS Receivers, in: Proc. 13th GPS/GNSS Symposium 2008, Nov. 11-14, Tokyo, Japan.
2. Trajkovski, K.K., Sterle, O., Stopar, B., 2010. Study positioning with high sensitivity GPS sensors under adverse conditions. *Sensors*, 10: 8332-8347.
3. Lee, H.K., 2010. An integration of GPS with INS sensors for precise long-baseline kinematic positioning. *Sensors*, 10: 9424-9438.
4. Hwang, J., Yun, H., Suh, Y., Cho, J., Lee, D., 2012. Development of an RTK-GPS Positioning Application with an Improved Position Error Model for Smartphones. *Sensors*, 12: 12988-13001; doi:10.3390/s121012988.
5. Hwang, J., Yun, H., Park, S.K., Lee, D., Hong, S., 2012. Optimal methods of RTK-GPS/Accelerometer integration to monitor the displacement of structures. *Sensors*, 12: 1014-1034.
6. Wisniewski, B., Bruniecki, K., Moszynski, M., 2013. Evaluation of RTKLIB's positioning accuracy using low-cost GNSS receiver and ASG-EUPOS, *TransNav: International Journal on Marine Navigation and Safety of Sea Transportation*, 7(1): 79-85, <https://doi.org/10.12716/1001.07.01.10>.
7. Pepe, M., 2018. CORS architecture and evaluation of positioning by low-cost GNSS receiver, *Geod. Cartography* 44(2): 36-44.
8. Parluhan Manurung, Hari Pramujo, Joshua BP Manurung, 2019. Development of GNSS Receiver for Mobile CORS with RTK Correction Services Using Cloud Server. *E3S Web of Conferences* 94, 01010.

9. Odolinski, R., Teunissen, P., 2016. Single-frequency, dual-GNSS versus dual-frequency, single-GNSS: a low-cost and high-grade receivers GPS-BDS RTK analysis, *J. Geod.* 90(11): 1255-1278.
10. Odolinski, R., Teunissen, P., 2017. Low-cost, high-precision, single-frequency GPS–BDS RTK Positioning, *GPS Solutions* 21, 1315-1330.
11. Odolinski, R., Teunissen, P., 2018. An assessment of smartphone and low-cost multi-GNSS single-frequency RTK positioning for low, medium and high ionospheric disturbance periods, *J. Geod.* <https://doi.org/10.1007/s00190-018-1192-5>.
12. Sioulis, A., Tsakiri, M., Stathas, D., 2015. Evaluation of low cost, high sensitivity GNSS receivers based on the ISO RTK standards, *Int. J. Geomatics Geosci.* 6(2): 1597-1606.
13. Tsakiri, M., Sioulis, A., Piniotis, G., 2017. Compliance of low-cost, single-frequency GNSS receivers to standards consistent with ISO for control surveying, *Int. J. Metrol. Qual. Eng.* 8(11): 1-12.
14. María, S., Garrido-Carretero, María, C., de Lacy-Pérez de los Cobos, María, J. Borque-Arancón, Antonio M. Ruiz-Armenteros, Rubén Moreno-Guerrero, Antonio J. Gil-Cruz, 2019. Low-cost GNSS receiver in RTK positioning under the standard ISO-17123-8: A feasible option in geomatics. *Measurement* 137: 168-178.
15. Pham Cong Khai, Le Van Canh, Nguyen Quoc Long, Nguyen Viet Nghia, Pham Van Chung, Vo Ngoc Dung, Nguyen Gia Trong, Le Duc Tinh, Nguyen Viet Ha, Nguyen Van Sang, 2019. Research on technology application continuous monitoring of displacement and deformation of works in area of Hanoi City. Final report of Science and Technology project of city level. Grant number 01C-04/08-2016-3. Hanoi Department of Science and Technology.
16. Pham, K.Cong 2020. Research on technical solution of displacement and deformation monitoring of high-rise buildings in real time. *Journal of Mining and Earth Sciences.* 61, 3 (Jun, 2020), 75-87. DOI:[https://doi.org/10.46326/JMES.2020.61\(3\).09](https://doi.org/10.46326/JMES.2020.61(3).09).
17. Pham, K.Cong and Nguyen, H.Van 2020. Investigation and design of monitoring systems in real time landslides at Xekaman 3 hydropower plant (in Vietnamese). *Journal of Mining and Earth Sciences.* 61, 1 (Feb, 2020), 11-20. DOI:[https://doi.org/10.46326/JMES.2020.61\(1\).02](https://doi.org/10.46326/JMES.2020.61(1).02).
18. Ta Hai Tung, et. al., 2016. Research and manufacture a system that provides real-time centimet accuracy GPS positioning services for fields requiring high accuracy. Report on research results, Project VT/CN-02/13-15.
19. Pham Cong Khai, Tran Dinh Trong, Nguyen Van Hai, 2020. GNSS/CORS-Based Technology for Real-Time Monitoring of Landslides on Waste Dump – A Case Study at the Deo Nai South Dump, Vietnam. *Journal of the Polish Mineral Engineering Society*, 2(46/1): 181–192.
20. Networked Transport of RTCM via Internet Protocol (Ntrip), Version 1.0. In: GDC (GNSS Data Center) [online]. Bundesamt für Kartographie und Geodäsie (BKG), 2004. [cit.26.05.2016]. Available from: http://igs.bkg.bund.de/root_ftp/NTRIP/documentation/NtripDocumentation.pdf/.
21. <http://store-drotek.com/891-rtk-zed-f9p-gnss.html>, 25/02/2021.
22. Hoang Ngoc Ha. Adjustment and calculation of geodetic and GPS/GNSS network. Science and Technology Publishing House, Hanoi, 2020.
23. Dang Nam Chinh, Do Ngoc Duong. Satellite navigation. Science and Technology Publishing House, Hanoi, 2014.
24. Ministry of Natural Resources and Environment of Vietnam. Decision on using the parameters to transform from the World Geodetic System – WGS-84 to Viet Nam National Coordinate System VN2000, No. 05/2007/QĐ-BTNMT.

Promoting Information and Communication Technology in Online Service Delivery in Vietnam

NGUYEN Thi Ngoc Mai^{1,*}, PHAM Ngoc Huong Quynh²

¹ National Academy of Public Administration, Hanoi, Vietnam

² VNU University of Economics and Business, Vietnam National University, Hanoi, Vietnam

Corresponding author: maingoc84@gmail.com

Abstract. Applying Information and Communication Technology (ICT) to public service delivery contributes to transparency, accountability, and cost-saving to improve administrative efficiency. This application has become an inevitable trend for administrative reform worldwide. This paper examines the policy of promoting ICT in public service delivery and its implementation in Vietnam. Recently, the Vietnamese government has created a thoroughly legal foundation to develop information infrastructure for public service delivery. However, online public service delivery results are still lower than expected, and the online service index in Vietnam has just reached the average level of the world. Therefore, to encourage citizens to use online public services, the government should improve the personal identification data system and promote propagating and popularize online public services. The government also should protect personal data and administrative system security to ensure organizational system safety and efficiency.

Keywords: Information and communication technology, Vietnam government, Online public service

1. Introduction

Applying ICT to government functions and procedures is essential in electronic government (e-government) policy implementation to increase efficiency, transparency, and citizen participation. Developing public service on Internet can facilitate citizens and business operations and lighten the pressure of paperwork for state management officials. This development helps individuals and enterprises save effort and working time while using public services. Instead of going to government agencies, people can directly access the administrative procedures and payment on the website with a computer connected to the Internet, then receive the results through the postal service.

According to the 2020 United Nations report, the world average online service index increased from 0.4178 in 2010 to 0.562. This index illustrates an uptrend in using online public services globally. The report also shows that the majority of local government portals can be accessed via mobile devices to raise the local governments' awareness of the importance of mobile technologies in multichannel service delivery. Especially in the COVID-19 pandemic, online public services are essential for communication, leadership, and collaboration between policymakers and society. However, the world average online service index in 2020 (0.562) is still less than expected. It implies that most local government portals are substandard (such as information provision but undersized or no services provision) and need to upgrade [1].

In Vietnam, the government issued a long-term plan for using ICT in public services for citizens and businesses in 2010. This strategy makes the online service index of Vietnam improved from 0.30476 in 2010 to 0.6529 in 2019 and was higher than the world average online service index (0.562 in 2020) [1]. However, in the government's report in 2018, the number of online filings was low. In the first quarter of 2018, this number accounted for 24.24% of the total public services provided by the central authorities and 9.69% by the local ones [2].

This paper aims to evaluate the ICT application in public service delivery implementation in Vietnam, show the advantages and disadvantages, and propose some strategies to boost ICT to increase the high quality of public services. The structure of the paper includes (i) Literature review on the importance and requirements of applying ICT in public service delivery towards higher effectiveness and efficiency in governmental tasks; (ii) Applying ICT in public service delivery in Vietnam; (iii) Proposals to develop ICT in public service delivery in Vietnam.

2. Literature review

By the beginning of the twenty-first century, due to a new e-government trend, many studies have

analyzed ICT applications in public service delivery.

Many authors agree that online public service significantly benefits economic development in both developing and developed countries. Applying ICT in public service delivery has offered ample benefits for citizens and the government in most developed countries. For example, in the EU countries, the increasing application of information technology brings the government closer to its citizens [3, 4]. Therefore, e-government continuously becomes a foundation for modern administration systems [5]. According to the 2020 United Nations' E-Government Survey, in developing countries and underdeveloped countries, more and more countries and municipalities are pursuing digital government strategies, some radically different from those guiding earlier e-government initiatives. The data from this report also shows that the global provision of online government services has improved significantly. More than 84% of worldwide countries now offer at least one online transactional service [6]. Information and communication technology can improve transparency by providing information access and increasing accountability by closely monitoring government activities [7, 8].

Besides, many studies show the influencing factors to the online public services development in different countries. These researches analyze three groups of factors that are (i) economic factors, (ii) social factors, and (iii) institutional factors.

Firstly, the economic factor includes technology and the level of economic development. Accordingly, technology has changed the methods of communication of people, leading people to require more precise information from the government. Therefore, the high technology creates more pressure on traditional administration systems to deliver transparent and efficient public service and avoid corruption [9]. Economic development also strongly influences online public services delivery. Studies show that online public services are more common in developed countries than in developing countries. Especially in developing and undeveloped countries, they have many financial, technological, and even cognitive challenges to improve online public services. For example, African countries have failed to develop online services because of the political, economic environment, and civil recognition [10].

Secondly, the social factor involves awareness of the network, gender, interests, age, education, and digital gap. In undeveloped and developing countries, the government and citizens have a limited understanding of applying technology to slow down online public services development. Besides, the digital gap (called digital knowledge) is also a factor leading to the failure to develop online public services in undeveloped countries. The larger the digital gap is, the slower the development of online public services is [11]. In addition, the adaptation or acceptance of using online public services also depends on people's preferences [12], gender, age, education, income, and understanding of the Internet [13]. However, undeveloped countries will overcome challenges to develop online public services in the long-time, regardless of their skills or sophisticated use. Therefore, some authors argue that undeveloped countries should invest in education to improve citizens' online public service use before investing in information and communication technology systems [14].

Thirdly, institutional factors are reflected through the national policies and legal system for online public services. The evidence provided by Igari's study (2014) shows that although Japan ranks first in broadband infrastructure quality, price, and speed, the percentage of Japanese citizens using online public services is less than in Denmark, where there is lower infrastructure [15]. It is because Denmark's government has successfully implemented (i) the national strategy on ICT application, (ii) the mechanism to promote ICT application, and (iii) the personal identification and digital signatures system toward user-oriented services. Therefore, Tangi et al. (2021) suggest that the government replace all traditional public services delivery, such as via telephone or the front desk, and develop the only online method. If the government provides both online and conventional administration systems, the e-government development may be slower. The traditional techniques are familiar to many citizens; thus, they often prefer the former [16]. For instance, in Netherland, formal administration is still preferred to online administration despite increasing the online transaction channel [17]. However, in the undeveloped country where many poor people do not know how to use technology and have very little opportunity to use technology, they will be restricted to using public services if the government only provides online public services.

Evaluating existing studies

Recently, e-government has been very prevalent. Many studies analyze the e-government and its contribution to economic development and the factors affecting e-government in both developed and developing countries. Although economic, social, and institutional factors influence the government's attempt to apply ICT in public service delivery, few studies appreciate the role of state management as an

influencing factor to online public service. Specifically, in developing countries where online public service is still new and unpopular, a state plays a vital role in popularizing the new form.

Reviewing the literature leads to the question: how should the government promote ICT in public service delivery? Therefore, this article examines the government's policy of applying ICT for providing public service and its implementation in Vietnam. This paper aims to show the advantages and disadvantages of this implementation and propose suggestions to promote online public services for Vietnamese.

3. Methodology and materials

This paper uses the comparative method successfully applied in Igari's studies in 2014 [15]. This method is helpful to analyze changes in the Vietnamese government's policy on using information technology to provide online public services in the two periods - 2010 to 2019 and 2019 to 2020. The advantages and disadvantages are shown to contribute to online public works management changes, especially in the COVID-19 pandemic context in Vietnam.

The paper uses secondary data of the online services index and the telecommunication infrastructure index collected by the United Nations. This data is input to analyze the effectiveness of government policy on providing online public services in Vietnam. In addition, the public administration performance index (PAPI) and provincial competitiveness index (PCI) are also used to illustrate the opinions of businesses and servants on the changes in public service delivery in Vietnam.

4. The application of information and communication technology to online public service in Vietnam

4.1. State's policy on applying information and communication technology to public services in Vietnam

From 2011 to 2019

In 2010, the Vietnamese government issued a plan to apply information technology in state agencies, a significant change in the administrative reform process, and establish ICT in public services delivery. Accordingly, state officials promulgate many legal regulations on digital signatures, online security, and digital documents. For example, Decision No. 28/2018/QĐ-TTg in 2018 on sending and receiving digital documents between state officials marked the critical step in administration system innovation. It is because that the legality of digital documents is recognized by the government and allowed to interchange between different state agencies simultaneously. As a result, state agencies saved a lot of time and costs, creating the first premise in using ICT to improve the efficiency of public administration work.

The digital signature is also one of the essential issues in online public services because of its security. In 2017, the Vietnamese government issued regulations on using digital signatures in Circular No. 41/2017/TT-BTTTT. Digital signatures have shortened time to approve and send documents for state agencies, saving much time requesting records for citizens. It is a turning point in online public service delivery in Vietnam.

The government's regulations on online public service delivery are implemented in all state offices in the whole country. For instance, Decree 43/2011/ND-CP in 2011 required all local and central officials to deliver public services on the state websites following the government's instructions. The Circular 10/2016/TT-BTTTT issued in 2016 was a national technical regulation on identifiers structure and packet data format for connection of document management systems.

From 2019 to 3/2021

The Covid-19 pandemic broke out worldwide, becoming a remarkable fact that negatively impacts all countries, including Vietnam. International governments must use social distancing measures to prevent its spread, leading to a global decline in economy, trade, and investment. Working online to maintain economic activity is the only method for all countries during the pandemic. Although the disaster came from the pandemic, countries have golden opportunities to promote online public services. The Vietnamese government has accelerated the application of information technology in state agencies to improve the quality of public service delivery. Accordingly, the government issued many legal and guiding documents for central and local agencies to switch to online public service delivery quickly.

Firstly, the government creates a unique system of digital transaction portal which would help citizens and public managers doing works easier. The traditional paper-text connection was replaced by the online-text connection system, including text connection between government to government (G-to-G), government to an individual (G-to-I), and government to business (G-to-B). It became essential in online

public service delivery, as state officials in any place can get the most updated text information with the fastest speed by online sharing. Similarly, businesses and citizens can easily access the central or local website addresses to get administrative procedures and data instead of state officials. It saves a lot of costs and time for people to have more time to focus on their professional tasks.

Besides, the government issued the important Project of National Document Linking Axis, No. 626/QĐ-VPCP approved on August 1st, 2019, and operated the national public service portal via the website link dichvucong.gov.vn, which notice one of the significant steps in providing online public services in the country. The national public service portal is a tool for government, ministries, and localities to evaluate and supervise the administrative procedures and improve transparency in the implementing administrative process, leading to avoiding corruption. In addition, The National Document Linking Axis saves time papers cost and reduces working time in state offices, contributing to speeding up administrative procedures reform.

In 2020, the government issued Decree No. 20/2020/ND-CP on digital identifiers for state officials to quickly share data between central and local agencies. Digital identifiers help agencies and citizens can easily search for personal identification on the website. Therefore, the government can promote the implementation of identification codes to citizens through chip-based ID cards, leading to manage population data easily.

The government also improved the infrastructure quality of public services delivery. Building a good infrastructure system for developing online public services is necessary for e-government, but costly to the state budget. The government significantly invested in infrastructure development by upgrading the Digital Government Architecture Framework (the document No. 11757/VPCP-KSTT version 2 in 2019).

Furthermore, the government also established the Digital Task Force, which vigorously promoted e-government strategies. Digital Task Force created the spider network, including horizontal and vertical connections among the central government, regions, and municipalities. This network could be cooperated with private-sector companies in necessary cases and encouraged all entities to coordinate and involve in e-government.

Generally, from 2011, the Vietnamese government actively issued legal conditions for online service provision. However, in 2011-2019, there were no detailed documents on applying ICT in public service delivery, except some regulations on digital signatures and documents. Since 2019, the government has promoted online service provision and launched the national public service portal. The government has also heavily invested in developing information technology infrastructure through Vietnam E-Government Architecture Framework.

4.2. The results of applying ICT in online public services in Vietnam

In 2010, Vietnam’s Online Service Index was only 0.30476, much lower than the world average of 0.4178. There was because of two following reasons. First, the economy was influenced by the 2008 world final crisis, causing the state’s financial setbacks in 2010, while improving ICT infrastructure required a large budget. Second, using new technology in administrative procedures was not preferred by state officials familiar with traditional methods, which means that public servants could not immediately adapt to working condition changes.

Tab. 1. Vietnam Online Service Index in the period of 2010-2020.

Year	2010	2012	2014	2016	2018	2020
Vietnam’s OSI	0.30476	0.42483	0.41732	0.57246	0.73610	0.65290
World’s average OSI	0.4178	0.4328	0.4712	0.4623	0.5691	0.5620

Table 1 shows that Vietnam’s online service index increased from 0.30476 to 0.42483 from 2010 to 2012 but slightly decreased in 2014. From 2010 to 2014, although the online service index rose, this was still lower than the world’s average index. However, both the index of Vietnam and the world recorded a decrease in 2016. It was because that there was a change in the calculation method by the United Nations. From 2016 to 2020, Vietnam’s online service index became higher than that of the world. (Vietnam’s online service index was 0.57246 in 2016, while the world’s average index was only 0.4623). In 2018, Vietnam’s online service index reached the highest rate, at 0.73610, higher than the international index of 0.5691. In 2020, the world’s online service index slightly increased from 0.5691 to 0.5620 while the index of Vietnam little decreased (from 0.73610 to 0.65290) [1].

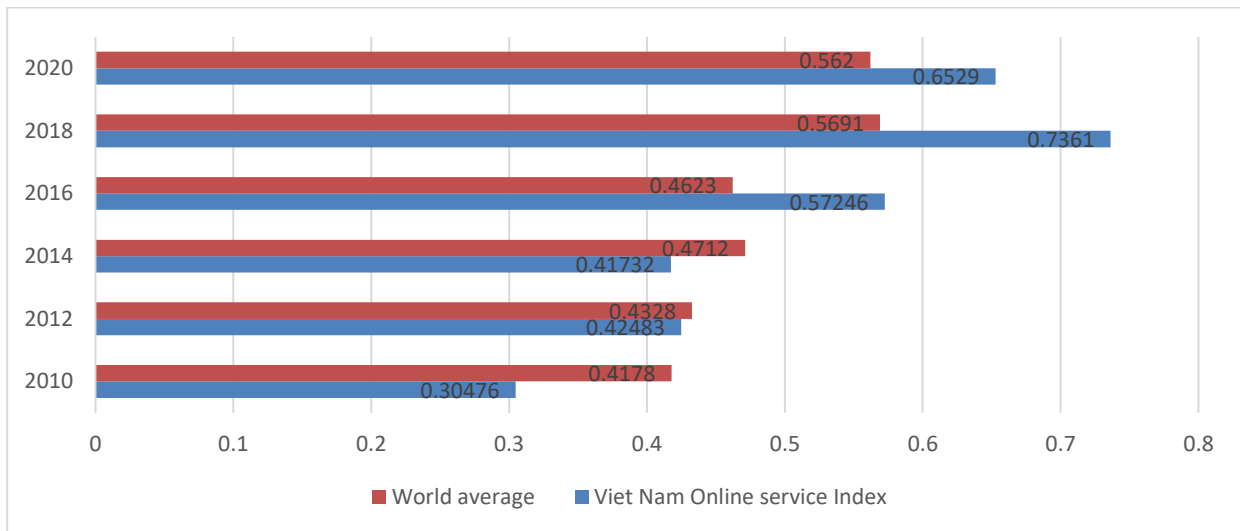


Fig. 1. Vietnam Online Service Index in the period of 2010-2020.

Fig. 1 illustrates the online service index between Vietnam and the world from 2010-2020. In general, there was an upward trend of the online service index of both. Vietnam’s index raised from 0.30476 in 2010 to 0.6529 in 2020, while the world’s index improved from 0.4178 in 2010 to 0.562 in 2020[1]. This figure also shows the Vietnamese online public service improvement between 2014 and 2016, as the index came from 0.41732 to 0.57246, respectively. In contrast, the world’s index fell 0.0089 points, from 0.4712 in 2014 to 0.4623 in 2016. This improvement in public service delivery in Vietnam resulted from Resolution 36a/NQ-CP in 2015 on e-government by the Vietnamese government. Accordingly, the government designed clear objectives and implementation solutions to promote ICT in public service delivery.

Tab. 2. Vietnam Telecommunication Infrastructure Index in the period 2010-2020.

Year	2010	2012	2014	2016	2018	2020
Vietnam Telecommunication Infrastructure Index	0.22606	0.39689	0.37923	0.37145	0.38900	0.66940
World average	0.232	0.3245	0.365	0.3711	0.4155	0.5464

Providing online public services requires good information infrastructure and high-quality human resources to use the Internet to perform their work proficiently. Since the ICT plan for online public service has been approved, the government has spent its budget improving information and communication infrastructure. Table 2 indicates the fluctuation of the telecommunication infrastructure index in Vietnam. The index of Vietnam showed an upward trend in infrastructure from 0.22606 in 2010 to 0.66940 in 2020. Compared to the world’s index, Vietnam’s index has consistently recorded a higher level in the whole period 2010-2020. Especially in 2020, Vietnam’s index was more significant than the world average. This data of Vietnam and the world was 0.6694 and 0.5464, respectively[2].

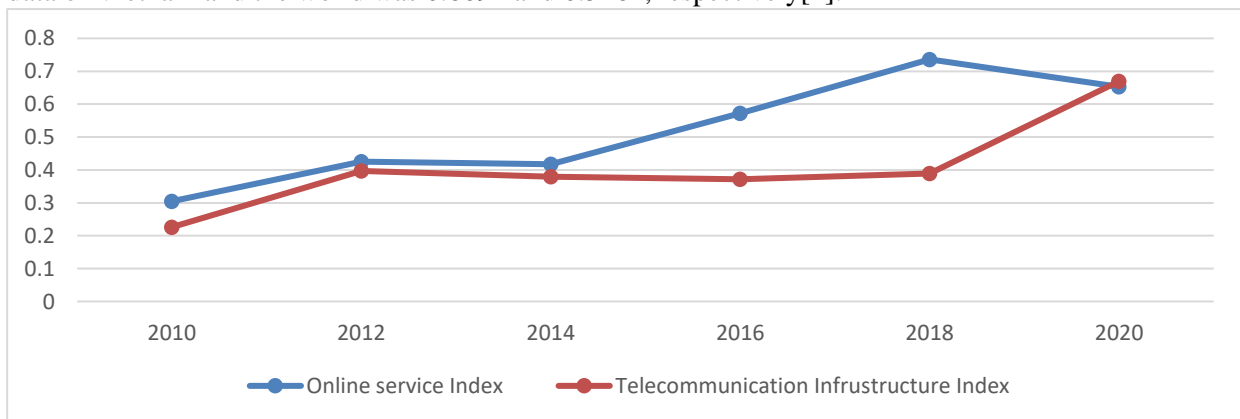


Fig. 2. Vietnam Telecommunication infrastructure Index and Online service Index.

Fig. 2 indicates the value of Vietnam’s telecommunication infrastructure index and online service index from 2010 to 2020. In general, the changing trend of the two indexes is not the same. From 2010 to 2012, there was an increase in the same direction of both indices. Although the two indices tended to increase, the online service index rose more than the telecommunication infrastructure index. From 2012 to 2018, the telecommunication infrastructure index did not fluctuate much, which was 0.39689 and 0.389 in 2012 and 2018, respectively. While the online service index significantly raised, from 0.42483 in 2012 to 0.7361 in 2018. During 2018-2020, there is an opposite change between these two indexes. The online service index decreased to 0.6529 in 2020, but the telecommunication infrastructure index increased significantly to 0.6694 in 2020 [3]. Thus, this figure demonstrates the improvement of information technology infrastructure, which has not uncertainly increased to contribute to the online public service delivery but sometimes in the opposite direction.

4.3. The evaluation of applying ICT in online public services in Vietnam

Tab. 3 indicates the enterprises’ evaluation of online public service delivery by state officials in Vietnam. A few enterprises agreed that applying information technology in business registration procedures at state agencies is good. However, this rate has improved over the years. In 2014, 28.57% of enterprises agreed with the good information technology application of registration procedures. This rate increased to 39% in 2020. Besides, the percentage of enterprises accessing provincial website fluctuated: 64.18% in 2014, increased to 76.84% in 2016, dropped to 65% in 2018 and fell to 53% in 2020 [4]. Generally, it can be seen that the province’s website is not helpful for businesses, thus the percentage of enterprises’ access to provincial websites decreased. Enterprises have not been interested in online public service for administrative procedures.

Tab. 3. The Provincial Competitiveness Index in Vietnam.

	Registration procedures: information technology application is good (%)	Percentage of firms have accessed provincial websites (%)
2014	28.57	64.18
2016	17.44	76.84
2018	36	65
2020	39	53

The enterprise evaluation on the openness and quality of provincial web pages from 2010-2020 is illustrated in Table 4. The score scale ranges from 0 to 100 points. Accordingly, most enterprises believe that the provincial web page is not open and of high quality, and their score is low during the period. However, this figure double increased from 15 in 2010 to 34.5 in 2020, bringing evidence for the government to further improve the information delivery on the local website [5].

Tab. 4. Openness and quality of the provincial webpage.

Year	Openness and quality of the provincial webpage
2010	15
2012	14
2014	29
2016	31
2018	35
2020	34.5

The advantages and disadvantages of the ICT application to online public services in Vietnam

There are some advantages in applying ICT to online public services in Vietnam. First, the government has spent a lot of effort to improve telecommunication infrastructure from 2010-2020 to create convenient conditions for applying ICT to online public services. Second, according to the data of the online service index, the telecommunication infrastructure index, and enterprises’ opinions. It is noticeable that the quality of online public service delivery improved in this period.

However, the rise of the online service index, the telecommunication infrastructure index is uncertain. Therefore, the improvement of information technology infrastructure is not certainly increased, influencing

the quality of online public service delivery. Moreover, the evaluation of enterprises on the provincial web page's quality shows the doubts for information security of administration transactions [6]. Besides, it is difficult for officials when there is a lack of a G-to-G link and population database system.

5. Conclusions and suggestions

Delivering online public service is an inevitable trend to enhance transparency and the administration system's efficiency in the process of administrative reform of worldwide countries. Recently, the Vietnamese government has issued and implemented many legal regulations and spent state budget to apply information communication technology to public service delivery. Although online public services have improved, citizens and enterprises were not satisfied and preferred to use online services.

In the context of the COVID-19 pandemic, governments and societies have been forced to promote using digital technologies to respond to the crisis, recover, and resolve socio-economic repercussions toward sustainable development. Therefore, the Government of Vietnam should (i) accomplish the population database system with identifiers, (ii) strengthen wide-spreading using online public service portals for citizens, and (iii) protect the privacy and mitigate the risk of over-surveillance associated with using technology.

6. Acknowledgements

The paper was presented during the 6th VIET-POL International Conference Scientific-Research Cooperation between Vietnam and Poland, 10-14.11.2021, HUMG, Hanoi, Vietnam.

7. References

1. <https://publicadministration.un.org/egovkb/en-us/Data/Country-Information/id/189-Viet-Nam>, 12/6/2021.
2. <https://pcivietnam.vn/du-lieu-pci>, 12/6/2021.
3. Pina, V., Torres, L., Royo, S., 2009. E-government evolution in E.U. local governments: a comparative perspective. *Online Information Review*, 33(6): 1137-1168, [https://doi: 10.1108/14684520911011052](https://doi.org/10.1108/14684520911011052).
4. Cepparulo, A., Zanfei, A., 2020. The diffusion of public eServices in European cities, *Government Information Quarterly*, 38(2), [https://doi: 10.1016/j.giq.2020.101561](https://doi.org/10.1016/j.giq.2020.101561).
5. Fakhoury, R., Aubert, B., 2015. Citizenship, trust, and behavioural intentions to use public e-services: The case of Lebanon, 2015. *International Journal of Information Management*, 35(3): 346-351, [https://doi: 10.1016/j.ijinfomgt.2015.02.002](https://doi.org/10.1016/j.ijinfomgt.2015.02.002).
6. Cepparulo, A., Zanfei, A., 2020. The diffusion of public eServices in European cities, *Government Information Quarterly*, 38(2), [https://doi: 10.1016/j.giq.2020.101561](https://doi.org/10.1016/j.giq.2020.101561).
7. Fedotova, O., Teixeira, L., Alvelos, A., 2012. E-participation in Portugal: evaluation of government electronic platforms, *Procedia Technology*, 5: 152-161, [https://doi: 10.1016/j.protcy.2012.09.017](https://doi.org/10.1016/j.protcy.2012.09.017).
8. Gasova, K., Stofkova, K., 2017. E-Government as a Quality Improvement Tool for Citizens Services, *Procedia Engineering*, 192: 225-230, [https://doi:10.1016/j.proeng.2017.06.039](https://doi.org/10.1016/j.proeng.2017.06.039).
9. Veeramootoo, N., Nunkoo, R., Dwivedi, Y.K., 2018. What determines success of an e-government service? Validation of an integrative model of e-filing continuance usage, *Government Information Quarterly*, 35(2): 161-174, [https://doi: 10.1016/j.giq.2018.03.004](https://doi.org/10.1016/j.giq.2018.03.004).
10. Kumar, R., Sachan, A., Mukherjee, A., 2018. Factors influencing e-government adoption in India: a qualitative approach, *Digital Policy, Regulation and Governance*, 20(5): 413-433, [https://doi: 10.1108/DPRG-02-2018-0007](https://doi.org/10.1108/DPRG-02-2018-0007).
11. United Nations Organizations, 2020. E-Government Survey 2020 Digital Government in the Decade of Action for Sustainable Development With addendum on COVID-19 Response, p 1-225.
12. Schuppan, T., 2009. E-Government in developing countries: Experiences from sub-Saharan Africa, *Government Information Quarterly*, 26(1), 118–127, [https://doi: 10.1016/j.giq.2008.01.006](https://doi.org/10.1016/j.giq.2008.01.006).
13. Ebberts, W.E., Jansen, M.G.M., van Deursen, J.A.M., 2016. Impact of the digital divide on e-government: Expanding from channel choice to channel usage, *Government Information Quarterly*, 33(4), 685–692, [https://doi: 10.1016/j.giq.2016.08.007](https://doi.org/10.1016/j.giq.2016.08.007).

14. Pleger, L.E., Mertes, A., Rey, A., Brüesch, C., 2020. Allowing users to pick and choose: A conjoint analysis of end-user preferences of public e-services,” *Government Information Quarterly*, 37(4), [https://doi: 10.1016/j.giq.2020.101473](https://doi.org/10.1016/j.giq.2020.101473).
15. Garín-Muñoz, T., López, R., Pérez-Amaral, T., Herguera, I., Valarezo, A., 2019. Models for individual adoption of eCommerce, eBanking and eGovernment in Spain, *Telecommunications Policy*, 43(1): 100-111.[https:// doi: 10.1016/j.telpol.2018.01.002](https://doi.org/10.1016/j.telpol.2018.01.002).
16. Igari, N., 2014. How to successfully promote ICT usage: A comparative analysis of Denmark and Japan, *Telematics and Informatics*, 31(1): 115-125, [https://doi: 10.1016/j.tele.2012.10.001](https://doi.org/10.1016/j.tele.2012.10.001).
17. Pieterse, W.J., Ebbers, W.E., 2020. Channel choice evolution: An empirical analysis of shifting channel behavior across demographics and tasks, *Government Information Quarterly*, 37(3), [https://doi: 10.1016/j.giq.2020.101478](https://doi.org/10.1016/j.giq.2020.101478).
18. Tangi, L., Benedetti, M., Gastaldi, L., Noci, G., Russo, C., 2021. Mandatory provisioning of digital public services as a feasible service delivery strategy: Evidence from Italian local governments, *Government Information Quarterly*, 38(1), [https://doi: 10.1016/j.giq.2020.101543](https://doi.org/10.1016/j.giq.2020.101543).
19. Vrabie, C., 2015. Education—A Key Concept for E-Administration, *Procedia - Social and Behavioral Sciences*, 186: 371-375, [https://doi: 10.1016/j.sbspro.2015.04.121](https://doi.org/10.1016/j.sbspro.2015.04.121).

Strengthening Inspection and Audit of Occupational Safety and Health in Coal Mining Enterprises in Vietnam

NGO Kim Tu^{1,*}

¹ University of Labour and Social Affairs, Hanoi, Vietnam

Corresponding author: tungokim@gmail.com

Abstract: Coal mining is one of the heavy, hazardous industries. Therefore, workers in this industry always face high risks of occupational accidents and diseases. According to the annual report of the Ministry of Labor, Invalids and Social Affairs (MoLISA), the situation of occupational accidents and illnesses in the mining sector in recent years has increased both in terms of number and severity, and this includes fatal occupational accidents in the coal mining industry. Currently, the authorities have been implementing inspection of occupational safety and health (OSH) to prevent and limit the situation. In the scope of this article, the author focuses on clarifying the position and the role of OSH inspecting while presenting and analyzing the results of the inspection of OSH legislation compliance within the coal mining industry nationwide. From there, proposing several solutions to strengthen inspection of OSH, prevent and limit occupational accidents and diseases in the coming time, contributing to improving the efficiency of state management of OSH in the coal mining industry in Vietnam today.

Keywords: Occupational safety and health (OSH), Inspection and audit of OSH, State management of OSH, Occupational accidents and diseases, Coal mining enterprises

1. Problem Statement

Coal mining is one of the crucial industries in ensuring national energy security. However, this is a heavy, toxic, and dangerous industry, with a high potential for occupational accidents, occupational diseases for workers [1]. According to statistics in recent years from the Ministry of Labor, Invalids, and Social Affairs, occupational accidents occurring in the country's mining industry are always at the "top" position compared to other sectors and fields. It's accounting for 15 to 16.5% of the total number of occupational accidents in the country, and thousands of people suffer from occupational diseases [2]. This includes fatal occupational accidents occurring at coal mining enterprises. Although state management agencies in charge of occupational safety and health (OSH) have organized and implemented many management solutions, the status of occupational accidents in coal mining enterprises, minerals are still high, and there is no sign of reduction. Against this background, strengthening inspection and examination of occupational safety and health in coal mining enterprises in Vietnam is considered one of the necessary measures today. This article uses secondary data from published reports, statistics, etc. and uses primary data made by the author to survey online for 17/22 coal mining companies belonging to Vietnam National Coal - Mineral Industries Holdings Corporation Limited (VINACOMIN), seven of which are underground mining companies, six are open-pit mining companies and the remaining four mine both underground and open-pit, all with the scale from 2000 to 5400 employees. The author selects coal mining companies belonging to Vinacomin for research because it is the largest domestic coal producer of Vietnam's coal industry, accounting for 85-90% of the total coal output of the whole industry in the country [3].

2. Introduction to the Occupational Safety and Health Inspection in Vietnam

2.1. Position, role, and function

The legal position of the Vietnam OSH inspectors has been specified in legal documents. The OSH Law 2015, Article 89, Clause 1 stipulates that OSH inspectors are specialized inspectors from agencies performing labour-related state management at central and provincial levels. In the Labour Law 2019, Article 215, Clause 2 stipulates: OSH inspectors are under specialized labour inspection and perform OSH inspection according to the provisions of the OSH Law. In the Law on Inspection 2010, Article 3, Clause 3 stipulates: *Specialized inspection* means inspection activities by competent state agencies by industry or sector applied to agencies, organizations, and individuals to inspect the compliance with specialized laws, professional and technical regulations, and management rules in such industry or sector [4].

Pursuant to the Law on Inspection 2010, According to Article 3, Decree No. 110/2017/ND-CP dated

October 4, 2017 of the Government stipulating the organization and operation of the Labour - Invalids and Social Affairs inspectorate: Agencies performing the functions of Labour - Invalids and Social Affairs inspection include: (i) State inspection agencies include: Inspectorate of the Ministry of Labour - Invalids and Social Affairs (referred to as Ministry Inspectorate) and Inspectorates of Departments of Labour - Invalids and Social Affairs (DoLISA) of the provinces and centrally-run cities (referred to as the Department Inspectorates); (ii) The agency assigned to perform the OSH specialized inspection functions is the Department of Work Safety [5].

From the above legal basis, it could be understood that:

At the national level:

Inspector of the Ministry of Labour, Invalids and Social Affairs: Decision No. 916/QD-LDTBXH of the Minister of Labor, Invalids and Social Affairs dated June 20, 2017 stipulates that the Ministry Inspectorate is an agency under the Ministry of Labor, War Invalids and Social Affairs. Labor - Invalids and Social Affairs, has the function to assist the Minister in implementing the provisions of the law on inspection work; conduct a specialized inspection of agencies, organizations, and individuals operating in the branches and domains under the Ministry's state management. On that basis, the Ministry Inspectorate shall carry out specialized inspections of OSH for corporations and economic groups throughout the country.

Department of Work Safety is a unit under the Ministry of Labour - Invalids and Social Affairs assigned to perform the functions of OSH specialized inspection. On that basis, the Director of the Department of Work Safety has issued the Decision No. 112/QD-ATLD dated October 5, 2017, stipulating that the Legal - Inspection Division - a unit under the Department of Work Safety is responsible for assisting the Director in implementing the function of state management in legal affairs, inspection, and audit of OSH.

At the provincial level: The People's Committee of the province/City under the Central Government stipulates that the Department of Labor, War Invalids and Social Affairs is a specialized agency, assisting the Provincial People's Committee in performing the advisory function and assisting the Provincial People's Committee in state management on Occupational Safety in the local area. In which, the Department Inspectorate is a unit under the local Department of Labor, War Invalids and Social Affairs, assisting the Director of the Department of Labor, War Invalids and Social Affairs in inspecting and inspecting OSH according to the provisions of law [6].

2.2. Responsibilities and authority

The OSH Inspectorates shall perform the responsibilities and authority prescribed in Articles 10 and 11 of the Government's Decree No. 07/2012/ND-CP stipulating agencies assigned to perform the specialized inspection functions and to operate specialized inspection activities. These include: (i) Develop inspection plans and submit them to the Ministry Inspectorate, Department Inspectorates to synthesize and submit to the Minister or DoLISA Directors for approval and arrangement of the implementation of such plans; (ii) Inspect the compliance with the specialized laws, regulations on professional and technical matters, rules on management in the related industries and sectors; (iii) Inspect the cases with signs of law violation as assigned by the Chief Inspector of the Ministry or Chief Inspector of the Department; (iv) Inspect other cases as assigned by the Minister or the DoLISA Director. (v) Monitor, urge and examine the implementation of their inspection conclusions, recommendations, and handling decisions; (vi) Summarize and report specialized inspection results to the Ministry Inspector, Department Inspector.

At the same time, the OSH Inspectorates also perform the responsibilities and authority prescribed in Articles 10 and 11 of the Government's Decree No. 110/2017/ND-CP stipulating the organization and operation of the inspectorates in the Labour - Invalids and Social Affairs sector. These include: (i) Carry out a specialized inspection within the scope of state management of the Department; (ii) Synthesize and report the results of the inspection, settlement of complaints and denunciations, and prevention and control of corruption in the fields under its management to the Ministry Inspectorate; (iii) Join the Ministry Inspectorate in guiding and training specialized inspectors in the fields under the scope of the Department's management; (iv) Detect, prevent and handle, under their competence or proposals of the competent state agencies, violations of the laws within the scope of state management according to regulations; (v) Other responsibilities and authorities as prescribed by law.

2.3. Scope, contents, and means of inspection

- *The scope of OSH specialized inspection is clearly defined in Article 89, Clause 2 of the OSH Law: OSH inspection in the fields of radiation, oil and gas exploration, and exploitation, railway, waterway, road, air transportation, or people's armed forces shall be implemented by state management agencies of such fields in collaboration with OSH inspectors.*

- *Regarding the inspection of the compliance with the law provisions on OSH:*

The labor law 2019, Article 214 stipulates that the contents of labor inspection include: (i) Inspecting the observance of labor laws; (ii) Investigate occupational accidents and violations of occupational safety and health; (iii) Participate in guiding the application of a system of standards and technical regulations on working conditions, occupational safety and health; (iv) To settle complaints and denunciations about labor in accordance with the law. (v) To handle according to their competence and propose competent agencies to handle labour law violations. [7]

Article 5, Clause 2 of Decree No. 110/2017/ND-CP includes the following contents: inspecting the implementation of measures to prevent and combat hazardous factors for employees; measures to handle technical incidents compromising OSH and causing occupational accidents and diseases; ensuring OSH for several specific types of work; ensuring OSH for production and business establishments; activities of OSH service providers.

- *Means of inspection:*

From 2006 to 2018, the Labour Inspectorate conducted the means of inspection according to Decision No.02/2006/QD-BLDTBXH dated February 16, 2006 of the Minister of Labour - Invalids and Social Affairs promulgating Regulations for using self-check forms for the implementation of labour laws by distributing the papers to each enterprise by post. These papers also includes self-check of the implementation of the OSH legislation. Since 2019, the Labour Inspectorate has been implementing the means of inspection as prescribed in Circular No.17/2018/TT-BLDTBXH of the Ministry of Labour - Invalids and Social Affairs promulgating the Regulation on using self-check forms for assessing the implementation of the labour law. According to this method, the Inspectorates of the provincial Departments of Labour - Invalids and Social Affairs guide enterprises to register for accounts and report self-check results online on the website. <http://tukiemtraphaplualaodong.gov.vn/>.

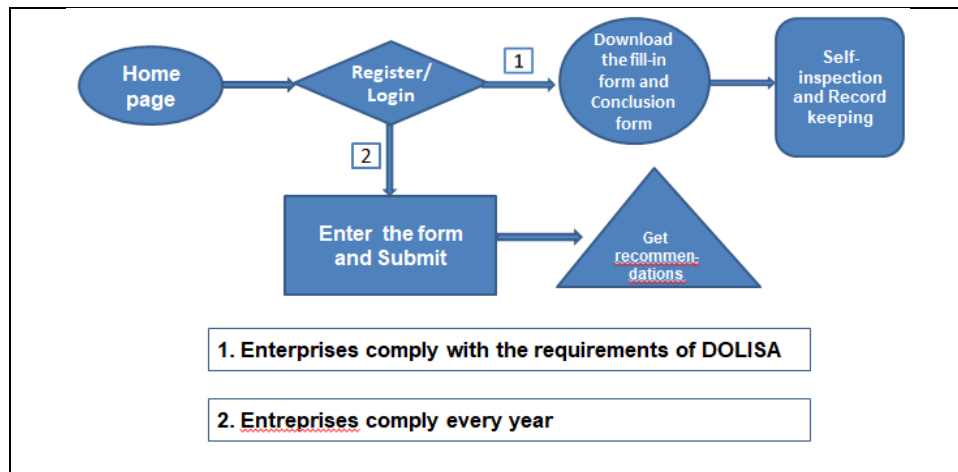


Fig. 1. Interface of the website.

The results of the online survey conducted by the author for 17 coal mining enterprises under TKV showed that: 100% of the survey respondents commented evaluated the reporting of the results of self-inspection on the implementation of the labor law online on the website is simple, convenient, and easy to use.

Assessing the necessity of reporting the results of self-inspection on the implementation of the labor law online on the website to help enterprises better comply with the law on OSH: 35.7% of the opinions is essential, 57.2% of the opinions are rated as necessary, and 7.1% of the results are quite necessary.

Thus, the method of using self-check sheets complies with modern labor laws, suitable for enterprises as well as keeping up with current management trends. That is, strengthen the remote consultation and guidance of the state management agency on OSH for enterprises in complying with the law on OSH.

In addition, the Ministry of Labour - Invalids and Social Affairs of Vietnam has issued Circular No. 20/2018/TT-BLDTBXH *guiding the coordination mechanism in carrying out specialized inspection of occupational safety and health at night, after business hours* with the primary purposes to: (i) Ensure the effectiveness and efficiency of specialized inspection in labour and OSH fields; (ii) Ensure violations of the law on labour and OSH must be prevented and addressed promptly; (iii) Promote the role of agencies and organizations in detecting and preventing violations of the law on labour and OSH; ensure the legitimate rights and interests of employees; (iv) Ensure the enforcement of the law on labour and OSH in production, business and service establishments operating at night or out of business hours [8].

2.4. Inspection force

In 2020, the number of inspectors of the entire Labour - Invalids and Social Affairs sector was 457 people. Of which, the Ministry Inspectorate and the agencies performing the specialized inspection function under the Ministry had 69 inspectors; 388 inspectors were working under Departments of Labour - Invalids and Social Affairs in localities. Regarding professional qualifications: 100% of inspectors have university degrees, 23.8% have master's degrees [9]. Up to now, Occupational Safety and Health Inspectors have been participating in many different training programs to improve their qualifications, expertise, and inspection skills and have been well implementing their tasks.

3. Inspection and audit of OSH in coal mining companies in Vietnam

3.1. Occupational accidents situation nationwide and in the VINACOMIN

According to the annual report of the Ministry of Labour - Invalids and Social Affairs, the number of occupational accidents occurring in the mining and mineral sectors in recent years has increased in both the number of cases and the number of deaths.

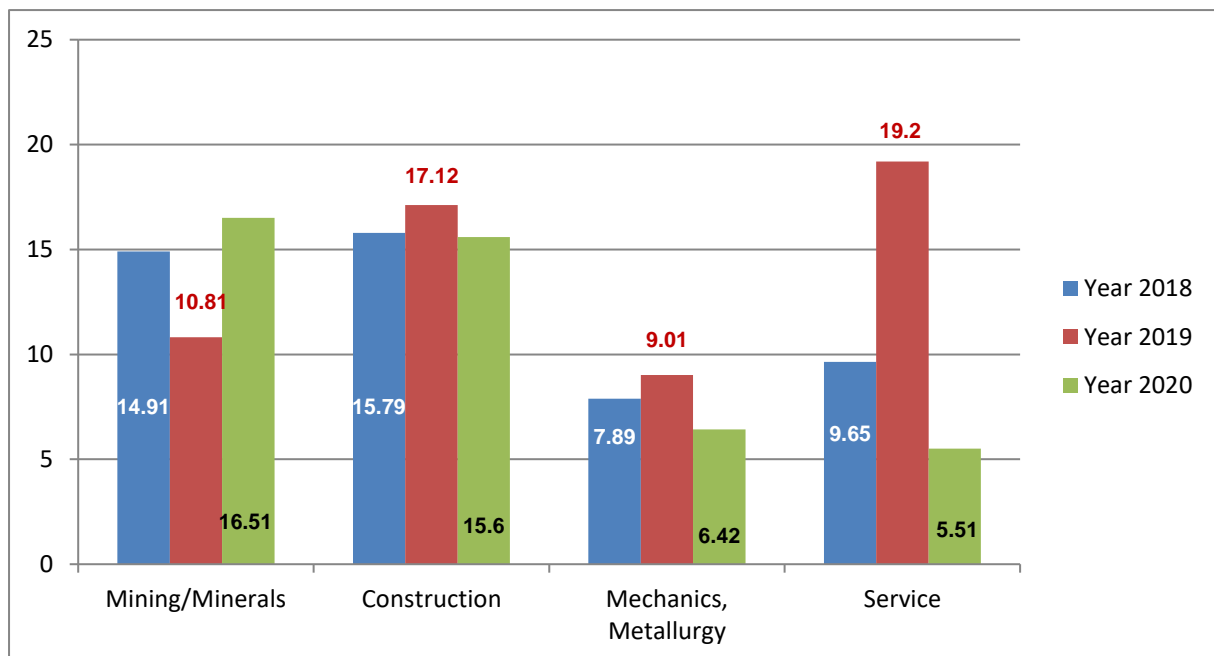


Fig. 2. Occupational accidents situation of nationwide and by sector.

Source: Annual summary report on Occupational accidents nationwide of DWS [2].

The figure above shows that, before 2020, the number of occupational accidents occurring in the mining and mineral sector was always lower than the number of occupational accidents occurring in the construction sector. But in 2020, the number of occupational accidents occurring in the mining and mineral sector was the highest and exceeded the number of occupational accidents occurring in the construction

sector by 0.87%. This number includes occupational accidents occurring in member entities of the Vinacomin.

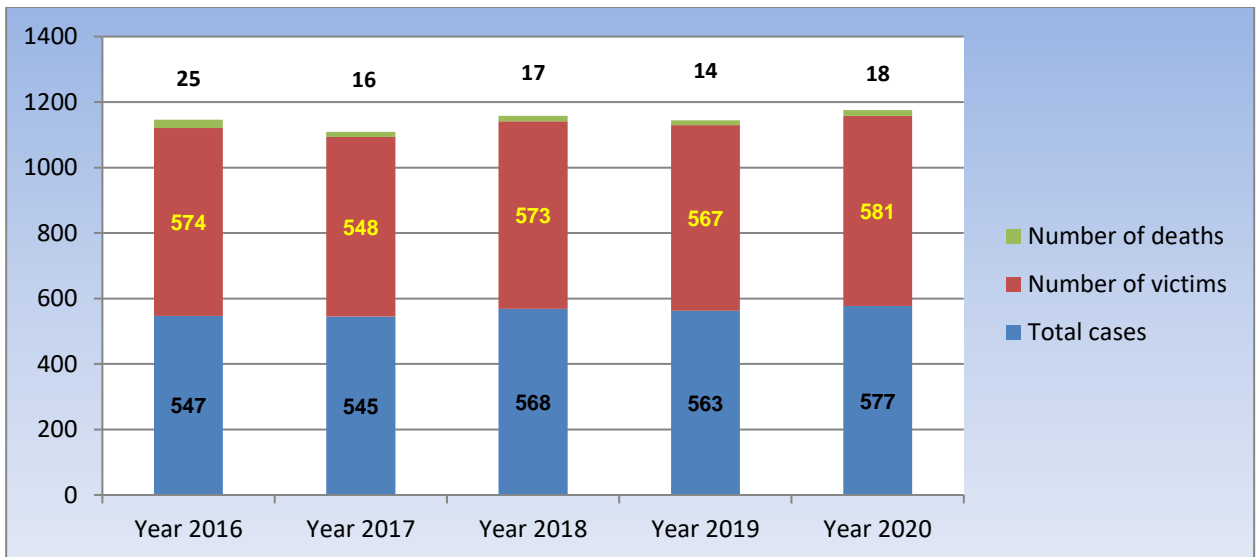


Fig. 3. Occupational accidents situation in the Vinacomin from 2016-2020.

Source: Annual report on Occupational accidents in 2016-2020 of VINACOMIN [10].

Analysis of the figure above shows that the number of occupational accidents and victims of Vinacomin increased slightly from 2017 to 2020. In particular, in 2016, there was the highest number of deaths due to occupational accidents with 25 people, and then it continued to decrease to 16 deaths in 2017 and 14 deaths in 2019. However, the number of deaths due to occupational accidents sharply increased to 18 people in 2020. Thus, from the OSH inspection four years ago to 2020, the situation of occupational accidents, especially fatal occupational accidents of VINACOMIN, has not been controlled or mitigated. According to the Occupational Safety Department of Vinacomin, the number of deaths from occupational accidents mainly occurred in underground coal mining units.

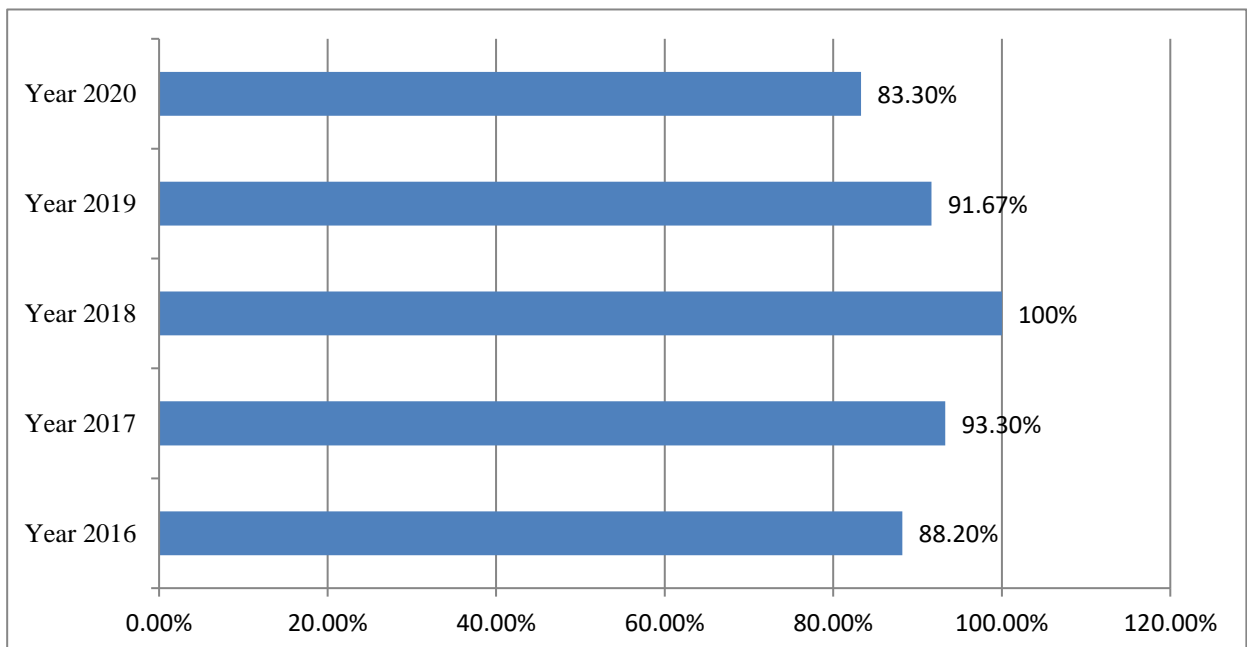


Fig. 4. The rate of fatal accidents in underground coal mining over time.

Source: Annual report on Occupational accidents in 2016-2020 of VINACOMIN [10].

The figure above shows that the fatal accident rate in underground mining from 2016 to 2020 of the Vinacomin was severe, accounting for 88.2% to 100% of the total number of occupational accidents. Notably, in 2018, eleven occupational accidents killed eleven people. This shows that underground coal mining is hazardous, with extremely high risks of being wounded or fatal because deep underground, the conditions are harsh with lack of oxygen, risk of tunnel collapse, landslide, water burst, asphyxiation, fire, and explosion, etc. While underground coal mining technology is far from modern, mechanization and automation have been applied in certain stages and procedures of mining. According to Vinacomin's annual OSH report, the leading causes of occupational accidents include: (i) Employees work subjectively, do not comply with the OSH rules and regulations; (ii) The persons in charge of direction and supervision of occupational safety are negligent and irresponsible. This situation shows that it is necessary to strengthen the OSH inspection and audit on coal mining activities by labor-related state management agencies at all levels.

3.2. OSH inspection and audit activities in coal mining companies

- Activities of OSH inspection/audit teams established by MoLISA

In 2016, the Ministry of Labour - Invalids and Social Affairs signed a Decision to establish an inspection team to inspect the observance of labour laws and OSH legislation in Vinacomin and 24 member companies. (Among them are 17 coal mining companies). The inspection team concluded several major violations: periodical OSH training for employees was not following regulations; using equipment with strict requirements on occupational safety that has not been verified; inadequate periodic health check for employees, etc. After announcing the inspection conclusions, Vinacomin and its member units have thoughtfully implemented the recommendations of the OSH inspection team. As a result, the number of deaths from occupational accidents in 2016 decreased from 25 to 14 in 2019. However, in 2020, the number of occupational accidents increased by 14 cases, from 563 in 2019 to 577. The number of injuries also increased to 581, and the death toll jumped to 18. Facing this situation, the Ministry Inspectorate promptly established an inspection team to inspect the observance of labour laws and OSH laws in 30 branches and units in the Vinacomin according to the Inspection Plan approved by the leadership of the Ministry of Labour - Invalids and Social Affairs in the Decisions from No. 228/QD-TTr to No.257/QD-TTr dated May 11 August 2020. Among the 30 branches and units subject to inspection, 43% were underground mining units, and 10% were open-pit mining units. The announcement of the results of the inspection team confirmed: (i) 100% of the inspected subjects had seriously complied with the OSH law. Specifically: they had established OSH apparatus and Health units as prescribed; a network of OSH officials had been established; they had based internal rules, regulations, and working procedures on OSH for working machines and equipment, etc. (ii) 100% of coal mining enterprises had fully complied with the legal regulations on OSH in coal mining activities such as safety in excavation and support of furnaces; protect and repair of furnace paths; propping and control of rocks/walls; ventilation, etc. At the same time, the occupational safety and health inspection team raised a number of shortcomings that Vinacomin and its member units need to overcome: (i) The production site still poses potential risks of compromising safety; (ii) Some construction solutions and measures are incomplete, irrelevant to actual production or each working position; (iii) There is still the phenomenon that staff directing production giving production orders (daily orders, shift orders) in a general way; (iv) work safety measures are still sketchy, etc.[11].

- Activities of the occupational safety and health inspection team established by the Department of Labour - Invalids and Social Affairs of Quang Ninh province

To date, the relevant authorities have granted 88.7% of the total number of coal mining licenses to the companies based in Quang Ninh province, and they are allowed to mine coal in Quang Ninh province [12]. Persuaded by the Law on Organization of Local Government and the Law on Occupational Safety and Health, Quang Ninh provincial government has hierarchical and decentralization the state management of OSH in its province. Thus, the Chairman of the People's Committee of Quang Ninh province has issued a document stipulating that the provincial Department of Labour - Invalids and Social Affairs is a specialized agency under the Provincial People's Committee, performing the function of advising and assisting the Provincial People's Committee in state management of OSH. On that basis, the Department of Labour - Invalids and Social Affairs of Quang Ninh province has the following responsibilities and authority in

operation: to inspect, audit, and address violations of the labour law and the law on occupational safety and health by organizations and individuals based in the province. They include units that are members of Vinacomin operating in coal mining, processing, and trading in Quang Ninh province.

In 2019, the Department of Labour - Invalids and Social Affairs of Quang Ninh province conducted a surprise inspection on OSH in 11 units under the Vinacomin and 20 contractors carrying out packages of loading, unloading, transporting soil and rock, digging pits according to Document No.7866/UBND-VX2 of the People's Committee of Quang Ninh province. The inspection team asked the units to implement 110 recommendations; temporarily stop 01 production position that does not ensure safety. At the same time, the Department of Labour - Invalids and Social Affairs of Quang Ninh province proposed to the Investigation Police Agency, the People's Procuracy of Quang Ninh province, and localities to investigate and address severe occupational accidents under their competence. Numerous typical cases of occupational accidents include: (i) The investigation police agency under Dong Trieu Town Police has issued a Decision to prosecute a criminal case No.52/QD due to violations of regulations on occupational safety related to the occupational accident that occurred on January 11, 2019 at transporting tunnel level -150 LC11(46) Project to expand the capacity of Trang Bach mine by Mining Construction Company-Vinacomin;(ii) The Investigation Police Agency of Cam Pha City Police has issued Decision No.09/QD-CSĐT on the prosecution of the criminal case "Violation of regulations on occupational safety and health, on safety in crowded places" related to an accident with one death on November 27, 2020 at the mine transportation route level -182, open-pit coal mining field of Deo Nai Coal Joint Stock Company - Vinacomin; prosecuted 01 defendant against Mr. Nguyen Chi Vu, operator of the Komatsu HD465-7R truck No.27 [13].

The inspection and examination of OSH in coal mining enterprises shall be carried out by state management agencies in charge of labor at all levels in accordance with the law, ensuring the detection, prevention, and timely handling of violations the law on OSH. Advanced and modern methods of inspection and examination of OSH. Forms of assessment and review of OSH are conducted in various ways: according to approved plans and programs, or irregularly inspected and tested under the direction of competent authorities. In addition, the Occupational Safety and Health Inspectorate also promotes consulting and guidance for enterprises to solve difficulties and problems in complying with the law on OSH. 90.4 % of the respondents said they had asked the State management agency on labor or the Youth Union to inspect OSH to advise and guide enterprises to solve difficulties problems in complying with OSH law, 9.6% of enterprises have never requested. Assessing the satisfaction of the results of support/advice/instruction from the state management agency on labor or from the Youth Union, inspecting OSH for enterprises on compliance with the OSH law, 41.2% of the opinions rated very satisfied, there were 47.0% of the comments rated the level of satisfaction, 5.9% of the comments rated the level of quite satisfied and 5.9% of the comments were less pleased.

The organization of occupational safety and health inspection teams at all levels is crucial to prevent and promptly handle violations of the law on OSH, thus contributing to ensuring the effectiveness and efficiency of specialized occupational safety and health inspection and at the same time ensure the legitimate rights and interests of the organization and employees. However, the occupational safety and health inspectorate still has the following shortcomings:

- Regulations on the duties and powers of inspectors when performing their official duties are limited, especially in case of detecting violations of the law on OSH;
- Resources for OSH inspection in the entire sector of Labour, Invalids and Social Affairs are still inadequate and do not meet current requirements;
- The number of occupational safety and health inspections carried out by enterprises is still tiny [14];
- The frequency of OSH inspections and examinations on the implementation of the law on OSH in enterprises in general as well as in coal mining enterprises, in particular, is still low;
- The coordination in investigating fatal occupational accidents and signs of crime among police agencies, procuracies, and occupational accident investigation teams in some places is not good [14].

These shortcomings significantly influence the effectiveness and efficiency of state management of OSH in coal mining enterprises in Vietnam today.

4. Proposal of several solutions to strengthen OSH inspection and audit in coal mining companies in Vietnam

4.1. Grounds for proposals

- *Directive 29-CT/TW dated September 18, 2013 of the Secretariat on promoting occupational safety and health in the period of industrialization, modernization, and international integration;*

- *Resolution No. 20-NQ/TW dated October 25, 2017 of the Party Central Committee on Strengthening the protection, care, and improvement of people's health in the new situation. It stated, "Implementing solutions synchronously for disaster prevention and control, ensuring order, traffic safety, and labour safety; prevention and control of accidents, injuries, fires, explosions, and occupational diseases";*

- *Decision No. 403/QĐ-TTg dated March 14, 2016 approving the adjustment of the development plan of Vietnam's coal industry to 2020, taking into account the prospect to 2030 from the development perspective of "ensuring safety in production";*

- *Decision No. 01/QĐ-LĐTBXH dated January 4, 2021 of the Minister of Labour - Invalids and Social Affairs promulgating the Action Plan of the Labour - Invalids and Social Affairs sector to implement Resolution No. 01/ NQ-CP and Resolution No. 02/NQ-CP dated January 1, 2021 of the Government: *Project on improving the inspection capacity of the Labour - Invalids and Social Affairs sector in the 2021-2026 period;**

- *Resolution No. 55-NQ/TW dated February 11, 2020 of the Politburo on orientations of Vietnam's national energy development strategy to 2030, with a vision to 2045: "Expanding search, exploration, promoting coal mining on the basis of ensuring safety, efficiency and saving resources";*

- Results of the inspection and audit of OSH in coal mining enterprises recently.

The above directions and strategies show that the Party, Government, and relevant agencies of Vietnam are very concerned about safety and health for workers and the social community in the coming time when coal mining activities vigorously develop. These are essential foundations in developing action plans and proposing solutions to strengthen inspection and audit of OSH in coal mining enterprises in Vietnam in the future.

4.2. Proposal of solutions

- Reviewing, amending, supplementing, and completing the legal provisions on: Occupational safety and health inspectors conduct independent inspection; Increased powers for inspectors when on duty; Strengthen the task of consulting and guiding enterprises in complying with the law on OSH; Strengthen supervision of the implementation of recommendations after inspection and examination of OSH;

- Strengthening the OSH inspection system, supplementing OSH inspection resources in the entire sector of Labour, Invalids and Social Affairs to meet current requirements such as: Increase staffing quotas based on increasing staffing quotas, position job placements from the Interior sector; Improve the capacity of the inspection team, inspecting OSH through professional training courses, soft skills,... Building a network of inspectors and inspectors from experts, experts professional and experienced managers;

- Increase the number of OSH inspections and inspections as well as the frequency of OSH inspections and audits on the observance of the OSH legislation in enterprises in general as well as in coal mining enterprises in particular, ensuring the inspection subjects are fair before the law as well as strengthen the form of irregular inspection and examination of OSH, avoiding the situation that the inspected subjects are prepared to cope;

- Continue to hierarchy and decentralize powers to local state management agencies in charge of labor to proactively develop programs and plans for inspection and inspection of OSH in accordance with local conditions and at the same time promote work. Cooperate in investigating fatal occupational accidents, with

signs of crime between police agencies, procuracies, and occupational accident investigation teams in those localities.

- Promote the application of information technology by online consultation, dissemination, and guidance of enterprises to comply with the law on OSH, publicizing the conclusions of inspection and examination of OSH, publicizing violations and penalties. treatment mode; Establishing a hotline to receive information: complaints and denunciations of violations of the law on OSH;

- Coordinate with relevant parties such as: Trade Union, Farmers' Union, Veteran's Association, Women's Union, etc. in propagating, disseminating, and educating the law on OSH.

5. Conclusion

The Vietnam Occupational Safety and Health Inspectors have specific positions and roles, clearly defined by law. At the same time, OSH Inspection is also an important function of labour-related state management agencies at all levels. Although the resources for OSH inspection in the entire Labour - Invalids and Social Affairs sector of Vietnam are still limited; the scope and targets of inspection are broad; and the contents of OSH inspection are complex and multi-sectoral in nature; OSH inspection and audit in coal mining enterprises have been implemented by labour-related state management agencies at all levels in accordance with the law, ensuring the detection, prevention and timely handling of violations against OSH law, contributing to the reduction of the frequency of fatal occupational accidents by 16.99% in the 2016-2019 period compared to the period 2011-2015 [14]. This ensures the achievement of the target of "Annual average reduction of the frequency of fatal occupational accidents by 5%" set out by the National Program on OSH for the period 2016-2020. In the coming time, the inspection and examination of OSH in coal mining enterprises should be further strengthened to improve the effectiveness of state management of OSH.

6. Acknowledgements

The author respectfully acknowledges and highly appreciates the results of the OSH inspection and testing missions in Vietnamese coal mining enterprises in the period 2016-2020. These are necessary activities of the state management agencies on OSH at all levels. Besides, the author also appreciates the survey opinions from 17 enterprises, representing in 22 coal mining enterprises nationwide today. From there, the author has more important grounds to make recommendations on some solutions to strengthen the inspection and examination of OSH in Vietnamese coal mining enterprises in the coming time. In addition, the author thanks scientists, experts and editorial board for helping us improve the quality of the manuscript.

7. References

1. International Labour Organization (ILO), 2009. Occupational, Safety and Health in mining, Project on capacity Building for Occupational Safety and Health in Vietnam (VIE/05/01/LUX), Labour-Social Publishing House.
2. Department of Work Safety (MoLISA), Annual summary report on Occupational accidents nationwide in 2016-2020.
3. <https://moit.gov.vn/tin-tuc/hoat-dong/bo-truong-nguyen-hong-dien-lam-viec-tai-tap-doan-cong-nghiep.html>
4. http://vanban.chinhphu.vn/portal/page/portal/chinhphu/hethongvanban?class_id=1&_page=1&mode=detail&document_id=180606
5. http://vanban.chinhphu.vn/portal/page/portal/chinhphu/hethongvanban?class_id=1&_page=1&mode=detail&document_id=98567
6. http://baucu.vinhphuc.gov.vn/ct/cms/chuyenmon/Lists/lichlehoitrongnam/View_detail.aspx?ItemID=27
7. http://vanban.chinhphu.vn/portal/page/portal/chinhphu/hethongvanban?class_id=1&_page=1&mode=detail&document_id=198540
8. <http://tukiemtraphapluatlaodong.gov.vn/Default/Index?ReturnUrl=%2F%3FAspxAutoDetectCookieSupport%3D1>
9. Inspector of the MOLISA (MoLISA), 2020. Final report: The implementation of the project "Improving inspection capacity".

10. Vietnam National Coal-Mineral Industries Holdings Corporation Limited (VINACOMIN), Annual report on Occupational accidents in 2016-2020.
11. Inspector of the MOLISA (MoLISA), 2020. Announcement of inspection results on the implementation of Labor law and OSH law in Vinacomin.
12. Ministry of Natural Resources and Environment, 2020. Department of Geology and Minerals, List of licenses for mining and mineral exploration.
13. Inspector of the DoLISA Quang ninh province, Annual summary report on OSH in 2019-2020.
14. Department of Work Safety (MoLISA), 2020. Summary report of the national program on OSH for the period 2016-2020.

Some Effects on the Temperature of the Mine Air at the Heading Face

NGUYEN Van Quang^{1,*}, NGUYEN Van Thinh¹, NGUYEN Cao Khai¹, PHAM Van Chung¹

¹ Hanoi University of Mining and Geology, 18 Vien street, Hanoi, Vietnam

Corresponding author: quangnv@hmg.edu.vn

Abstract. Currently, with the increase in mining output leading to deeper mining levels, the volume of heading face serving production has also increased. The thermal environment tends to worsen when digging deep due to the geothermal's effect, which increases the air temperature at the heading face. According to QCVN01/2011-BCT, the temperature at the heading face is not allowed to exceed 30°C. To ensure this, in Vietnam today, mainly forced ventilation method uses local fans to provide a clean amount of air to ensure a favorable environment for workers. With the forced ventilation method, the duct position is usually arranged on the side, and the distance from the duct mouth to the heading face is determined to ensure that $l < 6\sqrt{s}$. In this study, a numerical simulation method by Ansys CFX software is applied to study the influence of several factors such as duct position, air temperature of duct, and roughness characteristics of roadway on the temperature of the mine air at the heading face. The models are set up with six duct positions and four air temperature of duct parameters. Model 1 ($y = 1.1$ m) is better than models 2 to 6 in terms of temperature distribution and the lowest temperature values. Four models have different wind temperatures, and we can see the significant influence of the inlet air temperature of the duct on the thermal environment of the heading face. The results show that with the model $T = 297.15$ K, the temperature value on the roadway length is guaranteed as specified < 303 K. The result is a reference for determining the duct position and cool for the high-temperature heading face.

Keywords: Numerical modeling, CFX, Ventilation duct position, Heading face, Temperature of air mine

1. Introduction

With the need to develop the economy, the demand for coal minerals is constantly increasing. In recent years, coal mineral resources in the shallow part of Quang Ninh area are gradually depleting, leading to the trend of deep mining for natural resources with Vietnam's underground coal mines is very necessary. Currently, coal mines in Quang Ninh, Vietnam are prepared and exploited to the following levels: Mao Khe -400, Ha Lam -350, Khe Cham 2-4, -500; Mong Duong -400; This leads to an increase in the amount of preparatory excavation work and preparation at such depths, which means that the temperature of soil, rock, and coal will also gradually increase above 30°C along with the use of modern machinery and equipment. The air in the excavators also increases. As a result, the thermal environment deteriorates, affecting the working conditions of workers. Advance this to create favorable working conditions on wind speed, temperature, humidity, dust for mines as standard. At coal mines, the main method of local ventilation is the forced ventilation method. With the layout of the side ducts, the location depends on transport equipment with a distance of $L < 6\sqrt{s}$ for the roadway. There are many research works on working environment conditions in heading face in the general and thermal environment in particular. In general, the deterioration of the thermal environment in the heading face is mainly due to geothermal effects on machinery, equipment and inlet wind temperature. According to Agus, P.S et al., the three-dimensional blind heading model for studying the effects of the airflow velocity, the rock temperature and heat dissipation from mining equipment on the air temperature in the underground mine [1]. The heat transfer between the surrounding rock and the airflow in the underground mine is varied, including conduction heat from the rock to the airflow, thermal convection between the wall and the airflow, heat radiation from the wall to the airstream, and also includes heat transfer between the rock and the water, water and airflow [2, 3]. Len et al. stated that the high temperature of deep underground space is essentially influenced by the thermal characteristics of the surrounding rock [4]. QUAN Truong Tien et al. shows that the surface temperature affects the mine air temperature [5]. The mine temperature is affected by the geothermal, climate and heat radiation from mining equipment [6]. Other research indicated that mine air's important heat source effects are the heat from the rock, etc. [7]. In addition, many mathematical models have been proposed in the mine ventilation area, from one-dimensional heat transfer models to computational ventilation dynamics (CFD) models. In Vietnam, there are many typical studies on air temperature in underground mines. Dao Van Chi et al. [8] and Nguyen Van Quang et al. [9] analyzed the main factors that affect air temperature in the underground mine, such as the temperature of the surrounding rock, heat of

equipment, and airflow. However, this analysis and assessment is only qualitative and has not determined specific values. To improve microclimate conditions in underground mines, the authors proposed solutions to improve ventilation efficiency to ensure the velocity moves in the roadway and the mine air's temperature and humidity within the allowable limits [10, 11, 12]. Another study, determination of reasonable working mode for main fan to ensure the required air flow for heading face [13]. However, in specific geological conditions with specific area characteristics, the influence of factors on air temperature in the heading face is also different. In this paper, the author builds a numerical model showing the influence of duct position, inlet wind temperature, and especially taking into account the roughness of the roadway affecting the thermal environment in the heading face. From there, it can be used as a reference to choose the position of the duct, select the inlet temperature to ensure favorable environmental conditions, and save cooling costs when used. Thus, in addition to the influence of the heat source, the input temperature is critical, directly affecting the thermal conditions and the roughness of the heading face, increasing the heat exchange time between the rock and the air. The article builds 6 models with duct height ($y = 1.1 \text{ m}; 1.7 \text{ m}; 2.0 \text{ m}; 2.3 \text{ m}; 2.6 \text{ m}; 3.1 \text{ m}$) near the side of wall and 4 models with inlet air temperature ($t_{\text{duct}} = 297.15\text{K}; 299.15\text{K}; 301.15\text{K}; 302.15\text{K}$) vary with a 2 cm wall roughness.

2. Modeling

The simulation was based on the basic parameters of the roadway level -250 seam L7 of Mong Duong coal mine: the length of roadway $L > 40 \text{ m}$; the height of the roadway $y = 3.5 \text{ m}$, the width of the roadway $b = 4.5 \text{ m}$. The -250 level transport road uses the forced ventilation method with the following parameters ($\phi_{\text{duct}} = 0.6 \text{ m}$, $h_{\text{duct}} = 2.3$, $v = 9 \text{ m/s}$). From that, the article builds six positions of duct models (height of duct $y = 1.1 \text{ m}; 1.7 \text{ m}; 2.0 \text{ m}; 2.3 \text{ m}; 2.6 \text{ m}; 3.1\text{m}$). 4 models of inlet wind temperature ($t_{\text{duct}} = 297.15\text{K}; 299.15\text{K}; 301.15\text{K}; 302.15\text{K}$). The position of the duct is arranged in Figure 1.

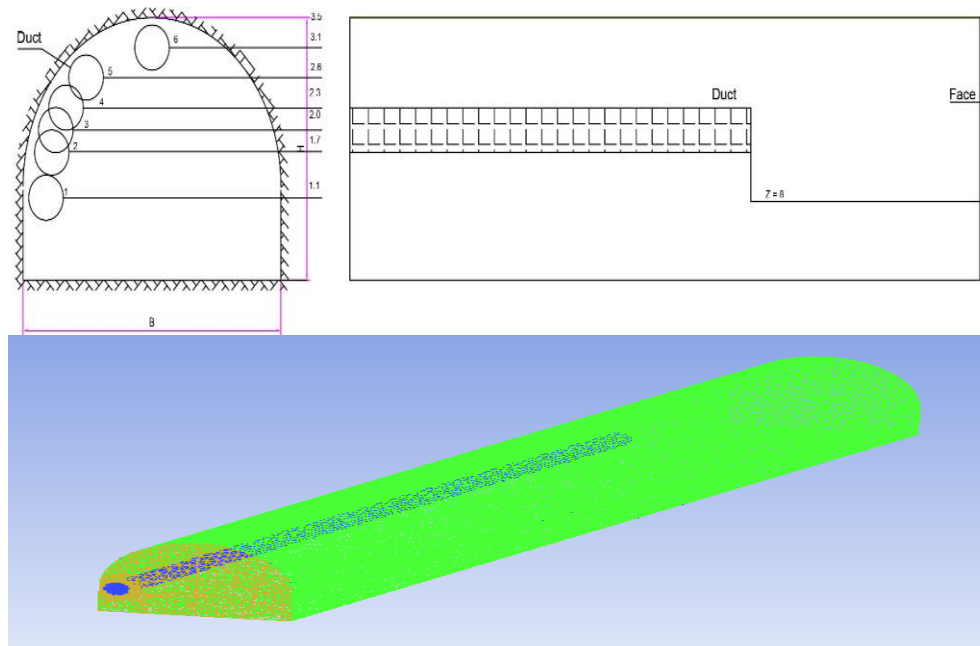


Fig. 1. Position of an air duct on heading face.

3. Computational model

3.1 Numerical model

The article uses numerical simulation (CFD) with geometric modeling and meshing done in ICFM-CFD software with the same geometric size as above, meshing with pipes of 0.03 and roadway of 0.3, the number of elements $2.2 \times 10^6 - 2.6 \times 10^6$ divide the boundary condition into two classes. The numerical simulations were carried out in ANSYS CFX. The turbulence model is K- ϵ .

3.2 Mathematical model

Numerical fluid mechanics is a method of simulations of phenomena related to the flow of gases, heat, and mass transfer. This paper uses this method to determine the influence of the parameters (duct position, inlet temperature) on the temperature distribution in the working area. Conservation equations for mass, momentum, and energy are expressed as:

- The continuity equation

$$\frac{\partial p}{\partial t} + \frac{\partial(pu)}{\partial x} + \frac{\partial(pv)}{\partial y} + \frac{\partial(pw)}{\partial z} = 0 \tag{1}$$

where: u,v,w is direction velocity (m/s); p is density (kg/m³); t is time (s).

- The momentum equation

$$\frac{\partial}{\partial t}(pv) + \nabla \cdot (vv) = -\nabla p + \nabla \mathcal{T} + pg + F \tag{2}$$

where: p is static pressure (pa) \mathcal{T} is stress tensor (pa), gravitationnal body force (m/s²); F is external body force (N).

- The energy equation

$$\frac{\partial}{\partial t}(pE) + \nabla \cdot (\overline{v}(pE + v)) = \nabla(k_{eff}\nabla T) + S_h \tag{3}$$

where: E is energy (J), T is temperature (K); k_{eff} is effective thermal conductivity; S_h is source term.

3.3 Boundary conditions

The boundary conditions and computational model settings for this study are presented in Table 1.

Tab. 1. Model parameters.

Real parameter	Model parameters	Real parameter	Model parameters
inlet air duct	Inlet	Temperature of air duct	302.15K
Velocity of air duct	9 m/s	Temperature off-air road	302.15K
Outlet	Outlet	Temperature of rock	305.15K
		Wall roughness	2 cm

4. Numerical simulation

4.1 Check the fit of the model

Measurement data, through field measurement with the temperature measuring equipment of the mine model "Kestrel -300", the measurement position is length from the face (z = 1 m, 2 m, 4 m, 10 m, 15 m, 20 m, 25 m, 30 m, 35 m) measure many positions on the cross-section to get the average result. Table 2. shows the measurement data result.

Tab. 2. Measurement and simulation data results.

Distance to face (m)	Measurement data (°K)	Simulation data (°K)	errors (°K)
1	303.4	303.506	0.1
2	303.6	303.57	0.03
4	303.9	303.678	0.22
10	303.9	303.878	0.02
15	304	303.837	0.16
20	304.3	304.017	0.28
25	304.6	304.332	0.27
30	304.6	304.587	0.06
35	304.7	304.596	0.1

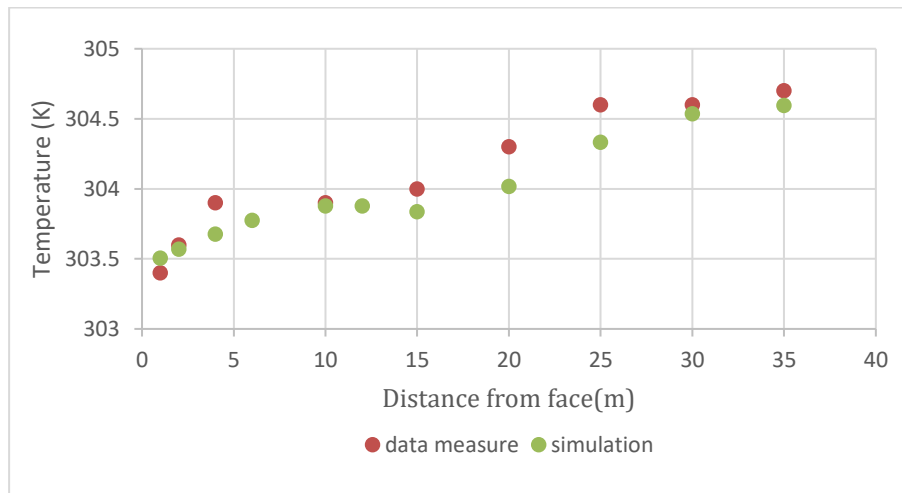


Fig. 2. Measurement and simulation results.

Figure 2 shows the numerical simulation results of the model ($y = 2.3$ m), and the field measurements show minor deviations, but they do not affect its accuracy. Therefore, the results of numerical simulations have a reference value.

4.2 Model with the variable position of the duct

From the software results, the article determines the average temperature of the cross-section on the roadway, then builds a graph with the average temperature value at the cross-sections with six models ($y = 1.1$ m; 1.7 m; 2.0 m; 2.3 m; 2.6 m; 3.1 m). The results are shown on the graphs corresponding to each model.

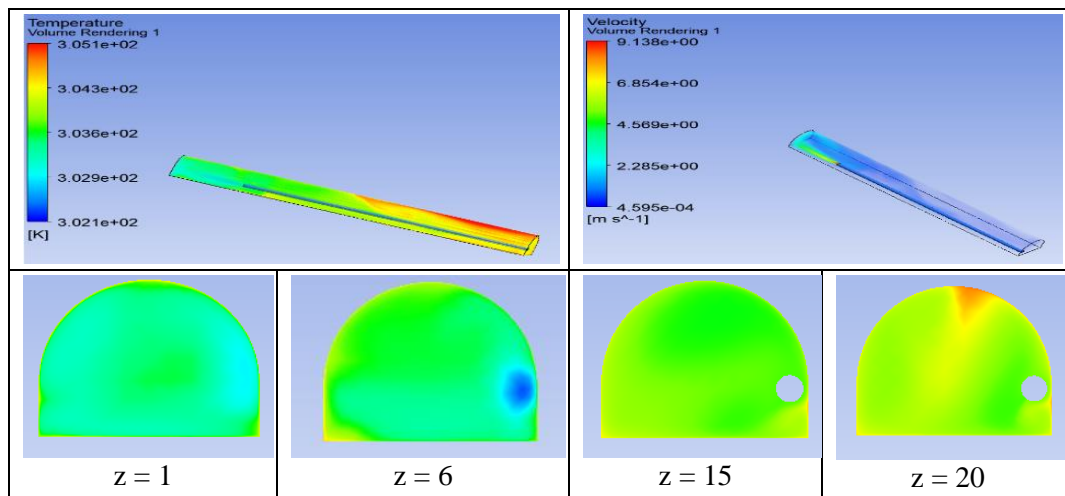


Fig. 3. Temperature distribution on the section and velocity on the road ($y = 1.1$ m).

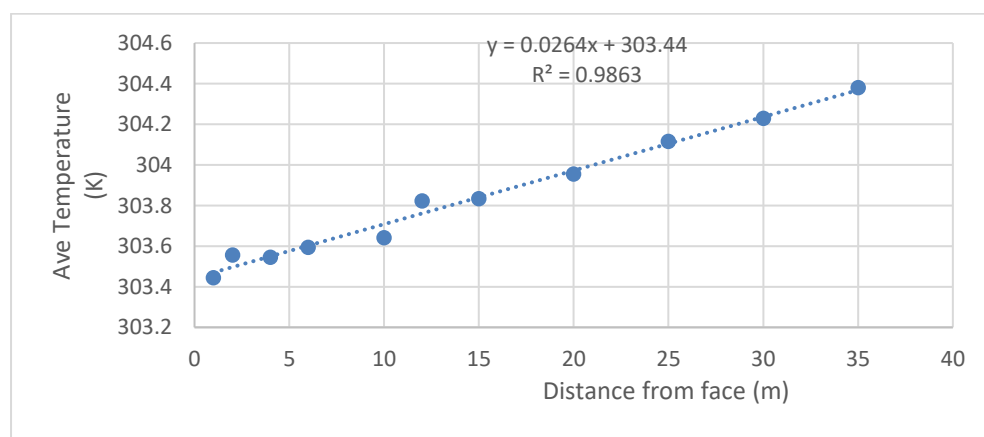


Fig. 4. Relationship between temperature and distance to face ($y = 1.1$ m).

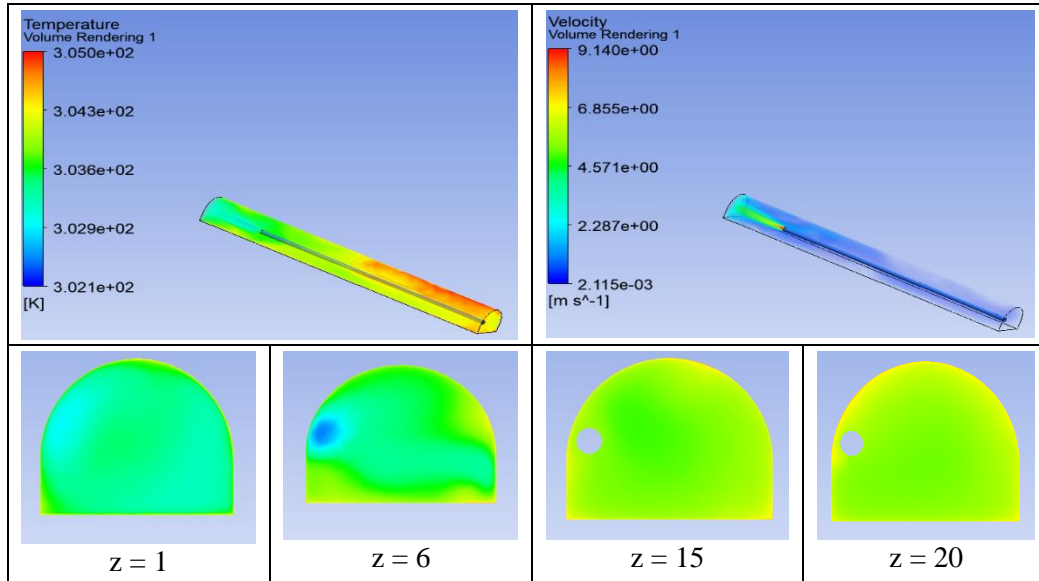


Fig. 5. Temperature distribution on the section and velocity on the road (y = 1.7 m).

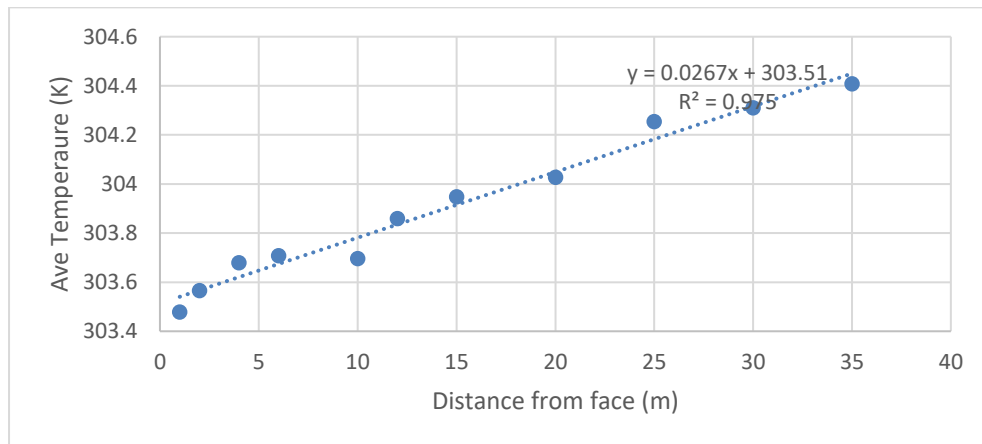


Fig. 6. Relationship between temperature and distance to face (y = 1.7 m).

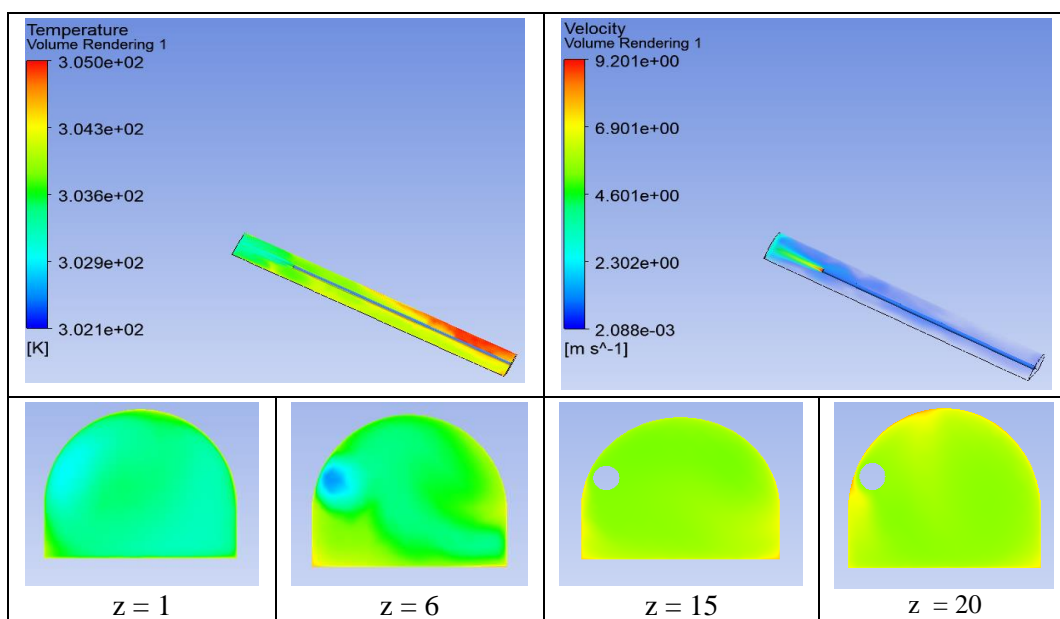


Fig. 7. Temperature distribution on section and velocity on the road (y = 2.0 m).

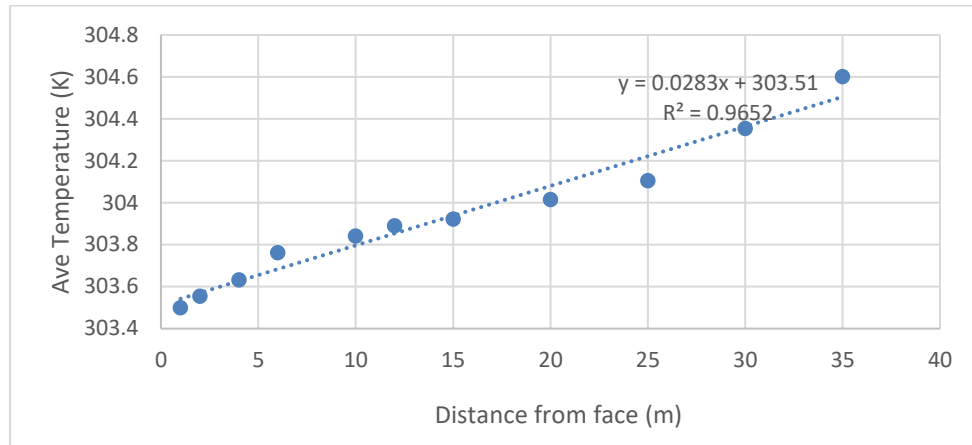


Fig. 8. Relationship between temperature and distance to face ($y = 2.0$ m).

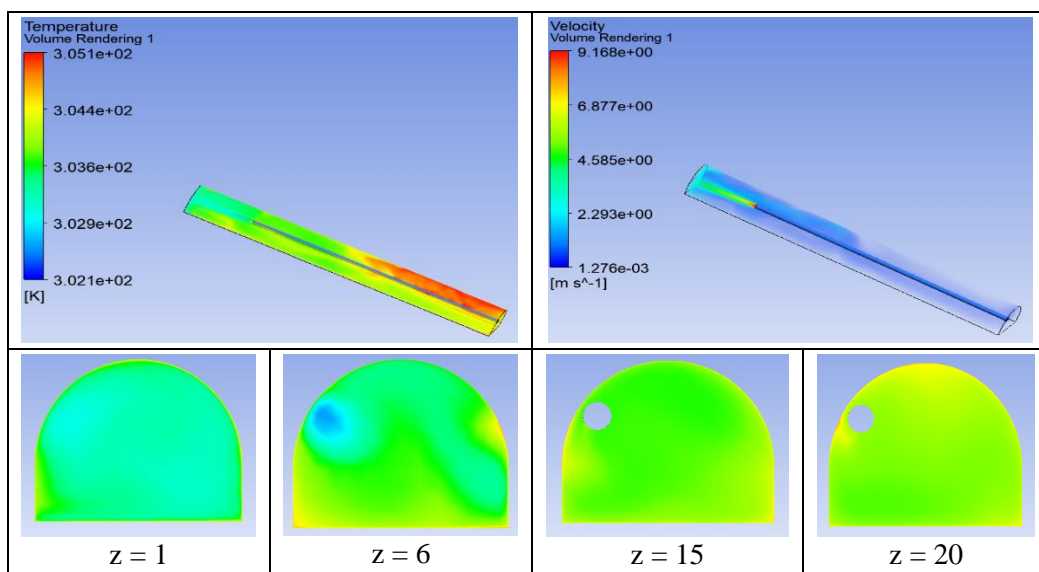


Fig. 9. Temperature distribution on cross-section of road ($y = 2.3$ m).

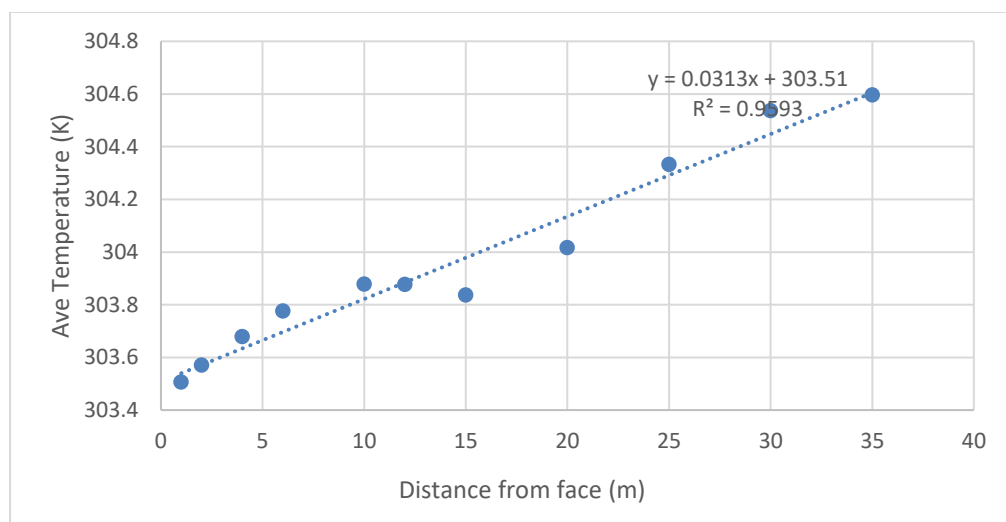


Fig. 10. Relationship between temperature and distance to face ($y = 2.3$ m).

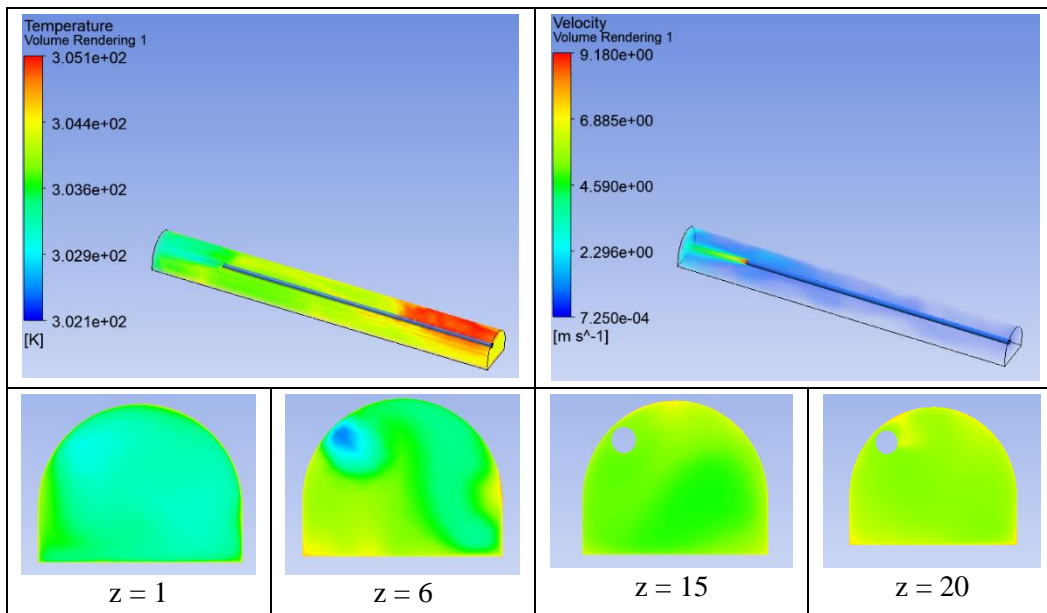


Fig. 11. Temperature distribution on cross-section of road ($y = 2.6$ m).

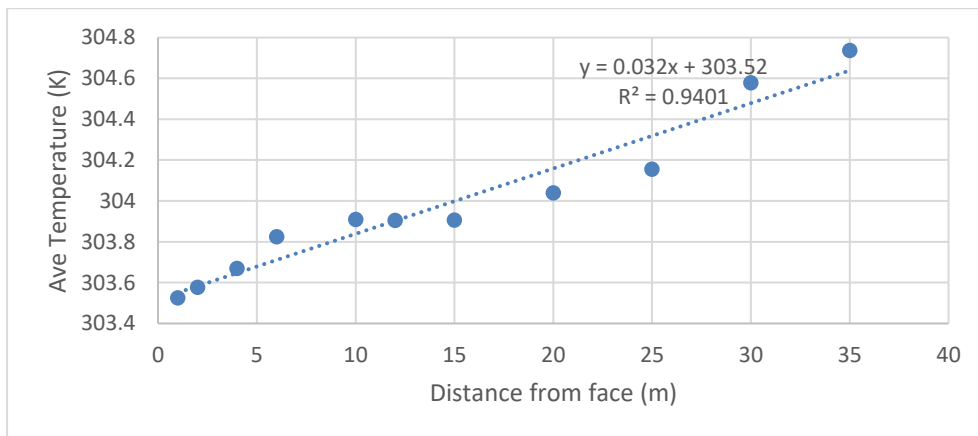


Fig.12. Relationship between temperature and distance to face ($y = 2.6$ m).

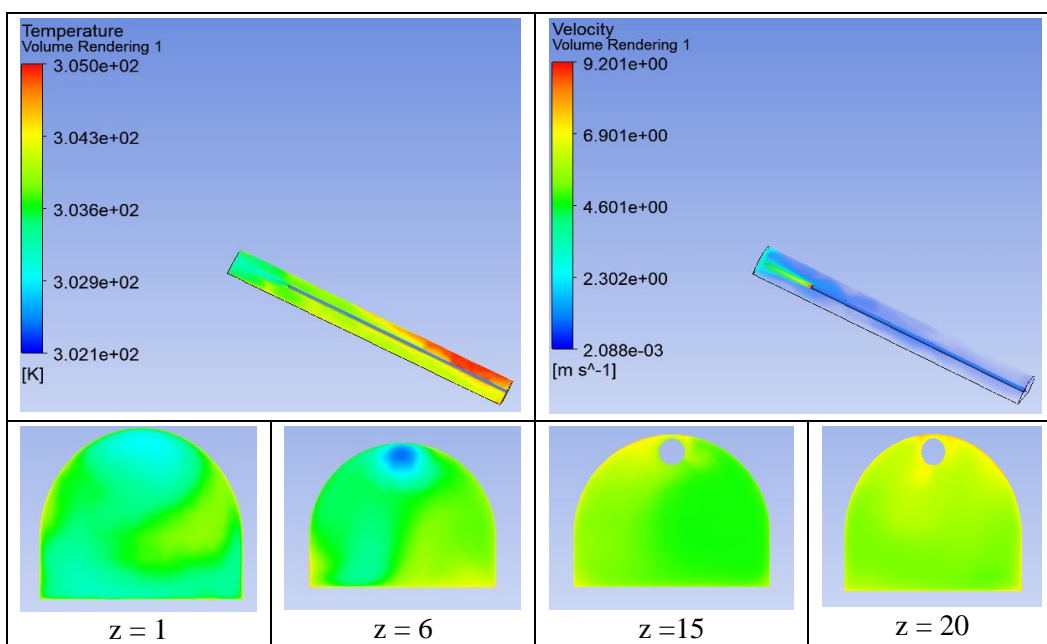


Fig. 13. Temperature distribution on cross-section of road ($y = 3.1$ m).

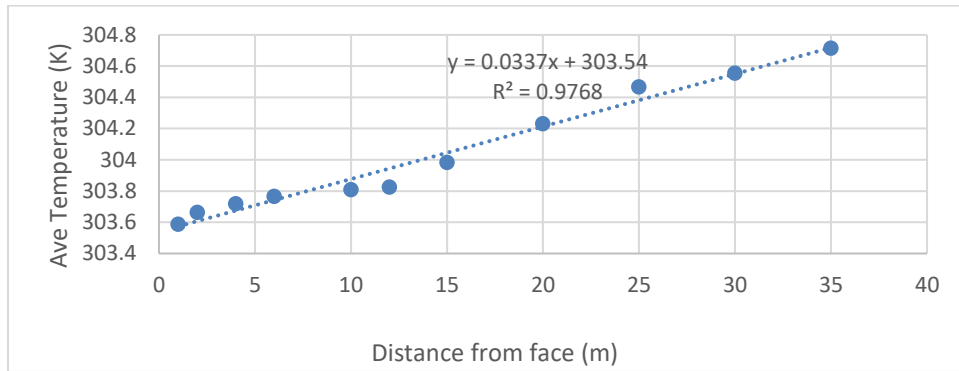


Fig. 14. Relationship between temperature and distance to face ($y = 3.1$ m).

4.3 Model with variable wind temperature in the air duct

For the heading road with a high-temperature environment and heat generation sources, the inlet wind temperature dramatically affects the thermal environment of the working area. Thus, the article built four models with temperature parameters.

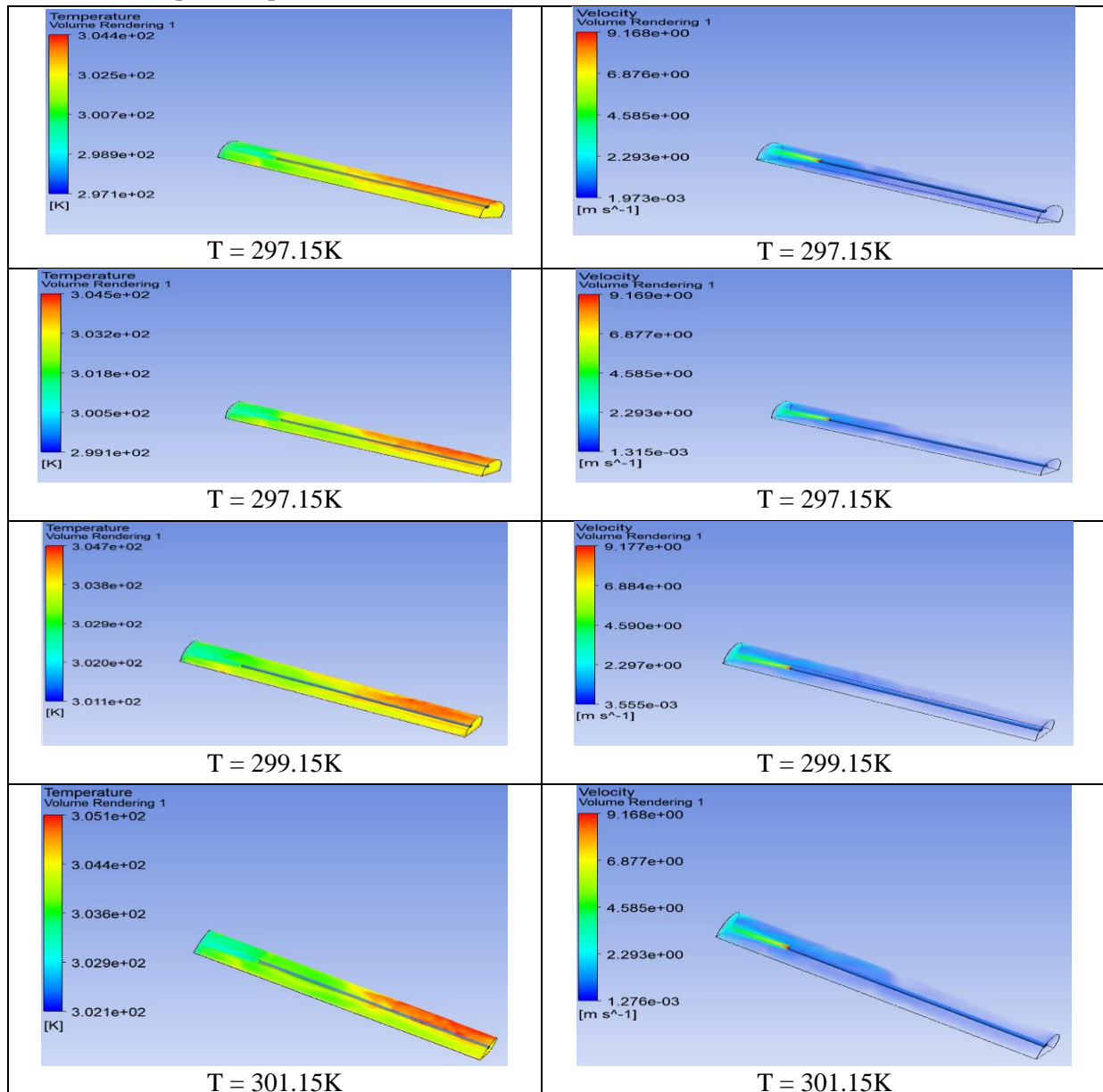


Fig. 15. Distribution of temperature and velocity fields with different wind temperatures.

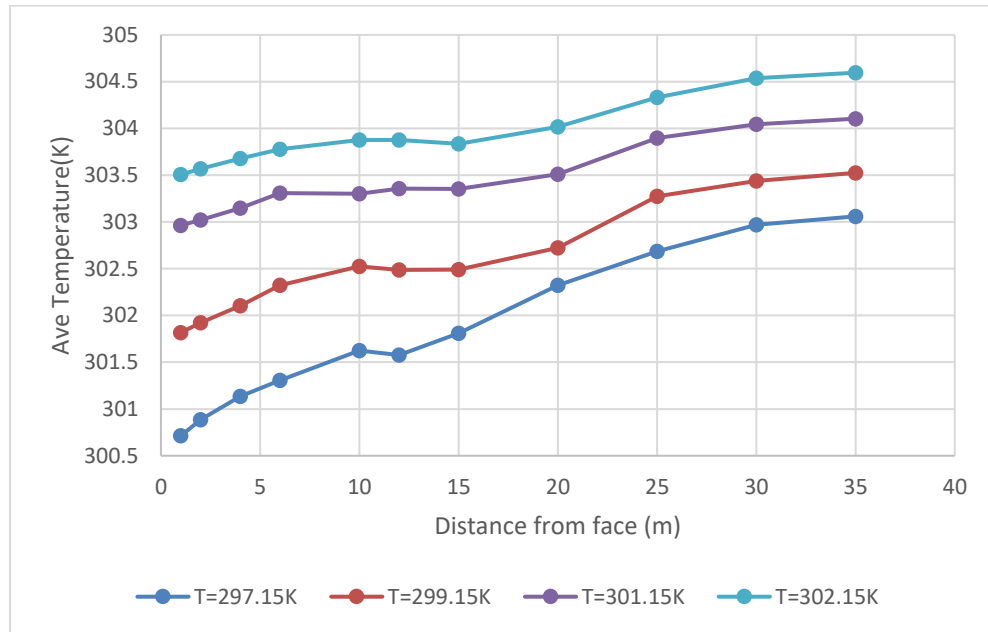


Fig. 16. Result of change of air temperature of road with inlet air temperature.

5. Results and discussions

Currently, with the increase in mining output leading to deeper mining levels, the volume of heading face serving production has also increased. The thermal environment tends to deteriorate when digging deep due to the geothermal's effect, which increases the air temperature at the heading face. This study evaluates and analyzes the influence of duct position and inlet temperature on air temperature in the heading face with a roughness of the roadway.

The simulation results of six models show that the temperature distribution on the cross-section was uneven and affects the comfort of the working environment. The air temperature near the wall is the highest because rock temperature and roughness increase the heat transfer time. As the distance from the mining face increased, the average temperature of the section increased almost linearly. The air temperature in front of the duct is lower than the behind, due to the influence of the duct's airflow. Therefore, the temperature in the roadway increases gradually due to the heat transfer of the surrounding rock and the airflow. Model 1 ($y = 1.1$ m) gives the most favorable temperature environment from 0-20 m in front of the face with average temperature $t_{tb} < 304$ K in which model 6 ($y = 3.1$ m) average temperature $t_{tb} < 304.2$ K is larger than other models. Fig. 4, 6, 8, 10, 12, and fig.14 shows that the thermal environment condition increases gradually from model 1 to model 6. With model 1, the temperature is distributed on the cross-sections more evenly than the remaining models. The environmental conditions in the working area are the best compared to the remaining positions.

The effect of inlet wind temperature on the thermal environment in the heading face is shown in Fig. 15,16. Model $T = 297.15$ K with a longer roadway are below 303K of 35 m. Model $T = 299.15$ K with a longer roadway are below 303K of 20 m. Model $T = 297.15$ K and $T = 299.15$ K with thermal environment was better than model $T = 301.15$ K and $T = 302.15$ K. Among them, the roadway air temperature of Model $T = 297.15$ K was the best. Besides, the other two models did not meet the standards ($T = 301.15$ K and $T = 302.15$ K). Model $T = 297.15$ K shows that the temperature value in the face area is the most comfortable from the measurement. Therefore, it has been found that the inlet air temperature is the biggest factor that affects mine temperature.

This study confirms the influence of geothermal, equipment, airflow, air temperature on the temperature field. However, this study shows the factors that affect the air temperature in the heading face, such as the duct's position and the inlet air temperature, and the roadway's roughness. Numerical modeling can represent the analysis of the temperature field with different conditions. The paper's findings provide a systematic understanding of the thermal environment, from which more effective thermal control strategies can be further developed.

6. Conclusions

This paper has studied six models of ventilation ducts on the heading face, four models with wind temperature, and analyzed the thermal environment of each model, combined with numerical simulation, to achieve a high-temperature environment more comfortable mining. Model 1 outperforms models 2 to 6 in terms of temperature distribution and lowest temperature values compared to the remaining models. Therefore, a layout like model 1 reduces costs when using the equipment cooler. From the model results of four models with different wind temperatures, we can see the significant influence of the inlet wind temperature on the thermal environment of the heading face. The results show that with the model $T = 297.15K$, the temperature value on the entire length of the roadway is guaranteed according to the regulations. As for model $T = 299.15K$, temperature conditions to ensure the standards only allowed within about 20 m from heading face. The rest of the models do not guarantee the standard requirements. Thus, creating a comfortable environment through ventilation is not enough. Therefore, with a high-temperature heading face, it is necessary to use cooling devices to reduce the temperature of the heading face to create a comfortable working environment for employees.

7. Acknowledgments

The paper was presented during the 6th VIET-POL International Conference Scientific-Research Cooperation between Vietnam and Poland, 10-14.11.2021, HUMG, Hanoi, Vietnam.

8. References

1. Agus, P.S., Jundika, C.K., Birgersson, E., Arun, S.M., 2015. Computational evaluation of thermal management strategies in an underground mine. *Appl. Therm. Eng.* 90: 1144-1150
2. Bao, T., Liu, Z., Meldrum, J., Green, C., Xue, P.F., Stan, V., 2018. Field tests and multiphysics analysis of a flooded shaft for geothermal applications with mine water. *Energy Conversion and Management*:169. <https://doi.org/10.1016/j.enconman.2018.05.065>
3. Zhao, Z.H., 2014. On the heat transfer coefficient between rock fracture walls and flowing fluid. *Computers and Geotechnics* 59:105-111. <https://doi.org/10.1016/j.compgeo.2014.03.002>
4. Chen, L., Li, J., Han, F., Zhang, Y., Liu, L., Zhang, B., 2019. Analysis of the thermal characteristics of surrounding rock in deep underground space. *Advances in Civil Engineering* 2019:1-9. <https://doi.org/10.1155/2019/2130943>
5. QUAN Truong Tien, Łuczak, R., Życzkowski, P., 2019. Climatic hazard assessment in selected underground hard coal mines in Vietnam. *Journal of the Polish Mineral Engineering Society*. <http://doi.org/10.29227/IM-2019-02-69>
6. Yang, X., Q. Han, J.P., Shi, X., Hou, D., Liu, C., 2011. Progress of heat-hazard treatment in deep mines, *Min. Sci. Technol. (China)* 21: 295-299.
7. Zhang, Y., Wan, Z.J., Gu, B., Zhou, C.B., Cheng, J.Y., 2017. Unsteady temperature field of surrounding rock mass in high geothermal roadway during mechanical ventilation. *J Cent South Univ* 24: 374-381. <https://doi.org/10.1007/s11771-017-3439-3>
8. Dao Van Chi, Le Van Thao, 2019. Research on solutions to prevent coal seam temperature rise in mechanized transport kilns area 7.3.1 zone I seam 7 Ha Lam coal mine. *Mining Industry Journal*. 4: 66-68 (in Vietnamese).
9. Nguyen Van Quang, Nguyen Van Thinh, Nguyen Cao Khai, Nguyen Thi Hong, 2020. Thermal control solution for underground coal mine in Quang Ninh. *Earth sciences and natural resources for sustainable development* (in Vietnamese).
10. Nguyen Cao Khai, Nguyen Van Thinh, Nguyen Phi Hung, Nguyen Van Quang, 2020. The current state of mine ventilation in Cao Thang area and future orientation. *Earth sciences and natural resources for sustainable development* (in Vietnamese).
11. Nguyen Cao Khai, 2020. Determine the operating mode of the main fan for Giap Khau coal mine, Hon Gai -TKV company, *Mining Industry Journal*, (in Vietnamese).
12. Dao, C.Van and Tran, H.Xuan 2020. Study on status and solution to improve the ventilation system of Quang Hanh coal mine (in Vietnamese). *Journal of Mining and Earth Sciences*. 61, 4 (Aug, 2020), 110-117. DOI:[https://doi.org/10.46326/JMES.2020.61\(4\).12](https://doi.org/10.46326/JMES.2020.61(4).12).
13. Dao, C.Van, Tran, H.Xuan and Le, D.Tien 2021. Determination of reasonable working mode for main fan stations during pilot operation of fan station VO - 22/14AR in Lo Tri area, Thong Nhat coal mine (in Vietnamese). *Journal of Mining and Earth Sciences*. 62, 4 (Aug, 2021), 15-20. DOI:[https://doi.org/10.46326/JMES.2021.62\(4\).02](https://doi.org/10.46326/JMES.2021.62(4).02).

Circular Economy Model and the Implementation in Vietnamese Coal Mining Industry

LE Dinh Chieu^{1,*}, DONG Thi Bich¹

¹ Hanoi University of Mining and Geology, 18 Vien street, Hanoi, Vietnam

Corresponding author: ledinhchieu@humg.edu.vn

Abstract. The circular economy is the economic model that has been applied for a long time in the world. This model is applied at all three levels: micro (enterprise-level), intermediate (industry level, industrial zone level), and macro-level (local level, regional level, or national level). Vietnamese Coal Mining Industry has been having important contributions to the socio-economic development of Vietnam. However, this industry also causes lots of issues about environmental pollution. In the context of resource depletion, environmental pollution and the cost of exploiting and processing increases with the deep exploiting process; the tastes of utilizing resources, minimizing environmental pollution, and creating more value-added for this industry are inevitable requirements. Because of the tasks, applying the circular economy model into this industry (both intermediate and micro-level) is the urgent solution for the sustainable development of the Vietnamese Coal Mining Industry. The paper uses a combination of research methods such as theoretical research, case study research, statistical data analysis, etc., to propose the circular economy model for the Vietnamese Coal Mining Industry and some solutions to deploy this model into the industry's operations towards sustainable development.

Keywords: Circular economy model, Vietnamese coal mining industry, Sustainable development

1. Introduction

In the context that the need of using natural resources is increasing to meet the need of humanity development. Along with the inadequacies of the linear economy such as resource waste and also the current state of resource depletion and environmental pollution, the circular economy model is being studied and applied widely in many developed countries in the world. In order for this model to maximize its effectiveness, it is necessary to apply synchronously at all three levels: the enterprise level, the industry level, and the local or national level. In Vietnam, the circular economy model has also begun to be researched and applied in some fields such as agriculture, industry, etc.

Vietnamese coal mining industry has formed and developed for hundreds of years. The industry has been being one of the key economic sectors of Vietnam. Besides the industry's achievements, such as providing mineral materials for other industries; exporting coal to receive foreign currency for the country, creating hundreds of thousands of jobs for the population, etc., the industry causes many negative impacts such as resource depletion and environmental degradation pollution. Especially in the current context that the coal mining industry is no longer the exclusive economic sector of Quang Ninh (The main coal mining area of Vietnam), the goals of sustainable development and harmony with other economic sectors, for example, tourism, services, etc., are being seriously considered by the Government and the Province. In that context, applying the circular economy model into the industry is the optimal solution to maximize using of mineral resources, reuse the unwanted output of the operation process to expand the value chain, and minimize the negative impact of this industry on the environment.

Meanwhile, there are not many studies about the circular economy model in the context of Vietnam and also Vietnamese coal mining industry. Therefore, it is necessary to establish a circular economy model suitable for the characteristics of the coal mining industry. It will create the basis for implementing solutions towards the sustainable development goals of the industry.

2. Theoretical basis of the circular economy model

2.1. The definition and roles of the circular economy

a) Definition

There are lots of different definitions of the circular economy. The circular economy describes an industrial economy that is designed to produce no waste or pollution [1]; the circular economy is a new economic model with huge economic potential in zero waste [2]; or the circular economy describes an economic system that based on business models that replace the concept of “end of life” by reducing,

reusing, recycling and recovering materials in manufacturing, distributing and consuming processes at the micro-level (products, companies, consumers), intermediate levels (eco-industrial parks) and macro levels (cities, regions, countries and furthermore) with the aim of sustainable development that based on ensuring environmental quality, economic prosperity, and social justice, serving the interests of both present and future generations [3].

Thus, it could be understood that the circular economy is an economy in which the undesired outputs (waste) of production processes are fully utilized. These undesired outputs will become inputs of the further production processes. So it could extend the value chain, and also reduce environmental pollution, towards sustainable development goals.

b) The roles of the circular economy

*) For businesses

This model helps businesses:

- Expanding the value chain by using unwanted outputs and recycling them as the inputs for further production processes.

- Reducing the cost by reusing some materials many times.

- Reducing economic losses and also negative impacts on workers' health that be caused by emission activities.

- It showed the social responsibility of companies. Thereby it is enhancing the reputation and competitive position of the companies.

*) For nations

- Using reasonably and efficiently resources, especially non-renewable ones.

Increasing more GDP/GNP by recycling or reusing unwanted outputs of companies in the economy creates more jobs for laborers.

- Reducing waste of manufacturing into the environment to reduce environmental pollution and also the consequences of them for the country.

In the context of resource depletion and environmental pollution, applying the circular economy model is an important measure to help the country achieve sustainable development goals.

2.2. The circular economy model

The circular economy model could be applied at all three levels: micro, intermediate and macro levels. However, in the paper, the authors present the application of the model to the Vietnamese coal mining industry. So the paper is mainly focused on the micro and intermediate levels. Therefore, the eco-industrial park model is a reference model to apply the circular economy model to this industry.

The eco-industrial park is a manufacturing and service-providing businesses community located in the same location. The companies that be the community members seek to improve economic, environmental, and social effectiveness through collaboration on the management of environmental and natural issues [4]. Businesses in the eco-industrial parks have industrial symbiosis. It means that there is a cooperation between businesses in an industrial park to optimize using of inputs and outputs such as raw materials, energy, water, waste, scrap, etc., in their operation process.

3. Research Methods

In this paper, the authors use some research methods:

3.1. Case study method

The method was used to research some specific cases to build the circular economy model that is suitable for the Vietnamese coal mining industry.

a) The case of using soil and rock waste from coal mining for leveling at sea encroachment projects in Quang Ninh, Vietnam

According to statistics, nowadays, Vinacomin manages about 1,210 million m³ of soil and rock waste; Dong Bac Corporation manages about 268.5 million m³ of soil and rock waste. The amount of soil and rock waste that is generated annually is about 150 million m³ [8]. Currently, soil and rock waste from the coal mining industry in Quang Ninh is being used for sea encroachment projects. From 2020 to 2025, the demand for soil and sand for leveling in Quang Ninh province is estimated at about 100 million m³/a years [8]. It will be a very potential market to consume the amount of soil and rock waste from coal mining.



Fig. 1. The dump of coal mining companies in Quang Ninh, Vietnam [8].



Fig. 2. Leveling activity for sea encroachment project at Phuong Dong urban area, Van Don - Quang Ninh [9].

Nowadays, soil and rock waste that from coal mining activities is causing very negative impacts on the environment, such as causing dust which greatly affects the residential areas around the mine. Therefore, using them for ground leveling in sea encroachment projects or traffic construction, etc., is a double-impact activity. It minimizes the negative impacts on the environment and also creates more value through being the input of the leveling operation.

b) The case of wastewater treatment at Viancomin - Vang Danh Coal Joint Stock Company

Coal mining activities generate a large amount of wastewater. The wastewater is acidic and also contains suspended solids, toxic heavy metals, etc. So it impacts so negatively on the environment. Faced with that situation, Vinacomin has built dozens of wastewater treatment stations, typically Vang Danh wastewater treatment stations. The station is designed with items such as the water route to the station, input monitoring chamber, reaction tank, settling tank, distribution tank, manganese filter tank, sludge condensate tank, and sludge press, etc. The station has a wattage of 3000 m³/h. All wastewater in Canh Ga and Vang Danh areas is collected and thoroughly treated at this station. Annually, the station treats about 10 million m³ of mine wastewater [10]. Mining wastewater after treatment is reused as domestic water for workers, and water sprayed to suppress dust, etc.

Thus, the treatment of mine wastewater helps reduce environmental pollution and also creates clean water to provide for the production and living of workers.

c) The case of methane treatment before, during, and after coal mining in some countries with developed coal mining industries in the world

According to estimates by the US Environmental Protection Agency (US EPA), the coal mining industry worldwide annually emits about 8-10% of total man-made methane. Thus, the emissions (including methane) from coal mining activities negatively impact the environment. Facing that situation, some countries with developed coal mining industries in the world, such as the USA, Australia, Russia, China, etc., have conducted methane recovery through drilling to remove methane before exploiting, during mining, and after the extraction process [7]. Thus, drilling to remove methane helps reduce the number of greenhouse gases released into the air and exploits large amounts of gas to provide input for the other production processes.

3.2. Statistical analysis methods

The methods were used to analyze the expected waste generated by the Vietnamese coal mining industry in the future.

a) Analysing the amount of soil and rock waste of coal mining activities

Tab. 1. The estimated amount of soil and rock waste from coal mining activities [5].

Areas	Total, 1000 m ³	Amount of soil and rock waste, 1000 m ³		
		2021÷2025	2026÷2030	After 2030
Uong Bi area	168,045	62,198	38,900	66,947
Hon Gai area	276,526	276,526	0	0
Cam Pha area	1,430,326	613,202	401,310	415,814
Other area	800,639	117,930	122,680	560,029
Total	2,675,536	1,069,856	562,890	1,042,790

Table 1 has shown that the amount of soil and rock waste from coal mining is very large. The waste of the Quang Ninh area (including Uong Bi, Hon Gai, Cam Pha) has a large proportion because it is still the main coal mining area in Vietnam. However, soil and rock waste tend to decrease over time in this area because open-pit coal mining is gradually shifting to underground mining. In the other areas, the amount of soil and rock waste has increased sharply because these mines are mainly small and are still exploited by open-pit mining technology.

In the future, the amount of soil and rock waste from coal mining is very large. So it is necessary to have treatment measures to both reuses the unwanted output and limit negative impacts on the environment.

b) Analysing the wastewater from coal mining operations

Tab. 2. The estimated amount of wastewater from coal mining in Vietnam [6].

Criteria	Unit	2021÷2025	2026÷2030
Amount of raw coal produced	Million tons/year	52.5	57.5
The average amount of mine wastewater	m ³ /ton	2	2
Amount mine wastewater	Million m ³ /year	105	115

Table 2 shows that the amount of wastewater is increasing with the increase of mining scale. This amount is also so large. Besides solid waste and wastewater, coal mining operations also emit many harmful gases such as CH₄, CO, SO_x, NO_x, etc. These wastes are required treatment not to cause environmental pollution. But it could also be a potential resource that could be used as an input for other economic activities.

4. The research results

From the above analysis, the authors propose the circular economy model that is suitable for the Vietnamese coal mining industry at both the industry level and the business level.

4.1. Industry-level model

Coal mining, processing, and trading activities in Vietnam are relatively concentrated and similar to industrial zones (in Quang Ninh, they are concentrated in three regions, including Uong Bi, Hon Gai, and Cam Pha). Based on the eco-industrial park model and the characteristics of the coal mining industry, the authors propose the circular economy model for the Vietnamese coal mining industry that is shown in Figure 3.

According to this model, the cooperation relationship between companies is shown that:

- Geological companies providing exploratory drilling services and methane recovery before, after, and also during the exploitation process;
- Environmental companies are providing wastewater and other waste treatment services to companies on coal mining, processing, trading, repairing, thermal power, etc.

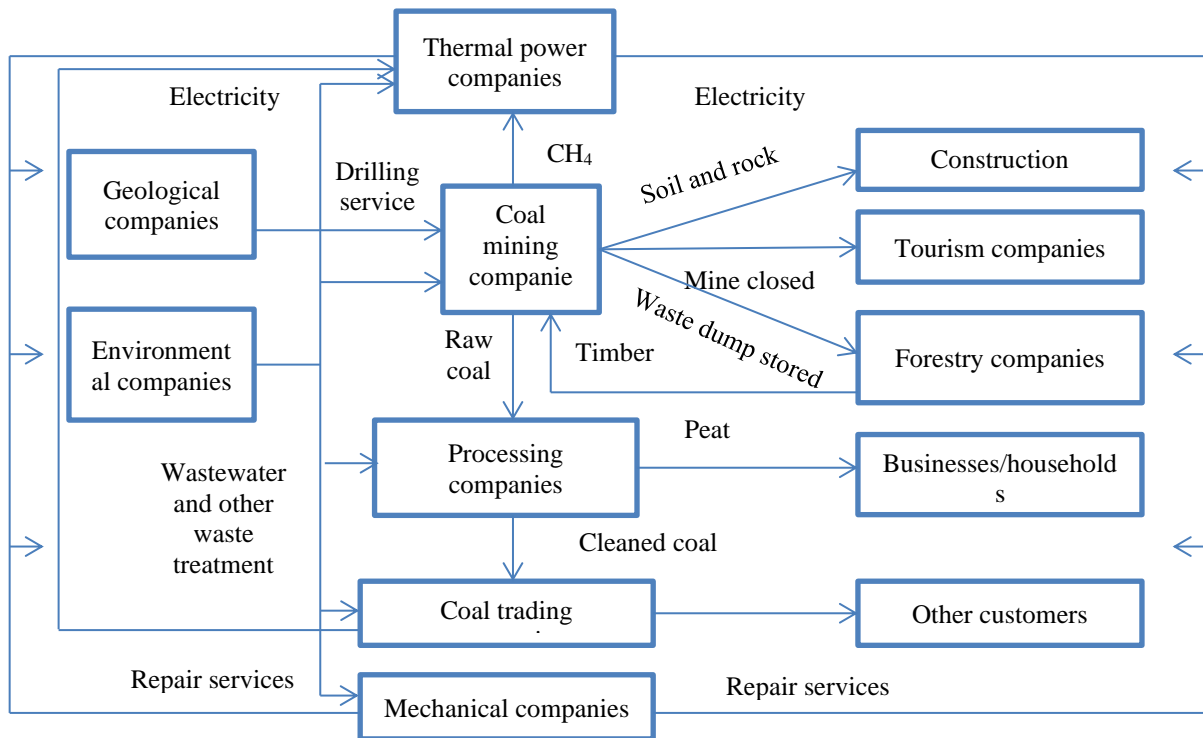


Fig. 3. The circular economy model applied to the Vietnamese coal mining industry.

- Coal mining companies supply raw coal to processing companies; provide soil and rock waste for construction companies (traffic works, ground leveling, sea encroachment, etc.); supply methane gas for thermal power companies. The restored waste dump could allow forestry companies to plant forests and buy timber from these companies for production. Mine after closing could be used for tourism.

- Processing companies supply cleaned coal for coal trading companies; provide peat (be salvaged of processing) to businesses/households.

- Mechanical companies provide repair services, restoration, and upgrading the production capacity of the equipment to other companies; thermal power companies supply electricity to other companies.

4.2. Enterprise-level model (for coal mining companies)

At the enterprise level (for coal mining companies), the authors propose the circular economy model shown in Figure 4.

According to this model, the recovered materials after each operation process and other unwanted outputs will be processed to continue for the future production cycle.

- For materials recovered after each operation process, companies will evaluate, repair, and restore to continue putting into future production; or reuse the parts and details of them as spare parts.

- The soil and rock waste will be used as ground leveling materials (for sea encroachment projects, traffic works, etc.). The rest is sent to the waste dump.

- The wastewater is treated to ensure standards of domestic water for workers and production water for dust suppression, road watering, watering plants, etc.

- The methane gas is recovered for electricity production.

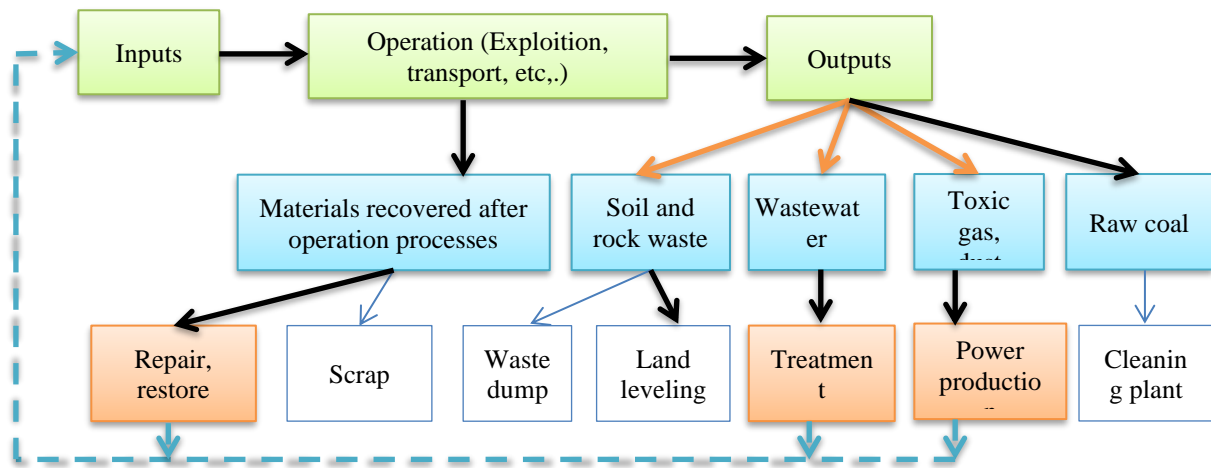


Fig. 4. The circular economy model is applied to coal mining companies.

Currently, some activities in the models (including industry-level model and enterprise-level model) have been performed at the companies in the industry. Such as using soil and rock waste for leveling, planting trees on waste dumps, etc.; some ideas have also started to be mentioned, such as using mines after closure for tourism; or reusing materials in the companies. However, these activities are carried out individually, without a systematic approach. The models in the paper systematized and closely linked the activities of the closed system. It helps to clearly define the outputs of each stage and visualize the recirculation of unwanted ones to minimize waste to the environment. This model also helps managers to establish development strategies for the industry towards sustainable development.

Besides Vietnamese coal mining industry is implemented by Vinacomin and Dong Bac Corporation (concentrated in Quang Ninh Province) and some small mines in other provinces. The models could be fully applied to the companies in Quang Ninh province (organized into concentrated industrial zones in the mining areas). For small mining areas in other provinces, depending on specific conditions, reduced models could be built from the models. For the future mining areas (Coal mining areas in the Red River Delta), the models could be used for master planning towards sustainable development.

5. Some solutions

Applying the circular economy model helps to use the unwanted outputs of production processes to create more value for businesses and society. It minimizes environmental pollution by reducing emissions into the environment. The paper suggests some solutions to able to apply the model to the Vietnamese coal mining industry.

- The Government needs to have the policy and orientation for developing the circular economy model and also has strict sanctions for using resources wastefully or causing environmental pollution.
- Companies must research or transfer modern technology from developed countries to apply in operations. This could be considered the most important solution because it is necessary to have modern technology to reproduce the unwanted outputs.
- The Government and also companies need to promote propaganda and education to raise the awareness of using natural resources reasonably and protecting the environment among people, businesses, and employees.
- Using waste for recycling could have low economic efficiency. However, it is effective in environmental protection and sustainable development. Therefore, the Government must apply at high levels the natural resource taxes and environmental protection taxes to get the budget and subsidizes for recycling waste.

6. Conclusions

The paper has synthesized the theory of the circular economy and the circular economy model; study some typical cases in the reuse of unwanted outputs of operations; and also analyzes some forecasting data on solid waste and wastewater of coal mining, processing, and trading activities in Vietnam in the

future. Based on those analyses, the paper proposes the Vietnamese coal mining industry's circular economy model (including industry level and business level). However, the paper mainly builds the management model. It is essential to research more specifically about technical-technology issues to apply the model to the industry effectively.

7. Acknowledgements

Paper was presented during the 6th VIET - POL International Conference Scientific-Research Cooperation between Vietnam and Poland, 10-14.11.2021, HUMG, Hanoi, Vietnam.

8. References

1. Littleboy, A., Cooksey, M., McGregor, K., 2016. The circular economy and its implications for natural resource supply and demand, UN Centre for Regional Development, seventh regional 3rd forum in Asia and the Pacific, 2-4 November, 2016, Adelaide, Sa, Australia.
2. Ellen MacArthur Foundation, Towards the circular economy: Economic and business rationale for an accelerated transition, 2013.
3. Kinnunen, P., 2019. Towards circular economy in the mining industry: implications of institutions on the drivers and barriers for tailings valorization. M.Sc Thesis, Tampere University, Finland.
4. Lowe, E., 1997. Eco-Industrial Parks: a handbook, Asian Development Bank, Manila, Philippines.
5. Vietnamese Government, Decision 403/2016/QĐ-TTg on master planning for developing the coal mining industry to 2030, Vietnam, 2016 (in Vietnamese).
6. Vinacomin Industry Investment Consulting JSC, Project on developing Vietnamese coal market in association with coal production and business following the market mechanism and ensuring national energy security, Hanoi, Vietnam, 2018 (in Vietnamese).
7. Website <http://congnghiepmoitruong.vn/giai-phap-kiem-soat-phat-thai-khi-me-tan-trong-nganh-cong-nghiep-khai-thac-than-ham-lo-o-viet-nam-5564.html>, 24/02/2020.
8. Website <https://nhandan.vn/vi-moi-truong-xanh/su-dung-dat-da-thai-mo-de-san-lap-cac-du-an--628552/>, 18/12/2020.
9. Website <https://nongnghiep.vn/chu-dau-tu-khu-do-thi-phuong-dong-co-y-tot-nhung-voi-vang-d284702.html>, 25/02/2021.
10. Website <http://www.vinacomin.vn/tin-tuc-vinacomin/xu-ly-nuoc-thai-mo-bao-ve-moi-truong-va-tai-su-dung-hieu-qua-201709201700344942.htm>, 20/09/2017.

Monitoring Vegetation Cover Changes by Sentinel-1 Radar Images Using Random Forest Classification Method

TRAN Van Anh^{1,*}, LE Thi Le², NGUYEN Nhu Hung³, LE Thanh Nghi¹, TRAN Hong Hanh¹

¹ Hanoi University of Mining and Geology, 18 Vien street, Hanoi, Vietnam

² Thu Dau Mot University, Binh Duong, Vietnam

³ Military of Technical Academy, 236 Hoang Quoc Viet, Hanoi, Vietnam

Corresponding author: tranvananh@hmg.edu.vn

Abstract. Vietnam is an Asian country with hot and humid tropical climate throughout the year. Forests account for more than 40% of the total land area and have a very rich and diverse vegetation. Monitoring the changes in the vegetation cover is obviously important yet challenging, considering such large varying areas and climatic conditions. A traditional remote sensing technique to monitor the vegetation cover involves the use of optical satellite images. However, in presence of the cloud cover, the analyses done using optical satellite image are not reliable. In such a scenario, radar images are a useful alternative due to the ability of radar pulses in penetrating through the clouds, regardless of day or night. In this study, we have used multi temporal C band satellite images to monitor vegetation cover changes for an area in Dau Tieng and Ben Cat districts of Binh Duong province, Mekong Delta, Vietnam. With a collection of 46 images between March 2015 and February 2017, the changes of five land cover types including vegetation loss and replanting in 2017 were analyzed by selecting two cases, using 9 images in the dry season of 3 years 2015, 2016 and 2017 and using all of 46 images to conduct Random Forest classifier with 100, 200, 300 and 500 trees respectively. The result in which the model with nine images and 300 trees gave the best accuracy with an overall accuracy of 98.4% and a Kappa of 0.97. The results demonstrated that using VH polarization, Sentinel-1 gives quite a good accuracy for vegetation cover change. Therefore, Sentinel-1 can also be used to generate reliable land cover maps suitable for different applications.

Keywords: Vegetation cover change, Sentinel-1, Random Forest, Binh Duong, Vietnam

1. Introduction

Over the past decade, Vietnam has seen a considerable transformation in the land use/ land cover due to multitude of reasons involving growing population, economy, urbanization and industrialization among others. Of all the land covers, vegetation cover is an important and a cyclical cover that is dependent on almost all the natural and anthropogenic parameters including the seasons, temperature and other climatic conditions. Kongtis [1] depicts that due to the population growth, the agriculture lands are getting reduced in Vietnam. Schaefer and Thinh (2019) [2] have mentioned a decrease in the agriculture land by 6% between 2000 and 2010, and an increase in residential area by 7% has been reported by Downes et al. (2016) [3]. Such a decrease in agriculture and overall vegetation cover may also trigger many disasters including floods[4], and urban heat waves [5]. Thus, detection of vegetation cover is necessary so as to understand and analyze the inter-relationships between the humans and their ecosystem[6] and for other national infrastructure planning and management applications[7].

The detection of changes in the vegetation cover are generally studied for larger areas and the results are required in considerably smaller amount of time. Therefore, remote sensing data is an effective tool to assist this task. Previously, only the optical satellite imageries were used to determine the change in land covers, mainly due to the free-availability of the imageries in the public domain. However, over the past one-two decades, researchers have addressed the limitations of the optical imageries in the change detection studies [8]. These include the limited results in case of cloud cover [9], but can be alleviated by image compositing [10]. Also, in optical image analysis, different species of trees or crops may be indistinguishable due to similar spectral reflectance. In addition, the optical imagery cannot penetrate the forest canopy and can sense only the topmost layer, thus affects the overall analysis. Therefore, radar remote sensing is now in vogue for many applications including land and forest cover classification [11]; [12], deforestation mapping [12], classification of agricultural areas [13], monitoring specific crops [14] etc. The radar remote sensing is free from the limitations of optical remote sensing but have its own limitations. Those limitations can be eliminated using several developed algorithms [14] [15]. Therefore, in this study, we have used Sentinel-1 imagery for our change detection analysis, primarily because of 1) the cloud cover over Vietnam due to the tropical climate and 2) free-availability of this imagery dataset.

The characteristics of land cover classification studies using radar satellite images (e.g. [16], [17], [18]) are to use multi-temporal and dual-polarized radar images to increase the accuracy of land cover change monitoring. For studies related to surface cover changes such as urban growth monitoring, forest monitoring and disaster management, images used to determine the changes are often ground-range images and are multi-polarization [19]. In the theory of change detection, the image classification or statistical analysis methods is one of the most important step. [20] used the Kullback-Leibler divergence while [21] used an unsupervised classification method of Hidden Markov Chain (HMC) to solve the angle difference when using single look complex images. [22] combined mean ratio and log ratio images and used wavelet networks method to determine the surface cover change in the time series, [23] used distance measurement and segmentation of images with the minimum error method for determining the change of objects on the multi-temporal and multi-polarization radar images.[24] used the Deep neural network method to identify changed and unchanged areas on multi-temporal SAR satellite images.

In general, the methods mentioned above have advantages and disadvantages when determining changes by using multi-temporal SAR images. In this study, we used a machine learning-based method, the Random Forest (RF), to classify the changes and unchanged vegetation in the images. Because our study area in Binh Duong province of Vietnam where has many types of perennial plants and forests, therefore RF method combined with statistical analysis on images between periods to detect the changes is quite appropriate. In addition, the problem of choosing parameters such as the number of trees for the RF model has not been analyzed in the published studies, so this study is an opportunity for us to evaluate the optimization of these parameters for RF model.

2. Study areas and data

2.1 Study area

The study area is two districts of Dau Tieng and Ben Cat located in the northwest of Binh Duong province. It borders on districts of Binh Phuoc province to the north, Thu Dau Mot city to the south, Trang Bang district to the southwest, and Duong Minh Chau district to the northwest, both of Tay Ninh province and to the southeast by Cu Chi district of Ho Chi Minh City. This area features many rubber plantations, fruit trees and also many changes in rubber planting areas within three years from 2015 to 2017.

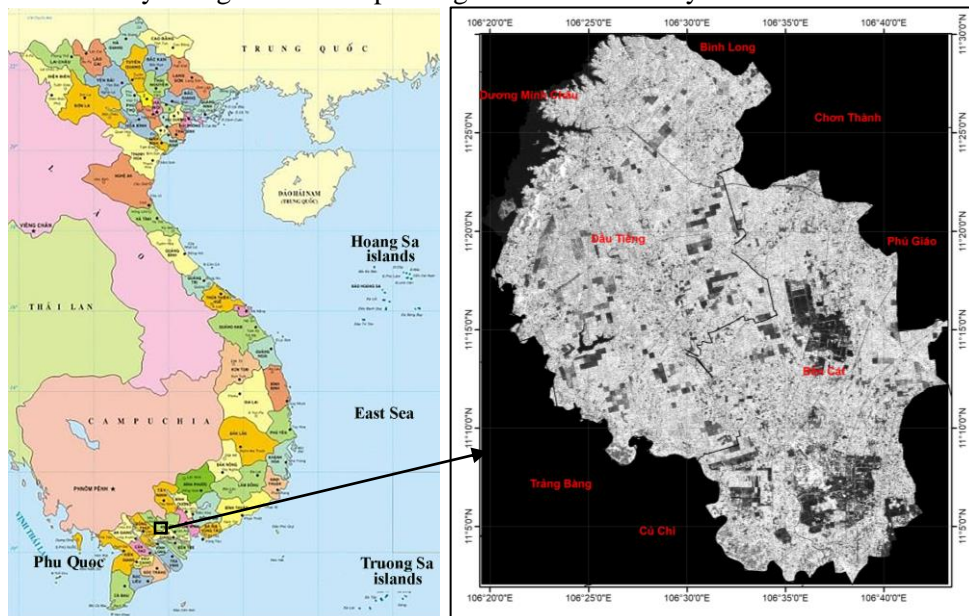


Fig. 1. The location of the study area and Sentinel-1 image acquired on March 23, 2015 was cut the boundary of Dau Tieng and Ben Cat districts, Binh Duong province.

2.2 Data used

The research material is Sentinel-1 satellite image, C band with a period of 12 days. This is a good data to assess the seasonal variation of land cover objects. Sentinel-1 data used is Level-1 ground range detected images (GRD), 10m resolution, dual polarization (VV and VH). The images were carried out with pre-processing steps on SNAP toolbox software includes calibration to compute sigma nought values; terrain correction; convert to dB value; noise filtering on multi-temporal images.

Sentinel -1A images are presented in Table 1, including 46 images from March 2015 to February 2017. The series of images was selected to see the change of backscatter of each type of vegetation in each plant's growth stage, thereby determining the type of short term crops or industrial crops and the change due to logging or replanting.

The study area has two seasons: dry season and rainy season. The rainy season starts from May to the end of November every year and the dry season starts from December to the end of April. According to the set of Sentinel-1 images used, there is about one image every 24 days. Because the objective of the study is a vegetation change, we focus on the dry season dates to see the difference of the plant objects from 2015 to 2017. Figure 2 is a color composite of 3 images in 3 dates: 2015-03-23, 2016-03-05 and 2017-02-04 with VH polarization. The reason for choosing the color combination of the VH is because VH polarization is mainly sensitive to volume scattering [25], but the study area is a large area of fruit trees and rubber trees, thus choosing VH for determining the vegetation change of this region is suitable.

Tab. 1. Sentinel -1A image set.

ID	Y-M-D	ID	Y-M-D	ID	Y-M-D	ID	Y-M-D	ID	Y-M-D
1	2015-03-23	11	2015-11-06	21	2016-03-05	31	2016-07-15	41	2016-12-06
2	2015-04-16	12	2015-11-18	22	2016-03-17	32	2016-07-27	42	2016-12-18
3	2015-05-10	13	2015-11-30	23	2016-03-29	33	2016-08-20	43	2016-12-30
4	2015-06-27	14	2015-12-12	24	2016-04-10	34	2016-09-01	44	2017-01-11
5	2015-07-21	15	2015-12-24	25	2016-04-22	35	2016-09-13	45	2017-01-23
6	2015-08-14	16	2016-01-05	26	2016-05-04	36	2016-09-25	46	2017-02-04
7	2015-09-07	17	2016-01-17	27	2016-05-16	37	2016-10-07		
8	2015-10-01	18	2016-01-29	28	2016-05-28	38	2016-10-19		
9	2015-10-13	19	2016-02-10	29	2016-06-09	39	2016-10-31		
10	2015-10-25	20	2016-02-22	30	2016-07-03	40	2016-11-12		

3. Methodology and processing

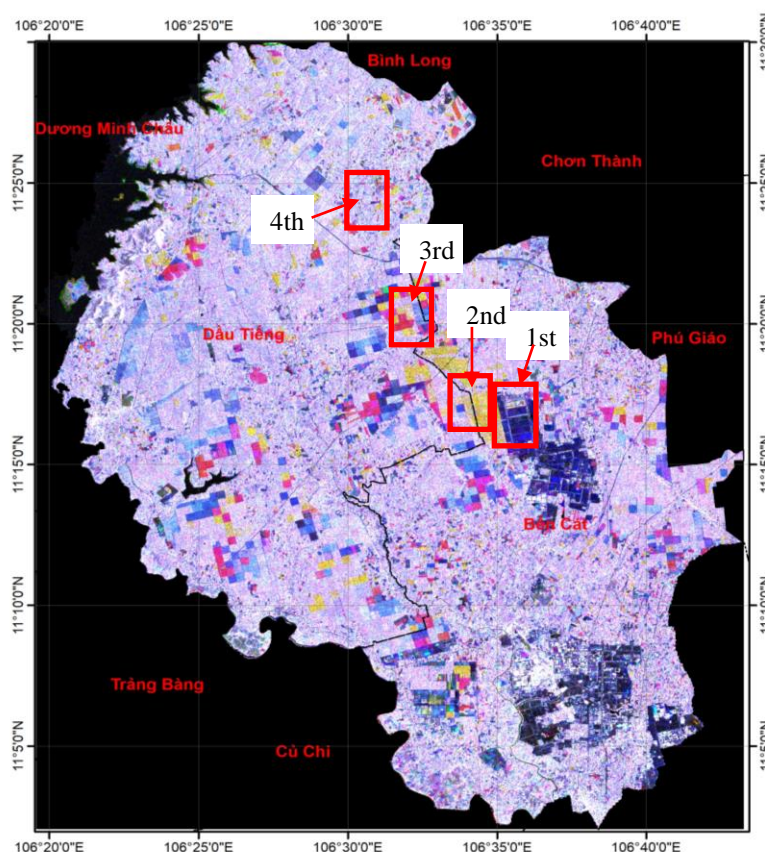


Fig. 2. RGB color composite image of Sentinel-1A VH polarization.

3.1 Characterization of land covers on multi-temporal SAR images

Analysis of multi-temporal SAR images of the study area (from March 2015 to February 2017), the land cover can be divided into two main groups: (i) the changed vegetation and (ii) The unchanged land cover (Fig. 2). The most vegetation changes mainly include perennial crop land that is rubber tree or other fruit trees. The unchanged land covers are usually residential areas or rubber lands. Fig. 2 shows the RGB color composite image of Sentinel-1 of three observation periods, March 2015, March 2016 and February 2017 with VH polarization. Different colors in the composite image are corresponding to the change of different types of land covers. The white or black colors in the RGB image are displayed as correspondingly unchanged objects because of the stability of the surface scattering in time series images. On the other hand, the different colors in the RGB image show the objects changed because of the different backscattering values of each pixel over time. To see the difference, the backscatter of some positions as blue, magenta, yellow, white and black color have been extracted through which help us can recognize the changes of the backscatter in three years through those charts.

In the blue areas, backscatter varied in the range of -12dB to -20 dB between March 2015 and July 2016, then scattering increased quite strongly indicating that within two years from 2015 to 2016, vegetation cover was available in this area, but then the vegetation in that area were clear-cut, so the scattering value increased (Fig. 3).

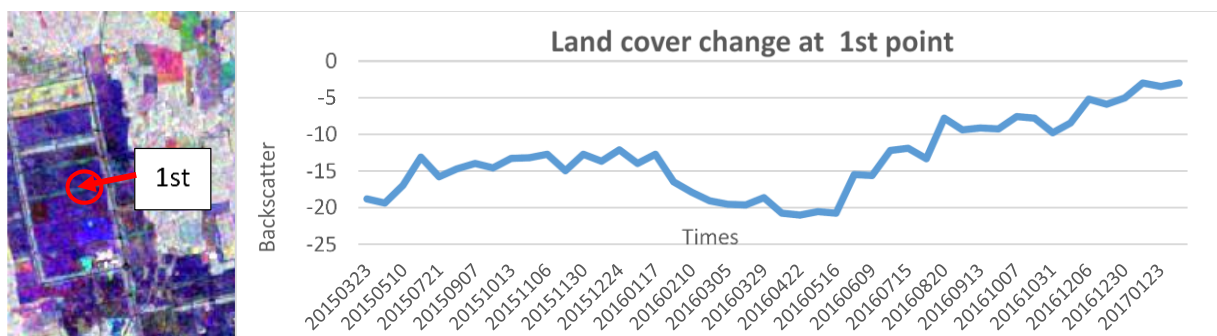


Fig. 3. Backscatter chart of the location of vegetation clear-cut in 2017.

At locations with light yellow color, the scattering value was high during the period from March 2015 to June 2016. This is possible that the previous period had no vegetation cover at this location but the later time was planted (Fig. 4).

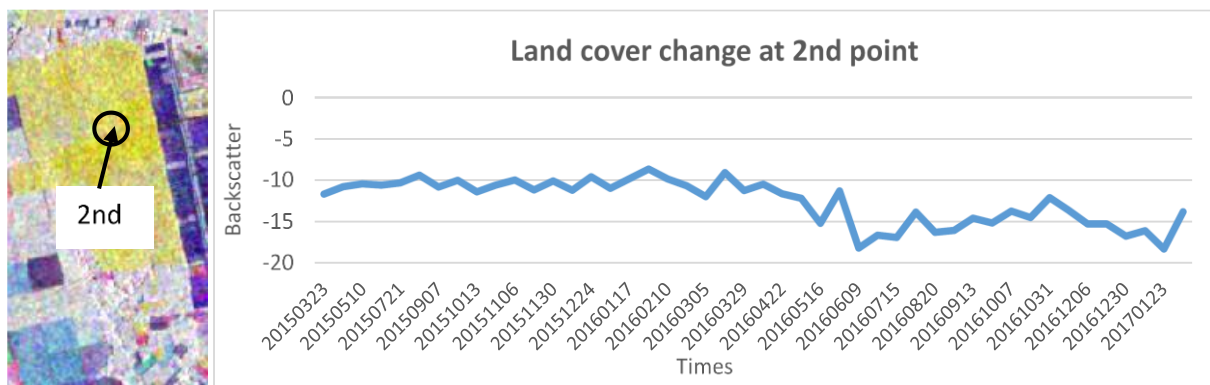


Fig. 4. Backscatter chart of replanting sites in 2017.

At the magenta locations, the scattering value decreased from December 2015 to June 2016. The vegetation here may be seasonal because the period before December 2015 and after June 2016 vegetation does not exist here.

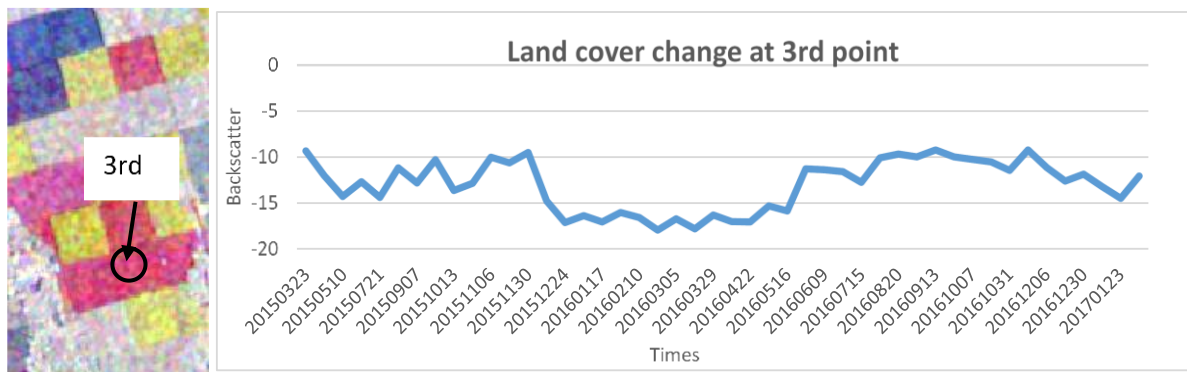


Fig. 5. Backscatter chart of seasonal crops.

At the fourth site, the backscattered signals almost varied in a narrow range from -11 dB to -7 dB showing the unchanged land cover in the area.

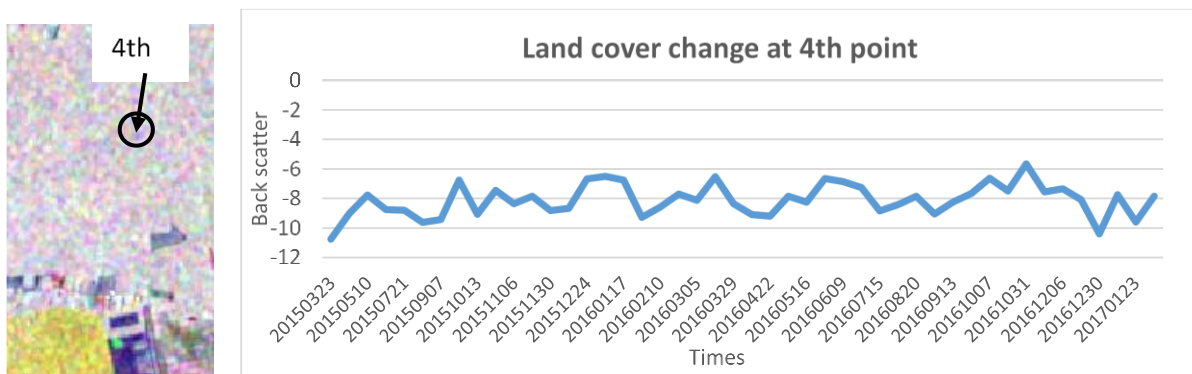


Fig. 6. Backscatter chart of unchanged land cover.

3.2 Research method

Through analysis of land cover changes on Sentinel-1 multi temporal images, the Random Forest (RF) method was selected for monitoring the vegetation change of the Dau Tieng, Binh Duong area (Fig. 4).

Overview of Random Forest method:

RF was proposed by Breiman in 2001 [26]. This is a supervised classifier based on decision trees and improved bagging and bootstrapping techniques. Bootstrapping is a very famous statistic method, was introduced by Efron in 1979 [27].

The Random Forest (RF) is an algorithm comprising of many single decision trees. Each tree is created from randomly selected training pixels (bootstrap). The two parameters that need to be defined in this classification algorithm are the number of trees to grow (ntree) and the number of variables to split at each node (mtry). The ntree selected depend on the shortest processing time to achieve the lowest error, ntree runs from 1 to 500 trees as default and mtry ranges from the minimum number of independent variables (equal to 1) to the maximum number of independent variables that used in the classifier.

After the Random Forest model is created, each result of the bootstraps in the set will vote for the most popular class and give a classification result. The model is formed based on the most voted classifier of each decision tree diagram [26] (Fig. 7).

Random Forest steps

- Step 1: From training data set D, random data are generated (bootstrap sample).
- Step 2: Using randomly sampled data subsets D1 , D2 , ..., Dk build trees T1 , T2 , ..., Tk. A decision tree consists of internal (or split) nodes and terminal (or leaf) nodes.
- Step 3: Combine the trees: Use the majority voting strategy for the classification.

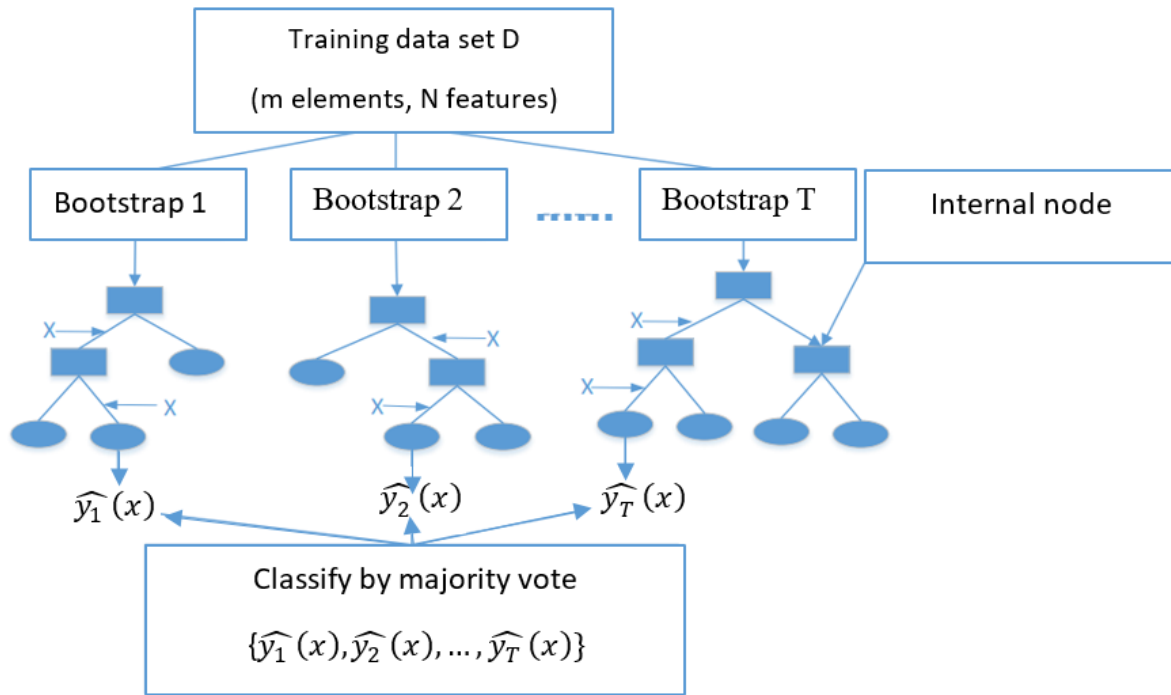


Fig. 7. Diagram of RF formation.

4. Results and discussion

4.1 Experimental procedure

- Pre-processing

The processing was conducted using SNAP and QGIS softwares as follow the processing flow chart in Figure 8. The Sentinel-1 images with GRD mode were calibrated, filtered by Multi-Temporal Speckle Filtering with 3x3 kernel and terrain corrected before application. The 30m SRTM data has been used for this purpose and the data was resampled to a pixel size of 20m ground resolution. The digital numbers values (DN) of SAR data were transformed into backscattering values in decibel (dB).

- Classification for change detection

Random Forest (RF) classification method has been carried out for mapping land cover changes. As a machine learning algorithm, RF has been widely applied and experimented with many times in optical images for land cover mapping. However, with the use of this RF method in terms of classifying vegetated cover changes by Radar images, not many scientists have done it yet.

Regarding the study area after analysing the differences in vegetation cover in the period from 2015 to 2017 above, we recognized some types of changes:

- Vegetation clear cut in 2017, mainly rubber trees. These areas are shown in a dark blue color image on RGB composite image and the backscatter chart at the first point (Fig. 3), corresponding to box number one in Figure 2.

- Vegetation replanting 2017 where the yellow color on RGB composite image, and the backscatter chart at the second point (Fig. 4) and inside the number two box in Figure 2.

- Another type of change is vegetation cover existed in 2016 and clear cut in 2015, 2017 where the magenta color was shown on RGB composite image, corresponding to the backscatter chart at third point in Figure 5. This type of vegetation is usually short-term agricultural crops.

- The unchanged objects will be grey color composite image and backscatter chart at the fourth point (Fig. 6)

- With water surface, the backscatters are very low and constant all the time and there is a black color in the color composite image.

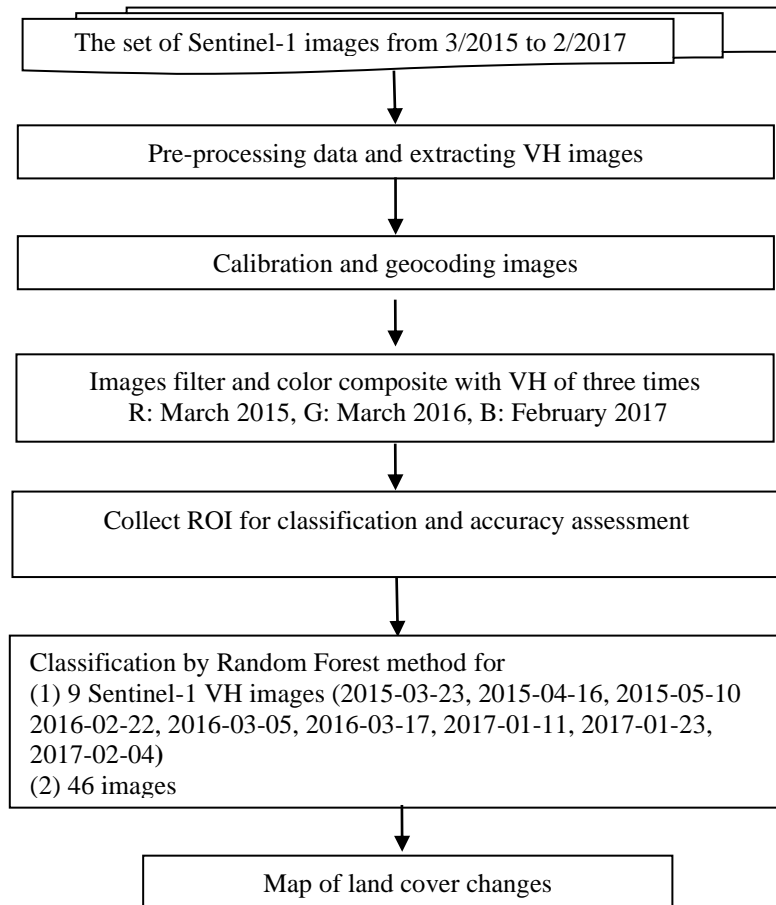


Fig. 8. Sentinel-1 VH image processing flow chart for land cover change detection.

Sentinel-1 VH color composite	Google Earth image 2017	Name of samples
		Clear cut 2017
		New planting 2017
		Seasonal crops
		Water
		No changes

Fig. 9. Samples selection base on the color composite and Google Earth images. (The unchanged areas can be whatever object exists during the 3 years of the survey, so it's does not have a feature pattern on the google image).

According to the flow chart, with 46 Sentinel-1 VH images in the period from March 2015 to February

2017, we processed two cases for RF classification, these are (1) 9 images, and (2) 46 images.

Case (1): Nine images were selected to be classified by RF method all fall in the dry seasons of 2015, 2016, and 2017, which is the period when vegetation changes are the best. Based on the above analysis, five land cover and vegetation change classes were selected to classify as clear cut in 2017, new planting in 2017, cropland, unchanged land, surface water. Then rely on different sources such as Google Earth history, color composite images of the three times mentioned above, training data were collected. Fig. 9 shows the selection of the samples on image composite and Google Earth history. A total of 3121 pixels were collected for sampling of which 925 pixels were used to validate the classification. The accuracy of the result is based on the overall accuracy (OA) and Kappa. The input data for classification is the training data set (N) which are 9 independent variables (denoted as B) in this case the 9 Sentinel-1 satellite images selected above. For each node of the tree, randomly select mtry as the division basis at that node. The default value of mtry=sqrt(B), in this study mtry=3.

Case (2): In the second case, forty-six images were used. Also, with the five classes used for classification mentioned above and the number of training samples is 3121, of which 925 pixels are used for validation. For a large number of images, the number of independent variables here will be chosen as 46 (B=46) and the number of nodes (mtree) is sqrt(46) which is approximately 7.

Each prediction (land cover type or vegetation changes) is made from each decision tree, it is labelled (labelled here is 1 of the 5 selected cover types above) for the end node of the classification scheme. The process will be performed through all the trees (ntree) and the land cover with the most votes of this classification scheme will represent that tree diagram participating in the combined results of the Random Forest model. In this study, the number of trees of 100, 200, 300, 500 we selected in turn and see the change in the error of each change.

4.2 Discussion

With the selected RF classification method and four times of selecting with different number of trees (ntree), the accuracy evaluation results including overall accuracy (AO) and Kappa for two sets of 9 images and 46 images on an independent sample set are 925 pixels mentioned above. Table 2 was obtained.

Tab. 2. Accuracy of two data sets in selection of different number of trees.

Number of images	Accuracy	100 trees	200 trees	300 trees	500 trees
9 images in dry seasons of 2015, 2016, 2017	OA	96.2%	97.1%	98.4%	98.4%
	Kapa	0.95	0.96	0.97	0.97
46 images in the period 2015-2017	OA	93.1%	93.2%	94.2%	94.2%
	Kapa	0.90	0.91	0.92	0.92

Table 2 shows that the OA of the RF classifier for both sets of images has high accuracy of over 94% and the difference between the results is not very large. However, as the number of ntree increases, the OA also increases. In the case of using 46 images, the accuracy is lower than the case of using 9 images, this can be explained because when too many independent variables are equivalent to the number of images, the information of the images does not differ much, so this leads to information redundancy and results in more errors in the RF model. In addition, when the number of trees increased to 300 and 500, the model gave the highest accuracy (98.4%) with a set of 9 images or 94.2% for a set of 46 images, this can be explained as the greater number of trees, the more stable the model, but the processing time will also be longer. However, the number of trees only needs to reach a certain limit, the accuracy does not change, so when the number of trees is up to 300, the AO is equivalent to the AO of setting 500 trees. Overall, the RF model with 300 trees in both sets of images is optimal for classification because the accuracy is similar to the 500 trees model while the processing time is lower. So, in this study, we decided to choose the model with the number of trees is 300, the set of images is 9 images.

With this option, the evaluation according to User’s accuracy (UA) and Producer’s accuracy (PA) also shows the reliability of the selected parameters, the results show these criteria of each layer is greater than 90% (Tab. 3). This shows that it is a promising method for classifying vegetation cover and its changes. The results also show the potential when using RF with 300 trees and 3 nodes to classify Sentinel-1 satellite image series into 5 types of vegetation cover and land cover changes, including 2017 clear cut, 2017 new planting, and seasonal crops, water surface and unchanged gave an accuracy of AO: 98.4%. The vegetation change monitoring experiment results for Dau Tieng and Ben Cat districts, Binh Duong province, from nine Sentinel-1 VH images with RF classification are shown in Figure 10.

Tab. 3. Accuracy of RF classification for a set of 9 images with 300 trees.

Accuracy			Confusion matrix					
Classes	UA (%)	PA (%)		Clear cut 2017	New planting 2017	Seasonal crops	No changes	Water
Clear cut 2017	98.7	97.5	Clear cut 2017	80	0	2	0	0
Replanting 2017	90.6	100	Replanting 2017	0	87	0	0	0
Seasonal crops	96.8	98.3	Seasonal crops	0	0	61	1	0
No changes	99.5	95.6	No changes	1	9	0	219	0
Water	100	100	Water	0	0	0	0	465
Over all accuracy: 98.4% and Kappa: 0.97								

Looking at the results, it is easy to recognize the areas of vegetation cover change are primarily new planting in 2017 which were shown in green. Besides, there were also some places that have removed vegetation in 2017 where magenta color. The areas of vegetation clear cut are mainly concentrated in Lai Uyen, Lai Hung and Thoi Hoa communes, Ben Cat district. With the data reported from the provincial committee, the new planting areas are mostly rubber trees. Those rubber tree regions are mainly distributed in An Lap, Long Tan, Long Hoa communes, Dau Tieng district. There have been 32.5 hectares of rubber trees newly planted under the Government's initiative. The tree planting campaign has been implemented since the beginning of 2016 so after planting when the trees are not high enough, the backscatter value is not high on the image until 2017 and this value is high and easily recognizable.

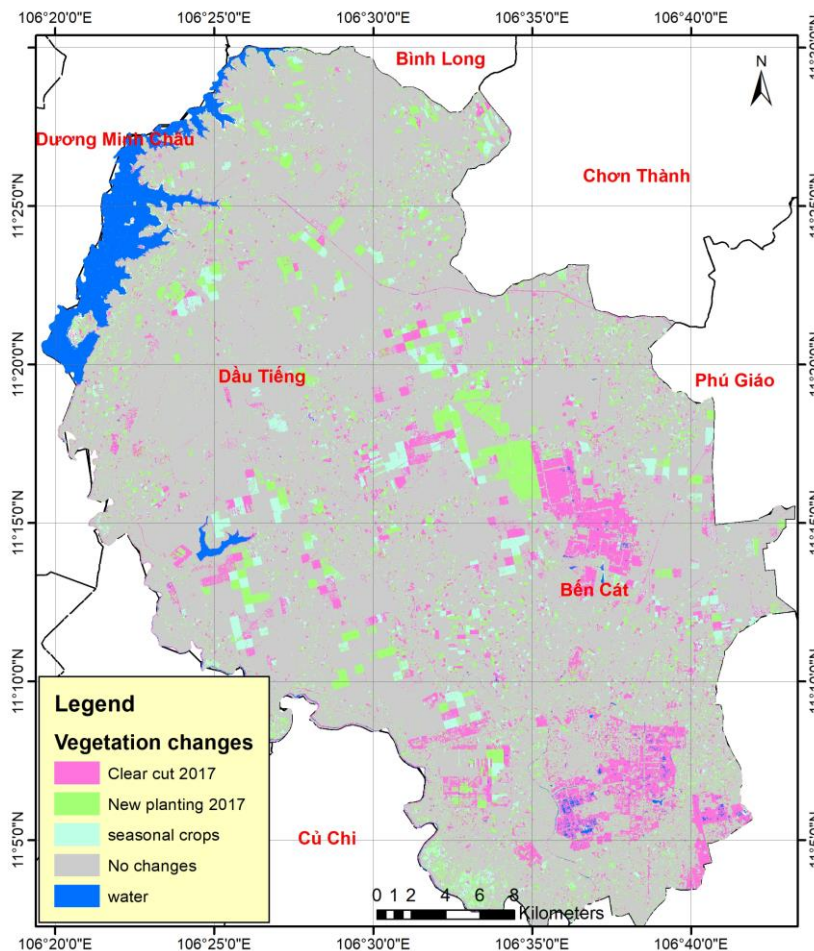


Fig.10. Land cover change monitoring at Dau Tieng and Ben Cat, Binh Duong province.

The areas cover with vegetation in 2016 are often short-term crops because the land was abandoned in

2015 and 2017. The areas under seasonal crops are shown by the cyan and are widely distributed in the communes of Long Tan, Long Nguyen, Thanh An, Dinh An, Dau Tieng district. In general, vegetation changes in Dau Tieng and Ben Cat Binh Duong areas are related to rubber tree because rubber trees are planted in rows and have quite square parcels. The areas of stable or little change are residential land or rubber trees or perennial fruit crops.

5. Conclusions

Through the analysis and testing of the Random Forest classification method, the changed and unchanged vegetation cover in Dau Tieng and Ben Cat, Binh Duong, Vietnam have been identified from Sentinel-1 polarized VH image data. The Sentinel-1 GRD image with a resolution of 10m is quite suitable for determining the land cover as well as the change of vegetation cover in tropical areas with cloud cover. In addition, this type of image is updated regularly and free download, so monitoring the changes of objects such as land cover and especially plants is very good.

The application of RF algorithm with combining images at different times of Sentinel-1 VH images is very important to evaluate the change of vegetation cover. When the number of images is large, the redundant information will slow down the processing speed and the accuracy will be worse than choosing a suitable number of images with large information differences. With a set of 9 images in the dry season of 3 years 2015, 2016 and 2017 and the number of trees of the RF model is 300, the accuracy of determining vegetation changes is the highest and achieving an OA accuracy of 98.4%.

This method offers promising results with free software and free images to be widely applicable at a low cost compared to most applications that used commercial images and software.

6. Acknowledgment

We would like to thank CESBIO, CNES, Toulouse, France provided Sentinel-1 images and some documents to process these results.

The paper was presented during the 6th VIET - POL International Conference on Scientific-Research Cooperation between Vietnam and Poland, 10-14.11.2021, HUMG, Hanoi, Vietnam.

7. References

1. Kontgis, C., Schneider, A., Fox, J., Saksena, S., Spencer, J.H., Castrence, M., 2014. Monitoring peri-urbanization in the greater Ho Chi Minh City metropolitan area. *Applied Geography*. 53: 377-388, <https://doi.org/10.1016/j.apgeog.2014.06.029>.
2. Schaefer, M., Think, N.X., 2019. Evaluation of land cover change and agricultural protection sites: A GIS and Remote Sensing approach for Ho Chi Minh city, Vietnam. *Heliyon*, 5(5): e01773, <https://doi.org/10.1016/j.heliyon.2019.e01773>.
3. Downes, N.K., Storch, H., Schmidt, M., Van Nguyen, T.C., Tran, T.N., 2016. Understanding Ho Chi Minh City's urban structures for urban land-use monitoring and risk-adapted land-use planning, in *Sustainable Ho Chi Minh City: Climate Policies for Emerging Mega Cities*, Springer. 89-116, https://doi.org/10.1007/978-3-319-04615-0_6.
4. Storch, H., Downes, N.K., 2011. A scenario-based approach to assess Ho Chi Minh City's urban development strategies against the impact of climate change. *Cities*. 28(6): 517-526, <https://doi.org/10.1016/j.cities.2011.07.002>.
5. Son, N.T., Chen, C.F., Chen, C.R., Thanh, B.X., Vuong, T.H., 2017. Assessment of urbanization and urban heat islands in Ho Chi Minh City, Vietnam using Landsat data. *Sustainable cities and society*. 30: 150-161, <https://doi.org/10.1016/j.scs.2017.01.009>.
6. Aly, A.A., Al-Omran A.M., Sallam A.S., Al-Wabel M.I., 2016. Vegetation cover change detection and assessment in arid environment using multi-temporal remote sensing images and ecosystem management approach. *Solid Earth*. 7(2): 713-725, <https://doi.org/10.5194/se-7-713-2016>.
7. Tran, H.Hong, Tran, A.Van and Le, N.Thanh., 2020. Study on land use changes, causes and impacts by remote sensing, GIS and Delphi methods in the coastal area of Ca Mau province in 30 years (in Vietnamese). *Journal of Mining and Earth Sciences*. 61, 4 (Aug, 2020), 36-45. DOI:[https://doi.org/10.46326/JMES.2020.61\(4\).04](https://doi.org/10.46326/JMES.2020.61(4).04).
8. Tran, A.Van, Nguyen, B.An, Dinh, T., Nguyen, Y.Hai Thi and Le, N.Thanh., 2020. Landslides detection in Bat Xat district, Lao Cai province, Vietnam using the Alos PalSAR time-series imagery by the SBAS method (in Vietnamese). *Journal of Mining and Earth Sciences*. 61, 4 (Aug, 2020), 1-10. DOI:[https://doi.org/10.46326/JMES.2020.61\(4\).01](https://doi.org/10.46326/JMES.2020.61(4).01).

9. Asner, G.P., 2001. Cloud cover in Landsat observations of the Brazilian Amazon. *International Journal of Remote Sensing*, 22(18): 3855-3862, <https://doi.org/10.1080/01431160010006926>.
10. Sannier, C., McRoberts, R.E., Fichet, L.V., Makaga, E.M.K., 2014. Using the regression estimator with Landsat data to estimate proportion forest cover and net proportion deforestation in Gabon. *Remote Sensing of Environment*, 151: 138-148, <https://doi.org/10.1016/j.rse.2013.09.015>.
11. Simard, M., Saatchi, S.S., De Grandi, G., 2000. The use of decision tree and multiscale texture for classification of JERS-1 SAR data over tropical forest. *IEEE Transactions on Geoscience and Remote Sensing*, 38(5): 2310-2321, DOI: 10.1109/36.868888.
12. Engdahl, M.E., Hyypä, J.M., 2003. Land-cover classification using multitemporal ERS-1/2 InSAR data. *IEEE Transactions on Geoscience and Remote Sensing*, 41(7): 1620-1628, DOI: 10.1109/TGRS.2003.813271.
13. Bargiel, D., Herrmann, S., 2011. Multi-temporal land-cover classification of agricultural areas in two European regions with high resolution spotlight TerraSAR-X data. *Remote sensing*, 3(5): 859-877, <https://doi.org/10.3390/rs3050859>.
14. Bouvet, A., Le Toan, T., 2011. Use of ENVISAT/ASAR wide-swath data for timely rice fields mapping in the Mekong River Delta. *Remote Sensing of Environment*, 115(4): 1090-1101, <https://doi.org/10.1016/j.rse.2010.12.014>.
15. Braun, A., Hochschild V., 2017. Potential and limitations of radar remote sensing for humanitarian operations. in *GI Forum*, DOI: 10.1553/giscience2017_01_s228.
16. Ajadi, O.A., Meyer, F.J., Webley, P.W., 2016. Change detection in synthetic aperture radar images using a multiscale-driven approach. *Remote Sensing*, 8(6): 482, <https://doi.org/10.3390/rs8060482>.
17. Longépé, N., et al., Assessment of ALOS PALSAR 50 m orthorectified FBD data for regional land cover classification by support vector machines. *IEEE Transactions on Geoscience and Remote Sensing*, 2011. 49(6): 2135-2150, DOI: 10.1109/TGRS.2010.2102041.
18. Niu, X., Ban, Y., 2013. Multi-temporal RADARSAT-2 polarimetric SAR data for urban land-cover classification using an object-based support vector machine and a rule-based approach. *International journal of remote sensing*, 34(1): 1-26, <https://doi.org/10.1080/01431161.2012.700133>.
19. Balzter, H., Cole, B., Thiel, C., Schmullius, C., 2015. Mapping CORINE land cover from Sentinel-1A SAR and SRTM digital elevation model data using random forests. *Remote Sensing*, 7(11): 14876-14898. <https://doi.org/10.3390/rs71114876>.
20. Ghanbari, M., Akbari, V., 2018. Unsupervised change detection in polarimetric SAR data with the Hotelling-Lawley trace statistic and minimum-error thresholding. *IEEE Journal of Selected Topics in Applied Earth Observations and Remote Sensing*, 11(12): 4551-4562, DOI: 10.1109/JSTARS.2018.2882412.
21. Inglada, J., Mercier, G., 2007. A new statistical similarity measure for change detection in multitemporal SAR images and its extension to multiscale change analysis. *IEEE transactions on geoscience and remote sensing*, 45(5): 1432-1445, DOI: 10.1109/TGRS.2007.893568.
22. Bouyahia, Z., Youssef, L.B., Derrode, S., 2008. Change detection in synthetic aperture radar images with a sliding hidden Markov chain model. *Journal of Applied Remote Sensing*, 2(1): 023526, <https://doi.org/10.1117/1.2957968>.
23. Gong, M., Cao, Y., Wu, Q., 2011. A neighborhood-based ratio approach for change detection in SAR images. *IEEE Geoscience and Remote Sensing Letters*, 9(2): 307-311, DOI: 10.1109/LGRS.2011.2167211.
24. Liu, M., Zhang, H., Wang, C., Shan, Z., 2012. Urban change detection for high-resolution fully polarimetric SAR using a modified heterogeneous clutter model. in *EUSAR 2012; 9th European Conference on Synthetic Aperture Radar*. VDE.
23. Gong, M., Zhao, J., Liu, J., Miao, Q., Jiao, L., 2015. Change detection in synthetic aperture radar images based on deep neural networks. *IEEE transactions on neural networks and learning systems*, 27(1): 125-138, DOI: 10.1109/TNNLS.2015.2435783
25. Nicolau, A.P., Flores-Anderson, A., Griffin, R., Herndon, K., & Meyer, F. J., 2021. Assessing SAR C-band data to effectively distinguish modified land uses in a heavily disturbed Amazon forest. *International Journal of Applied Earth Observation and Geoinformation*, 94: 102214, <https://doi.org/10.1016/j.jag.2020.102214>
26. Breiman, L., Random forests. *Machine learning*, 2001. 45(1): 5-32.
27. Efron, B., Bootstrap methods: another look at the jackknife. *The Annals of Statistics*, 7(1): 1-26. URL <http://www.jstor.org/stable/2958830>, 1979.

Doing Business in Vietnam from the Perspectives of Polish Entrepreneurs – the Role of Local Partners

NGUYEN Cao Son^{1,*}

¹ University of Lodz, Lodz, Poland

Corresponding author: son.ngcao@gmail.com

Abstract. The purpose of this paper is to investigate the challenges of expanding into an emerging market for multinational enterprises (MNEs) and the strategies they adopted to overcome these adversities. While interest in the expansion of MNEs into the Vietnamese market is increasing, there is a lack of research on this process from the Polish businesses' perspectives, which may differ from existing literature. The analysis of information obtained by a semi-structured interview method shows that the psychic/cultural distance is the most critical challenge the Polish enterprises must face when entering the Vietnamese market. The study also shows that the key success factor for the expansion of the Polish enterprises into this market is a local partner, i.e., acquiring an appropriate Vietnamese partner, good cooperation with him/her, and building mutual trust. As a result, among the available forms of internationalization, the Polish enterprises most often choose export and various forms of cooperation with local partners as the main ways to enter this market.

Keywords: Internationalization, International expansion, Local partner, Polish enterprises, Vietnam

1. Introduction

Nowadays, enterprises do not limit themselves to operating solely in domestic markets, but actively seek ways to expand their operations into foreign countries. Internationalization (or international expansion) can be defined as crossing the boundaries of the enterprises' home and setting up operations overseas [1]. It is worth noting that internationalization is not a new term, as it has been the subject of academic research since the 1960s [2]. Traditional explanations of international behaviors of enterprises proposed that internationalization occurs in stages (the Uppsala model) [3, 4]. This approach suggests that MNEs, especially the small- and medium-sized enterprises (SMEs) that frequently experience resource constraints, internationalize gradually, first experimentally exporting in geographically close markets, thereafter entering more distant countries or employing higher entry strategies. Such expansions are typically determined by enterprises' resources, including experiential knowledge and networks [5]. Subsequently, the emergence of the international entrepreneurship perspective placed a greater emphasis on the role played by enterprises' resources and capabilities in driving international activities [6]. The main focus of the international entrepreneurship perspective is to describe and analyze the phenomenon known as "International New Ventures" (INVs) or "Born Globals" (BGs) that has changed the internationalization process whereby enterprises become international from inception.

However, the challenges and barriers related to entering international markets, widely known in the literature as *liabilities of foreignness* [7, 8], remain significant for newcomers, regardless of whether an enterprise is a born-global or follows the Uppsala model. Overcoming the barriers to entering foreign markets is one of the most critical tasks of internationalizing enterprises, and a variety of factors may contribute to the success of internationalization. Hence, it is important for MNEs to be able to identify what are the key success factors in expansion into foreign markets.

The entry of Vietnam into the World Trade Organization (WTO) and membership of other plurilateral agreements have resulted in unprecedented investment in this new emerging economy [9]. While the interest in the expansion of foreign enterprises in the Vietnamese market is increasing, there is a lack of research on this process from the perspectives of Polish businesses participating in these international relationships. As Vietnam is a developing and emerging market with many institutional challenges, the investment decisions of MNEs in this country are complicated. In other words, Vietnam, like other emerging markets, has context-specific issues that may challenge the entry of MNEs into this market, beyond the understanding common in the extant literature. Thus, exploring the expansion of Polish enterprises into the Vietnamese market provides insights that can add to the broader internationalization literature on emerging markets. In this study, I investigate the challenges and barriers that the Polish enterprises must face in expansion into the Vietnamese market and how they overcame these barriers. Using the semi-structured interviews with Polish entrepreneurs, I attempt to answer the two following questions:

- (1) What are the challenges that hindered the expansion of Polish MNEs into the Vietnamese market from their perspectives?
- (2) What strategies did they employ to overcome these entry barriers in the Vietnamese market?

The rest of the paper is organized as follows. The next section reviews the literature on challenges of internationalization and entry strategies. The key features of the Vietnamese economy and the business activities of Polish MNEs in this market are then detailed. The paper proceeds with a description of the research methods applied in this study. Section 5 presents and discusses the key findings from this study, while Section 6 provides the conclusion, as well as a discussion of the study's limitations and the key directions for future research.

2. Literature review

Given that internationalization offers potential for economies of scales and enhanced competitive advantages [10, 11], enterprises are incentivized to internationalize their operations. Nevertheless, operating in foreign markets is risky [5, 12, 13] and may have influence on performance of enterprises [14], as they must face numerous challenges and barriers that create boundary conditions for internationalization. This is especially true in the context of investments in emerging markets, where the institutional environment is weak and the level of challenges faced by MNEs remains high [9].

Researchers identified five major factors that constitute challenges, namely, *psychic/cultural distance*, *political/legal factors*, *economic factors*, *human resources*, and *infrastructure*. The psychic/cultural distance plays a part in internationalization of MNEs, for instance, the cultural distance between the home and host country increases management costs and creates difficulty in management [15, 16]. The political/legal factors are related to laws regulating the international expansion of MNEs, and the political/legal stability. In turn, the economic factors as challenges are the issues such as recession, inflation, unemployment rate, and currency instability that impact the attractiveness of countries [17, 18]. Another challenge is inadequate skilled labor/ shortage of skilled labor in specific markets, which has negative impacts on international activities of MNEs [19]. Finally, the incomplete infrastructure (eg., energy and transportation) also hinders the international expansion of MNEs [20]. To mitigate these challenges, besides market selection, choices around entry strategies are central to the internationalization process of enterprises.

Indeed, operations in a foreign market depend on their choice of entry strategy (entry mode). An entry strategy is defined in the literature as an institutional arrangement chosen by an enterprise to operate in the international market [21]. As the most critical decision, entry strategy influences all future directions of MNEs [21]. A choice of entry strategy includes a choice of level of control. Control is the focus of internationalization literature because it is an antecedent for determining risk and return [22]. High-control modes can increase return and risk, while low-control modes minimize resource commitment and risk, but at the expense of profitability. Consequently, an enterprise can enter a foreign market via the following three categories of entry strategies in terms of the level of control [23]:

- (1) *Export strategies (low-control modes)*, including indirect and direct export strategies, which are characterized by low level of control, low risk, and high flexibility;
- (2) *Contractual strategies (intermediate modes)*, including contract manufacturing, licensing, franchising, joint ventures/strategic alliances, and management contracting, which are characterized by shared control and risk, as well as split ownership. Within this category of entry strategies, partners agree to share resources, technology, and supplement each other's needs for a long period of time. In such cooperation, the local partner provides valuable information on local market conditions (market-specific knowledge), contacts with suppliers and governmental institutions that are fundamental to MNE's operations in unfamiliar markets.
- (3) *Hierarchical strategies (investment modes, high-control modes)*, including foreign direct investment (FDI) in form of wholly-owned subsidiaries or branches, where the enterprise completely owns and controls the operations in overseas markets. Such entry strategies are characterized by high control and high risk, but low flexibility.

Each entry strategy has different implications according to the level of control that the enterprise can exert in the international expansion, and the resources and risk that it must assume to enter foreign markets. Hence, the choice of an appropriate entry strategy is a difficult and complex task for MNEs when expanding overseas [24].

3. The expansion of Polish enterprises into the Vietnamese market – an analysis of secondary sources

Nowadays, Polish enterprises are becoming increasingly active in expanding into foreign markets. In recent years, the number of Polish MNEs operating abroad has increased [25, 26, 27]. The main form of entering foreign markets used by Polish MNEs is exporting [28]. Notably, Polish enterprises more often decide to expand beyond European markets. Along with that, they are more and more attracted by Asian markets [27]. Among those markets, Vietnam has recently emerged as one of the most promising destinations in the world for the development of Polish investments and exports [29].

Indeed, today, Vietnam is a country with rapid economic development, where recently the GDP growth rate has been on average 7% per year. Although Vietnam has been hit by the ongoing COVID-19 pandemic, this country has shown remarkable resilience, as GDP grew by 2,9% in 2020 and is expected to grow 6,6% in 2021 on the back of successful control of the pandemic [30]. PricewaterhouseCoopers predicted that this Asian country could be one of the fastest growing economies in the world over the 2015–2050 period [31]. This is a relatively large sales market, as in 2019 the population of this country exceeded 96,5 million, and is expected to expand to 120 million by 2050 [30]. In 2016, Vietnam led the Southeast Asian region in terms of the Greenfield FDI Performance Index [32]. Today, Vietnam is one of the most attractive destinations for FDI and is host to some of the largest global MNEs [9]. Due to the geographical distance, Vietnam has not been a significant direction of expansion for Polish enterprises so far. Nevertheless, Polish exports to Vietnam are constantly growing: in 2014 it amounted to only EUR 110.8 million, in 2015 - EUR 129.9 million, and in 2016 - as much as EUR 213 million, and from that year Vietnam became the largest trading partner of Poland among the countries of Southeast Asia (ASEAN) in terms of turnover [33]. Hence, Vietnam has become one of the key markets in this region for Polish businesses.

Despite being a promising market and an important destination for Polish enterprises, to my best knowledge, research on the expansion of Polish MNEs into Vietnam is completely absent in the international business literature. Furthermore, like other developing and emerging markets, Vietnam has context-specific issues that may challenge the entry of MNEs, including the Polish enterprises, into this market, beyond the understanding common in the extant literature. As a new emerging market, Vietnam provides a good context to study the expansion activities of Polish MNEs in this country, which may very differ from their international operations in other markets, as well as the expansion of MNEs from other countries into Vietnam. Thus, the study fills this gap in the international business literature.

4. Research methods

The data for this study were collected through 33 semi-structured interviews with entrepreneurs or managers of Polish enterprises operating in the Vietnamese market. The use of the qualitative approach through interviews is a significant departure from previous studies that frequently employ quantitative methods to examine challenges of internationalization and entry strategies, which are not easily captured in quantitative data analysis [34]. Moreover, using the qualitative method would provide deeper insights and extend understanding of the subject.

The interviews were carried out between March 2017 and September 2019. The length of the interviews varied from 20 to 30 minutes. As all of the interviews were conducted in Polish and were then translated into English. Some of the interviewees did not want to be identified; consequently, all information that may lead to their identification is not revealed. The interviews focused on the background information, including two main parts: (1) the challenges and barriers that the Polish enterprises faced when entering the Vietnamese market; and (2) the strategies they adopted to overcome the challenges.

5. Results and discussions

The first part of each interview was devoted to getting information about the challenges and barriers that hindered the expansion of Polish enterprises into the Vietnamese market. All respondents indicated that the main challenges they faced when entering this market are *their lack of knowledge of local conditions, cultural differences, difficult cooperation with administration officials, corruption, and underdeveloped infrastructure*. Other less significant adversities, in their opinion, are *language barriers and work efficiency*.

It can be seen that the major challenges the Polish enterprises face during their expansion into the Vietnamese market are the psychic/cultural distance. The aforementioned challenges are difficulties that

hinder all foreign enterprises operating in this market. However, the respondents emphasized that foreign investors from Asian countries (e.g., Japan, South Korea, or China, etc.) may have fewer obstacles and have advantages over those of their Western counterparts due to geographical and cultural proximities.

The interviewees also indicated that the adversities and barriers could be more easily overcome if they establish a cooperation with a local partner, which is the second part of the interviews. One of the respondents very accurately specified it: *"The biggest problem of Polish investments in Vietnam is the unawareness of investors. They do not know that all major businesses are conducted by some large families. They also do not know that personal contacts are the basis of entering into contracts and that before we talk about business, we must first get to know and trust each other"*. This second part of the interviews focused on the importance of a local business partner in doing business in the Vietnamese market. Here are some selected opinions of respondents on this issue:

- *"Business activities in Vietnam require the participation of a Vietnamese person. It is imperative to find a partner you can trust to deal with local authorities, the community, and employees, as well as clients. Without a trusted Vietnamese partner, there is no chance to do anything"*.
- *"First, it is important to focus on building a stable relationship, because without it you will not gain trust, and without trust, there is little chance of success with such low effectiveness of state institutions, because the mere existence of regulations and their compliance with them do not guarantee anything. Second, it is also important to put effort into learning about the Vietnamese mentality in order to avoid surprises in formulating your own and understanding the other party's expectations"*.
- *"Patience and knowledge of Asian cultures. Be patient, understanding and get to know the local culture"*.
- *"Having a local business partner in this market is a key success factor. Only a Vietnamese partner knows the specifics of his market well and has the relationships necessary to develop business. However, it is not enough to establish a relationship with any local partner. You need a really good partner who knows all the elements of the game in his country and is characterized not only by the willingness but also the ability to act together"*.

It is simple to notice that all the opinions of the respondents indicated strong cultural differences, as the culture and mentality of the Vietnamese can be a "shock" to people from the West. One of the interviewees stated that: *"It is worth living here for three months before deciding to make any investment. The cultural difference is colossal, and the Vietnamese mentality is the biggest obstacle to doing business here. Stay and see if you will be able to cooperate with the Vietnamese!"*. Polish entrepreneurs emphasized the patience and the need to find a good local partner who can help to overcome the barriers of entry. In this part of the interviews, the respondents were also asked about the choice of the entry strategies adopted by them when entering the market. From the analysis of their answers, it can be concluded that the necessity to find an appropriate local partner causes the Polish enterprises, regardless of their size or branch, to choose export and various forms of cooperation with local partners as the main methods of entering this market. It can be explained by the fact that a local partner knows the specifics of his own country, understands the rules, mentality, and customs, which allows reducing the risk associated with entering an unfamiliar market.

Furthermore, in Vietnam, as in other Asian countries, interpersonal relation is of great importance in all aspects of life. For example, it is quite known in the literature under the slogan "guānxi" in China [35, 36], "kankei" in Japan [37], "kwankye" in Korea [37], or "jaan-Pechaan" in India [38], which means colloquially: "I know someone who knows someone who still knows someone... who can help you". Hence, building a network of connections and trust is the key success of doing business not only in Vietnam but also in other Asian countries. High personal culture, as well as knowledge of the mentality and habits of the local people also play an important role.

6. Conclusions

This study analyzes the expansion of Polish MNEs into the Vietnamese market, focusing on two main issues, i.e., the challenges the Polish MNEs faced when entering this market and how they overcame these challenges. Using the data collected via the semi-structured interviews of 33 entrepreneurs and managers of Polish enterprises, this study finds that the most critical challenge that hinders the expansion of the Polish enterprises into the Vietnamese market is the psychic/cultural distance. In their opinion, to overcome all challenges and barriers, it is crucial to find an appropriate local partner. The study also shows that among

the possible entry strategies, the Polish MNEs tend to choose export and various forms of cooperation with a local partner as the main way to enter this market.

Despite the contribution of this study, it is important to note that the study is based on the expansion of MNEs from a single country into a single emerging market, thus it may limit the extent to which these results are generalizable to cover all emerging markets. Furthermore, the small number of the Polish MNEs participating in the study also yields a small sample size that hinders the power of statistical testing and my ability to utilize more complex methods. Future research may use data collected from a number of MNEs in a cross-country context.

7. Acknowledgements

The paper was presented during the 6th VIET - POL International Conference on Scientific-Research Cooperation between Vietnam and Poland, 10-14.11.2021, HUMG, Hanoi, Vietnam.

8. References

1. Batsakis, G., Singh, S., 2019. Added distance, entry mode choice, and the moderating effect of experience: The case of British MNEs in emerging markets, *Thunderbird International Business Review*, 61(4), 581–594, <https://doi.org/10.1002/tie.22046>.
2. Kindleberger, C.P., *American business abroad*, Yale University Press, New Haven, 1969.
3. Johanson, J., Vahlne, J.E., 1977. The internationalization process of the firm: A model of knowledge development and increasing foreign market commitments, *Journal of International Business Studies*, 8(1), 23–32, <https://doi.org/10.1057/palgrave.jibs.8490676>.
4. Bilkey, W.J., Tesar, G., 1977. The export behavior of smaller-sized Wisconsin manufacturing firms, *Journal of international business studies*, 8(1): 93–98, <https://doi.org/10.1057/palgrave.jibs.8490783>.
5. Johanson, J., Vahlne, J.E., 2009. The Uppsala internationalization process model revisited: From liability of foreignness to liability of outsidership, *Journal of International Business Studies*, 40(9): 1411-1431, <https://doi.org/10.1057/jibs.2009.24>.
6. Brush, C.G., Edelman, L.F., Manolova, T., 2002. The impact of resources on small firm internationalization, *Journal of Small Business Strategy*, 13(1): 1–17, <https://libjournals.mtsu.edu/index.php/jsbs/article/view/490>.
7. Zaheer, S., 1995, Overcoming the Liability of Foreignness, *Academy of Management Journal*, 38(2): 341-363, <https://doi.org/10.2307/256683>.
8. Sethi, D., Judge, W., 2009. Reappraising liabilities of foreignness within an integrated perspective of the costs and benefits of doing business abroad, *International Business Review*, 18(4): 404-416, <https://doi.org/10.1016/j.ibusrev.2009.02.006>.
9. Dang, Q.T., Jasovska, P., Rammal, H.G., 2020. International business-government relations: The risk management strategies of MNEs in emerging economies, *Journal of World Business*, 55(1):101042, <https://doi.org/10.1016/j.jwb.2019.101042>.
10. Sapienza, H.J., Autio, E., George, G., Zahra, S.A., 2006. A capabilities perspective on the effects of early internationalization on firm survival and growth, *Academy of Management Review*, vol. 31(4): 914–933, <https://doi.org/10.5465/amr.2006.22527465>.
11. Porter, M.E., *Competition in global industries*, Harvard Business School Press, Boston, MA, 1986.
12. Brouthers, K.D., Brouthers, L.E., 2001. Explaining the national cultural distance paradox, *Journal of International Business Studies*, vol. 32, iss. 1, p 177–189, <https://doi.org/10.1057/palgrave.jibs.8490944>.
13. Bouncken, R.B., Cesinger, B., Kraus, S., 2014. The role of entrepreneurial risks in the intercultural context: A study of MBA students in four nations, *European Journal of International Management*, 8(1): 20–54, <https://doi.org/10.1504/EJIM.2014.058483>.
14. Kumar, V., Singh, N., 2008. Internationalization and performance of Indian pharmaceutical firms, *Thunderbird International Business Review*, 50(5): 321-330, <https://doi.org/10.1002/tie.20217>.
15. Richardson, C., 2014. Firm internationalisation within the Muslim world, *Journal of World Business*, 49(3): 386-395, <https://doi.org/10.1016/j.jwb.2013.07.005>.
16. Hutzschenreuter, T., Horstkotte, J., 2013. Performance effects of international expansion processes: The moderating role of top management team experiences, *International Business Review*, 22(1): 259-277, <https://doi.org/10.1016/j.ibusrev.2012.04.006>.

17. Lee, S.K., Jang, S.S., 2010. Internationalisation and exposure to foreign currency risk: An examination of lodging firms, *International Journal of Hospitality Management*, 29(4): 701–710, <https://doi.org/10.1016/j.ijhm.2010.02.003>.
18. Shieh, B.L., Wu, T.C., 2012. Equity-based entry modes of the Greater Chinese economic Area's foreign direct investments in Vietnam, *International Business Review*, 21(3): 508–517, <https://doi.org/10.1016/j.ibusrev.2011.06.001>.
19. Altinay, L., Brookes, M., Madanoglu, M., Aktas, G., 2014. Franchisees' trust in and satisfaction with franchise partnerships, *Journal of Business Research*, 67(5): 722–728, <https://doi.org/10.1016/j.jbusres.2013.11.034>.
20. Heung, V.C.S., Zhang, H., Jiang, C., 2008. International franchising: Opportunities for China's state-owned hotels?, *International Journal of Hospitality Management*, 27(3): 368–380, <https://doi.org/10.1016/j.ijhm.2007.10.002>.
21. Kumar, V., Subramaniam, V., 1997. A Contingency Framework for the Mode of Entry Decision, *Journal of World Business*, 32(1): 53-72, [https://doi.org/10.1016/S1090-9516\(97\)90025-0](https://doi.org/10.1016/S1090-9516(97)90025-0).
22. Anderson, E., Gatignon, H., 1986. Modes of Foreign Entry: A Transaction Cost Analysis and Propositions, *Journal of International Business Studies*, 17(3): 1-26, <https://doi.org/10.1057/palgrave.jibs.8490432>.
23. Hollensen, S., *Global Marketing*, sixth ed., Pearson Education Limited, Harlow, 2014.
24. Hill, C.W.L., Hwang, P., Kim, W.C., 1990. An eclectic theory of the choice of international entry mode, *Strategic Management Journal*, 11(2): 117-128, <https://doi.org/10.1002/smj.4250110204>.
25. PWC (2012), *Polski Czempion - Doświadczenia polskich firm inwestujących na rynkach zagranicznych*. <http://www.polskiczempion.pl> (accessed: 12.01.2021).
26. Business Consulting MDDP (2014), *Ekspansja międzynarodowa polskich przedsiębiorstw*. <http://www.mddp.pl>, 12.01.2021.
27. Poland, Go Poland, (2015), *Polskie firmy na globalnej scenie. Ekspansja w fazie wzrostu*, <http://www.polandgoglobal.pl>, 12.01.2021.
28. Grzegorzczak, W., 2018. Strategie ekspansji przedsiębiorstw województwa łódzkiego na rynki zagraniczne, *Handel Wewnętrzny*, 5(376): 81-89.
29. <https://www.prezydent.pl/aktualnosci/wizyty-zagraniczne/art,203,wietnam-dla-polski-brama-do-azji-a-polska-dla-wietnamu-brama-do-ue.html>, 12.01.2021.
30. <https://www.worldbank.org/en/country/vietnam/overview#1>, 07.04.2021.
31. <http://www.pwc.com/gx/en/issues/the-economy/assets/world-in-2050-february-2015.pdf>, 12.01.2021.
32. <https://www.fdiintelligence.com/Locations/Asia-Pacific/Vietnam/Vietnam-leads-emerging-market-greenfield-FDI-performance-index>, 12.01.2021.
33. <https://www.rp.pl/Dane-gospodarcze/312039922-Wietnam-przyciaga-polski-eksport.html>, 12.01.201.
34. He, W., Boateng, A., Ring, P., 2019. Motives, choice of entry mode, and challenges of bank internationalization: Evidence from China, *Thunderbird International Business Review*, 61(6): 897-909, <https://doi.org/10.1002/tie.22062>.
35. Barnes, B., Yen, D., Zhou, L., 2011. Investigating guanxi dimensions and relationship outcomes: Insights from Sino-Anglo business relationships, *Industrial Marketing Management*, 40(4): 510–521, <https://doi.org/10.1016/j.indmarman.2010.12.007>.
36. Berger, R., Herstein, R., 2012. The limits of guanxi from the perspective of the Israeli diamond industry, *Journal of Chinese Economic and Foreign Trade Studies*, 5(1): 29–41, <https://doi.org/10.1108/17544401211197940>.
37. Wilson, J., Ross Brennan, R., 2010. Doing business in China: is the importance of guanxi diminishing?, *European Business Review*, 22(6): 652-665, <https://doi.org/10.1108/09555341011082934>.
38. Chakrabolty, S., 1997. Business ethics in India, *Journal of Business Ethics*, 16(14): 1529–1538, <https://doi.org/10.1023/A:1005806913385>.

Genotype TNF- α (-308) and Silicosis on Factory Workers in Vietnam in 2020

NGUYEN Viet^{1,2}, NGUYEN Thi Thu Huyen^{3,*}, DAO Xuan Dat⁴, VU Xuan Quy⁴, PHAM Thi Quan⁴, LE Thi Kim Chung⁴, TRAN Huy Thinh⁴, LE Thi Huong⁴, NGUYEN Ngoc Anh⁴, NGUYEN Viet Nhung⁵, NGUYEN Ngoc Hong⁵, LUONG Mai Anh³, LE Thi Thanh Xuan⁴

¹ Vietnam National Cancer Institute, Vietnam National Cancer Hospital, Hanoi, Vietnam

² Hanoi University of Public Health, Hanoi, Vietnam

³ Health Environment Management Agency, Ministry of Health, Hanoi, Vietnam

⁴ Hanoi Medical University, Hanoi, Vietnam

⁵ National Lung Hospital, Hanoi, Vietnam

Corresponding author: thuhuyen80@yahoo.com

Abstract. The study aims to determine the TNF- α single-nucleotide polymorphism TNF- α (-308) and assess the association of TNF- α (-308) SNP with the risk of silicosis among workers directly exposed to silica dust in Vietnam. A study was undertaken among 78 cases with silicosis and 103 controls without silicosis in Vietnam. Blood samples were collected for genomic DNA extraction from each subject. The phenotyping of TNF- α (-308) was performed using polymerase chain reaction-based restriction fragment length polymorphism (PCR-RFLP) and dye termination sequencing. Results: The average exposure time of the case group was slightly higher than that of the control group (12.46 ± 6.732 years vs. 12.09 ± 7.854 years). The majority of genotypes in both silicosis and non-silicosis was GG. When analyzing the concentration of TNF- α in the study participants' blood, it is shown that the average concentration of TNF- α in the case group was higher than that in the control group. The genotype AG in the case group was 1.368 times higher than that in the control group. The percentage of all A alleles in the case group with silicosis was 1.342 times higher than the control group without the disease, similar to previous studies. Conclusion: The majority of genotypes in both groups was GG. The average concentration of TNF- α in blood, genotype AG, and the percentage of all A alleles in the case group was higher than that in the control group.

Keywords: Silicosis, Genotype, TNF- α , Vietnam

1. Introduction

Silicosis (also known as Potters Rot) is the most widespread form of pneumoconiosis. Silicosis is an occupational lung disease among workers who inhale silica dust daily. The manifestation of the disease is an irreversible diffuse lesion, which continues to develop after cessation of silica dust exposure [1].

Many theories explain the mechanism of silicosis, such as voltage theory, protein absorption theory, mechanical theory, immunology, etc. Among those, the "macrophage" theory is the most widely recognized. Accordingly, when silicon crystals into the alveoli were inhaled, they will be phagocytized by alveolar macrophages, activating the inflammatory response network, which leads to the secretion of cytokines of the inflammatory reaction into the alveoli spaces. The consequence of a chronic inflammatory response is that silicosis is developed.

In this chronic inflammation, there are many cytokines such as IL-1, IL-6, IL-10, TNF- α , etc... Among them, TNF- α is a cytokine due to macrophages. Alveolar secretory cells play an essential role in both the inflammatory response and the direct regulating factor stimulating fibroblasts and the collagenization of damaged tissue to form pulmonary fibrosis in silicosis. TNF- α gene regulates TNF- α production at transcription level [2]. Studies have shown that single nucleotide polymorphism in the promoter region increased TNF- α production. Recently, many studies worldwide show that this single polymorphism is related to the formation and progression of silicosis. In 2012, Wang et al. conducted a case-control study that showed the association of single nucleotide polymorphism TNF- α (-308) with silicosis. However, the results were still inconsistent, which requires further research [3]. Polymorphism at -308 nucleotides upstream from the transcription initiation site in the TNF- α promoter is associated with elevated TNF- α levels and disease susceptibilities. The molecular epidemiological studies of silicosis estimate the risk that the TNF- α gene variant is associated with the increased risk of silicosis [3, 4, 5, 6, 7, 8]. Since then, it helps to build strategies for prevention, screening, and early diagnosis for workers.

Studies on molecular epidemiology of silicosis in the world and Vietnam have still been inadequate; thus, it requires more effort. Therefore, this study was implemented to determine the TNF- α single-nucleotide polymorphism TNF- α (-308) in workers directly exposed to silica dust and to analyze the association between nucleotide monomorphism TNF-a 308) and silicosis.

2. Materials and Methods

2.1 Study Design, Case and Control Selection and Specimen selection

A descriptive study with a control group was undertaken from October 2018 to October 2020. The selected study participants were categorized into two groups. The control group included 103 workers exposed to silica dust with no diagnosis of silica dust. The case group was 78 workers exposed to silica dust and diagnosed with silicosis, following Circular 15/2016-QD-BYT of Ministry of Health guidance [1]. The study participants were selected with TNF- α higher than the threshold of diagnosis were selected from the list of 800 employees who quantified TNF- α under the study. The study participants selected with TNF- α higher than the diagnosis threshold were chosen from the list of 800 employees who quantified TNF- α under the study. The inclusion criteria for study participants included 1) direct exposure to silica dust for at least one year; 2) written informed consent for participation. The exclusion criteria were composed of 1) pregnant women; 2) those who were suffering from any inflammatory disease or tumours; 3) administrative staff.

A sample of blood (3mL) was collected in EDTA (Ethylene Diamine Tetracetic Acid) from each participant, and DNA was extracted using silica-res in method (Thermo Fisher Scientific, USA). The quality and quantity of genomic DNA samples were examined using Spectrophotometer.

2.2 Polymerase Chain Reaction-Based Restriction Fragment Length Polymorphism of TNF- α Fragments

Polymerase Chain Reaction-Based Restriction Fragment Length Polymorphism (PCR-RFLP) assays were designed to determine TNF- α genotypes. The primers sequences for TNF- α (-308) were described by Wang et al. (2012) with forwarding primer 5'-GAGGCAATAGGTTTTGAGGGCCAT-3', reverse primer 5'-CATCAAGGATACCCCTCACACT-3' (Thermo Fisher Scientific, USA) [3]. The polymerase chain reaction (PCR) was performed on Eppendorf™ Mastercycler™ Nexus Thermal Cycler (Eppendorf, Germany) in a 25 μ L reaction volume, which contained 12.5 μ L Dream Taq Green PCR (Thermo Fisher Scientific, USA), the paired primers for TNF- α (-308), H₂O and 3 μ L genomic DNA. DNA was heated to 95°C for 5 mins, and subject to 35 cycles of PCR at 94°C for 30 s, at 57°C for 40 s and 72°C for 30 s, finally extension at 72°C for 5 mins. PCR products were digested with NcoI at 37°C for 8 hours, and 3% agarose gel electrophoresis (Thermo Fisher Scientific, USA) was performed to check the status of the digested fragments. The results of electrophoresis assays were explained as follows, homozygous GG had one band sizing 114bp of restriction digested fragment PCR product on a gel, heterozygous GA had two bands sizing 114bp and 135 bp, respectively, and homozygous AA had one band sizing 135bp. Genotypes of TNF- α (-308) for selected samples were confirmed by dye termination sequencing method on ABI PRISM® 310 (Thermo Fisher Scientific, USA) in manufacturing. The representative sequencing results of ABI PRISM® 310 for the selected samples from each genotype of SNP were found in our study, which was shown in Figure 1.

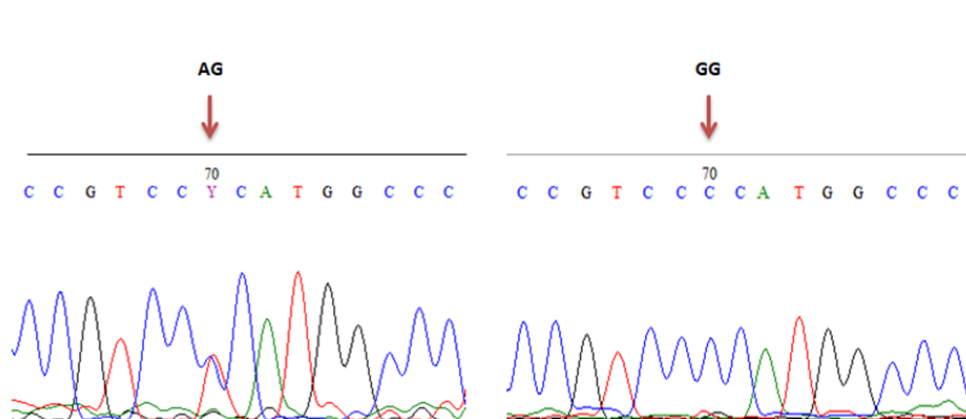


Fig. 1. The presentative sequences of TNF(-308) SNP genotypes.

2.3 Data analysis

Data were analyzed with SPSS 16.0 software (IBM, USA), and Review Manager 5.4 (Clicktime.com, Inc, USA) was used to evaluate the allele rate, genotypes, and their correlation with silicosis. The data are presented as frequencies and percentages for categorical variables and as mean \pm standard deviation (SD). χ^2 test or Fisher exact test was used to assess differences between the variables of workers with and without silicosis. Use the t-test to compare the mean age of the two disease groups and the control group.

To examine the association between the SNP TNF- α (-308) single polymorphism and the risk of silicosis, the Chi-Square test (χ^2) was applied to investigate the differences between genotype ratio and OR ratio and 95% CI. Since the genotype AA was not detected in this study, we only analyze AG and GG. P values < 0.05 were considered indicative of statistical significance.

3. Results

Baseline characteristics of the 78 silicosis patients and 103 workers without silicosis were described in Table 1. Most of the participants were male (92,3% in the case group and 88,3% in control). The mean age of the case group was $43.81 \pm 10,086$, which was higher than that in the control group ($39.46 \pm 7,543$). The average exposure time of the case group was 12.46 ± 6.732 years; it was similar in the control group ($12.09 \pm 7,854$ years). There was a non-significant difference between gender, age group, exposure time between the two groups of study participants.

Tab. 1. Characteristics of the study participants.

Variables	Cases (n,%)	Controls (n,%)	p values
<i>Gender</i>			0.457
Male	72 (92.3)	91 (88.3)	
Female	6 (7.7)	12 (11.7)	
Total	78 (100)	103 (100)	
<i>Age group</i>			0.195
>45 year-old	12 (15.4)	33 (32.0)	
35-45 year-old	38 (48.7)	45 (43.7)	
<35 year-old	28 (35.9)	25 (24.3)	
Age (Mean \pm SD)	43.81 ± 10.086	39.46 ± 7.543	
<i>Exposure time</i>			0.714
>10 years	11 (14.1)	25 (24.3)	
5-10 year	24 (30.8)	23 (22.3)	
<5 year	43 (55.1)	55 (53.4)	
Average year of exposure (Mean \pm SD)	12.46 ± 6.732	12.09 ± 7.854	

Characteristics of the TNF- α was presented in Table 2. It is shown that the average concentration of TNF- α in the case group was higher than that in the control group (Tab. 2). The mean blood concentration TNF- α in the case group was 15.81 pg/mL. The minimum and maximum values of TNF- α in this group were 0.17 pg/mL and 120.97 pg/mL. Whereas in the control group, the mean blood concentration TNF- α was 15.38 pg/mL with its minimum value being 2.56 pg/mL and 77.23 pg/mL, respectively. However, the difference in the average concentration of TNF- α in comparative groups was non-significant (p value > 0.05).

Tab. 2. Characteristics of the TNF- α concentration.

Characteristics of the TNF- α concentration (pg/mL)	Cases (n=78)	Controls (n=103)	p values*
Mean	15.81	15.38	0.2
Median	6.8182	8.358	
Standard deviation	22.34	17.12	
Max	120.97	77.23	
Min	0.17	2.56	

*t-test, comparing the mean of TNF- α concentration between case and control groups

Table 3 shows that GG genotype was the most common (87.2% in the case group and 90.3% in controls), following AG genotype. None of the study participants was detected with an AA genotype.

As for the allele ratio of the gene locus, in the disease group, the G allele was dominant with 93.6%. The A allele only accounts for 6.4%. Likewise, the control group's G and A alleles were 95.1% and 4.9%, respectively.

Tab. 3. Genotype ratio and allele ratio of locus SNP TNF- α (-308).

	Cases (n,%)	Controls (n,%)
TNF- α (-308) Genotype		
AA	0 (0)	0 (0)
AG	10 (12.8)	10 (9.7)
GG	68 (87.2)	93 (90.3)
Total	78 (100)	103 (100)
Allele ratio of the gene locus TNF- α (-308)		
G	146 (93.6)	196 (95.1)
A	10 (6.4)	10 (4.9)
Total	156 (100)	206 (100)

The risk of silicosis between genotypes AG and GG was evaluated in Table 4. The study found that the genotype AG in the case group was 1.368 times higher than that in the control group (OR = 1.368; 95% CI: 0.539-3.469). However, the correlation was non-significant, with a p-value > 0.05.

Tab. 4. Association of TNF- α (-308) . with risk of silicosis.

Allele	Cases (n,%)	Controls (n,%)	OR (95%CI)	p value
AG	10 (12.8)	10 (9.7)	1.368 (0.539-3.469)	0.508
GG	68 (87.2)	93 (90.3)		

When analyzing the A and G alleles of SNP TNF- α (-308) G/A on two groups of cases and controls, we found that the percentage of all A alleles in the case group with silicosis was 1.342 times higher than the control group without the disease (Tab. 5). However, this result was not statistically significant.

Tab. 5. Assessing the risk of silicosis between the alen A and alen G.

Allele	Cases (n,%)	Controls (n,%)	OR(A/G) (95%CI)	p
A	10 (6.4)	10 (4.9)	1.342 (0.545-3.310)	0.521
G	146 (93.6)	196 (95.1)		

4. Discussions

Silicosis is pneumoconiosis of lung fibrosis caused by inhalation of silica dust, usually for an extended period [9]. It is a common occupational disease among workers exposed to silica particles [9, 10]. The development of disease is related to the total dose and intensity of exposure to silica particles. Still, to date, the scientist cannot answer why some workers would get silicosis, while others did not in the same working environment. Many authors proposed strong evidence for individual variation in susceptibility to silicosis both in humans and in experimental animals [10, 11, 12, 13]. Despite the contribution of environmental factors, but in animal studies, it is shown that different strains have different susceptibility to disease, implying that susceptibility to silicosis is at least partly determined by genetic factors [12].

In our study, we investigated exposure time that is an essential factor in the pathogenesis of silicosis. Whereby 78 workers in the case group had an exposure time between 2 and 31 years, and the average exposure time of the case group was 12.46 ± 6.732 years. As for 103 subjects in the control group, their exposure time was ranged from 1 to 31 years with a mean of 12.09 ± 7.854 . The average exposure time of all the participants in our study is quite similar to R. Nadif's but lower than other studies carried out in South Africa, China, and Iran. This difference in exposure time between these studies may result from the epidemiological differences between Vietnamese people and others. It may also be influenced by the total amount of silica dust produced in the workplace due to the type of work with silica dust exposure in Vietnam that was different from other regions [3, 15, 16].

In silica dust-exposed persons and experimental model of fibrosis, TNF- α produced by macrophage is involved in the initial of chronic inflammation [9]. TNF- α is an inflammatory cytokine that plays a significant role in the pathogenesis of the pulmonary inflammatory disease. This hypothesis was demonstrated by some studies in animal experiments and population-based studies. In a case-control study in Chinese carried out with three different groups which are healthy group exposed to silicon dust with TNF- α concentration = 47.86 ± 16.52 pg/mL, another group diagnosed with silicosis having TNF- α = 109.11 ± 31.08 pg/mL, and silicosis patient group with the concentration TNF- α = 216.35 ± 51.03 pg/mL. This study shows that is not only significantly elevated TNF- α in exposed healthy donors and silicosis patients compared to healthy not exposed donors but also the TNF- α concentration of silicosis patients is higher than exposed healthy donors [17]. When we investigate the TNF- α concentration in silicosis, there is no significant difference between case and control. Still, it reflects the trend which is TNF- α concentration is higher in silicosis patients. These findings are similar to E. Slavov's study. It was implemented on Bulgarian populations with three groups which are the healthy population who were not exposed to silicon dust have concentration TNF- α = 14.8 ± 8.8 pg/mL, the healthy group with a history of silica dust exposure at concentrations TNF- α = 22.4 ± 11.1 pg/mL, and the case group diagnosed with silicosis with the concentrations TNF- α = 20.9 ± 12.9 pg/mL [18].

The regulation of TNF- α production occurred significantly at the transcription level [19]. Many authors proposed that the variant in the promoter of the TNF- α gene affected to enhance TNF- α production. The SNP TNF- α (-308) located in the promoter was thought to play an elevated TNF- α production. A case-control study in Indonesia with 336 workers shows that the AA/AG genotype of TNF- α (-308) affects elevated TNF- α concentration. Furthermore, this study also proved the AG genotype in silicosis patients higher than control donors, and AG genotype had a higher risk of silicosis than GG genotype in our study [7]. The results showed that the genotype AG in the case group was 1.368 times higher than that in the control group (OR = 1.368; 95% CI: 0.539-3.469). However, this finding has no significant meaning that the genotype AG increases the risk of silicosis in the study group. Our results are similar to those of Wang Yong Wei (2012) when the silicosis risk of AG genotype compared with GG was not statistically significant, or the study of Elizabeth L. Corbett on a South African population with 121 cases and 120 controls also showed no increased risk of silicosis of genotypes AA, AG compared with GG genotype. This result is similar to the study of author Yusesoy carried out on the European population and the author Isa Abdi RAD on the Iranian people [3, 4, 16, 20].

When analyzing the risk distribution of silicosis between subjects with the AG genotype and the subjects carrying the GG genotype in our study on the Vietnamese population with other studies in the world, we can see the AG genotype detection rate in the disease group was 1.37 times higher than that in the control group. This rate was similar to other studies in the world (Fig. 2).

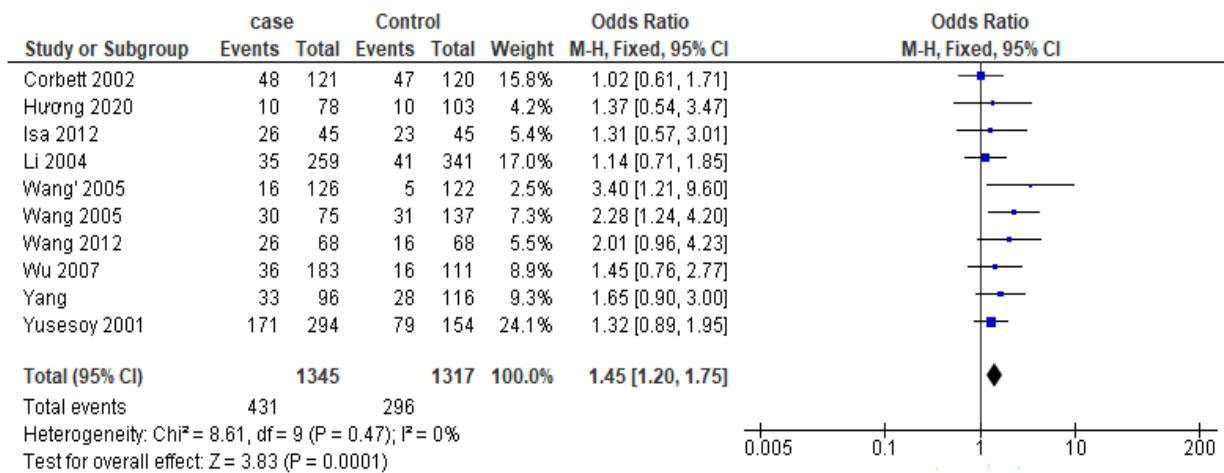


Fig. 2. Comparison of silicosis between genotypes AG and GG between our research and a number of studies around the world.

Regarding the study on the risk of allele A compared with the G allele in silicosis, different studies also show many inconsistent results. This study found that the percentage of all A alleles in the case group with silicosis was 1.342 times higher than the control group without the disease, which was similar to previous studies. Research by Kurniawidjaja shows that the rate of allele A in the disease group was statistically significantly higher than that in the control group ($p = 0.02$) [7]. Additionally, in the meta-analysis study of author Li Te Yang conducted on nine previous case-control studies of SNP TNF- α (-308) with risk of silicosis, it is identified that the allele A was 1.4 times more likely than the allele G to have a risk of silicosis (OR = 1.4; 95% CI: 1.11-1.78) [21]. In the study conducted by Yusesoy on the European population, the rate of allele A in the disease group was 1.32 times higher than that in the control group. However, some studies did not confirm the prominent allele A in silicosis patients. A study of the author Elizabeth L. Corbett did not prove that allele A increases the risk of silicosis compared to the allele G ($p = 0.15$). Our results can be easily compared with the results of Li Te Yang et al., where it shows that the association of SNP TNF- α (-308) with silicosis varies among various populations [4, 20].

As SNP TNF- α (-308) is in the promoter area of the cytokines protein TNF- α gene, there have been many studies on how allele changes at this SNP site affect the binding site of transcription initiation factors as well as cis factors, and the trans factor enhances the transcriptional enhancement of the TNF protein-encoding mRNA. - α in lymphocytes and macrophage cells can increase the concentration of TNF- α , essential cytokines in the pathogenesis of silicosis and pulmonary fibrosis diseases. However, studies on the role of this SNP in silicosis are still inconsistent. In our study, the percentage of allele A in the case group was higher than that in the control group. Although this difference was not statistically significant, it is still likely that this SNP is susceptible to silicosis because the SNP locus TNF- α (-308) is a gene with low permeability [22].

Our study had some strengths and limitations. It is the first study to determine the average concentration of TNF- α among the worker population directly exposed to silica dust. However, we cannot conclude the higher risk of TNF- α with silicosis that further study with larger sample size is needed.

5. Conclusions

Our study illustrates the majority of the genotype of TNF- α in both silicosis and non-silicosis was GG. When analyzing the concentration of TNF- α in the study participants' blood, it is shown that the average concentration of TNF- α in the case group was higher than that in the control group. The genotype AG in the case group was 1.368 times higher than that in the control group. The percentage of all A alleles in the case group with silicosis was 1.342 times higher than the control group without the disease, similar to previous studies. However, the result has not shown a statistically significant difference. Therefore, further studies with larger sample sizes are recommended.

6. Acknowledgements

The paper was presented during the 6th VIET - POL International Conference on Scientific-Research Cooperation between Vietnam and Poland, 10-14.11.2021, HUMG, Hanoi, Vietnam

The authors thank the Centres of Diseases Control/Preventive Health in 2 provinces, including Hai Duong and Thai Nguyen, for their support during field visits.

7. References

1. Ministry of Health of Viet Nam. TT15/2016 TT-BYT. Regulations on occupational diseases entitled to social insurance. 2016.
2. Lopes-Pacheco, M, Bandeira E, Morales MM.,2016. Cell-Based Therapy for Silicosis, *Stem Cells Int*, 2016, 509-518, <https://doi.org/10.1155/2016/5091838>.
3. Wang, Y.W., Lan, J.Y., Yang, L.Y., et al., 2012. TNF-alpha and IL-1RA polymorphisms and silicosis susceptibility in Chinese workers exposed to silica particles: a case-control study, *Biomedical and Environmental Sciences*, 2012, 25(5): 517-525. doi: 10.3967/0895-3988.2012.05.004.
4. Corbett, E.L., Mozzato-Chamay, N., Butterworth, A.E., et al., 2002. Polymorphisms in the tumor necrosis factor-alpha gene promoter may predispose to severe silicosis in black South African miners, *Am J Respir Crit Care Med*. 2002 Mar 1;165(5): 690-3. doi: 10.1164/ajrccm.165.5.2010050.
5. Li, Z., Xue, J., Yan, S., Chen, P., et al., 2013. Association between tumor necrosis factor- α 308G/A gene polymorphism and silicosis susceptibility: a meta-analysis, *PLoS One*, 8, 215-220, <https://doi.org/10.1371/journal.pone.0076614>.
6. Sullivan, K.E., Wooten, C., Schmeckpeper, B.J., et al.,1997. A promoter polymorphism of tumor necrosis factor alpha associated with systemic lupus erythematosus in African-Americans, *Arthritis and rheumatism*, 40(12): 2207-2211. <https://doi.org/10.1002/art.1780401215>.
7. Kurniawidjaja, L.M., et al., 2014. Silicosis and its progress influenced by genetic variation on TNF-alpha locus- 308, TNF-alpha and IL-10 cytokine on cement factory workers in Indonesia, *Pakistan journal of biological sciences : PJBS*, 17(3): 419-423. <https://doi.org/10.3923/pjbs.2014.419.423>.
8. Yucesoy, B., Vallyathan, V., Landsittel, D.P., et al., 2002. Cytokine polymorphisms in silicosis and other pneumoconioses, *Molecular and cellular biochemistry*, 234-235(1-2): 219-224.
9. Becklake, M.R.,1992. The mineral dust diseases, *Tubercle and lung disease : the official journal of the International Union against Tuberculosis and Lung Disease*, 73(1): 13-20. [https://doi.org/10.1016/0962-8479\(92\)90074-T](https://doi.org/10.1016/0962-8479(92)90074-T).
10. Leger, J.P., 1992. Occupational diseases in South African mines--a neglected epidemic?, *South African medical journal = Suid-Afrikaanse tydskrif vir geneeskunde*, 81(4): 197-201.
11. Ortiz, L.A., Lasky, J., Lungarella, G., et al., 1999. Upregulation of the p75 but not the p55 TNF-alpha receptor mRNA after silica and bleomycin exposure and protection from lung injury in double receptor knockout mice, *American journal of respiratory cell and molecular biology*, 20(4): 825-833. <https://doi.org/10.1165/ajrcmb.20.4.3193>
12. Ohtsuka, Y., Munakata, M., Ukita, H., et al.,1995. Increased susceptibility to silicosis and TNF-alpha production in C57BL/6J mice, *American journal of respiratory and critical care medicine*, 152 (6 Pt 1): 2144-2149. <https://doi.org/10.1164/ajrccm.152.6.8520788>.
13. Davis, G.S., Leslie, K.O., Hemenway, D.R., 1998. Silicosis in mice: effects of dose, time, and genetic strain, *Journal of environmental pathology, toxicology and oncology : official organ of the International Society for Environmental Toxicology and Cancer*, 17(2): 81-97.
14. Hassani, E., Bagheri, M., Rad, I.A., et al., 2017. Association between SNPs at IL-17A and IL-17F and susceptibility to accelerated silicosis, *Toxicology and Industrial Health*, 33: 673-680, <https://doi.org/10.1177/0748233717695431>
15. Nadif, R., Mintz, M., Marzec, J., et al., 2006. IL18 and IL18R1 polymorphisms, lung CT and fibrosis: a longitudinal study in coal miners, *European Respiratory Journal* 2006 28: 1100-1105; DOI: 10.1183/09031936.00031506
16. Rad, I.A., Mohebbi, I., Bagheri, M., et al., 2012. Molecular Evaluation of the IFN γ +874, TNF α -308, and IL-1Ra VNTR Sequences in Silicosis, *Maedica*,7(1),20-24.
17. Miao, R-M., Zhang, X-T., Yan, Y-L., et al., 2011. Change of serum TGF-beta1 and TNF-alpha in silicosis patients, *Chinese journal of industrial hygiene and occupational diseases*, (12): 606-607.

18. Slavov, E., Miteva, L., Prakova, G., et al., 2010. Correlation between TNF-alpha and IL-12p40-containing cytokines in silicosis, *Toxicology and industrial health*, 26(8): 479–486. <https://doi.org/10.1177/0748233710373082>
19. Economou, J.S., Rhoades, K., Essner, R., et al., 1989. Genetic analysis of the human tumor necrosis factor alpha/cachectin promoter region in a macrophage cell line, *The Journal of experimental medicine*, 170(1): 321–326. <https://doi.org/10.1084/jem.170.1.321>
20. Yucesoy, B., Vallyathan, V., Landsittel, D.P., et al., 2011. Association of tumor necrosis factor-alpha and interleukin-1 gene polymorphisms with silicosis, *Toxicology and applied pharmacology*, 172(1): 75–82. <https://doi.org/10.1006/taap.2001.9124>
21. Yang, L.T., Liu, X., Wu, G.H., et al., 2018. Association between tumor necrosis factor- α -308 G/AA polymorphism and risk of silicosis and coal workers pneumoconiosis in Chinese population, *Inhal Toxicol*, 30, 213-217.
22. Torres Puig-Gros, J., Alzuria Alos, R.M., et al., 2018. Concordance between the antecedents of influenza vaccination referred by pregnant women and those recorded in the medical record, *Revista espanola de salud publica*, 92, e201803005.

Assessing Impacts of Mining Activities on Land Use/Land Cover Change Using Remote Sensing and GIS Techniques: A Case Study in Campha City, Vietnam

LE Thi Thu Ha^{1,*}

¹Hanoi University of Mining and Geology, 18 Vien street, Hanoi, Vietnam

Corresponding author: lethithuha@humg.edu.vn

Abstract. Coal is one of the most mining commodities to date, especially to supply both national and international energy needs. Coal mining activities that are not well managed will have an impact on the occurrence of environmental damage. The present study was undertaken to analyze the process of human-induced landscape transformation in the coal mines affected areas of Cam Pha, northeast Vietnam by interpreting temporal remote sensing data and using Geographic Information System. This experiment revealed that most of the study area was dominated by forest in all the time sequence period. The forest cover has decreased about 21.3%, meanwhile having nine fold increase in mining area from 1990 to 2020. The forest area lost during the study period was 7983.45 ha due to land cover conversion into mining area. The mining activities were also detrimental to the bare land and water body cover. The results of this study are expected to be used to support government efforts and mining managers in post-mining coal activities.

Keywords: Land use/land cover change, Mining activities, Remote sensing, GIS

1. Introduction

Coal which is commonly called as the “black gold” of Vietnam, which contributes a major part to its commercial energy production and is widely used in the power industry to generate electricity. Mining of coal both surface and subsurface causes enormous damage to the flora, fauna, hydrological relations and soil biological properties [1]. Open-pit mining operations are processes of denudation, handling, and accumulation [2]. Therefore, open-pit mining areas are not only affected on the vegetation, soil, and terrain, but also created big pits, transit sites, solid waste, and changed in land use/land cover (LULC) [3, 4]. Although land is the natural resource of the utmost importance and original source of all material wealth of human being, the mining of natural resources is invariably associated with land use/land cover changes [5]. Modern techniques of mining using heavy equipment can produce dramatic alterations in land cover, both ecologically and hydrologically [6, 7]. In this context, it is essential to scrutinize the effect of mining on land use/land cover change to minimize its impact on environment as well as for proper land management and decision making [8, 9, 10]. To ascertain such changes, earth resource satellite data are critically important and useful for land use/land cover change studies [11].

Recently, integrated remote sensing (RS) and GIS technology has enabled environmentalists and natural resources managers to acquire multi-temporal data and detect periodical changes [12, 13]. Multi-temporal RS data associated with GIS tools have been used for the detection of the LULC dynamics [14, 15, 16]. Landsat TM, ETM+, and OLI with spectral channels are chosen specifically to map vegetation type, LULC, and other landscape features [17, 18]. These types of data are particularly relevant to the scope of the study and the free of charge of the data. GIS is an important tool for monitoring environment impacts from a wide coverage and a tool repetitive coverage of RS data [12, 16, 19]. Moreover, it can detect the change at multi-resolutions to generate multi-level information of LULC changes. This is to support the planning and cost-effective decision marking.

Coal mining has been most extensively practiced in all the area of Cam Pha city, northeast Vietnam, as a result of this, the original landscape have been converted to mine spoils. The total deposit of coal in Cam Pha city is approximately 2.2 billion tones spreading over patches of different sizes [20]. Coal extraction in the city is done mainly by primitive surface mining method commonly known as ‘open-pit’ mining. Mining operations in Cam Pha city consist of the fours largest open-cast mines in Vietnam (Deo Nai, Tay Nam Da Mai, Cao Son, and Coc Sau). Coal mining activities in Cam Pha city have had a great impact on the regional environment, including the LULC [21].

A detailed understanding of the impact of coal mining activities on changes of land use/land cover on time and space is pre-requisite for the city. Therefore, present study was undertaken to analyze the process

of human-induced land cover transformation in the coal mined affected areas of Cam Pha city of Quang Ninh, Northeast Vietnam by interpreting multi-temporal remote sensing data (in 1990, 2000, 2010 and 2020) and using geographic information system. In order to achieve this objective, the land cover types consists of forest, mining area, settlement, water body and bare land were taken into consideration to know the trend due to the impact of mining activities in different time periods.

2. Study areas

Cam Pha is a city of Quang Ninh province in the Northeast region of Vietnam (Fig. 1). Coal mining activities in Cam Pha started over 100 years ago. Cam Pha is also principally known for its proximity to extensive coal mines, and it is home to the largest mines in Vietnam, namely the Coc Sau, Cao Son, Deo Nai, Tay Nam Da Mai open-pit mines. The coal mining and processing industry are the primary economic sector generating income for the people. Its main economic activities are industry and construction (73.5 %), trade and service (25.1 %), and agroforestry and fishery for local consumption (1.4 %) [22].

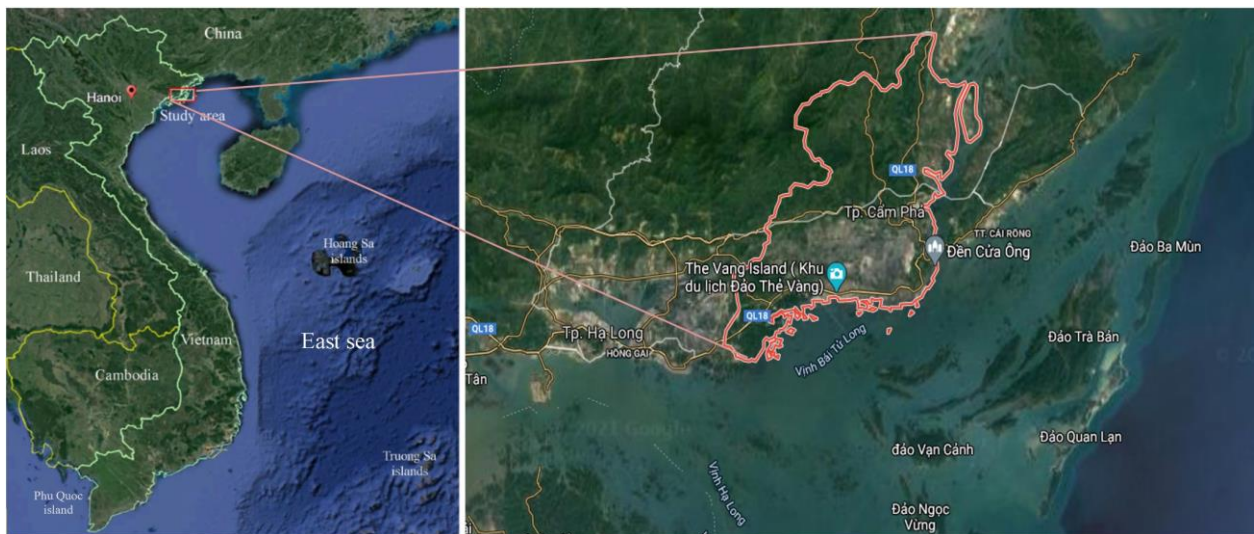


Fig. 1. Location of the study area.

3. Materials and Methods

3.1 Material and data sources

In this study, the satellite images used for extracting land use/land cover maps include: Landsat 5 Thematic Mapper (TM) images acquired in 1990, 2000, 2010 and Landsat 8 Operational Land Image (OLI) image acquired in 2020, which provided by the United States Geological Survey (USGS). Table 1 shows the details of satellite images with acquired time and resolution. Additionally, a topographic map (scale of 1:25,000) established by the Vietnamese Ministry of Natural Resources and Environment (MONRE) in 2020 was used for geocoding satellite images.

Tab. 1. List of Landsat data with acquired time and resolution (Source: USGS).

Sensor	Path/Row	Acquired Date	Local time	Resolution (m)
TM	126/045	26 November 1990	14h36'	30
TM	126/045	05 November 2000	14h56'	30
TM	126/045	03 September 2010	15h07'	30
OLI	126/045	12 November 2020	15h17'	30

3.2 Methodology

Procedure of image pre-processing is to remove distortions, precision and corrected terrain data (Level 1T) into the Universal Transverse Mercator (UTM) projection and WGS 84 datum (Zone 48, North). The images acquired in 1990, 2000 and 2010 were geo-referenced to the 2020 one. Then, the quality of the images was improved by using spectral enhancement tool.

An object-based approach was used to produce LULC map with 5 classes: Built-up, Mine area, Forest,

Water body and Bare land. As LULC spatial data became more widely available (either for sale or for free), such data (e.g. LANDSAT satellite images) could be more extensively used in developing countries. Object-based image analysis (OBIA) uses geographic objects as basic units for land cover classification. This approach reduces the within class variation and generally removes salt-and-pepper effects which result from isolated pixels mainly due to misclassification [23, 24, 25, 26]. OBIA has an advantage because it incorporates various sources of information like texture, shape and position as the basis for classification [23, 24]. A number of studies were conducted to compare the performance of object-based and pixel-based classification of Landsat imagery [27, 28]. In most of these studies, OBIA produced higher classification accuracies across various land cover types. Therefore, this paper further explores and demonstrates the capability of object-oriented image analysis software eCognition for landcover classification from Landsat imagery. The combination of complex object description, hierarchical image object network, and fuzzy system makes eCognition a challenge to knowledge-based image interpretation in a range of landcover classification applications.

Figure 3 shows the methodology flowchart adopted for the analysis. In the first step, the imagery was geometrically registered and radiometrically corrected. In the second step, land cover image objects were generated using an image segmentation algorithm. The training samples used for the former classification were carefully chosen after field investigation and reference were made to available ancillary maps. Finally, the accuracy of the classification results derived from this method was assessed using reliable reference data.

For detecting and analyzing the change on earth's surface, the most standard method used for land use land cover change detection is the post classification comparison method, which entails the comparison of independently produced classified images [29]. Post classification method is proved to be the most popular approach in change detection analysis [29, 30, 31, 32, 33]. This method requires the comparison between classification maps achieved from satellite images. The approach of this method is based on the rectification of the independently classified images, then the thematic maps generated is followed by the comparison of corresponding labels to identify the areas in which change has occurred. In this case LULC change detection study for opencast coal mining area in Cam Pha region was carried out by using post classification method. In addition, in order to obtain the dynamic changes of each class categories during the study period (i.e., from 1990 to 2020), the ArcMap 10.3 software were used to compute the trend, class total, net change, class change, percent change and rate of each LULC change between the years 1990, 2000, 2010, and 2020.

4. Results and discussion

4.1. Accuracy Assessment

The classification accuracy is achieved by comparing the ground truth data points sampled along roads, focusing on typical land-cover types in the region (Fig. 2) with the classified images. The accuracy of each classified image was provided by eCognition Developer 8.7 software using a stratified random sampling approach with a minimum per-class sample size of 20 points to ensure that classes. The overall accuracy is calculated by dividing the number of correctly classified pixels by the total number of reference and ground pixels [34]. Although it is simple, the overall accuracy has been the most conventional approach in accuracy assessment.

An improvement to the overall accuracy assessment is the Kappa coefficient of agreement which expresses the proportionate reduction in error generated by a classifier compared with the error of a completely random classification. Reference and ground samples were randomly generated, and then the respective informational classes were labeled by referring to the ortho-corrected digital land-use map. For this research, 128 references and ground sites were selected from high resolution Google Earth images, landuse/land cover map and fieldwork in December 2020. Results of accuracy assessment of the classified images showed that, the overall accuracy and kappa coefficient were found at 80.06% and 0.78 for classified image in 1990, 83.32% and 0.81 for classified image in 2000, 84.69% and 0.82 for classified image in 2010, 87.05% and 0.85 for classified image in 2020, respectively for LULC classified images.

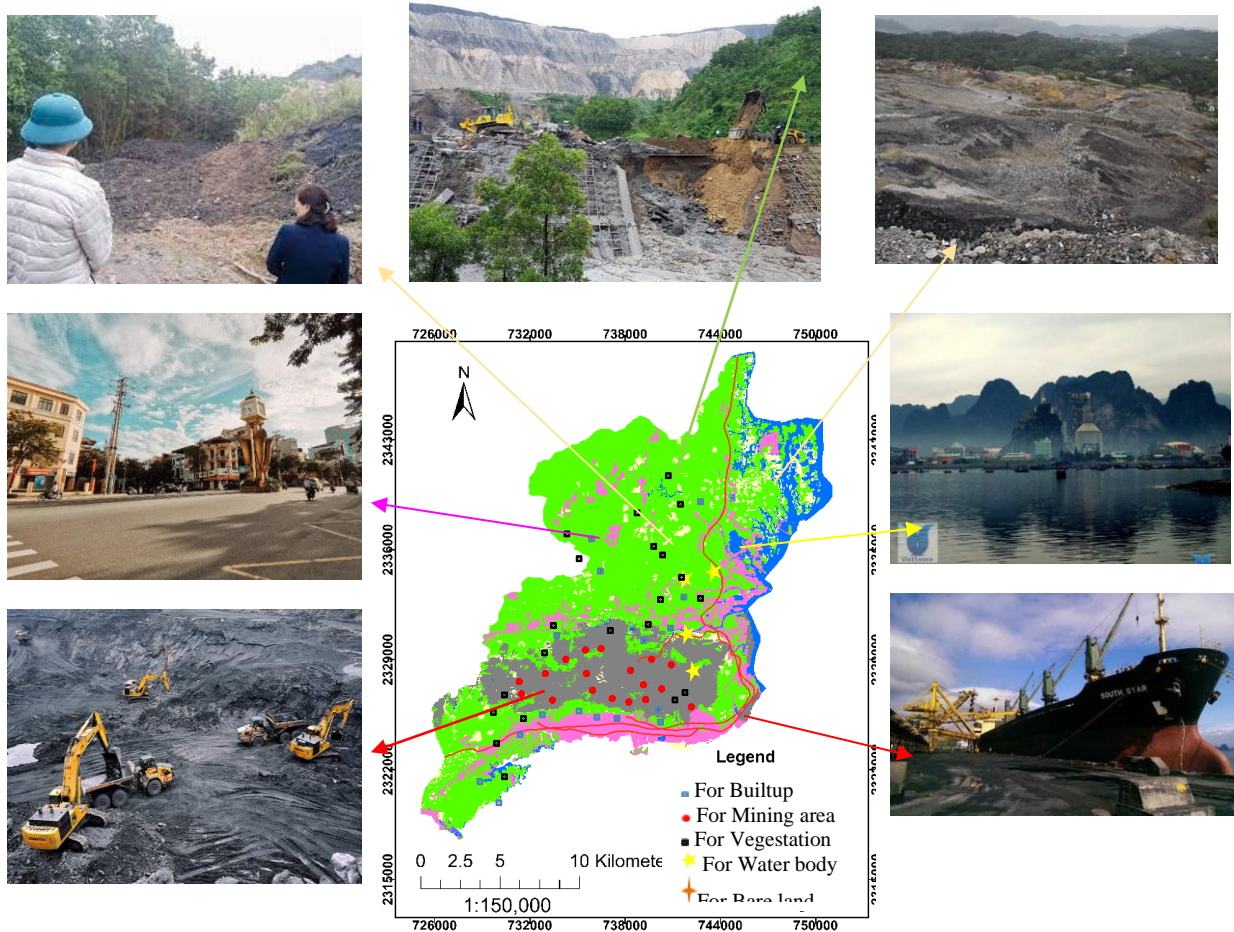


Fig. 2. Distribution of the ground truth points and field survey in the research.

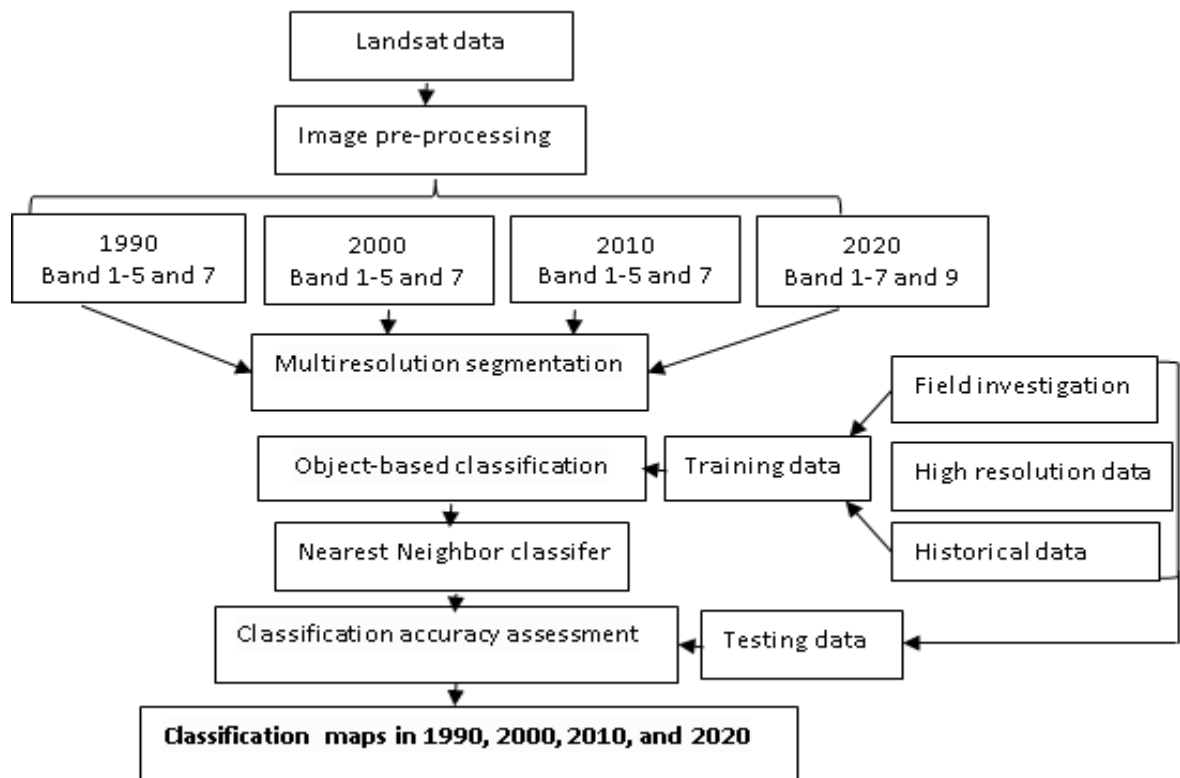


Fig. 3. Flowchart of image processing for land cover classification.

4.2 Land use/land cover maps in Campha city, Quang Ninh province, Viet Nam from 1990 to 2020

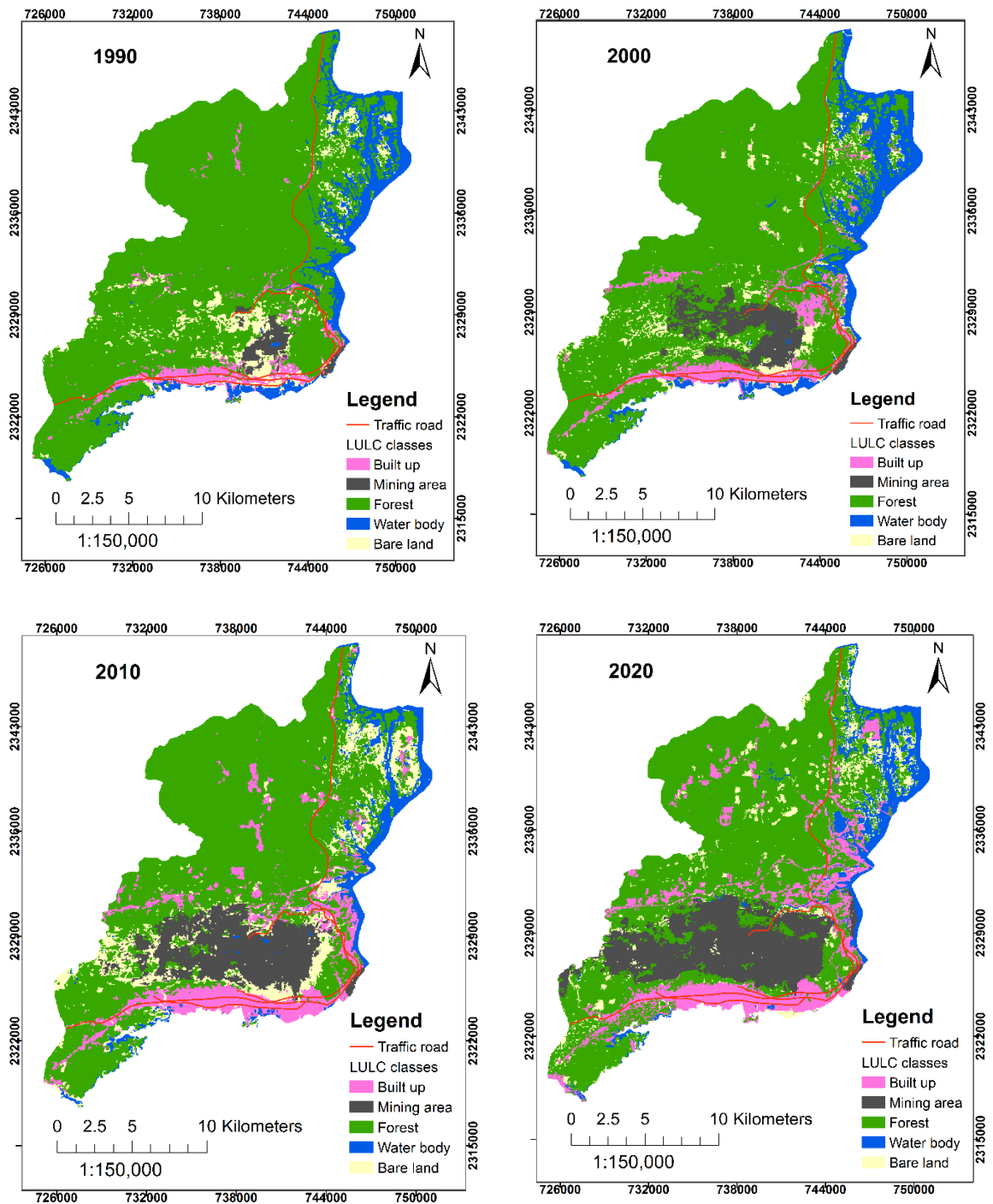


Fig. 4. Land use/land cover maps in Cam Pha city, Quang Ninh province, Viet Nam in 1990, 2000, 2010, and 2020.

The results on various land cover extents and their changes are presented in Figures 4, 5, and Table 2. Five major LULC classes: built up, forest, water body, mining area, and bare land were recognized in the study area. The LULC maps of the study area for four different years are presented in Fig. 4. Spatial distribution and area statistics of five LULC categories and the change of the area covered by each LULC category for each years are also shown in Table 2. Table 2 depicts the magnitude of change in different land use/ land cover categories in 4 period span from 1990 to 2000, 2000 to 2010, 2010 to 2020, and 1990 to 2020. Table 2 also shows the statistics of change detection analysis for the study period 1990-2020 for each class categories.

Figure 4 shows that coal mines area as a main part of the study was distributed mostly in the central or Cam Pha city. The forest area is the most biggest in the study area, and shows decreasing trend from 1990-2020. Forest cover land contains 29322.72 ha (78.41%) in the year 1990, however decreased to 21339.27 ha (57.06 %) in the year 2020.

The water body comprises the second largest class of the study area and forms an important land cover class. The rate of the water body is with area of 3494.34 ha (9.34%) in 1990, 3997.62 ha (10.69%) in 2000, and 2781.27 ha (7.43%) in 2020.

The coal mining area that had spread over 719.55 ha in 1990 (1.92%), increased to 2491.47 ha (6.66%) in 2000, and again increased to 6313.95 ha (16.89%) in 2020. The mining area comprises the opencast coal mines and overburden dumps showed constant increase in their aerial extents during the study period. The most mining extraction process and new mine coal pits are situated in forest land area.

On the other hand it can be observed from the data that there was a shrunken in the area of all of the land cover from 1990 to 2020, excepted mine and built up cover area (Tab. 2 and Fig. 5).

Tab. 2. Area of Land use/ land cover classes and its change from 1990 to 2020 in the Cam Pha coal mines area.

LULC classes	1990 (Ha)	2000 (Ha)	2010 (Ha)	2020 (Ha)	Changed 1990 -2000 (Ha)	Changed 2000 - 2010 (Ha)	Changed 2010 - 2020 (Ha)	Changed 1990 - 2020 (Ha)
Mining area	719.55	2491.47	4534.38	6313.95	+1771.92	+2042.91	+1779.57	+5594.4
Built up	1693.80	2415.78	4073.40	4842.18	+721.98	+1657.62	+768.78	+3148.20
Forest	29322.72	26708.49	22765.50	21339.27	-2614.41	-3942.99	-1426.23	-7983.45
Water body	3494.34	3997.62	2253.33	2781.27	+503.46	-1744.29	527.94	-712.89
Bare land	2165.67	1782.72	3769.47	2119.41	-382.95	+1986.75	-1650.06	-46.26
Total	37396.08	37396.08	37396.08	37396.08	0	0	0	0

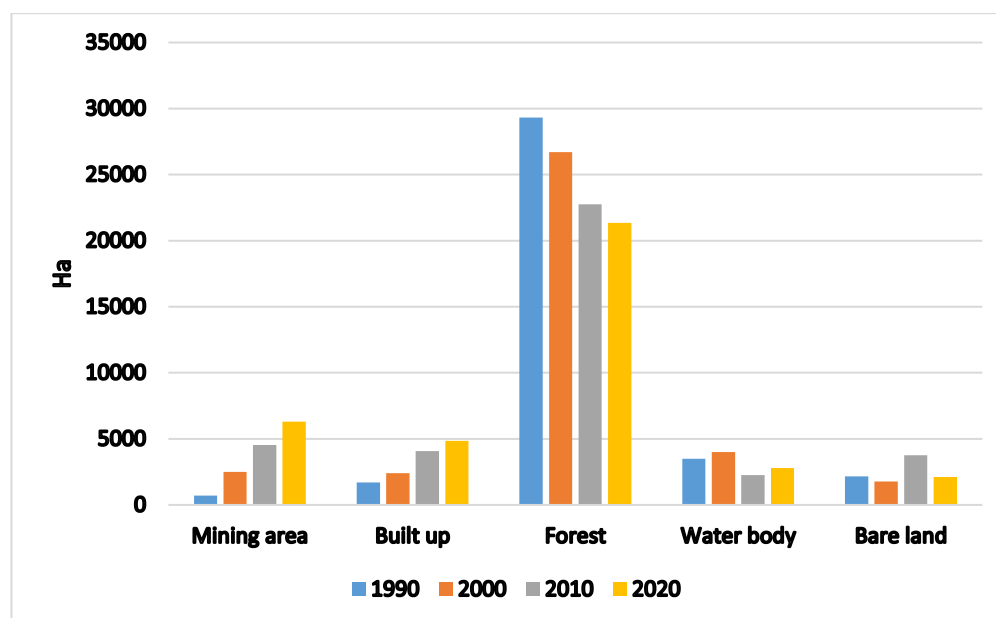


Fig. 5. Change in area under land use/land cover.

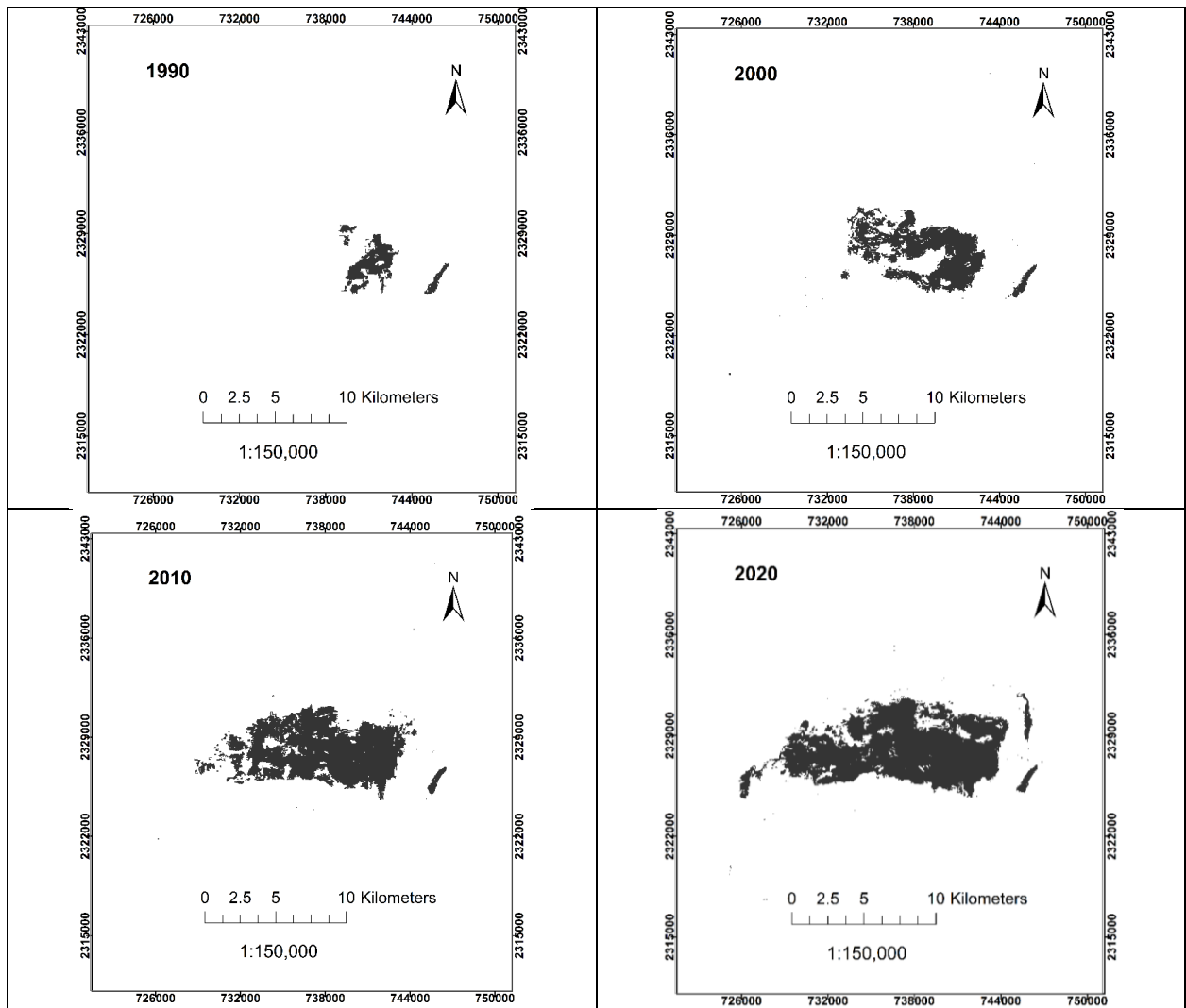


Fig. 6. The expansion of opencast coal mining areas in Cam Pha city from 1990 to 2020.

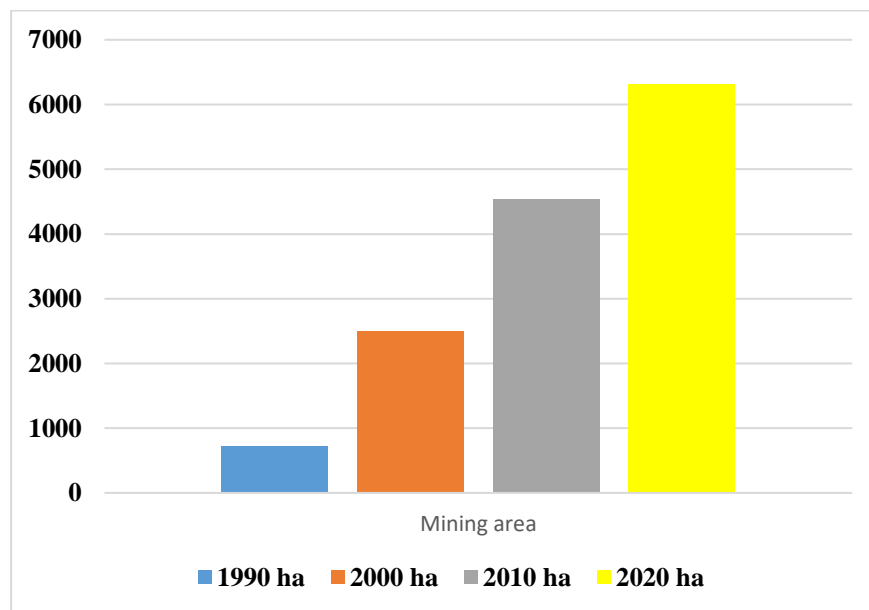


Fig. 7. Mining areal from 1990 to 2020 in Campha city, Quangninh province.

4.3. Impact of open-cast coal mines on land use/land cover change in Cam Pha city, Quang Ninh province, Viet Nam between 1990 and 2020

Land use dynamics were categorized in to five classes i.e., forest to mining, bare land to mining, water body to mining, no change and others were considered (Fig. 9). The result from the change analysis shows that there was impact of mining to different land uses/land cover, which were directly related to forest, bare land, and water body. About 43 km² of the forest of the study area was changed to the mining area from 1990 to 2020 and more than 10 km² area of bare land was converted into mining area during that period. The changes of about 3 percent of the total water body area revealed that much stress was on to the landscape during 30 years of time (Fig. 8).

The results of study revealed that from 1990 to 2020 maximum positive change is observed in the mining area, whereas maximum negative change recorded in forest land cover (Fig. 9 and Tab. 2). The mining activities in the area is a significant driver to decrease in LULC categories, and change their rates during the period from 1990 to 2020 (Fig. 8). The classified results of the forest area were the most victimized due to increasing in mining activity (from 719.55 ha in 1990 to 6313.95 ha in 2020). There was a loss 4321.620 ha of the forest area from 1990-2020 (approximate about 15%), meanwhile the water body converted 94.95 ha (about 3%) to mining area during 30 years (Fig. 8).

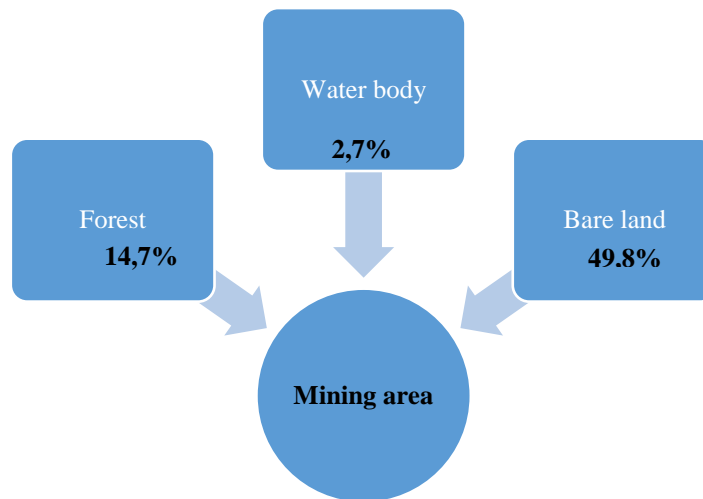


Fig. 8. The percentage of change (in %) of three LULC class converted to Mining area in the Cam Pha coalfield over time periods.

5. Conclusions

This study has revealed that considerable land use/land cover changes have taken place in Cam Pha city and around mines coal field from 1990 to 2020. Coal mining operation on large scale has significantly changed the mining environment. The mining area shows the increase of 5594.4 ha during 30 years due to the rapid increase in the coal production, meanwhile forest areas are decreasing but the plantations at overburden dumps under reclamation schemes have also been going on. It may be concluded that the land use/land cover change in the coal field has taken place due to the rapid expansion of mining and industrial activity the period of 1990 - 2020. This has resulted in the drastic changes in the land cover dynamics of the study area.

The use of multitemporal satellite data in the area has clearly demonstrated the potential of remote sensing imagery and its techniques in measuring the change pattern of LULC in the area characterized by the influx of mining. The use of remote sensing techniques can monitor the effect of opencast mining at local to regional scales due to the availability of past data, thereby helping us in reconstructing the effect of mining in the past few decades. A series of LULC maps generated by using multispectral and multitemporal remote sensing images acquired between 1990 and 2020 provides an understanding about how the LULC of an area evolved with time to its current form.

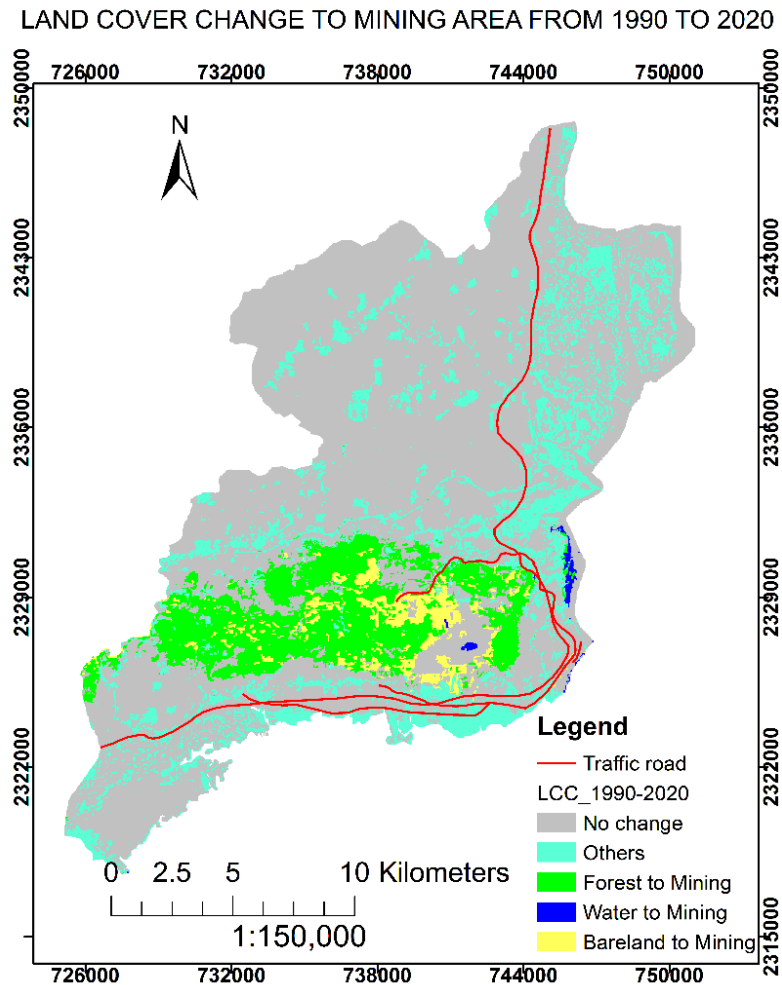


Fig. 9. Land use/land cover categories converted into mining area in Cam Pha city between 1990 and 2020.

6. Acknowledgements

The paper was presented during the 6th VIET - POL International Conference on Scientific-Research Cooperation between Vietnam and Poland, 10-14.11.2021, HUMG, Hanoi, Vietnam.

7. References

1. Sarma, K., Kushwaha, S.P.S., 2005. Coal mining impact on land use/land cover in Jaintia Hills district of Meghalaya, India using remote sensing and GIS technique. Conference Proceeding of National Conference on Geospatial Technologies, Geomatrix, 9(2005): 28-43.
2. Joshi, P.K., Kumar, M., Midha, N., Vijayanand and A. Paliwal, 2006. Assessing areas deforested by coal mining activities through satellite remote sensing images and gis in parts of Korba, Chattisgarh. Journal of the Indian Society of Remote Sensing, 34(4), Doi: 10.1007/BF02990926.
3. Prosper Laari Basommi, Qingfeng Guan, and Dandan Cheng, 2015. Exploring Land use and Land cover change in the mining areas of Wa East District, Ghana using Satellite Imagery. Open Geosci. 1(2015): 618–626, Doi: 10.1515/geo-2015-0058.
4. Chen, W., Li, X., He, H., Wang, L., 2018. A Review of Fine-Scale Land Use and Land Cover Classification in Open-Pit Mining Areas by Remote Sensing Techniques. Remote Sensing, 1(10): 15-20.
5. Prakash, A., Gupta, R.P., 1998. Land-use mapping and change detection in a coal mining area - A case study in the Jharia coalfield, India. International Journal of Remote Sensing, 3(19): 391-410, DOI: 10.1080/014311698216053.

6. Turner, M.G., Ruscher, C.L., 2004. Change in landscape patterns in Georgia. USA Land. Ecol., 4(2004): 251-421.
7. Singh, P. K., Singh, R., Singh, G., 2010. Impact of coal mining and industrial activities on land use pattern in Angul-Talcher region of Orissa, India. International Journal of Engineering Science and Technology, 2(12), 7771-7784.
8. Bocco, G., Mendoza, M., Velazquez, A., 2001. Remote sensing and GIS-based regional geomorphological mapping- a tool for land use planning in developing countries. Geomorphology, 39(3-4): 211-219.
9. Laskar, A., 2003. Integrating GIS and Multicriteria Decision Making Techniques for Land Resource Planning Master's thesis. International Institute for GeoInformation Science and Earth Observation, Enschede, Netherlands.
10. Turner, II, B.L., Lambin, E.F., Reenberg, A., 2007. The emergence of land change science for global environmental change and sustainability. Proc. Natl. Acad. Sci. U.S.A. 104(52): 20666-207671. Doi: 10.1073/pnas.0704119104.
11. Yuan, F., Sawaya, K.E, Loeffelholz, B.C., Bauer, M.E., 2005. Land cover classification and change analysis of the twin cities (Minnesota) Metropolitan Area by multitemporal Landsat remote sensing, Remote Sensing of Environment, 98(2005): 317-328.
12. Charou, E., Stefouli, M., Dimitrakopoulos, D., 2010. Using Remote Sensing to Assess Impact of Mining Activities on Land and Water Resources, Mine Water Environ, 29(1): 45-52.
13. Elsayed, A., El. Gammal, Salem M. Salem, Alaa Eldin A. El Gammal, 2010. Change detection studies on the world's biggest artificial lake (Lake Nasser, Egypt), The Egyptian Journal of Remote Sensing and Space Science, 13(2): 89-99.
14. Coppin, P., Jonckheere, I., Nackaerts, K., Muys, B., Lambin, E., 2004. Digital change detection methods in ecosystem monitoring: a review, International Journal of Remote Sensing, 25(9): 1565-1596.
15. Lu, D.S., Mausel, P., Brondízio, E.S., Moran, E., 2004. Change detection techniques, International Journal of Remote Sensing, 25(12): 2365-2407.
16. Ha Thu Thi Le, Nhat Dac Doan, Lam Thi Huynh, Thuy Thanh Thi Nguyen, Hiep Ngoc Thi Nguyen, Thuy Thanh Thi Luu, Chinh Cong Thi Vo, 2020. The influences of land cover structure on surface urban heat islands by using remote sensing and GIS, Journal of Mining and Earth Sciences, 61(2): 76-85.
17. Jensen, J.R., 2000. Remote Sensing of the Environment: An Earth Resource Perspective, 2nd Ed. Prentice-Hall, Inc.; Upper Saddle River, 544.
18. Mi, J., Yang, Y., Zhang, S., An, S., Hou, H., Hua, Y., Chen, F., 2019. Tracking the Land Use/Land Cover Change in an Area with Underground Mining and Reforestation via Continuous Landsat Classification. Remote Sensing, 11(14), 1719.
19. Meshesha, T.W., Tripathi, S.K., Khare, D., 2016. Analyses of land use and land cover change dynamics using GIS and remote sensing during 1984 and 2015 in the Beressa Watershed Northern Central Highland of Ethiopia. Model. Earth Syst. Environ., 2, (168), DOI 10.1007/s40808-016-0233-4.
20. Waldemar, M., 2018. Coal Mining and Coal Preparation in Vietnam. Journal of the Polish Mineral Engineering Society, 275-286, <http://doi.org/10.29227/IM-2018-01-40>.
21. Dung, L.V., 1994. Problems of beneficiation in coal preparation plants in Vietnam. New Trends in Coal Preparation Technologies and Equipment. Proceedings 5. of the 12th International Coal Preparation Congress, Cracow, Poland, 553-555. 6. ISBN 2-88449-139-2.
22. Mustafin, M.G., Tran Thanh-Son, Tran Manh-Hung, 2019. Comprehensive impact assessment development of the Coal field Campha in Vietnam to the coastal territory, IOP Conf. Series: Materials Science and Engineering 698, doi:10.1088/1757-899X/698/5/055014.

23. Hua Zhang, Yue Sun, Wenzhong Shi, Dizhou Guo & Nanshan Zheng, 2021. An object-based spatiotemporal fusion model for remote sensing images., *European Journal of Remote Sensing*, 54(1): 86-101, DOI: 10.1080/22797254.2021.1879683.
24. Sunil Bhaskaran, Shanka Paramananda, Maria Ramnarayan, 2010. Per-pixel and object-oriented classification methods for mapping urban features using Ikonos satellite data. *Applied Geography*, 30: 650 – 665, doi:10.1016/j.apgeog.2010.01.009.
25. Desheng Liu & Fan Xia, 2010. Assessing object-based classification: advantages and limitations. *Remote Sensing Letters*, 1(4): 187-194, Doi: 10.1080/01431161003743173.
26. Ha Thu Thi Le, Long Van Hoang, Trung Van Nguyen, 2021. Object-oriented classification for landcover of North Thang Long Industrial area using Worldview-2 data, *Journal of Mining and Earth Sciences*, 62(1): 10 -18.
27. Jing Qian, Qiming Zhoua, Quan Houa, 2007. Comparison of pixel-based and object-oriented classification methods for extracting built-up areas in aridzone, *ISPRS Workshop on Updating Geo-spatial Databases with Imagery & The 5th ISPRS Workshop on DMGIS*.
28. Sarmadian, F., 2007. Comparisons of Object-Oriented and Pixel-Based Classification of Land Use/Land Cover Types Based on Landsat7 ETM + Spectral Bands (Case Study: Arid Region of Iran). *American-Eurasian J. Agric. & Environ. Sci.*, 2(4): 448-456.
29. Anil, Z.C, Chitade, S.K., 2010. Impact analysis of open cast coal mines on land use/ land cover using remote sensing and GIS technique: a case study. *International Journal of Engineering Science and Technology*, 2(12): 7171-7176.
30. Giriraj, A., Babar, S., Reddy, C.S., 2008. Monitoring of Forest Cover Change in Pranahita Wildlife Sanctuary, Andhra Pradesh, India Using Remote Sensing and GIS. *Journal of Environmental Science and Technology*, 1: 73-79.
31. Al-shateri Hoshmand Ahmed Azeez1, Shuchrat Mukhitdinov, 2020. Land use land cover change detection in the mining areas of V. D. Yalovsky coal mine Russia. *International Scientific Conference “Problems of Complex Development of Georesources”*, 192, <https://doi.org/10.1051/e3sconf/202019204021>.
32. Anderson, P.R., Vinicius, A.S., Alex, M.S., Ana, C.F.X., Otto, C.R.F., Jorge, A.M., 2020. Impact of mining activities on areas of environmental protection in the southwest of the Amazon: A GIS- and remote sensing-based assessment. *Journal of Environmental Management*, 263, 110392.
33. Le Thi Thu Ha, Le Thi Van Anh, Pham Thi Lan, Nguyen Van Trung, 2018. Impact of urbanization on land surface temperature using remote sensing and GIS: A case of Tay Ho district, Hanoi city, Vietnam. *Journal of Mining and Earth Sciences*, 59(6): 64 -73.
34. Congalton, R.A., 1991. Review of assessing the accuracy of classifications of remotely sensed data, *Remote Sensing of Environment*, 37(1): 35 - 46, [https://doi.org/10.1016/0034-4257\(91\)90048-B](https://doi.org/10.1016/0034-4257(91)90048-B).

Research and Solution Proposals to Optimize Distribution Power Grids in Smart Grid Condition

PHAM Trung Son^{1,*}, NGUYEN Dinh Tien², NGUYEN Quang Thuan³, DANG Quang Khoa⁴

¹ Hanoi University of Mining and Geology, 18 Vien street, Hanoi, Vietnam

² Hanoi University of Industry, Hanoi, Vietnam

³ Thuyloi University, Hanoi, Vietnam

⁴ Vinh University of Technology Education, Nghe An, Vietnam

Corresponding author: phamtrungson@humg.edu.vn

Abstract. Smart Grid is a concept for transforming the electric power grid by using advanced automatic control and communications techniques and other forms of information technology. It integrates innovative tools and technologies from: generation, transmission and distribution. This also includes consumer appliances and equipment. This concept integrates energy infrastructure, processes, devices, information and markets into a coordinated and collaborative process. All allowing energy to be generated, distributed and consumed flexibly and efficiently. However, the Smart Grid with the integration of distributed generation itself also creates a several disadvantages. There can be problems with: stability and reliability, relay protection, isolation and operational isolation in which the problem is to create a burden on the distribution grid when transmitting electrical energy sources. Optimizing power flow and bringing high operating efficiency on Smart Grid conditions is an urgent issue. This paper focuses on researching and proposing solutions for optimal calculation of power flow on Smart Grid. The paper has researched, and analyzed calculation solutions to optimize power flow and proposed to use the Lagrange multiplier method. The study performed calculations for a typical Smart Grid model with three distributed generations. Calculation results have shown that the role of the method is to fully perform the optimal calculation of the power flow on the grid. This is in order to reduce power loss and energy loss as well as increasing operational efficiency while improving power quality in Smart Grid conditions.

Keywords: Smart grid, Power loss, Energy loss, Optimization, Distribution power grids

1. Introduction

The term Smart Grid refers to a modernization of the electrical network consisting of the integration of various technologies such as dispersed generation (DG), dispatchable loads, communication systems and storage devices utilized to efficiently deliver sustainable, economic and secure electricity. The Smart Grid concept is naturally associated with the integration of significant levels of Distributed Energy Resource (DER), including DGs, Demand Response (DR) [1, 2, 3], energy storage devices, and other energy sources into the electric grid. The Smart Grid scenario uses a two-way flow of electricity and information between power network and consumers in order to create an automated and widely distributed energy delivery network. The most important features of Smart Grid are the following: increasing the integration of renewable resources; increasing the participation of consumers in the network operation; decreasing the transmission and distribution losses, and lowering the energy cost for customers, subsequently; decreasing the electrical power consumption, and the emission of fossil fuels, concurrently; enabling consumers and electrical companies to control the demand.

Smart Grid or microgrid drivers are great in number, and linked to various factors. Such factors include: the necessity of controlling dispersed generation, ensuring power supply in remote areas, improving demand-side management, increasing energy efficiency, and creating self-healing electrical networks. The main objectives of Smart Grids are to increase supply reliability and improve power system security against contingencies or malicious attacks. Another important driver towards implementing Smart Grid is the higher integration of renewable energy resources on the distribution system level-which has substantially increased control problems in these systems [1, 4, 5].

Smart microgrids have served an integral role in the evolution of the Smart Grid [1, 6]. From this perspective, the Smart Grid can be divided into a system of integrated smart microgrids [1, 7, 8, 9]. In fact, the smart microgrid can be considered and exploited as the main building block of the smart grid [1, 10]. Therefore, Smart Grids and smart microgrids share common aspects such as interconnection with utility, interruptible loads, the use of different sources, employment of energy storage devices, optimal control based on customer requirements, optimal operation, the use of communications bandwidth for fast

applications and GPS, time-tagging, and cyber security [1, 11]. Based on these considerations, it follows that facing the problems of Smart Grids, and particularly smart microgrids, there should be revisions in traditional power system studies.

In current power systems, electrical losses are significant in the distribution of electrical energy, especially at lower voltage levels. Loss reduction can be achieved through the optimal control of power flow on the grid and the appropriate control of Distributed Generation (DG) resources in the distribution systems [1, 12], or more generally, through the control of dispatchable resources (DG, load, storage), which can be effectively assessed by using tools such as optimal power flow-like software. Connecting the new power sources to the current distribution systems leads to some technical and economic challenges [1, 13]. A possible solution for modern distribution systems consists of the creation of more or less independent cells which can interact in an internet-like structure. Microgrids can constitute the single element of this cellular structure in a large interconnected power system or be the natural answer to power supply in remote areas. In this regard, considering multi-microgrids as a system of microgrids would lead to different economic effects on the future Smart Grids [1, 14]. Also, preserving privacy of Optimal Power Flow models in this system is an important aspect which is discussed in [1, 15].

Operating the power transmission system when there is a high proportion of DG is really difficult and challenging. Most green energy sources rely on uncontrollable resources. In other words, generating electricity from renewable energy comes from natural resources such as sunlight, wind, or ocean waves. These types of sources generate intermittent and unstable power. Integrating large amounts of power from these types of sources- that cannot be regulated in a power supply system is a challenging task.

Optimizing power flow, bringing high operating efficiency under Smart Grid conditions is one of the urgent problems that need to be solved. The following content of the paper focuses on researching and proposing solutions for optimal calculation of power flow in order to reduce power loss and energy loss, increasing the improvement of operational efficiency while improving power quality in Smart Grid conditions.

2. Deterministic Optimal Power Flow

Power flow studies are necessary for planning, operating, and economic scheduling. This also includes other analysis; such as transient stability, voltage stability, and contingency studies. The tasks of power flow calculation are to solve the steady-state operating conditions of power systems based on the operation modes and the system's wiring.

Optimization of power flow is the task of identifying the optimal process from among others, compared by the criterion of optimality. Optimization can be distinguished as:

1. Determination of the optimal strategy for the development of power systems - construction or reconstruction of power systems and individual facilities (selection of location and capacity, setting the dates for commissioning new power plants, substations and transmission lines;
2. Selection of the best configuration of electrical networks;
3. Distribution of loads between individual power plants of an operating or projected system;
4. Choosing a strategy for the best use of material resources (types of fuel, etc.);

Therefore, the optimal power flow is necessary to minimize cost and energy losses ensuring increased revenue. The optimal power flow is a nonlinear characteristic optimization problem in a power system. The optimal power flow aims to minimize the total production cost by satisfying the load demand and system equality and inequality constraints [16, 17, 18]. The objective of optimal power flow is to find the setting of control variables at which objective function is optimized. Some of the possible objective functions in optimal power flow are power generation cost minimization, power transmission loss minimization, fuel emission during power generation, and minimum shift of generation from some optimum operation point [16, 19].

To solve the optimal power flow problem, many conventional and computer algorithms developed like lambda iteration method, base point, participation factors method, quadratic programming, nonlinear programming algorithm, gradient method Genetic Algorithm (GA), Evolutionary Programming (EP) [16, 20]. Optimal power flow has been used widely in planning and operation. Previously, several classical and modern optimization techniques have been proposed to solve the optimal power flow problem [16, 21] such as Particle Swarm Optimization (PSO) algorithm, Artificial Bee Colony (ABC) algorithm [16, 22], Firefly algorithm (FFL), Grasshopper Optimization Algorithm (GOA) [16, 23], Dynamic Programming (DP) [16, 24], Modified algorithm for finding the optimal nod of closed-medium voltage grids [25], Loop cutting algorithm [26].

According to the above discussion in optimal power flow, the objective is to optimize the power flow,

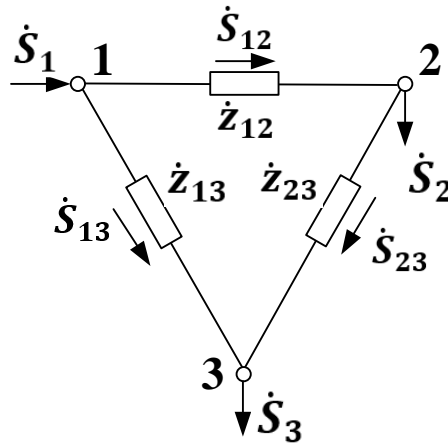


Fig. 1. Simple closed grid diagram.

Application of the Lagrange multiplier method to solve the problem of optimal distribution of power flows in the network consists in determining the minimum of the Lagrange function, which includes the active power losses:

$$\min \Delta P = \min \left(\frac{P_{12}^2 + Q_{12}^2}{U_{\text{norm}}^2} r_{12} + \frac{P_{23}^2 + Q_{23}^2}{U_{\text{norm}}^2} r_{23} + \frac{P_{13}^2 + Q_{13}^2}{U_{\text{norm}}^2} r_{13} \right) = \min \sum \frac{P_{kj}^2 + Q_{kj}^2}{U_{\text{norm}}^2} r_{kj} \quad (4)$$

and the equations of the first Kirchoff law:

$$\begin{cases} P_{12} - P_{23} = P_2; \\ P_{13} + P_{23} = P_3; \\ Q_{12} - Q_{23} = Q_2; \\ Q_{13} + Q_{23} = Q_3. \end{cases} \quad (5)$$

each of which is multiplied by the corresponding Lagrange multiplier. Consider the problem of optimizing the grid mode in Fig. 1, when the fluxes of reactive power in the lines Q_{kj} are equal to zero.

The equality of flows Q in lines 12, 23, 31 to zero means that at nodes 2 and 3 in Figure 1 full compensation of reactive power takes place. It is necessary to define

$$\min \Delta P = \min \left(\frac{P_{12}^2}{U_{\text{norm}}^2} r_{12} + \frac{P_{13}^2}{U_{\text{norm}}^2} r_{13} + \frac{P_{23}^2}{U_{\text{norm}}^2} r_{23} \right) \quad (6)$$

under the two equality constraints from (5)

$$\begin{cases} P_{12} - P_{23} = P_2 \\ P_{13} + P_{23} = P_3 \end{cases} \quad (7)$$

Lagrange function

$$F = \frac{P_{12}^2}{U_{\text{norm}}^2} r_{12} + \frac{P_{13}^2}{U_{\text{norm}}^2} r_{13} + \frac{P_{23}^2}{U_{\text{norm}}^2} r_{23} + \lambda_1 (P_{12} - P_{23} - P_2) + \lambda_2 (P_{13} + P_{23} - P_3) \quad (8)$$

where λ_1 and λ_2 are the Lagrange multipliers.

The conditional extremum problem (6), (8) with three variables P_{12} , P_{23} and P_{13} is reduced to the definition of an unconditional extremum (minimum) of the Lagrange function, which depends on five variables; three power flows and two Lagrange multipliers λ_1 and λ_2 . The minimum of the Lagrange function corresponds to the solution of the original problem and is determined by the equality to zero of five partial derivatives (equation 9).

To solve the system of linear algebraic equations (9), we transform its first three equations into the equation of the second Kirchoff law, excluding the Lagrange multipliers from them. As a result, we get the expression 10.

$$\left. \begin{aligned} \frac{\partial F}{\partial P_{12}} &= \frac{2P_{12}r_{12}}{U_{\text{norm}}^2} + \lambda_1 = 0 \\ \frac{\partial F}{\partial P_{23}} &= \frac{2P_{23}r_{23}}{U_{\text{norm}}^2} - \lambda_1 + \lambda_2 = 0 \\ \frac{\partial F}{\partial P_{13}} &= \frac{2P_{13}r_{13}}{U_{\text{norm}}^2} - \lambda_2 = 0 \\ \frac{\partial F}{\partial \lambda_1} &= P_{12} - P_{23} - P_2 = 0 \\ \frac{\partial F}{\partial \lambda_2} &= P_{13} + P_{23} - P_3 = 0 \end{aligned} \right\} \quad (9)$$

$$\frac{P_{12}}{U_{\text{norm}}^2} r_{12} + \frac{P_{13}}{U_{\text{norm}}^2} r_{13} + \frac{P_{23}}{U_{\text{norm}}^2} r_{23} = 0 \quad (10)$$

Solving the last two equations of system (9) together with this equation, we obtain

$$P_{12}r_{12} + (P_{12} - P_2)r_{23} + (P_{12} - P_2 - P_3)r_{13} = 0 \quad (11)$$

from here determine the optimal power flow running on the line

$$P_{12} = \frac{P_2(r_{23}+r_{13})+P_3r_{13}}{r_{12}+r_{23}+r_{13}} \quad (12)$$

From the formula, it is possible to adjust the optimal power flow on the line with any variation of the load and of the power supply. Through intelligent monitoring and control devices of Smart Grid, any changing working modes on the grid can be adjusted in a timely manner, keeping the mode parameters at an optimal level.

2.4 Test diagram used to calculate the optimal power flow

As examples of the application of the Lagrange multiplier method to optimize the power flow. The test diagram and detail parameters in Smart Grid condition are shown in Figure 2.

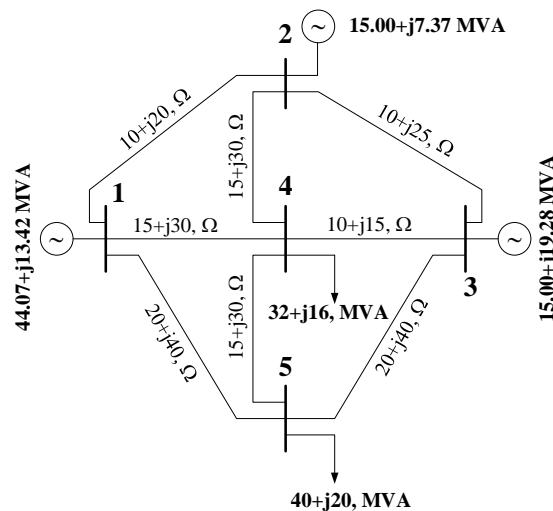


Fig. 2. The test calculation diagram.

Apply Lagrange multiplier method. The optimal power flow on the network segments is calculated and shown right on the Figure 3. The results of the optimal calculation of the power flow of the diagram are detailed in the Table 1.

The total active power loss on the grid is 2.07MW, the total active power transmission on the grid is 98.98MW. The optimal active power loss ratio is 2.09%. Thus, with the existing scheme, operating costs in the optimal mode of power flow will be reduced to the lowest level compared to other operating modes.

Through the optimal calculation results, corresponding to each operating mode, it is possible to determine the required power flow for transmission so that the loss on all lines is the lowest. Therefore, contributing to improving transmission efficiency, ensuring power quality while minimizing power system operating costs.

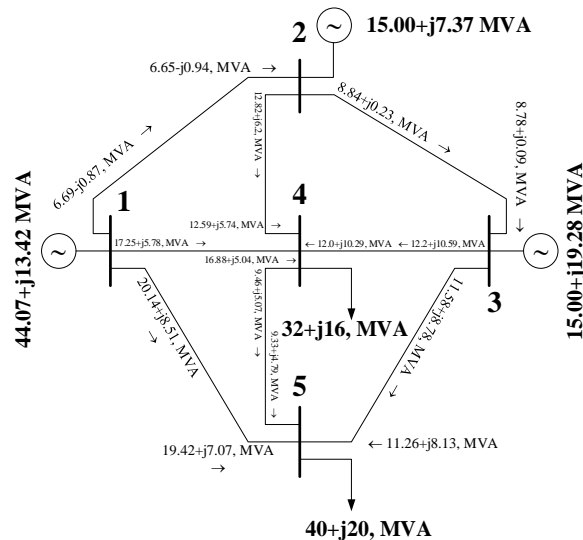


Fig. 3. Calculation results of the test diagram.

Tab. 1. Optimal calculation results of the test calculation diagram.

Network segment	Power at the beginning of the line, MVA	Power at the end of the line, MVA	Loss, MVA
1-2	6.69-j0.87	6.65-j0.94	0.04+j0.07
1-4	17.25+j5.78	16.88+j5.04	0.37+j0.74
1-5	20.14+j8.51	19.42+j7.07	0.72+j1.44
2-3	8.84+j0.23	8.78+j0.09	0.06+j0.14
2-4	12.82+j6.2	12.59+j5.74	0.23+j0.46
3-4	12.2+j10.59	12.0+j10.29	0.2+j0.3
3-5	11.58+j8.78	11.26+j8.13	0.32+j0.65
4-5	9.46+j5.07	9.33+j4.79	0.13+j0.28

The Smart Grid with the integration of distributed generation itself also creates several disadvantages. There can be problems with stability and reliability, relay protection, isolation and operational - in which the problem is to create a burden on the distribution grid when transmitting electrical energy sources. Therefore, optimizing power flow will bring high operating efficiency.

Smart Grid with the integration of distributed generation have unstable power sources, which cause power imbalances at nodes, which can result in large power losses and energy losses. It does not guarantee operational efficiency and leads to great economic loss. Thanks to the optimal calculation solution for the power flow, corresponding to any operating mode, Smart Grid's intelligent dispatching system -which uses the optimal calculation results of the power flow- will control it in time, so that the operating mode is consistently optimal.

Innovative Smart Grid solutions such as storage, will ensure stable power generation of distributed generations. The optimal power flow on the grid is determined by the optimal calculation through the Lagrange multiplier method, which will optimize the operating moderation.

3. Conclusions

The current energy transition is characterized by the desire to transition from traditional fossil fuels to more sustainable sources of electricity production. This transition necessitates the integration of new technologies such as renewable energy generators combined with the application of technology, equipment measurement, monitoring, control, and modern tools of communication. New electric production technologies have presented new design and implementation challenges due to the specificity of each resource. Traditional planning and operational strategies have solved these types of problems in the past by infrastructure reinforcements of the transmission or distribution grid. Innovative Smart Grid solutions such as storage, demand side management and curtailment were proposed as possible alternatives for infrastructure investments. These solutions require sophisticated power flow analysis tools. Existing power

analysis tools were presented including power flow analysis and optimal power flow analysis. Optimal power flow analysis was described in more detail to justify the choice of this tool as opposed to power flow analysis. These sophisticated algorithms present new mathematical challenges as well, which were discussed along with proposed solutions to overcome these challenges. This paper has presented work contributing to the advancement of power system analysis for Smart Grids in the presence of high renewable energy penetration. The solution used to calculate the optimal power flow is the Lagrange multiplier method. New sophisticated planning and operational tools are necessary to analyze the effects of high distributed generation penetration on existing architecture. The optimization of power flow of existing networks through automation and control has been discussed.

The Lagrange multiplier method was successfully designed and implemented to solve the optimal power flow problem. The comparison of results for the test diagram clearly shows that the Lagrange multiplier method is indeed capable of obtaining optimum solution efficiently for power flow problems. After finding the solution, the line losses have also been reduced by regulating the power flow on the grid. This indicates the significance of the Lagrange multiplier method to solve optimal power flow problems interconnected power system network.

4. Acknowledgements

The paper was presented during the 6th VIET - POL International Conference on Scientific-Research Cooperation between Vietnam and Poland, 10-14.11.2021, HUMG, Hanoi, Vietnam.

5. References

1. Hamdi Abdia, Soheil Derafshi Beigvanda, Massimo La Scalab, 2017. A review of optimal power flow studies applied to smart grids and microgrids. *Renewable and Sustainable Energy Reviews*. 71: 742-766.
2. Siano, P., 2014. Demand response and smart grids - A survey. *Renew Sustain Energy Rev*, 30: 461-78.
3. O'Connell, N., Pinson, P., Madsen, H., O'Malley, M., 2014. Benefits and challenges of electrical demand response: A critical review. *Renew Sustain Energy Rev*, 39: 686-99.
4. Mehrtash, A., Wang, P., Goel, L., 2013. Reliability evaluation of restructured power systems using a novel optimal power-flow-based approach. *IET Gener Transm Distrib*, 7: 192-9.
5. Lin, S.Y., Chen, J.F. Distributed optimal power flow for smart grid transmission system with renewable energy sources. *Energy* 2013; 56: 184-92.
6. Lidula, N.W.A, Rajapakse, A.D. Microgrids research: a review of experimental microgrids and test systems. *Renew Sustain Energy Rev* 2011; 15: 186-202.
7. Mohn, T. and Piasecki, R. A smarter grid enables communal microgrids. 2011 IEEE Green Technologies Conference (IEEE-Green), 1-6, 2011
8. Vasquez, J.C., Guerrero, J.M., Miret, J., Castilla, M., Vicuna, L.G.D., 2010. Hierarchical control of intelligent microgrids. *IEEE Ind Electron Mag* 4: 23-9.
9. Farhangi, H. The path of the smart grid. *IEEE Power Energy Mag* 2010; 8: p 18-28.
10. Mehrizi-Sani, A., Iravani, R. Potential-function based control of a microgrid in islanded and grid-connected modes. *IEEE Trans Power Syst* 2010; 25: 1883-91.
11. British Research. Smart grid (IEC61850) 2016. (<http://www.britishresearch.com/products/smart-grid-iec61850>) [accessed 06.06.16].
12. Bouzid, A.M., Guerrero, J.M., Cheriti, A., Bouhamida, M., Sicard, P., Benghanem, M. A survey on control of electric power distributed generation systems for microgrid applications. *Renew Sustain Energy Rev* 2015; 44: 51-66.
13. Fadaeenejad, M., Saberian, A.M., Fadaee, M., Radzi, M.A.M., Hizam, H., AbKadir, M.Z.A. The present and future of smart power grid in developing countries. *Renew Sustain Energy Rev* 2014; 29: 828-34.

14. Nikmehr, N., Najafi Ravadanegh, S. Optimal power dispatch of multi-microgrids at future smart distribution grids. *IEEE Trans Smart Grid* 2015; 6: 1648–57.
15. Wu, D., Lesieutre, B., Ramanathan, P., Kakunoori, B. Preserving privacy of AC optimal power flow models in multi-party electric grids. *IEEE Trans Smart Grid*. Volume: 7, Issue: 4, July 2016. Page(s): 2050 – 2060. [https:// DOI: 10.1109/TSG.2016.2544179](https://doi.org/10.1109/TSG.2016.2544179)
16. Hafiz Tehzeeb-Ul-Hassan, Muhammad Faizan Tahir, Kashif Mehmood, Khalid Mehmood Cheema, Ahmad H. Milyani, Qasim Rasool. Optimization of power flow by using Hamiltonian technique. *Energy Reports*. Volume 6, November 2020, 2267-2275.
17. Sinsuphun, N., Leeton, U., Kwannetr, U., Uthitsunthorn, D., Kulworawanich pong, T., 2011. Loss minimization using optimal power flow based on swarm intelligences. *ECTI Trans. Electr. Eng. Electron. Commun.* 9, 212–222.
18. Tahir, M.F., Saqib, M.A., 2016. Optimal scheduling of electrical power in energy deficient scenarios using artificial neural network and bootstrap aggregating. *Int. J. Electr. Power Energy Syst.* 83, 49–57
19. Khan, B., Singh, P., 2017. Optimal power flow techniques under characterization of conventional and renewable energy sources: A comprehensive analysis. *J. Eng.* Volume 2017. <https://doi.org/10.1155/2017/9539506>
20. Chan, K.Y., Pong, G., Chan, K. Investigation of hybrid particle swarm optimization methods for solving transient-stability constrained optimal power flow problems. *Proceedings of the World Congress on Engineering 2007. Vol I.* p 497-501, July 2 - 4, 2007, London, U.K.
21. Ebeed, M., Kamel, S., Jurado, F., 2018. Optimal power flow using recent optimization techniques. In: *Classical and Recent Aspects of Power System Optimization*. Elsevier, p 157–183.
22. Ayan, K., Kiliç, U., 2013. Solution of transient stability-constrained optimal power flow using artificial bee colony algorithm. *Turk. J. Electr. Eng. Comput. Sci.* 21, 360–372. <https://doi.org/10.3906/elk-1112-14>
23. Jumani, T.A., Mustafa, M.W., Md Rasid, M., Hussain Mirjat, N., Hussain Baloch, M., Salisu, S., Optimal power flow controller for grid-connected microgrids using grasshopper optimization algorithm. *Electronics* 2019, 8, 111; [doi:10.3390/electronics8010111](https://doi.org/10.3390/electronics8010111)
24. Bai, W., Lee, D., Lee, K.Y., 2017. Stochastic dynamic AC optimal power flow based on a multivariate short-term wind power scenario forecasting model. *Energies* 2017, 10, 2138; [doi:10.3390/en10122138](https://doi.org/10.3390/en10122138).
25. Thanh, L.Xuan 2017. Modified Algorithm for finding the optimal nod of closed-medium voltage grids. *Journal of Mining and Earth Sciences.* 58, 3 (Jun, 2017). Available from: <http://jmes.humg.edu.vn/en/archives?article=1191>
26. Dang, K.Quang and Tran, T.Trong 2019. Structural optimization of Ha Tinh city medium voltage grid by loop cutting algorithm (in Vietnamese). *Journal of Mining and Earth Sciences.* 60, 2 (Apr, 2019). Available from: <http://jmes.humg.edu.vn/en/archives?article=1000>
27. Michel Soustelle. *Phase Modeling Tools: Applications to Gases*. John Wiley & Sons. 2015.
28. Phil Lucht. *The Method of Lagrange Multipliers*. Rimrock Digital Technology, Salt Lake City, Utah 84103 last update: Oct 29, 2016. [online] Available at: <http://user.xmission.com/~rimrock/Documents/The%20Method%20of%20Lagrange%20Multipliers.pdf>
29. Salih, A., 2013. *Method of Lagrange Multipliers*. Department of Aerospace Engineering. Indian Institute of Space Science and Technology, Thiruvananthapuram – September 2013. [online] Available at: <https://www.iist.ac.in/sites/default/files/people/Lagrange-Multiplier.pdf>

Strategy in Dispatching Trucks and Shovels with Different Capacity to Increase the Operating Efficiency in Cao Son Surface Coal Mine, Vietnam

PHAM Van Hoa^{1,*}, TRAN Trung Chuyen¹, LE Hong Anh¹, LE Thi Thu Hoa¹, PHAM Van Viet¹,
NGUYEN Anh Tuan¹, LE Thi Huong Giang¹

¹ Hanoi University of Mining and Geology, 18 Vien street, Hanoi, Vietnam

Corresponding author: phamvanhoa@hmg.edu.vn

Abstract. In surface mining operations, the operating costs of truck-shovel system constitutes 50-60% of the total. Only a little save in the operation costs in this system will bring large profit for the mines. Due to many investment periods, the capacity of both trucks and shovels in Cao Son surface coal mine is different. This leads to the low efficiency and the difficulty in dispatching strategy for the mine. This paper presents the current situation and selection of advanced dispatching strategy for increasing the efficiency trucks and shovels at this surface coal mine. The results show the detailed match factor reflects the state of each team of loader and trucks and should be use as the indicator for dispatching decision for the heterogeneous truck and shovel fleet at Cao Son surface coal mine.

Keywords: Truck dispatching, Truck-shovel system, Dispatching strategy, Detailed match factor

1. Introduction

Cao Son surface coal mine is one of the biggest coal mines in Vietnam. Currently, the total volume of waste rock that need to be loaded and hauled is from 26 to 32 million m³/year. Trucks and shovels are used for loading and transporting of waste rock directly to the outside waste dumps or to the crusher of conveyor belt system. In 2017, there was about 50.58% of waste rocks transported by trucks to conveyor belt system (about 13 million m³). It was increased to 78.34% (17.8 million m³) in 2018. In 2020, the volume of waste rocks transported by the combination of trucks and conveyor belt in was increased to 20 million m³. Due to long operating time, the mine has invested many types of mining equipment and they are still operating together. There are both rope shovels and hydraulic excavators with different bucket's capacity from 3.3 m³ to 12 m³ using at the mine. About 20 electric rope shovels were invested about 40 years ago and the interruptions during shifts such as breakdown or maintenance may occur quite often. The other 11 newer hydraulic excavators are used for loading coal and waste rock. Due to the reduction in productivity of shovels and excavators over time, they are classified by into type A, type B and type C. The standard productivity of equipments type A is 110% higher than type B, and equipments type C is about 85% productivity of equipments type B. For the mining trucks, the capacity of truck has the range from 27 – 96 tons, but only the trucks with capacity from 55-96 tons are selected to transport waste rock. The modern of trucks is quite diversity such as: CAT 777D (96 tons), HD 785-5 (91 tons), HD 465 (58 tons), CAT 773 E (58 tons), HD 465 (55 tons), Belaz-7555B. There is total 121 trucks with capacity from 55-96 tons using for hauling waste rock. The average haulage distance is about 3.9 km. By increasing the volume of waste rock transported by the combination of trucks and conveyor belt system, the average haulage distance was decreased to nearly 3 km (in 2020). As the general rule, when the mine is going deeper, difficult working conditions increase. In order to complete the delivery output, the older equipments have to increase working hours, overcome the longer haulage distance, and the productivity of mining trucks decline in rainy season due to slippery routes (Figs. 1, 2) [1].

According to the data, the percentage of machine utilization for electric rope shovels EKG – 4.6, 5A (with bucket's capacity of 4.6-5 m³) is about 32%, meanwhile, nearly 70% of their time for repairing or maintenance or other reasons such as: power-off: 1%; stopped by damage: 4%; shift handover: 16%; repair time: 2%; stopped by other reasons: 45%. Other type of electric rope shovels, the rope shovel EKG 8i, also have low working time, about 38%. The situation is better for the hydraulic excavators with about 63% working time, and 37% waste time for other activities. There are also 8 types of loaders with the difference in bucket capacity. At this time, the dispatchers of the mine are usually based mostly on their experiences to allocate the trucks to these diversity types of excavators [2].

The operating costs for truck haulage usually takes about 50 to 60 percent [3]. Even a small improvement in this shovel-truck system will bring profit for the mine. For Cao Son surface coal mine, their

heterogeneous truck and loader fleet needs to select a suitable dispatching strategy. In this paper, the dispatching strategy is based on our GPS tracking app on smartphone which is placed in trucks and shovels for tracking their real time positions and other timing parameters for dispatching work. The GPS data are collected and sent directly to the management software for optimization calculation. The ability to increase the dispatching strategy of the mine can not do without the support of real time GPS information and with the help of new modern developed managing trucks and shovels software. Dispatching strategies for truck – shovel fleet in an open pit mine has important roles that will bring a good approach for operating this job on site.

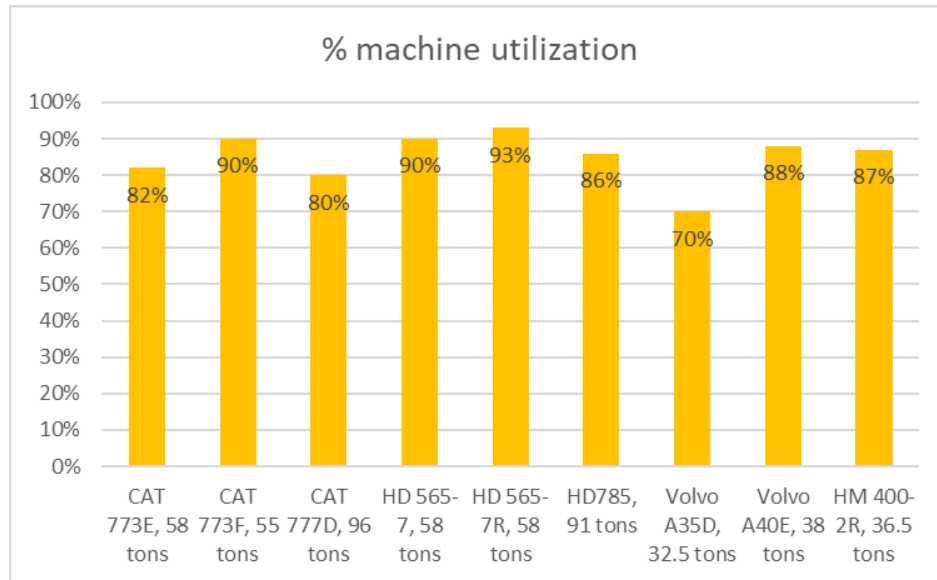


Fig. 1. The % machine utilization of some types of mining trucks at Cao Son surface coal mine [2].

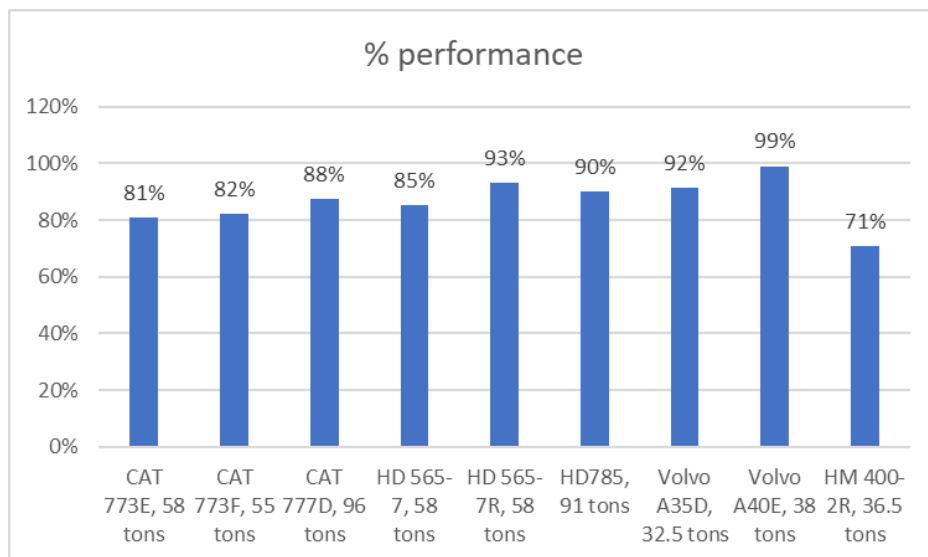


Fig. 2. The % performance of some mining trucks at Cao Son surface coal mine [2].

2. The hardware and software for managing and dispatching truck – shovel fleet

The management of a large truck -shovel fleet on a surface mine is always a priority for the improvements for many generations. These improvements on dispatching system are mostly based on the development of interdisciplinary fields such as: electronics, telecommunication, computer technology... From the computerized truck dispatching systems which were developed in late 1970's with higher price of hardware, to the cheaper systems due to the decrease in costs of computer hardware, the truck dispatching systems are classified into: manual, semi-automated and full automated. Today, lots of truck dispatching systems are based on current modern technologies. Based on current advantages, our project is to build a semi-automated truck – shovel dispatching system for Cao Son surface coal mine (Fig. 3).

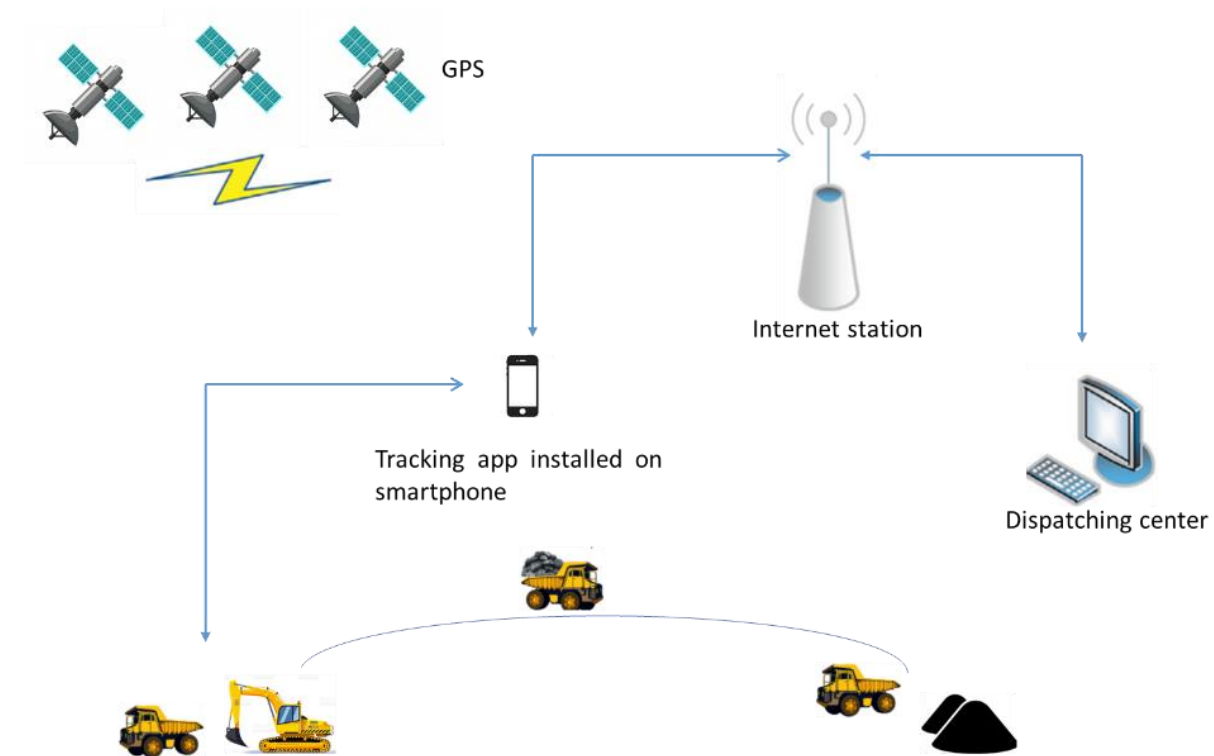


Fig. 3. Diagram of dispatching truck-shovel system for Cao Son surface coal mine [2].

The introduced system includes: software and hardware. The apps installed on smartphones and is placed on trucks or shovels for tracking the real time position, interacts between users and dispatching center and then send the data to dispatching center for analysis. The managing and dispatching software is installed on server and access by computer or other mobile devices such as ipad, tablet. The data from the trucks or shovels is transferred through communication network to the center dispatching software. Fig. 3 presents the diagram of dispatching truck-shovel system developed for Cao Son surface coal mine. When there are four or more satellites in the view, the GPS device integrated inside smartphones will calculate the information such as: velocity, position... The GPS device can work in any weather conditions, 24 hours per day and anywhere on earth [10, 11]. The realtime position of trucks and shovels and their timing data will be used for the next steps of analyzing and optimizing calculation. The dispatchers can monitor real time the loading and hauling activities of mine on the screens through the computer connected to internet.

The tracking apps installed smartphones with the function to monitor the timing parameters such as: loading time, truck cycle time, breakdown, unloading time, waiting time... These timing parameters is the basis for dispatchers and the system give a suitable dispatching decision for whole system.

3. Selection of dispatching strategy

Many dispatching strategies have been introduced such as: maximize truck, maximize shovel, match factor. In strategy of maximize truck, the available trucks are constantly reassigned to the shovel where they are most likely loaded first. When a truck is available for the calculation, many parameters such as: travel time of empty trucks end route, trucks waiting, and trucks being served of each shovel must be considered. The maximize truck strategy will increase the total productivity in comparison to fixed dispatching [4]. In this strategy, the utilization of shovel tends to disbalanced due to this dispatching procedure favors truck to shorter routes [5].

In strategy of maximize shovel, the truck is assigned to the shovel which has been waiting the longest or may be idle next [4]. The research from Sassos [6] showed this strategy brought a more uniform utilization of shovel.

Match factor is used as an indicator of productivity performance, and it is also a sign for the balance or unbalance of truck-shovel feet which strongly influenced on the performance of the system. The term match factor is defined as the ratio between truck arrival rate to loader service time. For the homogeneous truck and loader fleet (all the trucks are the same types and all the loader are the same type) [7]:

$$MF = \frac{\text{No. of trucks} \times \text{loader cycle time}}{\text{No. of loader} \times \text{truck cycle time}} \quad (1)$$

Match factor of 1.0 is used as balance point. At this value, the trucks are arriving at the loader at the same rate as they are being served. A match factor is bigger than 1.0, that means trucks are arriving faster than they are being served (over-trucking). If a match factor is smaller than 1.0, this indicates that trucks are arriving slower, and the loader can serve faster (under-trucking).

For heterogeneous haulage and homogenous loading fleet, the match factor can be defined [8]:

$$MF_i = \frac{x_i}{t_i \sum_{i'} \frac{x_{i'}}{t_{i,i'}}} \quad (2)$$

Where: MF_i - the match factor for heterogeneous haulage and homogenous loading fleet;

x_i – number of trucks of type i ;

t_i – cycle time for truck of type i ;

$x_{i'}$ - number of loaders of type i' ;

$t_{i,i'}$ - time taken to load truck type i with loader type i' ;

The match factor with some advantages such as: it is simple and can be applied to both homogeneous and heterogeneous, it can be predicted the mean waiting time. However, the disadvantages when using match factor are the performance of each loader can not be determined, the trucks cannot be precisely allocated to the loaders, can not control the grade and tonnage of a mine. To solve this problem, a detailed match factor (DMF) is determined for each loader individually and then used as a dispatched indicator for the fleet. According to Dabbagh A. & Bagherpour R. [9], the trucks and loaders may operate at their maximum capacity with the match factor of approximately 1.0, at this value the number of loading and haulage equipment is balanced. In a whole system with many loaders, the detailed match factor is determined for each loader separately. If the detailed match factor is bigger than 1, then the dispatcher will attempt to reduce the number of haulage equipments for this loader. In the opposite case, if the detailed match factor is smaller than 1.0, it means the loader needs to add haulage equipments to get the value of DMF as close to 1 as possible. It can be easily realized that if the detailed match factor of any loader is smaller than 1.0, the capacity of trucks and loaders is reduced without interrupting in the mining operation [9].

The Cao Son surface coal mine has the heterogeneous trucks and loaders fleet, in this research we focus on the dispatching strategy for the heterogeneous fleet of the mine.

The detailed match factor for a team of a loader and trucks can be determined [9]:

$$DMF_{i'} = \frac{\sum t_{i,i'} x_i}{\bar{t}_X} \quad (3)$$

x_i - number of truck type i

\bar{t}_X - average cycle time for the trucks

$$\bar{t}_X = \frac{\sum_i t_i x_i}{\sum_i x_i} \quad (4)$$

t_i - cycle time for truck of type $i \in X$;

X - group of available trucks

The overall match factor of heterogeneous truck and loader fleets [8]:

$$MF = \left(\bar{t}_X \sum_{i'} \frac{x_{i'}}{t_{i'}} \right)^{-1} \quad (5)$$

With the hypothesis that the detailed match factor of each team of loader and trucks will be an indicator for the dispatcher in allocating the trucks in working shift. In this paper, the relationship between detailed match factor and overall match factor for heterogeneous truck and loader fleet will be examined.

4. Selection of the dispatching strategy for truck – shovel fleet at Cao Son coal mine

The loaders and trucks which are mostly used for waste rock haulage at Cao Son coal surface mine are presented in Tables 1 and 2.

Tab. 1. Some loaders used for waste rock haulage at Cao Son mine.

No.	Type	Bucket capacity, m ³	Number
1	Rope shovels EКГ – 4,6; EКГ – 5A	4.6 to 5.0	11
2	Rope shovels EКГ – 8И	8	8
3	Rope shovel EКГ – 10	10	1
4	Komatsu PC1800-6	12	1
5	Komatsu PC1250	6.7	4

Tab. 2. Some trucks used for waste rock haulage at Cao Son mine.

No.	Type	Capacity, tons
1	CAT 777D	96
2	HD 785	91
3	HD 465 - 7	58
4	CAT 773 E, F	58
5	HD 465 -5	55

To analyze the influence of dispatching strategy on the truck-shovel, some combinations between loaders and trucks were examined. The examined teams of loader and trucks service for routes at Cao Son surface coal mine are presented in Table 3. The density of blasted waste rock is of 1.6 tons/m³. The bucket filling factor is 0.87, the bucket capacity of loader is exchanged unit into tons.

Tab. 3. Dispatching plan 1 for 3 teams of truck and shovel at Cao Son surface coal mine.

Team 1(route distance L ₁ = 3.5 km)	Parameters		Truck (loader) cycle time, s	Time required for full load of one truck, s	Detailed match factor DMF	Overall match factor MFE	
	Number of machines	Capacity, tons					
Loader EKG 8u	1	18	35		0.69	0.94	
Truck CAT 777	4	96	1764	210			
Truck CAT 773	2	91	1680	175			
Team 2 (route distance L ₁ = 3.7 km)							
Loader EKG 5A	1	11	35		0.96		
Truck CAT 777	3	96	1900	315			
Truck CAT 773	3	61	1800	280			
Team 3 (route distance L ₁ = 3.85 km)							
Loader PC-1250-8	1	15	35		1.1		
Truck CAT 773	7	58	1670	140			
Truck HD 465-5	6	55	1620	140			

In dispatching plan 1, team 1 has the DMF₁ of 0.69 (smaller 1.0), so this team is lack of truck and needs to add trucks. In team 2, the detailed match factor DMF₂ is of 0.96 (it's close to 1.0). In team 2, the number of trucks is nearly balanced with the service rate of the loader (a little undertruck). If the dispatcher adds 1 more truck to the team 2, then the value of DMF₂ is bigger than 1.0 that means this team will be overtrucked. In this case, the dispatcher should not change the number of trucks for team 2. For team 3, the detailed match factor DMF₃ is of 1.1, this means it is overtrucked. If the dispatcher withdraws 1 truck from this

team, then the detailed match factor DMF_3 will be equal to 1.0. This case it is a good dispatching decision, and the dispatcher should allocate 1 truck from team 3 to team 1.

Tab. 4. Dispatching plan 2 for 3 teams of truck and shovel at Cao Son surface coal mine.

Team 1 (route distance $L_1 = 3.5$ km)	Parameters		Truck (loader) cycle time, s	Time required for full load of one truck, s	Detailed match factor DMF	Overall match factor MF_{Σ}	
	Number of machines	Capacity, tons					
Loader EKG 8u	1	18	35		1.34	0.96	
Truck CAT 777	6	96	1764	210			
Truck CAT 773	6	91	1680	175			
Team 2 (route distance $L_1 = 3.7$ km)							
Loader EKG 5A	1	11	35		1.12		
Truck CAT 777	3	96	1900	315			
Truck CAT 773	4	61	1800	280			
Team 3 (route distance $L_1 = 3.85$ km)							
Loader PC-1250-8	1	15	35		0.6		
Truck CAT 773	3	58	1670	140			
Truck HD 465-5	4	55	1620	140			

In the dispatching plan 2, the detailed match factors of team 1 and team 2 are bigger than 1.0, they are of 1.34 and 1.12, respectively. That means, both team 1 and team 2 are overtrucked. However, in team 2, the detailed match factor is of 0.6 and it's largely undertrucked. It may need to add trucks from team 1 and/or team 2 to make the balance between truck service rate and loader service rate for each team of trucks and loader.

The overall match factor for dispatching plan 1 is of 0.94, and the overall match factor for dispatching plan 2 is of 0.96. If the dispatcher only looks at the values of the overall match factors in both dispatching plan 1 and 2, these overall indicators show the nearly balance between truck service rate and loader service rate for the fleet. In both plans, there is team of undertrucked loader with the detailed match factor much less than 1.0, and this team need to add more trucks to meet the requirement. There is also a team of overtrucked loader with the detailed match factor bigger than 1.0, and this team should reduce the number of trucks or dispatch the trucks to the teams with detailed match factor smaller than 1.0 (if is suitable).

From analyzing these above dispatching plans 1 and dispatching plan 2, it can be easy realized that the overall match factor does not show the effect inside of the truck-loader fleet. However, the detailed match factor for each team reflects the balance or unbalance of each team of loader and trucks. For the Cao Son surface coal mine with a heterogeneous truck and loader fleet, the dispatching strategy using detailed match factor of teams of loader and trucks as the indicator for dispatching procedure should be selected. The software bases on the detailed match factor to filter out the teams of loader and trucks that need to add or withdraw trucks. The dispatcher can choose the auto or semi-automated dispatching procedures for allocating trucks to loader with the purpose to balance the truck service rate and loader service rate (the detailed match factor for each team of loader and trucks should be as close as 1.0). Fig. 4 shows a diagram which presents an example that the trucks in team 2 can be dispatched to team 1 to make the balanced for the fleet. This can be done if the detailed match factor of team 1 is smaller than 1 and of team 2 is bigger than 1. In case the detailed match factors of team 1 and team 2 are smaller than 1, then the fleet have to add trucks.

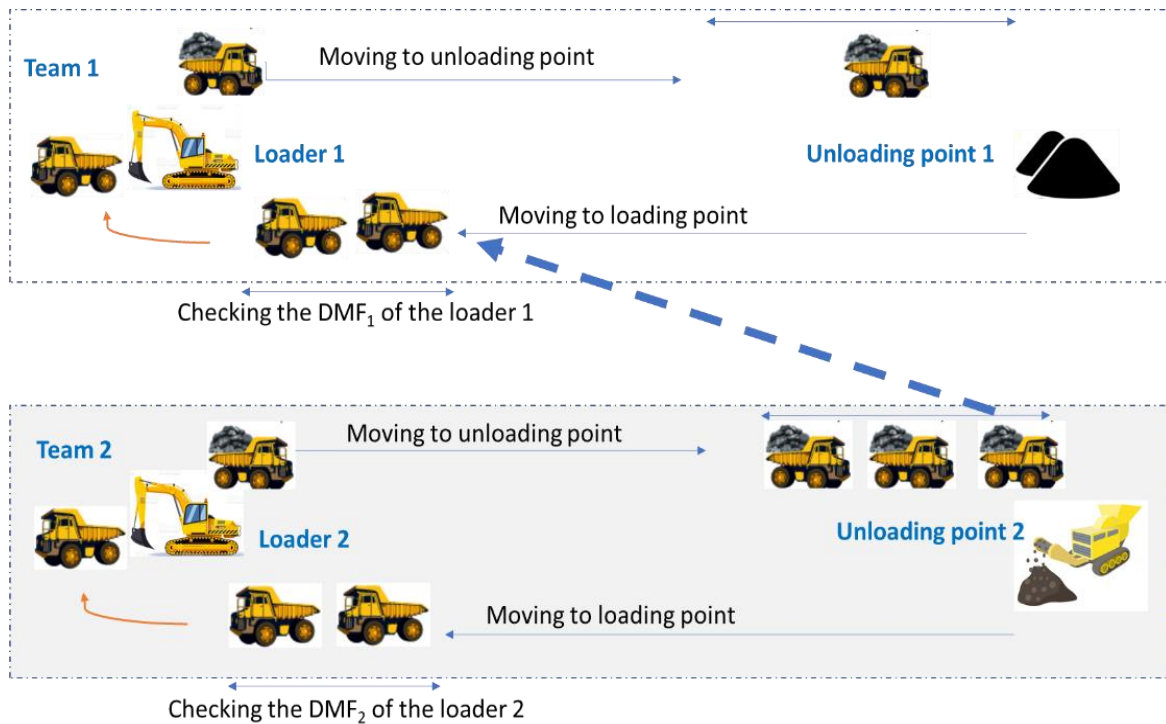


Fig. 4. Diagram presents the dispatching strategy for truck-shovel fleet for Cao Son surface coal mine.

5. Results and discussions

From the above analysis, it can be seen that the dispatching strategy using the detailed match factor reflects the state of each team of loader and trucks. With the realtime information of the trucks and loaders in the mines, any changes in truck cycle time, loader cycle time, waiting time, breakdown of the machines... that lead to the change in the detailed match factor of each team of loader and trucks. Therefore, the detailed match factor will be very helpful indicator for the dispatchers in effectively doing their work.

The balance point between loader service rate and trucks service rate or the detailed match factor is equal to 1.0 is the criterion for controlling the dispatching trucks in the system. In case of the heterogenous trucks and loaders fleet of Cao Son surface coal mine, the value of detailed match factor for each team of loader and trucks should be kept as close to 1.0 as possible. Mostly, the little undertrucked allocation can be accepted to keep the loaders time for auxiliary works at loading points.

6. Acknowledgements

The paper was presented during the 6th VIET - POL International Conference on Scientific-Research Cooperation between Vietnam and Poland, 10-14.11.2021, HUMG, Hanoi, Vietnam.

7. References

1. Pham Van Hoa, Bui Xuan Nam, Le Van Quyen, Le Thi Thu Hoa, and Pham Van Viet, 2019. Estimation of truck-shovel dispatching in Cao Son Open-Pit coal mine and the ability in applying information technology for increasing its efficiency, *Inżynieria Miner.*, 21(2): 21-27, 2019, <http://dx.doi.org/10.29227/IM-2019-02-53>.
2. Vinacomin, 2018, Technical data of Cao Son surface Coal mine (company document).
3. Alarie, S. and Gamache, M., 2002, Overview of solution strategies used in truck dispatching systems for open pit mines, *Int. J. Surf. mining, reclamation environment*, 16(1): 59-76, <https://doi.org/10.1076/ijsm.16.1.59.3408>.
4. Lizotte, Y., Bonates, E. and Leclerc, A., 1987, A design and implementation of a semi-automated truck/shovel dispatching system," *APCOM 87 Proc. 20th*, 1(3): 377-387, [Online]. Available: <http://www.saimm.co.za/Conferences/Apcom87Mining/377-Lizotte.pdf>.
5. Tu, J.H., Hucka V.J., 1985, Analysis of Open-Pit Truck Haulage Systems by Use of a Computer Model, *CIM Bull.*, 78(879): 53-59.

6. Sassos, M.P., 1984, Reserve's mine management system," E&MJ, pp. 42–49.
7. Burt, C.N. and Caccetta, L., 2007, Match factor for heterogeneous truck and loader fleets Int. J. Mining, Reclam. Environ., 21(4): 262–270, <https://doi.org/10.1080/17480930701388606>.
8. Burt, C.N., 2008, An Optimization Approach to Materials Handling in Surface Mines, Curtin University of Technology.
9. Dabbagh, A. and Bagherpour, R., 2019, Development of a Match Factor and Comparison of Its Applicability with AntColony Algorithm in a Heterogeneous Transportation Fleet in an Open-Pit Mine, J. Min. Sci., 55(1): 51–63, <https://doi.org/10.1134/S1062739119015287>.
10. Pham, K.Cong 2020. Research on technical solution of displacement and deformation monitoring of high-rise buildings in real time. Journal of Mining and Earth Sciences. 61, 3 (Jun, 2020), 75-87. DOI:[https://doi.org/10.46326/JMES.2020.61\(3\).09](https://doi.org/10.46326/JMES.2020.61(3).09).
11. Pham, K.Cong and Nguyen, H.Van 2020. Investigation and design of monitoring systems in real time landslides at Xekaman 3 hydropower plant (in Vietnamese). Journal of Mining and Earth Sciences. 61, 1 (Feb, 2020), 11-20. DOI:[https://doi.org/10.46326/JMES.2020.61\(1\).02](https://doi.org/10.46326/JMES.2020.61(1).02).

The capability of terrestrial laser scanning for monitoring the displacement of high-rise buildings

PHAM Trung Dung¹, PHAM Quoc Khanh^{1*}, CAO Xuan Cuong¹, NGUYEN Viet Hung², NGO Sy Cuong³

¹ Hanoi University of Mining and Geology, Department of Engineering Surveying, Hanoi, Vietnam

² University of Transport and Communications, Faculty of Information Technology, Hanoi, Vietnam

³ Vietnam Natural Resources and Environment Company

Corresponding author: phamquockhanh@hmg.edu.vn

Abstract. Recently, terrestrial laser scanner (TLS) has been increasingly used to monitor of displacement of high-rise buildings. The main advantages of this technique are time-saving, higher point density, and higher accuracy in comparison with GPS and conventional methods. While TLS is ordinary worldwide, there has been no study of the capability of TLS in monitoring the displacement of high-rise buildings yet in Vietnam. The paper's goal is to build a procedure for displacement monitoring of high-rise buildings and assess the accuracy of TLS in this application. In the experiments, a scanned board with a 60 cm x 60 cm mounted on a moveable monument system is scanned by Faro Focus^{3D} X130. A monitoring procedure using TLS is proposed, including three main stages: site investigation, data acquisition and processing, and displacement determination by the Cloud-to-Cloud method (C2C). As a result, the displacement of the scanned object between epochs is computed. In order to evaluate the accuracy, the estimated displacement using TLS is compared with the real displacement. The accuracy depends on scanning geometry, surface property, and point density conditions. Our results show that the accuracy of the estimated displacement is within ± 2 mm for buildings lower than 50 m of height. Thus, TLS completely meets the accuracy requirements of monitoring displacement in the Vietnam Standards of Engineering Surveying. With such outstanding performance, our workflow of using TLS could be applied to monitor the displacement of high-rise buildings in the reality of geodetic production in Vietnam.

Keywords: Terrestrial laser scanner, monitoring of displacement, the accuracy of displacement, high-rise buildings

1. Introduction

Monitoring the displacement of high-rise buildings has been a topic of great relevance. The displacement of these constructions is caused by the types of structure and the load's unpredictable and changing nature. Hence, monitoring of the high-rise buildings is needed to secure and preserve the safety of these constructions. In Vietnam, GPS and other conventional methods (e.g., levelling, theodolite, and total station) are widely used for monitoring displacement of the high-rise buildings. These methods can only monitor a specific number of points, restricting the estimation of the displacement of constructions. By contrast, TLS allows collecting massive points known as a point cloud from the monitoring object. A key element of monitoring displacement is transforming several epochs into one standard coordinate system. Typically, the standard coordinate system is a geodetic coordinate system that is determined by some reference points. At reference points, artificial targets like check boards or spheres are fixed on these points. The stable points are to detect an absolute displacement of the object that occurred in among epochs. In displacement monitoring by using TLS, the same monitoring object at different epochs is compared. Two basic algorithms normally used for identifying the displacement are test and comparison [1]. While the test method does not allow measuring the displacement quantitatively, the compare method enables us to solve this issue. The displacement of the monitoring object is measured by the distance between two-point clouds of different epochs.

TLS was widely applied in the field of deformation monitoring, such as structural monitoring [2], tunnel deformation monitoring [3], dam and tower monitoring [4], and deformation monitoring of a steel structure [5]. The deformation monitoring using TLS can also find in related studies [6, 7, 8, 9]. However, in this field, both a standard rule and a comprehensive evaluation of the accuracy of TLS is lack. Few published works applied TLS for monitoring displacement and deformation of construction based on conventional geodetic methods. That procedure includes site investigation, data acquisition, data processing, and data analysis. A procedure of the three-stage process model [10] is developed to compute the deformation of a dam by block

to point estimation and fine registration Iterative Closest Point (ICP). This procedure, then, is developed to become multiscale-model-to-model cloud comparison (M3C2), piecewise alignment, and block to point methods [8].

To evaluate the accuracy of TLS, Lindenbergh and Pfeifer [7] presented an investigation on the accuracy of Leica HDS2500 on the monitoring of a locked door. This issue can find in other evaluations of the accuracy of TLS for the health monitoring of structure [8, 11, 12]. The scanning geometry, materials, colour and roughness of properties, weather conditions such as wind, temperature, and humidity are important factors influencing the scan quality [13, 14, 15]. In the displacement monitoring of high-rise buildings, building characteristics that could affect scan quality should be considered, such as scanning geometry and the structure's surface material. This paper aims to develop a procedure for monitoring the displacement of high-rise buildings and evaluate the accuracy of TLS considering these influencing factors.

The paper presents the following structure and organization: after this introduction, Section 2 describes the methodology developed for displacement analysis and procedure for monitoring displacement of high-rise buildings. Section 3 presents the experiment. The influence of some potential factors on scan quality is investigated in section 4. The final section is conclusions, limitations, and future works of TLS for monitoring displacement of high-rise buildings.

2. Methodology

2.1. Displacement analysis

The displacement of an object can be computed directly by comparing the location of this scanned object at different epochs. Computation distance for two point-clouds can find in Lague, Brodu [16]. The point-to-point approach is widely used for displacement monitoring when the number of measured points is limited. This approach is called the point-wise comparison (see [17]) and is applied for monitoring mining excavation. Since a high point density can be acquired by TLS, the cloud-to-cloud (C2C) distance should be used [18]. This approach is the fast and straightforward direct comparison of point cloud because it does not require any data meshing. The C2C (Fig. 1) method applied in CC software estimates the distance between two-point clouds in which one of them is the reference or model cloud, and another is the compared cloud. Apart from C2C, the distance between two clouds can be computed by the cloud-to-mesh distance (C2M) [19], which is also a common techniques in inspection software. However, creating a surface mesh is complex for point clouds when a surface is not flat or missing data due to occlusion [16]. Hence, the C2M method is not discussed in the limitation of this study.

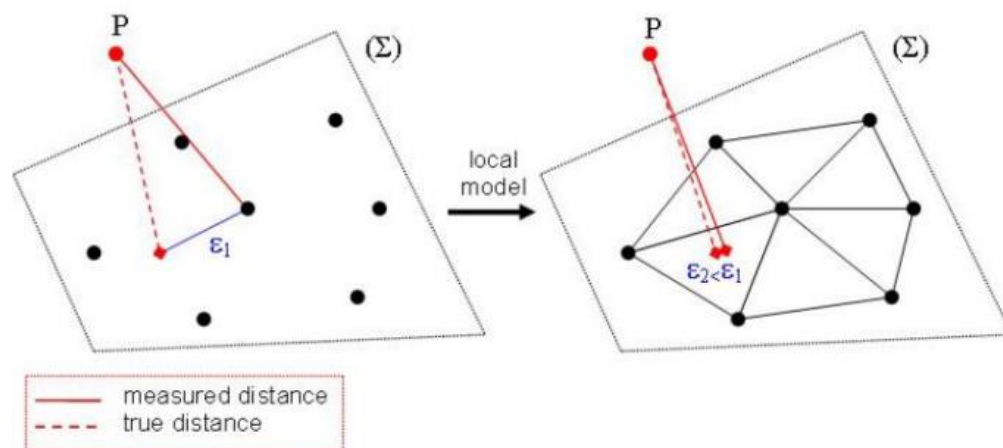


Fig. 1. The concept of local surface model of C2C method. The local surface allow us to better approximate measured distance ($\epsilon_2 < \epsilon_1$) [20].

The C2C approach applies the Hausdorff distance, which is defined by a max-min distance. The brief introduction of this distance can be described as follows. Given two finite point sets $A = \{a_1 \dots a_p\}$ and $B = \{b_1 \dots b_p\}$, the Hausdorff distance is defined as [21]:

$$H(A, B) = \max(h(A, B), h(B, A)), \quad (1)$$

where

$$h(A, B) = \max_{a \in A} \min_{b \in B} \|a - b\|, \quad (2)$$

and $\|\cdot\|$ is a norm on the points of A and B (e.g., the Euclidean norm).

Function $h(A, B)$ is called the directed Hausdorff distance from A to B. This approach is also used in cloud matching techniques such as ICP (Iterative closest points) [22].

2.2 Procedure of displacement monitoring

In displacement monitoring of high-rise buildings, the survey procedure is still an open question in TLS, and there have been no standard rules have in Vietnam yet. However, like any type of geodetic survey (e.g., theodolites, total station), initial planning is fundamental for deriving all necessary information on the objects scanned. Currently, to the author's best knowledge, a procedure for monitoring displacement of high-rise buildings includes the main stages as follows:

First, in the investigation stage, the information about the surveyed object needs to be collected. Large-scale maps and existing reference points are helpful in this respect. A preliminary scan with a low resolution is useful for further planning tasks if the surveyed area is large.

In the second stage, to acquire the expected resolution and accuracy of the point cloud, the parameters of resolution and quality should be set up [23]. The required accuracy in the determination of displacement depends on the types of constructions. According to the Vietnam construction standard (TCVN-9399), the accuracy for monitoring the displacement of high-rise buildings is 1/10.000 building's height (e.g., the accuracy of 10 mm with corresponding 100 m in high). Hence, the resolution and quality are set up at a considerable high level to meet the corresponding high accuracy requirement. Besides, the artificial targets (e.g., checkboard or sphere) are used to reduce errors in the registration and alignment. The types of targets and places for their locations to guarantee a good geometric configuration have to address. In the monitoring displacement of high-rise buildings (e.g., towers), the ground floor is assumed to be a stable area used to compute the displacement of unstable parts in higher floors. Because the displacement of a high-rise building is relative movement, a local coordinate system can be used instead of a geodetic reference coordinate system. Hence, we can be neglected georeferencing approach as well as its error.

The third stage of this procedure is to compute the displacement between two registered point clouds. The alignment between two point clouds is done by using pair points. At least three pairs are chosen at the stable area on the ground floor or by artificial targets centring on benchmarks. The alignment is to transform all epochs into a common coordinate system of the first epoch. Two different point clouds then are compared in which the point cloud at the first epoch is the reference cloud, and another one is compared cloud. In practice, the whole object is scanned, but only some parts of constructions are actual displacement. Some other parts are not actual displacement (e.g., setting up new equipment). Hence, segmentation that allows the automatical segmenting of several pieces from the point cloud is applied to solve this issue. The principle of segmentation is based on the same feature of objects. (e.g., properties, colour) [24]. This procedure is to extract the compared object that often planes, cylinders, etc. The segmentation had to be done in a similar procedure for all epochs. Then, segmented point clouds at corresponding epochs are compared using the C2C distance method described in section 2. Finally, the statistical parameters, including the mean of displacement and standard deviation of residuals, are estimated.

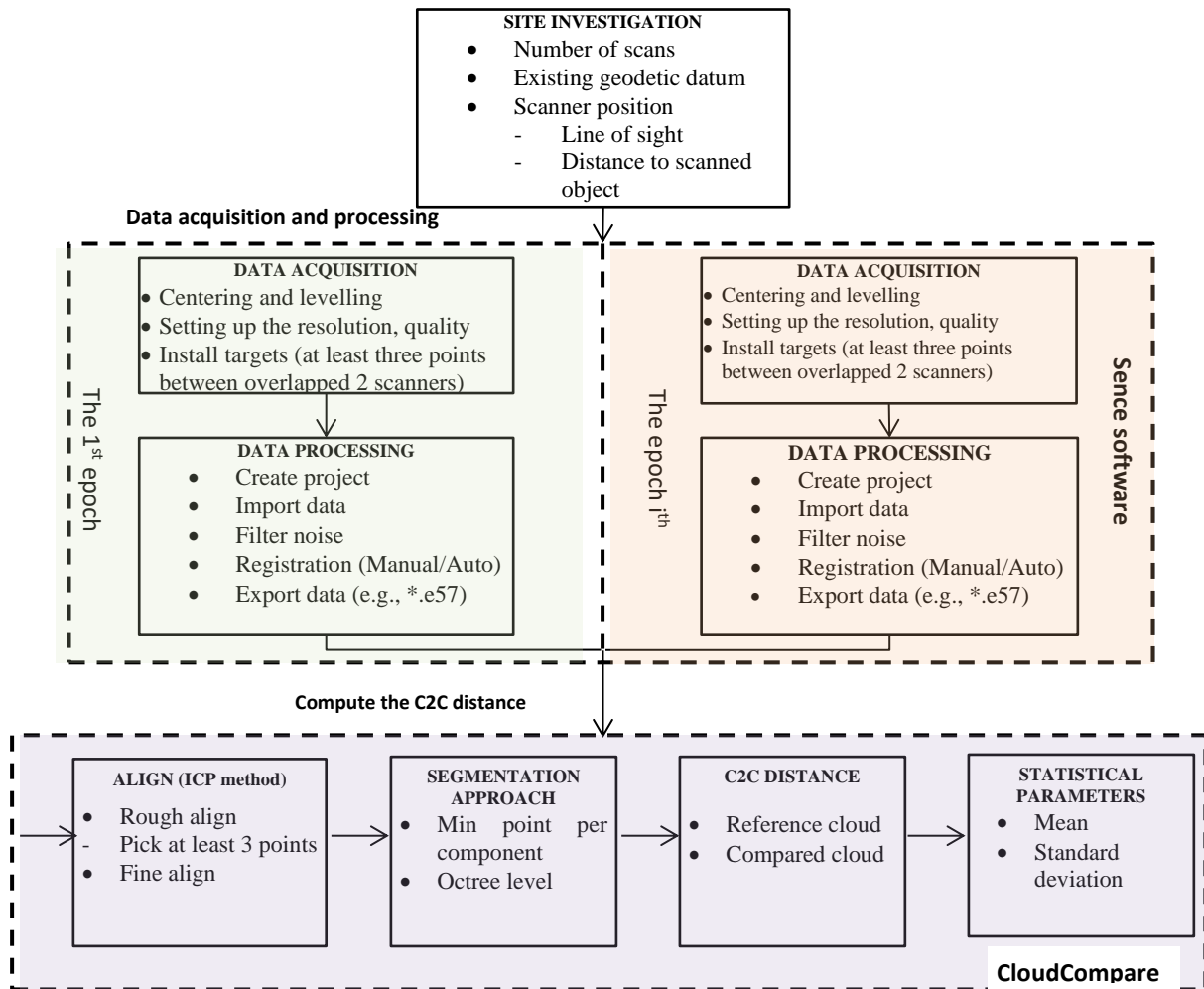


Fig. 2. The procedure for monitoring displacement of high-rise buildings using TLS.

3. Experiments

The displacement of an object can be determined by comparing its position at different times (epochs). In this study, the experimental data is collected by the Faro Focus^{3D} X130, that its specifications are listed in Tab. 1.

Tab. 1. Manufacturers' Specifications of Faro Focus^{3D} X 130.

Items	Character
Measure Technology	Phase shift
Vertical field of view	-60°-90°
field of view	0°-360°
Max. Range	0.6 m-130 m
Single point accuracy	±2 mm
Angular accuracy	0.005°
Max. Scan rate	976000 (pts/sec)
Max. resolution	1.5 x 1.5 mm at 10 m

The experimental measurements are carried out in three epochs at a high-rise building on the Hanoi University of Mining and Geology (HUMG) campus for three days (from 20th to 22nd February 2021). The artificial displacement is generated by using a movable board. This experimental board with a size of 60 cm x 60 cm is mounted on the steel monument. The steel monument can move on two parallel raids, and its displacement can be measured by a steel ruler with an accuracy of 0.2 mm (see Fig. 3). In the first epoch, the experimental measurement is scanned when scanned board is fixed at a certain position. In the second and third epochs, the experimental board is scanned after this moved back along the incident direction of the laser beam 10 and 20 mm, respectively. These artificial displacements are considered real displacements since errors in the determination of these displacements are sufficiently small.

TLS is a novel technique for monitoring of displacement of high-rise buildings in Vietnam. A reflectorless method is applied in TLS in which the reflectance that is defined as the ratio between reflected and incident laser power is the main factor influencing the scan quality. The potential factors that can impact the reflectance in the context of scanning high-rise buildings consist of the height of a scanned object, the incidence angle of the laser beam, the surface material of a scanned object. Thus, the experiment aims to investigate the influence of these factors on the scan quality. In addition, a sampling resolution strongly influencing the scan quality is evaluated in this experiment. The set of experiments and analysis results are presented in section 4. It is noting that the displacements between two epochs are computed by the C2C method using CloudCompare (CC) software in version 2.11.3.



Fig. 3. The experimental area and scanned board.

These experiments are to access the influence of some factors on the scan quality as follows:

The first experiment investigates the scanning geometry contribution due to the difference in the high of the scanned object on the scan quality. In the monitoring displacement of high-rise buildings, all construction parts in different high levels must be scanned to analyze the displacement and the bending line (e.g., a tower). In this study, an artificial displacement is created using the experimental board (more detail see in section 3), which is located at a distance of 20 m to the scanner. The board is placed on several floors with high levels of approximately 3 m, 6 m, 9 m, 12 m, 15 m, 52 m, as depicted in Fig. 5. It is worth noting that on the 14th floor, the distance from the scanner to the board is about 50 m. The high levels in this experiment are irregular due to the existing condition of HUMG's campus. Scanning geometry investigation could be helpful if object's scans have a complex shape or the difference in high, such as high-rise building structures like buildings and towers.

In the second experiment, the effect of the scanning geometry on the scanning quality is investigated by the incidence angle. The incidence angle is defined as the angle between the laser beam vector and the normal vector of the scanned surface [25]. This experiment simulates the case of a shortage of space for setting up scanning stations. High-rise buildings are usually built in an urban area where it is difficult or even impossible to find a suitable position to set up the scanner. Hence, the scanning geometries in monitoring high-rise buildings are bad in many cases. In this experiment, the experimental board is fixed at a certain position, while the scanner is changed in the range of 15 m and 20 m, respectively (Fig. 4).

The third experiment investigates the influence of surface materials of the scanned object on the scan quality. The reflectivity property of surface material is defined by the amount of light scattered relating to the wavelength of the laser light in use [15]. The surface materials of the scanned object are conducted by granite and concrete that are standard materials of high-rise building structures in Vietnam recently. The surface of granite is smoother than that surface of concrete, as depicted in Fig. 1. In this study, the evaluation is carried out by two surface materials of granite and concrete at six independent times. Each material is scanned from the same position. Other factors related to the surface of a scanned object like the clour are not discussed in the restriction of this study. This issue can find in [13, 26, 27].

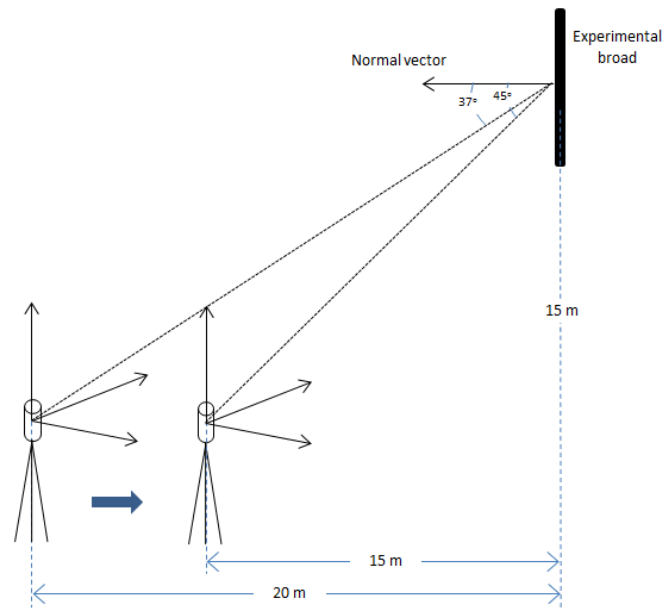


Fig. 4. Scanning geometry due to the incidence angle.

Lastly, the sampling resolution (or point density), another factor influencing scan quality, is investigated in this study. The higher the sampling resolution is set up, the more details of the scanned object can be acquired, but the scanning time also increases. Thus, the resolution parameter should be set for suitable to certain applications. This parameter can be set in the scanner before scanning, and it depends on manufacturers' specifications and scanned range. In general, the scanning resolution of phase-based scanners can provide a higher resolution than that of time-of-flight types. In this experiment, the resolution is examined in four different levels using Faro Focus^{3D} X130, which is a phase-based scanner. In Vietnam, other experiments of TLS for different applications (e.g., mining application) can find in [28,29].

4. Results

This section presents the influence of four potential factors as described in section 3 on the scan quality in the context of displacement monitoring for high-rise buildings. In the following analysis results, the difference value is compared between the real displacement and the distance estimated by the C2C method. It is reminded that the real displacements in the 2nd and 3rd epochs are 10 and 20 mm, respectively (see more details in section 3).

4.1 Influence of height of scanned objects on the scan quality

In this section, the influence of the scanning geometry is analyzed. The scanning geometry is investigated due to the difference in the height of the scanned object. Fig. 5 shows the displacement's mean and standard deviation values and the different values at the 2nd and 3rd epochs. The different value is small (between 0.2 and 0.6 mm) for both epochs. There is no significant different value when the height of the scanned object is less than 15 m (below 6th floors). The reason for this result is that the measured distances are not much different. In addition, the varying incidence angle (from 10° to 37°) in a short-range is insignificantly influenced by the scan quality. This result agrees with the investigation in [25]. The scan quality is not affected by the incidence angle between 0° to 40° with a 20 m measured distance. By contrast, on the 14th floor, the different value increases to approximately 2 mm in both epochs (2nd and 3rd epochs) due to poor scanning geometry. In this case, the distance from the scanner to the scanned object is about 50 m, and the incidence angle is 46°, leading to poor scanning geometry.

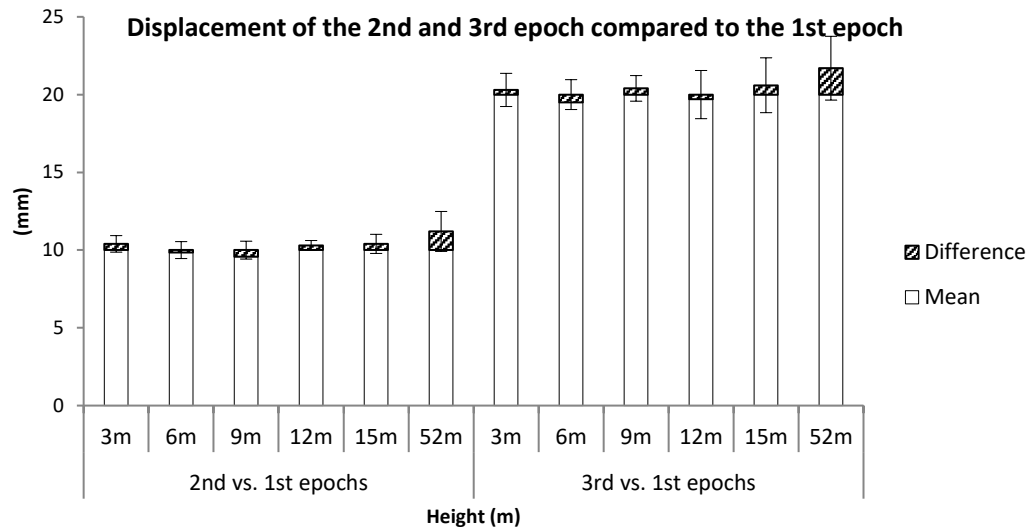


Fig. 5. The displacement measured by TLS with varying the height of a scanned object.

4.2 Influence of the incidence angle on the scan quality

Fig. 6 shows the influence of the incidence angle on the scan quality in two cases of 37° to 45° of the incidence angle. If the incidence angle is higher, the scan quality becomes worse. The different value in the displacement increases from approximately 0.5 to 1 mm. Similarly, an increased tendency of the standard deviation value can be seen in Fig. 6. These corresponding values increase from approximately 1 to 2 mm. These results agree with the theory that the received signal level influences the precision of the distance determination. Since the received signal level of measurements increases with decreasing incidence angles. However, this influence behaviour of the incidence angle on scan quality doesn't investigate in the scope of this study.

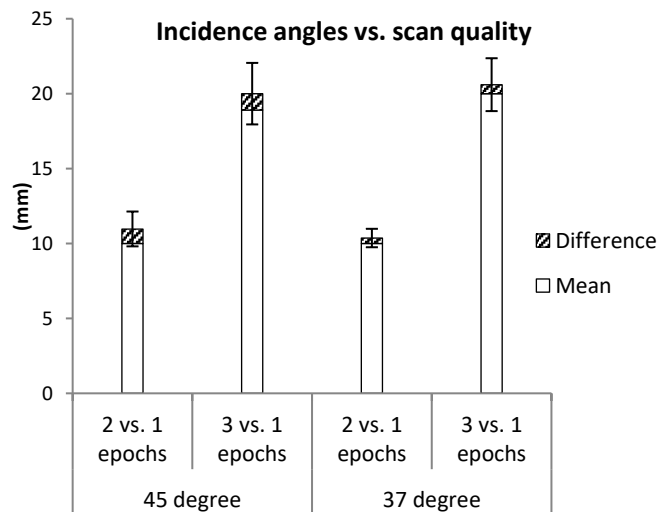


Fig. 6. Influence of incidence angle on scan quality.

4.3 Influence of surface materials of scanned objects on the scan quality

The influence of surface material on scan quality is pointed out by the displacement's mean and standard deviation values (Fig. 7). The displacement of the scanned object is compared between the 3rd epoch and the 1st one. Since the granite surface is smoother than the concrete surface (see Fig. 3), the reflectivity of the granite is better than the reflectivity of concrete. Thus, the determination of displacement using the granite material is approximately 1.5 to 3.0 times more accurate than that of concrete in this study.

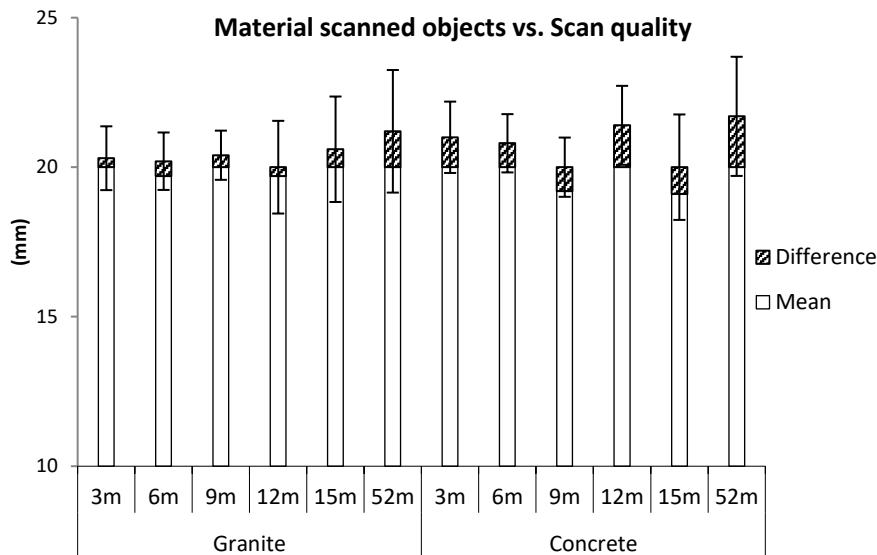


Fig. 7. Influence of surface material on scan quality.

4.4 Influence of Sampling resolution on the scan quality

The point density has a significant influence on the scan quality (Fig. 8). The difference in mean value between displacement calculated by the C2C method and the real one increases dramatically with decreasing the point density. This value increases from 0.1 to 3.3 mm when the point density reduces from 10000 to 750 points. Similarly, the STD also increases quickly from 1 to 3.2 mm by decreasing the density to 750 points.

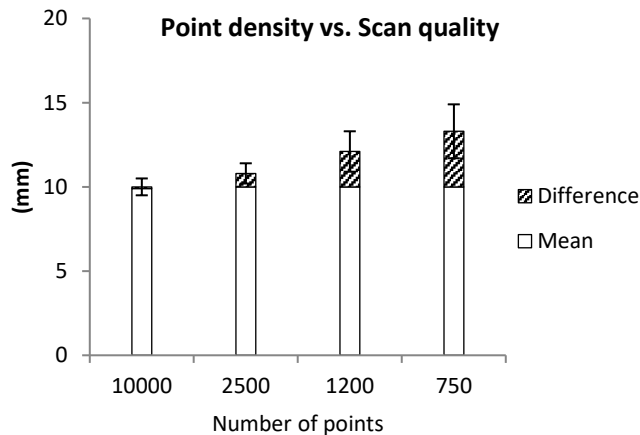


Fig. 8. The influence of sampling resolution on the scan quality.

5. Conclusions

The main goal of this paper is to assess the capacity of TLS on the displacement monitoring of high-rise buildings. This issue has been an initial stage in surveying engineering in Vietnam. In this paper, the main contributions are building a procedure for displacement monitoring of high-rise buildings using TLS and evaluating its accuracy for displacement monitoring.

First, the procedure for monitoring the displacement of high-rise buildings is proposed, including three main steps of site investigation, data acquisition, and processing, and compute the displacement through the distance between two-point clouds. In this procedure, a free coordinate system is used to avoid the error of georeferencing. Moreover, the artificial target is also utilized to improve the accuracy of both registration and alignment procedures.

Second, the accuracy of TLS is sufficient for monitoring the displacement of high-rise buildings according to the Vietnam construction standard. The displacement accuracy is smaller than 2 mm for a scanned object that is lower than 50 m in height. Although it takes a longer time to collect the data with

high point density, the author suggests that a moderately high resolution need to be used to meet the high requirement of accuracy in monitoring displacement. In addition, the paper indicates that the surface material and scanning geometry due to the distance and incidence angle are the main factors that influence the scan quality of TLS for a building higher than 20 m.

Several potential limitations of this study should be noted. First, the influence of error of registration and alignment procedures on displacement accuracy is not considered. Second, the scanned object in this experiment is limited to about 50 m in high. The behaviour impact of the incidence angle on scan quality is not studied in this paper.

In future work, other methods for estimating the distance between two different point clouds (e.g., mesh to cloud method) are worth investigating. The weather conditions, such as humidity, wind, and temperature, should be analyzed to monitor high-rise buildings' displacement.

6. Acknowledgements

This paper has been funded under the research program T21/20 of Hanoi University of Mining and Geology.

The paper was presented during the 6th VIET - POL International Conference on Scientific-Research Cooperation between Vietnam and Poland, 10-14.11.2021, HUMG, Hanoi, Vietnam.

7. References

1. Wujanz, D., 2016. Terrestrial laser scanning for geodetic deformation monitoring: Technische Universitaet Berlin (Germany).
2. González-Aguilera, D., J. Gómez-Lahoz, and J. Sánchez, 2008. A new approach for structural monitoring of large dams with a three-dimensional laser scanner. *Sensors*, 8(9): 5866-5883. <https://doi.org/10.3390/s8095866>
3. Van Gosliga, R., R. Lindenbergh, and N. Pfeifer, 2006. Deformation analysis of a bored tunnel by means of terrestrial laser scanning.
4. Schneider, D., 2006. Terrestrial laser scanning for area based deformation analysis of towers and water dams. in Proc. of 3rd IAG/12th FIG Symp., Baden, Austria, May.
5. Jatmiko, J. and P. Psimoulis., 2017. Deformation Monitoring of a Steel Structure Using 3D Terrestrial Laser Scanner (TLS). in Proceedings of the 24th International Workshop on Intelligent Computing in Engineering, Nottingham, UK.
6. Chrzanowski, A., A. Szostak, and R. Steeves., 2011. Reliability and efficiency of dam deformation monitoring schemes. in Proceedings of the CDA 2011 Annual Conference. Fredericton, NB. Canada. October.
7. Lindenbergh, R. and N. Pfeifer., 2005. A statistical deformation analysis of two epochs of terrestrial laser data of a lock. in Proceedings of the 7th Conference on Optical.
8. Mukupa, W., Robert, W., Hancock, M., Al-Manasir, K., 2017. A review of the use of terrestrial laser scanning application for change detection and deformation monitoring of structures. *Survey review*, 49(353): 99-116. <https://doi.org/10.1080/00396265.2015.1133039>
9. Wujanz, D., D. Krueger, and F. Neitzel., 2013. Defo Scan++: Surface based registration of terrestrial laser scans for deformation monitoring. in Proceedings of 2nd Joint International Symposium on Deformation Measurement (JISDM), Nottingham.
10. Wang, J., 2013. Block-to-point fine registration in terrestrial laser scanning. *Remote Sensing*, 5(12): 6921-6937. <https://doi.org/10.3390/rs5126921>
11. Jatmiko and P. Psimoulis, 2017. Deformation Monitoring of a Steel Structure Using 3D Terrestrial Laser Scanner (TLS), in 24th International Workshop on Intelligent Computing in Engineering. Nottingham, UK.
12. Park, H.S., H.M. Lee, and H. Adeli, 2007. A new approach for health monitoring of structures: Terrestrial Laser Scanning. *Computer-Aided Civil and Infrastructure Engineering*, 22(1): 19-30. <https://doi.org/10.1111/j.1467-8667.2006.00466.x>
13. Reshetyuk, Y., 2006. Investigation and calibration of pulsed time-of-flight terrestrial laser scanners. KTH.
14. Reshetyuk, Y., 2009 Self-calibration and direct georeferencing in terrestrial laser scanning. KTH.

15. Soudarissanane, S., 2016. The geometry of terrestrial laser scanning; identification of errors, modeling and mitigation of scanning geometry. <https://doi.org/10.4233/uuid:b7ae0bd3-23b8-4a8a-9b7d-5e494ebb54e5>
16. Lague, D., N. Brodu, and J. Leroux, 2013. Accurate 3D comparison of complex topography with terrestrial laser scanner: Application to the Rangitikei canyon (NZ). *ISPRS journal of photogrammetry and remote sensing*, 82(): 10-26. <https://doi.org/10.1016/j.isprsjprs.2013.04.009>
17. Little, M. 2006. Slope monitoring strategy at PPRust open pit operation. in *Proceedings of the international symposium on stability of rock slopes in open pit mining and civil engineering*. Southern African Institute of Mining and Metallurgy Johannesburg.
18. Jafari, B., A. Khaloo, and D. Lattanzi, 2017. Deformation tracking in 3D point clouds via statistical sampling of direct cloud-to-cloud distances. *Journal of Nondestructive Evaluation*. 36(4): 1-10. <https://doi.org/10.1007/s10921-017-0444-2>.
19. Oniga, V. and C. Chirila, 2013. Hausdorff distance for the differences calculation between 3D surfaces. *Journal of Geodesy and Cadastre RevCAD*, 15: 193-202.
20. Available from:
https://www.cloudcompare.org/doc/wiki/index.php?title=Distances_Computation#Local_modeling, 10/06/2021.
21. Huttenlocher, D.P., G.A. Klanderman, and W.J. Rucklidge, 1993. Comparing images using the Hausdorff distance. *IEEE Transactions on pattern analysis and machine intelligence*, 15(9): 850-863. <https://doi.org/10.1109/34.232073>
22. Besl, P.J. and N.D. McKay., 1992. Method for registration of 3-D shapes. in *Sensor fusion IV: control paradigms and data structures*. International Society for Optics and Photonics.
23. Bryan, P., D. Barber, and J. Mills, 2004. Towards a standard specification for terrestrial laser scanning in cultural heritage—one year on. *International Archives of the Photogrammetry, Remote Sensing and Spatial Information Sciences*, 35(B7): 966-971.
24. Vosselman, G. and H.-G. Maas, *Airborne and terrestrial laser scanning*. CRC press, 2010.
25. Soudarissanane, S., Linderbergh, R., Menenti, M., Teuissen, P. 2009. Incidence angle influence on the quality of terrestrial laser scanning points. in *Proceedings ISPRS Workshop Laserscanning*, 1-2 Sept 2009, Paris, France. ISPRS.
26. Voegtle, T., I. Schwab, and T. Landes. 2008. Influences of different materials on the measurements of a terrestrial laser scanner (TLS). in *Proc. of the XXI Congress, The International Society for Photogrammetry and Remote Sensing, ISPRS2008*.
27. Berenyi, A., T. Lovas, and A. Barsi, 2010. Terrestrial laser scanning—civil engineering applications. *International Archives of Photogrammetry, Remote Sensing and Spatial Information Sciences*, 38(Part 5): 80-85.
28. Nguyen, N.Viet, Nguyen, L.Quoc and Vu, L.Quoc 2017. Application of terrestrial laser scanner GeoMax Zoom 300 for 3D mapping of Vietnam's open-pit mines (in Vietnamese). *Journal of Mining and Earth Sciences*. 58(4):212-218 (in Vietnamese).
29. Nguyen, N.Viet and Vo, D.Ngoc 2016. The possibility applying of Terrestrial Laser Scanner 3D for construction - mining management in underground mines (in Vietnamese). *Journal of Mining and Earth Sciences*. 57: 65-73 (in Vietnamese).

Protection of Female Workers' rights in Employment and Incomes in Vietnam

NGUYEN Thi Hong Loan^{1,*}, PHAM Thu Trang¹, NGUYEN Thi Ngoc Anh¹,
BUI Thi Thu Thuy¹, NGUYEN Hong Thai²

¹ Hanoi University of Mining and Geology, 18 Vien street, Hanoi, Vietnam

² Hong Thai and Colleague International law firm Ltd, Hanoi, Vietnam

Corresponding author: nguyenthihongloan@hmg.edu.vn

Abstract. As an important task of the country's socio-economic development, protecting the rights of female workers in employment and income is concerned and implemented by international organizations and all countries in the world. The COVID-19 pandemic has been affecting the global economy and hurt the incomes and employment of many female workers. In Vietnam nowadays, there is an increase in the unemployment rate of female workers, gender inequality in employment and income, and the ability to secure their jobs and income. The article analyzes the current regulations and their implementation in the employment and income of Vietnamese female workers in the context of the COVID-19 pandemic. The article also proposes some recommendations on legal provisions related to training backup jobs, arranging and employing female employees, providing income support for female employees during leave due to the COVID-19 epidemic; and policies related to female workers' rights and their employers. These recommendations will improve Vietnam's labor law on female workers' rights in employment and income and enhance the efficiency of human resource use and socio-economic development.

Keywords: Rights of female workers, Employment and income, Labor Law, Covid-19 epidemic

1. Introduction

The rights of female workers in employment and income are legal capabilities suitable for gender specificities and confirmed, regulated, and ensured to implement for female employees. Globally, international laws recognize and guarantee citizens' rights and national laws protect the rights of female workers. The protection of female workers' rights aims to protect the labor force and their legitimate rights, ensures gender equality in employment, occupation, income, dignity, and their needs of rest. In recent times, the Vietnamese labor law system on the rights of female workers, the promulgation and implementation of related socio-economic policies have shown progress in legal thought and ensure protection efficiency.

According to the International Labour Organization (ILO), by the end of 2019, 70% of working-age women have joined the labor market and account for about 49% of the labor force of Vietnam [1]. In addition, their opportunities to learn, develop themselves, and promote to decision-making positions in organizations are increasingly expanding. The data also showed that many Vietnamese women is working in vulnerable employment areas with an average income of 13.7% lower than males in 2019 (with comparable working hours). Besides, the proportion of female workers is about 50% in the labor force but less than 25% of decision-making positions in organizations/enterprises [2]. Significantly, the COVID-19 pandemic led to the change in entrepreneurs, the demand in the labor market that will increase existing gender inequalities in the Vietnamese labor market, create new imbalances, and reduce the ability of female workers to implement their rights' employment and income.

As stated by the National General Statistics Office, by the end of 2020, the unemployment rate of female workers in ages of 15 to 24 was 9.2%, nearly twice that of male workers (5.2%), that of female workers over 25 is 2.1% in comparison with 1.1% of male workers [3]. Only a few new jobs are created and concentrated in the informal sector later; therefore, by the first quarter of 2021, female workers in this sector increased by 2.5 percentage points while male workers were 1.2 [3]. There are several explanations for these numbers, such as (1) the inequality in employment and income by genders; (2) the proportion of professionally trained female workers is lower; hence, female workers are often working in the informal or self-employed sectors, and it is complicated to change into other sectors; (3) regulations on the creation and use of reserve vocational training funds and provision of vocational training for female workers have not been implemented effectively or suitable with the COVID-19 pandemic context; (4) female workers have to spend more time on housework, especially when their children have to stay at home and learn online. The abovementioned causes are obstacles to their employment opportunities and their ability to meet the

requirements of employers. Thus, they have to accept less stable jobs as long as they can ensure their incomes.

From these facts, the article analyzes the current protection of the rights in employment and income of female workers in Vietnam, especially in the context of the COVID-19 pandemic, thereby recommending relevant policies to strengthen the protection of female workers' rights in employment and income.

2. Overview of regulations on women workers' rights and gender equality

2.1 The female workers' rights to equality on occupation

The Universal Declaration of Human Rights of 1948 declared that “Everyone has the right to work, to free choice of employment, to just and favourable conditions of work and to protection against unemployment. Everyone, without any discrimination, has the right to equal pay for equal work” (Articles 23 and 24) [4]. Therefore, the right to work is an inalienable right of all human beings, regardless of gender. Convention on the Elimination of All Forms of Discrimination against Women (CEDAW), which the United Nations General Assembly adopted in Article 11 also affirmed that “States Parties shall take all appropriate measures to eliminate discrimination against women in the field of employment in order to ensure, on a basis of equality of men and women, the same rights” [5]. According to the Article 11 of this Convention, the equal rights of women in the workplace include “(1) The right to the same employment opportunities, including the application of the same criteria for selection in matters of employment; (2) The right to free choice of profession and employment, the right to promotion, job security and all benefits and conditions of service and the right to receive vocational training and retraining, including apprenticeships, advanced vocational training and recurrent training; (3) The right to equal remuneration, including benefits, and to equal treatment in respect of work of equal value, as well as equality of treatment in the evaluation of the quality of work; (4) The right to social security, particularly in cases of retirement, unemployment, sickness, invalidity and old age and other incapacity to work, as well as the right to paid leave; (5) The right to protection of health and to safety in working conditions, including the safeguarding of the function of reproduction”

Article 3 of Labor Code of the Philippines ensures equal rights for women at work. “The State shall afford protection to labor, promote full employment, ensure equal work opportunities regardless of sex, race or creed and regulate the relations between workers and employers. The State shall assure the rights of workers to self-organization, collective bargaining, security of tenure, and just and humane conditions of work” [6]. Article 135 of this Code further clarifies that gender discrimination is illegal, significantly. “It shall be unlawful for any employer to discriminate against any woman employee with respect to terms and conditions of employment solely on account of her sex. The following are acts of discrimination: (a) Payment of a lesser compensation, including wage, salary or other form of remuneration and fringe benefits, to a female employee as against a male employee, for work of equal value; and (b) Favoring a male employee over a female employee with respect to promotion, training opportunities, study and scholarship grants solely on account of their sexes” [6].

Human rights and citizen rights are stipulated and protected by laws and the Constitution, including women and female workers' rights. The Constitution of the Social Republic of Vietnam (2013) stipulates “No one shall be discriminated in his or her political, civic, economic, cultural, and social life” (Article 16). The Constitution also clearly stipulates the role of the state, the society, and families in ensuring equal rights for women “(1) Male and female citizens have equal rights in all fields. The State has a policy to guarantee equal gender rights and opportunities, (2) The State, the society, and families create conditions for women’s comprehensive developments and promotion of their role in the society, (3) Sex discrimination is strictly prohibited” Article 26) [7]. Equal rights to work, to choose job and workplace are also affirmed “(1) Citizen has the right to work and to select career, job, and workplace, (2) Workers shall be provided equal and safe work conditions and shall be paid with salary and enjoy break policy, (3) Discrimination, forced labor, and employment of worker under the minimum age of labor are strictly prohibited” (Article 35) [8].

Vietnamese law also affirms that female workers have the right to choose jobs per their capacity and aspirations without being forced by any organization or individual [8]). Article 5 of this Code stipulates that “An employee has the rights to work; freely choose an occupation, workplace or occupation; participate in basic and advanced occupational training; develop professional skills; suffer no discrimination, forced labor and sexual harassment in the workplace”. According to this law, workers and female workers, in

particular, have the right to choose their own jobs, depending on their health and expertise. The State has policies to ensure the jobs for female workers: Article 135 stipulates that: “Necessary measures shall be implemented to create employment opportunities, improve working conditions, develop occupational skills, provide healthcare, and strengthen the material and spiritual welfare of female employees in order to assist them in developing effectively their vocational capacities and harmoniously combine their working lives with their family lives” [8]. In general, the provisions on woman workers’ right to work in Vietnam are similar to international conventions. These regulations aim at equal rights of female workers in training, work opportunities, recruitment, and employment.

Moreover, gender equality in workplace are also recognized in Article 13 of Law on Gender Equality in 2006, that “Man and woman are equal in terms of qualifications and age in recruitment, are treated equally in workplaces regarding work, wages, pay and bonus, social insurance, labour conditions and other working conditions”; and “Man and woman are equal in terms of qualifications and age when they are promoted or appointed to hold titles in the title-standard professions” [9].

Decree No. 145/2020/NĐ-CP, dated December 14, 2020 of the Government also details and guides the implementation of some articles of the Labour Code regarding gender equality, which states in Article 78: “Employers have the responsibility to ensure equality of male and female employees; implement measures for assurance of gender equality in terms of recruitment, employment, training, salary, rewarding, promotion, remuneration payment, social insurance, health insurance, unemployment insurance, working conditions, labor safety, working hours, rest periods, sick leave, maternal leave, other material and spiritual benefits”. Vietnam also encourages employing female workers by the statement: “The State encourages employers to: (a) Give priority to hiring females if they are qualified for works that are suitable for both genders; renew employment contracts with female employees when their employment contracts expire; (b) Provide benefits for female employees that are better than those prescribed by law” [10].

2.2 The female workers’ rights to equality on income

Universal declaration of the human right of 1948 set out: “Everyone, without any discrimination, has the right to equal pay for equal work”; and “Everyone who works has the right to just and favourable remuneration ensuring for himself and his family an existence worthy of human dignity, and supplemented, if necessary, by other means of social protection” [4] (Article 23). ILO Convention No. 100 of 1951 stipulate: “The term equal remuneration for men and women workers for work of equal value refers to rates of remuneration established without discrimination based on sex” [11]; and “This principle may be applied by means of: (a) national laws or regulations; (b) legally established or recognized machinery for wage determination; (c) collective agreements between employers and workers; or (d) a combination of these various means” [12].

Article 11 of the 1948 CEDAW recognizes the right to equal pay between women and men for work : “The right to equal remuneration, including benefits, and to equal treatment in respect of work of equal value, as well as equality of treatment in the evaluation of the quality of work” [5]. A salary is an amount the employer pays the employee under an agreement for work performed by the latter. Salary equals (=) base salary plus (+) allowances and other additional amounts. Article 90 of the Labour Code provides for wage equality and nondiscrimination for female workers: “Employers shall pay salaries fairly without discrimination against genders of employees who perform equal works.” [8]

Article 13 of Law on Gender Equality in 2006 stipulates: “Man and woman are equal in terms of qualifications and age in recruitment, are treated equally in workplaces regarding work, wages, pay and bonus, social insurance, labour conditions, and other working conditions”; Employers pay wage equally between male and female workers basing on the agreed salary, productivity, and work quality. Equal pay between female workers and male workers is also considered one of the most important factors ensuring the effective implementation of the equal rights of female workers [9].

The above-mentioned regulations have proved that international international conventions and Vietnam laws always provide female workers' equal pay for equal work..

2.3 The rights of female workers on guaranteeing employment and income

International conventions and Vietnam laws also protect women's right to work. Employers must not dismiss an employee or unilaterally terminate the employment contract with an employee due to her

marriage, pregnancy, maternity leave, or nursing a child. Recommendation R191 of ILO stipulates: “A woman should be entitled to return to her former position or an equivalent position paid at the same rate at the end of her leave in the maternity leave period; and “A pregnant or nursing woman should not be obliged to do night work if a medical certificate declares such work to be incompatible with her pregnancy or nursing” [13].

For the purpose of preventing discrimination against women due to her marriage, pregnancy, maternity leave, or nursing a child, ensuring the right to work of female workers; Article 11 of CEDAW stipulates: “In order to prevent discrimination against women on the grounds of marriage or maternity and to ensure their effective right to work, States Parties shall take appropriate measures: (a) To prohibit, subject to the imposition of sanctions, dismissal on the grounds of pregnancy or of maternity leave and discrimination in dismissals on the basis of marital status; (b) To introduce maternity leave with pay or with comparable social benefits without loss of former employment, seniority or social allowances; (c) To encourage the provision of the necessary supporting social services to enable parents to combine family obligations with work responsibilities and participation in public life, in particular through promoting the establishment and development of a network of child-care facilities; (d) To provide special protection to women during pregnancy in types of work proved to be harmful to them” [5].

Article 137 of the Philippine Labor Code also affirms that It shall be unlawful for any employer to discharge or refuse the admission of such woman upon returning to her work for fear that she may again be pregnant.

The Vietnam Labor Code in 2019 regulates: “The employer must not dismiss an employee or unilaterally terminate the employment contract with an employee due to his/her marriage, pregnancy, maternity leave, or nursing a child under 12 months of age”. To ensure employment and income of female employees when the labor contract expires during maternity leave, Article 137 of the Vietnam Labor Code 2019 stipulates: “Upon expiration of the employment contract with female employee who is pregnant or nursing a child under 12 months of age, conclusion of a new employment contract shall be given priority”. In case the labor contract has not expired and after the maternity leave, the female employee's right to maintain employment and income is specified in Article 140 of the Labor Code 2019: “An employee shall be reinstated to his/her previous work when he/she returns to work after the maternity leave prescribed without any reduction in his/her salary, rights and benefits before the leave. In case the previous work is no longer available, the employer must assign another work to the employee with a salary not lower than the salary he/she received prior to the maternity leave” [8].

The above regulations do not ensure only employment and income of female workers during pregnancy, maternity leave, or nursing a child, but also her mental and physical health. This helps women feel secure to perform their motherhood well.

3. The implementation of regulations on women workers' rights and gender equality

3.1 The implementation of female workers' rights to equality on occupation

Vietnam regulations on women workers' rights in the workplace comply with the international conventions, especially CEDAW. To help women workers overcome joblessness and ensure backup occupations for female employees, Vietnam Labor Code 2019 notes: “The State shall develop various forms of training to enable female employees to acquire additional occupational skills that are suitable to their physical and physiological characteristics and their motherhood roles” (Article 135). Besides, “necessary measures shall be implemented to create employment opportunities, improve working conditions, develop occupational skills, provide healthcare, and strengthen the material and spiritual welfare of female employees to assist them in developing their vocational capacities effectively and harmoniously combine their working lives with their family lives”. “Employers are encouraged to enable both male and female employees to work regularly, and to widely apply the systems of flexible working hours, part-time work, or outwork” [8].

Regulations and enforcement of rules on recruitment, employment, and training of workers in state-owned enterprises and large economic groups have ensured the equality of female workers at work, recruitment and promotion opportunities. However, female workers' equal rights have not been effectively implemented in private sector, especially small and medium enterprises, in terms of recruitment and

promotion opportunities. Currently, many enterprises have included gender and/or age criteria in their recruitment standards. This has created inequality between male and female workers in recruitment.

The provisions of Decree 145/2020/ND-CP, Circular 32/2018/TT – BLDTBXH, are guidelines for the implementation of several articles of the Labor Code 2019 on labor conditions, labor relations or appoints employees, providing financial support for female employees to participate in training courses at vocational training institutions [10]. As the government has not yet issued any regulation to encourage enterprises to provide advanced vocational training for female workers, small and medium enterprises have not yet developed plans and organized training for them. Currently, pre-employment training has almost met the needs of indirect workers working in specialized departments, and direct female workers receive on-the-job training. In contrast, advanced vocational training, primarily preventive vocational training for female workers, has not been paid attention. Survey results of Vietnam Women's Union show that nearly 60% of female workers who need vocational training to improve their professional qualifications have been trained. They often have to arrange their study in the evenings and weekends. Most of them have not received financial support from the business during advanced training. Due to lack of preventive vocational training for female employees, specific regulations and implementation solutions, by the end of 2020, i.e. after one year suffering from COVID-19, businesses have encountered a lot of problems. With financial difficulties leading measures to reduce labor costs, the unemployment rate of female workers tends to increase. In addition, in labor reduction, age and sex discrimination are clearly demonstrated, whereby 6.9% of employers choose the elderly group of pregnant and nursing young children workers to give up or resign during this period. Therefore, there is a relatively large gap in the unemployment rate between female (9.2% among ages of 15-24 and 2.1% over 25 years old) with male workers (with the respective rates of 5.2% and 1.1%) [1].

3.2 The implementation of female workers' rights to equality on income

The equal income rights of female workers in Vietnam are protected through the provisions of the labor law on wages, which are consistent with the recommendations of the ILO, the requirements of the CEDAW, and the national socio-economic conditions. Although enterprises often implement a standard salary system for employees, without discrimination on age or gender, the income of female workers is always lower than that of male workers with the same qualifications and positions. The average income of female workers is 10.7% lower than that of male workers. The higher the level of education, the greater this disparity is. In 2016, the income of untrained female workers was only 8.1% lower than that of men with the same qualifications, and this difference was up to 19.7% in the group of university graduates or higher [14]. On the other hand, due to the duty of motherhood, female workers hardly have opportunities to participate in jobs that require with strict time but well paid and higher promotion opportunities.

3.3 The situation of protecting the rights of female workers on guaranteeing employment and income

The rights to be guaranteed by employment and income of female workers in Vietnam are in provisions on similar job and income if employees return to work after maternity leave, prioritizing to re-signed the expired labor contract during pregnancy, salary for days off work, maternity leave, salary from work in the break between shifts during pregnancy and an under 12 months of age child-rearing, etc. However, the determination of wages for female workers from work in the break between shifts has not ensured the principles of the labor market as well as promoted the rights of female workers

Facing the problematic situations due to the COVID-19, the Vietnamese government has issued many policies to support employees and employers, such as (1) interest rate support for employers with the fund of VND 250,000 billion; (2) temporary exempt from the obligation to pay fees of union, pension, and death insurance fund; (3) income support for affected employees in the pandemic from the fund of 62,000 billion VND [15]. Additionally, there are many supplement programs of trade unions, women's unions, social organizations, and employers for income for employees. Nevertheless, the actual efficiency of the policy was not as expected because of the administrative procedures and regulations that make buffer

According to the data of the Ministry of Labor - Invalids and Social Affairs, only employees with labor contracts can be supported. Others who are in the informal sector, freelancers, and seasonal workers cannot obtain the favor. Besides, it takes long time for employers to access the low-level loan support (one million VND per month), thus, many employers do not apply for this support.

In addition, to support the procedures in salary payment during the stoppage due to the epidemic, there is the issued document No 1064 dated March 25, 2020 guiding the payment of stoppage wages and settlement of benefits for employees [16].

However, from 80% of surveyed small and medium enterprises, payments are for the vital labor force, other employees are eliminated. On the other hand, the regulation of stoppage wages: "wage during the stoppage due to the pandemic will be determined on the basis of an agreement between the employees and employers but not lower than the regional minimum wage prescribed by the Government " has not really ensured the effective in protecting the rights of female workers, who is the weak party in the relationship with the employer .

4. Recommendations to strengthen the protection of female workers' rights in employment and income

4.1 Recommendations to improve the legal provisions on the rights of female employees in employment and income

Firstly, regulations on vocational training need to be perfected, especially regulations on vocational training, creating and using vocational training funds for female employees at enterprises. To ensure that the female worker can meet the requirements of the market and perform their motherhood well, to help them being quickly employed again and reducing the unemployment rate in rapid changed demand for labors and in industry structure, more specific regulations on vocational training and handling of violations of regulations on vocational training them should be applied. However, as 93.5% of enterprises in Vietnam are small and medium-sized [17] so it is relatively difficult for them to set up and implement the training plan of vocation and back up occupations for employees. Thus, it is necessary to supplement regulations on training association between enterprises and vocational training centers and stipulates on the responsibility of enterprises in setting up and using the back up occupation training fund for female workers. In addition, it is also necessary to issue more regulations, encouraging enterprises to implement solutions to improve female workers' skills, providing additional training in suitable preventive occupations to their physical, physiological characteristics and motherhood.

Secondly, regulations on work arrangements for female employees should be supplemented to ensure jobs and income for female workers. The regulations on encouraging enterprises apply the part-time or flexible working regime, or assign jobs at home, ensure regular jobs for female workers, has demonstrated the State's policies on protecting the rights of female workers, and is suitable for the conditions of the economy being impacted by the Covid-19. However, there should be specific regulations and financial mechanisms to support employers in implementing solutions to ensure the government policies' energy, reducing the burden, and promoting companies in implementing the law's provisions. Moreover, to ensure the rights of female employees to work during pregnancy, childbirth, and child-rearing, it is advisable to empower them and their employers to make agreement on business traveling during pregnancy, the extra wages for the work during their break time due to raising children under 12 months of age. The regulations will promote their rights in employment and income, and ensure a balance between their rights and their employers' interests.

Thirdly, It is necessary to supplement to the labour law regulations on job and income security for female workers. Due to the social distancing in COVID-19, companies lessen their business. Consequently, employees' income has significantly decreased, although they are still provided supported income from employers. Therefore, it is necessary to have regulations on insurance or income support for employees due to the pandemic as well as force majeure reasons. Enterprises can ensure a financial balance in maintaining employees and income, life of female workers are also guaranteed

4.2 Recommendations on improving the efficiency of implementing female workers' rights in terms of employment and income

Firstly, it should be raising the awareness of female workers and employers about labor law, especially labor law on female workers' rights. It is necessary to flexibly apply various dissemination and training for female workers with labor law, such as direct dissemination activities, social networks (facebook, zalo, instagram, tiktok, etc.) or campaigns "for female workers' rights", etc. These measures help workers have full information, good awareness of the labor law and the rights of female workers, know how to protect their rights themselves, especially the rights in recruiting and appointing to important positions. Besides, to increase the knowledge of labor laws and female workers' rights, enterprises should regularly organize

periodic training for managers and leaders to promptly and adequately update legal regulations to raise gender awareness in employees' recruitment, training, and appointment.

Secondly, policies to support businesses and workers should be synchronously and effectively implementing in order to quickly restore production and restore the economy after the time of the COVID-19. Effectively enforce policies for supporting social security, creating jobs, training human resources and conditions for female workers to get the jobs rapidly, ensure the labor force for increasing production and business. These solutions ensure female workers' rights and promote economic development and recovery after COVID-19.

Thirdly, the inspection, examination and handling of violations of the labor law should be strengthening. In recent years, the review and investigation of violations of the labor law are not sufficient. Disadvantages are the handling of violations, gender inequality in recruitment and payment, the illegal firing of the employees, the violation in wages, working hours, etc. Therefore, it is necessary to improve the quality of inspection and examination by unifying the inspection order, promulgating clear regulations on assessment and evaluation, and strengthening the contingent of inspectors. Consequently, correct and sufficient implementation of the legal provisions in the rights of female workers will be ensured and effective.

Fourthly, it should be implementing income tax exemption and reduction policy on multi-field corporations such as e-commerce, digital technology, and communication corporations. The Law on Tax Administration stipulates that production, construction, and transportation enterprises with many female employees are entitled to a reduction in corporate income tax equal to the number of additional expenditures on female employees. However, the current reality is that the occupations in digital technology, telecommunications, e-commerce, etc are developing and attracting many female workers to join. Jobs in the Industry Revolution 4.0 require the application of high-tech knowledge and skills and a modern working environment suitable for female workers. The government should have more policies to encourage enterprises to use female workers to create more female workers to develop higher incomes for suitable working positions. The exemption and reduction of income tax for female employees encourage employers to recruit female employees, comply with specific regulations for female employees, and increase expenditures for training purposes for female workers' development.

Fifthly, it is necessary to raise the efficiency of policies in loan incentives for businesses to deal with difficulties due to Covid-19. The efficiency can be achieved by reforming administrative procedures in borrowing to shorten the loan duration or applying support measures for businesses to face difficulties due to Covid-19 such as prolonging repayment, favoring with loan interest and reducing fees, etc.,

5. Conclusions

The COVID-19 pandemic has badly affected the labor market of countries worldwide. It thereby affects the effectiveness of implementing the rights of female workers in general and the rights in employment and income in particular.

In Vietnam, the Labor Code was passed in 2019 and takes effect from 2021, when there are significant fluctuations on the labor market, many changes in the business methods, and the limitation of the female labor force in terms of conditions, working time, skills, etc. Thus, it is necessary to improve the regulations in the Labor Code and its relevant documents to ensure suitability and efficiency.

The article proposes some recommendations to improve the provisions of the Labor Law, which are focus on maintaining gender equality on employment and income, ensuring jobs and income for female labors during pregnancy, childbirth and child-rearing. The article also suggests solutions to ensuring jobs and income for female labors due to pandemic such as the COVID-19. In addition, the article proposes several recommendations for planning, carrying out Government policies, for applying Labor Laws regulations of female employees and employers. The recommendations will improve the implementation efficiency of female labors' rights, thereby contributing to promoting the rights of female laborers and strengthening the protection of their rights in employment and income. Paper was presented during the 6th VIET-POL International Conference Scientific-Research Cooperation between Vietnam and Poland, 10-14.11.2021, HUMG, Hanoi, Vietnam.

6. Acknowledgements

The paper was presented during the 6th VIET - POL International Conference on Scientific-Research Cooperation between Vietnam and Poland, 10-14.11.2021, HUMG, Hanoi, Vietnam.

7. References

1. International Labour Organization, 2021. Gender and the labour market in Vietnam: This is an analysis based on the Vietnam Labour Force Survey, <https://www.ilo.org>. 03/07/2021.
2. International Labour Organization, 2021. COVID-19 widens existing gender inequalities, creates new gaps in Vietnam, <https://www.ilo.org>. 03/07/2021.
3. General Statistics Office, 2020. Report on Labour force and employment in 3rd Quarter and 9 months in 2020, <https://www.gso.gov.vn> . 03/07/2021.
4. General Assembly of the United Nations, 1948. The Universal Declaration of Human Rights, <https://www.un.org>. 03/07/2021)
5. General Assembly of the United Nations, 1979. Convention on the Elimination of all forms of Discrimination against Women (CEDAW), <https://www.un.org>. 03/07/2021.
6. Department of Labor and Employment, 2017. Labor Code of the Philippines, <https://www.dole.gov.ph/>. 03/07/2021.
7. National Assembly, 2013. The constitution of the socialist republic of Vietnam on November 28th 2013, <https://thuvienphapluat.vn>. 05/07/2021.
8. National Assembly, 2019. Labor code No 45/2019/QH14 on November 20th, <https://thuvienphapluat.vn>. 06/07/2021.
9. National Assembly, 2006. The Law on Gender equality No 73/2006/QH11 on November 29th 2006, <https://thuvienphapluat.vn> 06/07/2021.
10. Vietnam Government, 2020. Decree No 145/2020/NĐ-CP on December 14th, 2020 about Elaboration of some articles of the labor code on working conditions and labor relations, <https://thuvienphapluat.vn>. 05/07/2021.
11. International Labour Organisation, 1951. Convention concerning Equal Remuneration for Men and Women Workers for Work of Equal Value, <https://www.ilo.org>. 05/08/2021.
12. <https://www.ilo.org/dyn/normlex/en/>, 05/08/2021.
13. 13.International Labour Organization, 2000. Maternity Protection Recommendation, (No 191).
14. <http://www.quanhelaodong.com/archives/2186?lang=vi>, 05/08/2021.
15. Chau Thanh, 2021. Summary of regimes and policies to support and overcome difficulties caused by Covid-19. <https://thuvienphapluat.vn/>. 03/07/2021.
16. Vietnam Ministry of Labour, Invalids and Social Affairs, 2020. Circular No 1064/LĐTBXH-QHLĐTL on March 25th, 2020 about Payment of wages and benefits for employees during work suspension due to Covid-19 pandemic. <https://thuvienphapluat.vn>. 03/07/2021.

Research, Calculation and Proposal of Ventilation Solution for Duong Huy Coal Mine when Mining Down to -250 m Depth

DAO Van Chi^{1,*}, LE Tien Dung¹, VU Thai Tien Dung¹, NGUYEN Hong Cuong¹

¹ Hanoi University of Mining and Geology, 18 Vien street, Hanoi, Vietnam

Corresponding author: daovanchi@hmg.edu.vn

Abstract. At present, according to the extraction plan in the year 2020 of Duong Huy Coal Company - Vinacomin, the mining is divided into three main zones: Central Zone extracts 06 faces; South Zone extracts 2 faces and Northeast Zone extracts 2 faces. The designated total production of all zones is 1,880,000 tons/year. To ensure the production of each mining zone, exhaust fan stations are installed at ventilation roadway adits with a total of 05 main fan stations. However, in the near future, to ensure and maintain production activities, the mine is being planned and operated using 03 main fan stations. The calculation results for the reasonable working mode of fan stations are as follows: for fan station FBCDZ-8-№32B at level +47 m, airflow is 167.69 m³/s and air pressure is 243.74 mm H₂O; for fan station 2K56-№30 level +40 m, airflow is 123.37 m³/s and air pressure is 324.79 mm H₂O; for fan station FBCDZ-8-№32B at level +44 m, airflow is 167.69 m³/s and air pressure is 354.99 mm H₂O.

Keywords: Main fan, Working mode, Ventilation, Airflow, Air pressure, Air velocity

1. Introduction

In Vietnam, underground mining areas mainly locate in Quang Ninh coal field. Vietnam National Coal - Mineral Industries Holding Corporation Limited (Vinacomin) are currently managing 13 coal companies with 17 mining sites. These sites are operated in small scale with coal production of 0.5-2.5 million tons per year. In general, mine sites are scattered, having complex geological conditions and low technological mechanisation. The ventilation is therefore very complicated. For example, Trang Bach - Trang Khe site of Uong Bi coal mine uses 07 main fan stations, or Quang Hanh coal mine uses 04 fan stations for underground mining ventilation. One critical ventilation problem for Quang Ninh underground coal mines is its difficulty at deeper mining. The roadways become greater and deeper that result in greater air pressure and higher temperature. As the fan stations are located far away from each other, their combination for overall ventilation is more difficult while “air-pulling” often occurs between the fans. During past years, Vinacomin has developed solutions for easy ventilation at deeper mining such as use of modern mining technology, reduction of fan station number and increase of fan power [1, 2]. At Duong Huy coal mine - Vinacomin, the mine operates in three main zones: Central Zone extracts 06 faces; South Zone extracts 02 faces, and Northeast Zone extracts 02 faces. The designated total production of all zones is 1,880,000 tons per year [3]. To ensure the production in each mining zone, exhaust fan stations are installed at ventilation roadway adits with a total of 05 main fan stations: 01 station using fan 2K56-№24, 01 fan station using two parallel fans 2K60-44-№16, 01 exhaust station using fan BD-II-6-№12/2x30, 01 station using fan 2K56-№30 and 01 station using exhaust fan FBCDZ-№12/2x45. In the near future, according to the Vinacomin’s approval, Duong Huy coal mine operates at greater depth of -250 m. The mine is designed to reduce fan station from five to three. Therefore, it is necessary to study and calculate the ventilation for mining at -250 m depth with only three main fan stations as designed. It should be noted that because the geo-mining conditions in Vietnam are complex and different from those in the world [4], oversea studies apparently have not focused on the reduction of fan station number in a combined system when mining at greater depth [5, 6, 7, 8].

2. Research and calculation of mine ventilation when mining down to -250 m depth

According to the mine design of Duong Huy coal mine for deeper mining approved by Vinacomin, the total fans are to reduce to only 03 main stations for overall ventilation. A simplified network of ventilation is shown in Figure 1. Based on this network, this paper presents a calculation and determination of main fan stations that are well combined with current underground workings.

2.1 Calculation of mine airflow

From the schedule when mining down to -250 m, the airflow calculated for faces, preparation roadways, stations and leaking airflow are as follows [9, 10, 11]:

Tab. 1. Required airflow for air-consumed excavation at -250 m depth.

Order	Name of air-consumed excavation	Airflow, m ³ /s	Note
1	Faces	175.4	
2	Roadway in reparation	119.6	
3	Underground stations	38.8	
4	Air leakage	24.6	

The corresponding total airflow is calculated as:

$$Q_m = 1.1 \times (Q_{lc} + Q_{cb} + Q_{ht} + Q_r) \tag{1}$$

Where: Q_m is total airflow of mine, m³/s; Q_{lc} is total airflow for all faces, m³/s; Q_{cb} is total airflow for roadway in reparation, m³/s; Q_{ht} is total airflow for underground stations, m³/s; Q_r is total leaking airflow through all excavations, m³/s.

Thus the total airflow is adjusted and calculated as:

$$Q_m = 1.1 \times (175.4 + 119.6 + 38.8 + 24.6) \approx 394 \text{ m}^3/\text{s} \tag{2}$$

2.2 Calculation of mine air pressure

The air pressure of mine is calculated according to PATH diagram network. The air pressure is calculated for each path according to the nodes identified in Fig. 1. Detailed information of the calculation method can be found in Tran, Le [9], Center for mining science [10] and Green Science Development Joint Stock Company [12], Green Science Development Joint Stock Company [13], Green Science Development Joint Stock Company [14]. The calculation result of maximum air pressure path over nodes having equal air pressure is as follows:

At point number 1 having air pressure $h_{max} = h_{min} = 0 \text{ mm H}_2\text{O}$;

At point number 5 having air pressure $h_{max} = h_{min} = 19.68 \text{ mm H}_2\text{O}$;

At point number 7 having air pressure $h_{max} = h_{min} = 22.18 \text{ mm H}_2\text{O}$;

At point number 8 having air pressure $h_{max} = h_{min} = 35.96 \text{ mm H}_2\text{O}$;

At point number 9 having air pressure $h_{max} = h_{min} = 36.88 \text{ mm H}_2\text{O}$;

At point number 11 having air pressure $h_{max} = h_{min} = 43.01 \text{ mm H}_2\text{O}$;

At point number 15 having air pressure $h_{max} = h_{min} = 48.00 \text{ mm H}_2\text{O}$;

At point number 24 having air pressure $h_{max} = h_{min} = 100.64 \text{ mm H}_2\text{O}$;

At point number 28 having air pressure $h_{max} = h_{min} = 134.53 \text{ mm H}_2\text{O}$;

At point number 32 having air pressure $h_{max} = h_{min} = 148.81 \text{ mm H}_2\text{O}$;

At point number 41 having air pressure $h_{max} = h_{min} = 158.21 \text{ mm H}_2\text{O}$;

At point number 44 having air pressure $h_{max} = h_{min} = 166.22 \text{ mm H}_2\text{O}$;

At point number 46 having air pressure $h_{max} = h_{min} = 168.49 \text{ mm H}_2\text{O}$;

At point number 56 having air pressure $h_{max} = h_{min} = 159.30 \text{ mm H}_2\text{O}$;

At point number 57 having air pressure $h_{max} = h_{min} = 268.09 \text{ mm H}_2\text{O}$;

At point number 60 having air pressure $h_{max} = h_{min} = 289.1 \text{ mm H}_2\text{O}$.

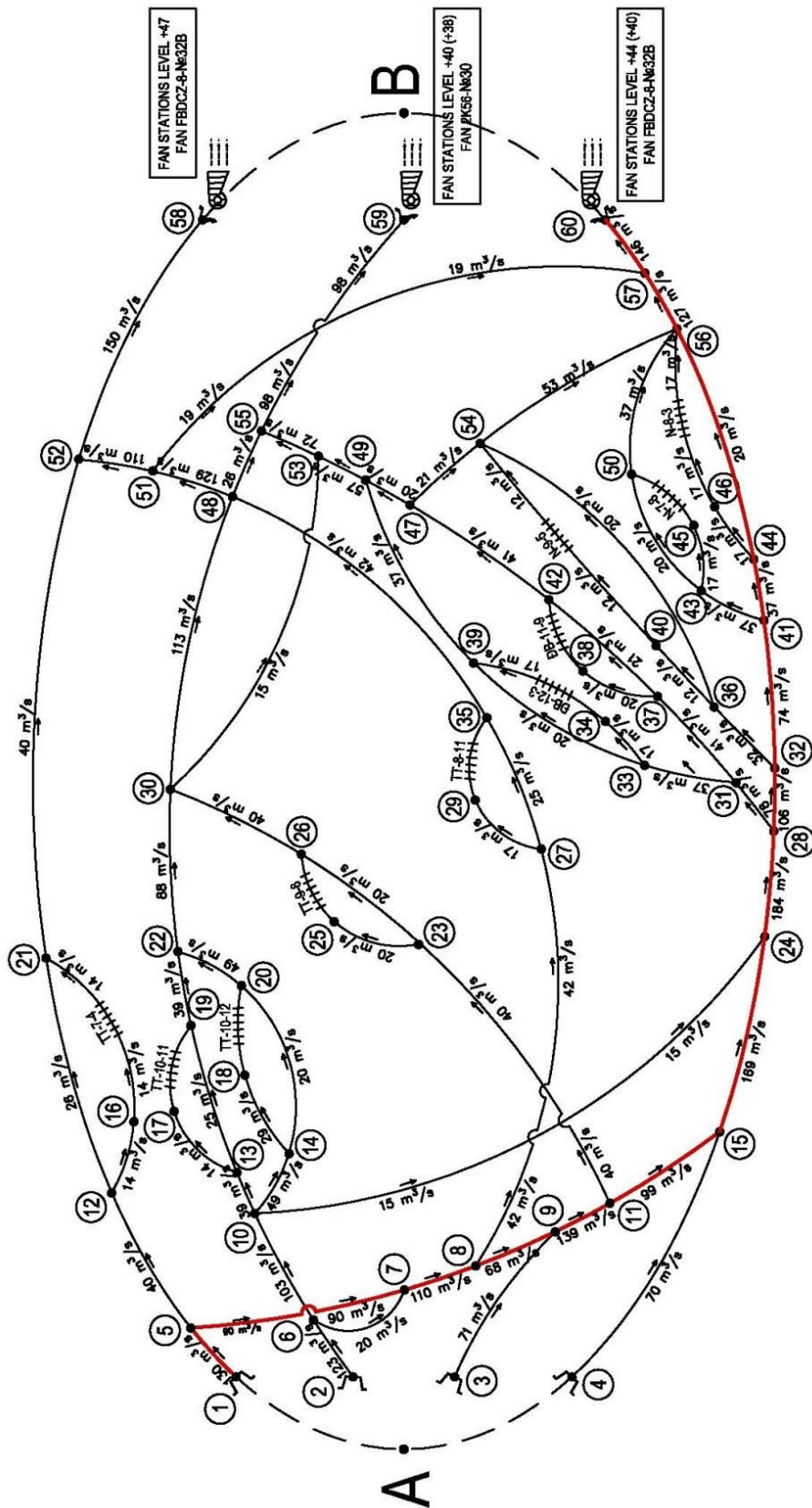


Fig. 1. Simplified ventilation network when 03 fan stations jointly working at -250 m depth.

Hence the maximum air pressure path is determined to go through paths: 1-5-7-8-9-11-15-24-28-32-41-44-46-56-57-60, as highlighted in red color and bold in Figure 1.

The maximum air pressure is: $H_{max} = 289.1 \text{ mm H}_2\text{O}$.

2.3 Calculation of main fan reasonable working mode at -250 m depth

a. Calculation of fan airflow

According to the above calculation, the required airflow for mining at -250 m depth is $394 \text{ m}^3/\text{s}$. Based on the determination of air-consumed excavations such as longwall, roadway or station for each fan station, the corresponding distribution for air consumptions and fan stations are as follows:

- Zone served by fan station level +47 m has $Q_1 = 150 \text{ m}^3/\text{s} \rightarrow Q_{q1} = 1.1 \times 150 = 165 \text{ m}^3/\text{s}$.
- Zone served by fan station level +40 m has $Q_2 = 98 \text{ m}^3/\text{s} \rightarrow Q_{q2} = 1.1 \times 98 = 107.8 \text{ m}^3/\text{s}$.
- Zone served by fan station level +44 m has $Q_3 = 146 \text{ m}^3/\text{s} \rightarrow Q_{q3} = 1.1 \times 146 = 160.6 \text{ m}^3/\text{s}$.

b. Calculation of fan air pressure

The fan stations work in combination and parallel in which each fan serves a separate air pressure for a mine site. Therefore, when being operated jointly, each fan air pressure is calculated according to the maximum air pressure from the area that fan serves. The air pressure of fan stations is calculated as follows:

* Air pressure to be created by fan station level +47 m

Based on the calculation result, a required air pressure H_{m1} of $199.1 \text{ mm H}_2\text{O}$ [10, 15, 16] is used to calculate mine resistance.

The resultant resistance is: $R_{m1} = 199.1/150^2 = 0.0088 \text{ k}\mu$.

The resistance created by fan is:

$$R_{tb1} = 0.05 \times 3.14/3.2^4 = 0.0015 \text{ k}\mu.$$

The air pressure served by fan station level +47 m is calculated as:

$$H_{q1} = (0.0088 + 0.0015) \times 165^2 = 280.42 \text{ mm H}_2\text{O}.$$

* Air pressure to be created by fan station level +40 m

Based on the calculation result, a required air pressure H_{m2} of $232.6 \text{ mm H}_2\text{O}$ is used to calculate mine resistance:

The mine resistance is: $R_{m2} = 232.2/98^2 = 0.024 \text{ k}\mu$

The resistance created by fan is:

$$R_{tb2} = 0.05 \times 3.14/3^4 = 0.0019 \text{ k}\mu.$$

The air pressure served by fan station level +40 is as follows:

$$H_{q2} = (0.024 + 0.0019) \times 107.8^2 = 280.42 \text{ mm H}_2\text{O}.$$

The air pressure needs to be created by fan is:

$$H_{q2} = (0.0139 + 0.0019) \times 154^2 = 300.98 \text{ mm H}_2\text{O}.$$

* Air pressure to be created by fan station level +44 m

Based on the calculation result, the required air pressure H_{m3} of $289.1 \text{ mm H}_2\text{O}$ is used to determine mine resistance

The mine resistance is: $R_{m3} = 289.1/146^2 = 0.0139 \text{ k}\mu$.

The resistance create by fan is:

$$R_{tb3} = 0.05 \times 3.14/3.2^4 = 0.0015 \text{ k}\mu$$

The air pressure served by fan station level +40 m is:

$$H_{q3} = (0.0139 + 0.0015) \times 160.6^2 = 397.22 \text{ mm H}_2\text{O}.$$

From the airflow and air pressure calculated for the above 03 fan stations, the fans are consequently chosen as follows:

- Fan station №1 level +47 m is fan FBCDZ-8-N₀32B with impeller blade angle of 43/35⁰ or equivalent.
- Fan station №2 level +40 m is fan 2K56-N₀30 with impeller blade angle of 40⁰.
- Fan station №3 level +44 m is fan FBCDZ-8-N₀32B with impeller blade angle of 40/32⁰ or equivalent.

3. Verification of working mode of fan stations when mining at -250 m depth

The airflow is distributed for air-consumed excavations as in Figure 1. In order to verify the working mode of 03 main fan station when jointly working in -250 m depth, this paper uses Kazamaru program for distribution of airflow. The results are shown in Figures 2, 3, 4, 5.

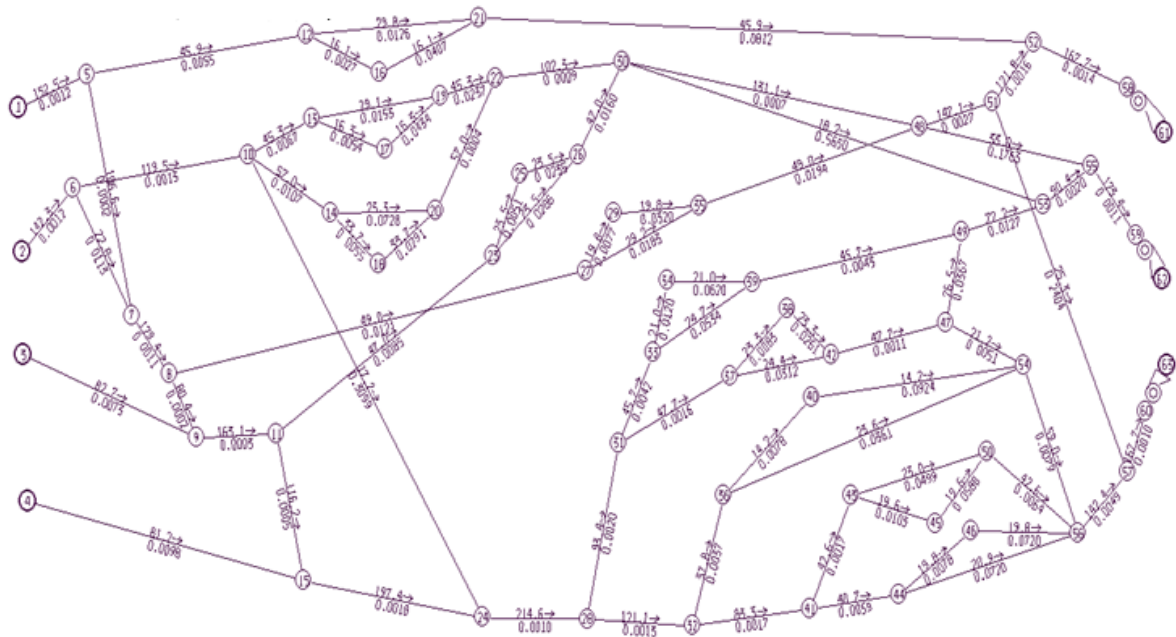


Fig. 2. Verification of working mode when 03 fan stations jointly working at -250 m mining depth.

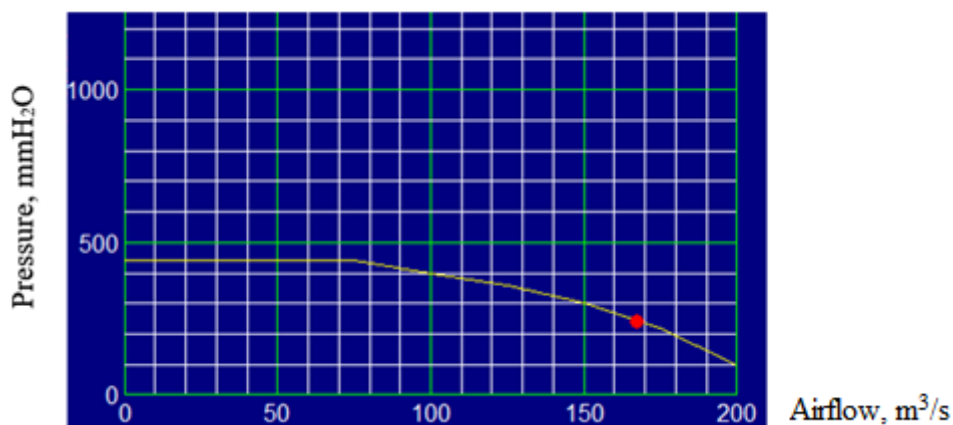


Fig. 3. Working point of Fan FBCDZ-8-N₀32B level +47 m.

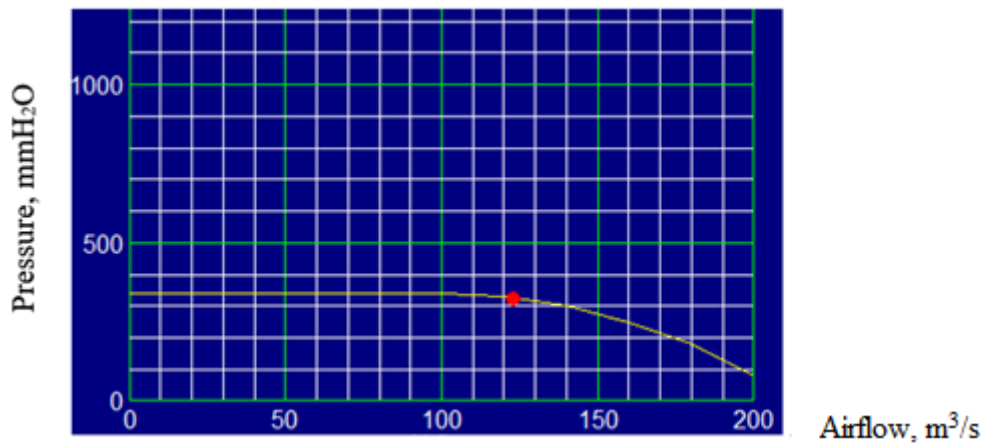


Fig. 4. Working point of Fan 2K56-№30 level +40 m.

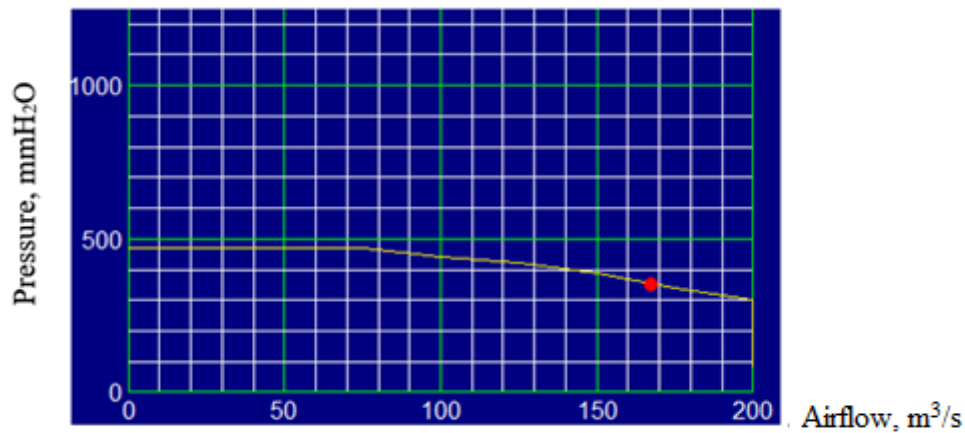


Fig. 5. Working point of Fan FBCDZ-8-№32B level +44 m.

The verification shows that the air pressure in ventilation paths satisfies the requirement. This indicates that the capacity of the above 3 fan stations completely fulfills the requirement when mining at depth of -250 m. The corresponding working mode of fans is as follows:

Tab. 2. Calculation of airflow, air pressure when 03 fan stations in use.

Order	Fan stations	Airflow $Q_{yc}, m^3/s$	Air pressure, $H, mm H_2O$
1	Fan station №1 level +47 m uses fan FBCDZ-8-№32B	167.69	243.74
2	Fan station №2 level +40 m uses fan 2K56-№30	123.37	324.79
3	Fan station №3 level +44 m uses fan FBCDZ-8-№32B	167.69	354.99

4. Proposal of solution to complete ventilation system at -250 m depth

To maintain the ventilation for the mining schedule at -250 m depth using current underground excavations, the following technical issues must be solved in the near future:

- The designated 3 fan stations ensure the ventilation of the mine down to -250 m. However, ventilation path 15-24 (railway-setting roadway -250 m Zone TT.II) has an air velocity of 8.45 and path 24-28 (in-rock roadway -250 m Zone DB.I) has a velocity of 9.2 m/s. The velocities exceed the maximum value of 8 m/s according to QCVN 01/2011-BCT [17]. Therefore, the roadways must be enlarged to reduce the velocity.

- Path 56-57 (in-seam roadway -100 m V8 and crosscut -100 m N.II) has the highest air pressure of 78.8 mmH₂O; its cross-sectional area should be enlarged for pressure reduction.

- To ensure the air velocity of paths 15-24 and 24-28 and to reduce the air pressure for roadways in path 56-57, it is suggested to enlarge roadway's cross-sectional area or to properly drive roadway from which the airflow through fan station +44 m reduces by 10 m³/s.

- An air window is additionally installed at -250 m to adjust airflow for each air-consumed excavation.

- According to the mine design for -250 m depth, the mine is ranked as Class III according to Ministry of Industry and Trade (2020) However, during the extraction, mining technology may change which accordingly changes the coal production. This results in a change in the methane gas emission of mine as well. Therefore, it is necessary to re-calculate the methane-class of mine for appropriate ventilation.

5. Conclusions

When mining down to -250 m, the reduction in main fan from 05 to 03 fan stations is to facilitate the mine management and to ensure a proper ventilation mode for mine. The calculation results have determined proper working mode of each fan station at +47 m, +40 m and +44 m as follows:

- Fan station FBCDZ-8-№32B level +47 m works with an airflow of 167.69 m³/s and air pressure of 243.74 mm H₂O;

- Fan station 2K56-№30 level +40 m works with an airflow of 123.37 m³/s and air pressure of 324.79 mm H₂O;

- Fan station FBCDZ-8-№32B level +44 m works with an airflow of 167.69 m³/s and air pressure of 354.99 mm H₂O.

To ensure the mine safety when operating the three main fan station without changing the current underground excavations, the cross-sectional area of the following roadways should be enlarged for legally air velocity and pressure: railway-setting roadway level -250 m Zone TT.II, curved roadway level -250 m, in-rock roadway -250 m Zone DB.I; roadway -100 m V8 and crosscut -100 m N.II.

6. Acknowledgements

The paper was presented during the 6th VIET - POL International Conference on Scientific-Research Cooperation between Vietnam and Poland, 10-14.11.2021, HUMG, Hanoi, Vietnam.

7. References

1. Dao, V.C., 2021. Study and development of method for determination of actual pressure characteristic curve and of reasonable working mode of main fan at Vinacomin underground coal mines, Quang Ninh (Vietnamese).
2. Dao, C.Van, Tran, H.Xuan and Le, D.Tien 2021. Determination of reasonable working mode for main fan stations during pilot operation of fan station VO - 22/14AR in Lo Tri area, Thong Nhat coal mine (in Vietnamese). *Journal of Mining and Earth Sciences*. 62, 4 (Aug, 2021), 15-20. DOI:[https://doi.org/10.46326/JMES.2021.62\(4\).02](https://doi.org/10.46326/JMES.2021.62(4).02).
3. Duong Huy Coal Company, Ventilation plan for Quarter III, IV 2020 and the year 2020, Quang Ninh, 2020 (Vietnamese).
4. Dao, C.Van and Tran, H.Xuan 2020. Study on status and solution to improve the ventilation system of Quang Hanh coal mine (in Vietnamese). *Journal of Mining and Earth Sciences*. 61, 4 (Aug, 2020), 110-117. DOI:[https://doi.org/10.46326/JMES.2020.61\(4\).12](https://doi.org/10.46326/JMES.2020.61(4).12).
5. Wallace, K., Prosser, B., Stinnette, J.D., 2016. The practice of mine ventilation engineering, *International Journal of Mining Science and Technology*, 25(2): 165-169.
6. Sasmito, A.P., et al., 2013. Some approaches to improve ventilation system in underground coal mines environment - A computational fluid dynamic study, *Tunnelling and Underground Space Technology*, 34: 82-95.
7. Bascompta, M., Sanmiquel, L., Zhang, H., 2018. Airflow Stability and Diagonal Mine Ventilation System Optimization: A Case Study, *Journal of Mining Science*, 54(5): 813-820.

8. Kursunoglu, N., Onder, M., 2015. Selection of an appropriate fan for an underground coal mine using the Analytic Hierarchy Process, *Tunnelling and Underground Space Technology*, 48: 101-109.
9. Tran, X.H., et al., *Mine Ventilation Manual - Underground Traffics and Fans*, Construction Publishing House, Hanoi, 2019 (Vietnamese).
10. Center for mining science - HUMG, *Verification and completion of current ventilation network and down to level -100/-250 of Duong Huy coal mine*, Hanoi, 2020 (Vietnamese).
11. Tran, X.H., et al., 2012. *Safety in underground mining*, Science and Technology Publishing House, Hanoi.
12. Green Science Development Joint Stock Company, *Verification of ventilation network and development of ventilation plan for level -350 of Khe Cham I - Ha Long Coal Company*, Hanoi, 2018.
13. Green Science Development Joint Stock Company, *Verification, air inverter and proper working mode of main fans - Improvement on ventilation efficiency at Nam Mau Coal Company - Vinacomin*, Hanoi, 2016.
14. Green Science Development Joint Stock Company, *Verification of ventilation network at Ha Rang - Ha Long Coal Company: ventilation calculation for year 2016*, Hanoi, 2016.
15. Wang, D.M., 2007. *Ventilation and Mine Safety*, China University of Mining Science and Technology, China.
16. Zhang, Q.Q., 1999. *Ventilation and safety*, CUMT Press, China.
17. Vietnam Ministry of Industry and Trade, *National technical regulations for safety in underground coal mining*, Hanoi, 2011.

The Impact of Coal Exploitation on Tidal Flat Changes, an Investigation Using Remote Sensing Data in Vietnam

PHAM Thi Lan¹, TONG Si Son^{2,*}, LE Thi Thu Ha¹, LE Thi Le³, HOANG Huu Duc⁴

¹Hanoi University of Mining and Geology, 18 Vien street, Hanoi, Vietnam

²University of Science and Technology of Hanoi, VAST, Hanoi, Vietnam

³Thu Dau Mot University, Binh Duong, Vietnam

Ho Chi Minh University of Natural Resources and Environment, Ho Chi Minh City, Vietnam

Corresponding author: tongson@gmail.com

Abstract. Tidal flat plays a crucial role in socio-economic development and ecological environment. Tidal flats in Ha Long-Cam Pha in Vietnam are impacted by human activities, especially coal mining activities. Using remote sensing data is able to detect, extract, and monitor the changes of tidal flats and exploited coal mine area with multi-temporal, in various scales, and for a large coverage. This study aims to investigate the impact of coal mining activities on the changes of tidal flats using remote sensing in Cam Pha, Ha Long, one of the biggest coal basins in Vietnam. Digital Elevation Models (DEMs) of tidal flats constructed by Landsat satellite images acquired in years 1989, 2001, and 2014 are compared to determine the volume changes. Besides, coal mining activities including coal production, waste rock dump area, and the expansion of open coal mine during the period 1989-2014 are investigated using correspondent Landsat images and the reports from the coal mine companies in the study area. Sediment samples in tidal flats are analyzed to determine the origin of the sediments. As the results, organic matter in the tidal flats is dominant with the concentration of 459 g/kg to 607 g/kg, which is evidence for the impact of coal exploitation on the coastal environment. In addition, the relationship between coal mine activities and tidal flat variation is well observed in this study.

Keywords: Tidal flat, Coal, Remote Sensing

1. Introduction

Tidal flats are the transition between land and sea, suffering by the interaction between tidal and other hydrodynamic forces to form areas in flat, fine-grained sediment and usually non-vegetated cover [1]. Tidal flat plays a crucial role in society, economy, and ecology. However, they are threatened by human activities and the phenomenon of climate change such as sea-level rise [2, 3]. One of the human activities affecting tidal flat change is coal mining activities in coastal area. Coal is known as one of the most mining commodities, especially to provide energy for the industrial development of countries [4]. Environmental problems arising from coal mining activities in Vietnam are normally caused by open cast mines. Generally, it is difficult to monitor the change of tidal flats because of muddy, soft ground, short time of exposure to the air [5]. With the ability of instantaneous observation on a large scale, repeatable data requirements at various detailed levels, remote sensing is recommended as the most effective method to detect changes in tidal flats.

As components of the remote sensing, satellite data, aerial photos have been majors data for studies related to environmental monitoring and reclamation of mining areas [6]. Based on broad spectral range, rapid coverage of large areas, and affordable cost, remote sensing data are promising data for the assessment of environmental impacts. Particularly, remote sensing data have been used to identify, outline, and monitor the pollution sources as well as their affected areas composing of land cover, water, and ecosystems [7]. Among these applications of remote sensing in tidal flats, some studies focused on quantifying the landform variation in tidal flats [8]. Several published works have attempted to extract the change information of the topography and sedimentation in tidal flats using Digital Elevation Models (DEMs) constructed from satellite images at different times [5, 8]. These intertidal DEMs have been generated using waterlines extracted from multi-temporal satellite data [9, 10, 11]. Previous studies have focused mainly on spatial and temporal changes of tidal flats. As a crucial indicator to evaluate the soil quality, organic matter plays a vital role in terrestrial ecosystems. Monitoring organic matter is a significant step to make plans for the environmental management and ecological restoration of mining areas [12]. Several papers have attempted to qualitatively analyze surface sediments to gain the information of grain size, organic matter in the relationship with tidal flat changes.

The main objective of this paper is such a combined analysis, in which the assessment of volume

change in the tidal flats is performed using multi-temporal remote sensing data. Besides, the study also investigates the impact of coal mining activities on tidal flat change. First, the DEMs of tidal flats are created using waterlines, which are extracted from multi-temporal Landsat images. Volume change of tidal flat is extracted by the comparison between the DEMs constructed at different times. Subsequently, the volume change of tidal flats is correlated to the statistical number of coal mining activities in the study area to figure out the effect of coal exploitation on the change of tidal flats. The experiment focuses on the tidal flat along Ha Long-Cam Pha coast.

2. Study areas

Ha Long Bay, one of seven wonder heritages recognized by UNESCO, is characterized by 1,600 limestone islands un-inhabited and unaffected by humans, located in the Gulf of Tonkin. An attractive sea landscape spreading in an area of 43,400 ha is the natural potentiality for the development of the tourism industry. The coastline of the Ha Long bay is the sea boundaries of Ha Long and Cam Pha cities which are known as the coal stock of Vietnam. With a special geological base, beneath Ha Long-Cam Pha is formed by petroleum and coal-bearing basins which have been exploited for more than 100 years. Cutting down from the top to create open pit mines is the main method to exploit coal, which makes the change of the topography by creating massive holes with a diameter of thousand meters. The unusable material as rocks, soil, and unqualified coal is piled up surrounding areas of the mines to create artificial mountains with a steep slope up to 8-20 degrees. Ha Long bay is in the tropical zone with a summer and a cold winter. The summer is the rainy season, specified by extreme precipitation with an average of 1,557 mm. Heavy rain falling on the unstable solid waste of the coal exportation, concentrated on steep slopes carries the coal particles to deposit them on the near-shore water area of Ha Long bay. Besides, the seawater in Ha Long is influenced by a tidal dominance regime because the wind, waves are obstructed by dense islands seaward. Calm water is a suitable condition to fate suspended coal sediments to form the coal tidal flat in the study area. Coal tidal flats are muddy, soft, and black with sparse benthos and mangroves. This study focuses on tidal flats along 10 km of coastline in the middle Ha Long and Cam Pha cities. The coastal areas are mainly fed by sediments transported from Nui Beo and Ha Tu coal mines via the Lo Phong and C2 rivers (Fig. 5). The two rivers are around 15 m to 30 m wide and 7 km long, but they are the unique drainage system in the study area.

3. Materials and Methods

3.1. Data in use

This study aims to assess the changes of tidal flats in Ha Long-Cam Pha area, Quang Ninh province, Vietnam by comparing the DEMs of tidal flats. DEMs are generated from a series of waterlines which are extracted from multi-temporal satellite images. Elevation of DEMs is synchronized from tidal levels. The accuracy of built DEMs depends on the accuracy of the waterlines extracted from satellite images. Besides, this study also accesses the relationship between coal mining activities and the tidal flat changes. Thus, the study needs not only the tide level and the satellite images but also the information on productivity, the coal mine expansion, and the area of waste rock dumps.

Satellite images and tidal levels

Remote sensing data used to analyze the variation of tidal flats are 37 Landsat images including 19 Landsat 5 TM, 13 Landsat 7 ETM+, and 5 Landsat 8 OLI. In those images, three scenes consisting of Landsat 5 acquired on 19th August 1989, Landsat 7 acquired on 09th August 2000, and Landsat 8 acquired on 21st June 2014 are used to determine the change of coal exploitation areas. Landsat images are collected from the United States Geological Survey (USGS) website in three periods 1989-1990, 1999-2001, and 2013-2014. These satellite images have been systematically processed at Landsat Surface Reflectance High-Level Data products (Tab. 1). It means that the acquired images are minimized the effects of atmosphere and the distortion related to topography. Simultaneously, these images have been adjusted to 30m spatial resolution in Universal Transverse Mercator (UTM) projection zone 48N. To minimize the effect of wind, waves on the accuracy of tidal level estimation, the satellite images acquired at the wind speed of greater than 10 m/s are not used in the experiment.

Tide level is the crucial parameter for tidal flat researches. In this study, tide levels are not only used as the criteria for selecting satellite images but also as the referent elevation for the DEMs. The tide level is real-time estimated using hydrological models from the Service Hydrographique et Océanographique

de la Marine (SHOM) service at the Hon Dau port in Do Son, which is located at Latitude 20°40'6.53"N, Longitude 106°48'53.50"E. Tidal levels are estimated at the acquisition time of every Landsat image (Tab. 1).

Tab. 1. Landsat image list (L7- Landsat 7 ETM+; L8 – Landsat 8; L5 - Landsat 5 TM).

Sensor	Acquisition date	Tidal level (m)	Sensor	Acquisition date	Tidal level (m)	Sensor	Acquisition date	Tidal level (m)
L8	20131109	3.21	L5	20001105	3.07	L 5	19901110	3.46
L7	20130914	3.01	L5	20001004	2.76	L5	19901025	3.25
L7	20130829	2.61	L7	20010929	2.49	L5	19881104	2.78
L7	20140104	2.5	L7	20000809	2.27	L5	19890920	2.56
L8	20131008	2.1	L5	20000630	2.09	L5	19891123	2.4
L8	20131227	1.9	L5	20001223	1.71	L5	19881120	2.21
L7	20131203	1.84	L7	20010524	1.58	L5	19890616	2.0
L8	20140621	1.61	L5	20010329	1.49	L5	19930915	1.79
L8	20130602	1.31	L5	20010820	1.22	L5	19900806	1.47
L7	20140731	1.23	L7	20010321	1.14	L5	19910606	1.24
L7	20130712	1.01	L7	20010711	0.83	L5	19890819	0.96
L7	20150413	0.75	L7	20000606	0.65	L5	19900518	0.81
						L5	19930526	0.5

Data of coal mining activities

Coal mining activities are presented by coal production, waste rock dump, and coal exploitation area. Coal production and waste rock stockpiles are collected from Ha Tu and Nui Beo mines as listed in Tab. 2. The values of coal mining activities are originated from official reports of the mines in the years 1989, 2000, and 2014. The coal exploitation area is extracted from corresponded Landsat images.

Tab. 2. Coal production of Ha Tu and Nui Beo mine.

Years	Ha Tu		Nui Beo	
	Waste rock dump (m ³)	Coal production (m ³)	Waste rock dump (m ³)	Coal production (m ³)
1989	2,959,353	66,468	586,860	48,342
2001	3,516,803	804,740	1,592,713	389,627
2014	19,594,611	1,460,054	14,352,410	1,751,676

3.2 Methodology

To figure out the impacts of coal mining activities on tidal flat changes in Ha Long- Cam Pha area, the satellite images, information of coal mining activities, and fieldwork data are combined in this study. Several methods are employed including the satellite image classification to detect coal mining areas, the waterline method to construct the DEM of tidal flats, spatial analysis methods to quantify the change of

tidal flats, and the sediment sample analysis to determine the organic matter, carbonat content and sediment size. Besides, the a field trip is carried out to collect samples. The overall processes are outlined in a flow chart in Figure 1.

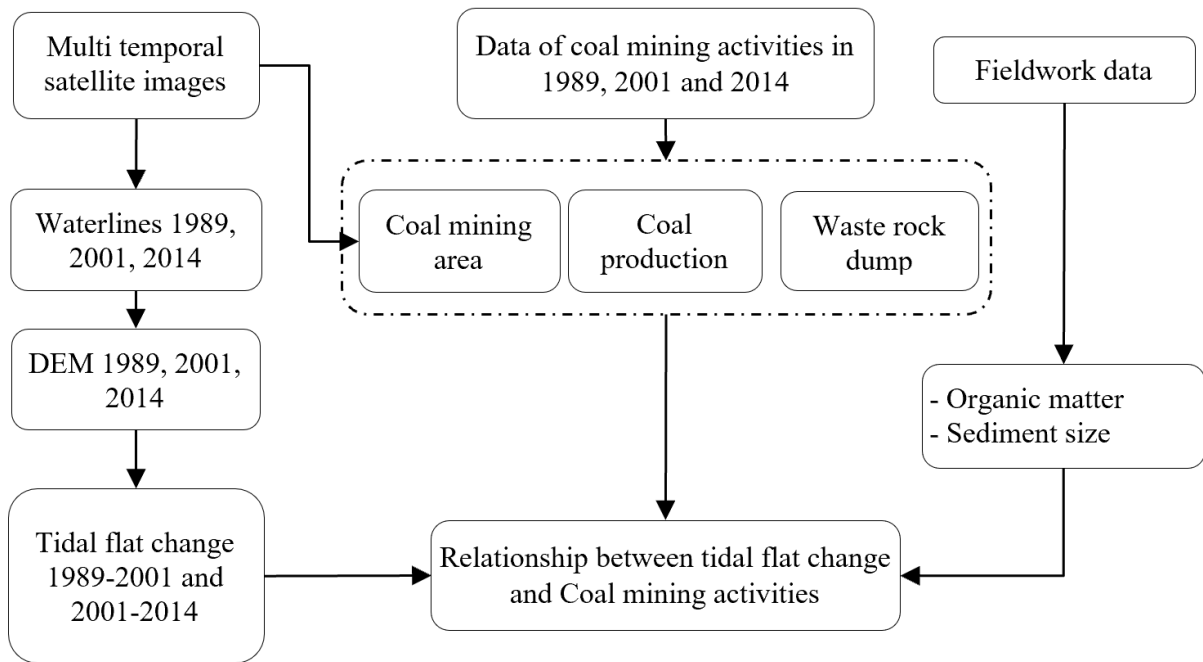


Fig. 1. Flow chart on methodology.

Mapping coal mines

The coal mining area is identified, based on the object-oriented classification method applied for Landsat images acquired in 1989, 2001, and 2014. The object-oriented classification method overcome the challenge caused by the spectral mixing between some surface objects in the coal exploitation area such as bare soil and waste rock dump [13,14]. The extraction of object-oriented features is processed with two steps; the image segmentation, and classification. Firstly, the image is discriminated into discrete segments based on statistical parameters of the image, which are compositing of the color, shape, compactness, and smoothness. Secondly, these segments are classified using features and criteria set by the user. The coal mining and waste rock dump areas in 1989, 2001, and 2014 are compared to each other to quantify the changes.

Constructing DEMs of tidal flats

To construct DEMs of tidal flats, we deploy the waterline method proposed by Mason et al., 1995 [8]. The ratio image calculated by dividing the short-wave infrared band from the green band, is used to extract the waterlines on satellite images in a coal tidal flat. The use of this ratio image is according to the suggestion from the previous study [5]. In total, 37 waterlines are generated from 37 free-cloud Landsat images acquired during the years 1989, 2001, and 2014. With an assumption that water levels at any location along a waterline are equal, these waterlines are assigned tidal levels at the acquisition times of satellite images to become contour lines. The contour lines are then used to construct a Triangular Irregular Network (TIN). The TIN model is a digital model to present geographic data by a triangular vector network of vertices. TINs created in 1989, 2001, and 2014 are then converted to corresponding DEMs with a 30 m pixel size using the linear interpolation method. Using the raster subtraction method, we subtract the DEM 2001 from DEM 2014 to quantify the erosion and deposition corresponding to negative values and positive values. The similar method is applied to the DEM 1989 and the DEM 2001 to observe the variation of tidal flats during the period 1989-2001.

Collecting and analyzing sediment samples

Sediment samples are collected and analyzed to discover the origin of the sediment. Along the 1.2 km transect counted from the coast to the lowest position of the tidal flat, we collect 5 samples at 5 positions named CP_River, CP1, CP2, CP3, CP4 (Fig. 2). In each position, we collected a sample with a 200 g weight on the top 5 cm deep layer of the tidal flats. Each sample is separated into 3 parts and dried at room temperature to analyse the grain size, organic matter, and carbonate content.

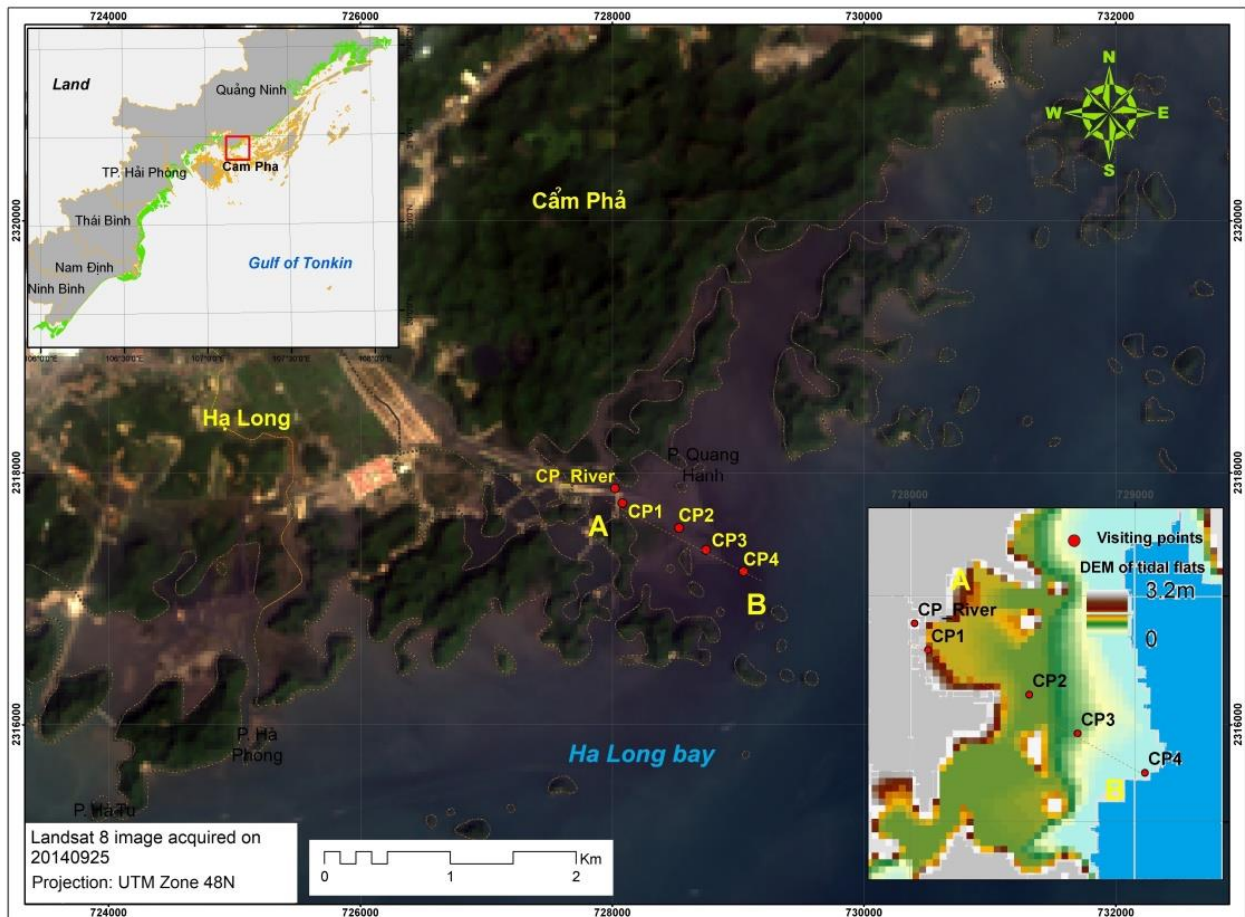


Fig. 2. Map of the study area and sample points on tidal flats in Ha Long-Cam Pha.

The sediment samples are dissolved in a solution before taking measurements using a Mastersizer device to detect the rain sizes. The Mastersizer uses a number of detector elements to capture the scattering pattern from the particles. The detectors take a "snap-shot" of the scattering pattern. Only particles passed through the analyzer beam at the time of snap-shot are captured. The measurement is repeatedly deployed in 3 snap-shots for each sample. The averaged results are used for the classification of particle sizes. Finally, sediment is classified into clay, silt, fine sand, medium sand, and coarse sand based on particle size (Fig. 3).

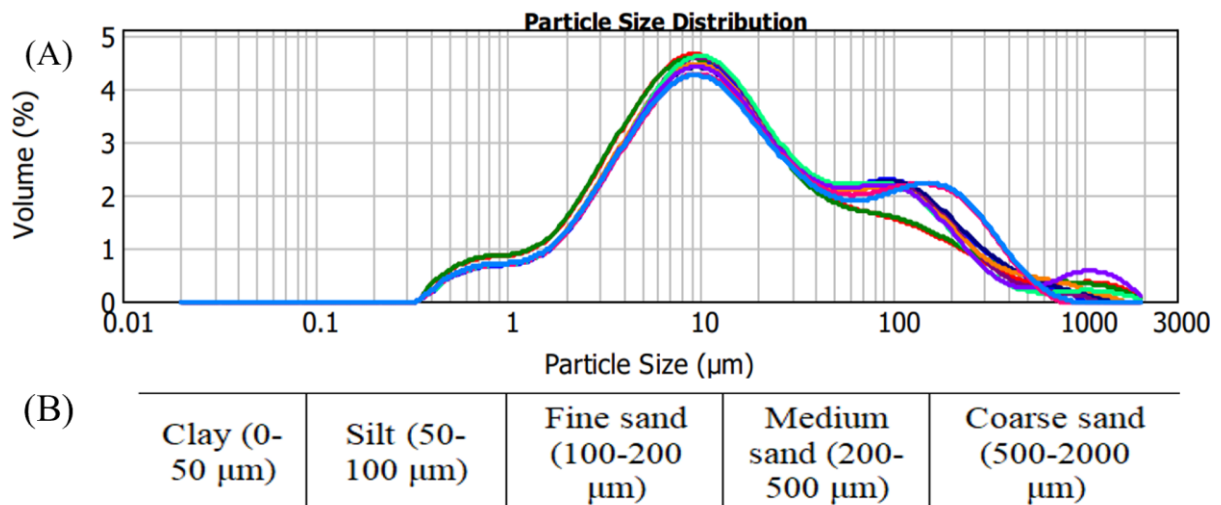


Fig. 3. (A) Sediment size statistics using the Mastersizer device with the colored curves corresponding to the number of measurements on a sample. (B) The scheme for classifying particle sizes.

Organic matter is strictly measured following standard ISO 12435 (1998). ISO 12435 is the international standard to specify a method for the spectrometric determination of organic carbon content in soil by oxidation in a sulfochromic medium. The standard is applicable to all types of air-dried soil samples with an exception of soils contained mineral reducing compounds, Cl^- or Fe^{2+} . Equipment for processing samples consists of 1/ Analytical balance with capable weighing 0.1mg. 2/ Heating block with capable maintaining $135^\circ\text{C} \pm 2^\circ\text{C}$, including 75 mL volumetric glass tubes. 4/ Centrifuge 5/ Glass fibre filters. 6/ Automatic pipette. 7/ Spectrophotometer (10 mm cuvette, 585 nm). To measure organic matter, each sample is dried at room temperature and milled until the particle size of samples is less than $250\ \mu\text{m}$. The organic matter of each sample is measured as the ratio of the amount of carbon in 1 kg of sample.

Carbonate minerals are mentioned as calcite (CaCO_3), aragonite, and dolomite (CaCO_3 and MgCO_3). Carbonate content is investigated following the standard ISO 10693 in 1995. Carbon content is measured following the principle that the carbon present in the soil is oxidized to carbon dioxide. This process is carried out by heating the samples to at least 900°C in a flow of oxygen-containing gas. The amount of carbon dioxide released is then measured by using the infrared detection method.

4. Results and discussions

4.1. The variation of coal mine exploitation

Figure 4 illustrates the coal production in m^3 , exploitation area in m^2 , and waste rock dump in m^3 of Nui Beo and Ha Tu coal mines in 1989, 2001, and 2014. Nui Beo coal mine has just started to be exploited at an industrial scale in 1989 with a small amount of waste rock dump and coal production. However, the exploitation area is around 400 ha due to it has been illegally exploited by local people for a long time (Fig. 4a). The exploitation has a gradual increase in the period 1989-2001 indicated by a slight change of exploitation parameters. In the period 2001-2014, we witness a shape increase in the coal exploitation with the mass of coal production and waste rock dump growing from around 0.4 million m^3 to 1.8 million m^3 and from 1.6 million m^3 to 14.4 million m^3 , respectively. Subsequently, the exploitation area rises doubly from around 500 ha to nearly 1000 ha in 2014. The expansion of exploitation area is observed mostly by the increase of soil dismantling and soil disposal area.

Figure 4b shows the variation of the waste rock dump and coal production in the relationship with the exploitation area of Ha Tu open pit mine. The mines in Ha Tu have been exploited for a long time before 1989, thus the statistic numbers of waste rock dumps and the exploitation area are large with 2.9 million m^3 and 770 ha in 1989, respectively. The waste rock dump is 3.5 million m^3 in 2001, lightly change compared to that in 1989, nevertheless, it dramatically rises to 19.6 million m^3 in 2014. On an opposite trend, the exploitation area increases by 130 ha during the period 1989-2001, but it gradually reduces by 50 ha from 950 ha in 2001 to 900 ha in 2014.

The continuous increase in all the activities of coal exploitation in Nui Beo during the period 2001-2014 denotes that the mine is in the exploiting outbreak state of the exploitation. The exploitation area is increasing along with the rise of the waste rock dump, is the typical characteristic of an open-pit mine which changes the landscape of the surrounding area. Inversely, the variation of statistic numbers in Ha Tu is an example of the exploitation at a stable stage. The dumping ground surrounding the exploitation center is gradually decreased by the plantation for environmental restoration. On the other hand, the coal production is collected from the official reports of coal mine companies which are joint-stock companies sharing the mines. For this reason, the number of production is normally including bias, thus it trend is not emphasized in this study.

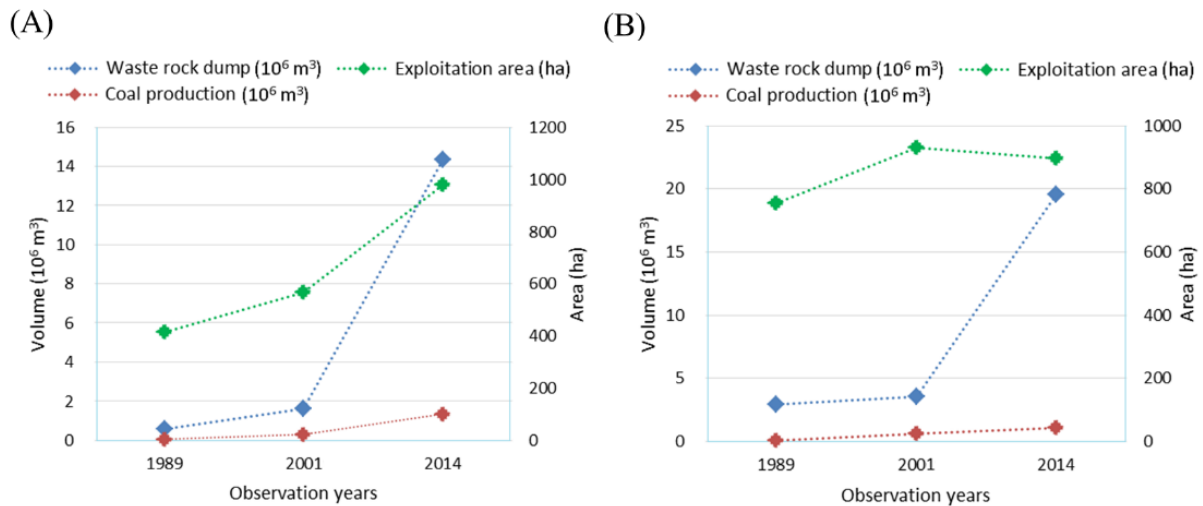


Fig. 4. (a) The variation of coal production, exploitation areas, and waste rock dump in 1989, 2001, and 2014 in (a) Nui Beo mine, and (b) Ha Tu mine.

4.2. The investigation of tidal flat changes

The changes of tidal flats are obtained by comparing DEMs of the tidal flats in 1989, 2001, and 2014. The DEM constructed in earlier years is subtracted from the one in later years to calculate the vertical changes of tidal flats. Negative values and positive values of the results correspond to vertical erosion and deposition. Vertical changes are multiplied with the area of a pixel-size (30 m x 30 m) to achieve the volume changes which indicates the amount of sediment loss or sediment concentration in m^3 unit. Fig. 5 illustrates the amount of sediment loss and sediment deposition on tidal flats during the period 1989-2014. The study area is characterized by numerous near-shore limestone islands which block suspended sediments to form tidal flats in the study areas. Accordingly, tidal flats are closer to the land and surrounded by islands, which tend to be higher deposition. Tidal flats in the Lo Phong river mouth with the red area have a higher rate of deposition than that of the C2 river mouth with the green areas.

To observe the cross-shore variation of tidal flats, 18 observation points are placed in even distribution along a cross-section of tidal flats at the C2 river mouth (Fig. 5). Figure 6 illustrates the volume changes of the tidal flat at 18 observation points in periods 1989-2001 and 2001-2014. The positive volume and negative volume correspond to the amount of sediment accretion and sediment loss in an 900 m^2 area during the periods. At the first observation point, the accretion occurs in both periods 1989-2001 and 2001-2014 with $1,008 \text{ m}^3$ and 621 m^3 positive volumes, respectively. The deposition is highest as the tidal flat is closest to the C2 river mouth. Tidal flats in the area from point 2nd to point 8th during two periods are similarly eroded with the maximum at more than 300 m^3 during 2001-2014. A contrasting variation of tidal flats between two periods is seen in the area from point 9th to the end of the tidal flat (point 18th). The tide flat from point 9th to point 14th experiences a strong deposition with the maximum accretion at 350 m^3 from 1989 to 2001, but it witnesses severe erosion during 2014-2020. Subsequently, an remarkable accretion is seen in the furthest area of tidal flat from point 15th to point 18th during the period 2001-2014, but the erosion is insignificantly observed during 1989-2001.

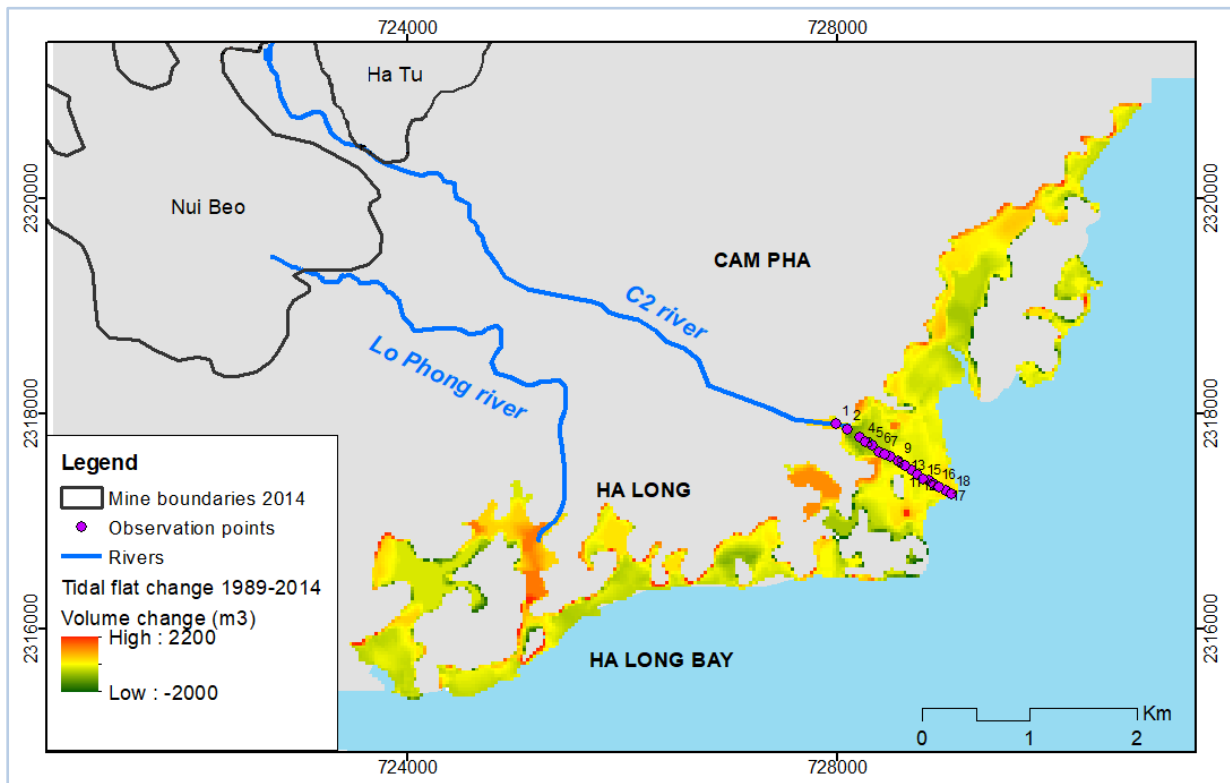


Fig. 5. Volume changes of tidal flats in the period 1989 – 2014 (m³).

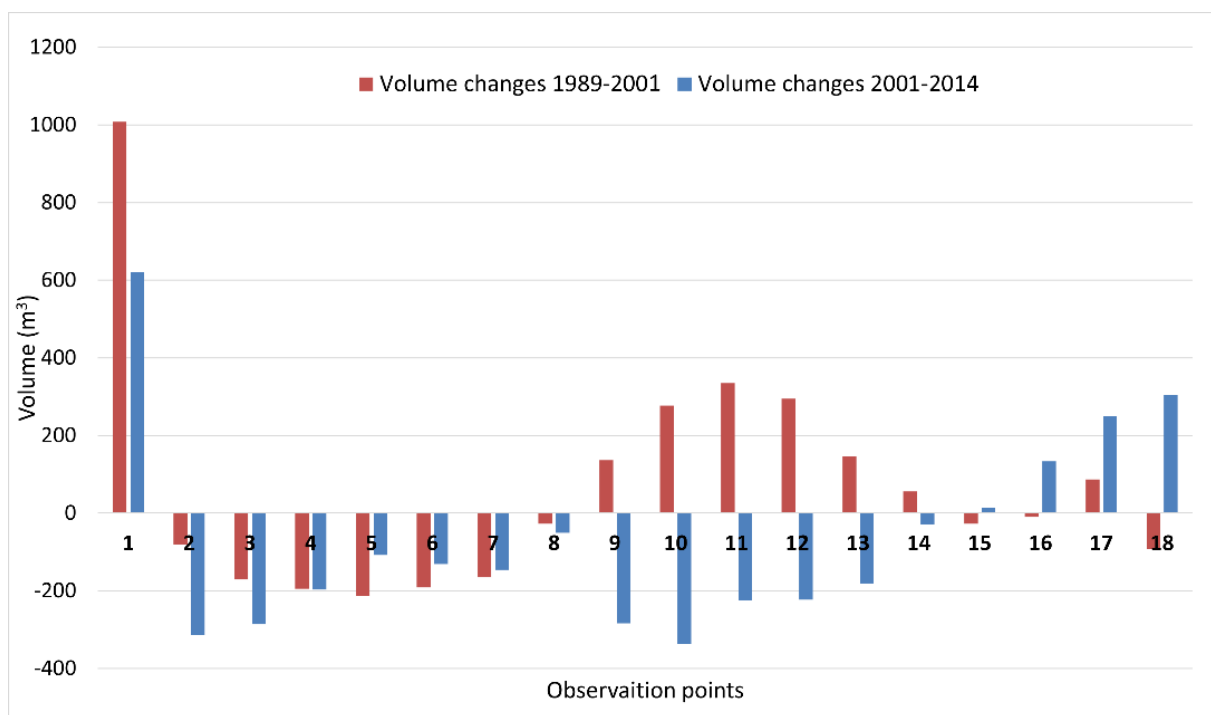


Fig. 6. The volume change of tidal flats along the observation points at the C2 River estuary during periods 1989-2001 and 2001-2014. The volume measured in m³, is calculated in a ground area of 900 m² (pixel size 30 m x 30 m).

4.3 Sediment characteristic of tidal flats

Three parameters of sediment samples in this study are analyzed including sediment size, organic matter, and carbonate content. However, the carbonate content is insignificant (below 1 %) thus it is

ignored and does not mention in other sections. Figure 7 illustrates the relationship between sediment characteristics and the topography along the cross-section in the tidal flat. The organic matter composed in sediment is from 459 g/kg to 607 g/kg (Fig. 7a). The CP_River sample is collected at the highest location of the tidal flats, closest to the C2 river mouth, which has the amount of 524 g organic matter per one kg sample. The farthest sample is collected at 1200 m from the C2 river mouth, at the lowest area of tidal flats, which has the highest concentration of organic matter with 607 g/kg. Generally, the organic matter in the tidal flat is gradually increasing from the mainland to the sea. The concentration of organic matter distributes oppositely with the elevation of tidal flats.

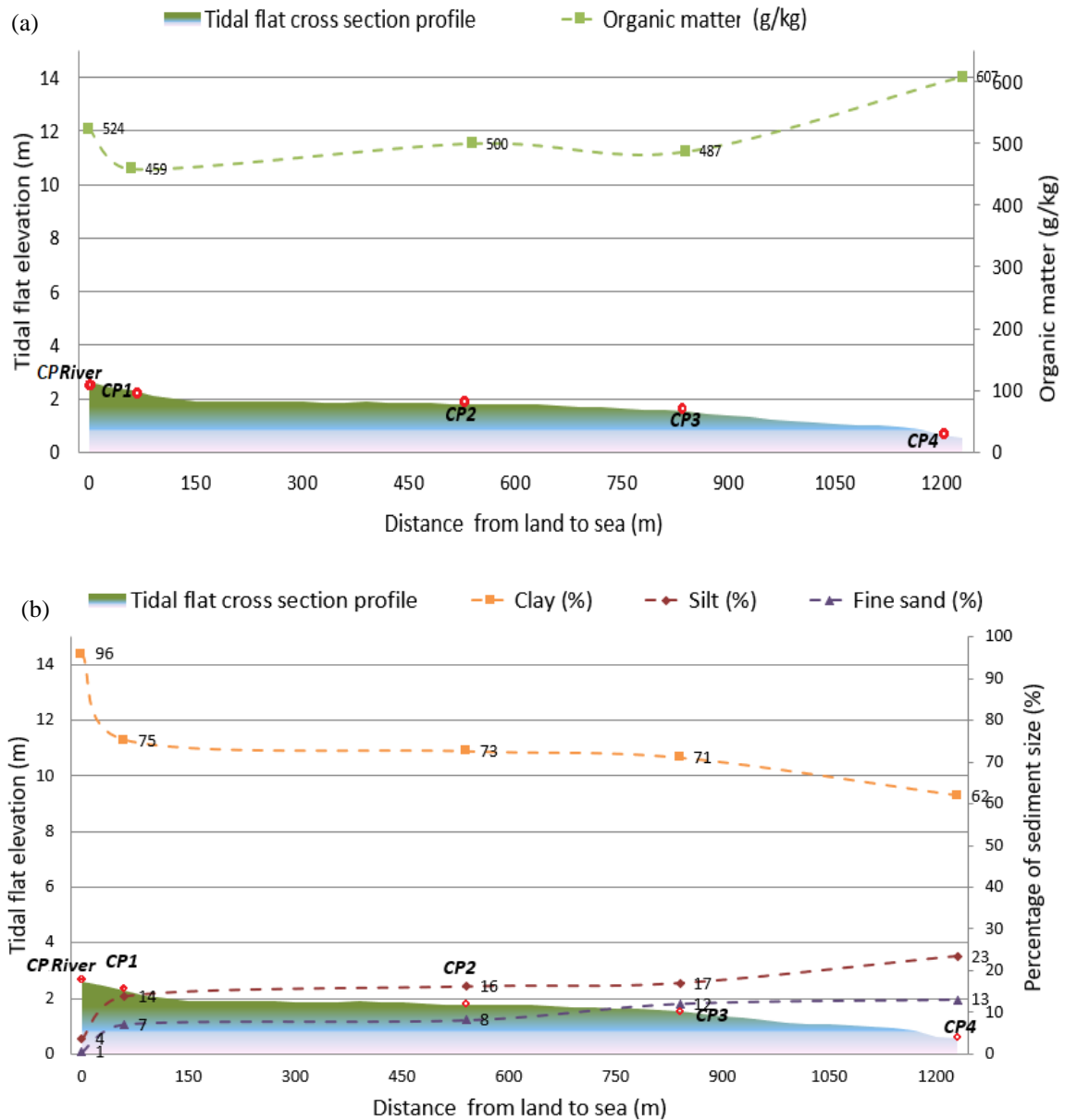


Fig. 7. (a) Organic matter and (b) sediment types distributing at 5 sample locations (CP River, CP1, CP2, CP3, CP4) in the tidal flat. Red points are the relative location of samples on tidal flats.

Figure 7b represents the distribution of sediment types in the correlation with the topography of the tidal flat. Only 3 types of sediment size are recognized in samples consisting of clay, silt, and fine sand. Clay with a size ranged from 0 to 50 μm , is predominant, which occupies more than 62 % of all the samples. Especially, the percentage of clay closing to the C2 river mouth reaches a maximum of 96 %. The concentration of the finer particles tends to gradually decrease seaward corresponding to the degradation of tidal flat elevation. The percentage of silt and fine sand occupies the small rest of the samples with a total from 5 % to 36 %. The concentration of these sediment types increases gradually seaward and correlates oppositely with the transition of tidal flat elevation.

4.4 Impact of coal exploitation on tidal flat changes

The impact of coal exploitation on the change of tidal flats is discussed in two aspects concerning 1/ the origin of sediment which forms the tidal flats and 2/ the correlation between the coal exploitation and the tidal flat variation.

To investigate the origin of the sediment forming the tidal flats, we attempt to analyze chemical and physical compounds in sediment samples collected in tidal flats. Organic matter, carbonate content, and particle size are three parameters that are measured in the study. The remains of the organism as animals, plants, and their waste products in the environment are the sources of organic matter [15]. Over millions of years, plant and mineral matter are undergone the processes of burial, compression, and heat to form coal. The rock is classified as coal since it must contain more than 50 % of organic matter [16]. As indicated in the previous sections, all sediment samples are composed of more than 50 % of organic matter, the rest of mineral such as carbonate content is insignificant. Besides, the sediment in the tidal flat is muddy and black [5]. Consequently, it is affirmed that the material forming tidal flats is coal particles, but we need to discuss more on the sources of coal particles which are originated from the ocean or from coal exploitation.

Ha Tu and Nui Beo are two open coal mines, occupies a large area of 1,400 ha, consisting of areas for coal exploitation, coal product storage, restoration area, rocky disposal, area for coal processing services, and transporting coal products, etc. All of these areas and relating coal mining activities disperse coal particles in various sizes into the water, soil, and atmospheric environment. These areas of the two mines are within the watersheds of the two rivers C2 and Lo Phong. Coal and other particles in the environment follow water flows to gather in these rivers then they are transported and spread out the near-shore water of the river mouths. The amount of suspended particles transported to the river mouths is extremely high during the rainy season. Besides, The coastal area of the study area suffers the effect of tide domination with calm water as the wind and waves are obstructed from the sea by thousands of islands in Ha Long bay. In calm conditions, suspended particles tend to settle in the shallow waters rather than moving offshore [17]. Moreover, the high percentage of organic matter containing in all sediment samples in tidal flats indicates the insufficiency of nutrients for animal habitats and plants that lead to little benthos and mangroves living in tidal flats [15]. The pure coal tidal flats with rare living things mean the tidal flats are continuously and instantaneously deposited or replaced with coal particles. For those reasons, the material which formed the tidal flats in the study area is of continental origin. According to the above discussions, it is concluded that the coal tidal flats in the study area are the consequence of coal exploitation activities in the land.

One of the objectives of this study is to figure out the relationship between the change of tidal flats and the variation of coal exploitations. Tidal flat changes in periods 1989-2001 and 2001-2014 are determined using corresponding satellite data. The quantity of coal exploitation is consisting of coal production, waste rock dump, which are collected from the reports of the mine managers. The exploitation area is determined on satellite images. During the period 1989-2001, the amount of waste rock dumps and coal production from both mines are small compared to that of the period 2001-2014 corresponding to $1.56 \times 10^6 \text{ m}^3$ and $28.84 \times 10^6 \text{ m}^3$ (Tab. 3). Simultaneously, the volume change of tidal flats is small with the sediment loss of $0.06 \times 10^6 \text{ m}^3$ from 1989 to 2001. According to Tong et. al. [5], the elevation error of DEM constructed in this study is 0.144 m, the uncertainty of volume changes in 122.4 ha tidal flats in the study area is $\pm 0.176 \times 10^6 \text{ m}^3$. The uncertainty is much greater than the change volume detected in tidal flats in 1989-2001, thus this change is insignificant. The sharp increase of waste rock dump and coal production in the period 2001-2014 may contribute to the accretion of tidal flats with $0.37 \times 10^6 \text{ m}^3$ positive changes. Although the more exposition of coal rubbishes to the environment, or more active coal mines generally boost up the amount of sediment transported to the near-shore water, it is hard to affirm the direct effect of coal mine exploitation on the quantitative changes of tidal flats using one or two observations. Besides, the sediment transport in tidal flats is controlled synthetically by 5 main forcing physical processes as the waves, the wind-induced circulation, the tide, the density-driven circulation, and the drainage [18]. Among these processes, the effect of drainage processes including sediment transport upon the tidal flat evolution has not been sufficiently indicated [19]. Consequently, the increase of coal mining activities is simultaneous with the deposition of the tidal flats in this experiment. However, the long-term effect of coal mining activities on the evolution of tidal flats is probably figured out since numerous temporal observations are investigated using remote sensing data. This research direction

should be continued in future studies.

Tab. 3. Tidal flat changes and the variation of coal mining activities calculated from both Nui Beo and Ha Tu mines.

Periods	Waste rock dump (10^6 m ³)	Coal production (10^6 m ³)	Exploited area (ha)	Tidal flat change (10^6 m ³)
1989-2001	1.56	0.81	327	-0.06
2001-2014	28.84	1.52	380	0.37

5. Conclusions

As an example for the assessment of the coal mining exploitation affecting the coastal area, this study attempts to determine the relationship between the tidal flat changes and the coal mining activities. Volume changes of tidal flats during two periods 1989-2001 and 2001-2014 are estimated using multi-temporal satellite images integrating instant tidal levels. Besides, the physical, chemical characteristics of sediments in tidal flats are analyzed. Coal mining activities of two open-pit mines are investigated according to three parameters consisting of waste rock dump, coal production, and exploitation area. The study has proved that the material constituted and formed the tidal flats are originated from the coal mining activities based on the characteristics of sediment samples. Although the increase of coal exploitation is simultaneous with the accretion of tidal flats in one period, it should be used numerous of observations to figure out the long-term impact of coal exploitation on the evolution of tidal flats. This issue opens a future study of applying the advance of information technology on a huge number of satellite data for long-term monitoring of the coal tidal flats changes.

6. Acknowledgements

We would like to express our thanks to the internal project coded T21-22, funded by the Hanoi University of Mining - Geology.

The paper was presented during the 6th VIET - POL International Conference on Scientific-Research Cooperation between Vietnam and Poland, 10-14.11.2021, HUMG, Hanoi, Vietnam.

7. References

1. Gao, S., *Geomorphology and sedimentology of tidal flat*, Coastal Wetlands, 2018.
2. Ryu, J.H., J.K. Choi, and Y.K. Lee, 2014. Potential of remote sensing in management of tidal flats: A case study of thematic mapping in the Korean tidal flats, *Ocean and Coastal Management*, 102(part B): 458-470, <https://doi.org/10.1016/j.ocecoaman.2014.03.003>.
3. Kirwan, M.L., G.R. Guntenspergen, A. D'Alpaos, J.T. Morris, S.M. Mudd, and S. Temmerman, 2010. Limits on the adaptability of coastal marshes to rising sea level, *Geophysical Research Letters*, 37(23), <https://doi.org/10.1029/2010GL045489>.
4. Suwarsono, N., Suryo Haryani, I. Prasasti, H.M. Listi Fitriana Priyatna, and M. Rokhis Khomarudin, 2017. Detecting the area damage due to coal mining activities using Landsat multitemporal (Case Study: Kutai Kartanegara, East Kalimantan), *International Journal of Remote Sensing and Earth Science*, 14(2): 151-158.
5. Tong, S.S., J.P. Derooin, and T.L. Pham, 2020. An optimal waterline approach for studying tidal flat morphological changes using remote sensing data: A case of the northern coast of Vietnam, *Estuarine, Coastal and Shelf Science*, 236(5): <https://doi.org/10.1016/j.ecss.2020.106613>.
6. Koruyan, K., A.H. Deliormanli, Z. Karaca, M. Momayez, H. Lu, and E. Yalçin, 2012. Remote sensing in management of mining land and proximate habitat Determining the expansion of marble quarries, *The Journal of The Southern African Institute of Mining and Metallurgy*, vol. 112(7): 667-672.

7. Charou, E., M. Stefouli, D. Dimitrakopoulos, E. Vasiliou, and O. D. Mavrantza, 2010. Using remote sensing to assess impact of mining activities on land and water resources, *Mine Water and the Environment*, 29(1): 45-52, <https://doi.org/10.1007/s10230-010-0098-0>.
8. Kim, Y., D.H. Jang, N.W. Park, and H.Y. Yoo, 2016. Assessment of landform changes in Baramarae tidal flat, Korea using combined analysis of multi-temporal remote sensing images and grain size measurement data, in *Journal of Marine Science and Technology (Taiwan)*, 24(6): 1070-1080. <https://doi.org/10.6119/JMST-016-0729-1>.
9. Heygster, G., J. Dannenberg, and J. Notholt, 2010. Topographic mapping of the german tidal flats analyzing SAR images with the waterline method, *IEEE Transactions on Geoscience and Remote Sensing*, 48(3): 1019-1030, <https://doi.org/10.1109/TGRS.2009.2031843>.
10. Lan, P.T., T.S. Son, K. Gunasekara, N.T. Nhan, and L.P. Hien, 2013. Application of Remote Sensing and GIS technology for monitoring coastal changes in estuary area of the Red river system, Vietnam, *Journal of the Korean Society of Surveying Geodesy Photogrammetry and Cartography*, 31(6): 529–538, <https://doi.org/10.7848/ksgpc.2013.31.6-2.529>.
11. Ryu, J.-H., J.-S. Won, and K. Duck Min, 2002. Waterline extraction from Landsat TM data in a tidal flat A case study in Gomso Bay, Korea, *Remote Sensing of Environment*, 83(3): 442-456, [https://doi.org/10.1016/S0034-4257\(02\)00059-7](https://doi.org/10.1016/S0034-4257(02)00059-7).
12. GreenFacts, 2019. Natural Organic Matter. <https://www.greenfacts.org/glossary/mno/natural-organic-matter-NOM.htm>.
13. Lan, T.P., Son, P.N., Nghia, V.N., Huong, V.D., Long, D.D., Nhung, H.T.V., Trang, T.T.N., Huan, V.T., 2020. Establishment of land cover map using objectoriented classification method for VNREDSat-1 data. *Journal of Mining and Earth Sciences*, 61(2): 134-144, DOI:10.46326/JMES.2020.61(2).15.
14. Lan, T.P., Ha, T.T.L., Luong, T.H., Hung, V.N., 2017. A Hierarchical object oriented method for land use classification of LANDSAT Imagery in Thai Thuy district, Thai Binh province. *Journal of Mining and Earth Sciences*, 58(4): 43-50.
15. Zhu, C., Z. Zhang, H. Wang, J. Wang, and S. Yang, 2020. Assessing soil organic matter content in a coal mining area through spectral variables of different numbers of dimensions, *Sensors (Switzerland)*, 20(6), <https://doi.org/10.3390/s20061795>.
16. Stanley, P.S., 2002. *Coal - A Complex Natural Resource*, U.S. Geological Survey.
17. Christie, M.C., Dyer, K.R., Turner, P., 2002. Sediment Flux and Bed Level Measurements from a Macro Tidal Mudflat, *Estuarine, Coastal and Shelf Science*, 49(5): 667-688.
18. Eisma, D., *Intertidal Deposits: River Mouths, Tidal Flats and Coastal Lagoons*, Marine Science Series, CRC Press, Boca Raton, 1997, 507.
19. Hir, P.L., W., Roberts, O., Cazaillet, M., Christiem, P., Bassoullet, Bacher, C., 2000. Characterization of intertidal flat hydrodynamics, *Continental Shelf Research*, 20(12-13): 1433-1459. [https://doi.org/10.1016/S0278-4343\(00\)00031-5](https://doi.org/10.1016/S0278-4343(00)00031-5)

A Solution to Ensure Ventilation when Expanding the Area of Cam Thanh Underground Coal Mine, Ha Long Coal Company, Vietnam

NGUYEN Cao Khai^{1,*}, NGUYEN Van Thinh¹, NGUYEN Phi Hung¹, NGUYEN Van Quang¹

¹ Hanoi University of Mining and Geology, 18 Vien street, Hanoi, Vietnam

Corresponding author: nguyencaokhai@humg.edu.vn

Abstract. In the process of underground mining, the mining system changes for various reasons. One of the main reasons is changes in the mining production plans, especially the scales and outputs. Nowadays, coal mines in Vietnam have been expanding in width and depth, and so have the mines' ventilation systems. Consequently, there will be changes in the alteration of the structure of the design ventilation system, which reduces the effectiveness of the ventilation and does not meet the main objective of mine ventilation, directly affect the safety of the working environment in the mine. Therefore, it is necessary to research the improvement of the ventilation system with the development and specific conditions of underground coal mines in Vietnam, improving the efficiency of the ventilation work and assuring the safety of the mine environment. Cam Thanh coal mine, Ha Long coal company, Vietnam, is the case study for this research. The article considers the plan of increases the mining output by more than 1.5 times, propose solutions to improve the ventilation system accordingly, helping the company proactively implement the production plan, ensure the working environment's safety, and reduce the costs of mine ventilation.

Keywords: Mine ventilation, Mine ventilation and safety, Cam Thanh mines area, Ventilation system adjustment, Fan operating points

1. Introduction

Ha Long Coal Company is a Vietnam National Coal and Minerals Holding Corporation Limited (Vinacomin) subsidiary. The company includes mining areas of Cam Thanh, Tan Lap, and Ha Rang, which coal output of 2020 is 1.75 million tons. Cam Thanh mining area plans to reach 400,000 tons per year, which requires three longwalls and eight preparation tunnels. Cam Thanh area will be a large area to increase production. After 2020, it is possible to increase the output to more or less 700,000 tons per year, with five longwalls [1, 2, 3]. It is imperative to develop a corresponding exploitation plan and, as a result, an appropriate ventilation system to increase the exploitation output of the area. This adaptation helps reduce natural hazards which may occur, such as fire and explosion due to accumulation of methane gas, suffocation due to accumulation of toxic gases, unsafe working environment conditions for workers, etc.

The study aims to apply appropriate solutions to complete the ventilation system for the mine in assuring environment and safety. The article helps to consider the economic efficiency of investment when the mine increases its production.

2. Research Methods

Cam Thanh mining area, Ha Long Coal Company, was selected as the research area. Statistics, inheritance, field studies, and theoretical studies are the main methods for detailed audit and assessment of the current mine ventilation system. The inspection results combined with the calculation of the planned ventilation requirements help us find suitable solutions and applied to improve ventilation efficiency to ensure mine safety.

3. Calculation of ventilation for Cam Thanh mine area

3.1. Calculate current of ventilation for the mining area

3.1.1. Diagrams of the current mine wind network

According to the current exploitation plan, to ensure 400,000 tons per year of output, Cam Thanh must operate three longwalls and eight preparation galleries. The plan of longwalls is shown in Table 1, and preparation galleries are in Table 2 [1].

Tab. 1. Characteristics of longwalls in Cam Thanh mine area.

No	Longwalls name	Length (m)	Cross-section of the tunnel used (m ²)	Productivity (tons /24h)	Number people working (people)	Maximum amount of explosives (kg)
1	Longwall XDY level -50/-20 V10 CB	55	4.5	260	20	4
2	Longwall TLD level -20/+40 V11B CB	94	4.5	253	22	4
3	Longwall TLD level -50/-20 V11B CB	60	4.5	260	22	4

Tab. 2. Parameters of preparation tunnel mirrors.

No	Name of preparation galleries	Length, L (m ³ /p)	Cross-section, S (m ²)	Explosives, A (kg)	Number people, n (people)
1	Preparation tunnel level -50/-20 CB V10	70	8.4	4.5	8
2	Preparation tunnel level +5 +HS +0/+5 V11b CB	30	6.5	4.5	8
3	Preparation tunnel KĐ level -50/+40 CB V11	125	9.4	5	10
4	Preparation tunnel leve -40 +HS -50/-40 CB V11	40	8.4	4.5	8
5	Preparation tunnel level +25 +HS +25/+40 CB V11	60	8.4	4.5	8
6	Preparation tunnel level -45, HS -50/-45 CB V10	20	6.5	4.5	8
7	Preparation tunnel level -45, HS -50/-45 CB V11	30	8.4	5	8
8	Preparation tunnel KĐLC level -50/-20 V10 CB	250	8.4	5	8

The diagram of the current wind network is structured from the faces with three longwalls, and eight preparation galleries (Fig. 1). In general, this ventilation network is relatively complex. The mine area is ventilated by suction ventilation with a BD-II-6-No15/2x55kW fan station.

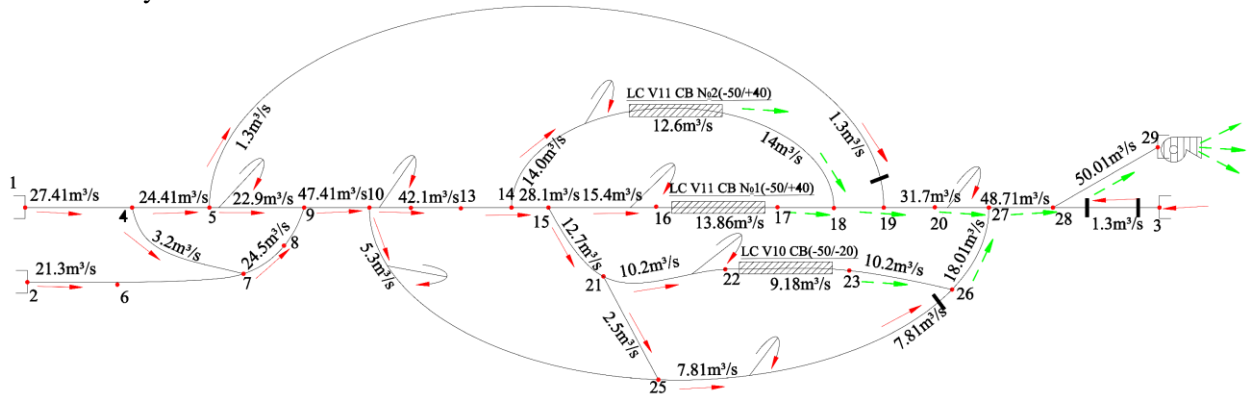


Fig. 1. Existing ventilation scheme in Cam Thanh mine area.

3.1.2. Calculation of current wind flow for the area

To calculate ventilation for Cam Thanh mine area, we apply the formula [4]:

$$Q_m = 1,1(K_{sl} \cdot \Sigma Q_{lc} + \Sigma Q_{cb} + \Sigma Q_{ht} + \Sigma Q_{rg}); m^3/s \tag{1}$$

Where:

1.1 - The coefficient refers to the uneven distribution of wind in wind currents.

K_{sl} - Coefficients to account for the increase in output of the longwall (select k_t = 1.1).

ΣQ_{rg} - Total leakage wind flow in mine, m³/s.

ΣQ_{lc} - Total amount of wind flow required for the furnace oven, m³/s.

ΣQ_{cb} - Total amount of wind flow needed for the digester mirror, m³/s.

ΣQ_{ht} - Total amount of wind flow required for the station, m³/s.

With the current mining status, we can calculate the wind flow for the site as follows:

$$Q_m = 1.1(1.1 \times 17.0 + 16.8 + 4.36 + 5.6) = 50.01 m^3/s$$

3.1.3. Calculation mine ventilation pressure

To calculate mine ventilation pressure, we calculate the low pressure of the wind currents and apply the formula [5]:

$$h_m = \sum h_{ms} + \sum h_{cb}, \text{ mmH}_2\text{O} \quad (2)$$

In which:

$\sum h_{ms}$ - The total hypotension caused by the frictional resistance of the segments, following each other in a wind flow, is calculated from the beginning to the endpoint. This pressure lowering is calculated according to the formula [4]:

$$h_{ms} = \alpha_i \frac{L_i \cdot P_i}{S_i^3} \cdot Q_i^2, \text{ mm H}_2\text{O} \quad (3)$$

In which:

α_i - The aerodynamic resistance coefficient in the i th tunnel on the airflow, kGS^2/m^4 ;

L_i, P_i, S_i - Length, circumference, the cross section of tunnel I , respectively;

Q_i - The amount of wind going through the i th tunnel, m^3/s .

$\sum h_{cb}$ - The total hypotension due to local resistance, calculated by a wind flow, is often taken from $(10 \div 25\%) H_{ms}$.

Replace the parameters and calculate the results of the mine pressure lowering as follows:

$h_1 = 85.03 \text{ mmH}_2\text{O}$ (flow lowering pressure 1);

$h_2 = 82.49 \text{ mmH}_2\text{O}$ (flow lowering pressure 2);

$h_3 = 78.80 \text{ mmH}_2\text{O}$ (flow lowering pressure 3)

and $h_4 = 67.26 \text{ mmH}_2\text{O}$ (flow lowering pressure 4).

Adjust the wind window is a method to balance the mine pressure. The lower pressure of the selected mine is $h_1 = 85.03 \text{ mmH}_2\text{O}$.

3.1.4. Determination of the current operating mode of the central blower

* Determine the airflow of the fans to create

To calculate the fan wind flow to be generated, we apply the following formula [4, 6]:

$$Q_q = K_r \cdot Q_m, \text{ m}^3/\text{s} \quad (4)$$

In which:

K_r - Leakage coefficient at fan station, semi-fixed fan station get $K_r = 1.15$

Q_m - Airflow required for the whole mine: $Q_m = 50.01 \text{ m}^3/\text{s}$

The results of calculating the airflow for fans are as follows: $Q_q = 57.51 \text{ m}^3/\text{s}$.

* Determine pressure the fans to create

Pressure the fans to create is calculated according to the formula [2, 6]:

$$H_q = (k_1 \cdot R_m + R_{tbq}) \cdot Q_q^2, \text{ mmH}_2\text{O} \quad (5)$$

In wich:

k_1 - the coefficient refers to the leakage at the fan station, $k_1 = 1/k_r^2$, $k_1 = 0.76$

R_m - mine resistance, $\text{k}\mu$; For the mine area, we have the mine resistance: $R_m = 0.033998 \text{ k}\mu$;

R_{tbq} - Resistance of fan equipment ($R_{tbq} = a \cdot \pi/D^4$): For the main fan of the mine, the fan resistance is as follows: $R_{tbq} = 0.0031$;

Instead we have: $h_q = 102.5 \text{ mmH}_2\text{O} = 1025 \text{ Pa}$;

* Determine the working mode of the main fans

The calculation to determine the operating mode of the main fans is calculated based on the general regulations and using the calculation method to determine the operating mode of the fans by the graph method [7, 8]. The calculation determines the operating mode of the main fans as follows:

- Equation curve characteristic mine: $h = 0.030978 \cdot Q^2$;

- Operating mode of the main blower

The determination result of the main wind fan is shown in Figure 2. The working point is point B, with

the fan working parameters as follows:

- Fan flow generated: $Q_{ct} = 59 \text{ m}^3/\text{s}$;
- Fan pressure: $h_{ct1} = 108.2 \text{ mmH}_2\text{O} = 1082 \text{ Pa}$;
- Impeller mounting angle of impeller: $\theta = +25^\circ$
- And Fan performance: $\eta = 0.54$.

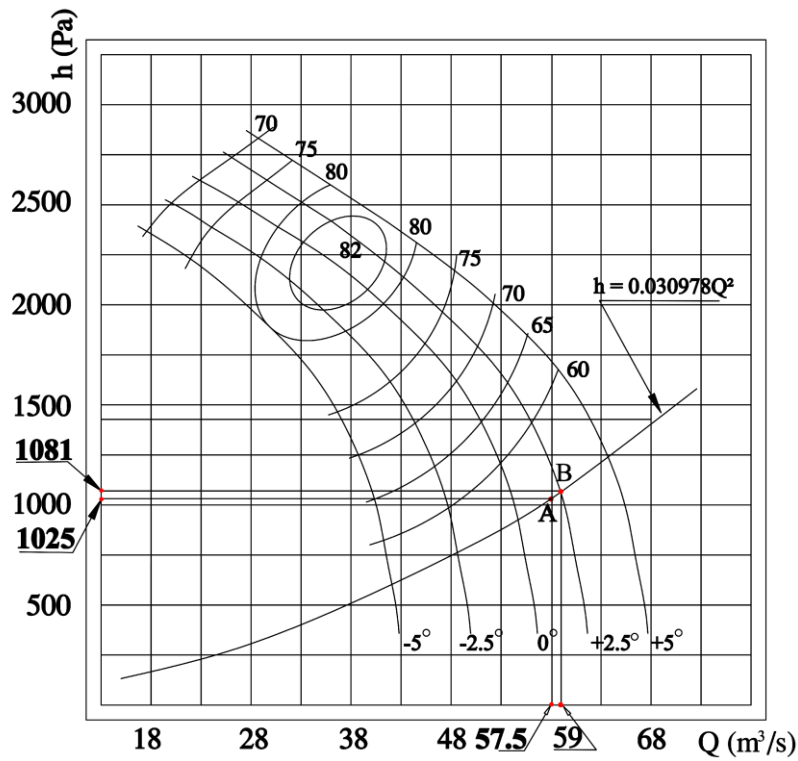


Fig. 2. Graph identifying the current operation mode of fan BD-II-6-No15 Mine area Cam Thanh, Ha Long Coal Company.

3.2. Calculate ventilation for the mine area when increasing production

The ventilation calculation of the mine area when increasing the mining output is similar to the current mine. However, the measure must take the parameters of the increasing mining output taken into account

3.2.1. Ventilation diagram of the mine site when increased production

To reach the output of the mine area to 700,000 tons per year, Cam Thanh exploits coal seams, including coal seam No10 and coal seam No11. The mine must operate five longwalls as shown in Table 3 and 10 preparation galleries as in Table 4 [2]. Figure 3. illustrates the mine ventilation diagram.

Tab. 3. Mobilization plan, longwall characteristics in production when increasing production.

No	Longwall name	Length (m)	Number of people	Explosives (kg)	Cross section (m ²)	Productivity (tons /24h)	
						Min	Max
1	XDY level -50/-20 V10 CB	55	20	4	4.5	240	270
2	XDY level -50/-20 V10 CN	80	22	4	4.5	240	300
3	TLD level -20/+40 V11B CB	94	22	4	4.5	240	300
4	TLD level -50/-20 V11B CB	60	10	4	3.2	240	270
5	XDY level -50/+40 V11CB	120	10	4	3.2	240	270

Tab. 4. Plans and characteristics of the preparation tunnel lines to meet when increasing production.

No	Preparation tunnel name	Anti-retention material	Cross section (m ²)	Length needs ventilation (m)	Explosives, A (kg)	Number people, n (people)

1	Level -25 (-25/-20) CBV10	iron	8.4	40	4.5	8
2	Level -50/-20 CB V10	iron	8.4	70	4.5	8
3	Level -40 (-50/-40) V11B CB	iron	8.4	50	4.5	8
4	Level +5 (+0/+5) V11B CB	iron	6.5	30	4.5	8
5	Level -40 (-50/-40) CB V11	iron	8.4	40	4.5	8
6	Level +25 (+25/+40) CB V11	iron	8.4	60	4.5	8
7	Level -45, (-50/-45) CBV10	iron	6.5	20	4.5	8
8	Level -20 LT.Cb V10	iron	6.5	70	4.5	8
9	Level -45, HS -50/-45 CB V11	iron	6.5	30	4.5	8
10	KDLC level -50/-20 V10 CB	iron	8.4	250	5	8

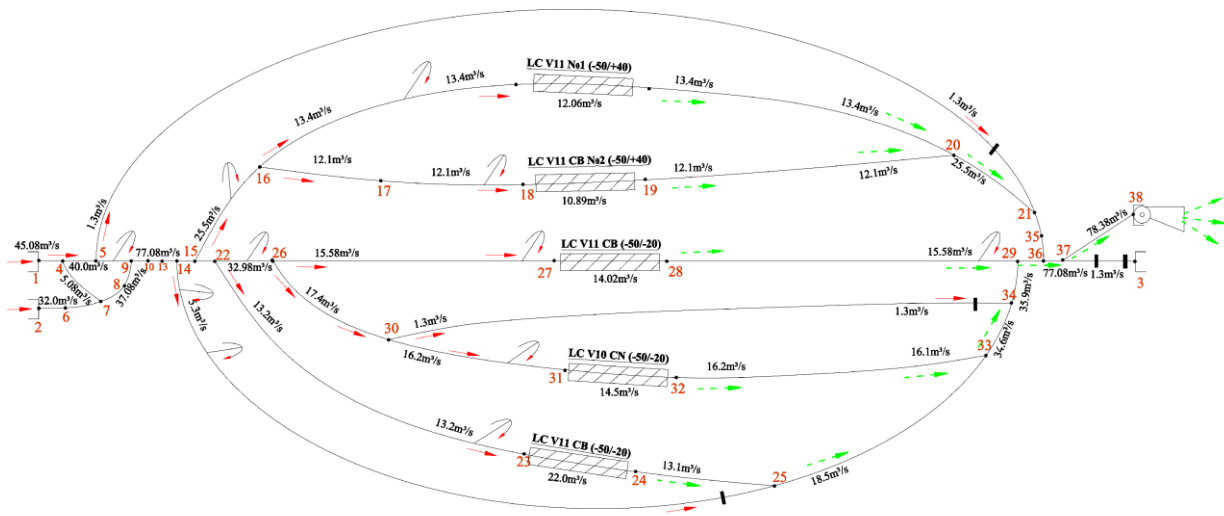


Fig. 3. Ventilation diagram of Cam Thanh mine area, when increasing exploitation output.

3.2.2. Calculate wind flow for the mine area when increasing production

With the condition that when increasing the mine area's exploitation output, the wind flow calculation results for the mine area are as follows:

$$Q_m = 1.1(1.1 \times 32.6 + 23.5 + 4.74 + 7.16) = 78.38 \text{ m}^3/\text{s}$$

3.2.3. Calculate pressure for the mine area when increasing output

As in Fig. 3, the wind network has five main air currents. Calculation results of the pressure of the specific wind flows are as follows: $h_1 = 118.81 \text{ mmH}_2\text{O}$ (XDY level -50/+40 V11CB); $h_2 = 113.45 \text{ mmH}_2\text{O}$ (XDY level -20/+40 V11CB); $h_3 = 126 \text{ mmH}_2\text{O}$ (XDY level -50/-20 V10 CB); $h_4 = 130.58 \text{ mmH}_2\text{O}$ (XDY level -50/-20 V10 CN); $h_5 = 125.81 \text{ mmH}_2\text{O}$ (TLD level -50/-20 V11B CB), in which the flow of h_4 is the largest. Hence, the $h_4 = 130.58 \text{ mmH}_2\text{O}$ is the pressure of the mine. The other flows are adjusted to pressure balance by setting the adjustment wind window.

3.2.4. Determine the operation mode of the central blower when increasing output

* Determine the wind flow of the fans to create

The calculation results of wind flow for the fans are as follows: $Q_q = 86.2 \text{ m}^3/\text{s}$.

* Determining the pressure fan to create

The pressure to create fan: $h_q = 161 \text{ mmH}_2\text{O} = 1610 \text{ Pa}$;

* Determine the reasonable working mode of the main fan

The technical characteristics and working capacity of the current BD-II-6-No15/2x55kW fans of the mine currently in use will not meet the ventilation demand of the mine if only one fan is used and the other

is in standby mode. Therefore, the plan to use existing BD-II-6-No15/2x55kW fans is only an immediate solution. In the long term, it is necessary to consider investing in a new type of fan.

When existing BD-II-6-No15/2x55kW fans are used, both fans must run in a combination of parallel modes close to each other with no backup. The result of determining working fan mode is as follows:

- Equation curve characteristic mine: $h = 0.0243 \cdot Q^2$;
- Operating mode of the main fan

The result of determining the operating mode of the main fan is in Fig. 4.

- + The common working point of the fan set is point B, with the working parameters as follows:

The total airflow generated by the fan set: $Q_c = 91.3 \text{ m}^3/\text{s}$;

Lower the pressure generated by the fan unit: $h_{ct} = 195.0 \text{ mmH}_2\text{O} = 1950 \text{ Pa}$;

- + The working point of the component fan is the B_{ct1} point, with the following working parameters:

Fan flow generated: $Q_{ct} = 45.6 \text{ m}^3/\text{s}$;

Lowering the fan pressure creates: $h_{ct} = 195 \text{ mmH}_2\text{O} = 1950 \text{ Pa}$;

Impeller angle of impeller: $\theta = 0^\circ$

And Fan performance: $\eta = 0.77$.

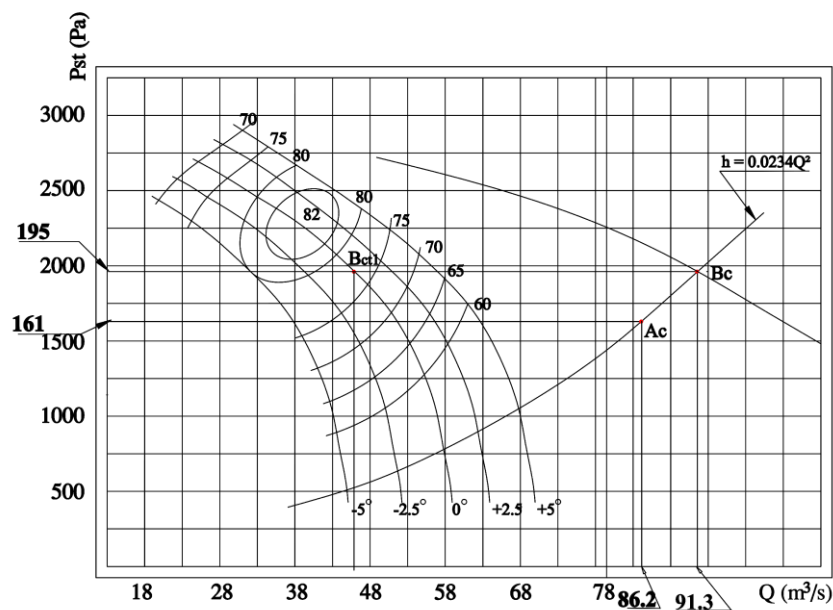


Fig. 4. Graph defining the operating mode of the main fan of Cam Thanh mine when increasing output. (using two BD-II-6-No15/2x55kW combined fans).

4. Solutions to complete the ventilation system of mine area when increasing exploitation output

With the research results and references from many research projects in mining [9, 10, 11, 12, 13, 14, 15, 16]. We propose several solutions to improve the operational efficiency of the mine ventilation system for Cam Thanh area nowadays and when the production output increase, as follows:

1- Orientation on ventilation method and fan placement

The work of ventilation for Cam Thanh mine area when continuing to exploit the plan from -50 to 40 is still carried out as at present. Specifically: General ventilation for the mine is still using the suction ventilation method, with 01 central fan station as today: type BD-II-6-No15/2x55kW) at the tunnel door of 117 level. However, if the catches of Cam Thanh mine area increase, this fan station will not meet, it is suggested: Raising the capacity of level +117 fan station from BD-II-6-N15/2x55kW up type fan 2K56-No24 or FBDCZ-6-No24/2x315 kW or fan with equivalent power.

2- Orientation of the general wind demand necessary to be put into the mine

The general wind flow of the mine needs to ensure the current clean wind demand (about $57.5 \text{ m}^3/\text{s}$) to maintain the production, and if Cam Thanh mine area mobilizes more longwall to increase the exploitation output. As planned, the demand for wind in Cam Thanh mine area will increase, so there must be appropriate calculation solutions.

3- Solutions to use the main fan

The estimated wind flow for the mine area is about 78.38 m³/s, which means that the central fan station needs to work with greater capacity, so the BD-II-6-No15/2x55kW fan type no longer responds. At that time, the mine area needs to change to other types of fan with higher capacity. Here, the research content considers the development needs of the mine until after 2025, so we will propose the use of 2K56-No24 fan (or a fan with a similar capacity). It is expected to calculate the operating mode of fan type 2K56-No24 when increasing exploitation output, as shown in Figure 5 [6].

The results determine the operating mode of the main fan, as shown in Fig. 5. With the fan working parameters as follows:

- The point is the job is the B_{ct2} point;
- Fan flow generated: Q_{ct} = 87 m³/s;
- Fan pressure generated: h_{ct} = 164.5 mmH₂O = 1645 Pa;
- Impeller mounting angle of impeller: θ = 2.5°
- And fan performance: η = 0.74.

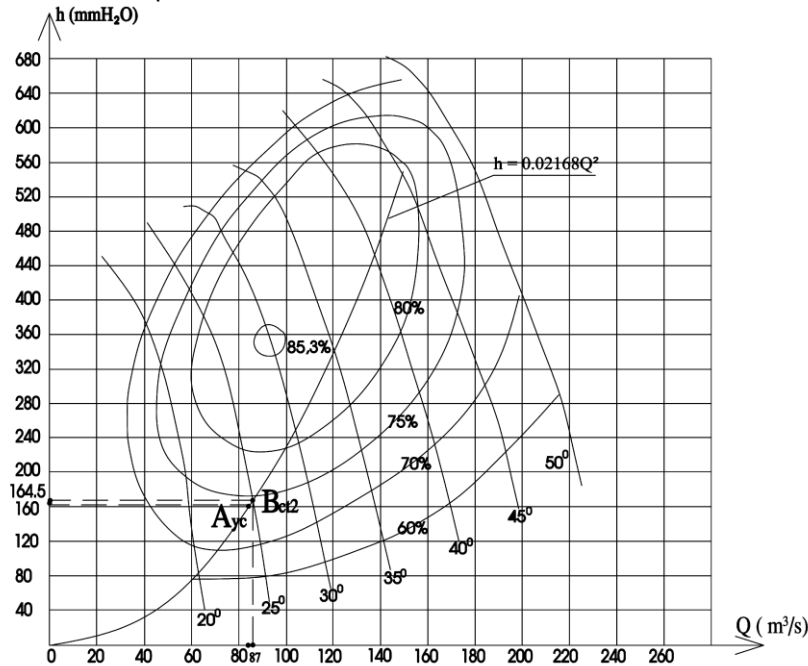


Fig. 5. Graph defining the operating mode of the central fan of Cam Thanh mine area when increasing output (plan to use fan 2K56-No24).

4- The optimal solution for the operating mode of the main fan

To improve the efficiency of mine ventilation and reduce the cost of mining, we propose a solution to use the inverter to adjust the operating mode of the fan and optimize the central fan to meet the needs of ventilation for mines. At the same time, it helps to economically and efficiently use of electricity and ensure environmental safety [5, 6, 17, 18, 19]. Here, with the conditions of the Cam Thanh mine, we recommend using a 3-Phase inverter LS LSLV5000H100-4COFD 500KW 380V and accompanying synchronous auxiliary equipment. Fig. 6. illustrates the model of automatic ventilation technology utilizing an inverter.

An inverter will adjust the fan's operating mode according to the required wind demand of the mine at each specific time. Here, the article takes data to change the operating mode of the main fan, so that the wind volume generated during holidays is 60% of the working days. The author's calculation software, and the results are shown in Figure 7. The efficiency when using the inverter to adjust the operating mode of the main fan will reduce power consumption by 41%, and according to current prices in Vietnam, the investment efficiency to over 90% [18].

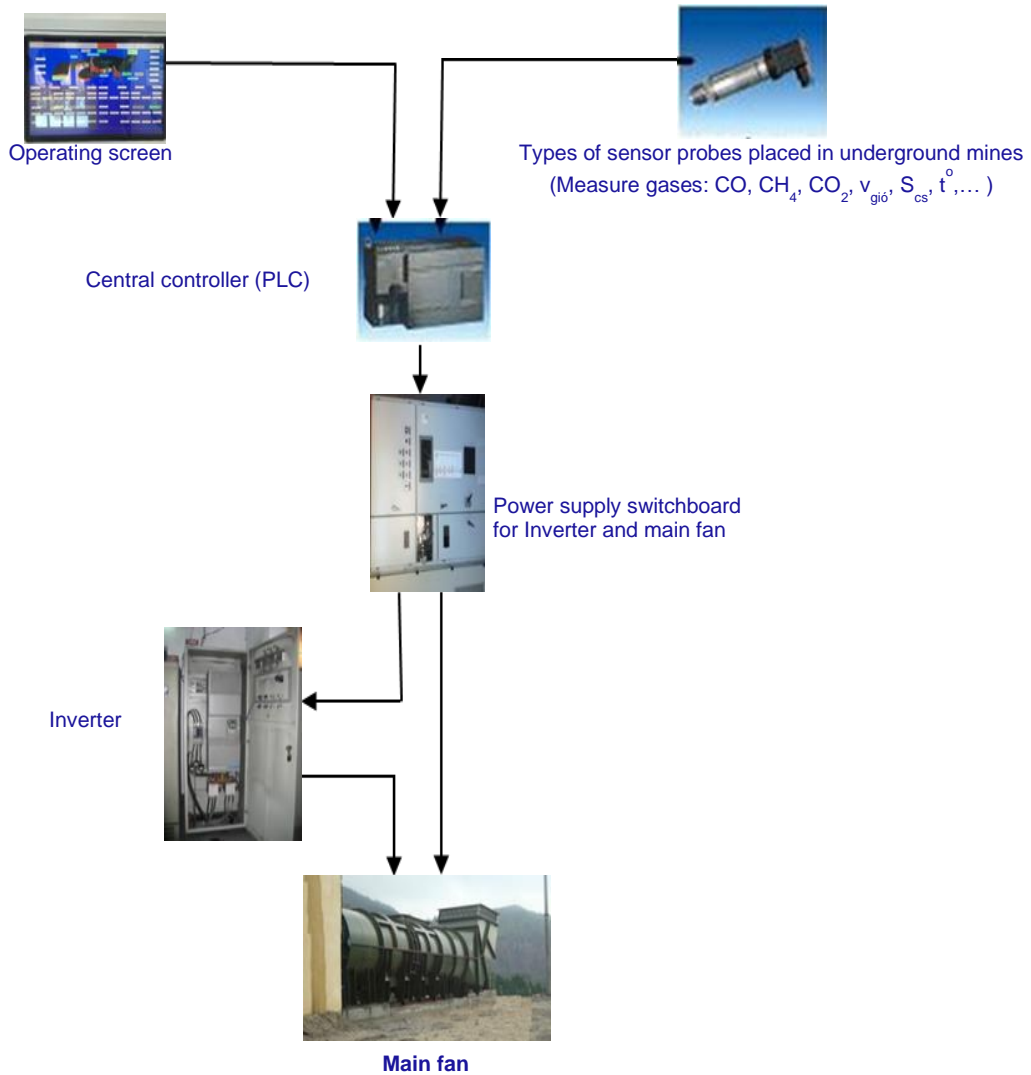


Fig. 6. Model of automatic ventilation technology using an inverter.

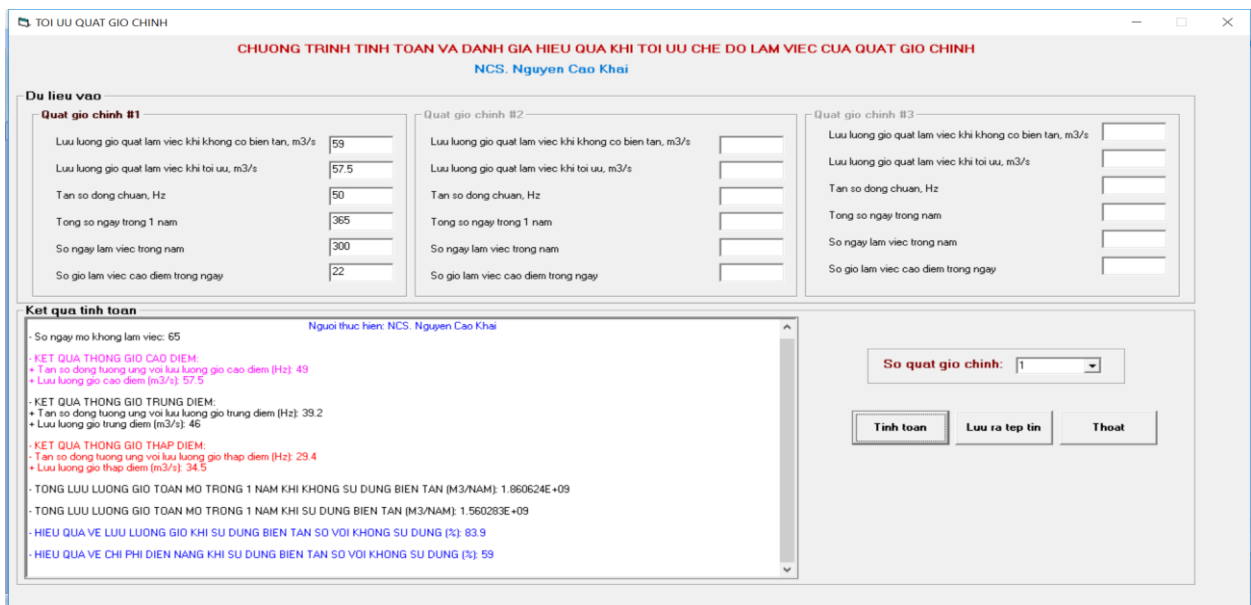


Fig. 7. The optimal calculation result of the current operating mode of fan type BD-II-6-No15/2x55kW.

5. Conclusion

The calculation of the current ventilation and the increase in mining output shows that the basic ventilation system of the mine still meets the requirements, such as the tunnel lines, wind shutters, etc. However, in the future, the wind flow needed for the mine will increase from 57.51 m³/s to 90.01m³/s, significantly affecting the ventilation capacity of the central fan station. To meet and further improve the efficiency of mine ventilation, the company needs to implement several solutions to perfect the ventilation system as follows:

1- The immediate solution

It is necessary to strengthen the management, especially the opening and closing of the wind doors, to ensure additional adjustment of the amount of wind shortage for the longwall, and improve working conditions. At the same time, it is always necessary to ensure the better quality of air ducts, reducing wind leaks to a minimum when ventilating the tunnel, building additional doors to check the operating mode of the central blower at the fan station. Processing and repairing windbreak doors, especially in the main fan station tunnel door, minimize leaking wind.

2- Orientation general direction for ventilation when increasing the exploitation output

When Cam Thanh mine area is put into longwall operation, to increase the output of the exploitation area up to five operating longwalls, it is necessary to replace the main fan type BD-II-6-No15 with a higher capacity fan, such as 2K56-No24 (or equivalent). Besides, the mine must invest in inverters to adjust the operating mode of the central blower to increase ventilation efficiency and reduce ventilation costs, contribute to reducing mining costs, improving safety and environmental conditions.

6. Acknowledgements

The paper was presented during the 6th VIET - POL International Conference on Scientific-Research Cooperation between Vietnam and Poland, 10-14.11.2021, HUMG, Hanoi, Vietnam.

7. References

1. Ha Long coal Company – Vietnam., 2020. Plan for production and ventilation of CamThanh mines area in 2020. Ha Long coal Company-TKV, 1-35.
2. Hon Gai coal Company – Vietnam., 2020. Plan for production and ventilation of HaLong coal Company in 2021 and planning directions to 2025. Ha Long coal Company, 1-65.
3. Nguyen Cao Khai., 2017. Studying to finalize the ventilation system for Cam Thanh mine, Ha Long Coal Company ensures to increase the output from 400,000 tons/year to 700,000 tons/year. Summary report of basic project code: T17-15, Hanoi University of Mining and Geology, 34-72.
4. Tran Xuan Ha., Dang Vu Chi., Nguyen Cao Khai., Nguyen Van Thinh., 2014. Mine ventilation curriculum. Science and Technology Publishing House, Hanoi, 357p.
5. Tran Xuan Ha., Dang Vu Chi., Nguyen Van Sung., Nguyen Cao Khai., Nguyen Van Thinh., Phan Quang Van., 2012. Occupational safety and sanitation in pit mining. Science and Technology Publishing House.
6. Babak G.A., K.P. Bocharov., AT Volokhiev., 1982. Main ventilation fans for underground mining. - M: Nedra, 296.
7. Nguyen Cao Khai., 2015. Determine the reasonable working regime of the main fan stations to improve the ventilation efficiency for some coal mines in Quang Ninh region. Journal of mining industry, 2: 25-29.
8. Dao, C.Van, Tran, H.Xuan and Le, D.Tien 2021. Determination of reasonable working mode for main fan stations during pilot operation of fan station VO - 22/14AR in Lo Tri area, Thong Nhat coal mine (in Vietnamese). Journal of Mining and Earth Sciences. 62, 4 (Aug, 2021), 15-20. DOI:https://doi.org/10.46326/JMES.2021.62(4).02.
9. Arnab Chatterjee., Lijun Zhang., Xiaohua Xia., 2015. Analyze the quantity and test the different ventilation systems in the deep mine. Energy application. 146: 65-73.
10. Nguyen Cao Khai., Nguyen Van Thinh., Nguyen Van Quang., 2019. Assessing the current status of underground mine ventilation system in ThanhCong-CaoThang area, Hon Gai coal company, Quang Ninh region, Vietnam. Journal of the Polish Mineral Engineering Society. 44-50.
11. Nguyen Cao Khai., Nguyen Van Thinh., Nguyen Phi Hung., Dao Van Chi., Nguyen Van Quang., 2020. Current Situation and Solutions to Advanced Ventilation Efficiency in Giap Khau Coal Mine Area, Hon Gai Coal Company of Viet Nam. Journal of the Polish Mineral Engineering Society. 209-219.

12. Dao, C.Van and Tran, H.Xuan 2020. Study on status and solution to improve the ventilation system of Quang Hanh coal mine (in Vietnamese). *Journal of Mining and Earth Sciences*. 61, 4 (Aug, 2020), 110-117. DOI:[https://doi.org/10.46326/JMES.2020.61\(4\).12](https://doi.org/10.46326/JMES.2020.61(4).12).
13. Marius Cornel Şuvar., Constantin Lupu., Victor Arad., Doru Cioclea., Vlad Mihai Păsculescu., Nelu Mija., 2014. Computerized simulation of mine ventilation networks for sustainable decision making process. *Environmental Engineering and Management Journal*. Gheorghe Asachi Technical University of Iasi, Romania. 1446-1451.
14. M. Shriwas., F. Calizaya., 2018. Automation in detection of recirculation in a booster fan ventilation network. *Int J Min Sci Technol*, 28: 513-517.
15. M.A. Moridi., Y. Kawamura., M. Sharifzadeh., E.K. Chanda., M. Wagner., H. Jang., 2015. Development of underground mine monitoring and communication system integrated ZigBee and GIS. *Int J Min Sci Technol*, 25: 811-818.
16. Nel. A.J.H, Vosloo J.C., Mathews. M. J., 2018. Evaluating complex mine ventilation operational changes through simulations. *J Energy South Africa*, 29: 22-32.
17. Nguyen Cao Khai., 2019. Ventilation of underground coal mines in Quang Ninh region approaches the 4.0 technology revolution. *Journal of mining industry*, 1: 82-86.
18. Nguyen Cao Khai., 2019. Optimizing working regime of main fan in underground coal mines in Quang Ninh. Doctoral thesis in engineering, University of Mining and Geology.
19. Pronko V.S., 2016. Structure and energy-saving control algorithms of the frequency-controlled electric drive of the main mine fans: Ph.D. dissertation abstract. St. Petersburg. 20p.

Prediction of Ground Subsidence During Underground Construction of Metro Line 2, Section 1, Ben Thanh - Tham Luong

VO Nhat Luan^{1,*}, NGUYEN Thi Nu², DO Minh Toan²

¹ Human Resources Training, Construction and Development Joint Stock Company, Ho Chi Minh City, Vietnam

² Hanoi University of Mining and Geology, 18 Vien street, Hanoi, Vietnam

Corresponding author: luancienco6@gmail.com

Abstract. Urban metro line No. 2 from An Suong station to Thu Thiem is one of the six metro lines that is planned to be built in Ho Chi Minh City (HCMC). The metro line goes through the area in which the stratigraphy consists of many units, distributed from 20-80 m. The hydrogeology mainly has 2 aquifers, namely Holocene, and Pleistocene which affecting the deep excavation. During construction, there will be some problems that will affect the work on the surface such as settlement, cracking, and damage. By finite element method on Plaxis software, the article forecasts the surface settlement during this metro line No.2. The results show that the ground settlement is relatively large in areas with soft ground structures. The settlement results depend on the geological structure characteristics, hydrogeological characteristics, and the shape and size of the tunnels.

Keywords: Ground subsidence, Underground construction, Metro line

1. Introduction

The metro line No. 2 Ben Thanh - Tham Luong is 11,322 km long, including 11 stations, with 9,315 km underground and ten underground stations. The metro line goes through the weak geological areas, low-lying terrain from the South, and gradually increasing to the Northwest.

The tunnel Boring Method (TBM) is commonly used for tunnel excavation. It is applied in complex hydrogeological conditions, weak and unstable soil, long tunnel, constant cross-section. This can be seen as a tunneling method using an excavation shield - a combination machine equipped with mechanized systems for excavation, loading, and unloading soil, assembling tunnel shells. It is also a strong temporary support frame, which has a protective effect when carrying out the main construction and installation stages. The shield can have a circular, rectangular, or elliptical cross-section, etc.

Using TBM, the tunnel is divided into sections and supported by a shell shield structure underneath the tunnel shell shield. It is built by an assembled structure or precast concrete to form a round retaining tunnel shell.

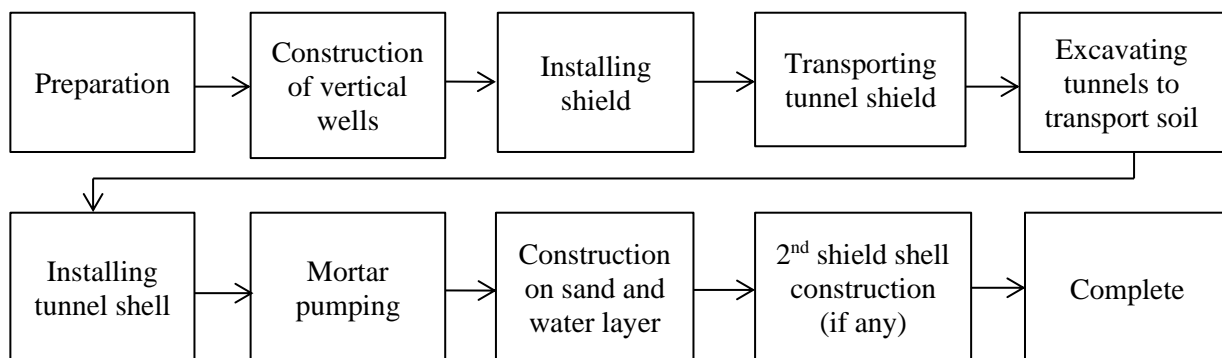


Fig. 1. TBM tunneling method process.

The advantage of this method is that it is unnecessary to divide the excavation face into many parts. Temporary support is not required, the movement of the surrounding soil is minimal, and the soil pressure is slight.

Currently, there have been much kinds of research on ground subsidence caused by tunnel construction in the world, also for Hochiminh City (HCMC) [1-3]. The results are different, but they share some similarities. Some of them showed that the surface settlement characteristics depend on the design, construction method, and technology as well as the geological conditions of the construction area. This paper studies the theoretical basis and selects the methodology to calculate the surface settlement

after excavating the double tunnel of Metro line 2 - HCMC by TBM shield in different construction conditions.

2. Methods of calculating surface settlement due to the influence of urban tunnel construction

2.1 Experimental method

There are many different methods to predict surface settlement [4-10].

The experimental method helps estimate these values when changing some data such as the depth, diameter of the tunnel, surface characteristics, and construction properties of soil during construction.

Surface settlement during tunnel construction is represented by the formation of funnel-shaped, which usually appears as a three-dimensional trough (Fig. 2a). The shape and displacement of the settlement conform to Gauss' law, which are characterized by the maximum settlement at the tunnel's center. The settlement decreases with the distance from the inflexion point of the curve outward in the building's horizontal section.

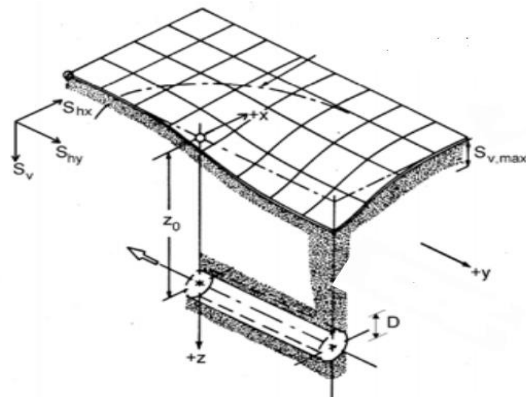


Fig. 2a. Funnel-shaped surface settlement [11]

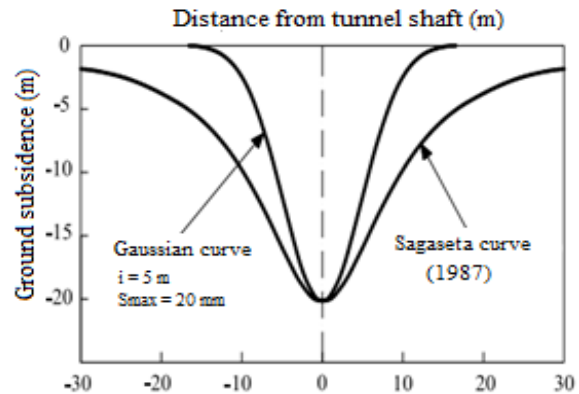


Fig. 2b. Funnel-shaped settlement cross-section [12].

However, in the case of double tunnel construction as of Metro Line 2, the surface settlement caused by the construction of the double tunnel can be predicted using different equations [4, 9, 13] with some adjustments. The surface settlement caused by a double tunnel is usually wider and larger than in a single tunnel (Fig. 3).

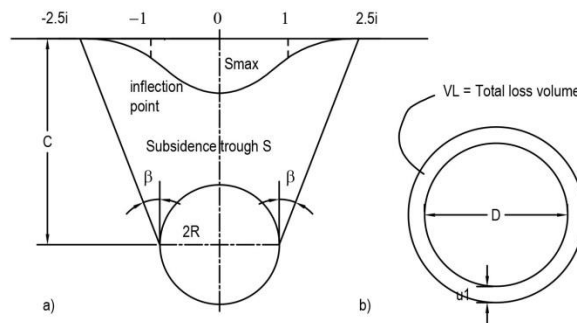


Fig. 3. The shape of the subsidence trough after excavating a single tunnel (a); Total loss volume V_L (b).

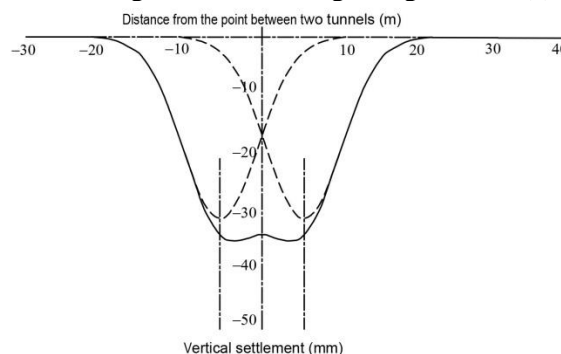


Fig. 4. The shape of subsidence trough after excavating a double tunnel.

In 1969 [4], Peck proposed a formula to calculate surface settlement (S_v) after excavating double tunnels:

$$S_v = S_{max} \left[\exp\left(-\frac{x_A^2}{2i^2}\right) + \exp\left(\frac{(x_A-d)^2}{2i^2}\right) \right] \quad (1)$$

In which:

d - the horizontal distance between the two centers of the tunnel.

x_A - the horizontal distance from the center of the first tunnel to the point of calculating settlement.

i – the standard deviation of the settlement curve. It is the horizontal distance from the inflection point of the settlement curve to the center of the tunnel, also known as the width of the surface settlement trough. There are various formulas to determine the value of i. Most of them are mainly obtained from the results of field observations. Accordingly, the value of i depends on the size (diameter) of underground constructions, geological conditions, and especially the depth of underground constructions (z_0).

$$i = 0.43z_0 + 1.1 \text{ (with consolidated soil)} \quad (2)$$

$$i = 0.28z_0 - 0.1 \text{ (with unconsolidated soil)} \quad (3)$$

In which: z_0 is the distance of the tunnel centerline to the ground.

2.2 Numerical Method

Today, with the vigorous development of software technology, numerical methods are increasingly dominant. The application of numerical methods to deal with ground subsidence caused by tunneling is the most appropriate. Numerical methods are not only used to predict surface settlement but also to simulate the entire construction progress, such as the tunneling stages; placement of tunnel segments; the interaction between tunnel segments and the surrounding soil; the influence on neighboring works, and the influence of seepage and consolidation, etc.

The finite element method is the most popular numerical method for estimating surface settlement due to tunnel construction. Simulating and forecasting surface settlement using specialized geotechnical software requires input data, such as geometric dimensions, material properties of the support system, construction methods, and geological conditions. The output results include surface settlement, internal forces in the tunnel shell (vertical pressure and bending moment in designing reinforcement of tunnel shell), and stress distribution diagrams.

The purpose of analysis plays an essential role in determining the model's elements, size, and complexity. Finite elements should be selected so that it is possible to closely simulate the actual process of the ground without being too complicated and beyond the capabilities of conventional calculation tools.

Currently, there are many software for geotechnical analysis and calculation in the world, such as Geostudio, Plaxis, or other software products from Rocscience. Each software has different strengths and weaknesses, which is applicable for various purposes. Plaxis 3D Tunnel software (Netherlands) is used to calculate surface settlement caused by the TBM tunneling process because of its ability to simulate the construction process accurately and calculate the stabilizing pressure at the face during the tunneling process. Therefore, this paper uses a numerical method based on Plaxis 3D Tunnel software to analyze and calculate the surface settlement caused by the influence of underground construction of Metro Line 2.

3. Analysis of surface settlement due to the influence of underground construction of Metro Line 2

3.1. Calculations of surface settlement due to the influence of underground construction of Metro Line 2

3.1.1. Material properties

Geological cross-section (vertical) alongside the center of Metro Line No. 2 is presented in Figure 5, including five soil layers as below:

- Layer 1: Gray clay, liquid to a plastic state.
- Layer 2: Gray, greenish-gray clay, semi-solid state.
- Layer 3: Small to medium sand particles, yellowish-gray, reddish-brown, medium dense sand.
- Layer 4: Patchy color, gray, yellowish-gray clay, semi-solid to solid-state.
- Layer 5: Gray, yellow, dense to the very dense clay-sand mixture.

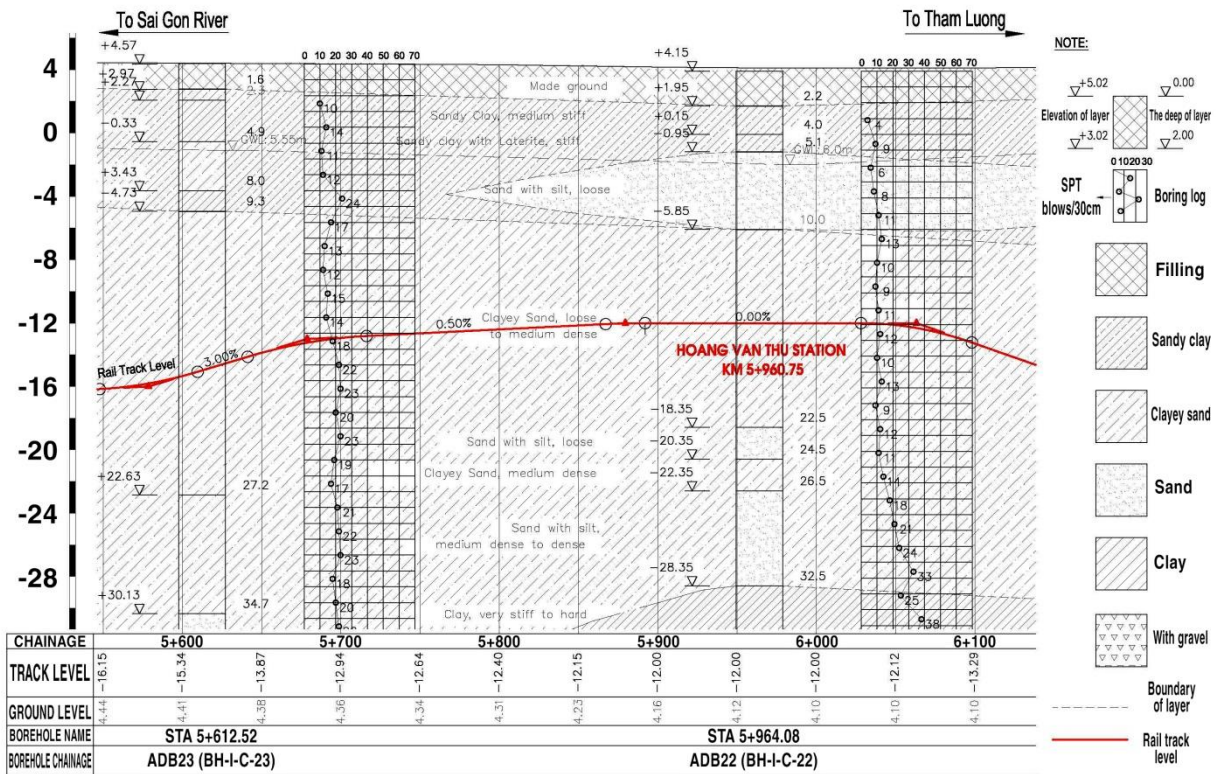


Fig. 5. Typical geological cross-section in location km 5+600 - km 6+100 of Metro Line No. 2.

Geological conditions of construction locations of the double tunnel line at the Km 0+200, Km 3+050, and Km 5+560 are shown in Table 1.

Tab. 1. Properties of soil layers at the location Km 0+200, Km 3+050, and Km 5+560.

No.	Parameters	Symbol	Value			Unit
			Layer 1	Layer 2	Layer 3	
1	Material sample	Model	Morh – Coulomb			-
2	Type of impact material	Type	Drained			-
3	Unit weight of soil above groundwater level	γ_{unsat}	15.8	20.8	19.6	kN/m ³
4	Unit weight of soil below the groundwater level	γ_{sat}	17.8	21	20.5	kN/m ³
5	Horizontal permeability coefficient	k_x	1.81×10^{-5}	0.5	0.5	m/day
6	Vertical permeability coefficient	k_y	0.9×10^{-5}	0.25	0.25	m/day
7	Young's modulus	E_{ref}	1000	30000	120000	kN/m ²
8	Unit adhesive force	c'	8.5	1.1	1.5	kN/m ²
9	Angle of internal friction	ϕ	15	28	21	degree
10	Dilation angle	ψ	0	4	3	degree
11	Poisson's coefficient	ν	0.33	0.3	0.3	-

Tunnel cross-section: Round tunnel, tunnel diameter D = 6.8m, tunnel cover thickness d = 0.6m. The material parameters of the shield and tunnel shell are shown in Table 2.

Tab. 2. Input parameters for tunnel shell concrete and TBM steel material.

No.	Parameters	Symbol	Value		Unit
			Tunnel shell concrete material	TBM excavator steel material	
1	Material Type	Expression	Elastic		-
2	Axial stiffness	EA	2.4×10^{10}	8.2×10^7	kN/m
3	Bending stiffness	EI	7.2×10^8	8.38×10^4	kNm ² /m
4	Equivalent thickness	d	0.6	0.111	m
5	Weight	w	14.4	38.15	kN/m/m
6	Poisson's coefficient	ν	0.15	0	-

3.1.2. Simulation using Plaxis 3D Tunnel

Building model using Plaxis 3D Tunnel to calculate the variation of surface settlement with the depth from the surface to the center of the double tunnel (-22.17m at location 0+200 and -11.48m at location 3+050) and the distance between the two centers of the double tunnel (16.5m at location 3+050 and 12.0m at location 5+650).

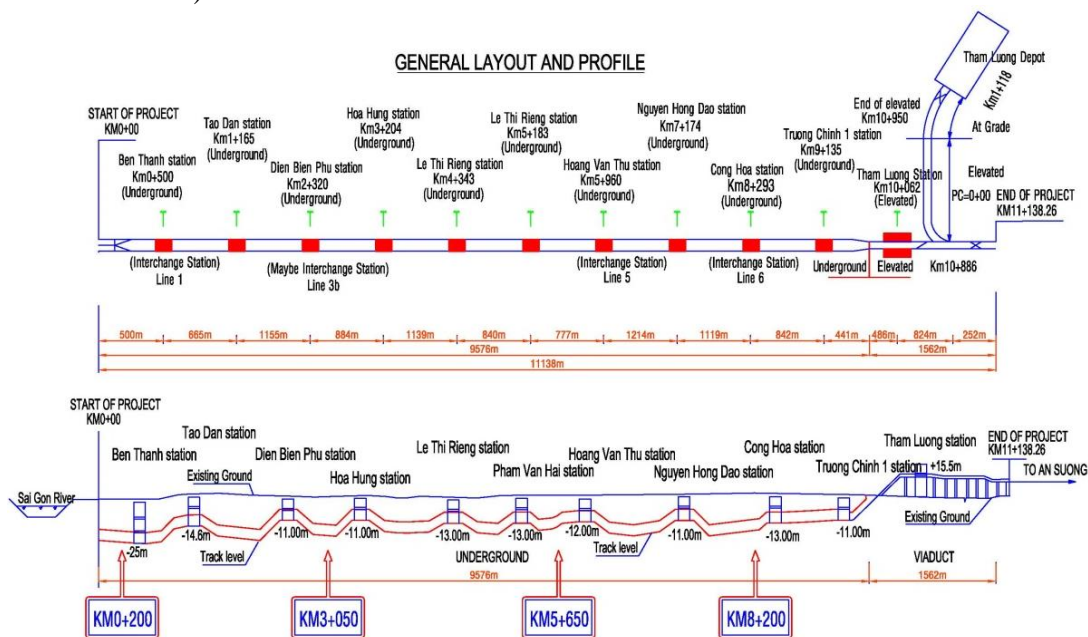


Fig. 6. Map of straight line and study locations.

Simulation process using 3D model includes 3 phases:

- Excavation face installation phase: a balanced pressure must be established for the face to ensure that the effect of volume loss on the face is insignificant. In other words, it can be assumed that this does not affect the surface settlement [14, 15].

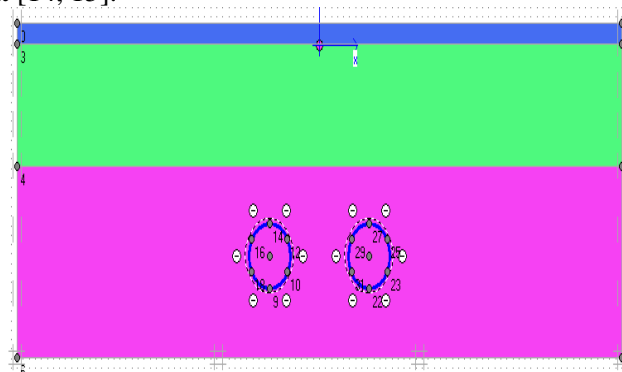


Fig. 7. Excavation face simulation.

- Excavating phase: establish the centripetal loss in the TBM tunneling process. The excavation face removes the soil in phase 1.

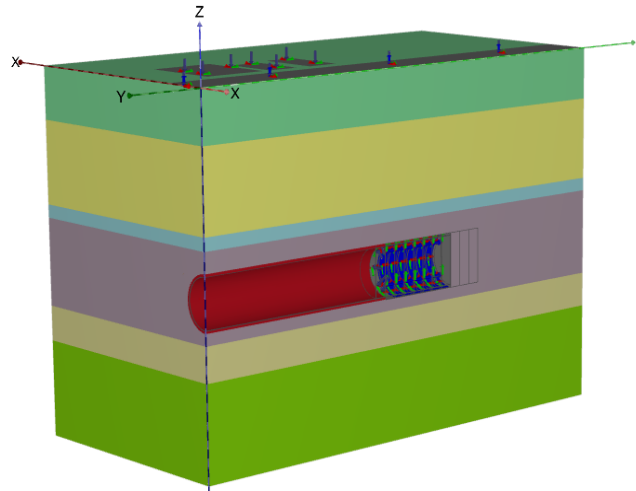


Fig. 8. Excavation process simulation.

- Tunnel shell installation phase: the tunnel shell is installed. Between the tunnel shell and the soil is a layer of mortar to avoid the settlement and waterproofing for the shell. This mortar is pumped into the end of the shield and creates pressure on the surrounding soil.

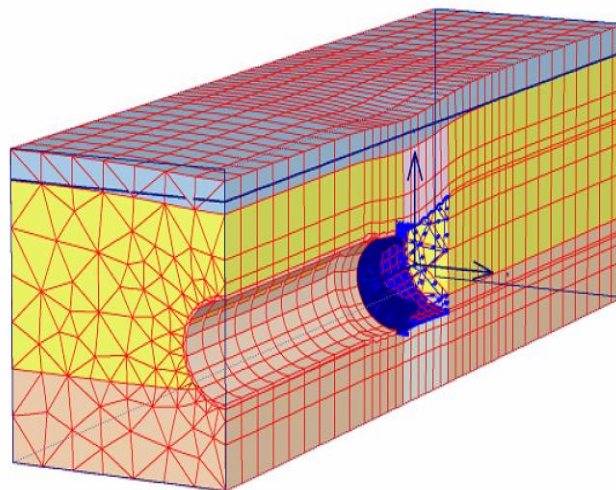


Fig. 9. Tunnel shell installation simulation.

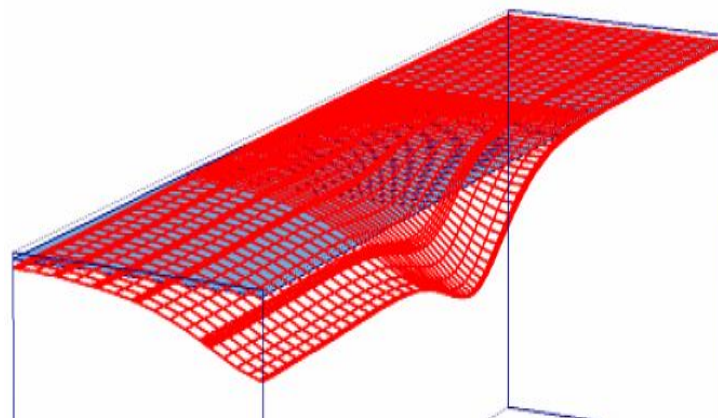


Fig. 10. Funnel-shaped settlement simulation after installing the tunnel shield.

3.2. Calculation results

- When the depth from the surface to the center of the double tunnels is different:

The authors used Plaxis 3D Tunnel software to simulate and calculate the surface settlement of the double tunnel at two locations 0+200 (depth from the surface to the center of the double tunnel is -

22.17m) and location 3+050 (depth: -11.48m). Together with geological conditions in Table 1, material parameters of the TBM and tunnel shell in Table 2, calculation results are as follows:

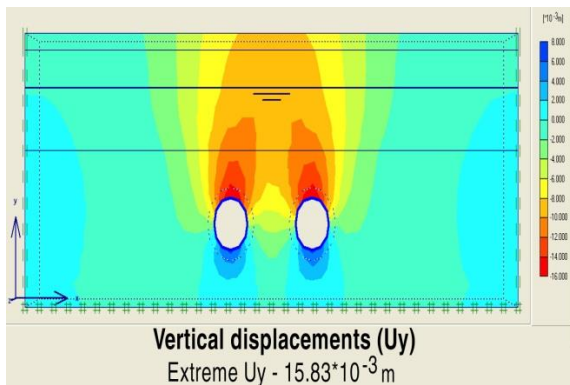


Fig. 11a. The final field of vertical surface displacement in case the distance between the double tunnels is 16.5m and located at a depth of -22.17m (location 0+200).

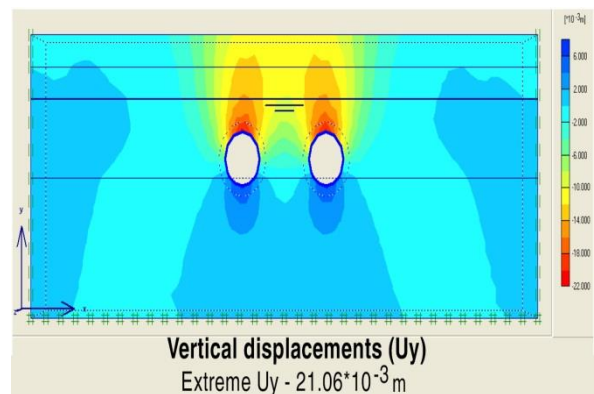


Fig. 11b. The final field of vertical surface displacement in case the distance between the double tunnels is 16.5m and located at a depth of -11.48m (location 3+050).

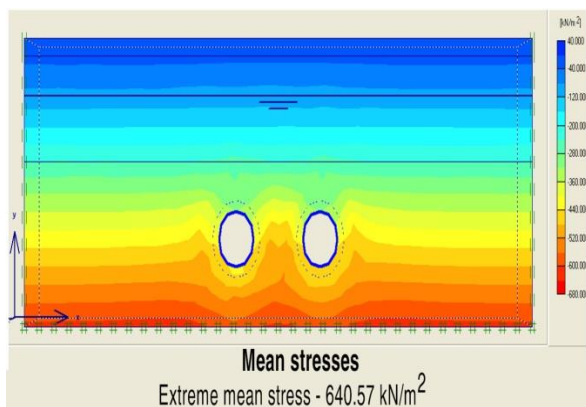


Fig. 12a. Effective stress at the location 0+200.

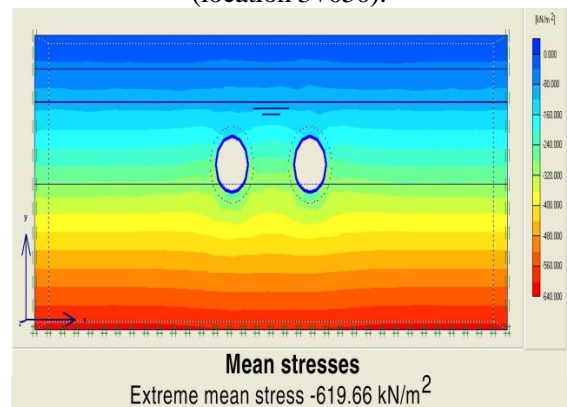


Fig. 12b. Effective stress at the location 3+050.

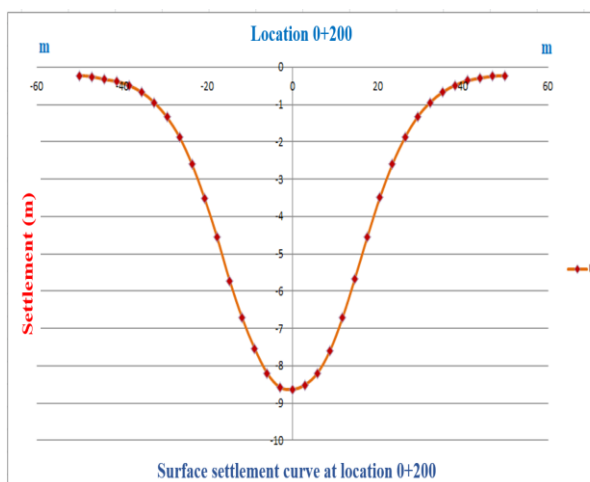


Fig. 13a. The surface settlement curve at location 0+200.

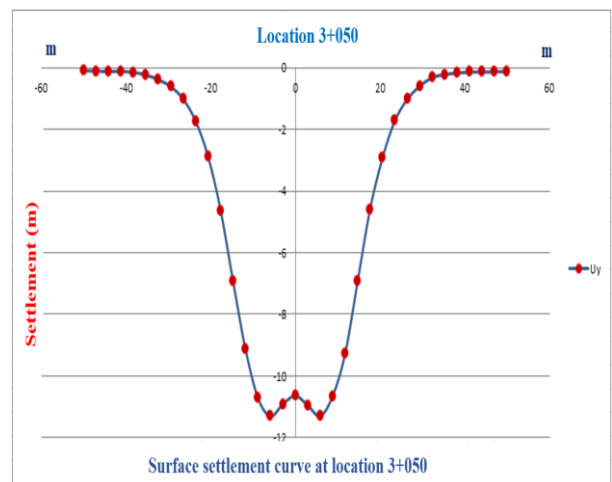


Fig. 13b. The surface settlement curve at location 0+050.

Results of the model analysis show that the deeper the double tunnel, the smaller the surface settlement. This is consistent with the fact that the increase of depth in the same geological conditions will increase the soil stress and reduce the surface settlement. However, the settlement curve shown in Figure 13a (location 0+200) and Figure 13b (location 3+050) are different. The settlement curve at the location 0+200 conforms to the theory of surface settlement of the single tunnel. In contrast, the settlement curve at the location 3+050 conforms to the theory of surface settlement of the double tunnel.

It can be explained that in the case of a double tunnel (Metro line 2) when the depth is too large (depending on geological conditions), the theoretical calculation will be suitable for the single tunnel because of the large soil stress. As a result, the difference in distance between the two tunnels is not significant regarding the influence on the construction work. In contrast, when the depth is suitable, the theoretical calculation perfectly matches with the model on Plaxis 3D Tunnel.

- When the tunnel has the same depth, the distance between the center of the double tunnel is different:

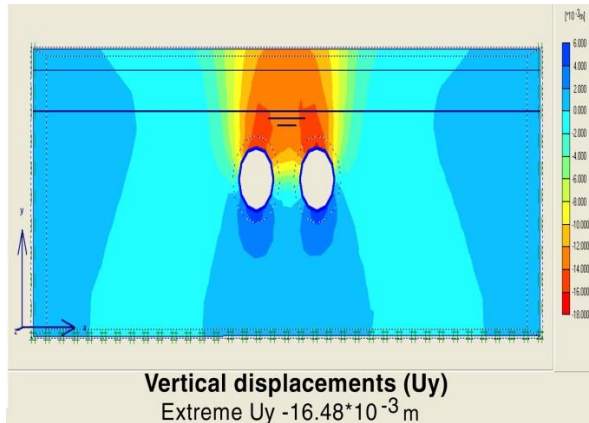


Fig. 14. The final field of vertical surface displacement in case the distance between the double tunnels is 12.0 m and located at a depth of -11.87 m (location 5+650).

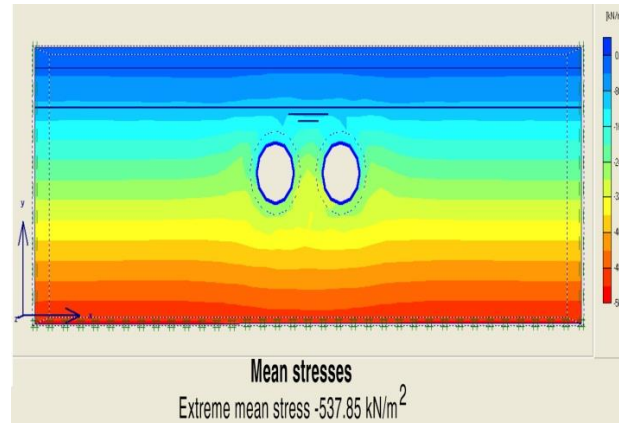


Fig. 15. Effective stress of the double tunnel at the location 5+650.

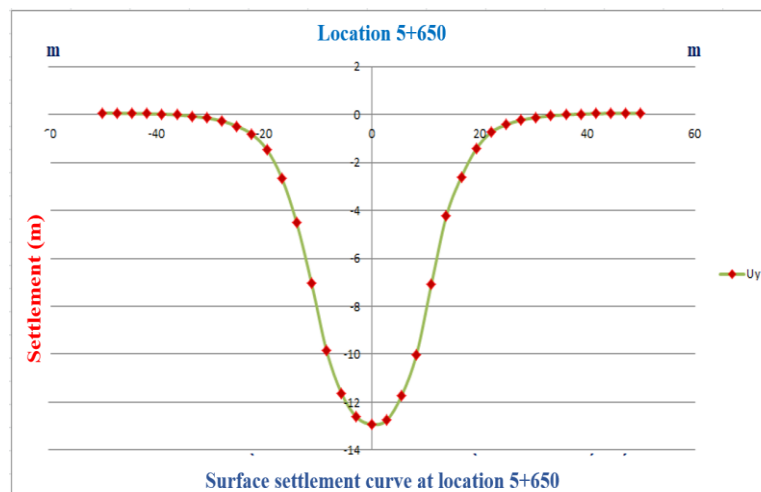


Fig. 16. Surface settlement at the location 5+650.

The results show that the surface settlement increases with the decrease of the distance between two tunnels. It is related to the soil stress at the surrounding location of each tunnel in the double tunnel. The larger the distance between the two tunnels, the greater the soil stress in the opposite case, so the surface settlement after excavating will be smaller (-11.30 mm at location 3+050 and -12.96 mm at location 5+060). The graph also shows that the surface settlement when the two tunnels are located closely to each other will be similar to the theoretical calculation of the single tunnel.

- When the tunnel has the same depth at different geological conditions:

The simulation is conducted at the location 8+200, the depth of the double tunnel is -11.21m, the geological conditions are as in Table 3:

Tab. 3. Properties of the soil layer.

No.	Parameters	Symbol	Value			Unit
			Layer 1	Layer 2	Layer 3	
1	Material sample	Model	Mohr - Coulomb			-

2	Type of impact material	Type	Drained			-
3	Unit weight of soil above ground water level	γ_{unsat}	16.0	17	17	kN/m ³
4	Unit weight of soil below the groundwater level	γ_{sat}	18.0	20	20	kN/m ³
5	Horizontal permeability coefficient	k_x	1.81×10^{-5}	0.5	0.5	m/day
6	Vertical permeability coefficient	k_y	0.9×10^{-5}	0.25	0.25	m/day
7	Elastic modulus	E_{ref}	10000	13000	75000	kN/m ²
8	Cohesion	c'	5	1	1	kN/m ²
9	Angle of internal friction	φ	25	31	31	degree
10	Expansion angle	ψ	0	0	0	degree
11	Poisson's coefficient	ν	0.35	0.30	0.30	-

The results of the calculation are as follows:

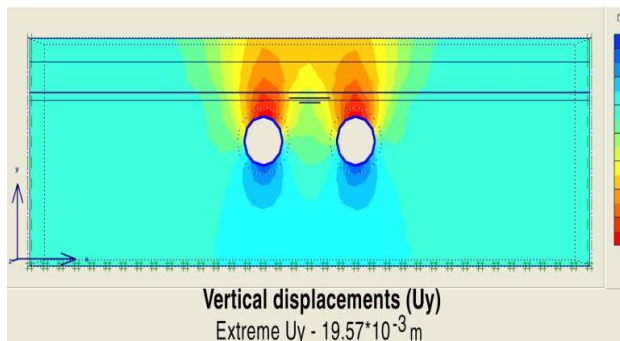


Fig. 17. The final field of vertical displacement of the subsoil in case the distance between the double tunnels is 16.5 m and located at a depth of -11.21 m (8+200).

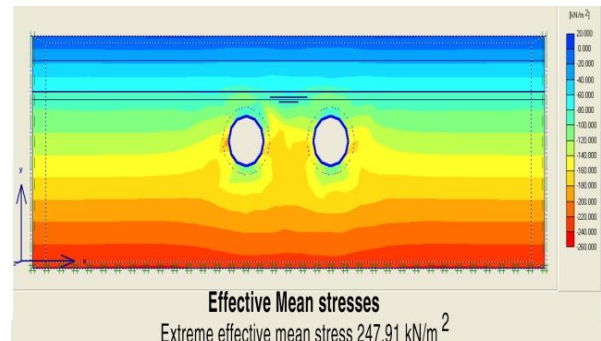


Fig. 18. Effective stress of the double tunnel at location 8+200.

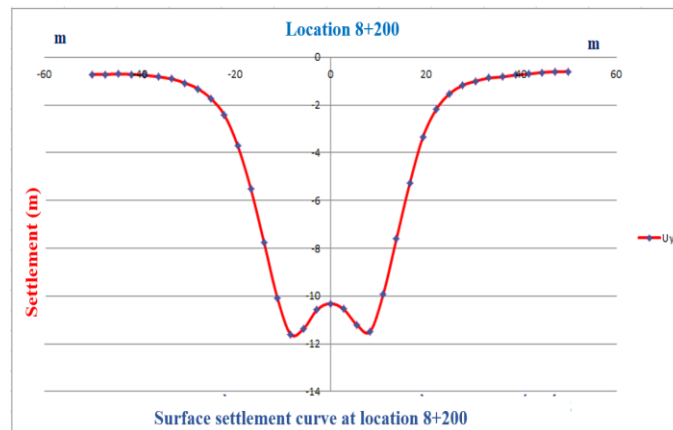


Fig. 19. Surface settlement at location 8+200.

The results show that the calculation of settlement on Plaxis 3D Tunnel model can be performed at many different locations with different geological conditions, and design parameters (depth of tunnel from the ground, distance between the center of the double tunnel two tunnels). Calculation results also show that the increase of the tunnel depth reduces the influence on the surface settlement. The decrease of the distance between the two tunnel centers will increase the surface settlement. These results are consistent with the fact that the soil stress varies when replaced by the tunnel shell volume, causing surface settlement.

Tab. 4. Combined results of the four cases above.

No.	Research location	Location 1	Location 2	Location 3	Location 4
1	Location	0+200	3+050	5+650	8+200

2	Depth of tunnel centerline (m)	-22.17	-11.48	-11.87	-11.21
3	Distance between two centers of double tunnel location (m)	16.5	16.5	12.0	16.5
4	Maximum vertical displacement (mm)	-15.83	-21.06	-16.48	-19.57
5	Maximum ground settlement (mm)	-8.63	-11.30	-12.96	-11.60
6	Maximum horizontal displacement (mm)	5.79	7.05	7.23	5.37
7	Maximum stress (kN/m ²)	-640.57	-619.66	-537.85	-247.91

4. Conclusions

The surface settlement caused by the construction of the double tunnels of Metro Line 2 can be predicted using various methods, including analytical and numerical methods. In particular, using numerical methods via simulation software such as Plaxis 3D gives the most suitable calculation results.

Research on surrounding surface settlement during the construction of metro line 2 in HCMC shows that when geological conditions are different, the surface settlement is different, which is consistent with the bearing capacity of the soil according to each geology area. The above results are only preliminary results. For final results, there must be a combination of calculations on the model, field observations, and laboratory work to determine soil pressure at the construction site and make an adjustment to the model to provide accurate results.

Before construction, investors and the construction contractors should consider the geological conditions of the area, design drafts, and make predictions to protect the existing works within the construction area and other neighboring works, avoiding possible consequences due to the influence of surface settlement.

5. Acknowledgments

The authors are thankful for the support of The Management Authority for Urban Railways (MAUR) and The Ho Chi Minh City Department of Transport.

The paper was presented during the 6th VIET - POL International Conference on Scientific-Research Cooperation between Vietnam and Poland, 10-14.11.2021, HUMG, Hanoi, Vietnam.

6. References

1. Minoru Kuriki, 2020. *Geotechnics for Sustainable Infrastructure Development*. Springer. Singapore, 1444.
2. Hieu, N.T., Giao, P.H., Phien-wej, N., 2020. *Geotechnics for Sustainable Infrastructure Development*. Springer. Singapore, 1444.
3. Kiet, H.N., Phien-wej, N., 2020. *Geotechnics for Sustainable Infrastructure Development*. Springer. Singapore, 1444.
4. Peck, R.B., 1969. Deep excavation and tunnelling in soft ground. *Proceedings of the 7th International Conference on Soil Mechanics and Foundation Engineering*. Mexico City, 225-290.
5. Schmidt, B., 1969. A method of estimating surface settlement above tunnels constructed in soft ground. *Canadian Geotechnical Journal*. 20: 11-22.
6. Cording, E.J., Hansmire, W.H., 1975. Displacements around soft ground tunnels. *Proceedings of the Fifth Panamerican Conference on Soil Mechanics and Foundation Engineering*. Buenos Aires, Argentina, 4: 571-633.
7. Attewell, P.B., 1977. Ground movements caused by tunneling in soil. *Proceedings of the Conference on Large Ground Movements and Structures*, Cardiff. July 1977, London, 812-948.

8. Clough, G.W., Hansen, L.A., 1981. Effects of clay Anisotropy on Braced Wall Behavior. *Journal of the Geotechnical Engineering Division, ASCE*. 107: 893-913.
9. O'Reilly, M.P., New, B.M., 1982. Settlement above tunnels in the United Kingdom - their magnitude and prediction. *Proceedings of the Third International Symposium, Institution of Mining and Metallurgy*. June 7-11, 1982, London, 173-181.
10. Rankin, W., 1988. Ground movements resulting from urban tunnelling: predictions and effects. *Proceedings of the 23rd Annual Conference of the Engineering Group of the Geological Society*. September 13 - 17, 1987, Nottingham, England, 79-92.
11. Do, T.Ngoc and Nguyen, T.Duc 2021. Prediction of ground surface settlement induced by twin shield tunnelling in urban conditions (in Vietnamese). *Journal of Mining and Earth Sciences*. 62, 2 (Apr, 2021), 47-56. DOI:[https://doi.org/10.46326/JMES.2021.62\(2\).05](https://doi.org/10.46326/JMES.2021.62(2).05).
12. Augarde, C.E., 1997. Numerical modelling of tunnelling processes for assessment of damage to buildings. PhD Thesis, Oxford University. England, 262.
13. Mair, R.J., Taylor, R.N., Bracegirdle, A., 1993. Subsurface settlement profiles above tunnels in clays. *Géotechnique*, 43(2): 315-320.
14. Do, T.Ngoc and Do, T.Duc 2020. Study of the influence of face pressure on surface settlements by shield tunneling (in Vietnamese). *Journal of Mining and Earth Sciences*. 61, 1 (Feb, 2020), 31-40. DOI:[https://doi.org/10.46326/JMES.2020.61\(1\).04](https://doi.org/10.46326/JMES.2020.61(1).04).
15. Pham, N.Thi and Nguyen, N.Viet 2021. The effects of dynamic pressure on the stability of prepared drifts near the working surface areas (in Vietnamese). *Journal of Mining and Earth Sciences*. 62, 1 (Feb, 2021), 85-92. DOI:[https://doi.org/10.46326/JMES.2021.62\(1\).10](https://doi.org/10.46326/JMES.2021.62(1).10).

Career Orientation of Students in the Faculty of Mining at Hanoi University of Mining and Geology

TRUONG Thi Hoa^{1,*}, NGUYEN Thuy Quynh¹, NGUYEN Thi Thanh Tra¹, NGUYEN Tat Thang²

¹ Hanoi National University of Education, Hanoi, Vietnam

² Vietnam National University of Agriculture, Hanoi, Vietnam

Corresponding author: truonghoa@hnue.edu.vn

Abstract. Career orientation has become significant in Vietnamese education recently. To students of the Mining Faculty of Hanoi University of Mining and Geology, this issue is more important as society changes its acceptance of mining. The research uses investigation, interview, and observation methods for 205 students to see their career orientation. The performance is on the following criteria: 1) Career choice based on individual interests, abilities, personalities, career values; 2) Understanding of the profession in aspects of quality and capacity, workplace, future working environment, the development trend, etc.; 3) The suitability of the profession with individual interests, abilities, personality, and values of the profession during the study; 4) Study plans to meet industry requirements; 5) Self-development plans in the future career. Research results show that the majority of students have the right and appropriate career. These students have clear and positive motivations and goals in the learning process. Only a few students have not determined the proper position in the profession due to their emotions, which are not stable and oriented.

Keywords: Student, Profession, Career orientation, Faculty of Mining.

1. Introduction

Career guidance is like a journey that requires correct awareness, a severe, positive attitude, and thoughtful preparation to decide their direction. A promising career is a career that matches individual interests, abilities, career values, personality, and intellectual capacity. It helps create motivation, joy, happiness, and success in studying and working in the future. Students who choose the wrong careers could be discouraged when entering school, lose motivation and study, and waste money and time. Thus, to choose the right career, with the suitable orientation, first and foremost, the students must understand themselves clearly, i.e., to understand their interests, abilities, learning abilities, personality, career values, etc. From that understanding, students must have a clear overview of the profession and vocational schools. Recently, there are some studies on vocational education, career counseling for students, and vocational education competencies, such as Le Thi Duyen's study on the status of education capacity of high school teachers [1], Truong Thi Hoa's publications about the vocational education competencies of pedagogical students and the ability to organize vocational education knowledge into subjects, and career counseling capacity of students [2, 3, 4, 5]. Dang Van Hai (2020) gave some recommendations to improve the effectiveness of vocational education in local education programs, such as 1) Promoting awareness about vocational education in the local educational curriculum; 2) Improving the effectiveness of consultancy and career orientation; 3) Implementing flexibly in organizing vocational education activities at schools; 4) Concretizing the content of vocational education in the implementation of local socio-economic development policies; 5) Increasing investment in resources; 6) Adapting experiences to promote vocational education for students [6]. Nguyen Thi Nhu Thuy, Lu Thi Mai Oanh (2020) researched and analyzed the basis of building an enrollment counseling model and the results of career counseling and enrollment to help students in choosing their careers based on their interests and personal capacity, and social value of the profession [7].

According to Jesus Bravo et al., career orientation is best represented by a six-dimension factor structure, which contains entrepreneurial creativity, security, managerial competence, lifestyle, technical competence, and service to a cause. Five of the six factors that emerged were correlated as expected with proactive personality, ambition, career self-management behaviors, mentoring relationships, and workplace attitudes, providing support for our conceptualization and a measure of career orientation [8]. William Donald et al. researched early steps along the pathway of exploring the student perception of graduate

employability. The neo-liberalization of higher education has been studied, characterized by increased participation, diversity, employability, and work-integrated learning. Subsequently, the evolving nature of careers was detailed, providing coverage of traditional and contemporary careers, with a particular focus on boundaryless and protean career constructs [9]. E. Polyanskaya, O. Fisenko, V. Kulakova research on Strong-Willed Character Traits in Students' Career Orientation in the Labor Market and Self-Realization mentions psychological factors such as initiative, perseverance, and aspiration of students affect their career orientation. The more students have a strong desire to overcome obstacles and solve difficult tasks in their career, the higher their initiative, and perseverance. And when orienting career, the most preferred career orientations are "stability of work", "management", "service", and the least popular are "professional competence" and "stability of the residence" [10]. Angela Ulrich, Kerstin Helker and Katharina Losekamm research on "What Can I Be When I Grow Up?"—The Influence of Own and Others' Career Expectations on Adolescents' Perception of Stress in Their Career Orientation Phase. Their research is based on the possible selves approach and aims at understanding how far imbalance between adolescents' own and their social environments' expectations for their vocational future will cause stress. Results showed a variety of expectations for future careers held by participants and their social environment and emotions regarding these expectations. Positive deactivating emotions (satisfaction and relief) negatively predicted adolescents' stress and strain, and the older and closer to final job choice participants were, the more they reported stress and strain. These findings suggest including adolescents' social environment in the career choice process [11].

To summarize, most articles on career guidance focus on students but hardly mention their career orientation in technical schools. This article concentrates on the career orientation of students in the Faculty of Mining, Hanoi University of Mining and Geology, to narrow that gap. Some recommendations are proposed to help students get better orientation at the university and workplaces.

2. Research content

2.1 Research methods

Investigation method was used in surveys to evaluate the career orientation of students by the following criteria: 1) Occupation chosen based on individual interests, capability, personality, and career values; 2) Understanding of the profession regarding the quality and capacity of the profession, workplace, future working environment, and development trend of the profession; 3) The suitability of the profession with individual interests, abilities, personality, and career values during the study; 4) The study plan to meet industry requirements; 5) The plan of professional self-development. The survey presented the highest level (5 points) and the lowest level (1 point). We evaluate five levels: The data processing results are mainly based on the average results by the formula: "Value of distance" = (Maximum – Minimum)/n. Therefore, the designed questionnaire with five levels of responses, "Value of the distance" = (5-1)/5 = 0.8, divided into five scales: Level 1 (Very low): 1.00 to 1.80 points; Level 2 (Low): 1.8 to nearly 2.6 points; Level 3 (Average): 2.6 to almost 3.4 points, Level 4 (High): 3.4 to almost 4.2 points, Level 5 (Very high): 4.2 to 5.00 points.

The interview method was used to directly interview students through open-ended questions to find out deeply and thoroughly the relevance to the student's career orientation.

Besides, the authors collected lecturers' observation results of on-site students' attitudes in the study while doing assigned tasks.

2.2. Research subjects

We studied on 205 students in Faculty of Mining: 28 (11.2%) female students, 177 (89.8%) male students, 55 (26.8%) freshmen, 52 (25.4%) sophomore students, 53 (25.9%) junior students, and 45 (21.9%) senior students. Fig. 1 shows the distribution of students in the Faculty of Mining by age.

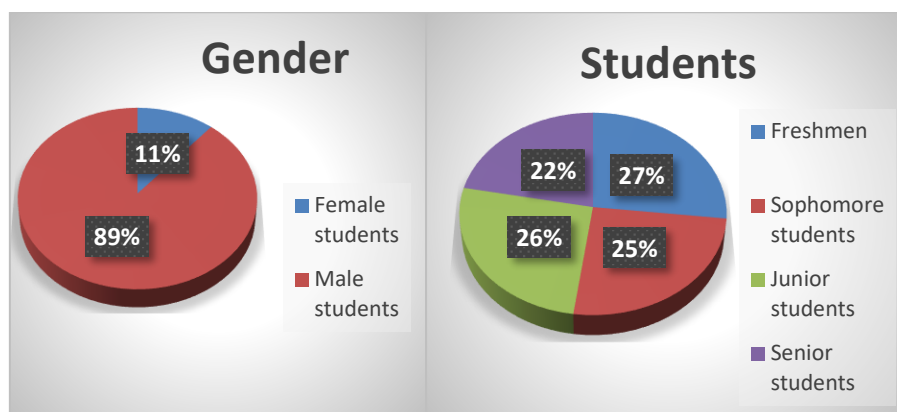


Fig. 1. The distribution of students in the Faculty of Mining by age.

2.3. Results and discussion

2.3.1. Understanding criteria of an exemplary career selection

To prepare for the right career, students have to choose an appropriate major to enroll in a university or college, considering their interests, abilities, intellectual capacity, characteristics, personality, and career value. To find out if students have a right or wrong understanding and to their extent about the criteria, we used the question: according to you, to choose the right major, which of the following criteria is the most important? Table 1 shows the results.

Tab. 1. Current status of correct understanding criteria of career selection.

No.	Criterion	Percentage (%)					Avg.	Var.	Rank
		1	2	3	4	5			
1	Personal interests	4.4	1.5	13.7	28.8	51.7	4.22	1.032	5
2	Personal capability	1.5	4.4	15.1	25.9	53.2	4.25	0.966	2
3	Academic capability	1.5	4.4	10.7	35.6	47.8	4.24	0.916	3
4	Characteristics, Personality	2.9	2.9	17.1	21.0	56.1	4.24	1.029	3
5	Career value	1.5	4.4	11.7	35.1	47.3	4.22	0.923	5
6	Labor market demand	1.5	2.9	11.7	30.2	53.7	4.32	0.898	1
7	Family background	2.9	5.9	15.1	28.8	47.3	4.12	1.055	7
8	Advice from parents/others	5.4	4.4	23.4	26.8	40.0	3.92	1.137	8

Results from the Table 1 show that most students correctly assessed the above criteria when choosing a career with a very high average score (average score from 4.22 to 4.23). Although the requirements do not differ much, if we look at the order of the criteria, we see a difference, as follows:

Labor market demand (average = 4.32) ranks first, showing that students are concerned about the industry’s needs for labor, the unemployment rate, the employment rate, and recruitment.

Personal capability (average = 4.25) ranks second, mentioning individual forte, strength, and self-confidence. Therefore, students choose this criterion at a high level.

Following these two criteria is academic ability. When choosing a career, students need to consider their advantages in studying, relevant to subjects they are good at, prerequisites for other university majors.

Ranked in the same third position are personality and characteristics. These two categories show that when choosing a career, students need to consider and evaluate their characters and aspects to find suitable professions, as each job requires specific features.

The profession’s value is reflected in the dedication to society, working for the community, not thinking about self-interest ranked fifth place.

The family background ranked seventh place. Family background also affects career choice such as family’s economy, family’s support for that career choice.

The last position is advice from parents or others. However, this is not a criterion for choosing the right profession, which shows that some students do not adequately understand the criteria for choosing a career. If students rely on the advice of their parents or others, they cannot determine their interests and abilities.

In the interview, Tran Thanh T, a sophomore student, said: “In my opinion, choosing a career must

come from my abilities and interests. Therefore, I choose the criteria of interests and personal capability”. Another student, Nguyen The N, a senior student, said: “I think that all criteria are appropriate at each stage. For me, I feel it needs to base on the labor market demand”. Comparison the understanding of the criteria of students in year 1, 2, 3, and 4, the Oneway ANOVA test with the coefficients $sig. > 0.05$ shows no statistically significant difference in mean scores between groups of students in all eight variables of the question. Thus, the above results show that most students have the correct understanding and assessment of the criteria for choosing their fitting careers, beside a small percentage has not.

2.3.2. The current status of students’ career choice

With this content, we confirm the understanding of whether the criteria for choosing a career are consistent with the student’s actual career choice, using the question: What are the reasons for your choice of a job? Table 2 shows the results.

Tab. 2. The current status of students’ career choices.

No.	Explanation	Freshmen		Sophomores		Juniors		Seniors		Avg.	Var.	Rank
		Avg.	Var.	Avg.	Var.	Avg.	Var.	Avg.	Var.			
1	Personal interests	3.09	1.442	3.48	1.334	3.56	.814	4.25	1.135	3.67	1.324	8
2	Personal capability	3.54	1.421	3.52	1.052	3.38	1.025	4.20	1.123	3.69	1.187	7
3	Academic capability	3.37	1.190	3.73	1.169	3.38	1.025	4.20	1.123	3.80	1.182	5
4	Characteristics, Personality	2.97	1.445	3.71	1.114	3.38	1.025	4.38	0.756	3.78	1.179	6
5	Career value	3.63	1.262	4.11	0.880	3.81	0.750	4.25	1.090	4.01	1.050	2
6	Labor market demand	3.80	1.132	4.01	0.966	3.81	0.981	4.15	1.152	3.97	1.075	3
7	Family background	3.11	1.659	3.92	1.154	3.81	0.981	4.20	1.166	3.87	1.289	4
8	Friends’ suggestion	1.69	1.255	2.79	1.370	2.69	1.250	3.85	1.314	2.94	1.517	10
9	Advice from parents/others	3.63	1.457	4.19	1.226	4.00	1.095	4.30	1.101	4.12	1.233	1
10	Family’s tradition	3.14	1.309	3.58	1.438	3.63	1.025	4.05	1.244	3.67	1.357	8

Table 2 shows that the majority of students made the right choices to study mining. Comparing students of different courses, Oneway ANOVA test with coefficients $sig. < 0.05$ indicates a statistically significant difference in student mean score across most of the years across the variables. Fourth-year students scored higher on the criteria than the first, second, and third-year students. However, the hierarchical results are prominent, as follows:

In the first place, students choose this major because of the advice of parents or others (average = 4.12). If the perception is correct, this result shows that the action will be right, but the results are very different from Table 1. As can be seen, here, there is no consistency and correlation between understanding the criteria for choosing a major and the actual reason for choosing the major you are studying. In Table 1, labor market demand ranked first place, and advice from parents/others ranks the last. Thus, there is a disparity between awareness and actual action. In this criterion, there is no difference among students.

Career value (average = 4.01) ranks second position, orienting to the social value of the profession, which can be both material and spiritual values. This criterion has a difference between first-year and fourth-year students: first-year students rated much lower than fourth-year ones (average = 3.63 vs. 4.25).

The last position is students’ abilities and interests when entering the mining industry. It can be seen that students choose a career that does not match their interests and skills. There is a difference between first, second, and fourth-year students. The reason for following peers ranked last. Surprisingly, some students enrolled at the university under the suggestion of friends, which is a student’s mistake: choosing a career without understanding himself and the industry. There is a diversity among first-year students, sophomores, and seniors: in freshman year, average = 1.69 and in sophomores year, average = 2.79, but in senior year, average = 3.85; and there is also a difference between third and fourth-year students.

In discussion with students, Phan Ngoc L, a freshman, said: “I chose to enter this industry because my parents worked in this industry, so they follow their advice.” A sophomore student, Nguyen Nhat M, said: “I chose this major because I found it suitable for my ability”.

Thus, the above results show that a good percentage of students choose a career according to their interests and abilities. The others’ choice depends on labor market needs and their career value. There is a

variation among freshman, sophomore, junior, and senior students.

2.3.3 Understanding of professional information

After identifying students' abilities, interests, and learning capacity and understanding who they are, the next step is to find out about the suitable profession. To assess how students understand their jobs, we asked the following question: Before enrolling in your major, how have you understood the industry? The results are in Table 3.

Tab. 3. Understanding a profession before enrolling.

No.	Profession information	Percentage (%)					Avg.	Var.	Rank
		1	2	3	4	5			
1	Requirements on competency for people working in the profession	1.5	5.4	10.2	36.6	46.3	4.21	0.934	8
2	Requirements on ethical qualities for people working in the profession	1.5	5.4	8.8	32.2	52.2	4.28	0.938	4
3	Recruiting demand	1.5	3.9	10.7	31.2	52.7	4.30	0.915	2
4	Working position	1.5	3.9	11.7	27.3	55.6	4.32	0.930	1
5	Industry development	1.5	4.9	14.1	31.2	48.3	4.20	0.957	9
6	Vocational training schools	1.5	5.4	11.7	35.1	46.3	4.20	0.945	9
7	Basic salary	1.5	3.9	12.2	33.2	49.3	4.25	0.919	7
8	Working environment	1.5	2.0	15.6	29.3	51.7	4.28	0.900	4
9	Recruitment conditions of companies	1.5	2.0	14.1	31.2	51.2	4.29	0.886	3
10	Job hunting opportunities	0.0	5.9	11.2	31.7	51.2	4.28	0.884	4

The above results show that the students understood their profession at a high level (average score from 4.32-4.2). Knowledge about working positions ranked first place with average = 4.32 means that students are interested in their jobs after graduation.

Recruitment demand ranked second, which is critical information because the higher demand for recruitment, the more chances for new postgraduates to find jobs.

The third position is companies' recruitment conditions, which shows students' concern about their job opportunities.

The qualifications of people working in the sector are not very important, as students put it at the eighth position.

There is no difference among freshman, sophomore, junior and senior students.

Through discussion, senior student Nguyen Trung K said: "Choosing to join the mining industry, I surfed many websites to find information about it. Only after considering it carefully can I make the right choice".

Students learned about the profession with interests from the above results to see if it is easy to apply for a job later. They were afraid of unemployment after graduation, so they continuously learned about the recruitment needs of companies. They did not pay much attention to other information such as the requirements of the capacity of the profession.

2.3.4. The student's suitability with the field of study

In this part, we want to see if the industry is suitable for students by the question: When entering this major, do you find your field of study right for you? In which of the following criteria?

The results obtained are in Table 4.

Tab. 4. Degree of the field of study suitability according to industry selection criteria.

No.	Cause	Freshmen		Sophomores		Juniors		Seniors		Avg.	Var.	Rank
		Avg.	Var.	Avg.	Var.	Avg.	Var.	Avg.	Var.			
1	Personal interests	3.57	1.243	3.61	1.215	3.63	0.500	4.26	0.947	3.97	0.975	4
2	Personal capability	3.77	0.910	3.88	0.970	3.81	0.750	4.21	1.035	4.01	1.012	3
3	Academic capability	3.86	0.974	3.91	1.056	4.00	0.632	4.21	1.035	3.94	1.069	6
4	Characteristics, Personality	3.69	1.231	3.88	1.069	3.63	0.500	4.21	1.035	4.05	1.053	1
5	Career value	3.74	1.268	3.98	1.060	3.81	0.750	4.36	0.913	4.05	0.991	1

6	Labor market demand	4.03	1.014	3.90	1.017	3.81	0.750	4.31	0.958	3.95	1.147	5
7	Family background	3.63	1.239	3.81	1.150	3.44	1.365	4.41	0.864	3.82	1.138	7

The above table shows that the suitability of the study field compared to students' characteristics is at a reasonable level. Most students find their field of study suitable.

The first place is appropriate for career value and labor market demand (average = 4.05). When students enter the profession, they only care about the opportunities to find a job quickly after graduation with a high salary. And this is also the topic that students consistently talk about during the study.

The suitability between academic ability and field of study ranked third. It means that students realize it is not difficult to learn in their major compared to their learning capability. They can absorb the knowledge of the subject relatively easily.

Their abilities ranked fourth, which shows that students' choice of majors does not depend on their knowledge and skills.

In line with interests only ranked in the seventh position, the last post in the order.

Comparison among different students through Oneway ANOVA test with coefficients sig. <0.05 shows a statistically significant difference in mean scores on the variables, specifically as follows: personal preferences: among first, second, and fourth-year students; career value: among first and fourth-year students; family background: among all students.

Comparing the correlation among students' causes for choosing a major and the degree of job suitability, we found a close correlation. That is, students choose according to any criteria; those criteria are suitable for them. For example, students who choose a career because of their interests learn they like; Students who choose a career because of their ability learn comfortably and quickly.

In the interview, Duong Duc H, a freshman student, said: "When I entered mining engineering, I found it quite difficult, but I also tried to overcome difficulties, to get a good job in a good company". Nguyen Van T, a senior student, said: "I chose this major because I heard about it from some students, so I think it's good. During my study, it is fortunate that it matches my ability. Now I like mining engineering, so I am very interested in the subjects of our major".

Thus, most students find that they are studying in a suitable course, leading to better learning.

2.3.5. The level of interest in the industry students are studying

Again, this content aims to know when students have entered the school and how much they care about the industry's information. To figure it out, we gave the students the following question: How well do you understand the industry you are studying?

Tab. 5. The degree of understanding of the profession in the studying process.

No.	Career information	Percentage (%)					Avg.	Var.	Rank
		1	2	3	4	5			
1	Companies you want to work for in the future	0.0	2.0	20.0	37.1	41.0	4.17	0.814	10
2	Requirements of profession competency	0.0	3.4	14.6	35.1	46.8	4.25	0.831	5
3	Qualities of people working in the profession	0.0	2.0	16.1	39.5	42.4	4.22	0.785	7
4	Industry development trends	0.0	2.0	18.0	37.6	42.4	4.20	0.803	8
5	Job position	0.0	2.0	17.1	35.6	45.4	4.24	0.804	6
6	Basic salary	0.0	2.0	18.5	37.1	42.4	4.20	0.807	8
7	Working environment	0.0	0.0	21.5	31.2	47.3	4.26	0.790	3
8	Recruitment conditions	0.0	0.0	17.6	34.1	48.3	4.31	0.753	1
9	Job opportunities	0.0	2.0	17.1	31.7	49.3	4.28	0.815	2
10	Courses in studying program	0.0	2.0	18.5	31.2	48.3	4.26	0.826	3

Table 5 shows that students learn information related to the profession they are studying at a higher level. Students are very interested in the major. However, there are differences in their priorities of information.

First and foremost, students wanted to know about the conditions of employment, which are requirements of qualifications, health, professional fields, and specific jobs. These pieces of information are helpful for them in preparation for the recruitment before their graduation.

Job opportunities are secondly concerned. The desire to get a job after graduation is natural to any student.

Courses in the training program and the working environment in the future are in the third positions.

The competency requirements of the profession, which ranked at fifth place, show that although students should pay attention to this factor, it is not a top priority. This thing will be enjoyable to the image to and development the power they are in to the learning.

As ranked in the last positions, the information about the company that students will work for after graduation shows that not all students have a clear goal of working in the company.

Comparison among students of different courses through Oneway ANOVA Test with sig. coefficients. > 0.05 shows no statistically significant difference in mean scores in all ten variables in the above content.

Thus, there is no difference in the student’s understanding of the profession before and after studying this major.

2.3.6. Student learning activities

In this part, we want to find out about the perception, attitude, and behavioral manifestations in the learning of students. We want to find out the correlation relationship between students’ career choices and student’s activities. To explore this content, we asked: How do you perceive the subjects during the learning process? Results of answers are in Table 6.

Tab. 6. Current status of students’ learning activities.

No.	Content	Freshmen		Sophomores		Juniors		Seniors		Avg.	Var.	Rank
		Avg.	Var.	Avg.	Var.	Avg.	Var.	Avg.	Var.			
1	Easy to learn major subjects	3.74	1.067	3.67	1.142	3.63	0.500	4.28	0.799	3.86	1.020	9
2	Interested in major subjects	3.86	1.089	3.83	1.041	4.00	0.632	4.43	0.763	4.04	0.977	5
3	Try to get good grades in learning	4.26	0.852	4.14	0.894	4.19	0.750	4.43	0.763	4.26	0.840	2
4	Going to class is a big effort for me	3.80	1.346	4.03	0.953	4.19	0.750	4.18	0.992	4.06	1.029	4
5	Listen attentively to the teachers’ lectures	4.20	0.964	4.00	0.936	4.19	0.750	4.48	0.698	4.20	0.878	3
6	Committed to completing my studies at school, no matter how difficult it is	4.26	0.780	4.10	0.949	4.38	0.806	4.52	0.698	4.29	0.852	1
7	Study just enough to pass subjects	3.34	1.371	3.79	1.055	4.00	0.894	4.28	0.915	3.88	1.098	8
8	Take time to study difficult subjects thoroughly	3.63	1.190	3.89	1.086	3.81	0.750	4.43	0.694	4.01	1.017	7
9	Always enjoy new lessons and learning challenges	3.57	1.145	3.93	1.036	3.81	0.403	4.43	0.763	4.02	0.987	6
10	Find the subjects interesting and meaningful	3.29	1.487	3.63	1.311	3.63	0.806	4.13	1.024	3.73	1.250	10

In Table 6, there are some prominent pieces of information:

- Awareness of subjects: Although students have good awareness about the training program, “Easy to learn major subjects”, and “Find the subjects interesting and meaningful” ranked the last positions. It is not easy for students to understand specialized knowledge, but they have to during the study. Once students understand the lessons, they can find the course exciting and meaningful.

- Attitude towards the subjects: The students of Mining Engineering have a good attitude in studying.

Although courses are challenging, the students have a positive attitude as they are interested in learning important topics and always attentively listening to the teacher’s lectures.

- Behavioral manifestations in learning: In this content, the students’ great determination is shown in specific actions. “Committed to completing my studies at school, no matter how difficult it is”, “Try to achieve good grades in studying”, and “always listen attentively to the teachers’ lectures” are top answers. These answers show the high determination of students, no matter what challenges they scope to complete their study at HUMG.

Besides, a negative criterion that we evaluate is “going to class is a great effort for me” ranking fourth place. There are a few students whose goal of studying is to pass the courses. They are not interested in their study. In other words, they lack motivation in learning.

Comparison among first, second, and fourth-year students through Oneway ANOVA test with coefficient sig. < 0.05 shows a statistically significant difference in mean scores.

Tab. 6.1. Correlation between career suitability and student learning activities.

		The major suitable for their ability	Interest in studying major subjects
The major suitable for their ability	Pearson Correlation	1	.742**
	Sig. (2-tailed)		.000
	N	205	205
Interest in studying major subjects	Pearson Correlation	.742**	1
	Sig. (2-tailed)	.000	
	N	205	205

** . Correlation is significant at the 0.01 level (2-tailed).

There is a correlation between the suitability of the profession they choose (Tab. 4) and the students’ strong learning attitude (Tab. 6). The learning attitude will be positive and exciting for those who have chosen a career that follows their interests (Tab. 6.1). Students who find the major suitable for their ability find the study more straightforward and faster (Tab. 6.2).

Tab. 6.2. The correlation between career suitability and students’ learning activities.

		The major suitable for their ability	Easy to learn major subjects
The major suitable for their ability	Pearson Correlation	1	.724**
	Sig. (2-tailed)		.000
	N	205	205
Easy to learn major subjects	Pearson Correlation	.724**	1
	Sig. (2-tailed)	.000	
	N	205	205

** . Correlation is significant at the 0.01 level (2-tailed).

In discussions, Le Truong G, a sophomore student, said: “This major is good and I like it. Thus, every class I am interested in, I will try to study well. I hope I can have a good career with high income in the future”. A junior student, Nguyen The B, said: “Sometimes I also feel pressure, studying this major is not suitable for me. Hence, it is a big effort to go to class.”

Thus, students in the Faculty of Mining of Hanoi University of Mining and Geology have been active in their learning activities. This statement is reflected in their awareness, attitude, and behavior.

2.3.7. Preparing for the future career

We questioned: How have you prepared for your work in the future? This question aims to know how students prepare for their future work. The results are in Table 7 below:

Tab. 7. Students' preparation for their future career.

No.	Content	Freshmen		Sophomores		Juniors		Seniors		Avg.	Var.	Rank
		Avg.	Var.	Avg.	Var.	Avg.	Var.	Avg.	Var.			
1	I have plenty of time so preparing is unnecessary	3.80	1.158	3.73	0.992	2.69	1.078	3.64	1.317	3.64	1.153	10
2	Have goals and development plans	4.14	0.810	4.14	0.815	3.81	0.403	4.28	0.799	4.17	0.789	1
3	Have been implementing the plan towards goals	4.14	0.810	3.98	0.848	4.00	0.632	4.30	0.782	4.12	0.814	2
4	Participate in club activities on and off campus	3.83	0.954	4.06	0.853	3.81	0.750	4.39	0.802	4.11	0.870	5
5	Attend advanced courses	3.74	1.221	3.97	0.867	3.63	0.500	4.34	0.854	4.03	0.939	8
6	Attend seminars and talks relevant to the industry	3.80	1.158	4.08	0.738	3.81	0.403	4.39	0.802	4.12	0.849	2
7	Participate in teachers' projects	3.91	1.011	4.08	0.824	3.81	0.403	4.30	0.782	4.11	0.833	5
8	Attend soft skills classes	4.14	1.004	3.99	0.786	3.63	0.500	4.28	0.915	4.09	0.864	7
9	Attend foreign language classes	4.37	0.731	4.03	0.917	3.63	0.500	4.18	0.992	4.12	0.900	2
10	Ready to make job applications	3.74	1.172	3.63	1.231	3.06	1.124	4.23	1.007	3.80	1.189	9

Students have relatively well prepared for their future careers. "Having goals and development plans" is the most important for students. "Participate in seminars and talks relevant to the industry" to learn more and improve industry knowledge, and "attend foreign language class" to improve languages skills ranked second. Students prioritize those above activities. "Participate in club activities on and off-campus" and "participate in teachers' projects" are also necessary activities for students. Also, most students are "ready to make job applications."

Tran Gia B, a senior student, shared his opinion: "I have prepared a lot for my job applications regarding necessary skills and a proactive mindset."

Comparing among first, second, third, and fourth-year students through One-way ANOVA test with coefficient sig. < 0.05 indicates a statistically significant difference in mean scores. Fourth-year students prepared at a higher level than other year students in the following criteria: participate in club activities on and off-campus, participate in advanced training courses, participate in seminars and talks relevant to the industry, participate in teachers' projects, and be ready to make job applications. The rest of the other criteria showed no difference.

Thus, students have consciously prepared for their future careers in various ways. However, some students do not know how to prepare for their future careers, and they have no motivation to set goals in the learning process. Fourth-year students prepare at a higher level than first, second, and third-year students.

2.3.8. Students' confidence in their professional abilities

We asked the question: Are you now confident in your professional capability? The results are in Table 8:

Tab. 8. Confidence in students’ professional competence.

No.	Content	Freshmen		Sophomores		Juniors		Seniors		Avg.	Var.	Rank
		Avg.	Var.	Avg.	Var.	Avg.	Var.	Avg.	Var.			
1	I feel I can get a job right after graduation	3.60	0.976	3.67	1.091	4.00	0.894	4.08	0.900	3.82	1.019	3
2	I feel I still lack a lot of industry knowledge	3.80	0.901	4.02	0.912	3.63	0.500	4.18	0.827	4.00	0.863	1
3	I feel I still lack many professional skills	3.97	0.891	3.96	0.947	3.63	0.500	4.13	0.866	4.00	0.891	1
4	I am not confident because I feel this profession is not suitable for me	3.91	1.040	3.79	1.195	2.50	1.265	3.74	1.413	3.70	1.278	4

Results show students’ confidence in their abilities is relatively high. The criteria “I can get a job right after graduation” (average = 3.82) shows their belief. These students are confident in their expertise and skills. Besides, some students still think that they lack a lot of knowledge and professional skills. Therefore, they do not have enough knowledge and skills to apply for jobs immediately.

Some students are not confident because “this profession is not suitable for me”. It is because students choose a major without motivation, learning goals, and confidence. Consequently, they cannot achieve high results and lack sufficient knowledge and skills for further work.

Comparison of confidence among first, second, third, and fourth-year students through One-way ANOVA test with coefficient sig. < 0.05 indicates no statistically significant difference in mean scores. It means there is no difference in students’ confidence in career. This fact seems contradictory because fourth-year students should have more confidence than first, second, and third-year students.

In addition, we compared the correlation between students’ preparation for their future careers (Tab. 7) with confidence in their abilities (Tab. 8) and found a close relationship (Tab. 9). With good preparation of knowledge, skills, and skills at a high level, their confidence in their abilities is also correspondingly high.

Tab. 9. The correlation between preparation for a future career and confidence in personal ability.

		Preparation for future career	Confidence in personal ability
Preparation for future career	Pearson Correlation	1	.713**
	Sig. (2-tailed)		.000
	N	205	205
Confidence in personal ability	Pearson Correlation	.713**	1
	Sig. (2-tailed)	.000	
	N	205	205

** . Correlation is significant at the 0.01 level (2-tailed).

Thus, students are confident in their abilities to a reasonable level, while students who are not confident in themselves are also at a reasonable level. Significantly, there is no difference between the students of the courses because, as a rule, the fourth-year students must be more confident than first, second, and third-year students.

2.3.9. Orientation of students’ future work

We aim to determine how graduation students choose a career through the question: How do you choose your future job? The results are in Table 10:

Tab. 10. Orientation of students' future work.

No.	Content	Freshmen		Sophomores		Juniors		Seniors		Avg.	Var.	Rank
		Avg.	Var.	Avg.	Var.	Avg.	Var.	Avg.	Var.			
1	Good working environment	4.29	0.860	3.94	0.879	4.19	0.911	4.20	0.833	4.10	0.863	1
2	High income	4.34	0.838	4.03	0.893	3.88	1.204	4.07	0.998	4.08	0.938	2
3	Potential for promotion	4.09	1.173	3.59	1.244	4.06	1.124	3.97	1.110	3.83	1.186	6
4	Good compensation policy	3.97	1.014	3.72	1.028	3.94	0.998	3.95	1.087	3.86	1.036	5
5	Work brings joy and happiness	4.11	0.993	3.99	0.841	4.00	0.894	4.03	0.894	4.02	0.877	3
6	Work brings social values	4.09	1.011	4.00	0.848	3.94	0.998	3.97	0.948	4.00	0.907	4
7	Creative, challenging work	3.71	1.405	3.57	1.281	3.44	1.504	3.82	1.285	3.67	1.313	7

The results show that students' choices are also diverse, and each student has a different career value.

Ranked first is the students' choice of a "good working environment" reflected in the workplace atmosphere, such as suitable work, happy and harmonious colleagues in the company, etc.

The second best choice is high income. Indeed, many students choose this criterion, which means salaries and bonuses of the company help them have a more comfortable life.

The third popular choices are "work brings joy and happiness" and "work brings social value". These are the spiritual values that students aspire. One-way ANOVA test with coefficient sig. < 0.05 indicates no statistically significant difference in mean scores among first, second, third, and fourth-year students.

Thus, we see no difference in choosing future jobs. Most students chose "good working environment" and "high income" as the two criteria earned the highest score.

3. Conclusions

The above research shows that most students in the Faculty of Mining, Hanoi University of Mining and Geology, have good career orientation. The majority of students have identified the proper criteria when choosing a career. They have carefully researched information about the industry, such as labor market demand, working environment, job position, capability requirements, and quality of the profession they are studying. The information and decision motivate them to form the awareness, attitude, and behavior in learning. Many students prepare well for their future careers by setting goals, planning and implementing plans, and participating in other activities to enhance understanding and build skills. As a result, many students are confident in their professional ability to work in the industry after graduation successfully. However, a few students determined relatively wrong criteria for choosing a career, depending on the advice of friends or others. Hence, they do not find the field of study suitable for them, which downgrades their motivation and goals in the learning process. Consequently, they are not excited to study.

Students need to understand their strengths, interests, and career values clearly and actively learn about the profession to have a proper choice for studying. It is important to improve career orientation in high schools and universities. Consequently, students can develop their responsibility in their studying and self-improvement to meet the needs of the industry. Especially, it is necessary to proactively discuss with career counselors when they have difficulties at the university.

4. Acknowledgements

The paper was presented during the 6th VIET - POL International Conference on Scientific-Research Cooperation between Vietnam and Poland, 10-14.11.2021, HUMG, Hanoi, Vietnam.

5. References

1. Le Thi Duyen., 2019. Current situation of vocational training capacity teachers of high schools.
2. Truong Thi Hoa., 2018. Define the ability of career counseling ability of students in the education department.

3. Truong Thi Hoa., 2018. The reality of Hanoi National University of Education's students' ability to organize experiential activities for vocational education.
4. Truong Thi Hoa., 2018. The reality of pedagogical students' capacity of integrating vocational education knowledge into subjects.
5. Truong Thi Hoa., 2018. The reality of career counseling capability of Hanoi National University of Education's students
6. Dang Van Hai., 2020. Vocation education for high school students under the education program in Nghe An province.
7. Nguyen Thi Nhu Thuy., Lu Thi Mai Oanh., 2020. Career counseling and enrollment for high school students on the research results at Ho Chi Minh city university of technology and education.
8. Jesus Bravo., Scott E. Seibert., Maria L. Kraimer., Sandy J. Wayne., Robert C. Liden., 2015. Measuring Career Orientations in the Era of the Boundaryless Career: Results suggest that career orientation is best represented by a six-dimension factor structure, Article in Journal of Career Assessment, November 2015 DOI: 10.1177/1069072715616107
9. William Donald., Yehuda Baruch., Melanie Ashleigh., 2017. Boundaryless and Protean Career Orientation: A Multitude of Pathways to Graduate Employability. DOI: 10.1057/978-1-137-57168-7_6.
10. E. Polyanskaya., O. Fisenko., V. Kulakova., 2018. Strong-Willed Character Traits in Students' Career Orientation in the Labor Market and Self-Realization, Article in European Research Studies Journal. DOI: 10.11214/thalassinus.21.06.062.
11. Angela Ulrich., Kerstin Helker., Katharina Losekamm., 2021. What Can I Be When I Grow Up?"- The Influence of Own and Others' Career Expectations on Adolescents' Perception of Stress in Their Career Orientation Phase, 13: 912. <https://doi.org/10.3390/su13020912>.

Exploring the Relation between Seismic Coefficient and Rock Properties Through Field Measurements and Empirical Model for Evaluating the Effect of Blast-Induced Ground Vibration in Open-Pit Mines: A Case Study at the Thuong Tan III Quarry (Vietnam)

TRAN Quang Hieu^{1,*}

¹ Hanoi University of Mining and Geology, 18 Viet street, Hanoi, Vietnam

Corresponding author: tranquanghieu@humg.edu.vn

Abstract Blasting is one of the most effective methods for fragmenting rock in quarries. Nevertheless, its adverse effects are significant, especially blast-induced ground vibration. Field measurement and empirical equations are simple methods to determine and estimate the intensity of blast-induced ground vibration. However, we cannot evaluate the effects of blast-induced ground vibration on the surrounding environment based on these outcomes. Therefore, this study explores the relation between seismic coefficient and rock properties through field measurements and an empirical model for evaluating the effect of blast-induced ground vibration in open-pit mines. Accordingly, the seismic coefficient (K) is considered the main objective in this study. Firstly, it was determined based on the rock properties. Subsequently, an empirical model for estimating blast-induced ground vibration was developed based on field measurements. This empirical equation was then expanded to determine K to check whether it matches the determined K by the rock properties. Finally, it was used as the threshold to determine the maximum explosive charged per delay to ensure the safety of the surrounding environment from blast-induced ground vibration. For this aim, the Thuong Tan III quarry (in Binh Duong province, Vietnam) was selected as a case study. Fifth-teen blasting events with a total of 75 blast-induced ground vibration values were recorded and collected. An empirical equation for estimating blast-induced ground vibration was then developed based on the collected dataset, and K was determined in the range of 539 to 713 for the Thuong Tan III quarry. Based on the measured blast-induced ground vibrations, developed empirical model, and K values, the Phase 2 software was applied to simulate the effects of blast-induced ground vibration on the stability of slopes as one of the impacts on the surrounding environment. From the simulation results, we can determine the maximum explosive charged per delay for each type of rock to ensure the stability of the slope.

Keywords: Ground vibration; Seismic coefficient; Thuong Tan III quarry; Simulation; Vietnam.

1. Introduction

Blasting is one of the most popular and helpful in fragmenting rocks in open-pit mines. Although the advantages of blasting for rock breakage are undeniable, however, the hazards impacts with blasting are not trivial, such as ground vibration, air overpressure, back-break, fly rock, etc. [1, 2, 3, 4]. Of these undesirable effects, ground vibration is the most dangerous, with many severe impacts, including instability of benches and slopes, disrupting structures, cracks or collapses houses, the vibration of roads and railways, underground water, to name a few. Peak particle velocity (PPV) is well-known as an indicator for measuring ground vibration. It is generated by the wasted energy of explosions and spreads in rocky environments. At high frequencies in a short time, the PPV can significantly affect the structure of the building. Although oscillation is a gradual decrease in the distance, in the case of PPV fluctuations coincide with the natural oscillation of the systems, resonance oscillation will occur and significantly affect cracks, collapses, and subsidence. Consequently, blast-induced PPV evaluation and control are essential to minimize adverse impacts on the environment. Many scholars have studied empirical approaches; however, most models developed for predicting blast-induced PPV were mainly based on the linear relationship between explosive charge per delay and monitoring distance [5, 6, 7].

Therefore, when choosing safe blasting modes, one proceeds from the level of the seismic action of the explosion that does not exceed the maximum permissible value, the existing regulatory data, the actual state of protected objects, their service life, degree of responsibility, etc.

2. Study area and materials

Thuong Tan III quarry is located in Thuong Tan commune, Bac Tan Uyen District, Binh Duong province of Vietnam (Fig. 1). The approved mine reserve is 16.727 million m³, and the authorized area is 42 ha to

cote -70 m. The deepest mining site reaches -50 m, the soil layer is 4÷5 m thick, and the rock layer is 8÷10 m wide. The stone processing area is located in the south and southwest of the mining area, with the stone crushers in operation. This quarry was selected as a case study because it is close to the Thuong Tan IV quarry with a distance of 180÷200 m [8]. Therefore, blasting operations in the Thuong Tan III quarry were recommended as high risks for the Thuong Tan IV quarry slopes.

In small surveying projects, rotary-wing UAVs such as DJI Phantom 3, 4, or DJI Inspire 2 are often utilized widely [9-16]. Mine terrain for this study is collected in this study is DJI Inspire 2. The camera mounted on the drone is crucially important as it directly contributes to the resulting 3D models' accuracy. The results are shown in Fig. 1.

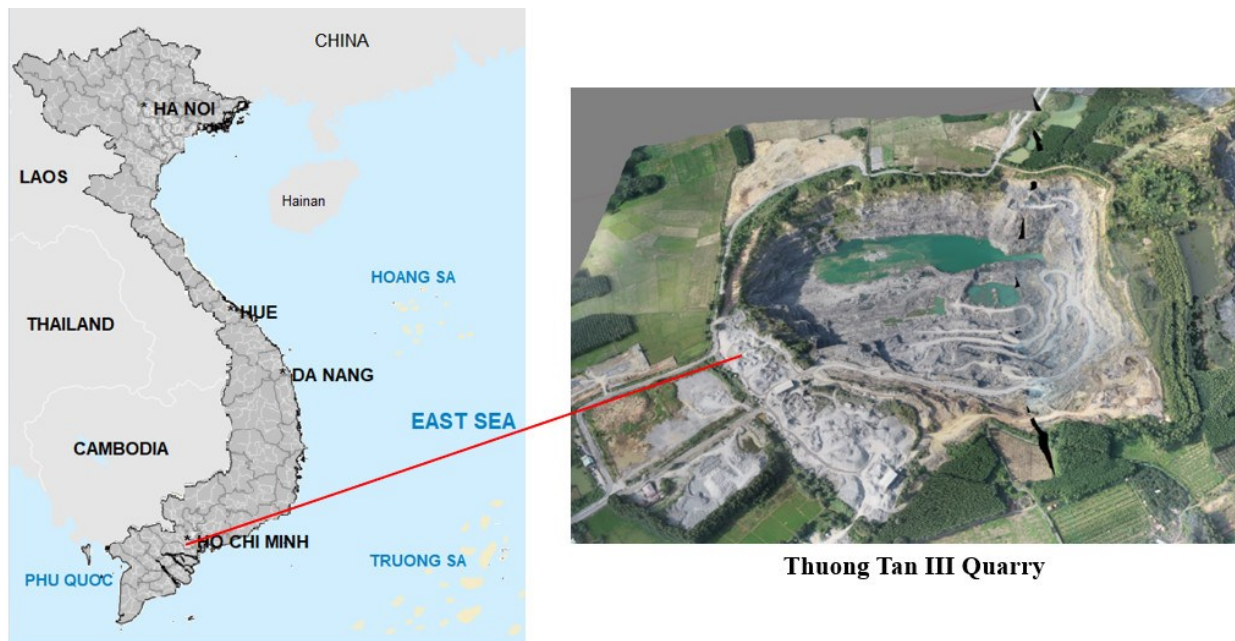


Fig. 1. Location of the Thuong Tan III quarry in Binh Duong province, Vietnam.

In this study, 15 blasting events were performed with a total of 75 explosion-induced ground vibration records at the sensitive environmental objects. The study aimed to determine the attenuation coefficient of blasting vibration (K) to predict the ground vibration caused by the explosion and blast-induced ground vibration at the Thuong Tan III, Thuong Tan IV quarry. We used a multipoint blasting vibration monitoring system (Vibration wireless sensor provides real-time monitoring data- Wireless Mesh Sensor (WMS-02) (Fig. 2):

- Real-Time Wireless Sensors: Sensor products are built to be deployed on mining and construction sites, tunnels, bridges, pathways, and other structures. Sensors also can monitor both vibration and tilt simultaneously. Thanks to this ability, the effects of blasting vibration on structural safety can be understood in real-time [17-19].

- Sensor & Gateway for monitoring & routing: Vibration wireless sensor provides real-time monitoring data. Gateway products quickly route data and alerts to the desired locations (i.e., mobile phones, FTP Server, GIS). USB Management Node is a dongle attached to a PC and establishes a wireless mesh network. It enables bi-directional communication with a maximum of 100 sensors. Sensors have been designed for easy installation and wireless remote management to provide readings and alerts when a user-defined allowable limit is exceeded (Fig. 2).

- Sensors can be positioned over a large area as each sensor can act as a repeater; the sensor network can span kilometers. Multiple sensors are deployed at target locations. Readings are transmitted to the Management Node (Management dongle) connected to the PC. Since our sensors have a built-in router function, all tasks are sent to the detector near the Management Node and, in turn, to the Node (Fig. 3).

Eight blasting events of the mine were conducted, and four seismographs monitored each blasting event. Finally, a total of 75 records of PPV were collected for predicting and simulating the effects of PPV, including the explosive charge per blast (Q), monitoring distance (D), and PPV. It is worth noting that the

Wireless Mesh Sensor (WMS-02) seismograph was used to monitor PPV, and a GPS device was used to measure D. The details of the datasets are summarized in Tab. 1. In this quarry, the borehole diameter of 105 mm, bench height of 8÷10 m, powder factor of 0.35÷0.34 kg/m³, the burden of 10÷11.5 m, spacing of 2.8÷3.2 m, sub drilling of 105 mm, and stemming of 4.9÷5.2 m; maximum charge per delay Q_{dl}= 20÷40 kg; Total explosives in the blast Q= 1000÷3000 kg; Distance between the blasting and measuring locations R= 100÷500 m. The details of the dataset are presented in Tab. 1.



Fig. 2. Seismograph for monitoring blast-induced ground vibration in the Thuong Tan III quarry.

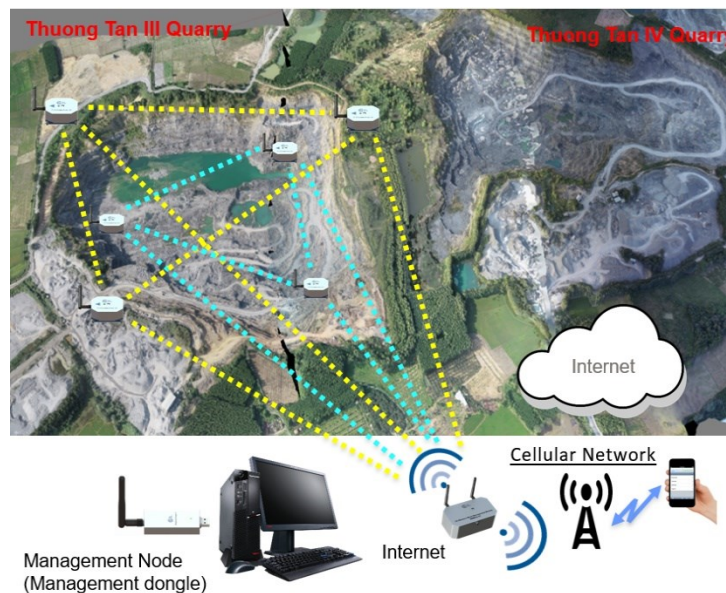


Fig. 3. Scheme for monitoring blast-induced ground vibration in the Thuong Tan III quarry.

Tab. 1. The dataset collected in this study.

Q/Q _{dl}	D	V	Q/Q _{dl}	D	V	Q/Q _{dl}	D	V
2275/ 40	98.25	5.62	2250/ 30	51.3	6.85	1860/ 62	57.4	5.58
	102.93	2.94		75.1	3.55		51.3	6.10
	120.35	1.93		75.3	2.87		32.8	2.80
	56.64	16.85		110.4	1.91		33.9	5.90
	56.14	18.63		24.5	44.84		44.9	3.65
1950/ 27	98.6	1.78	2000/ 38.8	75.1	1.28	1464/ 23	48.3	5.88
	85.7	2.75		62.3	3.64		39.8	12.00
	126.7	1.29		72.0	3.04		44.3	6.13
	93.1	2.08		47.2	5.57		45.3	7.62
	125.3	1.40		31.8	7.08		77.9	5.63
2880/ 36	54.4	6.98	2000/ 31.2	52.4	11.80	2236/ 40	68.4	7.85
	93.4	3.22		50.8	13.05		55.6	14.66
	128.4	4.48		77.5	2.26		33.0	22.68

	78.2	5.37		68.6	2.29		66.2	8.74
	48.7	8.70		63.4	4.87		60.1	9.70
1538/ 48	69.7	6.78	2675/ 29	102.1	3.81	1788/ 40	46.7	3.55
	40.5	13.12		52.0	17.50		43.0	10.20
	65.4	8.30		90.6	14.30		86.5	4.01
	81.3	3.25		74.2	4.12		51.6	3.00
	69.6	3.81		43.0	5.91		33.7	22.20
1760/ 20	44.8	13.05	2625/ 29	73.7	2.43	2700/ 25	84.8	5.04
	64.8	4.87		85.9	24.40		52.5	2.23
	97.3	2.29		71.0	34.20		133.4	4.16
	108.1	1.98		51.8	4.83		161.2	3.10
	78.2	2.26		57.2	3.57		87.0	4.60

3. Methodology

3.1. P-wave and S-wave Velocity Theory in rock

To study the issue more simply, we use methods to analyze the kinematic and dynamic characteristics of elastic waves (deformations) generated in the well by an impulse source. The rock is viewed mainly as a flexible body [20-22]. An elastic body is characterized by the deformations' restoration when the applied forces are removed. In a homogeneous isotropic medium, waves of two types arise and propagate longitudinal wave P and shear wave S (Figs. 4, 5).

- Waves P arise during deformations of the volume of an elastic body. In the P wave, the particles of the medium move in the direction of wave propagation in the applied forces F. The wave is an alternation of compression and extension zones. These zones move at a speed V_p , which is longitudinal wave velocity.

- Waves S waves arise during deformations of the shape (shear) of an elastic body. In the S wave, the particles of the medium move perpendicular to the wave propagation in the direction of the applied forces F. An alternation of stripes with the opposite direction of particle motion is observed. These zones (stripes) move at a speed of V_s . V_s is the speed of the transverse wave.



Fig. 4. Forces and deformations applied (Waves P and waves S).

$$E = (F / S) / (\Delta l / l) \quad (1)$$

$$\mu = (\Delta d / d) / (\Delta l / l) \quad (2)$$

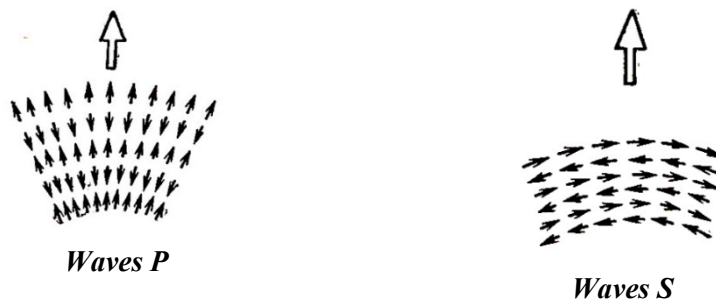


Fig. 5. Wave direction and particle movement (Waves P and waves S).

Shear modulus G , Young's modulus E , and Poisson's ratio μ are related. μ - Poisson's ratio can be determined based on measuring the velocities V_p and V_s .

$$G = \frac{E}{2(1 + \mu)} \quad (3)$$

$$\mu = \frac{V_p^2 - 2V_s^2}{2(V_p^2 - V_s^2)} \quad (4)$$

- Longitudinal wave P- translational motion of particles of the medium in the direction of propagation of elastic vibrations (waves). Longitudinal waves propagate at a speed V_p determined by the elastic and density properties of the medium [23, 24]:

$$V_p = \sqrt{\frac{E(1 - \mu)}{\sigma(1 + \mu)(1 - 2\mu)}} = \sqrt{\frac{\lambda + 2\mu}{\sigma}}, \text{ m/s} \quad (5)$$

Transverse wave S - motion of particles of the medium in the direction perpendicular to the propagation of elastic vibrations. Transverse waves propagate at speed V_s determined by the elastic and density properties of the medium [17, 18]:

$$V_s = \sqrt{\frac{E}{\sigma 2(1 + \mu)}} = \sqrt{\frac{\mu}{\sigma}}, \text{ m/s} \quad (6)$$

Where: σ - density of the medium, kg/m^3 ; λ - Lamé constant.

$$\lambda = \frac{\sigma E}{(1 + \sigma)(1 - 2\sigma)} \quad (7)$$

μ - Poisson's ratio (characterizes the resistance of the rock to shape change).

$$\mu = \frac{E}{2(1 + \sigma)} \quad (8)$$

E - Young's modulus (Characterizes the resistance of the rock to volume change).

V_p - Longitudinal wave P, m/s

V_s - Transverse wave S, m/s

The constants λ and μ , which determine the rigidity of the medium, grow faster than the density σ during the compaction of rocks. Therefore, an increase in density is usually accompanied by an increase in acoustic velocity. The constants λ and μ are always positive. Consequently, the speeds of the longitudinal waves are always more significant than the velocities of the transverse ones.

Seismic coefficient (K) changes depending on the change in the blasting conditions. K is determined based on specific measurements of the velocity with known Q and R . When calculating the seismic effect of short-delay explosions, if there is no data on the maximum weight of the charge in the group, the values of the seismicity coefficients can be determined through the function of reducing the seismic effect of explosions. Then the value of the seismicity coefficient is found by the formula:

$$K = 1000 \cdot \sqrt[3]{\frac{V_p}{\sigma} \left(1 - \frac{4}{3} \frac{V_s}{V_p}\right)^2} \quad (9)$$

3.2. Empirical model for estimating blast-induced ground vibration

To estimate blast-induced ground vibration by empirical methods, the well-known formula of M.A. Sadovsky [25-27] was used in this study and is described in Eq. 10.

$$V = K \left(\frac{R}{\sqrt[3]{Q_{dl}}} \right)^{-\alpha}, \text{ mm/s} \quad (10)$$

where: V - peak particle velocity, mm/s; Q_{dl} - maximum charge per delay, kg; R - the distance between the blasting and measuring locations, m; K - seismic coefficient, α - specific geological constant; D -scaled

distance, $D = R / \sqrt[3]{Q_{dl}}$.

3.3. Simulation of blast-induced ground vibration effects

To evaluate the effects of blast-induced ground vibration on the surrounding environment, the slope stability in the Thuong Tan III quarry [28-30] was simulated through the numerical analysis model using the Phase 2 software. For this aim, the equivalent blasting pressure (P_f) is calculated based on Eq. 11:

$$P_f = 0.0037 \rho v^2 \tag{11}$$

where ρ - Density of explosion; v - Velocity of the explosion, fps.

It is worth mentioning that P_f is calculated and used in the Phase 2 software under the effects of Q_{dl} , which is one of the simulation model inputs.

4. Results and discussion

4.1. Determination of the seismic coefficient (K) based on rock properties

Through exploration results up to cote -100m, it was shown that the mineral body of the stone-built in the mine is siltstone, claystone, claystone contains little lime accounted for 68 %. The thickness of the layer of siltstone containing lime is from a few cm to >10m. The siltstone containing little lime are rocks with technological properties that meet the standards for use as building materials for concrete aggregates requiring high bearing properties (type I stone). The remaining rocks include siltstone clay containing little lime, having lower compressive strength (grade II rock), accounted for 32 % that meets the standard for being used as common building materials for construction (Fig. 6).



Fig. 6. Rock properties of the Thuong Tan III quarry.

The thickness of the siltstone layer, siltstone containing lime, is from a few cm to >10 m. The siltstone, siltstone containing little lime, siltstone, and siltstone containing little lime are rocks with technological properties that meet the standards for use as building materials for concrete aggregates requiring high bearing properties (type I stone). The remaining rocks include siltstone clay, siltstone clay containing little lime, claystone, claystone containing less lime, having lower compressive strength (grade II rock) accounted for 32% that meets the standard for being used as common building materials for construction, civil construction, and rural transport.

- Siltstone: $V_p = 3540$ m/s; $V_s = 1880$ m/s; $\sigma = 2720$ kg/m³
- Clay-Siltstone: $V_p = 3260$ m/s; $V_s = 1722$ m/s; $\sigma = 2680$ kg/m³
- Claystone: $V_p = 3015$ m/s; $V_s = 1690$ m/s; $\sigma = 2540$ kg/m³

In the Thuong Tan III quarry, the majority rocks are siltstone, clay-siltstone, and claystone. Eq. 9 was applied to calculate the K values, as shown in Tab. 2.

Tab. 2. Seismic coefficient of the Thuong Tan III quarry based on the rock properties.

Value	Type of stone		
	Siltstone	Clay-Siltstone	Claystone
σ , kg/m ³	2720	2680	2540
V_p , m/s	3240	2855	2515
V_s , m/s	1880	1722	1690
K	713	656	539

From Tab. 1, it can be seen that K when blasting with siltstone is higher (1.02÷1.11) times than that of clay-siltstone and claystone.

4.2. Determination of the seismic coefficient (K) based on the empirical model

To determine the K based on the empirical model, the empirical equation (10) can be expanded as follows:

$$K = \frac{VR^\alpha}{Q_{dl}^{\frac{\alpha}{3}}} \tag{12}$$

Based on the experimental datasets and empirical equation (10), blast-induced ground vibration can be calculated according to Eq. 13, and the relationship between V and D (Fig. 7).

$$V = 626.13 \left(\frac{R}{\sqrt[3]{Q}} \right)^{-1.14}, \text{ mm/s} \tag{13}$$

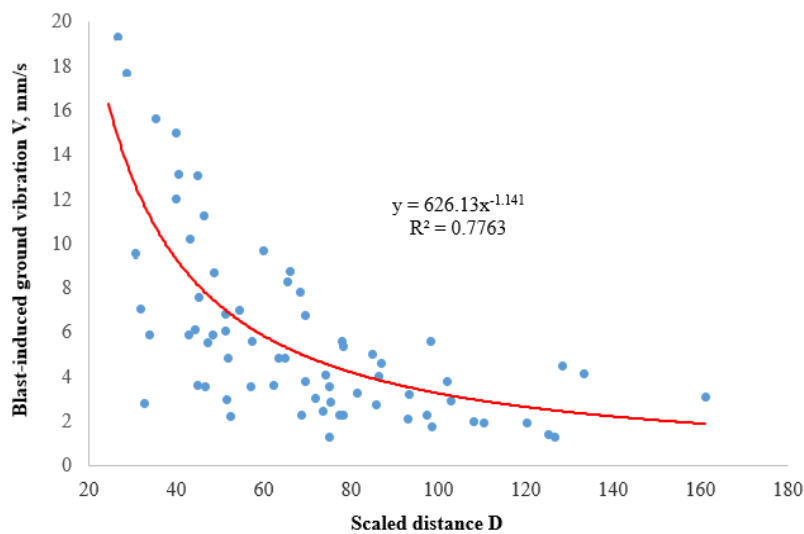


Fig. 7. Relationship between V and Scaled distance D.

Based on Eq. 13, it is easy to see that K= 626.13 and the specific geological constant $\alpha = -1.14$. Next, Eq. 12 was applied to calculate K values, as listed in Tab. 3.

Tab. 3. The dataset collected for this study.

Q/Q _{dl}	D	V	K	Q/Q _{dl}	D	V	K	Q/Q _{dl}	D	V	K
2275/ 40	98.25	5.62	1054	2250/ 30	51.3	6.85	612	1860/ 62	57.4	5.58	566
	102.93	2.94	582		75.1	3.55	490		51.3	6.10	545
	120.35	1.93	456		75.3	2.87	398		32.8	2.80	150
	56.64	16.85	1686		110.4	1.91	410		33.9	5.90	329
	56.14	18.63	1846		24.5	44.84	1724		44.9	3.65	280
1950/ 27	98.6	1.78	335	2000/ 38.8	75.1	1.28	177	1464/ 23	48.3	5.88	490
	85.7	2.75	442		62.3	3.64	406		39.8	12.00	804
	126.7	1.29	322		72.0	3.04	400		44.3	6.13	463
	93.1	2.08	367		47.2	5.57	453		45.3	7.62	591
	125.3	1.40	347		31.8	7.08	367		77.9	5.63	811
2880/ 36	54.4	6.98	667	2000/ 31.2	52.4	11.80	1081	2236/ 40	68.4	7.85	974
	93.4	3.22	570		50.8	13.05	1153		55.6	14.66	1436
	128.4	4.48	1142		77.5	2.26	323		33.0	22.68	1227
	78.2	5.37	777		68.6	2.29	285		66.2	8.74	1045
	48.7	8.70	733		63.4	4.87	554		60.1	9.70	1039

1538/ 48	69.7	6.78	859	2675/ 29	102.1	3.81	747	1788/ 40	46.7	3.55	285
	40.5	13.12	896		52.0	17.50	1590		43.0	10.20	746
	65.4	8.30	980		90.6	14.30	2445		86.5	4.01	651
	81.3	3.25	491		74.2	4.12	560		51.6	3.00	270
	69.6	3.81	483		43.0	5.91	432		33.7	22.20	1229
1760/ 20	44.8	13.05	1000	2625/ 29	73.7	2.43	329	2700/ 25	84.8	5.04	800
	64.8	4.87	569		85.9	24.40	3927		52.5	2.23	204
	97.3	2.29	425		71.0	34.20	4426		133.4	4.16	1106
	108.1	1.98	414		51.8	4.83	437		161.2	3.10	1023
	78.2	2.26	327		57.2	3.57	361		87.0	4.60	751

4.3. Simulation of slope stability based on the K and blast-induced ground vibration

Slope stability is considered one of the most adverse effects of blast-induced ground vibration on the surrounding environment. A slope failure in a mine working area can give rise to significant economic losses and safety impacts. The fundamental failure modes are varied and complex. Such mechanisms are governed by engineering geology conditions of rock mass which are almost always unique to a particular site. Using a numerical analysis model of the finite element method under the Phase 2 environment, we simulated the effects of blast-induced ground vibration on slope stability.

Accordingly, Eq. 11 was applied based on the maximum explosive charged per blast for this aim. Based on Eq. 11, ground vibration, and K, different scenes can be applied to simulate the equivalent blasting pressure. As an example, $Q = 1000 \text{ kg}$, $P_f = 3.325 \text{ MPa}$. The results are simulated in Fig. 8.

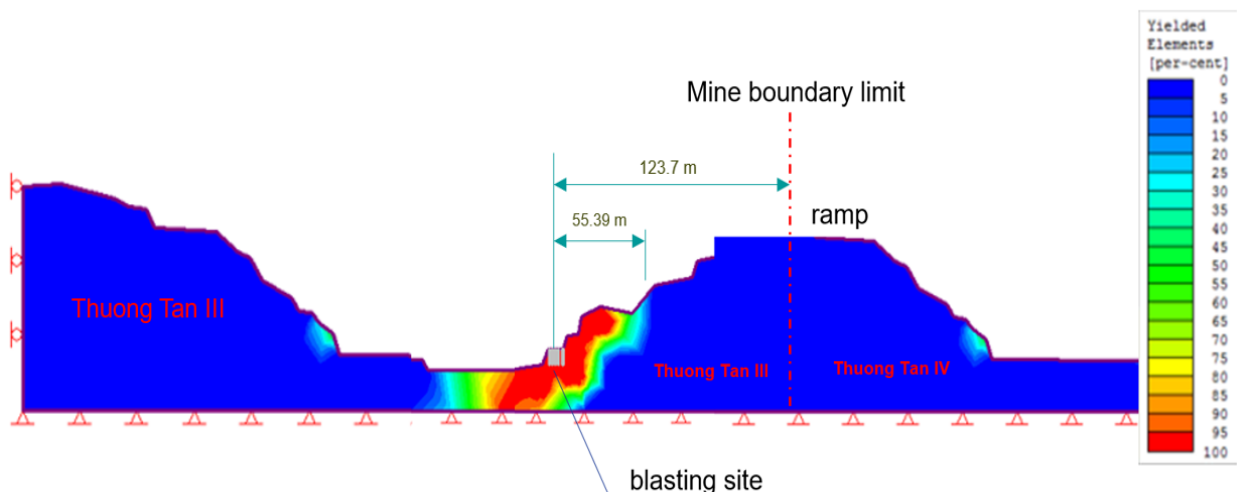


Fig. 8. Simulation of slope stability with $Q = 1000 \text{ Kg}$.

As shown in Fig. 8, it is clear that the impact zone of blast-induced ground vibration with the $Q_{\max} = 1000 \text{ kg}$ is in the range of 0 to 55.39 m. Therefore, the safety distance for slopes in the Thuong Tan III quarry with $Q_{\max} = 1000 \text{ kg}$ is $R > 55.39 \text{ m}$ (Tab. 4).

Tab. 4. The blasting distance ensures the safety and stability of the slope for Thuong Tan III.

N ^o	Parameter	Safety distance	
1	Distance from blasting site to slope stability	$R \geq 55.39 \text{ m}$	$R < 55.39 \text{ m}$
2	Maximum charge per delay	$Q_{dl} \leq 40 \text{ kg}$	$Q_{dl} \leq 30 \text{ kg}$
3	Maximum explosive charged per blast	$1000 \text{ kg} < Q \leq 3000 \text{ kg}$	$Q \leq 1000 \text{ kg}$ (Presplit Blasting)

5. Conclusions

Blasting is a crucial stage in the mining process; nevertheless, its side effects, especially blast-induced ground vibration, need to accurately predict and controlled to reduce the damages induced by blasting operations. Based on the results of this study, we draw some conclusions:

- Attenuation coefficient of blasting vibration (K) changes depending on the change in the blasting conditions. K is determined based on specific measurements of the velocity with known Q and R. We can determine the vibration attenuation coefficient due to blasting ($K= 539\div 713$) when blasting for each different type of rock (Siltstone, Clay-siltstone, Claystone). As a result, we can predict a safe zone of earthquake vibration due to the above explosion affecting the stamina slope stability.

- In this study, we used a multipoint blasting vibration monitoring system (Vibration wireless sensor provides real-time monitoring data). It is possible to determine the attenuation coefficient of blasting vibration K to predict the intensity and safety zone of blast-induced ground vibration in a quarry from test blasting results.

- Using a numerical analysis model of the finite element method (Phase 2), we simulate the effect of the blasting pressure values on the slope stability of the Thuong Tan III quarry as well as the safety zone of blast-induced ground vibration in the quarry. Based on the obtained results, sensitive environmental objects can be protected and safe during the mining process.

Several techniques are used to improve wall stability in open-pit mines. Pre-split blasting is the most pragmatic and practical approach for tackling this issue in open-pit mines.

6. Acknowledgements

The author would like to acknowledge and appreciate the opinions and judgments of researchers, scientists, and professors who came from Dong-A University, Korea, and Hanoi University of Mining and Geology. This paper would not have been possible without experiences and support from professors, experts, researchers, and engineers. In addition, the author thanks peer-reviewers for their valuable comments, which helped us improve the manuscript's quality.

The paper was presented during the 6th VIET - POL International Conference on Scientific-Research Cooperation between Vietnam and Poland, 10-14.11.2021, HUMG, Hanoi, Vietnam.

7. References

1. Bui, X.-N., Choi, Y., Atrushkevich, V., Nguyen, H., Tran, Q.-H., Long, N. Q., et al., 2020. Prediction of Blast-Induced Ground Vibration Intensity in Open-Pit Mines Using Unmanned Aerial Vehicle and a Novel Intelligence System. *Natural Resources Research*, 29(2): 771-790, doi:10.1007/s11053-019-09573-7.
2. Nguyen, H., Bui, X.-N., & Moayed, H., 2019a. A comparison of advanced computational models and experimental techniques in predicting blast-induced ground vibration in open-pit coal mine. [journal article]. *Acta Geophysica*, 67(4): 1025-1037, doi:10.1007/s11600-019-00304-3.
3. Nguyen, H., Bui, X.-N., Tran, Q.-H., Le, T.-Q., & Do, N.-H., 2019b. Evaluating and predicting blast-induced ground vibration in open-cast mine using ANN: A case study in Vietnam. *SN Applied Sciences*, 1(1): 125.
4. Ding, Z., Nguyen, H., Bui, X.-N., Zhou, J., & Moayed, H., 2020. Computational Intelligence Model for Estimating Intensity of Blast-Induced Ground Vibration in a Mine Based on Imperialist Competitive and Extreme Gradient Boosting Algorithms. *Natural Resources Research*, 29(2): 751-769, doi:10.1007/s11053-019-09548-8.
5. Armaghani, D. J., Momeni, E., Abad, S. V. A. N. K., & Khandelwal, M., 2015. Feasibility of ANFIS model for prediction of ground vibrations resulting from quarry blasting. *Environmental Earth Sciences*, 74(4): 2845-2860.
6. Khandelwal, M., & Singh, T., 2006. Prediction of blast induced ground vibrations and frequency in opencast mine: a neural network approach. *Journal of sound and vibration*, 289(4): 711-725.
7. Monjezi, M., Hasanipanah, M., & Khandelwal, M., 2013. Evaluation and prediction of blast-induced ground vibration at Shur River Dam, Iran, by artificial neural network. *Neural Computing and Applications*, 22(7-8): 1637-1643.

8. Evaluation of the impact during and after mining on the cote -100m of Thuong Tan III and Thuong Tan IV quarries, Thuong Tan commune, Bac Tan Uyen district, Binh Duong province, Code 3209/QD-UBND Binh Duong, Chairman, Acceptance 24/01/2019.
9. Bui Xuan Nam., Lee Changwoo., Nguyen Quoc Long., Adeel Ahmad., Cao Xuan Cuong., Nguyen Viet Nghia., Le Van Canh., Nguyen Hoang., Le Qui Thao., Duong Thuy Huong., Nguyen Van Duc., 2019. Use of Unmanned Aerial Vehicles for 3D topographic Mapping and Monitoring the Air Quality of Open-pit Mines, *Inzynieria Mineralna*, 2: 222-238.
10. Nguyen Quoc Long., Ropesh Goyal., Bui Khac Luyen., Le Van Canh., Cao Xuan Cuong., Pham Van Chung., Bui Ngoc Quy., Xuan-Nam Bui., 2020. Influence of Flight Height on The Accuracy of UAV Derived Digital Elevation Model of Complex Terrain, *Inzynieria Mineralna*, 1: 179-187.
11. Le Van Canh., Cao Xuan Cuong., Le Hong Viet., Dinh Tien., 2020. Volume computation of quarries in Vietnam based on Unmanned Aerial Vehicle (UAV) data (in Vietnamese). *Journal of Mining and Earth Sciences*. 61, 1: 21-30. DOI:[https://doi.org/10.46326/JMES.2020.61\(1\): 03](https://doi.org/10.46326/JMES.2020.61(1): 03).
12. Nguyen Quoc Long., Vo Ngoc Dung., Vo Chi My., 2020. Advanced Mining Geomatic Technologies Serving Open-Pit Mining Operation in Vietnam (in Vietnamese). *Journal of Mining and Earth Sciences*. 61(5): 125-133. DOI:<https://doi.org/10.46326/JMES.KTLT2020.11>.
13. Nguyen Viet Nghia., 2020. Building DEM for deep open-pit coal mines using DJI Inspire 2 (in Vietnamese). *Journal of Mining and Earth Sciences*. 61(1): 1-10. DOI:[https://doi.org/10.46326/JMES.2020.61\(1\).01](https://doi.org/10.46326/JMES.2020.61(1).01).
14. L. Q. Nguyen, 2021. Accuracy assessment of open - pit mine's digital surface models generated using photos captured by Unmanned Aerial Vehicles in the post - processing kinematic mode (in Vietnamese). *Journal of Mining and Earth Sciences*, Vol. 62, no. 4, Aug. 2021, p 38-47, doi:[10.46326/JMES.2021.62\(4\).05](https://doi.org/10.46326/JMES.2021.62(4).05).
15. Nguyen, Q. L., Le, T. T. H., Tong, S. S., Kim, T. T. H., (2020). UAV Photogrammetry-Based For Open Pit Coal Mine Large Scale Mapping, Case Studies In Cam Pha City, Vietnam. *Sustainable Development of Mountain Territories*, 12(4), 501-509. DOI: [10.21177/1998-4502-2020-12-4-501-509](https://doi.org/10.21177/1998-4502-2020-12-4-501-509).
16. Nguyen Q. L., Ropesh G., Bui, K. L., Cao X. C., Le V. C., Nguyen Q. M., Xuan-Nam B., (2021). Optimal Choice of the Number of Ground Control Points for Developing Precise DSM using Light-Weight UAV in Small and Medium-Sized Open-Pit Mine. *Archives of Mining Sciences*, 66 (3), p 369-384, doi: [10.24425/ams.2021.138594](https://doi.org/10.24425/ams.2021.138594).
17. Tran Quang Hieu., Hoang Nguyen., Xuan-Nam Bui., Carsten Drebenstedt., Belin Vladimir Arnoldovich., Victor Atrushkevich., 2021. Evaluating the Effect of Meteorological Conditions on Blast-Induced Air Over-Pressure in Open Pit Coal Mines, Xuan-Nam Bui et al. (Eds.): *Proceedings of the International Conference on Innovations for Sustainable and Responsible Mining*. 1, Springer (indexed by Scopus), https://doi.org/10.1007/978-3-030-60839-2_9.
18. Nguyen Hoang., Bui Xuan Nam., Tran Quang Hieu., Le Thi Huong Giang., 2020. A novel soft computing model for predicting blast - induced ground vibration in open - pit mines using gene expression programming (in Vietnamese). *Journal of Mining and Earth Sciences*. 61(5): 107-116. DOI:<https://doi.org/10.46326/JMES.KTLT2020.09>.
19. Tran Quang Hieu., Bui Xuan Nam., Nguyen Hoang., Nguyen Anh Tuan., Nguyen Quoc Long., 2020. Applicable possibility of advanced technologies and equipment in surface mines of Vietnam. *Journal of Mining and Earth Sciences*. 61(5): 16-32. DOI:<https://doi.org/10.46326/JMES.KTLT2020.02>.
20. Carcione, J.M., Tinivella, U., 2000. Bottom simulating reflectors: seismic velocities and AVO effects. 65: 54-67.
21. С.В. Густов., Л.В., 2012. Суровицкий. Влияние диаметра заряда на коэффициент, характеризующий кдельный сейсмический эффект в управнении садовооского, – 61 с.
22. Лобова Г.А., 2012. Полевая геофизика и геофизические исследования скважин: методические указания по выполнению домашнего задания по дисциплинам «Полевая геофизика» и «Геофизические исследования скважин» (заочная форма обучения). – Томский политехнический университет, 16с.

23. J.P.Castagna., M.L. Batzle., and R.L.Eastwood., 1985. Relationship between compressional-wave and shearwave velocities in elastic silicate rocks, *Geophysics*, 50: 571-581.
24. Per Avseth., et al., 2008. "Quantitative Seismic Interpretation", Cambridge University Press, 2005P.F. Anderson and L.R. Lines, "A comparison of inversion techniques for estimating Vp/Vs from 3D seismic data", CREWES Research Report. 20.
25. Dam Trong Thang., Bui Xuan Nam., Tran Quang Hieu., 2014, *Blasting in mining and structures*. Publishing house of natural and technology science. Ha Noi. 454.
26. QCVN 01:2019/BCT., National technical regulation on safety in the storage, transportation, use and disposal of industrial explosive materials.
27. Садовский М.А., 2004. Оценка сейсмически опасных зон при взрывах // В кн. М.А.Садовский. Избранные труды: Геофизика и физика взрыва. - М.: Наука. С. 93-102.
28. Le Dinh Tan., 2000. The dynamic calculation of underground structures under impacting of blasting wave. Doctor thesis. Military Technical Academy. Ha Noi.
29. Martin Stolárik., Modeling of vibration effect within small distances, *Acta Geodyn. Geomater.* 2008. 5(2): 137-146.
30. Tran Tuan Minh., Bui Xuan Nam., Tran Quang Hieu., Nguyen Quang Huy., 2018. Research on the effects of the blasting pressure values on the stability of concrete lining in the existing tunnel during expansion auxiliary tunnel in Hai Van pass project of Viet Nam, *Журнал «Устойчивое развитие горных территорий»*, 3(37): 411-419.

Improvement of State Institution on Mineral Resources Management and Exploitation in Vietnam

PHAM Ngoc Huyen¹, NGUYEN Thi Hoai Nga², NGUYEN Quoc Long^{2,*}
NGUYEN Quoc Cuong³, NGUYEN Ngoc Bich⁴

¹ National Academy of Public Administration, 77 Nguyen Chi Thanh street, Hanoi, Vietnam

² Hanoi University of Mining and Geology, 18 Vien street, Hanoi, Vietnam

³ Thu Dau Mot University, Binh Duong, Vietnam

⁴ Hanoi University of Public Health, Hanoi, Vietnam

Corresponding author: nguyenuoclong@humg.edu.vn

Abstract. Vietnam's mining industry has a long history with mines distributed throughout the country. It has contributed significantly to national economic growth. However, it also causes negative impacts on the environment, thereby affecting sustainable development and mineral resource management. Therefore, mineral resource management is one of the most critical tasks of state management. The factors that directly affect this issue are the institutional system and state management tools by the law. State institutions are an essential tool to regulate behaviors and establish social orders and disciplines in all fields, including mineral resources management. This article presents the current law on managing and exploiting mineral resources to provide orientations and solutions to improve the state institution on these activities in Vietnam. Based on clarifying the theory of state institutions and analyzing the current legal document systems in Viet Nam, the paper emphasizes the role of appraisal in improving the quality of legal documents and perfecting state institutions.

Keywords: State institution, Mineral resources management, Evaluation of legal documents, minerals, mining activities

1. Introduction

The institution is humanly devised constraints that structure political, economic, and social interactions [1]. State institution includes legal standards established by the state, forming a system of legal documents regulate and create acts and relationships among the state, individuals, and organizations to develop the social discipline. The institution provides a system of rules, principles, and laws [2] of state management. The state institutions have been studied in many fields [3] and different countries [4]. In Vietnam, the state institution on mineral resources management and exploration is a system of legal documents that regulate the behavior of management subjects and objects in the management and exploitation of minerals.

Over the years, the Vietnamese legal system and its quality requirements have been studied and analyzed from various angles [5, 6]. The authorities' responsibility is to ensure the legal document system's uniformity and consistency [7], in which authors studied the conditions and criteria [8, 9, 10, 11]. The solutions to improve the legal system are given to ensure sustainable development [12]. The requirements on feasibility [13] and solutions to enhance the feasibility of legal documents [14] are also studied and interpreted.

At the international, appraisal plays an essential role in improving legal documents' quality [15] and is an indispensable step in elaborating and promulgating legal documents [16, 17], such as in Russia [18], and France [19].

In this study, the article develops the role of appraisal in improving the quality of legal documents, developing criteria for assessing the quality of legal documents in Vietnam, creating a basis for perfecting the state regulation in mineral resources' management.

Vietnam has rich reserves of mineral ores. The exploitation of minerals brings high economic value. It causes specific impacts on the environment and climate change, creating problems for interest groups and giving rise to other complex issues in state management. Therefore, it is critical to managing the mineral resources' exploitation effectively. However, in recent years, mining activities mainly rely on manual and semi-mechanized methods, which has significantly impacted environmental degradation and ecological imbalance [20]. Besides, as investors aim to earn profits quickly, mining enterprises, primarily small and

medium sizes, only focus on exploiting export at the level of ores and concentrates. However, the Mineral Law has stipulated restrictions on the export of raw minerals, which leads to significant loss of resources, low economic value and efficiency, and waste of resources. Inadequate sanctions in policies and laws on mineral resources’ management and exploitation lead to violations of mineral management [21]. The level of transparency in the Vietnamese mining industry in 2017 ranks 45 out of 89 countries, from current policies and regulations on the tax system, financial reporting regimes, management process, licensing, level of state participation, and benefit-sharing methods [22]. To overcome the above shortcomings, improving state institutions is a crucial task and a top priority. The system of policies and laws is a requisite for publicity and transparency on mineral resources’ management and exploitation. The article builds a standard framework for assessing the quality of legal documents, the legal document system and using case studies and randomized controlled trials to improve the quality of the assessment of legal documents before promulgating.

2. Study areas

In Vietnam, the Ministry of Natural Resources and Environment (MONRE) is assigned the primary responsibility for managing and exploiting mineral resources [23]. In addition, the Ministry of Industry and Trade (MOIT) [24], the Ministry of Construction (MOC), and the Ministry of Finance (MOF) [25] jointly manage. The article studies the legal documents promulgated by the National Assembly, the government, MONRE, MOIT, and other competent entities regulating mineral resources’ management in Vietnam.

3. Methodology

The study examined 518 legal documents in force out of 988 promulgated by the National Assembly, the government, and ministries to regulate mineral resources’ management in Vietnam, focusing on evaluating documents issued from 2016 to 2020 with 130 legal documents. Sample documents were surveyed on the National Database of Legal Documents. Based on determining the characteristics of the samples, the authors designed a sampling mechanism with a layered sampling method, which is random sampling in a predetermined group. The appraisal document samples are classified by the issues and issuing agencies.

4. Criteria for assessing the legal documents’ quality

The legal documents’ quality is the achievement level of the draft legal documents according to each quality evaluation criterion of the proposed draft documents before promulgation [26]. This study builds a system of criteria for evaluating the quality of legal documents to improve the quality of legal documents in promulgating, as in Table 1:

Tab. 1. A standard framework for assessing the quality of draft legal documents.

No.	Criteria	Criteria components
1	The necessity of document	1) Objectives of document 2) To specify practical issues by documents or contents of assigned policies, laws to concretize 3) To list reasons for issues settled by documents 4) To see reasons for issues are settled by documents 5) To propose changes of issues when documents take effect
2	Governing subjects of document drafts	1) Subject groups governed by documents
3	Governing scope of document drafts	1) Scope governed by documents
4	Appropriateness of document draft contents with guidelines of the	1) To specify legal bases of documents 2) To specify laws, legal documents decrees containing contents that documents are responsible for concretizing

No.	Criteria	Criteria components
	Party and policies of the state	3) To specify contents of policies that legal documents are assigned to issue and implement policies 4) To specify documents assigned by the government to issue legal documents for implementing tasks assigned
5	A process on the compilation of document drafts	1) To consider whether document drafts are compiled under the prescribed process 2) Appropriateness of profession of document compiling units to contents of document drafts
6	Constitutionality and legality of document drafts	1) To determine whether document contents violate any article of the Constitution 2) To determine whether document contents are within contents of authority to issue documents
7	Consistency of document drafts with law system of Vietnam	1) System of documents with contents related to document drafts in order of legality and time 2) System of legal norms prescribing contents of legal normative document drafts.
8	Assessment of compatibility with related international treaties participated by the Socialist Republic of Vietnam	1) To specify international treaties related to contents of legal normative document drafts 2) To specify a relationship between international treaties and contents of legal normative document drafts.
9	Feasibility of document drafts	1) Content and appearance structure of documents for proving of document logicalness 2) Structure of norms: assumptions, regulations, sanctions 3) Logical diagram of documents 4) Assessment products show sufficiency and appropriateness on necessary financial resource conditions for assurance of document effect and effectiveness and other necessities for the actual implementation of documents. 5) To consider reports on document draft impact assessment, specify achievements and limits of reports on impact assessment, issues not specified or non-comprehensively specified by reports on impact assessment. + Time and location of impact assessment + Sequence of impact assessment + Method for impact assessment + Impact assessment documents + Subjects assessing impacts + Cost of impact assessment + Contents and structure of reports on impact assessment.
10	Effective period of documents	1) To determine whether the time that documents take effect changes or affect current activities.

No.	Criteria	Criteria components
		2) Subject groups affected by impacts of legal norms when documents officially take effect
11	Assessment of administrative procedures in document drafts (if any)	1) To determine whether appraisal products show feasibility and effectiveness of managerial procedures in document drafts (if any)
12	Integration of gender equality into legal documents	1) Beneficial subject group when records take effect 2) To make document drafts practical, to determine which subjects are responsible for deploying and implementing documents 3) Gender fairness in contributing opinions to drafts 4) Gender fairness in getting benefits of documents
13	Collection of opinions for document drafts	1) List of subjects, subject groups giving opinions 2) List of subjects, subject groups giving opinions and summary table of opinions of each topic and subject groups 3) Contribution opinions of related Ministries and departments 4) To assess documents on contribution opinion summary and documents on explanation and receipt of contribution opinions for document drafts 5) To consider issues with many opposite opinions ➔ Assessment results show sufficiency, authentication of opinions, and sufficiency of subject groups giving opinions
14	Assessment of document appearance	1) The appearance of documents complies with current legal provisions
15	Assessment of Vietnamese language standard in document drafts	1) Spelling mistakes 2) Word mistakes 3) Sentence mistakes 4) Punctuation mistakes

5. Quality of the legal documents’ institutional system on mineral resources’ management in Vietnam

5.1 Advantages

According to the Law on Minerals provisions in 2010, the system of agencies responsible for state management of minerals includes the government, MONRE, MOIT, MOC, MOF, People’s Committees at all levels [24]. The government performs the unified state management of minerals. MONRE is responsible to the government for achieving the state management of minerals nationwide, promulgating and organizing the implementation of legal documents on minerals, technical regulations, norms, and prices in geological exploration of minerals, and other tasks. MOIT and MOC are responsible for elaborating and submitting the planning on minerals assigned by the government, coordinating with MONRE in state management of minerals. People's Committees at all levels shall perform the tasks within their given competence.

In the past, elaborating and promulgating legal documents were carried out under the Law on Promulgation of Legal Documents in 2015 and Decree 34/2016/ND-CP. Depending on the form of legal documents and the competence to promulgate corresponding legal documents, each type of legal document has the order and promulgating procedures that are different and implemented following current law provisions. In recent years, building and perfecting institutions and laws on mineral resources’ management and exploitation have been a workload with more complex contents and policies. However, the promulgated

legal documents confirm their necessity, clarifying the subject matter of regulation and the draft document's scope, ensuring compliance with the development and issuance of documents (Criteria 1, 2, 3, 5).

In 518 legal documents regulating the management and exploitation of minerals, MONRE issued 258 as in Table 2 [25]:

Tab. 2. Number of legal documents promulgated from 2016 to 2020.

No	Type of legal document	Number of legal documents for 2016 – 2020	Number of legal documents in 2020
1	Law	02	01
2	Resolution	01	01
3	Decree	29	07
4	Decision	11	04
5	Circular, Joint-Circular	215	17
Total		258	30

Following the Law on Minerals in 2010, many legal documents and normative legal documents have been promulgated by the National Assembly, the Government and competent ministries to direct and administer mineral resources' management. MONRE has submitted the Law on Surveying and Mapping (2018) and the Law on Environmental Protection (2020) to the National Assembly. These two important laws contribute to perfecting the state institutional system on mineral resources' management and exploitation. Other documents detailing and guiding the management and exploitation of natural resources, including mineral resources, are also actively developed. The Law on Minerals has strengthened the decentralization of state management for the local authorities to grant licenses for mineral exploration, exploitation, and processing. The promulgated documents are consistent with the Party's guidelines and policies and the state's policies and laws on mineral resources' management (Criteria 4).

The provisions of the law on administrative procedures and business investment conditions in natural resources are also amended and perfected. Contradictory, overlapping, inconsistent, and unsuitable regulations are handled and resolved gradually. Notably, Decree No. 158/2016/ND-CP has been a critical legal basis in geology and minerals. It contributes to solving the shortcomings and inadequacies in mineral resources' management in a fundamental, comprehensive, and relatively radical way, removing difficulties and obstacles in implementing the Law on Minerals [27]. It also creates favorable conditions for enterprises when participating in mineral activities such as obtaining mining license documents, exploration permissions, etc., in a clear, transparent, and convenient way. Moreover, it clarifies the responsibilities of relevant subjects in appraising dossiers, organizations, and individuals applying for mineral activity licenses when participating in the editing, supplementing, and completing documents. The regulations on the auction of mineral exploration rights and mining rights are added to enhance the initiative and self-responsibility of organizations and individuals in mineral activities. The administrative procedures in the draft document are increasingly being improved to be convenient for people and enterprises (Criteria 11).

The results of the legal dictionary on minerals, chaired by MONRE, and coordinated with the ministries and branches, determined that there are 86 documents relevant to mineral activities [28]. The constitutionality, legitimacy, consistency of draft legal documents with the Vietnamese legal system, and compatibility with applicable international treaties are increasingly guaranteed (Criteria 6, 7, 8).

Recently, many policies and legal regulations on mineral activities have focused on developing and perfecting. The draft legal documents and projects on mineral resources' management are built, focusing on the active participation of experts, scientists, and managers, ensuring that documents must meet the criteria of uniformity, consistency, feasibility, publicity, and transparency when promulgated. The system of legal documents is regularly reviewed and published a list of legal documents that have expired or ceased to be effective in whole or in part (Criteria 10). In addition, the criteria for mainstreaming gender equality in the draft legal documents (if any), collecting comments on the draft documents, its format, and the standardization of Vietnamese language in the draft document (Criteria 12, 13, 14, 15) is also increasingly

improved. Formulating and perfecting policies and laws on mineral activities have achieved specific results, removing obstacles and barriers from practice, promoting the mineral resources, contributing to environmental protection in sustainable socio-economic development. The legal documents' system is increasingly improved in quantity and quality, creating a reasonably complete and strict legal framework.

5.2. Limitations

The construction and improvement of legal institutions still pose some problems, especially assessing the feasibility of the draft document (Criteria 9). Issues of legal regulations, inadequacies in practice, lack of synchronization and connection remain. The harmonization of interests among the states, localities, businesses, and communities is also a challenge with the current system of legal regulations. Continue to improve legal documents' quality, feasibility, stability, and longevity to create stability and order in mineral resources' management.

Besides, some legal documents, technical regulations, and rules are issued postponed in promulgation, such as the Law on Minerals and other guidance Decrees. Some contents have also been stipulated in the Law on Minerals but have been slow to be promulgated, such as regulations on bidding for mineral exploration and exploitation, regulations on procedures for state capital allocation, tax on the transfer of exploration rights, rights mining excavation.

The current regulations of the legal system are not powerful. Mining rights and mining licenses become prominent issues regarding fee collection, as the sanctions are not sufficient. It also takes time to receive and appraise mineral mining licenses. The local authorities have not yet strictly implemented the current regulations on mineral exploitation. Some mines have been licensed by the locality but do not carry out mining. There are still illegal mining, over-exploitation, and mining beyond the licensed area.

The existing sanctions to deal with violations in mining activities are not sufficiently strong, slowly implemented, and do not match the reality conditions. For example, the price bracket for calculating natural resource tax for some minerals promulgated in Circular No. 44/2017/TT-BTC of the Ministry of Finance is inappropriate, causing problems in collecting mineral mining rights of previously exploited reserves.

The master plan of mineral exploration and mining areas is not synchronized, bringing difficulties for extractive companies, affecting the auction progress of mineral exploration and mining rights by the current Mineral Law.

Surveying, summarizing, and assessing data help to form the quality of legal normative document drafts as in Fig. 1.

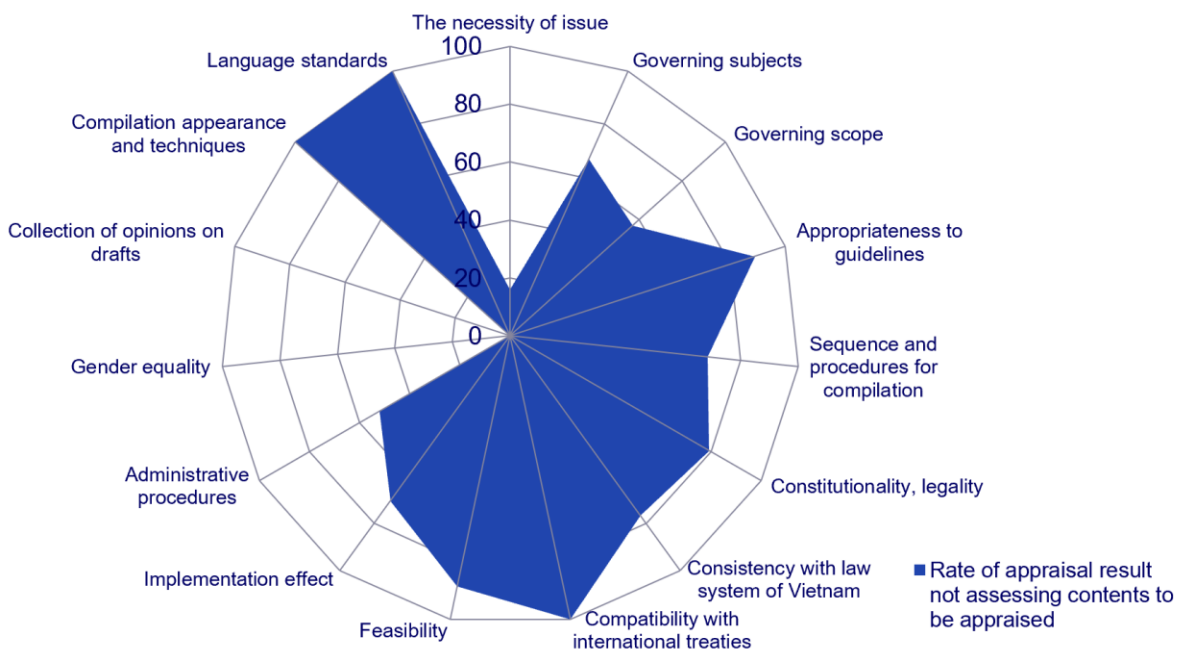


Fig. 1. Assessment quality of normative legal documents (Via 130 surveyed samples).

The inadequacies of the current legal system on mineral resources' management and exploitation are for many reasons, affecting the effectiveness and efficiency of the legal system. One of the reasons is that the appraisal of documents has not yet been promoted.

6. Conclusions

The system of legal documents and its quality is an essential factor in any state institution. The regulations on the form, authority to issue documents, orders, and procedures for the development and issuance of documents are increasingly complete in Viet Nam nowadays. The activities to evaluate documents before and after promulgation are gradually focused on implementation. In this process, the document appraisal is a pre-examination activity, which can detect unreasonable issues that need to be better. The appraisal activities with practical methods and tools will improve the quality of legal documents, perfecting state institutions in various fields, including management and mining of mineral resources.

An appraisal is a helpful tool to evaluate and improve the quality of legal documents when promulgating, avoiding overlapping regulations, significantly contribute to perfecting state institutions in various fields, especially the mineral sector in Vietnam today. Based on clarifying the theory of state institutions, the role of appraisal in improving the quality of legal documents and perfecting state institutions, analyzing the current situation of legal document systems.

The result of this research will contribute to perfecting and recommendations for improving the quality of Vietnam's state institutions on the management and exploitation of mineral resources in particular and the entire Vietnamese institutional system in general.

7. Acknowledgements

We thank anonymous reviewers for their comments that were very valuable for revising the manuscript.

The paper was presented during the 6th VIET - POL International Conference on Scientific-Research Cooperation between Vietnam and Poland, 10-14.11.2021, HUMG, Hanoi, Vietnam.

References

1. Douglass C. North, 1990. Institutions, institutional change and economic Performance. Washington University. Political Economy of Institutions and Decisions, ISBN 9780521397346
2. B. A. Garner, 2019. Black's Law Dictionary, USA. ISBN-13: 978-1539229759
3. Norman, Schofield, Gonzalo, Caballero, 2017. State, Institutions and Democracy, Springer. ISBN 978-3-319-44582-3
4. Nguyen Chu Duong, 2005. State institutions of countries in the world, Judicial Publishing House, Hanoi.
5. Nguyen Minh Tam, 2003. Building and perfecting the Vietnamese legal system – Theoretical and practical issues, People's Public Security Publishing House.
6. Nguyen Minh Doan, 2005. Building and perfecting the Vietnamese legal system in the context of building a socialist rule of law state, National Political Publishing House.
7. Nguyen Nhu Phat, 2014. Building a unified, synchronous, transparent and effective legal system in the rule of law in Vietnam, Social Science Publishing House.
8. Phan Trung Ly, 2011. Ensuring the consistency of the Vietnamese legal system”, Judicial Publishing House.
9. Phan Thanh Ha, 2010. Some basic criteria to ensure the consistency of the legal system, Journal of the State and Law No. 8/2010.
10. Nguyen Dinh Tho, 2011. What solutions to improve the unity of the legal system?, Journal of Legislative Research.

11. Le Thi Nga, 2011. Requirements for the consistency of the legal system, *Journal of Legislative Research* No. 196.
12. Nguyen Van Dong, 2010. Building and perfecting the legal system to ensure sustainable development in Vietnam today", *Judicial Publishing House*.
13. Phan Trung Hien, Nguyen Thi My Tien, 2014. Feasibility of legal documents and proposed solutions, *Journal of Legislative Research*.
14. Nguyen Van Cuong, 2014. Some solutions to enhance the feasibility of legal documents, *Journal of State Organization*.
15. J. Raz, 1990. *The Concept of a Legal System*, Clarendon Press. ISBN 978-0198253631.
16. A.I. Stavseva, editor, 1985. *Legal documents*, Moscow Legal Document Publishing House.
17. N.N. Kusnarenko, 2000. *Textology*, Knowledge Publishing House, Kiev.
18. Kevin R.Murphy, Jeanette N.Clevel and Madison E.Hanscom, 2018. *Performance appraisal and management*, SAGE Publications, Inc; ISBN-13: 978-1506352909.
19. L. Moktar, B. Jessica, 2015. *Analyse D' impact Resglementaire*, University of Québec, France. ISBN 978-2-7605-4259-4
20. Institute of Consulting and Development, 2010. *Status of management, exploitation and use of mineral resources in the context of sustainable development in Vietnam*, Science and Technology Publishing House.
21. Nguyen Mai Vinh, 2019. Inadequacies in the management of mineral resources from an audit perspective, *Electronic State Audit Journal*, 17+18st, 25.4.2019
22. Natural Resource Governance Institute (NRGI), 2017. *Resource Governance Index*. Learn more at www.resourcegovernance.org
23. Government, 2013. Decree No. 21/2013/ND-CP defining the functions, tasks, powers and organizational structure of the Ministry of Natural Resources and Environment, issued on March 4, 2013.
24. Government, 2012. Decree No. 95/2012/ND-CP defining the functions, tasks, powers and organizational structure of the Ministry of Industry and Trade, issued on November 12, 2012.
25. Government, 2013. Decree No. 62/2013/ND-CP defining the functions, tasks, powers and organizational structure of the Ministry of Construction, issued on June 25, 2013.
26. Pham Ngoc Huyen, 2017. *Quality of appraisal of legal normative document drafts by ministers*, National Academy of Public Administration.
27. Government, 2016. Decree No. 158/2016/ND-CP detailing the implementation of several articles of the Law on Minerals, issued on November 29, 2016.
28. <https://phapdien.moj.gov.vn/qt/tintuc/Pages/ngbien-cuu-trao-doi.aspx?ItemID=208>, 17.3.2021.

Applying Artificial Pillar to Replace the Coal Pillar Protecting Roadway to Increase Production Efficiency and Sustainable Development in the Vietnamese Coal Industry

DINH Van Cuong^{1,*}, NGUYEN Anh Tuan², TRAN Van Thanh³, NGUYEN Thi Hoai Nga³, DUONG Duc Hai⁴

¹ Institute of Mining Science and Technology – Vinacomin, Hanoi, Vietnam

² Vietnam National Coal – Mineral Industries Holding Corporation Limited, Hanoi, Vietnam

³ Hanoi University of Mining and Geology, Hanoi, Vietnam

⁴ Central Mining Institute, Katowice, Poland

Corresponding author: *dinhcuongvimsat@gmail.com*

Abstract. Vietnam's domestic coal production is growing fast and is expected to reach 68.9 million tons in 2030, nearly 1.5 times higher than today. Open-pit mines will gradually reduce production and close, and underground mining coal output will increase progressively year by year and take a leading role. Besides the investment in new mines to achieve these goals, it is necessary to maximize the coal reserve exploited annually of existing underground mine projects, which its coal reserve in pillars protecting roadways currently accounts for 12–15%. The further exploitation of this coal reserve will decrease the costs of preparation of underground mines and granting mining rights and depreciation of infrastructure assets. Moreover, it will help reduce the loss of non-renewable resources and contributing to the sustainable development of Vietnam's coal industry.

Keywords: coal pillar protecting roadways; coal loss; artificial pillar; underground mine

1. Introduction

In the last twenty-five years, Vietnam's total annual coal production increased rapidly from 9.4 million tonnes in 1995 to 34.9 million tonnes in 2005 and to 45.1 million tonnes in 2020 (which grew about 4.8 times). According to the Master Plan of Coal Industry Development in Vietnam by 2020, outlook to 2030 (Decision No.403/QD-TTg dated March 14, 2016), the domestic coal production will increase to 63.22 million tonnes in 2025, in which the open-pit's output will decrease from 15.3 million tonnes in 2020 to 13.27 million tonnes in 2025. However, coal production of underground mines is growing faster, from 29.8 million tonnes in 2020 to 49.94 million tonnes in 2025, an increase of 1.7 times compared to the present and accounted for nearly 80% of the national coal output.

Figure 1 illustrates details of the Vietnamese coal production during 1995–2020 and outlook to 2025.

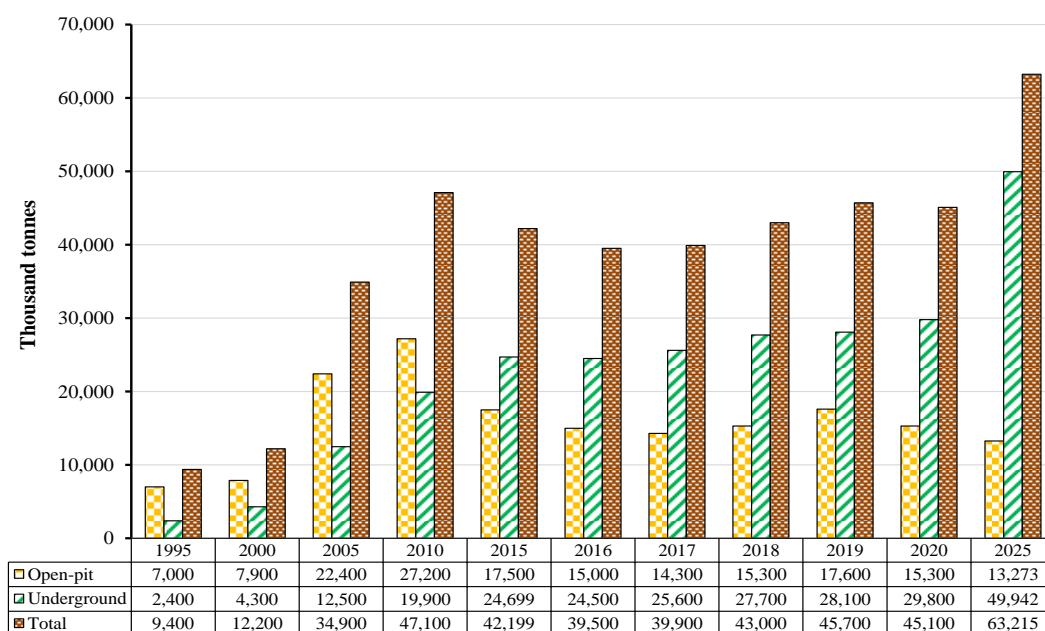


Fig. 1. Vietnamese coal production during 1995–2020, outlook to 2025 [1].

To achieve this goal, along with opening new mines, the maximum exploitation of coal reserves in underground mines is also an important issue. The most feasible way is to exploit coal reserves in pillars protecting roadways, which account for 12–15% of total coal reserves of mining projects. There are available coal reserves that are considered inevitable losses due to a lack of appropriate mining technology. Suppose coal reserves in pillars are exploited, in addition to reducing the loss of non-renewable resources. In that case, it will bring a wide range of economic efficiency for mining companies, such as reducing the cost of preparing excavation, depreciation costs of opening mines, infrastructure, cost of granting mineral mining rights. Experience in some countries with mineral development, such as Russia, Poland, and China, showed an appropriate and feasible direction to increase the coal industry's production efficiency and sustainable development.

2. Current situation of underground mining cost of Vietnam National Coal - Mineral Industries Holding Corporation Limited

In Vietnam, coal is exploited by Vietnam National Coal-Mineral Industries Holding Corporation Limited (VINACOMIN), Dong Bac Corporation (a military-run economic unit under the Ministry of National Defense), and a few private companies. VINACOMIN is the leading producer and supplier, with an annual output accounting for about 85% of the national coal output. In this paper, the authors research the technology of production of underground coal mines of VINACOMIN.

Currently, underground coal companies/mines of VINACOMIN are mainly located in Quang Ninh province (13 coal mines), with a length of nearly 100 km from Dong Trieu district (Mao Khe and Uong Bi coal mines) to Cam Pha city (Khe Cham coal mine and Mong Duong coal mine). The majority of exploited coal from underground mines (raw coal) is delivered to a transportation company for central processing plants to be ready for consumption. Therefore, in underground coal mines of VINACOMIN, the cost of coal production will be mainly direct production costs and a small ratio of consumption and management cost. From the production and business plans of some underground coal mines in Quang Ninh province, the production costs depend on production conditions (geological conditions, mining technologies applied in the production lines, etc.) and volume of infrastructure investment, ranged from 49.3 Euros to 52.7 Euros per ton in 2020. It is worth noting that direct costs reach 89.6–91.4%, consumption, and management costs are only 8.55% or 10.48%. Details of the total cost of coal mining are in Table 1.

Tab. 1. The total cost of coal production by production stages in underground coal mines of VINACOMIN in 2020 [2].

No	Cost	Value (VND per ton)			Ratio compared to I	
		Smallest	Largest	Medium		
I	Direct production costs	1,231,023	1,297,761	1,275,746	100%	
1	Cost of driving prepared roadways	146,338	293,816	204,539	16.03%	
2	Cost of mining coal in longwall	257,992	285,105	270,145	21.18%	
3	Cost of infrastructure depreciation	37,360	118,613	81,573	6.39%	
4	Cost for mining rights	26,120	26,120	26,120	2.05%	
5	Others	671,676	729,257	693,370	54.35%	
II	Consumption cost	2,141	2,622	2,483	-	
III	Cost for enterprise management and other costs	118,251	149,139	133,970	-	
IV	Total cost of coal production by stages (I + II + III)	1,355,078	1,449,477	1,412,199	-	
V	Proportion (%)	I/IV	89.53	91.42	90.35	-
		II/IV	0.16	0.19	0.18	-
		III/IV	8.39	10.29	9.47	-

The results in Table 1 show that VINACOMIN is maintaining its advantage of mass production. Costs account for a large proportion, including the cost of driving prepared roadways (204,539 VND per ton, accounting for 16.03% of production costs), the cost of mining coal in longwall (270,145 VND per ton, 21.18%), depreciation (81,573 VND per ton, 6.39%), and mining rights (26,120 VND per ton, 2.05%). These costs accumulate 582,377 VND per ton, account for 45.65% of direct production costs (see Figure 2). Thus, it is necessary to research and apply new technologies to exploit coal reserves in pillars protecting prepared roadways in underground coal mines.

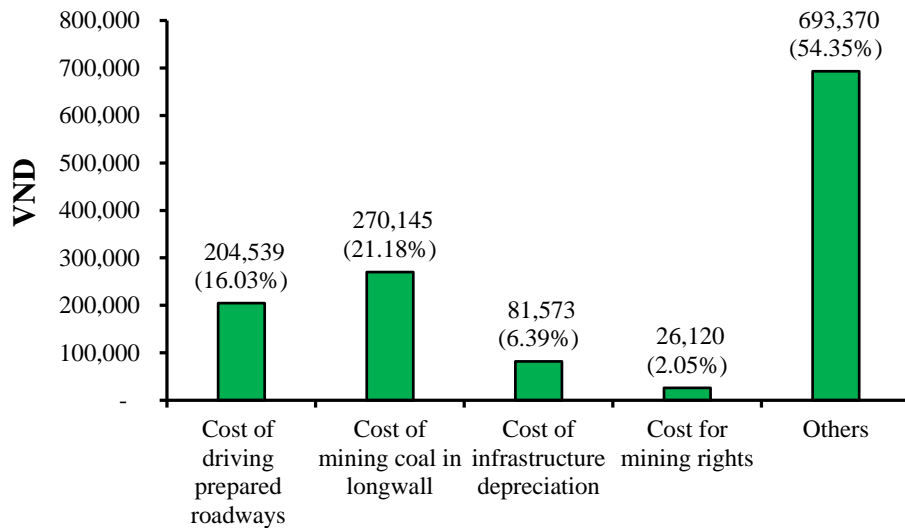


Fig. 2. Structure of direct production costs.

3. Evaluate the potential of using artificial pillar to replace the coal pillar protecting roadway in underground coal mines in Quang Ninh province

3.1 Experience in using artificial pillars to replace the coal pillar protecting roadway in the world

Underground mining in Quang Ninh is mainly longwall, mining along the strike of the coal seams. The preparation method can be generalized as 121 (Figure 3a). Each (1) longwall will have two (2) roadways (ventilation roadway, transport roadway) and one (1) coal pillar to protect from 15–18m to maintain the transportation roadway as a ventilation roadway for the next longwall. The length of longwall in underground mines of VINACOMIN is from 100–150m, an average of 120m. The rate of coal loss due to technical requirements of protection pillars accounts for 12–15% of the total coal reserves in the longwall mining area. Hence, not only the rate of coal loss but also production costs increase.

Countries such as Russia, China, Poland [3, 4, 5, 6] have successfully applied artificial pillars to replace coal pillars protecting preparation roadways to overcome the rise of coal loss and production costs. Accordingly, to simultaneously extract coal in the protection pillar and maintain the transport roadway as a ventilation roadway of the next longwall, the protected coal pillar will be replaced by artificial pillars. The materials used to construct the pillars can be clustered columns, wooden/metal cribs, stone cribs, brick/rock blocks, or chemical materials. With diagram 121, each (1) longwall only has one (1) prepared road and one (1) artificial pillar to replace the coal pillar (the preparation and exploitation scheme of this type is generalized to 111 in Figure 3b). Thus, compared to diagram 121, the type 111 scheme has allowed reducing the rate of coal loss in the protection pillar and the driving cost of prepared roadway (reduction 01 roadway). Meanwhile, the ability to isolate the roadway from the mining area to reduce the impacts of water, toxic gas and prevent endogenous fire is well-performed. It is because the artificial pillar is constructed continuously on the side of the roadway.

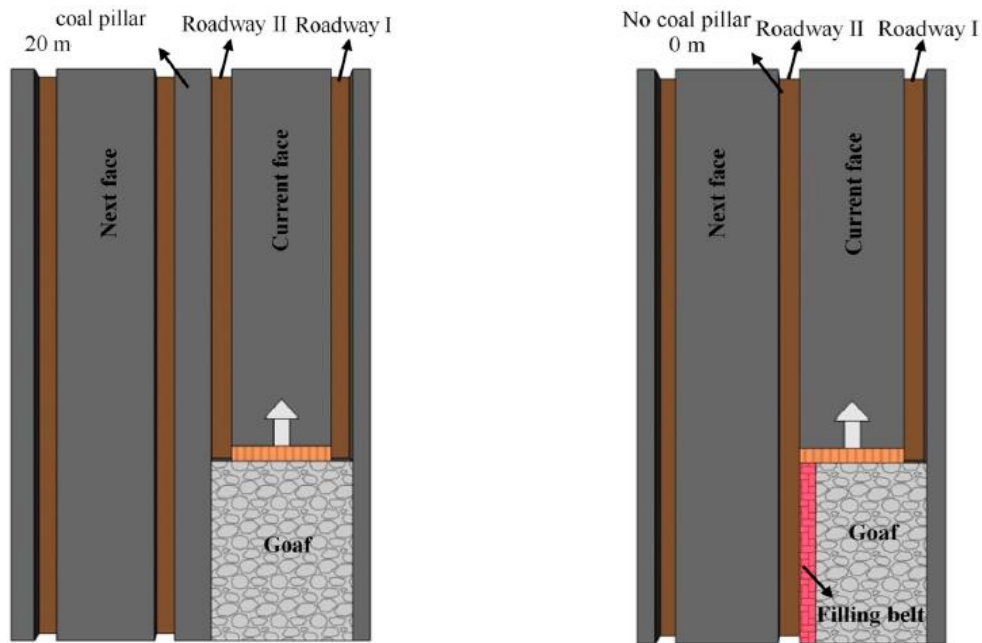
Recently, coal mining companies in China [7, 8] have applied the scheme of preparing roadways for longwalls to exploit coal without protection pillars (referred to as 110). With this solution, each (1) longwall has only one (1) roadway without (0) a protected coal pillar. The essence of technological solution is that the preparation roadway of longwall is maintained without the support of coal pillars or artificial pillars. Roadways maintained by the overall solution are actively implemented to reduce the pressure while enhancing its load capacity. Firstly, directional pre-splitting roof cutting is used to cut down the

transmission passage of ground pressure in part of the overlying rock strata. The gob-side roadway should be maintained by cable bolt or anchor with Constant Resistance and Large Deformation (CRLD) to keep the gateway roof stable during the advance roof caving. Finally, the gangue of the gateway roof will be blocked by using hydraulic props and barbed wire, which are closed to the gob-side (Figure 4).

However, solution 110 also has some disadvantages:

- The protected side of the roadway contacts directly to the mining area with poor isolation. If the site is highly affected by water and coal is self-igniting, safety becomes critical.

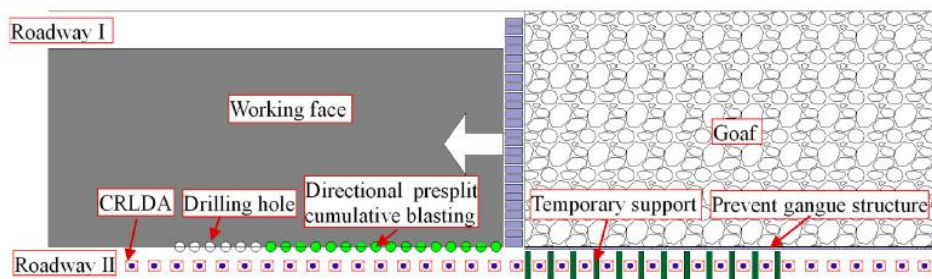
- The technological method is only effective for mining coal seams with thickness from thin to medium (≤ 3.5 m) and dip up to 15° .



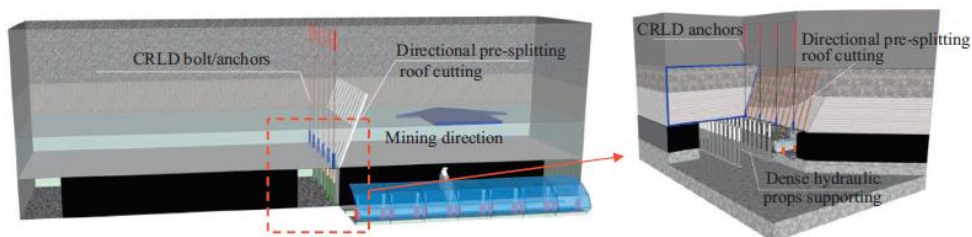
a. Preparation diagram of type 121

b. Preparation diagram of type 111

Fig. 3. Illustration of the preparation for longwall mining type 121 and 111.



a. Coal mining diagram in preparation roadway - longwall type 110



b. Diagram of layout principles because cable belt increase the ability to carry the load of the roadway along the seam and arrange the hole to cut the main roof

Fig. 4. Illustration of the preparation roadway for longwall mining type 110.

Preliminary assessment, both mining solutions 111 and 110 can be applied in underground coal mines in Quang Ninh province to reduce coal loss and the costs associated with the preparation roadways, discounting the mine depreciation, thereby contributing to lower production costs. In Quang Ninh, most coal seams have thicknesses over 3.5 m and dip angles over 15°. Furthermore, due to a specific tropical climate, long annual rainy season, and a large amount of rainfall, many mines scope risks when exploiting the upper floors, such as collapse rock walls or displacing cracks to connect the surface to the terrain. Hence, there is a problem of surface water infiltrating/flowing into the mining area, then exporting to the lower mining floor is inevitable. Besides, some mines face fire problems in the excavation due to arising spontaneous combustion of coal (such as Ha Lam and Uong Bi mines). Thus, solution type 111 is widely used owing to the good isolation of the roadway, which is protected with the previous mining area.

Figure 5 illustrated the results of the application of solution type 111 in Changcun mine (China) [4]. The strip pillar is applied to protect the transport roadway of the longwall S511 as a ventilation roadway of the lower longwall (S510). The transport roadway has a rectangular section, 4.5 m wide, 3.5 m high, resisting by reinforced plastic anchors combining cable anchors on the roof of the roadway. The coal seam has a thickness of 6.1 m, dip angle of 4°. The roadway was driven along the seam floor. On the roof of the roadway is a layer of coal with a thickness of 2.6 m.

Artificial pillars protecting roadways are formed from a mixture of mineralized materials labeled C30 (30 MPa - compressive strength, 30 GPa - elastic modulus, Poisson coefficient 0.2, see Table 2). The artificial pillars strip is 1.6 m wide, 3.5 m high, located in the mining area, and is contacting the transport roadway. The artificial pillars consist of blocks (3.0 m × 1.6 m × 3.0 m), constructed adjacent to each other using a specialized mold bag of the same size. The mixture of materials is pumped into the bag. To increase the load capacity is steel bolt is added to the artificial pillars strip through its body. With the length of the experimental roadway of 300 m in the Changcun coal mine, 100 bags were used, corresponding to 100 artificial pillars forming artificial pillars strip.

Tab. 2. Specifications of some types of construction materials for pillars.

Type	Young's Modulus	Poisson's Ratio	Compressive strength	Tensile strength
C10	20 GPa	0.2	10 MPa	0.75 MPa
C20	25.5 GPa	0.2	20 MPa	1.1 MPa
C30	30 GPa	0.2	30 MPa	1.45 MPa

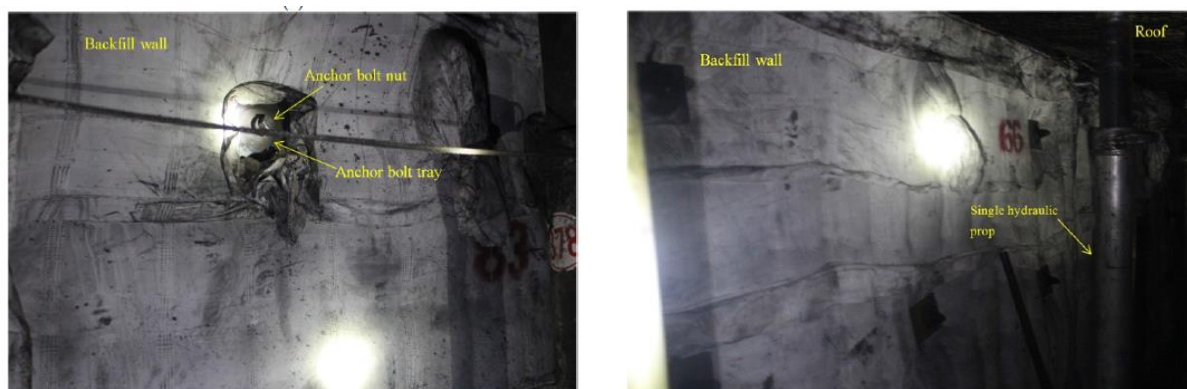


Fig. 5. Artificial pillar protecting transportation roadway of longwall S511 in underground coal mine Changcun, China.

The monitoring results show that the most considerable mine pressure impacts the pillar at the range of 5.0 m from the longwall face, reaching 37–37.9 MPa, gradually decreasing to about 30 MPa at the position of 60 m away from the face (Figure 6). In general, the solution has been successfully applied with the following consequences: the mine pressure on the pillar range is at the allowed level, and the pillar strip meets the protection and maintenance requirements of the transport roadway of longwall S511. Along with the technical efficiency, the solution also brings economic benefits to Changcun mine through saving coal

resources and reducing preparation roadway costs. More importantly, with only 300 m of roadway kept as a ventilation roadway for the next longwall, this mine saved about 638 thousand USD.

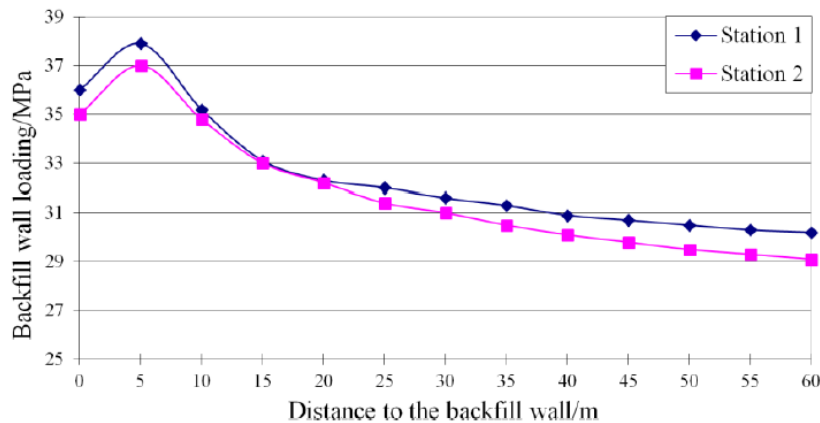


Fig. 6. Mine pressure changes acting on artificial mine pillars in Changcun.

3.2 Potential of applying the technological solution in underground mines in Quang Ninh province

According to [9], coal reserves of seams, with medium thickness (from 1.2–3.5 m with about 184,327 thousand tons), thickness over 3.5 m (about 280,080 thousand tons), and dip up to 35° are mobilized and operated in 12 large underground mine projects in Quang Ninh province (Mao Khe, Uong Bi, Vang Danh, Nam Mau, Ha Lam, Nui Beo, Ha Long, Quang Hanh, Duong Huy, Thong Nhat, Khe Cham and Mong Duong). The total reserves account for 464,407 thousand tons, nearly 74% of total coal reserves (630,645 thousand tons - only in the longwall area, details shown in Figure 7). This is the range of reserves expected to apply the longwall mining technology, protecting the roadway along the seam strike by coal pillar. If only temporarily calculated by 12% of the coal reserves in the longwall mining area, the coal reserves left in the protection pillars were 55,729 thousand tons (22,119 thousand tons of average thick seams, 33,610 thousand tons of thick seams). This reserve equivalent equals to total reserves of a large underground mine. Thereby, there is a potential of applying new technology solutions (111 and 110) for mining coal in protected pillars of underground coal mines in Quang Ninh province, and suitable to the strategy of Vietnam coal sector.

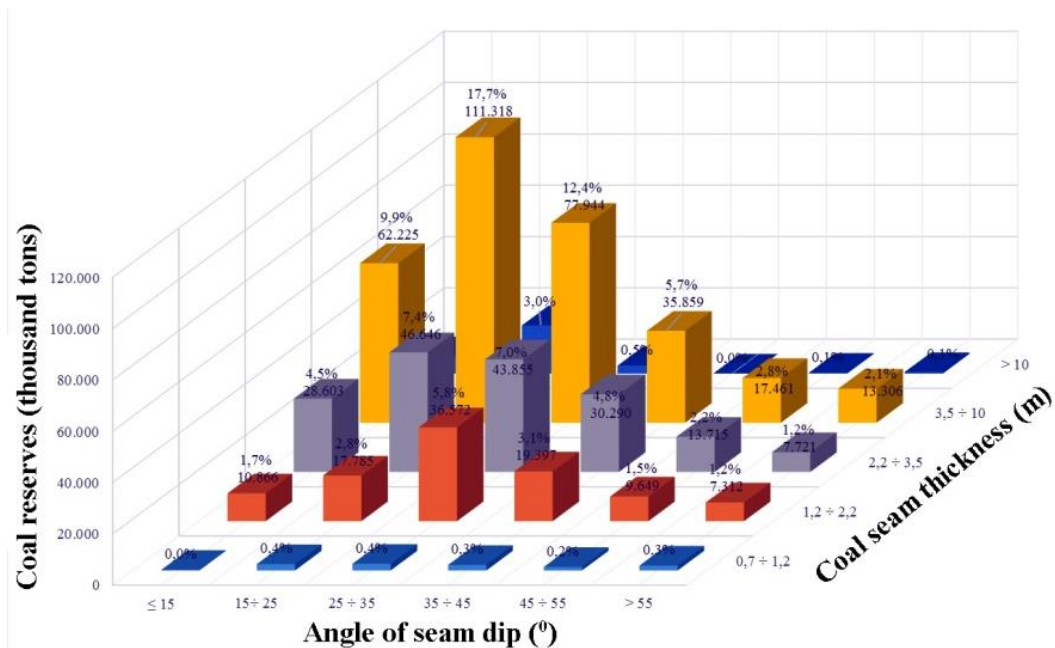


Fig. 7. Coal reserves of 12 underground mine projects in Quang Ninh province [9].

4. Implementing and evaluating the effectiveness of artificial pillars to replace coal pillars protecting prepared roadways in underground coal mines

4.1 Choose the location and design to apply artificial pillar

To accurately assess the efficiency of using artificial pillars to protect the preparation roadways, the authors calculated and designed a specific underground mine of VINACOMIN. The selected design site is a longwall 14.5-19 level -190/-150 of seam No 14.5, Khe Cham III coal mine of Khe Cham Coal Company - VINACOMIN. The thickness of the coal seam design is 5.6 m. The dip angle is 12°. The floor and roof of the longwall are stable aggregates of rock. The longwall ranks type I of methane gas, and the coal of seam is not spontaneous combustion. According to the plan of Khe Cham Coal Company, the longwall is prepared with a face length of 65 m and the strike length of 171 m. A coal pillar of 18 m width remains to protect and maintain the transport roadway as a ventilation roadway for the next longwall (14.5-20) (Figure 8). Then, the actual length of the longwall is only 45 m.

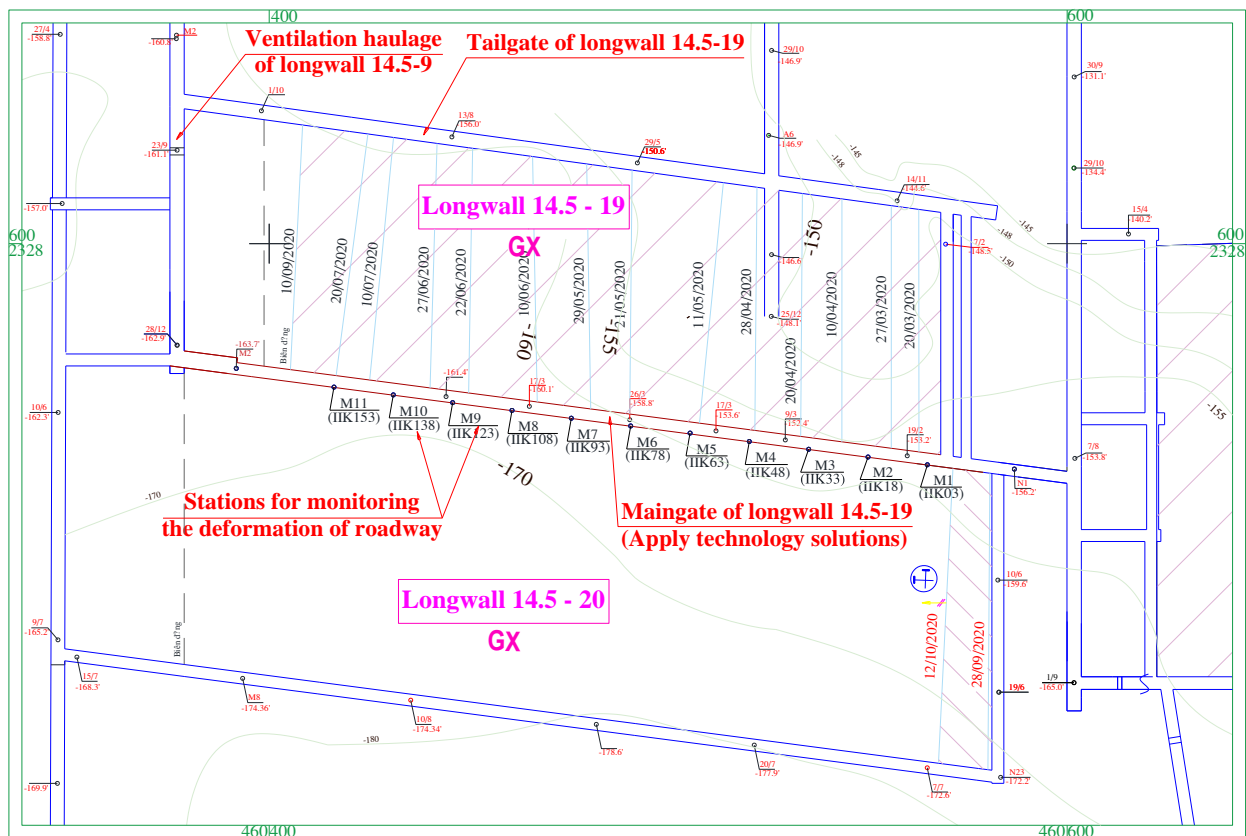


Fig. 8. Location map of the designed longwall 14.5-19 in Khe Cham coal mine III.

The transport roadway of longwall 14.5-19 was driven along the seam floor and lies entirely in the seam 14.5 with arch cross-section (3.24 m high, 4.03 m wide, excavated area 11.2 m², and usable area 8.5 m²). This roadway is supported by flexible anti-steel. The structure consists of 5 SVP-27 steel sections with a wave of 0.5 m. Because the transport roadway within the coal seam is large, it is not suitable to apply artificial pillars made from stone strips, supporting pillars, or mining without protective pillars. Accordingly, in this case, artificial pillars with continuous strip and crib construction are applicable.

The longwall 14.5-19 had been completed and must be put into operation soon at the time of evaluation. The authors assessed the current technical conditions, the ability to supply materials for reinforcement, and the production progress in the longwall 14.5-19 of coal seam 14.5. At the results, the authors chose artificial pillars with wooden crib structure combined with steel columns (pillar structure made of more modern and superior materials will be deployed later). Accordingly, the intersection of the longwall will be supported and kept by the cribs with suitable compression capacity. At the same time, the inside area of the transport roadway of longwall 14-5-19 also needs additional reinforcement. The application will allow the company to mine more coal in pillars protecting the prepared roadways (about 19,951 tons). The coal output of the design longwall increased to 67,451 tons. The rate of coal loss from 39% decreased to 14%. The roadway

per 1000 tons decreased by nearly 23%, from 8.19 m per 1000 tons to 6.3 m per 1000 tons. Figure 9 illustrates the schematic constructed support the transport roadway of longwall 14.5-19 and artificial pillars. Table 3 shows some technical and economic indicators of the technology.

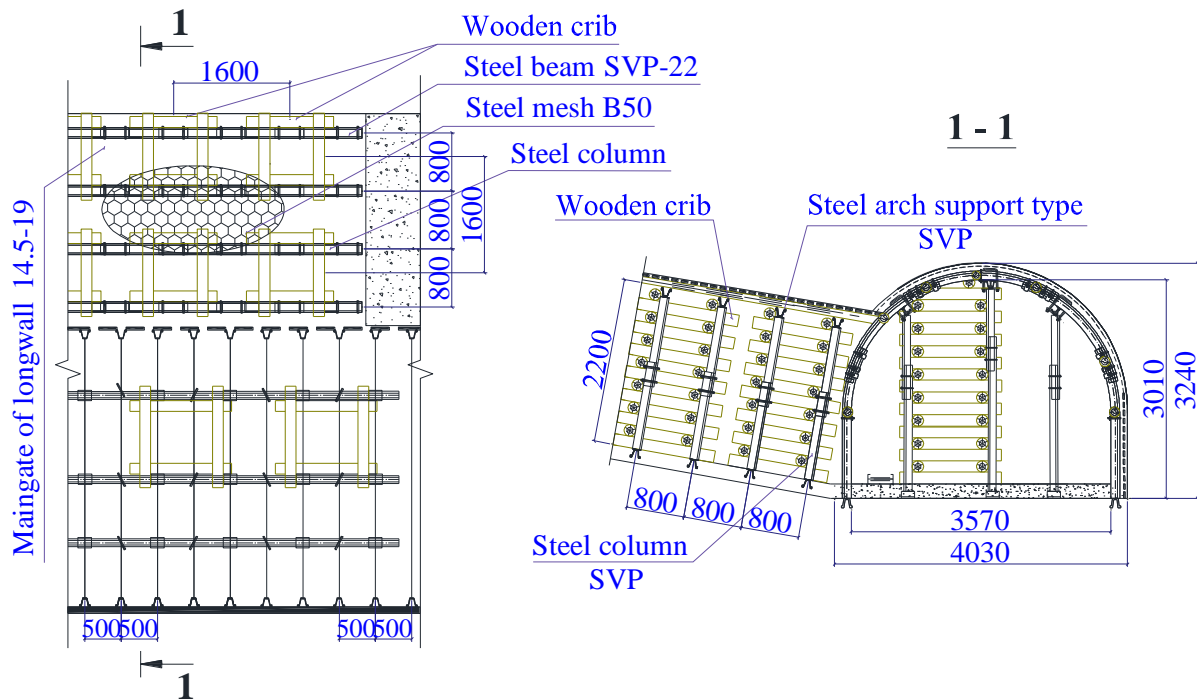


Fig. 9. Illustration of artificial pillars constructed in underground.

Tab. 3. Summary of main economic and technical indicators for longwall according to the options of protecting the transport roadway 14.5-19.

No	Name of indicator	Unit	Amount		Difference (increase '+'; reduction '-')
			Leaving protection coal pillar	Using artificial pillar	
1	Coal seam thickness	m	5.60	5.60	
2	The dip angle of the coal seam	degree	12	12	
3	Face length	m	45	65	+20
4	Length of coal pillars protecting the transportation roadway	m	18	0	-18
5	Length in retreat longwall	m	171	171	0
6	Coal reserves				
a	of the design area	thousand tons	81,255	81,255	0
b	of coal pillar protecting transportation roadway	thousand tons	25,807	-	-25,807
c	of the design longwall	thousand tons	61,442	87,249	+25,807
7	Volume meter of preparation roadway from designed area	m	432	472	40
8	Mining capacity	ton/year	150,000	150,000	0
9	Equipment depreciation time	year	5	5	0
10	Output of coal extracted from designed longwall (technology coal loss 5%)	ton	52,777	74,945	+22,168
11	Cost for a meter of preparation roadway	m/1000 ton	8.19	6.30	-1.89
12	Coal loss rate	%	39%	14%	-25%
13	Coal commercial product	ton	47,500	67,451	+19,951

In the economic aspect, the price of one ton of consumption coal in traditional pillars to protect the transport roadway is 1,617,844 VND. Using artificial pillars to replace coal pillars makes it possible to reduce the costs of driving roadways, infrastructure depreciation, and mining rights fees by mining more coal reserves from the pillars. Therefore, the price can be reduced to 1,583,929 VND per ton. Thus, for each ton of mined coal from the longwall 14.5-19 using artificial pillars, Khe Cham Coal Company can benefit 33,915 VND. The total benefit value for Khe Cham Coal Company in just one area of the longwall 14.5-19 is calculated by 67.45 thousand tons × 33,915 VND per ton = 2,287,610 thousand VND (about 83,185 Euros). Table 4 and Figure 10 show details of economic indicators's comparison.

Tab. 4. Comparison of economic indicators between two options.

No	Name of indicator	Unit	Amount		Difference (increase '+'; reduction '-')
			Leaving protection coal pillar	Using artificial pillar	
1	2	3	4	5	6=5-4
1	Coal commercial product	Ton	47,500	67,451	+19,951
2	Total cost of coal production	million VND	76,847	106,837	-29,990
3	Coal price	VND/ton	1,617,844	1,583,929	-33,915
-	Cost for driving roadways	VND/ton	165,777	126,440	-39,337
-	Cost of coal mining in longwall	VND/ton	421,436	511,660	+ 90,224
-	Cost of depreciation of mine opening and infrastructure	VND/ton	152,451	107,358	-45,093
-	Cost for mining rights	VND/ton	37,259	26,238	-11,021
-	Others	VND/ton	840,922	812,233	-28,688
4	Total benefit value of the artificial pillar option (V.1 x VI.3)	thousand VND	2,287,610		

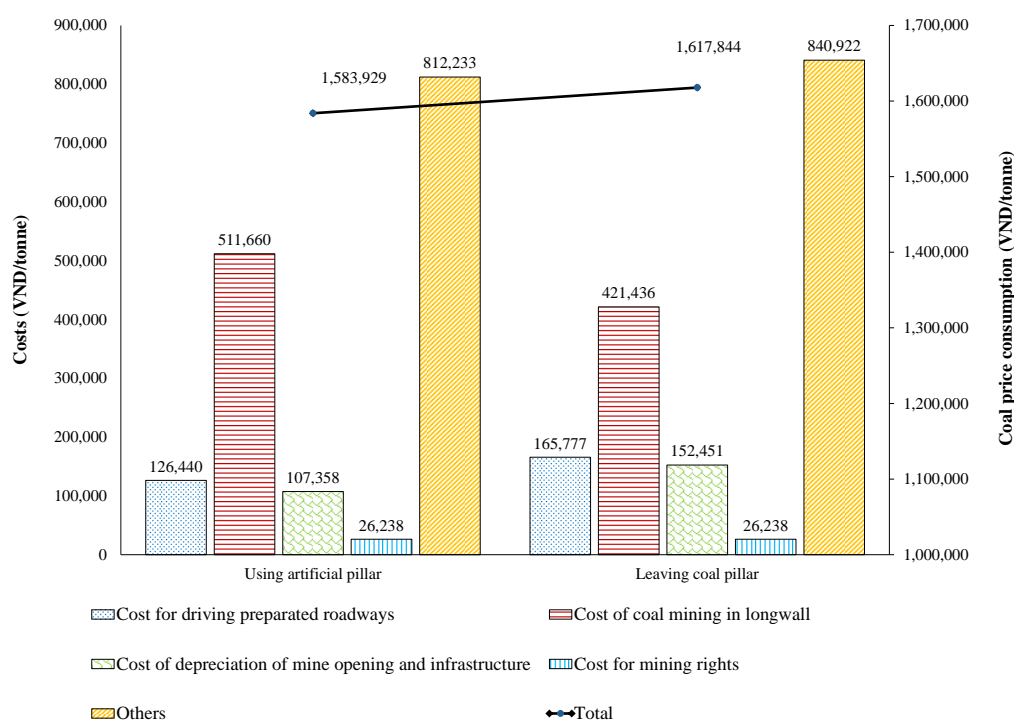


Fig. 10. Comparison of consumption price between two technological solutions.

4.2 Evaluating the stability of the roadway protected by artificial pillars

To evaluate the stability of the transport roadway protected by artificial pillars, during the exploitation of longwall 14.5-19, the authors collaborated with Khe Cham Coal Company to set up stations monitoring deformation on the transport roadway of longwall 14.5-19. There are 11 measuring stations located at a distance of 3, 18, 33, 48, 63, 78, 93, 109, 123, 138, and 153 meters from the first position of longwall face 14.5-19 along the strike to the last mining position.

The monitoring results show that the roadway's deformation rate was the strongest and fastest within about 40 m in front of and behind the longwall face (vertical deformation rate was from 7 to 10 mm/day-night; horizontal deformation from 8 to 20 mm/day-night). In the advanced direction of the longwall face, in the gob area from the 40th meter in the opposite direction of the face forward, this rate gradually decreased (the vertical deformation rate was only from 0 to 4 mm/day-night, vertical deformation from 0 to 6 mm/day-night). From the 100th meter behind the longwall face towards the gob, the roadway was no longer deformed and became stable.

The total deformation value of the roadway during the monitoring period reached a maximum of 300 mm vertically (measurement station No.1) and 350 mm horizontally (measurement station No. 3). It corresponds to a reduction of its cross-section of about 9.8–9.97%, ensuring the parameter according to safety regulations to serve ventilation and production of the longwall 14.5-20 (see Figure 11).

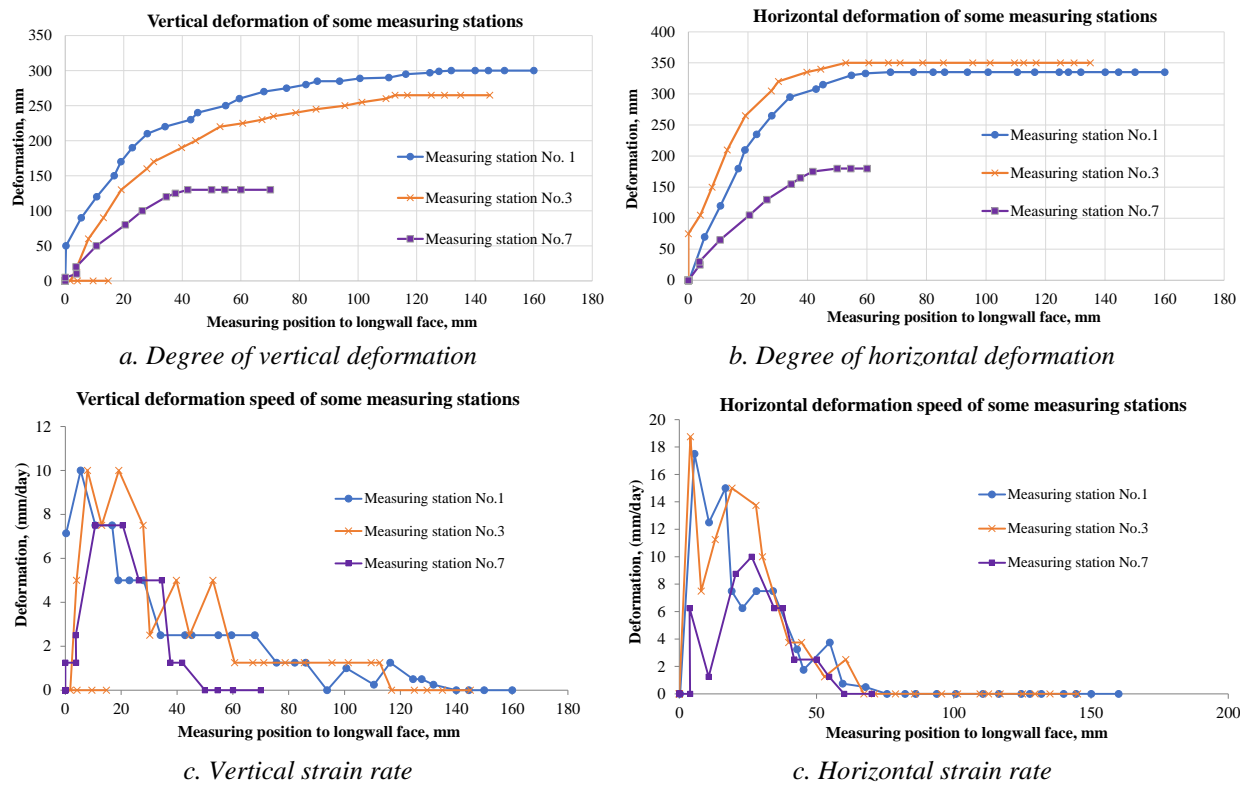


Fig. 11. The result of deformation monitoring of roadway, longwall 14.5-19.

5. Conclusions

Applying artificial pillars to replace coal pillars protecting prepared roadways during the mining process will reduce the loss of coal resources, the cost of driving roadways, and direct labor. Therefore, the company can gain better economic efficiency. New underground coal mines' investment requires many procedures and cannot be deployed soon. Thus, it is an excellent way to apply different mining technology with a high level of mechanization and significant capacity to meet the increasing coal demand of the country. The technological solution using artificial pillars to replace coal pillars protecting the prepared roadway can potentially ensure the sustainable development goal of VINACOMIN and Vietnam's coal industry regarding economic benefits, the utilization of coal resources, and the safety of the labor.

6. Acknowledgments

The paper was presented during the 6th VIET - POL International Conference on Scientific-Research Cooperation between Vietnam and Poland, 10-14.11.2021, HUMG, Hanoi, Vietnam.

7. References

1. VIMCC, 2016. Planning on development of Vietnam's coal industry to 2020, outlook to 2030 approved by the Prime Minister in Decision No. 403/QĐ-TTg dated March 14, 2016, Ha Noi.
2. VINACOMIN, 2020. Business plan for 2020 of underground mines of VINACOMIN, Ha Noi.
3. Dinh, V. C.; Tran V. T.; Nguyen, A. T., 2018. Evaluating the possibility of using artificial pillars to replace coal pillars to protect preparation roadways in underground mines of Quang Ninh. Scientific conference "21st Century Mining Industry - Science, Technology and Environment Issues", Vietnam Mining Science and Technology Association, 243-251.
4. Wu, R.; He, Q; Oh, J.; Li, Z.; Zhang, C., 2018. A New Gob-Side Entry Layout Method for Two-Entry Longwall Systems, *Journal Energies*, vol. 11, iss. 8, <https://doi.org/10.3390/en11082084>.
5. Nielacny, P., 2009. Selection of technology for maintaining gate roadways of longwall in one-sided surroundings of goafs based on measurements of rock mass displacements, Doctoral Thesis, AGH University of Science and Technology, Cracow, Poland.
6. ZiZheng, Z., 2016. Research on roof control technology and stability of immediate roof in filling area of gob-side roadway, Doctoral Thesis, China University of Mining and Technology, Xuzhou, China.
7. He, M; Zhu, G.; Guo, Z., 2015. Longwall mining “cutting cantilever beam theory” and 110 mining method in China–The third mining science innovation, *Journal of Rock Mechanics and Geotechnical Engineering*, vol. 7, iss. 5, p. 483-492, <https://doi.org/10.1016/j.jrmge.2015.07.002>.
8. Tao, Z; Song, Z.; He, M.; Meng, Z.; Pang, S., 2018. Principles of the roof cut short-arm beam mining method (110 method) and its mining-induced stress distribution, *International Journal of Mining Science and Technology*, 28,(3): 391-396, <https://doi.org/10.1016/j.ijmst.2017.09.002>.
9. Dang, T. H., 2016. Developing the application of mining technology and driving roadway in underground mines of Quang Ninh coalfield in the period of 2013–2015, outlook to 2020, Technical report, edited by Institute of Mining Science and Technology, Hanoi.

Using the Potential of The Employees' Expertise and Awareness of Occupational Hazards in The Mining Industry

Dagmara Nowak-Senderowska¹, Michał Patyk²

¹ Ph.D., Eng. AGH University of Science and Technology, Faculty of Civil Engineering and Resource Management, Av. Mickiewicza 30, PL-30-059 Cracow, Poland; email: nowaksen@agh.edu.pl, tel. 12 617 20 75.

² Ph.D., Eng. AGH University of Science and Technology, Faculty of Civil Engineering and Resource Management, Av. Mickiewicza 30, PL-30-059 Cracow, Poland; email: mpatyk@agh.edu.pl, tel. 12 617 21 10.

Abstract. The paper highlights the results of a study that examined the employees' expertise and awareness of occupational hazards in their work environment. The research involved a survey conducted in the form of a short questionnaire among employees responsible for loading and hauling of excavated material in an opencast mine. Among 23 major hazards that were thus identified, there were global hazards (affecting the entire mining process) as well as local, task-specific hazards. Depending on the number of responses, 10 local and 3 global hazards were identified in the analyzed area, involving noise, stress and dust. Active participation of the crew in the risk identification process helped in the assessment of their criticality levels, according to employees carrying out various task, highlighting the benefits of such approach for effective work safety management in a mining company. The conducted research demonstrated yet another goal to be achieved - i.e. the comparison of criticality levels of hazards as identified by employees and those reported in occupational risk assessment reports in the mine.

Keywords: hazard identification, occupational risk assessment, survey, surface mining.

1. Introduction

The mining sector still ranks among the most hazardous industries, due to unfavourable operating conditions and in the case of miners, the working conditions are variable, both in terms of specific tasks or operations to be performed and complexity of the mining production process and diversity of operating conditions. In many cases miners are faced with high job demands (excessive workloads), negatively impacting on their health condition or life-threatening. Occupational hazard is defined as the probability of undesirable events and impacts (consequences) associated with the specified operation or task carried out, taking into account the criticality of these events. It is associated with the probability of a job-related undesirable event resulting in material losses and producing negative impacts on humans (their health and safety at work). According to the current legislation, it is the employer's responsibility to conduct the occupational risk assessment at workplace and to provide the employees with relevant information on hazards and risks within the workplace (Dz.U. 2020.1320).

The first stage of the occupational risk assessment procedure involves the collecting of necessary data for identification of all potential hazards to be encountered at work. There are two major steps yielding the data for further analysis and having a direct influence on the assessment results. The main aim of this study is to highlight a new source of information about the potential hazards and risks at work, namely the employees' expertise and experience of surface mining and their perception of the criticality of occupational hazards and risks within the worksite.

2. Risk assessment procedure in Polish companies - general outline

Generally, the aim of the occupational risk assessment is to identify all hazards and risks within the workplace and to establish the associated risk level. Every specific task or operation, regardless of its type and the place where it is carried out, involves an exposure to risk. It is the employer's responsibility to provide employees with information on occupational hazards and risks within the workplace and to put in place the control measures to eliminate or control their negative impacts. The employer's responsibilities in this respect are set forth in the Labour Code. Art 226 of the Law of 26th June 1974 "Labour Code", imposes a duty on the employer 1) to evaluate and document the risks associated with the performed tasks and operations, and to put in place the control measures aimed to minimise the risk exposure; 2) to provide employees with information on hazards and risks affecting specific tasks and operations carried out by them and to instruct them in the use of protective measures (Dz.U. 2020.1320).

The definition of the occupational risk is provided in the Regulation by the Minister of Labour and Social Policy on General Provisions on Occupational Safety and Health of 26th September 1997 (Dz.U.03.169.1650). Occupational risk is defined as the probability of an undesirable event related to the performed task or operation, resulting in material loss and, specifically, having negative impact on humans due to occupational hazards present in the work environment or related to the working method. In accordance with paragraph 39 of the said Regulation, the employer is obligated to evaluate and document the hazards and risks affecting specific tasks and operations to be carried out and to put in place necessary preventive measures aimed to minimise the risk exposure. The principle whereby the occupational risk exposure should be minimised can be summarised in terms of a safety triad model, incorporating three basic

components: avoiding hazards, adopting solutions on the level of organisation and adoption of group protection measures, providing information about residual risks and application of individual protection equipment (Gierasimiuk 2009). These principles stem directly from the above-mentioned Regulation having relevance to general occupational health and safety requirements, specifically from Art 39 wherein the employer's responsibilities in the context of occupation risk management are listed in this order.

In the final stage of the risk evaluation procedure, the risk levels obtained from analyses are compared with the risk tolerability levels. The results of occupational risk evaluation are used to facilitate the decision-making in matters relating to risk tolerance or management (PN - N-18002 (2000)).

Prior to the occupation risk evaluation it has to be established whether it should concern a specific worksite, a process, or an object as a whole or their sections or parts, which might require a separate analysis. In the first stage of the risk evaluation procedure the worksite (an object or process) are described, its extent defined and all relevant data are compiled.

Identification of hazards and risks within the workplace, which is a major step in the occupational risk evaluation, requires a systematic approach to detect the largest possible numbers of potential hazards and unfavorable, hazardous conditions that may lead to an exposure to risk. Several methods have been developed to facilitate full and exhaustive identification of potential hazards (HAZOP, WHAT-IF, CHECK LIST) which provide a detailed procedure to be adopted for hazard detection.

The final stage consists in the risk evaluation whereby specific hazards are aligned with the associated risk levels, in accordance with the adopted measure. Each method provides the principles used to establish the risk level depending on the probability of the hazard occurrence and severity of its impacts (Rączkowski 2020). All these methods differ in the level of specificity and detail, and the relevant regulations do not stipulate the use of any particular risk assessment method. Widely used methods include that specified in the technical standard PN-N-18002, alongside the Risk Score, Five Steps or the PHA (Preliminary Hazard Analysis) approach. Amongst the most popular methods is that provided in the standard PN-N-18002 and the Risk Score approach. Risk assessment in accordance with these methods involves the examination of each potential hazard which in turn may produce certain impacts (Romanowska-Słomka and Słomka 2018).

Occupational risk assessment ought to be conducted at regular intervals and whenever the information and data on which the procedure relies have become outdated; moreover, the risk assessment is requisite when:

- a new job position is being designed;
- job positions are to be changed or modified;
- after a change of conditions and requirements relating to the job positions being evaluated
- after a change of the adopted protective measures.

3. Risk assessment procedure in Polish companies - general outline

Identification of hazards involves a reconnaissance to find out whether a given hazard is present at workplace and to determine its characteristic: 'Hazards include all aspects that have negative impact on employees' health or put their health in jeopardy - machinery and equipment, working methods and organisation, chemical substances, electricity, as well as psychosocial hazards and factors associated with strenuous effort while lifting or moving heavy objects, static or monotone tasks' (Górska and Kossobudzka-Górska 2019). The awareness and knowledge of the hazards present and their extent is requisite for the occupational risk assessment, incident rate analyses, employee training or optimisation of tasks and operations (Dzeng et al 2016; Klimecka-Tatar et al 2020; Niciejewska et al 2020; Niciejewska et al 2021).

4. Sources of information about hazards and risk within the workplace

Main sources of information on hazards and risks in the given work environment include:

- Technical specifications of objects (systems) or processes
- Procedures and instruction manuals
- Statistics of the rate of accidents and incidents at work, job-related illnesses and events that may potentially result in an accident
- Observations of tasks and operations carried by the person within the given workplace
- Interviews with employees
- Measurements of hazardous factors within the workplace
- Observation of external factors which may affect the employee's behaviour at workplace

- Analysis of psychosocial or physical hazards and factors giving rise to stress
- Analysis of organisational activities aimed to ensure the adequate working conditions (Rączkowski 2020).

Data collection is based on a variety of methods and techniques, including the examination of company documents, control reports and questionnaires (Nowak-Senderowska 2014; Niciejewska and Kiriliuk 2020), collective observations (Hasanzadeh et al 2017), case studies (Namian et al 2016), surveys (including questionnaires, discussions, brainstorming, expert opinions) (Eiter et al 2016).

Studies investigating the safety risks perception and handling by employees (including the mining crews) have revealed that for most employees identification of hazards within the workplace is problematic, hence the difficulty with the correct assessment of associated risks. Of particular importance, on the other hand, is professional experience of employees (their knowledge of tasks and operations to be performed), supervision, participation in employee training – all these enhance the ability to predict the hazard occurrence and calculate the risk (Bahn 2013; Haas et al 2014; Eiter et al 2016; Namian et al 2016; Bae et al 2021).

5. Methodology

The study concerned an surface mine and the related mining operations, loading and hauling of the excavated material, as well as processing operations. The main focus was on two activities: loading and hauling of the excavated material and on job positions directly related to these activities, supervisory positions and those involving the control of machinery and equipment (Fig 1).

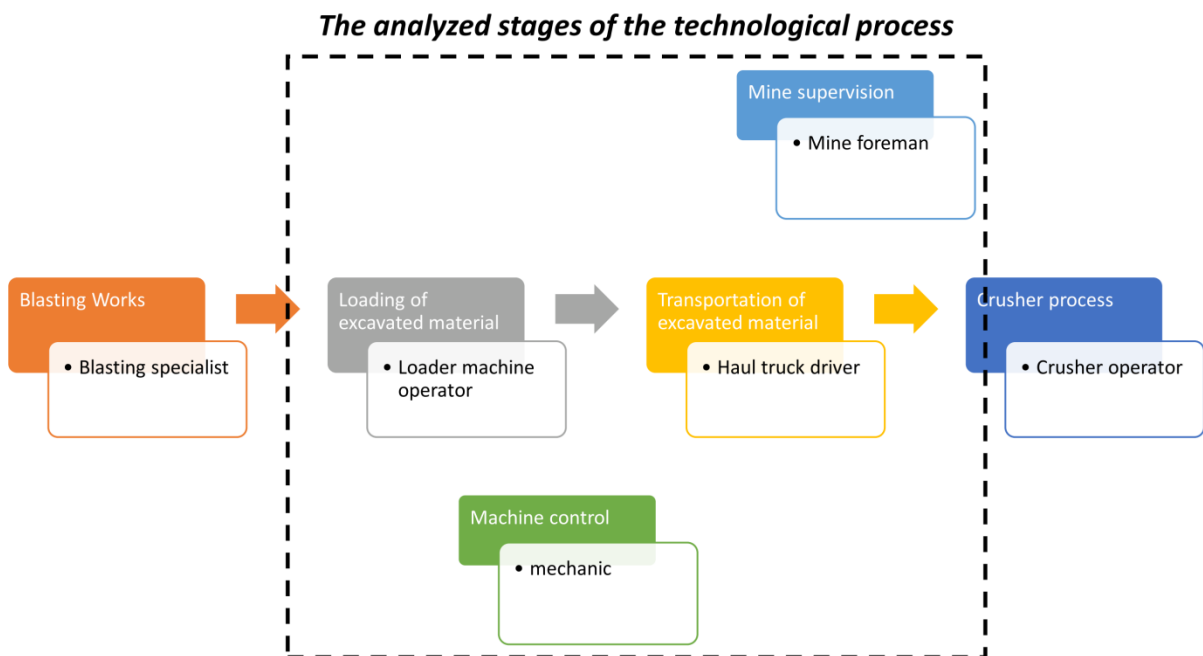


Fig. 1. Activities and operations in an surface mine, with the specified job positions

Rys. 1. Proces technologiczny w kopalni odkrywkowej z wyszczególnionymi stanowiskami pracy

Identification of hazards and risks and specification of related jobs and job positions was based on the employees’ questionnaire whereby the respondents, being crew members occupying the given positions, were asked to point out 5 most critical safety hazards or factors that were present or were likely to emerge in the work environment as well as those which affected the specific tasks and operations carried out by those persons (Fig 2).

Survey questionnaire

The objective of the questionnaire is to answer the question to which hazard or safety risk the employees are exposed while performing their duties

Dear employees

All answers are anonymous and the questionnaire is a part of studies aimed at identification of occupational risks related to specified job positions. The results of the questionnaire will be used to identify the most critical hazards/risks related to mining activities in the entire mining process.

Specify your job position:

Enter your job position

Point out 5 most critical hazards/risks which are present or are likely to occur or to which you are exposed while performing your duties (the actual order of listed hazards is of no consequence):

Please enter 1st hazard here
Please enter 2nd hazard here
Please enter 3rd hazard here
Please enter 4th hazard here
Please enter 5th hazard here

Fig. 2. Questionnaire model - List of 5 most critical hazards (Patyk 2019)

Rys. 2. Wzór ankiety - określenie 5 najbardziej istotnych zagrożeń (Patyk 2019)

6. Criticality of hazards in the work environment on the basis of the questionnaire

The survey conducted at the mining company had 15 respondents occupying 4 different positions (Table 1):

- Hauling truck drivers – 6 employees
- Loader machine operators – 3 employees
- Mechanics – 4 employees
- Mine foremen (deputies) – 2 employees

This number of respondents is closely related with the number of crew members in an surface mine. The largest group were dump truck drivers, who were able to identify the largest number and a wide range of hazards. Next in line came the mechanics (13 hazards) and loader machine operators (13 hazards). The smallest group were the mine foremen who identified 5 identical hazards (Table 1).

Tab. 1. Survey results

Tab. 1. Otrzymane wyniki z przeprowadzonych ankiet.

Job/position	Mechanic	Haul truck driver	Mine foreman	Loader machine operator
The number of employees	4	6	2	3
The number of identified hazards	13	18	5	13

Altogether, 15 workers were able to identify 23 diverse hazards (Fig 3). Amongst the frequently listed hazards and factors were:

- Dust (10)
- Noise (8)
- High fall (8)
- Stress (7)
- Mechanical vibration (6):

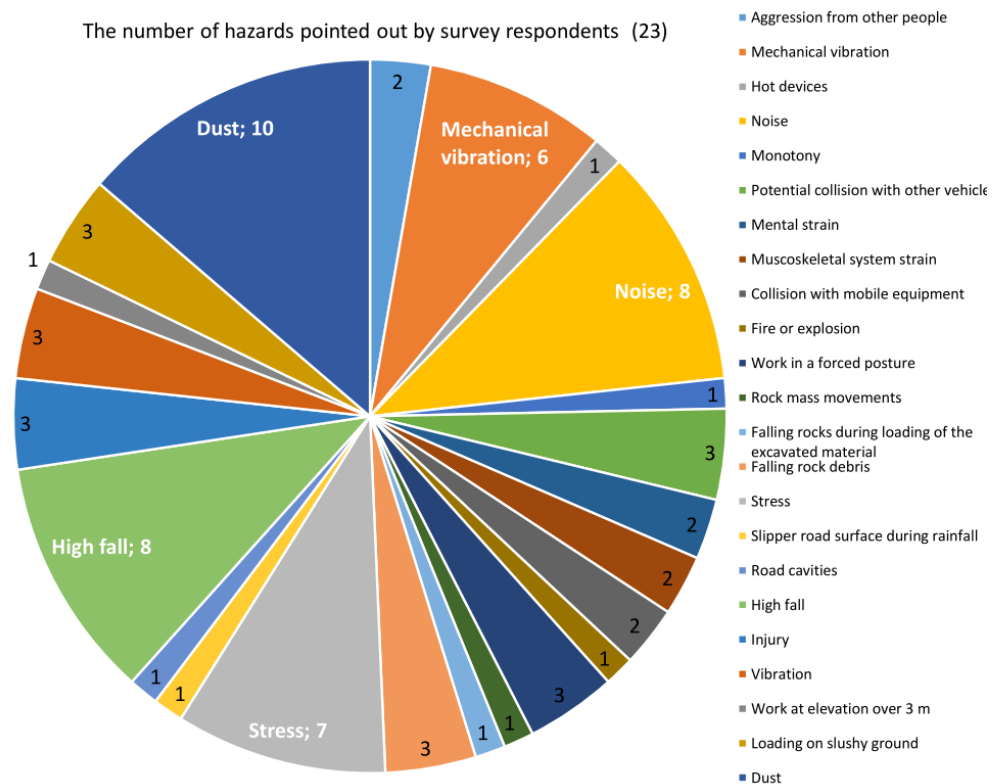


Fig. 3. The number of hazards pointed out by survey respondents
 Rys. 3. Ilość zagrożeń wskazana przez ankietowanych pracowników

The actual distribution of hazards and factors pointed out by those taking part in the survey is shown in Fig 4, highlighting those hazards and factors that are perceived as most critical in their jobs.

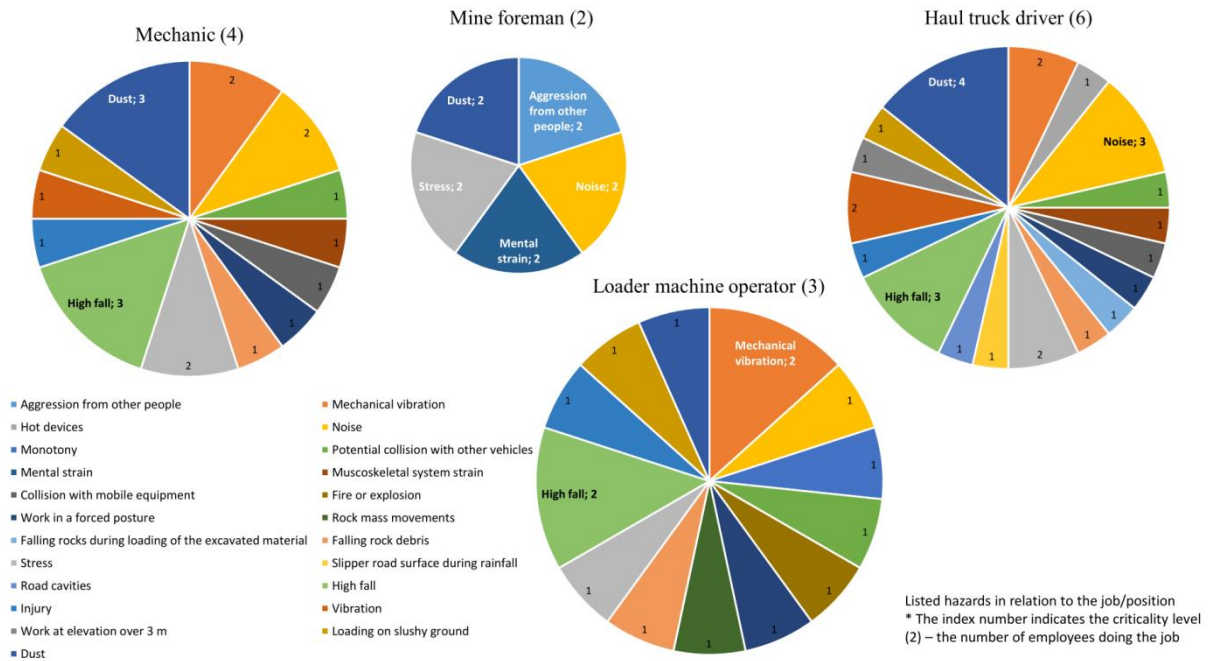


Fig. 4. Distribution of hazards and factors associated with given jobs

Rys. 4. Rozkład zagrożeń występujących na danych stanowiskach pracy

In the case of the most numerous group: dump truck drivers, amongst the most critical hazards listed were the dust- pointed out by 4 employees (66% employees doing the given job), high fall and noise- each listed by 3 employees (50%). The next in line came the mechanics, who pointed out to dust and high falls as the most critical hazards- each listed by 3 employees (75%). Loader machine operators pointed out to high falls and mechanical vibration as the most critical hazards- each listed by 2 employees (66%). The only group of employees whose lists of hazards were found to be identical were mine foremen (deputies), who pointed out to dust, stress, noise, mental strain and aggression from other people.

Certain hazards and factors were pointed out only by those doing the specified job (occupying one position), which indicates that these hazards and factors are local, task-related. On the other hand, there are some hazards and factors which affect 2,3 or even 4 jobs. Those hazards and factors that are identified on all analysed worksites can be regarded as inherent in the mining process in its entirety, and referred to as ‘global’ (Fig 5).

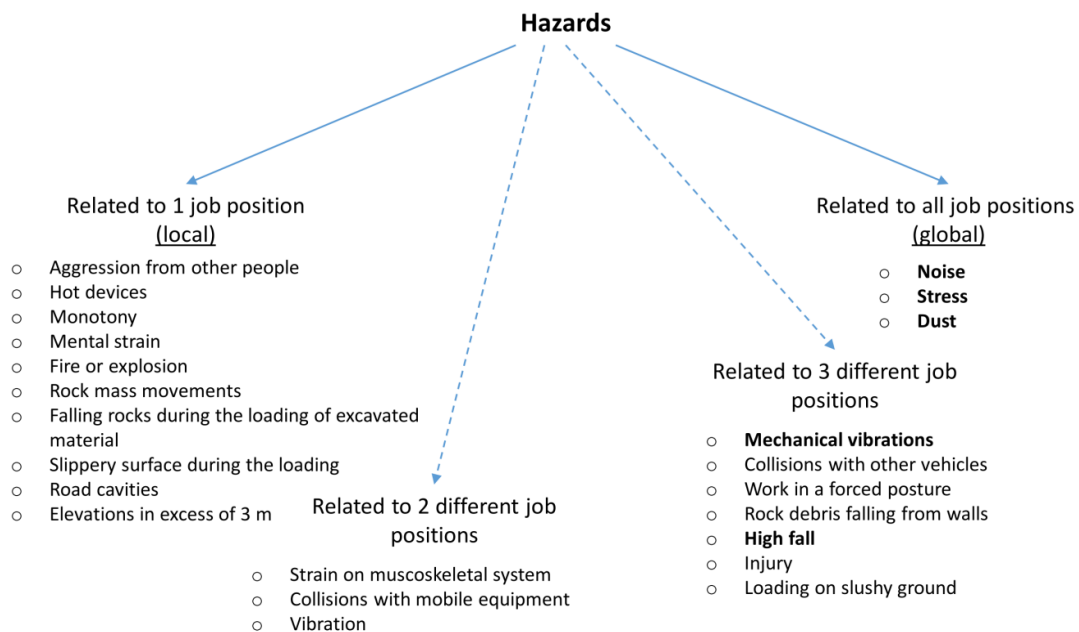


Fig. 5. Impacts of individual hazards at various stages of the surface mining process

Rys. 5. Charakter oddziaływania poszczególnych zagrożeń w analizowanych etapach procesu technologicznego w kopalni odkrywkowej

Global hazards related to each task and job position include noise, stress and dust. Moreover., these particular hazards were most frequently pointed out by the respondents in the survey. The other group includes hazards and factors emerging at some stages of the surface mining process (related to 3 out of 4 analysed job positions), such as mechanical vibrations, high fall, work in a forced posture, potential collisions with other vehicles, falling rock debris and loading of the excavated material on slushy grounds. The first two hazards from the second group (indicated in bold in Fig 5) are among those most frequently pointed out by all survey respondents.

Another important aspect is the specification of hazards pointed out by employees in relation to their tasks /job positions. Thus, the summary of results provides a compilation of hazard criticality levels as perceived by employees and the scale of their impacts in relation to the number of analysed job positions (Table 2). Thus the local hazards are highlighted – for example, dump truck drivers pointed out to 5 hazards related to their job. Similarly, loader machine operators pointed out to 3 such hazards whilst mine foremen identified 2 hazards (as well as 3 global hazards, related to the entire mining process). Mechanics, as survey respondents, did not point out any hazards affecting only the tasks and operations carried out by them (Table 2).

Tab. 2. Summary of a research study on identification of hazards
 Tab. 2. Podsumowanie wykonanych badań dotyczących identyfikacji zagrożeń

Type of hazard	Total times indicated	Hazard level of impact				Job position			
		Related to 1 job position (local)	Related to 2 different job positions	Related to 3 different job positions	Related to all job positions (global)	Mechanic	Haul truck driver	Mine foreman	Loading machines operator
Dust	10	NO	NO	NO	YES	YES	YES	YES	YES
Noise	8	NO	NO	NO	YES	YES	YES	YES	YES
High fall	8	NO	NO	YES	NO	YES	YES	NO	YES
Stress	7	NO	NO	NO	YES	YES	YES	YES	YES
Mechanical vibrations	6	NO	NO	YES	NO	YES	YES	NO	YES
Possibility of collision with other vehicles	3	NO	NO	YES	NO	YES	YES	NO	YES
Work in a forced posture	3	NO	NO	YES	NO	YES	YES	NO	YES
Rock debris falling from walls	3	NO	NO	YES	NO	YES	YES	NO	YES
Injuries	3	NO	NO	YES	NO	YES	YES	NO	YES
Vibrations	3	NO	YES	NO	NO	YES	YES	NO	NO
Loading on slushy ground	3	NO	NO	YES	NO	YES	YES	NO	YES
Aggression from other people	2	YES	NO	NO	NO	NO	NO	YES	NO
Mental strain	2	YES	NO	NO	NO	NO	NO	YES	NO
Strain on the musculoskeletal system	2	NO	YES	NO	NO	YES	YES	NO	NO
Collision with mobile equipment	2	NO	YES	NO	NO	YES	YES	NO	NO
Hot devices	1	YES	NO	NO	NO	NO	YES	NO	NO
Monotony	1	YES	NO	NO	NO	NO	NO	NO	YES
Conflagration or explosion	1	YES	NO	NO	NO	NO	NO	NO	YES
Rock mass movements	1	YES	NO	NO	NO	NO	NO	NO	YES
Falling rocks during loading of the excavated material	1	YES	NO	NO	NO	NO	YES	NO	NO
Slippery road surface during rainfall	1	YES	NO	NO	NO	NO	YES	NO	NO
Road cavities	1	YES	NO	NO	NO	NO	YES	NO	NO
Height over 3m	1	YES	NO	NO	NO	NO	YES	NO	NO

7. Conclusions

The study summarises the result of a research study in which the employees were invited to contribute to the hazard identification being a part of the occupational risk evaluation procedure in an surface mine. Employees occupying various positions in a surface mine were thus encouraged to actively participate in a survey. Identification of hazards in the occupational risk evaluation by the mining crew is a dynamic process because the working conditions tend to change, new hazards may emerge with the advancement of mining operations (including natural hazards) and, last but

not least, because of complexity of operations involved in the surface mining process in the natural surroundings. The respondents – employees in the mine duly identified 23 occupational hazards and factors, pointing out those which they perceived as most critical within their worksite. The survey results suggest that the analysed mining process is affected by 10 local and 3 global hazards, depending on the actual listing by crew members responsible for loading and hauling of excavated material. Additionally, the survey revealed that:

- Those employed as mechanics pointed out mostly to hazards affecting at least 2 operations (job positions);
- Mine foremen pointed out 2 hazards affecting their job positions only and three global hazards, i.e. those related to the entire mining process;
- Only those responsible for hauling of the excavated material pointed out to hazards or factors affecting each level of operations. They were able to identify hazards related to one, two, three or even four operations and job positions.

The approach outlined in the study whereby the employees' expertise and experience is recalled in the risk identification is a move towards ensuring the crew's active participation in the occupation risk assessment, provides an additional source of information on hazards and risks within the workplace, highlights a large number of potential hazards to be analysed in the occupational risk assessment procedure. Thus the risk assessment results become more reliable, which is of primary importance in the context of planning further actions as a part of the occupational risk management in the mining industry.

The study highlights the need and directions for further research to verify whether the hazards and factors pointed out by employees can also be found in the occupational risk evaluation reports and to find out how the respective criticality levels should compare.

Similar surveys are planned to be conducted in other surface mines to establish the level of employees' awareness of hazards and risks within the workplace..

8. Acknowledgements

This research was funded by AGH University of Science and Technology, Faculty of Civil Engineering and Resource Management; subsidy number: 16.16.100.215

9. References

1. Act of June 26, 1974; Labor Code. Dz.U. 2020.1320
2. Bae H., Simmons D.R., Polmear M., 2021. Promoting the Quarry Workers' Hazard Identification Through Formal and Informal Safety Training, *Safety and Health at Work*, <https://doi.org/10.1016/j.shaw.2021.02.003>
3. Bahn S., 2013. Workplace hazard identification and management: The case of an underground mining operation, *Safety Science* 57, 129–137. doi:10.1016/j.ssci.2013.01.010
4. Dzung, R.J., Lin, C.T., Fang, Y.C., 2016. Using eye-tracker to compare search patterns between experienced and novice workers for site hazard identification. *Safety Science* 82, 56–67. doi:10.1016/j.ssci.2015.08.008
5. Eiter, B.M., Kosmoski, C.L., Connor, B.P., 2016. Defining hazard from the mine worker's perspective. *Mining Engineering* 68, 50–54. doi:10.19150/me.6832
6. Gierasimiuk J., 2009. Ogólna charakterystyka zagrożeń oraz zasad oceny i ograniczania ryzyka zawodowego, CIOP – Centralny Instytut Ochrony Pracy - Państwowy Instytut Badawczy: https://www.ciop.pl/CIOPPortalWAR/appmanager/ciop/pl?_nfpb=true&_pageLabel=P30001831335539182278&html_tresc_root_id=27410&html_tresc_id=27434&html_klucz=19558&html_klucz_spis=03.06.2021
7. Górka E., Kossobudzka-Górka A., 2019. Interaktywne podejście do oceny ryzyka zawodowego w mikroprzedsiębiorstwie, *Zeszyty Naukowe Małopolskiej Wyższej Szkoły Ekonomicznej w Tarnowie*, 41(1), 83-102
8. Haas E.J., Hoebbel C.L., Rost K.A., 2014. An analysis of trainers' perspectives within an ecological framework: Factors that influence mine safety training processes, *Safety and Health at Work* 5, 118–124. doi:10.1016/j.shaw.2014.06.004
9. Hasanzadeh S., Esmaceli B., Dodd M.D., 2017. Impact of Construction Workers' Hazard Identification Skills on Their Visual Attention, *Journal of Construction Engineering and Management* 143(10), 04017070. doi:10.1061/(asce)co.1943-7862.0001373

10. Klimecka-Tatar D., Matevž O., 2020. The Level of Occupational Health and Safety in European Enterprises Providing Transport and Logistics Services in Terms of Quality Management Principles, Multidisciplinary Aspects of Production Engineering 3, 394–404. doi:10.2478/mape-2020-0034
11. Management System Occupational Health and Safety. General guidelines for risk assessment (PN-N-18002 (2000))
12. Namian M., Albert A., Zuluaga C., Behm M., 2016. Role of Safety Training: Impact on Hazard Recognition and Safety Risk Perception, Journal of Construction Engineering and Management 142, 04016073. doi:10.1061/(asce)co.1943-7862.0001198
13. Niciejewska M., Idzikowski A., Škurková K.L., 2021. Impact of Technical, Organizational and Human Factors on Accident Rate of Small-Sized Enterprises, Management Systems in Production Engineering 29, 139–144. doi:10.2478/mspe-2021-0018
14. Niciejewska M., Kiriliuk O., 2020. Occupational health and safety management in “small size” enterprises, with particular emphasis on hazards identification, Production Engineering Archives 26, 195–201. doi:10.30657/pea.2020.26.34
15. Niciejewska M., Obrecht M., 2020. Impact of Behavioral Safety (Behavioural-Based Safety – BBS) on the Modification of Dangerous Behaviors in Enterprises, System Safety: Human - Technical Facility - Environment 2, 324–332. doi:10.2478/czoto-2020-0040
16. Nowak-Senderowska D., 2014. Metodyka kompleksowego szacowania ryzyka szkody na zdrowiu pracowników na wybranych górniczych stanowiskach pracy, Rozprawa doktorska, Akademia Górniczo-Hutnicza, Kraków
17. Patyk M., 2020. Ryzyko zawodowe procesu technologicznego, Praca dyplomowa – Studia podyplomowe w zakresie Bezpieczeństwa i higieny pracy, Akademia Górniczo-Hutnicza, Kraków - not published
18. Rączkowski B., 2020. BHP w praktyce, Ośrodek Doradztwa i Doskonalenia Kadr Sp. z o.o. Gdańsk, ISBN 978-83-7426-554-6
19. Regulation of the Minister of Labor and Social Policy of September 26, 1997 on general provisions on health and safety at work. Dz.U.03.169.1650
20. Romanowska-Słomka I., Słomka A., 2018. Ocena ryzyka zawodowego, Wydawnictwo: Tarbonus, ISBN 978-83-7394-665-1



Cretaceous Granitic Magmatism in South-Central Vietnam: Constraints from Zircon U–Pb Geochronology	7
NGUYEN Huu Hiep, PHAM Nhu Sang, HOANG Van Long, ANDREW Carter, BUI Vinh Hau, BUI Hoang Bac, TRINH Thanh Trung, NGUYEN Lam Anh	
Automatic Monitoring System Designed for Controlling the Stability of Underground Excavation	15
MAŁKOWSKI Piotr, NIEDEBALKSI Zbigniew, BEDNAREK Łukasz	
Applying Electrical Impedance Tomography Techniques for Detection of Decay Inside Trees	31
KIEU Duy Thong, VU Hong Duong, NGUYEN Thi Thu Hang, NGUYEN Thu Tuy	
Mining-induced Land Subsidence Detected by Sentinel-1 SAR Images: An Example from the Historical Tadeusz Kościuszko Salt Mine at Wapno, Greater Poland Voivodeship, Poland	41
KIM Thi Thu Huong, TRAN Hong Ha, BUI Khac Luyen, LIPECKI Tomasz	
Riverbank Filtration – A Potential Water Source Exploitation for the Red River Delta Region	53
NGUYEN Trung Hieu, DOAN Thu Ha, HOANG Van Duy, TONG Thanh Tung	
The Influence of the Sample Preparation on the Result of Coal Propensity to Spontaneous Combustion in the High-temperature Adiabatic Method	65
Dariusz OBRACAJ, Marek KORZEC, VU Tien Tung	
Artificial Neural Network Optimized by Modified Particle Swarm Optimization for Predicting Peak Particle Velocity Induced by Blasting Operations in Open Pit Mines	79
BUI Xuan-Nam, NGUYEN Hoang, NGUYEN Truc Anh	
Integration of Delphi Technique and Analytical Hierarchy Process Method in Assessment the Groundwater Potential Influence Criteria: A Case Study of the Ba River Basin	91
DANG Tuyet Minh, NGUYEN Le Tung Duong	
Rule-based Classification of Airborne Laser Scanner Data for Automatic Extraction of 3D Objects in the Urban Area	103
BUI Ngoc Quy, LE Dinh Hien, DUONG Anh Quan, NGUYEN Quoc Long	
Development of Integrated Reporting in Poland	115
BARTOSZ Rymkiewicz	
Identifying Correlation of Coal Seams in the Tien Hai Area, Northern Vietnam by Using Multivariate Statistic Methods	129
KHUONG The Hung, NGUYEN Phuong, NGUYEN Thi Cuc, PHAM Nhu Sang, NGUYEN Danh Tuyen	
Influence of Harmonics on the Working Efficiency of a 6/1.2 kV Transformer in a Pit Mine	149
NGO Xuan Cuong, DO Nhu Y	
Stabilization of Deep Roadways in Weak Rocks Using the System of Two-level Rock Bolts	157
TRAN Tuan Minh, DO Ngoc Thai, DANG Trung Thanh, NGUYEN Duyen Phong, VO Trong Hung	
Stress Distribution Around Mechanized Longwall Face at Deep Mining in Quang Ninh Underground Coal Mine	167
BUI Manh Tung, LE Tien Dung, VO Trong Hung	
Geometrical Tests of Powered Roof Support Positioning in a Longwall Complex	177
SZURGACZ Dawid, ZHIRONKIN Sergey, TRZOP Konrad, VÖTH Stefan, SOBIK Leszek, CEHLÁR Michal	
General Geometric Model of GNSS Position Time Series for Crustal Deformation Studies – A Case Study of CORS Stations in Vietnam	183
TRAN Dinh Trong, NGUYEN Quoc Long, NGUYEN Dinh Huy	
Phase Diagrams of the Excitonic Insulator State: Analyzing the Excitonic Susceptibility	199
DO Thi Hong Hai, NGUYEN Thi Hau	
Geotechnical Properties of Soft Marine Soil at Chan May Port, Vietnam	207
NGUYEN Thi Nu, NGUYEN Thanh Duong, BUI Truong Son	
Applying the Lessons Learned from the Economics Nobel Prize 2020 to Land Use Right Auction in Vietnam	217
PHAM Ngoc Huong Quynh, NGUYEN Thi Ngoc Mai	
An Overview of Rare Earth Ores Beneficiation in Vietnam	227
NHU Thi Kim Dung, PHAM Van Luan, VU Thi Chinh, TRAN Van Duoc	
Technological and Economic Analysis of the Application of Surface Miner on the Example of a Limestone Deposit in Poland	237
ZAJĄCZKOWSKI Maciej	
Determination of Land Fund for the Development of Static Road Traffic Demand in Hanoi (Vietnam)	243
PHAN Anh, VO Thi Hong Lan, PHAN Huy Duong	
Assessment of Change in Urban Green Spaces Using Sentinel 2 MSI Data and GIS Techniques: A Case Study in Thanh Hoa City, Vietnam	251
NGUYEN Viet Nghia, TRINH Le Hung, NGUYEN Thi Thu Nga, LE Thi Le	
Mineralogical and Geochemical Characteristics of Lead-zinc Ore Deposits, and Potential Accompanying Components in the Cho Don – Cho Dien Area, Bac Kan Province, Vietnam	261
NGUYEN Tien Dung, NGUYEN Khac Du, NGUYEN Ngoc Thom	
State Governance of Coal Mining Industry towards Sustainable Development in Vietnam	275
CHU Thi Khanh Ly, PHAM Ngoc Huong Quynh, PHAM Tu Phuong, NGUYEN Quynh Nga	
Life Cycle Inventory (LCI) Stochastic Approach Used for Rare Earth Elements (REEs), Considering Uncertainty	283
SALA Dariusz, BIEDA Boguslaw	
Estimation of Suspended Sediment Concentration in Downstream of the Ba River Basin using Remote Sensing Images	293
NGUYEN Ba Dung, BUI Ngoc An, DANG Tuyet Minh	
A Numerical Method for the Design of the U-Shaped Segmental Tunnel Lining under the Impact of Earthquakes: A Case Study of a Tunnel in the Hanoi Metro System	305
NGUYEN Chi Thanh, DO Ngoc Anh, PHAM Van Vi, GOSPODARIKOV Alexandr	
Development of Support Plan and Operation Scheme for Semi-mechanized Longwall Face of Coal Seam 10T, Nam Khe Tam Mine – 86 Company, Dong Bac Corporation	321
VU Trung Tien, LE Tien Dung, VU Thai Tien Dung	
Research about Integration of Geodetic and Geotechnical Methods in Monitoring the Horizontal Displacement of Diaphragm Walls	331
PHAM Quoc Khanh, TRAN Ngoc Dong, NGUYEN Thi Kim Thanh, PHAM Van Chung	
Influence of Single Phase Voltage Loss and Load Carrying Mode on Mine Drainage Pump Motor in Vietnam	341
DO Nhu Y, NGO Xuan Cuong	
Method of Air Temperature Forecast in Mechanized Longwall Workings in the Conditions of Vietnamese Mines	353
TRUONG Tien Quan, Rafał ŁUCZAK, Piotr ŻYCZKOWSKI, Marek BOROWSKI	

VISION ZERO – Tools for Safety, Health, and Well-being Management and the Application in the Vietnamese Coal Mining Industry	365
NGUYEN Nga, MEESMANN Ulrich, TRUONG Ngoc-Linh, TRINH Vu-Hoa	
Current Status of Coal Mining and Some Highlights in the 2030 Development Plan of Coal Industry in Vietnam	373
NGUYEN Quynh Nga, NGUYEN Van Hau, PHAM Tu Phuong, CHU Thi Khanh Ly	
Cause and Solution to Roadway Deformation in Vietnam Underground Coal Mines	381
LE Quang Phuc	
Research and Development of Real-time High-Precision GNSS Receivers: A Feasible Application for Surveying in Coal Mines in Vietnam	391
PHAM Cong Khai, NGUYEN Gia Trong, NGUYEN Van Hai, TRAN Trong Xuan	
Promoting Information and Communication Technology in Online Service Delivery in Vietnam	405
NGUYEN Ngoc Mai, PHAM Ngoc Huong Quynh	
Strengthening Inspection and Audit of Occupational Safety and Health in Coal Mining Enterprises in Vietnam	413
NGO Kim Tu	
Studying the Effects of Some Factors on the Temperature of the Mine Air at the Heading Face	423
NGUYEN Van Quang, NGUYEN Van Thinh, NGUYEN Cao Khai, PHAM Van Chung	
Circular Economy Model and the Implementation in Vietnamese Coal Mining Industry	433
LE Dinh Chieu, DONG Thi Bich	
Monitoring Vegetation Cover Changes by Sentinel-1 Radar Images using Random Forest Classification Method	441
TRAN Van Anh, LE Thi Le, NGUYEN Nhu Hung, LE Thanh Nghi, TRAN Hong Hanh	
Doing Business in Vietnam from the Perspectives of Polish Entrepreneurs – the Role of Local Partners	453
NGUYEN Cao Son	
Genotype TNF-α(-308) and Silicosis on Factory Workers in Vietnam in 2020	459
NGUYEN Viet, NGUYEN Thi Thu Huyen, DAO Xuan Dat, VU Xuan Quy, PHAM Thi Quan, LE Thi Kim Chung, TRAN Huy Thinh, LE Thi Huong, NGUYEN Ngoc Anh, NGUYEN Viet Nhung, NGUYEN Ngoc Hong, LUONG Mai Anh, LE Thi Thanh Xuan	
Assessing Impacts of Mining Activities on Land Use/Land Cover Change Using Remote Sensing and GIS Techniques: A Case Study in Campha City, Vietnam	467
LE Thi Thu Ha	
Research and Solution Proposals to Optimize Distribution Power Grids in Smart Grid Condition	479
PHAM Trung Son, NGUYEN Dinh Tien, NGUYEN Quang Thuan, DANG Quang Khoa	
Strategy in Dispatching Trucks and Shovels with Different Capacity to Increase the Operating Efficiency in Cao Son Surface Coal Mine, Vietnam	487
PHAM Van Hoa, TRAN Trung Chuyen, LE Hong Anh, LE Thi Thu Hoa, PHAM Van Viet, NGUYEN Anh Tuan, LE Thi Huong Giang	
The Capability of Terrestrial Laser Scanning for Monitoring the Horizontal Displacement of High-Rise Buildings	495
PHAM Trung Dung, PHAM Quoc Khanh, CAO Xuan Cuong, NGUYEN Viet Hung, NGO Sy Cuong	
Protection of Female Workers' rights in Employment and Incomes in Vietnam	505
NGUYEN Thi Hong Loan, PHAM Thu Trang, NGUYEN Thi Ngoc Anh, BUI Thi Thu Thuy, NGUYEN Hong Thai	
Research, Calculation and Proposal of Ventilation Solution for Duong Huy Coal Mine when Mining Down to -250 m Depth	513
DAO Van Chi, LE Tien Dung, VU Thai Tien Dung, NGUYEN Hong Cuong	
The Impact of Coal Exploitation on Tidal Flat Changes, an Investigation Using Remote Sensing Data in Vietnam	521
PHAM Thi Lan, TONG Si Son, LE Thi Thu Ha, LE Thi Le, HOANG Huu Duc	
Solution to Ensure Ventilation when Expanding the Area of Cam Thanh Underground Coal Mine, Ha Long Coal Company, Vietnam	533
NGUYEN Cao Khai, NGUYEN Van Thinh, NGUYEN Phi Hung, NGUYEN Van Quang	
Prediction of Ground Subsidence During Underground Construction of Metro Line 2, Section 1, Ben Thanh - Tham Luong	543
VO Nhat Luan, NGUYEN Thi Nu, DO Minh Toan	
Career Orientation of Students in the Faculty of Mining at Hanoi University of Mining and Geology	555
TRUONG Thi Hoa, NGUYEN Thuy Quynh, NGUYEN Thi Thanh Tra, NGUYEN Tat Thang	
Exploring the Relation between Seismic Coefficient and Rock Properties Through Field Measurements and Empirical Model for Evaluating the Effect of Blast-Induced Ground Vibration in Open-Pit Mines: A Case Study at the Thuong Tan III Quarry (Vietnam)	567
TRAN Quang Hieu	
Improvement of State Institution on Management and Exploitation of Mineral Resources in Vietnam	579
PHAM Ngoc Huyen, NGUYEN Hoai Nga, NGUYEN Quoc Long, NGUYEN Quoc Cuong, NGUYEN Ngoc Bich	
Applying artificial pillar to replace the coal pillar protecting roadway to increase production efficiency and sustainable development in the Vietnamese coal industry	587
DINH Van Cuong, NGUYEN Anh Tuan, TRAN Van Thanh, NGUYEN Thi Hoai Nga, DUONG Duc Hai	
Using The Potential Of The Employees' Expertise And Awareness Of Occupational Hazards In The Mining Industry	567
Dagmara NOWAK-SENDEROWSKA, Michał PATYK	

